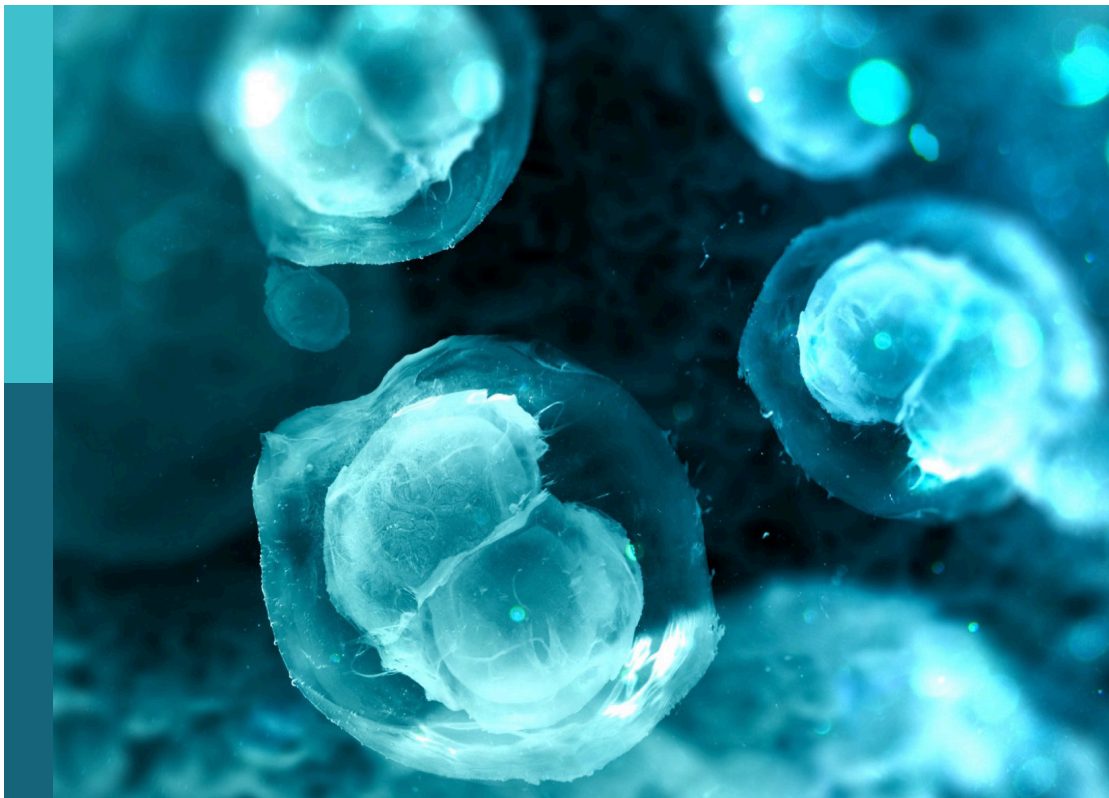
frontiers | Research Topics

Cancer cell reprogramming: Impact on carcinogenesis and cancer progression

Edited by
Ira Ida Skvortsova, Elvira V. Grigorieva, Simona Kranjc Brezar and Yue Zhao

Published in
Frontiers in Cell and Developmental Biology
Frontiers in Oncology



FRONTIERS EBOOK COPYRIGHT STATEMENT

The copyright in the text of individual articles in this ebook is the property of their respective authors or their respective institutions or funders. The copyright in graphics and images within each article may be subject to copyright of other parties. In both cases this is subject to a license granted to Frontiers.

The compilation of articles constituting this ebook is the property of Frontiers.

Each article within this ebook, and the ebook itself, are published under the most recent version of the Creative Commons CC-BY licence. The version current at the date of publication of this ebook is CC-BY 4.0. If the CC-BY licence is updated, the licence granted by Frontiers is automatically updated to the new version.

When exercising any right under the CC-BY licence, Frontiers must be attributed as the original publisher of the article or ebook, as applicable.

Authors have the responsibility of ensuring that any graphics or other materials which are the property of others may be included in the CC-BY licence, but this should be checked before relying on the CC-BY licence to reproduce those materials. Any copyright notices relating to those materials must be complied with.

Copyright and source acknowledgement notices may not be removed and must be displayed in any copy, derivative work or partial copy which includes the elements in question.

All copyright, and all rights therein, are protected by national and international copyright laws. The above represents a summary only. For further information please read Frontiers' Conditions for Website Use and Copyright Statement, and the applicable CC-BY licence.

ISSN 1664-8714
ISBN 978-2-83251-794-9
DOI 10.3389/978-2-83251-794-9

About Frontiers

Frontiers is more than just an open access publisher of scholarly articles: it is a pioneering approach to the world of academia, radically improving the way scholarly research is managed. The grand vision of Frontiers is a world where all people have an equal opportunity to seek, share and generate knowledge. Frontiers provides immediate and permanent online open access to all its publications, but this alone is not enough to realize our grand goals.

Frontiers journal series

The Frontiers journal series is a multi-tier and interdisciplinary set of open-access, online journals, promising a paradigm shift from the current review, selection and dissemination processes in academic publishing. All Frontiers journals are driven by researchers for researchers; therefore, they constitute a service to the scholarly community. At the same time, the *Frontiers journal series* operates on a revolutionary invention, the tiered publishing system, initially addressing specific communities of scholars, and gradually climbing up to broader public understanding, thus serving the interests of the lay society, too.

Dedication to quality

Each Frontiers article is a landmark of the highest quality, thanks to genuinely collaborative interactions between authors and review editors, who include some of the world's best academicians. Research must be certified by peers before entering a stream of knowledge that may eventually reach the public - and shape society; therefore, Frontiers only applies the most rigorous and unbiased reviews. Frontiers revolutionizes research publishing by freely delivering the most outstanding research, evaluated with no bias from both the academic and social point of view. By applying the most advanced information technologies, Frontiers is catapulting scholarly publishing into a new generation.

What are Frontiers Research Topics?

Frontiers Research Topics are very popular trademarks of the *Frontiers journals series*: they are collections of at least ten articles, all centered on a particular subject. With their unique mix of varied contributions from Original Research to Review Articles, Frontiers Research Topics unify the most influential researchers, the latest key findings and historical advances in a hot research area.

Find out more on how to host your own Frontiers Research Topic or contribute to one as an author by contacting the Frontiers editorial office: frontiersin.org/about/contact

Cancer cell reprogramming: Impact on carcinogenesis and cancer progression

Topic editors

Ira Ida Skvortsova — Innsbruck Medical University, Austria

Elvira V. Grigorieva — Institute of Molecular Biology and Biophysics FRC FTM, Russia

Simona Kranjc Brezar — Senior Research Associate, Institute of Oncology Ljubljana, Department of Experimental Oncology, Slovenia

Yue Zhao — University of Cologne, Germany

Citation

Skvortsova, I. I., Grigorieva, E. V., Brezar, S. K., Zhao, Y., eds. (2023). *Cancer cell reprogramming: Impact on carcinogenesis and cancer progression*. Lausanne: Frontiers Media SA. doi: 10.3389/978-2-83251-794-9

Table of contents

06 Editorial: Cancer cell reprogramming: Impact on carcinogenesis and cancer progression
Yue Zhao, Simona Kranjc Brezar, Elvira V. Grigorieva and Ira-ida Skvortsova

09 Downregulation of METTL7B Inhibits Proliferation of Human Clear Cell Renal Cancer Cells *In Vivo* and *In Vitro*
Wei Li, Shi Xu, Naixiong Peng, Zejian Zhang, Hua He, Ruoyu Chen, Dong Chen, Jiqing Fan and Xisheng Wang

21 LECT 2 Antagonizes FOXM1 Signaling via Inhibiting MET to Retard PDAC Progression
Xin Li, Pingping Lin, Ye Tao, Xin Jiang, Ting Li, Yunshan Wang, Chenjing Wang and Yu Cao

35 The Deubiquitinase USP39 Promotes ESCC Tumorigenesis Through Pre-mRNA Splicing of the mTORC2 Component Rictor
Yuan Zhao, Huiwu Geng, Gang Liu, Qiang Ji, Xiaomin Cheng, Xinying Li, Wei Liu, Rick F. Thorne, Renquan Zhang and Xiaoying Liu

47 Conditional Cell Reprogramming in Modeling Digestive System Diseases
Ruihua Zhao, Rui Li, Tianqi An and Xuefeng Liu

56 MAPK-RAP1A Signaling Enriched in Hepatocellular Carcinoma Is Associated With Favorable Tumor-Infiltrating Immune Cells and Clinical Prognosis
Hailin Li, Guangyu Han, Xing Li, Bowen Li, Bo Wu, Hongyuan Jin, Lingli Wu and Wei Wang

71 PDE2 Inhibits PKA-Mediated Phosphorylation of TFAM to Promote Mitochondrial Ca^{2+}-Induced Colorectal Cancer Growth
Yilin Zhao, Yaya Wang, Jing Zhao, Zhaohui Zhang, Mingpeng Jin, Feng Zhou, Chao Jin, Jing Zhang, Jinliang Xing, Nan Wang, Xianli He and Tingting Ren

83 Genome Instability-Derived Genes Are Novel Prognostic Biomarkers for Triple-Negative Breast Cancer
Maoni Guo and San Ming Wang

96 NAP1L1 Functions as a Tumor Promoter *via* Recruiting Hepatoma-Derived Growth Factor/c-Jun Signal in Hepatocellular Carcinoma
Ye-wei Zhang, Qian Chen, Bo Li, Hai-Yang Li, Xue-Ke Zhao, Yan-yi Xiao, Shu Liu and Shi Zuo

110 PARP1 Inhibitor Combined With Oxaliplatin Efficiently Suppresses Oxaliplatin Resistance in Gastric Cancer-Derived Organoids via Homologous Recombination and the Base Excision Repair Pathway
Huafu Li, Chunming Wang, Linxiang Lan, Wenhui Wu, Ian Evans, E. Josue Ruiz, Leping Yan, Zhijun Zhou, Joaquim M. Oliveira, Rui L. Reis, Zhenran Hu, Wei Chen, Axel Behrens, Yulong He and Changhua Zhang

129 Kill and Clearance in HCC: An Approach Based on NK Cells and Macrophages
Maryam Mehrabi, Fatemeh Amini and Shima Mehrabi

142 ASF1B Promotes Oncogenesis in Lung Adenocarcinoma and Other Cancer Types
Wencheng Zhang, Zhouyong Gao, Mingxiu Guan, Ning Liu, Fanjie Meng and Guangshun Wang

159 Circular RNA hsa_circ_0000073 Enhances Osteosarcoma Cells Malignant Behavior by Sponging miR-1252-5p and Modulating CCNE2 and MDM2
Zhijing Ren, Qinqin Yang, Jiajia Guo, Haifeng Huang, Bo Li, Zhen Yang and Xiaobin Tian

172 Classification of Estrogen Receptor-Positive Breast Cancer Based on Immunogenomic Profiling and Validation at Single-Cell Resolution
Xianxiong Ma, Hengyu Chen, Ming Yang, Zunxiang Ke, Mengyi Wang, Tao Huang and Lei Li

188 RFWD2 Knockdown as a Blocker to Reverse the Oncogenic Role of TRIB2 in Lung Adenocarcinoma
Ruimin Hao, Jinxia Hu, Yuemei Liu, Dongmin Liang, Yan-Mei Li, Ranran Wang, Shucui Zhang, Pingyu Wang, You-Jie Li and Shuyang Xie

202 NR2F1-AS1 Promotes Pancreatic Ductal Adenocarcinoma Progression Through Competing Endogenous RNA Regulatory Network Constructed by Sponging miRNA-146a-5p/miRNA-877-5p
Dong Luo, Yunfei Liu, Zhiqiang Li, Hongwei Zhu and Xiao Yu

219 The Prognostic Model Based on Tumor Cell Evolution Trajectory Reveals a Different Risk Group of Hepatocellular Carcinoma
Haoren Wang, Shizhe Yu, Qiang Cai, Duo Ma, Lingpeng Yang, Jian Zhao, Long Jiang, Xinyi Zhang and Zhiyong Yu

233 A Novel ZNF304/miR-183-5p/FOXO4 Pathway Regulates Cell Proliferation in Clear Cell Renal Carcinoma
Li-Xin Ren, Bo-Wen Zeng, Meng Zhu, An-Ning Zhao, Bei Shi, Hong Zhang, Dan-Dan Wang, Jun-Fei Gu and Zhan Yang

245 MiRNA-146a/AKT/β-Catenin Activation Regulates Cancer Stem Cell Phenotype in Oral Squamous Cell Carcinoma by Targeting CD24
Sangeeta Ghuwalewala, Dishari Ghatak, Sumit Das, Stuti Roy, Pijush Das, Ramesh Butti, Mahadeo Gorain, Somsubhra Nath, Gopal C. Kundu and Susanta Roychoudhury

262 Overexpression of NREP Promotes Migration and Invasion in Gastric Cancer Through Facilitating Epithelial-Mesenchymal Transition
Yuan-jie Liu, Shu-hong Zeng, Yi-dou Hu, Yong-hua Zhang and Jie-pin Li

279 Extrachromosomal Circular DNA (eccDNA): From Chaos to Function
Shanru Zuo, Yihu Yi, Chen Wang, Xueguang Li, Mingqing Zhou, Qiyao Peng, Junhua Zhou, Yide Yang and Quanyuan He

287 SIPA1 Enhances Aerobic Glycolysis Through HIF-2α Pathway to Promote Breast Cancer Metastasis
Chenguang Yao, Jun Weng, Lingyun Feng, Wanjun Zhang, Yan Xu, Peijing Zhang, Yoshimasa Tanaka and Li Su

301 Disruption of LTBP4 Inhibition-Induced TGFβ1 Activation Promoted Cell Proliferation and Metastasis in Skin Melanoma by Inhibiting the Activation of the Hippo-YAP1 Signaling Pathway
Lina Wang, Dongrun Tang, Tong Wu and Fengyuan Sun

318 An Aging-Related Gene Signature-Based Model for Risk Stratification and Prognosis Prediction in Lung Squamous Carcinoma
Wen-Yu Zhai, Fang-Fang Duan, Si Chen, Jun-Ye Wang, Ze-Rui Zhao, Yi-Zhi Wang, Bing-Yu Rao, Yao-Bin Lin and Hao Long

332 The Emerging Role of PRMT6 in Cancer
Zhixian Chen, Jianfeng Gan, Zhi Wei, Mo Zhang, Yan Du, Congjian Xu and Hongbo Zhao

347 Recent Advances of Autophagy in Non-Small Cell Lung Cancer: From Basic Mechanisms to Clinical Application
Weina Guo, Keye Du, Shanshan Luo and Desheng Hu

frontiers | Frontiers in Oncology

TYPE Editorial
PUBLISHED 15 February 2023
DOI 10.3389/fonc.2023.1152402

Check for updates

OPEN ACCESS

EDITED AND REVIEWED BY
Tao Liu,
University of New South Wales, Australia

*CORRESPONDENCE
Yue Zhao
yue.zhao@uk-koeln.de
Ira-ida Skvortsova
Ira.Skvortsova@i-med.ac.at

SPECIALTY SECTION
This article was submitted to Molecular and Cellular Oncology, a section of the journal Frontiers in Oncology

RECEIVED 27 January 2023
ACCEPTED 30 January 2023
PUBLISHED 15 February 2023

CITATION
Zhao Y, Kranjc Brezar S, Grigorieva EV and Skvortsova I-i (2023) Editorial: Cancer cell reprogramming: Impact on carcinogenesis and cancer progression.
Front. Oncol. 13:1152402.
doi: 10.3389/fonc.2023.1152402

COPYRIGHT
© 2023 Zhao, Kranjc Brezar, Grigorieva and Skvortsova. This is an open-access article distributed under the terms of the Creative Commons Attribution License (CC BY). The use, distribution or reproduction in other forums is permitted, provided the original author(s) and the copyright owner(s) are credited and that the original publication in this journal is cited, in accordance with accepted academic practice. No use, distribution or reproduction is permitted which does not comply with these terms.

Editorial: Cancer cell reprogramming: Impact on carcinogenesis and cancer progression

Yue Zhao[1]*, Simona Kranjc Brezar[2], Elvira V. Grigorieva[3] and Ira-ida Skvortsova[4]*

[1]Department of General, Visceral, Tumor and Transplantation Surgery, University Hospital of Cologne, Cologne, Germany, [2]Department of Experimental Oncology, Institute of Oncology Ljubljana, Ljubljana, Slovenia, [3]Institute of Molecular Biology and Biophysics Federal Research Center of Fundamental and Translational Medicine (FRC FTM), Timakova, Novosibirsk, Russia, [4]Laboratory for Experimental and Translational Research on Radiation Oncology (EXTRO-Lab), Department of Therapeutic Radiology and Oncology, Innsbruck Medical University, Innsbruck, Austria

KEYWORDS

cell reprogramming, cancer stem cell, cancer metabolism, cancer metastasis, carcinogenesis

Editorial on the Research Topic
Cancer cell reprogramming: Impact on carcinogenesis and cancer progression

The transformation of normal cells into cancerous cells is a multi-stage process which progresses from a pre-cancerous lesion to a malignant tumor. There were an estimated almost 10.0 million deaths from cancer worldwide in 2020 (1). Currently challenges in cancer managements major due to late diagnosis, metastasis, recurrence, tumor heterogeneity and therapy resistance (2), All these failures could be explained by the characteristics of tumor heterogeneity and the existence of cancer stem cells (CSCs) (3). The concept of cellular plasticity was first proposed by Gurdon et al. (4). Cancer cells are also showing genetically and epigenetically plasticity, so cancer cell reprogramming could cover a board of cellular and molecular alterations, having significant impact on carcinogenesis and cancer progression and will also provide promising therapeutic strategies to convert the tumor malignancy (5, 6). In this Research Topic: '*Cancer Cell Reprogramming: Impact on Carcinogenesis and Cancer Progression*', we aim to collect and discuss the studies on this topic based on 5 review articles, 13 original articles and 7 bioinformatic centralized studies.

First of all, signaling pathways and key modulators in cancer reprogramming are still the hot topics in cancer research. Knowing biological targets or biomarkers enables us to develop an effective and specific treatment approach in melanoma, lung, gastric and hepatocellular cancer (7, 8). Zhang et al. demonstrated the NAP1L1 as a potentially significant oncogene that could be used as a prognostic factor in hepatocellular carcinoma (HCC). Indeed, the upregulation of NAP1L1 promotes disease progression and predicts poor prognosis of HCC in patients. Silencing of NAP1L1 expression significantly decreased cell proliferation and cell

cycle transformation *in vitro* and *in vivo*. The reversion of these suppressive effects in NAP1L1 cells after transfecting HDGF or c-Jun, clearly indicates for the first time NAP1L1 as a potential oncogene that acts *via* HDGF/c-Jun signaling pathway in HCC.

Despite different treatment approaches, surgery, immunotherapy, radiation therapy, chemotherapy, or combination therapy, malignant melanoma is the most invasive and fatal skin carcinoma. Thus, the time of melanoma diagnosis and the use of specific biological markers are crucial. Wang et al. focused on a gene encoding a subtype of Latent transforming growth factor binding protein 4 (LTBP4), an extracellular matrix glycoprotein belonging to the LTBP/fibrillins superfamily that is involved in the development of skin melanoma. Down-regulation of LTBP4 expression in cells and melanoma tissues predicted poor prognosis of melanoma patients. Furthermore, the authors indicated the crucial role of the molecular signaling pathway LTBP4-TGFβ1-Hippo-YAP1 in the progression of skin melanoma *in vitro* and *in vivo* by switching it on/off. LTBP4 may function as a possible new biomarker for melanoma skin.

Nowadays treatment options for gastric cancer are still limited (9, 10). Resistance to chemotherapeutic drugs represents a great challenge in cancer treatment. To provide survival benefits to patients with oxaliplatin combined therapies, Li et al. studied the mechanisms of resistance to oxaliplatin in human organoids grown *in vitro* and subcutaneously *in vivo* and compared the data to patients' follow-ups. This study greatly represents the development of personalized therapy. Overexpressed PARP1 was shown as an important gene involved in oxaliplatin resistance by inhibiting the base excision repair pathway. Additionally, for the first time, it was shown that oxaliplatin inhibited homologous recombination by CDK1 activity and made cancers with normal BRCA1 function sensitive to PARP inhibition. Importantly, they demonstrated that combining oxaliplatin with a PARP1 inhibitor can overcome the oxaliplatin resistance, suggesting a potential new treatment modality for patients with gastric cancer without BRCA1 mutations. This observation can be helpful in clinical practice to evaluate the efficacy of PARP1 inhibitors in combination with platinum compounds in gastric cancer patients.

The new aspect in the personalized medicine of gastric cancer is focused on targeting the tumor microenvironment which includes a variety of cellular and non-cellular components such as non-malignant host cells, immune, blood, and endothelial cells, fibroblasts, mesenchymal stromal cells, and extracellular matrix. Unfortunately, targeting drugs for the first-line treatment of gastric cancer are still unavailable. Liu et al. assume that the reason for this situation is due to the lack of the biomarkers and complexity of the tumor microenvironment in gastric cancer. The authors suggested to consider the Neuronal Regeneration Related Protein (NREP) as a key regulator of gastric cancer progression. It was shown that NREP is involved in EMT activation, CAF mibilization, actin cytoskeleton remodeling, and M2 macrophage infiltration resulting in tumor development and progression.

Non-small cell lung cancer (NSCLC) represents approximately 85% of subtypes of lung cancer, which is the leading cause of cancer death worldwide. In this issue, Guo et al. elucidated autophagy, an important physiological activity that controls cell survival and death, affecting cell homeostasis and clinical therapeutics. The authors give us a nice historical overview through the preclinical and clinical data in NSCLC demonstrating that autophagy modifies the tumor microenvironment, participates in metabolic reprogramming, eliminates ROS, promotes resistance to chemotherapeutic drugs and tumor evasion in antitumor immune responses. Additionally, a brief description of autophagy biomarkers NSCLC and already used agents in the inhibition of autophagy enlighten us on how to further develop new treatment options for NSCLC. In a translational study of lung adenocarcinoma, Hao et al. found that knock down of RFWD2, an E3 ubiquitin ligase, may reverse the oncogenic role of the tribble (TRIB) pseudokinase protein family member- TRIB2. TRIB2 was reported as an oncogene and promoted cancer cell proliferation and migration (11). In this study, they further demonstrated that TRIB2 regulated the lung cancer cell growth by modulating the proteasome-mediated degradation of proteins *via* interaction with RFWD2.

Recently, continuously growing number of studies on the role of the mitochondrial Ca^{2+} in the progression of malignant tumors leads to the increasing interest of basic researchers to investigate the molecular regulation of mitochondrial calcium homeostasis in cancer progression. It is currently known that mitochondrial Ca^{2+} uptake is markedly enhanced in a variety of malignancies, but the exact mechanisms orchestrating the levels of Ca^{2+} in mitochondria are not fully elucidated. Zhao et al. have shown that Ca^{2+} uptake can be upregulated by the mitochondrial calcium uniporter (MCU). Augmented Ca^{2+} concentration results in increased mitochondrial biogenesis accompanied by suppressing the phosphorylation of mitochondrial transcription factor A (TFAM). Authors have focused on the molecular mechanisms underlying the inhibition of TFAM phosphorylation by MCU-related mitochondrial Ca^{2+} uptake. It was found that PDE2/cAMP/PKA axis contributed tot he TFAM stability and colorectal cancer cell growth.

Several articles are devoted to the study of molecular mechanisms of the development of such aggressive urologic tumors as clear cell renal cell carcinoma (ccRCC) and the search for new biomarkers for proper adjuvant therapy selection (12, 13). Li et al. demonstrated the involvement of a poorly studied member of the methyltransferases family - METTL7B in ccRCC tumorigenesis. METTL7B knockdown inhibited the growth of ccRCC *in vitro* and *in vivo* by inhibiting the expression of genes involved in the regulation of cell cycle and invasion, for the first time identifying METTL7B as a biomarker of poor clinical outcome and potential therapeutic target in ccRCC patients.

In addition, Ren et al. paid special attention to the genes, which are downregulated in ccRCC, so not being cancer biomarker candidates, although the genes are also important for carcinogenesis. The authors demonstrated that transcriptional repressor zinc-finger protein 304 (ZNF304) is down-regulated in ccRCC tissue, and a lower level of this protein is associated with poor prognosis of patient survival. A molecular mechanism of ZNF304 involvement in RCC progression is realized through ZNF304/miR-183-5p/FOXO4 axis, suggesting key components of this pathway as potential therapeutic targets in ccRCC.

Metabolic reprogramming of cancer cells is one of the most important hallmarks of cancer (14). Yao et al. demonstrated the important role of signal-induced proliferation-associated 1 (SIPA1) in aerobic glycolysis. SIPA1 may alter the main source of ATP production from oxidative phosphorylation to glycolysis by

promoting the transcription of EPAS1 (a gene encoding hypoxia-inducible factor-2α (HIF-2α)) and interacting with multiple glycolysis-related genes in breast cancer models. Developing new strategies targeting SIPA1 and blocking aerobic glycolysis may provide promising insight in treating breast cancer patents.

Cancer cell reprogramming supported the existence of CSCs, which are characterized by the permanent processes of differentiation and dedifferentiation. Therefore, there is a need to know more about the molecular regulation of the processes of CSC differentiation/dedifferentiation. The manuscript by Ghuwalewala et al. demonstrates that CD24 is a functional target of miR-146a. miR-146a can modulate CSC properties through CD24-AKT-β-catenin axis. It opens new perspectives in the development of more precise diagnostic tools and personalized medicine approaches to be used in the management of HNSCC patients.

A little part in this issue is an interesting review by Zuo et al., devoted to a special aspect of cell physiology as the presence and functional significance of such underestimated structure as extrachromosomal circular DNA (eccDNA). The authors give a brief discovery history of eccDNA, describe several models of the eccDNA biogenesis and their important role in a variety of normal physiological processes and carcinogenesis. The high stability of extracellular free eccDNAs and their presence in cancer tissues and peripheral blood of cancer patients suggest the potential applying them as a novel type of biomarkers in liquid biopsy for the early detection of diseases, the monitoring of drug treatment response, and cancer survival.

Interestingly, in this Research Topic, there is an article systematically discussed conditional reprogramming (CR) cell culture technology in cell reprogramming research of digestive System diseases. It is based on using irradiated Swiss-3T3-J2 mouse fibroblast cells and the Rho-associated kinase (ROCK) inhibitor Y-27632. This technology may work as a promising model for drug sensitivity tests, gene profile analyses, and even tissue regeneration-associated applications. Never or less, the limitations of CR were also summarized. In particular, the authors' team shared the experience of establishing the Next Generation Living Biobank (NGLB) based on 2D and 3D culture systems with the potential of combining CR technology (Zhao et al.).

Conclusion

This Research Topic sought to collect promising translational studies, new mechanisms and molecular signatures, highlighting the importance of understanding the molecular mechanism and the clinical impact of cancer cell reprogramming in carcinogenesis and malignancy progression. Developing new therapeutic strategies and promising approaches which regulate the cancer cell plasticity may provide insights to overcome the therapy resistance and propose successful management of the metastatic disease.

Author contributions

All authors have made a substantial contribution to this editorial work, and approved the context for publication.

Acknowledgments

All of the topic editors would like to express their sincere gratitude to all the authors and institutions for their full dedication of the manuscripts in this Research Topic.

Conflict of interest

The authors declare that the research was conducted in the absence of any commercial or financial relationships that could be construed as a potential conflict of interest.

Publisher's note

All claims expressed in this article are solely those of the authors and do not necessarily represent those of their affiliated organizations, or those of the publisher, the editors and the reviewers. Any product that may be evaluated in this article, or claim that may be made by its manufacturer, is not guaranteed or endorsed by the publisher.

References

1. Ferlay J, Colombet M, Soerjomataram I, Parkin DM, Pineros M, Znaor A, et al. Cancer statistics for the year 2020: An overview. *Int J Cancer* (2021) 149(4):778–89. doi: 10.1002/ijc.33588

2. Batlle E, Clevers H. Cancer stem cells revisited. *Nat Med* (2017) 23(10):1124–34. doi: 10.1038/nm.4409

3. Reya T, Morrison SJ, Clarke MF, Weissman IL. Stem cells, cancer, and cancer stem cells. *Nature* (2001) 414(6859):105–11. doi: 10.1038/35102167

4. Gurdon JB, Elsdale TR, Fischberg M. Sexually mature individuals of xenopus laevis from the transplantation of single somatic nuclei. *Nature* (1958) 182(4627):64–5. doi: 10.1038/182064a0

5. Gong L, Yan Q, Zhang Y, Fang X, Liu B, Guan X. Cancer cell reprogramming: a promising therapy converting malignancy to benignity. *Cancer Commun (Lond)* (2019) 39(1):48. doi: 10.1186/s40880-019-0393-5

6. Yang L, Shi P, Zhao G, Xu J, Peng W, Zhang J, et al. Targeting cancer stem cell pathways for cancer therapy. *Signal Transduct Target Ther* (2020) 5(1):8. doi: 10.1038/s41392-020-0110-5

7. Hanahan D. Hallmarks of cancer: New dimensions. *Cancer Discov* (2022) 12(1):31–46. doi: 10.1158/2159-8290.CD-21-1059

8. Wang DR, Wu XL, Sun YL. Therapeutic targets and biomarkers of tumor immunotherapy: response versus non-response. *Signal Transduct Target Ther* (2022) 7(1):331. doi: 10.1038/s41392-022-01136-2

9. Yuan L, Xu ZY, Ruan SM, Mo S, Qin JJ, Cheng XD. Long non-coding RNAs towards precision medicine in gastric cancer: Early diagnosis, treatment, and drug resistance. *Mol Cancer* (2020) 19(1):96. doi: 10.1186/s12943-020-01219-0

10. Wei L, Sun J, Zhang N, Zheng Y, Wang X, Lv L, et al. Noncoding RNAs in gastric cancer: implications for drug resistance. *Mol Cancer* (2020) 19(1):62. doi: 10.1186/s12943-020-01185-7

11. Zhang YX, Yan YF, Liu YM, Li YJ, Zhang HH, Pang M, et al. Smad3-related miRNAs regulated oncogenic TRIB2 promoter activity to effectively suppress lung adenocarcinoma growth. *Cell Death Dis* (2016) 7(12):e2528. doi: 10.1038/cddis.2016.432

12. Fitzgerald KN, Motzer RJ, Lee CH. Adjuvant therapy options in renal cell carcinoma - targeting the metastatic cascade. *Nat Rev Urol* (2022). doi: 10.1038/s41585-022-00666-2

13. Berg SA, McGregor BA. The continuing question of adjuvant therapy in clear cell renal cell carcinoma. *Cancers (Basel)* (2022) 14(24):6018. doi: 10.3390/cancers14246018

14. Hanahan D, Weinberg RA. Hallmarks of cancer: The next generation. *Cell* (2011) 144(5):646–74. doi: 10.1016/j.cell.2011.02.013

frontiers in Oncology

ORIGINAL RESEARCH
published: 26 February 2021
doi: 10.3389/fonc.2021.634542

Downregulation of METTL7B Inhibits Proliferation of Human Clear Cell Renal Cancer Cells *In Vivo* and *In Vitro*

Wei Li[1*†], *Shi Xu*[2†], *Naixiong Peng*[1], *Zejian Zhang*[1], *Hua He*[1], *Ruoyu Chen*[3], *Dong Chen*[1], *Jiqing Fan*[1] *and Xisheng Wang*[1*]

[1] Department of Urology, Shenzhen Longhua District Central Hospital, The Affiliated Central Hospital of Shenzhen Longhua District, Guangdong Medical University, Shenzhen, China, [2] Department of Burn and Plastic Surgery, Shenzhen Longhua District Central Hospital, The Affiliated Central Hospital of Shenzhen Longhua District, Guangdong Medical University, Shenzhen, China, [3] Department of Proctology, Shenzhen Longhua District Central Hospital, The Affiliated Central Hospital of Shenzhen Longhua District, Guangdong Medical University, Shenzhen, China

Clear cell renal cell carcinoma (ccRCC) is the most aggressive urologic tumor, and its incidence and diagonosis have been continuously increasing. Identifying novel molecular biomarker for inhibiting the progression of ccRCC will facilitate developing new treatment strategies. Although methyltransferase-like 7B (METTL7B) was identified as a Golgi-associated methyltransferase, the function and mechanism of METTL7B in ccRCC development and progression has not been explored. METTL7B expression were significantly upregulated in ccRCC tissues (n = 60), which significantly associated with TNM classification, tumor size, lymph node metastasis, and poor prognosis for ccRCC patients. Functional studies showed downregulation of METTL7B inhibited cell proliferation, migration *in vitro*, and xenograft tumor formation *in vivo*. In addition, METTL7B knockdown promoted cell cycle arrest at G0/G1phase and induced cellular apoptosis. Taken together, downregulation of METTL7B inhibits ccRCC cell proliferation and tumorigenesis *in vivo* and *in vitro*. These findings provide a rationale for using METTL7B as a potential therapeutic target in ccRCC patients.

Keywords: METTL7B, methyltransferase, ccRCC, proliferation, tumorigenesis

OPEN ACCESS

Edited by:
Ira Ida Skvortsova,
Innsbruck Medical University, Austria

Reviewed by:
Zhanjun Guo,
Fourth Hospital of Hebei Medical University, China
Miriam Galvonas Jasiulionis,
Federal University of São Paulo, Brazil

****Correspondence:***
Xisheng Wang
18923877315@163.com
Wei Li
qwer_214@163.com

[†]These authors have contributed equally to this work

Specialty section:
This article was submitted to Molecular and Cellular Oncology, a section of the journal Frontiers in Oncology

Received: *28 November 2020*
Accepted: *14 January 2021*
Published: *26 February 2021*

Citation:
Li W, Xu S, Peng N, Zhang Z, He H, Chen R, Chen D, Fan J and Wang X (2021) Downregulation of METTL7B Inhibits Proliferation of Human Clear Cell Renal Cancer Cells In Vivo and In Vitro. Front. Oncol. 11:634542. doi: 10.3389/fonc.2021.634542

INTRODUCTION

Renal cell carcinoma (RCC) is a malignant tumor originated from the proximal tubules of the nephrons (1). Clear cell RCC (ccRCC) is the most prevalent pathological subtype and accounts for approximately 70% of all diagnosed RCC cases (2). Approximately 15–20% of ccRCC patients had metastatic lesions at primary diagnosis, and 30% eventually developed metastatic after surgery (1, 3). Once metastasized, the prognosis for patients is poor. The most critical causes of the poor outcome are the lack of sensitive biomarkers for early diagnosis and effective treatments (4). Therefore,it is needed to identify novel molecular targets, especially previously unrecognied molecules that can monitor the progression of ccRCC and develop more effective treatment strategies.

Methyltransferases (METTL) are a large group of enzymes that transfer a methyl group to lysine or arginine side chains on nuclear and cytoplasmic proteins (5). So the funtions of this protein family were predicted to methylate RNA (METTL3, METTL14, METTL1), DNA (METTL4), or protein (METTL10 and METTL11A) (6–8). Many studies have demonstrated that METTL proteins play a central role in the development of genetic diseases, cancers, and metabolic diseases through regulating signaling pathways (9, 10). For example, METTL14 suppresses proliferation and metastasis of colorectal cancer by downregulating oncogenic long non-coding RNA XIST (11). Upregulated METTL3 promotes metastasis of colorectal cancer *via* miR-1246/SPRED2/MAPK signaling pathway (12). Howerver, most METTL proteins are still poorly characterized.

METTL7B was originally identified as a Golgi-associated methyltransferase which methylates Golgi-associated proteins using multidimensional protein identification technology in 2004 (13). However, few study has investigated the function and mechanism of METTL7B in cancer development and progression. METTL7B might serve as a biomarker for diagnosis and tumor progression in papillary thyroid carcinoma (14). METTL7B also enhanced migration and invasion of thyroid carcinoma cells through promote TGF-β1-induced epithelial-mesenchymal transition (EMT) (15). Our previous study also showed that METTL7B is required for cancer cell proliferation and tumorigenesis in non-small cell lung cancer (16). Therefore, we planned to characterize the role and mechanism of METTL7B in ccRCC. In this study, we showed that METTL7B is involved in the regulation of cell cycle progression and essential for ccRCC development. We suggested that METTL7B might serve as a potential therapeutic target for ccRCC.

MATERIALS AND METHODS

Clinical Samples and Immunohistochemistry (IHC) Staining

The tissue array containing a total of 60 pairs of ccRCC samples and matched adjacent normal renal tissues with follow-up data was obtained from Shenzhen Longhua District Central Hospital (Shenzhen, China). This study was approved by the Ethics Committee of Shenzhen Longhua District Central Hospital. IHC assays were performed on tissue microarray chips according to a standard protocols by Abclonal description. Briefly, sections were incubated with anti-METTL7B polyclonal antibody (Abclonal, #A7200, 1:100) overnight at 4°C, and subsequently incubated with streptavidin-conjugated horseradish peroxidase. Sections were visualized with DAB kit and counterstained with hematoxylin, mounted in neutral gum, and analyzed using a brightfield microscope. All IHC samples were assessed by two independent pathologists blinded to both the sample origins and the subject outcomes. For survival analyses, patient overall survivals stratified by METTL7B expression, were presented as the Kaplan–Meier plots and tested for significance using log-rank tests. Differences were considered significant when P value was less than 0.05.

Cell Lines and Cultures

The human ccRCC cell line (786-O, A498, Caki-1,796-P, and ACHN) were purchased from the American Type Culture Collection (ATCC). HK 2 cell line was purchased from Shanghai Cell Bank, Chinese Academy of Sciences. The three ccRCC cell line(A498, Caki-1, and ACHN)were cultured in in Eagle's Minimum Essential Medium (DMEM, Gibco) medium. The 786-O and 796-P were cultured in RPMI 1640 (Gibco). The normal proximal tubule epithelial cell line HK-2 was DMEM/F-12 1:1 (Gibco). All the cells were cultured in 10% fetal bovine serum (Hyclone) at 37°C in an incubator with 5% CO_2. All lines were measured to be confirm negative of mycoplasma contamination.

Cell Transfection

Cells were seeded on six-well plates at a density of 2×10^5 cells/well. After 80% confluence was reached, shMETTL7B (METTL7B shRNA: 5'- GGGAAAGGCTGTCAAATAA -3') and a negative control shRNA (shNC: 5'- TTCTCCGAACGTG TCACGT -3') were transfected into cells using SuperFectin shRNA Transfection Reagent (Pufei, Shanghai, China). After 48 h, quantitative RT-PCR and Western blot were performed to determine the transfection efficiency.

Cell Viability and Proliferation Assay

The living cell population was analyzed using Trypan Blue dye exclusion assay and MTT assay according to our previous report (17).

Colony Formation Assay

METTL7B shRNA or negative control shRNA was transfected into 796-P and ACHN cells. Subsequently, cells were seeded in six-well plates at a density of 10^3 cells/well. After incubation at 37°C for 14 days, colonies were fixed with 4% paraformaldehyde and stained by crystal violet (0.1%) for 15 min at room

Abbreviations: METTL7B, Methyltransferase 7B; RCC, Renal cell carcinoma; ccRCC, Clear cell RCC; PCR, Polymerase Chain Reaction; shRNA, Short hairpin RNA; BSA, Bovine Serum Albumin; h, hour; CCK8, Cell Counting Kit; S.D., standard deviation; EMT, Epithelial-mesenchymal transition; CDKN2D, cyclin dependent kinase inhibitor 2D; PCNA, proliferating cell nuclear antigen.

temperature and photographed by a camera. Macroscopic colonies of each well were counted.

Flow Cytometry Analysis of Apoptosis and Cell Cycle Distribution

METTL7B shRNA or negative control shRNA was transfected into 796-P and ACHN cells. For apoptosis assays, cells were collected and treated with 500 μl Annexin V/PI binding buffer and then incubated for 15 min at room temperature. For cell cycle assays, cells were collected and fixed in 75% ethanol for 24 h. Then the cells were washed by cold PBS, stained with Annexin V- FITC and PI for 20 min, and then analyzed by flow cytometer (BD Bioscineces, Bedford, MA, USA).

Cell Migration and Invasion Assays

The transwell insert for 24-well plate (8 μm-pore size, Corning, NY, USA) was used to measure the migratory and invasive ability of cells. For transwell migration assays, cells (2.5×10^4) with shMETTL7B or negative control shRNA were seeded into the transwell insert with serum-free medium and the culture medium with 10% FBS was added in the lower chamber for chemo-attractant. The invasion assays were performed similarly except that the upper chambers of 24-well cell culture inserts were coated with 200 mg/ml of Matrigel (BD Biosciences, Bedford, MA). Following culture for 48 h at 37˚C, the cells in the bottom chamber were stained with 0.1% crystal violet (Beyotime Biotech, China). The cells were then evaluated by a light microscopy (CK40; Olympus Corporation, Tokyo, Japan) at the magnification at ×100. Images were captured, then the cells were counted randomly in five fields and the average was calculated.

RNA Extraction and Real-Time Quantitative PCR Assays

Total RNA was extracted from cells using Trizol Reagent (Invitrogen, USA), and cDNA was synthesized from 1 μg of RNA with the M-MLV Reverse Transcriptase Kit (Promega, USA) as recommended by the manufacturer. Real-time quantitative PCR reactions for the quantification of gene expression were performed with Bio-Rad iQ5 Real Time PCR System. The primers for METTL7B and β-acin sequences used according to our previous report (16).

Western Blot

Total protein was extracted as described previously (16, 18). Protein concentration was determined with the BCA Protein Assay Kit (Pierce, Rockford, IL, USA). Equivalent amounts of protein samples were uploaded and separated by 12% SDS-PAGE and then electro-transferred to polyvinylidene difluouride (PVDF) membranes (Millipore Corp, Atlanta, GA, USA). The membranes were blocked in 5% non-fat dry milk powder at room temperature for 1 h, and then incubated with primary antibodies as following: anti-METTL7B (Abclonal, 1:800), anti-N-cadherin (Abcam, 1:1,000), anti-vimentin (Abcam, 1:1,000), anti-slug (abcam, 1:1,000), anti-snail (CST, 1:800), anti-twist (CST, 1:800), anti-CDK1 (CST, 1:1,000), anti-CCND1 (CST, 1:1,000), anti-CCNB1 (CST,1:1,000), anti-CDKN2D (CST, 1:1,000) for overnight at 4°C, followed by HRP-conjugated secondary antibodies at room temperature for 1 h. The housekeeper gene β-actin was employed as an internal control. The signals of bands were detected by ECL reagents.

In Vivo Tumorigenesis Assay

Male BALB/c nu/nu mice (4–5 weeks old) purchased from the Laboratory Animal Center of Shanghai, Academy of Science Chinese (Shanghai, China), were housed under specific pathogen-free conditions. Mice were randomly divided into two groups with five mice in each group. 796-P transfected with METTL7B shRNA or negative control shRNA (1×10^6 cells/mice) were injected subcutaneously into the flanks of mice. Ten days after cell injection, the length (L) and width (W) of tumor xenografs were measured at a 3-day intervals with a vernier caliper. Tumor volumes were calculated ($V = W^2 \times L/2$). The animals were sacrificed under general anesthesia with chloral hydrate (5%, 100 μl/10 g). All the experiments complied with the guidelines of the Guangdong Medical University Institutional Animal Care and Use Committee on Animal Care and Use.

Statistical Analysis

All data were expressed as mean ± standard deviation (S.D). SPSS 19.0 (SPSS, Chicago, IL, USA) was used to conduct all the statistical analysis. Kaplan-Meier for survival analysis. Student's t-test were used to evaluate the differences between variables. Chi-square test or Spearman's rank test (as appropriate) were used for correlation between METTL7B expression and clinicopathological characteristics. The correlation between gene expression and clinicopathologic features were and P value less than 0.05 was regarded as statistically significant.

RESULTS

METTL7B Is Upregulated in ccRCC and Correlates With Poor Clinical Outcomes

Firstly, to analyze the expression pattern of METTL7B in ccRCC, we compared METTL7B expression between normal renal tissues and ccRCC tissues using TCGA data. The results showed that METTL7B was significantly upregulated in ccRCC tissues (**Figure 1A**). To further investigate the clinical significance of METTL7B expression in RCC tumorigenesis, the expression of METTL7B was further evaluated in 60 pairs of ccRCC tissues and their matched non-tumor tissues by qRT-PCR and IHC staining. The results showed that the expression of METTL7B was significantly higher in ccRCC tissues compared to their matched normal renal tissues (**Figure 1B**). IHC staining

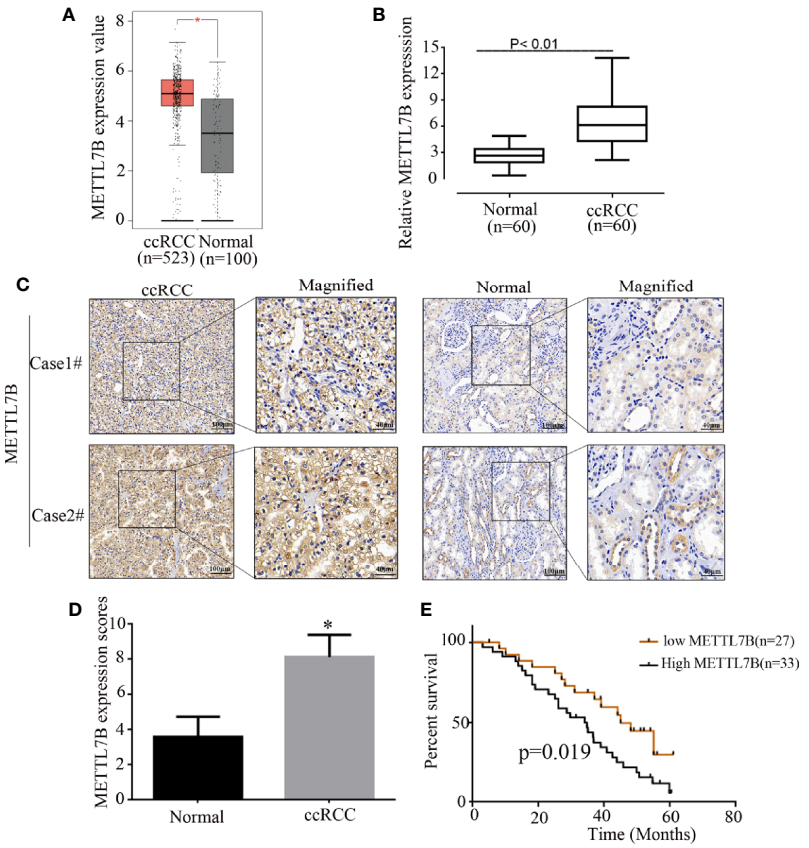


FIGURE 1 | METTL7B is highly expressed in human ccRCC tissues. **(A)** The expressions of METTL7B in ccRCC tissues and normal renal tissues were analyzed based on TCGA database. Data are presented as the mean ± SD. **(B)** The expression of METTL7B mRNA were evaluated in 60 pairs of ccRCC tissues and normal renal tissues by qRT-PCR. Data are presented as the mean ± SD of three independent experiments. **(C)** The expressions of METTL7B in ccRCC and paired normal renal tissues were tested by IHC staining. **(D)** METTL7B staining scores in ccRCC tumors and the corresponding non-tumor tissues (n = 60). **(E)** Kaplan–Meier survival curves showed that METTL7B expression level was negatively correlated with prognosis prediction of ccRCC analyzed. *p < 0.05.

analysis also indicated that the high expression of METTL7B in ccRCC tissues (**Figures 1C, D**).

The correlation of METTL7B expression with various clinicopathologic features was investigated and the result showed that upregulation of METTL7B was significantly associated with TNM classification (P = 0.048), Tumor size (P = 0.031), Lymph node metastasis (P = 0.046) (**Table 1**). Furthermore, the Kaplan-Meier survival analysis revealed that the patients harboring higher METTL7B expression showed significantly shorter overall survival than did patients with lower METTL7B expression (P < 0.019, **Figure 1E**). Taken together, the initial findings indicate that upregulation of METTL7B may play an important role in ccRCC tumorigenesis.

Downregulation of METTL7B Inhibits ccRCC Cell Proliferation *In Vitro*

To further investigate the role of METTL7B in ccRCC progression, we examined the expression of METTL7B in five ccRCC cell lines: 786-O, 796-P, A498, ACHN and Caki-1, and human normal proximal tubule epithelial cell line HK-2. Consistent with the result of ccRCC tissues, we found that METTL7B was upregulated in RCC cells compared with human normal proximal tubule epithelial cell HK-2 (**Supplementary Figure 1**). Among these ccRCC cells, 796-P and ACHN cell was predominantly upregulated. Therefore, we used 796-P and ACHN cells for further investigation in the following studies.

Our previous study have designed and validated two different shRNAs targeting METTL7B (16). One of them was used in this study. Firstly, 786-P and ACHN cells were transfected with lentivirus carrying a specific shRNA targeting METTL7B (shMETTL7B) and control (shCtrl). Lentivirus for knockdown efficiency was also examined by qPCR and western blot. The results showed that the mRNA and protein expressions of METTL7B were significantly decreased compared to that in the control group (shCtrl) (**Figures 2A, B**). Furthermore, the trypan blue rejection method and MTT assay were used to measure the cell proliferation and viability. Cell growth assay showed that

TABLE 1 | The correlation between METTL7B expression and clinical characteristics of patients with ccRCC.

Characteristics	Cases(n = 60)	METTL7B Expression		*P value*
		Low	High	
Gender				
Male	26	11	15	0.714
Female	34	16	18	
Age				
>60 years	33	16	17	0.236
≤60 years	27	9	18	
Fuhrman Grade				
1–2	31	12	19	0.455
3–4	29	14	15	
TNM classification				
I-II	25	15	10	**0.048***
III-IV	35	12	23	
Tumor size				
≤5cm	34	20	14	**0.031***
>5cm	26	8	18	
Lymph node metastasis				
Negative	15	9	6	**0.046***
Positive	45	14	31	

**means statistically significant.*
The meaning of the bold values is highlighted and less than 0.05.

METTL7B knockdown can significantly inhibit proliferation capabilities and viability (**Figures 2C, D**).

Downregulation of METTL7B Induces ccRCC Cell Cycle Arrest At G1/S Transition

Furthermore, we subsequently performed the colony formation assay to determine whether knocking down METTL7B could inhibit the colony formation capacity. Results demonstrated that knocking down METTL7B significantly reduced the number of colonies when compared with control cells (**Figure 3A**). Then we characterized the cell cycle transition and cellular apoptosis by flow cytometry analysis, and found that knocking down METTL7B increased the percentage of cells in G0/G1 phase from 55.51, 50.23% in shNC (796-P and ACHN) cells to 73.23, 69.18%, respectively in shMETTL7B cells (796-P and ACHN) (**Figure 3B**). In addition, based on the AnnexinV-FITC/PI staining assay, the percentages of apoptotic cells in shMETTL7B cells were significantly higher than that in shNC cells (**Figure 3C**). These data indicated that METTL7B is important for both ccRCC cell cycle transition and apoptotic signaling.

To investigate how METTL7B regulates cell cycle, the expression of G1/S transition regulators were measured by Western blot. The results showed that knocking down METTL7B significantly decreased the expression of CCND1 (Cyclin D1), but increased CDKN2D(cyclin dependent kinase inhibitor 2D) (**Figure 4**).

Downregulation of METTL7B Inhibits ccRCC Cell Migration and Invasion

Because METTL7B expression levels correlated with lymph node metastasis, the effect of METTL7B on ccRCC metastasis was also investigated. Transwell migration and invasion assays showed that knocking down METTL7B could significantly decrease cell motility and invasion (**Figure 5**). EMT was shown to strongly enhance cancer cell motility and metastasis, so the expression of several EMT-associated proteins were measured by Western blot. The results showed that knocking down METTL7B could significantly increase the expression of the epithelial markers E-cadherin, and inhibit the expression of mesenchymal markers N-cadherin, Vimentin, and Slug without affecting Snail and Twist expression in 796-P cells (**Figure 6**). In ACHN cells, knocking down METTL7B also inhibits Snail expression (**Figure 6**). These data indicated that knocking down METTL7B can inhibit ccRCC cell migration and invasion by inhibiting EMT.

Downregulation of METTL7B Represses ccRCC Tumor Growth *In Vivo*

To further study the biological functions of METTL7B *in vivo*, shMETTL7B-796-P and shNC-796-P cells were subcutaneously inoculated into BALB/c nude mice and tumor growth was monitored. The results showed that knocking down METTL7B significantly inhibited tumor growth compared with shNC group (**Figure 7A**). The tumor volume and weight from knockdown METTL7B tumor group was significantly smaller than shNC group (**Figures 7B, C**). However, there was no significant loss in body weight in the experimental mice. Taken together, these findings indicated that knocking down METTL7B can suppress ccRCC cells growth *in vivo*. Expression of Ki-67 antigen and proliferating cell nuclear antigen (PCNA) was assessed immunohistochemically in specimens from xenografts. The results showed that the expression level of Ki-67 and PCNA in shMETTL7B exnograft tumors was dramatically decreased (**Figure 8**). These findings demonstrated that METTL7B knockdown inhibited the growth of ccRCC *in vivo*.

DISCUSSION

METTL7B was firstly identified as a Golgi-associated methyltransferase (13). However, there was no report on the function of METTL7B in ccRCC cancer development. In the present study, we found that METTL7B is frequently upregulated in ccRCC tissues, which significantly associated with TNM classification, Tumor size, Lymph node metastasis, and poor prognosis for ccRCC patients. We further analyzed the role of METTL7B in ccRCC cell proliferation, tumorigenesis *in vitro* and *in vivo*, and explored the molecular mechanisms.

In the past, studies on molecular mechanisms of ccRCC tumorigenesis mainly focused on the oncogenes or tumor suppressor genes that coded proteins (2, 19). However, aberrant methylation may be the most common mechanism inactivating cancer-related genes in ccRCC. Previous studies

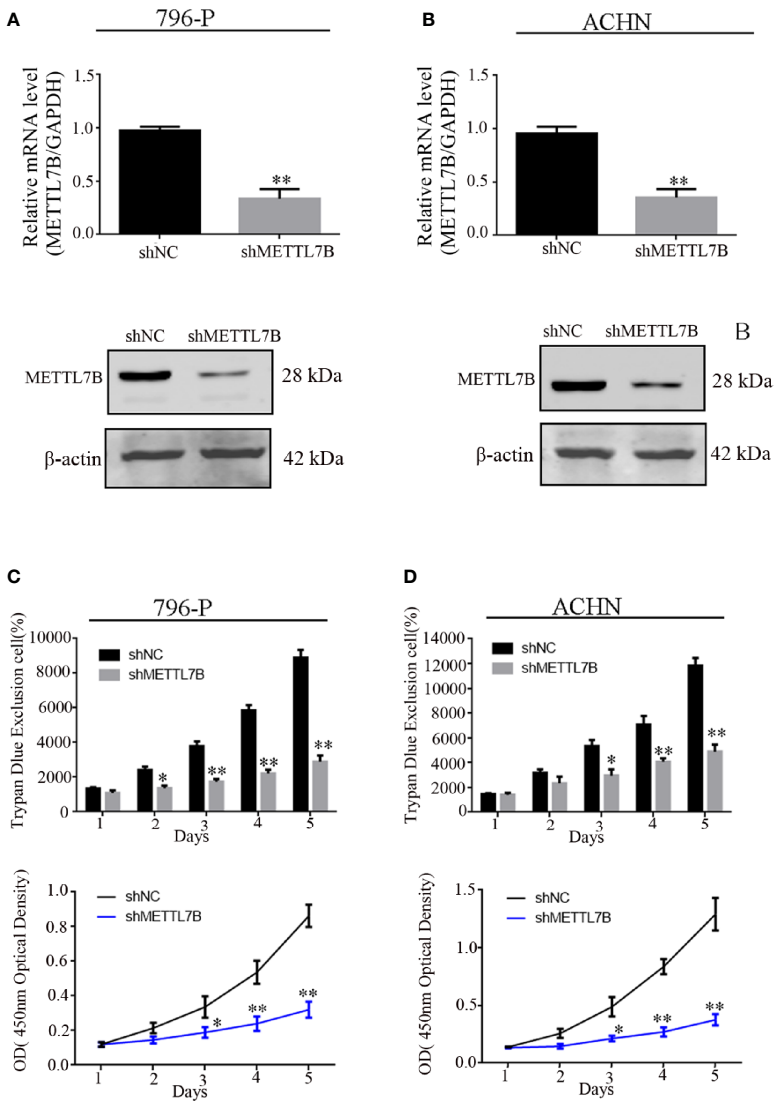


FIGURE 2 | Knockdown of METTL7B inhibits the proliferation of ccRCC cells *in vitro*. 796-p and ACHN cells transfected with sh-METTL7B (shMETTL7B) or sh-Control (shNC) for 48 h. The transfection efficiency confirmed by qRT-PCR **(A)** and Western blot **(B)**. **(C)** The living cell population was analyzed using Trypan Blue dye exclusion assay. **(D)** the cell viability were measured using MTT assay. Data are presented as the mean ± SD of three independent experiments. **p < 0.01, *p < 0.05 *vs.* shNC group.

have demonstrated that methylation links to cancer development as methylation of tumor suppressor genes promotes tumorigenesis (20, 21). In this study, we identified that both mRNA and protein of METTL7B is upregulated ccRCC tissues. Furthermore, overexpression of METTL7B was significantly associated with TNM classification, Tumor size, Lymph node metastasis, and poor prognosis for ccRCC patients. Previous studies have showed that m6A related genes (METTL3, METTL14, and HNRNPA2B1) may predict the prognosis of ccRCC patients (22). This results indicated that METTL7B might be a potential prognostic biomarker in ccRCC in the further.

We analyzed the function of METTL7B in the growth of ccRCC cells. The results showed that knockdown METTL7B significantly inhibited cell proliferation, clone formation. Furthermore, knockdown METTL7B promotes cell cycle arrest at G0/G1 phase and cellular apoptosis. These results suggested that METTL7B affect cell cycle progression through inhibiting or increasing cell cycle related-genes expression. We examined the expression of G0/G1 related genes using Western blot. The results showed that the expression of CCND1 were significantly downregulated in shMETTL7B cells, while cyclin dependent kinase inhibitor 2D (CDKN2D) was significantly upregulated without

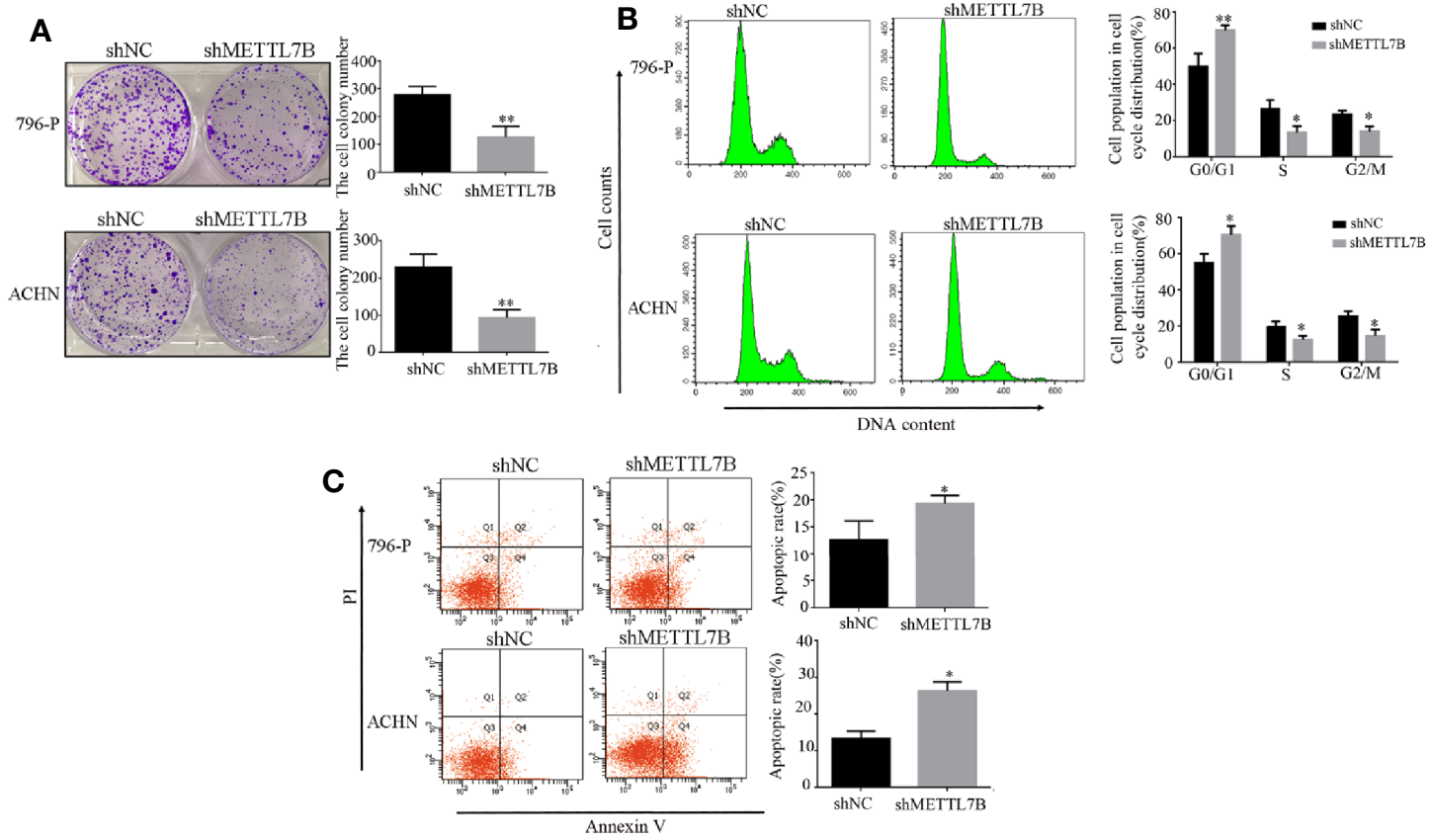


FIGURE 3 | Knockdown of METTL7B promotes ccRCC cell cycle arrest and cellular apoptosis. **(A)** Colony-formation assay of 796-p and ACHN cells transfected with sh-METTL7B (shMETTL7B) or sh-Control (shNC). After incubation for 14 days, colonies were stained and photographed. *P < 0.05, *vs.* shNC group. **(B, C)** 796-p and ACHN cells transfected with sh-METTL7B (shMETTL7B) or sh-Control (shNC) were collected and analyzed using flow cytometry for cell apoptosis and cell cycle. Data are presented as the mean ± SD of three independent experiments. **p < 0.01, *p < 0.05 *vs.* shNC group.

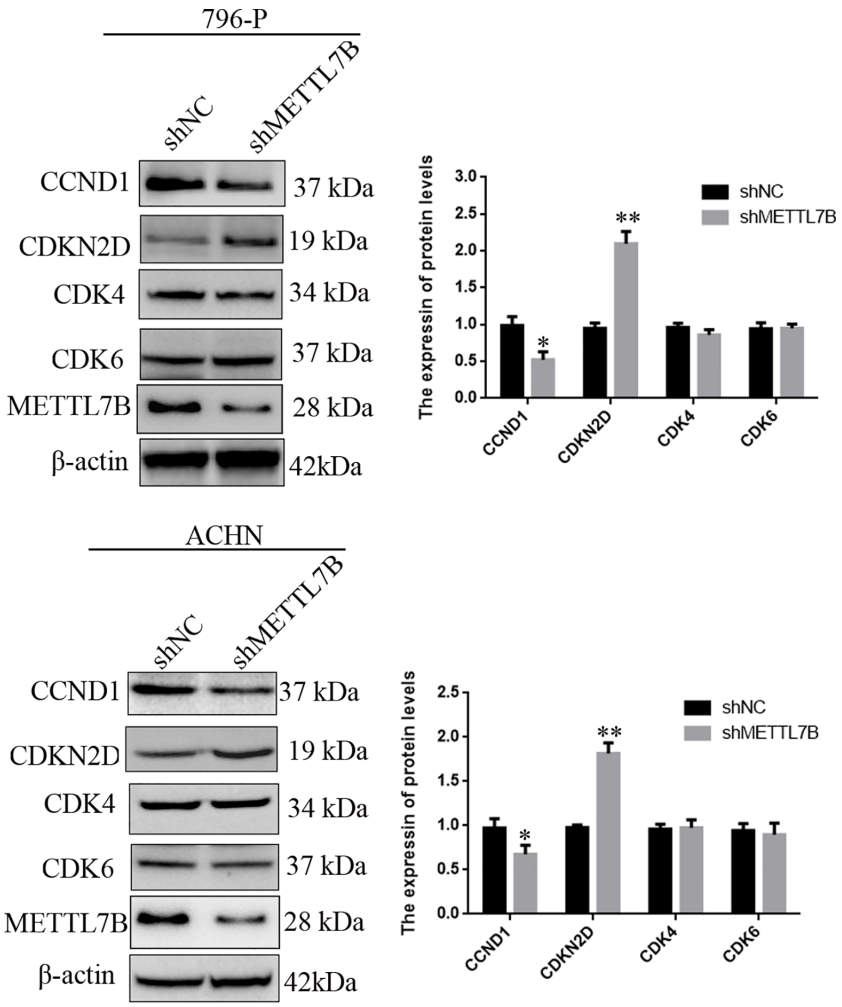


FIGURE 4 | Knockdown of METTL7B inhibited G0/G1 realted protein expression. 796-p and ACHN cells transfected with sh-METTL7B (shMETTL7B) or sh-Control (shNC) for 48 h. The total protein was extracted and subjected to SDS-PAGE, followed by western blot analysis. Beta-actin was used as an internal control. Data are presented as means ± SD of three independent experiments. *P < 0.05, **P < 0.01 *vs* shCtrl group.

affecting CDK4 and CDK6 expression. These results were consistent with cell cycle arrest in our study and previous reports. Previous studies have demonstrated that CCND1 can bind with CDK4 to control cell proliferation and migration (23). CCND1 and CDK4–mediated cell cycle progression provides a competitive advantage for human hematopoietic stem cells *in vivo* (24). CCND1 paly significant roles in the regulation of RCC cell proliferation and tumorigenesis. LINC00511 can promote the malignant phenotype of ccRCC by increasing CCND1 expression (25). Furthmore, high amounts of CDKN2D also can inhibit CDK4/6 activity and further arrest the cell cycle progression from G1 to S phase (26). miR-451 inhibits esophageal carcinoma proliferation by targeting CDKN2D expression (27). These results suggested that METTL7B may function as a oncogene and play a critical role in ccRCC formation and progression.

Epithelial-mesenchymal transition (EMT) plays an important role in both development, cancer progression, and metastasis (28). We further investigate the effect of METTL7B on ccRCC cell invasion. The results were consistent with previous report that knockdown METTL7B significantly inhibited cell invasion and migration (15). Loss of component molecules of cell adhesion and tight junctions is the hallmark of EMT in cancer (28, 29). We then examined changes in expression levels of key EMT-related transcription factors and markers in ccRCC cells after METTL7B knockdown. The results showed that knockdown METTL7B increased the expression of E-cadherin, but reduced the expression of N-cadherin, and vimentin. In addition, the expression of Slug (transcription factors) was significantly repressed in METTL7B knockdown cells, whereas the expression of Twist1, Snail, Zeb1, or Zeb2 was not changed in this context. However, mechanisms of how METTL7B up- or

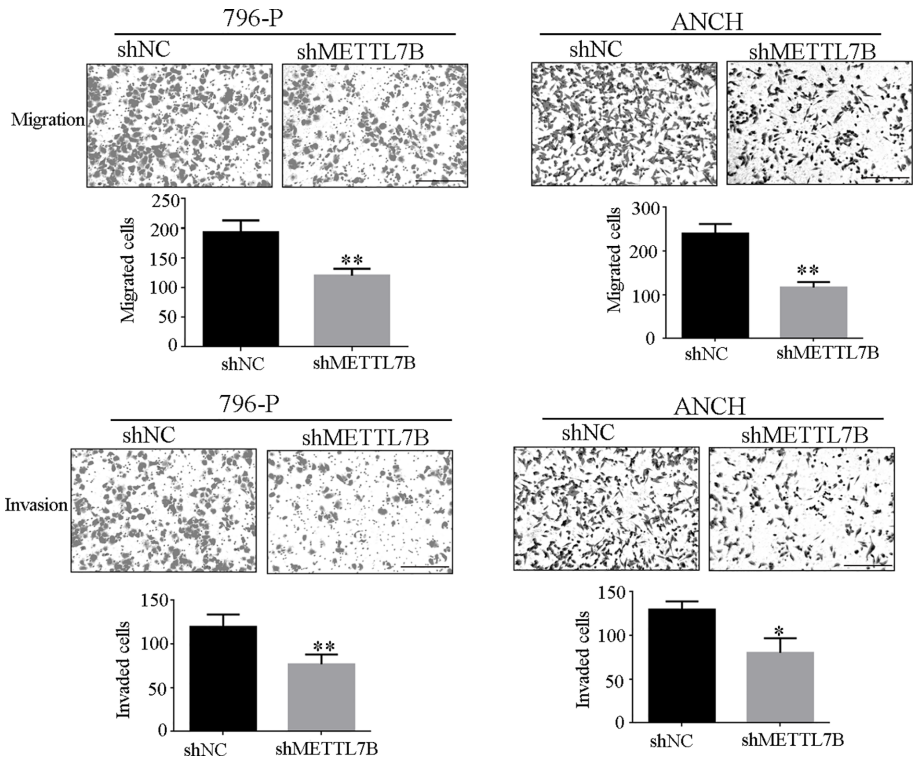


FIGURE 5 | Knockdown of METTL7B inhibits ccRCC invasion and migration. 796-p and ACHN cells transfected with sh-METTL7B (shMETTL7B) or sh-Control (shNC) for 48 h. Invasion and migration assays were measured using Transwell champers. **(A)** Knockdown of METTL7B could inhibit cell migration in 796-p and ACHN cells. **(B)** Knockdown of METTL7B could inhibit cell invasion in 796-p and ACHN cells. Data represent mean ± S.D. of three independent experiments. Scale bar = 100 μm, *P < 0.05, **P < 0.01 *vs* shCtrl group.

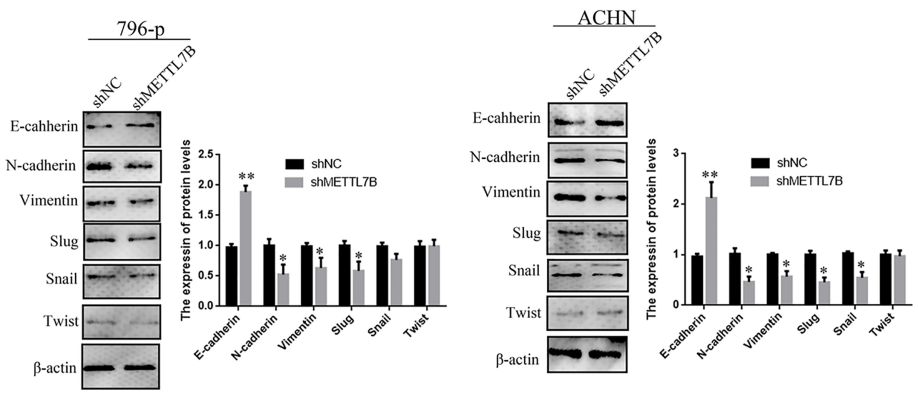


FIGURE 6 | Knockdown of METTL7B inhibited EMT in ccRCC cells. A significant reduction of vimentin and N-cadherin but increase E-cadherin was detected in shMETTL7B cells compared to shNC cells by Western blotting. Beta-actin was used as an internal control. Data are presented as means ± SD of three independent experiments. *P < 0.05, **P < 0.01 *vs* shCtrl group.

downregulates the expression of these genes needs to be further investigated.

Prvious studies have demonstrated that METTL proteins play a important role in tumorgenesis through methylate RNA, DNA or protein (6–8). In addition, Gene Ontology (GO) annotations showed METTL7B has methyltransferase activity and S-adenosylmethionine-dependent methyltransferase activity. So we think that

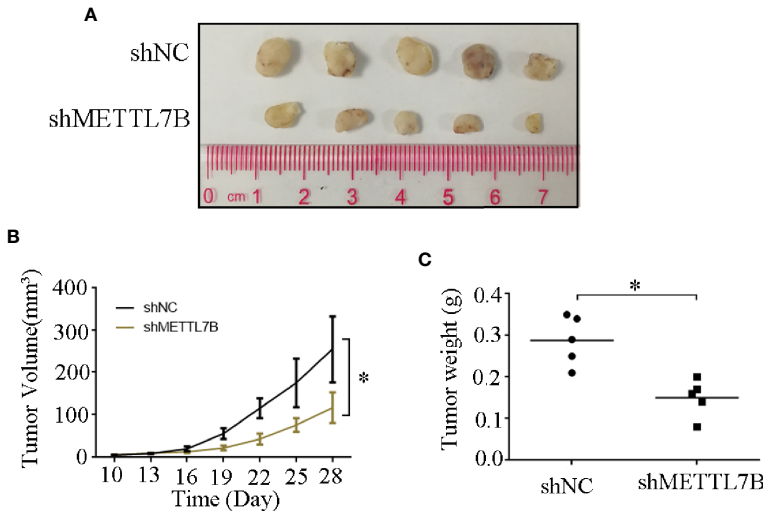


FIGURE 7 | Knockdown of METTL7B inhibits xenograft tumor formation *in vivo*. **(A)** Representative xenograft tumors for indicated cells were shown. **(B)** METTL7B knockdown significantly reduced xenograft tumor growth in male nude mice by tumor volume examination. **(C)** Depletion of METTL7B significantly suppressed xenograft tumor weights. *P < 0.05 *vs* shCtrl group.

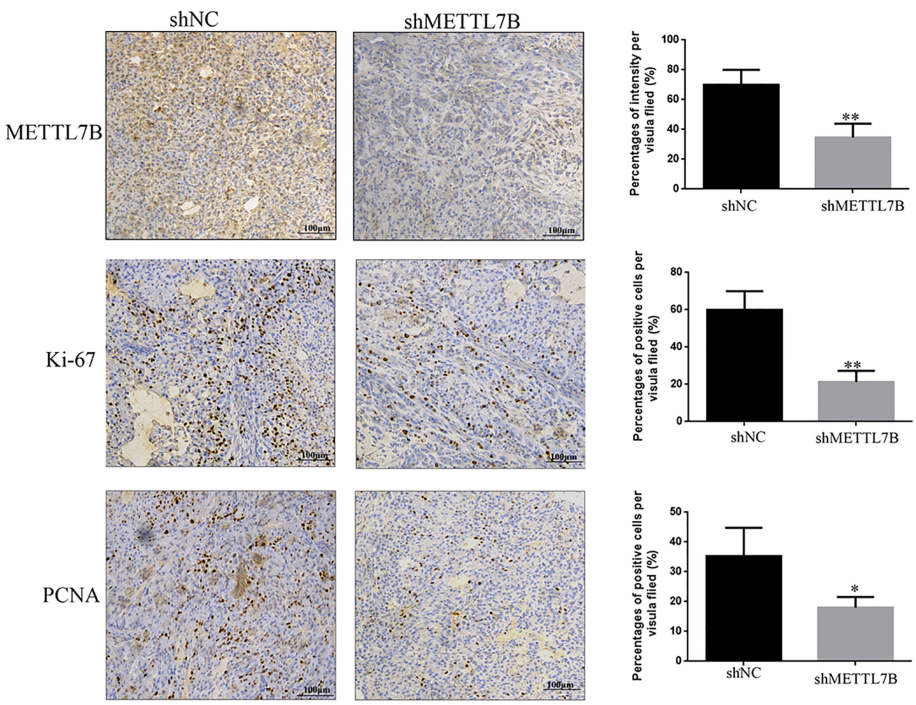


FIGURE 8 | Knockdown of METTL7B inhibits the expression of Ki67 and PNCA in xenograft tumor tiusses. IHC staining were used to measured the expression of Ki67 and PNCA in xenograft tumor tiusses. The intensities of Ki-67 and PCNA were both decreased in xenograft tumors from shMETTL7B-transfected 796-p cells. *P < 0.05 vs shCtrl group.

METTL7B might affects protein, DNA or RNA methylation. In the following study, We will further study the molecular regulatory mechanism through whole genome methylation sequencing and RNA methylation sequencing to confirm that how METTL7b can regulate cell cycle or EMT-related gene expression.

In conclusions, our study demonstrated that METTL7B is aberrantly overexpressed in ccRCC tissues. Knocking down METTL7B can significantly reduce ccRCC cell proliferation both *in vivo* and *in vitro*. The oncogenic role of METTL7B is achieved by inhibiting the expression of genes involved in the regulation of cell-cycle (such as CDK1, CCND1, and CCNB1) and invasion (E-cadherin, N-cadherin, Vimentin, and Slug).

DATA AVAILABILTIY STATEMENT

The original contributions presented in the study are included in the article/**Supplementary Material**. Further inquiries can be directed to the corresponding authors.

ETHICS STATEMENT

This study was approved by the Ethics Committee of Shenzhen Longhua District Central Hospital. The patients/participants provided their written informed consent to participate in this study.

AUTHOR CONTRIBUTIONS

WL, SX, and XW developed the project. WL, RC, and NP performed experiments and wrote the manuscript. ZZ,HH, DC, and JF supervised the work. All authors contributed to the article and approved the submitted version.

FUNDING

The work was supported by grants from the National Natural Science Foundation of China (No. 81702889).

SUPPLEMENTARY MATERIAL

The Supplementary Material for this article can be found online at: https://www.frontiersin.org/articles/10.3389/fonc.2021.634542/full#supplementary-material

Supplementary Figure 1 | Relative METTL7B expression in five ccRCC cell lines (786-O, A498, Caki-1, 796-P, and ACHN) and one normal human renal cell line (HK-2) was measured by RT-pPCR and Western blot, *P < 0.05 *vs* HK-2 group.

REFERENCES

1. Linehan WM, Ricketts CJ. The Cancer Genome Atlas of renal cell carcinoma: findings and clinical implications. *Nat Rev Urol* (2019) 16(9):539–52. doi: 10.1038/s41585-019-0211-5
2. Chen W, Hill H, Christie A, Kim MS, Holloman E, Pavia-Jimenez A, et al. Targeting renal cell carcinoma with a HIF-2 antagonist. *Nature* (2016) 539 (7627):112–7. doi: 10.1038/nature19796
3. Makhov P, Joshi S, Ghatalia P, Kutikov A, Uzzo RG, Kolenko VM. Resistance to Systemic Therapies in Clear Cell Renal Cell Carcinoma: Mechanisms and Management Strategies. *Mol Cancer Ther* (2018) 17(7):1355–64. doi: 10.1158/1535-7163.mct-17-1299
4. Xiong Y, Yuan L, Chen L, Zhu Y, Zhang S, Liu X, et al. Identifying a Novel Biomarker TOP2A of Clear Cell Renal Cell Carcinoma (ccRCC) Associated with Smoking by Co-Expression Network Analysis. *J Cancer* (2018) 9 (21):3912–22. doi: 10.7150/jca.25900
5. Horning BD, Suciu RM, Ghadiri DA, Ulanovskaya OA, Matthews ML, Lum KM, et al. Chemical Proteomic Profiling of Human Methyltransferases. *J Am Chem Soc* (2016) 138(40):13335–43. doi: 10.1021/jacs.6b07830
6. Lan Q, Liu PY, Haase J, Bell JL, Hüttelmaier S, Liu T. The Critical Role of RNA m(6)A Methylation in Cancer. *Cancer Res* (2019) 79(7):1285–92. doi: 10.1158/0008-5472.can-18-2965
7. Heyn H, Esteller M. An Adenine Code for DNA: A Second Life for N6-Methyladenine. *Cell* (2015) 161(4):710–3. doi: 10.1016/j.cell.2015.04.021
8. Shimazu T, Barjau J, Sohtome Y, Sodeoka M, Shinkai Y. Selenium-based S-adenosylmethionine analog reveals the mammalian seven-beta-strand methyltransferase METTL10 to be an EF1A1 lysine methyltransferase. *PloS One* (2014) 9(8):e105394. doi: 10.1371/journal.pone.0105394
9. Bohnsack KE, Höbartner C, Bohnsack MT. Eukaryotic 5-methylcytosine (m^5C) RNA Methyltransferases: Mechanisms, Cellular Functions, and Links to Disease. *Genes (Basel)* (2019) 10(2):102. doi: 10.3390/genes10020102
10. Rogawski DS, Grembecka J, Cierpicki T. H3K36 methyltransferases as cancer drug targets: rationale and perspectives for inhibitor development. *Future Med Chem* (2016) 8(13):1589–607. doi: 10.4155/fmc-2016-0071
11. Yang X, Zhang S, He C, Xue P, Zhang L, He Z, et al. METTL14 suppresses proliferation and metastasis of colorectal cancer by down-regulating oncogenic long non-coding RNA XIST. *Mol Cancer* (2020) 19(1):46. doi: 10.1186/s12943-020-1146-4
12. Peng W, Li J, Chen R, Gu Q, Yang P, Qian W, et al. Upregulated METTL3 promotes metastasis of colorectal Cancer via miR-1246/SPRED2/MAPK signaling pathway. *J Exp Clin Cancer Res* (2019) 38(1):393. doi: 10.1186/s13046-019-1408-4
13. Wu CC, MacCoss MJ, Mardones G, Finnigan C, Mogelsvang S, Yates JR3rd3rd, et al. Organellar proteomics reveals Golgi arginine dimethylation. *Mol Biol Cell* (2004) 15(6):2907–19. doi: 10.1091/mbc.e04-02-0101
14. Cai WY, Chen X, Chen LP, Li Q, Du XJ, Zhou YY. Role of differentially expressed genes and long non-coding RNAs in papillary thyroid carcinoma diagnosis, progression, and prognosis. *J Cell Biochem* (2018) 119(10):8249–59. doi: 10.1002/jcb.26836
15. Ye D, Jiang Y, Sun Y, Li Y, Cai Y, Wang Q, et al. METTL7B promotes migration and invasion in thyroid cancer through epithelial-mesenchymal transition. *J Mol Endocrinol* (2019) 63(1):51–61. doi: 10.1530/jme-18-0261
16. Liu D, Li W, Zhong F, Yin J, Zhou W, Li S, et al. METTL7B Is Required for Cancer Cell Proliferation and Tumorigenesis in Non-Small Cell Lung Cancer. *Front Pharmacol* (2020) 11:178. doi: 10.3389/fphar.2020.00178
17. Li W, Yu KN, Ma J, Shen J, Cheng C, Zhou F, et al. Non-thermal plasma induces mitochondria-mediated apoptotic signaling pathway via ROS generation in HeLa cells. *Arch Biochem Biophys* (2017) 633:68–77. doi: 10.1016/j.abb.2017.09.005
18. Li W, Yu KN, Bao L, Shen J, Cheng C, Han W. Non-thermal plasma inhibits human cervical cancer HeLa cells invasiveness by suppressing the MAPK pathway and decreasing matrix metalloproteinase-9 expression. *Sci Rep* (2016) 6:19720. doi: 10.1038/srep19720
19. Barth DA, Slaby O, Klec C, Juracek J, Drula R, Calin GA, et al. Current Concepts of Non-Coding RNAs in the Pathogenesis of Non-Clear Cell Renal Cell Carcinoma. *Cancers (Basel)* (2019) 11(10):1580. doi: 10.3390/cancers11101580
20. Shenoy N, Vallumsetla N, Zou Y, Galeas JN, Shrivastava M, Hu C, et al. Role of DNA methylation in renal cell carcinoma. *J Hematol Oncol* (2015) 8:88. doi: 10.1186/s13045-015-0180-y
21. Xing T, He H. Epigenomics of clear cell renal cell carcinoma: mechanisms and potential use in molecular pathology. *Chin J Cancer Res* (2016) 28(1):80–91. doi: 10.3978/j.issn.1000-9604.2016.02.09

22. Zhao Y, Tao Z, Chen X. Identification of a three-m6A related gene risk score model as a potential prognostic biomarker in clear cell renal cell carcinoma. *PeerJ* (2020) 8:e8827. doi: 10.7717/peerj.8827
23. Bienvenu F, Jirawatnotai S, Elias JE, Meyer CA, Mizeracka K, Marson A, et al. Transcriptional role of cyclin D1 in development revealed by a genetic-proteomic screen. *Nature* (2010) 463(7279):374–8. doi: 10.1038/nature08684
24. Mende N, Kuchen EE, Lesche M, Grinenko T, Kokkaliaris KD, Hanenberg H, et al. CCND1-CDK4-mediated cell cycle progression provides a competitive advantage for human hematopoietic stem cells in vivo. *J Exp Med* (2015) 212 (8):1171–83. doi: 10.1084/jem.20150308
25. Deng H, Huang C, Wang Y, Jiang H, Peng S, Zhao X. LINC00511 promotes the malignant phenotype of clear cell renal cell carcinoma by sponging microRNA-625 and thereby increasing cyclin D1 expression. *Aging (Albany NY)* (2019) 11(16):5975–91. doi: 10.18632/aging.102156
26. Sherr CJ, Roberts JM. CDK inhibitors: positive and negative regulators of G1-phase progression. *Genes Dev* (1999) 13(12):1501–12. doi: 10.1101/gad.13.12.1501
27. Zang WQ, Yang X, Wang T, Wang YY, Du YW, Chen XN, et al. MiR-451 inhibits proliferation of esophageal carcinoma cell line EC9706 by targeting CDKN2D and MAP3K1. *World J Gastroenterol* (2015) 21(19):5867–76. doi: 10.3748/wjg.v21.i19.5867
28. Lamouille S, Xu J, Derynck R. Molecular mechanisms of epithelial-mesenchymal transition. *Nat Rev Mol Cell Biol* (2014) 15(3):178–96. doi: 10.1038/nrm3758
29. Zhang Y, Weinberg RA. Epithelial-to-mesenchymal transition in cancer: complexity and opportunities. *Front Med* (2018) 12(4):361–73. doi: 10.1007/s11684-018-0656-6

Conflict of Interest: The authors declare that the research was conducted in the absence of any commercial or financial relationships that could be construed as a potential conflict of interest.

Copyright © 2021 Li, Xu, Peng, Zhang, He, Chen, Chen, Fan and Wang. This is an open-access article distributed under the terms of the Creative Commons Attribution License (CC BY). The use, distribution or reproduction in other forums is permitted, provided the original author(s) and the copyright owner(s) are credited and that the original publication in this journal is cited, in accordance with accepted academic practice. No use, distribution or reproduction is permitted which does not comply with these terms.

frontiers in Cell and Developmental Biology

ORIGINAL RESEARCH
published: 15 April 2021
doi: 10.3389/fcell.2021.661122

LECT 2 Antagonizes FOXM1 Signaling via Inhibiting MET to Retard PDAC Progression

Xin Li[1†], Pingping Lin[1†], Ye Tao[1], Xin Jiang[1], Ting Li[1], Yunshan Wang[2], Chenjing Wang[1] and Yu Cao[1]*

[1] Department of Pharmacy, The Affiliated Hospital of Qingdao University, Qingdao, China, [2] Department of Clinical Laboratory, The Second Hospital of Shandong University, Jinan, China

OPEN ACCESS

Edited by:
Ira Ida Skvortsova, Innsbruck Medical University, Austria

Reviewed by:
Guoxiong Zhou, Affiliated Hospital of Nantong University, China
Kuirong Jiang, Nanjing Medical University, China
Rui Kong, First Affiliated Hospital of Harbin Medical University, China

***Correspondence:**
Yu Cao
caoyu1767@126.com

[†] These authors have contributed equally to this work

Specialty section:
This article was submitted to Molecular and Cellular Oncology, a section of the journal Frontiers in Cell and Developmental Biology

Received: *30 January 2021*
Accepted: *30 March 2021*
Published: *15 April 2021*

Citation:
Li X, Lin P, Tao Y, Jiang X, Li T, Wang Y, Wang C and Cao Y (2021) LECT 2 Antagonizes FOXM1 Signaling via Inhibiting MET to Retard PDAC Progression. Front. Cell Dev. Biol. 9:661122. doi: 10.3389/fcell.2021.661122

Pancreatic ductal adenocarcinoma (PDAC) is one of the most lethal cancers with minimally effective treatments, highlighting the importance of developing novel biomarkers and therapeutic targets. Here, we disclosed the mechanisms that leukocyte cell-derived chemotaxin-2 (LECT2) modulates PDAC development using in vitro and in vivo models. LECT2 is downregulated in metastatic PDACs compared with the primary tumor, and its expression is correlated with multiple clinical pathologic features and prognosis. The absence promotes multiple malignant behaviors, including cell proliferation, epithelial-mesenchymal transition, migration, and invasion. In vivo studies showed that LECT2 overexpression inhibits tumor growth and lung metastasis. Mechanistically, LECT2 inhibits FOXM1 signaling by targeting HGF/MET to retard PDAC progression, revealing LECT2 as a promising biomarker and therapeutic target for PDAC in the future.

Keywords: PDAC, LECT2, HGF/MET, FOXM1 signaling, tumor growth

INTRODUCTION

Pancreatic ductal adenocarcinoma (PDAC) is the most common form of pancreatic cancer worldwide. Despite the progress in surgical techniques and medical treatment, the overall prognosis is still weak, as the 5-year relative survival rate is only 9% (Siegel et al., 2020). It is typically diagnosed at a distant stage resulting in limited treatment options, and the available therapies are mostly unsuccessful due to frequent recurrence and metastasis. In this case, there is an urgent need to identify new biomarkers or therapeutic targets to improve the diagnosis and prognosis of this malignancy.

As a 16-kDa secreted protein, leukocyte cell-derived chemotaxin-2 (LECT2) was initially isolated in humans from phytohemagglutinin-stimulated T-cell leukemia SKW-3 cells and identified as a chemotaxin of neutrophils (Yamagoe et al., 1996; Ito et al., 2003). Recently, it has been reported to have a batch of other functions in many pathological conditions, including arthritis (Okumura et al., 2008), cancer (Chen et al., 2014; Okabe et al., 2014), immune modulation (Ando et al., 2012; Lu et al., 2013), liver fibrosis (Xu et al., 2019), neuronal development (Koshimizu and Ohtomi, 2010), glucose metabolism and metabolic syndrome (Lan et al., 2014; Hwang et al., 2015).

In terms of cancer, LECT2 has been shown to act as a tumor suppressor in multiple cancers, such as hepatocellular carcinoma, non-small cell lung cancer, and intestinal cancer (Chen et al., 2014, 2016; Greenow et al., 2018; Hung et al., 2018; L'Hermitte et al., 2019). Moreover, in combination with CYP1A1 and CETN1, LECT2 could be predictive for breast carcinoma recurrence, and it can also be predictive of survival among female smokers (Andres et al., 2015). However, the role of LECT2 in the development of PDAC and the underlying mechanisms are not entirely understood.

In this study, LECT2's expression was detected in tissue samples from *in situ* and metastatic PDACs, which is related to the prognosis and clinical pathological characteristics. We also assessed the suppressive effect of LECT2 on various malignant behaviors of PDAC cell lines, both in vivo and in vitro. Besides, potential signaling pathways and target proteins involved in the molecular mechanism underlying the regulatory effect of LECT2 were also investigated. This work may give some clues to the potential of LECT2 as a biomarker or therapeutic target in tumor formation and metastasis of PDAC.

MATERIALS AND METHODS

Cell Lines

Human pancreatic cancer cell lines HPNE, S2-007, BxPC3, S2-013, Panc-1, MiaPaca-2, and AsPC-1 were purchased from the ATCC (Amerian Type Culture Collection, ATCC). HPNE, BxPC3, Panc-1, S2-007, and S2-013 cells were cultured in DMEM (Biological Industries, Cat. No. 06-1055-57-1A) + 10% FBS (Biological Industries, Cat. No. 04-007-1A) + 1% penicillin/streptomycin (Solarbio, P1400); MiaPaca-2 and AsPC-1 cells were cultured in RPMI-1640 (Biological Industries, Cat. No. 01-101-1A) + 10% FBS (Biological Industries, Cat. No. 04-007-1A) + 1% penicillin/streptomycin. All cells were cultured at 37°C with 5% CO2 and saturated humidity.

Antibodies and Reagent

Leukocyte cell-derived chemotaxin-2 antibody (Cat. No. ab119429), FOXM1 antibody (Cat. No. ab17379), MET antibody (Cat. No. ab51067), Cyclin D1 antibody (Cat. No. ab134175), Cyclin B1 antibody (Cat. No. ab32053), c-Myc antibody (Cat. No. ab185656), and Fibronection antibody (Cat. No. ab32419) were purchased from Abcam. E-cadherin antibody (Cat. No. #14472), β-catenin antibody (Cat. No. #8480), N-cadherin antibody (Cat. No. #13116), N-cadherin antibody (Cat. No. #13116), Vimentin antibody (Cat. No. #5741), Phospho-Met (Tyr1234/1235) antibody (Cat. No. #3077), mouse IgG antibody (Cat. No. #7076), and rabbit IgG antibody (Cat. No. #7074) were purchased from CST (Cell Signaling Technology). Hepatocyte Growth Factor (HGF) (Cat. No. H0536) was purchased from Merck. Selumetinib (AZD6244) (S1008) was purchased from Selleck.

Plasmids and Short Hairpin RNAs

The cDNAs of LECT2 and FOXM1 were obtained from GeneCopoeia, and the cDNAs were constructed on a lentiviral vector. The shRNA sequence of LECT2 and FOXM1 was obtained from the Sigma website: shLECT2 #1: CCGGGCAGAAA GTTTATCCTGGCATCTCGAGATGCCAGGATAAACTTTCT GCTTTTTTG; shLECT2 #2: CCGGTTCTACATTAAGCCAA TTAAGCTCGAGCTTAATTGGCTTAATGTAGAATTTTTTG; shFOXM1: CCGGTTGCAGGGTGGTCCGTGTAAACTCGAGT TTACACGGACCACCCTGCAATTTTTG. The shRNA sequence was synthesized and constructed on a lentiviral vector.

Western Blotting

The cells were lysed by RIPA lysate (Beyotime Biotechnology, Cat. No. P0013B) containing protease inhibitor (Roche, Cat. No. 11206893001), and the protein supernatant was collected after centrifugation; the protein supernatant was added to the protein loading buffer to denature the protein. Prepare 10 or 8% SDS-PAGE gel. After the protein is electrophoresed, transferred, and blocked, add the corresponding primary antibody and incubate at 4°C overnight. After washing, add the corresponding secondary antibody (CST, #7076, or #7074) and incubate at room temperature for 1 h. After washing, add ECL (Millipore, Cat. No. WBULS0500) for exposure; use the BioImaging Systems instrument to obtain protein expression pictures, and use ImageJ software to count gray values. Ratio to β-Actin % represents the ratio of the gray value of LECT2 to the gray value of β-Actin and then multiplied by 100.

qRT-PCR

The cells were extracted with total RNA by the Trizon (ThermoFisher, A33250) method and reverse transcribed into cDNA using EasyScript® Reverse Transcriptase (TRAN, AE101-02). Perform qRT-PCR with the following primers: 5′-CCAATGAGATCCGGACGTGT-3′ (LECT2 Forward) and 5′-TCCTGGCCCACAATCATTCC-3′ (LECT2 Reverse); 5′-GA GAAGGCTGGGGCTCATTT-3′ (GAPDH Forward) and 5′-A GTGATGGCATGGACTGTGG-3′ (GAPDH Reverse); 5′-GGGG TCTGTCATGGAAGGTG-3′ (E-cadherin Forward) and 5′-CA AAATCCAAGCCCGTGGTG-3′ (E-cadherin Reverse); 5′-AGG CGTTATGTGTGTATCTTCACT-3′ (N-Cadherin Forward) and 5′-GGAGGGATGACCCAGTCTCT-3′ (N-Cadherin Reverse); 5′-TCGTGCTTTGACCCCTACAC-3′ (Fibronection Forward) and 5′-CGGGAATCTTCTCTGTCAGCC-3′ (Fibronection Reverse); 5′-GGACCAGCTAACCAACGACA-3′ (Vimentin Forward) and 5′-AAGGTCAAGACGTGCCAGAG-3′ (Vimentin Reverse). The ratio to GAPDH represents the number of cycles of LECT2 minus the number of cycles of GAPDH.

Immunohistochemistry

Sections of pancreatic cancer tissues were dewaxed, citric acid antigen repaired, and 3% hydrogen peroxide treated. Tissues were removed and then serum-blocked and antibody-incubated. Tissue-stained sections were analyzed by Image-Pro software for positive or negative areas.

MTT and Cell Proliferation

Cells were counted and seeded in 96-well plates. After 48 h of culture, MTT (0.5 mg/ml) (Solarbio, M8180) was added

and incubated for 4 h. 150 μl DMSO was added and mixed to obtain the OD value. After counting, the cells were plated in 6-well plates, cultured for 14 days. Fresh medium was changed twice a week. Cells were fixed with methanol, and crystal violet stained. The number of cell clones was photographed to count.

Migration and Invasion

Transwell was covered with Migration gel and incubated at 37°C for 30 min. After adding an appropriate number of cells for 12 h, the cells were fixed and stained, and then the number of cell invasions was counted. After counting the cells, they were seeded in the Transwell cell in a 24-well plate, fixed for staining after 12 h in culture, and then counted the number of cell migration. Relative migration or invasion cells/per area means selecting five areas randomly and counting the number of cells in them.

In vivo Tumorigenesis and Metastasis Assay

Collect pancreatic cancer cell lines that overexpress or knock LECT2, count and inject them into the skin of nude mice, and measure the xenograft tumor volume every week; The pancreatic cancer cell lines that overexpressed or knocked LECT2 were collected and injected into the tail vein of nude mice. Thirty days later, the lung tissues of nude mice were collected to observe the pancreatic cancer cell lung metastasis.

RNA-Seq Analysis

For the BXPC3 cell line overexpressing LECT2, total RNA was extracted by Triton. Total RNA was sequenced using Illumina HiSeq and subsequently matched to the genome using TopHat2 software. Differential genes were analyzed using HTseq software and DESeq2 software. The RNA sequencing data has been uploaded to the GEO database (GSE168611).

Specimens

Tissue samples from patients with pancreatic cancer were collected by the General Surgery of the Affiliated Hospital of Qingdao University, and pancreatic cancer *in situ* and metastases were recorded. Metastases are PDAC with lymph node metastasis. Pancreatic cancer tissue is stored in liquid nitrogen. The staging of pancreatic cancer patients strictly follows the American Cancer Society, the American Joint Committee on Cancer TNM system staging standards. Twenty-two primary (*in situ*) and twenty-two metastatic (Met) PDACs tissue samples were used to extract total RNA and total protein, and detect the mRNA and protein expression levels of LECT2. Besides, the expression of LECT2 in PDACs was also detected by immunohistochemistry. The cancer tissue used complies with the regulations of the Ethics Committee of Qingdao University.

Statistical Analysis

All data were statistically analyzed using the Student's *t*-test in SPSS software. Data are presented as mean ± SD, and $p < 0.05$ was considered statistically significant.

RESULTS

LECT2 Expression Is Downregulated in Metastatic PDACs Compared With Primary Tumor

The LECT2 expression was measured in paired primary tumors and metastatic tumors (Lymph node metastasis), respectively (**Figures 1A,B**). *In situ*, primary tumors showed higher mRNA levels of LECT2 than paired metastatic samples. Similarly, we also found that LECT2 protein levels were remarkably higher in primary PDACs compared with those of the paired metastatic specimens (**Figures 1C–E**). Moreover, Kaplan-Meier analysis indicated that low levels of LECT2 predicted poor clinical outcome in PDAC (**Figure 1F**). LECT2 expression was also correlated with multiple clinical pathologic features, including TNM staging, tumor size, lymph node metastasis, and distant metastasis (**Table 1** and **Supplementary Figure 1A**). Moreover, the expression level of LECT2 is negatively correlated with tumor size, lymph node metastasis, and distant metastasis. Collectively, the results mentioned above implied that LECT2 might play a tumor-suppressive role in PDAC progression. Finally, we also analyzed the expression level of LECT2 in the PADC tumor and the adjacent area of the tumor. Immunohistochemical staining showed that the expression level of LECT2 in the tumor was significantly lower than that in the adjacent area of the tumor (**Supplementary Figure 1B**).

LECT2 Inhibits PDAC Tumor Growth Both *in vitro* and *in vivo*

To explore whether LECT2 acts as a tumor suppressor in pancreatic cancer, PDAC cell lines BXPC-3 and ASPC-1 were transfected with lentiviral vectors encoding human LECT2 inserts, whereas MiaPaca-2 and Panc-1 cells were transfected with shRNAs targeting LECT2 based on the endogenous expression of LECT2 (**Supplementary Figure 2**). The transfection efficiency was confirmed by immunoblotting and RT-qPCR (**Supplementary Figure 3**). Subsequently, cell viability and colony formation assays were performed to examine the effect of LECT2 on tumor proliferation. As expected, the ectopic expression of LECT2 suppressed cell viability and clonal forming abilities in BXPC-3 and ASPC-1 cells (**Figures 2A,C**). Conversely, LECT2 deficiency notably promoted these oncogenic behaviors in MiaPaca-2 and Panc-1 cells (**Figures 2B,D**). To further assess the function of LECT2 in tumor suppression, xenograft mice injected with BXPC-3 cells bearing LECT2 inserts or MiaPaca-2 cells bearing shLECT2 were established, respectively. In agreement with the in vitro findings, xenograft mice injected with BXPC-3 cells displayed reduced tumor volume and weight compared to control models (**Figures 2E–G**). In contrast, the deficiency of LECT2 in the MiaPaca-2 cells markedly speeded

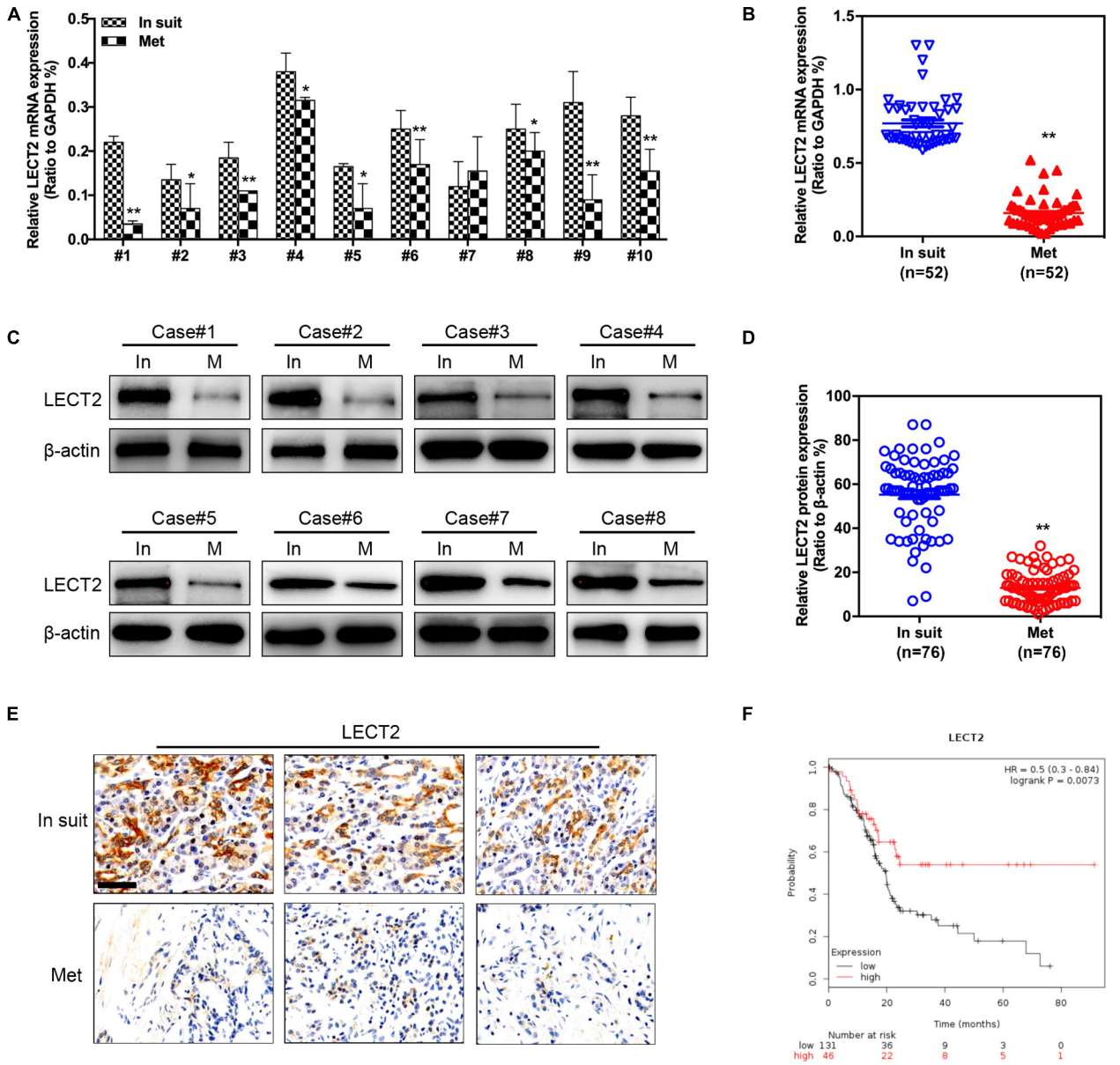


FIGURE 1 | LECT2 expression in primary (*in situ*) and metastatic (Met) PDACs. **(A)** Representative qRT-PCR results of LECT2 expression in paired primary and metastatic (Lymph node metastasis) PDACs. **(B)** Quantification of qRT-PCR results in paired primary ($n = 52$) and metastatic ($n = 52$) PDACs. **(C)** Representative immunoblotting results of LECT2 protein levels in paired primary and metastases (Lymph node metastasis) PDACs. **(D)** Quantification of immunoblotting results in paired primary ($n = 76$) and metastatic ($n = 76$) PDACs. **(E)** Representative images of immunohistochemistry (IHC) staining for LECT2 in sections from paired primary and metastatic PDACs (Scale bar: 100 μm). **(F)** Kaplan-Meier analysis indicating the overall survival of PDAC patients with low (black) or high (red) LECT2 expression. $^{*}p < 0.01$ and $^{**}p < 0.01$.

up tumor growth in vivo (**Figures 2H–J**). Together, these findings indicate that LECT2 detains PDAC tumorigenesis both in vitro and in vivo.

LECT2 Inhibits Epithelial-Mesenchymal Transition in PDAC

Since LECT2 expression is downregulated in metastatic PDACs compared with the primary tumor, we speculated that LECT2 might be involved in the regulation of PDAC metastasis. To test the above notion, we first examined the morphology and epithelial-mesenchymal transition (EMT) markers like E-cadherin, N-cadherin, α-catenin, fibronectin, and vimentin in transformed BXPC-3 and ASPC-1 cells (**Figures 3A–C** and **Supplementary Figure 4A**). Phase-contrast images clearly showed that BXPC-3 and ASPC-1 cells overexpressing LECT2 displayed epithelial morphology. Consistently, immunofluorescence, immunoblotting, and qPCR

TABLE 1 | Correlations between LECT2 expression and clinicopathologic features in PDCA patients.

Variable	Expression of LECT2		Total	P^a
	Low	High		
Age (years)				
°≤65	65	31	96	0.163
°>65	110	37	147	
Gender				
°Male	32	98	130	0.317
°Female	25	68	113	
Tumor location				
°Head	115	44	159	0.102
°Body tail	63	19	84	
TNM (AJCC)				
°I, II	104	61	165	0.026
°III, IV	53	25	78	
Tumor size				
°≤3 cm	39	42	81	<0.001
°>3 cm	113	49	162	
Tclassification				
°T1, 2	98	44	142	0.076
°T3, 4	77	24	101	
Lymph node metastasis				
°Absent	95	81	176	0.012
°Present	54	13	67	
Distant metastasis				
°Absent	114	103	217	<0.001
°Present	22	4	26	
Vascular Invasion				
°Absence	132	77	209	0.253
°Present	26	8	34	
Histological differentiation				
°Well/Moderate	121	40	161	0.321
°Poor	61	22	83	

[a]*p-value < 0.05 was considered statistically significant. p-values were calculated using the Pearson chi-square test.*

analysis indicated high levels of epithelial markers (E-cadherin and α-catenin) and lowered expression of mesenchymal markers (N-cadherin, fibronectin, and vimentin) in LECT2-overexpressing BXPC-3 and ASPC-1 cells. On the other hand, cells devoid of LECT2 manifested the opposite trends (**Figures 3D–F** and **Supplementary Figure 4B**). In other words, LECT2-deficient MiaPaca-2 and Panc-1 cells displayed mesenchymal morphology and high levels of mesenchymal markers as well as low levels of epithelial markers. The data mentioned above suggest that LECT2 manages the plasticity between epithelial and mesenchymal states in PDAC cells.

LECT2 Inhibits PDAC Migration, Invasion, and Distant Lung Metastasis

As EMT is considered to be a fundamental process involved in cancer metastasis, the role of LECT2 in migration and invasion was thus investigated. BXPC-3 and ASPC-1 cells with excessive expression of LECT2 were subjected to cell migration and invasion assessment (**Figure 4A** and **Supplementary Figure 5A**). As expected, LECT2 overexpression impaired the migratory and invasive abilities of BXPC-3 and ASPC-1 cells. Conversely, ablation of LECT2 promoted migration and invasion in MiaPaca-2 and Panc-1 cells (**Figure 4B** and **Supplementary Figure 5B**). These findings together indicated that LECT2 inhibited migration and invasion in PDAC cells. To further explore the effect of LECT2 on metastasis in a physiologic tumor context, we developed a xenograft model, employing BXPC-3 cells expressing LECT2 vectors. In line with in vitro results, LECT2 overexpression reduced considerably the number of mice with lung metastasis (7 of 10, BxPC-3-Vector; 3 of 10, BxPC-3-LECT2), and the number of metastatic lung foci per section as shown by the H&E staining of lung tissues from mice after intravenous injection (**Figures 4C,D**). Meanwhile, LECT2 knockdown increased those numbers compared to control (4 of 10, MiaPaca-2-shControl; 9 of 10, MiaPaca-2-shLECT2#1) (**Figures 4E,F**). Hence, LECT2 regulates not only EMT but also regulates both migration and invasion of PDAC cells, consequently influencing in vivo metastasis.

LECT2 Negatively Correlates With Forkhead Box M1 Signaling Pathway and Downregulates FOXM1 Expression

Next sought to explore how LECT2 regulates the tumorigenesis and metastasis of PDAC. To decipher the underlying mechanism of PDAC development and progression impeded by LECT2, we performed RNA-seq with BXPC-3 cells bearing empty vectors or LECT2 inserts (**Figure 5A**). The RNA-seq results showed that there were 215 up-regulated genes and 173 down-regulated genes (**Supplemental Table 1**). Gene set enrichment analysis (GSEA) revealed the forkhead box M1 (FOXM1) signaling pathway as the enriched signature reversely correlated with endogenous LECT2-dependent transcription in PDAC (**Figure 5B**). Protein-Protein-Interaction Network further showed the enriched genes in the FOXM1 signaling pathway (**Figure 5C**).

To investigate LECT2's effect on FOXM1 expression, qRT-PCR and immunoblotting were applied to total RNA and protein extracted from BXPC-3 and ASPC-1 cells with excessive expression of LECT2 or LECT2-deficient MiaPaca-2 and Panc-1 cells (**Figures 6A–D**). In BXPC-3 and ASPC-1 cells, LECT2 overexpression led to lower levels of FOXM1 and its downstream target genes, such as cyclin D1, cyclin B1, and c-Myc (**Figures 6A,C**, and **Supplementary Figure 6A**). Likewise, the depletion of LECT2 resulted in enhanced expression of FOXM1 and its downstream target genes in MiaPaca-2 and Panc-1 cells (**Figures 6B, D**, and **Supplementary Figure 6B**). These findings were further supported by the immunochemistry evidence from transformed PDAC cells and pancreatic cancer tissues showing the inverse correlation between LECT2 and FOXM1 (**Figures 6E–H**). Also, we found that overexpression of FOXW1 significantly increased the cell viability, clone formation ability, and invasion/migration ability of BxPC-3 cells (**Supplementary Figure 7**). Collectively, these findings suggested that LECT2 negatively mediated the FOXM1 signaling pathway in PDAC.

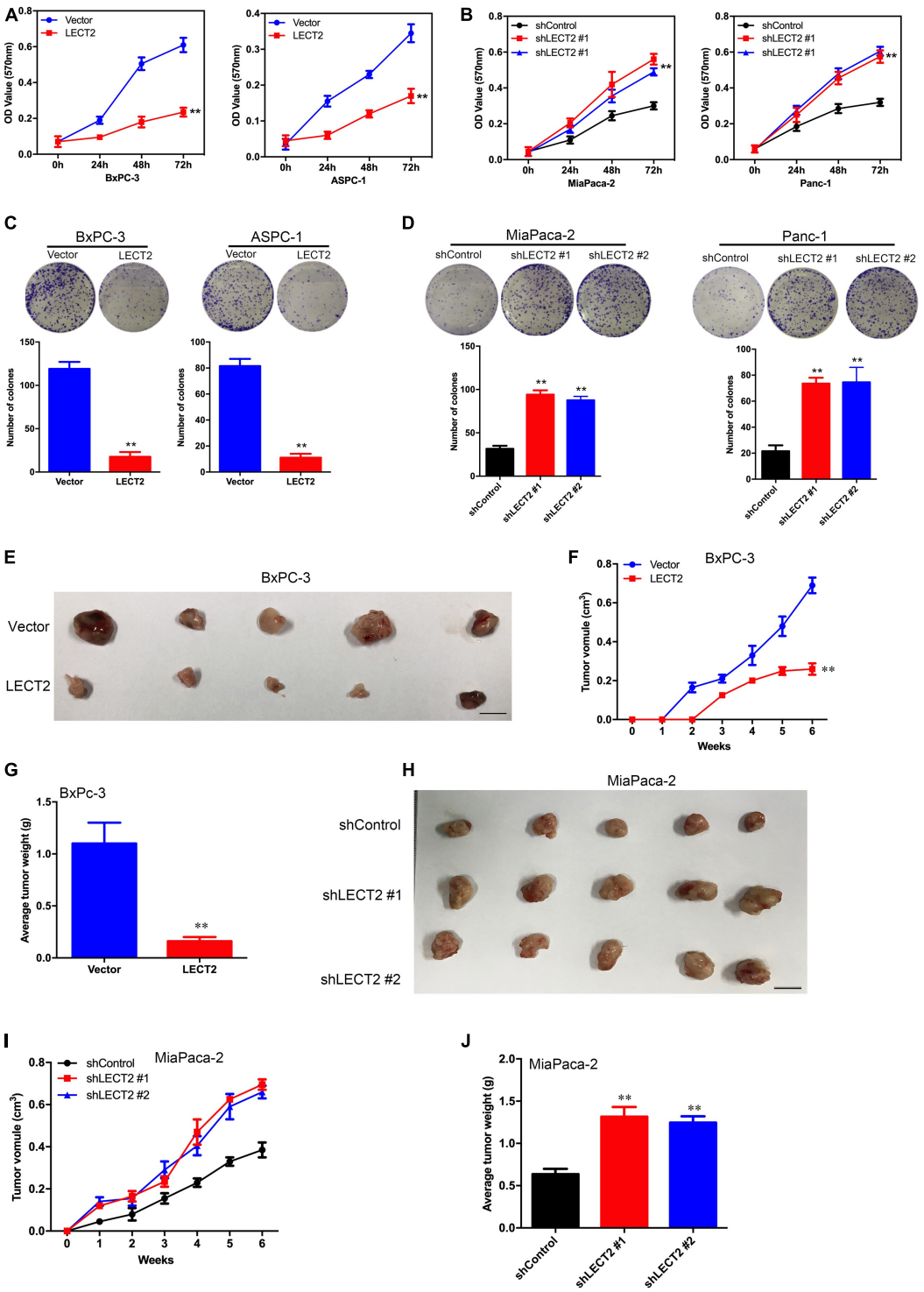


FIGURE 2 | LECT2 regulates cell proliferation, colony formation, and tumor growth in PDAC. **(A)** Cell proliferation of BxPC-3 (left) and ASPC-1 (right panel) cells transfected with control (blue) or LECT2 (red) vector. **(B)** Cell proliferation of MiaPaca-2 (left) and Panc-1 (right panel) cells transfected with shControl (black) or shLECT2 (red and blue) vectors. **(C)** Colony formation of BxPC-3 (left) and ASPC-1 (right panel) cells as described in **(A)**. **(D)** Colony formation of MiaPaca-2 (left) and Panc-1 (right panel) cells as described in **(B)**. **(E–G)** BxPC-3 cells (1×10^6), as described above, were injected subcutaneously into the mice ($n = 5$ for each group), and the resulting tumors in each group were measured once a week. Photographs of tumors isolated from the mice **(E)**, the tumor volume **(F)**, and the weights of the tumors **(G)** are shown. **(H–J)** MiaPaca-2 cells (1×10^6), as described above, were injected subcutaneously into the mice ($n = 5$ for each group), and the resulting tumors in each group were measured once a week. Photographs of tumors isolated from the mice **(H)**, the tumor volume **(I)**, and the weights of the tumors **(J)** are shown. Scale bar = 1 cm in **(E)** and **(H)**. $^{**}p < 0.01$.

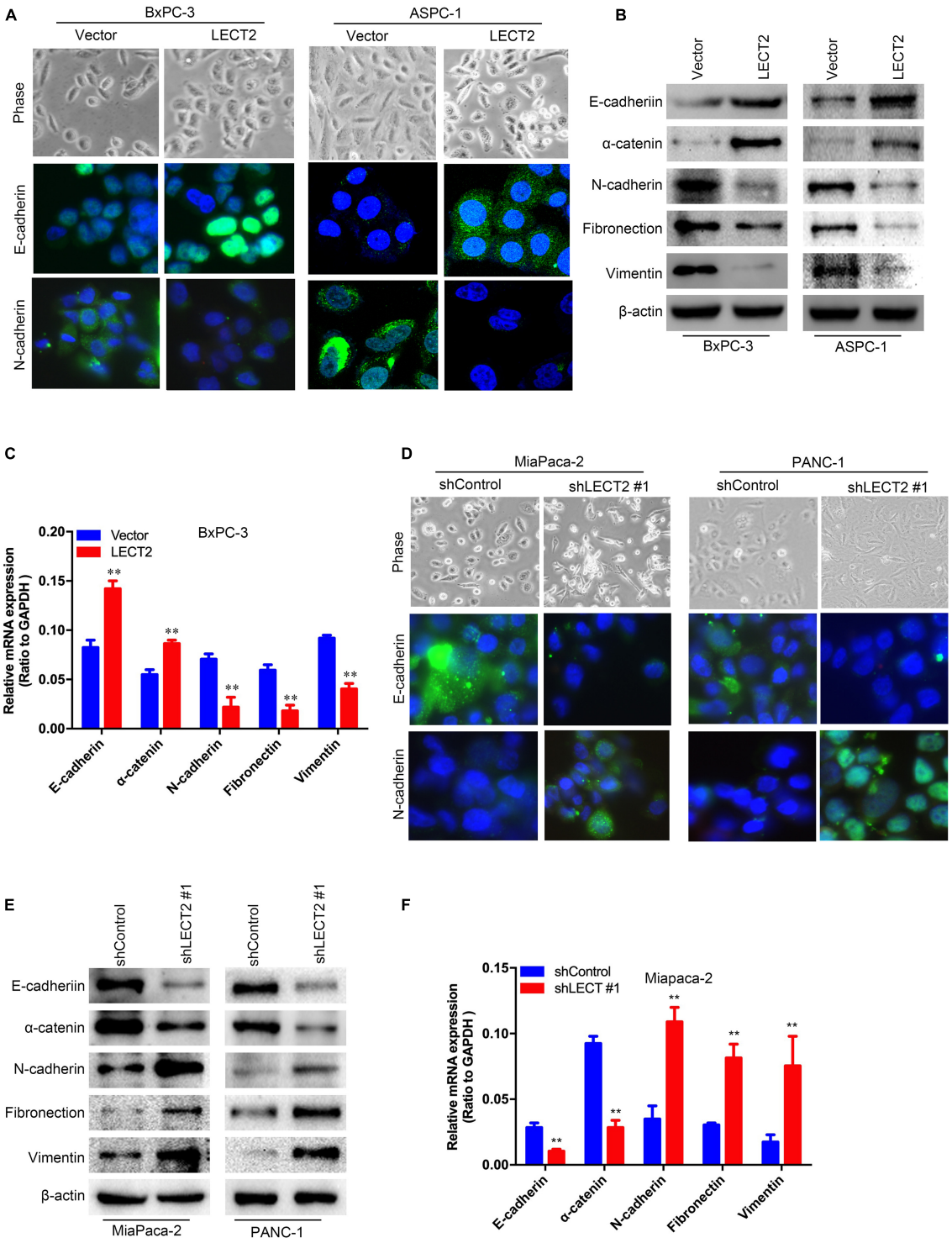


FIGURE 3 | LECT2 inhibits epithelial-mesenchymal transition (EMT) in PDAC. **(A)** Phase-contrast images (top) and immunofluorescence images of transformed BxPC-3 (left) and ASPC-1 (right) cells stained with antibodies against E-cadherin (middle), or N-cadherin (bottom panel). BxPC-3 and ASPC-1 cells were transfected with control or LECT2 vector, as described in **Figure 2**. **(B)** Immunoblotting analysis of expression of E-cadherin, α-catenin, N-cadherin, Fibronectin, and Vimentin proteins in the cells shown in **(A)**. β-actin was used as a loading control. **(C)** mRNA expression of E-cadherin, α-catenin, N-cadherin, Fibronectin, and Vimentin in transformed BxPC-3 cells as described above. **(D)** Phase-contrast images (top) and immunofluorescence images of transformed MiaPaca-2 (left) and Panc-1 (right) cells stained with antibodies against E-cadherin (middle), or N-cadherin (bottom panel). MiaPaca-2 and Panc-1 cells were transfected with shControl or shLECT2 vector, as described in **Figure 2**. **(E)** Immunoblotting analysis of expression of E-cadherin, α-catenin, N-cadherin, Fibronectin, and Vimentin proteins in the cells shown in **(D)**. β-actin was used as a loading control. **(F)** mRNA expression of E-cadherin, α-catenin, N-cadherin, Fibronectin, and Vimentin in transformed MiaPaca-2 cells as described above. Scale bar = 20 μm in **(A)** and **(D)**. $^{**}p < 0.01$.

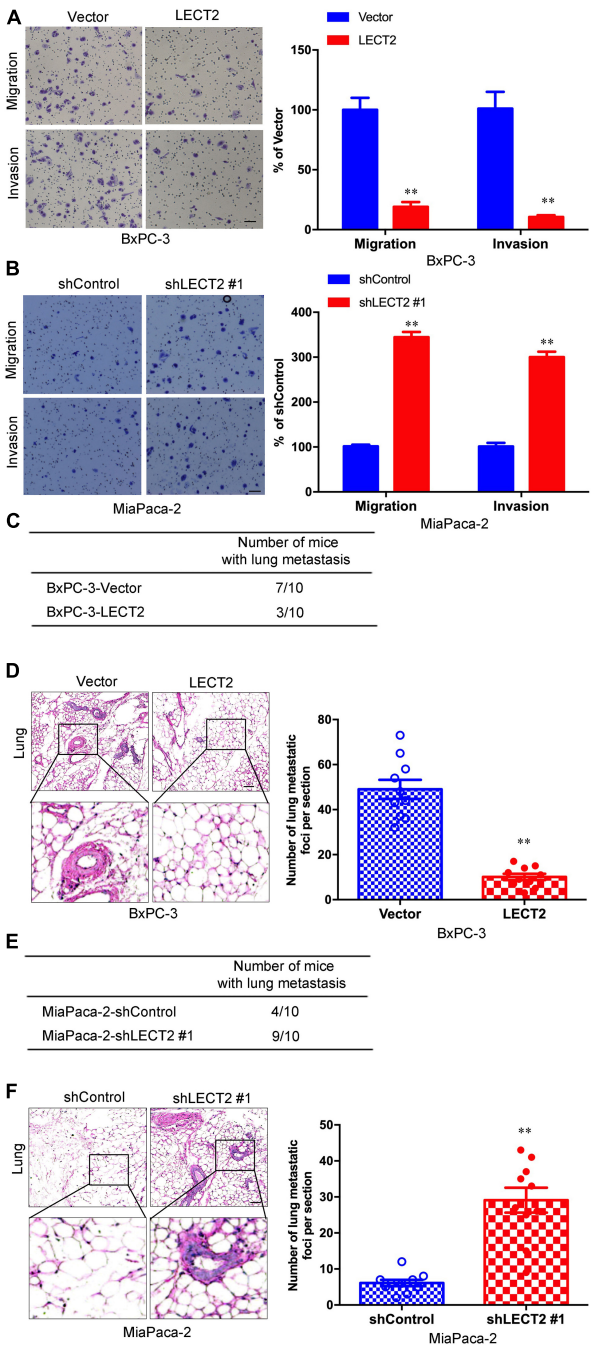


FIGURE 4 | LECT2 inhibits PDAC migration, invasion, and distant lung metastasis. **(A,B)** Representative images of migration (top) and invasion (bottom) of transformed BxPC-3 **(A)** and MiaPaca-2 **(B)** cells described above (left) with corresponding quantifications (right). **(C)** Number of mice with distant lung metastasis following intravenous injections of transformed BxPC-3 cells as described above. **(D)** Representative H&E staining images (left) of metastatic lung foci per section from allograft mice described in **(C)** with corresponding quantifications (right). **(E)** Number of mice with distant lung metastasis following intravenous injections of transformed MiaPaca-2 cells as described above. **(F)** Representative H&E staining images (left) of metastatic lung foci per section from allograft mice described in **(E)** with corresponding quantifications (right). Scale bar = 50 μm in **(A,B)**. Scale bar = 200μm in **(D,E)**. $^{**}p < 0.01$.

FOXM1 Is Necessary for the Suppressive Impact of LECT2 on PDAC Malignancy

To prove whether FOXM1 is required for the inhibitory effect of LECT2 on PDAC malignancy, we established two stable cell lines, BXPC-3 cells expressing LECT2 as well as FOXM1 insert, and MiaPaca-2 cells transfected with shRNAs that target LECT2 as well as FOXM1. Subsequently, cell viability and colony formation assays were performed to examine the involvement of FOXM1 in the effect of LECT2 on tumor proliferation (**Figures 7A–D**). As anticipated, the ectopic expression of FOXM1 in BXPC-3 cells almost completely abolished the inhibitory effect of LECT2 overexpression on cell viability and colony formation (**Figures 7A,C**). In contrast, FOXM1 deficiency dramatically reduced the impact of LECT2 knockdown on cell viability and sphere formation in MiaPaca-2 cells (**Figures 7B,D**). Similarly, migration and invasion assay showed that the reintroduction of FOXM1 restored the aggressive abilities of BXPC-3 cells undermined by LECT2 overexpression (**Figure 7E**). Besides, we found that the promoting effect of LECT2 deficiency on cell migration and invasion was impaired when FOXM1 was also knocked down (**Figure 7F**). Since LECT2 mediated the transition between epithelial and mesenchymal states, immunoblotting was thus applied to evaluate the function of FOXM1 on EMT markers (**Figures 7G,H**). The data showed that epithelial phenotype favored by excessive expression of LECT2 was revoked by FOXM1 the overexpression in BxPC-3 cells, whereas FOXM1 knockdown abolished the mesenchymal states induced by LECT2 deficiency in MiaPaca-2 cells.

Most Importantly, in vivo evidence from mouse xenografts injected with the transformed BxPC-3 orMiaPaca-2 cells revealed that reintroduction of FOXM1 reversed the inhibitory effects of LECT2 on distant metastasis. In contrast, the ablation of FOXM1 attenuated the lung metastasis induced by LECT2 deficiency (**Figures 7I,J**). The results, as mentioned above, demonstrated that LECT2 might suppress the malignant behaviors of PDAC cells via downregulating FOXM1 expression.

Hepatocyte Growth Factor/MET Is Involved in the Regulation of FOXM1 by LECT2

The co-presence of both MET and FOXM1 is common in patients with gastric cancer (Francica et al., 2016). Besides, a positive feedback loop between FOXM1 and HGF/MET has been identified in PDAC, which contributes to PDAC growth (Cui et al., 2016). Since LECT2 was reported to antagonize MET receptor activation in hepatocellular carcinoma and non-small cell lung cancer (Chen et al., 2014; Hung et al., 2018), we speculated that LECT2 might regulate FOXM1 signaling by targeting MET. To test the notion mentioned above, two stable cell lines were established, MiaPaca-2 cells transfected with shRNAs that target LECT2 as well as MET, and BXPC-3 cells expressing LECT2, as well as MET, insert. Immunoblotting, migration, and invasion assays were performed, respectively, to measure the function of MET on LECT2 affected malignant behaviors (**Figure 8**). As expected, MET knockdown had a slight effect on LECT2 but completely

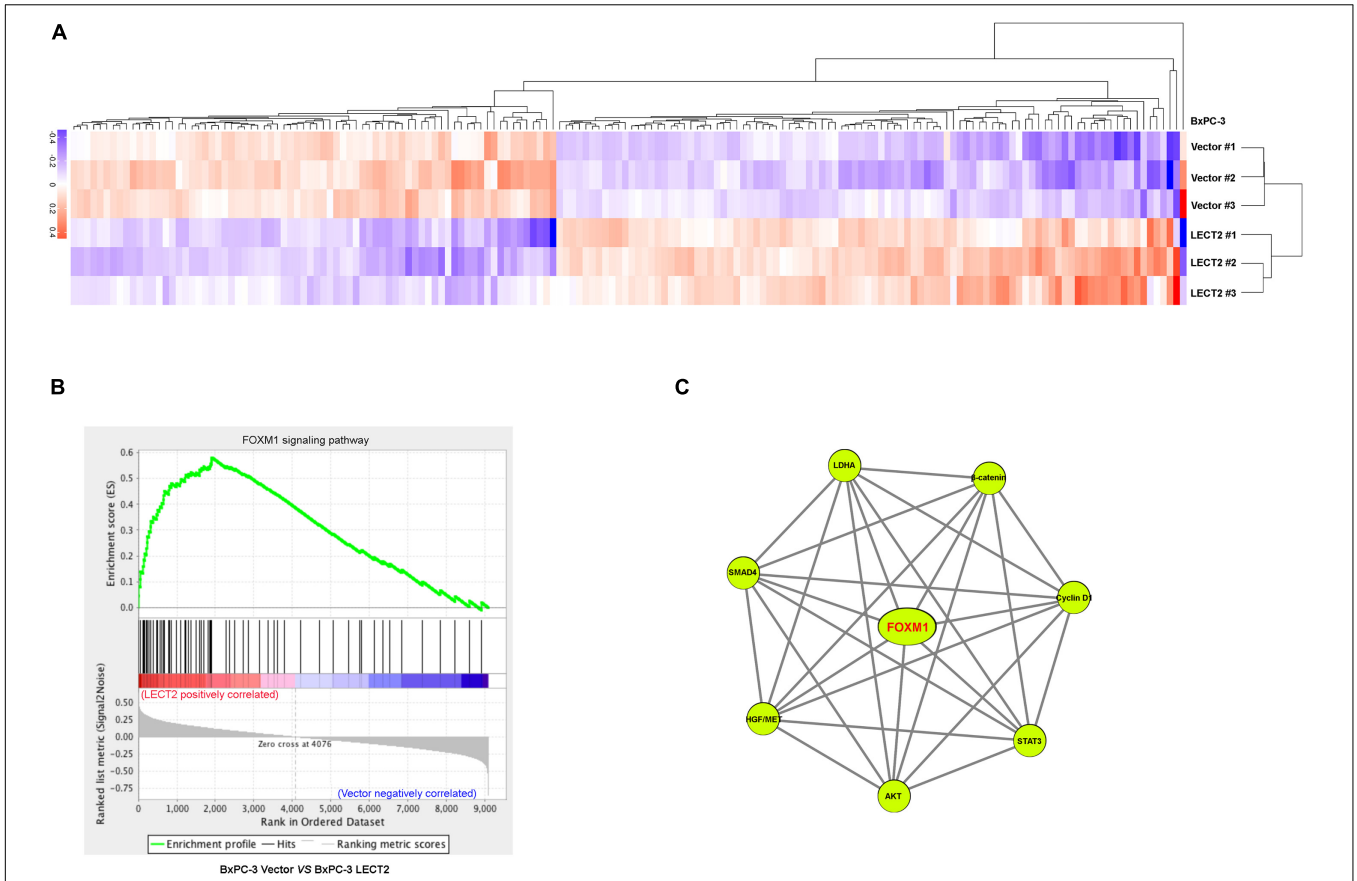


FIGURE 5 | LECT2 negatively correlates with the FOXM1 signaling pathway. **(A)** Heatmap summarizing genes that differentially expressed in BxPC-3 cells transfected with control or LECT2 vectors. Up-regulated genes were labeled in red, and downregulated genes were shown in purple. **(B)** Enrichment of the FOXM1 signaling pathway in Gene Set Enrichment Analysis (GSEA) of genes altered as described above. **(C)** Protein-Protein-Interaction Network, including the enriched genes in the FOXM1 signaling pathway.

blocked the expression of FOXM1 (**Figure 8A**). Additionally, coincident observations were achieved by immunoblotting together with migration and invasion assay that MET deficiency completely abrogated the promoting effects of LECT2 loss on these malignant behaviors in MiaPaca-2 cells (**Figures 8A,B**). However, knocking out LECT2 did not affect MET protein levels. Therefore, we also tested the phosphorylation level of MET after knockout or overexpression of LECT2. The experimental results showed that knocking out LECT2 significantly increased the expression level of p-MET. At the same time, the overexpression of LECT2 inhibited the expression level of p-MET (**Supplementary Figures 8A,B**). Furthermore, a MET inhibitor (Selumetinib) was used to treat MiaPaca-2 cells knocked out of LECT2. The experimental results showed that the effect of knocking out LECT2 on the increase of cell migration and invasion was reversed (**Supplementary Figures 8C,D**). On the other hand, HGF partially recovered the FOXM1 expression and the migratory and invasive abilities in BXPC-3 cells expressing LECT2 (**Figures 8C,D**). Overall, these observations indicated that LECT2 might antagonize FOXM1 signaling via targeting HGF/MET, which affects multiple biological processes and slow down PDAC tumor formation and metastasis (**Figure 8E**). Finally, we also stably overexpress HGF in BxPC-3 cells overexpressing LECT2 (**Supplementary Figure 8E**). BxPC-3 cells co-overexpressing LECT2 and HGF reversed the inhibitory effect of LECT2 on cell invasion and migration (**Supplementary Figures 8F,G**). These results indicate that LECT2 inhibits FOXM1 by negatively regulating HGF/MET, leading to an inhibitory effect on the metastasis of pancreatic cancer cells.

DISCUSSION

The incidence of PDAC is steadily increasing, with the highest mortality-to-incidence ratio amongst all solid organ cancers (Mizrahi et al., 2020). However, the diagnosis and prognosis are still miserable, highlighting the necessity of novel biomarkers and therapeutic targets. However, accumulated evidence showed that the clinical implications of LECT2 in various malignancies, the molecular mechanisms of LECT2 in PDAC progression remain mostly unclear. In this study, we showed that LECT2 serves as a tumor suppressor in PDAC progression as follows: (1) LECT2 is downregulated in metastatic PDACs compared with

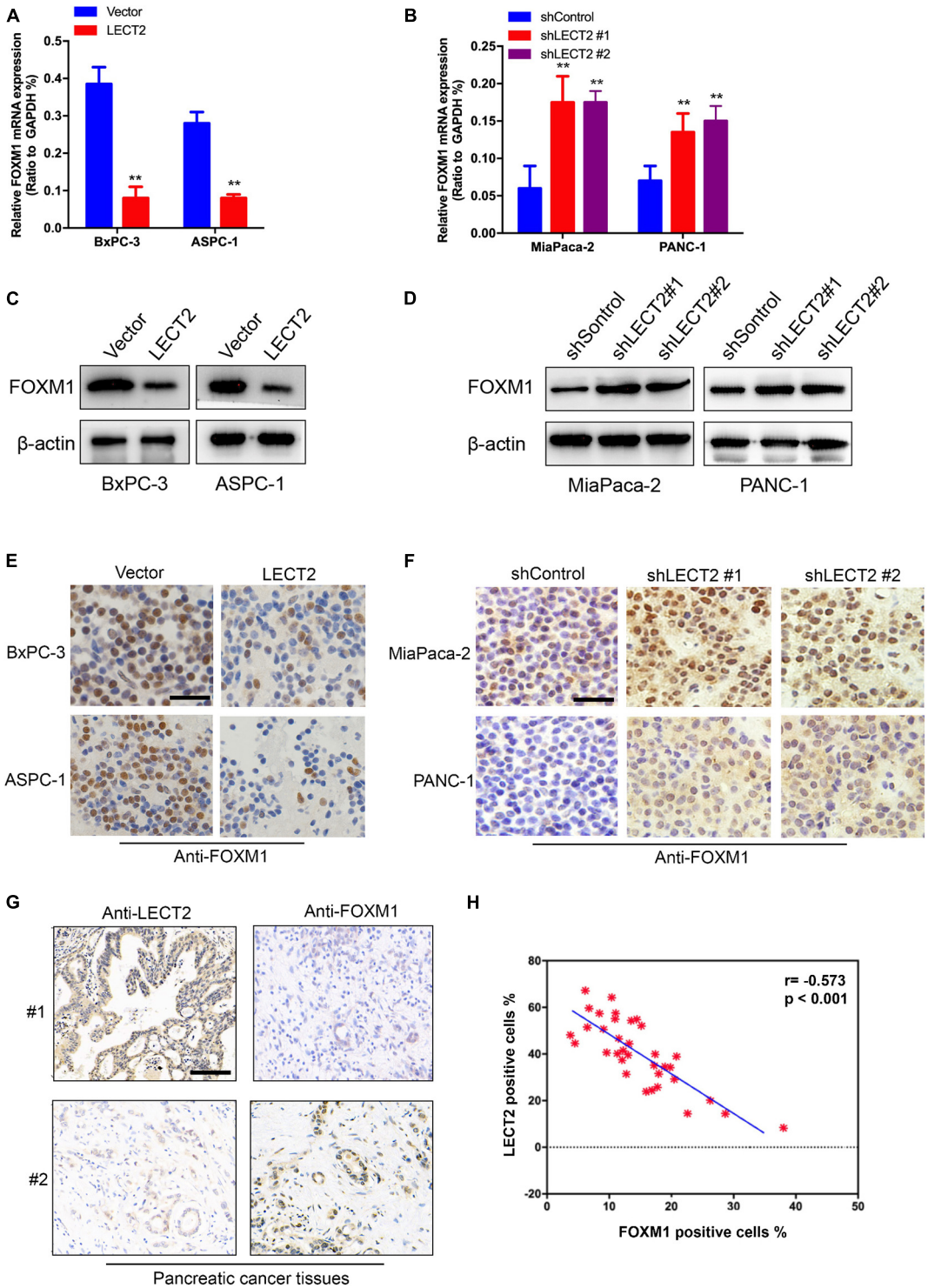


FIGURE 6 | LECT2 downregulates FOXM1 expression. **(A)** mRNA expression of FOXM1 in BxPC-3 and ASPC-1 cells transfected with control (blue) or LECT2 (red) vector. **(B)** mRNA expression of FOXM1 in MiaPaca-2 and Panc-1 cells transfected with shControl (blue) or shLECT2 (red and magenta) vector. **(C)** Immunoblotting to measure FOXM1 protein levels in BxPC-3 (left) and ASPC-1 (right) cells described in **(A)**. **(D)** Immunoblotting to measure FOXM1 protein levels in MiaPaca-2 (left) and Panc-1 (right) cells described in **(B)**. **(E)** Representative IHC staining images of FOXM1 in BxPC-3 (top) and ASPC-1 (bottom) cells described in **(A)**. **(F)** Representative IHC staining images of FOXM1 protein levels in MiaPaca-2 (top) and Panc-1 (bottom) cells described in **(B)**. **(G)** Representative IHC staining images of LECT2 and FOXM1 in pancreatic cancer tissues from 2 patients. **(H)** Quantification of **(G)**. Scale bar = 400 μm in **(E,F)**. Scale bar = 200 μm in **(G)**. $^{**}p < 0.01$.

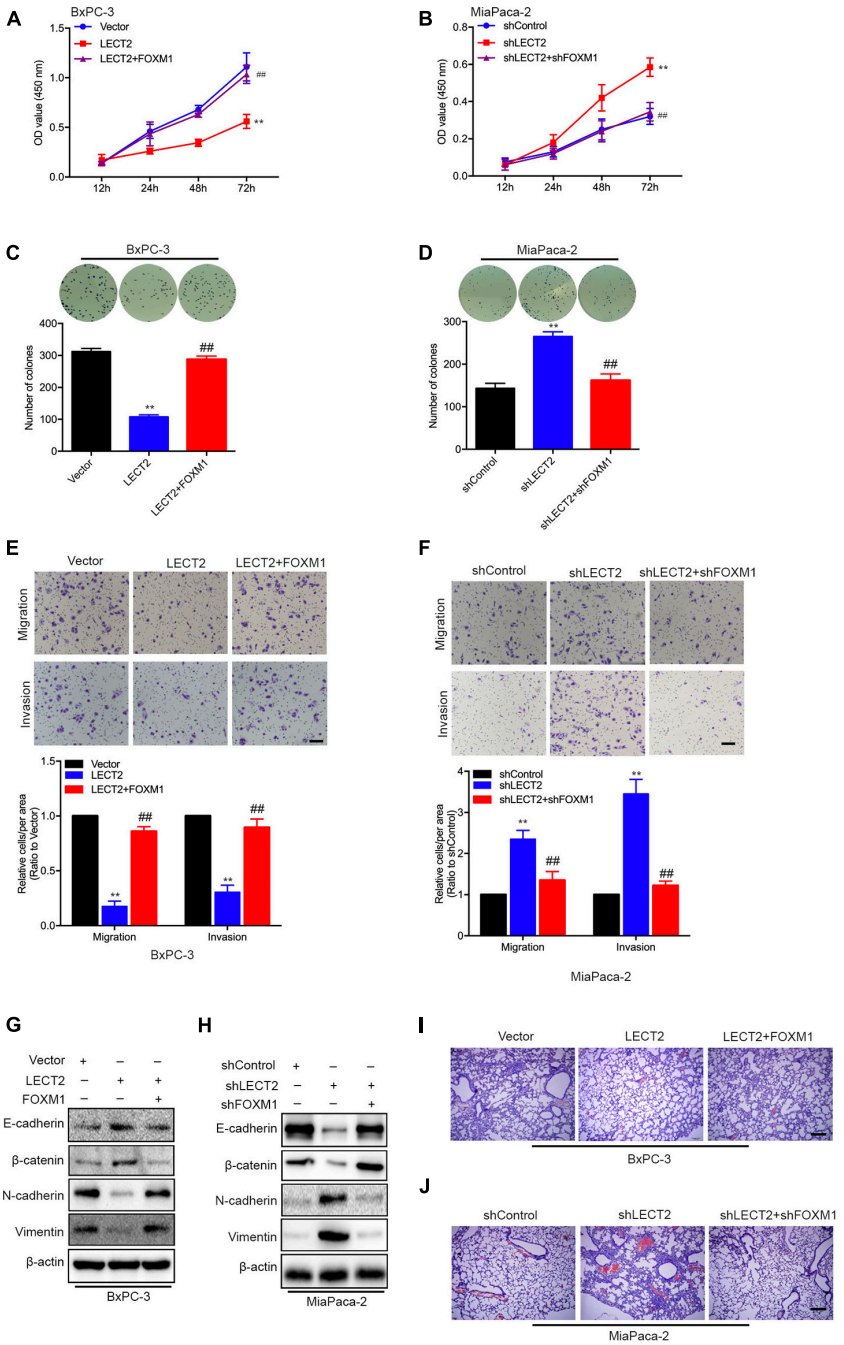


FIGURE 7 | LECT2 suppresses malignant behaviors depending on FOXM1. **(A)** Cell proliferation of BxPC-3 cells transfected with control (blue), LECT2 (red), or LECT2 together with FOXM1 (magenta) vectors. **(B)** Cell proliferation of MiaPaca-2 cells transfected with shControl (blue), shLECT2 (red), or shLECT2 together with shFOXM1 (magenta) vectors. **(C,D)** Colony formation of BxPC-3 **(C)** and MiaPaca-2 **(D)** cells as described in **(A,B)**. **(E,F)** Migration (top) and invasion (middle) of BxPC-3 **(E)** and MiaPaca-2 **(F)** cells as described above with corresponding quantifications (bottom). **(G,H)** Immunoblotting analysis of E-cadherin, β-catenin, N-cadherin, and Vimentin protein levels in BxPC-3 **(G)** and MiaPaca-2 **(H)** cells as described above. **(I,J)** Representative H&E staining images of metastatic lung foci per section from allograft mice injected with BxPC-3 **(I)** and MiaPaca-2 **(J)** cells as described above. Scale bar = 50 μm in **(E,F)**. Scale bar = 200 μm in **(I,J)**. $^{**}p < 0.01$ and $^{\#\#}p < 0.01$.

the primary tumor, and its expression is negatively correlated with multiple clinical pathologic features and prognosis. (2) Overexpression of LECT2 attenuates PDAC tumor growth and metastasis in vitro and in vivo. (3) Mechanistically, LECT2 inhibits FOXM1 signaling by targeting HGF/MET, which retards PDAC progression.

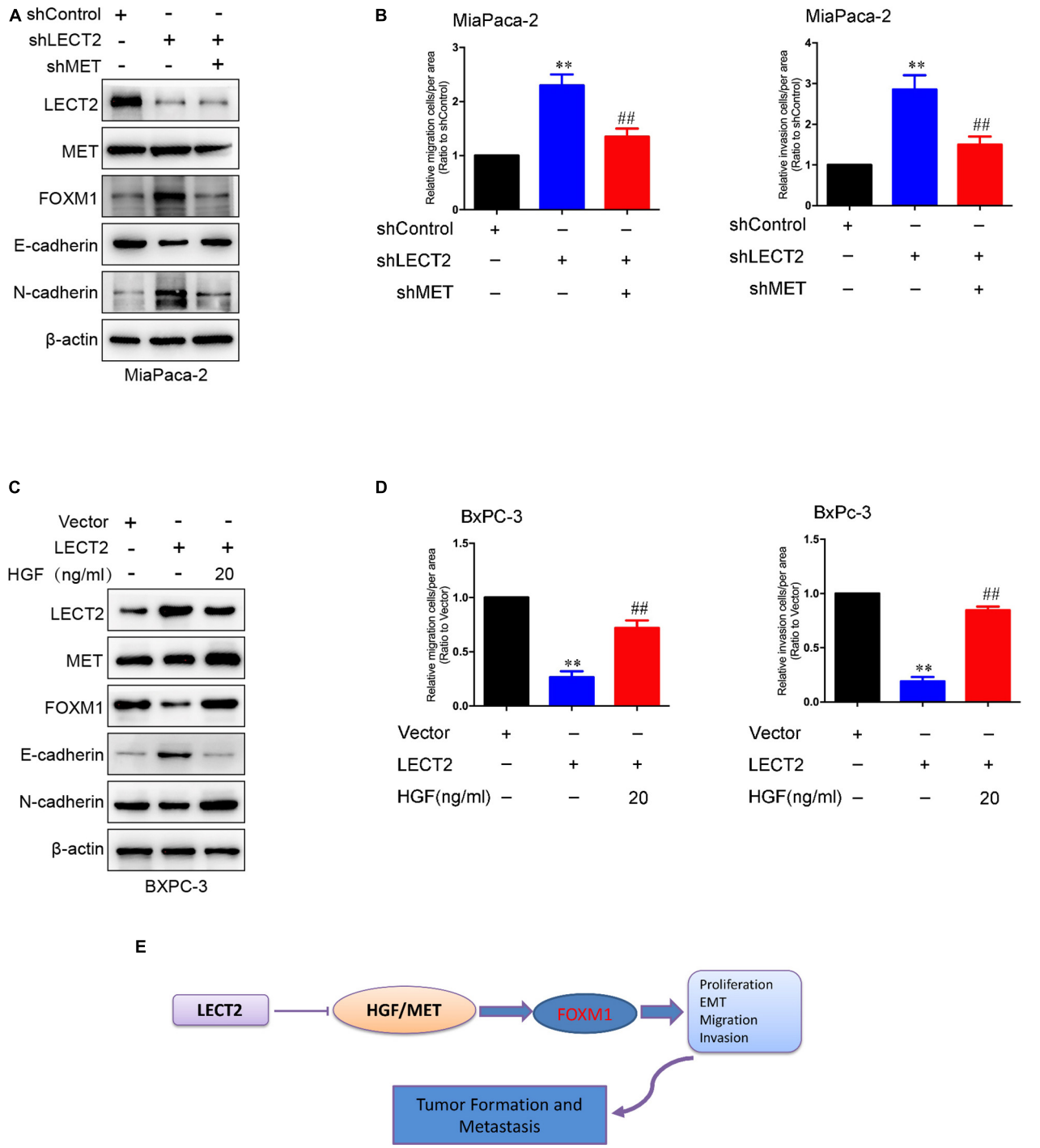


FIGURE 8 | HGF/MET is involved in the regulation of FOXM1 by LECT2. **(A)** Immunoblotting analysis of LECT2, MET, FOXM1, E-cadherin, and N-cadherin protein levels in MiaPaca-2 cells transfected with shControl, shLECT2, and shMET. **(B)** Migration (left) and invasion (right) of MiaPaca-2 cells described in **(A)**. **(C)** Immunoblotting analysis of LECT2, MET, FOXM1, E-cadherin, and N-cadherin protein levels in BxPC-3 cells transfected with Control, LECT2, and/or HGF vectors. **(D)** Migration (left) and invasion (right) of BxPC-3 cells described in **(C)**. **(E)** Schematic model illustrating the biological processes regulated by LECT2 in PDAC. $^{**}p < 0.01$ and $^{\#\#}p < 0.01$.

To explore whether LECT2 is involved in PDAC development, we first detected LECT2 expression in cell lines and tissues from PDAC patients. LECT2 expression significantly decreased in PDACs, especially the metastatic tumors, indicating the potential suppressive role of LECT2 in this malignancy. Moreover, by using PDAC cell lines bearing LECT2 inserts or shRNAs targeting this

protein, as well as the corresponding xenografts injected with the transformed cells, we demonstrated that LECT2 overexpression markedly alleviated cell proliferation, EMT, migration, and invasion. In contrast, ablation of LECT2 had the opposite effects. These results suggest the potential application of LECT2 as a promising biomarker or clinical therapeutic target for the diagnosis and treatment of PDAC in the future.

FOXM1 is a member of the fork headbox (Fox) protein superfamily, which is characterized by a conserved winged-helix DNA-binding domain (Clark et al., 1993). As a critical proliferation-associated transcription factor, FOXM1 is a master factor involved in cell cycle transition and directly or indirectly transactivates the expression of target genes that are strictly involved in the processes of cell proliferation, self-renewal, and tumorigenesis (Wierstra, 2013; Laissue, 2019). Increased expression of FOXM1 is identified in multiple human cancers, including ovarian cancer, breast cancer, prostate cancer, hepatocellular carcinoma, colorectal cancer, melanoma, lung cancer, and gastric cancer, which indicates a poor prognosis in most solid tumors. Meanwhile, inhibition of FOXM1 in cancer cells represses cell proliferation, EMT, migration, metastasis, angiogenesis, and drug resistance (Liao et al., 2018). Given its explicit oncogenic nature, FOXM1 has emerged as a promising target for cancer treatment (Xu et al., 2015). However, drugs targeting FOXM1 have yet to be fully explored, which is likely due to the poor current understanding of the mechanism underlying FOXM1 dysregulation. Here, we discovered that LECT2 negatively correlates with the FOXM1 signaling pathway and downregulates FOXM1 expression and its downstream target genes, which contributed to the suppressive impact of LECT2 on PDAC malignancy. Considering the positive feedback loop between FOXM1 and HGF/MET in PDAC, the implication of HGF/MET in the mediation of FOXM1 by LECT2 was also assessed, which may facilitate a comprehensive understanding of FOXM1 regulation in solid tumor.

In conclusion, the current study provides validating evidence that LECT2 acts as a tumor suppressor in PDAC, and the expression of LECT2 in PDAC cells and tissue is significantly lower, which predicts reduced survival. LECT2 significantly inhibits the viability, colony formation, migration, and invasion of PDAC cells in vitro. It retards tumor growth and metastasis in vivo. On the mechanic level, FOXM1 signaling is critical for the inhibitory effects of LECT2 on the malignant behaviors in PDAC. LECT2 regulates FOXM1 expression through targeting HGF/MET. LECT2 could thus serve as a promising biomarker and target for PDAC prognosis and treatment.

DATA AVAILABILITY STATEMENT

The datasets presented in this study can be found in online repositories. The names of the repository/repositories and accession number(s) can be found below: NCBI GEO; GSE168611.

ETHICS STATEMENT

The studies involving human participants were reviewed and approved by the cancer tissue used complies with the regulations of the Ethics Committee of Qingdao University. The patients/participants provided their written informed consent to participate in this study. The animal study was reviewed and approved by the mice used complied with the rules of the Qingdao University Ethics Committee on the correct use of animals.

AUTHOR CONTRIBUTIONS

XL and PL contributed equally to this work and completed relevant experiments. YT, XJ, and TL completed part of the experiment and processed part of the experimental data. YW completed the revision of the manuscript. CW and YC designed the work and preparation of the manuscript. All authors contributed to the article and approved the submitted version.

FUNDING

This research was funded by the Natural science foundation of Shandong province, grant number ZR2019MH101.

SUPPLEMENTARY MATERIAL

The Supplementary Material for this article can be found online at: https://www.frontiersin.org/articles/10.3389/fcell.2021.661122/full#supplementary-material

REFERENCES

Ando, K., Kato, H., Kotani, T., Ozaki, M., Arimura, Y., and Yagi, J. (2012). Plasma leukocyte cell-derived chemotaxin 2 is associated with the severity of systemic inflammation in patients with sepsis. *Microbiol. Immunol.* 56, 708–718. doi: 10.1111/j.1348-0421.2012.00488.x

Andres, S. A., Bickett, K. E., Alatoum, M. A., Kalbfleisch, T. S., Brock, G. N., and Wittliff, J. L. (2015). Interaction between smoking history and gene expression levels impacts survival of breast cancer patients. *Breast Cancer Res. Treat.* 152, 545–556. doi: 10.1007/s10549-015-3507-z

Chen, C. K., Yang, C. Y., Hua, K. T., Ho, M. C., Johansson, G., Jeng, Y. M., et al. (2014). Leukocyte cell-derived chemotaxin 2 antagonizes MET receptor activation to suppress hepatocellular carcinoma vascular invasion by protein tyrosine phosphatase 1B recruitment. *Hepatology* 59, 974–985. doi: 10.1002/hep.26738

Chen, C. K., Yu, W. H., Cheng, T. Y., Chen, M. W., Su, C. Y., Yang, Y. C., et al. (2016). Inhibition of VEGF165/VEGFR2-dependent signaling by LECT2 suppresses hepatocellular carcinoma angiogenesis. *Sci. Rep.* 6:31398. doi: 10.1038/srep31398

Clark, K. L., Halay, E. D., Lai, E., and Burley, S. K. (1993). Co-crystal structure of the HNF-3/fork head DNA-recognition motif resembles histone H5. *Nature* 364, 412–420. doi: 10.1038/364412a0

Cui, J., Xia, T., Xie, D., Gao, Y., Jia, Z., Wei, D., et al. (2016). HGF/Met and FOXM1 form a positive feedback loop and render pancreatic cancer cells resistance to Met inhibition and aggressive phenotypes. *Oncogene* 35, 4708–4718. doi: 10.1038/onc.2016.14

Francica, P., Nisa, L., Aebersold, D. M., Langer, R., Bladt, F., Blaukat, A., et al. (2016). Depletion of FOXM1 via MET targeting underlies establishment of a DNA damage-induced senescence program in gastric cancer. *Clin. Cancer Res.* 22, 5322–5336. doi: 10.1158/1078-0432.CCR-15-2987

Greenow, K. R., Zverev, M., May, S., Kendrick, H., Williams, G. T., Phesse, T., et al. (2018). Lect2 deficiency is characterised by altered cytokine levels and promotion of intestinal tumourigenesis. *Oncotarget* 9, 36430–36443. doi: 10.18632/oncotarget.26335

Hung, W. Y., Chang, J. H., Cheng, Y., Chen, C. K., Chen, J. Q., Hua, K. T., et al. (2018). Leukocyte cell-derived chemotaxin 2 retards non-small cell lung cancer progression through antagonizing MET and EGFR activities. *Cell Physiol. Biochem.* 51, 337–355. doi: 10.1159/000495233

Hwang, H. J., Jung, T. W., Hong, H. C., Seo, J. A., Kim, S. G., Kim, N. H., et al. (2015). LECT2 induces atherosclerotic inflammatory reaction via CD209 receptor-mediated JNK phosphorylation in human endothelial cells. *Metabolism* 64, 1175–1182. doi: 10.1016/j.metabol.2015.06.001

Ito, M., Nagata, K., Kato, Y., Oda, Y., Yamagoe, S., Suzuki, K., et al. (2003). Expression, oxidative refolding, and characterization of six-histidine-tagged recombinant human LECT2, a 16-kDa chemotactic protein with three disulfide bonds. *Protein Expr. Purif.* 27, 272–278. doi: 10.1016/s1046-5928(02)00634-4

Koshimizu, Y., and Ohtomi, M. (2010). Regulation of neurite extension by expression of LECT2 and neurotrophins based on findings in LECT2-knockout mice. *Brain Res.* 1311, 1–11. doi: 10.1016/j.brainres.2009.11.010

Laissue, P. (2019). The forkhead-box family of transcription factors: key molecular players in colorectal cancer pathogenesis. *Mol. Cancer* 18:5. doi: 10.1186/s12943-019-0938-x

Lan, F., Misu, H., Chikamoto, K., Takayama, H., Kikuchi, A., Mohri, K., et al. (2014). LECT2 functions as a hepatokine that links obesity to skeletal muscle insulin resistance. *Diabetes* 63, 1649–1664. doi: 10.2337/db13-0728

L'Hermitte, A., Pham, S., Cadoux, M., Couchy, G., Caruso, S., Anson, M., et al. (2019). Lect2 controls inflammatory monocytes to constrain the growth and progression of hepatocellular carcinoma. *Hepatology* 69, 160–178. doi: 10.1002/hep.30140

Liao, G. B., Li, X. Z., Zeng, S., Liu, C., Yang, S. M., Yang, L., et al. (2018). Regulation of the master regulator FOXM1 in cancer. *Cell Commun. Signal.* 16:57. doi: 10.1186/s12964-018-0266-6

Lu, X. J., Chen, J., Yu, C. H., Shi, Y. H., He, Y. Q., Zhang, R. C., et al. (2013). LECT2 protects mice against bacterial sepsis by activating macrophages via the CD209a receptor. *J. Exp. Med.* 210, 5–13. doi: 10.1084/jem.20121466

Mizrahi, J. D., Surana, R., Valle, J. W., and Shroff, R. T. (2020). Pancreatic cancer. *Lancet* 395, 2008–2020. doi: 10.1016/s0140-6736(20)30974-0

Okabe, H., Delgado, E., Lee, J. M., Yang, J., Kinoshita, H., Hayashi, H., et al. (2014). Role of leukocyte cell-derived chemotaxin 2 as a biomarker in hepatocellular carcinoma. *PLoS One* 9:e98817. doi: 10.1371/journal.pone.0098817

Okumura, A., Saito, T., Otani, I., Kojima, K., Yamada, Y., Ishida-Okawara, A., et al. (2008). Suppressive role of leukocyte cell-derived chemotaxin 2 in mouse anti-type II collagen antibody-induced arthritis. *Arthritis Rheum* 58, 413–421. doi: 10.1002/art.23215

Siegel, R. L., Miller, K. D., and Jemal, A. (2020). Cancer statistics, 2020. *CA Cancer J. Clin.* 70, 7–30. doi: 10.3322/caac.21590

Wierstra, I. (2013). FOXM1 (Forkhead box M1) in tumorigenesis: overexpression in human cancer, implication in tumorigenesis, oncogenic functions, tumor-suppressive properties, and target of anticancer therapy. *Adv. Cancer Res.* 119, 191–419. doi: 10.1016/B978-0-12-407190-2.00016-2

Xu, M., Xu, H. H., Lin, Y., Sun, X., Wang, L. J., Fang, Z. P., et al. (2019). LECT2, a ligand for tie1, plays a crucial role in liver fibrogenesis. *Cell* 178, 1478–1492.e20. doi: 10.1016/j.cell.2019.07.021

Xu, X. S., Miao, R. C., Wan, Y., Zhang, L. Q., Qu, K., and Liu, C. (2015). FoxM1 as a novel therapeutic target for cancer drug therapy. *Asian Pac. J. Cancer Prev.* 16, 23–29. doi: 10.7314/apjcp.2015.16.1.23

Yamagoe, S., Yamakawa, Y., Matsuo, Y., Minowada, J., Mizuno, S., and Suzuki, K. (1996). Purification and primary amino acid sequence of a novel neutrophil chemotactic factor LECT2. *Immunol. Lett.* 52, 9–13. doi: 10.1016/0165-2478(96)02572-2

Conflict of Interest: The authors declare that the research was conducted in the absence of any commercial or financial relationships that could be construed as a potential conflict of interest.

Copyright © 2021 Li, Lin, Tao, Jiang, Li, Wang, Wang and Cao. This is an open-access article distributed under the terms of the Creative Commons Attribution License (CC BY). The use, distribution or reproduction in other forums is permitted, provided the original author(s) and the copyright owner(s) are credited and that the original publication in this journal is cited, in accordance with accepted academic practice. No use, distribution or reproduction is permitted which does not comply with these terms.

frontiers in Oncology

ORIGINAL RESEARCH
published: 26 May 2021
doi: 10.3389/fonc.2021.667495

The Deubiquitinase USP39 Promotes ESCC Tumorigenesis Through Pre-mRNA Splicing of the mTORC2 Component Rictor

Yuan Zhao[1†], Huiwu Geng[2†], Gang Liu[2†], Qiang Ji[2,3], Xiaomin Cheng[2], Xinying Li[2], Wei Liu[1], Rick F. Thorne[3], Renquan Zhang[1] and Xiaoying Liu[2,3*]*

[1] Department of Thoracic Surgery, The First Affiliated Hospital, Anhui Medical University, Hefei, China, [2] Biology Department, School of Life Sciences, Anhui Medical University, Hefei, China, [3] Translational Research Institute of Henan Provincial People's Hospital and People's Hospital of Zhengzhou University, Molecular Pathology Centre, Academy of Medical Sciences, Zhengzhou University, Zhengzhou, China

OPEN ACCESS

Edited by:
Simona Kranjc Brezar, Institute of Oncology Ljubljana, Slovenia

Reviewed by:
Estela Jacinto, University of Medicine and Dentistry of New Jersey, United States
Min Deng, Mayo Clinic, United States

***Correspondence:**
Renquan Zhang
zhangrenquan@live.cn
Xiaoying Liu
liuxiaoying@ahmu.edu.cn
orcid.org/0000-0003-3450-5683

[†]These authors have contributed equally to this work

Specialty section:
This article was submitted to Molecular and Cellular Oncology, a section of the journal Frontiers in Oncology

Received: *13 February 2021*
Accepted: *05 May 2021*
Published: *26 May 2021*

Citation:
Zhao Y, Geng H, Liu G, Ji Q, Cheng X, Li X, Liu W, Thorne RF, Zhang R and Liu X (2021) The Deubiquitinase USP39 Promotes ESCC Tumorigenesis Through Pre-mRNA Splicing of the mTORC2 Component Rictor. Front. Oncol. 11:667495. doi: 10.3389/fonc.2021.667495

Spliceosomes are large RNA-protein molecular complexes which mediate splicing of pre-mRNA in eukaryotic cells. Their function is frequently altered in cancer, providing opportunities for novel therapeutic approaches. The ubiquitin specific protease 39 (USP39) is a highly conserved deubiquitylation family member that plays an essential role in pre-mRNA splicing where it serves to assemble the mature spliceosome complex. Previous studies have reported that USP39 acts in an oncogenic manner where it contributes to cancer progression and predicts poor prognosis in various human tumor types. Here we report that USP39 is differentially upregulated in human esophageal squamous cell carcinoma (ESCC) and its expression is significantly associated with clinicopathological characteristics including differentiation status and TNM stage. We found the USP39 upregulation was maintained in ESCC cell lines where it functioned to promote cancer cell growth *in vitro* and in xenografts. RNA-seq analyses identified that mTOR pathway activation was affected by shRNA-mediated silencing of USP39. Subsequent biochemical analyses demonstrated that USP39 regulates the activity of mTORC2 by selectively enhancing the splicing and maturation of Rictor mRNA, although not other key mTORC components. Together, our report proposes USP39 as a biomarker and oncogenic factor in ESCC, with a potential for targeting the USP39/mTOR2/Rictor axis as a therapeutic strategy. Furthermore, our study adds ESCC to the list of cancers where USP39 contributes to tumorigenesis and progression.

Keywords: esophageal squamous cell carcinoma (ESCC), ubiquitin specific protease 39 (USP39), mammalian target of rapamycin (mTOR), RNA splicing, rictor

INTRODUCTION

With an increasing incidence worldwide, esophageal cancer represents one of the most aggressive and fatal cancers (1, 2). In the highest-risk areas, 90% of cases are esophageal squamous cell carcinoma (ESCC), the major histopathological type of this disease. Despite advances in treatment, five-year survival rates are less than 20% and these poor outcomes are associated with late stage

diagnosis, frequent metastasis and therapeutic resistance (3, 4). Therefore, ESCC research is focused on understanding the molecular mechanisms governing disease initiation and progression with the goal of identifying novel therapeutic targets.

Spliceosomes are large RNA-protein molecular complexes which mediate splicing of pre-mRNA in eukaryotic cells. Major spliceosome components consist of different combinations of small nuclear RNAs (snRNAs) designated U1, U2, U4, U5 and U6 which form stable ribonuclear protein complexes (snRNPs), each involved at different stages of the splicing process. Other accessory proteins including recruiting factors such as the serine and arginine-rich (SR) proteins are also involved (5). The genes encoding spliceosome assembly components such as SF3B1, ZRSR2, U2AF1 and SRSF2 have been found to have frequent and recurrent somatic mutations in various types of cancers whereas other components may be overexpressed, collectively suggesting roles in oncogenesis (6–10). Notably, knockdown of spliceosome-related genes results in growth inhibition of breast, lung, and melanoma cancer cells, but has had little effect on the survival of the normal epithelial cells (11). Therefore, studies on the spliceosome and its related proteins may offer novel opportunities to enhance the efficacy of cancer therapies.

The ubiquitin specific protease 39 (USP39) is a highly conserved deubiquitylation family member (also known as Sad1p in yeast) and component of the U4/U6-U5 tri-snRNP. Each member of USPs contains a zinc finger ubiquitin binding domain and a ubiquitin C-terminal hydrolase (UCH) domain (12) although USP39 is notably deprived of ubiquitin protease activity due to the absence of three active site residues in its UCH-domain (13). USP39 plays an essential role in pre-mRNA splicing with studies showing it functions in the assembly of mature spliceosome complex, although not in the maintenance of complex stability (12). In particular, USP39 was shown to be involved in the splicing of Aurora B and other mRNAs essential for proper spindle checkpoint function (14). Consistently, mutation of zebrafish USP39 induces Rb1 splicing defects which induces G1/S arrest (15). Moreover, other studies have suggested that USP39 functions as an oncogenic factor in numerous cancers including breast (16), liver (17), medullary thyroid (18), lung (19), prostate (20), oral squamous cell (21) and renal cell carcinomas (22). For example, USP39 promotes prostate cancer cell tumorigenesis by facilitating EGFR mRNA maturation and transcriptional elongation (20), whereas in glioma it promotes progression by facilitating TAZ mRNA maturation (23). Our previous research in melanoma also implicated USP39 in disease progression through regulating cell cycle and apoptosis *via* ERK1/2 signaling (24).

To our knowledge, USP39 has not yet been previously investigated in ESCC. Here we report that USP39 is differentially upregulated in human ESCC compared with adjacent normal tissues and find that its expression is significantly associated with clinicopathological characteristics. We also found US39 upregulation was maintained in ESCC cell lines and showed it impacted measures of tumorigenesis both *in vitro* as well as xenograft experiments. We further demonstrate this oncogenic activity is due to USP39's role in regulating the maturation of Rictor mRNA. Our data define USP39 as a biomarker and oncogenic factor in ESCC, with a potential for targeting USP39/mTOR2/Rictor pathway as a therapeutic strategy.

MATERIALS AND METHODS

Cell Culture

The human ESCC cell line ECA109 was obtained from the Culture Collection of the Chinese Academy of Sciences (Shanghai, China); ESCC cell lines KYSE30, KYSE70, TE13 and the normal esophageal epithelial cell line Het-1A were all obtained from Kebai Biological Technology (Nanjing, China). Cells were cultured in RPMI 1640 medium (Gibco BRL, Rockville, MD, USA) with 5% fetal bovine serum, 100 U/ml of penicillin and 100 mg/ml streptomycin. Primary cultures of esophageal epithelial cells were prepared by modification of established methods. All cells were maintained at 37°C in a humidified chamber containing 5% CO_2.

Datasets

To investigate the clinical significance of USP39 in ESCC, we retrieved and analyzed the expression of USP39 in ESCC tissues and adjacent normal tissues using published data from public Gene Expression Omnibus (GEO) database (http://www.ncbi.nlm.nih.gov/geo) and normalized using Robust Multichip Average (RMA). Subsequently, we also acquired gene expression data from TCGA (https://portal.gdc.cancer.gov/projects/TCGA-LIHC) and analyzed the relationship between USP39 expression and disease-free survival.

Clinical Specimens and Ethics

Fresh tumor tissues and paired adjacent normal tissues were collected from patients who underwent radical esophagectomy at the Department of Thoracic Surgery, the First Affiliated Hospital of Anhui Medical University between March 2014 and January 2017. Tissue samples were fixed in formalin and embedded in paraffin (FFPE). The patient's clinicopathological characteristics were obtained from surgical and pathological records. The tumor stage utilized in the present study was according to the 8th edition of the American Joint Committee on Cancer (AJCC) TNM classification system. Patients received neither chemotherapy nor radiotherapy before resection. All human tumor tissues were obtained with written informed consent with a signature from patients or their guardians prior to participation in the study. This study was approved by the institutional review board of Anhui Medical University (20190402).

Immunohistochemistry

Deparaffinized and hydrated FFPE tissue sections (5 μm) were subject to antigen retrieval using microwaving at 130°C

for 10 min. Sections were then incubated for 15 min in 3% H_2O_2 to eliminate endogenous peroxidase before subsequent incubation with USP39 primary antibodies (1:100; Abcam, ab131332) overnight at 4°C. Secondary antibody incubations were performed at 37°C for 30 min, washed with three times with phosphate-buffered saline (PBS) for 5 min, then incubated with DAB and hematoxylin. Immunoreactivity was blindly evaluated by two professional pathologists to according to immunoreactivity score (IRS) system, which is based on the proportion and intensity of positively stained cells. The percentage of positive cells was scored as 0-4 where positive stained cells ≤5% (0), 6–25% (1), 26–50% (2), 51–75% (3), and >75% (4); while the intensity of staining was scored as 0-3: colorless (0), bright yellow (1), yellow (2), and brown (3). The overall staining scores were then calculated by multiplying the percentage and intensity staining scores. The staining score index was designated as negative (-, 0), weak positive (+, 1-4), moderate positive (++, 5-8), and strong positive (+++, 9-12). For analysis, we combined weak positive and negative staining cases as low USP39 expression, and moderate and strong positive staining as high USP39 expression.

Lentiviral Transduction

The lentivirus particles containing shRNA constructs targeting USP39 (sh-USP39-1, shUSP39-2) or negative control (sh-control) were obtained from GeneChem (Shanghai, China). Transduction of ECA109 and KYSE30 cells was performed in the presence of polybrene (Sigma, USA) at a final concentration of 5 μg/ml according to the manufacturer's instructions. Two days after transduction, GFP fluorescence was confirmed and cells further selected with 4-6 μg/ml puromycin. The sequences of the shRNAs and negative control used are as follow: sh-control, 5′-TTCTC CGAACGTGTCACGT-3′; sh-USP39-1, 5′-TTTGGAAGAG GCGAGATAA-3′; sh-USP39-2, 5′-CAAGTTGCCTCCATAT CTA-3′.

Plasmid Vectors and Transfection

A pcDNA3.1-based expression plasmid was constructed containing HA epitope-tagged USP39 cDNA and used to transfect ECA109 and KYSE30 cells using Lipofectamine 2000 reagent in Opti-MEM medium for 6h. The medium was replaced with fresh complete medium before conducting the indicated experiments.

Quantitative Real-Time PCR (qRT-PCR)

Total RNA was extracted from the cells using Trizol reagent (Invitrogen, USA). Isolated total RNA was quantified and used to generate cDNA using a reverse transcription kit (Toyobo; Osaka, Japan). The mRNA levels were quantified by real-time PCR. The data were interpreted using the $2^{-\Delta\Delta Ct}$ method with GAPDH serving as a reference gene for normalization. All experiments were repeated at least 3 times. The primers used are shown in **Table 4**.

Western Blotting Analysis

Total cell lysates were resolved on 12% denaturing polyacrylamide gels and electro-transferred to PVDF membranes. Membranes were blocked in TBST solution containing 5% (w/v) fat-free dry milk followed by triple washing in TBST and incubation with primary antibodies against human USP39 (#ab131332, abcam), mTOR (#2972s, CST), Raptor (20984-1-AP, proteintech), Rictor (#53A2, CST), Akt (#2920, CST), p-Akt (Thr308) (#9275s, CST), p-Akt (Ser473) (#4060, CST), S6K1 (#2217s, CST), p-Rps6 (#5364s, CST) or GAPDH (#60004-1-IG, proteintech), respectively, overnight at 4°. After washing three times, the membranes were incubated with horseradish peroxidase-conjugated secondary antibodies for 1h at room temperature. Proteins were detected using ECL reagent (Pierce, USA) and band intensities were normalized to GAPDH. Each experiment was performed for three times.

Cell Proliferation Assay

Cells were plated into 96-well culture plates and after overnight culture, CCK-8 solution (Dojindo; Kumamoto, Japan) was added to evaluate cell proliferation every 24 hours for 4 consecutive days. The absorbance of the samples was measured at 450 nm in a microplate reader. Experiments were repeated at least three times.

Colony Formation Assay

Cells were seeded at 1000 cells/well in 6-well plates and cultured at 37°C. Twelve days later, cells were washed twice with PBS, fixed with 4% formaldehyde, stained with 0.5% crystal violet for 10 min and washed with ddH_2O for three times. Colonies were photographed with a digital camera.

RNA-Seq Analysis

Total RNA from ECA109 cells (triplicates) bearing control or USP39 shRNA was extracted by the Qiagen RNeasy kit (Qiagen, Cat #74104). Libraries were prepared using VAHTS® Total RNA-seq (H/M/R) Library Prep Kit (Vazyme) according to the manufacturer's instructions. Samples were sequenced on an Illumina HiSeq6000 with paired-end 150 bp reads. Reads were then filtered for adapter contamination using cutadapt and so that at least 90% of bases of each read had a quality score >20. Reads were aligned to the reference genome (hg19) using STAR version 2.5.2b retaining only primary alignments. Reads overlapping blacklisted regions of the genome were then removed. Transcript abundance was then estimated using salmon, and differential expression was detected using DESeq2. Pathway analyses were then performed on significantly upregulated and significantly downregulated gene sets independently according to the KEGG (Kyoto Encyclopedia of Genes and Genomes) database (25).

RNA Immunoprecipitation (RIP) Assay

RIP analysis was performed using the Magna RIP RNA-binding protein immunoprecipitation kit (Millipore, Billerica, MA, USA)

and the USP39 antibody (#ab131332, Abcam) following the manufacturer's protocol. Co-precipitated RNAs were isolated, purified, and subjected to qRT-PCR analysis.

Animal Studies

Male BALB/c nude mice (at age 3-4 weeks; GemPharmatech Co., Ltd; Nanjing, China) were randomly divided into the indicated groups. ECA109 cells (6×10^6) with or without USP39 shRNA knockdown were injected subcutaneously into the right flank of each mouse. Tumor sizes were measured by calipers every 3 days. Mice were killed and tumors were weighed at 28 days after tumor cell transplantation. Tumors were collected and either immediately snap-frozen and preserved at -80°C, or fixed in 10% formalin for 48 h before paraffin embedding and sectioning. Animal studies were also approved by the Animal Research Ethics Committee of Anhui Medical University.

Statistical Analysis

Statistical analysis was performed using the SPSS 17.0 software package. Differences in categorical variables between two groups were analyzed by Chi-square test or Mann-Whitney U test. Analysis of variance and Student's t test were used for comparison among different treatment groups. $P < 0.05$ was considered statistically significant. All experiments were carried out with at least three replicates.

RESULTS

USP39 Is Upregulated in ESCC

We first analyzed gene expression data from ESCC cases determined from microarray-based studies in the GEO database (GDS3838 and GSE23400). The analyses of two independent cohorts showed consistently that USP39 expression was elevated in tumor tissues compared with their paired adjacent normal tissues (**Figures 1A, B**). To verify this observation, Western blotting analyses were conducted in a small cohort of matched pairs of ESCC tissues (T) and adjacent normal tissues (N). Instructively, USP39 protein was decisively upregulated in all eight ESCC cases compared with normal tissues (**Figure 1C**). We then extended these studies to include immunohistochemical (IHC) examination of 120 pairs of ESCC samples (**Figures 1D, E**). Here strong staining for USP39 was detected in 82 (68.3%) of ESCC tissues but only in 33 (27.5%) of normal tissues (**Table 1**). Moreover, we analyzed whether the expression of USP39 was associated with ESCC clinicopathological characteristics. As shown in **Table 2**, the upregulation of USP39 in ESCC was found to be associated with tumor differentiation, invasion, lymph node metastasis and TNM stage. In contrast, other demographic factors, including age, gender and tumor location were independent of USP39 expression. We also performed Kaplan-Meier survival analysis using TCGA dataset. The results showed patient disease free survival (DFS) was significantly shorter in ESCC cases with high USP39 expression compared with low USP39 expression (**Figure 1G**), which suggests that upregulation of USP39 is correlated with the poor prognosis of ESCC. This proposes USP39 as a potential biomarker for ESCC.

We also examined USP39 expression in ESCC cell lines (ECA109, KYSE30, KYSE70 and TE13) compared with normal esophageal epithelial cell line (Het-1A) using Western blotting. Consistent with the *ex vivo* analyses of ESCC tissues, the protein levels of USP39 were significantly higher in the ESCC cell lines compared with normal esophageal epithelial cells (**Figure 1F**).

USP39 Promotes Proliferation of ESCC Cells *In Vitro*

Based on findings in the previous Section, we sought to investigate the biological function of USP39 in ESCC cells. We first established that USP39 could be effectively suppressed in the ECA109 and KYSE30 cell lines by RNAi using independent short hairpin RNAs (shRNAs) delivered as lentiviral particles. Measurement of USP39 levels by qPCR confirmed reductions in USP39 mRNA in both cell lines with the sh-USP39-1 shRNA construct being more efficient than the other used (**Figures 2A, B**). Along with negative controls the USP39 knockdown cell lines were then subjected to cell growth measurements using both the CCK-8 and colony formation assays. Knockdown of USP39 in both ESCC cell lines resulted in decisive reductions in the ability of cells to proliferate as well as establish colonies (**Figures 2C–E**). Conversely, overexpression of USP39 in ECA109 and KYSE30 cells increased their ability to proliferate and establishing colonies compared with the vector control (**Figures 2F–I**). Together these data indicate that USP39 promotes ESCC cell proliferation *in vitro*.

USP39 Modulates ESCC Growth *In Vivo*

We then turned to investigate whether knockdown of USP39 also reduces ESCC cell growth in the more physiologically relevant *in vivo* context. Equal cell numbers of ECA109 cells bearing control or USP39 shRNA stable knockdown were inoculated into the flanks of nude mice and allowed to establish xenografts over four weeks. Tracking tumor growth by volume measurements showed that the growth rate of sh-USP39-1 was significantly less with the final tumor weights being consistently less than their control counterparts (**Figures 3A–C**). These results indicated that USP39 is also critical for ESCC cell proliferation and tumorigenicity *in vivo*.

USP39 Regulates mTORC2 Signaling Through Rictor

Having established that USP39 contributes to a growth promoting phenotype in ESCC cells we sought to explore the potential mechanisms involved. We therefore conducted comparative transcriptomic analyses on control versus USP39 shRNA stable knockdown cells using RNA-seq.

Analyses of differentially regulated pathways using KEGG suggested that mTOR was one of the most significant pathways altered by USP39 knockdown (**Figure 4A**). mTOR is a serine/

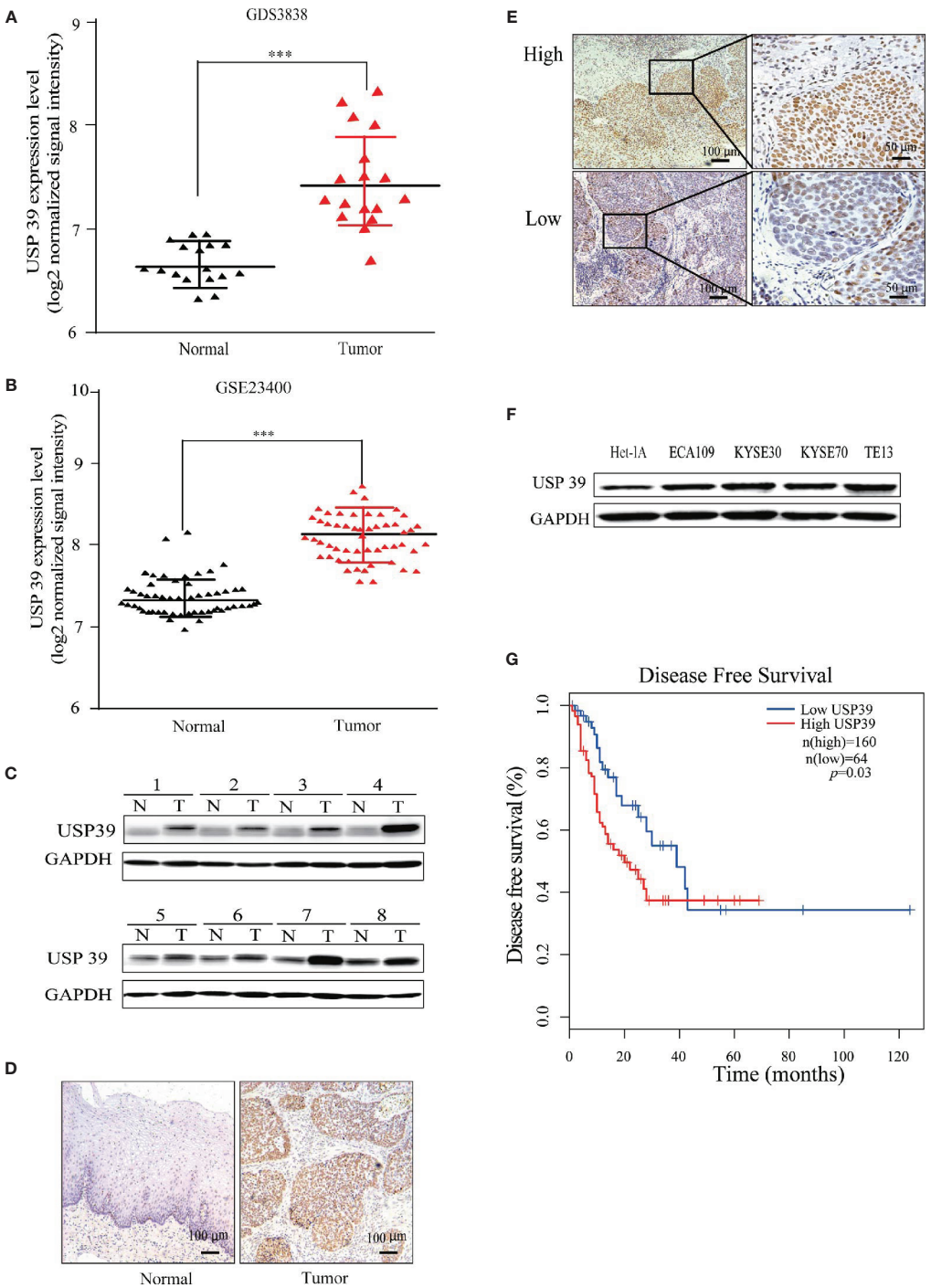


FIGURE 1 | USP39 is upregulated in ESCC tissues and cell lines. **(A, B)** The relative expression of USP39 in ESCC tissues compared with normal tissues was analyzed using GEO datasets GDS3838 **(A)** and GSE23400 **(B)**. Student's t-test: *** $p < 0.001$. **(C)** Western blotting analyses of USP39 protein expression in ESCC (T) and paired adjacent normal tissues (N). USP39 protein expression levels were normalized to the GADPH loading control (n = 8 per group). **(D, E)** Representative immunohistochemical staining of USP39 expression in a matched pair of adjacent normal versus tumor tissues **(D)** and examples of high and low IRS scores in ESCC cancer tissues **(E)**. **(F)** Western blotting analyses for USP39 expression in ESCC cell lines ECA109, KYSE30, KYSE70 and TE-13 compared with normal esophageal cell line Het-1A. **(G)** Kaplan-Meier curve showing a correlation of USP39 expression with disease free survival rate in ESCC patients.

TABLE 1 | IHC staining of USP39 expression in ESCC tissues.

	# of cases	Expression		*P*
		Low (-/+)	High (++/+++)	
Normal	120	87	33	P<0.001
ESCC	120	38	82	

P value was estimated by Chi-square test.

TABLE 2 | Relationship of USP39 expression and clinicopathological characteristics in patients.

	# of cases	Expression		*P*
		Low (-/+%)	High (++/+++%)	
Age				
≥65	72	23	49	0.936
≥65	48	15	33	
Gender				
male	87	28	59	0.843
female	33	10	23	
Tumor location				
Ut	19	6	13	0.950#
Mt	56	17	39	
Lt	45	15	30	
Differentiation status				
Well	26	21	5	<0.001
Moderate	63	15	48	
Poor	31	2	29	
Invasion				
T1+T2	47	25	22	<0.001
T3+T4	73	13	60	
Lymph node metastasis				
Absent	69	29	40	0.005
Present	51	9	42	
TNM stage				
I+ II	65	31	34	<0.001
III+ IV	55	7	48	

Lt, lower thoracic esophagus; Mt, middle thoracic esophagus; Ut, upper thoracic esophagus. P value was estimated by Chi-square test, #P value was estimated by Mann-Whitney U test.

threonine kinase that regulates cell growth and proliferation and interacts with several proteins to form two distinct complexes named mTORC1 and mTORC2, distinguished by mTORC1 containing Raptor and mTORC2 containing Rictor. Instructively, Western blotting analysis showed that the expression of Rictor, but not mTOR or Raptor, was reduced in USP39 deficient cells compared to control cells (**Figure 4B**). We further observed that USP39 knockdown reduced the phosphorylation of Akt at its hydrophobic motif (Ser473), while the phosphorylation of S6K1, a downstream target of mTORC1, exhibited little change (**Figure 4B**). These results show that targeting USP39 by RNAi inhibits mTORC2 but not mTORC1 in ESCC cells.

As a spliceosome component, we anticipated that USP39 was likely impacting Rictor expression at the mRNA level. Indeed, evaluation by qRT-PCR showed that knockdown of USP39 significantly reduced the Rictor mRNA expression in ECA109 and KYSE30 cells (**Figure 4C**). Furthermore, we performed IHC of Rictor on human ESCC samples (n = 50) and found that IHC scores for Rictor were significantly correlated with USP39 expression ($p < 0.01$; **Figure 4D**, **Table 3**). Thus, USP39 and Rictor are positively correlated in both ESCC cell lines and tissues. Collectively, these results demonstrated that loss of USP39 led to selective decreases in Rictor expression but did not affect other major components of the mTOR signaling pathway.

USP39 Regulates Rictor Protein Expression Through Pre-mRNA Splicing and Maturation

Since USP39 is involved in the pre-mRNA splicing of certain genes (20, 23), we hypothesized that USP39 also regulates Rictor pre-mRNA splicing. To test this, we designed qRT-PCR primers that would distinguish the levels of unspliced pre-mRNA (intron 4-5) and mature spliced mRNA (exon 4-5 junction) (**Figure 5A**). Using this assay we found that knockdown of USP39 significantly increased the levels of unspliced mRNA transcripts compared with the controls, together with corresponding decreases in spliced mRNA (**Figure 5B**). Calculating the splicing efficiency expressed as the ratio of spliced to unspliced transcripts indicated that targeting USP39 by RNAi reduced the splicing efficiency of Rictor pre-mRNA (**Figure 5C**). In comparison, the splicing of S6K1 was not affected by USP39 knockdown (**Figure 6**).

Additionally, we performed RNA-binding protein immunoprecipitation assays (RIP) against USP39 using extracts prepared from ESCC cell lines. Analysis of the samples by qRT-PCR showed that Rictor pre-mRNA was significantly enriched in USP39 immunoprecipitates compared with IgG controls (**Figure 5D**). These results suggest that USP39 may directly regulate the splicing and maturation of Rictor pre-mRNA in ESCC cells.

DISCUSSION

Previous studies have reported that USP39 contributes to cancer progression and predicts poor prognosis in various human tumor types. Analyses of public datasets together with our cohort of tissues now add ESCC to the list of cancers where USP39 likely contributes to disease progression. Indeed, immunohistochemical analyses showed the upregulation of USP39 in ESCC was positively correlated with tumor differentiation status, invasion, lymph node metastasis and TNM stage. In functional experiments, we demonstrated that the upregulation of USP39 promotes cell proliferation *in vitro*, and knockdown of USP39 suppressed the tumorigenicity of ECA109 cells in a mouse xenograft model. Together these results are consistent with an oncogenic role for USP39 in the development and/or progression of ESCC.

Based on the RNA-seq analysis, we found that downstream activation of the mTOR pathway was dramatically affected by USP39 deficiency. The central element of this pathway is mTOR, a serine/threonine kinase that regulates cell growth and proliferation in response to the availability of growth factors and nutrients (26). However, mTOR exists in two functionally distinct complexes: mTORC1 and mTORC2, which have

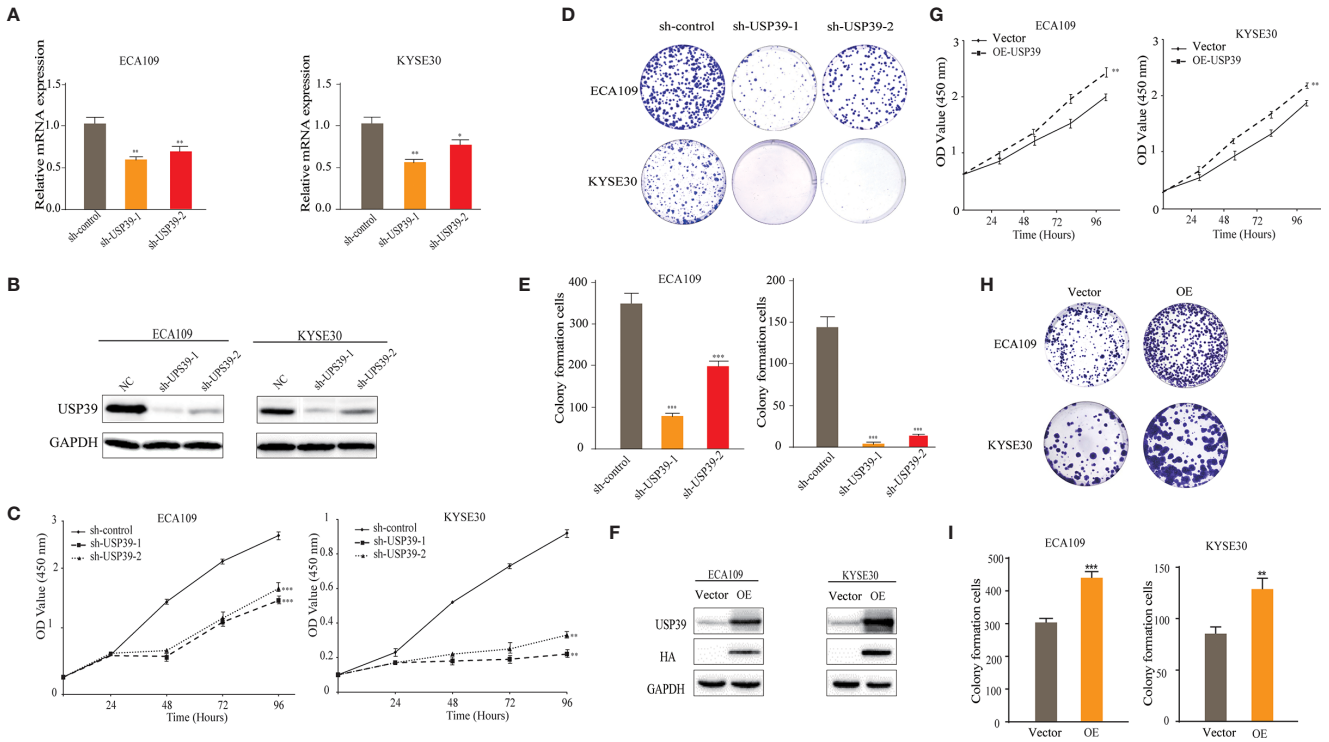


FIGURE 2 | Silencing USP39 expression in ESCC cells inhibits proliferation. **(A, B)** USP39 levels were measured in the ESCC cell lines ECA109 and KYSE30 by qRT-PCR **(A)** and Western blotting **(B)** after stable knockdown with negative control shRNA or two different shRNAs targeting USP39, sh-USP39-1 and sh-USP39-2. **(C–E)** Proliferation of the cells from **(A)** was measured from 0-96 h using CCK-8 assays **(C)** or colony formation assays **(D, E)**. **(F–I)** Proliferation in vector control or USP39 overexpressing cells **(F)** was measured by CCK-8 assays **(G)** or colony formation assays **(H–I)**. The results are shown as mean ± S.D. of three independent experiments. Student's t-test: $^{*}p < 0.05$, $^{**}p < 0.01$, $^{***}p < 0.001$.

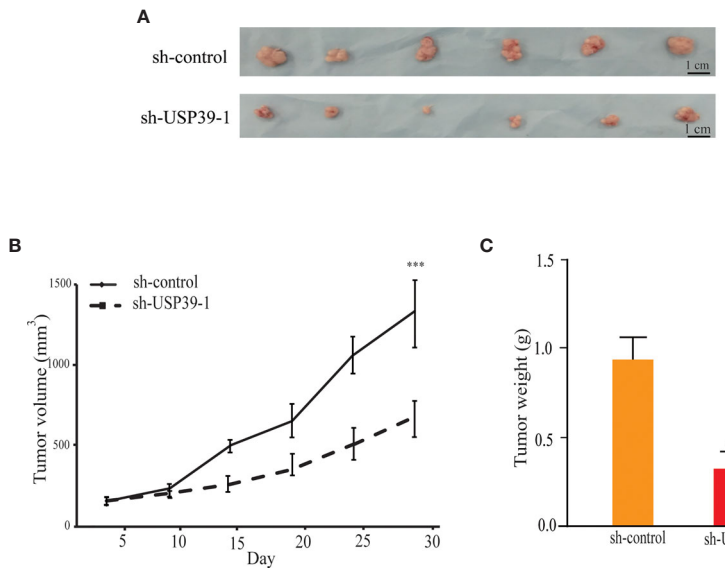


FIGURE 3 | USP39 shRNA knockdown decreases xenograft growth of ESCC cells. **(A)** Representative photographs of tumor xenografts removed from nude mice at 28 days post-injection with ECA109 cells transduced with sh-control or sh-USP39-1. **(B, C)** Caliper-based measurements of tumor size measured at the indicated intervals **(B)** and final tumor weights **(C)**. The results are shown as mean ± S.D. of three independent experiments. Student's t-test: $^{***}p < 0.001$.

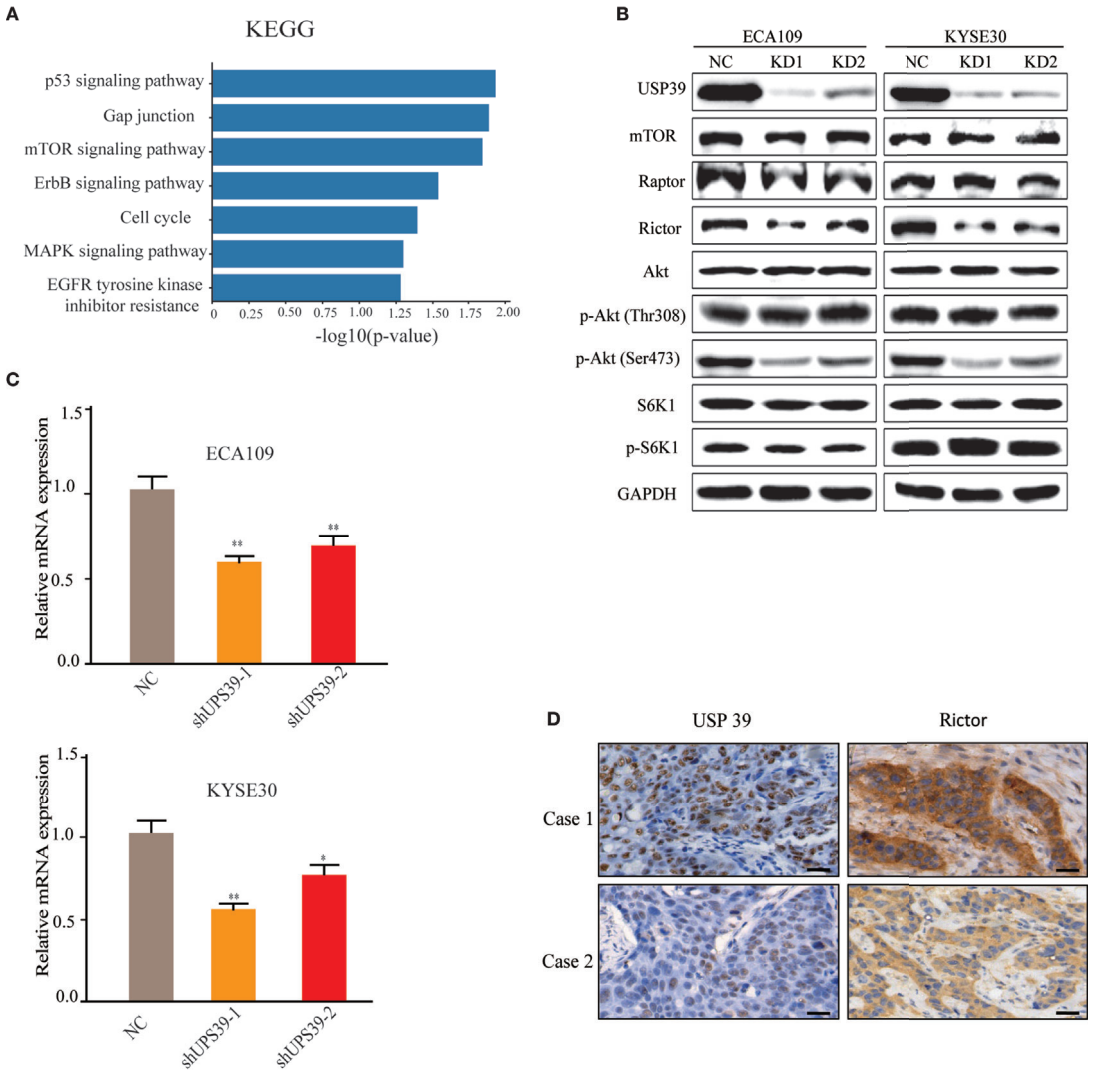


FIGURE 4 | Rictor is downregulated by USP39 silencing. **(A)** RNA-seq analysis conducted on control versus USP39 shRNA-bearing ECA109 cells identified differentially regulated KEGG pathways. **(B)** Western blotting analyses of key components of mTOR signaling pathways in ECA109 and KYSE30 cells stably transduced with sh-control or sh-USP39-1, sh-USP39-2. GAPDH was used as a loading control. **(C)** qRT-PCR analyses of Rictor mRNA levels in ECA109 and KYSE30 cell lines after USP39 knockdown. The results are shown as mean ± S.D. of three independent experiments. Student's t-test: $^{*}p < 0.05$, $^{**}p < 0.01$. **(D)** Representative images of IHC staining of USP39 versus Rictor in high USP39 (Case 1) and low USP39 (Case 2) IRS examples of ESCC tissues.

different functions. The mTORC1 complex is composed of mTOR, mLST8, PRAS40, Deptor and Raptor and enhances cell growth and proliferation through various mechanisms, whereas mTORC2 contains mTOR, mLST8, mSIN1, Deptor, Protor-1 and Rictor (27). In contrast to mTORC1, relatively little is known about the functions of mTORC2 although it has been described that mTORC2 regulates cell survival through Akt activation by S473 phosphorylation (28). Like mTORC1, recent reports also demonstrated that dysregulation of mTORC2 signaling often occurs in a variety of human malignant tumors, rendering it a crucial and validated target in cancer treatment (29–31).

TABLE 3 | Correlation of USP39 and Rictor protein expression in ESCC samples.

		USP39		*P*
		Low	High	
Rictor	Low	11	6	0.005
	High	8	25	

P value was estimated by Chi-square test.

The functions of mTORC1 and mTORC2 are distinguished by their differential activation of downstream effectors, mTORC1-S6K1 and mTORC2-Akt, respectively. We therefore investigated the relationship between USP39 and mTOR signaling through analysis of key mTORC1 and mTORC2

TABLE 4 | The primers for qRT-PCR used in this study.

	forward	reverse
USP39	5'-GGCAGTAAAACTTGAGGGTGT-3'	5'-TTGAAGTCTCACGCCTACATTC-3'
GAPDH	5'-TGACTTCAACAGCGACACCCA-3'	5'-CACCCTGTTGCTGTAGCCAAA-3'
Rictor unspliced mRNA	5'-TTGTGTGGCTTGGAGTGAGT-3'	5'-AGTTTTGCTGCACAGGTTTCA-3'
Rictor spliced mRNA	5'-AACTGGGCTTTCACTATGAGGA-3'	5'-TGGATGAGATATCGAAGCGCT-3'
S6K1 unspliced mRNA	5'-ATGAGGTCACACTGTTGCCC-3'	5'-AATTTTGGGCTGGGTGTGGT-3'
S6K1 spliced mRNA	5'-AAGAAGATGATGTCCGCCAGT-3'	5'-AGATTTCTGTGGAGGGGCAAA-3'
Rictor	5'-GGAAGCCTGTTGATGGTGAT-3'	5'-GGCAGCCTGTTTTATGGTGT-3'

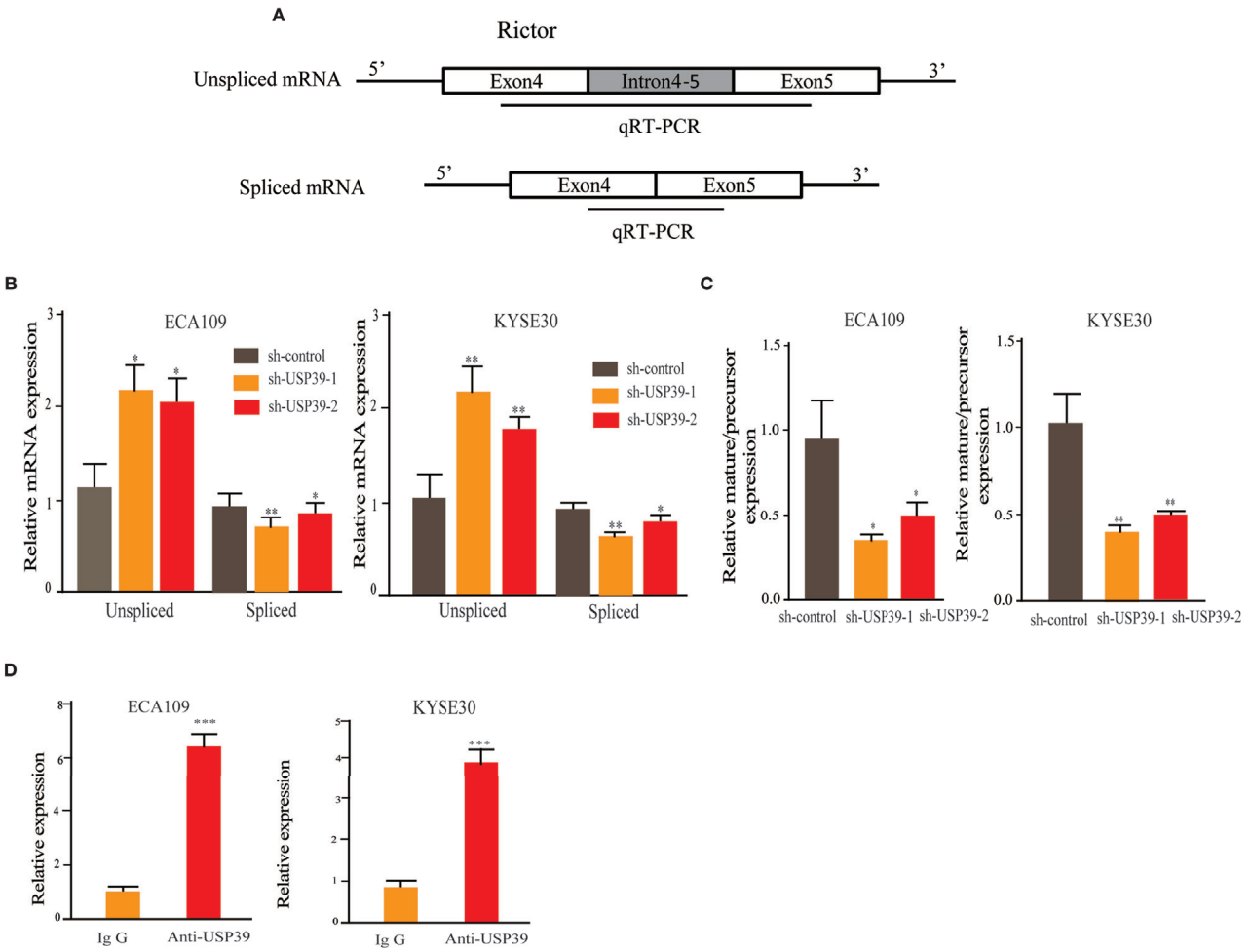


FIGURE 5 | USP39 is involved in Rictor pre-mRNA splicing and maturation. **(A)** Schematic illustrating the qPCR primer pairs used to measure pre-mRNA and mature mRNA species based on the Rictor gene sequence in the Ensembl database. **(B, C)** qRT-PCR analyses showing relative mRNA levels of spliced and unspliced Rictor RNA transcripts in ECA109 and KYSE30 cells with or without USP39 shRNA knockdown **(B)**. Splicing efficiency is expressed as the ratio between mature/pre-mRNA levels **(C)**. GAPDH was used for normalization. **(D)** RNA immunoprecipitations (RIP) performed using antibodies against USP39 or an IgG control. qRT-PCR were used to measure relative Rictor mRNA levels recovered in the immunoprecipitated complex. The results are shown as mean ± S.D. of three independent experiments. Student's t-test: $^{*}p < 0.05$, $^{**}p < 0.01$, $^{***}p < 0.001$.

components. The protein levels of mTOR were unchanged with USP39 knockdown although there was a reduction in Rictor but not Raptor, proposing effects on mTORC2. Indeed, we found a positive correlation between USP39 and Rictor expression in our cohort using IHC. Furthermore, examining the levels and activation of their respective downstream elements, S6K1 and Akt, revealed that USP39 silencing reduced the levels of Ser473 phosphorylated Akt, but not the levels or phosphorylation status of S6K1. Interestingly, it has been previously shown that Rictor contributes to mTORC2-medicated phosphorylation of Akt in

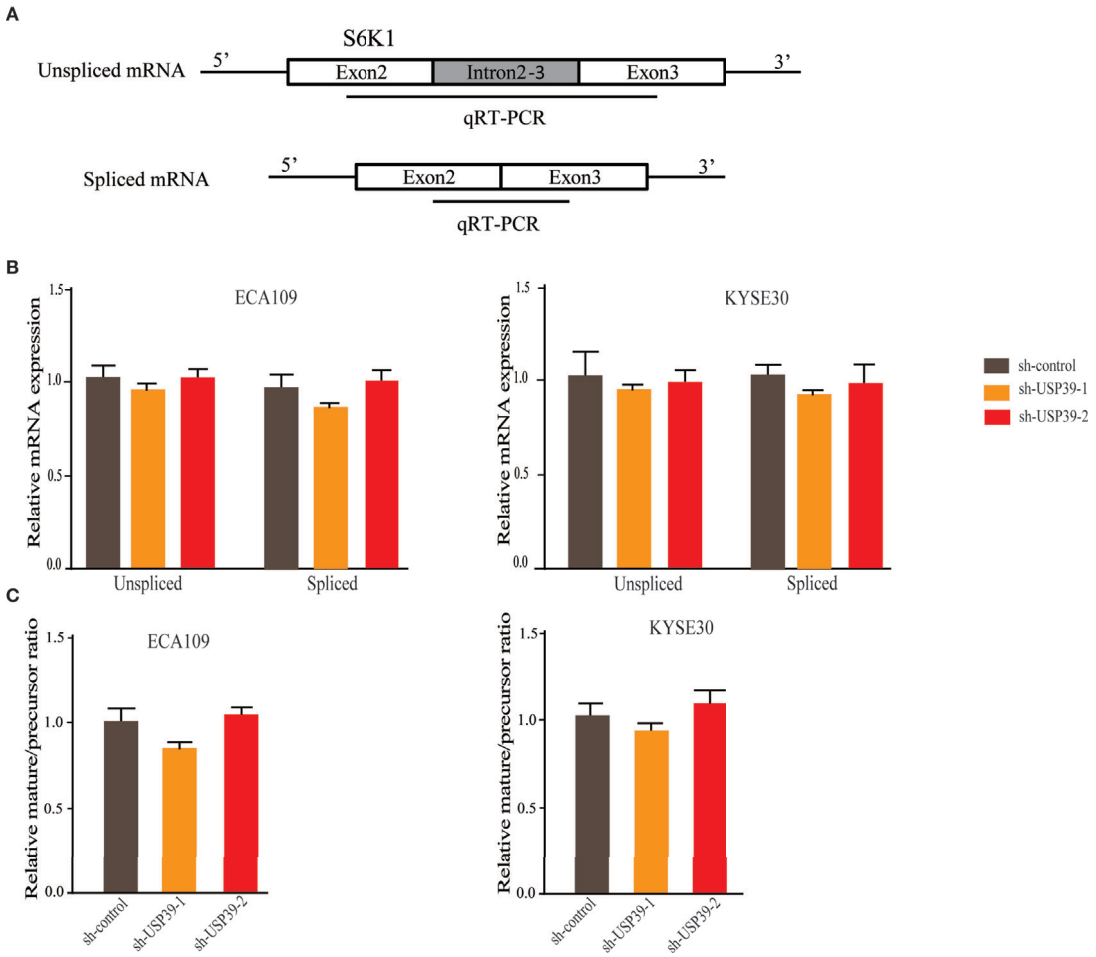


FIGURE 6 | USP39 is not involved in the splicing of S6K1. **(A)** Schematic illustrating the qPCR primer pairs used to measure pre-mRNA and mature mRNA species based on the S6K1 gene sequence in the Ensembl database. **(B, C)** qRT-PCR analyses showing relative mRNA levels of spliced and unspliced S6K1 RNA transcripts in ECA109 and KYSE30 cells with or without USP39 shRNA knockdown **(B)**. Splicing efficiency is expressed as the ratio between mature/pre-mRNA levels **(C)**. GAPDH was used for normalization. The results are shown as mean ± S.D. of three independent experiments. Student's t-test: $p > 0.05$.

ESCC cell lines (32). Moreover, Rictor has recently been shown to be amplified in cancer, and plays an important role in cell proliferation and cell survival (33–36). Here the overexpression of Rictor has also been reported in ESCC where it positively correlated with American Joint Committee on Cancer (AJCC) disease stage and negatively impacted survival (37). Moreover, stable knockdown of Rictor inhibited the proliferation of ESCC cells *in vitro* and *in vivo* (38). Thus, our results propose that Rictor constitutes a key target of USP39 in ESCC where it plays an essential role in regulating mTORC2-mediated signaling to promote tumor cell proliferation.

A fundamental question that remained was how USP39 drives increased Rictor expression. USP39, also known as the 65 kDa SR-related protein from early studies, has been implicated in the function of the spliceosome-complex (12). Although USP39 is a component of the U4/U6-U5 tri-snRNP, it is not necessary for tri-snRNP complex stability. Rather USP39 is necessary for spliceosome maturation and function (12). Because USP39 has been shown to be necessary for pre-mRNA splicing in particular genes including aurora B and Rb1 (14, 15), it was natural to examine for changes in Rictor mRNA splicing. One approach used to determine the splicing rate of pre-mRNA involves comparing pre-mRNA and mature mRNA transcript levels by examining the presence of transcripts containing or lacking intronic sequences (20, 23, 39). Focusing on the intron 4-5/exon 4-5 ratio we found that Rictor pre-mRNA was upregulated following USP39 knockdown, indicating a role for USP39 in the efficient maturation of Rictor mRNA. In support, we found that Rictor pre-mRNA was associated with USP39. Thus, USP39 likely regulates Rictor protein expression through effects on processing of Rictor mRNA (**Figure 7**).

CONCLUSION

In conclusion, we demonstrated that USP39 is commonly upregulated in ESCC, and that it promotes malignant tumor

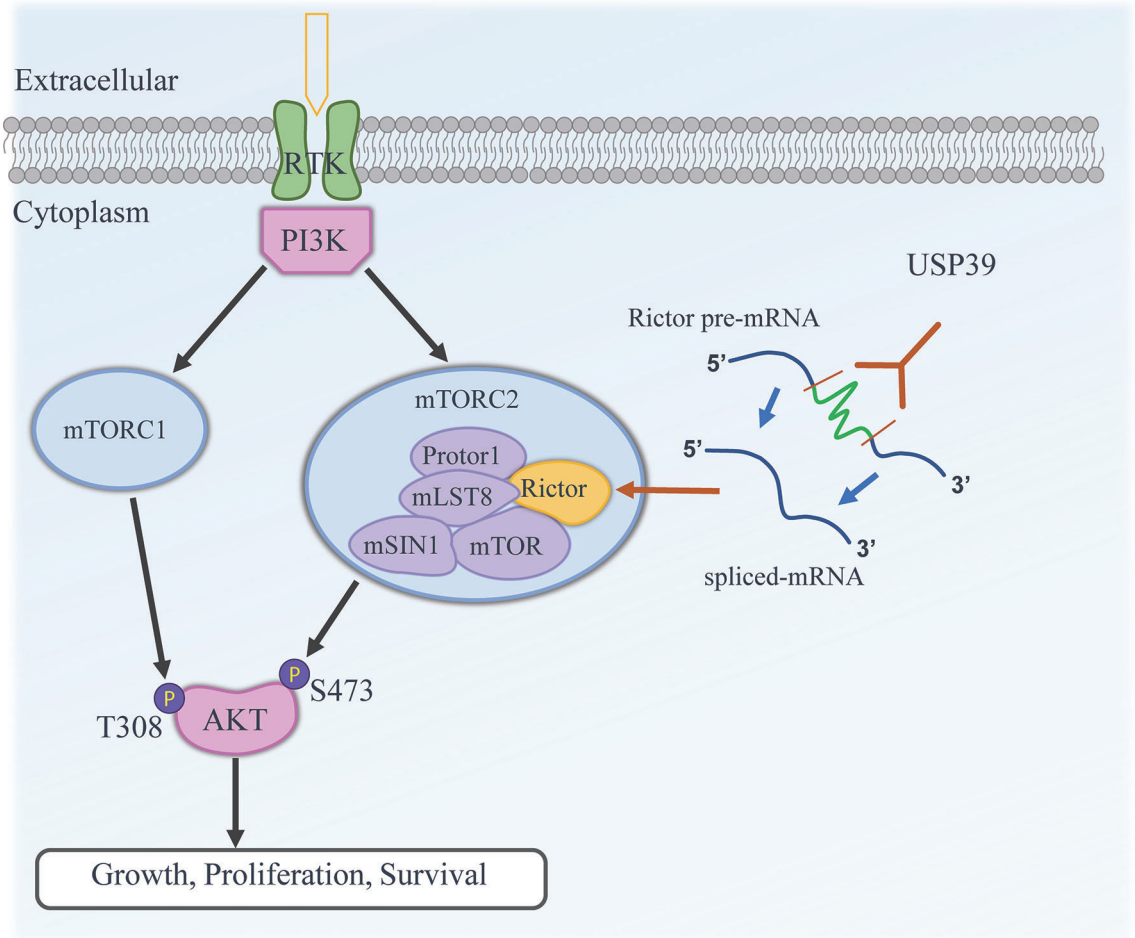


FIGURE 7 | Working model illustrating the functional contribution of USP39 in regulating the activity of mTORC2 by selectively enhancing the splicing and maturation of Rictor mRNA in ESCC.

properties in ESCC both *in vitro* and *in vivo*. Herein, USP39 appears to be an oncogenic driver in the progression of human ESCC. Functionally, we discovered a new role of USP39 in regulating mTORC2 signaling pathway due to its ability to enhance splicing and maturation of Rictor mRNA. Finally, our work provides an important basis for the development of diagnostic and therapeutic approaches in the treatment of ESCC patients by targeting USP39.

DATA AVAILABILITY STATEMENT

The original contributions presented in the study are included in the article/supplementary material, further inquiries can be directed to the corresponding author/s.

ETHICS STATEMENT

The studies involving human participants were reviewed and approved by Anhui Medical University. The patients/participants provided their written informed consent to participate in this study. The animal study was reviewed and approved by Anhui Medical University.

AUTHOR CONTRIBUTIONS

XLiu, YZ and RZ designed the research. YZ, HG, GL, QJ and XC performed the experiments. YZ, HG, GL, XLi and WL analyzed the data. YZ, RZ, XLiu and RT wrote the manuscript. All authors contributed to the article and approved the submitted version.

FUNDING

This work was supported by the National Natural Science Foundation of China [Grant numbers 81772908, 81201368, 31702030], and Anhui Provincial Natural Science Foundation [Grant number 1808085QH271], the Natural Science Foundation of Universities of Anhui Province [Grant number KJ2019ZD22].

REFERENCES

1. Parkin DM, Bray F, Ferlay J, Pisani P. Global Cancer Statistics, 2002. *CA: Cancer J Clin* (2005) 55(2):74–108. doi: 10.3322/canjclin.55.2.74
2. Bray F, Ferlay J, Soerjomataram I, Siegel RL, Torre LA, Jemal A. Global Cancer Statistics 2018: GLOBOCAN Estimates of Incidence and Mortality Worldwide for 36 Cancers in 185 Countries. *CA: Cancer J Clin* (2018) 68 (6):394–424. doi: 10.3322/caac.21492
3. Reichenbach ZW, Murray MG, Saxena R, Farkas D, Karassik EG, Klochkova A, et al. Clinical and Translational Advances in Esophageal Squamous Cell Carcinoma. *Adv Cancer Res* (2019) 144:95–135. doi: 10.1016/bs.acr.2019.05.004
4. Lagergren J, Smyth E, Cunningham D, Lagergren P. Oesophageal Cancer. *Lancet* (2017) 390(10110):2383–96. doi: 10.1016/S0140-6736(17)31462-9
5. Wahl MC, Will CL, Luhrmann R. The Spliceosome: Design Principles of a Dynamic RNP Machine. *Cell* (2009) 136(4):701–18. doi: 10.1016/j.cell.2009.02.009
6. Wang L, Lawrence MS, Wan Y, Stojanov P, Sougnez C, Stevenson K, et al. SF3B1 and Other Novel Cancer Genes in Chronic Lymphocytic Leukemia. *New Engl J Med* (2011) 365(26):2497–506. doi: 10.1056/NEJMoa1109016
7. Rossi D, Bruscaggin A, Spina V, Rasi S, Khiabanian H, Messina M, et al. Mutations of the SF3B1 Splicing Factor in Chronic Lymphocytic Leukemia: Association With Progression and Fludarabine-Refractoriness. *Blood* (2011) 118(26):6904–8. doi: 10.1182/blood-2011-08-373159
8. Yoshida K, Sanada M, Shiraishi Y, Nowak D, Nagata Y, Yamamoto R, et al. Frequent Pathway Mutations of Splicing Machinery in Myelodysplasia. *Nature* (2011) 478(7367):64–9. doi: 10.1038/nature10496
9. Graubert TA, Shen D, Ding L, Okeyo-Owuor T, Lunn CL, Shao J, et al. Recurrent Mutations in the U2AF1 Splicing Factor in Myelodysplastic Syndromes. *Nat Genet* (2012) 44(1):53–7. doi: 10.1038/ng.1031
10. Das S, Krainer AR. Emerging Functions of SRSF1, Splicing Factor and Oncoprotein, in RNA Metabolism and Cancer. *Mol Cancer Res MCR* (2014) 12(9):1195–204. doi: 10.1158/1541-7786.MCR-14-0131
11. Quidville V, Alsafadi S, Goubar A, Commo F, Scott V, Pioche-Durieu C, et al. Targeting the Deregulated Spliceosome Core Machinery in Cancer Cells Triggers mTOR Blockade and Autophagy. *Cancer Res* (2013) 73(7):2247–58. doi: 10.1158/0008-5472.CAN-12-2501
12. Makarova OV, Makarov EM, Luhrmann R. The 65 and 110 kDa SR-related Proteins of the U4/U6.U5 tri-snRNP are Essential for the Assembly of Mature Spliceosomes. *EMBO J* (2001) 20(10):2553–63. doi: 10.1093/emboj/20.10.2553
13. Lygerou Z, Christophides G, Seraphin B. A Novel Genetic Screen for snRNP Assembly Factors in Yeast Identifies a Conserved Protein, Sad1p, Also Required for pre-mRNA Splicing. *Mol Cell Biol* (1999) 19(3):2008–20. doi: 10.1128/MCB.19.3.2008
14. van Leuken RJ, Luna-Vargas MP, Sixma TK, Wolthuis RM, Medema RH. USP39 is Essential for Mitotic Spindle Checkpoint Integrity and Controls mRNA-levels of Aurora B. *Cell Cycle* (2008) 7(17):2710–9. doi: 10.4161/cc.7.17.6553
15. Rios Y, Melmed S, Lin S, Liu NA. Zebrafish USP39 Mutation Leads to Rb1 mRNA Splicing Defect and Pituitary Lineage Expansion. *PloS Genet* (2011) 7 (1):e1001271. doi: 10.1371/journal.pgen.1001271
16. Wang H, Ji X, Liu X, Yao R, Chi J, Liu S, et al. Lentivirus-Mediated Inhibition of USP39 Suppresses the Growth of Breast Cancer Cells In Vitro. *Oncol Rep* (2013) 30(6):2871–7. doi: 10.3892/or.2013.2798
17. Yuan X, Sun X, Shi X, Jiang C, Yu D, Zhang W, et al. USP39 Promotes the Growth of Human Hepatocellular Carcinoma In Vitro and In Vivo. *Oncol Rep* (2015) 34(2):823–32. doi: 10.3892/or.2015.4065
18. An Y, Yang S, Guo K, Ma B, Wang Y. Reduced USP39 Expression Inhibits Malignant Proliferation of Medullary Thyroid Carcinoma In Vitro. *World J Surg Oncol* (2015) 13(1):255. doi: 10.1186/s12957-015-0669-4
19. Lin Z, Xiong L, Lin Q. Ubiquitin-Specific Protease 39 is Overexpressed in Human Lung Cancer and Promotes Tumor Cell Proliferation In Vitro. *Mol Cell Biochem* (2016) 422(1-2):97–107. doi: 10.1007/s11010-016-2809-8
20. Huang Y, Pan XW, Li L, Chen L, Liu X, Lu JL, et al. Overexpression of USP39 Predicts Poor Prognosis and Promotes Tumorigenesis of Prostate Cancer Via Promoting EGFR mRNA Maturation and Transcription Elongation. *Oncotarget* (2016) 7(16):22016–30. doi: 10.18632/oncotarget.7882
21. Li KY, Zhang J, Jiang LC, Zhang B, Xia CP, Xu K, et al. Knockdown of USP39 by Lentivirus-Mediated RNA Interference Suppresses the Growth of Oral Squamous Cell Carcinoma. *Cancer Biomarkers section A Dis Markers* (2016) 16(1):137–44. doi: 10.3233/CBM-150549
22. Xu Y, Zhu MR, Zhang JY, Si GM, Lv JJ. Knockdown of Ubiquitinspecific Peptidase 39 Inhibits the Malignant Progression of Human Renal Cell Carcinoma. *Mol Med Rep* (2018) 17(3):4729–35. doi: 10.3892/mmr.2018.8421
23. Ding K, Ji J, Zhang X, Huang B, Chen A, Zhang D, et al. RNA Splicing Factor USP39 Promotes Glioma Progression by Inducing TAZ mRNA Maturation. *Oncogene* (2019) 38(37):6414–28. doi: 10.1038/s41388-019-0888-1
24. Zhao Y, Zhang B, Lei Y, Sun J, Zhang Y, Yang S, et al. Knockdown of USP39 Induces Cell Cycle Arrest and Apoptosis in Melanoma. *Tumour Biol J Int Soc Oncodevelopment Biol Med* (2016) 37(10):13167–76. doi: 10.1007/s13277-016-5212-x
25. Kanehisa M, Goto S, Kawashima S, Okuno Y, Hattori M. The KEGG Resource for Deciphering the Genome. *Nucleic Acids Res* (2004) 32(Database issue): D277–80. doi: 10.1093/nar/gkh063
26. Kim LC, Cook RS, Chen J. mTORC1 and mTORC2 in Cancer and the Tumor Microenvironment. *Oncogene* (2017) 36(16):2191–201. doi: 10.1038/onc.2016.363
27. Guertin DA, Sabatini DM. Defining the Role of mTOR in Cancer. *Cancer Cell* (2007) 12(1):9–22. doi: 10.1016/j.ccr.2007.05.008
28. Laplante M, Sabatini DM. mTOR Signaling in Growth Control and Disease. *Cell* (2012) 149(2):274–93. doi: 10.1016/j.cell.2012.03.017
29. Hua H, Kong Q, Zhang H, Wang J, Luo T, Jiang Y. Targeting mTOR for Cancer Therapy. *J Hematol Oncol* (2019) 12(1):71. doi: 10.1186/s13045-019-0754-1
30. Zou Z, Chen J, Yang J, Bai X. Targeted Inhibition of Rictor/mTORC2 in Cancer Treatment: A New Era After Rapamycin. *Curr Cancer Drug Targets* (2016) 16(4):288–304. doi: 10.2174/1568009616666151113120830
31. Gkountakos A, Pilotto S, Mafficini A, Vicentini C, Simbolo M, Milella M, et al. Unmasking the Impact of Rictor in Cancer: Novel Insights of mTORC2 Complex. *Carcinogenesis* (2018) 39(8):971–80. doi: 10.1093/carcin/bgy086
32. Hou G, Zhao Q, Zhang M, Fan T, Liu M, Shi X, et al. Down-Regulation of Rictor Enhances Cell Sensitivity to PI3K Inhibitor LY294002 by Blocking mTORC2-medicated Phosphorylation of Akt/PRAS40 in Esophageal Squamous Cell Carcinoma. *Biomed Pharmacother = Biomed Pharmacother* (2018) 106:1348–56. doi: 10.1016/j.biopha.2018.07.075
33. Morrison Joly M, Hicks DJ, Jones B, Sanchez V, Estrada MV, Young C, et al. Rictor/mTORC2 Drives Progression and Therapeutic Resistance of HER2-Amplified Breast Cancers. *Cancer Res* (2016) 76(16):4752–64. doi: 10.1158/0008-5472.CAN-15-3393
34. Roulin D, Cerantola Y, Dormond-Meuwly A, Demartines N, Dormond O. Targeting mTORC2 Inhibits Colon Cancer Cell Proliferation In Vitro and Tumor Formation In Vivo. *Mol Cancer* (2010) 9:57. doi: 10.1186/1476-4598-9-57
35. Masri J, Bernath A, Martin J, Jo OD, Vartanian R, Funk A, et al. mTORC2 Activity is Elevated in Gliomas and Promotes Growth and Cell Motility Via Overexpression of Rictor. *Cancer Res* (2007) 67(24):11712–20. doi: 10.1158/0008-5472.CAN-07-2223
36. Cheng H, Zou Y, Ross JS, Wang K, Liu X, Halmos B, et al. Rictor Amplification Defines a Novel Subset of Patients With Lung Cancer Who may Benefit From Treatment With mTORC1/2 Inhibitors. *Cancer Discovery* (2015) 5(12):1262–70. doi: 10.1158/2159-8290.CD-14-0971
37. Jiang WJ, Feng RX, Liu JT, Fan LL, Wang H, Sun GP. RICTOR Expression in Esophageal Squamous Cell Carcinoma and its Clinical Significance. *Med Oncol* (2017) 34(3):32. doi: 10.1007/s12032-017-0894-5
38. Lu Z, Shi X, Gong F, Li S, Wang Y, Ren Y, et al. RICTOR/mTORC2 Affects Tumorigenesis and Therapeutic Efficacy of mTOR Inhibitors in Esophageal Squamous Cell Carcinoma. *Acta Pharm Sin B* (2020) 10(6):1004–19. doi: 10.1016/j.apsb.2020.01.010
39. Chen J, Crutchley J, Zhang D, Owzar K, Kastan MB. Identification of a DNA Damage-Induced Alternative Splicing Pathway That Regulates p53 and Cellular Senescence Markers. *Cancer Discovery* (2017) 7(7):766–81. doi: 10.1158/2159-8290.CD-16-0908

Conflict of Interest: The authors declare that the research was conducted in the absence of any commercial or financial relationships that could be construed as a potential conflict of interest.

Copyright © 2021 Zhao, Geng, Liu, Ji, Cheng, Li, Liu, Thorne, Zhang and Liu. This is an open-access article distributed under the terms of the Creative Commons Attribution License (CC BY). The use, distribution or reproduction in other forums is permitted, provided the original author(s) and the copyright owner(s) are credited and that the original publication in this journal is cited, in accordance with accepted academic practice. No use, distribution or reproduction is permitted which does not comply with these terms.

frontiers in Cell and Developmental Biology

REVIEW
published: 03 June 2021
doi: 10.3389/fcell.2021.669756

Conditional Cell Reprogramming in Modeling Digestive System Diseases

Ruihua Zhao[1†], Rui Li[1,2†], Tianqi An[1] and Xuefeng Liu[3,4,5,6]*

[1] Department of Oncology, The First Affiliated Hospital of Zhengzhou University, Zhengzhou, China, [2] Department of Oncology, Tongji Hospital, Huazhong University of Science and Technology, Wuhan, China, [3] Department of Pathology, Center for Cell Reprogramming, Georgetown University Medical Center, Washington, DC, United States, [4] Department of Oncology, Lombardi Comprehensive Cancer Center, Georgetown University Medical Center, Washington, DC, United States, [5] Departments of Pathology and Urology, The Ohio State University School of Medicine, Columbus, OH, United States, [6] James Comprehensive Cancer Center, The Ohio State University, Columbus, OH, United States

Digestive diseases have become an important source of morbidity and mortality. The considerable financial and health burdens caused by digestive diseases confirm the importance of extensive research to better understand and treat these diseases. The development of reliable preclinical models is essential for understanding the pathogenesis of digestive diseases and developing treatment and prevention methods. However, traditional established cell lines and animal models still have many limitations in the study of the digestive system. Conditional reprogramming (CR) cell culture is a newly developed primary technology that uses irradiated Swiss-3T3-J2 mouse fibroblast cells and the Rho-associated kinase (ROCK) inhibitor Y-27632 to rapidly and efficiently generate many cells from diseased and normal tissues. CR cells (CRCs) can be reprogrammed to maintain a highly proliferative state and recapitulate the histological and genomic features of the original tissue. Moreover, after removing these conditions, the phenotype was completely reversible. Therefore, CR technology may represent an ideal model to study digestive system diseases, to test drug sensitivity, to perform gene profile analysis, and to undertake xenograft research and regenerative medicine. Indeed, together with organoid cultures, CR technology has been recognized as one of the key new technologies by NIH precision oncology and also used for NCI human cancer model initiatives (HCMI) program with ATCC. In this article, we review studies that use CR technology to conduct research on diseases of the digestive system.

Keywords: conditional cell reprogramming, digestive system diseases, cell model, CR technology, cell culture technology

OPEN ACCESS

Edited by:
Ira Ida Skvortsova,
Innsbruck Medical University, Austria

Reviewed by:
Komal S. Rathi,
Children's Hospital of Philadelphia, United States
Kyoung-Ho Pyo,
Yonsei University, South Korea

****Correspondence:***
Xuefeng Liu
xuefeng.liu@georgetown.edu

[†] These authors have contributed equally to this work

Specialty section:
This article was submitted to Molecular and Cellular Oncology, a section of the journal Frontiers in Cell and Developmental Biology

Received: *19 February 2021*
Accepted: *27 April 2021*
Published: *03 June 2021*

Citation:
Zhao R, Li R, An T and Liu X (2021) Conditional Cell Reprogramming in Modeling Digestive System Diseases. Front. Cell Dev. Biol. 9:669756. doi: 10.3389/fcell.2021.669756

INTRODUCTION

The digestive system involves the gastrointestinal tract, including the oral cavity, pharynx, esophagus, stomach, small and large intestines, as well as auxiliary organs, namely, the liver, gallbladder, and pancreas. The digestive system is a continuous anatomical structure that can swallow, digest, absorb food nutrients, and expel the remaining waste. It also mediates interactions between the host and resident bacteria (Matuchansky and Beauchant, 1982). Digestive system diseases (including infections, inflammation, and cancers) have become important sources of morbidity and mortality. Globally, the burden of digestive system diseases is increasing annually

(GBD 2017 Pancreatic Cancer Collaborators, 2019; GBD 2017 Inflammatory Bowel Disease Collaborators, 2020; GBD 2017 Oesophageal Cancer Collaborators, 2020). Colorectal and stomach cancers are the third and fourth most common malignancies worldwide, each accounting for approximately 800,000 victims per year (Siegel and Miller, 2020). Other common benign digestive system diseases, such as acute and chronic gastroenteritis caused by bacteria or other pathogens, inflammatory bowel disease (IBD), and functional gastrointestinal disorders, not only cause pain, disability and even death but also carry an enormous financial burden to both families and society. Indeed, the direct costs for care of patients with IBD singly were estimated to be €4.6–5.6 billion annually in Europe, and the incidence of IBD is still increasing steadily in Western countries (Burisch et al., 2013). The enormous financial and health burdens resulting from digestive system diseases confirm the importance of great research efforts to better understand and treat these diseases.

Developing reliable preclinical models that can accurately recapitulate the complex physiology and pathophysiology of different digestive system organs is essential to understand the developmental processes and mechanisms of diverse disorders of the digestive system organs, such as infection, inflammation, and cancer, to develop drug therapy. Conventionally, traditional established cell lines cultured in 2-dimensional (2D) or animal models have been widely used as digestive system models. Although these models have significantly contributed to the development of digestive system research, they still have many limitations. Only 1–10% of cell lines (depending on the source tissue and disease progression status) can be successfully established to be transformed immortalized or cancerous cell lines, and most primary cells, especially normal cells, are hard to culture because of their limited life span (Giard et al., 1973). More importantly, after being artificially cultured on glass or plastic plates with undefined medium for the long term, the genes of the established cell lines have undergone tremendous changes, making it impossible to recapitulate the complex characteristics of the primary tissue. Therefore, the results obtained in 2D cultures may not represent the true host response (Gillet et al., 2013). Animal models, especially recently emerged engineered mouse models and primary patient-derived xenografts (PDXs), may overcome the limitations of cell lines and better mimic human disease and treatment response (Ito et al., 2018). However, the application of animal models might be limited by high costs, low throughput, and technical challenges; more importantly, differences in specific species cause inaccurate recapitulation of biological and therapeutic responses. Recently, *in vitro* three-dimensional (3D) organoid culture techniques for various cell types, such as induced pluripotent stem cells (iPSCs), pluripotent embryonic stem (ES) cells, and immortalized cell lines, have been successfully developed (Kretzschmar and Clevers, 2016; Sato et al., 2009). Three-dimensional organoid models contain multicellular organ structures, which are thought to closely mimic complex original structures and functions. They can also be maintained for a long time and are easily manipulated (Clevers, 2016). Digestive system organoids have been established using cells from the stomach, small intestine, colon, and other organs (Pan et al., 2018). Organoids have advantages in understanding the mechanisms and biological processes of digestive diseases (such as cancer, infectious disease, and IBD), thereby helping to promote the development of personalized and regenerative medicine. However, they are not suitable for high-throughput screening because in general, 28–42 days are needed to grow enough cells (Xinaris, 2019). There is still an urgent need for a single model of the digestive system that is fast, easy to execute, and easily successful.

Recently, Liu et al. (2017) developed a new primary cell culture technology, called conditional reprogramming (CR), using irradiated Swiss-3T3-J2 mouse fibroblast cells and Y-27632, a Rho-associated kinase (ROCK) inhibitor, to rapidly and efficiently generate indefinite epithelial cells (**Figure 1**). Cells processed by this method are called conditionally reprogrammed cells (CRCs). The CR method can rapidly and efficiently generate large numbers of primary epithelial cells from different tissues, such as fresh or cryopreserved surgical specimens, fine-needle aspiration (FNA), core biopsies, and PDX tissues (Palechor-Ceron et al., 2019). CRCs can be reprogrammed to maintain a highly proliferative state, known as "reprogrammed stem-like" (Suprynowicz et al., 2012), and recapitulate the histological characteristics and genomic characteristics of the original tissue (Alamri et al., 2016). Moreover, after removing these conditions, the phenotype is completely reversible (Liu et al., 2012, 2020). Therefore, CR technology might be an ideal model to study digestive system diseases, to test drug sensitivity, to perform gene profile analysis, and in xenograft research and regenerative medicine. In this article, we review studies that use CR technology for digestive system disease research (**Table 1**).

DEVELOPMENT OF CR TECHNOLOGY

The *in vitro* life spans of primary cells, including normal human epithelial cells and human embryonic stem cells (hESCs), are very short, which is an obstacle to research (Reubinoff et al., 2000). Different efforts have been made to optimize the cultivation of primary cells. Initially, H Green developed a keratinocyte/feeder coculture system. By using lethally irradiated feeder cells at the correct density, keratinocytes can be continuously propagated (Rheinwald and Green, 1975). The method was further developed by adding an epidermal growth factor (Stanley and Dahlenburg, 1984). Y-27632 was initially proven to significantly improve the cloning efficiency of human embryonic stem (ES) cells (Watanabe et al., 2007), and a study found that using Y-27632 during primary culture can effectively prepare large numbers of human epithelial stem cells from various primitive epithelial tissues (Terunuma et al., 2010). Sandra et al. also reported that treatment of primary keratinocytes with Y-27632 can greatly improve the proliferation and immortality of these cells (Chapman et al., 2010; Liu et al., 2012). More importantly, immortalized cells showed typical characteristics of primary keratinocytes. Later, Liu and colleagues proved that the combination of Y-27632 and fibroblast cells, called CR technology, can induce indefinite proliferation of many epithelial and nonkeratinocyte normal cells and tumor cells *in vivo* (Liu et al., 2012, 2017; Tricoli et al., 2018). The

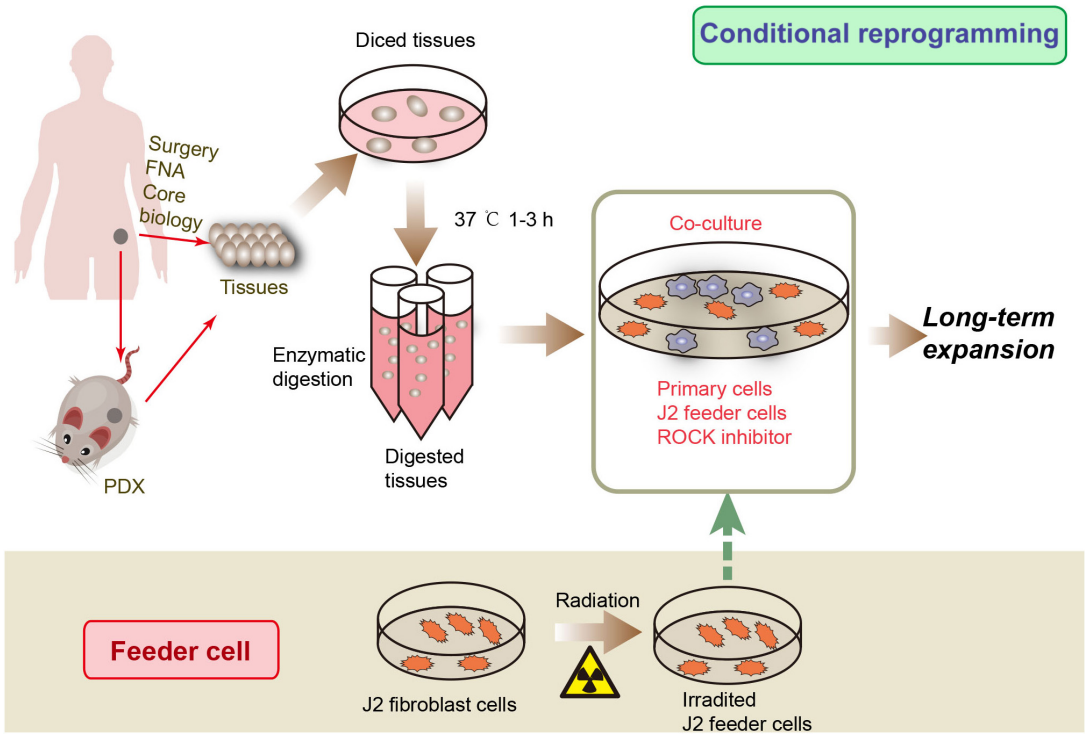


FIGURE 1 | CRC development processes. Tissue samples can be obtained from surgical core biopsies, fine-needle aspiration (FNA) or patient-derived xenograft (PDX). The tissue is then cut into small pieces and digested to produce primary cells. Then the primary cells were co-cultured with irradiated J2 feeder cells and ROCK inhibitor to obtain CR cells.

CR method has been shown to be rapid and efficient in the establishment of cell cultures capable of unlimited growth from normal and cancer tissues. Most importantly, CRCs maintain the developmental potential of the original tissue and can restore the differentiation ability of the cells after these conditions are removed. Additionally, the CR method can rapidly generate cultures from small biopsy specimens and cryopreserved tissue. Recently, the technology has been modified and can be used to cultivate cells from the skin, prostate, lung, breast, kidney, and even neuroendocrine and endocrine tissues (Gao et al., 2017; Liu et al., 2017; Palechor-Ceron et al., 2019; Timofeeva et al., 2017; Urbaniak et al., 2019). Therefore, the CR method has potential applications in basic research and diagnosis, treatment, and regenerative medicine.

APPLICATION IN DIGESTIVE DISEASES RESEARCH

Modeling Diseases

CRCs have been established quickly and efficiently from a variety of human normal and tumor specimens, including the colon. There is no need to use exogenous viruses or genetic manipulation. CRCs can maintain the characteristics of their primary tissues. After removing these conditions, the differentiation ability of the cells can be restored, and they can be grown in 2D and 3D systems, making CR an ideal *in vitro* model of digestive diseases. Emily C et al. applied CR technology to establish a 2D monolayer model of mouse intestinal epithelial cells (IEC monolayers) from both wild-type and genetic mouse models. IEC monolayers can form epithelial colonies and maintain their genetic characteristics during the long passage process. They can also form 3D spheres in medium, including Matrigel (Moorefield et al., 2018). This study indicates that CR technology could be used to culture numerous genotype-specific mouse small intestinal epithelial cells for further functional studies. Recently, using CR technology, Su et al. successfully isolated human primary hepatocytes from fresh liver tissues of patients of different ages and with different hepatic diseases. They achieved a high success rate in the long-term culture of primary hepatocytes *in vitro* with various hepatic diseases (Su et al., 2019b). They also established a primary human hepatocyte culture with liver function from patients with ornithine transcarbamylase deficiency (Su et al., 2019a). Therefore, the study showed that the use of CR technology in patient-derived hepatic cell culture can be a valuable and viable model for studying mechanisms related to hepatic diseases. Using CR technology, a group of well-differentiated porcine pancreatic ductal epithelial cells with bicarbonate secretion capacity have been established, which will improve our knowledge of pancreatic physiology and bicarbonate secretion mechanisms (O'Malley et al., 2018). For the establishment of preclinical cancer models, it is essential to obtain enough tumor tissues. However, tissue samples can only be obtained from many advanced cancer

TABLE 1 | Comparison of the model systems for digestive system diseases.

	Conventional cell lines	Primary cells	PDX model	3D organoid	CRC
Sample origin					
FNA	No	No	No	No∼+	+++
Core biopsy	No	No∼+	-	+	+++
Surgical specimens	+	++	++	+++	+++
Cryopreserved tissue	No∼+	+∼++	No∼+	+++	+++
Cancerous tissue	+++	++	++	+++	+++
Noncancerous tissue	No	No∼+	No	+	+
Timing	Several days	1∼4 weeks	1∼5 months	1∼4 weeks	1–10 days
Success rate	+	++	++	+++	+++
Rapid expansion	+++	++	+	++	+++
Genetic stability	+	++	++	++	++
Cost	+	++	+++	++	+
HT screening	+++	+	No	++	+++
Representation of primary tissue	+	++	++	++	++
Life span	+++	+	+	++	+++
Difficulty of differentiation	+++	+	+++	+	+
biobanking	No	+	++	+++	+++
Tissue-specific	+	+++	+++	+++	+++
Genetic manipulation	+++	No∼+	No	++	++
Tumor–stroma interaction	No	No	++	+	No

This table was adapted and modified from Liu and Mondal (2020).

patients through fine-needle or core needle biopsy. Research by Lee et al. (2019, 2021) showed that CR technology can be used to establish pancreatic cancer cell lines through biopsies guided by endoscopic ultrasound. CRCs from pancreatic cancer tissues have the same genetic characteristics as those from the primary tumor and can be used for genomic research and drug sensitivity studies and can identify new diagnostic and therapeutic targets for pancreatic cancer (Lee et al., 2019, 2021). The PDX model has become an important tool for translational research, but there are some limitations, including unsustainable *in vitro* growth. Researchers used CR technology to successfully generate and amplify stable cell lines from PDX tumors of human bladder, lung, and ovaries without compromising the basic biological characteristics of the model (Borodovsky et al., 2017). Therefore, CR technology can be used for *in vitro* amplification of PDX cells for subsequent studies. CR cells can be produced from organoid and xenograft tissues and can also form CR cell-derived xenograft (CDX) tumors and be cultured in spheres or organoids (Timofeeva et al., 2017; Moorefield et al., 2018; Mondal et al., 2019; Palechor-Ceron et al., 2019), demonstrating that these three platforms can work together to provide platforms for digestive system disease study.

Precision Medicine and Drug Discovery

Precision medicine is a newly developed method for the treatment and prevention of diseases based on the patients' biological information and their clinical signs and symptoms (Collins and Varmus, 2015). Recently, in oncology, the treatment and classification of cancer have changed due to genetic testing. Targeted therapy is a treatment method that uses drugs to target specific genes and proteins related to the survival and growth of cancer cells, and this is the foundation of precision medicine. Targeted therapy is a rapidly developing field of cancer research. Researchers are studying many new targets and drugs through basic and clinical research (Baudino, 2015). Although the outcomes of certain cancer patients, including patients with lung and breast cancers, have been greatly improved due to targeted therapies (Gu et al., 2016; Hirsch et al., 2017), the results of evaluating new targeted drugs in digestive system cancer clinical trials are usually frustrating. In the past 20 years, targeted therapy for gastrointestinal cancer has made little progress (Narita and Muro, 2017; Aslan et al., 2018; DeLeon et al., 2018; Dzunic et al., 2019). A particular limitation in identifying new and effective targets and drugs for digestive system cancers is that the results are only based on studies in long-term cultured cell lines or xenograft models (Garnett et al., 2012); thus, the results of most clinical trials are usually disappointing. Currently, the use of patient-derived models with the advantages of stable genotype, high-throughput screening, immortality, and xenotransplantation is urgently needed for target discovery and drug screening. CR technology can be used in primary cell cultures from normal and tumor tissues of different species and to maintain the phenotypic and genotypic characteristics and intratumoural heterogeneity of the primary tissues. CR cells can also be cultured in PDX models and 3D conditions. Therefore, CR technology provides a new platform for evaluating the effectiveness and toxicity of new drugs and developing individualized treatment plans in digestive system diseases. Recently, Alamri et al. used CR technology to cultivate CRCs from primary tissue of low-grade mucoepidermoid carcinoma (MEC) and used them to detect candidate therapeutic pathways. They demonstrated that the amphiregulin-mechanistic target of rapamycin-protein kinase B (AKT; AKT1) pathway was activated in MECs and that the growth of MECs could be inhibited

by MK2206 (allosteric AKT inhibitor) in 2D and 3D cultures (Alamri et al., 2018). The CR technique was used for the first time to determine the important role of the MYC-ERCC3 interaction in pancreatic ductal adenocarcinoma (PDAC), and triptolide (a covalent ERCC3 inhibitor) was found to be a potential treatment target in MYC-dependent PDAC (Beglyarova et al., 2016). Another group used PDAC cell lines and CR-cultured primary cells to identify the role of the low-immunogenicity anti-mesothelin immunotoxin RG7787 in pancreatic cancer (Hollevoet et al., 2014). Wang et al. established a novel individualized CR system (termed i-CR) from colorectal cancer tissues. By high-throughput i-CR drug screening, they discovered that inhibition of the EGFR and MEK or CDK4/6 pathways exerted a synergistic inhibitory effect against colorectal cancer and supersynergistic effects when EGFR, MEK, and CDK4/6 inhibitors were used simultaneously. Their study showed that the novel i-CR system combined with PDX models will enable individualization of therapy and drug discovery (Wang et al., 2020). Using CRCs from colorectal cancer patients, Kim et al. (2018) found that ATP6V0C encoding lysosomal V-ATPase V0 subunit C and IDF-11774 (a new clinical drug candidate for the treatment of colorectal cancer) are synthetically lethal and that this effect was associated with the expression of B-cell CLL/lymphoma 2 (Bcl-2) and PIK3CA mutations. Adenoid cystic carcinoma (ACC) is a rare salivary adenocarcinoma and has a high rate of metastasis. Currently, we still do not have a research model suitable for this disease (Bradley, 2017). Chen et al. (2017) successfully cultured ACC cells from two separate ACC PDX tumors using modified CR medium conditions (which can maintain the characteristic MYB translocation). They also developed a method to rapidly verify the ability of cultured CR cells to metastasize *in vivo* using zebrafish. Using the CR/zebrafish model, they identified regorafenib as a potential drug for this cancer. In another study using CR technology, Panaccione et al. (2016) found that ACC features previously unidentified CD133+ cells with neural stem characteristics. These cells were driven by FABP7, NOTCH1, and SOX10 expression. They also found that these cells were sensitive to Notch inhibition, which may provide a new target for the treatment of ACC. In addition, some groups have used patient-derived CRCs from other cancers for comprehensive drug testing (Saeed et al., 2017; Kettunen et al., 2019). A recently published article explored the clinical feasibility of using CRC to guide chemotherapy for patients with colorectal cancer. They generated CRC cells and paired them with a PDX mouse model of primary colorectal tumor cells to establish the correlation between drug sensitivity *in vitro* and the patient's clinical response. They showed that the use of CRC screening chemical drug screening is comparable to the PDX model. More importantly, it was shown to be highly consistent with the clinical results of the enrolled colorectal cancer patients (Li et al., 2021). Therefore, we believe that this technology will be used for high-throughput drug screening of digestive system diseases, especially digestive system tumors. Su et al. (2019a) established CRCs from fresh human liver tissues and determined that the cells still reserve 1A1, 2C9, and CYP3A4 activities. CYPs are essential for drug metabolic enzymes in the human body. Therefore, CRCs from primary normal cells might be used as a model for evaluating drug toxicity and metabolism.

Regenerative Medicine

Regenerative medicine is a science and technology that uses biological and engineering methods to create lost or functionally damaged tissues and organs to establish their normal function. The field mainly includes cell therapy, immunomodulatory therapy (separate administration or secretion by injection of cells and regeneration of bioactive molecules), and tissue engineering (transplantation of organs and tissues grown in the laboratory). This technology provides new treatments for patients suffering from clinical problems such as end-stage organ failure and serious injuries (Atala, 2012). In recent years, stem cells, including adult stem cells (ASCs), induced pluripotent stem cells (iPSCs), and embryonic stem cells (ESCs), have been studied intensely to explore their value in regenerative medicine (Riazi et al., 2009). However, there is some difficulty in efficiently inducing the functional differentiation of stem cells. CR technology can generate cells from very few donor tissues and can rapidly expand them *in vitro* in large quantities; more importantly, the cells can be well differentiated into the native cell type after CR conditions are eliminated. Therefore, CR technology has application potential in the field of regenerative medicine. Using CR-cultured cells for tissue engineering and regenerative medicine has aroused great interest among scientists. Cells can be cultured using CR technology and engineered methodologies, particularly 3D scaffold materials, to generate tissues that exquisitely recapitulate their original structures and functions. Another method of using CR technology for regeneration is to promote their maturation into functional tissues and then implant them in the host. Hamilton et al. implanted a combination of airway epithelial CR cells and a fibroblast-containing graft in a rabbit model of revascularization, featuring decellularized tracheal stents and implanted structures with the function of revascularization. They found keratin-positive cells throughout the scaffold (Hamilton et al., 2019). Their research showed that CR cells can improve the repair of host epithelium and/or directly promote mucosal regeneration, which can be used in regenerative medicine. One study showed that CR technology can indefinitely expand normal oesophageal epithelial cells from endoscopic biopsy samples of pediatric patients (Jensen et al., 2017). Therefore, the cells can be combined with synthetic or natural scaffolds to provide treatment options for patients with defects, trauma, or diseases. Having a large number of cells will help to construct a fully regenerated oesophageal epithelial cell cavity to help promote the regeneration of the remaining cell types. Therefore, rapid amplification of patient-derived cells with stable genetic characteristics based on CR technology will meet the unmet needs of tissue engineering for personalized regenerative medicine in digestive system disease. Further research in these subfields may lead to the development of treatment options to use different types of CR cells in regenerative medicine for human digestive system diseases.

TABLE 2 | Applications of CR technology in digestive system diseases.

Origination	Tissue	Cells	Application	References
			Cell model	
Genetic mouse model	Intestinal	Normal intestinal epithelium	Genotype-specific mouse intestinal epithelial cells	Moorefield et al., 2018
Human	Liver	Hepatocytes	Hepatic cells from different liver diseases: OTCD; Citrullinemia type 1 disease; Cirrhosis; Hepatitis C virus-induced liver failure; Maple syrup urine disease	Su et al., 2019a,b
Sus scrofa	Pancreas	Pancreatic ductular epithelium cell	Pancreatic ductular epithelial cells	O'Malley et al., 2018
Human	Pancreas	Pancreatic cancer cell	Pancreatic cancer cells obtained by EUS-FNB.	Lee et al., 2019
			Precision medicine and drug discovery	
Human	Pancreas	Pancreatic ductal adenocarcinoma cell	Determine the important role of the MYC-ERCC3 interaction in PDAC, found triptolide may be a potential target treatment for MYC-dependent PDAC	Beglyarova et al., 2016
Human	Pancreas	Pancreatic ductal adenocarcinoma cell	Identify the role of the low immunogenicity anti-mesothelin immunotoxin RG7787 in pancreatic cancer	Hollevoet et al., 2014
Human	Salivary gland	Salivary gland neoplasms	Demonstrated AKT; the AKT1 pathway was activated in MEC, and the growth of MEC cells can be inhibited by MK2206	Alamri et al., 2018
Human	Large intestine	Colorectal cancer	Identify synergistic effects of EGFR, MEK, and CDK4/6 inhibitors in the colorectal cancer	Wang et al., 2020
Human	Large intestine	Colorectal cancer	Identified that ATP6V0C and IDF-11774 were synthetically lethal and this effect was associated with low Bcl-2 expression and PIK3CA mutations	Kim et al., 2018
Human	Large intestine	Colorectal cancer	For rapid screening of individualized chemotherapy for colorectal cancer patients	Wang et al., 2020
Human	Salivary gland	Adenoid cystic carcinoma	Identified regorafenib as a potential therapeutic drug	Chen et al., 2017
Human	Salivary gland	Adenoid cystic carcinoma	Characterized the majority population of CD133+ cells in ACC and found these cells were sensitive to Notch inhibition	Panaccione et al., 2016
			Regenerative medicine	
Human	Oesophageal	Oesophageal epithelial cells	Might help to engineer an oesophageal construct with a completely reseeded oesophageal epithelial cell lumen	Riazi et al., 2009

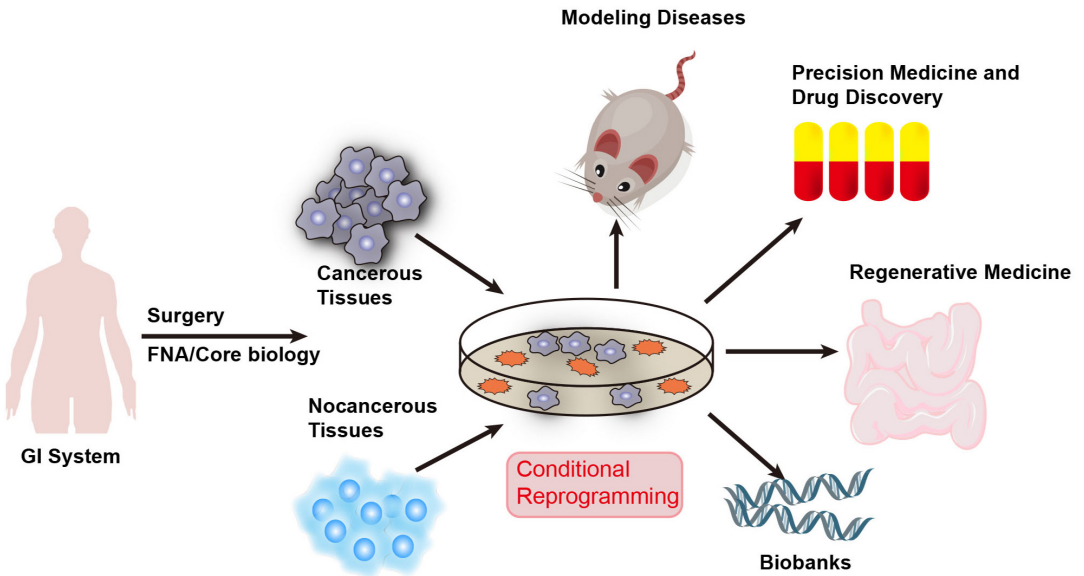


FIGURE 2 | Applications of CR technology in human digestive system diseases. CR technology can quickly generate cultures from fresh and cryopreserved normal and diseased human tissue samples obtained through surgery, core biopsy, and fine-needle aspiration (FNA). Therefore, CR technology can be used as an ideal *in vitro* model for digestive system diseases and facilitate precision medicine and drug discovery. It will also aid in tissue engineering for personalized regenerative medicine and provides an exciting opportunity to build a living biobank for digestive system disease.

OTHERS

Biobanks play vital roles in innovative clinical medicine and translational biomedical research. The latest scientific advances in cryopreservation have made it possible to establish living biobanks, which enable long-term collection and storage of viable functional tissues and proliferating cell types (Li et al., 2020). The ability to quickly and efficiently build a stable CRC from normal and diseased tissue provides an exciting opportunity to build a living biobank (Liu et al., 2012; Coppola et al., 2019). Our team proposed establishing the Next Generation Living Biobank (NGLB), which collects and stores tissues from surgery, core needle or fine-needle biopsy, and cells from scrub or liquid, such as urine and blood. Corresponding omics (e.g., genomics, transcriptomics, proteomics, metabolomics) and clinical information should be gathered together. At the same time, CR technology is being used to grow large numbers of cells to meet the needs of disease modeling, drug discovery, and regenerative medicine in the future (Palechor-Ceron et al., 2019). Compared with traditional living biobanks, NGLB enables us to use CR technology to generate cells in rare diseases for which cell lines or cell models are not currently available (**Table 2**).

Limitations of CR Technology

The results of CR technology studies have proven that it may play an important role in digestive system disease. However, some limitations need improvement. The CR method cannot lack stromal components such as matrix, vascular immune, or endothelial cells. Therefore, we were unable to analyze the effect of stromal cells on tumor cell growth and their response to therapeutic agents (Liu et al., 2017). However, CR technology can be cultured in 3D organoids, and there are already several models that combine 3D organoid systems and stromal cells. In the future, it is necessary to establish models that integrate multiple stromal cell types into the 3D culture system with CR technology to check direct epithelial/matrix interactions (Liu et al., 2017). Another limitation is the inability to distinguish tumors from normal epithelial cells because the CR method allows normal and tumor epithelial cells to grow outward. Normal cells sometimes replicate more than tumor cells, so normal cells eventually surpass culture. However, the standard CR method has some modifications and may be a selective expansion of tumor cells *in vitro* (Wang et al., 2020). Despite these limitations, CR technology still has very good application prospects in digestive system diseases. There is no a single perfect model for biomedical research including *in vitro* or *ex vivo* cell cultures and *in vivo* animal assays since every method or system have its own unique properties, advantages and limitations/disadvantages. One chooses a model which is appropriate for his/her specific question. In many cases, scientists or researchers must choose combination of the technologies at variety of levels from molecules, cells, organs, to individual or population for their research purpose. For example, combination of CRC (2D), organoids (3D) and PDX (*in vivo*) is highly recommended from NCI (National Cancer Institute) to establish patient-derived model repository.

CONCLUSION

The development of CR technology creates exciting possibilities for digestive system research. The CR method can quickly and efficiently establish cell cultures from normal and diseased tissues. Most importantly, CRCs maintain the developmental potential of the original tissue and can restore the differentiation ability of the cells after removing these conditions. Additionally, it can quickly generate cultures from small biopsies and cryopreserved tissues. CR cells can also be produced from xenografts and organoid tissues. It can also form CDX tumors and be cultured in spheroids or organoids. Therefore, CR technology might be an ideal *in vitro* model for digestive system diseases and could facilitate precision medicine and drug discovery (**Figure 2**). Future studies using CR technology will also aid in tissue engineering for personalized regenerative medicine and provide an exciting opportunity to build a living biobank for digestive system disease. The use of CR technology has created great opportunities for the advancement of diagnosis, development of new treatments, and prevention of digestive system disease.

AUTHOR CONTRIBUTIONS

XL had the idea for the article and revised the manuscript. RZ and RL performed the literature search and drafted the manuscript. TA revised the manuscript. All authors contributed to the article and approved the submitted version.

FUNDING

This work was supported by internal support from HPV Vaccine Royalty in Center for Cell Reprogramming/Department of Pathology, Georgetown University Medical Center. The funders had no role in the data analysis, the decision to publish, or preparation of the manuscript, and Henan Natural Science Foundation (202300410383).

REFERENCES

Alamri, A. M., Kang, K., Groeneveld, S., Wang, W., Zhong, X., Kallakury, B., et al. (2016). Primary cancer cell culture: mammary-optimized vs conditional reprogramming. *Endocr. Relat. Cancer* 23, 535–554. doi: 10.1530/erc-16-0071

Alamri, A. M., Liu, X., Blancato, J. K., Haddad, B. R., Wang, W., Zhong, X., et al. (2018). Expanding primary cells from mucoepidermoid and other salivary gland neoplasms for genetic and chemosensitivity testing. *Dis. Model. Mech.* 11:dmm031716.

Aslan, M., Shahbazi, R., Ulubayram, K., and Ozpolat, B. (2018). Targeted therapies for pancreatic cancer and hurdles ahead. *Anticancer Res.* 38, 6591–6606. doi: 10.21873/anticanres.13026

Atala, A. (2012). Regenerative medicine strategies. *J. Pediatr. Surg.* 47, 17–28.

Baudino, T. A. (2015). Targeted cancer therapy: the next generation of cancer treatment. *Curr. Drug. Discov. Technol.* 12, 3–20. doi: 10.2174/1570163812666150602144310

Beglyarova, N., Banina, E., Zhou, Y., Mukhamadeeva, R., Andrianov, G., Bobrov, E., et al. (2016). Screening of conditionally reprogrammed patient-derived carcinoma cells identifies ercc3-myc interactions as a target in pancreatic cancer. *Clin. Cancer. Res.* 22, 6153–6163. doi: 10.1158/1078-0432.ccr-16-0149

Borodovsky, A., McQuiston, T. J., Stetson, D., Ahmed, A., Whitston, D., Zhang, J., et al. (2017). Generation of stable PDX derived cell lines using conditional reprogramming. *Mol. Cancer* 16:177.

Bradley, P. J. (2017). Adenoid cystic carcinoma evaluation and management: progress with optimism! *Curr. Opin. Otolaryngol. Head Neck Surg.* 25, 147–153. doi: 10.1097/moo.0000000000000347

Burisch, J., Jess, T., Martinato, M., and Lakatos, P. L. (2013). The burden of inflammatory bowel disease in Europe. *J. Crohns Colitis* 7, 322–337.

Chapman, S., Liu, X., Meyers, C., Schlegel, R., and McBride, A. A. (2010). Human keratinocytes are efficiently immortalized by a Rho kinase inhibitor. *J. Clin. Invest.* 120, 2619–2626. doi: 10.1172/jci42297

Chen, C., Choudhury, S., Wangsa, D., Lescott, C. J., Wilkins, D. J., Sripadhan, P., et al. (2017). A multiplex preclinical model for adenoid cystic carcinoma of the salivary gland identifies regorafenib as a potential therapeutic drug. *Sci. Rep.* 7:11410.

Clevers, H. (2016). Modeling development and disease with organoids. *Cell* 165, 1586–1597. doi: 10.1016/j.cell.2016.05.082

Collins, F. S., and Varmus, H. (2015). A new initiative on precision medicine. *N. Engl. J. Med.* 372, 793–795. doi: 10.1056/nejmp1500523

Coppola, L., Cianflone, A., Grimaldi, A. M., Incoronato, M., Bevilacqua, P., Messina, F., et al. (2019). Mirabelli, Biobanking in health care: evolution and future directions. *J. Transl. Med.* 17:172.

DeLeon, T. T., Ahn, D. H., Bogenberger, J. M., Anastasiadis, P. Z., Arora, M., Ramanathan, R. K., et al. (2018). Novel targeted therapy strategies for biliary tract cancers and hepatocellular carcinoma. *Future Oncol.* 14, 553–566. doi: 10.2217/fon-2017-0451

Dzunic, M., Petkovic, I., Cvetanovic, A., Vrbic, S., and Pejcic, I. (2019). Current and future targets and therapies in metastatic colorectal cancer. *J. BUON* 24, 1785–1792.

Gao, B., Huang, C., Kernstine, K., Pelekanou, V., Kluger, Y., Jiang, T., et al. (2017). Non-malignant respiratory epithelial cells preferentially proliferate from resected non-small cell lung cancer specimens cultured under conditionally reprogrammed conditions. *Oncotarget* 8, 11114–11126. doi: 10.18632/oncotarget.14366

Garnett, M. J., Edelman, E. J., Heidorn, S. J., Greenman, C. D., Dastur, A., Lau, K. W., et al. (2012). Systematic identification of genomic markers of drug sensitivity in cancer cells. *Nature* 483, 570–575.

GBD 2017 Inflammatory Bowel Disease Collaborators (2020). The global, regional, and national burden of inflammatory bowel disease in 195 countries and territories, 1990-2017: a systematic analysis for the Global Burden of Disease Study 2017. *Lancet Gastroenterol. Hepatol.* 5, 17–30.

GBD 2017 Oesophageal Cancer Collaborators (2020). The global, regional, and national burden of oesophageal cancer and its attributable risk factors in 195 countries and territories, 1990-2017: a systematic analysis for the Global Burden of Disease Study 2017. *Lancet Gastroenterol. Hepatol.* 5, 582–597.

GBD 2017 Pancreatic Cancer Collaborators (2019). The global, regional, and national burden of pancreatic cancer and its attributable risk factors in 195 countries and territories, 1990-2017: a systematic analysis for the Global Burden of Disease Study 2017. *Lancet Gastroenterol. Hepatol.* 4, 934–947.

Giard, D. J., Aaronson, S. A., Todaro, G. J., Arnstein, P., Kersey, J. H., Dosik, H., et al. (1973). In vitro cultivation of human tumors: establishment of cell lines derived from a series of solid tumors. *J. Natl. Cancer Inst.* 51, 1417–1423. doi: 10.1093/jnci/51.5.1417

Gillet, J. P., Varma, S., and Gottesman, M. M. (2013). The clinical relevance of cancer cell lines. *J. Natl. Cancer Inst.* 105, 452–458. doi: 10.1093/jnci/djt007

Gu, G., Dustin, D., and Fuqua, S. A. (2016). Targeted therapy for breast cancer and molecular mechanisms of resistance to treatment. *Curr. Opin. Pharmacol.* 31, 97–103. doi: 10.1016/j.coph.2016.11.005

Hamilton, N. J. I., Hynds, R. E., Gowers, K. H. C., Tait, A., Butler, C. R., Hopper, C., et al. (2019). Using a three-dimensional collagen matrix to deliver respiratory progenitor cells to decellularized trachea in vivo. *Tissue Eng. Part C Methods* 25, 93–102. doi: 10.1089/ten.tec.2018.0241

Hirsch, F. R., Scagliotti, G. V., Mulshine, J. L., Kwon, R., Curran, W. J. Jr., Wu, Y. L., et al. (2017). Lung cancer: current therapies and new targeted treatments. *Lancet* 389, 299–311. doi: 10.1016/s0140-6736(16)30958-8

Hollevoet, K., Mason-Osann, E., Liu, X. F., Imhof-Jung, S., Niederfellner, G., and Pastan, I. (2014). In vitro and in vivo activity of the low-immunogenic antimesothelin immunotoxin RG7787 in pancreatic cancer. *Mol. Cancer Ther.* 13, 2040–2049. doi: 10.1158/1535-7163.mct-14-0089-t

Ito, R., Takahashi, T., and Ito, M. (2018). Humanized mouse models: application to human diseases. *J. Cell. Physiol.* 233, 3723–3728. doi: 10.1002/jcp.26045

Jensen, T. J., Foster, C., Sayej, W., and Finck, C. M. (2017). Conditional reprogramming of pediatric human esophageal epithelial cells for use in tissue engineering and disease investigation. *J. Vis. Exp.* 121:55243.

Kettunen, K., Boström, P. J., Lamminen, T., Heinosalo, T., West, G., Saarinen, I., et al. (2019). Personalized drug sensitivity screening for bladder cancer using conditionally reprogrammed patient-derived cells. *Eur. Urol.* 76, 430–434. doi: 10.1016/j.eururo.2019.06.016

Kim, B. K., Nam, S. W., Min, B. S., Ban, H. S., Paik, S., Lee, K., et al. (2018). Bcl-2-dependent synthetic lethal interaction of the IDF-11774 with the V0 subunit C of vacuolar ATPase (ATP6V0C) in colorectal cancer. *Br. J. Cancer* 119, 1347–1357. doi: 10.1038/s41416-018-0289-1

Kretzschmar, K., and Clevers, H. (2016). Organoids: modeling development and the stem cell niche in a dish. *Dev. Cell* 38, 590–600. doi: 10.1016/j.devcel.2016.08.014

Lee, H. S., Kim, E., Lee, J., Park, S. J., Hwang, H. K., Park, C. H., et al. (2021). Profiling of conditionally reprogrammed cell lines for in vitro chemotherapy response prediction of pancreatic cancer. *EBioMedicine* 65:103218. doi: 10.1016/j.ebiom.2021.103218

Lee, H. S., Lee, J. S., Lee, J., Kim, E. K., Kim, H., Chung, M. J., et al. (2019). Establishment of pancreatic cancer cell lines with endoscopic ultrasound-guided biopsy via conditionally reprogrammed cell culture. *Cancer Med.* 8, 3339–3348. doi: 10.1002/cam4.2210

Li, S., Wang, M., and Zhou, J. (2020). Brain organoids: a promising living biobank resource for neuroscience research. *Biopreserv. Biobank.* 18, 136–143. doi: 10.1089/bio.2019.0111

Li, Y., Guo, D., Zhang, Y., Wang, L., Sun, T., Li, Z., et al. (2021). Rapid screening for individualized chemotherapy optimization of colorectal cancer: a novel conditional reprogramming technology-based functional diagnostic assay. *Transl. Oncol.* 14:100935. doi: 10.1016/j.tranon.2020.100935

Liu, W., Ju, L., Cheng, S., Wang, G., Qian, K., Liu, X., et al. (2020). Conditional reprogramming: modeling urological cancer and translation to clinics. *Clin. Transl. Med.* 10:e95.

Liu, X., Krawczyk, E., Suprynowicz, F. A., Palechor-Ceron, N., Yuan, H., Dakic, A., et al. (2017). Conditional reprogramming and long-term expansion of normal and tumor cells from human biospecimens. *Nat. Protoc.* 12, 439–451. doi: 10.1038/nprot.2016.174

Liu, X., and Mondal, A. M. (2020). Conditional cell reprogramming for modeling host-virus interactions and human viral diseases. *J. Med. Virol.* 92: 2440–2452. doi: 10.1002/jmv.26093

Liu, X., Ory, V., Chapman, S., Yuan, H., Albanese, C., Kallakury, B., et al. (2012). ROCK inhibitor and feeder cells induce the conditional reprogramming of epithelial cells. *Am. J. Pathol.* 180, 599–607.

Matuchansky, C., and Beauchant, M. (1982). [The digestive system and pancreas in 1982]. *Biomed. Pharmacother.* 36, 407–414.

Mondal, A. M., Ma, A. H., Li, G., Krawczyk, E., Yuan, R., Lu, J., et al. (2019). Fidelity of a PDX-CR model for bladder cancer. *Biochem. Biophys. Res. Commun.* 517, 49–56. doi: 10.1016/j.bbrc.2019.06.165

Moorefield, E. C., Blue, R. E., Quinney, N. L., Gentzsch, M., and Ding, S. (2018). Generation of renewable mouse intestinal epithelial cell monolayers and organoids for functional analyses. *BMC Cell. Biol.* 19:15. doi: 10.1186/s12860-018-0165-0

Narita, Y., and Muro, K. (2017). Challenges in molecular targeted therapy for gastric cancer: considerations for efficacy and safety. *Expert Opin. Drug Saf.* 16, 319–327.

O'Malley, Y., Rotti, P. G. I, Thornell, M., Vanegas Calderón, O. G., Febres-Aldana, C., Durham, K., et al. (2018). Development of a polarized pancreatic ductular cell epithelium for physiological studies. *J. Appl. Physiol. (1985)* 125, 97–106.

Palechor-Ceron, N., Krawczyk, E., Dakic, A., Simic, V., Yuan, H., Blancato, J., et al. (2019). Conditional reprogramming for patient-derived cancer models and next-generation living biobanks. *Cells* 8:1327. doi: 10.3390/cells8111327

Pan, Y., Zhao, S., and Cao, Z. (2018). Organoid models of gastrointestinal neoplasms: origin, current status and future applications in personalized medicine. *Genes Dis.* 5, 323–330. doi: 10.1016/j.gendis.2018.09.002

Panaccione, A., Chang, M. T., Carbone, B. E., Guo, Y., Moskaluk, C. A., Virk, R. K., et al. (2016). NOTCH1 and SOX10 are essential for proliferation and radiation resistance of cancer stem-like cells in adenoid cystic carcinoma. *Clin. Cancer Res.* 22, 2083–2095. doi: 10.1158/1078-0432.ccr-15-2208

Reubinoff, B. E., Pera, M. F., Fong, C. Y., Trounson, A., and Bongso, A. (2000). Embryonic stem cell lines from human blastocysts: somatic differentiation in vitro. *Nat. Biotechnol.* 18, 399–404. doi: 10.1038/74447

Rheinwald, J. G., and Green, H. (1975). Serial cultivation of strains of human epidermal keratinocytes: the formation of keratinizing colonies from single cells. *Cell* 6, 331–343. doi: 10.1016/s0092-8674(75)80001-8

Riazi, A. M., Kwon, S. Y., and Stanford, W. L. (2009). Stem cell sources for regenerative medicine. *Methods Mol. Biol.* 482, 55–90. doi: 10.1007/978-1-59745-060-7_5

Saeed, K., Rahkama, V., Eldfors, S., Bychkov, D., Mpindi, J. P., Yadav, B., et al. (2017). Comprehensive drug testing of patient-derived conditionally reprogrammed cells from castration-resistant prostate cancer. *Eur. Urol.* 71, 319–327. doi: 10.1016/j.eururo.2016.04.019

Sato, T., Vries, R. G., Snippert, H. J., van de Wetering, M., Barker, N., Stange, D. E., et al. (2009). Single Lgr5 stem cells build crypt-villus structures in vitro without a mesenchymal niche. *Nature* 459, 262–265. doi: 10.1038/nature07935

Siegel, R. L., and Miller, K. D. (2020). Cancer statistics, 2020. *CA Cancer J. Clin.* 70, 7–30.

Stanley, M. A., and Dahlenburg, K. (1984). The effect of choleragen and epidermal growth factor on proliferation and maturation in vitro of human ectocervical cells. *In Vitro* 20, 144–151. doi: 10.1007/bf02626655

Su, S., Di Poto, C., Kroemer, A. H., Cui, W., Roy, R., Liu, X., et al. (2019a). Establishment of ornithine transcarbamylase deficiency-derived primary human hepatocyte with hepatic functions. *Exp. Cell. Res.* 384:111621. doi: 10.1016/j.yexcr.2019.111621

Su, S., Di Poto, C., Roy, R., Liu, X., Cui, W., Kroemer, A., et al. (2019b). Long-term culture and characterization of patient-derived primary hepatocytes using conditional reprogramming. *Exp. Biol. Med. (Maywood)* 244, 857–864. doi: 10.1177/1535370219855398

Suprynowicz, F. A., Upadhyay, G., Krawczyk, E., Kramer, S. C., Hebert, J. D., Liu, X., et al. (2012). Conditionally reprogrammed cells represent a stem-like state of adult epithelial cells. *Proc. Natl. Acad. Sci. U.S.A.* 109, 20035–20040. doi: 10.1073/pnas.1213241109

Terunuma, A., Limgala, R. P., Park, C. J., Choudhary, I., and Vogel, J. C. (2010). Efficient procurement of epithelial stem cells from human tissue specimens using a Rho-associated protein kinase inhibitor Y-27632. *Tissue Eng. Part A* 16, 1363–1368. doi: 10.1089/ten.tea.2009.0339

Timofeeva, O. A., Palechor-Ceron, N., Li, G., Yuan, H., Krawczyk, E., Zhong, X., et al. (2017). Conditionally reprogrammed normal and primary tumor prostate epithelial cells: a novel patient-derived cell model for studies of human prostate cancer. *Oncotarget* 8, 22741–22758. doi: 10.18632/oncotarget.13937

Tricoli, L., Naeem, A., Parasido, E., Mikhaiel, J. P., Choudhry, M. U., Berry, D. L. I, et al. (2018). Characterization of the effects of defined, multidimensional culture conditions on conditionally reprogrammed primary human prostate cells. *Oncotarget* 9, 2193–2207. doi: 10.18632/oncotarget.23363

Urbaniak, A., Jousheghany, F., Yuan, Y., Piña-Oviedo, S., Huczyński, A., Delgado, M., et al. (2019). The response of phyllodes tumor of the breast to anticancer therapy: an in vitro and ex vivo study. *Oncol. Lett.* 18, 5097–5106.

Wang, Y., Liao, H., Zheng, T., Wang, J., Guo, D., Lu, Z., et al. (2020). Conditionally reprogrammed colorectal cancer cells combined with mouse avatars identify synergy between EGFR and MEK or CDK4/6 inhibitors. *Am. J. Cancer Res.* 10, 249–262.

Watanabe, K., Ueno, M., Kamiya, D., Nishiyama, A., Matsumura, M., Wataya, T., et al. (2007). A ROCK inhibitor permits survival of dissociated human embryonic stem cells. *Nat. Biotechnol.* 25, 681–686. doi: 10.1038/nbt1310

Xinaris, C. (2019). Organoids for replacement therapy: expectations, limitations and reality. *Curr. Opin. Organ Transplant.* 24, 555–561. doi: 10.1097/mot.0000000000000680

Conflict of Interest: Several patents for conditional reprogramming technology has been awarded to Georgetown University by the United States Patent Office. The license for this technology has been given to a Maryland-based start-up company for commercialization. The inventor, XL and Georgetown University receive potential royalties and payments from the company. Several organizations and companies (Propagenix, ATCC, STEMCELL Technologies, etc.) are selling CR cells, media and related reagents.

The remaining authors declare that the research was conducted in the absence of any commercial or financial relationships that could be construed as a potential conflict of interest.

Copyright © 2021 Zhao, Li, An and Liu. This is an open-access article distributed under the terms of the Creative Commons Attribution License (CC BY). The use, distribution or reproduction in other forums is permitted, provided the original author(s) and the copyright owner(s) are credited and that the original publication in this journal is cited, in accordance with accepted academic practice. No use, distribution or reproduction is permitted which does not comply with these terms.

frontiers in Oncology

ORIGINAL RESEARCH
published: 10 June 2021
doi: 10.3389/fonc.2021.649980

MAPK-RAP1A Signaling Enriched in Hepatocellular Carcinoma Is Associated With Favorable Tumor-Infiltrating Immune Cells and Clinical Prognosis

*Hailin Li[1], Guangyu Han[1], Xing Li[1], Bowen Li[2], Bo Wu[3], Hongyuan Jin[3], Lingli Wu[4] and Wei Wang[1]**

[1] Department of General Surgery, Hongqi Hospital Affiliated to Mudanjiang Medical University, Mudanjiang, China, [2] Department of Oncology and Laparoscopy Surgery, The First Affiliated Hospital of Harbin Medical University, Harbin, China, [3] Department of General Surgery, The Fourth Affiliated Hospital of China Medical University, Shenyang, China, [4] Department of Cardiology, China–Japan Union Hospital of Jilin University, Changchun, China

OPEN ACCESS

Edited by:
Ira Ida Skvortsova, Innsbruck Medical University, Austria

Reviewed by:
Prasanna Ekambaram, University of Pittsburgh, United States
Shuyun Rao, George Washington University, United States

***Correspondence:**
Wei Wang
Doctorwu8962@hotmail.com

Specialty section:
This article was submitted to Molecular and Cellular Oncology, a section of the journal Frontiers in Oncology

Received: 06 January 2021
Accepted: 10 May 2021
Published: 10 June 2021

Citation:
Li H, Han G, Li X, Li B, Wu B, Jin H, Wu L and Wang W (2021) MAPK-RAP1A Signaling Enriched in Hepatocellular Carcinoma Is Associated With Favorable Tumor-Infiltrating Immune Cells and Clinical Prognosis. Front. Oncol. 11:649980. doi: 10.3389/fonc.2021.649980

Background: MAPK-RAP1A signaling, which is involved in cancer progression, remains to be defined. Upregulation of MAPK-RAP1A signaling accounts for most cancers that harbor high incident rate, such as non-small cell lung cancer (NSCLC) and pancreatic cancer, especially in hepatocellular carcinoma (HCC). MAPK-RAP1A signaling plays an important function as clinical diagnosis and prognostic value in cancers, and the role of MAPK-RAP1A signaling related with immune infiltration for HCC should be elucidated.

Methods: Microarray data and patient cohort information from The Cancer Genome Atlas (TCGA; n = 425) and International Cancer Genome Consortium (ICGC; n = 405) were selected for validation. The Cox regression and least absolute shrinkage and selection operator (LASSO) were used to construct a clinical prognostic model in this analysis and validation study. We also tested the area under the curve (AUC) of the risk signature that could reflect the status of predictive power by determining model. MAPK-RAP1A signaling is also associated with tumor-infiltrating immune cells (TICs) as well as clinical parameters in HCC. The GSEA and CIBERSORT were used to calculate the proportion of TICs, which should be beneficial for the clinical characteristics (clinical stage, distant metastasis) and positively correlated with the survival of HCC patients.

Results: HCC patients with enrichment of MAPK-RAP1A signaling were associated with clinical characteristics and favorable T cell gamma delta (VδT cells), and STMN1, RAP1A, FLT3, HSPA8, ANGPT2, and PGF were used as candidate biomarkers for risk scores of HCC. To determine the molecular mechanism of this signature gene association, Gene Set Enrichment Analysis (GSEA) was proposed. Cytokine–cytokine receptor interaction, TGF-β signaling pathway, and Intestinal immune network for IgA production gene sets

were closely related in MAPK-RAP1A gene sets. Thus, we established a novel prognostic prediction of HCC to deepen learning of MAPK-RAP1A signaling pathways.

Conclusion: Our findings demonstrated that HCC patients with enrichment of MAPK-RAP1A signaling were associated with clinical characteristics and favorable T cell gamma delta (Vδ T cells), which may be a novel prognostic prediction of HCC.

Keywords: hepatocellular carcinoma, MAPK-RAP1A signaling, tumor-infiltrating immune cells, gamma delta T cell, prognosis

INTRODUCTION

Hepatocellular carcinoma (HCC) is the sixth leading cancer and accounts for the second highest number of lethal malignant cancer globally (1). HCC accounts for most primary malignancy of liver cancers and is biologically heterogeneous. Despite treatment advances in surgery, liver transplantation, and radiofrequency ablation, the 5-year survival rate for HCC is still less due to heterogeneous tumor (2). At present, the development of sorafenib represented the main treatment for advanced liver cancer (3). However, a larger proportion of patients will have recurrence or metastasis (4). Thus, it is worth identify that distinct molecular genes and pathways, which accelerate molecular studies with the prognostic outcomes of HCC (5).

Among them, the MAPK and RAP1A are the mediator pathways in regulating cell biology of cancer cells (6, 7). MAPKs are best-characterized regulators of extracellular signals that are transduced to the nucleus; MAPKs include three important protein kinase families: extracellular signal-regulated protein kinases (ERKs), c-Jun NH2-terminal kinases (JNKs), and p38 family of kinases (8). Ras-associated protein-1 A (RAP1A), a small GTPase that belongs to the Ras-related protein family, was observed to regulate oncogenic Ras phenotype and Rho GTPase mediated actin cytoskeleton. RAP1A signaling is involved in cell proliferation, differentiation, and cell–cell junction in several cancer types (9–11). It was also reported that RAP1A regulates cancer through activating MAPK signaling in order to regulate motility and metastasis (12). The upregulation of RAP1A induced the MAPK signaling, which indicated that p38 may be identified as the counterparts of the RAP1A-dependent biological function (7, 12). Therefore, the clinical involved in the expression of MAPK-RAP1A signaling should be strongly considered.

The tumor microenvironment (TME), which contains stromal and immune cells, is thought to be a determinant factor in the advance of HCC (13, 14). Immune stroma plays a major role in the TME and development of tumor growth to the metastasis of HCC (15). Meanwhile, recent evidence indicates that immune cells may also play a role in cancer *via* ERK, another pathway of MAPK, thus probably essential for the development of therapeutic processes (16). Pancreatic cancer cells have been reported to be taken up by T lymphocytes to activate p38 MAPK *via* secreting exosomes, which ultimately causes immunosuppression (17). HCC-derived exosomes carried HMGB1 and activated TIM-1$^+$ Breg cell; this delivery led to increase in angiogenesis by TLR and MAPK signaling pathways (18). To our knowledge, Ubc9 acts as a functional binding partner of ADAP and plays a selective role in TCR-mediated Rac1 activation *via* modulation of the membrane targeting of RAP1A and RapL (19). Therefore, the construction of MAPK-RAP1A signaling is known to involve the tumor microenvironment that can improve HCC prognosis.

In the present study, we constructed tumor-infiltrating immune cells (TICs) closely related to MAPK-RAP1A signaling through bioinformatics methods. Next, MAPK-RAP1A related signature genes significantly related to clinical features were detected to validate diagnosis and prognosis. Then we identified TICs by integrating MAPK-RAP1A related signature genes for HCC. We here aimed to provide potential marker for assessment of HCC clinical prognosis and playing a key role in TME.

MATERIALS AND METHODS

HCC Patients

From January 2020 to December 2020, 20 human liver cancer tissue samples and corresponding para-carcinoma tissue samples were collected from patients with HCC in Hongqi Hospital Affiliated to Mudanjiang Medical University. The sample collection was approved by the research ethics committee of Hongqi Hospital Affiliated to Mudanjiang Medical University. Each patient provided informed consent to participate in the study. All collected samples were immediately frozen in liquid nitrogen until subsequent analysis.

TCGA and ICGC Data Source

All eligible sequencing datasets, clinical characteristics, and follow-up information in The Cancer Genome Atlas (TCGA) (https://gdc.cancer.gov/about-data/publications/pancanatlas) and International Cancer Genome Consortium (ICGC) database (https://icgc.org/) were downloaded. Gene sets with HCC were used to perform KEGG analyses. The KEGG pathway in the TCGA database was used as the training set, and data in the ICGC data sets were used for the validation set. Meanwhile, MAPK-RAP1A related genes were selected using the R package "limma" from the pre-processed data with log2(x + 1) transformation, and the adjusted P value <0.05 was considered statistically significant.

Construction of a Risk Signature Associated With MAPK-RAP1A Signaling

To screen the association between clinical stage and risk signature, multivariate cox regression models were used to assess the clinical characteristics of MAPK-RAP1A signaling in R language. The data in the TCGA database were used as the training sets, and data in the ICGC data sets were used for the validation sets to establish a nomogram. The HCC patients' information identified the relationship between clinical stage and risk scores, and Wilcoxon rank test as the significance test. LASSO regression was used to set precision power gene combination to identify key modules (20). R language survival and survminer were applied for the survival analysis and time-dependent receiver operating characteristic (ROC) curve to assess the efficiency of the risk signature.

Association of Hub Genes' Expression With Tumor Purity and Tumor-Infiltrating Immune Cells

The ssGSEA and CIBERSORT tools were used to estimate tumor-infiltrating immune cells (TICs) for sample by R language (21, 22); the final estimate outcome was sum up to three kinds of scores: stromal score, immune score, and ESTIMATE Score, which correlated with the larger ratio of the immune infiltration. Moreover, the infiltration of T gamma delta showed a relatively lower risk signature in MAPK-RAP1A signaling. Next, we applied Tumor Immune Estimation Resource (TIMER) to integrate the results of those hub gene expression of HCC hub genes and both tumor purity, TICs. Interestingly, STMN1, RAP1A, FLT3, HSPA8, ANGPT2, and PGF were all positively associated with tumor purity. Furthermore, a relationship was observed between the six hub genes and infiltration of immune cells (23, 24). Combined with the above results, we suggested that the prognostic evaluation based on the high abundance of MAPK-RAP1A signaling assessed through ssGSEA or CIBERSORT analysis is reliable.

Functional Enrichment Analysis

Gene set enrichment analysis (GSEA) was performed to investigate the MAPK-RAP1A signature gene potential mechanisms (21). The gene set "c2.cp.kegg.v6.2.symbols.gmt", downloaded from the Molecular Signature Database (MSigDB, http://software.broadinstitute.org/gsea/msigdb/index.jsp), was selected as the reference gene set. GSEA was used to elucidate biological processes associated with the significant survival difference; R package "ClusterProfiler" was utilized for GSEA analysis of the hub genes between low expression group and high expression group in R with adjusted $P < 0.05$ and $|\log_2 FC| > 0.5$ (25).

Immunohistochemical Staining

Each resected specimen was fixed with 10% formalin, dehydrated, and embedded in paraffin. Paraffin sections were 3 μm thick and placed on glass slides. Firstly, the sections were deparaffined and incubated in an oven at 70°C for 1 h and 30 min. Then sections were carried out in xylene, and rehydration was carried out after gradient ethanol dehydration. Afterwards, the sections were incubated in 1× EDTA solution at low strength of microwave for 15 min to keep the endogenous peroxidase activity. Then, the sections were washed with PBS for three times and were then incubated with primary antibodies against STMN1 (1:200; Proteintech, 11157-1-AP), RAP1A (1:100; Abcam, ab197673), FLT3 (1:180; Abcam, ab52648), ANGPT2 (1:100; Proteintech, 24613-1-AP), PGF (1:200; Proteintech, 10642-1-AP), and HSPA8 (1:400; Proteintech, 10654-1-AP), CD276 (B7H3) (1:100; Abcam, ab105922), CD274 (PD-L1) (1:100; CST, #13684) at 4°C overnight. A secondary goat anti-rabbit antibody (1:200; ab205718, Abcam, UK) further incubated the slides at 37°C for 30 min. Binding of the primary antibodies was visualized *via* diaminobenzidine method (DAB, Boster Biological Technology, USA). Finally, these sections were counterstained with hematoxylin, dehydrated by a gradient ethanol, followed by xylene, and mounted. The staining of each specimen was evaluated through two independent investigators blinded to the clinicopathological information.

When it was present in the membrane or cytoplasm, the expression of proteins was considered positive. The staining score was assessed according to parameters of intensity and extension, and scored to determine the protein expression profiles. The staining-based expression levels were divided into four categories: positive, moderate, low, and negative; the scoring system used is based on the proportion of stained cells (>75, 25–75, or <25%); and the intensity of staining was also categorized into four: strong, moderate, weak, or negative. A final combined score of 0–12 was obtained by multiplying the intensity and percentage scores. Patients were classified into high or low protein expression groups based on median expression scores.

Real-Time Quantitative Polymerase Chain Reaction

Tumor specimens and adjacent normal tissues were collected from recruited HCC patients. Total RNAs were extracted from tissues with TRIzol reagent (Invitrogen, Carlsbad, CA, USA). About 500 ng of purified RNA was reverse transcribed into complementary DNAs (cDNAs) using SuperScript ™II (Life Technologies, Darmstadt, Germany), and underwent SYBR green-based real-time polymerase chain reaction using a standard protocol with specific primers (Applied Biosystems, Carlsbad, CA, USA). In the PCR amplification process, samples were predenaturated at 95°C for 10 min, then 40 cycles of denaturation at 95°C, and annealing at 60°C for 1 min. The $2^{-\Delta\Delta CT}$ method was used to calculate the results, which are presented as the x-fold increase with the adjacent normal tissues as control. All primer sequences used in our study are the following:

ERK forward, 5′-TGGATTCCCTGGTTCTCTCTAAAG-3′; reverse, 5′-GGGTCTGTTTTCCGAGGATGA-3′; JNK forward, 5′-TGTGTGGAATCAAGCACCTTC-3′; reverse, 5′-AGGCGTCATCATAAAACTCGTTC-3′; RAP1A forward, 5′-TGTCTCACTGCACCTTCA-3′; reverse, 5′-GACTTCCCAACG CCTCCT-3′; P38 forward, 5′-CGACTTGCTGGAGAAGATGC-3′; reverse, 5′-GGCACAAAGCTGATGACTTC-3′.

Western Blot

The total protein was extracted from four cell lines Huh7, HepG2, Hepa1-6 in ice by RIPA lysis buffer (Beyotime, Shanghai, China) with protease and phosphatase inhibitor cocktail (Roche, Basel, Switzerland). The protein concentration was detected by BCA Protein Assay Kit (Beyotime, Shanghai, China); proteins were separated by SDS-PAGE and transferred onto polyvinylidene difluoride membranes (Millipore, Bedford, MA). Then incubated in 5% Bovine Serum Albumin at room temperature for 2 h. The membranes were exposed to primary antibodies against ERK, p-ERK, JNK, p-JNK, p38, p-p38, and RAP1A (1:1,000 dilution; Santa Cruz Biotechnology, Santa Cruz, CA) or β-actin (1:1,000 dilution; Cell Signaling Technology, USA) at 4°C overnight. After that, the membranes were incubated with secondary antibody (1:5,000 dilution; Cell Signaling Technology, USA), and protein blots were detected by Automatic Chemiluminescence Imaging Analysis System (Tanon, Shanghai, China).

Statistical Analyses

All statistical tests including Cox regression models, LASSO regression, ROC curve analysis and K–M survival analyses were conducted using Rversion 3.5.1 (https://www.r-project.org/). Statistical differences between distributions were computed by independent t test between two groups and Kruskal–Wallis for multigroup comparison. P <0.05 was considered statistically significant. The charts, forest plots, and calibration plots were drawn using R language. This study finally selected to build the diagnostic prediction model or diagnosis guidelines using a logistic regression method.

RESULTS

Construction of A Nomogram for Predicting Prognostic Risk of MAPK-RAP1A

In order to detect the MAPK-RAP1A pathway, we detected the expression of ERK, JNK, p38, and RAP1A by tissue RT-qPCR and found that the expression of ERK, JNK, p38, and RAP1A in HCC tumor tissues was higher than that in adjacent tissues (**Figure 1A**). We also detected the expression of ERK, JNK, p38, and RAP1A by western blot and found that the expression of phosphorylated ERK, JNK, p38, and RAP1A in Huh7, HepG2, and Hepa1-6 was higher than in L02 (**Figure 1B**). To better confirm the MAPK-RAP1A related genes with risk signature, we evaluated HCC patients with detailed clinical sample information (gender, age, histological grade, pathologic stage, and TNM stage) and follow-up information in the TCGA platform. Firstly, multivariate cox regression analyses were conducted to assess the independent predictive power in the training cohort, revealing that the risk signature remained as an independent risk factor correlated with HCC patients' prognosis ($p < 0.05$) (**Figure 1C**). Second, risk signature was significantly correlated with TNM stages and overall survival (**Figures 1D, E**). Subsequently, multivariate Cox regression analyses was tested in the validation cohort by the ICGC datasets, indicating that gender, stage, and risk scores were independent risk factors for HCC patients ($p < 0.05$) (**Figure 1F**). Finally, a nomogram integrating the factors was constructed for predicting clinical features of HCC. It was noted that the nomogram model demonstrated the probability accuracy for predicting HCC (**Figure 1G**). We considered that a nomogram integrating MAPK-RAP1A risk signature might act as accurate predictive power.

Six-Related Genes Were Screened Out for Constructing a Risk Signature

Through the LASSO algorithm, 328 MAPK-RAP1A related gene were performed to build the prognostic risk signature in the TCGA training cohort, and 11 genes (STMN1, RAP1A, FLT3, HSPA8, FGF9, EFNA5, IRAK1, RAC3, DUSP10, ANGPT2, and PGF) were filtered out because of shrinking parameters (**Figure 2A**). Subsequently, six genes (STMN1, RAP1A, FLT3, HSPA8, ANGPT2, and PGF) were selected to establish a prognostic model (**Figure 2B**). Risk score = 1.5962 * (the expression level of STMN1) + 1.7459 * (the expression level of RAP1A) + 2.2693* (the expression level of FLT3) + 1.3980 * (the expression level of HSPA8) + 1.462 * (the expression level of ANGPT2) + 1.7673 * (the expression level of PGF). Finally, a nomogram integrating the six signatures was demonstrating the performance of the risk signature in predicting HCC (**Figure 2C**). The mentioned nomogram revealed ta better predictive accuracy by the total points obtained by adding up (**Figure 2D**).

Stratification of TCGA Training and ICGC Validation Cohorts Using the Risk Signature

According to the median risk score, we divided the cohort patients into high-risk and low-risk groups. The high-risk group exhibited a higher frequency of poorer overall survival (OS) than the low-risk group in the TCGA platform by K–M curve (**Figure 3A**). To further assess the predictive accuracy of this MAPK-RAP1A risk signature, we performed a time-dependent ROC curve analysis. The AUC was 0.75, 0.805, and 0.65 at 1, 3, and 5 years for survival in the training cohort of TCGA (**Figure 3C**). The ICGC dataset protocols were used for the validation of the risk signature for this purpose, which indicated that higher scores exhibited markedly worse overall survival (OS) (**Figure 3B**). The AUCs for OS in the validation cohort were 0.75, 0.805, and 0.65 at 1, 3, and 5 years, respectively (**Figure 3D**). Thus, we considered that the clinical prognostic model successfully stratified cohort patients from TCGA into high and low-risk groups with predicting the clinical prognosis of HCC.

Validation of Signature Genes in the MAPK-RAP1A Datasets

Among the 11 genes screened above, six signature genes (STMN1, RAP1A, FLT3, HSPA8, ANGPT2, and PGF) were identified to validate prognostic and diagnostic value and clinical features. All of them, which were significantly

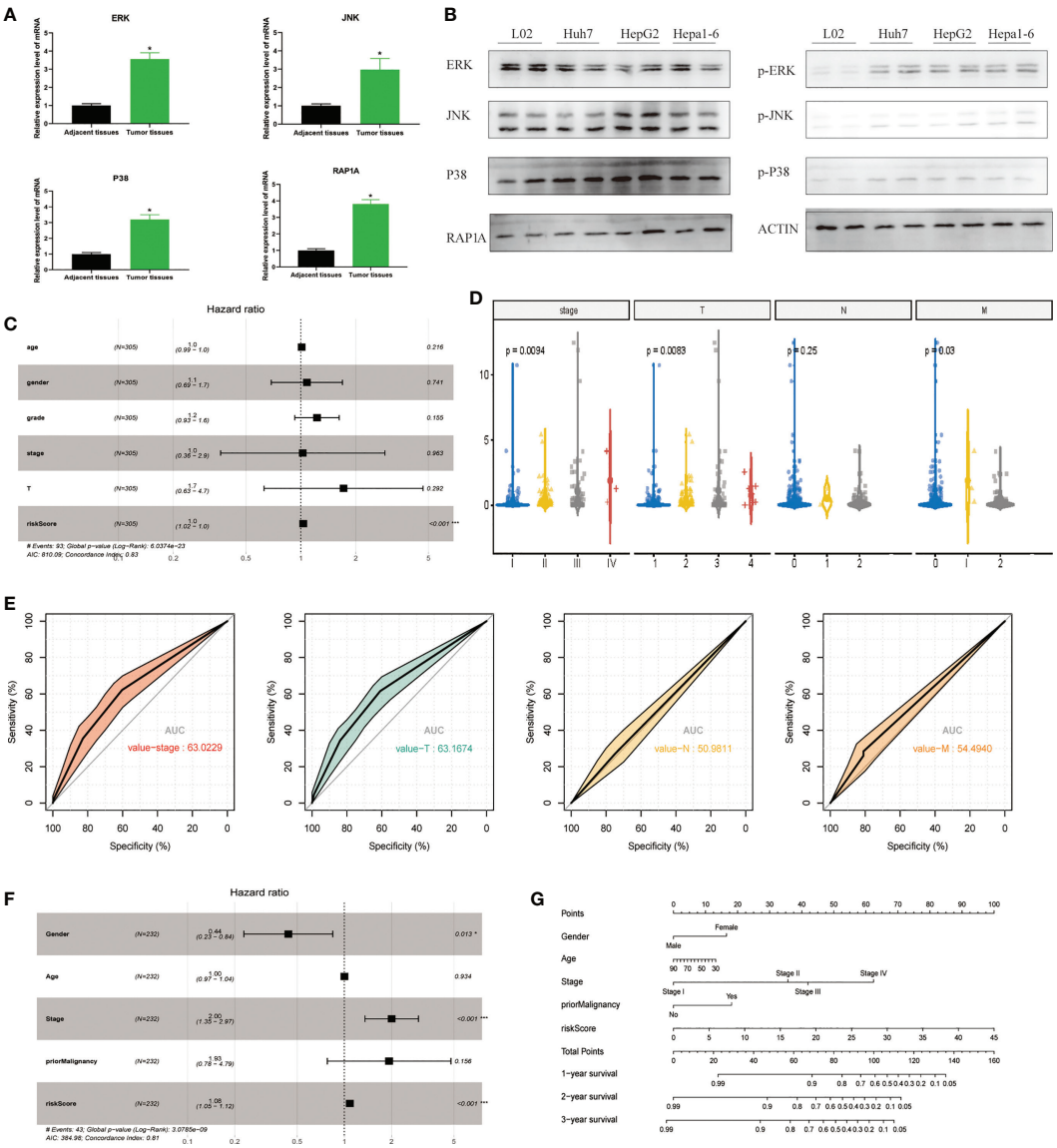


FIGURE 1 | Establishment of the risk signature with MAPK-RAP1A related genes in the training (TCGA) and validation database (ICGC). **(A)** RT-qPCR was used to detect the expression of ERK, JNK, p38, RAP1A in 20 cases HCC tumor tissues and adjacent tissues. **(B)** Western blot was used to detect the expression of ERK, JNK, p38, RAP1A in Huh7, HepG2, Hepa1-6, and L02 cell lines. **(C)** Multivariate Cox regression analysis to validate prognosis related clinicopathological characters. **(D)** The correlation of our MAPK-RAP1A risk signature with the clinicopathological characters (TNM stage) of HCC from the training set. **(E)** ROC curves of AUC evaluated the efficiency of the risk signature for predicting TNM stage in training set. **(F)** Multivariate Cox regression analysis to validate prognosis related clinicopathological characters. **(G)** Nomogram for predicting 1-, 3-, and 5-year OS of LIHC patients in the ICGC cohort. *$p < 0.05$; ***$p < 0.001$.

upregulated ($p < 0.05$) in HCC samples, can potentially act as oncogenes compared with normal controls. In addition, STMN1, RAP1A, FLT3, HSPA8, ANGPT2, and PGF were identified as the key oncogenic components in HCC samples with different TNM stage, T classification, lymph node metastasis, and distant metastasis, with higher expression levels indicating higher stage (**Figures 4A–D**). Conversely, all six signature genes in the module might act as potential prognostic values.

The Categories of Immunity and Tumor Purity of MAPK-RAP1A Datasets

The immunity of the MAPK-RAP1A signaling was used in the principal components analysis (PCA) for assigning patients to low- and high-immunity categories (**Figures 5A, B**). Further comparison analysis showed that tumor purity had significantly higher expression levels in low-immunity compared with high-immunity (**Figure 5C**). Regarding prognosis, K–M curves

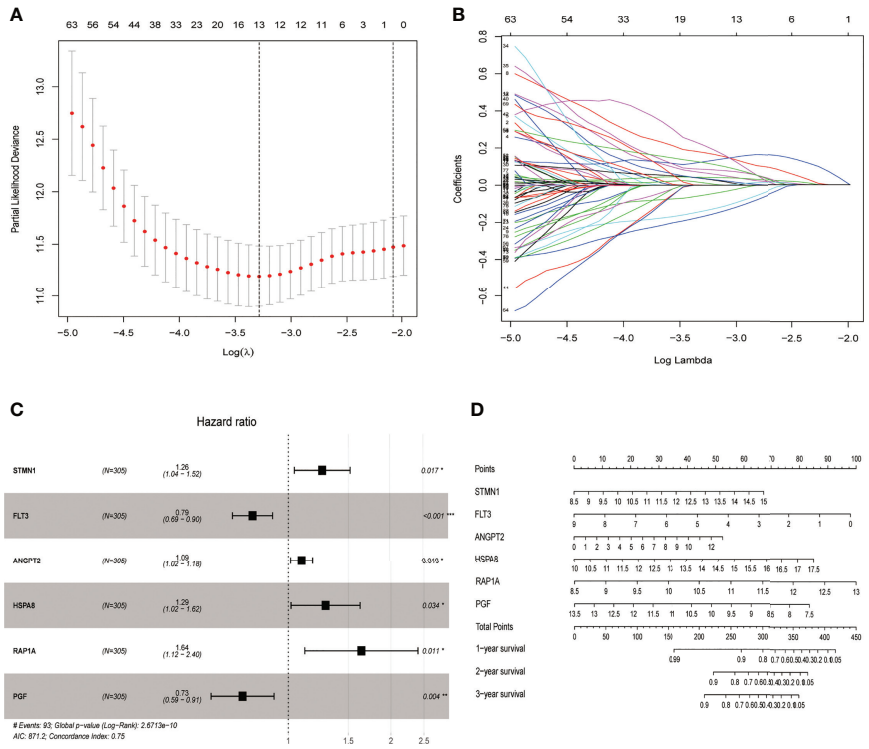


FIGURE 2 | Screening out genes for constructing a risk signature. **(A)** Log (Lambda) value of the 11 genes in LASSO model. **(B)** The most proper log (Lambda) value in LASSO model. **(C)** Six genes (STMN1, FLT3, ANGPT2, HSPA8, RAP1A, and PGF) were selected for constructing a risk signature using multivariate Cox regression model. **(D)** A nomogram for predicting 1-, 3- and 5-year survival rate of HCC patients was established. *$p < 0.05$; **$p < 0.01$; ***$p < 0.001$.

showed that higher tumor purity of MAPK-RAP1A signaling was associated significantly with worse OS (**Figure 5D**).

Association of Stromal Score, Immune Score, and ESTIMATE Score With Several Clinical Features

The immune components and clinicopathological characteristics were positively correlated; we analyzed the corresponding stromal score, immune score, and estimate score of MAPK-RAP1A gene sets from TCGA-LIHC database (**Figure 6A**). Among them, stromal score and estimate score are key proportion of advanced TNM stages. The representative images of the immune score were only negatively correlated with T classification of TMN stages ($p = 0.007$), and estimate score significantly declined with T and M classification of TMN stages ($p = 0.028$ and $p = 0.021$). Whereas there was no correlation between ESTIMATE algorithm and lymph node metastasis ($P = 0.776$). These results suggested that the ratio of immune components was correlated with the progress of HCC, especially in metastasis (**Figures 6B–E**).

Association of Risk Signature With Tumor Purity and Tumor Immune Cell Infiltration

It was demonstrated that the levels of TICs, including Tregs, T-cells gamma delta (VδT cells), and monocytes were significantly higher in the normal patient group compared with the HCC patient group (**Figure 7A**). As shown in **Figure 7B**, two immune infiltration cell subpopulations were significantly enriched in the low-risk patient group (Macrophage 0 and VδT cells). To characterize the TICs, the contents of infiltrating immune cells were investigated. We utilized TIMER website source to identified potential associations between the expression of signature genes and immune purity of tumor, infiltrating immune cells (**Figures 7C–G**). Interestingly, STMN1 and ANGPT2 were significantly positively correlated with tumor purity, whereas RAP1A, FLT3, HSPA8, and PGF were all significantly negatively correlated with tumor purity. Consequently, the present study reveals relationships linking these six genes and infiltration of VδT cells (**Figures 7C–G**).

GSEA Reveal a Close Relationship Between Hub Genes and Tumor Proliferation

To explore the molecular mechanisms of STMN1, RAP1A, FLT3, HSPA8, ANGPT2, and PGF in HCC, we detected GSEA on the TCGA-LIHC RNA-seq data. This work confirmed that the role of hub genes in high expression groups of RAP1A, FLT3, HSPA8, ANGPT2, and PGF were all enriched in "cytokine–cytokine receptor interaction" pathways. Additionally, the "ECM –receptor interaction" and "TGF–beta signaling pathway" gene set were enriched in high expression groups of ANGPT2 and HSPA8, whereas "Intestinal immune network for IgA

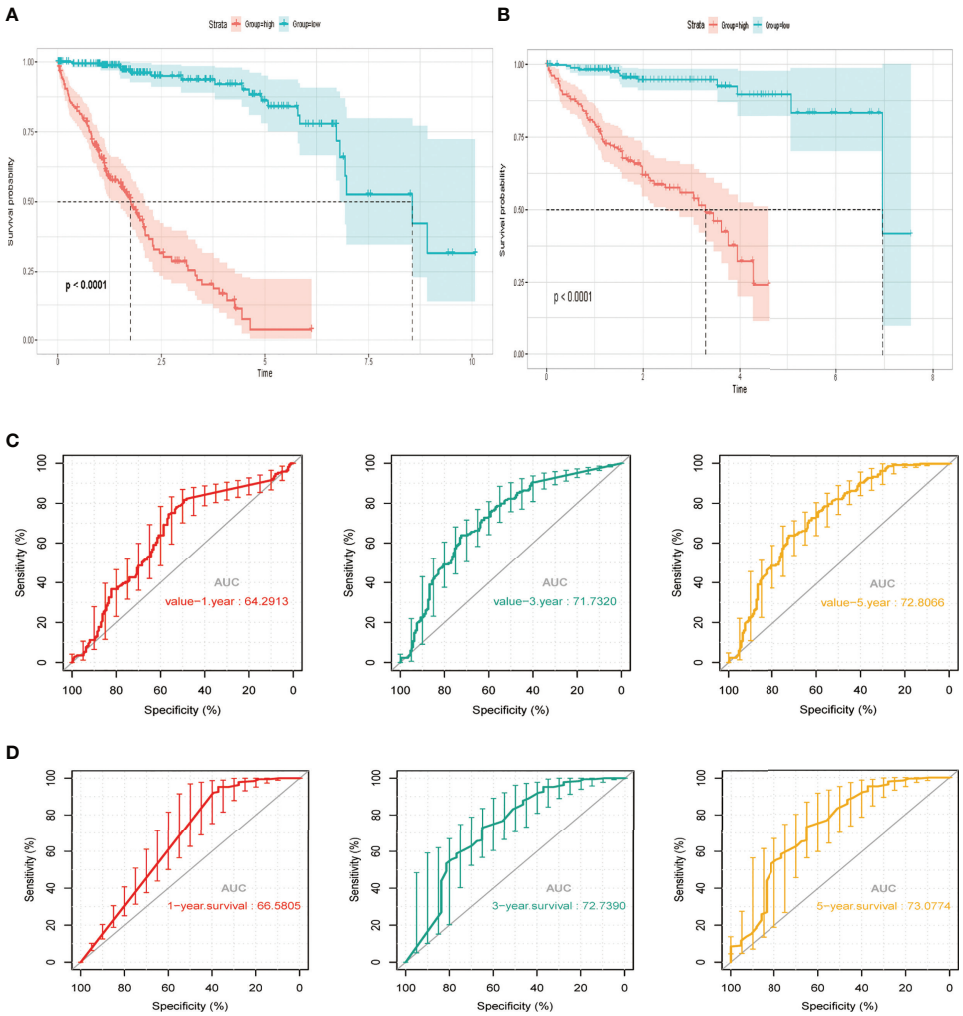


FIGURE 3 | The risk signature in HCC from the training set, the independent external validation cohort. **(A, C)** The Kaplan–Meier curves of the MAPK-RAP1A related risk signature. **(B, D)** Time-dependent ROC curves at 1, 3, and 5 years. AUC, area under the ROC; HCC, hepatocellular carcinoma; ROC, receiver-operating characteristic.

production" was enriched in the PGF, FLT3, and STMNI high-expression groups, respectively, which suggest that these hub gene sets were all closely involved in tumor proliferation (**Figures 8A–F**).

Correlation of the Signature With B7 Therapy-Related Molecule

Moreover, B7(CD80) served as specific markers for T cell gamma delta (VδT), respectively. As shown in **Figure 9A**, the hub genes of ANGPT2, FLT3, PGF, STMN1, RAP1A, and HSPA8 were significantly positively correlated with immune checkpoint B7 (CD80) in the TCGA database (p =1.41e-11 for ANGPT2, p <2.2e-16 for FLT3, p <2.2e-16 for PGF, p <1.9e-9 for STMN1, p <2.2e-16 for RAP1A, p =2.6e-15 for HSPA8) (**Figure 9A**). Subsequently, the relationships between the risk signature with MAPK-RAP1A signaling and the expression levels of B7 were found. The data here indicated that higher immune checkpoint gene of B7 may be significantly observed in high-risk patients (p = 0.012) (**Figure 9B**). Interestingly, the expression levels of PGF, STMN1, ANGPT2, FLT3, RAP1A, and HSPA8 were all significant positively correlated with B7 in HCC tissues (**Figure 9C**) (**Supplement Figure**). To further access the prognostic model between risk signature and B7 on patients' OS, a survival comparison was made among the four groups based on the combination of risk signature and immune checkpoint gene of B7. Comparison results revealed that HCC patients with risk signature and B7 in the predictive models are able to distinguish the overall survival (p <0.0001) (**Figure 9D**). Finally, the present study reveals relationships linking B7(CD80) and PDL1 in HCC tissues compared with adjacent tissues (**Figure 9E**).

DISCUSSION

In the current study, a novel network was developed that enabled the identification of the MAPK-RAP1A risk signature for the

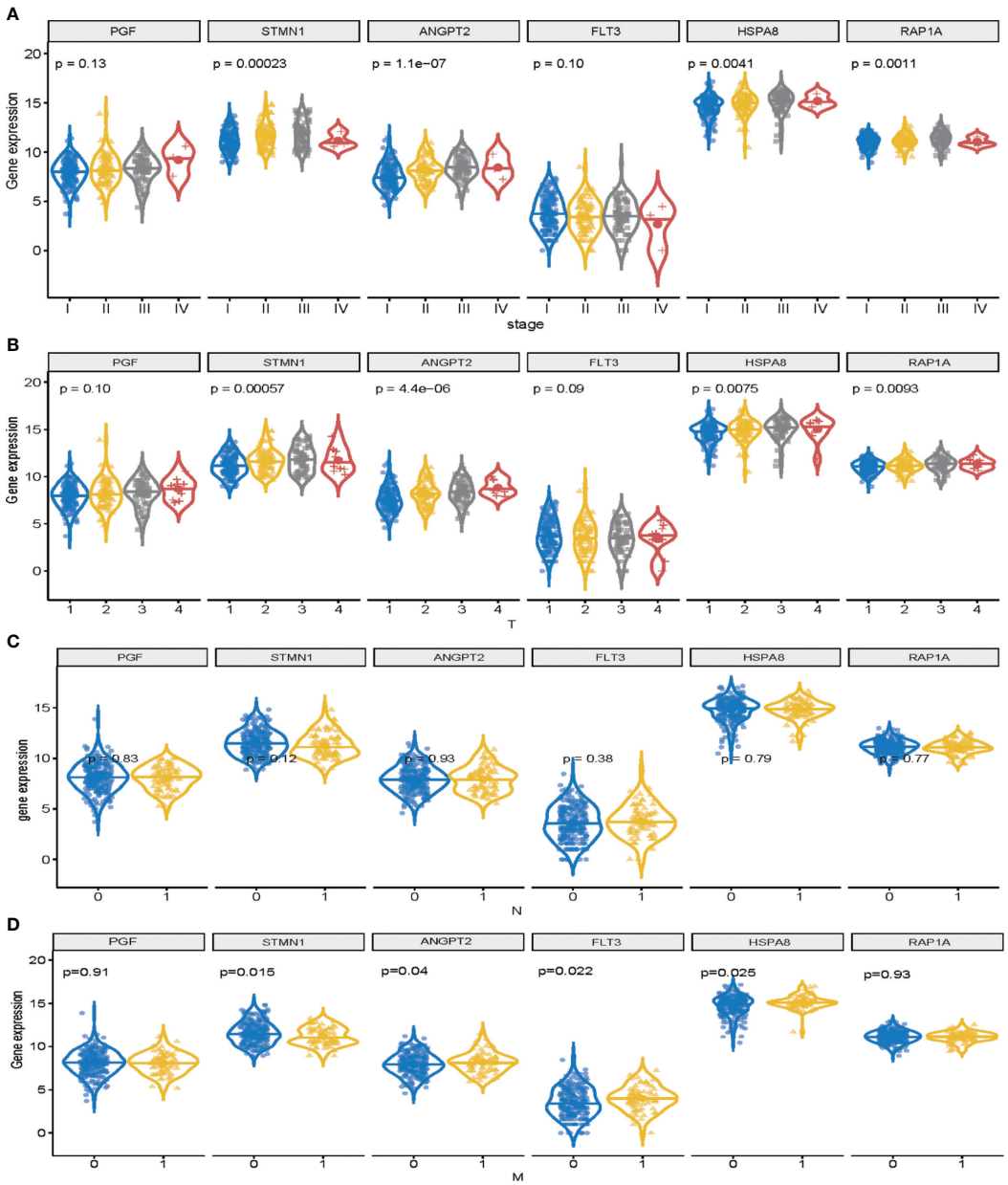


FIGURE 4 | Validation of signature genes in the MAPK-RAP1A dataset. **(A)** Expression of STMN1, FLT3, ANGPT2, HSPA8, RAP1A, and PGF in HCC samples with different TNM stages. **(B)** Expression of STMN1, FLT3, ANGPT2, HSPA8, RAP1A, and PGF in HCC samples with different T stages. **(C)** Expression of STMN1, FLT3, ANGPT2, HSPA8, RAP1A, and PGF in HCC samples with different N stages. **(D)** Expression of STMN1, FLT3, ANGPT2, HSPA8, RAP1A, and PGF in HCC samples with different M stages.

evaluation of clinical feature, and its clinical feature was associated with tumor-infiltrating immune cells (TICs). As expected, KEGG pathways were mostly concentrated on MAPK and RAP1A signaling. The reliable and effective MAPK-RAP1A risk signature accurately predicts the diagnosis of HCC patients. Computation analysis among TICs of MAPK-RAP1A risk signature, were preferentially observed in T cell gamma delta compared with other immune cells. Based on the analysis of TCGA and ICGC dataset, a risk signature was identified. The risk signature was composed of six signature genes which were screened out from 374 cases of HCC and 50 normal tissues. To characterize the results of the GSEA, the signature genes were associated with immune and inflammation mechanisms.

In order to further elucidate the role of the risk signatures in cancer, the association of the risk signature and clinical model

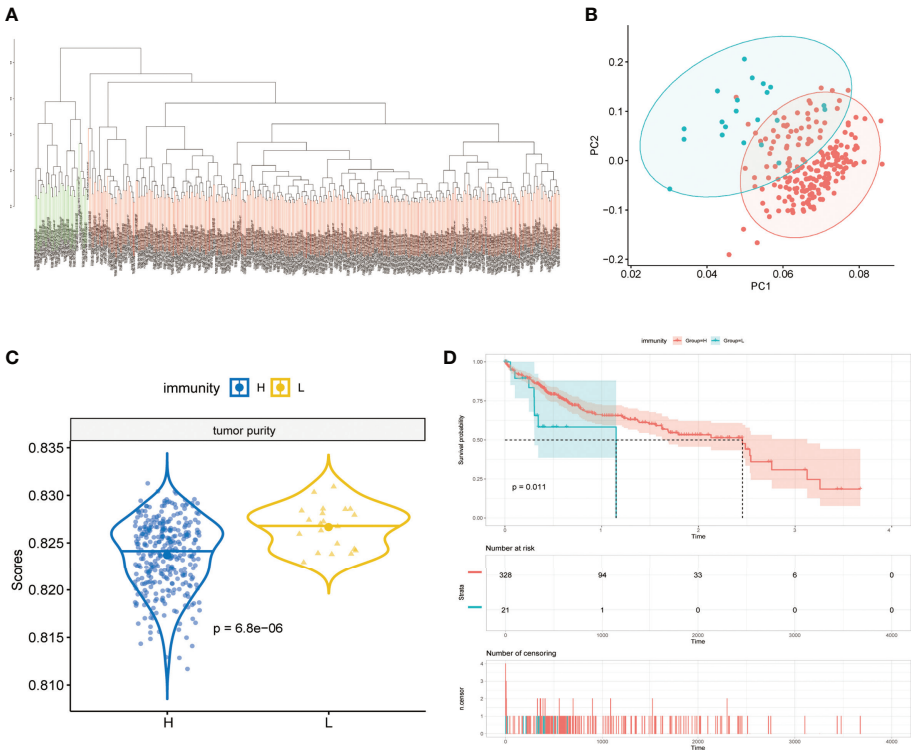


FIGURE 5 | Establishment of the MAPK-RAP1A with immunity in the TCGA database. **(A, B)** PCA based on MAPK-RAP1A gene signature between low-immunity group and high-immunity group. **(C)** Tumor purity in different immunity subgroups. **(D)** Kaplan–Meier curves of overall survival according to immunity groups in the training cohort.

was assessed. For example, a recent study indicated that the immune related nine-gene signature is involved in the status of tumor immune microenvironment (26). Another study also constructed a known lncRNAs prognostic signature for cancer and may aid in the field of tumor immunity and immunotherapy (27). Studies conducted so far concluded that investigating the prognostic value of tumor-infiltrating B lymphocytes lncRNA signature (TILBlncSig) in bladder cancer identified and validated biomarkers of immunotherapy response (28). However, these studies did not use the signaling pathway of samples to comprehensively explore the relationship between TICs and prognosis of HCC.

To probe the signaling events in HCC expression, this is the first study to reveal the relationships linking MAPK-RAP1A signaling pathway and TICs. We obtained a number of prognostic MAPK-RAP1A signature genes and established a novel patient prognosis and clinical feature model. Consistently, we have linked prognostic model to poor OS, which is consistent with other studies in HCC. Consequently, the MAPK-RAP1A related prognostic model provides a more reliable tool, which was a good prognostic factor with HCC. In addition, such model that consists of six signature genes was then successfully validated as a prognostic factor. Based on this overall hypothesis, we revealed that MAPK-RAP1A prognostic model could act as a more reliable tool for HCC prognosis prediction.

In addition, we identified MAPK-RAP1A signature genes (STMN1, RAP1A, FLT3, HSPA8, ANGPT2 and PGF) which were related with HCC worse clinical phenotype and prognosis. STMN1 is an oncogene that is a highly conserved cytosolic phosphoprotein, was found to be over-expressed in various types of cancer such as lung, breast, gastric cancer, and HCC. It plays an important role in cell differentiation, proliferation, drug resistance, and cancer stem cell properties and as an emerging target for tumor therapy (29). STMN1 regulated cancer-associated fibroblast (CAF) features through HSC by triggering the HGF/MET signaling pathway (30).

RAP1A is a small G protein that is similar to Ras oncogene and associated with different cellular processes. Other studies also showed that RAP1A may be a potential target for cell proliferation, adhesion, and invasion in different types of cancers (9, 31, 32). Recent clinical studies reported that RAP1A also correlated with the clinical characteristics of the advanced tumor stage in Oral Cavity Squamous Cell Carcinoma (OCSCC) (33). Another study showed that RAP1A disrupts aberrant tumor suppressor of EYA4 in HCC cells, which was associated with promoting growth and invasion (34).

FLT-3 belongs to the receptor tyrosine kinase family, which is encoded by the FLT3 gene. FLT3 has been found to control the function of normal and malignant hematopoiesis (34). Activating mutations of FLT3 associated with a poor prognosis in acute

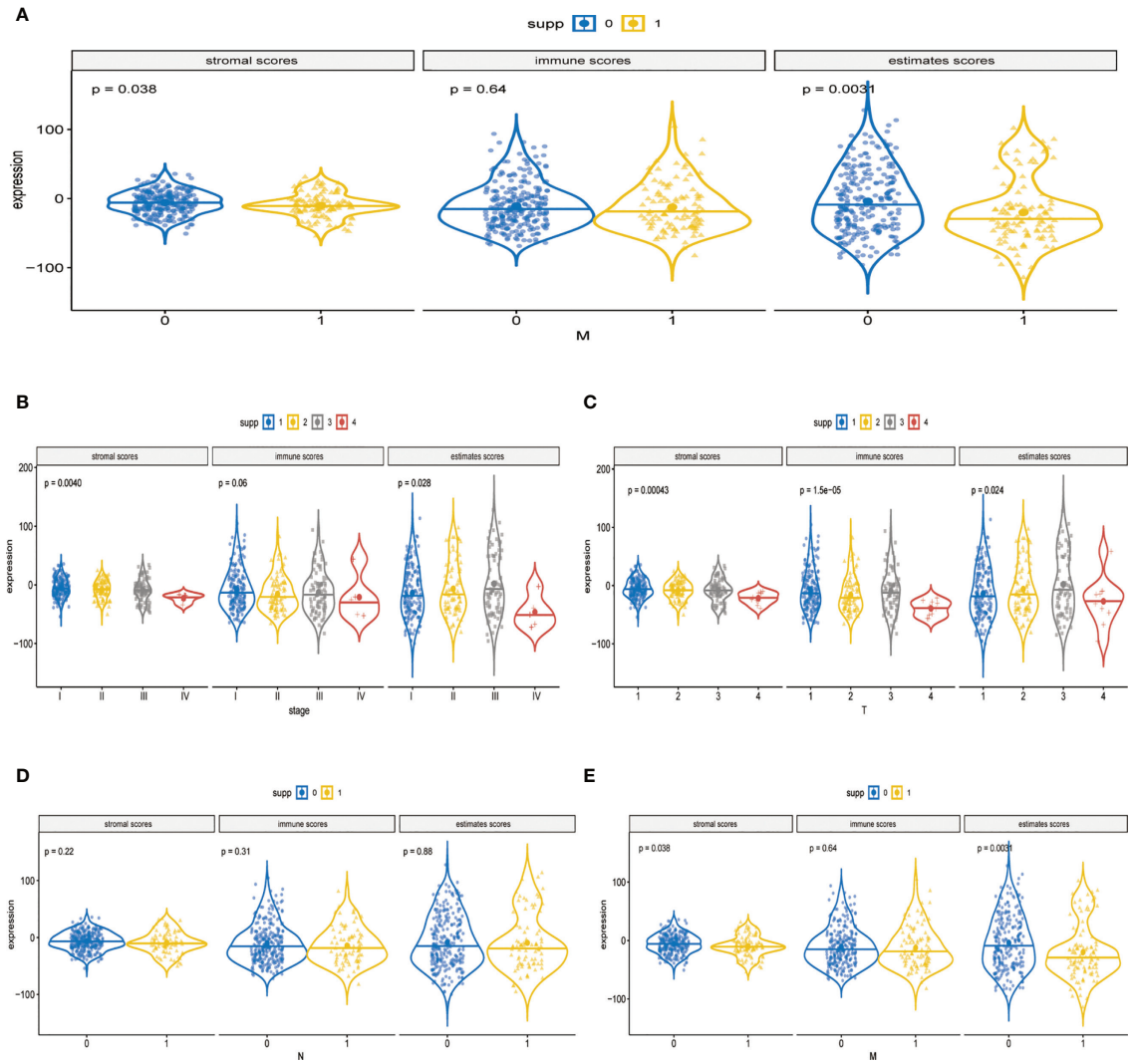


FIGURE 6 | Validation of immune estimate in the MAPK-RAP1A dataset. **(A)** The corresponding stromal score, immune score, and estimated score of MAPK-RAP1A gene signature between low-immunity group and high-immunity group. **(B)** Scores of stromal, immune, and ESTIMATE in HCC samples with different TNM stages. **(C)** Scores of stromal, immune, and ESTIMATE in HCC samples with different T stages. **(D)** Scores of stromal, immune, and ESTIMATE in HCC samples with different N stages. **(E)** Scores of stromal, immune, and ESTIMATE in HCC samples with different M stages.

myeloid leukemia (AML) and FLT3 inhibitors have an important role in high-risk patients (35). Targeting a tyrosine kinase receptor, sorafenib is now routinely required to provide therapy benefits in FLT3 of HCC patients (36, 37). Moreover, the association between patients treated with sorafenib and high FLT3 levels could be a novel predictor to improve OS in HCC patients (38).

The HSPA8 protein integrates compensatory mechanisms to drive cellular growth and is dysregulated in multiple chronic stress diseases, including cancer. Mechanistically, the molecular chaperone HSPA8, also known as Hsc70c, and directed to lysosomes, selectively degrades cellular proteins to sustain cellular homeostasis (39). The role of HSPA8 is expressed abnormally in early liver cancer, and its expression increases with cancer initiation and progression (40). So, HSPA8 detection may improve early detection of liver cancer sensitive indicators, but whether and how HSPA8 is involved in cancer initiation and development has been explored.

ANGPT2 is available in the extracellular signals that play a crucial role in angiogenesis and resistance to antiangiogenic therapy (41, 42). ANGPT2 is an angiogenic factor that binds Tie2 receptor and emerged as an attractive vascular drug target with the vascular endothelial growth factor (VEGF) pathway (43). Currently, ANGPT2 has been playing an important role in tumor angiogenesis and might confer resistance to sorafenib therapy (44–46). Furthermore, a study reveals that HCC cell secreted exosomal ANGPT2 was recycled by recipient HUVECs that suppressed the epithelial–mesenchymal transition (EMT) activation (47).

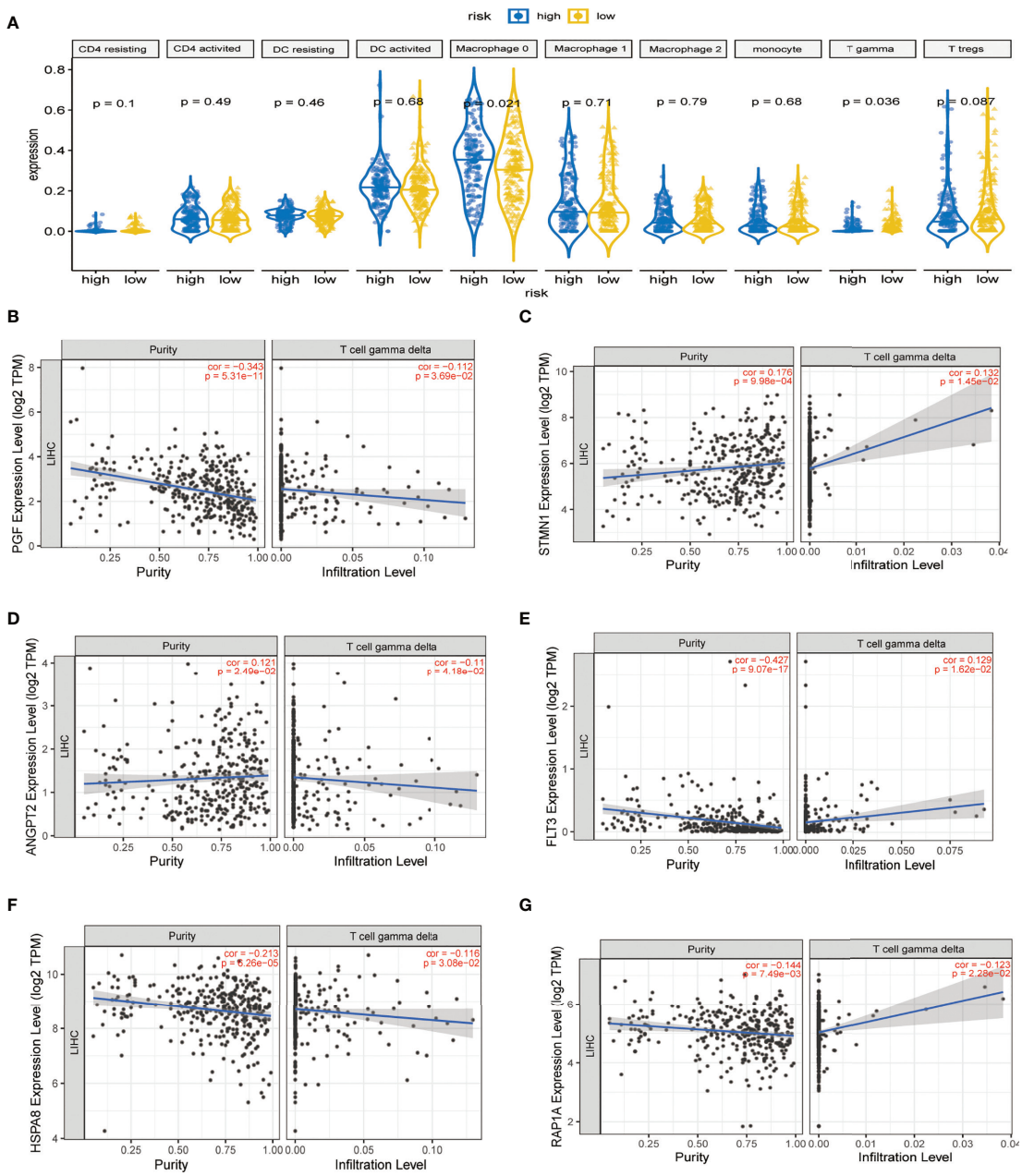


FIGURE 7 | Immune infiltration construction and validation in HCC. **(A)** Plot for comparison of the immune cell fraction difference between high risk and low risk. Fractions of each immune cell type were compared. Association of hub genes' expression with immune infiltration in HCC. **(B)** PGF **(C)** STMN1, **(D)** ANGPT2, **(E)** FLT3, **(F)** HSPA8, and **(G)** RAP1A. *P* <0.05 denotes significance. Each dot represents a sample in the TCGA-LIHC dataset.

Placenta growth factor (PGF), a member of the VEGF family, also plays an important role in the current anti-angiogenesis therapy. In this way, the present study has generated that patients with higher PGF had poorer response to chemotherapy and poorer prognosis and identified biomarkers in epithelial ovarian cancer (EOC) (48). PGF has been involved in elevated NF-kB signaling pathway in cervical cancer (49), but its role in HCC remains unclear.

To characterize the tumor-infiltrating immune cells' (TICs') status, the relationships between risk signature model and immune cell were analyzed by GSEA and CIBERSORT. The high abundance of TICs for risk signature may also affect clinical features and survival analysis. In addition, the data here indicated that higher infiltration levels of T cell gamma delta (Vδ T cells) were independent prognostic protective factors in HCC. Similar to previous reports (50, 51), our data confirmed that the infiltration

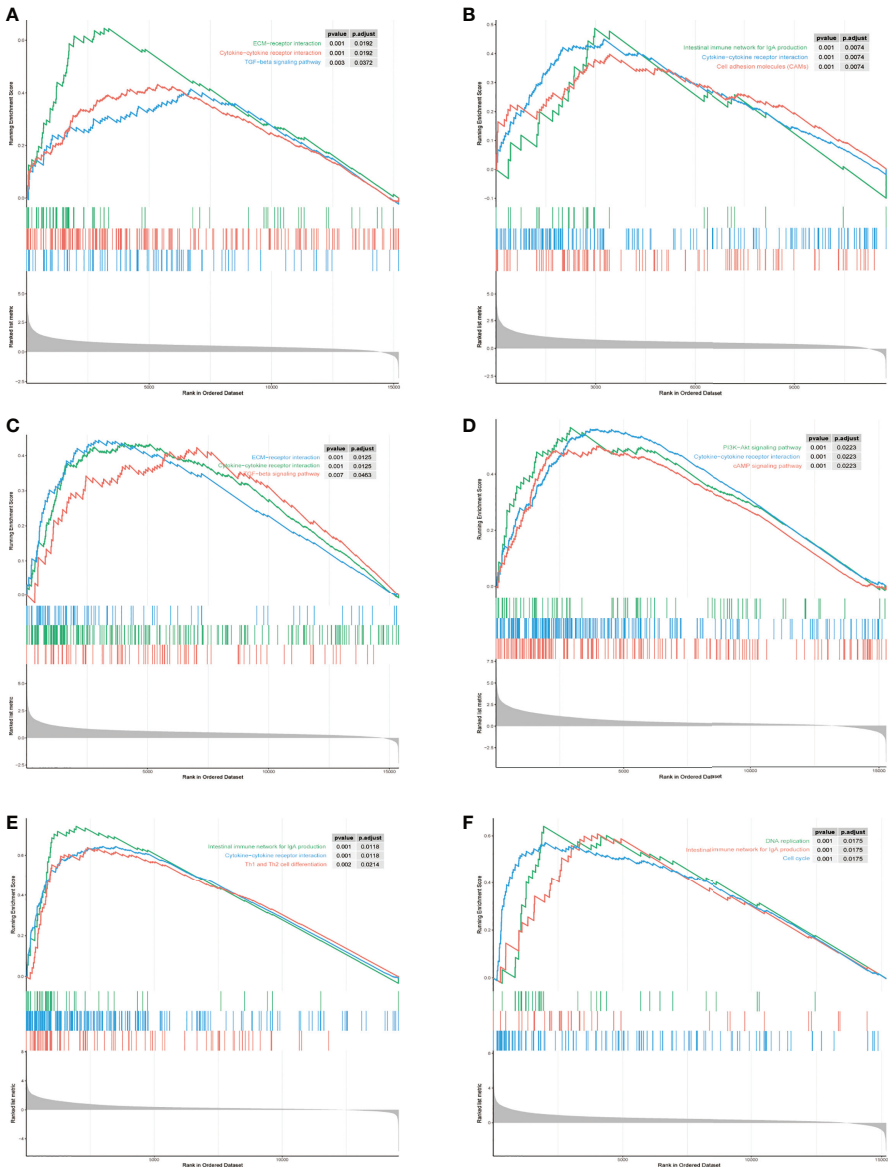


FIGURE 8 | Gene set enrichment analysis (GSEA) of hub genes in the TCGA-LIHC MAPK-RAP1A dataset. **(A–F)** Top three gene sets (according to GSEA enrichment score) enriched in the high-expression group of single hub genes. **(A)** PGF, **(B)** STMN1, **(C)** ANGPT2, **(D)** FLT3, **(E)** HSPA8, and **(F)** RAP1A.

of VδT cells was an independent prognostic factor. VδT cells play a critical role in the solid tumor microenvironment, but the effectiveness in killing various tumor cells present has been shown to be limited (50–52). Vδ2 T cells infiltrate several types of tumors, including the liver, and could serve as a prognostic factor (53). Activated Vδ2 T cells can exhibit the functions and characteristics of dendritic cells (54). On the one hand, Vδ2 T cells not only express the chemokine receptor CCR7 on the surface, but also upregulate the expression levels of MHCI and MHCII molecules, as well as co-stimulating molecules CD80 (B7) and CD86 (55).

In order to elucidate the role of the signature genes' biological functions, the association of STMN1, RAP1A, FLT3, HSPA8, ANGPT2, and PGF was positively associated with tumor purity in HCC. Based on the exploration from TIMER website, of the risk signature, six signature genes (STMN1, RAP1A, FLT3, HSPA8, ANGPT2, and PGF) were associated with infiltrating immune cells. Characterization of immune regulation by the GSEA indicated significantly different immune function among different expression groups classified by the hub gene. The results of GSEA were in accordance with this speculation. Also, many immune-related KEGG pathways, such as cytokine–cytokine receptor interaction, ECM–receptor interaction and TGF–beta signaling pathway, suggested a signature contribution to immunity regulation.

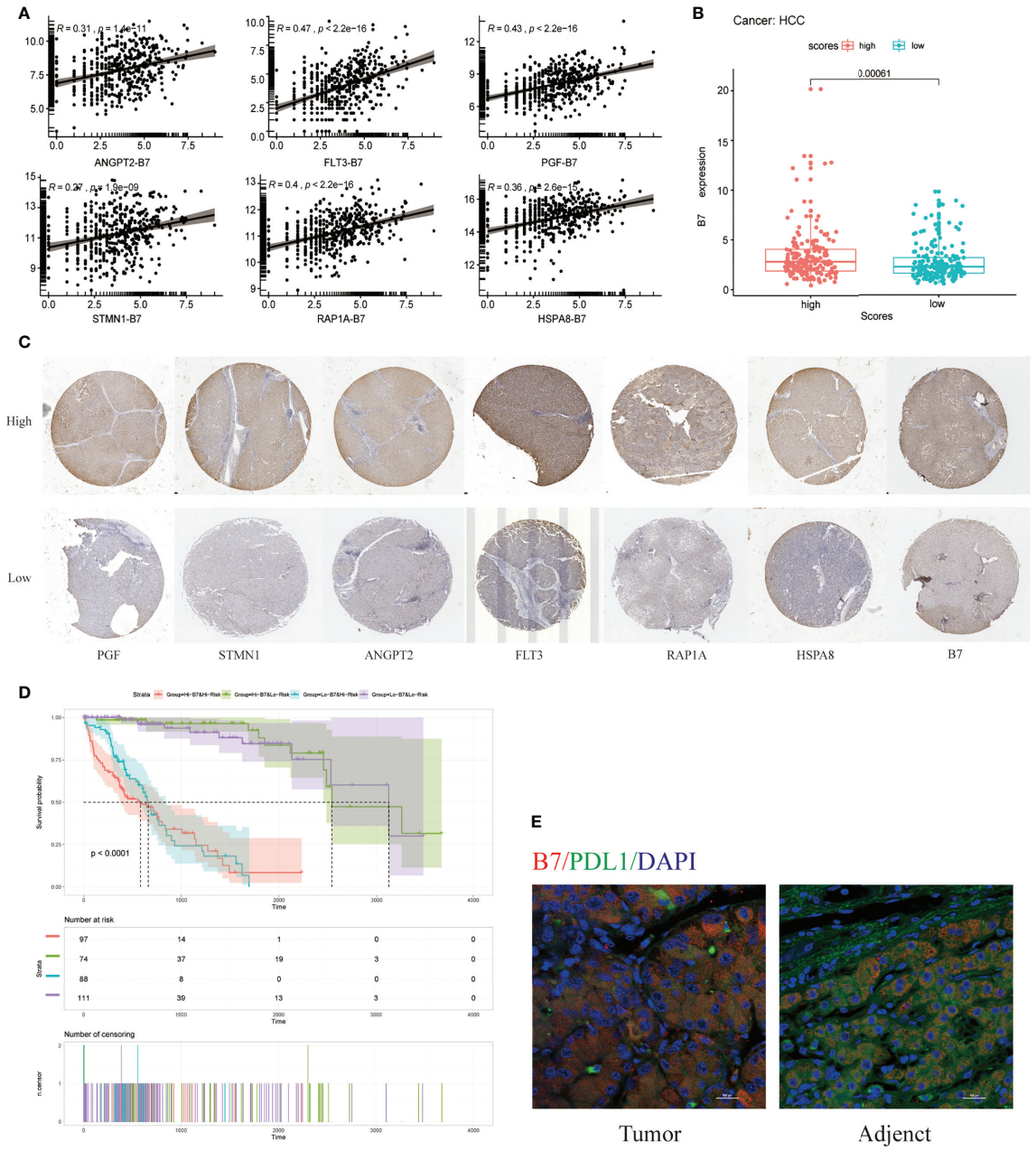


FIGURE 9 | Effect of the risk signature and immune checkpoint gene expression on patient survival. **(A)** Association between the risk signature and immune checkpoint gene expression. **(B)** Association between the hub gene and immune checkpoint gene expression. **(C)** Immunohistochemical staining was used to compare the expression of PGF, STMN1, ANGPT2, FLT3, RAP1A, HSPA8 with B7 in HCC tissues. **(D)** Kaplan–Meier survival curves of OS among patient groups stratified by the risk signature and immune checkpoint gene expression. **(E)** Association between B7 (CD80) and PDL1 in HCC tissues compared with adjacent tissues. Supplemental Figure Immunohistochemistry was used to detect the negative control, high and low expression of PGF, STMN1, ANGPT2, FLT3, RAP1A, HSPA8, and B7 in HCC tissues at high and low magnification.

In summary, taken together, all the above research suggested that the MAPK-RAP1A risk signature maybe a potential prognostic molecular marker for HCC patients. Furthermore, the predictive value of the risk signature was validated in available clinical information and RNAseq data. The MAPK-RAP1A risk signature was not only shown to have prognostic value for HCC patients but was also related to immune cell infiltration (T cell gamma delta) and the immunotherapy signature. The MAPK-RAP1A risk signature added significant predictive power to CD80 (B7) expression, which led to a

significant overall survival. Altogether, these results suggested that the risk signature could shed light on the mechanisms of immunotherapeutic targeting.

DATA AVAILABILITY STATEMENT

The datasets presented in this study can be found in online repositories. The names of the repository/repositories and accession number(s) can be found in the article/**Supplementary Material**.

ETHICS STATEMENT

The studies involving human participants were reviewed and approved by the research ethics committee of Hongqi Hospital Affiliated to Mudanjiang Medical University. The patients/participants provided their written informed consent to participate in this study. Written informed consent was obtained from the individual(s) for the publication of any potentially identifiable images or data included in this article.

AUTHOR CONTRIBUTIONS

HL, GH, XL, BL, and LW contributed to the bioinformatics analysis. BW and HJ performed the experiment. WW reviewed the article and provided comments. All authors contributed to the article and approved the submitted version.

SUPPLEMENTARY MATERIAL

The Supplementary Material for this article can be found online at: https://www.frontiersin.org/articles/10.3389/fonc.2021.649980/full#supplementary-material

REFERENCES

1. Llovet JM, Zucman-Rossi J, Pikarsky E, Sangro B, Schwartz M, Sherman M, et al. Hepatocellular Carcinoma. *Nat Rev Dis Primers* (2016) 2:16018. doi: 10.1038/nrdp.2016.18
2. Allemani C, Weir HK, Carreira H, Harewood R, Spika D, Wang XS, et al. Global Surveillance of Cancer Survival 1995-2009: Analysis of Individual Data for 25,676,887 Patients From 279 Population-Based Registries in 67 Countries (CONCORD-2). *Lancet* (2015) 385(9972):977–1010. doi: 10.1016/S0140-6736(14)62038-9
3. Joliat GR, Allemann P, Labgaa I, Demartines N, Halkic N. Treatment and Outcomes of Recurrent Hepatocellular Carcinomas. *Langenbecks Arch Surg* (2017) 402(5):737–44. doi: 10.1007/s00423-017-1582-9
4. Bruix J, Gores GJ, Mazzaferro V. Hepatocellular Carcinoma: Clinical Frontiers and Perspectives. *Gut* (2014) 63(5):844–55. doi: 10.1136/gutjnl-2013-306627
5. Lin DC, Mayakonda A, Dinh HQ, Huang P, Lin L, Liu X, et al. Genomic and Epigenomic Heterogeneity of Hepatocellular Carcinoma. *Cancer Res* (2017) 77(9):2255–65. doi: 10.1158/0008-5472.CAN-16-2822
6. Wagner ER, Nebreda AR. Signal Integration by JNK and P38 MAPK Pathways in Cancer Development. *Nat Rev Cancer* (2009) 9(8):537–49. doi: 10.1038/nrc2694
7. Nussinov R, Jang H, Zhang M, Tsai CJ, Sablina AA. The Mystery of Rap1 Suppression of Oncogenic Ras. *Trends Cancer* (2020) 6(5):369–79. doi: 10.1016/j.trecan.2020.02.002
8. Cowan KJ, Storey KB. Mitogen-Activated Protein Kinases: New Signaling Pathways Functioning in Cellular Responses to Environmental Stress. *J Exp Biol* (2003) 206(Pt 7):1107–15. doi: 10.1242/jeb.00220
9. Xiang J, Bian C, Wang H, Huang S, Wu D. MiR-203 Down-Regulates Rap1A and Suppresses Cell Proliferation, Adhesion and Invasion in Prostate Cancer. *J Exp Clin Cancer Res* (2015) 34:8. doi: 10.1186/s13046-015-0125-x
10. Anuja K, Kar M, Chowdhury AR, Shankar G, Padhi S, Roy S, et al. Role of Telomeric RAP1 in Radiation Sensitivity Modulation and its Interaction With CSC Marker KLF4 in Colorectal Cancer. *Int J Radiat Biol* (2020) 96(6):790–802. doi: 10.1080/09553002.2020.1721609
11. Gaonac'h-Lovejoy V, Boscher C, Delisle C, Gratton JP. Rap1 is Involved in Angiopoietin-1-Induced Cell-Cell Junction Stabilization and Endothelial Cell Sprouting. *Cells* (2020) 9(1):15. doi: 10.3390/cells9010155
12. Lu L, Wang J, Wu Y, Wan P, Yang G. Rap1A Promotes Ovarian Cancer Metastasis Via Activation of ERK/p38 and Notch Signaling. *Cancer Med* (2016) 5(12):3544–54. doi: 10.1002/cam4.946
13. Angell H, Galon J. From the Immune Contexture to the Immunoscore: The Role of Prognostic and Predictive Immune Markers in Cancer. *Curr Opin Immunol* (2013) 25(2):261–7. doi: 10.1016/j.coi.2013.03.004
14. Gentles AJ, Newman AM, Liu CL, Bratman SV, Feng W, Kim D, et al. The Prognostic Landscape of Genes and Infiltrating Immune Cells Across Human Cancers. *Nat Med* (2015) 21(8):938–45. doi: 10.1038/nm.3909
15. Grivennikov SI, Greten FR, Karin M. Immunity, Inflammation, and Cancer. *Cell* (2010) 140(6):883–99. doi: 10.1016/j.cell.2010.01.025
16. Shin MH, Kim J, Lim SA, Kim J, Lee KM. Current Insights Into Combination Therapies With MAPK Inhibitors and Immune Checkpoint Blockade. *Int J Mol Sci* (2020) 21(7):2531. doi: 10.3390/ijms21072531
17. Shen T, Huang Z, Shi C, Pu X, Xu X, Wu Z, et al. Pancreatic Cancer-Derived Exosomes Induce Apoptosis of T Lymphocytes Through the P38 MAPK-mediated Endoplasmic Reticulum Stress. *FASEB J* (2020) 34(6):8442–58. doi: 10.1096/fj.201902186R
18. Ye L, Zhang Q, Cheng Y, Chen X, Wang G, Shi M, et al. Tumor-Derived Exosomal HMGB1 Fosters Hepatocellular Carcinoma Immune Evasion by Promoting TIM-1(+) Regulatory B Cell Expansion. *J Immunother Cancer* (2018) 6(1):145. doi: 10.1186/s40425-018-0451-6
19. Xiong Y, Ye C, Yang N, Li M, Liu H. Ubc9 Binds to ADAP and Is Required for Rap1 Membrane Recruitment, Rac1 Activation, and Integrin-Mediated T Cell Adhesion. *J Immunol* (2017) 199(12):4142–54. doi: 10.4049/jimmunol.1700572
20. Tibshirani R. The Lasso Method for Variable Selection in the Cox Model. *Stat Med* (1997) 16(4):385–95. doi: 10.1002/(SICI)1097-0258(19970228)16:4<385::AID-SIM380>3.0.CO;2-3
21. Subramanian A, Tamayo P, Mootha VK, Mukherjee S, Ebert BL, Gillette MA, et al. Gene Set Enrichment Analysis: A Knowledge-Based Approach for Interpreting Genome-Wide Expression Profiles. *Proc Natl Acad Sci U S A* (2005) 102(43):15545–50. doi: 10.1073/pnas.0506580102
22. Newman AM, Liu CL, Green MR, Gentles AJ, Feng W, Xu Y, et al. Robust Enumeration of Cell Subsets From Tissue Expression Profiles. *Nat Methods* (2015) 12(5):453–7. doi: 10.1038/nmeth.3337
23. Li B, Severson E, Pignon JC, Zhao H, Li T, Novak J, et al. Comprehensive Analyses of Tumor Immunity: Implications for Cancer Immunotherapy. *Genome Biol* (2016) 17(1):174. doi: 10.1186/s13059-016-1028-7
24. Li T, Fan J, Wang B, Traugh N, Chen Q, Liu JS, et al. Timer: A Web Server for Comprehensive Analysis of Tumor-Infiltrating Immune Cells. *Cancer Res* (2017) 77(21):e108–10. doi: 10.1158/0008-5472.CAN-17-0307
25. Yu G, Wang LG, Han Y, He QY. clusterProfiler: An R Package for Comparing Biological Themes Among Gene Clusters. *OMICS* (2012) 16(5):284–7. doi: 10.1089/omi.2011.0118
26. Wang Z, Zhu J, Liu Y, Liu C, Wang W, Chen F, et al. Development and Validation of a Novel Immune-Related Prognostic Model in Hepatocellular Carcinoma. *J Transl Med* (2020) 18(1):67. doi: 10.1186/s12967-020-02255-6
27. Xu S, Wang Q, Kang Y, Liu J, Yin Y, Liu L, et al. Long Noncoding Rnas Control the Modulation of Immune Checkpoint Molecules in Cancer. *Cancer Immunol Res* (2020) 8(7):937–51. doi: 10.1158/2326-6066.CIR-19-0696
28. Zhou M, Zhang Z, Bao S, Hou P, Yan C, Su J, Sun J. Computational Recognition of lncRNA Signature of Tumor-Infiltrating B Lymphocytes

With Potential Implications in Prognosis and Immunotherapy of Bladder Cancer. *Brief Bioinform* (2020) 2020:bbaa047. doi: 10.1093/bib/bbaa047
29. Hsieh SY, Huang SF, Yu MC, Yeh TS, Chen TC, Lin YJ, et al. Stathmin1 Overexpression Associated With Polyploidy, Tumor-Cell Invasion, Early Recurrence, and Poor Prognosis in Human Hepatoma. *Mol Carcinog* (2010) 49(5):476–87. doi: 10.1002/mc.20627
30. Zhang R, Gao X, Zuo J, Hu B, Yang J, Zhao J, et al. STMN1 Upregulation Mediates Hepatocellular Carcinoma and Hepatic Stellate Cell Crosstalk to Aggravate Cancer by Triggering the MET Pathway. *Cancer Sci* (2020) 111 (2):406–17. doi: 10.1111/cas.14262
31. Sayyah J, Bartakova A, Nogal N, Quilliam LA, Stupack DG, Brown JH. The Ras-related Protein, Rap1A, Mediates Thrombin-Stimulated, Integrin-Dependent Glioblastoma Cell Proliferation and Tumor Growth. *J Biol Chem* (2014) 289(25):17689–98. doi: 10.1074/jbc.M113.536227
32. Chen CH, Chuang HC, Huang CC, Fang FM, Huang HY, Tsai HT, et al. Overexpression of Rap-1A Indicates a Poor Prognosis for Oral Cavity Squamous Cell Carcinoma and Promotes Tumor Cell Invasion Via Aurora-A Modulation. *Am J Pathol* (2013) 182(2):516–28. doi: 10.1016/j.ajpath.2012.10.023
33. Mo SJ, Hou X, Hao XY, Cai JP, Liu X, Chen W, et al. EYA4 Inhibits Hepatocellular Carcinoma Growth and Invasion by Suppressing NF-kappaB-dependent RAP1 Transactivation. *Cancer Commun (Lond)* (2018) 38(1):9. doi: 10.1186/s40880-018-0276-1
34. Stirewalt DL, Radich JP. The Role of FLT3 in Haematopoietic Malignancies. *Nat Rev Cancer* (2003) 3(9):650–65. doi: 10.1038/nrc1169
35. Perl AE. Availability of FLT3 Inhibitors: How do We Use Them? *Blood* (2019) 134(9):741–5. doi: 10.1182/blood.2019876821
36. Levis M. Midostaurin Approved for FLT3-mutated Aml. *Blood* (2017) 129 (26):3403–6. doi: 10.1182/blood-2017-05-782292
37. Daver N, Schlenk RF, Russell NH, Levis MJ. Targeting FLT3 Mutations in AML: Review of Current Knowledge and Evidence. *Leukemia* (2019) 33 (2):299–312. doi: 10.1038/s41375-018-0357-9
38. Sun W, Li SC, Xu L, Zhong W, Wang ZG, Pan CZ, et al. High FLT3 Levels May Predict Sorafenib Benefit in Hepatocellular Carcinoma. *Clin Cancer Res* (2020) 26(16):4302–12. doi: 10.1158/1078-0432.CCR-19-1858
39. Robert G, Jacquel A, Auberger P. Chaperone-Mediated Autophagy and Its Emerging Role in Hematological Malignancies. *Cells* (2019) 8(10):1260. doi: 10.3390/cells8101260
40. Xiang X, You XM, Li LQ. Expression of HSP90AA1/HSPA8 in Hepatocellular Carcinoma Patients With Depression. *Onco Targets Ther* (2018) 11:3013–23. doi: 10.2147/OTT.S159432
41. Valenzuela DM, Griffiths JA, Rojas J, Aldrich TH, Jones PF, Zhou H, et al. Angiopoietins 3 and 4: Diverging Gene Counterparts in Mice and Humans. *Proc Natl Acad Sci U S A* (1999) 96(5):1904–9. doi: 10.1073/pnas.96.5.1904
42. Maisonpierre PC, Suri C, Jones PF, Bartunkova S, Wiegand SJ, Radziejewski C, et al. Angiopoietin-2, a Natural Antagonist for Tie2 That Disrupts In Vivo Angiogenesis. *Science* (1997) 277(5322):55–60. doi: 10.1126/science.277.5322.55
43. Jayson GC, Kerbel R, Ellis LM, Harris AL. Antiangiogenic Therapy in Oncology: Current Status and Future Directions. *Lancet* (2016) 388 (10043):518–29. doi: 10.1016/S0140-6736(15)01088-0
44. Morse MA, Sun W, Kim R, He AR, Abada PB, Mynderse M, et al. The Role of Angiogenesis in Hepatocellular Carcinoma. *Clin Cancer Res* (2019) 25 (3):912–20. doi: 10.1158/1078-0432.CCR-18-1254
45. Marisi G, Petracci E, Raimondi F, Faloppi L, Foschi FG, Lauletta G, et al. ANGPT2 and NOS3 Polymorphisms and Clinical Outcome in Advanced Hepatocellular Carcinoma Patients Receiving Sorafenib. *Cancers (Basel)* (2019) 11(7):1023. doi: 10.3390/cancers11071023
46. Scholz A, Plate KH, Reiss Y. Angiopoietin-2: A Multifaceted Cytokine That Functions in Both Angiogenesis and Inflammation. *Ann N Y Acad Sci* (2015) 1347:45–51. doi: 10.1111/nyas.12726
47. Xie JY, Wei JX, Lv LH, Han QF, Yang WB, Li GL, et al. Angiopoietin-2 Induces Angiogenesis Via Exosomes in Human Hepatocellular Carcinoma. *Cell Commun Signal* (2020) 18(1):46. doi: 10.1186/s12964-020-00535-8
48. Meng Q, Duan P, Li L, Miao Y. Expression of Placenta Growth Factor is Associated With Unfavorable Prognosis of Advanced-Stage Serous Ovarian Cancer. *Tohoku J Exp Med* (2018) 244(4):291–6. doi: 10.1620/tjem.244.291
49. Tilborghs S, Corthouts J, Verhoeven Y, Arias D, Rolfo C, Trinh XB, et al The Role of Nuclear Factor-Kappa B Signaling in Human Cervical Cancer. *Crit Rev Oncol Hematol* (2017) 120:141–50. doi: 10.1016/j.critrevonc.2017.11.001
50. Gebhardt T, Mueller SN, Heath WR, Carbone FR. Peripheral Tissue Surveillance and Residency by Memory T Cells. *Trends Immunol* (2013) 34 (1):27–32. doi: 10.1016/j.it.2012.08.008
51. Chien YH, Meyer C, Bonneville M. Gammadelta T Cells: First Line of Defense and Beyond. *Annu Rev Immunol* (2014) 32:121–55. doi: 10.1146/annurev-immunol-032713-120216
52. Fisher J, Anderson J. Engineering Approaches in Human Gamma Delta T Cells for Cancer Immunotherapy. *Front Immunol* (2018) 9:1409. doi: 10.3389/fimmu.2018.01409
53. Lo Presti E, Pizzolato G, Corsale AM, Caccamo N, Sireci G, Dieli F, et al. Gammadelta T Cells and Tumor Microenvironment: From Immunosurveillance to Tumor Evasion. *Front Immunol* (2018) 9:1395. doi: 10.3389/fimmu.2018.01395
54. Willcox CR, Davey MS, Willcox BE. Development and Selection of the Human Vgamma9vdelta2(+) T-Cell Repertoire. *Front Immunol* (2018) 9:1501. doi: 10.3389/fimmu.2018.01501
55. Dar AA, Patil RS, Patil RS and Chiplunkar SV. Insights Into the Relationship Between Toll Like Receptors and Gamma Delta T Cell Responses. *Front Immunol* (2014) 5:366. doi: 10.3389/fimmu.2014.00366

Conflict of Interest: The authors declare that the research was conducted in the absence of any commercial or financial relationships that could be construed as a potential conflict of interest.

Copyright © 2021 Li, Han, Li, Li, Wu, Jin, Wu and Wang. This is an open-access article distributed under the terms of the Creative Commons Attribution License (CC BY). The use, distribution or reproduction in other forums is permitted, provided the original author(s) and the copyright owner(s) are credited and that the original publication in this journal is cited, in accordance with accepted academic practice. No use, distribution or reproduction is permitted which does not comply with these terms.

frontiers in Oncology

ORIGINAL RESEARCH
published: 21 June 2021
doi: 10.3389/fonc.2021.663778

PDE2 Inhibits PKA-Mediated Phosphorylation of TFAM to Promote Mitochondrial Ca^{2+}-Induced Colorectal Cancer Growth

Yilin Zhao[1,2†], Yaya Wang[3†], Jing Zhao[2†], Zhaohui Zhang[4], Mingpeng Jin[2], Feng Zhou[2,5], Chao Jin[4], Jing Zhang[6], Jinliang Xing[2], Nan Wang[4], Xianli He[4*] and Tingting Ren[6*]*

[1] Department of Clinical Oncology, Xijing Hospital, Fourth Military Medical University, Xi'an, China, [2] State Key Laboratory of Cancer Biology and Department of Physiology and Pathophysiology, Fourth Military Medical University, Xi'an, China, [3] College of Chemistry and Chemical Engineering, Xi'an University of Science and Technology, Xi'an, China, [4] Department of General Surgery, Tangdu Hospital, Fourth Military Medical University, Xi'an, China, [5] Department of General Surgery, Huaihai Hospital, Xuzhou Medical University, Xuzhou, China, [6] State Key Laboratory of Cancer Biology and Experimental Teaching Center of Basic Medicine, Fourth Military Medical University, Xi'an, China

Growing evidence indicates that the dysregulation of mitochondrial calcium (Ca^{2+}) plays a critical role in the growth of tumor cells, including colorectal cancer (CRC). However, the underling mechanism is not fully elucidated. In this study, the regulatory effects of mitochondrial Ca^{2+} on phosphodiesterase 2 (PDE2)/cAMP/PKA axis and the phosphorylation of mitochondrial transcription factor A (TFAM) as well as the growth of CRC cells were systematically investigated both *in vitro* and *in vivo*. Our findings demonstrated that MCU-induced mitochondrial Ca^{2+} uptake activated mitochondrial PDE2 in CRC cells. Moreover, overexpression MCU in CRC led to a 1.9-fold increase in Ca^{2+} uptake compared to control cells. However, knockdown of MCU resulted in 1.5-fould decrease in Ca^{2+} uptake in mitochondria compared to the controls. Activation of mitochondrial PDE2 significantly inhibited the activity of mitochondrial protein kinase A (PKA), which subsequently leads to decreased phosphorylation of TFAM. Our data further revealed that PKA regulates the phosphorylation of TFAM and promotes the degradation of phosphorylated TFAM. Thus, TFAM protein levels accumulated in mitochondria when the activity of PKA was inhibited. Overall, this study showed that the overexpression of MCU enhanced CRC growth through promoting the accumulation of TFAM proteins in mitochondria. Conversely, knockdown of MCU in CRC cells resulted in decreased CRC growth. Collectively, these data suggest that the mitochondrial Ca^{2+}-activated PDE2/cAMP/PKA axis plays a key role in regulating TFAM stability and the growth of CRC cells.

Keywords: mitochondrial Ca^{2+}, colorectal cancer, mitochondrial transcription factor A, mitochondrial calcium uniporter, phosphodiesterase 2

OPEN ACCESS

Edited by:
Ira Ida Skvortsova, Innsbruck Medical University, Austria

Reviewed by:
Harish Chinna Konda Chandramoorthy, King Khalid University, Saudi Arabia
Giulietta Di Benedetto, Neuroscience Institute (CNR), Italy

***Correspondence:**
Tingting Ren
rtt419@fummu.edu.cn
Xianli He
wanghe@fummu.edu.cn
Nan Wang
wangnandoc@163.com

†These authors contributed equally to this work

Specialty section:
This article was submitted to Molecular and Cellular Oncology, a section of the journal Frontiers in Oncology

Received: *03 February 2021*
Accepted: *26 April 2021*
Published: *21 June 2021*

Citation:
Zhao Y, Wang Y, Zhao J, Zhang Z, Jin M, Zhou F, Jin C, Zhang J, Xing J, Wang N, He X and Ren T (2021) PDE2 Inhibits PKA-Mediated Phosphorylation of TFAM to Promote Mitochondrial Ca^{2+}-Induced Colorectal Cancer Growth. Front. Oncol. 11:663778. doi: 10.3389/fonc.2021.663778

INTRODUCTION

Colorectal cancer (CRC) is one of the most deadly and commonly diagnosed cancers worldwide (1). Moreover, the incidence of CRC is steadily rising, especially in developing countries that are adopting the "western" way of life (1, 2). Although substantial progress has been achieved in the treatment of CRC, the mortality of CRC is still high. Therefore, the mechanism underlying the progression of CRC needs to be explored urgently.

Mitochondria harbor a Ca^{2+} buffering system and thus play a critical role in regulating intracellular calcium homeostasis (3). Over the past decade, a growing number of studies have shown that dysregulation of mitochondrial calcium homeostasis is closely linked with the progression of various types of cancers (4, 5). For example, our and other groups have demonstrated that mitochondrial calcium uniporter (MCU), a key mediator of mitochondrial Ca^{2+} uptake, is upregulated in several cancer cell types, including CRC (6), breast cancer (7), hepatocellular carcinoma (HCC) (8) and glioblastoma (GBM) (9). Moreover, a series of studies clearly indicate that the suppression of the mitochondrial Ca^{2+} uptake by the MCU inhibitor causes proliferation arrest, compromised migration, and cell death in several types of cancer cells (10, 11). Among them, our recent study has demonstrated that upregulated MCU enhances mitochondrial calcium uptake to promote mitochondrial biogenesis and colorectal cancer growth by suppressing phosphorylation of mitochondrial transcription factor A (TFAM) (6). However, the mechanism underlying the inhibition of TFAM phosphorylation by MCU-mediated mitochondrial Ca^{2+} uptake remains to be explored.

TFAM is a key regulator of mitochondrial DNA (mtDNA) replication and mitochondrial biogenesis (12). Altered mtDNA replication and mitochondrial biogenesis are closely associated with cancer cell proliferation and metastasis (13, 14). Thus, deregulation of TFAM has been implicated in various types of cancer, including CRC. For instance, TFAM is found to be aberrantly expressed in CRC cells and a high TFAM expression can serve as a useful marker for tumor progression in CRC patients (15). Because the fact that TFAM plays a significant role in carcinogenesis, the expression of TFAM is strictly controlled in cells. A study suggests that TFAM protein levels is regulated by phosphorylation (16). A detailed investigation revealed that TFAM is phosphorylated by cAMP-dependent protein kinase A (PKA) and that phosphorylated TFAM is degraded by Lon protease (16). Moreover, another study revealed that prune, localized in the mitochondrial matrix, is responsible for stabilizing TFAM by inhibiting the mitochondrial cAMP/PKA signaling pathway (17). A growing number of studies have indicated that PDE2, which is responsible for hydrolyzing the phosphodiester bond in the second messenger molecule cyclic adenosine monophosphate (cAMP) and cyclic guanosine monophosphate (cGMP), is instrumental for the growth and invasion of human malignant melanoma cells and osteosarcoma cells (18, 19). Although the significance of PDE2 in carcinogenesis has been investigated, the biological function of PDE2/cAMP/PKA axis-mediated TFAM stability in CRC growth remains to be explored.

In the present study, the regulatory effects of mitochondrial Ca^{2+} on mitochondrial PDE2/cAMP/PKA axis and the phosphorylation of TFAM, as well as the growth of colorectal cancer cells with MCU overexpression and knockdown were systematically investigated both *in vitro* and *in vivo*.

MATERIALS AND METHODS

Cell Line and Animal Model

The normal human colorectal epithelial cell line FHC and CRC cell lines T84, SW1116, LS174T, HCT116 and RKO were purchased from the American Type Culture Collection. Cells were cultured in RPMI-1640 medium or DMEM supplemented with 10% fetal bovine serum and 1% penicillin/streptomycin solution.

LS174T cells with MCU knockdown or MCU overexpression were injected into five-week-old male Balb/c nude mice (six per group) to generate *in vivo* subcutaneous xenograft models. Tumor volume was measured every three days for 30 days and mice were sacrificed to measure of the wet weight of the excised tumors. All animal experiments were performed in compliance with the policies of the Institutional Animal Care and Use Committee of the Fourth Military Medical University (Permission number: IACUC-20170105; date issued: 2017-01-01).

Antibodies and Reagents

The primary antibodies and their working concentrations used in this study are listed in **Supplementary Material Table 1.2.3**. The Mitochondria Fractionation Kit (Cat# C3601) was purchased from Beyotime (Biotechnology, China). PDE2 Activity Assay Kit (Cat# ab139460), PKA Kinase Activity Assay Kit (Cat# ab139435), cAMP Assay (Cat# ab65355) and ODQ (Cat# ab120022) were all purchased from Abcam (Abcam, United Kingdom). Go 6983 (Cas# 133053-19-7) inhibitor was from MCE (MCE, USA). The CellTiter 96® Aqueous One Solution Cell Proliferation Assay was purchased from Promega (Cat# G3581, Promega, USA) and 5-ethynyl-2'-deoxyuridine (EdU)-incorporation assay kit was purchased from Ribobio (Cat# C10310, Ribobio, China). Bay 60-7550 (Cat# HY-14992) and H89 (Cat# HY-15979) were purchased from Med Chemexpress (Med Chemexpress, USA).

Overexpression and Knockdown of Target Genes

To overexpress human MCU, PDE2A and TFAM proteins, the cDNA extracted from LS174T cells was used as a template to amplify the *MCU*, *PDE2A* and *TFAM* genes the primers listed in **Supplementary Material**. The PCR-amplified target genes were then cloned into the pcDNA™ 3.1 (+) vector (Invitrogen, USA). To generate shRNA expression vectors, a small hairpin RNA (shRNA) containing sequences targeting the human PDE2A, PKA or MCU was cloned into the pSilencer™ 3.1 puro vector

(Ambion, USA). The shRNA control vector was generated by cloning a control shRNA into the pSilencer™ 3.1 puro vector. Cells were transfected with siRNA and plasmids using Lipofectamine 2000 transfection reagent (Invitrogen, USA) following the protocols recommended by the manufacturer. The siRNA sequences were synthesized (GenePharma, China) and are listed in **Supplementary Material**.

Western Blot Analysis

Western blot experiments were carried out using the standard protocol described previously (20). Briefly, cells were lysed using RIPA buffer (Xi'an JingCai Biotechnology Company, China) with addition of protease and phosphatase inhibitors (Roche, Switzerland). The SDS-polyacrylamide gel was utilized to separate the target protein from the total proteins extracted from the lysed cells, followed by transferring the separated proteins to a PVDF membrane. The membrane was incubated with the primary antibody at 4°C overnight and then probed with a horseradish peroxidase-conjugated secondary antibody for 2h at room temperature. An enhanced chemiluminescence system was employed to detect the protein. Phosphorylated TFAM was detected using a previously described method (6). The band intensity in Western blot analyses was analyzed by Image J software (NIH, Bethesda, MD) and represented as the fold change of corresponding control value. The dilutions of antibodies are listed in **Supplementary Material**.

Preparation of Mitochondrial Subcompartments and Proteinase K Protection Assays

The Mitochondria Fractionation Kit for Cultured Cells (Beyotime Biotechnology Cat# ab139460, China) was employed to isolate the mitochondria mainly according to the manufactures' protocols. Firstly, 2×10^7 cells were collected and centrifuged at 1000× rcf for 5 min. Secondly, Mitochondria Isolation Reagents were used to isolate mitochondria according to the manufactures' protocols. All operations were performed on ice. Mitochondrial matrix was obtained by removing its outer membrane following the method reported previously (21). Briefly, isolated mitochondria were washed and suspended in STE containing 0.1% (w/v) fat-free BSA. The mitochondria were diluted with STE/BSA to a final concentration of 50 mg.ml-1 and stirred on ice. 0.5 ml of digitonin (6.25 mg.ml-1) was added dropwise over 2 min and the solution was kept on ice for a further 13 min. Three volumes of STE/BSA were added and the mixture was homogenized 4 times with a tight homogenizer. The mitochondria matrix fraction was collected by centrifugation for 10 min at 10,000 g.

The protease K protection assays were performed according to the method published previously (22). Briefly, 20μg/ml protease K (PK) were added into 20μg mitochondria protein for 20 minutes on ice. Then PK was inactivated with 2mM phenylmethanesulfonyl fluoride (PMSF) for min on ice. The mitochondria was solubilized with 1% Triton X-100 for 15 min on ice prior to PK treatment.

Drug Administration

Bay 60-7550 (Cat# HY-14992, Med Chemexpress, USA), a PDE2 specific inhibitor, was employed in this study. Bay 60-7550 was dissolved in 1% dimethyl sulfoxide (DMSO), freshly prepared before administration. Mice under diethyl ether anesthesia received a single dose of Bay 60-7550 (1mg/kg) through intraperitoneal injection. The Bay 60-7550 inhibitor was injected into mice every other day for 30 days.

Measurement of Mitochondrial Ca^{2+}

The amount of mitochondrial Ca^{2+} was measured following the experimental protocol described previously (6). In brief, the plasmid containing the mitochondrial matrix-targeted fluorescent tagged inverse pericam was used to transfect CRC cells. The cells were then visualized under a confocal laser scanning microscope FV1000 (Olympus Corporation, Japan). Histamine (10μM) was added to trigger mitochondrial Ca^{2+} uptake after 30 s of baseline recording. Confocal images were recorded every 10 s at 545 nm excitation. All instrument settings (laser power, confocal slit opening, spectral bandwidth pixel excitation time, and photomultiplier sensitivity) were identical with control cells using custom-made software.

Activity Assays of Mitochondrial PDE2 and PKA

The enzymatic activities of mitochondrial PDE2 and PKA were determined with the PDE2 Activity Assay Kit and PKA Kinase Activity Assay Kit (Abcam, United Kingdom), respectively, following the manufacturers' protocols. Briefly, cells were harvested in a 15 mL conical tube (1 x 10^7/mL). The cells were lysed with the reagent in the kit and subsequently the protein concentration was measured. Then the enzymatic activities of mitochondrial PDE2 and PKA were assayed using the reagent kit according to the manufacturers' protocols. All values were normalized to total cellular protein concentration.

Immunohistochemical (IHC) Staining

Immunohistochemical (IHC) experiments were carried out following the experimental procedure described previously (20). In brief, sections were deparaffinized and hydrated. Antigen was retrieved by treating with hot citrate buffer (pH = 6.0) under pressure. Then, sections were incubated with primary antibody overnight at 4°C. Color was developed using DAB substrate followed by hematoxylin counterstaining. The expression levels in terms of IHC score were independently assessed by two pathologists according to the intensity and percentage of positive cells.

Cell Viability and Cell Proliferation Assays

Cell viability and cell proliferation assays were carried out using the methods described methods (23). Briefly, the proliferation of CRC cells and non-cancerous colon cells were measured using the CellTiter 96® Aqueous One Solution Cell Proliferation Assay (Promega, USA) according to the manufacturers' instructions. CRC cells and non-cancerous colon cells were seeded with 2000

cells on a 96-well plate and incubated for 4 days. Cell proliferation was detected daily based on the absorbance at 490 nm. To assess cell proliferation, the 5-ethynyl-2'-deoxyuridine (EdU)-incorporation assay kit (Ribobio, China) was used according to manufactures' protocols.

Site-Directed Mutagenesis

Plasmid constructs expressing mutant TFAM proteins including $TFAM^{S55D}$ and $TFAM^{S55A}$, which are also referred to as pcDNA-$TFAM^{S55D}$ and pcDNA-$TFAM^{S55A}$, were generated previously in our lab (6).

Statistical Analysis

SPSS 17.0 software (SPSS. Inc., USA) was utilized to analyze the data. Values are shown as the mean ± SEM from three independent experiments, where appropriate. Student's t-test was employed to analyze significant differences between two groups or multiple groups. A *P-Value* <0.05 was considered statistically significant.

RESULTS

MCU-Mediated Mitochondrial Ca^{2+} Uptake Activates Mitochondrial PDE2 to Inhibit PKA Activity

To explore whether MCU-mediated mitochondrial Ca^{2+} uptake was involved in regulating the activity of mitochondrial PDE2 and PKA, MCU was overexpressed or knocked down in CRC cells. We first determined the expression level of MCU in one normal human colorectal epithelial cell line (FHC) and a series of CRC cell lines including T84, SW116, LS174T, HCT116 and RKO. The qRT-PCR and Western blot analysis revealed that the expression level of MCU is significantly higher in CRC cell lines compared to normal colorectal epithelial cell line (**Supplementary Material Figures 1A, B**). To further explore the biological functions of MCU in CRC cells, the expression of MCU was knocked down or over-expressed in LS174T cells which had relatively high levels of MCU expression. As shown in **Figures 1A, B**, successful knockdown and overexpression of mitochondrial MCU at both

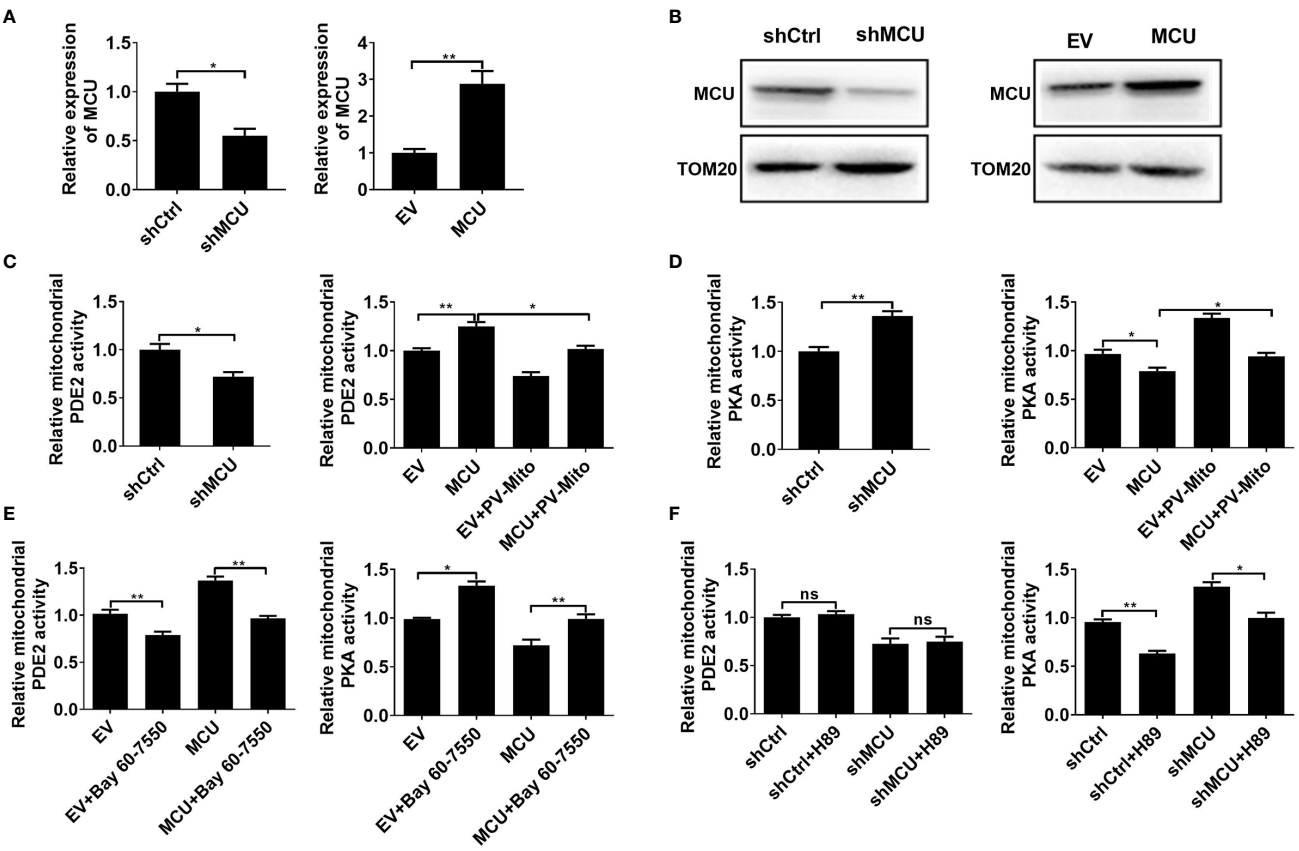


FIGURE 1 | MCU-mediated mitochondrial Ca2+ uptake activates mitochondrial PDE2 to inhibit mitochondrial PKA activity. **(A)** QRT-PCR analysis for the mRNA level in LS174T cells treated as indicated. **(B)** Western blot analysis of protein level of mitochondrial MCU in LS174T cells treated as indicated. **(C)** Relative mitochondrial PDE2 activity in LS174T cells treated as indicated. **(D)** Relative mitochondrial PKA activity in LS174T cells treated as indicated. **(E)** Relative activities of mitochondrial PDE2 and PKA in LS174T cells treated as indicated (Bay 60-7550, 4.7nM PDE2 inhibitor for 24h). **(F)** Relative activities of mitochondrial PDE2 and PKA in LS174T cells treated as indicated (H89, 1μM PKA inhibitor for 24h). MCU, expression vector encoding mitochondrial calcium uniporter; shCtrl, expression vector encoding control shRNA; shMCU, expression vector encoding shRNA against MCU; EV, empty vector; PV-Mito, expression vector encoding parvalbumin with mitochondria target sequence. *P < 0.05; **P < 0.01; ns, not significant.

mRNA and protein levels were confirmed. As expected, the data showed that the resting matrix Ca^{2+} level was lower in CRC cells with MCU knockdown compared to the controls, whereas the resting matrix Ca^{2+} level was remarkably higher in MCU-overexpressed CRC cells compared to the controls (**Supplementary Material Figure 1C**). Moreover, the overexpression of MCU in CRC cells markedly enhanced mitochondrial Ca^{2+} uptake, while knockdown of MCU decreased mitochondrial Ca^{2+} uptake (**Supplementary Material Figure 1D**). These two experimental groups showed statistically significant difference. Overexpression MCU in CRC led to a 1.9-fold increase in Ca^{2+} uptake compared to control cells. However, knockdown of MCU resulted in 1.5-fould decrease in Ca^{2+} uptake in mitochondria compared to the controls. Then mitochondria were isolated from MCU-overexpressing and MCU-knockdown CRC cells. The knockdown of MCU alone or in combination with PDE2 overexpression were confirmed by Western blot (**Figure S1E**). Moreover, the overexpression of MCU alone or in combination with PDE2 inhibition were validated by Western blot as well (**Figures S1F, G**).

Then the enzymatic activity of PDE2 and PKA in mitochondria was measured. As shown in **Figures 1C, D**, the knockdown of MCU resulted in decreased mitochondrial PDE2 activity and increased mitochondrial PKA activity in CRC cells compared with the control group. However, overexpression of MCU exhibited the opposite effect. The $[Ca^{2+}]_m$ buffering by PV-Mito significantly reversed the effects caused by MCU overexpression. Moreover, we found that the PDE2 inhibitor BAY60-7550 remarkably increased the activity of mitochondrial PKA by inhibiting PDE2 activity in CRC cells with or without MCU overexpression compared with the corresponding controls (**Figure 1E**). In contrast, the PKA inhibitor H89 only inhibited the activity of mitochondrial PKA, but had no effect on the activity of mitochondrial PDE2 in CRC cells (**Figure 1F**). These results indicate that MCU-mediated mitochondrial Ca^{2+} uptake increases the activity of mitochondrial PDE2 and subsequently inhibits the activity of mitochondrial PKA in CRC cells.

Due to the low expression of MCU in FHC cells, we measured the activity of PDE2 and PKA in a non-cancerous colon cell line FHC with MCU overexpression. We found that these results in FHC cells are similar to those obtained in CRC cells treated with MCU overexpression (**Supplementary Material Figures 2A–D**). Given that overexpression or down-regulation of MCU impinges on mitochondrial PDE2 activity. We measured the level of cAMP in isolated mitochondria from CRC cells with MCU overexpression and knockdown. Our data indicated that the knockdown of MCU resulted in an increase of the levels of cAMP in CRC cells compared with the control group, whereas the overexpression of MCU exhibited the opposite effect (**Supplementary Material Figure 2E**). Furthermore, we used the phospho-PKA substrate antibody to directly assess the mitochondrial PKA activity in the mitochondria isolated from CRC cells treated with MCU overexpression. The data showed that the phosphorylation level of PKA substrates was decreased in CRC cells with MCU overexpression. Conversely, the addition of PV-Mito and bay 60-7550 significantly decreased the phosphorylation level of PKA substrates (**Supplementary Material Figures 2F, G**).

Previous studies showed that PDE2 is a cGMP-activated PDE2, degrading both cGMP and cAMP (24). Moreover, it has been reported that Ca^{2+} can activate the soluble guanylate cyclase (sGC) through GCAP1(Guanylyl Cyclase Activator Protein 1) and GCAP2(Guanylyl Cyclase Activator Protein 2), and this, through cGMP production, could activate PDE2 (24). We used of siRNA of GCAP1 and inhibitors of sGC to verify this hypothesis. Western blot analysis showed that the protein level of PDE2A was not obviously changed when the expression of GCAP1 was inhibited in MCU-overexpressed CRC cells. However, the activity of PDE2 was significantly inhibited in CRC cells (**Supplementary Material Figures 3A, B**). Furthermore, it has been reported that PDE2 could also be activated by protein kinase C (PKC) (25). We tested this hypothesis by adding PKC inhibitor into CRC cells with MCU downregulation. Our data indicated that the addition of PKC inhibitor did not cause a change in mitochondrial PDE2 activity, suggesting that Ca^{2+} may regulate the activity of PDE2 through GCAP1 (**Supplementary Material Figures 3A, B**).

PDE2-Mediated Inhibition of PKA Activity Is Essential for Mitochondrial Ca^{2+} Induced Dephosphorylation of TFAM

Considering that our previous study demonstrated the regulation of mitochondrial Ca^{2+} in TFAM phosphorylation, which is essential for controlling TFAM stability (6), we examined whether the PDE2/cAMP/PKA axis is engaged in regulating TFAM phosphorylation in human CRC cells. Our data showed that the decreased protein level of TFAM and increased TFAM phosphorylation, which were mediated by MCU knockdown, were significantly reversed when the activity of PKA was suppressed by siRNA or a PKA inhibitor, H89 (**Figures 2A, B**). Furthermore, the protein level and phosphorylation level of TFAM shown in **Figures 2A**, **B** had been quantified using the ImageJ software (**Supplementary Material Figures 4A, B**). Our data suggested that phosphorylation of TFAM leads to its degradation, which is consistent with previous studies (6, 16). In the meantime, we also examined the activities of mitochondrial PKA and PDE2 in MCU knocked-down CRC cells with addition of siPKA or H89. We found that the activity of mitochondrial PKA was restored to normal in CRC cells treated with MCU knockdown in combination with siPKA or H89 (**Figures 2C, D**). Similar results were obtained when the phospho-PKA substrate antibody was used to determine the PKA activity (**Supplementary Material Figure 4C**). However, the activity of PDE2 displayed no remarkable change, irrespective of the change of PKA (**Figures 2C, D**).

Furthermore, the inhibition of PDE2 activity either by siRNA or a PDE2 inhibitor Bay 60-7550 notably restored the phosphorylation of TFAM and then resulted in downregulation of TFAM in MCU-overexpressing CRC cells compared with controls (**Figures 2E, F**). The protein expression level and phosphorylation level of TFAM shown in **Figures 2E**, **F** had been quantified using the ImageJ software (**Supplementary Material Figures 4D, E**). Overexpression of MCU in CRC cells led to an increase in the activity of mitochondrial PDE2, whereas the activity of mitochondrial PKA was decreased compared with the control group. Similar results were obtained when the phospho-PKA substrate antibody was used to determine the

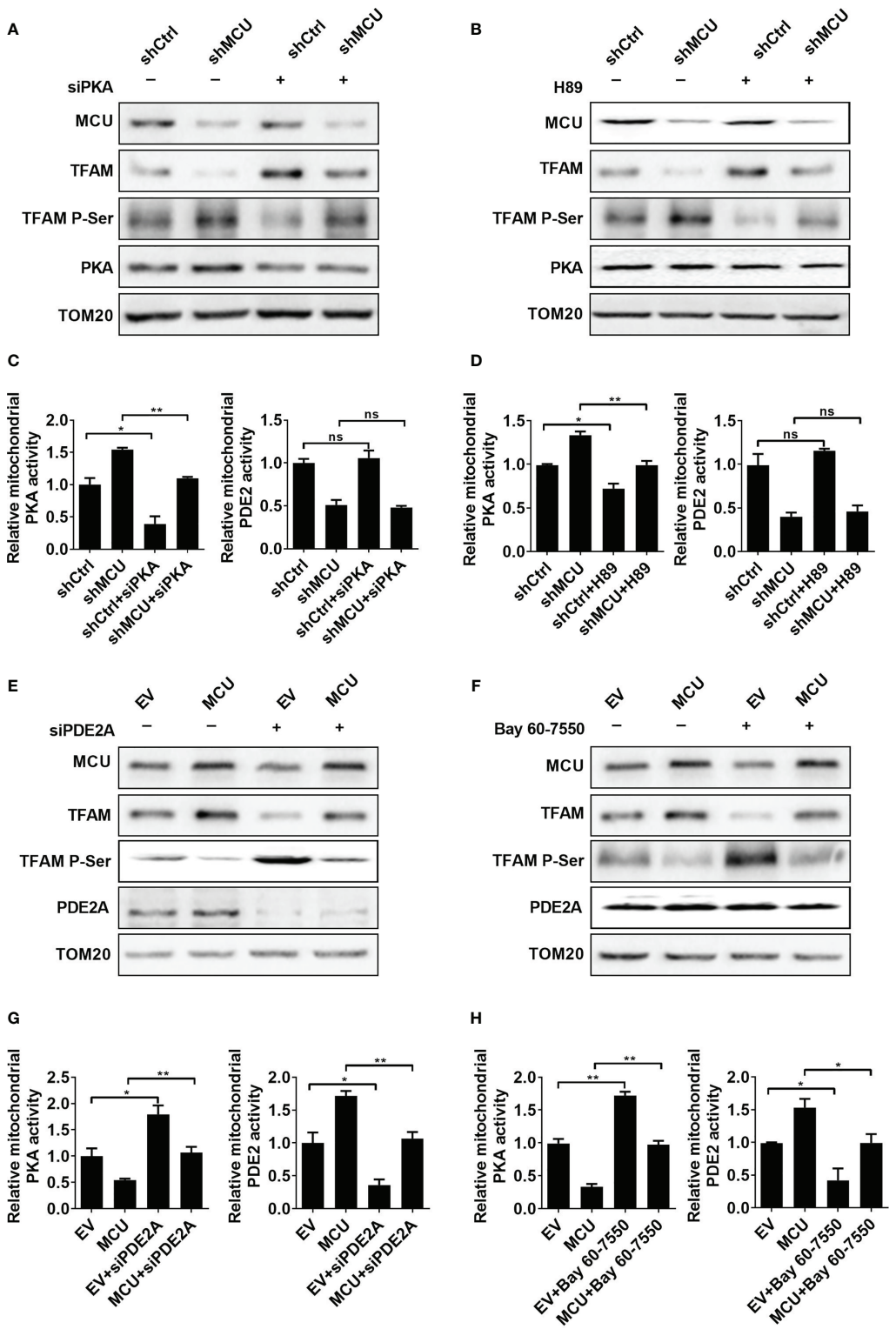


FIGURE 2 | PDE2-mediated inhibition of PKA activity is essential for mitochondrial Ca2+ induced dephosphorylation of TFAM. **(A, B)** Western blot analysis for protein levels of mitochondrial MCU and PKA, TFAM and phosphorylated TFAM in LS174T cells treated as indicated. siPKA: siRNA against PKA. PKA inhibitor H89 (1 μM) was used. **(C, D)** Relative activities of mitochondrial PDE2 and PKA in LS174T cells treated as indicated. **(E, F)** Western blot analysis for protein levels of mitochondrial MCU, PDE2, TFAM and phosphorylated TFAM in LS174 cells treated as indicated. **(G, H)** Relative activities of mitochondrial PDE2 and PKA in LS174T cells treated as indicated. siPDE2A: siRNA against PDE2A. PDE2 inhibitor Bay 60-7550 (4.7 nM) was used. *P < 0.05; **P < 0.01; ns, not significant.

PKA activity (**Supplementary Material Figure 4F**). However, the addition of siPDE2A or Bay 60-7550 significantly reversed the effect caused by MCU overexpression in CRC cells (**Figures 2G, H**). Additionally, we determined the phosphorylation of TFAM in CRC cells treated with siPKA in combination with siPDE2A. Our data indicated that TFAM phosphorylation is dependent on PKA (**Supplementary Material Figure 4G**).

The mitochondrial outer membrane was removed from the isolated mitochondria and then the matrix proteins were examined by Western blot experiments to detect the expression of the PDE2A and PKA. Our data demonstrated the presence of PDE2A and PKA in mitochondrial matrix (**Supplementary Material Figure 4H**). Collectively, these findings provide supporting evidence that the PDE2/cAMP/PKA axis participates in MCU-mediated regulation of TFAM phosphorylation in CRC cells.

Activation of PDE2 Is Essential for Mitochondrial Ca^{2+}-Mediated CRC Cell Growth

To explore the functional roles of PDE2-mediated decrease of TFAM phosphorylation in CRC cell growth, we first examined the effect of PDE2 activity on CRC growth *in vitro*. As shown in **Figures 3A, B**, the overexpression of PDE2 significantly promoted cell proliferation and increased the percentage of EDU-positive cells compared with the corresponding controls. In addition, the overexpression of PDE2 notably reversed the effect of MCU knockdown in CRC cells (**Figures 3A, B**). Consistently, inhibition of PDE2 activity by siRNA or inhibitor Bay 60-7550 significantly suppressed cell proliferation and decreased the percentage of EDU-positive cells (**Figures 3C–F**). Moreover, the inhibition of PDE2 activity clearly reversed the effect of MCU overexpression in CRC cells (**Figures 3C–F**). Meanwhile, we also explored the functional roles of PDE2-mediated decrease of TFAM phosphorylation in non-cancerous colon cell growth. The results showed that cell viability and cell proliferation were enhanced in normal human colorectal epithelial cells with MCU overexpression. In addition, inhibition of PDE2 activity by siPDE2A or PDE2 inhibitor significantly suppressed cell viability and decreased the percentage of EDU-positive cells in FHC cells (**Supplementary Material Figures 5A–D**).

We further investigated the physiological role of PDE2-mediated decrease of TFAM phosphorylation in CRC growth *in vivo*. the xenograft nude mice models were established with CRC

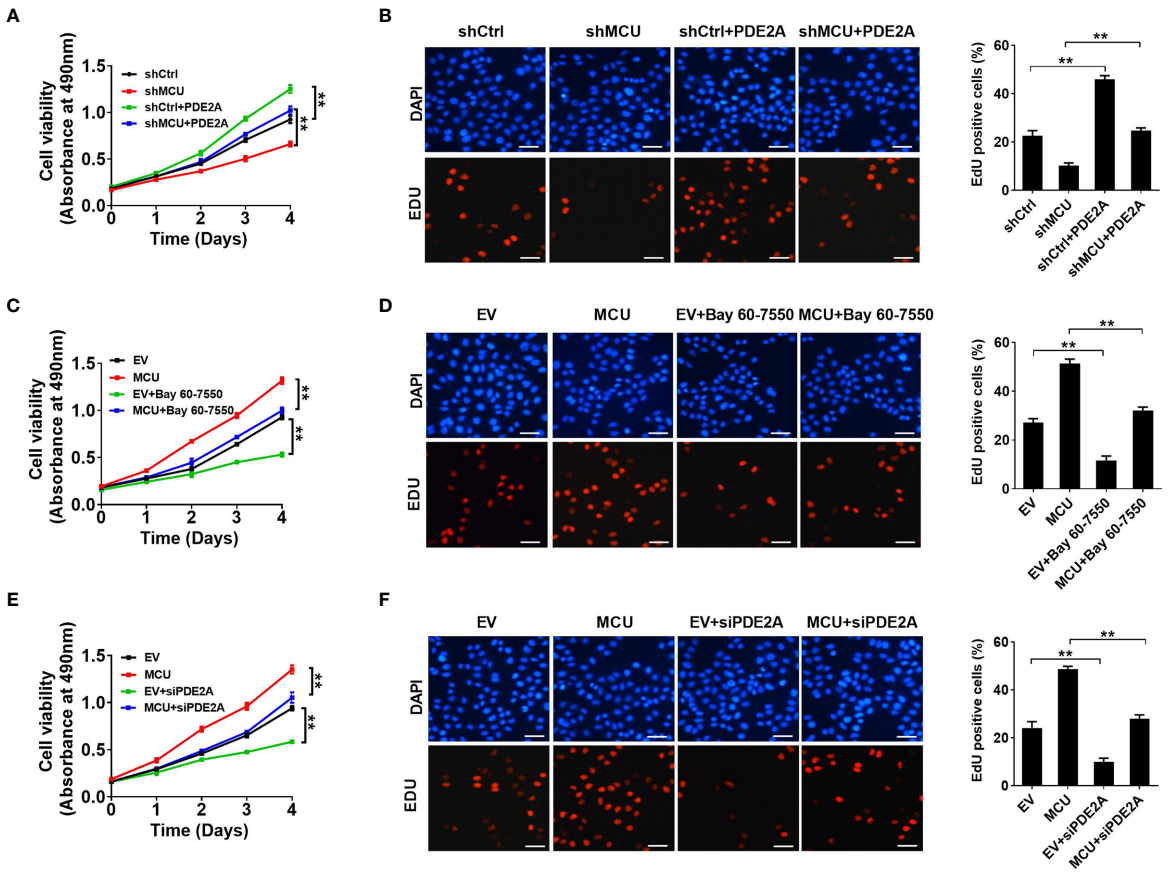


FIGURE 3 | Activation of PDE2 is essential for mitochondrial Ca2+-mediated CRC cell proliferation *in vitro*. **(A, C, E)** MTS assay for cell viability and **(B, D, F)** EdU incorporation assays for cell proliferation in LS174T cells with treatments as indicated (scale bar, 20 μm). PDE2A, expression vector encoding PDE2A; siPDE2A, siRNA against PDE2A. **P < 0.01.

cells. Our data showed that treatment with the PDE2 inhibitor Bay 60-7550 markedly suppressed the growth of CRC xenografts and clearly reversed the effect of MCU overexpression on CRC growth (**Figures 4A, B**). Consistently, IHC analysis indicated that CRC xenograft treated with Bay 60-7550 had a lower percentage of Ki67-positive cells compared with the corresponding controls (**Figures 4C, D**). Collectively, these findings indicate that PDE2 harbors a vital role in mitochondrial Ca^{2+}-regulated CRC growth both *in vitro* and *in vivo*.

Decreased Phosphorylation of TFAM Is Involved in Mitochondrial Ca^{2+}-Mediated CRC Growth

We then sought to explore the effect of TFAM and its phosphorylation on MCU-regulated CRC growth *in vitro* and *in vivo*. As shown in **Figures 5A–D**, TFAM overexpression promoted cell proliferation and increased the rate of EDU-positive cells in CRC cells compared with the corresponding controls. A previous study revealed that TFAM was phosphorylated at serine-55 (23). Thus, the mutation of serine-55 to alanine ($TFAM^{S55A}$) abolished its PKA-dependent phosphorylation, whereas the mutation of serine-55 to aspartic acid ($TFAM^{S55D}$) mimics the sustained phosphorylation of TFAM (26). Furthermore, we found that the overexpression of $TFAM^{S55D}$ resulted in a lower cell proliferation and EDU-positive cell percentage in CRC cells compared with cells overexpressed with wild type (WT) TFAM. On the contrary, the overexpression of $TFAM^{S55A}$, which inhibits TFAM phosphorylation, exhibited the opposite effect on cell growth in CRC cells (**Figures 5A–D**). Consistent with the *in vitro* experiments, similar results were obtained in *in vivo* CRC xenograft nude mice models (**Figures 6A–D**). These data implied that TFAM overexpression resulted in a faster growth and higher percentage of Ki67-positive cells in CRC xenografts compared with the corresponding controls. Conversely, we found that the overexpression of $TFAM^{S55D}$ led to a slower growth and lower Ki67-positive cell percentage in CRC xenografts than in those overexpressing WT TFAM. Moreover, the overexpression of $TFAM^{S55A}$ exhibited the opposite effect (**Figures 6A–D**). To sum up, these data support the notion that TFAM phosphorylation plays a vital role in MCU-regulated CRC growth.

DISCUSSION

In this study, our results demonstrated that MCU-induced mitochondrial Ca^{2+} uptake significantly enhanced the activity

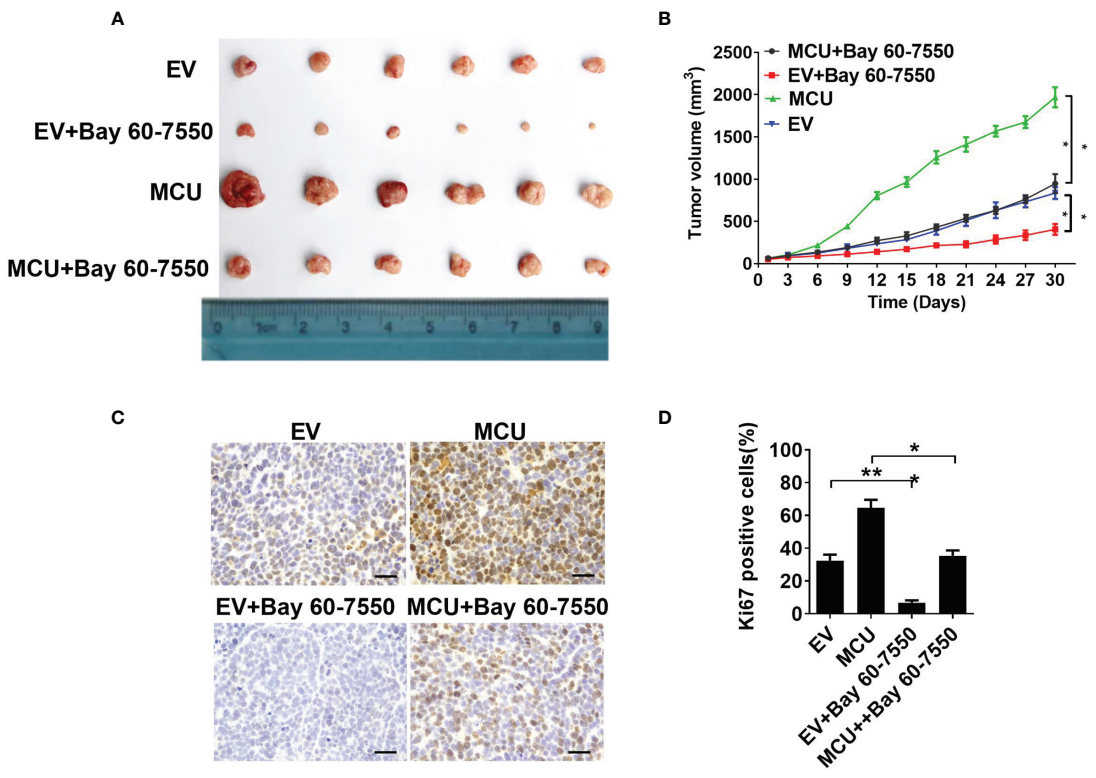


FIGURE 4 | Activation of PDE2 is essential for mitochondrial Ca2+-mediated CRC cell proliferation *in vivo*. **(A)** Dissected tumors from sacrificed mice and **(B)** tumor growth curves of subcutaneous xenograft tumor developed from LS174T cells with treatments as indicated. **(C)** Representative IHC staining images of Ki67 and **(D)** percentage of Ki67-positive cells in xenograft tumor developed from LS174T cells with treatments as indicated (scale bar, 50 μm). *P < 0.05; **P < 0.01.

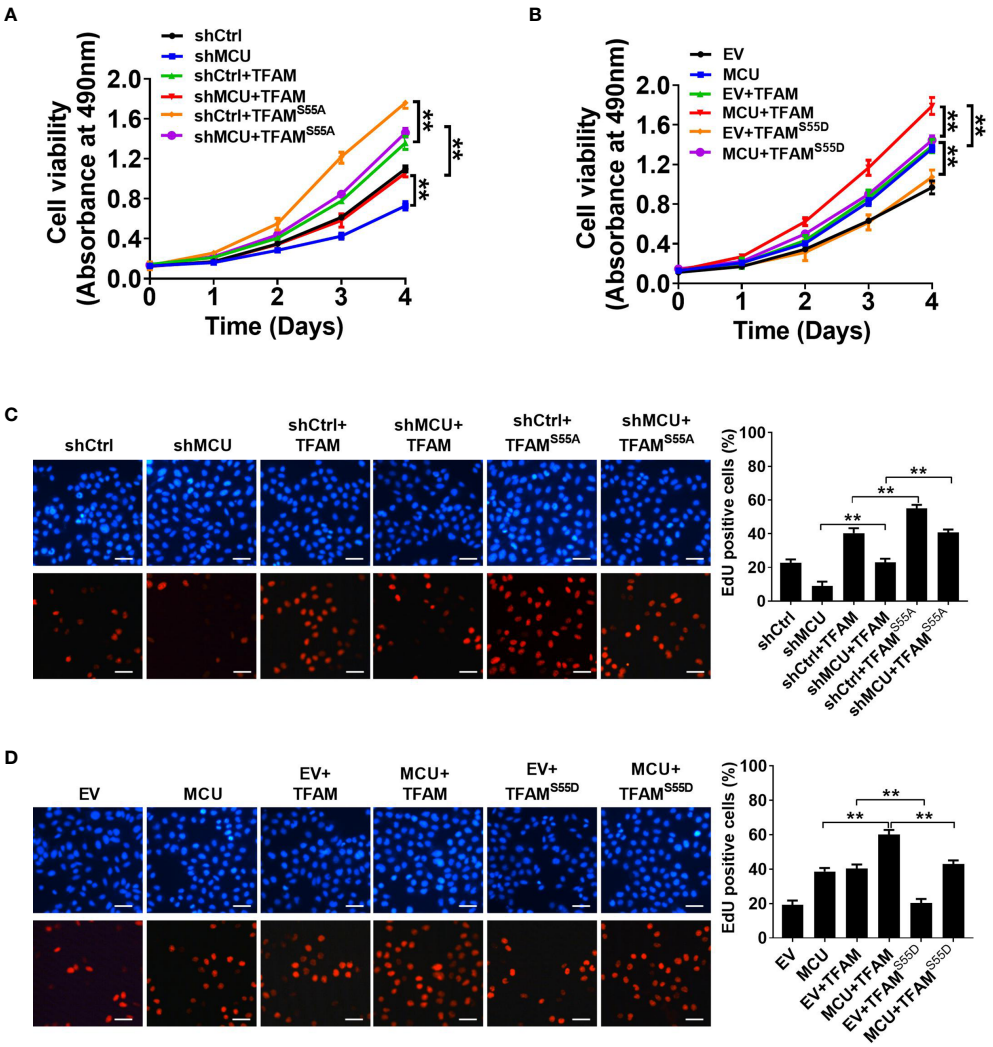


FIGURE 5 | Decreased phosphorylation of TFAM is involved in mitochondrial Ca2+-mediated CRC growth *in vitro*. **(A, B)** MTS assay for cell viability and **(C, D)** EdU incorporation assays for cell proliferation in LS174T cells with treatments as indicated (scale bar, 20 μm). **P < 0.01.

of the mitochondrial PDE2/cAMP/PKA axis, which subsequently led to decreased phosphorylation of TFAM and thus accumulation of TFAM. Consistently, a previous study demonstrated that a phosphodiesterase prune, a cAMP-degrading enzyme, stabilizes TFAM to promote mtDNA replication by inhibiting mitochondrial cAMP/PKA signaling (17). Moreover, our results indicated that both PDE2 and TFAM play critical roles in mitochondrial Ca^{2+}-induced CRC growth.

It has been well established that Ca^{2+} is critical for activating several family members of PDEs. For instance, studies have shown that the enzymatic activity of PDE1 and the localization of PDE4 are mediated by an increase in $[Ca^{2+}]_i$ (27, 28). Our findings establish that MCU-mediated Ca^{2+} uptake plays essential roles in regulating mitochondrial PDE2, which is known to possess dual substrate specificity for cAMP and cGMP (29). Thus, PDEs are considered to play vital roles in modulating the cross-talk between cAMP and Ca^{2+} signaling (27). Moreover, it has been suggested that cAMP harbors a significant role in activating PKA, which in turn regulates diverse physiological processes (30, 31).

Further investigation revealed that activation of the PDE2/cAMP/PKA axis by Ca^{2+} possesses a key role in regulating the stability of TFAM. Our data imply that downregulation of mitochondrial PKA activity mediated by mitochondrial PDE2 resulted in a decrease in the phosphorylation of TFAM, which then leads to accumulation of TFAM protein in mitochondria. These findings are consistent with a previous report, which suggests that PKA-mediated TFAM phosphorylation is crucial for the stability of TFAM (16). The overexpression and/or knockdown of mitochondrial MCU, TFAM, $TFAM^{S55A}$ and $TFAM^{S55D}$ in LS174T cells were confirmed

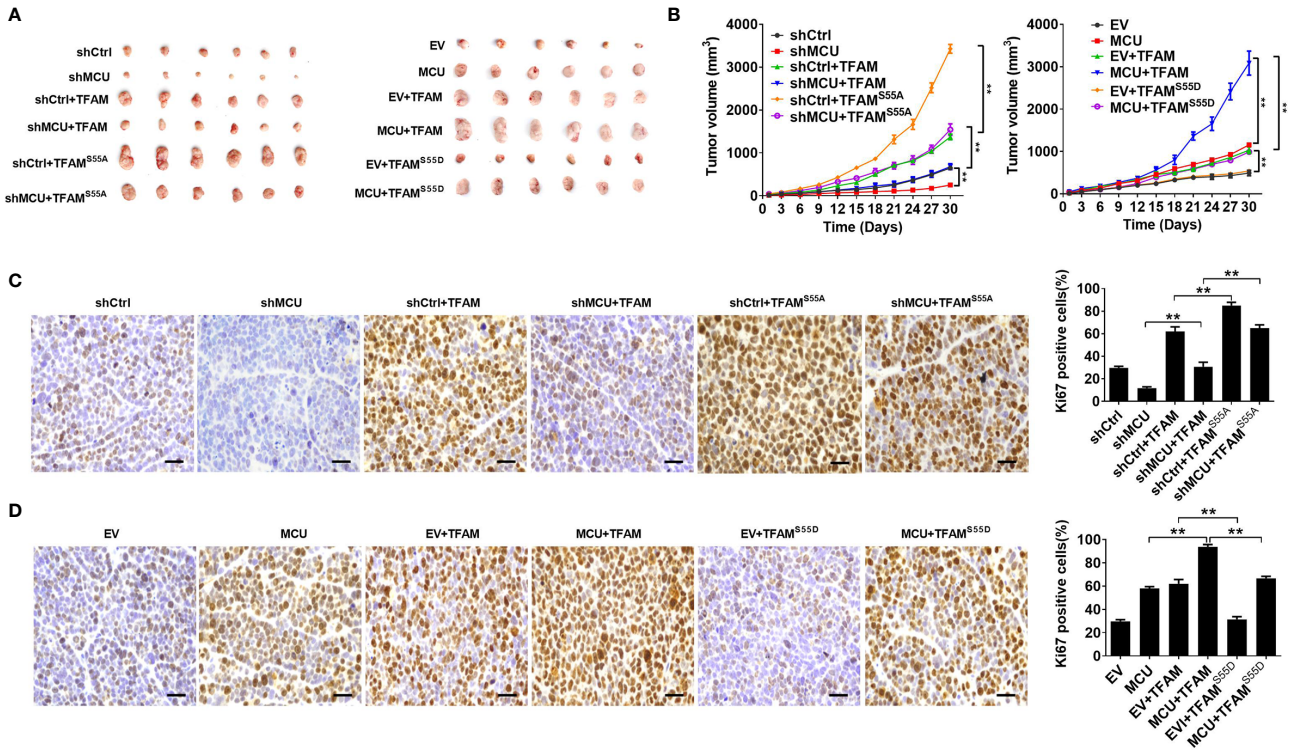


FIGURE 6 | Decreased phosphorylation of TFAM is involved in mitochondrial Ca2+-mediated CRC growth *in vivo*. **(A)** Dissected tumors from sacrificed mice and **(B)** tumor growth curves of subcutaneous xenograft tumor developed from LS174T cells with treatments as indicated. **(C, D)** Representative IHC staining images of Ki67 and (shMCU and MCU group) percentage of Ki67-positive cells in xenograft tumor developed from LS174T cells with treatments as indicated (scale bar, 50 μm). ** $P < 0.01$.

by western blot (**Supplementary Material Figures 6A, B**). Our data further showed that phosphorylation of TFAM led to its degradation, whereas inhibiting the phosphorylation of TFAM resulted in its accumulation in mitochondria.

Moreover, compartmentalized mitochondrial cAMP signaling mediated by the PDE/PKA axis has been demonstrated to be important for TFAM stabilization (17), which is also consistent with the findings of the current study.

The biological functions of several PDE family members have been intensively studied in CRC. For instance, one study showed that cAMP/PDE4B signals possess an important role in mediating the malignant phenotype of CRC cells by regulating the mammalian target of rapamycin (mTOR) signaling (32). Furthermore, PDE4D has been demonstrated to play an essential role in modulating cAMP levels in DLD-1 CRC cells, which in turn mediates the expression of Myc in CRC cells (33). Similarly, in the present study, we demonstrated that mitochondrial PDE2 also harbor a key role in promoting CRC growth by mediating the phosphorylation of TFAM. Furthermore, Monterisi et al. indicated that the cAMP/PKA signaling domain is localized at mitochondrial membranes and regulated by PDE2 (34), which is in agreement with our findings. Detailed investigations revealed that PDE2 mediates mitochondrial morphology and apoptotic cell death through local regulation of cAMP/PKA signaling (34). It has also been reported that erythro-9-(2-hydroxy-3-nonyl) adenine (EHNA), a PDE2 inhibitor, is capable of suppressing the growth of the human malignant melanoma PMP cell line (19). Collectively, these findings suggest that PDEs are important players in CRC.

Growing evidence indicates that TFAM is closely associated with CRC. For example, one study showed that the expression of TFAM is frequently upregulated in colon adenocarcinoma tissues compared with the corresponding paracancerous tissues (35). Additionally, a positive correlation between TFAM expression and TNM stage exists in CRC (15). Additionally, truncating mutation of TFAM is found to be frequently occurred in CRC, resulting in mtDNA depletion and cisplatin-induced apoptotic resistance of most microsatellite-unstable CRC (36). Collectively, these studies indicate that high TFAM expression can be a potential marker for tumor progression in CRC patients. Several studies also suggest that microRNAs, including microRNA-214 (miR-214) and microRNA-204 (miR-204), may play a pivotal in regulating the proliferation of CRC cells by mediating TFAM expression (37, 38). In the current study, our data uncovered a novel mechanism underlying TFAM-mediated CRC growth.

In conclusion, our findings uncover that MCU-induced mitochondrial calcium (Ca^{2+}) uptake activated PDE2 in mitochondria, which in turn inhibited the activity of

mitochondrial PKA. This subsequently led to decreased phosphorylation of TFAM and increased accumulation of TFAM in mitochondria. Taken together, our data indicate that the mitochondrial Ca^{2+}-activated PDE2/cAMP/PKA axis is instrumental in regulating TFAM stability and the growth of CRC cells. These findings imply that targeting PDE2/cAMP/PKA axis-mediated TFAM accumulation could be a promising therapeutic strategy for CRC treatment.

DATA AVAILABILITY STATEMENT

The raw data supporting the conclusions of this article will be made available by the authors, without undue reservation.

ETHICS STATEMENT

This study was performed with the approval from the Ethics Committee of Fourth Military Medical University (Permission number: KY20173189-1; Date issued: 2017-03-06). The patients/participants provided their written informed consent to participate in this study. All animal experiments were conducted according to the guidelines of the Institutional Animal Care and Use Committee of the Fourth Military Medical University (Permission number: IACUC-20170105; Date issued: 2017-01-01). Written informed consent was obtained from the owners for the participation of their animals in this study.

AUTHOR CONTRIBUTIONS

YZ, FZ, NW, ZZ, MJ, CJ, and JZhao performed the experiments and analyzed the data. YW, JZhang, and JX wrote the paper. TR, JX, XH, YW, and JZhao supervised and revised the paper. All authors contributed to the article and approved the submitted version.

FUNDING

This study was supported by the China Postdoctoral Science Foundation (2020M683751, 2019M663985 and 2019M663984) and Basic Research Plan of Shanxi Natural Science (2021JQ-559). Key Research and Development Projects of Shanxi Province (2017SF-188), Natural Science Foundation of Shaanxi Provincial Department of Education (JM8020) and the National Natural Science Foundation of China (81872302, 82002511, 81802345, 81672340 and 82072722).

ACKNOWLEDGMENTS

The authors thank Peng Yuan at the Experimental Teaching Center of Basic Medicine for helpful discussions.

SUPPLEMENTARY MATERIAL

The Supplementary Material for this article can be found online at: https://www.frontiersin.org/articles/10.3389/fonc.2021.663778/full#supplementary-material

REFERENCES

1. Zhang Y, Chen Z, Li J. The Current Status of Treatment for Colorectal Cancer in China: A Systematic Review. *Med (Baltimore)* (2017) 96:e82425. doi: 10.1097/md.0000000000008242
2. Chen W, Zheng R, Baade PD, Zhang S, Zeng H, Bray F, et al. Cancer Statistics in China, 2015. *CA Cancer J Clin* (2016) 66:115–325. doi: 10.3322/caac.21338
3. Bravo-Sagua R, Parra V, López-Crisosto C, Díaz P, Quest AF, Lavandero S. Calcium Transport and Signaling in Mitochondria. *Compr Physiol* (2017) 7:623–345. doi: 10.1002/cphy.c160013
4. Maycotte P, Marin-Hernandez A, Goyri-Aguirre M, Anaya-Ruiz M, Reyes-Leyva J, Cortes-Hernandez P. Mitochondrial Dynamics and Cancer. *Tumour Biol* (2017) 39:10104283176983915. doi: 10.1177/1010428317698391
5. Vultur A, Gibhardt CS, Stanisz H, Bogeski I. The Role of the Mitochondrial Calcium Uniporter (Mcu) Complex in Cancer. *Pflugers Arch* (2018) 470:1149–635. doi: 10.1007/s00424-018-2162-8
6. Liu Y, Jin M, Wang Y, Zhu J, Tan R, Zhao J, et al. Mcu-Induced Mitochondrial Calcium Uptake Promotes Mitochondrial Biogenesis and Colorectal Cancer Growth. *Signal Transduct Target Ther* (2020) 5:595. doi: 10.1038/s41392-020-0155-5
7. Tosatto A, Sommaggio R, Kummerow C, Bentham RB, Blacker TS, Berecz T, et al. The Mitochondrial Calcium Uniporter Regulates Breast Cancer Progression Via Hif-1α. *EMBO Mol Med* (2016) 8:569–855. doi: 10.15252/emmm.201606255
8. Ren T, Zhang H, Wang J, Zhu J, Jin M, Wu Y, et al. Mcu-Dependent Mitochondrial Ca(2+) Inhibits Nad(+)/sirt3/sod2 Pathway to Promote Ros Production and Metastasis of Hcc Cells. *Oncogene* (2017) 36:5897–9095. doi: 10.1038/onc.2017.167
9. Li X, Spelat R, Bartolini A, Cesselli D, Ius T, Skrap M, et al. Mechanisms of Malignancy in Glioblastoma Cells are Linked to Mcu Upregulation and Higher Intracellular Calcium Level. *J Cell Sci* (2020) 133(6):1–34. doi: 10.1242/jcs.237503
10. Curry MC, Peters AA, Kenny PA, Roberts-Thomson SJ, Monteith GR. Mitochondrial Calcium Uniporter Silencing Potentiates Caspase-Independent Cell Death in mda-mb-231 Breast Cancer Cells. *Biochem Biophys Res Commun* (2013) 434:695–7005. doi: 10.1016/j.bbrc.2013.04.015
11. Tang S, Wang X, Shen Q, Yang X, Yu C, Cai C, et al. Mitochondrial Ca^{2+} Uniporter is Critical for Store-Operated Ca^{2+} Entry-Dependent Breast Cancer Cell Migration. *Biochem Biophys Res Commun* (2015) 458:186–935. doi: 10.1016/j.bbrc.2015.01.092
12. Picca A, Lezza AM. Regulation of Mitochondrial Biogenesis Through Tfam-Mitochondrial DNA Interactions: Useful Insights From Aging and Calorie Restriction Studies. *Mitochondrion* (2015) 25:67–755. doi: 10.1016/j.mito.2015.10.001
13. Lin CS, Lee HT, Lee MH, Pan SC, Ke CY, Chiu AW, et al. Role of Mitochondrial DNA Copy Number Alteration in Human Renal Cell Carcinoma. *Int J Mol Sci* (2016) 17:814–28. doi: 10.3390/ijms17060814
14. Sun X, Zhan L, Chen Y, Wang G, He L, Wang Q, et al. Increased Mtdna Copy Number Promotes Cancer Progression by Enhancing Mitochondrial Oxidative Phosphorylation in Microsatellite-Stable Colorectal Cancer. *Signal Transduct Target Ther* (2018) 3:85. doi: 10.1038/s41392-018-0011-z
15. Abe Y, Nakayama Y, Katsuki T, Inoue Y, Minagawa N, Torigoe T, et al. The Prognostic Significance of the Expression of Monocarboxylate Transporter 4 in Patients With Right- or Left-Sided Colorectal Cancer. *Asia Pac J Clin Oncol* (2019) 15:e49–e555. doi: 10.1111/ajco.13077

16. Lu B, Lee J, Nie X, Li M, Morozov YI, Venkatesh S, et al. Phosphorylation of Human Tfam in Mitochondria Impairs DNA Binding and Promotes Degradation by the Aaa+ Lon Protease. *Mol Cell* (2013) 49:121–325. doi: 10.1016/j.molcel.2012.10.023
17. Zhang F, Qi Y, Zhou K, Zhang G, Linask K, Xu H. The Camp Phosphodiesterase Prune Localizes to the Mitochondrial Matrix and Promotes Mtdna Replication by Stabilizing Tfam. *EMBO Rep* (2015) 16:520–75. doi: 10.15252/embr.201439636
18. Murata T, Shimizu K, Kurohara K, Tomeoku A, Koizumi G, Arai N. Role of Phosphodiesterase2a in Proliferation and Migration of Human Osteosarcoma Cells. *Anticancer Res* (2019) 39:6057–625. doi: 10.21873/anticanres.13812
19. Hiramoto K, Murata T, Shimizu K, Morita H, Inui M, Manganiello VC, et al. Role of Phosphodiesterase 2 in Growth and Invasion of Human Malignant Melanoma Cells. *Cell Signal* (2014) 26:1807–175. doi: 10.1016/j.cellsig.2014.03.031
20. Gao T, Zhang X, Zhao J, Zhou F, Wang Y, Zhao Z, et al. Sik2 Promotes Reprogramming of Glucose Metabolism Through Pi3k/Akt/Hif-1α Pathway and drp1-Mediated Mitochondrial Fission in Ovarian Cancer. *Cancer Lett* (2020) 469:89–1015. doi: 10.1016/j.canlet.2019.10.029
21. Mercer TR, Neph S, Dinger ME, Crawford J, Smith MA, Shearwood AM, et al. The Human Mitochondrial Transcriptome. *Cell* (2011) 146:645–585. doi: 10.1016/j.cell.2011.06.051
22. Acin-Perez R, Russwurm M, Günnewig K, Gertz M, Zoidl G, Ramos L, et al. A Phosphodiesterase 2a Isoform Localized to Mitochondria Regulates Respiration. *J Biol Chem* (2011) 286:30423–325. doi: 10.1074/jbc.M111.266379
23. Huang Q, Zhan L, Cao H, Li J, Lyu Y, Guo X, et al. Increased Mitochondrial Fission Promotes Autophagy and Hepatocellular Carcinoma Cell Survival Through the Ros-Modulated Coordinated Regulation of the Nfkb and tp53 Pathways. *Autophagy* (2016) 12:999–10145. doi: 10.1080/15548627.2016.1166318
24. Sakurai K, Chen J, Kefalov VJ. Role of Guanylyl Cyclase Modulation in Mouse Cone Phototransduction. *J Neurosci* (2011) 31:7991–80005. doi: 10.1523/JNEUROSCI.6650-10.2011
25. Geoffroy V, Fouque F, Nivet V, Clot JP, Lugnier C, Desbuquois B, et al. Activation of a cGMP-Stimulated Camp Phosphodiesterase by Protein Kinase C in a Liver Golgi-Endosomal Fraction. *Eur J Biochem* (1999) 259:892–9005. doi: 10.1046/j.1432-1327.1999.00123.x
26. Quirós PM, Bárcena C, López-Otín C. Lon Protease: A Key Enzyme Controlling Mitochondrial Bioenergetics in Cancer. *Mol Cell Oncol* (2014) 1:e9685055. doi: 10.4161/23723548.2014.968505
27. Goraya TA, Cooper DM. Ca2+-calmodulin-dependent Phosphodiesterase (Pde1): Current Perspectives. *Cell Signal* (2005) 17:789–975. doi: 10.1016/j.cellsig.2004.12.017
28. Baillie GS, Huston E, Scotland G, Hodgkin M, Gall I, Peden AH, et al. Tapas-1, a Novel Microdomain Within the Unique N-Terminal Region of the pde4a1 Camp-Specific Phosphodiesterase That Allows Rapid, ca2+-Triggered Membrane Association With Selectivity for Interaction With Phosphatidic Acid. *J Biol Chem* (2002) 277:28298–3095. doi: 10.1074/jbc.M108353200
29. Zhang KY, Card GL, Suzuki Y, Artis DR, Fong D, Gillette S, et al. A Glutamine Switch Mechanism for Nucleotide Selectivity by Phosphodiesterases. *Mol Cell* (2004) 15:279–865. doi: 10.1016/j.molcel.2004.07.005
30. Bers DM, Xiang YK, Zaccolo M. Whole-Cell Camp and Pka Activity are Epiphenomena, Nanodomain Signaling Matters. *Physiol (Bethesda)* (2019) 34:240–495. doi: 10.1152/physiol.00002.2019.
31. Patriarchi T, Buonarati OR, Hell JW. Postsynaptic Localization and Regulation of Ampa Receptors and cav1.2 by Beta2 Adrenergic Receptor/Pka and Ca(2+)/Camkii Signaling. *EMBO J* (2018) 37:1–24. doi: 10.15252/embj.201899771
32. Kim DU, Kwak B, Kim SW. Phosphodiesterase 4b Is an Effective Therapeutic Target in Colorectal Cancer. *Biochem Biophys Res Commun* (2019) 508:825–315. doi: 10.1016/j.bbrc.2018.12.004
33. Kim DU, Nam J, Cha MD, Kim SW. Inhibition of Phosphodiesterase 4d Decreases the Malignant Properties of Dld-1 Colorectal Cancer Cells by Repressing the Akt/Mtor/Myc Signaling Pathway. *Oncol Lett* (2019) 17:3589–985. doi: 10.3892/ol.2019.9996
34. Monterisi S, Lobo MJ, Livie C, Castle JC, Weinberger M, Baillie G, et al. Pde2a2 Regulates Mitochondria Morphology and Apoptotic Cell Death Via Local Modulation of Camp/Pka Signalling. *Elife* (2017) 6:1–20. doi: 10.7554/eLife.21374
35. Wen S, Gao J, Zhang L, Zhou H, Fang D, Feng S. P53 Increase Mitochondrial Copy Number Via Up-Regulation of Mitochondrial Transcription Factor a in Colorectal Cancer. *Oncotarget* (2016) 7:75981–955. doi: 10.18632/oncotarget.12514
36. Guo J, Zheng L, Liu W, Wang X, Wang Z, Wang Z, et al. Frequent Truncating Mutation of Tfam Induces Mitochondrial DNA Depletion and Apoptotic Resistance in Microsatellite-Unstable Colorectal Cancer. *Cancer Res* (2011) 71:2978–875. doi: 10.1158/0008-5472.can-10-3482
37. Wu K, He Y, Li G, Peng J. Expression and Proliferative Regulation of mir-204 Related to Mitochondrial Transcription Factor a in Colon Cancer. *Zhonghua Wei Chang Wai Ke Za Zhi* (2015) 18:1041–65.
38. Wu K, Ma J, Zhan Y, Liu K, Ye Z, Chen J, et al. Down-Regulation of microRNA-214 Contributed to the Enhanced Mitochondrial Transcription Factor a and Inhibited Proliferation of Colorectal Cancer Cells. *Cell Physiol Biochem* (2018) 49:545–5. doi: 10.1159/000492992

Conflict of Interest: The authors declare that the research was conducted in the absence of any commercial or financial relationships that could be construed as a potential conflict of interest.

Copyright © 2021 Zhao, Wang, Zhao, Zhang, Jin, Zhou, Jin, Zhang, Xing, Wang, He and Ren. This is an open-access article distributed under the terms of the Creative Commons Attribution License (CC BY). The use, distribution or reproduction in other forums is permitted, provided the original author(s) and the copyright owner(s) are credited and that the original publication in this journal is cited, in accordance with accepted academic practice. No use, distribution or reproduction is permitted which does not comply with these terms.

frontiers in Cell and Developmental Biology

ORIGINAL RESEARCH
published: 12 July 2021
doi: 10.3389/fcell.2021.701073

Genome Instability-Derived Genes Are Novel Prognostic Biomarkers for Triple-Negative Breast Cancer

*Maoni Guo and San Ming Wang**

Cancer Centre and Institute of Translational Medicine, Faculty of Health Sciences, University of Macau, Macau, China

Background: Triple-negative breast cancer (TNBC) is an aggressive disease. Recent studies have identified genome instability-derived genes for patient outcomes. However, most of the studies mainly focused on only one or a few genome instability-related genes. Prognostic potential and clinical significance of genome instability-associated genes in TNBC have not been well explored.

Methods: In this study, we developed a computational approach to identify TNBC prognostic signature. It consisted of (1) using somatic mutations and copy number variations (CNVs) in TNBC to build a binary matrix and identifying the top and bottom 25% mutated samples, (2) comparing the gene expression between the top and bottom 25% samples to identify genome instability-related genes, and (3) performing univariate Cox proportional hazards regression analysis to identify survival-associated gene signature, and Kaplan–Meier, log-rank test, and multivariate Cox regression analyses to obtain overall survival (OS) information for TNBC outcome prediction.

Results: From the identified 111 genome instability-related genes, we extracted a genome instability-derived gene signature (GIGenSig) of 11 genes. Through survival analysis, we were able to classify TNBC cases into high- and low-risk groups by the signature in the training dataset (log-rank test $p = 2.66e{-}04$), validated its prognostic performance in the testing (log-rank test $p = 2.45e{-}02$) and Molecular Taxonomy of Breast Cancer International Consortium (METABRIC) (log-rank test $p = 2.57e{-}05$) datasets, and further validated the predictive power of the signature in five independent datasets.

Conclusion: The identified novel signature provides a better understanding of genome instability in TNBC and can be applied as prognostic markers for clinical TNBC management.

Keywords: TNBC, mutation, copy number variation, genome instability, prognosis

OPEN ACCESS

Edited by:
Ira Ida Skvortsova, Innsbruck Medical University, Austria

Reviewed by:
Lili Zhang, Beijing Hospital, China
Song Guo, Shanghai Institute of Nutrition and Health (CAS), China

***Correspondence:**
San Ming Wang
sanmingwang@um.edu.mo

Specialty section:
This article was submitted to Molecular and Cellular Oncology, a section of the journal Frontiers in Cell and Developmental Biology

Received: *27 April 2021*
Accepted: *10 June 2021*
Published: *12 July 2021*

Citation:
Guo M and Wang SM (2021) Genome Instability-Derived Genes Are Novel Prognostic Biomarkers for Triple-Negative Breast Cancer. Front. Cell Dev. Biol. 9:701073. doi: 10.3389/fcell.2021.701073

INTRODUCTION

Triple-negative breast cancer (TNBC) accounts for ∼15% of all breast cancer cases and is characterized by the absence of estrogen receptor (ER), progesterone receptor (PR), and epidermal growth factor receptor 2 (HER2) (Oakman et al., 2010). TNBC often occurs at a young age, highly aggressive, and metastatic with a poor prognosis (Haffty et al., 2006; Dent et al., 2007). A part of TNBC is related with the germline mutation in *BRCA1* and *BRCA2*, but the cause for most of the TNBC remains unclear (Song et al., 2014). With its unusual clinic outcome, a TNBC-specific prognostic signature will be highly valuable for clinical management of TNBC cases (Mersin et al., 2008; Tan and Swain, 2008).

Genomic instability is a major hallmark in cancer and an important prognostic factor associated with cancer progression and survival (Suzuki et al., 2003; Negrini et al., 2010). Genome instability-associated signatures have been identified in certain types of cancer. For example, a genomic instability-derived three-miRNA signature was used as a risk predictor for invasive breast cancer (Bao et al., 2021); a 12-genomic instability-derived gene expression signature was identified as a clinical outcome predictor for breast cancer (Habermann et al., 2009). Genome instability-related mutation and copy number variation (CNV) were also identified in TNBC (Schmitt et al., 2012). For instance, germline mutations in *BRCA1*, *BRCA2*, *ATM*, *PALB2*, *RAD51D*, and *RAD50* disrupted DNA damage repair pathways in TNBC (Wu et al., 2019); *FOSL1* had significantly higher CNV gains in TNBC than in other types of breast cancer (Serino et al., 2019); *PIK3CA* had high mutation frequency and copy number gains and highly ethnic-specific in TNBC (Jiang et al., 2019); somatic mutation and CNV-derived genomic metrics were significantly associated with immune prognostic category in TNBC (Karn et al., 2017). Furthermore, somatic mutations and CNVs were associated with dysregulation of multiple genes in TNBC. For example, mutations in *MYH9* and *HERC2* were both associated with lower lymphocyte-specific kinase (LCK) metagene expression in TNBC (Safonov et al., 2017); *JAK2* and *PD-L1* amplifications upregulated *PD-L1* expression by disturbing the JAK/STAT1 pathway in TNBC (Chen M. et al., 2018); high expression of *PD-L1* was associated with significant *CD274* gene copy number gain in TNBC (Guo et al., 2016). However, the clinical impact of these abnormalities as prognostic markers in TNBC remains largely unclear.

We hypothesized that there could be a genome instability-derived signature involved in the tumorigenesis and development of TNBC. We further reasoned that genomic instability-derived somatic mutation and CNV in TNBC could disturb gene expression in TNBC; therefore, expression difference in TNBC could be used as prognostic markers to predict clinical outcome of TNBC.

In this study, we first calculated the accumulative counts of somatic mutation and CNV in TNBC cases and selected the top and bottom 25% of the ranked cases. We then identified 111-genomic instability-derived genes to divide the cases into genomic unstable (GU) and genomic stable (GS) groups. Furthermore, we identified a genome instability-derived gene signature (GIGenSig) of 11 genes to classify TNBC cases into high- and low-risk groups. We validated the results using multiple independent TNBC datasets. Our study provides a GIGenSig as a prognosis marker to predict the clinical outcome of TNBC.

MATERIALS AND METHODS

Datasets Used for the Study

We downloaded the METABRIC (Molecular Taxonomy of Breast Cancer International Consortium) breast cancer datasets (Pereira et al., 2016) from the cBioPortal database[1], including clinical information, gene expression, somatic mutation, and CNV data. The expression profile was processed as log intensity level of Illumina Human v3 microarray. We also downloaded the version 19 gene annotation file from the GENCODE database[2]. Then, we randomly divided the TNBC cases into the training dataset and the testing dataset with the same size of living and deceased overall survival (OS) status in each dataset. The training dataset consisting of 150 TNBC samples was used to identify the prognostic signature and build the prognostic risk model; the testing dataset consisting of 149 TNBC patients was used to validate the prognostic model. Clinical characteristics for the training, testing, and METABRIC datasets are summarized in **Table 1**. The Cancer Genome Atlas (TCGA[3]), Shanghai TNBC data[4] (Jiang et al., 2019; Goldman et al., 2020), and three additional independent datasets of GSE21653, GSE31448, and GSE25066 from the GEO database[5,6,7] were used to validate the performance of the prognostic risk model (Hatzis et al., 2011; Sabatier et al., 2011a,b). For TCGA and Shanghai RNAseq datasets, we downloaded or processed the gene-level transcription estimates in log2($x + 1$) transformed RSEM normalized count. For the other three GEO microarray datasets, they were processed using the robust multichip average (RMA) algorithm for background adjustment (Irizarry et al., 2003a,b), and the Affymetrix GeneChip probe-level data were log2 transformed. The platform information for Affymetrix Human Genome U133 Plus 2.0 Array was downloaded from the Affymetrix website[8]. Gene expression data from the Affymetrix-based expression profiling were obtained by repurposing microarray probes based on the platform information and the gene annotation file from the GENCODE database (release 19, see text footnote 2).

Identification of Genome Instability-Related Genes in TNBC

To identify genome instability-related genes in TNBC, we first processed gene expression and genomic alteration profiles. For gene expression profile, we extracted the expression log intensity

[1]https://www.cbioportal.org/

[2]https://www.gencodegenes.org

[3]http://xena.ucsc.edu/

[4]https://www.ncbi.nlm.nih.gov/sra/?term=SRP157974

[5]https://www.ncbi.nlm.nih.gov/geo/query/acc.cgi?acc=GSE21653

[6]https://www.ncbi.nlm.nih.gov/geo/query/acc.cgi?acc=GSE31448

[7]https://www.ncbi.nlm.nih.gov/geo/query/acc.cgi?acc=GSE25066

[8]http://www.affymetrix.com

TABLE 1 | Clinical information for triple-negative breast cancer (TNBC) patient datasets used in this study.

Characteristics		Training dataset ($N = 150$)	Testing dataset ($N = 149$)	Molecular Taxonomy of Breast Cancer International Consortium (METABRIC) dataset ($N = 299$)	*p*-Value*
Age (%)	Age < 55	68(45.33)	75(50.34)	143(47.83)	0.687
	Age ≥ 55	82(54.67)	74(49.66)	156(52.17)	
Menopausal_status (%)	Pre	49(32.67)	58(38.93)	107(35.79)	0.529
	Post	101(67.33)	91(61.07)	192(64.21)	
Tumor stage (%)	I/II	100(66.67)	92(61.74)	192(64.21)	0.532
	III/IV	16(10.67)	9(6.04)	25(8.36)	
	Unknown	34(22.67)	48(32.21)	82(27.42)	
Grade (%)	G1/2	17(11.33)	22(14.77)	39(13.04)	0.664
	G3	132(88.00)	125(83.89)	257(85.95)	
	Unknown	1(0.67)	2(1.34)	3(1.01)	
OS_status (%)	Living	69(46.00)	69(46.31)	138(46.15)	0.999
	Deceased	81(54.00)	80(53.69)	161(53.85)	

**p-value: Chi square test.*

levels (Illumina Human v3 microarray) for 16,331 protein-coding genes; for mutations, silent mutations were removed; for CNV profile, we only retained high-level amplification and homozygous deletion evaluated by GISTIC2 segment (Mermel et al., 2011). Then, we integrated TNBC gene expression and genomic alteration data as shown in **Supplementary Figure 1**: (1) extracted gene expression, somatic mutation, and CNV profiles in the 299 TNBC cases; (2) constructed a binary matrix by integrating somatic mutation and CNV profiles; (3) calculated the accumulated alterations for each case; (4) took the top 25% and the bottom 25% of alternated cases as GU group and GS group; (5) compared the gene expression between GU and GS groups by using the R package "limma"; and (6) identified genome instability-related genes with a Benjamini and Hochberg (BH) adjusted p-value < 0.05 and logFC (fold-change) > 1 or < -1 between GU group and GS group.

Functional Enrichment Analysis

We applied enrichGO and enrichKEGG functions in the Bioconductor package "clusterProfiler" to identify the functions and pathways of the genome instability-related genes (Yu et al., 2012). We also performed Gene Ontology (GO) and Kyoto Encyclopedia of Genes and Genomes (KEGG) functional enrichment annotation using the Database for Annotation, Visualization and Integrated Discovery (DAVID tool[9], version 6.8) (Huang da et al., 2009). The Benjamini p-adjust < 0.05 was considered as statistically significant in "clusterProfiler" and p-value < 0.05 for DAVID analyses.

Statistical Analysis

To identify the genes predictive for TNBC OS, a univariate Cox proportional hazards regression analysis was performed to evaluate the relationship between the expression level of each gene and patient OS in the training dataset. Only the genes with a p-value < 0.05 were taken as statistically significant survival predictors. To construct a predictive model, a multivariate Cox regression model was applied for these selected genes with OS in the training dataset. A risk score formula was built to evaluate the risk of each patient to develop TNBC as follows:

$$\text{Overall risk score (ORS)} = \sum_{i=1}^{N} (Exp_i \times Coe_i)$$

where, N is the number of prognostic genes, Exp is the gene expression value, and Coe is the estimated regression coefficient of the gene. A risk score for each patient was calculated by including the expression values of each selected gene, weighed by their estimated regression coefficients in the multivariate Cox regression analysis. The patients were divided into high- and low-risk groups using the median of the risk scores as the threshold. The receiver operating characteristic (ROC) curves were used to compute the sensitivity and specificity of overall prediction of the selected gene expression-based overall risk scores (ORSs) using the R package "survivalROC." The area under curve (AUC) value was also calculated. The Kaplan–Meier method was applied to generate OS curves, and the log-rank test was used to assess the differences in OS between the high- and low-risk groups using the R package "survival." Additionally, univariate and multivariate Cox proportional hazards regression, and data stratification analyses were performed to test whether the ORS was independent of other clinical features. Statistical significance was based on p-value < 0.05 and 95% confidence interval (CI) estimates.

To evaluate the performance of the risk model prediction, we randomly chose samples from the high- and low-risk group and trained a support vector machine (SVM) classifier based on the expression level of the selected genes in the risk model using the R package "e1071." The 10-fold cross-validation method was used to evaluate the performance of the classifier. Plots of the ROC curve of the classifier and the calculation of the AUC were fulfilled using the R verification package. In addition, Chi-square test and Wilcoxon rank-sum test were also used in the study, and a p-value < 0.05 was considered as statistically significant. In differential expression analysis, the genes with the cutoff of

[9]http://david.abcc.ncifcrf.gov/

p-value < 0.05 and logFC > 1 or < -1 between the two groups were regarded as statistically significant. All statistical analyses were performed using R version 3.6.3.

RESULTS

Identification of Genome Instability-Related Genes in TNBC

We identified 299 TNBC samples from the METABRIC breast cancer dataset and performed a systematic analysis (**Supplementary Figure 1**). To identify the genes associated with genomic instability, we calculated the cumulative count of alterations including somatic mutations and CNVs in each patient and sorted these counts in decreased order. The top 25% of TNBC patients ($n = 75$) were named as the GU group and the bottom 25% ($n = 75$) as the GS group. We performed differential expression analysis between the GU and GS groups. We identified 111 differentially expressed genes between the two groups, 63 upregulated and 48 downregulated in the GU group (**Supplementary Table 1**). We performed unsupervised hierarchical clustering analysis for all 299 TNBC samples by the 111 genes and compared our GU/GS groups with the PAM50 and claudin-low subtype available from the METABRIC dataset. The results showed that 69.1% (143/207) of the samples in the GU group were classified as basal subtype and 65.2% (60/92) samples in the GS group as the claudin-low subtype (**Figure 1A**). We found that all patients were classified into either the GU group or the GS group, in which the cumulative alterations in the GU group were significantly higher than that of the GS group (**Figure 1B**, Wilcox test $p < 0.001$). We further compared the expression level of *FOXM1*, a genome

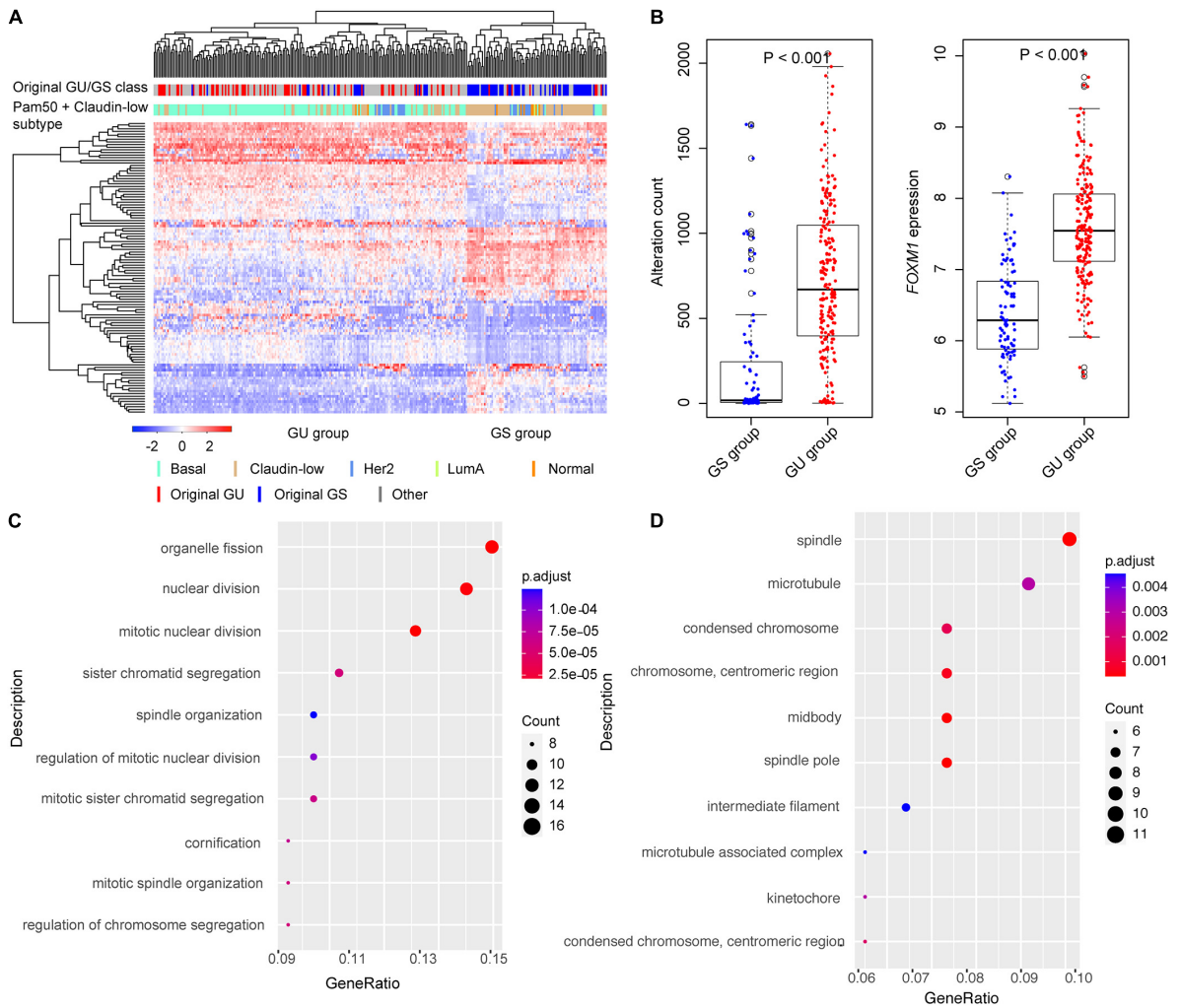


FIGURE 1 | Identification of genome instability-related genes in triple-negative breast cancer (TNBC). **(A)** Hierarchical clustering of all the 299 Molecular Taxonomy of Breast Cancer International Consortium (METABRIC) TNBC cases using the expression of 111-genomic instability-related genes. The patients were divided into genomic unstable (GU) and genomic stable (GS) groups. **(B)** Boxplots of alteration count and *FOXM1* expression in GU and GS groups. The alteration counts and *FOXM1* expression in GU group were significantly higher than that in GS group. **(C)** The top 10 Gene Ontology Biological Process (GOBP) terms of functional enrichment results. **(D)** The top 10 Gene Ontology Cellular Component (GOCC) terms of functional enrichment results.

instability-related driver gene (Teh et al., 2010; Kim et al., 2013; Senfter et al., 2019), between the GU and GS groups. We found that the expression of *FOXM1* in the GU group was significantly higher than that in the GS group (**Figure 1B**, Wilcox test $p < 0.001$) and observed the expression of the classical proliferation gene *MKI67* was significantly higher in the GU group than that in the GS group (**Supplementary Figure 2A**, Wilcox test $p < 0.001$). To validate our defined GU/GS groups, we performed clustering analysis for the 111 genes in the 235 Shanghai TNBC samples and found that all samples were also significantly classified into the GU (191/235, 81.3%) and GS (44/235, 18.7%) groups (**Supplementary Figure 3A**). Besides, we compared the homologous recombination deficiency (HRD) levels between the GU/GS groups in the Shanghai dataset and observed that HRD level in the GU group was significantly higher than that in the GS group (**Supplementary Figure 3B**). We performed the same analysis using top 10% and bottom 10% as the cutoff for the GU/GS groups and received similar results from using the top 25% and bottom 25% as the cutoff (**Supplementary Figure 2B**).

To test whether these 111 differentially expressed genes were involved in important biological processes and pathways associated with genome instability, we performed functional enrichment analysis using R package "clusterProfiler" with BH adjustment for multiple testing. We identified multiple pathways associated with genomic instability, such as mitotic nuclear division, organelle fission, nuclear division, sister chromatid segregation, regulation of chromosome segregation, etc. (**Figures 1C,D**). We also performed DAVID analysis using the 111 genes. The results also showed that these genes were largely involved in cell cycle process, cell proliferation, and immune response (**Supplementary Figure 4A**), and some genes (such as *SFRP4*, *PRKCB*, *FZD9*, and *RAC2*) were known in involving TNBC development (**Supplementary Figure 4B**). The results highlight that the 111 differentially expressed genes were involved in tumorigenesis and development process of TNBC.

Identification of GIGenSig for Prognostic Prediction

To explore the potential prognostic value of the above genome instability-related genes, we divided all the METABRIC TNBC cases into two subsets, the training dataset ($n = 150$) and the testing dataset ($n = 149$). To identify prognostic-associated genes, we conducted univariate Cox regression analysis to calculate the relationship between the 111 gene expression and OS in the training dataset. The result showed that 11 of the genes were associated with OS in TNBC (**Table 2**, $p < 0.05$). We named these 11 genes as GIGenSig. To evaluate the prognostic potential of GIGenSig, we constructed a prognostic risk model for OS based on the expression of GIGenSig and coefficients of multivariate Cox analysis: ORS = (0.137 × *PRKCB* expression) + (0.037 × *TFF3* expression) + (−0.008 × *ART3* expression) + (−0.071 × *CD52* expression) + (−0.030 × *CD79A* expression) + (−0.155 × *FZD9* expression) + (−0.010 × *GABRP* expression) + (−0.145 × *IRF8* expression) + (−0.187 × *ITM2A* expression) + (−0.038 × *SOX10* expression) + (−0.072 × *VGLL1* expression). Among the GIGenSig, the coefficients of *PRKCB* and *TFF3* were positive, suggesting that they were risk factors for TNBC, and their high expression was associated with poor survival of TNBC. In contrast, the coefficients for the other nine genes (*ART3*, *CD52*, *CD79A*, *FZD9*, *GABRP*, *IRF8 ITM2A*, *SOX10*, and *VGLL1*) were negative, suggesting that these were protective factors, and their higher expression was associated with better survival.

Based on ORS values, TNBC patients in the training datasets were classified into two groups by their median ORS (−4.602), named as high-risk group and low-risk group. Survival plot showed that the OS survival in the low-risk group was significantly better than those of the high-risk group (**Figure 2A**, log-rank test $p = 2.66e{-}04$; HR = 2.718, 95% CI: 1.699–4.350), the 5-year survival rate in the low-risk group (73%) was higher than that in high-risk group (48%), and the 5-year ROC curve analysis provided an AUC of 0.648 (**Figure 2B**). In addition, SVM and 10-fold cross-validation showed that our risk model was robust to classify TNBC patients into high- and low-risk groups (**Supplementary Figure 5A**, AUC = 0.987, $p = 7.62e{-}33$).

We ranked the ORS for patients in the training dataset to explore the differences of GIGenSig expression, alteration count, and *FOXM1* expression between low score and high score groups (**Figure 2C**). Clustering analysis showed that *PRKCB* and *TFF3* were upregulated in the high score group, whereas the other nine genes were upregulated in the low score group (**Figure 2C**). The differences of alteration count and *FOXM1* expression were both significant between the high-risk and low-risk groups (**Figure 2D**). The count of alterations in the high-risk group was significantly higher than that in the low-risk group (**Figure 2D**, Wilcoxon test $p = 0.024$). Additionally, *FOXM1* had significantly higher expression in the high-risk group than in the low-risk group (**Figure 2D**, Wilcoxon test $p < 0.001$).

Validation of GIGenSig for Prognostic Prediction in Testing and Molecular Taxonomy of Breast Cancer International Consortium Datasets

To explore the prognostic performance of GIGenSig, we tested it using the testing dataset of 149 TNBC cases. Based on the ORS cutoff in the training dataset, the cases in the testing dataset were classified into high-risk group ($n = 73$) and low-risk group ($n = 76$). The OS of the low-risk group was significantly higher than that of the high-risk group (**Figure 3A**, log-rank test $p = 2.45e{-}02$; HR = 1.820, 95% CI: 1.099–3.023). Similarly, the 5-year survival rate in the low-risk group (72%) was also higher than that in the high-risk group (60%), and the 5-year ROC analysis yielded an AUC of 0.607 (**Supplementary Figure 6A**). Additionally, the SVM and 10-fold cross-validation showed that our risk model was robust to classify TNBC patients into high- and low-risk groups in the testing dataset (**Supplementary Figure 5B**, AUC = 0.980, $p = 8.64e{-}32$). We also displayed the clustering of GIGenSig, alteration count, and *FOXM1* expression level according to the increasing order of the ORS for each patient in the testing dataset (**Figure 3C**). The alteration count and *FOXM1* expression level were both significantly higher in the high-risk group than in the low-risk group (**Figure 3E**, Wilcoxon

TABLE 2 | Univariate Cox regression analysis for the 11 of 111-genome instability-related genes associated with overall survival in TNBC.

Gene	Genomic location	Coefficient	HR	95% CI	*p*-Value
ART3	chr4:76932337–77033955	−0.126	0.882	0.778–0.999	0.048
CD52	chr1:26644448–26647014	−0.171	0.843	0.715–0.993	0.042
CD79A	chr19:42381190–42385439	−0.150	0.860	0.751–0.986	0.031
FZD9	chr7:72848109–72850450	−0.187	0.829	0.689–0.999	0.049
GABRP	chr5:170190354–170241051	−0.115	0.891	0.817–0.971	0.009
IRF8	chr16:85932409–85956215	−0.228	0.796	0.646–0.982	0.033
ITM2A	chrX:78615881–78623164	−0.188	0.829	0.690–0.997	0.046
PRKCB	chr16:23847322–24231932	−0.212	0.809	0.657–0.996	0.045
SOX10	chr22:38366693–38383429	−0.154	0.857	0.755–0.973	0.017
TFF3	chr21:43731777–43735761	0.106	1.112	1.011–1.224	0.029
VGLL1	chrX:135614311–135638966	−0.160	0.852	0.739–0.983	0.028

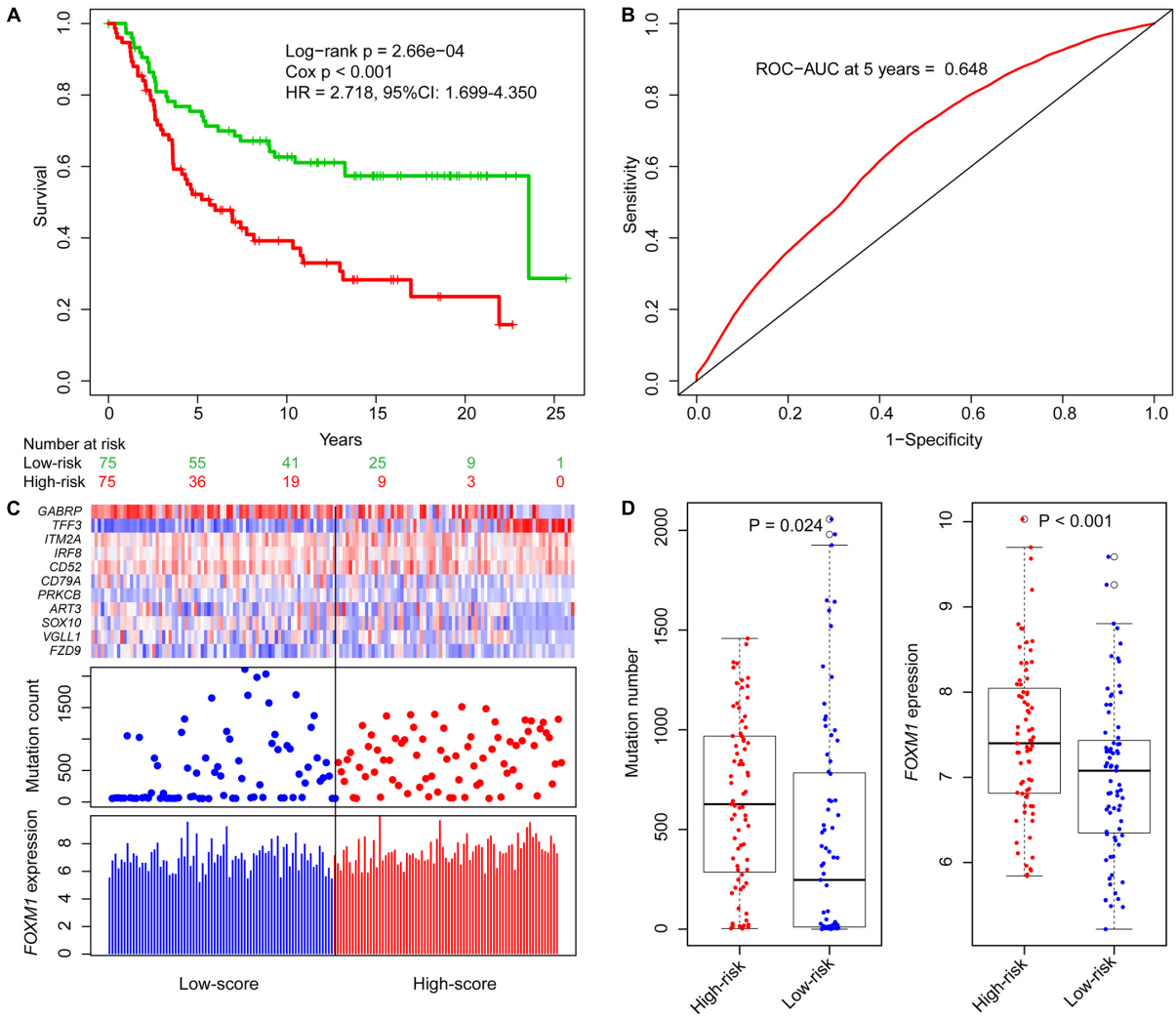


FIGURE 2 | Identification of genome instability-derived gene signature (GIGenSig) for prognostic prediction. **(A)** Survival curve of overall survival of TNBC patients in the training dataset. Patients were significantly classified into high- and low-risk groups; **(B)** 5-year receiver operating characteristic (ROC) curve for the GIGenSig in the training dataset; **(C)** GIGenSig gene expression pattern and alteration distribution and *FOXM1* expression level with the increasing overall risk score (ORS) scores for the patients in the training dataset. The blue and red represent the low- and high-risk groups, respectively; **(D)** distribution of accumulative alteration number and *FOXM1* expression in the high- and low-risk groups in the training dataset. The blue and red represent the low- and high-risk groups, respectively.

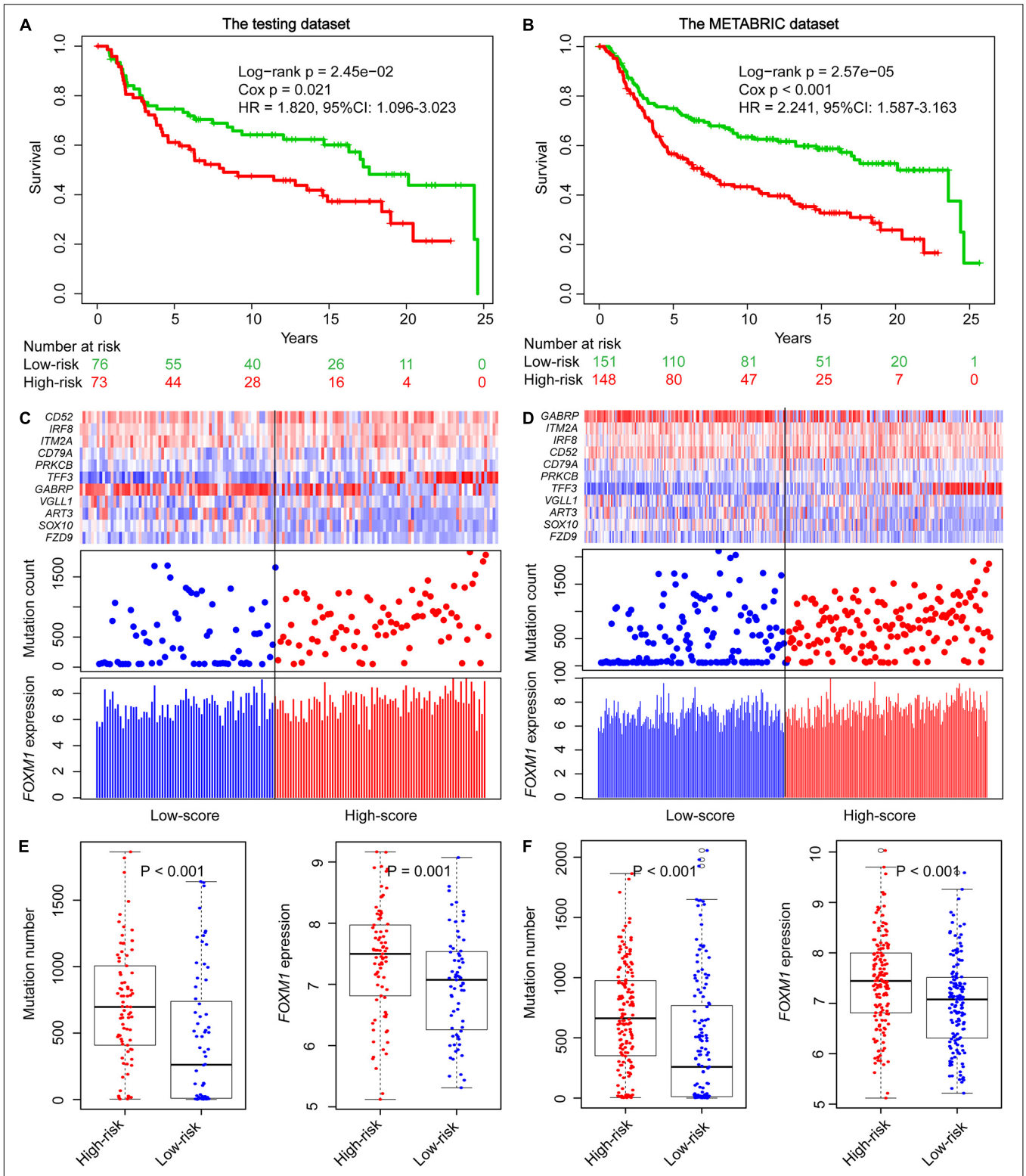


FIGURE 3 | Validation of GIGenSig for prognostic prediction in the testing and METABRIC datasets. **(A,B)** Survival curves of overall survival of patients in the testing and METABRIC datasets. Patients were significantly classified into high- and low-risk groups. **(C,D)** The GIGenSig gene expression pattern, alteration distribution, and *FOXM1* expression level with the increasing ORS scores for the patients in the testing and METABRIC dataset. The blue and red represent the low- and high-risk groups, respectively. **(E,F)** The distribution of accumulative alteration number and *FOXM1* expression in the high- and low-risk groups in the testing and METABRIC datasets. The blue and red represent the low- and high-risk groups, respectively.

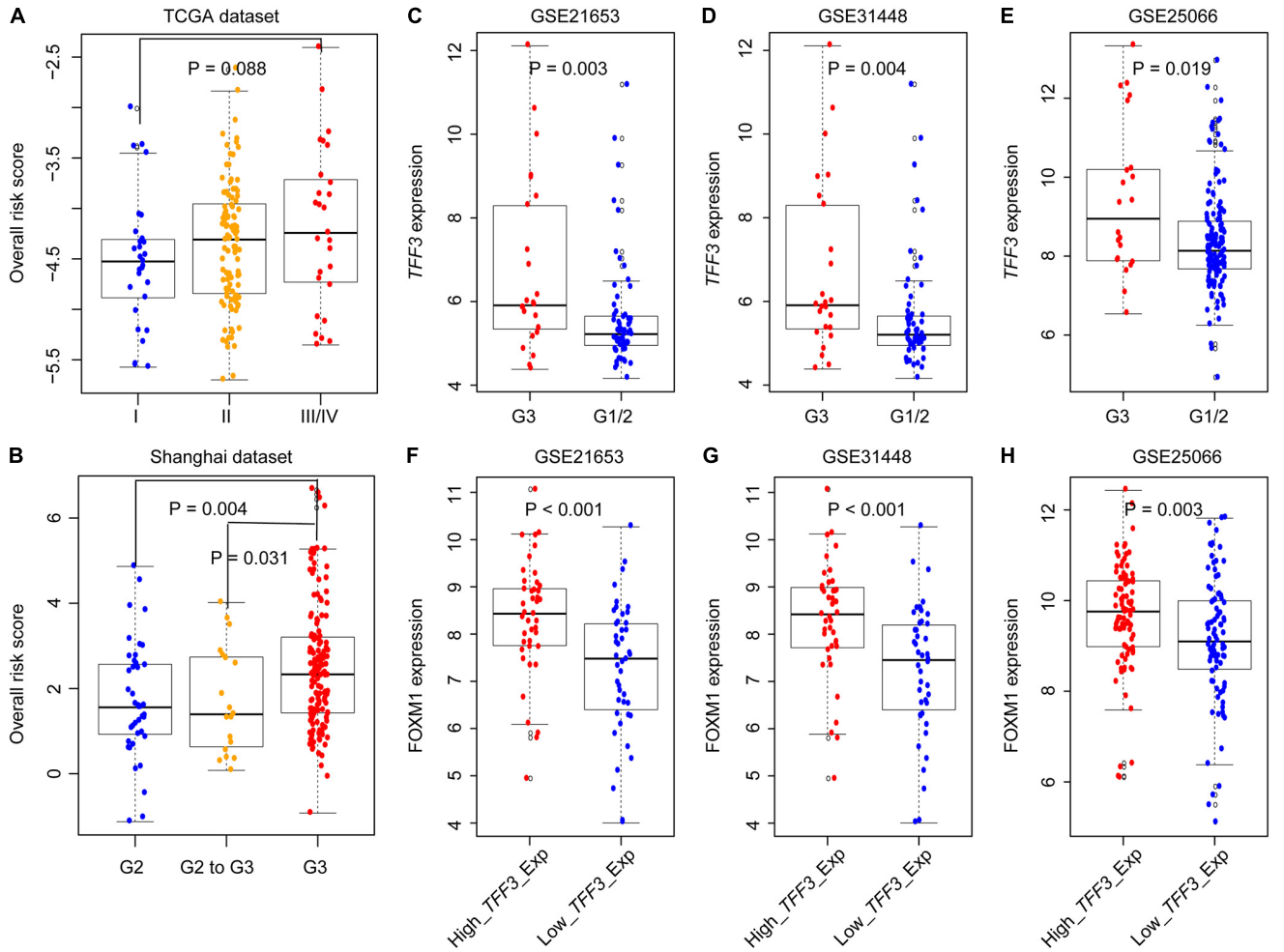


FIGURE 4 | Validation of GIGenSig in five additional datasets. **(A,B)** Boxplots for ORS for TNBC patients with different stage and grade in The Cancer Genome Atlas (TCGA) and Shanghai dataset. **(C–E)** Boxplots for *TFF3* expression among patients with different grade in GSE21653, GSE31448, and GSE25066. **(F–H)** Boxplots for *FOXM1* expression among patients with high and low *TFF3* expression in GSE21653, GSE31448, and GSE25066. The comparisons between any two different groups were performed by Wilcox test.

test $p < 0.001$ for alteration count; Wilcoxon test $p = 0.001$ for *FOXM1* expression level).

We also validated the prognostic power of GIGenSig in the METABRIC TNBC dataset. The patients were classified into two groups. The median survival time of the low-risk group was significantly higher than that of the high-risk group (**Figure 3B**, median: 23.6 vs. 7 years; log-rank test $p = 2.57e{-}05$; HR = 2.241, 95% CI: 1.587–3.63). The 5-year survival rate in the low-risk group was longer (72%) than that in the high-risk group (54%), and the 5-year ROC gave an AUC of 0.627 (**Supplementary Figure 6B**). In addition, the SVM and 10-fold cross-validation showed that our risk model was robust to classify TNBC patients into high- and low-risk groups in the METABRIC dataset (**Supplementary Figure 5C**, AUC = 0.980, $p = 5.30e{-}62$). A similar pattern was observed in the METABRIC dataset as in the training and testing datasets for the clustering of GIGenSig, alteration count, and *FOXM1* expression (**Figure 3D**). Additionally, both significant differences were present for alteration count and *FOXM1* expression between the high-risk and low-risk groups (**Figure 3F**, Wilcoxon test $p < 0.001$ for alteration count; Wilcoxon test $p < 0.001$ for *FOXM1* expression level).

Validation of GIGenSig in Five Additional Datasets

We compared GIGenSig using two independent datasets, the TCGA and Shanghai TNBC data, to test if clinical stage and grade could have an impact on the prognosis of TNBC. As shown in **Figure 4A**, there was a close relationship between the stage of TNBC and ORS but not reaching a significant level in the TCGA dataset (**Figure 4A**, Wilcoxon test $p = 0.088$). ORS was also associated with TNBC grade in Shanghai dataset that ORS of grade 3 was significantly higher than that of grade 2 and grades 2–3 (**Figure 4B**, $p = 0.004$ for comparing with grade 2; $p = 0.031$ for comparing with grades 2–3; Wilcoxon test). We

TABLE 3 | Univariate and multivariate Cox regression analyses of the genome instability-derived gene signature (GIGenSig) and overall survival in different patient datasets.

Characteristics	Univariable analysis			Multivariable analysis		
	HR	95% CI	*p*-value	HR	95% CI	*p*-Value
Training dataset						
GIGenSig	2.718	1.699–4.350	<0.001	2.184	1.218–3.915	0.009
Age	1.022	1.004–1.041	0.019	1.042	1.007–1.079	0.018
Menopausal status	0.887	0.549–1.433	0.625	2.656	1.024–6.886	0.045
Tumor stage	1.358	0.691–2.672	0.375	0.963	0.458–2.024	0.921
Grade	1.187	0.593–2.375	0.629	1.870	0.822–4.255	0.135
Testing dataset						
GIGenSig	1.820	1.096–3.023	0.021	1.354	0.683–2.682	0.038
Age	1.024	1.008–1.040	0.004	1.035	1.000–1.072	0.052
Menopausal status	0.640	0.395–1.037	0.070	2.215	0.754–6.508	0.148
Tumor stage	4.682	2.255–9.721	<0.001	4.976	2.266–10.926	<0.001
Grade	0.899	0.504–1.605	0.719	1.485	0.689–3.203	0.313
METABRIC dataset						
GIGenSig	2.241	1.587–3.163	<0.001	1.647	1.080–2.512	0.020
Age	1.024	1.012–1.036	0.000	1.037	1.013–1.062	0.002
Menopausal status	0.736	0.525–1.031	0.075	2.270	1.137–4.531	0.020
Tumor stage	2.180	1.332–3.569	0.002	1.851	1.093–3.134	0.022
Grade	1.011	0.649–1.573	0.962	1.456	0.842–2.515	0.178

further validated GIGenSig in another three independent breast cancer datasets generated by the microarray platform (GSE21653, GSE31448, and GSE25066). We reannotated the microarray data to obtain the gene expression data and extracted the common clinical characteristics from the three datasets. We then examined the association of GIGenSig with TNBC genomic instability information in these three independent datasets. Among all the 111 genes in GIGenSig, we found that *TFF3* presented significantly higher expression level in grade 3 than in grades 1 and 2 in all three datasets (**Figures 4C–E**, $p = 0.003$ for GSE21653; $p = 0.004$ for GSE31448; and $p = 0.019$ for GSE25066; Wilcoxon test). Furthermore, we tested the relationship between *TFF3* expression and *FOXM1* expression in the three datasets. We observed that *FOXM1* expression in patients with high *TFF3* expression was significantly higher than that with low *TFF3* expression in all three datasets (**Figures 4F–H**, $p < 0.001$ for GSE21653; $p < 0.001$ for GSE31448; and $p = 0.003$ for GSE25066; Wilcoxon test).

Prognostic Prediction by GIGenSig Is Independent of Clinical Features

To explore whether the prognostic ability of GIGenSig was independent of age, menopausal status, and tumor stage, we performed univariate and multivariate Cox regression analysis. The results showed that the GIGenSig was significantly associated with TNBC OS in the three datasets when adjusted by age, menopausal status, tumor stage, and grade (**Table 3**). The METABRIC patients were divided into two groups according to age with <55 and ≥55, pre- and post-status of menopause, and tumor stage with I/II and III/IV. The patients were classified into high- and low-risk groups according to the median risk scores in the training dataset. The results revealed that the patients were significantly classified into two groups by age (**Figures 5A,B**; log-rank test $p = 0.019$ for age < 55 group; log-rank test $p = 0.002$ for age ≥ 55 group), menopausal (**Figures 5C,D**; log-rank test $p = 0.074$ for premenopausal group; log-rank test $p < 0.001$ for postmenopausal group), and stage subset (**Figures 5E,F**; log-rank test $p < 0.001$ for stage I/II group; log-rank test $p = 0.387$ for stage III/IV group). The classification for patients in the stage III/IV group was not significant probably due to the smaller sample size ($n = 25$) in this group. These results indicated that GIGenSig served as a prognostic signature for TNBC independent of age, menopausal status, and tumor stage.

Genome Instability-Derived Gene Signature Performs Better Than Other Prognostic Signatures

To further explore the prognostic performance of the GIGenSig, we compared GIGenSig with other TNBC prognostic signatures including the two-gene signature (Alsaleem et al., 2020), the five-gene signature (Wang et al., 2018), the eight-gene signature (Kim et al., 2019), and the 19-gene signature (Qian et al., 2017) using the METABRIC dataset. The result showed that the 5-year AUC (0.627) of OS for GIGenSig was significantly higher than that of the two-gene signature (AUC = 0.534), the five-gene signature (AUC = 0.571), the eight-gene signature (AUC = 0.546), and the 19-gene signature (AUC = 0.615) (**Figure 6**). The results demonstrated that the GIGenSig provided better prognostic prediction for TNBC than the other four signatures.

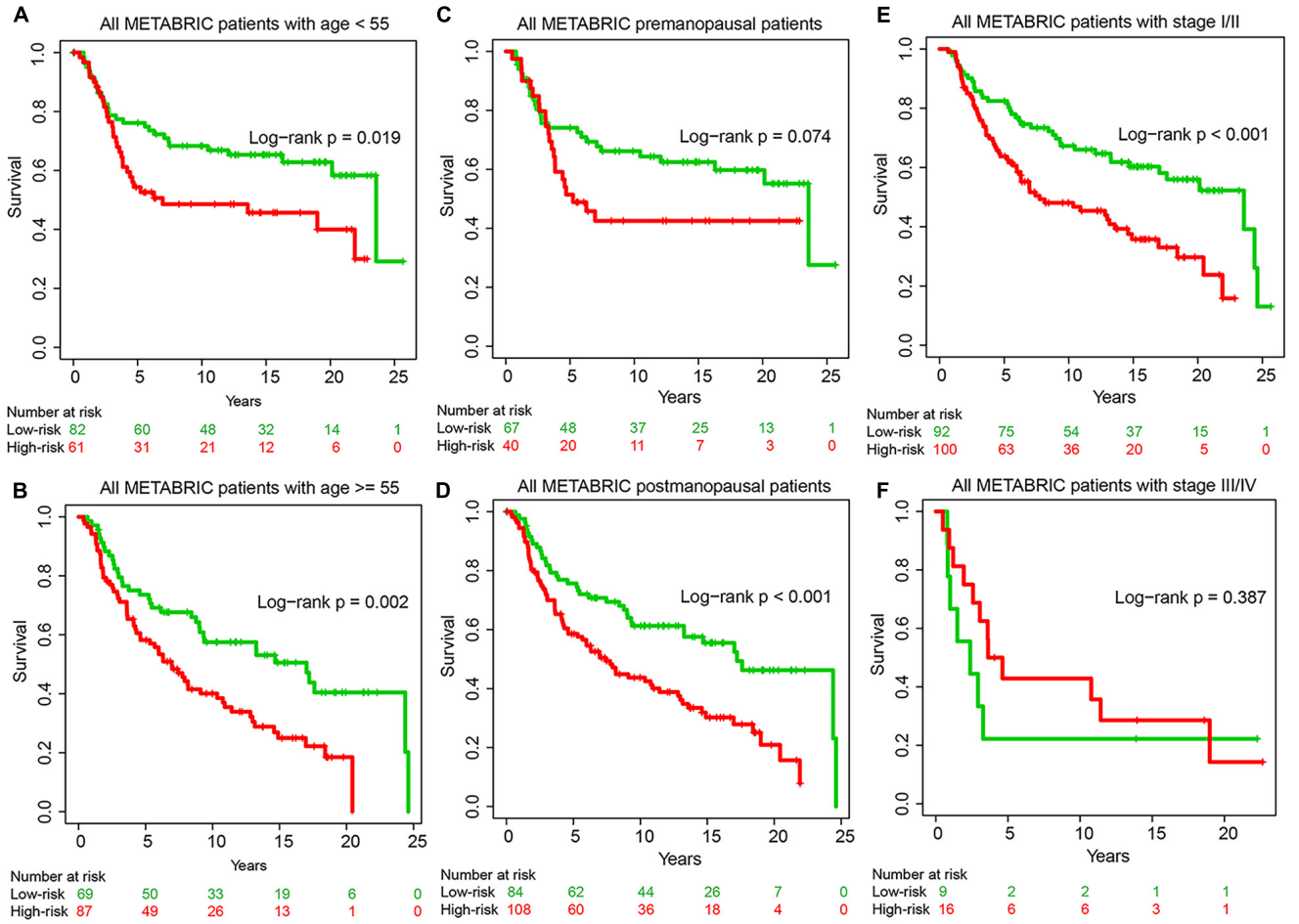


FIGURE 5 | Prognostic prediction by GIGenSig is independent of clinical features. **(A,B)** Survival curve of overall survival (OS) for patients with age <55 and ≥55 in the METABRIC datasets. Patients were significantly classified into high- and low-risk groups. **(C,D)** Survival curve of OS for patients with premenopausal and postmenopausal status in the METABRIC datasets. Patients were classified into high- and low-risk groups; **(E,F)** Survival curve of OS for patients with stages I and II and stages III and IV in the METABRIC datasets. Patients were classified into high- and low-risk groups.

DISCUSSION

Compared with TNBC treatment, limited progress has been made in TNBC prognosis (Sulaiman et al., 2018a,b; Mou and Wang, 2019; Zhang et al., 2019). Prognostic study usually evaluates clinical features, such as tumor size, stage, grade, etc., which provide limited mechanistic information to understand the relationship between prognosis and the disease (Echavarria et al., 2018; Johansson et al., 2018; Park et al., 2019). Genome instability and abnormal gene expression are common features in cancer (Telli et al., 2016; Tutt et al., 2018; Huang et al., 2019). While the relationship between genome instability and dysregulation of gene expression in cancer has been studied, genome-wide characterization for its prognostic value in TNBC has not been systematically analyzed (Grady and Carethers, 2008; Rao et al., 2017; Kalimutho et al., 2019).

As shown from our current study, molecular evidence from genome instability and abnormal gene expression is a rich resource to identify prognostic signatures as the prognostic marker for TNBC. In our study, we identified 111 genome instability-related genes by integrating mutation, CNV, and gene expression from TNBC. Functional analysis showed that these 111 genomic instability-related genes were enriched in the pathways associated with mitotic process. Dysregulation of mitotic processes can impact DNA replication involving mitotic nuclear division, nuclear division, and organelle fission, contributing to genome instability and OS of TNBC (Chen L. et al., 2018; Si et al., 2020; Suo et al., 2020). For example, the feedback loop between Drp1-mediated mitochondrial fission and Notch signaling pathway can promote TNBC cell survival via increasing survivin expression (Chen L. et al., 2018), and silibinin-induced mitochondrial fission can cause mitophagy preventing silibinin-induced apoptosis in TNBC (Si et al., 2020). Functional annotation with DAVID tool revealed that these 111-genomic instability-related genes play important roles in carcinogenetic pathways, such as affecting cell cycle (Kastan and Bartek, 2004), uncontrolled cell proliferation

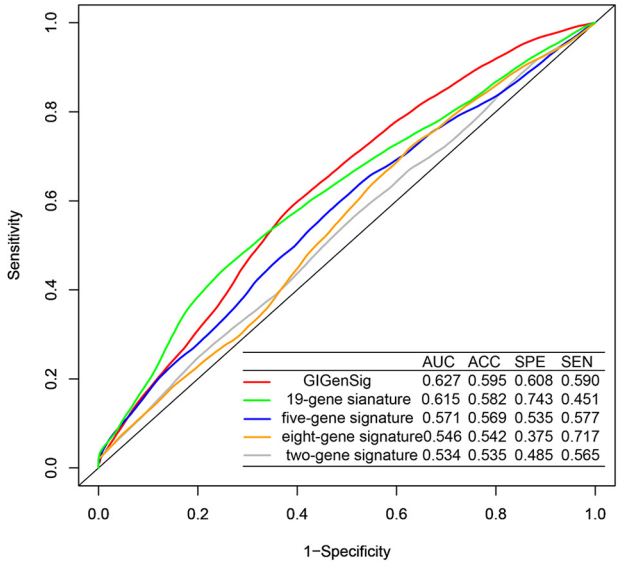


FIGURE 6 | Better performance of GIGenSig than other prognostic signatures. Five-year ROC comparison of overall survival between GIGenSig signature and other four signatures from AUC (area under the curve), ACC (accuracy), SPE (specificity), and SEN (sensitivity).

(Evan and Vousden, 2001), and abnormal immune response (Desrichard et al., 2016).

From the 111 genes, we further identified a GIGenSig with 11 genes (*ART3*, *CD52*, *CD79A*, *FZD9*, *GABRP*, *IRF8*, *ITM2A*, *PRKCB*, *SOX10*, *TFF3*, and *VGLL1*). Our study demonstrated that the GIGenSig effectively divided TNBC into high- and low-risk groups in the training dataset and its prognostic value was validated independently in multiple testing datasets. Besides, GIGenSig was significantly associated with genomic alteration pattern and *FOXM1* expression, which are important predictors of genome instability. Certain genes in GIGenSig are known to be closely related to tumorigenesis and development of TNBC. For example, *ART3* overexpression regulated TNBC cell functions by activating AKT and ERK pathways (Tan et al., 2016); *GABRP* and *VGLL1* were present in basal-like/triple-negative phenotype, and their expression levels were associated with OS of TNBC (Castilla et al., 2014; Sizemore et al., 2014); and *ITM2A* and *SOX10* were prognostic biomarkers for TNBC and potential therapeutic targets (Harbhajanka et al., 2018; Abuderman et al., 2020).

Furthermore, our identified GIGenSig can have clinical significance in TNBC treatment. It has been reported that Ki67 encoded by *MKI67* plays an important role in the prognosis and treatment of breast cancer (Yerushalmi et al., 2010; Li et al., 2015; Jurikova et al., 2016). Using the METABRIC dataset, we also observed that older TNBC patients had significantly lower *MKI67* expression than younger TNBC patients (**Supplementary Figure 7A**, Wilcox test $p = 2.59e{-}3$). However, Ki67 did not show prognostic value for patients used in our study (**Supplementary Figure 7B**). This implies that a combination of multiple genes provides better prognostic power than does a single gene. Our study also found that TNBC patients with chemotherapy treatment had low risk (84 vs. 73 with chemotherapy in the low-risk and high-risk groups, **Supplementary Figure 7C**), demonstrating the effectiveness of chemotherapy as the main therapeutic strategy in TNBC treatment (Denkert et al., 2017; Chaudhary et al., 2018; Lyons, 2019).

In conclusion, our study provides a genome instability-based TNBC prognostic signature to predict the clinical outcome of TNBC. Further tests with more datasets and clinical information will validate its value for clinical TNBC applications.

DATA AVAILABILITY STATEMENT

Publicly available datasets were analyzed in this study. These are included in the article/**Supplementary Material**.

AUTHOR CONTRIBUTIONS

MG and SW conceptualized the study and reviewed and edited the manuscript. MG formulated the methodology, performed the investigation and visualization, and wrote the original draft. SW supervised and secured the funding. Both authors contributed to the article and approved the submitted version.

FUNDING

This study was supported by grants from the Macau Science and Technology Development Fund (085/2017/A2 and 0077/2019/AMJ), the University of Macau (SRG2017-00097-FHS and MYRG2019-00018-FHS), and the Faculty of Health Sciences, the University of Macau (FHSIG/SW/0007/2020P, Startup fund) (SW).

ACKNOWLEDGMENTS

We are thankful to the Information and Communication Technology Office (ICTO), University of Macau, for providing the High-Performance Computing Cluster (HPCC) resources and facilities for the study.

SUPPLEMENTARY MATERIAL

The Supplementary Material for this article can be found online at: https://www.frontiersin.org/articles/10.3389/fcell.2021.701073/full#supplementary-material

REFERENCES

Abuderman, A. A., Harb, O. A., and Gertallah, L. M. (2020). Prognostic and clinicopathological values of tissue expression of MFAP5 and ITM2A in triple-negative breast cancer: an immunohistochemical study. *Contemp. Oncol. (Pozn)* 24, 87–95. doi: 10.5114/wo.2020.97520

Alsaleem, M. A., Ball, G., Toss, M. S., Raafat, S., Aleskandarany, M., Joseph, C., et al. (2020). A novel prognostic two-gene signature for triple negative breast cancer. *Mod. Pathol.* 33, 2208–2220. doi: 10.1038/s41379-020-0563-7

Bao, S., Hu, T., Liu, J., Su, J., Sun, J., Ming, Y., et al. (2021). Genomic instability-derived plasma extracellular vesicle-microRNA signature as a minimally invasive predictor of risk and unfavorable prognosis in breast cancer. *J. Nanobiotechnol.* 19:22. doi: 10.1186/s12951-020-00767-3

Castilla, M. A., Lopez-Garcia, M. A., Atienza, M. R., Rosa-Rosa, J. M., Diaz-Martin, J., Pecero, M. L., et al. (2014). VGLL1 expression is associated with a triple-negative basal-like phenotype in breast cancer. *Endocr. Relat. Cancer* 21, 587–599. doi: 10.1530/ERC-13-0485

Chaudhary, L. N., Wilkinson, K. H., and Kong, A. (2018). Triple-negative breast cancer: who should receive neoadjuvant chemotherapy? *Surg. Oncol. Clin. N. Am.* 27, 141–153. doi: 10.1016/j.soc.2017.08.004

Chen, L., Zhang, J., Lyu, Z., Chen, Y., Ji, X., Cao, H., et al. (2018). Positive feedback loop between mitochondrial fission and Notch signaling promotes survivin-mediated survival of TNBC cells. *Cell Death Dis.* 9:1050. doi: 10.1038/s41419-018-1083-y

Chen, M., Pockaj, B., Andreozzi, M., Barrett, M. T., Krishna, S., Eaton, S., et al. (2018). JAK2 and PD-L1 amplification enhance the dynamic expression of PD-L1 in triple-negative breast cancer. *Clin. Breast Cancer* 18, e1205–e1215. doi: 10.1016/j.clbc.2018.05.006

Denkert, C., Liedtke, C., Tutt, A., and von Minckwitz, G. (2017). Molecular alterations in triple-negative breast cancer-the road to new treatment strategies. *Lancet* 389, 2430–2442. doi: 10.1016/S0140-6736(16)32454-0

Dent, R., Trudeau, M., Pritchard, K. I., Hanna, W. M., Kahn, H. K., Sawka, C. A., et al. (2007). Triple-negative breast cancer: clinical features and patterns of recurrence. *Clin. Cancer Res.* 13(15 Pt 1), 4429–4434. doi: 10.1158/1078-0432.CCR-06-3045

Desrichard, A., Snyder, A., and Chan, T. A. (2016). Cancer Neoantigens and Applications for Immunotherapy. *Clin. Cancer Res.* 22, 807–812. doi: 10.1158/1078-0432.CCR-14-3175

Echavarria, I., Lopez-Tarruella, S., Picornell, A., Garcia-Saenz, J. A., Jerez, Y., Hoadley, K., et al. (2018). Pathological response in a triple-negative breast cancer cohort treated with neoadjuvant carboplatin and docetaxel according to lehmann's refined classification. *Clin. Cancer Res.* 24, 1845–1852. doi: 10.1158/1078-0432.CCR-17-1912

Evan, G. I., and Vousden, K. H. (2001). Proliferation, cell cycle and apoptosis in cancer. *Nature* 411, 342–348. doi: 10.1038/35077213

Goldman, M. J., Craft, B., Hastie, M., Repecka, K., McDade, F., Kamath, A., et al. (2020). Visualizing and interpreting cancer genomics data via the Xena platform. *Nat. Biotechnol.* 38, 675–678. doi: 10.1038/s41587-020-0546-8

Grady, W. M., and Carethers, J. M. (2008). Genomic and epigenetic instability in colorectal cancer pathogenesis. *Gastroenterology* 135, 1079–1099. doi: 10.1053/j.gastro.2008.07.076

Guo, L., Li, W., Zhu, X., Ling, Y., Qiu, T., Dong, L., et al. (2016). PD-L1 expression and CD274 gene alteration in triple-negative breast cancer: implication for prognostic biomarker. *Springerplus* 5:805. doi: 10.1186/s40064-016-2513-x

Habermann, J. K., Doering, J., Hautaniemi, S., Roblick, U. J., Bundgen, N. K., Nicorici, D., et al. (2009). The gene expression signature of genomic instability in breast cancer is an independent predictor of clinical outcome. *Int. J. Cancer* 124, 1552–1564. doi: 10.1002/ijc.24017

Haffty, B. G., Yang, Q., Reiss, M., Kearney, T., Higgins, S. A., Weidhaas, J., et al. (2006). Locoregional relapse and distant metastasis in conservatively managed triple negative early-stage breast cancer. *J. Clin. Oncol.* 24, 5652–5657. doi: 10.1200/JCO.2006.06.5664

Harbhajanka, A., Chahar, S., Miskimen, K., Silverman, P., Harris, L., Williams, N., et al. (2018). Clinicopathological, immunohistochemical and molecular correlation of neural crest transcription factor SOX10 expression in triple-negative breast carcinoma. *Hum. Pathol.* 80, 163–169. doi: 10.1016/j.humpath.2018.06.007

Hatzis, C., Pusztai, L., Valero, V., Booser, D. J., Esserman, L., Lluch, A., et al. (2011). A genomic predictor of response and survival following taxane-anthracycline chemotherapy for invasive breast cancer. *JAMA* 305, 1873–1881. doi: 10.1001/jama.2011.593

Huang, Y., Li, W., Yan, W., Wu, J., Chen, L., Yao, X., et al. (2019). Loss of PICH promotes chromosome instability and cell death in triple-negative breast cancer. *Cell Death Dis.* 10:428. doi: 10.1038/s41419-019-1662-6

Huang da, W., Sherman, B. T., and Lempicki, R. A. (2009). Systematic and integrative analysis of large gene lists using DAVID bioinformatics resources. *Nat. Protoc.* 4, 44–57. doi: 10.1038/nprot.2008.211

Irizarry, R. A., Bolstad, B. M., Collin, F., Cope, L. M., Hobbs, B., and Speed, T. P. (2003a). Summaries of Affymetrix GeneChip probe level data. *Nucleic Acids Res.* 31:e15. doi: 10.1093/nar/gng015

Irizarry, R. A., Hobbs, B., Collin, F., Beazer-Barclay, Y. D., Antonellis, K. J., Scherf, U., et al. (2003b). Exploration, normalization, and summaries of high density oligonucleotide array probe level data. *Biostatistics* 4, 249–264. doi: 10.1093/biostatistics/4.2.249

Jiang, Y. Z., Ma, D., Suo, C., Shi, J., Xue, M., Hu, X., et al. (2019). Genomic and transcriptomic landscape of triple-negative breast cancers: subtypes and treatment strategies. *Cancer Cell* 35, 428–440.e425. doi: 10.1016/j.ccell.2019.02.001

Johansson, A. L. V., Andersson, T. M., Hsieh, C. C., Jirstrom, K., Cnattingius, S., Fredriksson, I., et al. (2018). Tumor characteristics and prognosis in women with pregnancy-associated breast cancer. *Int. J. Cancer* 142, 1343–1354. doi: 10.1002/ijc.31174

Jurikova, M., Danihel, L., Polak, S., and Varga, I. (2016). Ki67, PCNA, and MCM proteins: markers of proliferation in the diagnosis of breast cancer. *Acta Histochem.* 118, 544–552. doi: 10.1016/j.acthis.2016.05.002

Kalimutho, M., Nones, K., Srihari, S., Duijf, P. H. G., Waddell, N., and Khanna, K. K. (2019). Patterns of genomic instability in breast cancer. *Trends Pharmacol. Sci.* 40, 198–211. doi: 10.1016/j.tips.2019.01.005

Karn, T., Jiang, T., Hatzis, C., Sanger, N., El-Balat, A., Rody, A., et al. (2017). Association between genomic metrics and immune infiltration in triple-negative breast cancer. *JAMA Oncol.* 3, 1707–1711. doi: 10.1001/jamaoncol.2017.2140

Kastan, M. B., and Bartek, J. (2004). Cell-cycle checkpoints and cancer. *Nature* 432, 316–323. doi: 10.1038/nature03097

Kim, E. K., Park, A. K., Ko, E., Park, W. Y., Lee, K. M., Noh, D. Y., et al. (2019). Risk stratification of triple-negative breast cancer with core gene signatures associated with chemoresponse and prognosis. *Breast Cancer Res. Treat.* 178, 185–197. doi: 10.1007/s10549-019-05366-x

Kim, Y. H., Choi, M. H., Kim, J. H., Lim, I. K., and Park, T. J. (2013). C-terminus-deleted FoxM1 is expressed in cancer cell lines and induces chromosome instability. *Carcinogenesis* 34, 1907–1917. doi: 10.1093/carcin/bgt134

Li, J., Chen, Z., Su, K., and Zeng, J. (2015). Clinicopathological classification and traditional prognostic indicators of breast cancer. *Int. J. Clin. Exp. Pathol.* 8, 8500–8505.

Lyons, T. G. (2019). Targeted therapies for triple-negative breast cancer. *Curr. Treat. Options Oncol.* 20:82. doi: 10.1007/s11864-019-0682-x

Mermel, C. H., Schumacher, S. E., Hill, B., Meyerson, M. L., Beroukhim, R., and Getz, G. (2011). GISTIC2.0 facilitates sensitive and confident localization of the targets of focal somatic copy-number alteration in human cancers. *Genome Biol.* 12:R41. doi: 10.1186/gb-2011-12-4-r41

Mersin, H., Yildirim, E., Berberoglu, U., and Gulben, K. (2008). The prognostic importance of triple negative breast carcinoma. *Breast* 17, 341–346. doi: 10.1016/j.breast.2007.11.031

Mou, E., and Wang, H. (2019). LncRNA LUCAT1 facilitates tumorigenesis and metastasis of triple-negative breast cancer through modulating miR-5702. *Biosci. Rep.* 39:BSR20190489. doi: 10.1042/BSR20190489

Negrini, S., Gorgoulis, V. G., and Halazonetis, T. D. (2010). Genomic instability–an evolving hallmark of cancer. *Nat. Rev. Mol. Cell Biol.* 11, 220–228. doi: 10.1038/nrm2858

Oakman, C., Viale, G., and Di Leo, A. (2010). Management of triple negative breast cancer. *Breast* 19, 312–321. doi: 10.1016/j.breast.2010.03.026

Park, J. H., Jonas, S. F., Bataillon, G., Criscitiello, C., Salgado, R., Loi, S., et al. (2019). Prognostic value of tumor-infiltrating lymphocytes in patients with early-stage triple-negative breast cancers (TNBC) who did not receive adjuvant chemotherapy. *Ann. Oncol.* 30, 1941–1949. doi: 10.1093/annonc/mdz395

Pereira, B., Chin, S. F., Rueda, O. M., Vollan, H. K., Provenzano, E., Bardwell, H. A., et al. (2016). The somatic mutation profiles of 2,433 breast cancers refines their genomic and transcriptomic landscapes. *Nat. Commun.* 7:11479. doi: 10.1038/ncomms11479

Qian, J., Chen, H., Ji, X., Eisenberg, R., Chakravarthy, A. B., Mayer, I. A., et al. (2017). A 3q gene signature associated with triple negative breast cancer organ specific metastasis and response to neoadjuvant chemotherapy. *Sci. Rep.* 7:45828. doi: 10.1038/srep45828

Rao, C. V., Asch, A. S., and Yamada, H. Y. (2017). Frequently mutated genes/pathways and genomic instability as prevention targets in liver cancer. *Carcinogenesis* 38, 2–11. doi: 10.1093/carcin/bgw118

Sabatier, R., Finetti, P., Adelaide, J., Guille, A., Borg, J. P., Chaffanet, M., et al. (2011a). Down-regulation of ECRG4, a candidate tumor suppressor gene, in human breast cancer. *PLoS One* 6:e27656. doi: 10.1371/journal.pone.0027656

Sabatier, R., Finetti, P., Cervera, N., Lambaudie, E., Esterni, B., Mamessier, E., et al. (2011b). A gene expression signature identifies two prognostic subgroups of basal breast cancer. *Breast Cancer Res. Treat.* 126, 407–420. doi: 10.1007/s10549-010-0897-9

Safonov, A., Jiang, T., Bianchini, G., Gyorffy, B., Karn, T., Hatzis, C., et al. (2017). Immune gene expression is associated with genomic aberrations in breast cancer. *Cancer Res.* 77, 3317–3324. doi: 10.1158/0008-5472.CAN-16-3478

Schmitt, M. W., Prindle, M. J., and Loeb, L. A. (2012). Implications of genetic heterogeneity in cancer. *Ann. N. Y. Acad. Sci.* 1267, 110–116. doi: 10.1111/j.1749-6632.2012.06590.x

Senfter, D., Samadaei, M., Mader, R. M., Gojo, J., Peyrl, A., Krupitza, G., et al. (2019). High impact of miRNA-4521 on FOXM1 expression in medulloblastoma. *Cell Death Dis.* 10:696. doi: 10.1038/s41419-019-1926-1

Serino, L. T. R., Jucoski, T. S., Morais, S. B., Fernandes, C. C. C., Lima, R. S., Urban, C. A., et al. (2019). Association of FOSL1 copy number alteration and triple negative breast tumors. *Genet. Mol. Biol.* 42, 26–31. doi: 10.1590/1678-4685-gmb-2017-0267

Si, L., Fu, J., Liu, W., Hayashi, T., Mizuno, K., Hattori, S., et al. (2020). Silibinin-induced mitochondria fission leads to mitophagy, which attenuates silibinin-induced apoptosis in MCF-7 and MDA-MB-231 cells. *Arch. Biochem. Biophys.* 685:108284. doi: 10.1016/j.abb.2020.108284

Sizemore, G. M., Sizemore, S. T., Seachrist, D. D., and Keri, R. A. (2014). GABA(A) receptor pi (GABRP) stimulates basal-like breast cancer cell migration through activation of extracellular-regulated kinase 1/2 (ERK1/2). *J. Biol. Chem.* 289, 24102–24113. doi: 10.1074/jbc.M114.593582

Song, H., Cicek, M. S., Dicks, E., Harrington, P., Ramus, S. J., Cunningham, J. M., et al. (2014). The contribution of deleterious germline mutations in BRCA1, BRCA2 and the mismatch repair genes to ovarian cancer in the population. *Hum. Mol. Genet.* 23, 4703–4709. doi: 10.1093/hmg/ddu172

Sulaiman, A., McGarry, S., Lam, K. M., El-Sahli, S., Chambers, J., Kaczmarek, S., et al. (2018a). Co-inhibition of mTORC1, HDAC and ESR1alpha retards the growth of triple-negative breast cancer and suppresses cancer stem cells. *Cell Death Dis.* 9:815. doi: 10.1038/s41419-018-0811-7

Sulaiman, A., McGarry, S., Li, L., Jia, D., Ooi, S., Addison, C., et al. (2018b). Dual inhibition of Wnt and Yes-associated protein signaling retards the growth of triple-negative breast cancer in both mesenchymal and epithelial states. *Mol. Oncol.* 12, 423–440. doi: 10.1002/1878-0261.12167

Suo, H. D., Tao, Z., Zhang, L., Jin, Z. N., Li, X. Y., Ma, W., et al. (2020). Coexpression network analysis of genes related to the characteristics of tumor stemness in triple-negative breast cancer. *Biomed. Res. Int.* 2020:7575862. doi: 10.1155/2020/7575862

Suzuki, K., Ohnami, S., Tanabe, C., Sasaki, H., Yasuda, J., Katai, H., et al. (2003). The genomic damage estimated by arbitrarily primed PCR DNA fingerprinting is useful for the prognosis of gastric cancer. *Gastroenterology* 125, 1330–1340. doi: 10.1016/j.gastro.2003.07.006

Tan, A. R., and Swain, S. M. (2008). Therapeutic strategies for triple-negative breast cancer. *Cancer J.* 14, 343–351. doi: 10.1097/PPO.0b013e31818d839b

Tan, L., Song, X., Sun, X., Wang, N., Qu, Y., and Sun, Z. (2016). ART3 regulates triple-negative breast cancer cell function via activation of Akt and ERK pathways. *Oncotarget* 7, 46589–46602. doi: 10.18632/oncotarget.10306

Teh, M. T., Gemenetzidis, E., Chaplin, T., Young, B. D., and Philpott, M. P. (2010). Upregulation of FOXM1 induces genomic instability in human epidermal keratinocytes. *Mol. Cancer* 9:45. doi: 10.1186/1476-4598-9-45

Telli, M. L., Timms, K. M., Reid, J., Hennessy, B., Mills, G. B., Jensen, K. C., et al. (2016). Homologous recombination deficiency (HRD) score predicts response to platinum-containing neoadjuvant chemotherapy in patients with triple-negative breast cancer. *Clin. Cancer Res.* 22, 3764–3773. doi: 10.1158/1078-0432.CCR-15-2477

Tutt, A., Tovey, H., Cheang, M. C. U., Kernaghan, S., Kilburn, L., Gazinska, P., et al. (2018). Carboplatin in BRCA1/2-mutated and triple-negative breast cancer BRCAness subgroups: the TNT trial. *Nat. Med.* 24, 628–637. doi: 10.1038/s41591-018-0009-7

Wang, S., Beeghly-Fadiel, A., Cai, Q., Cai, H., Guo, X., Shi, L., et al. (2018). Gene expression in triple-negative breast cancer in relation to survival. *Breast Cancer Res. Treat.* 171, 199–207. doi: 10.1007/s10549-018-4816-9

Wu, J., Mamidi, T. K. K., Zhang, L., and Hicks, C. (2019). Integrating germline and somatic mutation information for the discovery of biomarkers in triple-negative breast cancer. *Int. J. Environ. Res. Public Health* 16:1055. doi: 10.3390/ijerph16061055

Yerushalmi, R., Woods, R., Ravdin, P. M., Hayes, M. M., and Gelmon, K. A. (2010). Ki67 in breast cancer: prognostic and predictive potential. *Lancet Oncol.* 11, 174–183. doi: 10.1016/S1470-2045(09)70262-1

Yu, G., Wang, L. G., Han, Y., and He, Q. Y. (2012). clusterProfiler: an R package for comparing biological themes among gene clusters. *OMICS* 16, 284–287. doi: 10.1089/omi.2011.0118

Zhang, B., Shetti, D., Fan, C., and Wei, K. (2019). miR-29b-3p promotes progression of MDA-MB-231 triple-negative breast cancer cells through downregulating TRAF3. *Biol. Res.* 52:38. doi: 10.1186/s40659-019-0245-4

Conflict of Interest: The authors declare that the research was conducted in the absence of any commercial or financial relationships that could be construed as a potential conflict of interest.

Copyright © 2021 Guo and Wang. This is an open-access article distributed under the terms of the Creative Commons Attribution License (CC BY). The use, distribution or reproduction in other forums is permitted, provided the original author(s) and the copyright owner(s) are credited and that the original publication in this journal is cited, in accordance with accepted academic practice. No use, distribution or reproduction is permitted which does not comply with these terms.

frontiers in Cell and Developmental Biology

ORIGINAL RESEARCH
published: 23 July 2021
doi: 10.3389/fcell.2021.659680

NAP1L1 Functions as a Tumor Promoter *via* Recruiting Hepatoma-Derived Growth Factor/c-Jun Signal in Hepatocellular Carcinoma

Ye-wei Zhang[1†], Qian Chen[1†], Bo Li[1†], Hai-Yang Li[1,2], Xue-Ke Zhao[3], Yan-yi Xiao[4], Shu Liu[5] and Shi Zuo[1,2*]*

[1] Department of Clinical Medicine, Guizhou Medical University, Guiyang, China, [2] Department of Hepatobiliary Surgery, The Affiliated Hospital of Guizhou Medical University, Guiyang, China, [3] Department of Infectious Diseases, The Affiliated Hospital of Guizhou Medical University, Guiyang, China, [4] Department of Obstetrics and Gynecology, The Third Affiliated Hospital of Southern Medical University, Guangzhou, China, [5] Department of Breast Surgery, The Affiliated Hospital of Guizhou Medical University, Guiyang, China

OPEN ACCESS

Edited by:
Simona Kranjc Brezar, Institute of Oncology Ljubljana, Slovenia

Reviewed by:
Avik Choudhuri, Harvard University, United States
Xina Xie, Shenzhen Second People's Hospital, China

***Correspondence:**
Shu Liu
308659546@qq.com
Shi Zuo
drzuoshi@gmc.edu.cn

[†] These authors have contributed equally to this work

Specialty section:
This article was submitted to Molecular and Cellular Oncology, a section of the journal Frontiers in Cell and Developmental Biology

Received: 28 January 2021
Accepted: 08 June 2021
Published: 23 July 2021

Citation:
Zhang Y-w, Chen Q, Li B, Li H-Y, Zhao X-K, Xiao Y-y, Liu S and Zuo S (2021) NAP1L1 Functions as a Tumor Promoter via Recruiting Hepatoma-Derived Growth Factor/c-Jun Signal in Hepatocellular Carcinoma. Front. Cell Dev. Biol. 9:659680. doi: 10.3389/fcell.2021.659680

NAP1L1 has been reported to be significantly involved in the carcinogenesis of hepatocellular carcinoma (HCC). Yet, its detailed molecular basis is still to be determined. Based on the analysis of The Cancer Genome Atlas (TCGA) database, NAP1L1 mRNA was found to be upregulated and predicted the poor prognosis initially. Subsequently, consistent with the prediction, the upregulated expression of NAP1L1 mRNA and protein levels was confirmed by quantitative polymerase chain reaction (qPCR), Western blot, and immunohistochemistry assays. Upregulated NAP1L1 protein positively promoted the disease progression and poor prognosis of HCC. In addition, NAP1L1 protein expression was considered as an independent prognostic factor in HCC. Inhibition of NAP1L1 expression by siRNA or shRNA pathway significantly reduced the cell proliferation and cell cycle transformation *in vitro* and *in vivo*. Mechanism analysis first showed that the function of NAP1L1 was to recruit hepatoma-derived growth factor (HDGF), an oncogene candidate widely documented in tumors. Furthermore, the latter interacted with c-Jun, a key oncogenic transcription factor that can induce the expression of cell cycle factors and thus stimulate the cell growth in HCC. Finally, transfecting HDGF or c-Jun could reverse the suppressive effects on HCC growth in NAP1L1-suppressed HCC cells. Our data indicate that NAP1L1 is a potential oncogene and acts *via* recruiting HDGF/c-Jun in HCC.

Keywords: hepatocellular carcinoma (HCC), HDGF, c-Jun, proliferation, NAP1L1

INTRODUCTION

Liver cancer is one of the leading causes of cancer-related deaths in the world (Akinyemiju et al., 2017), also causing the fourth deaths in most common malignancy and the third deaths in leading tumor-related deaths in China. Liver cancer is classified as primary and metastatic liver cancer. In China, hepatocellular carcinoma (HCC) accounts for about 85–90% of primary liver cancer (Zhou et al., 2018). Therefore, we focused on HCC in this study.

Hepatocellular carcinoma is a type of heterogeneous cancer with a lot of factors implicated in its development, with chronic infection and cirrhosis by hepatitis B virus (HBV) being the most prevalent (Beasley, 1988; McGlynn et al., 2015; Yamashita and Kaneko, 2016). Cirrhosis due to metabolic dysfunction, excessive alcohol consumption, non-alcoholic fatty liver disease (NAFLD), and hepatitis C virus (HCV) infection are also involved in HCC development (Venook et al., 2010; Morgan et al., 2013; Calzadilla and Adams, 2016; Yamashita and Kaneko, 2016). These factors alone or together lead to the imbalance of gene expression in the normal liver, inducing the occurrence and development of HCC (Lin et al., 2019, 2020; Liu et al., 2020).

NAP1L1 belongs to the human counterpart of the yeast NAP-I protein, a histone-binding factor involved in the cumulative nucleosome formation. NAP1L1 has been shown as a potential tumor promoter and participates in the pathogenesis of several tumors including colorectal cancer, renal cancer, and pancreatic neuroendocrine neoplasm (Schimmack et al., 2014; Zhai et al., 2018; Queiroz et al., 2020). Recent studies on HCC showed that PRDM8 suppresses the occurrence of tumor *via* interacting with NAP1L1 (Chen et al., 2018). Furthermore, NAP1L1 is modulated by the LncRNA CDKN2B-AS1/NAP1L1 axis and participates in the pathogenesis of HCC. However, the molecular basis of NAP1L1 in modulating HCC proliferation is still unclear (Huang et al., 2018).

Here, we found that the NAP1L1 protein level was significantly elevated in both HCC patients and HCC cell lines. It was an unfavorable factor, boosting the clinical progression and poor prognosis of HCC patients. Further, NAP1L1 was shown to be an oncogene that recruits hepatoma-derived growth factor (HDGF). The latter interacts with c-Jun, thus stimulating cell cycle signal transition and thus finally inducing HCC proliferation. The data indicate that NAP1L1 is a tumor promoter, significantly involved in the pathogenesis of HCC.

MATERIALS AND METHODS

Bioinformatics Assay

BIOGRID web[1] was used to find the potential biomarker interacting with NAP1L1 and HDGF. UALCAN web[2] was used to analyze the differential expression of NAP1L1 in HCC cancer based on The Cancer Genome Atlas (TCGA) database.

Cell Culture

Normal liver cell lines (LO2) and HCC cell lines (HCCLM3, PLC/PRF-5, Huh-7, 97H, Hep-G2, and Hep-3B) were purchased from the Cell Bank of the Chinese Academy of Sciences (Shanghai, China) and cultured in Dulbecco's modified Eagle medium (DMEM) (HyClone, Logan, UT, United States) supplemented with 10% fetal bovine serum (FBS; PAN-Biotech, Aidenbach, Germany). The cell lines were incubated with a 5% CO_2 humidified chamber at 37°C.

[1]https://thebiogrid.org/

[2]http://ualcan.path.uab.EdU/

RT-PCR and QPCR

Total RNA was isolated from the HCC cell lines using a TRIzol Kit (Foregene, Chengdu, China). cDNA was synthesized using a cDNA synthesis kit (Vazyme, Nanjing, China), and the cDNA was used as a template for amplification using specific primers (GAPDH genes were used as internal gene controls). The primers used in this study are shown in **Supplementary Table 1**. RT-PCR and quantitative polymerase chain reaction (qPCR) were performed following the manufacturer's instructions using Bio-Rad T100 and Bio-Rad CFX96 detection systems.

Immunohistochemistry

This study was approved by the Research Ethics Committee of The Affiliated Hospital of Guizhou Medical University (No. 2018005). In this study, a total of 10 HCC tissues and 10 adjacent tissues were obtained from HCC patients undergoing surgical treatment.

Tissue array was purchased from Shanghai Tufei Biotech (Shanghai Tufeibio, Shanghai, China). It was used to examine NAP1L1 protein expression. The indirect streptavidin–peroxidase method was used following the manufacturer's standard experiment guidelines. Cell staining was scored separately by two pathologists blinded to the clinical parameters. The extent of staining, defined as the percentage of positively stained tumor cells with respect to the whole tissue area, was scored on a scale of 0–4 as follows: 0, <10%; 1, 10–25%; 2, 26–50%; 3, 50–75%; and 4, >75%. The staining intensity was scored as 0–3 (Negative: 0; Weak expression: 1; Positive expression: 2; Strong expression: 3). The score represents the product of positive staining score, and the color intensity score was used as the final staining score for NAP1L1 (Abcam, Cambridge, MA, United States), Ki-67 (Cell Signaling Technology, Danvers, MA, United States), and PCNA (Proteintech, Wuhan, China) (0–12). For statistical analysis, final staining scores of 0–6 and 8–12 were considered to show low and high expressions, respectively. The Cat numbers, origins, and dilution concentrations used for all antibodies are listed in **Supplementary Table 2**.

Lentivirus Infection

ShRNA-NAP1L1 lentiviral particles were constructed by GeneChem (Shanghai, China). HCCLM3 and Huh-7 cells were infected with the lentiviral vector. Silencing efficiency for NAP1L1 was measured by Western blot analysis. Transient and stable disturbance sequences are shown in **Supplementary Table 3**.

SiRNA and Plasmid Transfection

SiRNAs for NAP1L1 were designed and synthesized by RiboBio (Guangzhou, China). Plasmids for HDGF were purchased from Vigene Biosciences. Twelve hours before transfection, the HCC cells were plated into six-well plates (Nest Biotech, Wuxi, China) and cultured to 30–50% confluence. SiRNAs or plasmids were then transfected at a working concentration of 100 nM using the Lipofectamine 2000 Transfection Reagent (Invitrogen, Carlsbad, CA, United States) following the manufacturer's protocol. Then, DMEM was supplemented with 10% FBS after 4 h.

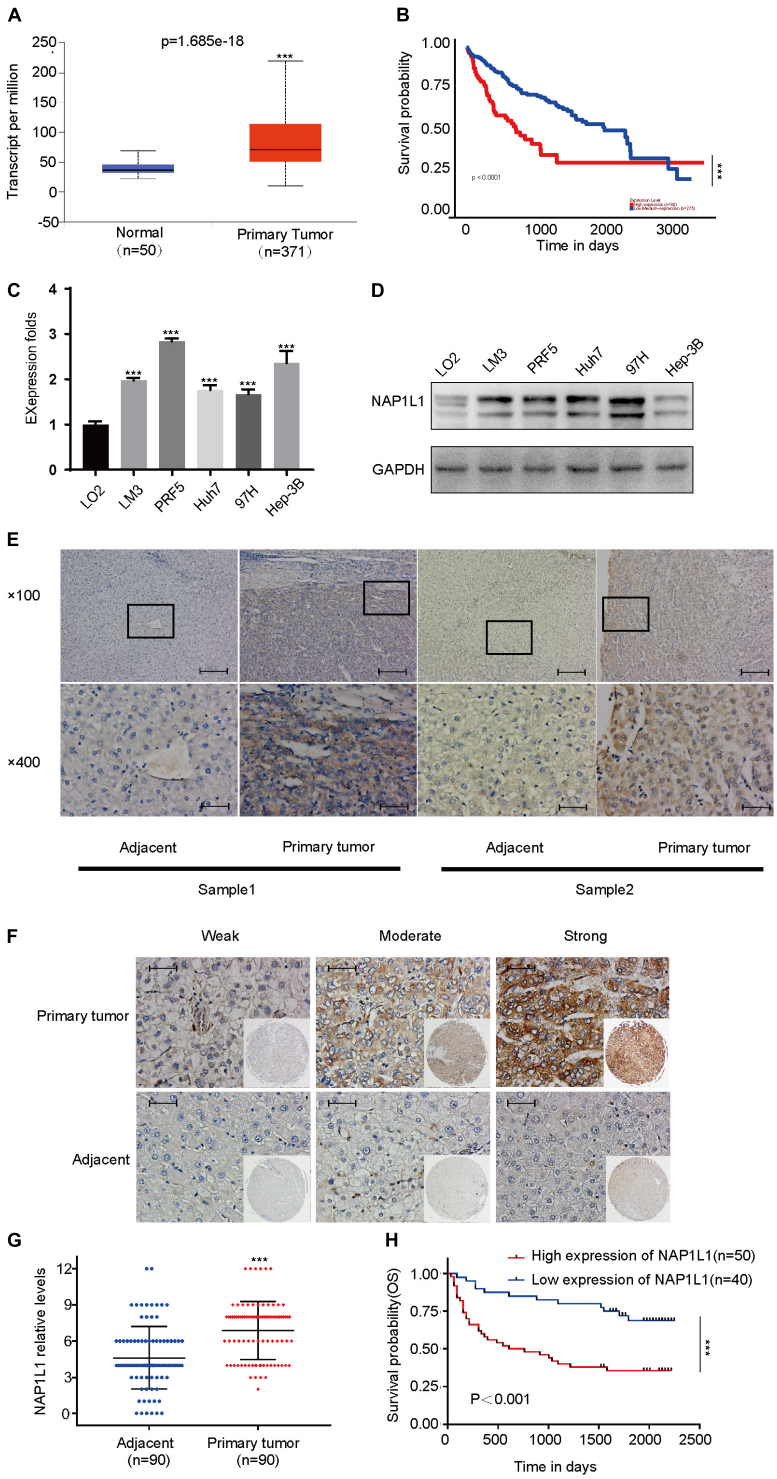


FIGURE 1 | NAP1L1 was upregulated in HCC, and high expression reduced the overall survival. **(A)** NAP1L1 mRNA expression in liver cancer tissue and peritumoral tissue among the HCC patients obtained from the TCGA database (http://ualcan.path.uab.edu/). **(B)** Kaplan–Meier survival analysis for overall survival based on the NAP1L1 expression data. **(C)** RT-qPCR analysis of NAP1L1 mRNA expression in normal hepatocytes and HCC cell lines. **(D)** Western blot analysis of expression levels in normal hepatocytes and HCC cell lines. **(E)** NAP1L1 expression was measured *via* immunohistochemical staining in HCC and paracarcinoma tissues (×100 visual field, scale bar: 200 μm, ×400, scale bar: 50 μm). **(F)** NAP1L1 expression performed in TMA (scale bar: 50 μm). **(G)** TMA immunohistochemical cell staining score. **(H)** Kaplan–Meier survival analysis for overall survival in TMA showing NAP1L1 expression. Data are presented as mean ± SD from three independent experiments. *$p < 0.05$ vs. control; **$p < 0.01$; ***$p < 0.001$.

MTT Cytotoxicity

The HCC cancer cells (5,000/well) were seeded into 96-well plates. For lentivirus-mediated shNAP1L1 expression, the cells were incubated for a week. For transient transfections with si-NAP1L1, the cells were cultured for up to 4 days. Subsequently, 20 μl of MTT (5 μg/μl in PBS) (Sigma, St. Louis, MO, United States) solution was added to each well and incubated for 4 h. Then, the formazan crystals formed by viable cells were solubilized in 150 ml dimethyl sulfoxide (Sigma, St. Louis, MO, United States), and the absorbance value (OD) was measured at 490 nm. All the experiments were repeated at least three times.

Colony Formation Assay

Cloning is based on the previous study (Lin et al., 2019). The cells were seeded in six-well culture plates at 200–500 cells/well (the number of inoculations was determined following the minimum of population dependence of cell lines). After incubation for 14 days, the cells were washed twice with PBS solution and stained with hematoxylin solution. The number of colonies was counted under a microscope. All the experiments were repeated at least three times.

EdU Staining

In the EdU incorporation assay, the proliferating HCC cells were examined using a Cell-Light EdU Apollo 488 or 567 *In Vitro* Imaging Kit (RiboBio) following the manufacturer's protocol. After incubation with 10 mM EdU for 2 hours, the HCC cells were treated with 4% paraformaldehyde, permeabilized in 0.3% Triton X-100, and stained with Apollo fluorescent dyes. A total of 5 mg/ml of DAPI was used to stain the cell nuclei for 10 min. The number of EdU-positive cells was counted under a fluorescence microscope in five random fields. All the assays were independently performed three times.

Subcutaneous Tumorigenesis in Nude Mice

A total of 5×10^6 logarithmically growing HCC cells of NAP1L1 downregulated and their corresponding negative control (NC) cells were injected into the subcutaneous tissues of nude mice (BALB/C, nu/nu, female 3–4 weeks old) (one group = 5). The animals were fed an autoclaved laboratory rodent diet. On the 21st day, the tumor tissues were excised and weighed. All the animal studies were conducted in accordance with the principles and procedures outlined in the Guizhou Medical University Guide for the Care and Use of Animals.

Western Blot Assays

The extracted proteins were separated by 10% SDS-PAGE and further transferred onto PVDF membranes (Millipore, Bedford, MA, United States). Antibodies including NAP1L1 (Abcam), CCND1 (Abcam), HDGF (Proteintech), and c-Jun (Proteintech) were used in the Western blot assays following the manufacturer's instructions. Detection was performed using ECL Plus Western blotting detection reagents (Millipore, United States). The specific protein expression levels of the blots were normalized to GAPDH (Santa). The Cat numbers, origins, and dilution concentrations used for all antibodies are listed in **Supplementary Table 2**.

Co-Immunoprecipitation (Co-IP) Assay

Co-Immunoprecipitation (Co-IP) assay was carried out using Pierce Co-IP Kit (Thermo Scientific, United States) following the manufacturer's instructions. The total protein was extracted and quantified. A total of 3,000 μg protein in 400 μl supernatant was incubated with 10 μg anti-NAP1L1 (Abcam), anti-HDGF (Proteintech), anti-c-Jun (Proteintech), or anti-IgG antibodies for 12 h at 4°C. The beads were washed, eluted in a sample buffer, and boiled for 10 min at 100°C. The immune complexes were subjected to Western blot analysis. Anti-IgG was used as an NC. The Cat numbers, origins, and dilution concentrations used for all antibodies are listed in **Supplementary Table 2**.

Confocal Microscopy

HCCLM3 and Huh-7 cells were cultured overnight (2×10^5/immunofluorescence well) and then treated with

TABLE 1 | Correlation of NAP1L1 expression with clinicopathological characteristics of patients with HCC.

Characteristics	*n*	NAP1L1 expression		
		High	Low	*p*
Gender				
Male	70	37(52.86%)	33(47.14%)	0.335
Female	20	13(65.00%)	7(35.00%)	
Age(year)				
≤50	40	24(60.00%)	16(40.00%)	0.448
>50	50	26(52.00%)	24(48.00%)	
Clinical stage				
I	58	25(43.10%)	33(56.90%)	0.001
II∼III	32	25(78.13%)	7(21.88%)	
Tumor scale				
≤5 cm	47	24(51.06%)	23(48.94%)	0.37
>5cm	43	26(60.47%)	17(39.53%)	
Histological Grade				
I∼II	54	22(40.74%)	32(59.26%)	<0.001
III	36	28(77.78%)	8(22.22%)	
Vital states				
Alive	46	18(39.13%)	28(60.87%)	0.001
Die	44	32(72.73%)	12(27.27%)	
Recurrence				
No	22	16(72.73%)	6(27.27%)	0.062
Yes	68	34(50.00%)	34(50.00%)	
HBsAg				
Positive	70	40(57.14%)	30(42.86%)	0.571
Negative	20	10(50.00%)	10(50.00%)	
Tumor thrombus				
No	65	29(44.62%)	36(55.38%)	<0.001
Yes	25	21(84.00%)	4(16.00%)	
Lymph metastasis metastasismetastasis				
No	86	48(55.81%)	38(44.19%)	0.819
Yes	4	2(50.00%)	2(50.00%)	
AFP stage				
≤200 μg/L	45	15(33.33%)	30(66.67%)	<0.001
>200 μg/L	45	35(77.78%)	10(22.22%)	

4% paraformaldehyde and permeabilized with 0.5% Triton X-100 at room temperature. The cells were incubated with anti-NAP1L1 (Abcam), anti-HDGF (Proteintech), and anti-c-Jun (Proteintech) antibodies for 60 min at 37°C. After incubation for 30 min at 37°C with a secondary antibody, coverslips were mounted onto the slides with a mounting solution containing 0.2 mg/ml DAPI. The images were captured by laser scanning confocal microscopy (Zeiss LSM 800). The Cat numbers, origins, and dilution concentrations used for all antibodies are listed in **Supplementary Table 3**.

Statistical Analysis

Statistical analyses were carried out using SPSS 22.0 statistical software package (SPSS, Chicago, IL, United States). The data are shown as the mean ± SD obtained from at least three independent experiments. Two-tailed Student's *t*-test was applied for comparisons between groups. Survival analysis was performed using the Kaplan–Meier method. All statistical tests were two-sided; single, double, and triple asterisks indicate statistical significance (*$p < 0.05$, **$p < 0.01$, and ***$p < 0.001$).

RESULTS

NAP1L1 Level Is Upregulated in HCC and Correlates With Poor Prognosis

According to the analysis of the TCGA database, NAP1L1 mRNA was upregulated and predicted poor prognosis (**Figures 1A,B**). Subsequently, consistent with the prediction, the upregulated expression of NAP1L1 mRNA and protein levels was confirmed by real-time quantitative PCR (qRT-PCR), Western blot analysis of the human HCC and normal liver cell lines, and immunohistochemistry assay on the clinic human HCC tissue sections (**Figures 1C–E**). Immunohistochemical analysis of NAP1L1 was performed in tissue microarrays (TMA) containing 90 paired HCC samples and adjacent non-tumor tissues of human HCC, and cell staining was scored (**Figures 1F,G**). Survival analysis showed that overexpressed NAP1L1 is an unfavorable factor, reducing the overall survival time of HCC patients (**Figure 1H**), and then the clinical significance of NAP1L1 expression was assessed (**Table 1**). Features associated with the survival in univariate Cox regression analysis were as follows: clinical stage ($p < 0.001$), histological grade ($p = 0.023$), tumor scale ($p = 0.008$), recurrence ($p = 0.035$), tumor thrombus ($p < 0.001$), lymph metastasis ($p = 0.009$), AFP stage ($p < 0.001$), and NAP1L1 expression ($p = 0.001$). However, multivariate Cox regression analysis indicated that clinical stage ($p = 0.007$) was a predictor for poor survival compared with high NAP1L1 level (**Table 2**).

NAP1L1 Knockdown Inhibits Cell Proliferation *in vitro* and *in vivo*

To investigate the NAP1L1 effects on HCC proliferation, lentivirus-carrying shRNA-NAP1L1 was infected into HCCLM3 and Huh7 cells (**Supplementary Figure 1A**). The transfection efficiency was first analyzed by a qRT-PCR analysis (**Figure 2A**), and Western blot analyses were used to further verify this result (**Figure 2B**). Subsequently, the MTT (**Figure 2C**), plate clone (**Figure 2D**), and EdU staining assays confirm that shNAP1L1 inhibits cell proliferation *in vitro* (**Figure 2E**). A preliminary *in vivo* study was carried out. The average weight and volume of tumors significantly decreased in those xenograft mice injected with NAP1L1-level-decreased HCC cells compared with the NC group (**Figure 2F** and **Supplementary Figure 1B**). Then, ki-67 and PCNA expressions in xenograft tumors in nude mice were detected, and it was confirmed that in the group injected with shRNA-NAP1L1, the content of tumors was significantly smaller than that of the NC xenograft group (**Figure 2G**).

SiRNA-NAP1L1 Reduces Cell Proliferation *in vitro*

The HCC cancer cells were transfected with siRNA-NAP1L1, and their knockdown efficiency was verified (**Figures 3A,B**). SiRNAs which significantly repressed the expression of NAP1L1 were selected to perform MTT and EdU assays. The MTT assay shows that the reduced NAP1L1 protein level significantly decreased the cell growth (**Figure 3C**). EdU staining assay confirms the results obtained in the MTT assay (**Figure 3D**). We also assessed the

TABLE 2 | Summary of univariate and multivariate Cox regression analysis.

Parameter	Univariate analysis			Multivariate analysis		
	Hazard Ratio	95.0% CI	*p*	Hazard Ratio	95.0% CI	*p*
Gender	1.448	0.745-2.814	0.275			
Age(year)	0.702	0.388-1.271	0.243			
Clinical stage	5.203	2.809-9.639	<0.001	2.97	1.349-6.536	0.007
Tumor scale	2.291	1.246-4.214	0.008	1.752	0.906-3.390	0.096
Histological grade	1.995	1.102-3.611	0.023	0.851	0.429-1.689	0.645
Recurrence	0.501	0.263-0.954	0.035	0.495	0.237-1.035	0.062
HBsAg	0.947	0.468-1.917	0.88			
Tumor thrombus	3.614	1.973-6.622	<0.001	1.375	0.671-2.819	0.385
Lymph metastasis	4.007	1.424-11.273	0.009	3.159	0.947-10.535	0.061
AFP stage	3.124	1.648-5.923	<0.001	1.764	0.803-3.871	0.157
NAP1L1 expression	3.135	1.609-6.110	0.001	2.016	0.871-4.667	0.102

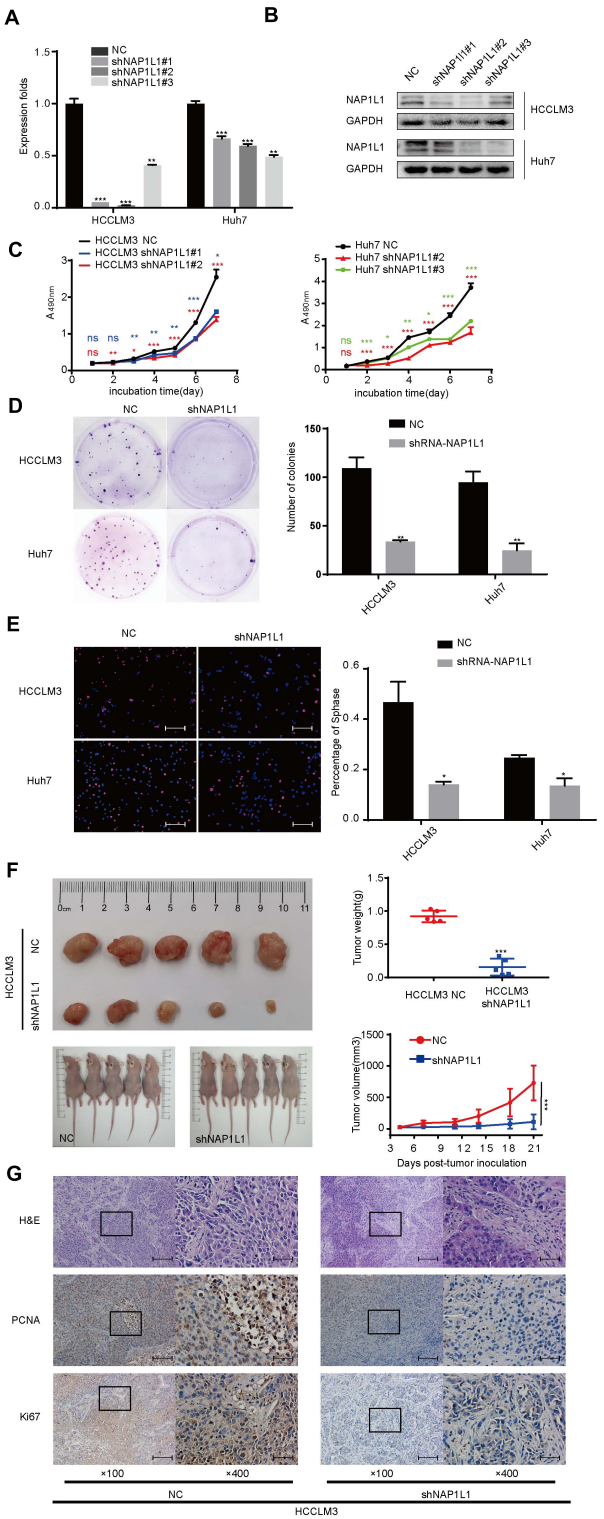


FIGURE 2 | Downregulated NAP1L1 expression attenuated cell proliferation. **(A)** Quantitative RT-qPCR data to measure gene expression after shRNA-NAP1L1 lentivirus or NC lentivirus transfection into HCCLM3 and Huh7 cells. **(B)** Efficiency of silencing NAP1L1 by Western blot analysis. **(C)** MTT assays indicated that shRNA-NAP1L1 inhibited the proliferation *(Continued)*

FIGURE 2 | Continued
in vitro. **(D)** Downregulated NAP1L1 expression suppressed plate clone formation. **(E)** EdU assay showed that the downregulation of NAP1L1 suppressed the proliferation *in vitro* (scale bar: 200 μm). **(F)** Xenograft tumor of nude mice showed that the average weight and volume of tumors decreased in the shRNA-NAP1L1 group compared with the NC group. **(G)** Hematoxylin–eosin staining in xenograft tumor of nude mice and expression of PCNA and Ki-67 were measured *via* IHC staining in the xenograft tumor of nude mice (×100 visual field, scale bar: 200 μm, ×400, scale bar: 50 μm). Data are presented as mean ± SD from three independent experiments. $^{*}p < 0.05$ vs. control; $^{**}p < 0.01$; $^{***}p < 0.001$.

effect of NAP1L1 in downregulation on cell cycle distribution by flow cytometry. The results show that the knockdown of NAP1L1 inhibited the S phase of HCC cells *in vitro* (**Figure 3E**).

Moreover, we also assessed the effect of NAP1L1 overexpression on downstream signaling. This was associated with the increase in the expression of HDGF, c-Jun, and CCND1 (**Supplementary Figures 1A,B**). The MTT and EdU assay showed that the increased NAP1L1 protein level significantly promoted the cell growth (**Supplementary Figures 1C,D**). Overexpression of NAP1L1 promoted HCC proliferation by promoting G1/S transition (**Supplementary Figure 1E**).

NAP1L1 Interacts With HDGF

Interestingly, a previous study in our group had found that NAP1L1 is a potential candidate of HDGF interaction proteins in endometrial carcinoma using exogenous Co-IP combined with mass spectrometry (unpublished data). In this study, we confirmed that NAP1L1 binds to HDGF by an endogenous Co-IP assay (**Figures 4A,B**). Furthermore, the confocal microscopic images showed the colocalization of NAP1L1 and HDGF in the cytoplasm of HCC cells (**Figure 4C**).

NAP1L1 Recruits c-Jun

Furthermore, we observed that HDGF interacted with c-Jun by Co-IP assay both in the cytoplasm and in the nucleus, predominantly in the cytoplasm (**Figure 5A**). c-Jun is an oncogenic transcription factor significantly participating in many tumor pathogeneses by transcription or suppressing the expression of some genes. Previous studies have shown that c-Jun regulates the proliferation of non-small cell lung cancer by targeting CCND1 (Zhao et al., 2018). The Co-IP assay in this study showed the interaction between c-Jun and HDGF in HCC (**Figures 5B,C**).

Transfecting HDGF Increases c-Jun/CCND1 Signal and Restores Cell Proliferation in NAP1L1-Suppressing HCC Cells

In this study, the NAP1L1 knockdown efficiencies and change in downstream were validated by Western blot assays (**Figure 6A**). The HDGF cDNA plasmid was transfected to NAP1L1-suppressing cells, to explore the role of HDGF in NAP1L1-mediated pathogenesis of HCC cancer. The knockdown efficiency was verified by qRT-PCR and western blot analysis

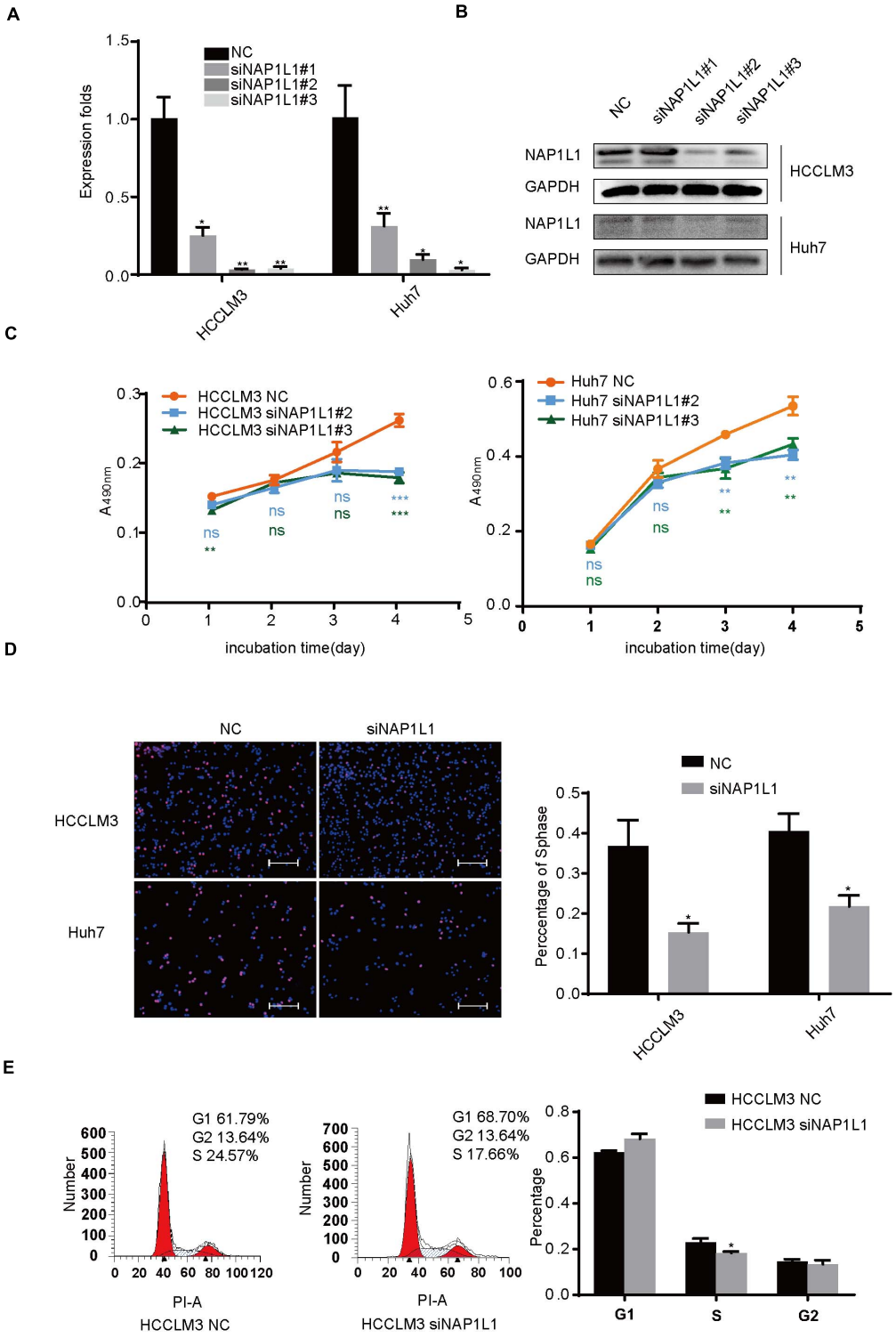


FIGURE 3 | SiRNA-NAP1L1 reduces cell proliferation *in vitro*. **(A)** Quantitative RT-qPCR data to measure gene expression after siRNA-NAP1L1 or NC lentivirus transfection into HCCLM3 and Huh7 cells. **(B)** Expression levels of NAP1L1 were detected by Western blot analysis to screen effective transfection fragments. **(C)** MTT assays showed that the inhibition of NAP1L1 reduces proliferation *in vitro* in HCCLM3 and Huh7. **(D)** EdU assay indicated that the downregulation of NAP1L1 suppressed the proliferation *in vitro* (scale bar: 200 μm). **(E)** Cell cycle distribution was subjected to flow cytometry, and quantified histograms show the effect of NAP1L1 downregulation on cell cycle distribution. Data are presented as mean ± SD from three independent experiments. $^{*}p < 0.05$ vs. control; $^{**}p < 0.01$; $^{***}p < 0.001$.

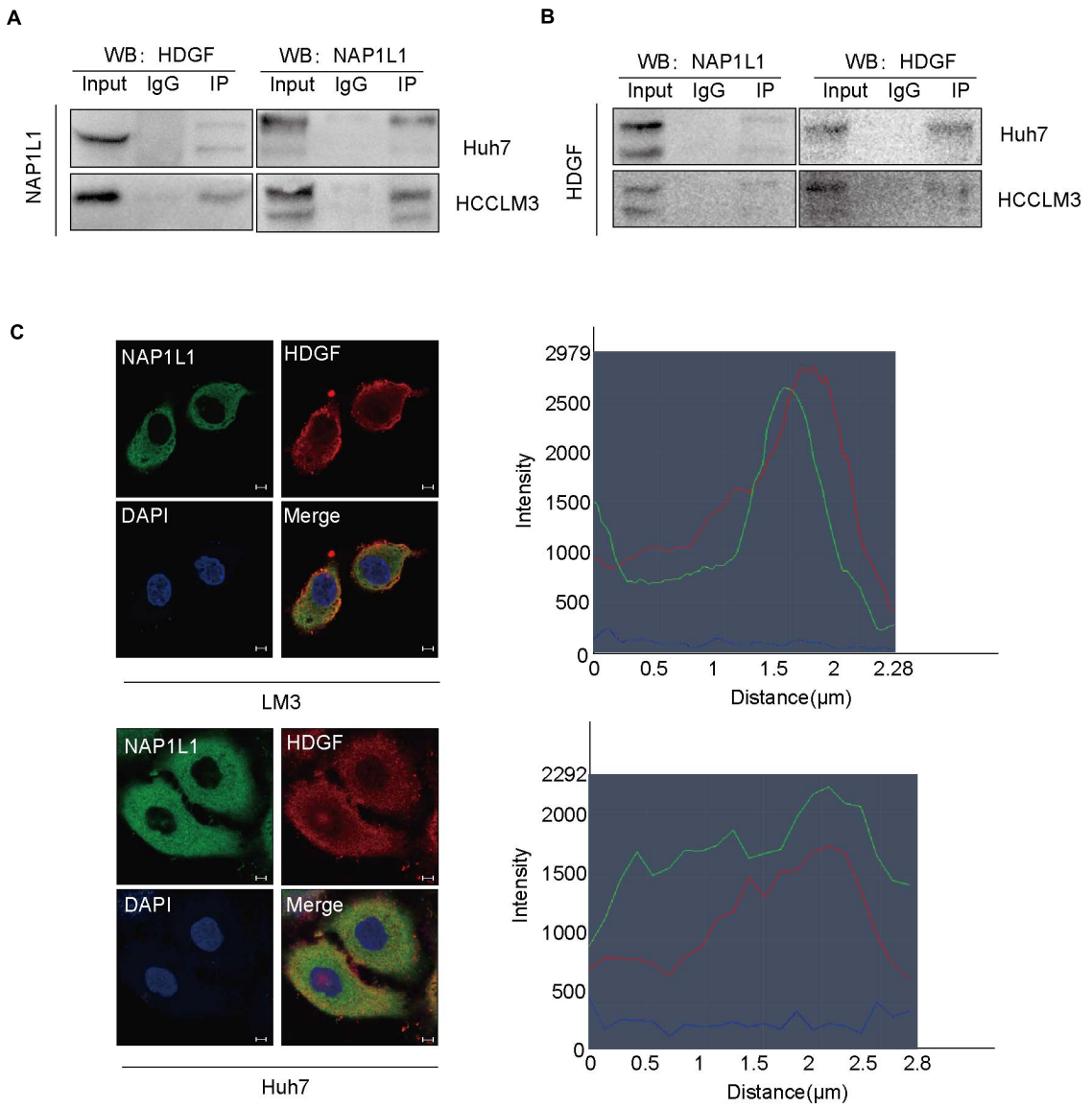


FIGURE 4 | NAP1L1 interacts with HDGF. **(A,B)** Co-IP assay identified NAP1L1 coprecipitated with HDGF. **(C)** Confocal microscopic images showed the colocalization of NAP1L1 and HDGF in the cytoplasm in HCCLM3 and Huh7 cells (scale bar: 5 μm).

(**Figures 6B,C**), and according to our observation *in vitro*, the ability of cell proliferation (**Figure 6D**) and EdU staining (**Figure 6E**) was restored. Western blot assay indicated that the c-Jun/CCND1 signal was significantly increased (**Figure 6C**).

Transfecting c-Jun Increases CCND1 Signal and Restores Cell Proliferation in NAP1L1-Suppressing HCC Cells

In addition, we transfected the c-Jun cDNA plasmid to NAP1L1-suppressing cells. qRT-PCR and Western blot analysis (**Figures 7A,B**) verified the knockdown efficiency, and the ability of cell proliferation (**Figure 7C**) and EdU staining (**Figure 7D**) was restored *in vitro*.

DISCUSSION

Hepatocellular carcinoma accounts for most liver cancers. This type of cancer occurs more often in men than in women. It is usually diagnosed in people of age 50 or older. In China, HCC is one of the common malignant tumors and mostly correlated with chronic HBV infection and subsequent liver cirrhosis formation. In the pathogenesis of HCC, a large number of genes and signal pathways show abnormal expression (Chen et al., 2019; Luiken et al., 2020). Therefore, exploring the pathogenesis of HCC will help to further improve the treatment of HCC, improving the survival prognosis and prolonging the survival time of patients.

The human NAP1-like protein (NAP1L) family comprises NAP1L1, NAP1L2, NAP1L3, NAP1L4, NAP1L5, and NAP1L6

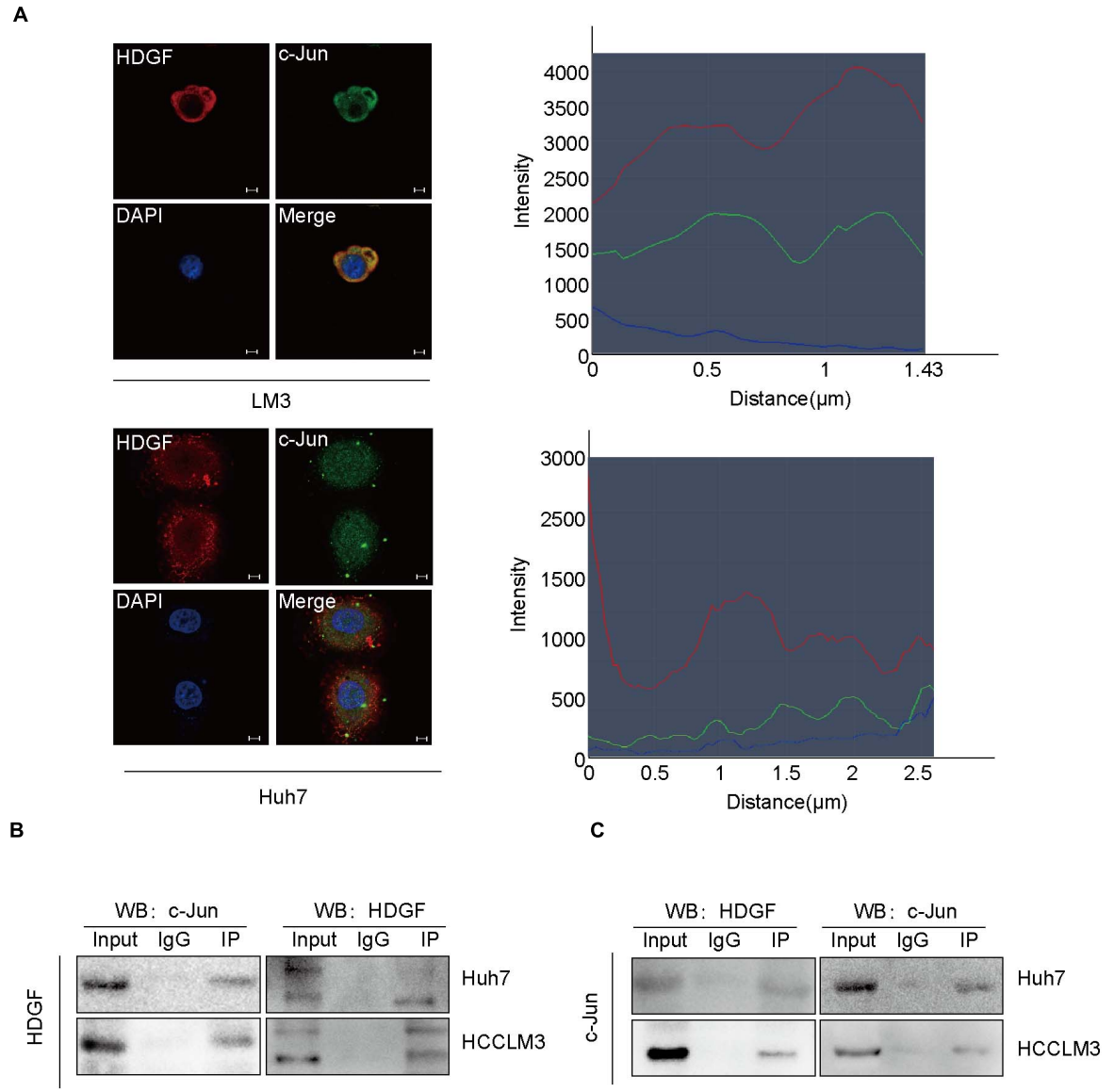


FIGURE 5 | NAP1L1 interacts with HDGF to recruit c-Jun. **(A)** Confocal microscopic images showed the colocalization of HDGF and c-Jun in the cytoplasm and nucleus (predominantly in the cytoplasm) in HCCLM3 and Huh7 cells (scale bar: 5 μm). **(B,C)** Co-IP assay was performed to determine that HDGF co-precipitated with c-Jun.

proteins (Attia et al., 2013). In recent studies, NAP1L1 has been shown as a promoter of tumor pathogenesis. NAP1L1 participates in the miR-532-5p-mediated suppression of renal cancer cell proliferation. In colorectal cancer and pancreatic neuroendocrine neoplasm, NAP1L1 was found to be a biomarker, involved in the pathogenesis of these two types of cancers (Schimmack et al., 2014; Zhai et al., 2018; Queiroz et al., 2020). In HCC, NAP1L1 acts as a tumor promoter and is repressed by PRDM8 and let-7c-5p. However, the molecular basis of NAP1L1 in modulating HCC proliferation is still undermined.

In this study, we first analyzed the expression of NAP1L1 mRNA in the TCGA database. The data showed that the NAP1L1 expression level increased in HCC. Furthermore, the higher the malignant grade of HCC, the higher the expression level of NAP1L1. Survival analysis showed that a high expression of NAP1L1 significantly shortened the overall survival time of HCC patients. These data indicate that NAP1L1 is a potentially significant oncogene in HCC. To confirm these data, qPCR was used to examine the NAP1L1 mRNA expression in HCC tissues and cells compared with liver tissues and cells. The results are consistent with the TCGA data of NAP1L1. Furthermore, immunohistochemistry was used to test the NAP1L1 protein expression. Consistent with the mRNA data, the expression of NAP1L1 was found to be higher in HCC cell lines and tissues. Our results are similar to other reports of NAP1L1 in HCC cancer,

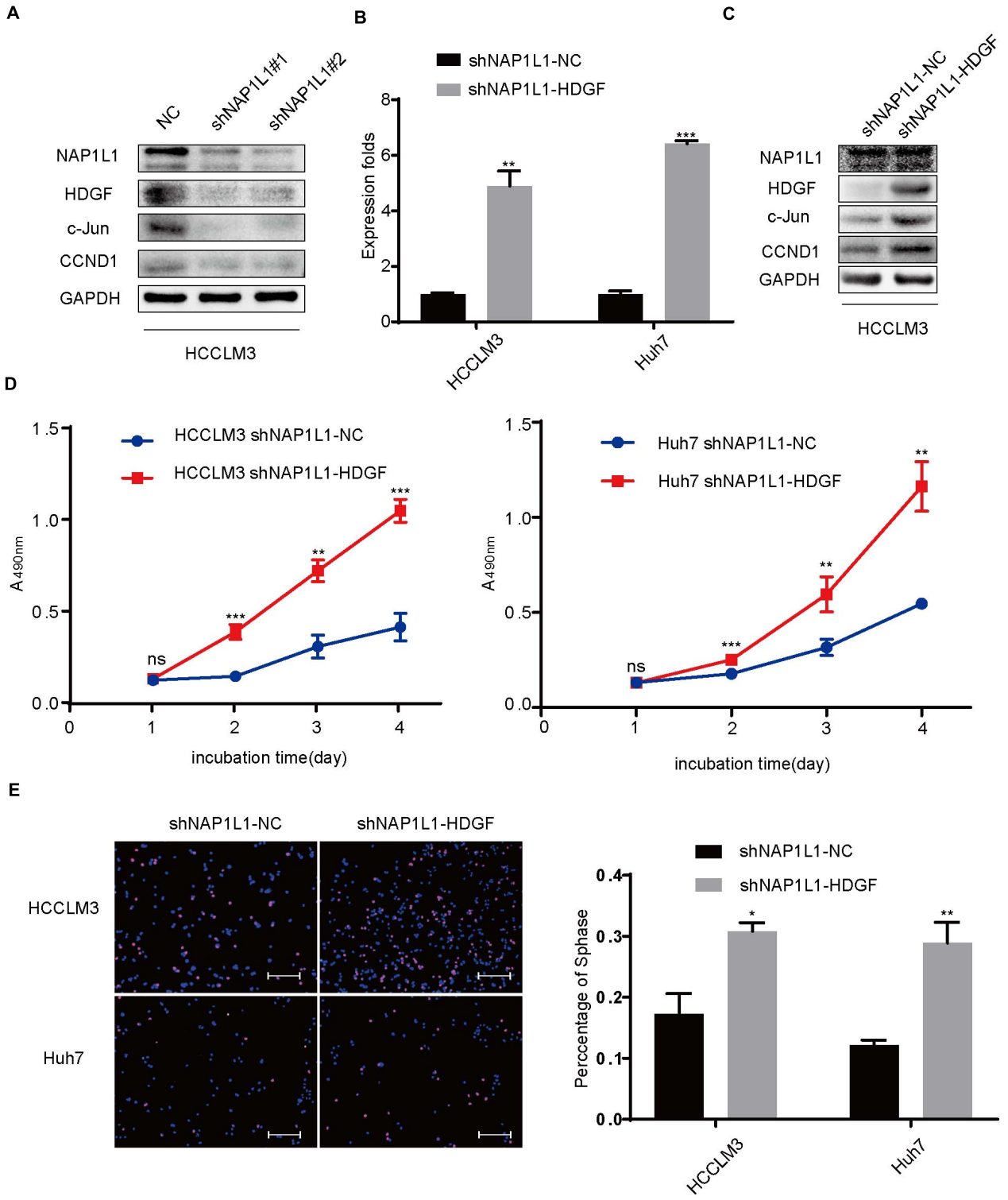


FIGURE 6 | Transfecting HDGF restores cell proliferation in NAP1L1-suppressing HCC cells through the c-Jun/CCND1 signal. **(A)** NAP1L1, HDGF, c-Jun, and CCND1 protein expression in NC and shNAP1L1 cells in HCCLM3. **(B)** RT-qPCR data to measure HDGF expression after HDGF is restored in shNAP1L1 HCC cells. **(C)** NAP1L1, HDGF, c-Jun, and CCND1 protein sequences in HDGF restored shNAP1L1 HCCLM3. **(D)** MTT assays indicated that transfecting HDGF restores cell proliferation. **(E)** EdU assay indicated that transfecting HDGF restores cell proliferation (scale bar: 200 μm). Data are presented as mean ± SD from three independent experiments. $^{*}p < 0.05$ vs. control; $^{**}p < 0.01$; $^{***}p < 0.001$.

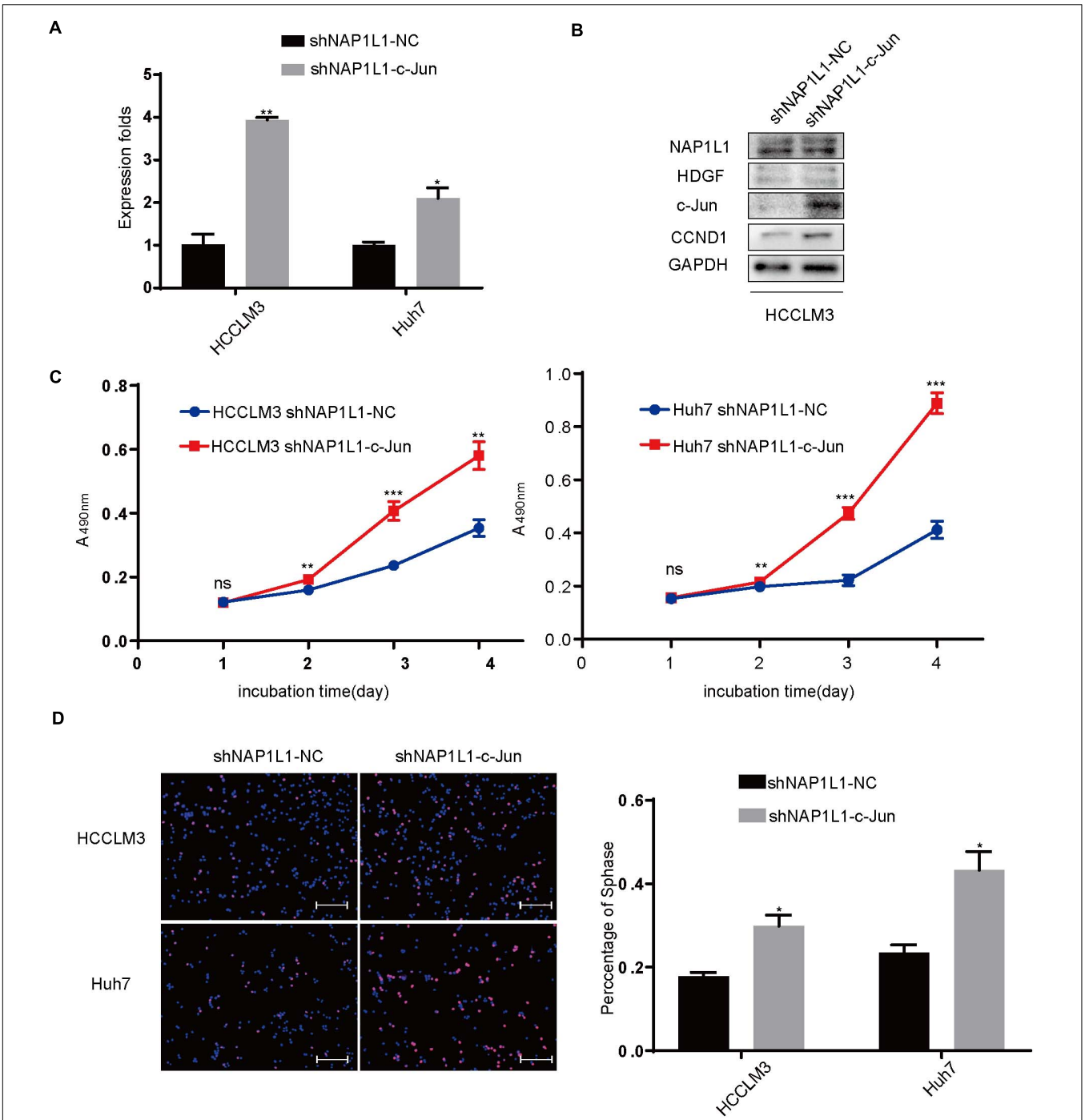


FIGURE 7 | Transfecting c-Jun increases the CCND1 signal and restores cell proliferation in NAP1L1-suppressing HCC cells. **(A)** Quantitative RT-qPCR data to measure c-Jun expression after restoring c-Jun in shNAP1L1 HCC cells. **(B)** NAP1L1, HDGF, c-Jun, and CCND1 protein sequences in HDGF restored shNAP1L1 HCCLM3 (scale bar: 200 μm). **(C)** MTT assays showed that transfecting c-Jun restores cell proliferation. **(D)** EdU assay showed that transfecting c-Jun restores cell proliferation (scale bar: 200 μm). $^{*}p < 0.05$ vs. control; $^{**}p < 0.01$; $^{***}p < 0.001$.

indicating that NAP1L1 is a tumor promoter participating in HCC pathogenesis.

In previous studies, NAP1L1 has been reported to be involved in promoting tumor pathogenesis (Schimmack et al., 2014; Zhai et al., 2018; Queiroz et al., 2020), but few studies have shown its role in cancers. Here, the role and molecular basis of NAP1L1 in HCC were further explored. It was observed that the suppression of NAP1L1 by siRNA or shRNA significantly decreased the cell cycle transition and cell proliferation *in vivo* and *in vitro* by MTT assay, plate clone formation, EdU staining, and subcutaneous

tumorigenesis in nude mice. These data further support that NAP1L1 is a potential oncogene in HCC.

Previous studies showed that NAP1L1 is repressed by PRDM8 and let-7c-5p (Chen et al., 2018; Huang et al., 2018) involved in HCC pathogenesis. Here, we found a new molecular basis for NAP1L1 to modulate HCC growth. HDGF was primarily obtained from the conditioned media of Huh-7 hepatoma cells (Nakamura et al., 1989). HDGF has been widely documented as an oncogene, inducing tumor occurrence and development including endometrial cancer, nasopharyngeal carcinoma, non-small cell lung cancer, liver cancer, and breast cancer (Wang and Fang, 2011; Chen et al., 2012; Fu et al., 2017; Min et al., 2018; Liu C. et al., 2019; Xiao et al., 2019).

Use of HDGF antibody therapy has significantly increased the antineoplastic activity of gemcitabine, bevacizumab, and chemotherapy in non-small cell lung cancer (Ren et al., 2009; Zhao et al., 2013). These studies show the significance of HDGF in the occurrence of malignant tumors.

Interestingly, previous studies in our lab had found that NAP1L1 is a potential candidate of HDGF interaction proteins in endometrial carcinoma using exogenous Co-IP assay combined with mass spectrometry (unpublished data). Furthermore, endogenous Co-IP assay and microconfocal colocalization assay were used to determine that NAP1L1 interacted with HDGF and colocalized in the cytoplasm and nucleus. To further elucidate the molecular mechanism of NAP1L1 for promoting cell cycle transition and cell proliferation *via* HDGF, the BioGrid database was used to predict the interacting proteins of HDGF and observed that c-Jun is a potential candidate. c-Jun is an oncogenic transcription factor, significantly participating in many tumor pathogeneses by transcription or suppressing the expression of some genes (Lin et al., 2019, 2020; Liu Y. et al., 2019; Liu et al., 2020; Zou et al., 2020). In HCC, c-Jun has been reported to modulate cell cycle signals, promoting malignant phenotypes of HCC (Eferl et al., 2003; Machida et al., 2010; Min et al., 2012), indicating the key role of c-Jun in HCC. Then, by consulting the BioGrid database, a combination was found between Jun and HDGF (Wang et al., 2011). In subsequent study, endogenous Co-IP assay showed that HDGF binds to c-Jun. Furthermore, HDGF and c-Jun were shown to be colocalized in the cytoplasm and nucleus. The results indicate that HDGF recruits c-Jun to participate in HCC carcinogenesis.

Finally, HDGF or c-Jun cDNA plasmid was transfected into shNAP1L1-treated HCC cells, and it was found that the cell cycle transition signal was significantly increased in shNAP1L1-treated HCC cells. Furthermore, the cell proliferation ability was also restored in NAP1L1-suppressed HCC cells. These data revealed that HDGF or c-Jun positively participated in NAP1L1-induced HCC proliferation.

In summary, elevated NAP1L1 protein level is a significantly unfavorable outcome for HCC patients. It acts as a tumor promoter that binds to HDGF. The latter recruits c-Jun to stimulate cell cycle signal transition and thus induces HCC carcinogenesis.

However, the results reported in this study are not sufficient to determine whether NAP1L1 interacts with HDGF and c-Jun to form a protein complex, or interacts with HDGF, further affecting the interaction between HDGF and c-Jun. This will be studied further in the future.

DATA AVAILABILITY STATEMENT

The datasets presented in this study can be found in online repositories. The names of the repository/repositories and accession number(s) can be found in the article/ **Supplementary Material**.

ETHICS STATEMENT

The studies involving human participants were reviewed and approved by the Research Ethics Committee of The Affiliated Hospital of Guizhou Medical University. The patients/participants provided their written informed consent to participate in this study. The animal study was reviewed and approved by the Research Ethics Committee of The Affiliated Hospital of Guizhou Medical University. Written informed consent was obtained from the individual(s) for the publication of any potentially identifiable images or data included in this article.

AUTHOR CONTRIBUTIONS

SZ and SL planned the experiments and revised the manuscript. Y-wZ, QC, and BL performed the experiments and prepared a draft of the manuscript. H-YL and X-KZ performed the statistical analysis. Y-wZ conceived the project and edited the manuscript. Y-yX and Y-wZ discussed the results. All the authors read and approved the final manuscript.

FUNDING

This work was financed by grants received from the Natural Science Foundation of Guizhou Province [(2018)1127], The 12th Special Fund for Young Scientist of Guizhou Province [(2019)5647], and National Natural Science Foundation of Guizhou Medical University (gzwjkj2020-1-101).

SUPPLEMENTARY MATERIAL

The Supplementary Material for this article can be found online at: https://www.frontiersin.org/articles/10.3389/fcell.2021.659680/full#supplementary-material

Supplementary Figure 1 | (A) Quantitative RT-qPCR data to measure the gene expression after NAP1L1 overexpression plasmid transfection into HCCLM3 and Huh7 cells. **(B)** Expression levels of NAP1L1 were detected by Western blot analysis to screen effective transfection fragments. **(C)** MTT assays showed that the upregulation of NAP1L1 promoted the proliferation *in vitro* in HCCLM3 and Huh7. **(D)** EdU assay indicated that the upregulation of NAP1L1 promoted the proliferation *in vitro* (scale bar: 200 μm). **(E)** Cell cycle distribution was subjected to flow cytometry, and quantified histograms show the effect of NAP1L1 overexpression on cell cycle distribution. Data are presented as

mean ± SD from three independent experiments. *$P < 0.05$ vs. control; **$P < 0.01$; ***$P < 0.001$.

Supplementary Figure 2 | (A) Representative images of HCC cells stably transfected with fluorescently labeled lentivirus under bright-field and fluorescence microscopy (scale bar: 250 μm). Both HCCLM3 and Huh7 cells were transfected with NC lentivirus or shNAP1L1 lentivirus. **(B)** Xenograft tumor in nude mice in shRNA-NAP1L1 group compared with NC group.

Supplementary Figure 3 | (A) EdU assay for the downregulation of NAP1L1 with shRNA-NAP1L1 lentivirus *in vitro* (scale bar: 200 μm). **(B)** EdU assay for the downregulation of NAP1L1 with siRNA-NAP1L1 *in vitro* (scale bar: 200 μm). **(C)** EdU assay indicated that transfecting HDGF restores the cell proliferation *in vitro* (scale bar: 200 μm). **(D)** EdU assay showed that transfecting c-Jun restores the cell proliferation *in vitro* (scale bar: 200 μm). **(E)** EdU assay indicated that the upregulation of NAP1L1 promoted the proliferation *in vitro* (scale bar: 200 μm).

REFERENCES

Akinyemiju, T., Abera, S., Ahmed, M., Alam, N., Alemayohu, M. A., Allen, C., et al. (2017). The burden of primary liver cancer and underlying etiologies from 1990 to 2015 at the global, regional, and national level: results from the global burden of disease study 2015. *JAMA Oncol.* 3, 1683–1691. doi: 10.1001/jamaoncol.2017.3055

Attia, M., Rachez, C., Avner, P., and Rogner, U. C. (2013). Nucleosome assembly proteins and their interacting proteins in neuronal differentiation. *Arch. Biochem. Biophys.* 534, 20–26. doi: 10.1016/j.abb.2012.09.011

Beasley, R. P. (1988). Hepatitis B virus. The major etiology of hepatocellular carcinoma. *Cancer* 61, 1942–1956. doi: 10.1002/1097-0142(19880515)61:10<1942::aid-cncr2820611003<3.0.co;2-j

Calzadilla, B. L., and Adams, L. A. (2016). The natural course of non-alcoholic fatty liver disease. *Int. J. Mol. Sci.* 17:774. doi: 10.3390/ijms17050774

Chen, J., Gingold, J. A., and Su, X. (2019). Immunomodulatory TGF-beta signaling in hepatocellular carcinoma. *Trends Mol. Med.* 25, 1010–1023. doi: 10.1016/j.molmed.2019.06.007

Chen, S. C., Kung, M. L., Hu, T. H., Chen, H. Y., Wu, J. C., Kuo, H. M., et al. (2012). Hepatoma-derived growth factor regulates breast cancer cell invasion by modulating epithelial–mesenchymal transition. *J Pathol.* 228, 158–169. doi: 10.1002/path.3988

Chen, Z., Gao, W., Pu, L., Zhang, L., Han, G., Zuo, X., et al. (2018). PRDM8 exhibits antitumor activities toward hepatocellular carcinoma by targeting NAP1L1. *Hepatology* 68, 994–1009. doi: 10.1002/hep.29890

Eferl, R., Ricci, R., Kenner, L., Zenz, R., David, J. P., Rath, M., et al. (2003). Liver tumor development. c-Jun antagonizes the proapoptotic activity of p53. *Cell* 112, 181–192. doi: 10.1016/s0092-8674(03)00042-4

Fu, Q., Song, X., Liu, Z., Deng, X., Luo, R., Ge, C., et al. (2017). miRomics and proteomics reveal a miR-296-3p/PRKCA/FAK/Ras/c-Myc feedback loop modulated by HDGF/DDX5/beta-catenin complex in lung adenocarcinoma. *Clin. Cancer Res.* 23, 6336–6350. doi: 10.1158/1078-0432.CCR-16-2813

Huang, Y., Xiang, B., Liu, Y., Wang, Y., and Kan, H. (2018). LncRNA CDKN2B-AS1 promotes tumor growth and metastasis of human hepatocellular carcinoma by targeting let-7c-5p/NAP1L1 axis. *Cancer Lett.* 437, 56–66. doi: 10.1016/j.canlet.2018.08.024

Lin, X., Li, A. M., Li, Y. H., Luo, R. C., Zou, Y. J., Liu, Y. Y., et al. (2020). Silencing MYH9 blocks HBx-induced GSK3beta ubiquitination and degradation to inhibit tumor stemness in hepatocellular carcinoma. *Signal Transduct. Target. Ther.* 5:13. doi: 10.1038/s41392-020-0111-4

Lin, X., Zuo, S., Luo, R., Li, Y., Yu, G., Zou, Y., et al. (2019). HBX-induced miR-5188 impairs FOXO1 to stimulate β-catenin nuclear translocation and promotes tumor stemness in hepatocellular carcinoma. *Theranostics* 9, 7583–7598. doi: 10.7150/thno.37717

Liu, C., Peng, X., Li, Y., Liu, S., Hou, R., Zhang, Y., et al. (2020). Positive feedback loop of FAM83A/PI3K/AKT/c-Jun induces migration, invasion and metastasis in hepatocellular carcinoma. *Biomed. Pharmacother.* 123:109780. doi: 10.1016/j.biopha.2019.109780

Liu, C., Wang, L., Jiang, Q., Zhang, J., Zhu, L., Lin, L., et al. (2019). Hepatoma-derived growth factor and DDX5 promote carcinogenesis and progression of endometrial cancer by activating beta-catenin. *Front. Oncol.* 9:211. doi: 10.3389/fonc.2019.00211

Liu, Y., Jiang, Q., Liu, X., Lin, X., Tang, Z., Liu, C., et al. (2019). Cinobufotalin powerfully reversed EBV-miR-BART22-induced cisplatin resistance via stimulating MAP2K4 to antagonize non-muscle myosin heavy chain IIA/glycogen synthase 3beta/beta-catenin signaling pathway. *Ebiomedicine* 48, 386–404. doi: 10.1016/j.ebiom.2019.08.040

Luiken, S., Fraas, A., Bieg, M., Sugiyanto, R., Goeppert, B., Singer, S., et al. (2020). NOTCH target gene HES5 mediates oncogenic and tumor suppressive functions in hepatocarcinogenesis. *Oncogene* 39, 3128–3144. doi: 10.1038/s41388-020-1198-3

Machida, K., Tsukamoto, H., Liu, J. C., Han, Y. P., Govindarajan, S., Lai, M. M., et al. (2010). c-Jun mediates hepatitis C virus hepatocarcinogenesis through signal transducer and activator of transcription 3 and nitric oxide-dependent impairment of oxidative DNA repair. *Hepatology* 52, 480–492. doi: 10.1002/hep.23697

McGlynn, K. A., Petrick, J. L., and London, W. T. (2015). Global epidemiology of hepatocellular carcinoma: an emphasis on demographic and regional variability. *Clin. Liver Dis.* 19, 223–238. doi: 10.1016/j.cld.2015.01.001

Min, L., Ji, Y., Bakiri, L., Qiu, Z., Cen, J., Chen, X., et al. (2012). Liver cancer initiation is controlled by AP-1 through SIRT6-dependent inhibition of survivin. *Nat. Cell Biol.* 14, 1203–1211. doi: 10.1038/ncb2590

Min, X., Wen, J., Zhao, L., Wang, K., Li, Q., Huang, G., et al. (2018). Role of hepatoma-derived growth factor in promoting de novo lipogenesis and tumorigenesis in hepatocellular carcinoma. *Mol. Oncol.* 12, 1480–1497. doi: 10.1002/1878-0261.12357

Morgan, R. L., Baack, B., Smith, B. D., Yartel, A., Pitasi, M., and Falck-Ytter, Y. (2013). Eradication of hepatitis C virus infection and the development of hepatocellular carcinoma: a meta-analysis of observational studies. *Ann. Intern. Med.* 158(5 Pt 1), 329–337. doi: 10.7326/0003-4819-158-5-201303050-00005

Nakamura, H., Kambe, H., Egawa, T., Kimura, Y., Ito, H., Hayashi, E., et al. (1989). Partial purification and characterization of human hepatoma-derived growth factor. *Clin. Chim. Acta* 183, 273–284. doi: 10.1016/0009-8981(89)90361-6

Queiroz, C., Song, F., Reed, K. R., Al-Khafaji, N., Clarke, A. R., Vimalachandran, D., et al. (2020). NAP1L1: a novel human colorectal cancer biomarker derived from animal models of Apc inactivation. *Front. Oncol.* 10:1565. doi: 10.3389/fonc.2020.01565

Ren, H., Chu, Z., and Mao, L. (2009). Antibodies targeting hepatoma-derived growth factor as a novel strategy in treating lung cancer. *Mol. Cancer Ther.* 8, 1106–1112. doi: 10.1158/1535-7163.MCT-08-0779

Schimmack, S., Taylor, A., Lawrence, B., Alaimo, D., Schmitz-Winnenthal, H., Buchler, M. W., et al. (2014). A mechanistic role for the chromatin modulator, NAP1L1, in pancreatic neuroendocrine neoplasm proliferation and metastases. *Epigenetics Chromatin* 7:15. doi: 10.1186/1756-8935-7-15

Venook, A. P., Papandreou, C., Furuse, J., and de Guevara, L. L. (2010). The incidence and epidemiology of hepatocellular carcinoma: a global and regional perspective. *Oncologist* 15(Suppl. 4), 5–13. doi: 10.1634/theoncologist.2010-S4-05

Wang, J., Huo, K., Ma, L., Tang, L., Li, D., Huang, X., et al. (2011). Toward an understanding of the protein interaction network of the human liver. *Mol. Syst. Biol.* 7:536. doi: 10.1038/msb.2011.67

Wang, S., and Fang, W. (2011). Increased expression of hepatoma-derived growth factor correlates with poor prognosis in human nasopharyngeal carcinoma. *Histopathology* 58, 217–224. doi: 10.1111/j.1365-2559.2010.03739.x

Xiao, Y. Y., Lin, L., Li, Y. H., Jiang, H. P., Zhu, L. T., Deng, Y. R., et al. (2019). ZEB1 promotes invasion and metastasis of endometrial cancer by interacting with HDGF and inducing its transcription. *Am. J. Cancer Res.* 9, 2314–2330.

Yamashita, T., and Kaneko, S. (2016). [Liver Cancer]. *Rinsho Byori* 64, 787–796.

Zhai, W., Ma, J., Zhu, R., Xu, C., Zhang, J., Chen, Y., et al. (2018). MiR-532-5p suppresses renal cancer cell proliferation by disrupting the ETS1-mediated positive feedback loop with the KRAS-NAP1L1/P-ERK axis. *Br. J. Cancer* 119, 591–604. doi: 10.1038/s41416-018-0196-5

Zhao, J., Ma, M. Z., Ren, H., Liu, Z., Edelman, M. J., Pan, H., et al. (2013). Anti-HDGF targets cancer and cancer stromal stem cells resistant to chemotherapy. *Clin. Cancer Res.* 19, 3567–3576. doi: 10.1158/1078-0432.CCR-12-3478

Zhao, M., Xu, P., Liu, Z., Zhen, Y., Chen, Y., Liu, Y., et al. (2018). Dual roles of miR-374a by modulated c-Jun respectively targets CCND1-inducing PI3K/AKT

signal and PTEN-suppressing Wnt/beta-catenin signaling in non-small-cell lung cancer. *Cell Death Dis.* 9:78. doi: 10.1038/s41419-017-0103-7

Zhou, J., Sun, H. C., Wang, Z., Cong, W. M., Wang, J. H., Zeng, M. S., et al. (2018). Guidelines for diagnosis and treatment of primary liver cancer in China (2017 edition). *Liver Cancer* 7, 235–260. doi: 10.1159/000488035

Zou, Y., Lin, X., Bu, J., Lin, Z., Chen, Y., Qiu, Y., et al. (2020). Timeless-stimulated miR-5188-FOXO1/beta-Catenin-c-Jun feedback loop promotes stemness via ubiquitination of beta-catenin in breast cancer. *Mol. Ther.* 28, 313–327. doi: 10.1016/j.ymthe.2019.08.015

Conflict of Interest: The authors declare that the research was conducted in the absence of any commercial or financial relationships that could be construed as a potential conflict of interest.

Publisher's Note: All claims expressed in this article are solely those of the authors and do not necessarily represent those of their affiliated organizations, or those of the publisher, the editors and the reviewers. Any product that may be evaluated in this article, or claim that may be made by its manufacturer, is not guaranteed or endorsed by the publisher.

Copyright © 2021 Zhang, Chen, Li, Li, Zhao, Xiao, Liu and Zuo. This is an open-access article distributed under the terms of the Creative Commons Attribution License (CC BY). The use, distribution or reproduction in other forums is permitted, provided the original author(s) and the copyright owner(s) are credited and that the original publication in this journal is cited, in accordance with accepted academic practice. No use, distribution or reproduction is permitted which does not comply with these terms.

frontiers in Cell and Developmental Biology

ORIGINAL RESEARCH
published: 23 August 2021
doi: 10.3389/fcell.2021.719192

PARP1 Inhibitor Combined With Oxaliplatin Efficiently Suppresses Oxaliplatin Resistance in Gastric Cancer-Derived Organoids via Homologous Recombination and the Base Excision Repair Pathway

Huafu Li[1,2,3,4†], Chunming Wang[1,4†], Linxiang Lan[2,3†], Wenhui Wu[1†], Ian Evans[2,3], E. Josue Ruiz[2,3], Leping Yan[5], Zhijun Zhou[6], Joaquim M. Oliveira[7,8], Rui L. Reis[7,8], Zhenran Hu[6], Wei Chen[1], Axel Behrens[2,3], Yulong He[1,4]* and Changhua Zhang[1]**

[1] Digestive Diseases Center, The Seventh Affiliated Hospital of Sun Yat-sen University, Shenzhen, China, [2] Adult Stem Cell Laboratory, The Francis Crick Institute, London, United Kingdom, [3] The Institute of Cancer Research, London, United Kingdom, [4] Department of Gastrointestinal Surgery, The First Affiliated Hospital of Sun Yat-sen University, Guangzhou, China, [5] Center of Scientific Research, The Seventh Affiliated Hospital of Sun Yat-sen University, Shenzhen, China, [6] Department of Medicine, The University of Oklahoma Health Sciences Center, Oklahoma City, OK, United States, [7] 3B's Research Group, I3Bs – Research Institute on Biomaterials, Biodegradables and Biomimetics, Headquarters of the European Institute of Excellence on Tissue Engineering and Regenerative Medicine, AvePark, Parque de Ciência e Tecnologia, Zona Industrial da Gandra, University of Minho, Guimarães, Portugal, [8] ICVS/3B's – PT Government Associate Laboratory, Guimarães, Portugal

Oxaliplatin (OXA) resistance in the treatment of different types of cancer is an important and complex problem. The culture of tumor organoids derived from gastric cancer can help us to provide a deeper understanding of the underlying mechanisms that lead to OXA resistance. In this study, our purpose was to understand the mechanisms that lead to OXA resistance, and to provide survival benefits to patients with OXA through targeted combination therapies. Using sequence analysis of OXA-resistant and non-OXA-resistant organoids, we found that PARP1 is an important gene that mediates OXA resistance. Through the patients' follow-up data, it was observed that the expression level of PARP1 was significantly correlated with OXA resistance. This was confirmed by genetic manipulation of PARP1 expression in OXA-resistant organoids used in subcutaneous tumor formation. Results further showed that PARP1 mediated OXA resistance by inhibiting the base excision repair pathway. OXA also inhibited homologous recombination by CDK1 activity and importantly made cancers with normal BRCA1 function sensitive to PARP inhibition. As a result, combination of OXA and Olaparib (PARP-1/2/3 inhibitor), inhibited *in vivo* and *in vitro* OXA resistant organoid growth and viability.

Keywords: gastric cancer, L-OHP resistance, homologous recombination, PARP1 inhibitors, organoid

OPEN ACCESS

Edited by:
Ira Ida Skvortsova,
Innsbruck Medical University, Austria

Reviewed by:
Laura Lafon-Hughes,
Universidad de la Republica, Uruguay
David A. Alagpulinsa,
Massachusetts General Hospital and Harvard Medical School, United States
Wael Jdey,
Onxeo, France

***Correspondence:**
Changhua Zhang
zhchangh@mail.sysu.edu.cn
Yulong He
heyulong@mail.sysu.edu.cn
Axel Behrens
Axel.Behrens@crick.ac.uk

†These authors share first authorship

Specialty section:
This article was submitted to Molecular and Cellular Oncology, a section of the journal Frontiers in Cell and Developmental Biology

Received: *02 June 2021*
Accepted: *19 July 2021*
Published: *23 August 2021*

Citation:
Li H, Wang C, Lan L, Wu W, Evans I, Ruiz EJ, Yan L, Zhou Z, Oliveira JM, Reis RL, Hu Z, Chen W, Behrens A, He Y and Zhang C (2021) PARP1 Inhibitor Combined With Oxaliplatin Efficiently Suppresses Oxaliplatin Resistance in Gastric Cancer-Derived Organoids via Homologous Recombination and the Base Excision Repair Pathway. Front. Cell Dev. Biol. 9:719192. doi: 10.3389/fcell.2021.719192

INTRODUCTION

Currently, the standard treatment for gastric cancer is surgical resection. However, the opportunity for surgery is often lost as the majority of cases are diagnosed at an advanced stage (Yuan et al., 2020). Alternative therapies such as radiotherapy and chemotherapy can be considered yet are often ineffective. Available chemotherapy, based on cisplatin and 5-fluorouracil (5-FU) or their combined derivatives, such as oxaliplatin (OXA) and capecitabine, fail in 95% of non-surgical gastric tumors (Wei et al., 2020). In order to advance in the treatment of gastric cancer, there is an urgent need to gain a better understanding of the mechanisms of chemoresistance. This is necessary to provide a more "personalized" treatment to patients and to develop new strategies to overcome chemotherapy resistance.

The use of patient-derived cell lines or xenografts may facilitate the discovery of new therapies because they are closely related to the clinical disease, allowing them to be used to guide chemotherapy selection (Remy et al., 2020). Tumor organoids is an emerging technology that can better mimic primary tumors and provide better tools for *in vitro* research.

Organoids are a three-dimensional (3D) cell culture system derived from primary tissue or stem cells. Compared with most other primary cell cultures, the main advantage of the organoid culture system is that it can maintain the genomic stability of the cell over the long term while maintaining the characteristics of tissue origin (Huch et al., 2015; Liu and Meltzer, 2017). Individual cancer-like organoids can be used to predict therapeutic responses to certain drugs, and the establishment of large gastric cancer organoids biobases in combination with drug screening may help outline new therapeutic strategies for gastric cancer (Lo et al., 2021; Seidlitz et al., 2021). When gastric cancer organoids are exposed to commonly used chemotherapy agents, there are varying degrees of response, comparable to the clinical response of the patient (Wang et al., 2014; Yan et al., 2018). Thus we can use patient derived organoids to investigate the mechanisms of OXA resistance.

In this study, we aim to analyze the clinical samples of patients and conduct drug sensitivity experiments with gastric cancer organoids. Clinical specimens of four gastric cancer patients were obtained and organoid cultures established, two from patients who had responded well to OXA treatment and two whose tumors were OXA-resistant.

In vivo and *in vitro* studies using the organoids mirrored the clinical data in terms of OXA sensitivity. Sequencing data suggested PARP1 as a key gene involved in mechanisms of OXA resistance and this was confirmed using a range of *in vitro* and *in vivo* approaches. Importantly, we demonstrated that combining OXA with a PARP1 inhibitor is able overcome the OXA resistance and points the way to a potential new therapeutic modality for the treatment of GC.

RESULTS

PARP1 Is an Important Core Gene Leading to OXA Resistance

In order to investigate the mechanisms behind the chemotherapuetic resistance, we used four patient-derived organiods (sGC1, sGC2, rGC1, and rGC2), rGC1 and rGC2 were derived from patients whose GC recurred after postoperative chemotherapy, while sGC1 and sGC2 were from patients without recurrence after postoperative chemotherapy. In a viability assay, rGC1 (IC50 = 19.95 $\mu m.L^{-1}$) and rGC2 (IC50 = 63.09 $\mu m.L^{-1}$) were found to be more resistant to OXA than sGC1 (IC50 = 0.93 $\mu m.L^{-1}$) and sGC1 (IC50 = 3.03 $\mu m.L^{-1}$) (**Supplementary Figure 1A**). In order to explore the regulation of core genes that may mediate OXA-resistance, we performed mRNA sequencing on the patient derived organoids. The data was anlysed by PPi network construction. **Figure 1A** shows their differentially expressed genes (DEGs) and fold change (FC). Compared with non-drug-resistant patients, the main enrichment pathways for drug-resistant patients include homologous recombination (HR), DNA replication, base excision repair (BER), and cell cycle regulation (**Figure 1B**). Finally, we searched for the core genes using String and found that PARP1 was a candidate gene affecting drug resistance (**Figures 1C,D**).

PARP1 Is Upregulated in Gastric Cancer OXA Resistance Organoid

Through our experiments on OXA resistance of rGC1, rGC2, sGC1 and sGC2 *in vitro* and *in vivo*, it was found that the tolerance of rGC1 and rGC2 to OXA was significantly higher than that of sGC1 and sGC2 (**Supplementary Figure 1D** and **Figures 2A–F**). Moreover, it was found that the expression level of PARP1 in rGC1 and rGC2 of OXA-resistant organoid was significantly higher than that in sGC1 and sGC2 of OXA-sensitive organoid ($P < 0.05$) (**Figures 2G–I**).

PARP1 Plays an Important Role in Maintaining OXA Resistance

To confirm the role of PARP1 in OXA resistance, we overexpressed PARP1 in the OXA-sensitive organoids and found that this increased their tolerance to OXA. Conversely, PARP1 knockdown in OXA-resistant organoid, showed decreased tolerance to OXA ($P < 0.05$) (**Figures 3A–C** and **Supplementary Figure 3A**). Similar results were seen *in vivo* when PARP1 was overexpressed in the OXA-sensitive organoid before subcutaneous implantation, and it was found that the tolerance of the resulting tumors to OXA was significantly increased. Moreover, PARP1 knockdown was performed on the OXA-resistant rGC1 and rGC2 organoids and it was found that the tolerance of tumors to OXA *in vivo* was reduced ($P < 0.05$) (**Figures 3D–F**). These results indicate that

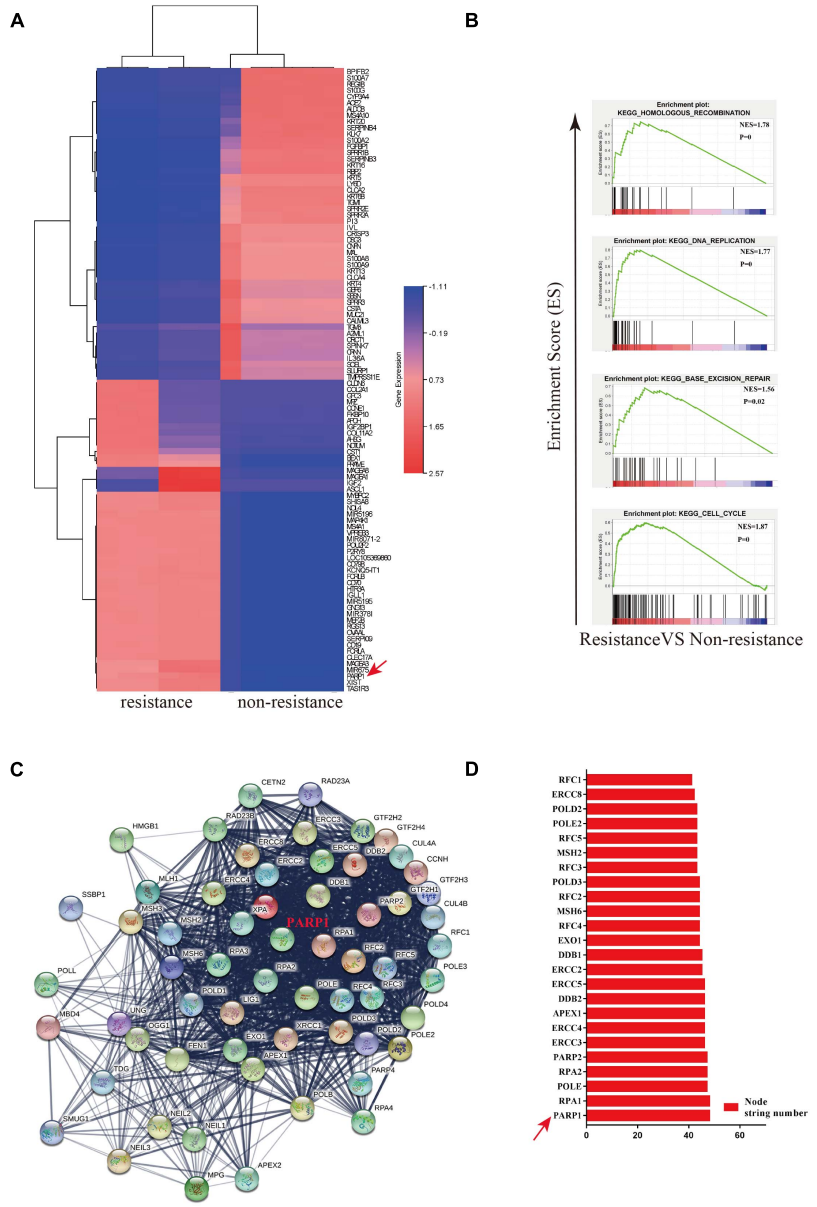


FIGURE 1 | PARP1 is the central gene of Oxaliplatin resistance in gastric cancer. **(A)** Heatmap of mRNA differential expression of sGC1 and sGC2 tumors against rGC1 and rGC2 tumors. The abscissa represents the gene name. Red represents High and blue represents Low. **(B)** Analysis of enrichment of mRNA differential expression of sGC1 and sGC2 tumors against rGC1 and rGC2 tumors. **(C)** STRING database protein interaction network diagram of mRNA differential expression in sGC1 and sGC2 tumors compared to rGC1 and rGC2 tumors. Edges represent protein-protein associations. Cambridge blue, curated databases; Violet, experimentally determined; Green, gene neighborhood; Red, gene fusions; Blue, gene co-occurrence; Reseda, text mining; Black, co-expression; Lilac, protein homology. **(D)** Comparison of NODE string number of two gene sets in core genes of **(C)**. All experiments were repeated three times.

PARP1 plays a pivotal role in OXA resistance *in vitro* and *in vivo*.

PARP1 Inhibition by Olaparib Sensitizes Gastric Cancer to OXA

Since PARP1 appears be an important gene for OXA resistance we wanted to determine whether a PARP1 inhibitor combined with OXA can effectively inhibit OXA resistance. Using both the PARP1 inhibitor, Olaparib, and OXA in combination effectively inhibited the viability, size, cell count, and proliferation of the organoids derived from the OXA resistance gastric cancers (rGC1 and rGC2) ($P < 0.05$) (**Figures 4A–C**). This drug combination also significantly inhibited the activity and proliferation of a range of OXA resistance gastric cancer cell lines (**Supplementary Figures 2A,B**). BALB/C NUDE mice *in vivo* tumorigenesis experiments also confirmed that these drugs when used in combination could effectively inhibit tumor growth when

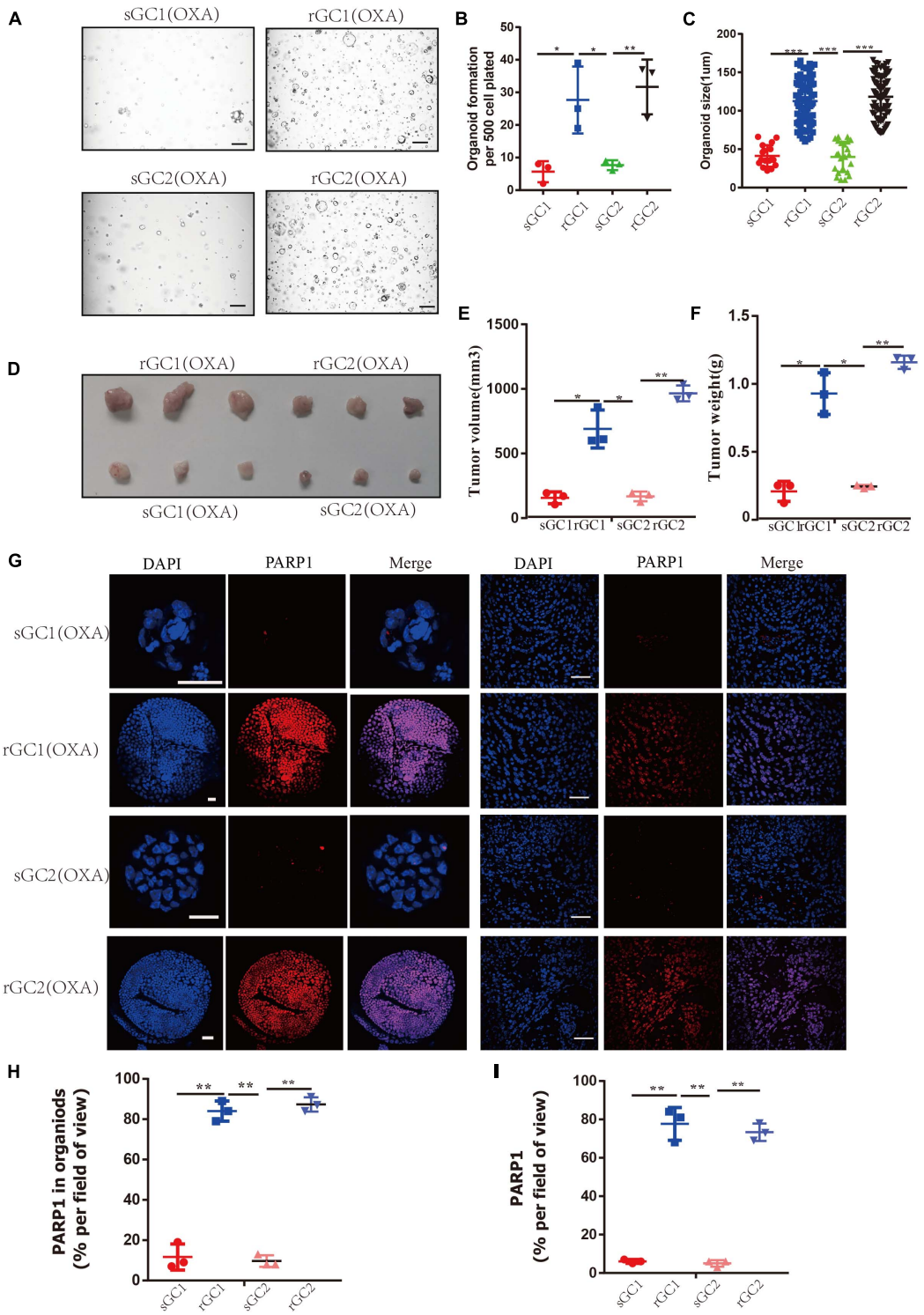


FIGURE 2 | PARP1 is upregulated in oxaliplatin resistance gastric cancer. **(A–C)** sGC1, sGC2, rGC1, and rGC2 organoids were treated with Oxaliplatin before imaging **(A)**, number of organoids **(B)**, and size of organoids **(C)**. **(D)** Representative images of tumorigenesis in BALB/C NUDE mice treated with Oxaliplatin. The ruler represents 1 cm. **(E)** Tumour growth curves of organoids in PDOX BALB/C Nude mice. The curve shows the average tumor volume. Error bars represent mean ± standard deviation. **(F)** Mass of tumors of PDOX in BALB/C NUDE mice. The curve shows the average tumor mass. **(G)** Representative images of PARP1 levels stained by immunofluorescence in organoid and tumors. The scale bar represents 20 μm for tumour images, 200 μm for organoid images. **(H)** Proportion of PARP1 + cells in organoid **(G,I)**, proportion of PARP1 + cells in tumor **(G)**. The Student's *t* test was used for statistical analysis. Error bars indicate mean ± standard deviation. *<0.05, **<0.01, and ***<0.001. All experiments were repeated three times.

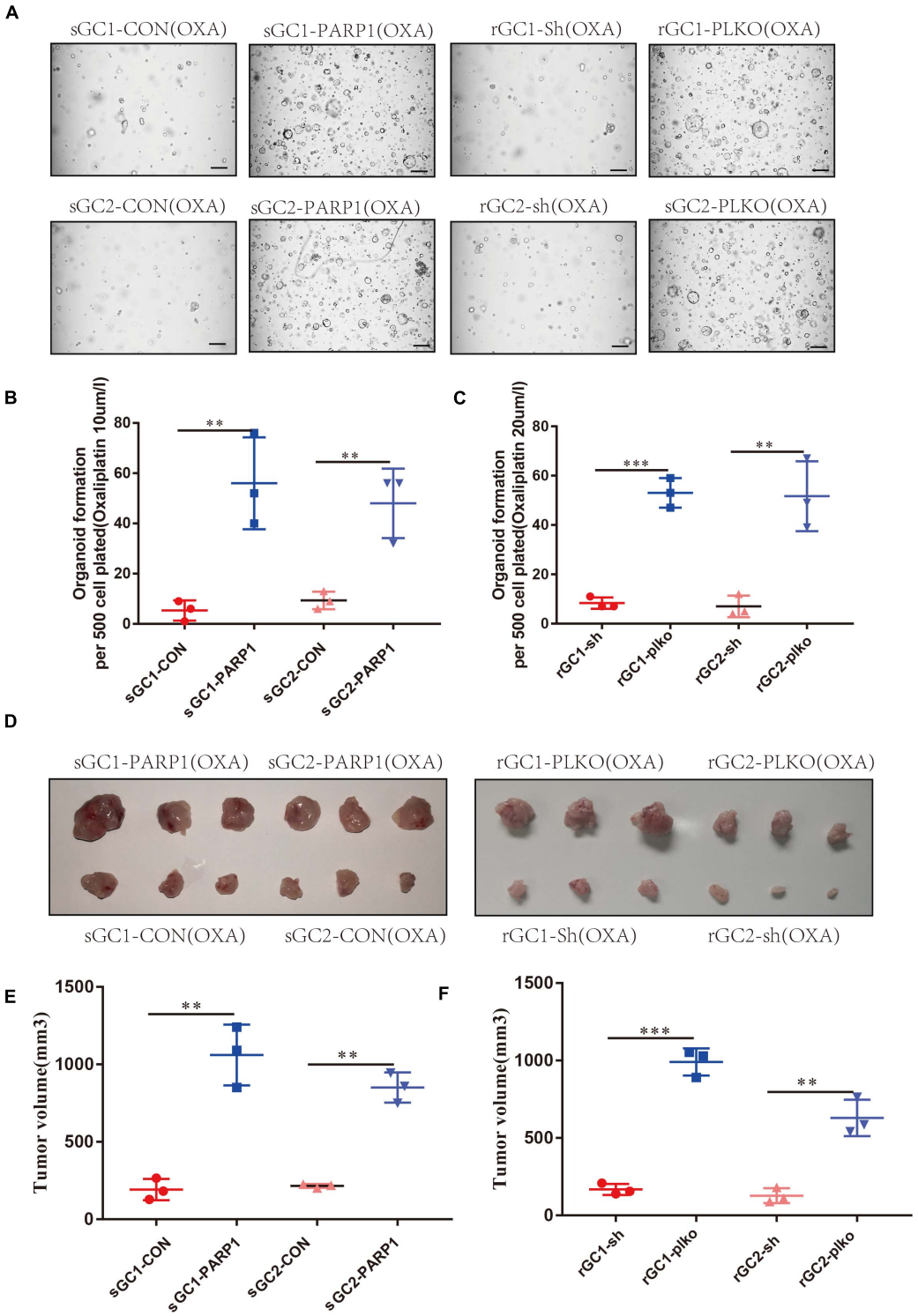


FIGURE 3 | PARP1 is required for Oxaliplatin resistance development. **(A–C)** sGC1, sGC2 and sGC1 PARP1 overexpression, sGC2 overexpression,rGC1, rGC2 and rGC1 PARP1 knock-down, and rGC2 knock-down organoids were treated with Oxaliplatin before imaging **(A)** number of organoids **(B,C)**. **(D)** Representative images of tumorigenesis in BALB/C NUDE mice with Oxaliplatin. The ruler represents 1 cm. **(E)** Tumor growth curves of PDOX BALB/C NUDE mice of sGC1, sGC2 and sGC1 PARP1 overexpression, and sGC2 overexpression. The curve shows the average tumor volume. Error bars represent mean ± standard deviation. **(F)** Tumor growth curves of PDOX BALB/C NUDE mice of rGC1, rGC2 and rGC1 PARP1 knock-down, and rGC2 knock-down. The curve shows the average tumor volume. Error bars represent mean ± standard deviation. Three mice carried xenografts and one xenograft per mouse. All experiments were repeated three times. *<0.05, **<0.01, and ***<0.001.

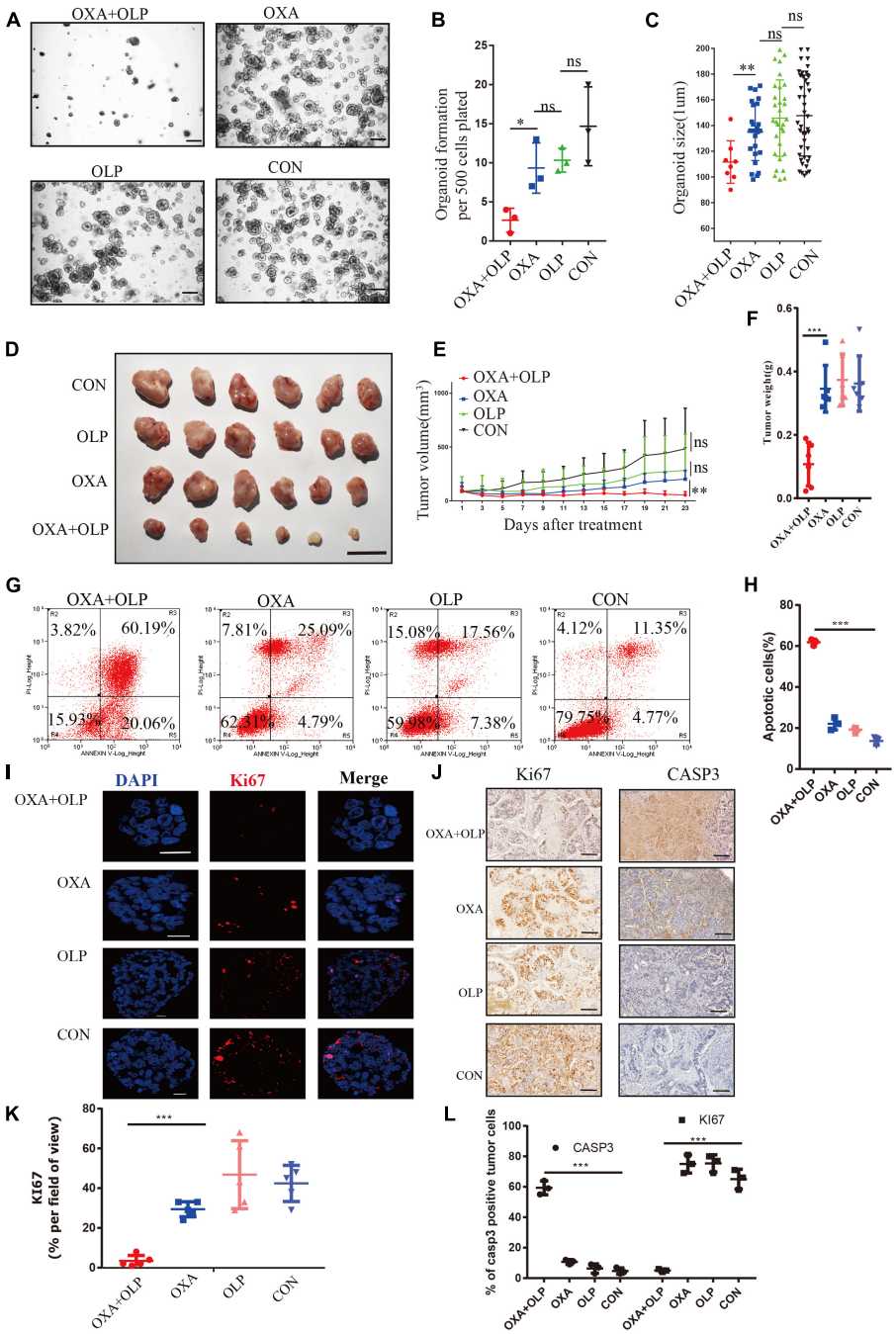


FIGURE 4 | PARP1 inhibition by Olaparib sensitizes gastric cancer to Oxaliplatin. **(A–C)** rGC1 organoids were treated with Olaparib + Oxaliplatin, Oxaliplatin, and Olaparib, respectively, before imaging **(A)**, number of organoids **(B)**, and size of organoids **(C)**. The scale represents 500 μm. Different drug concentrations were used to act on cells and before cell viability tests **(A,E)**. Drug action time was 36 h. **(D)** Representative images of tumorigenesis in BALB/C NUDE mice with Olaparib + Oxaliplatin, Oxaliplatin, Olaparib and a blank control group of rGC1. The ruler represents 1 cm. **(E)** Tumor growth curves of PDOX BALB/C NUDE mice of rGC1 organiod. The curve shows the average tumor volume. Error bars represent mean ± standard deviation. **(F)** Mass of tumors of PDOX in BALB/C NUDE mice of rGC1 organiod. The curve shows the average tumor mass. **(G)** The effect of different medication groups on the apoptosis of rGC1 organoids. **(H)** Comparison of the proportion of apoptosis in different groups. **(G,I)** Representative images of KI67 stained by IF staining of rGC1 organoids treated with olaparib + oxaliplatin, oxaliplatin, Olaparib, and a blank control group. The red stains indicate KI67 positive. The scale represents 2 um. **(J)** Representative images of KI67 and Caspase3 stained by IHC staining after tumorigenesis of BALB/C NUDE mice treated with Olaparib + Oxaliplatin, Oxaliplatin, Olaparib, and a blank control group of rGC1. The brown stains indicate KI67 and Caspase3 positive. The scale represents 200 um. **(K)** Statistical analysis of KI67 + cells. **(I,L)** Comparison of the percentage of positive cells stained with KI67 and Caspase3. Student's *t* test was used for statistical analysis. Error bars indicate mean ± standard deviation. OXA, Oxaliplatin. OLP, Olaparib. CON, control group. *<0.05, **<0.01, and ***<0.001. All experiments had repeated three times. PDOX, patient-derived organiod culture xenograft. ns, no significant.

compared with their use individually ($P < 0.05$) (**Figures 4D–F**), and can induce cell apoptosis and affect proliferation of tumor cells ($P < 0.05$) (**Figures 4G–L**). By comparing Olaparib + OXA versus OXA alone, it was found that the Olaparib + OXA group was mainly enriched in oxidative phosphorylation and PPAR signaling pathway (**Supplementary Figures 2C,D**). These two pathways are primarily important enrichment pathways for tumor apoptosis after chemotherapy-induced DNA damage (Yang and Frucht, 2001; Yadav et al., 2015). The main pathways enriched in the OXA group were JAK-STAT, MAPK, NOTCH, and WNT signaling pathways (**Supplementary Figures 2E–H**). In fact, these pathways are not only related to drug resistance in tumors, but also closely related to proliferation.

Combined Oxaliplatin With Olaparib Inhibits BER and HR Repair Pathways via Blocking Both CDK1-BRCA1 and PARP1-Related Activities

Through the study above, the increase in PARP1 expression was found to be an important mediating factor for OXA resistance. We then investigated the mechanims of PARP1 mediated OXA resistance. PARP1 is usually used to repair single base breaks in DNA, which are a type of commonly occurring DNA damage, and not normally harmful to cells. However, when these broken bases are transcribed or replicated, they will destroy and cause damage to the new DNA copies. The activation of PARP1 can promote DNA base excision repair (BER) and inhibit the binding of transcription factors to single-stranded DNA, thus inhibiting the transcription of damaged DNA (Slyskova et al., 2018). PARP1 is highly likely to mediate OXA resistance through its regulation of DNA repair mechanisms. First, the effect of OXA on DNA damage (increase of γH2AX) in OXA resistant cells and sensitive cells was studied and the results showed that the resistant cells were able to effectively repair DNA (decrease of γH2AX) after the damage by OXA (**Figure 5A**). However, when PARP1 was inhibited in these cells, DNA repair was significantly impaired ($P < 0.05$) (**Figures 5B,C**). The role of BER in cancer drug resistance had been proposed by many studies (Horton et al., 1995; Faivre et al., 2003; Preston et al., 2009; Yang et al., 2010; Sawant et al., 2017), and PARP1 plays an important role in the BER pathway (Ronson et al., 2018). To this end, the effect of PARP1 inhibiton combined with OXA on the BER pathway marker, XRCC1 was studied, and Olaparib + OXA was found to significantly inhibit the BER pathway when compared to OXA alone (**Figures 5A,D,E**). However, the transcription levels of XRCC1 in OXA resistance patients and non-resistant patients, and XRCC1 of OXA resistance and non-resistant cell lines did not change significantly (**Supplementary Figures 3B,C**).

The role of PARP1 is to bind to DNA damage sites (mostly single-stranded DNA breaks) and catalyze the synthesis of poly ADP ribose chains on protein substrates (Mateo et al., 2019). In order to study the core target of PARP1 interaction, weighted gene co-expression network analysis (WGCNA) was used to find the core gene that interacted with PARP1. The data indicated that CDK1 (Cyclin-dependent kinase) played a key role in the high expression of PARP1 (**Supplementary Figure 4** and **Supplementary Table 1**). CDK 1 is a core component of the cell cycle mechanism, forming a complex with cyclin A and B to promote the progression of S phase, G2 phase and M phase. Recently, CDK1 and its other family members have been shown to be involved in the DNA damage response pathway (Myers et al., 2007). Studies have found that CDK1 can inhibit homologous recombination by inhibiting the phosphorylation of BRCA1 (Johnson et al., 2009, 2011). Thus, we next determined whether OXA can directly act on BRCA1 or CDK1 to inhibit BRCA1 and cause homologous recombination failure.

To do this, we investigated the interaction of OXA with BRCA1 and CDK1. First, the Olaparib + OXA drug combination was compared with single drug OXA. OXA was seen to significantly inhibit the phosphorylation of BRCA1 and CDK1 (**Figures 6A,B**), but Olaparib had no significant effect (**Figures 6A**, **7A–C**, **8A–F**). In addition to affecting the functions of BRCA1 and CDK1, OXA also decreased the expression level of RAD51 ($P < 0.05$) (**Figures 6A**, **Figure 7D,E**). RAD51 is an important marker in homologous recombination. OXA may be able to inhibit homologous recombination by affecting the function of BRCA1, which in turn leads to a decrease in RAD51 and ultimately aggravating DNA damage (such as increased expression of H2AX). But whether OXA indirectly inhibited BRCA1 function by inhibiting CDK1 or directly inhibiting BRCA1 function remains unclear. So their relationship was compared by inhibiting CDK1. **Figure 6A** showed that CDK1 inhibitors significantly decreased the phosphorylation of BRCA1, and the effect was similar to that of OXA. In order to examine whether OXA can bypass CDK1 and directly inhibit BRCA1, the functional effects of cisplatin, which is also a platinum-based drug, was used on CDK1 and BRCA1 and compared to that of OXA. It was found that cisplatin did not inhibit the functions of CDK1 and BRCA1 (**Figure 6A**). Moreover, it was shown through proliferation and colony formation assay that the effect of cisplatin combined with PARP1 and CDK1 inhibitors was not significantly different from the effect of OXA combined with PARP1 inhibition (**Figures 6C,D**). Thus CDK1 plays an important role in killing tumor cells in platinum-based chemotherapy. In fact, although the principle of action of Cisplatin and OXA is basically the same, cisplatin is less effective than that of OXA (Liu et al., 2019) and CDK1 may be the main reason for this difference. Since OXA, in combination with olaparib, works by inhibiting both BER and HR. We further verified our results by comparing their effects on BER and HR markers as well as DNA damage markers through combination of drugs (**Supplementary Figures 5A–D**). It was found that that OXA inhibited HR and olaparib inhibited BER, which together leads to the aggravation of DNA damage in cells.

PARP1 Expression Predicts the Relapse of Human Gastric Cancer After Surgery

In order to clinically verify the importance of PARP1 in the recurrence of gastric cancer after curative surgery and adjuvant chemotherapy, we enrolled gastric cancer patients undergoing adjuvant chemotherapy in Sun Yat-sen University's Gastric Cancer Research Center. Through immunohistochemistry and

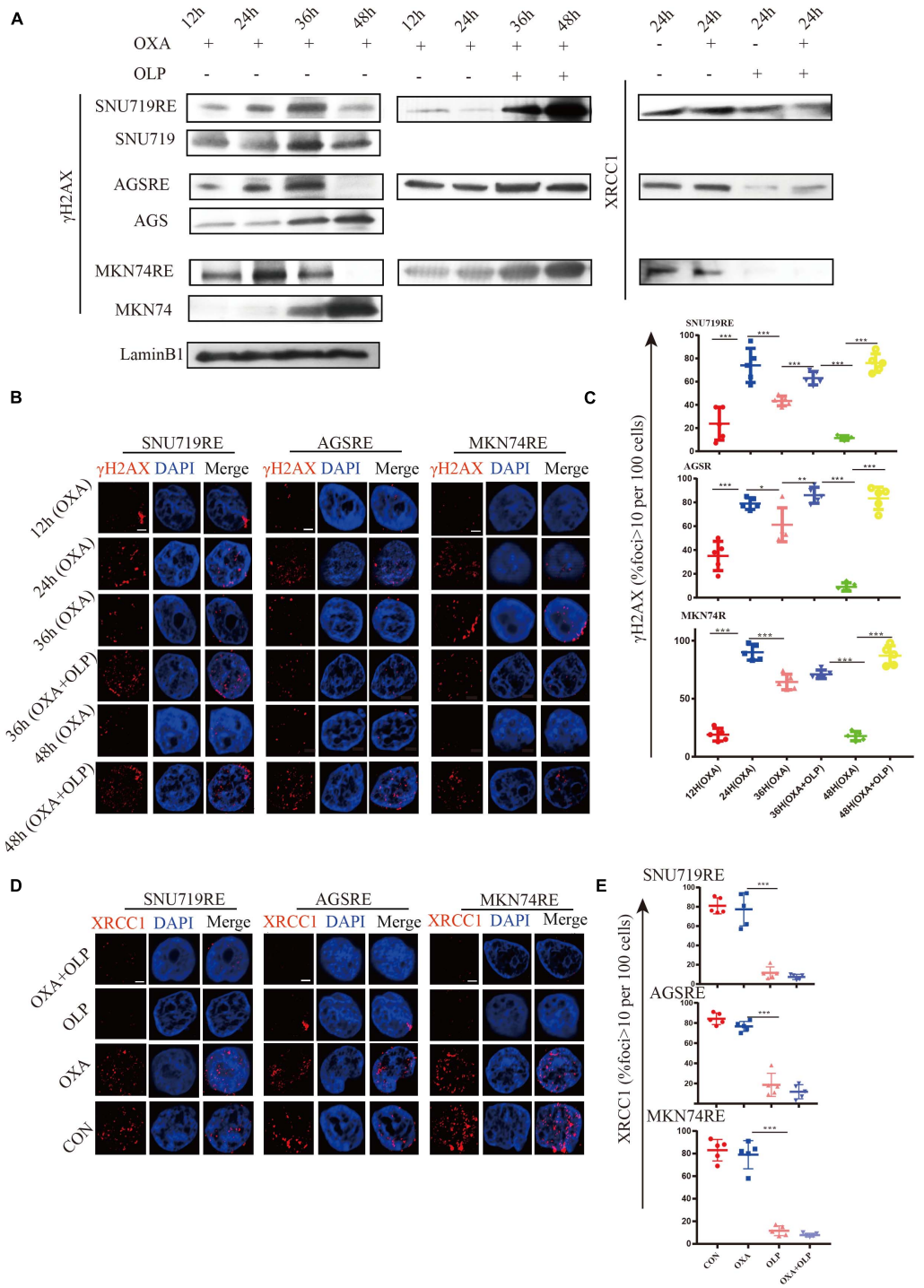


FIGURE 5 | The inhibition of PARP1 can significantly enhance the DNA damage and inhibit BER of Oxaliplatin-resistant GC. **(A)** Comparison of γH2AX expression in Olaparib + Oxaliplatin, Oxaliplatin, Olaparib, and the blank control group and the MKN74, SNU719, AGS resistant strains, and their corresponding wild-type cell lines at different times. Comparison of XRCC1 expression in Olaparib + Oxaliplatin, Oxaliplatin, Olaparib, and the blank control group in MKN74, SNU719, and AGS Oxaliplatin resistance strains. **(B)** Immunofluorescent comparison of γH2AX expression in Olaparib + Oxaliplatin, Oxaliplatin, Olaparib, and the blank control group and the MKN74, SNU719, AGS resistant strains, and their corresponding wild-type cell lines at different times. **(C)** Ratio of γH2AX + cells in MKN74, SNU719, AGS Oxaliplatin resistance strains, and their corresponding wild-type cell line **(B,D)** immunofluorescent comparison of XRCC1 expression in Olaparib + Oxaliplatin, Oxaliplatin, Olaparib, and the blank control group in MKN74, SNU719, and AGS Oxaliplatin resistance strains. The scale represents 2 um. **(E)** Ratio of XRCC1 cells in MKN74, SNU719, AGS Oxaliplatin resistance strain and their respective wild-type cell lines **(D)**, respectively. The Student's *t* test was used for statistical analysis. Error bars indicate mean ± standard deviation. OXA, Oxaliplatin. OLP, Olaparib. CON, control group. AGSR, AGS Oxaliplatin resistance. SNU719R, SNU719 Oxaliplatin resistance. MKN74R, MKN74 Oxaliplatin resistance. *<0.05, **<0.01, and ***<0.001. All experiments were repeated three times.

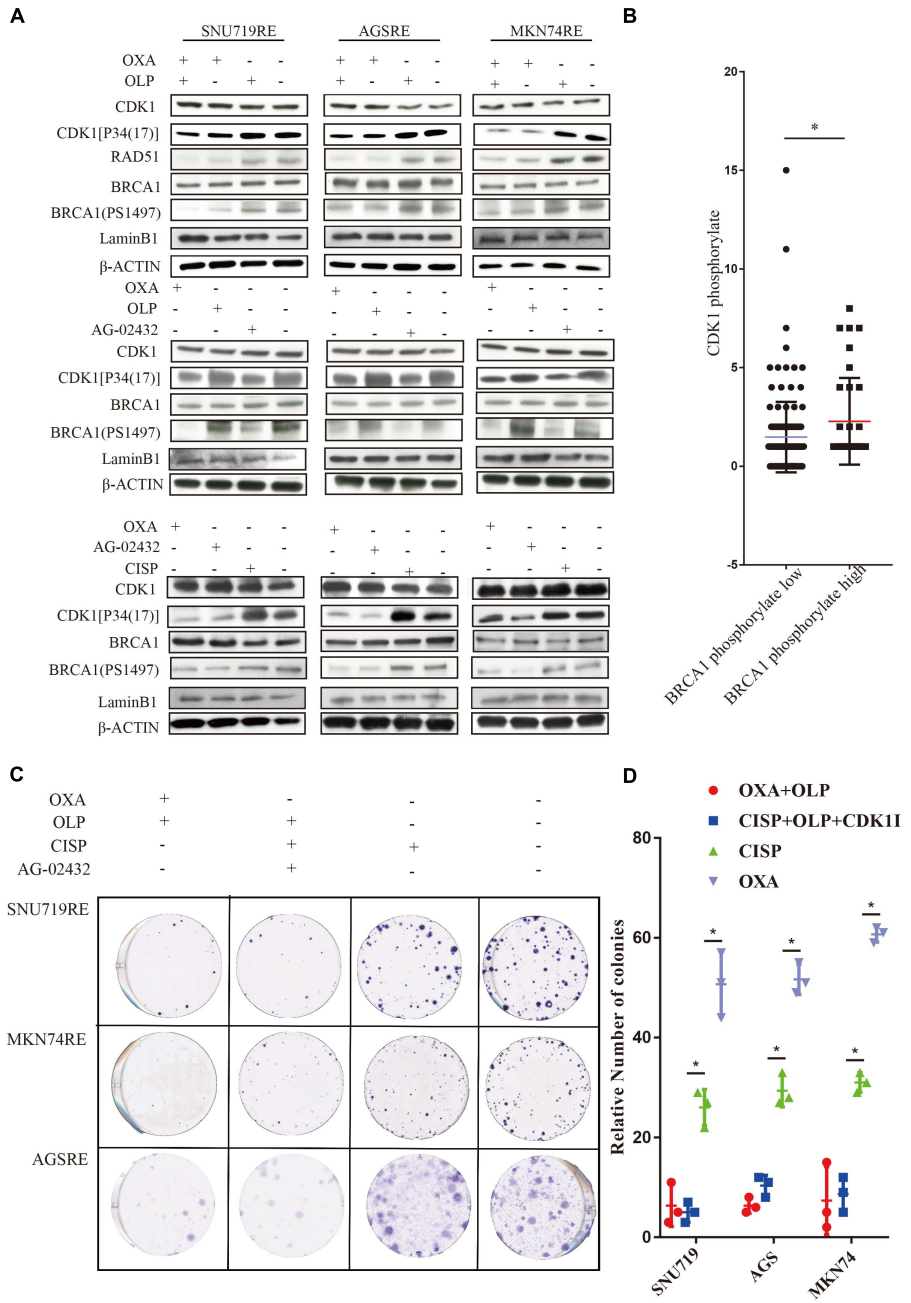


FIGURE 6 | Treatment of Oxaliplatin inhibits HR repair pathways via blocking CDK1-BRCA1 activities in Oxaliplatin resistance cell line. **(A)** Verification by WB on the effects of Olaparib + Oxaliplatin, Oxaliplatin, Olaparib, AG-02432 and cisplatin on CDK1 expression and its phosphorylation, BRCA1 expression and its phosphorylation, RAD51 expression in SNU719, MKN74, and AGS Oxaliplatin resistance strains. Drug action time was 36 h. **(B)** Histochemical results of protein phosphorylation in gastric cancer patients. **(C,D)** The effects of Olaparib + Oxaliplatin and cisplatin combined with CDK1 inhibitor Olaparib on colony formation of overexpressed PARP1 and normally expressed PARP1 cell lines in SNU719, MKN74, and AGS Oxaliplatin resistance strains. Colonies were stained with crystal violet. The Student's *t* test was used for statistical analysis. Error bars indicate mean ± standard deviation. OXA, Oxaliplatin. OLP, Olaparib. CON, control group. CISP, cisplatin. PCDK1, CDK1 phosphorylation antibody. PBRCA1, BRCA1 phosphorylation antibody. AGSR, AGS Oxaliplatin resistance. SNU719R, SNU719 Oxaliplatin resistance. MKN74R, MKN74 Oxaliplatin resistance. *<0.05. All experiments were repeated three times.

recurrence status of patients after adjuvant chemotherapy, we found that PARP1 was highly expressed in the tumors of patients who relapsed after adjuvant chemotherapy (**Figures 9A–C**). Moreover, the recurrence time of patients with high PARP1 expression was significantly shorter than that of patients with low expression (**Figures 9A–C**). Thus PARP1 can be used as an important indicator to clinically predict recurrence in postoperative adjuvant chemotherapy patients,

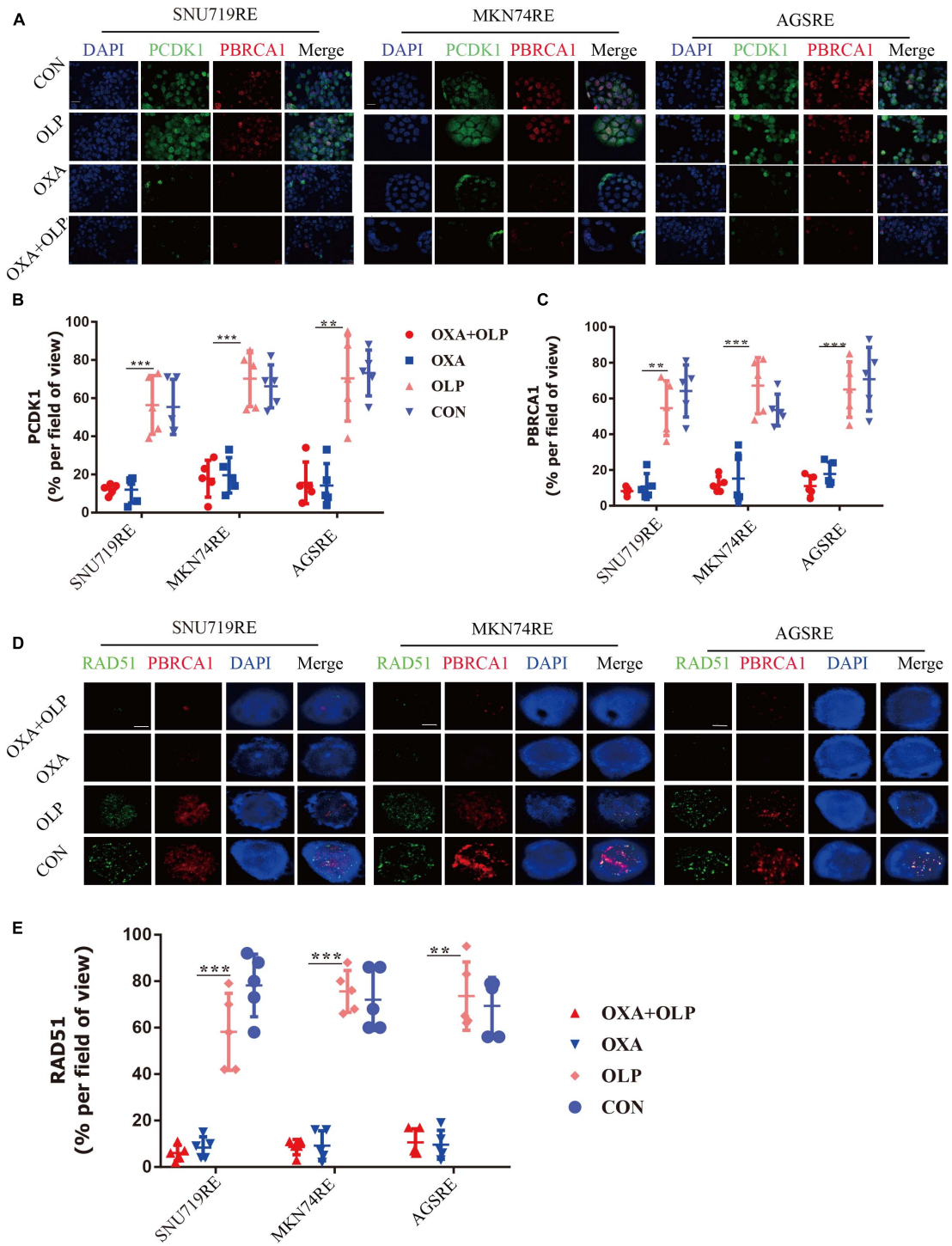


FIGURE 7 | Oxaliplatin inhibits HR repair pathways via blocking both CDK1-BRCA1. **(A)** Representative images of immunofluorescent CDK1 phosphorylation and BRCA1 phosphorylation staining of Olaparib + exaliplatin, Oxaliplatin, Olaparib, and blank control group in MKN74, SNU719, AGS Oxaliplatin resistance cell lines. The scale represents 20 um. Drug action time was 36 h. **(B,C)** Proportion of CDK1 phosphorylation and BRCA1 phosphorylation positive cells **(A)**, respectively. **(D)** Representative images of immunofluorescent phosporylation staining comparisons of Olaparib + Oxaliplatin, Oxaliplatin, Olaparib and blank control group and immunofluorescent phosphorylation staining of RAD51 and BRCA1 of MKN74, SNU719, AGS resistant strains RAD51, and BRCA1 at different time. The scale represents 2 um. **(E)** Statistical analysis of RAD51 + cells in **(D)**. The Student's *t* test was used for statistical analysis. Error bars indicate mean ± standard deviation. OXA, Oxaliplatin. OLP, Olaparib. CON, control group. PCDK1, CDK1 phosphorylation antibody. PBRCA1, BRCA1 phosphorylation antibody. AGSRE, AGS Oxaliplatin resistance. SNU719RE, SNU719 Oxaliplatin resistance. MKN74RE, MKN74 Oxaliplatin resistance. *<0.05, **<0.01, and ***<0.001. All experiments were repeated three times.

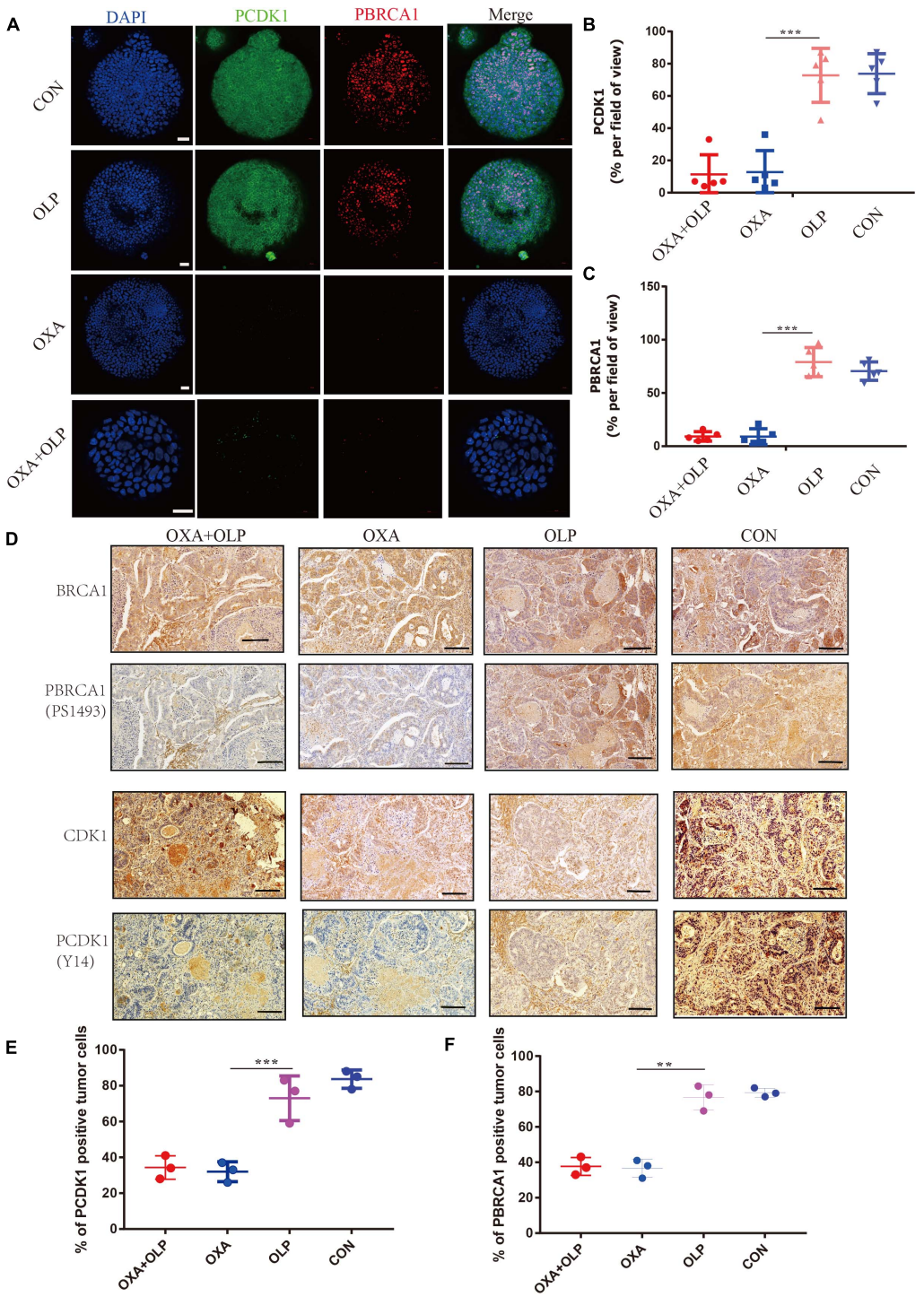


FIGURE 8 | Treatment of Oxaliplatin inhibits HR repair pathways via blocking CDK1-BRCA1 activities in Oxaliplatin resistance gastric cancer Organoid and PDOX. **(A)** Representative images of immunofluorescent staining comparison of CDK1 phosphorylation and BRCA1 phosphorylation in öxaliplatin resistance gastric cancer organoids under the effects of Olaparib + Oxaliplatin, Oxaliplatin, Olaparib, and the blank control group. The scale represents 20 μm. Drug action time was 36 h. **(B,C)** Proportion of CDK1 phosphorylation and BRCA1 phosphorylation positive cells **(A)**, respectively. **(D)** Representative images of comparison of IHC staining of CDK1 and its phosphorylation and BRCA1 and its phosphorylation in BALB/C NUDE mice after tumorigenesis under the effects of Olaparib + Oxaliplatin, Oxaliplatin, Olaparib, and blank control group. The scale represents 200 um. **(E,F)** Proportion of CDK1 phosphorylation and BRCA1 phosphorylation positive cells in **(D)**, respectively. The Student's *t* test was used for statistical analysis. Error bars indicate mean ± standard deviation. OXA, Oxaliplatin. OLP, Olaparib. CON, control group. CISP, cisplatin. PCDK1, CDK1 phosphorylation antibody. PBRCA1, BRCA1 phosphorylation antibody. PDOX, patient-derived organotipic culture xenograft. **<0.01, and ***<0.001. All experiments were repeated three times.

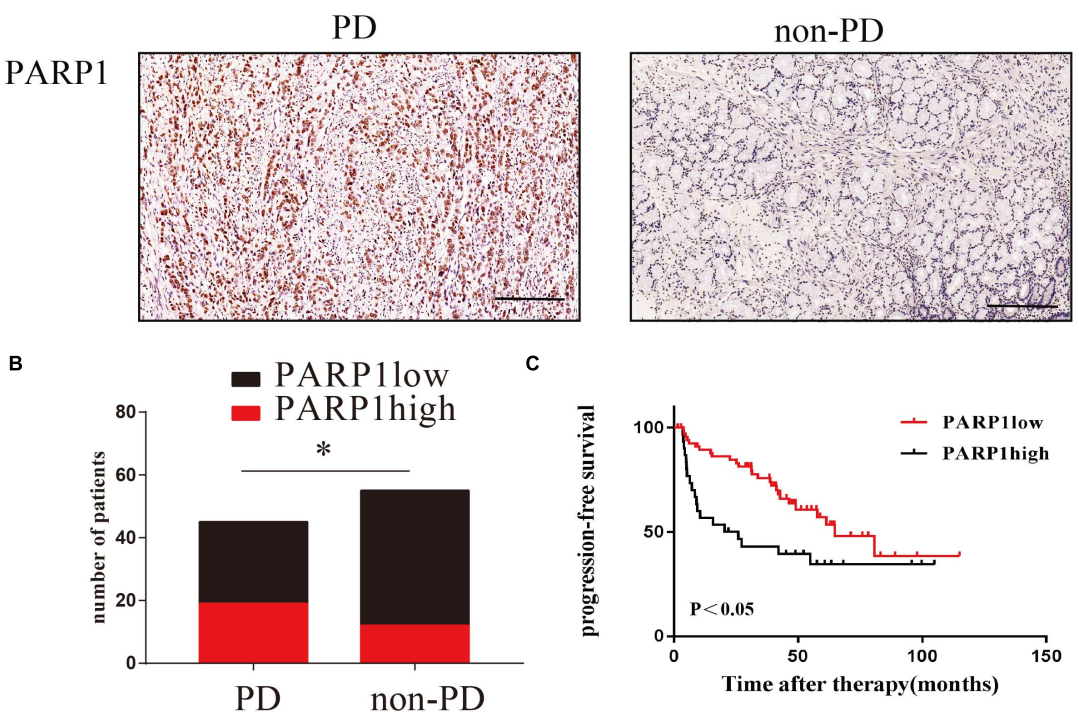


FIGURE 9 | PARP1 expression predicts the relapse of human gastric cancer after surgery. **(A)** Representative images of IHC stained PARP1 in PD tumors (left) and non-PD tumors (right). The brown nucleus is positive for PARP1. The scale represents 200 um. **(B)** Comparison of the number of patients with PARP1 positive and negative staining. **(C)** Comparison of PARP1 expression and tumor recurrence time after chemotherapy. Kaplan–Meier survival plot was used. *<0.05. PD, progressed disease.

and provides confirmation that PARP1 play an important role in chemotherapy resistance.

DISCUSSION

We used sequence analysis of tumors from patients who relapsed after OXA chemotherapy and the patients with a good chemotherapy response. It was found that PARP1 was significantly increased in relapsed patients after postoperative chemotherapy. We then verified that PARP1 played a pivotal role in OXA resistance using OXA resistant cell lines and organoid patient derived xenografts *in vivo* BALB/C NUDE mice. In order to explore the relationship between PARP1 and OXA resistance, we inhibited PARP1 to significantly enhance the ability of OXA to kill cancer and OXA resistance cells. The combined use of PARP1 inhibitors with OXA can significantly inhibit activity of GC organoids, which affects their tumor initiation ability. *In vivo* experiments also showed that inhibiting PARP1 significantly overcame the resistance to OXA. Subsequently, we found that PARP1 mediates the DNA repair ability of OXA resistance cells by regulating the DNA repair pathway BER, and after the combination of PARP1 inhibitor, Olaparib, the joint effect allowed the drugs to effectively cause homologous recombination failure through impaired CDK1 and BRCA1 function, eventually leading to tumor cell apoptosis.

PARP1 is a multifunctional protein post – translational modifier found in most eukaryotic cells. It is activated by recognizing fragments of DNA that are structurally damaged and is thought to be a DNA damage receptor. It also performs polyadenosine diphosphate ribosylation of many nucleoproteins. Proteins modified by PARP1 include histones, RNA polymerase, DNA polymerase, and DNA ligase. ADP-ribosylation of histones results in their detachment, which is helpful to repair the binding of proteins and repair DNA damage (Alemasova and Lavrik, 2019). PARP1 plays a very important role in the BER pathway, and studies have shown that PARP1 can directly regulate the repair process during DNA single strand breakage or base resection repair (BER) (Ronson et al., 2018). The breakdown of PARP1 function inhibits the BER process (Reynolds et al., 2015). BER pathway is an important signaling pathway leading to oxaliplatin resistance (Sharma and Dianov, 2007). Our study also found that PARP1 expression could cause oxaliplatin resistance through BER by inhibiting the XRCC1. The XRCC1 also participates in MMEJ (an alternative pathway to NHEJ) but we found no significant changes in ERCC1, an important marker of MMEJ (Sfeir and Symington, 2015; Seol et al., 2018).

PARP1 inhibitors can enhance the efficacy of radiotherapy, alkylating agents and platinum-based chemotherapy by

inhibiting DNA damage repair and promoting apoptosis of tumor cells (Wang et al., 2017). It wasn't until 2014 that olaparib, the world's first PARP (polyADP ribosome polymerase) inhibitor, was approved for the treatment of ovarian cancer, followed by the Pani family of Rucaparib, niraparib and tarazoparib (Wang et al., 2019). PARP and BRCA are both regulators of DNA repair, and PARP is responsible for single-strand repair. When PARP is inhibited, the single-strand breaks of cells continue to increase and gradually develop into double-strand breaks. At this time, BRCA is required for high-Fi precision repair (homologous recombination) of double-strand breaks to prevent cell death caused by DNA instability (D'Andrea, 2018). Although most studies have shown that PARP1 inhibitors can effectively enhance the efficacy of chemotherapy drugs, the mutation rate of BRCA1 mutations in most gastrointestinal tumors is actually not high (Narod and Foulkes, 2004).

Our study found that PARP1 inhibitors in combination with OXA have a powerful anti-tumor effect in gastric cancer patients without BRCA1 mutations. We found that CDK1 was an important factor affecting the function of PARP1 when we searched for the core gene influencing PARP1 function by means of WGCNA. Cell cycle progression is controlled by cyclin-dependent kinases (CDKs) and is a tightly regulated process in eukaryotic cells. Genomic integrity is maintained through the precise activation of CDKs and the correct timing coordination of DNA synthesis. CDK2 and CDK1 co-mediate the S and G2 phases, while CDK1 regulates the G2/M phase and mitotic progression. The deletion of CDKs in a single shRNA-mediated transformed cell suggests that they can easily complement each other (Cai et al., 2006). Exposure to genotoxic damage leads to activation of a checkpoint cascade that downregulates CDK activity and imposes cell cycle arrest to prevent the reproduction of damaged DNA. Delayed cell cycle progression is caused by DNA-induced activation of phosphatidylinositol 3 kinase-like protein kinase ATM (ataxia – telangiectasia mutation) and ATR (ATM and RAD3 associated) (Abraham, 2001). BRCA1 is an important component of ATM- and ATR-mediated checkpoint signaling and is hyperphosphorylated by ATM and ATR during DNA damage. BRCA1 acts as a scaffold to promote ATM/ATR phosphorylation of a set of substrates including CHK1 and CHK2 (Foray et al., 2003). Although CDK2 and CDK1 can compensate for each other during cell cycle progression, allowing a single CDK-depleted cell to proliferate, it is unclear whether they play a non-overlapping role in DNA damage-induced checkpoint control. In this study, we found that in the response of cisplatin to gastric cancer cells, selective inhibition of CDK1 could affect the function of BRCA1, while OXA could play an independent role, indicating that OXA could inhibit CDK1 and thus exert the function of inhibiting BRCA1. This is the first time that oxaliplatin has been found to play a role in gastric cancer by inhibiting CDK1 phosphorylation.

CONCLUSION

Our study found that PARP1 inhibitors in combination with oxaliplatin have a powerful anti-tumor effect in gastric cancer patients without BRCA1 mutations. However, our study found that oxaliplatin itself can affect BRCA1 by inhibiting the function of CDK1, causing BRCA1 dysfunction and allowing PARP1 inhibitors to function effectively.

MATERIALS AND METHODS

Cell Culture

GC cell lines AGS (ATCC® CRL-1739™) and MKN74 (ABC-TC0689) were ordered from the Francis Crick Institute Cell Services, SNU719 cells were provided by Nanjing Kegen Biotechnology Co., Ltd. All GC cell lines were grown in complete medium containing 10% FCS and RPMI.

In order to cultivate a stable OXA-resistant GC cell line, AGS, SNU719 and MKN74 cells were exposed to RPMI with an initial OXA (No. S1224, Selleckchem) concentration of 1 μmol.L^{-1} and 10% fetal bovine serum. The surviving cell population was grown to a concentration of 80% and passaged twice within 9 days to ensure survival. The above process was repeated for the surviving cells with consecutively higher OXA concentrations of 10 μmol.L^{-1} (15 days), 20 μmol.L^{-1} (30 days), 50 μmol.L^{-1} (60 days), 100 μmol.L^{-1} (90 days), and finally 200 μmol.L^{-1} (120 days). Afterward, resistance to OXA was confirmed by IC50 and a colony forming test (see **Supplementary Figures 1A–C**).

Human Tissue and Organoids

Human GC tissues were taken from patients who underwent gastric cancer surgery in The First Affiliated Hospital of Sun Yat-sen University, PRC. They agreed and signed a donation and research consent form. This was approved by the Clinical Research and Animal Experiment Ethics Committee of The First Affiliated Hospital of Sun Yat-sen University [Ethical Review (2017) No. 208]. This research complied with all the ethics of human participation in research.

Biopsies were obtained from the surgery of gastric cancer patients treated by the Gastric Cancer Research Center of Sun Yat-sen University, for GC organoid culture. According to the patient's postoperative clinical history, we included two cases of recurrence of GC after chemotherapy (named rGC1 and rGC2 repectively) and two cases of satisfactory post-chemotherapy outcomes for our organoid cultures (named sGC1 and sGC2). The organoids were screened through the Scientific Research Center of the Seventh Affiliated Hospital of Sun Yat-sen University and organoid strains of 4 patients were finally selected to be included in the experiment.

The organoids were generated as follows, the GC sample was placed in 50 U.mL^{-1} penicillin-streptomycin (Thermo Fisher Scientific) ice-cold G solution, was minced on ice and incubated in DMEM containing 1 mg.ml^{-1} collagenase V (Sigma-Aldrich) for 1 h at 37°C. Ice-cold PBS was added to stop the digestion, and the mixture was then centrifuged at 4°C (300 G, 5 min). The samples were further digested with TrypLE (Thermo Fisher Scientific) at 37°C for 5 min, which was then stopped with a large quantity of PBS. The suspension was filtered through 40 μm nylon mesh, centrifuged, and the cells were resuspended in the medium. Organoids were passaged with TrypLE every 2 weeks.

The medium for establishing and culturing human GC organoids was as described in the literature (Seidlitz et al., 2019).

Lentivirus Production and Infection of Organoids

Control and shRNA_PARP1-expressing pLKO vectors were purchased from Sigma (China). PARP1 overexpression vectors designed to generate the lentivirus were obtained from Shanghai Genechem Co., Ltd. All lentiviral particles were produced in HEK293T cells by standard procedures, concentrated by ultracentrifugation at 100,000*g* for 2 h and resuspended in sterile PBS. Organoids were extracted from Matrigel using TrypLE Express (Thermo Fisher Scientific), resuspended in OptiMEM with 10 $\mu g.mL^{-1}$Polybrene, and then mixed with the virus solution in an incubator for 6 h. Cells were plated back into Matrigel and split 72 to 168 h later when antibiotic selection was started.

Quantitative Real-Time PCR

When the number of cells were less than 10^3 we used MagMAX-96 Total RNA Isolation Kit (Ambion) to extract RNA, for higher cell numbers, RNeasy Mini Kit (Qiagen) was used. Random hexamer primers (Invitrogen) were used with the SuperScript III First-Strand cDNA synthesis kit or iScript cDNA synthesis kit (BioRad) according to the manufacturer's instructions to generate cDNA. cDNA was diluted with distilled water to 2 mol/L and RT-qPCR was performed using the Express SYBR GreenER (Thermo Fisher Scientific) ABI7500 (Applied Biosystems). The primers were designed using the Universal Probabilistic Analysis and Design Center (Roche) to ensure that they span the exon-exon junction. Actin was used for normalization. The list of RT-qPCR primers is provided in **Supplementary Table 2**.

Western Blotting

The total protein of the extracted cells was lysed in ice-cold cell lysis buffer (NEB) containing 1 mM PMSF and 1:100 protease inhibitor cocktail (Sigma). The lysate was pre-cleared with 15 × l protein A Sepharose 4B beads (Sigma) at 4°C for 30 min. NE-PER^{TM} Nuclear and Cytoplasmic Extraction Reagents (Thermo Fisher Scientific, 78833) were used to extract nucleoprotein from cells. The BCA protein assy (Pierce, Rockford, IL, United States) and Western Blot procedures were performed as described previously (Ruiz et al., 2019). Antibodies used included Anti-beta Actin antibody (1:50000, Abcam, ab49900), Anti-gamma H2A.X (phospho S139) antibody (1:1000, Abcam, ab2893), PARP-1 antibody (F-2) (1: 500, Santa Cruz, sc-8007), Cdc2 p34 antibody (17) (1:500, Santa Cruz, sc-54), BRCA1 antibody (D-9) (1:500, Santa Cruz, sc-6954), Phospho-cdc2 (Tyr15) Antibody (1:1000, Cellsignal, #9111), Phospho-BRCA1 (Ser1497) Polyclonal Antibody (1:1000, Thermo Fisher Scientific, # PA5-64621), Rad51 Antibody (G-5) (1:500, Santa Cruz, sc-133089), XRCC1 (1:1000, Abcam, ab44830), and Lamin B1 (1: 20000, Proteintech, 66095-1-Ig).

Flow Cytometry

Annexin V-PI apoptosis assay was performed using Annexin V-FITC Apoptosis Detection Kit (Sigma-Aldrich), following the protocol provided by the manufacturers. FlowJo 10 software was used to analyze the data.

Colony Formation Assay and Cell Viability

Control (DMSO), Olaparib (No.S1060, Selleckchem) (25 μM.mL-1), OXA (10 uM.mL-1), cis Platinum (5 μM.mL-1) and CDK1 inhibitor (AG-024322, BIOQUOTR, and 837364-57-5) (0.12 μM.mL-1) were added to cells (500/well) in a 6-well plate. After 2 weeks of culturing, the formation of colonies or colosphere was evidently visible, the cell colonies were then fixed, stained with 0.1% crystal violet in 20% methanol solution, and counted. This process was repeated three times per solution type.

In a 96-well transparent bottom blackboard, 3,000 cells were planted in each well (organoids were planted in Matrigel). The drug was then added to each well according to a 10-fold concentration gradient. Cell viability as determined by Adenosine triphosphate (ATP) levels (Promega, Madison, WI, United States) were assayed by CellTiter-Glo using a luminometer (PerkinElmer Life and Analytical Sciences, Boston, MA, United States) 48 h later.

Immunohistochemical Staining

The tissues were collected, fixed with 10% neutral buffered formalin (NBF, Sigma) for 16 h, dehydrated with 70% ethanol, and embedded in 4 × m paraffin sections. H&E staining was performed according to standard procedures. After heat-mediated antigen extraction in 10 mM sodium citrate buffer (pH 6.2), the endogenous peroxidase was blocked with 1.6% hydrogen peroxide, and PARP-1 (Proteintech, 13371-1 -AP), KI67 (Abcam, ab15580), Caspase 3 (Proteintech, 19677-1-AP), BRCA1 (Affinity Biosciences, AF6289), Phospho-BRCA1-Ser1497 (Affinity Biosciences, AF8204), CDK1 (Abcam, ab133327), and Phospho-CDK1-Y15 (Abclonal, AP0016) were stained with DAB according to manufacturer's manual. Positive cells were counted in 5 random fields of view per slide.

Immunofluorescent Staining

Cell/organoids were grown in a glass bottom tissue culture plate (Ibidi, lot:191218/2), fixed with 5% NBF for 10 min, and blocked with PBS containing 10% FCS, 1% BSA (Sigma) and 0.2% Triton-X. The primary antibody was incubated in blocking buffer at 4°C for 16 h. The fluorescent secondary antibody was incubated with 3 μM DAPI in blocking buffer at 20°C for 1–6 h. Fluorescence staining was imaged on a Zeiss LSM 780 confocal microscope. Tissues were prepared as detailed for Immunohistochemical staining. Secondary antibodies were fluorophore-conjugated and incubated with 3μM DAPI in the dark. Before mounting, slides were incubated in 0.1% (w/v) Sudan black B (Sigma) in 70% ethanol to reduce background signal. Antibodies include Anti-gamma H2A.X (phospho S139) antibody (1:1000, Abcam, ab2893), PARP-1 antibody (F-2) (1: 500, Santa Cruz, sc-8007), Phospho-cdc2 (Tyr15) Antibody (1:1000, Cellsignal,

#9111), Phospho-BRCA1 (Ser1497) Polyclonal Antibody (1:1000, Thermo Fisher Scientific, # PA5-64621), Rad51 Antibody (G-5) (1:500, Santa Cruz, sc-133089), XRCC1 (1:1000, Abcam, ab44830), and XRCC1 (1:1000, Abcam, ab235196).

The PDOX Mouse Model

In vivo experiments were performed in accordance with the Institutional Animal Care and Use Committee (IACUC) regulations. The experimental protocol was approved by the Clinical Research and Animal Experiment Ethics Committee of The First Affiliated Hospital of Sun Yat-sen University [Ethical Review (2017) No. 208]. The experiment was performed by the staff of the Animal Center of the First Affiliated Hospital of Sun Yat-sen University. In order to study the tumorigenesis ability of OXA resistance, 100,000 cells previously selected were inoculated into BALB/C NUDE female mice with Matrigel (BD, 354230). After 25 days, 6 mice with organoids transplantation tumors received a treatment of OXA (Selleckchem, s1224) at a dose of 5 $mg.kg^{-1}$ twice a week for the period of 4 weeks.

For the other 6 mice, PBS were injected intraperitoneally. The cancer-bearing BALB/C NUDE mice were sacrificed 4 weeks later, and tumors were harvested for measuring and weighing. In order to study the drug resistance of PARP1 expression, 100,000 cells of plko and PARP1-sh1 (rGC1 and rGC2) were inoculated into BALB/C NUDE mice with Matrigel (BD, 354230). After 25 days, 6 mice with organoids transplantation tumors received OXA treatment as before. The cancer-bearing BALB/C NUDE mice were sacrificed 4 weeks later, and tumors were harvested for measuring and weighing. we inoculated 200,000 cells of control and PARP1 overexpression (sGC1 and sGC2) into BALB/C NUDE mice with Matrigel (BD, 354230). After 25 days, 6 mice with organoids transplantation tumors received a treatment of OXA (Selleckchem, s1224) at a dose of $mg.kg^{-1}$ twice a week for the period of 4 weeks. The cancer-bearing BALB/C NUDE mice were sacrificed 4 weeks later, and tumors were harvested for measuring and weighing.

The organoids of rGC1 and rGC2 were digested into single cells by TrypLE and then counted, and 100,000 cells were mixed with Matrigel and inoculated subcutaneously into BALB/C NUDE mice (6 per group). After 25 days, the organoids transplanted BALB/C NUDE mice received intraperitoneal injection of either OXA (Selleckchem, s1224) + Olaparib (Selleckchem, AZD2281, s1060), OXA, Olaparib, or PBS. OXA dose was 5 $mg.kg^{-1}$, Olaparib dose was 50 $mg.kg^{-1}$, combined group dose was $mg.kg^{-1}$ of OXA and 25 $mg.kg^{-1}$ of Olaparib twice per week, each treatment lasting for the period of 4 weeks. The tumor size and body mass of the mice were measured every 3 days. The mice were sacrificed 1 month later, and tumors were removed. All tumors were photographed and the mass and volume determined. Tumor volume (mm^3) $= 0.5 \times width^2 \times length$.

RNA Isolation and Microarray

Total RNA was extracted from tissue samples, and Nanodrop 2000 was used to detect the concentration and purity of the RNA. Agarose gel electrophoresis was used to detect RNA integrity, and Agilent 2100 was used to determine the RIN value. A single library construction required that the total amount of RNA was no less than 5 μg, the concentration $\geq$ 200 $ng.\mu L^{-1}$, and the OD260/280 between 1.8 and 2.2. The mRNA capture and library preparation were completed by the advanced sequencing equipment of Shanghai Origin-gene Biomedical Technology Co., Ltd. using KAPA mRNA HyperPrep kit (Roche). The biological triplicate libraries were sequenced on the Illumina Truseq TM RNA sample prep Kit platform of the facility, and each sample produced an average of 25 million single-ended reads of 75 bp. The designated reference genome was used to align the high-quality sequence with post quality control. The PDOX sample was first compared with mouse reference genome. After removing mice-related data, it was then compared with human reference genome. The human reference genome was obtained from Ensembl database, genome version GRCh38, gene annotation information was Ensemble 92. Before alignment, cutadapt (version 1.9.1) was used for quality control and adaptor trimming of the original reading. Annotation release 86 was used to sequence the reads of the human genome GRCh38 using RSEM 1.3.0 and STAR 2.5.2, and count the subsequent gene levels. In version 3.6.1 of R package, the DESeq2 package (version 1.24.0) was used for normalization and differential expression analysis of raw count data. Regularized logarithmic transformation was performed on the rlog function.

Clinical GC Patient Samples

From May 2010 to February 2020, the progressive GC tissue samples before the start of OXA treatment were collected from the First Affiliated Hospital of Sun Yat-sen University ($n = 100$) through surgical specimens or biopsy, and the patients' research consent form were signed and documented. This study was approved by the Ethics Committee of The First Affiliated Hospital of Sun Yat-sen University [Ethical Review (2018) No. 087]. The OXA group received at least 6 cycles of OXA treatment. The detailed clinical characteristics of the patients can be found in **Table 1**. The tumor response to chemotherapy was evaluated by the three-dimensional volume reduction rate or tumor response rate (radiological evaluation), and evaluated in accordance with the response evaluation criteria in the solid tumor (RECIST) guidelines (Eisenhauer et al., 2009). In the validation phase, patients with worsening symptoms, new lesions, or radiologically assessed tumor regeneration $\geq$ 25% were assigned to the progressive disease (PD) group ($n = 45$) and the remaining non-PD group ($n = 55$). PFS is defined as the duration from tumor resection to PD. Follow-up was performed every 3 months (for the initial 0–2 years), 6 months (subsequent 2–4 years), and once a year until death or February 2020. The follow-up study included abdominal computed tomography and postoperative physical examination.

Patient Information in Public Databases

The transcriptome data of patients with gastric adenocarcinoma confirmed by pathology was downloaded from the TCGA website[1] in June 2020, including data from 416 patients with gastric adenocarcinoma and general information of the

[1]https://portal.gdc.cancer.gov/

TABLE 1 | Demographics of GC patients of SYSU.

	Non-progress (55)	Progress (45)	*P*
Gender			
Male	29	24	0.952
Female	26	21	
Age			
≤65	15	20	0.060
>65	40	24	
M staging			
M0	55	45	–
M1	0	0	
T staging			
T1	1	3	0.370
T2	19	2	
T3	31	31	
T4	4	9	
N staging			
N0	27	10	0.343
N1	20	15	
N2	5	9	
N3	3	11	
Differentiation			
High	31	31	0.130
Moderately	18	11	
Poorly	6	3	
Undifferentiation	0	0	
PARP1			
High	43	26	0.032
Low	12	19	
CD133			
High	39	22	0.025
Low	16	23	

corresponding cases. Data that did not list survival time were excluded, leaving 416 cases of gastric cancer and 33 cases of adjacent tissues. Inclusion criteria: (a) diagnosis age ≥ 8 years old; (b) tumor site: stomach; (3) cases with clear pathology. The exclusion criteria are as followed: (a) multiple tumor; (b) carcinoma *in situ*; (c) incomplete follow-up data; and (d) deaths within 30 days. Proteomics data of patients with gastric adenocarcinoma were downloaded from the CPTAC website[2] in June 2020, including data and corresponding general information of 130 gastric adenocarcinoma patients.

Gene Set Enrichment Analysis (GSEA)

Gene set enrichment analysis was performed using software (GSEA V4.0.3) developed by the Broad Institute of MIT and Harvard University[3]. The RNA-seq datasets of OXA resistance patients, normalized RNA read counts were used for analysis, and the following settings were applied: permutation number = 1000, permutation type = gene set, enrichment statistics = weighting, a measure of gene ranking = signal noise. For the TCGA gastric cancer dataset, the samples were grouped according to their expression above or below the median value. The normalized RSEM read count was used for analysis, and the following settings were applied: number of permutations = 1000, permutation type = phenotype, enrichment statistics = weighting, measurement of gene ranking = signal 2 noise. Recognized marker gene set 40, KEGG pathway or gene ontology (GO) terms, and false discovery rate (FDR q) < 0.05 were considered significant enrichment.

Screening of Differentially Expressed Genes (DEGs)

The expectation-maximization method RNA-Seq was used to normalize the 3-level transcriptome data of the data set, and the logarithmic transformation of all gene expression values was performed. Approximate data were normally distributed after normalization by quantiles (Li and Dewey, 2011). In this study, the R package limma program v3.28.14 was used to analyze the differential genes of gene expression data, and its mRNA satisfied $P < 0.01$, false discovery rate (FDR) < 0.01 and $|\log2 \text{ fold change (FC)}| > 1.5$, where $P < 0.05$ indicated that the hypothesis test was statistically significant. FDR is a control indicator for the error rate of the hypothesis test. As an evaluation index of the selected differential genes, the number of false rejections was proportional to the number of rejected invalid hypotheses. FC was usually used to describe the degree of change from the initial value to the final value. In this study, the ratio of tumor tissue gene expression value to normal tissue gene expression value was used, also known as the fold change. The heatmap and volcano map of the differential genes were constructed in R language for visual comparison.

WGCNA Co-expression Network Construction

Gene expression data (mRNA-seq data) was downloaded from the TCGA database. A total of 24,991 genes were identified in each sample. Analysis of variance was performed and then sorted from largest to smallest. The SD value of each gene was calculated and sorted from largest to smallest, and then the top 5000 genes were selected for WGCNA. WGCNA package in R software was used to construct a gene co-expression network from the expression data map of these 5000 genes (Luo et al., 2015). Using the adjacency function in WGCNA, an adjacency matrix was constructed by calculating the Pearson correlation between all pairs of genes in the selected sample. In this study, $\beta = 7$ (scale-free $R2 = 0.9$) was used as the soft threshold parameter to ensure a scale-free network. In order to further identify the functional modules in the co-expression network of these 5000 genes, the adjacency matrix was used to calculate the Topological Overlap Measure (TOM), which represents the overlap in the shared neighborhood. We identified related modules by calculating the correlation between MEs and PARP1 expression levels. Then the log10 transformation of the p value (GS = lgP) in the linear regression of gene expression and clinical PARP1 expression level information was defined as gene significance (GS). In addition, module significance (MS) is defined as the average GS of all genes

[2]https://cptac-data-portal.georgetown.edu/study-summary/S025

[3]https://www.gseamsigdb.org/gsea/index.jsp

in a module. In general, among all the selected modules, the module with the highest absolute value of MS was considered to be the module related to the level of PARP1 expression.

PPI Network Construction of Key Module Gene

The Hub gene, which is highly interconnected with the nodes in the module, is considered to have important functions. We selected the top 30 Hub genes in the module network as candidate genes for further analysis and verification. The STRING data set is an online biological resource that can decode the interaction between proteins and proteins to obtain the actual precise functions of proteins (Snel et al., 2000). The candidate gene was submitted to the protein interaction of STRING, and the binding confidence interval of the cutoff value was set to 0.4. In the plugin, Molecular Complex Detection (MCODE), the significant models with strong protein-protein connection were calculated and selected with the default parameters (degree cut ≥ 2, node score cut ≥ 2, K-core ≥ 2, maximum depth $= 100$). $P < 0.05$ was considered statistically significant.

Statistical Analysis

The images and graphs shown represent several experiments repeated on different individuals at different times. Each experiment was repeated independently at least three times. All statistics were performed using SPSS and R software. The statistical test was explained in the figure legend. All results were statistically different based on the mean $\pm$ SD, $P < 0.05$.

DATA AVAILABILITY STATEMENT

The datasets presented in this study can be found in online repositories. The names of the repository/repositories and accession number(s) can be found below: BioProject PRJNA669415.

ETHICS STATEMENT

This study was approved by the Ethics Committee of The First Affiliated Hospital of Sun Yat-sen University [Ethical Review (2018) No. 087] and the Clinical Research and Animal Experiment Ethics Committee of The First Affiliated Hospital of Sun Yat-sen University [Ethical Review (2017) No. 208].

AUTHOR CONTRIBUTIONS

AB, YH, CZ, HL, and CW designed the study. HL, CW, and LL contributed to development of methodology. HL, CW, LL, IE, and ZZ contributed to acquisition of data (provided animals, acquired and managed patients, and provided facilities, etc.). HL, CW, LL, and ER contributed to analysis and interpretation of data (e.g., statistical analysis, biostatistics, and computational analysis). JO, RR, HL, CW, WC, ZH, and LY contributed to cultivation and development organoid. All authors contributed to writing the manuscript.

FUNDING

This study was supported by the National Natural Science Foundation of China (Grant No. 82073148), The Sanming Project of Medicine in Shenzhen (SZSM201911010), and International Program for Ph.D. Candidates, Sun Yat-sen University. This work was also supported by the Guangdong Provincial Key Laboratory of Digestive Cancer Research (No. 2021B1212040006).

ACKNOWLEDGMENTS

The authors would like to thank Antonio Tedeschi (Adult Stem Cell Laboratory, The Francis Crick Institute) for valuable comments on this article and Prof. Qiao Su (Laboratory Animal Center, The First Affiliated Hospital of Sun Yat-sen University) for technical assistance.

SUPPLEMENTARY MATERIAL

The Supplementary Material for this article can be found online at: https://www.frontiersin.org/articles/10.3389/fcell.2021.719192/full#supplementary-material

Supplementary Figure 1 | Verifying the drug resistance level in GC resistant strains. **(A–C)** indicate the comparison of cell viability between AGS, SNU719, and MNK74 Oxaliplatin resistance strains and wild-type cell strains under the effects of Oxaliplatin, respectively. **(D)** indicate the comparison of cell viability between sGC1, sGC2 and rGC1, rGC2 under the effects of Oxaliplatin, respectively. The Student's *t* test was used for statistical analysis. Error bars indicate mean ± standard deviation. OXA, Oxaliplatin. OLP, Olaparib. CON, control group. PCDK1, CDK1 phosphorylation antibody. PBRCA1, BRCA1 phosphorylation antibody. AGSRE, AGS Oxaliplatin resistance. SNU719RE, SNU719 Oxaliplatin resistance. MKN74RE, MKN74 Oxaliplatin resistance. All experiments had repeated three times.

Supplementary Figure 2 | PARP1 expression is an important mediating factor for Oxaliplatin resistance. **(A,B)** The effects of Olaparib + Oxaliplatin and Oxaliplatin on colony formation of overexpressed and normally expressed PARP1 in SNU719, MKN74, and AGS stable strains. Colonies are stained with crystal violet. **(C,D)** After treatment with Olaparib + Oxaliplatin, the BALB/C NUDE mice expression was enriched in oxidative phosphorylation, PPAR Signaling pathway. **(E–H)** After treatment with Oxaliplatin, the BALB/C NUDE mice expression was enriched in JAK STAT signaling pathway, MAPK signaling pathway, NOTCH signaling pathway, and WNT Signaling pathway. Student's *t* test was used for statistical analysis. Error bars indicate mean ± standard deviation. AGSRE, AGS Oxaliplatin resistance. SNU719RE, SNU719 Oxaliplatin resistance. MKN74RE, MKN74 Oxaliplatin resistance. ***<0.001. All experiments had repeated three times.

Supplementary Figure 3 | PARP1 was significantly expression than XRCC1 in oxaliplatin resistant GC. **(A)** Verification by WB on the PARP1 knock-down and overexpression. **(B)** Volcano plot for the statistical significance (*Y*-axis, −log2 transformation) versus the fold change of gene expression (*X*-axis, log2 transformation) between sGC1 and sGC2, and rGC1 and rGC2 populations determined by RNA-seq ($n = 3$). FC, fold change; padj, false-discovery-rate adjusted *p* value. **(C)** RT-qPCR was used to compare PARP1 mRNA expression in SNU719, MKN74, and AGS resistant strains and wild-type cell lines. Student's *t* test was used for statistical analysis. Error bars indicate mean ± standard deviation. OXA, Oxaliplatin. OLP, Olaparib. CON, control group. AGSRE, AGS Oxaliplatin resistance. SNU719RE, SNU719 Oxaliplatin resistance. MKN74RE, MKN74 Oxaliplatin resistance. ns, No significant. All experiments had repeated three times.

Supplementary Figure 4 | CDK1 is an important target of Oxaliplatin combined with PARP1 inhibitor that can effectively kill Oxaliplatin resistance cells. **(A)** The

clustering was based on the expression data in TCGA. The top 5000 genes with the highest SD values were used for the analysis by WGCNA. The color intensity was proportional to expression status (PARP1 low and PARP1 high). **(B)** Analysis of the scale-free fit index for various soft-thresholding powers (β). Analysis of the mean connectivity for various soft-thresholding powers. In all, 3 was the most fit power value. **(C)** The cluster dendrogram of module eigengenes. **(D)** The cluster dendrogram of genes in TCGA. Each branch in the figure represents one gene, and every color below represents one co-expression module. **(E)** Heatmap of the correlation between module eigengenes and the expression status of PARP1. The dark orange module was the most positively correlated with PARP1 high expression. **(F)** Hierarchical clustering of module hub genes that summarizes the modules yielded in the clustering analysis. **(G)** Heatmap plot of the adjacencies in the hub gene network. Scatter plot of module eigengenes in the Brown module. **(H)** STING database protein interaction network diagram of Brown module. Edges represent protein-protein associations. Cambridge blu, curated databases; Violet, experimentally determined; Green, gene neighborhood; Red, gene fusions; Blue, gene co-occurrence; Reseda, text mining; Black, co-expression; Lilac, protein homology. **(J)** statistical ranking of **(I)** in accordance to the number of interactive network nodes. The abscissa represents the number of nodes. All experiments had repeated three times.

Supplementary Figure 5 | Treatment of Oxaliplatin inhibits HR repair pathways via blocking CDK1-BRCA1 activities in Oxaliplatin resistance gastric cancer **(A)** representative images of immunofluorescent phosporylation staining comparisons of Olaparib + Oxaliplatin, Oxaliplatin, Olaparib, and blank control group and immunofluorescent phosphorylation staining of RAD51, XRCC1 and γH2AX of MKN74, SNU719, AGS resistant strains. The scale represents 2 um. **(B)** Statistical analysis of RAD51 + cells in A. **(C)** Statistical analysis of γH2AX + cells in **(A)**. **(D)** Statistical analysis of XRCC1 + cells in A. The Student's *t* test was used for statistical analysis. Error bars indicate mean ± standard deviation. OXA, Oxaliplatin; OLP, Olaparib; CON, control group; AGSRE, AGS Oxaliplatin resistance; SNU719RE, SNU719 Oxaliplatin resistance; MKN74RE, MKN74 Oxaliplatin resistance. **<0.01, and ***<0.001. All experiments had repeated three times.

REFERENCES

Abraham, R. T. (2001). Cell cycle checkpoint signaling through the ATM and ATR kinases. *Genes Dev.* 15, 2177–2196. doi: 10.1101/gad.914401

Alemasova, E. E., and Lavrik, O. I. (2019). Poly(ADP-ribosyl)ation by PARP1: reaction mechanism and regulatory proteins. *Nucleic Acids Res.* 47, 3811–3827. doi: 10.1093/nar/gkz120

Cai, D., Latham, V. M. Jr., Zhang, X., and Shapiro, G. I. (2006). Combined depletion of cell cycle and transcriptional cyclin-dependent kinase activities induces apoptosis in cancer cells. *Cancer Res.* 66, 9270–9280. doi: 10.1158/0008-5472.can-06-1758

D'Andrea, A. D. (2018). Mechanisms of PARP inhibitor sensitivity and resistance. *DNA Repair* 71, 172–176. doi: 10.1016/j.dnarep.2018.08.021

Eisenhauer, E. A., Therasse, P., Bogaerts, J., Schwartz, L. H., Sargent, D., Ford, R., et al. (2009). New response evaluation criteria in solid tumours: revised RECIST guideline (version 1.1). *Eur. J. Cancer* 45, 228–247. doi: 10.1016/j.ejca.2008.10.026

Faivre, S., Chan, D., Salinas, R., Woynarowska, B., and Woynarowski, J. M. (2003). DNA strand breaks and apoptosis induced by oxaliplatin in cancer cells. *Biochem. Pharmacol.* 66, 225–237. doi: 10.1016/s0006-2952(03)00260-0

Foray, N., Marot, D., Gabriel, A., Randrianarison, V., Carr, A. M., Perricaudet, M., et al. (2003). A subset of ATM- and ATR-dependent phosphorylation events requires the BRCA1 protein. *Embo J.* 22, 2860–2871. doi: 10.1093/emboj/cdg274

Horton, J. K., Srivastava, D. K., Zmudzka, B. Z., and Wilson, S. H. (1995). Strategic down-regulation of DNA polymerase beta by antisense RNA sensitizes mammalian cells to specific DNA damaging agents. *Nucleic Acids Res.* 23, 3810–3815. doi: 10.1093/nar/23.19.3810

Huch, M., Gehart, H., Van Boxtel, R., Hamer, K., Blokzijl, F., Verstegen, M. M., et al. (2015). Long-term culture of genome-stable bipotent stem cells from adult human liver. *Cell* 160, 299–312. doi: 10.1016/j.cell.2014.11.050

Johnson, N., Cai, D., Kennedy, R. D., Pathania, S., Arora, M., Li, Y. C., et al. (2009). Cdk1 participates in BRCA1-dependent S phase checkpoint control in response to DNA damage. *Mol. Cell* 35, 327–339. doi: 10.1016/j.molcel.2009.06.036

Johnson, N., Li, Y. C., Walton, Z. E., Cheng, K. A., Li, D., Rodig, S. J., et al. (2011). Compromised CDK1 activity sensitizes BRCA-proficient cancers to PARP inhibition. *Nat. Med.* 17, 875–882. doi: 10.1038/nm.2377

Li, B., and Dewey, C. N. (2011). RSEM: accurate transcript quantification from RNA-Seq data with or without a reference genome. *BMC Bioinformatics* 12:323. doi: 10.1186/1471-2105-12-323

Liu, Q., Zeng, X., Wang, W., Huang, R. L., Huang, Y. J., Liu, S., et al. (2019). Awareness of risk factors and warning symptoms and attitude towards gastric cancer screening among the general public in China: a cross-sectional study. *BMJ Open* 9:e029638. doi: 10.1136/bmjopen-2019-029638

Liu, X., and Meltzer, S. J. (2017). Gastric cancer in the era of precision medicine. *Cell Mol. Gastroenterol. Hepatol.* 3, 348–358.

Lo, Y. H., Kolahi, K. S., Du, Y., Chang, C. Y., Krokhotin, A., Nair, A., et al. (2021). A CRISPR/Cas9-engineered ARID1A-deficient human gastric cancer organoid model reveals essential and nonessential modes of oncogenic transformation. *Cancer Discov.* 11, 1562–1581. doi: 10.1158/2159-8290.cd-20-1109

Luo, Y., Coskun, V., Liang, A., Yu, J., Cheng, L., Ge, W., et al. (2015). Single-cell transcriptome analyses reveal signals to activate dormant neural stem cells. *Cell* 161, 1175–1186. doi: 10.1016/j.cell.2015.04.001

Mateo, J., Lord, C. J., Serra, V., Tutt, A., Balmaña, J., Castroviejo-Bermejo, M., et al. (2019). A decade of clinical development of PARP inhibitors in perspective. *Ann. Oncol.* 30, 1437–1447. doi: 10.1093/annonc/mdz192

Myers, J. S., Zhao, R., Xu, X., Ham, A. J., and Cortez, D. (2007). Cyclin-dependent kinase 2 dependent phosphorylation of ATRIP regulates the G2-M checkpoint response to DNA damage. *Cancer Res.* 67, 6685–6690. doi: 10.1158/0008-5472.can-07-0495

Narod, S. A., and Foulkes, W. D. (2004). BRCA1 and BRCA2: 1994 and beyond. *Nat. Rev. Cancer* 4, 665–676. doi: 10.1038/nrc1431

Preston, T. J., Henderson, J. T., Mccallum, G. P., and Wells, P. G. (2009). Base excision repair of reactive oxygen species-initiated 7,8-dihydro-8-oxo-2'-deoxyguanosine inhibits the cytotoxicity of platinum anticancer drugs. *Mol. Cancer Ther.* 8, 2015–2026. doi: 10.1158/1535-7163.mct-08-0929

Remy, C., Borniard, J., and Perez, J. (2020). Analysis of unscheduled telephone calls received by a specialized cancer pain nurse. *Pain Manag. Nurs.* 21, 255–258. doi: 10.1016/j.pmn.2019.07.009

Reynolds, P., Cooper, S., Lomax, M., and O'neill, P. (2015). Disruption of PARP1 function inhibits base excision repair of a sub-set of DNA lesions. *Nucleic Acids Res.* 43, 4028–4038. doi: 10.1093/nar/gkv250

Ronson, G. E., Piberger, A. L., Higgs, M. R., Olsen, A. L., Stewart, G. S., Mchugh, P. J., et al. (2018). PARP1 and PARP2 stabilise replication forks at base excision repair intermediates through Fbh1-dependent Rad51 regulation. *Nat. Commun.* 9:746.

Ruiz, E. J., Diefenbacher, M. E., Nelson, J. K., Sancho, R., Pucci, F., Chakraborty, A., et al. (2019). LUBAC determines chemotherapy resistance in squamous cell lung cancer. *J. Exp. Med.* 216, 450–465. doi: 10.1084/jem.20180742

Sawant, A., Floyd, A. M., Dangeti, M., Lei, W., Sobol, R. W., and Patrick, S. M. (2017). Differential role of base excision repair proteins in mediating cisplatin cytotoxicity. *DNA Repair* 51, 46–59. doi: 10.1016/j.dnarep.2017.01.002

Seidlitz, T., Koo, B. K., and Stange, D. E. (2021). Gastric organoids-an in vitro model system for the study of gastric development and road to personalized medicine. *Cell Death Differ.* 28, 68–83. doi: 10.1038/s41418-020-00662-2

Seidlitz, T., Merker, S. R., Rothe, A., Zakrzewski, F., Von Neubeck, C., Grützmann, K., et al. (2019). Human gastric cancer modelling using organoids. *Gut* 68, 207–217.

Seol, J. H., Shim, E. Y., and Lee, S. E. (2018). Microhomology-mediated end joining: good, bad and ugly. *Mutat. Res.* 809, 81–87. doi: 10.1016/j.mrfmmm.2017.07.002

Sfeir, A., and Symington, L. S. (2015). Microhomology-mediated end joining: a back-up survival mechanism or dedicated pathway? *Trends Biochem. Sci.* 40, 701–714. doi: 10.1016/j.tibs.2015.08.006

Sharma, R. A., and Dianov, G. L. (2007). Targeting base excision repair to improve cancer therapies. *Mol. Aspects Med.* 28, 345–374. doi: 10.1016/j.mam.2007.06.002

Slyskova, J., Sabatella, M., Ribeiro-Silva, C., Stok, C., Theil, A. F., Vermeulen, W., et al. (2018). Base and nucleotide excision repair facilitate resolution of platinum drugs-induced transcription blockage. *Nucleic Acids Res.* 46, 9537–9549. doi: 10.1093/nar/gky764

Snel, B., Lehmann, G., Bork, P., and Huynen, M. A. (2000). STRING: a web-server to retrieve and display the repeatedly occurring neighbourhood of a gene. *Nucleic Acids Res.* 28, 3442–3444. doi: 10.1093/nar/28.18.3442

Wang, K., Yuen, S. T., Xu, J., Lee, S. P., Yan, H. H., Shi, S. T., et al. (2014). Whole-genome sequencing and comprehensive molecular profiling identify new driver mutations in gastric cancer. *Nat. Genet.* 46, 573–582. doi: 10.1038/ng.2983

Wang, Q., Xiong, J., Qiu, D., Zhao, X., Yan, D., Xu, W., et al. (2017). Inhibition of PARP1 activity enhances chemotherapeutic efficiency in cisplatin-resistant gastric cancer cells. *Int. J. Biochem. Cell Biol.* 92, 164–172. doi: 10.1016/j.biocel.2017.08.001

Wang, S., Han, L., Han, J., Li, P., Ding, Q., Zhang, Q. J., et al. (2019). Uncoupling of PARP1 trapping and inhibition using selective PARP1 degradation. *Nat. Chem. Biol.* 15, 1223–1231. doi: 10.1038/s41589-019-0379-2

Wei, L., Sun, J., Zhang, N., Zheng, Y., Wang, X., Lv, L., et al. (2020). Noncoding RNAs in gastric cancer: implications for drug resistance. *Mol. Cancer* 19:62.

Yadav, N., Kumar, S., Marlowe, T., Chaudhary, A. K., Kumar, R., Wang, J., et al. (2015). Oxidative phosphorylation-dependent regulation of cancer cell apoptosis in response to anticancer agents. *Cell Death Dis.* 6:e1969. doi: 10.1038/cddis.2015.305

Yan, H. H. N., Siu, H. C., Law, S., Ho, S. L., Yue, S. S. K., Tsui, W. Y., et al. (2018). A comprehensive human gastric cancer organoid biobank captures tumor subtype heterogeneity and enables therapeutic screening. *Cell Stem Cell* 23, 882–897.e11.

Yang, J., Parsons, J., Nicolay, N. H., Caporali, S., Harrington, C. F., Singh, R., et al. (2010). Cells deficient in the base excision repair protein, DNA polymerase beta, are hypersensitive to oxaliplatin chemotherapy. *Oncogene* 29, 463–468. doi: 10.1038/onc.2009.327

Yang, W. L., and Frucht, H. (2001). Activation of the PPAR pathway induces apoptosis and COX-2 inhibition in HT-29 human colon cancer cells. *Carcinogenesis* 22, 1379–1383. doi: 10.1093/carcin/22.9.1379

Yuan, L., Xu, Z. Y., Ruan, S. M., Mo, S., Qin, J. J., and Cheng, X. D. (2020). Long non-coding RNAs towards precision medicine in gastric cancer: early diagnosis, treatment, and drug resistance. *Mol. Cancer* 19:96.

Conflict of Interest: The authors declare that the research was conducted in the absence of any commercial or financial relationships that could be construed as a potential conflict of interest.

Publisher's Note: All claims expressed in this article are solely those of the authors and do not necessarily represent those of their affiliated organizations, or those of the publisher, the editors and the reviewers. Any product that may be evaluated in this article, or claim that may be made by its manufacturer, is not guaranteed or endorsed by the publisher.

Copyright © 2021 Li, Wang, Lan, Wu, Evans, Ruiz, Yan, Zhou, Oliveira, Reis, Hu, Chen, Behrens, He and Zhang. This is an open-access article distributed under the terms of the Creative Commons Attribution License (CC BY). The use, distribution or reproduction in other forums is permitted, provided the original author(s) and the copyright owner(s) are credited and that the original publication in this journal is cited, in accordance with accepted academic practice. No use, distribution or reproduction is permitted which does not comply with these terms.

frontiers in Oncology

OPINION
published: 07 September 2021
doi: 10.3389/fonc.2021.693076

Kill and Clearance in HCC: An Approach Based on NK Cells and Macrophages

Maryam Mehrabi[1]*, *Fatemeh Amini*[2] *and Shima Mehrabi*[3]

[1] Independent Researcher, Newcastle, United Kingdom, [2] Vitaccess, Oxford, United Kingdom, [3] Internal Medicine, Iran University of Medical Sciences, Tehran, Iran

Keywords: NK, macrophage, monocyte, myeloid-derived suppressor cell, hypoxia, phagocytosis, liver homeostasis, hepatocellular carcinoma

INTRODUCTION

In our previous perspective, we investigated the role of hypoxic lesions in the development of necrotic zone in solid tumors (1). We suggested the increased infiltration of macrophages/monocytes to the pre-necrotic zone and under the influence of chemoattractants (VEGF, CCL2, and CCL5), danger signals, and a trail of necrotic debris as a mechanism to maximize their opportunity to clear the lesion. They continuously sample and mediates recognition of damage-associated molecular patterns (DAMPs), including heat shock proteins, cytokines, DNA, RNA, metabolic ATP, HMGB1, histones, altered carbohydrate, and negatively exposed phosphatidylserine (PS) on the surface of necrotic corpses or apoptotic cells. We suggested gradual alteration of gene expression in macrophages eventually turns off their phagocytic machinery leaving uncleared cell corpses as a rich source of building blocks for cancer stem cells. Even subtle differences in the internalized ligands could have far-reaching consequences on cytokine production and antigen presentation to NK cells.

Here, we propose a synergistic act of kill and clearance by NK cells and macrophages as a therapeutic strategy in HCC. We have provided a comprehensive mechanism underlying human NK cell and macrophage dysfunction in HCC, investigated the crosstalk between NK cells and a group of myeloid-derived suppressor cells (MDSCs) with a typical monocytic phenotype (CD14+ HLA-DR-/low), and the immunosuppressive role of hypoxia in HCC. We have also outlined the possible future research directions to target the crosstalk between NK cells and macrophage/MDSC to enhance kill and clearance by NK cells and macrophages in HCC and other solid tumors.

OPEN ACCESS

Edited by:
Simona Kranjc Brezar, Institute of Oncology Ljubljana, Slovenia

Reviewed by:
Denisa Baci, University of Milano-Bicocca, Italy

***Correspondence:**
Maryam Mehrabi
maryam.a.mehrabi@gmail.com

Specialty section:
This article was submitted to Molecular and Cellular Oncology, a section of the journal Frontiers in Oncology

Received: *09 April 2021*
Accepted: *23 August 2021*
Published: *07 September 2021*

Citation:
Mehrabi M, Amini F and Mehrabi S (2021) Kill and Clearance in HCC: An Approach Based on NK Cells and Macrophages. Front. Oncol. 11:693076. doi: 10.3389/fonc.2021.693076

Abbreviations: BM, Bone Marrow; DAMPs, Damage-Associated Molecular Patterns; EMT, Epithelial-Mesenchymal Transition; GI tract, Gastrointestinal tract; HCC, Hepatocellular Carcinoma; HIF, Hypoxia-inducible Factor; HSCs, Hematopoietic Stem Cells; KC, Kupffer Cell; MDSC, Myeloid Derived Suppressor Cell (only monocytic); MHC-I, Histocompatibility Complex Class I; NK cell, Natural Killer cell; SDF-1, Stromal Cell-derived Factor-1; STAT, Signal Transducers and Activators of Transcription, TAM, Tumor Associated Macrophage; TCGA, The Cancer Genome Atlas; TME, Tumor Microenvironment; H&E, Hematoxylin-Eosin.

IMMUNOLOGY OF LIVER DURING HOMEOSTASIS AND HCC

The adult human liver receives a mixture of 75% deoxygenated blood from the portal vein and 25% oxygen-rich blood from the aorta. The former contains digested nutrients from the entire gastrointestinal (GI) tract, the spleen, and the pancreas. During homeostasis, the liver is constantly bombarded with gut-derived products in a strictly regulated microenvironment, which removes dangerous stimuli and resolves inflammation. This organ maintains a balance between pro-inflammatory (e.g. TNF-α, IL-1β, IL-2, IL-12, IL-15, and IFNγ) and anti-inflammatory (e.g. IL-10, IL-13, and TGFβ) cytokines in the absence of pathological inflammation or infection (**Figure 1**) (2). Production of these cytokines through normal physiological processes is controlled by a network of hepatic lymphoid, myeloid, and non-hematopoietic cell populations (3). With enormous regeneration capacity, differentiated hepatocytes can enter the cell cycle and repair the injured tissue after acute damage (**Figure 1**) (4, 5). Failure to clear dangerous stimuli due to any dysregulated inflammation could drive chronic infection and pathology (**Figure 3**).

Tumorigenesis is generally believed to be the consequence of accumulated mutations. Genetic changes in mature hepatocytes are a common condition caused by multifactorial processes such as metabolic liver disease, and alcoholic or non-alcoholic liver disease (6, 7). Despite variable causes, primary liver cancers arise almost exclusively in the setting of chronic inflammation, in which stress stimuli within hepatocytes initiate the death of liver cells, the production of DAMPs, and the influx of activated immune cells (8, 9). The sequence of chronic necroinflammation and release of DAMPs during tumor growth results in the upregulation of a number of immune regulatory pathways aimed at compensatory liver regeneration. Meanwhile, the cycle of orchestrated events including expansion and accumulation of tumor-promoting immunoregulatory cell populations like myeloid-derived suppressor cells (MDSCs), epigenetic and metabolic changes resulting in immune cell tolerance, induction of negative regulators of pro-inflammatory signaling pathways, and development of T-cell exhaustion results into the induction of liver fibrosis and/or subsequent cirrhosis, which often precedes hepatocarcinogenesis.

Recent Genomic profiling has provided an overview of significant drivers of HCC (10–12) with about 40 somatic alterations in coding regions, including the genes encoding the tumor suppressor p53 and cell-cycle regulators, as well as molecules involved in WNT-β-catenin signaling, epigenetic modification, oxidative-stress pathways, the RAS–RAF–MAPK, and PI(3)K–AKT–mTOR pathways (13). The frequency of these mutations depends on underlying risk factors. Despite all the development in the molecular characterization of HCC, little progress was achieved in stratifying patients and developing predictive biomarkers for targeted therapies.

In search of new therapeutic strategies, an extensive immunogenomic analysis of diverse cancer types are published

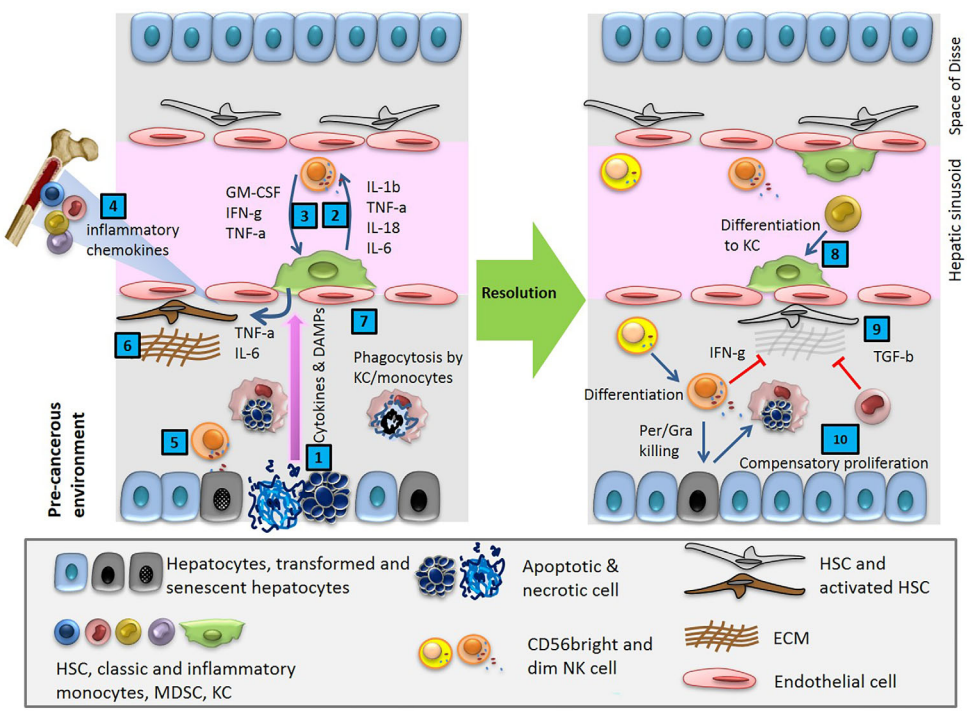


FIGURE 1 | Cytokines and DAMPs released in pre-cancerous environment activate innate immune cells, resident macrophages (KC) and NK cells, and induces HSCs trafficking from BM. After a cycle of cytotoxic NK cell mediated cell death and phagocytosis of debris by macrophages, the tissue reaches homeostasis.

in "The immune landscape of cancer". Using TCGA molecular platforms and Hematoxylin-Eosin (H&E) staining data analysis of 10,000 clinical samples including HCC, the research predicts intrinsic and extrinsic regulators of tumors with a critical role in the leukocyte population and infiltration in the TME (14). The collective intrinsic data suggest the influence of seven immune-related transcription factors, including interferon and STAT-family. The extracellular networks imply direct cell-to-cell contact between immune cells or communication *via* soluble molecules. Proinflammatory cytokines, such as IL-6 and TNF, which activate the transcription factors STAT3 and nuclear factor-κB (NF-κB), respectively, have been reported to be important for the development and progression of HCC. Hepatocyte-specific inhibition of STAT3 has been shown to inhibit tumor growth in a mouse model of chemically induced HCC (15). The role of key receptors and ligands, such as transforming growth factor-β1 (TGFβ1), CXCL10, CXCR3, and receptor-ligand pairs, such as the CCL2-CCR2 axis, is highlighted in the cellular communication network. An important key point manifested in the immune subtypes is that the immune system context can dictate the immune cell interactions. Interestingly, a dramatic increase in the number of macrophages and the rarity of NK cells is an obvious trend in all the HCC studies.

MACROPHAGES AND NK CELLS IN HEALTHY LIVER

The liver is a tightly controlled immunological network with one of the largest populations of innate immune cells. Additionally, intrahepatic lymphocytes are often present in the sinusoidal lumen. Deregulation of this network is a hallmark of chronic liver disease and HCC. As key components of the innate immune system, resident macrophages known as Kupffer cells (KC) and NK cells play vital roles in maintaining organ homeostasis and rapid response to potentially dangerous stimuli. They continuously survey their microenvironment for danger and are ready to respond by entering an activated state characterized by cytokine secretion, phagocytosis, and, on occasions, direct cytotoxicity (**Figures 1** and **3**) (16).

Resident Macrophages (Kupffer Cells)

The liver sinusoid has a lining of discontinuous endothelium and KCs, allowing for the removal and degradation of immunogenic molecules in the liver (17). Resident macrophages, KCs, constitute a third of the liver non-parenchymal cells and located within the hepatic sinusoids, in close contact with both the sinusoidal endothelium and hepatocytes. Having the largest population of resident macrophages, the liver has 80–90% of total resident macrophages present in the body. They are capable of responding to cytokines, Toll-like receptor (TLR), RIG-like receptor, and NOD-like receptor signaling, and express a variety of receptors, including the scavenger receptor cysteine-rich (SRCR) superfamily members (18). KCs are equipped with a massive array of PPRs, complement receptors, and Fc receptors, through which they respond with increased phagocytic activity and production of inflammatory cytokines. The liver microenvironment alters the physiologic function, population density, and cytologic characteristics of KCs. For example, periportal KCs at the first point of contact for incoming blood have a greater phagocytic capacity than smaller KCs from midzonal and perivenous regions (19, 20). KCs play a central role in the liver systemic immune responses, have essential roles in immune regulation, tissue repair, and liver regeneration. In liver disease, they have a phagocytic function and release cytokines such as TNFα and IL-6, both important mediators in hepatic inflammation and fibrogenesis. There is cumulative evidence from murine transplantation experiments that KCs can derive from the bone marrow (BM) monocytes (21–24). Monocytes in tissue also participate in tissue healing, clearance of pathogens and dead cells, and initiation of adaptive immunity.

Hepatic NK cells

Human NK cells are derived from BM and phenotypically defined as $CD3^{-}CD56^{+}$ large granular lymphocyte. They are part of the innate immune system and a key player in cancer immune surveillance. NK cells form up to 50% of the intrahepatic lymphocytes, approximately 5 times higher than the proportion in peripheral blood. Hepatic NK cells are constitutively activated, displaying significantly higher cytotoxic activity against tumor cells compared with circulating NK cells (3, 25). Two subsets of NK lymphocytes, CD56bright and CD56dim, with different functional outcomes contribute to the liver NK cells. Cytolytic activity is mostly confined to the CD56dim subset, whereas cytokine production is generally assigned to CD56bright cells. Hepatic NK cells can control the progression of HCC *via* two mechanisms, killing tumor cells and targeting liver fibrosis.

NK cells express a wide array of germline-encoded inhibitory and activating receptors in a stochastic pattern that bind and detect various tumor ligands, contrary to T and B cells which require somatic gene rearrangements to generate receptor diversity and specificity. They are involved in nonspecific, intrahepatic cell killing due to downregulation of the major histocompatibility complex class I (MHC-I) on tumor cells. The MHC-I downregulation leads to loss of the NK cell inhibitory signal and activation of killing pathways (26). Recognition of DNA damage in cancer cells by the activatory receptor, NKG2D, is another detection pathway (27), while some others remain unknown. NK cells exert antitumor effects by exocytosis of perforin/granzyme-containing granules, induction of apoptosis in target cells, and production of various cytokines that augment the functions of other immune cells (28, 29), and can change the course of tumor development (30–32).

Hepatic NK cells can also control the progression of HCC *via* anti-fibrotic properties. Liver fibrosis is characterized by the differentiation of hepatic stellate cells to myofibroblast and excessive deposition of extracellular matrix proteins in the liver. It is a common scarring response to various forms of chronic liver disease and is associated with excess hepatocellular death (33). The anti-fibrotic property of NK cells through targeting activated hepatic stellate cells is a major pathway they

provide immunosurveillance to HCC (34–37). However, this property is often suppressed in human HCC. There are several possible explanations for this, including STAT3-mediated upregulation of immunosuppressive cytokines IL-10 and TGFβ (38), phagocytosis of NK cells by hepatic stellate cells (39), NK cell exhaustion, and the dysregulation of NK cell-activating ligands (40).

HCC is associated with a dramatic decrease in the frequency of circulating and intrahepatic NK cells as well as their impairment in cytotoxicity and cytokine production (41, 42). This is mainly reflected in the reduction of CD56dim NK cell subset rather than CD56bright and tends to decrease further in advanced-stage HCC patients (43, 44). It has been shown that low intratumoral NK cells among tumor-infiltrating lymphocytes (TILs) have shorter disease-free survival (DFS) and overall survival (OS) and restoration of NK cell activity after curative surgery in clinical trials is associated with recurrence-free survival (45).

TRAFFICKING AND ACCUMULATION OF MONOCYTIC CELLS IN HCC

Monocyte Trafficking in HCC

Molecular alterations of hepatic gene expression mediate microenvironment changes that favour tumour cell colonization. The tumour-derived secreted factors in an inflammatory microenvironment induce rapid infiltration of BM progenitor cells to the liver and dictate their differentiation programs. For example, stress stimuli in TME upregulate the gene expression of hepatic SDF-1 localised to the biliary epithelium. SDF-1 is a potent HSC chemoattractant, and plays a key role in their migration from BM to circulation and eventually homing to the site of insult in a concentration-dependent manner (46). Gene expression of SDF-1 is directly regulated by the transcription factor HIF-1, resulting in selective surface expression of SDF-1 protein in direct proportion to reduced oxygen tension. As a result, migration and homing of circulating CXCR4-positive progenitor cells increase to the hypoxic area of tissue. It has been shown that blockade of SDF-1 or CXCR4 on circulating cells prevents progenitor cell recruitment to the sites of inflammation (47). The recruited BM cells play an important role in the generation of fibrosis and tumor progression. In a complex coordinated process, these cells together with liver cell compartments, express a specific set of growth factors and cytokines, which allows the immune escape of tumor cells in an immune-suppressive environment (**Figure 2A**).

During homeostasis, monocyte trafficking from BM is under the control of chemoattractants, such as IL-3, stem cell factor (SCF), and macrophage colony-stimulating factor (M-CSF). Monocytes stay in circulation for about 3 days; then randomly leave to tissues, where they play a key role in clearance and phagocytosis. There is also a continuous loss of Kupffer cells in the healthy liver, which is balanced by the formation of new macrophages from circulating monocytes and to a small extent from the self-renewal of existing KCs (**Figure 1**). The network of cells concerned with macrophage production in the liver is part of the mononuclear phagocyte system.

Emergency hematopoiesis during liver disease is characterized by a shift in cell fate resulting in higher production of particular immune cells at the expense of others, as such increased production of monocytes compared to lymphocytes (48, 49). The half-life of BM-derived monocytes in this condition temporarily reduces to 12 h. They contribute to immune defence by direct recruitment to the injured tissue and subsequent entry into lymph nodes *via* afferent lymphatic channels (50, 51). This process is accompanied by long-lasting effects and results in an altered activation state and increased number of monocytes even weeks after inflammation, a phenomenon called "trained immunity" (52). It has been proposed that cytokines, like IFNγ and IL-1β, secreted in BM by immune or non-immune cells are crucial for these long-lasting training effects (53). There is no doubt that these cells are "trained" through epigenetic changes since HSCs isolated from animals injected with β-glucan preserved their capacity to generate more myeloid cells 12 weeks post-transfer into untrained animals (54).

Understanding the relationship between progenitor cell products derived from BM and monocyte-to-macrophages differentiation is of great interest (55). Recent studies in human and transgenic mouse models suggest that different subsets of macrophages in tissue originate from a distinct population of monocytes in peripheral blood (21–24). The main monocyte-associated antigen marker is CD14, the LPS receptor, being the most specific (56). During maturation, human monocytes gain a progressive increase in CD14, CD11b, CD13, CD36, and CD45 expression, with a mild decrease in HLA-DR and CD15. Mature monocytes show expression of bright CD14, CD33, CD36, CD38, CD64, variably bright CD13, and low CD15 (57, 58). Another marker antigen, CD68, is broadly expressed in all mononuclear phagocytes and related to the lysosome-associated membrane protein (LAMP) family. However, its function is still obscure. Apart from marker antigens, levels of chemokine receptors for fractalkine (CX3CR1) and CCR2 (MCP1) seem to distinguish monocyte subsets that give rise to inflammatory and resident macrophages. The majority of the cells migrate to the site of inflammation under the influence of Soluble mediators including vascular endothelial growth factor (VEGF), platelet-derived growth factor (PDGF), transformation growth factor-β (TGFβ), chemokine (C-C motif) ligand (CCL2), and macrophage colony-stimulating factor (M-CSF). The expression of glypican-3 (GPC-3) on the surface of HCC cells may also promote monocyte recruitment (59). The rationale is that distinct subsets of monocytes are recruited at different stages of liver injury and tumor progression, with the first wave of monocytes facilitating the removal of dead hepatocytes and debris and the later phase promoting the resolution of inflammation and tissue repair (50, 60).

In the context of HCC metastasis, increased level of M-CSF and extensive infiltration of macrophages have been associated with intrahepatic metastasis and recurrence (61). Moreover, pharmacological approaches to directly target TAMs,

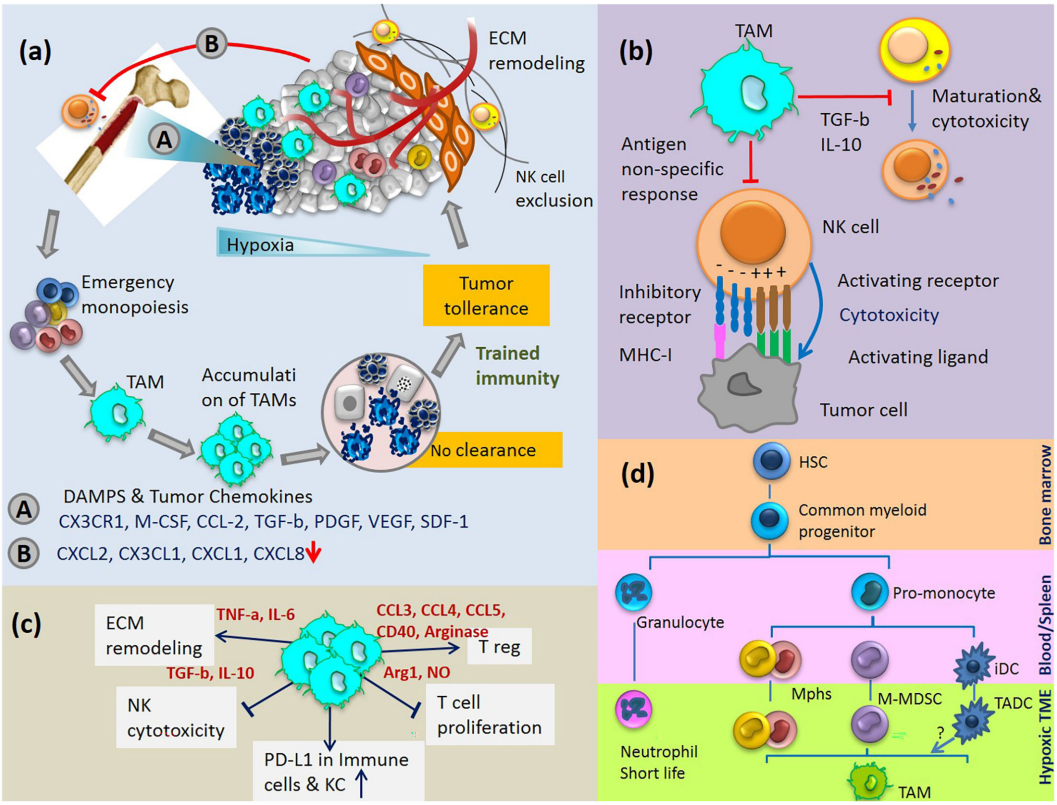


FIGURE 2 | **(A)** Cycle of emergency monopoiesis, accumulation of immature suppressive macrophages in TME, inhibition of CD56dim NK cell egress from BM and their exclusion from tumor are part of the synchronize program which causes immune tolerance to HCC. **(B)** TAM inhibits NK cell cytotoxicity and maturation. **(C)** Immunosuppressive activities of TAMs. **(D)** TAMs differentiation pathway: myeloid cells originate from HSCs in the BM and differentiate into various myeloid cell lineages in blood, spleen and tumor tissue. Various monocytic cells in TME change to polarized phenotypes between M1-M2. iDC, immature dendritic cells; TADC, tumor-associated dendritic cells.

via knocking out CCL2 or other TAM-specific chemokines, reduced migration and invasion of HCC cell lines (17).

Myeloid-Derived Suppressor Cells in HCC

In patients with HCC, a group of myeloid-derived suppressor cells has been identified based on the expression of CD14 low level of HLA-DR, with a typical monocytic phenotype. The number and percentage of these cells increases in blood and the site of insult as time passing after tumor inoculation (62). They can induce liver damage and hepatocyte apoptosis. These cells also contribute significantly to the immunosuppressive microenvironment of tumors using multiple mechanisms, including suppression of T cell proliferation, generation of induced regulatory T cells, and upregulation of inhibitory surface protein, PD-L1, in KC. They repress the antitumor activity of NK cells by inhibiting perforin-dependent cytotoxicity.

It appears that the migration of MDSC to the site of the tumor is governed by the same mechanisms as monocytes and neutrophils. Currently, there is no clear evidence that MDSCs may have a unique pattern of migration distinct from their control counterparts (63). However, this issue needs to be formally investigated.

MDSCs are present in the healthy liver and expand during chronic liver disease (64). The expansion of MDSCs is well known for acute bacterial and viral infection as well as other stress stimuli. However, they quickly differentiate to mature macrophages, neutrophils, or DCs, rather than accumulating in the site of insult. This phenomenon is only common in cancer where MDSCs maturation is affected by multiple unknown factors produced by tumor and tumor stroma. The extended stimulation of MDSCs by various growth factors and cytokines in TME blocks their terminal differentiation and they expand variably to immature phenotypes of TAMs consistent with tumor heterogeneity (**Figures 2A, D**) (65–67).

TRAFFICKING AND DIFFERENTIATION OF NK CELLS IN HCC

NK Cell Trafficking in HCC

HCC is associated with a dramatic decrease in the number of NK cells and impairment in their cytotoxicity. This is partly dictated by the chemokine milieu in TME, which preferably attracts

CD56bright subset of NK cells rather than CD56dim. Moreover, reduced expression of CXCL2, CX3CL1, CXCL1, and CXCL8 results in a reduced number of CD56dim subsets in TME (68). Another important driving factor for these changes is TGFβ1 in TME. TGFβ1-mediated increase of the miR-23a-27a-24-2 cluster in NK cells induces downregulation of the surface expression of CX_3CR1 (69). CX3CR1 is a receptor to CX3CL1 (fractalkine) and one of the main regulators of NK cell egress from BM and extravasation to the site of tissue. This ligand is selectively expressed by CD56dim NK cells (70). Moreover, the miR-23a-27a-24-2 cluster hampers NK cell cytotoxicity through downregulation of perforin/granzyme B expression. Interestingly, TGFβ1 is also responsible for upregulation of the mentioned microRNA axis in hepatocellular carcinoma cells (71), as well as in CD8 T cells. Given that this is not limited to HCC and has been reported in several tumors, makes the miR-23a-27a-24-2 axis a potential target for the treatment of HCC (72).

NK Cell Differentiation in HCC

Besides receiving myeloid and lymphoid cells from BM, the adult human liver contains populations of HSCs, which form colonies upon *in vitro* culture. These cells may contribute to the local HSC differentiation under stress (73, 74). Lymphocytes extracted from the adult human liver contain a high level of recombinase-activated genes 1 and 2 (RAG1 and RAG2). These enzymes are involved in lymphocyte gene rearrangement and recombination, suggesting lymphocyte differentiation can occur in the adult liver (75). Murine models of liver transplant also well describe this phenomenon (19, 76), and c-kit+ stem cells in adult mice liver have the potential to reconstitute multiple lineages and BM stem cells (76–78).

Complete maturation of NK cells in HCC is accompanied by the chemokine receptor repertoire, which would define their re-circulation toward the site of insult. There is a substantial number of NK cells in afferent lymphatic vessels. This is like naïve T cells and supports the hypothesis that tumor lymphatic organ is the site for NK cell maturation, acquisition of cytotoxic properties, and tolerance to self (KIR expression). Alternatively, NK cells could mature to effector NK cells during the local immune response in the malignant tissue (79).

MDSCs and NK cells

In vitro culture of NK cells, isolated from blood or tumor in human HCC, with autologous M-MDSCs ($CD14^+$ $HLA\text{-}DR^{-/low}$) significantly reduces the cytotoxicity and release of IFNγ in NK cells. This phenomenon in the liver, MDSC-mediated NK cell impairment, is a general mechanism in all types of liver disease, but the frequency and accumulation of MDSCs in blood and the site of insult happens only in cancer (80).

Several *in-vitro*, clinical, and preclinical studies have investigated the pathways to reduce MDSC accumulation in TME and the consequences on NK cell cytotoxicity (81). As a valuable source of data, these cases shed light on the future therapeutic strategies for kill and clearance based on NK cells and macrophages. A few notable examples are as follow:

The mechanism of MDSC accumulation in HCC is shown to be activated by direct contact between NKp30, the NK-activating receptor, and unknown ligands/factors on MDSC. This inhibitory process causes a significant reduction in surface expression of NKp30; but is not dependent on NKG2D, CD16, CD94, NKp44, CD69, and NKp80. Also, blocking arginase activity or the production of NO in MDSC does not affect this process (62). Blocking NKP30 interaction with its counterparts on MDSC can inhibit the trafficking of MDSC to the site of tumor, reduce the NO production by MDSC, and results in the enhancement of NK cell cytotoxicity in HCC.

Blocking MDSC chemoattractants, such as CCL2 and CCR5, is another strategy to reduce MDSC migration and homing to TME. As an example, inhibition of CCL2 produced by MDSCs, inhibits JAK/STAT3 pathway and reduces MDSC trafficking to the site of tumor (82), while targeting STAT3 in tumor-bearing mice, exhibits a higher expression of the NK activation markers NKG2D, CD69, Fas ligand (FasL), granzyme B, perforin, and IFNγ, resulting in reduced tumor growth (38, 83).

Another approach, the improvement of MDSC differentiation using vitamin A, D, and E in clinical trials, provided promising results (84). While vitamin D3 decreased the level of immature MDSCs, patients with vitamin D deficiency had lower NK-mediated cytotoxicity (85). Vitamin E treatment also can target this cross-talk, enhances immune responses through decreasing NO production by MDSCs (86), and it is known that MDSCs impair NK cell function *via* the production of NO (87). Thus, inhibition of NO production offers a strategy for targeting MDSC-NK crosstalk and their role in the kill and clearance of solid tumors.

THE ROLE OF HYPOXIA IN TUMOR PROGRESSION

The hypoxic microenvironment in advanced solid tumors is the result of tumor cell outgrowth and imbalanced vascularization (88). This phenomenon plays a critical role in metabolism, phenotypic regulation of the cancer stem cells, and epithelial-mesenchymal transition (EMT) (89). Responses to hypoxia are nearly instant and include short-term changes in the activity of biomolecules to long-term adaptations of global gene-expression programs at the cellular, tissue, and organismal level. Strong nuclear accumulation of the transcription factor HIF-1α at the cellular level modulates the expression of nearly 1000 genes involved in hypoxic adaptations, blood vessel formation, cell differentiation, and inflammation. In HCC, the high expression level of HIF-1α strongly correlates with the adverse prognosis and progressive stages of the tumor. It has been established that HIF proteins activate specific signaling pathways, such as Hedgehog and Wnt/β-catenin, which accelerate the EMT and aggressive capacity of HCC cells (90, 91). Hypoxia also leads to the accumulation of intracellular reactive oxygen species (ROS), which induces GLI1-dependent EMT progress (90, 91). Conversely, developed HIF inhibitors show immense promise for further development of anti-cancer drugs (92).

Hypoxic effects are not limited to hepatocytes and alter immune cell functions by metabolic reprogramming and switching from oxidative phosphorylation to aerobic glycolysis. This metabolic switch in macrophages is essential for the production of proinflammatory mediators like IL1β and causes activation of HIF-1α (93). However, such influence on liver KC function is presently unknown. Cells in healthy liver receive 75% of blood from the portal vein and are in a constant state of low oxygen tension (94). The fact a hypoxic response is not induced during homeostasis suggests that cells in the liver need a higher threshold of oxygen deficiency to respond or they may have a unique pattern of response to hypoxia.

Recent studies from several groups implicate hypoxia as a very important mechanism that converts monocytes, myeloid cells, macrophages, and MDSC into much more potent immune suppressive cells (**Figure 2D**). These cells differentiate into tumor-associated macrophages quite quickly with profound immunosuppressive activity (95).

Macrophage activation *in vitro* is typically classified as two polarized states, M1 and M2 (96). However, TAMs are phenotypically and functionally placed in a spectrum between M1 and M2, rather than fitting one of them (97, 98). Polarization of TAMs reflects differential changes in TME (99). Changes including oxygen tension and production of lactic acid inhibit glycolysis and derive TAMs metabolic changes towards oxidative phosphorylation (OXPHOS) (100). Upregulation of HIF-1 in hypoxic condition induces production of NO by TAMs, which further promote genetic instability and malignant transformation of cancer cells (100). This master transcription factor is regulated by NF-κB and induces profound changes in the expression level of angiogenesis- and metastasis-related genes, such as VEGF, FGF2, MMP7, and MMP9 (101, 102). Consequent to this is the recruitment of more macrophages, and release of pro-inflammatory cytokines, such as TNFα, IL-1β, MIF, CCL3, and COX2, as well as M2 markers, such as IL-10 and arginase 1. The continued upregulation of HIF is part of the regenerative and immunosuppressive response (103).

Hypoxic alterations result in more potent nonspecific immunosuppressive activity of monocyte/macrophages inside the tumor compare to lymphoid organs. HIF-1 directly binds to a transcriptionally active hypoxia response element in the PD-L1 promoter and increases PD-L1 expression in MDSCs, TAMs, DCs, and tumor cells (104). MDSC lacking HIF-1 did not differentiate into TAM within the TME but instead acquired markers of DC (105, 106).

Hypoxia causes an increase in CD45 tyrosine phosphatase activity of monocytes and MDSCs, which results in the selective decrease of STAT3 activity in the hypoxic region of the tumor. The upregulation of CD45 phosphatase activity is mediated by the disruption of CD45 protein dimerization caused by increased sialylation of CD45. Treatment with sialidase abrogates the effect of hypoxia on STAT3 activity and differentiation of MDSCs to TAM (107). Changes in oxidative phosphorylation and glycolysis in tumors also affect the function of MDSCs. It is now established that activation of myeloid cells leads to a switch towards Warburg metabolism (108).

ACCUMULATION OF SENESCENT CELLS AND TAMS IN HCC

Transient senescent hepatocytes, at a state of stable cell-cycle arrest, appear frequently in different types of liver disease and pre-cancerous microenvironments. These cells are subject to immune-mediated clearance, which depends on an intact immune response. By contrast, the accumulation of persistent senescent cells at the site of insult is specific to an already established tumor (**Figure 2A**). Secreting chemokines and cytokines like CCL2, these cells induce trafficking and homing of CCR2+ myeloid cells to the liver. In a pre-cancerous environment, the immature myeloid cells differentiate into macrophages and clear the senescent hepatocytes, a process termed ''senescence surveillance'' (**Figure 1**). However, in an already established tumor, the maturation of myeloid cells to macrophages is blocked by multiple factors and mechanisms, such as tumor-derived growth factors (STAT3, IRF8, C/EBPβ, Notch, adenosine receptors A2B signaling, NLRP3), hypoxia, and negative feedback loops (1, 80). Histopathological samples from HCC patients show a positive correlation between areas of the tumor with senescent hepatocytes (P16+) and myeloid-derived cells (CCR2+). This data suggests the impaired phagocytic machinery of TAMs in HCC which leads to the accumulation of senescent cells. In fact, the secreted factors by senescent hepatocytes suppress liver cancer initiation while accelerating the growth of fully established HCC. To date, many questions remain regarding the specific role of macrophages in the clearance of senescent cells in TME, such as (i) how do macrophages interact with senescent cells, (ii) how does this interaction changes at the different stages of tumor formation and progression, (iii) what is the threshold of senescent cell accumulation and at what threshold of senescent cells accumulation macrophages lose their phagocytic activity? Future comprehensive research is needed to identify other factors linked to senescent accumulation in HCC and their interaction with macrophages.

STRATEGIES TO ENHANCE NK CELLS AND MACROPHAGES KILL AND CLEARANCE IN HCC

To identify the potential targets to unleash the power of NK cells and macrophages in killing the cancer cells and clearing the dead bodies, debris, and senescent cells in TME, it is rational to focus on the key molecular determinants of NK-macrophage crosstalk. In a reciprocal regulation, human macrophages/monocytes produce cytokines which dictate the activation of NK cells, in turn, NK cells orchestrate the macrophage immunity by producing immunomodulatory factors. In the therapeutic strategy based on kill and clearance, the goal is to enhance the phagocytic activity of macrophages and increase number of activated cytotoxic NK cells in HCC (**Figures 2B, C**).

A notable example is the direct interaction between NKP30 and its counterparts on MDSCs, which facilitates the trafficking

and accumulation of MDSCs at the site of tumor (62). Blocking this interaction is a potential candidate to boost NK-macrophage kill and clearance in HCC.

The immune checkpoints between macrophages and NK cells may also provide new opportunities to explore the therapeutic effect of their blocking on kill and clearance in TME. As an example, data from patients with B-cell lymphoma suggest that PD-L1/PD-1 signaling on TAMs impairs their phagocytic capacity through SIRPα, an inhibitory receptor expressed mainly by myeloid cells. The data suggest the interruption of the PD-1/PD-L1 axis is sufficient to activate NK cells and enhance cancer cell lysis through degranulation of CD107a (109).

Another strategy to target the crosstalk between macrophages and NK cells is to cut off TAMs replenishment at the site of tumor. Most of these cells migrate from the bone marrow and recruit into TME under the influence of chemoattractants. Therefore, their trafficking is highly dependent on signaling axis like CCL2/CCR2, CCL5/CCR5, CSF-1/CSF-1R and the Soluble mediators including vascular endothelial growth factor (VEGF), platelet-derived growth factor (PDGF), transformation growth factor-β (TGFβ), and macrophage colony-stimulating factor (M-CSF). The expression of glypican-3 (GPC-3) on the surface of HCC cells may also promote monocyte recruitment (59). An implication of this is the possibility to inhibit the establishment of an immunosuppressive pre-metastatic niche *via* TAM suppression and filtration of NK cells *via* blocking these signaling pathways or reducing the soluble mediators (110, 111). Ongoing clinical trials and preclinical models of solid tumors based on this method reported comprehensive advantageous including the increase of NK cells infiltration and improved efficacy of chemotherapy, radiation therapy, and immunotherapy (112). Also, targeting the CSF1–CSF1R pathway improves the efficacy of immune checkpoint inhibitors for the treatment of HCC (CTLA4, PD1) (113), and pharmacological approaches to directly target TAMs, *via* knocking out CCL2 or antibodies and fusion proteins against other TAM-specific chemokines, reduced migration and invasion of HCC cell lines (17).

The new tools like production of human induced pluripotent stem cells (iPSC) derived lymphocytes and genetic engineering give the opportunity to expand the favourite phenotype of immune cells to ex-vivo clinical scale. Bioreactor-derived iPSC-macrophages represent a highly pure population of $CD45^+CD11b^+CD14^+CD163^+$ cells with the functional features of professional phagocytes, and iPSC-NK cell offers advantages over the T cell immunotherapy. The Chimeric antigen receptor (CAR) constructs now can provide standardized, targeted off-the-shelf NK cells and macrophages for kill and clearance immunotherapy. As example, researchers have designed CAR-M, which express the intracellular domain of FcRv and promote the phagocytic potential of target antigens. Linking the PI3K p85 subunit to CAR-M-FcRv forms a tandem which has better whole-cell phagocytosis[28]. CAR-NK constructs containing the transmembrane domain of NKG2D, the 2B4 co-stimulatory domain, and the CD3ζ signaling domain offer improved NK cell-mediated killing of tumor cells (114). Nonetheless, critical aspects of cell-based therapies in clinical trials are long-term safety, tolerability, efficacy as well as the tumorigenic potential of the iPSC-derived cell-based treatments.

Several studies implicate hypoxia as a very important mechanism that alters immune cell functions (92). Hypoxia represses NK activation receptors, including NKp46, NKp44, NKp30, and NKG2D, preventing NK cell-mediated cancer cell killing, while enhances the level of MHC class I molecules on cancer cells and their binding to inhibitory receptors on NK cells. In monocytes and myeloid-derived cells, hypoxia causes an increase in CD45 tyrosine phosphatase activity and a decrease in STAT3 activity. Treatment with sialidase abrogates the effect of hypoxia on STAT3 activity and differentiation of MDSCs to TAM (99, 107). MDSCs lacking HIF-1 did not differentiate into TAM within the TME but instead differentiated to DC (105, 106). There has been enormous growing interest in the development of inhibitors to target HIF-1α and the related downstream genes. Therapeutic strategies to disrupting HIF-1α and the related downstream genes would be able to switch TME for kill and clearance by NK cells and macrophages and improve cancer immunotherapies in non-responder HCC patients.

Nanorobots can present potential therapeutic tools for kill and clearance in TME. The recent advances of robotics and nanotechnology can lead to the development of cell-type nanorobots with specific functions. For example, microbivore is a nanorobot designed as artificial phagocyte. It can achieve complete clearance of the most sever septicemic infections in hours or less, far better than the weeks needed for antibiotic-assisted phagocytic defence. Field of nanorobotics can open up new horizons for abundant research which could lead to an amazing range of kill and clearance devices in combination or as substitute for NK cells and macrophages.

CONCLUSION

Hepatocellular carcinoma is a complex medical condition associated with a poor prognosis. Symptoms of liver cancer often do not appear until the cancer is at an advanced stage and 70% of patients at diagnosis are ineligible for the curative treatments (resection, liver transplantation, and ablation therapies) (115). The only standard treatment for advanced cancer (sorafenib) also develops long-term drug resistance (116, 117). Therefore, there is a desperate need for new therapeutic strategies in HCC. Spontaneous immune responses against tumor antigens in HCC make it an attractive target for immunotherapy. The principles of current immune-based therapies in cancer are harnessing the potential of the immune system to destroy malignant cells. Unfortunately, the existing immunotherapies for solid cancers rarely cure the disease once it has become metastatic.

In our recent publication, we investigated the role of the necrotic zone and potential mechanisms involved in disarming macrophage phagocytic machinery in solid tumors (1). We suggested that further accumulation of dying, dead, and disintegrating cancer cells in this region makes the tumor

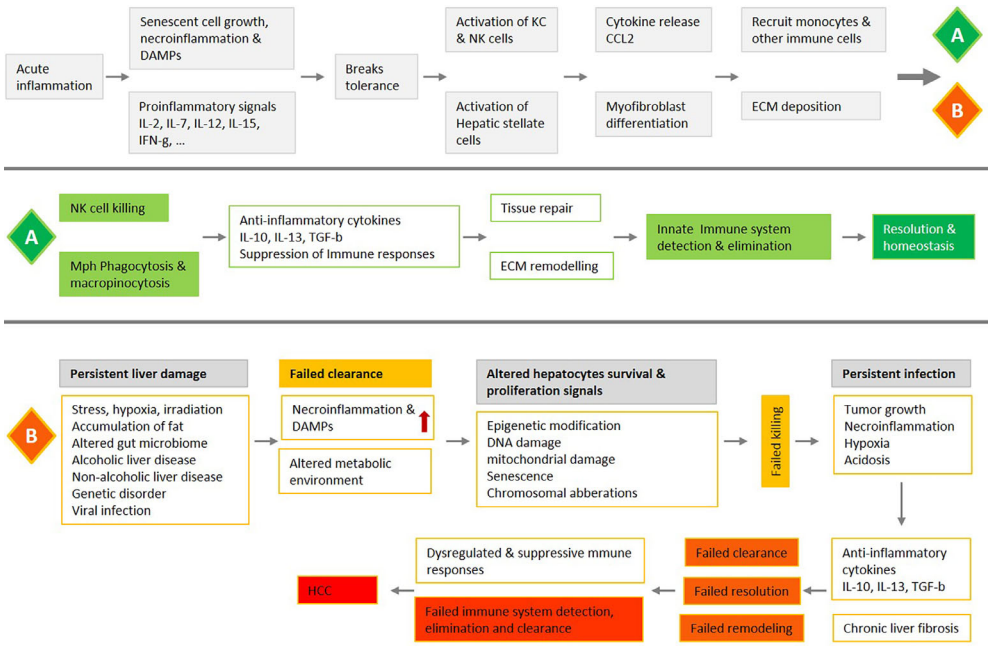


FIGURE 3 | An overview of liver acute inflammation and two possible processes, resolution **(A)** or chronic inflammation and HCC **(B)**, with a focus on the NK-macrophage kill and clearance. Liver acute inflammation must be resolved for homeostasis to be stored. An array of diverse mediators regulates NK cells and monocytes/macrophages trafficking and blunt production of inflammatory mediators, while also promoting clearance of tissue. Failure in NK cells killing, and macrophage clearance are associated with chronic unresolved inflammation, which is the central causative factor in the development of HCC.

proinflammatory and potentially provides a rich source of building blocks for the anaerobic metabolism of cancer stem cells as well as immune cells. The phagocytic clearance in the liver is fundamental for tissue homeostasis, controlling important aspects of inflammation and the immune response (**Figures 1**–**3**) (118). Herein, we discussed observations that support a synergistic act of NK-macrophage kill and clearance as a therapeutic strategy in HCC and other solid tumors. The key aspects of observations can be listed as follows:

- NK cells and macrophages have a primordial role in cancer immune surveillance.
- Synergistic act of kill and clearance by NK cells and macrophages is the centre point of innate and adaptive immunity, and therapeutic manipulation of this crosstalk provides an attractive strategy for HCC treatment.
- Excessive and persistent accumulation of necrotic and apoptotic corpses, debris, and senescent cells in TME support NK-macrophage kill and clearance strategy as a therapeutic tool in HCC (119, 120).
- NK cell deficiencies characterised by the absence of NK cells or their function and accumulation of TAMs with redundant phagocytic machinery indicate the importance of NK-macrophage kill and clearance is in tumor immune surveillance.

Further in-vitro and in-vivo experimental investigations could produce interesting findings that help to better understand the innate immune networking in HCC and increase therapeutic efficacy. Herein, our suggestive approaches to develop therapeutic methods based on NK-macrophage kill and clearance in solid tumors include: (i) The production of human-induced pluripotent stem cells derived NK cells and macrophages with the favorite functional features, (ii) chimeric antigen receptor (CAR) constructs of NK cells and macrophages that kill and clear efficiently, (iii) targeting the crosstalk between NK cells and macrophages, such as NKP30, to boost kill and clearance in HCC, (iv) immune checkpoint blockade, such as PD-L1/PD-1, and activation of cancer cell lysis and phagocytosis, (iv) blocking signaling axis like CCL2/CCR2 and CSF-1/CSF-1R to inhibit cell trafficking from bone marrow and TAMs accumulation in TME, (v) strategies to disrupting or inhibit HIF-1α and the related downstream genes to control metabolic switch in TME, (vi) and using nanorobots as a counterpart or substitute for immune cells to improve kill and clearance in TME (**Figures 2A–D** and **3**).

AUTHOR CONTRIBUTIONS

MM: conception and design of the manuscript, research of supporting evidence, writing and design of figures. FA and SM: editing, research of supporting evidence, critical revision of content, and final approval. All authors contributed to the article and approved the submitted version.

REFERENCES

1. Mehrabi M, Amini F, Mehrabi S. Active Role of the Necrotic Zone in Desensitization of Hypoxic Macrophages and Regulation of CSC-Fate: A Hypothesis. *Front Oncol* (2018) 8:235. doi: 10.3389/fonc.2018.00235
2. Kelly A, Goldenmason L, Traynor O, Geoghegan J, Mcentee G, Hegarty J, et al. Chananti Ges in Hepatic Immunoregulatory Cytokines in Patients With Metastatic Colorectal Carcinoma: Implications for Hepatic Anti-Tumour Immunity. *Cytokine* (2006) 35(3-4):171–9. doi: 10.1016/j.cyto.2006.07.019
3. Tu Z, Bozorgzadeh A, Crispe IN, Orloff MS. The Activation State of Human Intrahepatic Lymphocytes. *Clin Exp Immunol* (2007) 149(1):186–93. doi: 10.1111/j.1365-2249.2007.03415.x
4. Jörs S, Jeliazkova P, Ringelhan M, Thalhammer J, Dürl S, Ferrer J. Lineage Fate of Ductular Reactions in Liver Injury and Carcinogenesis. *Z Für Gastroenterol* (2015) 53(01):2445–57. doi: 10.1055/s-0034-1397072
5. Ringelhan M, Pfister D, O'Connor T, Pikarsky E, Heikenwalder M. The Immunology of Hepatocellular Carcinoma. *Nat Immunol* (2018) 19:222–32. doi: 10.4254/wjh.v7.i17.2080
6. Hernandez–Gea V, Toffanin S, Friedman SL, Llovet JM. Role of the Microenvironment in the Pathogenesis and Treatment of Hepatocellular Carcinoma. *Gastroenterology* (2013) 144(3):512–27. doi: 10.1053/j.gastro.2013.01.002
7. Fattovich G, Stroffolini T, Zagni I, Donato F. Hepatocellular Carcinoma in Cirrhosis: Incidence and Risk Factors. *Gastroenterology* (2004) 127:S35–50. doi: 10.1053/j.gastro.2004.09.014
8. Nakagawa H, Umemura A, Taniguchi K, Font-Burgada J, Dhar D, Ogata H, et al. ER Stress Cooperates With Hypernutrition to Trigger TNF-Dependent Spontaneous HCC Development. *Cancer Cell* (2014) 26(3):331–43. doi: 10.1016/j.ccr.2014.07.001
9. Loomba R, Sanyal AJ. The Global NAFLD Epidemic. *Nat Rev Gastroenterol Hepatol* (2013) 10(11):686–90. doi: 10.1038/nrgastro.2013.171
10. Totoki Y, Tatsuno K, Covington KR, Ueda H. Trans-Ancestry Mutational Landscape of Hepatocellular Carcinoma Genomes. *Nat Genet* (2014) 46:1267–73. doi: 10.1038/ng.3126
11. Lee J. The Mutational Landscape of Hepatocellular Carcinoma. *Clin Mol Hepatol* (2015) 21(3):220. doi: 10.3350/cmh.2015.21.3.220
12. Schulze K, Imbeaud S, Letouzé E, Alexandrov LB, Calderaro J, Rebouissou S, et al. Exome Sequencing of Hepatocellular Carcinomas Identifies New Mutational Signatures and Potential Therapeutic Targets. *Nat Genet* (2015) 47(5):505–11. doi: 10.1038/ng.3252
13. Llovet JM, Zucman-Rossi J, Pikarsky E, Gores G. Hepatocellular Carcinoma. *Nat Rev Dis Prim* (2016) 2:16018. doi: 10.1038/nrdp.2016.18
14. Thorsson V, Gibbs DL, Brown SD, Wolf D, Bortone DS. The Immune Landscape of Cancer. *Immunity* (2018) 48:812–30.e14. doi: 10.1016/j.immuni.2018.03.023
15. Subramaniam A, Shanmugam MK, Perumal E, Li F, Nachiyappan A, Dai X, et al. Potential Role of Signal Transducer and Activator of Transcription (STAT)3 Signaling Pathway in Inflammation, Survival, Proliferation and Invasion of Hepatocellular Carcinoma. *Biochim Et Biophys Acta (BBA) - Rev Cancer* (2013) 1835(1):46–60. doi: 10.1016/j.bbcan.2012.10.002
16. Gao B, Jeong W, Tian Z. Liver: An Organ With Predominant Innate Immunity. *Hepatology* (2007) 47(2):729–36. doi: 10.1002/hep.22034
17. Haybaeck J, Zeller N, Wolf MJ, Weber A, Wagner U, Kurrer MO, et al. A Lymphotoxin-Driven Pathway to Hepatocellular Carcinoma. *Cancer Cell* (2009) 16(4):295–308. doi: 10.1016/j.ccr.2009.08.021
18. Bilzer M, Roggel F, Gerbes AL. Role of Kupffer Cells in Host Defense and Liver Disease. *Liver Int* (2006) 26(10):1175–86. doi: 10.1111/j.1478-3231.2006.01342.x
19. Robinson MW, Harmon C, O'Farrelly C. Liver Immunology and Its Role in Inflammation and Homeostasis. *Cell Mol Immunol* (2016) 13(3):267–76. doi: 10.1038/cmi.2016.3
20. Wang SC. Kupffer Cell Activation by Lipopolysaccharide in Rats: Role for Lipopolysaccharide Binding Protein and Toll-Like Receptor 4. *Hepatology* (2000) 31(4):932–6. doi: 10.1053/he.2000.5634
21. Ziegler-Heitbrock L. The CD14 CD16 Blood Monocytes: Their Role in Infection and Inflammation. *J Leukocyte Biol* (2006) 81(3):584–92. doi: 10.1189/jlb.0806510
22. Fogg DK. A Clonogenic Bone Marrow Progenitor Specific for Macrophages and Dendritic Cells. *Science* (2006) 311(5757):83–7. doi: 10.1126/science.1117729
23. Geissmann F, Jung S, Littman DR. Blood Monocytes Consist of Two Principal Subsets With Distinct Migratory Properties. *Immunity* (2003) 19 (1):71–82. doi: 10.1016/s1074-7613(03)00174-2
24. Tacke F, Randolph GJ. Migratory Fate and Differentiation of Blood Monocyte Subsets. *Immunobiology* (2006) 211(6-8):609–18. doi: 10.1016/j.imbio.2006.05.025
25. Norris S, Collins C, Doherty DG, Smith F, Mcentee G, Traynor O, et al. Resident Human Hepatitis Lymphocytes Are Phenotypically Different From Circulating Lymphocytes. *J Hepatol* (1998) 28(1):84–90. doi: 10.1016/s0168-8278(98)80206-7
26. Morvan MG, Lanier LL. NK Cells and Cancer: You Can Teach Innate Cells New Tricks. *Nat Rev Cancer* (2015) 16(1):7–19. doi: 10.1038/nrc.2015.5
27. Gasser S, Orsulic S, Brown EJ, Raulet DH. The DNA Damage Pathway Regulates Innate Immune System Ligands of the NKG2D Receptor. *Nature* (2005) 436(7054):1186–90. doi: 10.1038/nature03884
28. Nakatani K, Kaneda K, Seki S, Nakajima Y. Pit Cells as Liver-Associated Natural Killer Cells: Morphology and Function. *Med Electron Microsc* (2004) 37(1):29–36. doi: 10.1007/s00795-003-0229-9
29. Orange JS. Formation and Function of the Lytic NK-Cell Immunological Synapse. *Nat Rev Immunol* (2008) 8(9):713–25. doi: 10.1038/nri2381
30. Herberman RB, Reynolds CW, Ortaldo JR. Mechanism of Cytotoxicity by Natural Killer (NK) Cells. *Annu Rev Immunol* (1986) 4(1):651–80. doi: 10.1146/annurev.iy.04.040186.003251
31. Anfossi N, André P, Guia S, Falk CS, Roetynck S, Stewart CA, et al. Human NK Cell Education by Inhibitory Receptors for MHC Class I. *Immunity* (2006) 25(2):331–42. doi: 10.1016/j.immuni.2006.06.013
32. Basile GD, Ménasché G, Fischer A. Molecular Mechanisms of Biogenesis and Exocytosis of Cytotoxic Granules. *Nat Rev Immunol* (2010) 10(8):568–79. doi: 10.1038/nri2803
33. Pinzani M. Pathophysiology of Liver Fibrosis. *Dig Dis* (2015) 33(4):492–7. doi: 10.1159/000374096
34. Gur C, Doron S, Kfir-Erenfeld S, Horwitz E, Abu-Tair L, Safadi R, et al. NKp46-Mediated Killing of Human and Mouse Hepatic Stellate Cells Attenuates Liver Fibrosis. *Gut* (2011) 61(6):885–93. doi: 10.1136/gutjnl-2011-301400
35. Björkström NK, Ljunggren H, Michaëlsson J. Emerging Insights Into Natural Killer Cells in Human Peripheral Tissues. *Nat Rev Immunol* (2016) 16(5):310–20. doi: 10.1038/nri.2016.34
36. Doherty DJ, Norris S, Madrigal-Estebas L, McEntee G, Traynor O, Hegarty JE, et al. The Human Liver Contains Multiple Populations of NK Cells, T Cells, and CD3 CD56 Natural T Cells With Distinct Cytotoxic Activities and Th1, Th2, and Th0 Cytokine Secretion Patterns. *J Immunol* (1999) 16 (3):2314–21.
37. Harmon C, Robinson MW, Fahey R, Whelan S, Houlihan DD, Geoghegan J, et al. Tissue-Resident Eomes(hi) T-Bet(Lo) CD56bright NK Cells With Reduced Proinflammatory Potential Are Enriched in the Adult Human Liver. *Eur J Immunol* (2016) 46(9):2111–20. doi: 10.1002/eji.201646559
38. Sui Q, Zhang J, Sun X, Zhang C, Han Q, Tian Z. NK Cells Are the Crucial Antitumor Mediators When STAT3-Mediated Immunosuppression Is Blocked in Hepatocellular Carcinoma. *J Immunol* (2014) 193(4):2016–23. doi: 10.4049/jimmunol.1302389
39. Muhanna N, Doron S, Wald O, Horani A, Eid A, Pappo O, et al. Activation of Hepatic Stellate Cells After Phagocytosis of Lymphocytes: A Novel Pathway of Fibrogenesis. *Hepatology* (2008) 48(3):963–77. doi: 10.1002/hep.22413
40. Coulouarn C, Factor VM, Conner EA, Thorgeirsson SS. Genomic Modeling of Tumor Onset and Progression in a Mouse Model of Aggressive Human Liver Cancer. *Carcinogenesis* (2011) 32(10):1434–40. doi: 10.1093/carcin/bgr133
41. Tian Z, Chen Y, Gao B. NK Cells in Liver Disease. *Hepatology* (2013) 57 (4):1654–62. doi: 10.1002/hep.26115
42. Sun C, Sun H, Xiao W, Zhang C, Tian Z. Natural Killer Cell Dysfunction in Hepatocellular Carcinoma and NK Cell-Based Immunotherapy. *Acta Pharmacol Sin* (2015) 36(10):1191–9. doi: 10.1038/aps.2015.41

43. Cai L, Zhang Z, Zhou L, Wang H, Fu J, Zhang S, et al. Functional Impairment in Circulating and Intrahepatic NK Cells and Relative Mechanism in Hepatocellular Carcinoma Patients. *Clin Immunol* (2008) 129(3):428–37. doi: 10.1016/j.clim.2008.08.012
44. Wu Y, Kuang D, Pan W, Wan Y, Lao X, Wang D, et al. Monocyte/macrophage-Elicited Natural Killer Cell Dysfunction in Hepatocellular Carcinoma Is Mediated by CD48/2B4 Interactions. *Hepatology* (2013) 57 (3):1107–16. doi: 10.1002/hep.26192
45. Moroso V, Metselaar HJ, Mancham S, Tilanus HW, Eissens D, Meer AV, et al. Liver Grafts Contain a Unique Subset of Natural Killer Cells That Are Transferred Into the Recipient After Liver Transplantation. *Liver Transplant* (2010) 16(7):895–908. doi: 10.1002/lt.22080
46. Dalakas E, Newsome PN, Harrison DJ, Plevris JN. Hematopoietic Stem Cell Trafficking in Liver Injury. *FASEB J* (2005) 19(10):1225–31. doi: 10.1096/fj.04-2604rev
47. Ceradini DJ, Kulkarni AR, Callaghan MJ, Tepper OM, Bastidas N, Kleinman ME, et al. Progenitor Cell Trafficking Is Regulated by Hypoxic Gradients Through HIF-1 Induction of SDF-1. *Nat Med* (2004) 10(8):858–64. doi: 10.1038/nm1075
48. Liu A, Wang Y, Ding Y, Baez I, Payne KJ, Borghesi L. Cutting Edge: Hematopoietic Stem Cell Expansion and Common Lymphoid Progenitor Depletion Require Hematopoietic-Derived, Cell-Autonomous TLR4 in a Model of Chronic Endotoxin. *J Immunol* (2015) 195(6):2524–8. doi: 10.4049/jimmunol.1501231
49. Pietras EM, Mirantes-Barbeito C, Fong S, Loeffler D, Kovtonyuk LV, Zhang S, et al. Chronic Interleukin-1 Exposure Drives Haematopoietic Stem Cells Towards Precocious Myeloid Differentiation at the Expense of Self-Renewal. *Nat Cell Biol* (2016) 18(6):607–18. doi: 10.1038/ncb3346
50. Shi C, Pamer EG. Monocyte Recruitment During Infection and Inflammation. *Nat Rev Immunol* (2011) 11(11):762–74. doi: 10.1038/nri3070
51. Randolph GJ, Inaba K, Robbiani DF, Steinman RM, Muller WA. Differentiation of Phagocytic Monocytes Into Lymph Node Dendritic Cells *In Vivo*. *Immunity* (1999) 11(6):753–61. doi: 10.1016/s1074-7613(00)80149-1
52. Netea MG, Joosten LA, Latz E, Mills KH, Natoli G, Stunnenberg HG, et al. Trained Immunity: A Program of Innate Immune Memory in Health and Disease. *Science* (2016) 352(6284):1–23. doi: 10.1126/science.aaf1098
53. Boettcher S, Manz MG. Regulation of Inflammation- and Infection-Driven Hematopoiesis. *Trends Immunol* (2017) 38(5):345–57. doi: 10.1016/j.it.2017.01.004
54. Mitroulis I, Ruppova K, Wang B, Chen L, Grzybek M, Grinenko T, et al. Modulation of Myelopoiesis Progenitors Is an Integral Component of Trained Immunity. *Cell* (2018) 172(1-2):147–61.e12. doi: 10.1016/j.cell.2017.11.034
55. Geissmann F, Manz MG, Jung S, Sieweke MH, Merad M, Ley K. Development of Monocytes, Macrophages, and Dendritic Cells. *Science* (2010) 327(5966):656–61. doi: 10.1126/science.1178331
56. GS Firestein, SE Gabriel, IB McInnes, JR ODell eds. "Mononuclear Phagocytes. Siamon Gordon, Annette Plüddemann". In: *Kelley and Firesteins Textbook of Rheumatology*. Philadelphia, PA: Elsevier.
57. Steinman RM. Identification Of A Novel Cell Type In Peripheral Lymphoid Organs Of Mice: I. Morphology, Quantitation, Tissue Distribution. *J Exp Med* (1973) 137(5):1142–62. doi: 10.1084/jem.137.5.1142
58. Chitu V, Stanley ER. Colony-Stimulating Factor-1 in Immunity and Inflammation. *Curr Opin Immunol* (2006) 18(1):39–48. doi: 10.1016/j.coi.2005.11.006
59. Yukihiro H, Hiroaki K. Glypican-3 Is a Prognostic Factor and an Immunotherapeutic Target in Hepatocellular Carcinoma. *World J Gastroenterol* (2016) 22:275–83. doi: 10.3748/wjg.v22.i1.275
60. Nahrendorf M, Pittet MJ, Swirski FK. Monocytes: Protagonists of Infarct Inflammation and Repair After Myocardial Infarction. *Circulation* (2010) 121(22):2437–45. doi: 10.1161/circulationaha.109.916346
61. Zhu X, Zhang J, Zhuang P, Zhu H, Zhang W, Xiong Y, et al. High Expression of Macrophage Colony-Stimulating Factor in Peritumoral Liver Tissue Is Associated With Poor Survival After Curative Resection of Hepatocellular Carcinoma. *J Clin Oncol* (2008) 26(16):2707–16. doi: 10.1200/jco.2007.15.6521
62. Hoechst B, Voigtlaender T, Ormandy L, Gamrekelashvili J, Zhao F, Wedemeyer H, et al. Myeloid Derived Suppressor Cells Inhibit Natural Killer Cells in Patients With Hepatocellular Carcinoma via the NKp30 Receptor. *Hepatology* (2009) 50(3):799–807. doi: 10.1002/hep.23054
63. Murdoch C. Mechanisms Regulating the Recruitment of Macrophages Into Hypoxic Areas of Tumors and Other Ischemic Tissues. *Blood* (2004) 104 (8):2224–34. doi: 10.1182/blood-2004-03-1109
64. Pallett LJ, Gill US, Quaglia A, Sinclair LV, Jover-Cobos M, Schurich A, et al. Metabolic Regulation of Hepatitis B Immunopathology by Myeloid-Derived Suppressor Cells. *Nat Med* (2015) 21(6):591–600. doi: 10.1038/nm.3856
65. Maenhout SK, Lint SV, Emeagi PU, Thielemans K, Aerts JL. Enhanced Suppressive Capacity of Tumor-Infiltrating Myeloid-Derived Suppressor Cells Compared With Their Peripheral Counterparts. *Int J Cancer* (2013) 134(5):1077–90. doi: 10.1002/ijc.28449
66. Haverkamp JM, Crist SA, Elzey BD, Cimen C, Ratliff TL. In Vivo Suppressive Function of Myeloid-Derived Suppressor Cells Is Limited to the Inflammatory Site. *Eur J Immunol* (2011) 41(3):749–59. doi: 10.1002/eji.201041069
67. Corzo CA, Condamine T, Lu L, Cotter MJ, Youn JI, Cheng P, et al. HIF-1alpha Regulates Function and Differentiation of Myeloid-Derived Suppressor Cells in the Tumor Microenvironment. *J Exp Med* (2010) 207:2439–53. doi: 10.1084/jem.20100587
68. Castriconi R, Carrega P, Dondero A. Molecular Mechanisms Directing Migration and Retention of Natural Killer Cells in Human Tissues. *Front Immunol* (2018) 9:2324. doi: 10.3389/fimmu.2018.02324
69. Castriconi R, Dondero A, Bellora F, Moretta L, Castellano A, Locatelli F, et al. Neuroblastoma-Derived Tgfβ1 Modulates the Chemokine Receptor Repertoire of Human Resting NK Cells. *J Immunol* (2013) 190(10):5321–8. doi: 10.4049/jimmunol.1202693
70. Ponzetta A, Sciumè G, Benigni G, Antonangeli F, Morrone S, Santoni A, et al. CX3CR1 Regulates the Maintenance of KLRG1 NK Cells Into the Bone Marrow by Promoting Their Entry Into Circulation. *J Immunol* (2013) 191 (11):5684–94. doi: 10.4049/jimmunol.1300090
71. Huang S, He X, Ding J, Liang L, Zhao Y, Zhang Z, et al. Upregulation of miR-23a~27a~24 Decreases Transforming Growth Factor-Beta-Induced Tumor-Suppressive Activities in Human Hepatocellular Carcinoma Cells. *Int J Cancer* (2008) 123(4):972–8. doi: 10.1002/ijc.23580
72. Chhabra R, Dubey R, Saini N. Cooperative and Individualistic Functions of the microRNAs in the miR-23a~27a~24-2 Cluster and Its Implication in Human Diseases. *Mol Cancer* (2010) 9(1):232. doi: 10.1186/1476-4598-9-232
73. Golden-Mason L, Curry MP, Nolan N, Traynor O, Mcentee G, Kelly J, et al. Differential Expression of Lymphoid and Myeloid Markers on Differentiating Hematopoietic Stem Cells in Normal and Tumor-Bearing Adult Human Liver. *Hepatology* (2000) 31(6):1251–6. doi: 10.1053/jhep.2000.7713
74. Crosbie OM, Reynolds M, Mcentee G, Traynor O, Hegarty JE, Ofarrelly C. In Vitro Evidence for the Presence of Hematopoietic Stem Cells in the Adult Human Liver. *Hepatology* (1999) 29(4):1193–8. doi: 10.1002/hep.510290402
75. Collins C, Norris S, Mcentee G, Traynor O, Bruno L, Boehmer HV, et al. RAG1, RAG2 and Pre-T Cell Receptor α Chain Expression by Adult Human Hepatic T Cells: Evidence for Extrathymic T Cell Maturation. *Eur J Immunol* (1996) 26(12):3114–8. doi: 10.1002/eji.1830261243
76. Taniguchi H, Toyoshima T, Fukao K, Nakauchi H. Presence of Hematopoietic Stem Cells in the Adult Liver. *Nat Med* (1996) 2(2):198–203. doi: 10.1038/nm0296-198
77. Watanabe H. C-Kit Stem Cells and Thymocyte Precursors in the Livers of Adult Mice. *J Exp Med* (1996) 184(2):687–93. doi: 10.1084/jem.184.2.687
78. Ogawa M. Expression and Function of C-Kit in Hemopoietic Progenitor Cells. *J Exp Med* (1991) 174(1):63–71. doi: 10.1084/jem.174.1.63
79. Carrega P, Ferlazzo G. Natural Killer Cell Distribution and Trafficking in Human Tissues. *Front Immunol* (2012) 3:347. doi: 10.3389/fimmu.2012.00347
80. Medina-Echeverz J, Eggert T, Han M, Greten TF. Hepatic Myeloid-Derived Suppressor Cells in Cancer. *Cancer Immunol Immunother* (2015) 64:931–40. doi: 10.1007/s00262-015-1736-y

81. Bruno A, Mortara L, Baci D, Noonan DM, Albini A. Myeloid Derived Suppressor Cells Interactions With Natural Killer Cells and Pro-Angiogenic Activities: Roles in Tumor Progression. *Front Immunol* (2019) 10:771. doi: 10.3389/fimmu.2019.00771
82. Liu JF, Deng WW, Chen L, Li YC, Wu L, Ma SR, et al. Inhibition of JAK2/STAT3 Reduces Tumor-Induced Angiogenesis and Myeloid-Derived Suppressor Cells in Head and Neck Cancer. *Mol Carcinog* (2018) 57:429–39. doi: 10.1002/mc.22767
83. Sun X, Sui Q, Zhang C, Tian Z, Zhang J. Targeting Blockage of STAT3 in Hepatocellular Carcinoma Cells Augments NK Cell Functions via Reverse Hepatocellular Carcinoma-Induced Immune Suppression. *Mol Cancer Ther* (2013) 12:2885–96. doi: 10.1158/1535-7163.MCT-12-1087
84. Wiers KM, Lathers DM, Wright MA, Young MR. Vitamin D3 Treatment to Diminish the Levels of Immune Suppressive $CD34^+$ Cells Increases the Effectiveness of Adoptive Immunotherapy. *J Immunother* (2000) 23:115–24. doi: 10.1097/00002371-200001000-00014
85. Mortara L, Gariboldi MB, Bosi A, Bregni M, Pinotti G, Guasti L, et al. Vitamin D Deficiency has a Negative Impact on Cetuximab-Mediated Cellular Cytotoxicity Against Human Colon Carcinoma Cells. *Target Oncol* (2018) 13:657–65. doi: 10.1007/s11523-018-0586-x
86. Lee GY, Han SN. The Role of Vitamin E in Immunity. *Nutrients* (2018) 10:10111614. doi: 10.3390/nu10111614
87. Stiff A, Trikha P, Mundy-Bosse B, McMichael E, Mace TA, Benner B, et al. Nitric Oxide Production by Myeloid-Derived Suppressor Cells Plays a Role in Impairing Fc Receptor-Mediated Natural Killer Cell Function. *Clin Cancer Res* (2018) 24:1891–904. doi: 10.1158/1078-0432.CCR-17-0691
88. Williams KJ, Cowen RL, Brown LM, Chinje EC, Jaffar M, Stratford IJ. Hypoxia in Tumors: Molecular Targets for Anti-Cancer Therapeutics. *Adv Enzyme Regul* (2004) 44(1):93–108. doi: 10.1016/j.advenzreg.2003.11.019
89. Imai T, Horiuchi A, Wang C, Oka K, Ohira S, Nikaido T, et al. Hypoxia Attenuates the Expression of E-Cadherin via Up-Regulation of SNAIL in Ovarian Carcinoma Cells. *Am J Pathol* (2003) 163(4):1437–47. doi: 10.1016/s0002-9440(10)63501-8
90. Diebold I, Petry A, Hess J, Görlach A. The NADPH Oxidase Subunit NOX4 Is a New Target Gene of the Hypoxia-Inducible Factor-1. *Mol Biol Cell* (2010) 21(12):2087–96. doi: 10.1091/mbc.e09-12-1003
91. Cichon MA, Radisky DC. ROS-Induced Epithelial-Mesenchymal Transition in Mammary Epithelial Cells Is Mediated by NF-κb-Dependent Activation of Snail. *Oncotarget* (2014) 5(9):2827–38. doi: 10.18632/oncotarget.1940
92. Ferguson JE, Matin SF. Re: Targeting Renal Cell Carcinoma With a HIF-2 Antagonist. *Eur Urol* (2017) 71(6):987. doi: 10.1016/j.eururo.2017.02.015
93. Tannahill GM, Curtis AM, Adamik J, Palsson-McDermott EM, McGettrick AF, Goel G. Succinate Is an Inflammatory Signal That Induces IL-1β Through HIF-1α. *Nature* (2013) 496(7444):238–42. doi: 10.1038/nature11986
94. Wilson GK, Tennant DA, Mckeating JA. Hypoxia Inducible Factors in Liver Disease and Hepatocellular Carcinoma: Current Understanding and Future Directions. *J Hepatol* (2014) 61(6):1397–406. doi: 10.1016/j.jhep.2014.08.025
95. Gabrilovich DI, Nagaraj S. Myeloid-Derived Suppressor Cells as Regulators of the Immune System. *Nat Rev Immunol* (2009) 9(3):162–74. doi: 10.1038/nri2506
96. Biswas SK, Mantovani A. Macrophage Plasticity and Interaction With Lymphocyte Subsets: Cancer as a Paradigm. *Nat Immunol* (2010) 11 (10):889–96. doi: 10.1038/ni.1937
97. Franklin RA, Liao W, Sarkar A, Kim MV, Bivona MR, Liu K, et al. The Cellular and Molecular Origin of Tumor-Associated Macrophages. *Science* (2014) 344(6186):921–5. doi: 10.1126/science.1252510
98. Qian B, Pollard JW. Macrophage Diversity Enhances Tumor Progression and Metastasis. *Cell* (2010) 141(1):39–51. doi: 10.1016/j.cell.2010.03.014
99. Biswas SK, Allavena P, Mantovani A. Tumor-Associated Macrophages: Functional Diversity, Clinical Significance, and Open Questions. *Semin Immunopathol* (2013) 35(5):585–600. doi: 10.1007/s00281-013-0367-7
100. Biswas S. Metabolic Reprogramming of Immune Cells in Cancer Progression. *Immunity* (2015) 43(3):435–49. doi: 10.1016/j.immuni.2015.09.001
101. Burke B, Tang N, Corke KP, Tazzyman D, Ameri K, Wells M, et al. Expression of HIF-1a by Human Macrophages: Implications for the Use of Macrophages in Hypoxia-Regulated Cancer Gene Therapy. *J Pathol* (2002) 196(2):204–12. doi: 10.1002/path.1029
102. Semenza GL. Regulation of Mammalian O2 Homeostasis by Hypoxia-Inducible Factor 1. *Annu Rev Cell Dev Biol* (1999) 15(1):551–78. doi: 10.1146/annurev.cellbio.15.1.551
103. Imtiyaz HZ, Simon MC. Hypoxia-Inducible Factors as Essential Regulators of Inflammation. *Curr Topics Microbiol Immunol* (2010) 345:105–20. doi: 10.1007/82_2010_74
104. Noman MZ, Desantis G, Janji B, Hasmim M, Karray S, Dessen P, et al. PD-L1 Is a Novel Direct Target of HIF- 1alpha, and Its Blockade Under Hypoxia Enhanced MDSC-Medi-Ated T Cell Activation. *J Exp Med* (2014) 211:781–90. doi: 10.1084/jem.20131916
105. Corzo CA, Condamine T, Lu L, Cotter MJ, Youn J, Cheng P, et al. HIF-1α Regulates Function and Differentiation of Myeloid-Derived Suppressor Cells in the Tumor Microenvironment. *J Exp Med* (2010) 207(11):2439–53. doi: 10.1084/jem.20100587
106. Liu G, Bi Y, Shen B, Yang H, Zhang Y, Wang X, et al. SIRT1 Limits the Function and Fate of Myeloid-Derived Suppressor Cells in Tumors by Orchestrating HIF-1 -Dependent Glycolysis. *Cancer Res* (2013) 74(3):727–37. doi: 10.1158/0008-5472.can-13-2584
107. Kumar V, Cheng P, Condamine T, Mony S, Languino LR, Mccaffrey JC, et al. CD45 Phosphatase Inhibits STAT3 Transcription Factor Activity in Myeloid Cells and Promotes Tumor-Associated Macrophage Differentiation. *Immunity* (2016) 44(2):303–15. doi: 10.1016/j.immuni.2016.01.014
108. Pearce EJ, Everts B. Dendritic Cell Metabolism. *Nat Rev Immunol* (2014) 15 (1):18–29. doi: 10.1038/nri3771
109. Vari F, Arpon D, Keane C, Hertzberg MS, Talaulikar D, Jain S, et al. Immune Evasion via PD-1/PD-L1 on NK-Cells and Monocyte/Macrophages Is More Prominent in Hodgkin Lymphoma Than DLBCL. *Blood* (2018) 131:1809–19. doi: 10.1182/blood-2017-07-796342
110. Mitchem JB, Brennan DJ, Knolhoff BL, Belt BA, Zhu Y, Sanford DE, et al. Targeting Tumor-Infiltrating Macrophages Decreases Tumor-Initiating Cells, Relieves Immunosuppression, and Improves Chemotherapeutic Responses. *Cancer Res* (2013) 73:1128–41. doi: 10.1158/0008-5472.CAN-12-2731
111. Sceneay J, Chow MT, Chen A, Halse HM, Wong CS, Andrews DM, et al. Primary Tumor Hypoxia Recruits $CD11b^+$/Ly6Cmed/$Ly6G^+$ Immune Suppressor Cells and Compromises NK Cell Cytotoxicity in the Premetastatic Niche. *Cancer Res* (2012) 72:3906–11. doi: 10.1158/0008-5472.CAN-11-3873
112. Nywening TM, Belt BA, Cullinan DR, Panni RZ, Han BJ, Sanford DE, et al. Targeting Both Tumour-Associated CXCR2(+) Neutrophils and CCR2(+) Macrophages Disrupts Myeloid Recruitment and Improves Chemotherapeutic Responses in Pancreatic Ductal Adenocarcinoma. *Gut* (2017). doi: 10.1136/gutjnl-2017-313738
113. Wang Y, Zhang X, Yang L, Xue J, Hu G. Blockade of CCL2 Enhances Immunotherapeutic Effect of Anti-PD1 in Lung Cancer. *J Bone Oncol* (2018) 11:27–32. doi: 10.1016/j.jbo.2018.01.002
114. Li Y, Hermanson DL, Moriarity BS, Kaufman DS. Human iPSC-Derived Natural Killer Cells Engineered With Chimeric Antigen Receptors Enhance Anti-Tumor Activity. *Cell Stem Cell* (2018) 23:181–92. doi: 10.1016/j.stem.2018.06.002
115. Clark HP, Carson WF, Kavanagh PV, Ho CPH, Shen P, Zagoria RJ, et al. Staging and Current Treatment of Hepatocellular Carcinoma. *Radiographics* (2005) 25(Suppl 1):S3–23. doi: 10.1148/rg.25si055507
116. Llovet JM, Ricci S, Mazzaferro V, Hilgard P, Gane E, Blanc JF, et al. Sorafenib in Advanced Hepatocellular Carcinoma. *N Engl J Med* (2008) 359:378–90. doi: 10.1056/NEJMoa0708857
117. Cheng AL, Guan Z, Chen Z, Tsao CJ, Qin S, Kim JS, et al. Efficacy and Safety of Sorafenib in Patients With Advanced Hepatocellular Carcinoma According to Baseline Status: Subset Analyses of the Phase III Sorafenib Asia-Pacific Trial. *Eur J Cancer* (2012) 48:1452–65. doi: 10.1148/rg.25si055507
118. Arandjelovic S, Ravichandran KS. Phagocytosis of Apoptotic Cells in Homeostasis. *Nat Immunol* (2015) 16(9):907–17. doi: 10.1038/ni.3253
119. Malhi H, Gores GJ, Lemasters JJ. Apoptosis and Necrosis in the Liver: A Tale of Two Deaths? *Hepatology* (2006) 43(S31):1–14. doi: 10.1002/hep.21062
120. Vick B, Weber A, Urbanik T, Maass T, Teufel A, Krammer PH, et al. Knockout of Myeloid Cell Leukemia-1 Induces Liver Damage and Increases

Apoptosis Susceptibility of Murine Hepatocytes. *Hepatology* (2008) 49 (2):627–36. doi: 10.1002/hep.22664

Conflict of Interest: Author FA was employed by company Vitaccess.

The remaining authors declare that the research was conducted in the absence of any commercial or financial relationships that could be construed as a potential conflict of interest.

Publisher's Note: All claims expressed in this article are solely those of the authors and do not necessarily represent those of their affiliated organizations, or those of the publisher, the editors and the reviewers. Any product that may be evaluated in this article, or claim that may be made by its manufacturer, is not guaranteed or endorsed by the publisher.

Copyright © 2021 Mehrabi, Amini and Mehrabi. This is an open-access article distributed under the terms of the Creative Commons Attribution License (CC BY). The use, distribution or reproduction in other forums is permitted, provided the original author(s) and the copyright owner(s) are credited and that the original publication in this journal is cited, in accordance with accepted academic practice. No use, distribution or reproduction is permitted which does not comply with these terms.

frontiers in Oncology

ORIGINAL RESEARCH
published: 09 September 2021
doi: 10.3389/fonc.2021.731547

ASF1B Promotes Oncogenesis in Lung Adenocarcinoma and Other Cancer Types

*Wencheng Zhang[1], Zhouyong Gao[2], Mingxiu Guan[3], Ning Liu[4], Fanjie Meng[5] and Guangshun Wang[1]**

[1] Department of Oncology, Tianjin Baodi Hospital, Baodi Clinical College of Tianjin Medical University, Tianjin, China, [2] Department of Thoracic Surgery, Baodi Clinical College of Tianjin Medical University, Tianjin, China, [3] Department of Laboratory, Tianjin Baodi Hospital, Baodi Clinical College of Tianjin Medical University, Tianjin, China, [4] Department of Pathology, Tianjin Baodi Hospital, Baodi Clinical College of Tianjin Medical University, Tianjin, China, [5] Department of Thoracic Surgery, The Second Hospital of Tianjin Medical University, Tianjin, China

OPEN ACCESS

Edited by:
Simona Kranjc Brezar, Institute of Oncology Ljubljana, Slovenia

Reviewed by:
Pranshu Sahgal, Dana–Farber Cancer Institute, United States
Lucillia Bezu, Gustave Roussy Cancer Campus, France

***Correspondence:**
Guangshun Wang
wgsmed@163.com

Specialty section:
This article was submitted to Molecular and Cellular Oncology, a section of the journal Frontiers in Oncology

Received: *27 June 2021*
Accepted: *19 August 2021*
Published: *09 September 2021*

Citation:
Zhang W, Gao Z, Guan M, Liu N, Meng F and Wang G (2021) ASF1B Promotes Oncogenesis in Lung Adenocarcinoma and Other Cancer Types. Front. Oncol. 11:731547. doi: 10.3389/fonc.2021.731547

Anti-silencing function 1B histone chaperone (ASF1B) is known to be an important modulator of oncogenic processes, yet its role in lung adenocarcinoma (LUAD) remains to be defined. In this study, an integrated assessment of The Cancer Genome Atlas (TCGA) and genotype-tissue expression (GTEx) datasets revealed the overexpression of ASF1B in all analyzed cancer types other than LAML. Genetic, epigenetic, microsatellite instability (MSI), and tumor mutational burden (TMB) analysis showed that ASF1B was regulated by single or multiple factors. Kaplan-Meier survival curves suggested that elevated ASF1B expression was associated with better or worse survival in a cancer type-dependent manner. The CIBERSORT algorithm was used to evaluate immune microenvironment composition, and distinct correlations between ASF1B expression and immune cell infiltration were evident when comparing tumor and normal tissue samples. Gene set enrichment analysis (GSEA) indicated that ASF1B was associated with proliferation- and immunity-related pathways. Knocking down ASF1B impaired the proliferation, affected cell cycle distribution, and induced cell apoptosis in LUAD cell lines. In contrast, ASF1B overexpression had no impact on the malignant characteristics of LUAD cells. At the mechanistic level, ASF1B served as an indirect regulator of DNA Polymerase Epsilon 3, Accessory Subunit (POLE3), CDC28 protein kinase regulatory subunit 1(CKS1B), Dihydrofolate reductase (DHFR), as established through proteomic profiling and Immunoprecipitation-Mass Spectrometry (IP-MS) analyses. Overall, these data suggested that ASF1B serves as a tumor promoter and potential target for cancer therapy and provided us with clues to better understand the importance of ASF1B in many types of cancer.

Keywords: lung adenocarcinoma, immune infiltration cells, prognosis, ASF1B, profiling

INTRODUCTION

Lung cancer is one of the most common and deadliest forms of malignant cancer throughout the world (1). Approximately 40% of lung cancer cases are of the most common LUAD histopathological subtype (2). LUAD is associated with high rates of tumor recurrence and a poor prognosis owing to the combination of adverse factors that span a range of different biological and clinical behaviors and the increased resistance to anti-lung cancer drugs. Moreover, existing targeted drugs have shown unsatisfactory efficacy (3). Further research is thus needed to better understand the mechanisms underlying LUAD development and progression. Genetic mutation is the primary process that drives oncogenesis (4, 5), with gene-specific overexpression or silencing being additionally associated with epigenetic mechanisms such as changes in histone post-translational modification or DNA methylation (6–8). Aberrant activation or expression of chromatin-regulating proteins such as histone-modifying enzymes, histone variants, effector proteins, histone chaperones, and chromatin remodeling proteins is closely tied to cancer onset and progression (9–11). Histone H3–H4 chaperone anti-silencing function 1 (ASF1) is a key histone chaperone involved in regulating processes including DNA replication, DNA damage repair, and transcription (12, 13). There are two paralogous forms of ASF1: Anti-Silencing Function 1A Histone Chaperone (ASF1A) and ASF1B. While ASF1A is primarily involved in regulating DNA repair and cellular senescence, ASF1B serves as a preferential regulator of cellular proliferation (13, 14). Increased ASF1B expression levels have been linked to the prognosis of LUAD and breast cancer patients (15, 16). Prior work suggests that ASF1B is a key regulator of proliferation, apoptosis, and the cell cycle in prostate cancer, cervical cancer, clear cell renal cell carcinoma, and breast cancer (16–19). Even so, the role of this gene in LUAD and many other cancers has yet to be definitively established. Herein, we explored the expression and prognostic relevance of ASF1B across cancers, in addition to evaluating the association between ASF1B expression levels and molecular pathways, immune infiltration, methylation, Copy number variations (CNV), MSI, and TMB. Lastly, we examined the impact of knocking down and overexpressing ASF1B on proliferation, cell cycle progression, apoptosis, and potential mechanism of LUAD. Our data provide novel insights into the functional importance of ASF1B in LUAD and indicate ASF1B as a potential target for the therapeutic management of cancers.

MATERIALS AND METHODS

Dataset Analyses

To evaluate the expression of ASF1B in 33 different cancers, TCGA was queried to download RNA-seq gene expression data and clinical records pertaining to 11,058 cases (http://xena.ucsc.edu/welcome-to-ucsc-xena/) (Workflow Type: HTSeq FPKM) (20), with the GTEx data similarly being downloaded (21). Samples for which data pertaining to age, gender, TNM stage, distant and lymph node metastases, or OS were not recorded were excluded from subsequent analyses, as were patient samples with an Overall Survival (OS) <30 days. GSE31210 and GSE62254 datasets was downloaded from GENE EXPRESSION OMNIBUS (GEO). ICGC_ARRAY dataset was downloaded from International Cancer Genome Consortium (ICGC). Levels of ASF1B expression in Pan-cancer and normal tissue datasets were additionally evaluated with the Oncomine database (http://www.oncomine.org) (22–48). Relationships between methylation and patient outcomes were assessed with the MethSurv database (https://biit.cs.ut.ee/methsurv/) (49). Associations between ASF1B expression, methylation, and CNVs were examined using the GSCALite platform (http://bioinfo.life.hust.edu.cn/web/GSCALite/) (50). Correlations between ASF1B and molecular-or immune-related subtypes were assessed with the TISIDB platform (TISIDB (hku.hk)) (51).

Immune Infiltration Analysis

The CIBERSORT algorithm was used to approximate the infiltration of different immune cell types into patient tumors, followed by quality filtering. Additionally, the R ESTIMATE algorithm was utilized to assess tumor purity for all samples (52).

Cell Culture and Transfection

H1299, H1975, H1650 cells were grown in RPMI-1640 (Gibco BRL, MD, USA), while A549 cells were cultured in DMEM (Gibco BRL). In both cases, media contained 10% fetal bovine serum (Gibco BRL), 50 IU/mL penicillin, and 50 mg/mL streptomycin (Invitrogen, CA, USA), and cells were grown in humidified 5% CO_2 incubators at 37°C. Three different ASF1B-specific small-interfering RNA (siRNA) constructs were synthesized (siASF1B-1: CAACGAGUACCUCA ACCCUTT, siASF1B-2: GACGACCUGGAGUGGAAUUTT, siASF1B-3: UCAACUGCACUC CUAUCAATT. GenePharma, Shanghai, China), another siRNA derives from the literature (siASF1B-4: CCCUUGAGUACCAUUGAUCUU) (53). They were transiently transfected into cells using Lipofectamine 2000 (Invitrogen) based on provided directions. At 60 h post-transfection, Western blotting was used to select the most effective siRNA. Next, short hairpin RNAs (shRNA) constructs were synthesized based upon the most effective siRNA sequence (Gene Pharma). ASF1B overexpression and negative control lentiviral factors were obtained from FENGHUISHENGWU (Changsha, Hu Nan Province, China), while lentiviruses encoding ASF1B-shRNA and corresponding negative controls were from Gene Pharma. LUAD cells were transduced with these lentiviral vectors at stock concentrations of 1×10^8 –1×10^9 particles/ml. The H1975 and H1650 cell lines were used for gain-of-function studies, whereas H1299 and A549 cells were utilized when conducting loss-of-function studies. Cellular transduction was performed when cells were 60–70% confluent, with lentiviruses being administered at a dose of 1×10^7/ml together with 6 μg/ml polybrene (Sigma-Aldrich,

H9268). After transduction, puromycin (0.6 μg/mL, Sigma) was used to select for stably transduced cells.

EdU Assay

Cells were incubated for 2 h with EdU (Ribobio, Guangzhou, China), after which they were process sed based on provided directions. Cells were washed thrice with phosphate buffered saline (PBS), treated for 50 min with 100μl of 1×Apollo® reaction cocktail, and stained for 30 min with 100 μl of Hoechst 33342 prior to fluorescent microscopic visualization.

CCK-8 Assay

Cell viability was assessed *via* CCK-8 assay (gene-protein link, Beijing, China) Briefly, cells were added to 96-well plates ($2x10^3$/well) for 24, 48, 72, or 96 h, after which 10 μl of CCK-8 solution was added per well and plates were incubated for an additional 2 h at 37°C. Absorbance at 450 nm was then assessed with an iMark microplate reader (Bio-Rad), with six wells per treatment group being analyzed.

Flow Cytometry

Cell cycle progression was assessed by fixing cells overnight with chilled 70% ethanol at 4°C. Cells were then washed in PBS and suspended in 415 ul of propidium iodide (PI, gene-protein link) for 30 min at 37°C while protected from light. A flow cytometer (BD Accuri C6, BD Biosciences, USA) was then used to assess the cells, with the resultant data being analyzed using ModFit LT. Cellular apoptosis was assessed with an Annexin V-AF647/PI kit (Gene-Protein Link) based on provided directions. Briefly, cells were washed twice with chilled PBS, resuspended in binding buffer, and $2x10^5$ cells in 100 ul were stained with 5μL of Annexin V-AF647. Samples were gently mixed for 5 min at room temperature, after which 10 uL of PI was added. Finally, 400 uL of PBS was added, and samples were assessed *via* flow cytometry.

Western Blotting

Nuclear proteins were isolated from cells with the NE-PER™ Nuclear and Cytoplasmic Extraction Reagents (Thermo Fisher), and a NanoDrop ONE instrument was used to quantify protein levels in each sample. Protein from ~$1x10^6$ appropriately treated cells was then extracted with 1x SDS loading buffer, and Western blotting was conducted as described previously (54). Briefly, equal protein amounts were separated *via* 10% or 15% SDS-PAGE and transferred onto PVDF membranes (0.22u m, Bio-rad), which were blocked for 1 h using 5% non-fat dry milk in Tris buffered saline (TBS) containing 0.05% tween-20 (TBST) (Solarbio Life Sciences, Beijing, China) at room temperature, followed by overnight incubation at 4°C with appropriate primary antibodies. Blots were then stained with secondary antibody (1:5000, ZSGB-BIO, ZB-2305, ZB-2301) for 1 h at room temperature, and ECL reagents (CWBIO) were used to detect protein bands. Anti-ASF1B was purchased from Santa Cruz Biotechnology (1:200, sc-393169), while anti-POLE3 was from Proteintech (1:2000, 15278-1-AP), and anti-CASP-3 was from Cell Signaling (1:1000, 9662).

Immunofluorescent Staining

H1975 Cells were added to glass coverslips in 6-well plates, fixed with 4% formaldehyde, permeabilized with 0.5% Triton X-100/PBS, blocked for 30 min with 5% Albumin Bovine V (BSA) at room temperature, and incubated overnight with anti-ASF1B (1:100, Santa Cruz Biotechnology, Inc. sc-393169.) at 4°C. Cells were then probed with a secondary fluorescently conjugated antibody (1:300,bs-0295G) for 2 h, followed by DAPI counterstaining (Solarbio Life Science), after which images were captured *via* inverted fluorescence microscopy (Nikon, Japan).

Proteomic Profiling

Proteomic analyses were performed as in prior reports (55). Briefly, following protein isolation and trypsin treatment, peptides were dissolved in water containing 0.1% formic acid in water and analyzed *via* liquid chromatography-tandem mass spectrometry (LC-MS/MS). Raw MS data were converted into a generic Mascot file using Proteome Discoverer (Thermo Scientific, v 2.0), and were processed with the Mascot search engine (Matrix Science, v.2.3.02).

IP-MS

Nuclear proteins were extracted from control and ASF1B-3x Flag-expressing A549 cells using the NE-PER™ Nuclear and Cytoplasmic Extraction Reagents to which protease and phosphatase inhibitors had been added. Supernatants were mixed for 2 h with anti-Flag at 4°C, after which they were mixed for 1 h with A/G agarose beads (Thermo Fisher Scientific) at 4°C. Protein complexes were then rinsed four times using NETN, one time with PBS, and separated *via* 10% SDS-PAGE. Coomassie blue was used to stain gels in order to visualize proteins, with gel lanes then being excised for in-gel tryptic digestion. Peptides were then extracted, concentrated, and analyzed *via* LC-MS/MS (EASY nLC 1200-Orbitrap Fusion Lumors+ETD, Thermo Fisher Scientific).

qRT-PCR

TRIzol (Invitrogen) was used to extract RNA from appropriate cells based on provided directions, after which SuperScript III First-strand (Thermo Fisher) was used to prepare cDNA. Primers used in Quantitative Real-time PCR (qPCR) assays are shown in **Table S1**. All qPCR reactions were conducted with SYBR Green Master Mix (Thermo Fisher) using the following conditions: 95°C for 5min; 40 cycles of 95°C for 30 s and 60°C for 1 min. β-actin served as a normalization control.

Statistical Analysis

Data were analyzed using R v 3.6.3. Wilcoxon tests were used to compare ASF1B expression levels in normal and tumor tissues, while Kruskal-Wallis tests were used to evaluate relationships between ASF1B expression and patient clinical stage. Kaplan-Meier curves were used to assess survival outcomes, and correlations were evaluated with Spearman's correlation coefficients. A two-sided $P < 0.05$ was the threshold of significance.

RESULTS

Assessment of ASF1B Expression in Cancer

We began by querying the GTEx and TCGA databases, revealing pronounced ASF1B upregulation in all cancers other than Acute Myeloid Leukemia (LAML) (**Figure 1A**), as further confirmed using Oncomine data (**Figure 1B**). We also found that ASF1B expression levels varied significantly among different clinical stages in patients with Adrenocortical carcinoma (ACC), Breast invasive carcinoma (BRCA), Colon adenocarcinoma (COAD), Kidney Chromophobe (KICH), Kidney renal clear

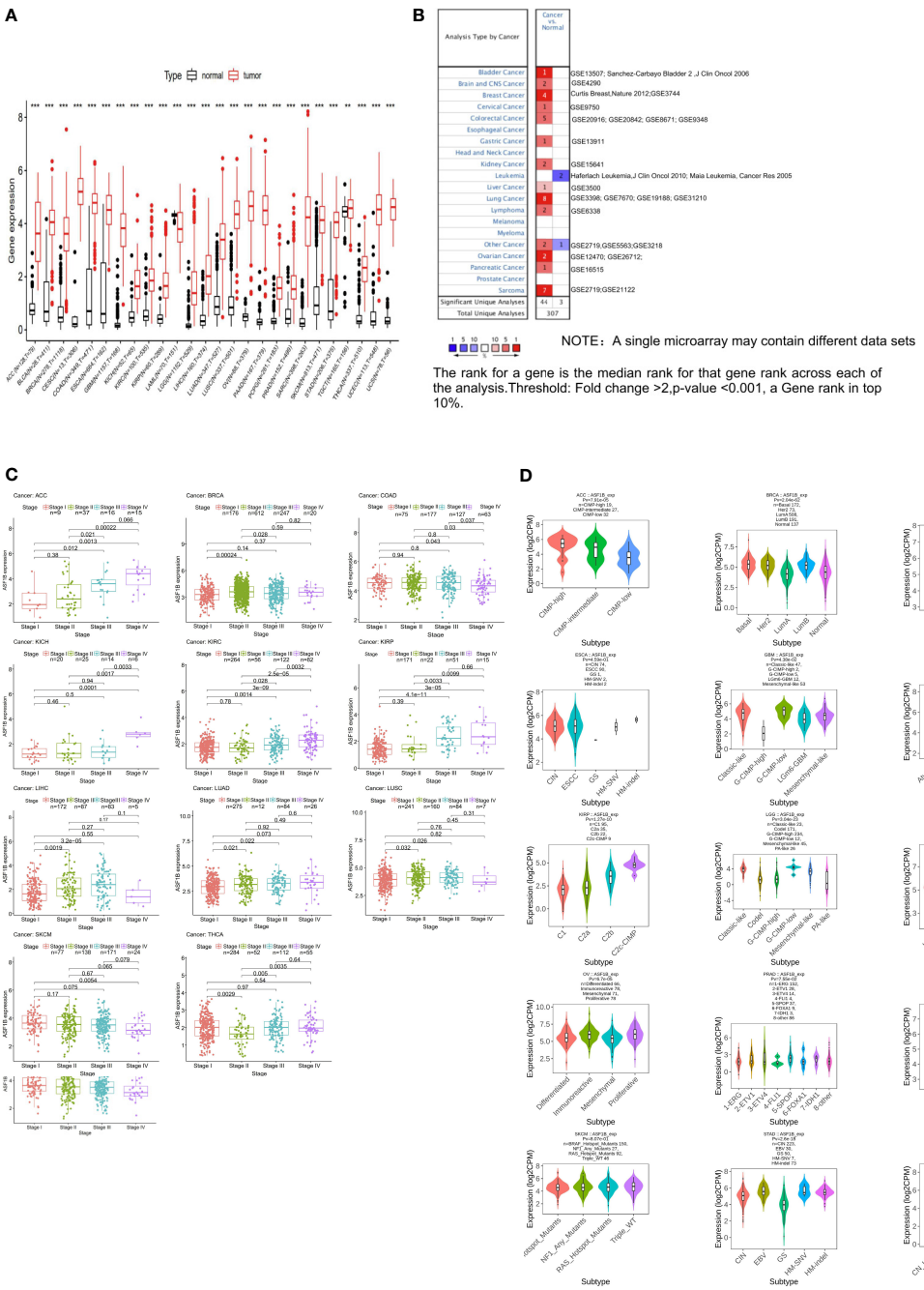


FIGURE 1 | The transcription levels of ASF1B in human cancers. **(A)** The mRNA expression of ASF1B between tumor and normal tissues was analyzed by using tissues from TCGA and GTEx. **(B)** The mRNA expression of ASF1B between tumor and normal tissues was analyzed by using tissues from Oncomine. **(C)** Correlations of ASF1B expression with different clinical stages in patients with different cancers from TCGA. **(D)** ASF1B expression in different molecular subtypes of cancers *via* TISIDB database (**p value ≤ 0.01; ***p value ≤ 0.001).

cell carcinoma (KIRC), Kidney renal papillary cell carcinoma (KIRP), Liver hepatocellular carcinoma (LIHC), LUAD, Lung squamous cell carcinoma (LUSC) and Skin Cutaneous Melanoma (SKCM) (**Figure 1C**). In addition, ASF1B expression in different molecular subtypes of ACC, BRCA, COAD, Esophageal carcinoma (ESCA), Glioblastoma multiforme (GBM), Head and Neck squamous cell carcinoma (HNSC), KIRP, Brain Lower Grade Glioma (LGG), LUSC, Ovarian serous cystadenocarcinoma (OV), Prostate adenocarcinoma (PRAD), Rectum adenocarcinoma (READ), SKCM, Stomach adenocarcinoma (STAD), Uterine Corpus Endometrial Carcinoma (UCEC) was significantly different (**Figure 1D**).

Evaluation of the Prognostic Relevance of ASF1B in Different Cancers

Next, we examined the prognostic relevance of ASF1B in different cancer types in order to determine whether it was consistently associated with particular cancer patient outcomes. Elevated ASF1B expression was linked to poorer OS in ACC, KIRC, KIRP, LGG, LIHC, LUAD, Mesothelioma (MESO), and Pancreatic adenocarcinoma (PAAD), whereas it was associated with better OS in Cervical squamous cell carcinoma and endocervical adenocarcinoma (CESC), STAD, and Thymoma (THYM) patients (**Figure 2A**). Subsequent GSE31210, GSE62254 and ICGC_ARRAY datasets analysis supported results of LUAD、PAAD and STAD (**Figure 2B**).

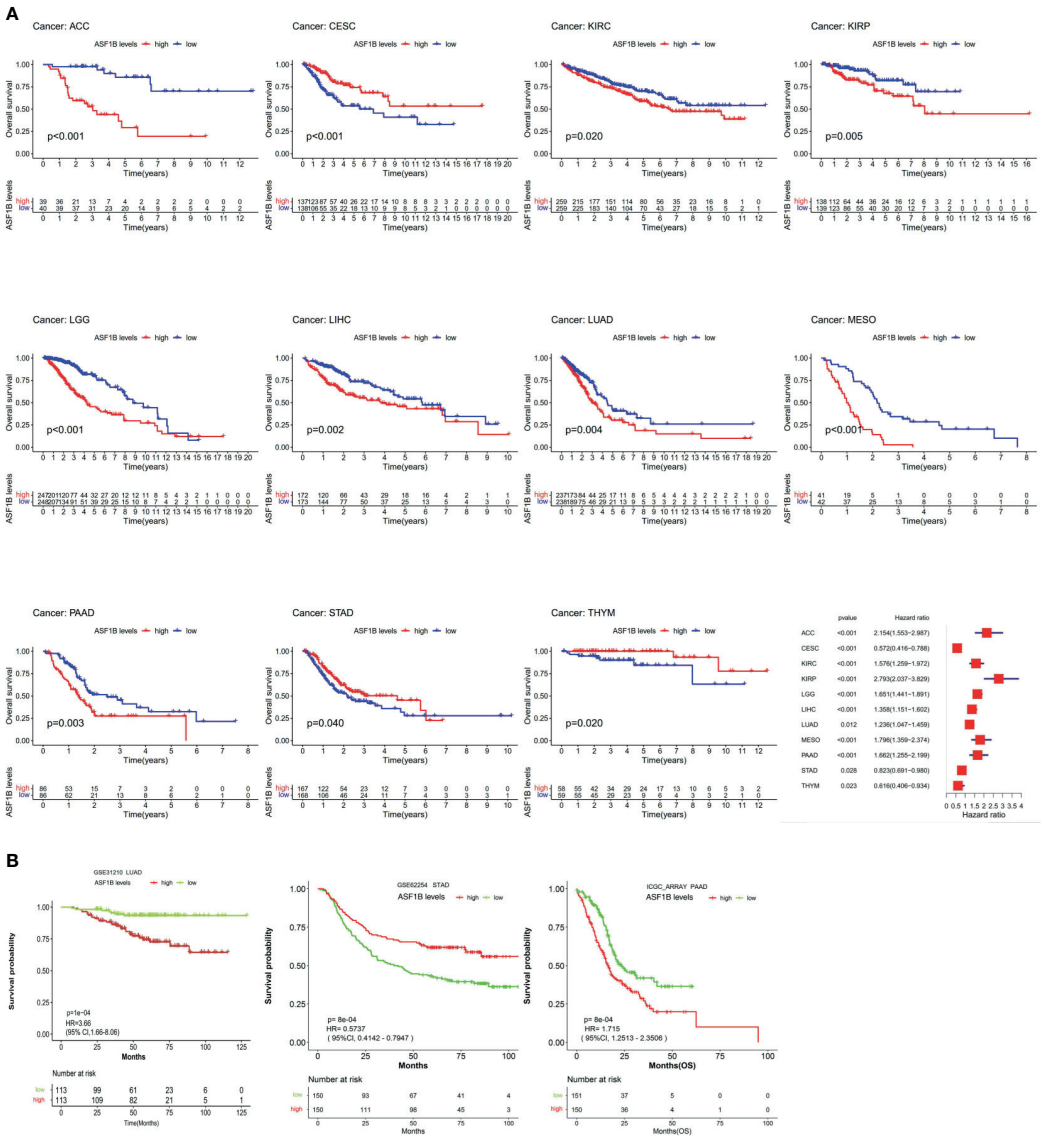


FIGURE 2 | The association between ASF1B expression and cancer patient prognosis. **(A)** The correlation between ASF1B expression and the prognosis of various cancer types were evaluated by The TCGA database. **(B)** The Relationship between ASF1B expression and the prognosis of various cancer types were analyzed.

Assessment of the Association Between ASF1B Expression and Methylation, MSI, TMB, and Genetic Alteration Status in Different Cancers

We next sought to explore whether ASF1B expression patterns and prognostic relevance were related to patterns of DNA methylation in different cancer types. A negative association between ASF1B expression levels and DNA methylation were observed in ACC, Bladder Urothelial Carcinoma (BLCA), CESC, COAD, LGG, LIHC, LUSC, MESO, PAAD, READ, PRAD, Sarcoma (SARC), SKCM, STAD, Testicular Germ Cell Tumors (TGCT), Thyroid carcinoma (THCA), and UCEC (P<0.05) (**Figure 3A**). When we further evaluated methylated sites associated with prognostic

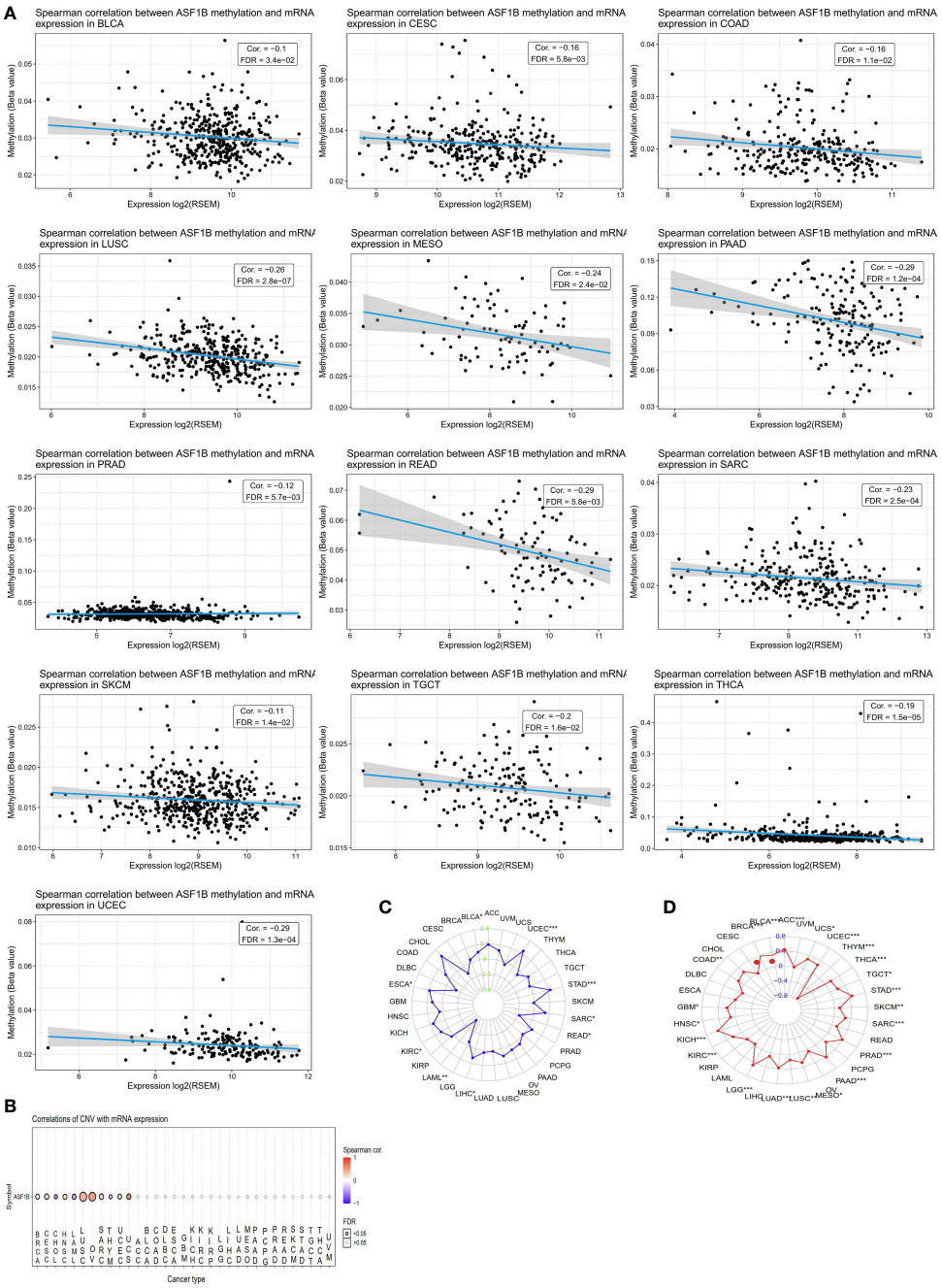


FIGURE 3 | CNV, DNA methylation, MSI and TMB of ASF1B in human cancers. **(A)** The relationship between methylation and ASF1B expression. DNA methylation beta values ranging from 0(unmethylated) to 1(fully methylated). **(B)** Correlations of CNV and ASF1B expression. **(C)** Correlations of TMB and ASF1B expression. **(D)** Correlations of MSI and ASF1B expression. *p value ≤0.05; **p≤0.01; *** p value ≤0.001.

outcomes in different cancers, we found that cg2527424, cg26259181, cg25274248, cg06391548, and cg26259181 were related to poorer survival in KIRP, LGG, LIHC, STAD, and LUAD (P<0.05), respectively (**Supplementary Figure 1**). To assess the degree of variability in ASF1B expression attributable to CNVs we additionally conducted correlation analyses revealing a positive association between ASF1B expression and CNVs in BRCA, CESC, HNSC, LUSC, OV, SARC, UCEC, and Uterine Carcinosarcoma (UCS), whereas this correlation was negative in ACC, LAML, and THYM (P<0.05) (**Figure 3B**). MSI referred to the spontaneous loss or gain of nucleotides from short tandem repeat DNA tracts (56), and we thus examined correlations between ASF1B expression and MSI status, indicating a positive association between these variables in BLCA, UCEC, STAD, SARC, LIHC, KIRC, and ESCA, whereas they were negatively correlated in READ, and LAML (P<0.05) (**Figure 3C**). TMB is emerging as a profound biomarker for predicting immunotherapy effect and is calculated as total amount of mutations per DNA megabases, in which the detected variants are defined as insertions, base substitutions, or deletions across bases (57). We also assessed the relationship between TMB and ASF1B expression, revealing them to be positively correlated in ACC, BLCA, BRCA, COAD, GBM, HNSC, KICH, KIRC, LGG, LUAD, LUSC, MESO, PAAD, PRAD, SARC, STAD, TGCT, THCA, UCEC, and UCS, but negatively correlated with THYM (P<0.05) (**Figure 3D**). As such, aberrant ASF1B expression and associated prognostic relevance in different cancers may be partially attributable to the above mechanisms.

The Association Between ASF1B Expression and Immune Cell Infiltration

Next, we employed the CIBERSORT algorithm to assess relationships between immune cell infiltration and ASF1B expression in tumor and normal tissue samples. GEO and TCGA results revealed ASF1B expression to be positively correlated with levels of M1 and M0 macrophages as well as with levels of activated memory CD4+ T cells, whereas it was negatively correlated with resting memory CD4+ T cells and resting Mast cells in LUAD (**Figures 4A, B**). In lung tissue samples from the GTEx database, ASF1B expression was

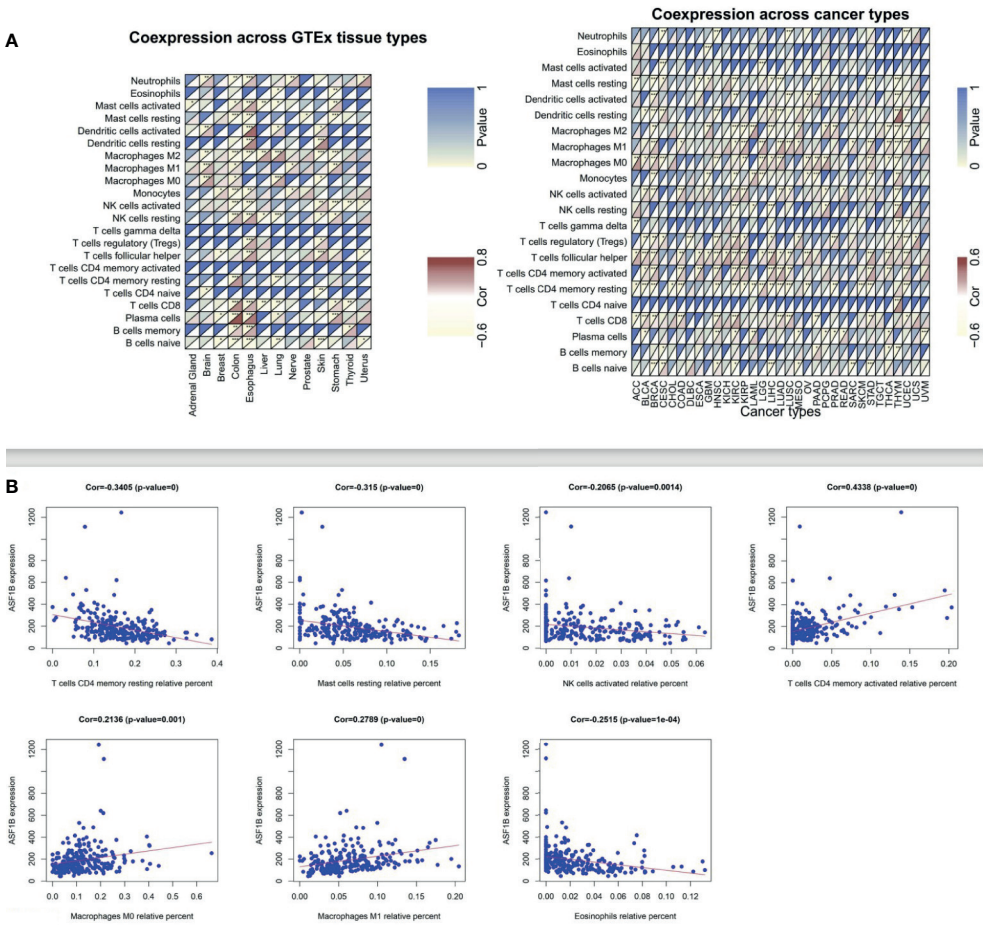


FIGURE 4 | Correlation analysis between ASF1B and tumor-infiltrating immune cell. **(A)** Correlation analysis of ASF1B mRNA expression with 22 types of immune cells were explored across cancers and normal tissues from TCGA and GTEx by CIBERSORT. **(B)** Correlation analysis of ASF1B mRNA expression with immune cells were further investigated in LUAD from GEO by CIBERSORT. *p value ≤0.05; **p≤0.01; *** p value ≤0.001.

positively correlated with resting memory CD4+ T cells and negatively correlated with M0 macrophages. When we expanded these results to other tumors and normal tissue types, we found ASF1B to be unrelated to gamma delta T cell or activated memory CD4+ T cell infiltration in normal tissues, and it was similarly unrelated to naïve CD4+ T cell infiltration in analyzed cancers. ASF1B was associated with M2 macrophages in 7 cancers, resting Mast cells and activated NK cells in 6 cancers, M0 and M1 macrophages in 7 cancers, T follicular helper cells in 11 cancers, and resting memory CD4+ T cells in 10 cancers. ASF1B was also associated with resting Mast cells, neutrophils, activated Mast cells, B cells, CD8+ T cells, and naïve CD8+ T cells in 5 normal tissues, M0 macrophages in 3 normal tissues, plasma cells and M1 macrophages in 4 normal tissues, and activated NK cells and M2 macrophages in 6 normal tissues (**Figure 4A**). Through molecular immune subtyping, we further observe significant differences in ASF1B expression levels across C1(wound healing), C1(IFN-γ dominant), C3(inflammatory), C4 (lymphocyte deplete), C5(immunologically quiet), and C6 (TGF-β dominant) subtypes for most analyzed cancers (**Supplementary Figure 2**).

Examination of Pathways Significantly Associated With ASF1B

To more fully explore the functional roles of ASF1B, we conducted a KEGG GSEA assessment across tumor and normal tissue types, with the resultant heatmap exhibiting a clear clustering pattern (P<0.05, NES>1, NES<-1). Immune-related pathways were highly enriched in normal tissues, with ASF1B being significantly related to JAK/STAT signaling in 7 normal tissues, cytosolic DNA sensing and RIG-I-like receptor signaling in 9 normal tissues, cytokine-cytokine receptor interactions in 5 normal tissues, antigen processing and presentation in 4 normal tissues, autophagy regulation in 10 normal tissues, and the cell cycle and oocyte meiosis in 4 normal tissues (**Figure 5A**). In pan-cancer analyses, ASF1B was significantly associated with Toll-like receptor signaling in 11 cancers, NK cell-mediated cytotoxicity in 14 cancers, chemokine signaling in 10 cancers, JAK/STAT signaling in 3 cancers, Cytosolic DNA sensing in 20 cancers, cytokine-cytokine receptor interactions in 9 cancers, antigen processing and presentation in 19 cancers, autophagy regulation in 20 cancers, the cell cycle in 21 cancers, cell adhesion molecules

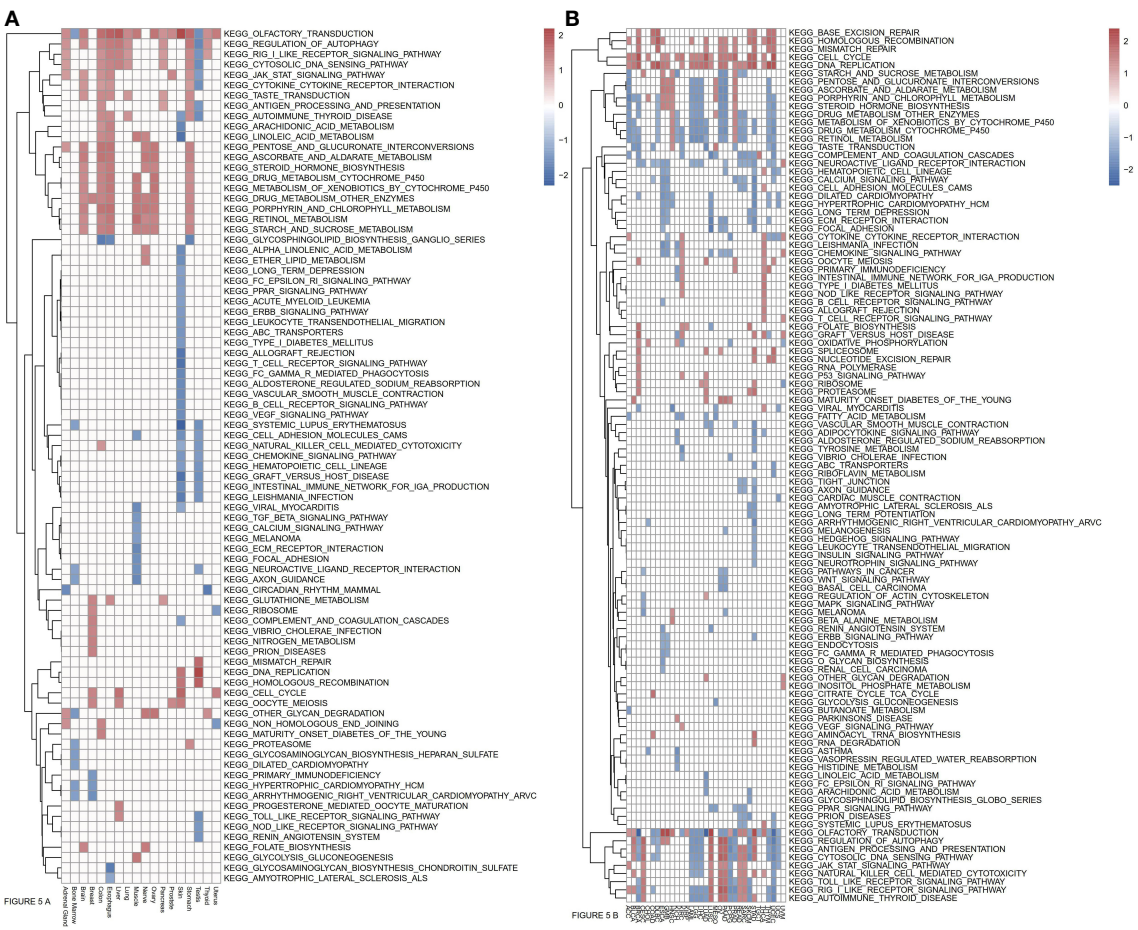


FIGURE 5 | **(A)** Relationships between ASF1B and KEEG pathways in normal tissues from GTEx analyzed by GSEA. **(B)** Relationships between ASF1B and KEEG pathways in cancers from TCGA analyzed by GSEA. (NES≥1.0, p-value<0.05).

in 6 cancers, DNA replication in 22 cancers, vascular smooth muscle contraction in 4 cancers, homologous recombination in 15 cancers, mismatch repair in 8 cancers, and ECM receptor interaction in 8 cancers. We further identified four pathways that were only evident in different cancers, with ASF1B being significantly involved in the regulation of base excision repair in 7 cancers, pathways in cancer in 3 cancers, P53 signaling pathway in 3 cancers, and the spliceosome in 5 cancers (**Figure 5B**).

ASF1B Regulates Lung Cancer Cell Line Phenotypes

Next, we measured ASF1B expression levels in different LUAD cell lines (A549, NCI-H1975, NCI-H1299, NCI-H1650) using data from the Cancer Cell Line Encyclopedia (CCLE) database, revealing that these levels ranged from low (A549 cells) to very high (H1650 cells) (**Supplementary Figure 3**). To understand the functional role of this gene in LUAD, we knocked it down in H1975 and H1650 cells and overexpressed it in two other cell lines. The efficiency of ASF1B knockdown was assessed using four different siRNA constructs, with subsequent Western blotting revealing siRNA-4 to be the most effective in H1975 cells (**Supplementary Figure 4**). Lentiviral vectors were then used to generate stable cell lines (**Figure 6**).

In CCK-8 assays, ASF1B knockdown markedly impaired H1975 and H1650 cell viability relative to scramble controls ($P<0.05$) (**Figure 7A**). Consistently, in an EdU uptake assay these ASF1B-knockdown cells exhibited impaired proliferation ($P<0.05$) (**Figures 7B, C**). Flow cytometric analyses additionally indicated that such knockdown was associated with a significant increase in the percentage of cells in the S phase only in H1650 cells ($P<0.05$) and with a significant reduction in the frequency of cells in the G1 phase ($P<0.05$) relative to scramble control in H1650 and H1975 cells (**Figure 8**).

In addition, ASF1B knockdown was linked to an increase in apoptotic cell death as measured *via* flow cytometry (**Figure 9A**). To confirm that ASF1B is associated with apoptosis in LUAD cells, we analyzed caspase-3 levels therein, revealing a significant increase in caspase-3 levels in H1975 and H1650 cells following ASF1B knockdown (**Figure 9B**). Overall, these findings indicated that ASF1B downregulation can inhibit proliferation, modulate

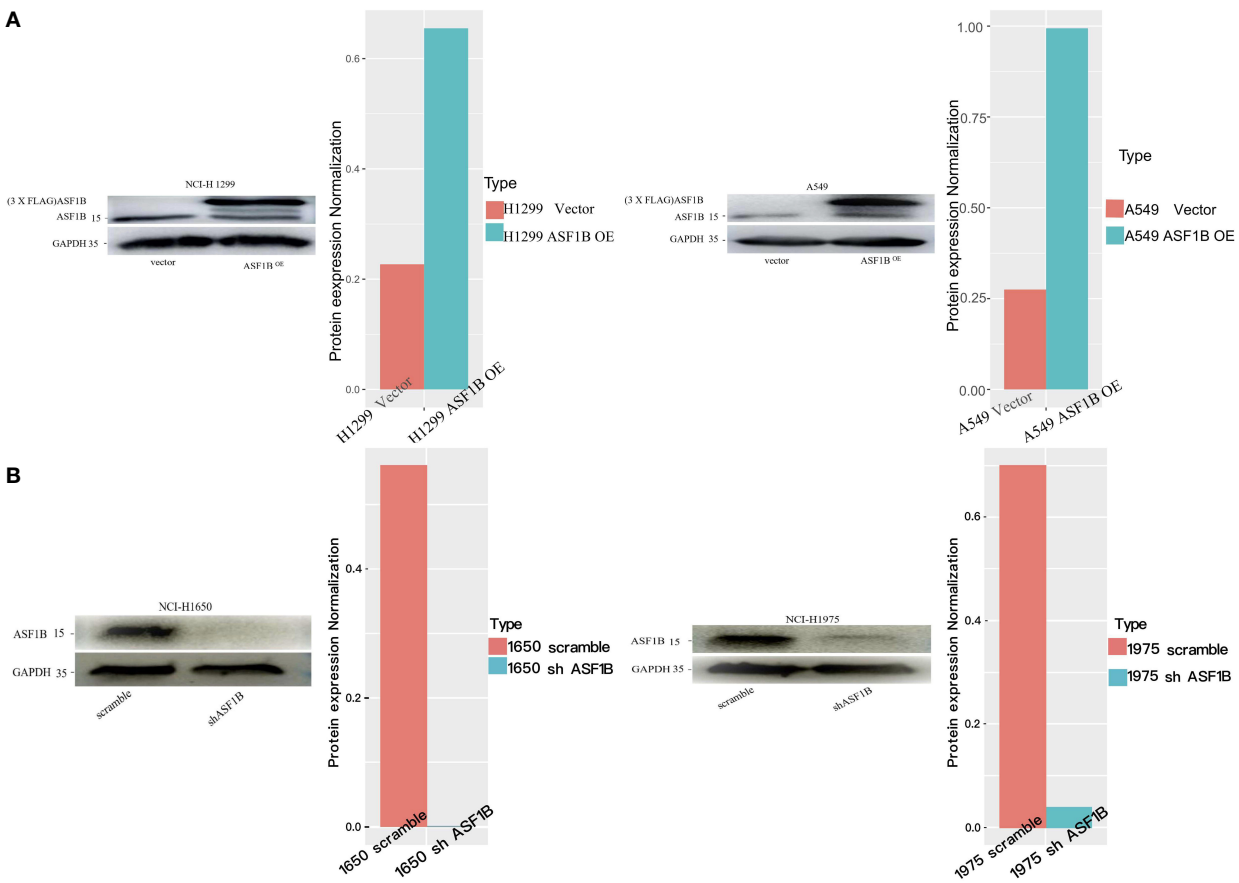


FIGURE 6 | Knockdown or overexpression of ASF1B in LUAD cell lines. **(A)** ASF1B protein expression in stable ASF1B-OE cells. Western blot detecting higher ASF1B protein levels in stable ASF1B-OE-H1299 or ASF1B-OE-A549 cells than those in control cells. The density levels were quantified and represented as a bar graph. **(B)** ASF1B protein expression in stable ASF1B-shRNA-cells. Western blot detecting lower ASF1B protein levels in stable ASF1B-shRNA-H1975 or ASF1B-shRNA-H1650 cells than those in control cells.

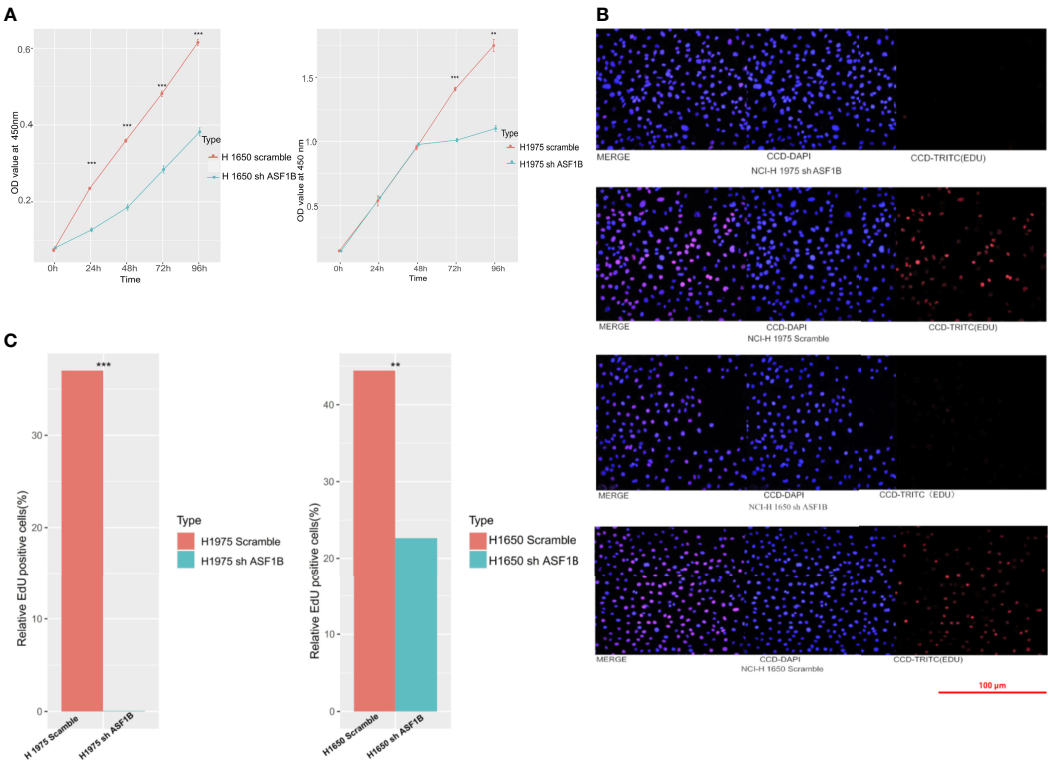


FIGURE 7 | **(A)** Cell viability assay of H1975 and H1650 cells. **(B)** Cell proliferation assay of H1975 and H1650 cells. **(C)** Accumulated analysis of the cell proliferation. **p vaule ≤0.01; ***p vaule ≤0.001.

cell cycle progression, and promote apoptosis. In lung cancer cells. ASF1B overexpression did not affect these processes (data not shown).

Proteomic Profiling-Based Identification of ASF1B Downstream Signaling Target Proteins

To explore the downstream mechanisms whereby ASF1B may influence the above pathways, an LC-MS analysis was conducted to screen for ASF1B target proteins in four cell lines (**Figure 10**). A total of 58 proteins were co-regulated by ASF1B after the LC-MS were intersected (**Supplementary Figure 5**). Further study found POLE3, CKS1B, DHFR, ribosomal protein S29(RPS29), and transmembrane protein 230 (TMEM230) were affected by different biological background of cell lines (**Supplementary Table 1**). To confirm these results, we conducted Western blotting analyses of ASF1B-shRNA-H1975 and scrambled cells, revealing significant decreases in POLE3 expression consistent with these proteomic results (**Supplementary Figure 6**). ASFB1 expression was also associated with POLE3, CKS1B, and DHFR expression in most normal tissues and in many cancers including LUAD ($R>0.4$, $p<0.05$) (**Supplementary Figure 7**).

Immunofluorescent staining revealed ASF1B and POLE3 to localize to the nucleus, while CKS1B was present in the nucleus and cytoplasm (**Supplementary Figure 8**). We thus conducted an IP-MS experiment, which failed to reveal direct interaction between ASF1B and POLE3 or CKS1B (**Supplementary Figure 9**).

When we examined CKS1B expression in LUAD samples in the TCGA dataset, we found it was an independent predictor of poor LUAD patient prognosis and correlated with patient age, gender, T, N, M, and clinical stage (**Supplementary Figure 10**). POLE3 was unrelated to LUAD patient prognosis or clinicopathological parameters in LUAD. Therefore, we detected the mRNA expression of CKS1B in stable knockdown ASF1B cells and scramble cells. ASF1B knockdown reduced CKS1B mRNA expression, indicating ASF1B regulate CKS1B independent of post-transcriptional regulation (**Supplementary Figure 11**).

DISCUSSION

Herein, we examined the expression and prognostic relevance of ASF1B across many cancer types. In a TCGA analysis, we observed TCGA upregulation in 25 cancers other than LAML relative to corresponding normal tissue samples. Oncomine results were largely consistent with the results of these analyses. Many genes play different roles in different cancers (58–60), thus explaining the variable prognostic significance of ASF1B observed among cancer types and subtypes. Such tumor heterogeneity is a significant barrier to reliable tumor treatment

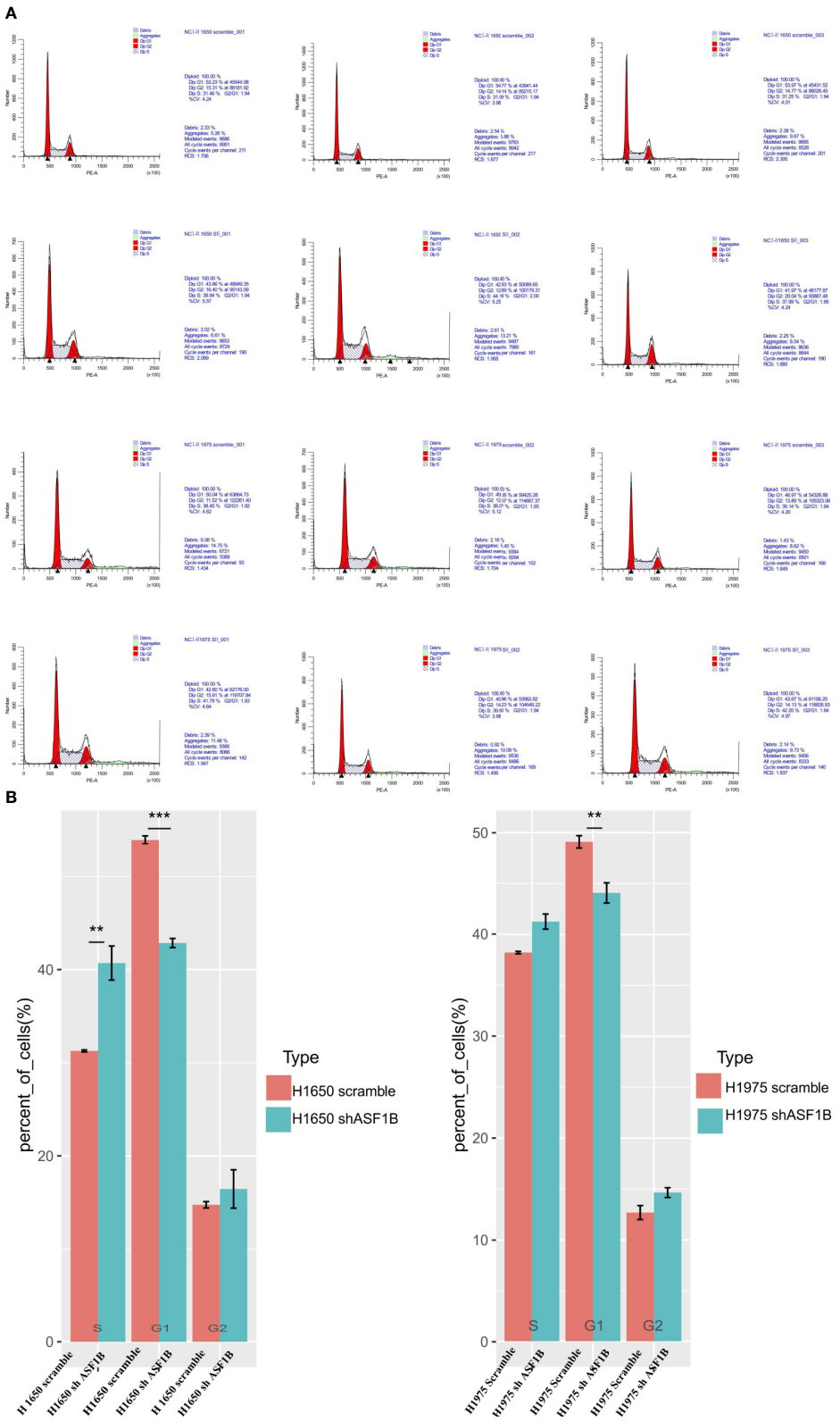


FIGURE 8 | ASF1B knockdown influence the cell cycle. **(A)** Flow cytometry was used to detect the cell cycle changes in H1975 and H1650. **(B)** Accumulated analysis of the cell cycle. **p vaule ≤0.01; ***p vaule ≤0.001.

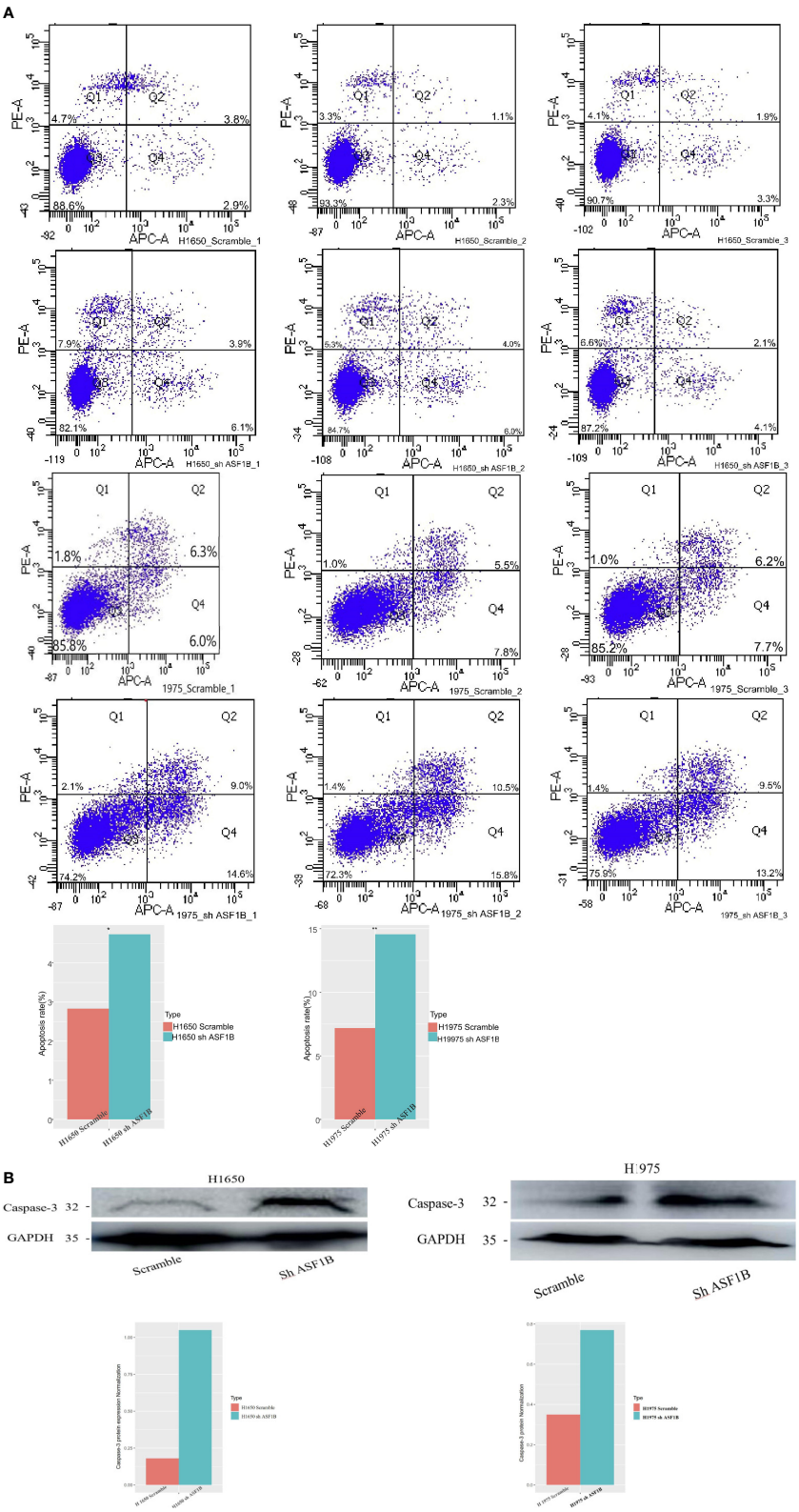


FIGURE 9 | **(A)** Flow cytometry was used to detect the early apoptosis changes in H1975 and H1650. **(B)** Western blot was used to detect the protein levels of apoptosis-3 in H1650 and H1975 cells treated with knockout-ASF1B and untreated control cells. *p vaule ≤0.05; **p vaule ≤0.01.

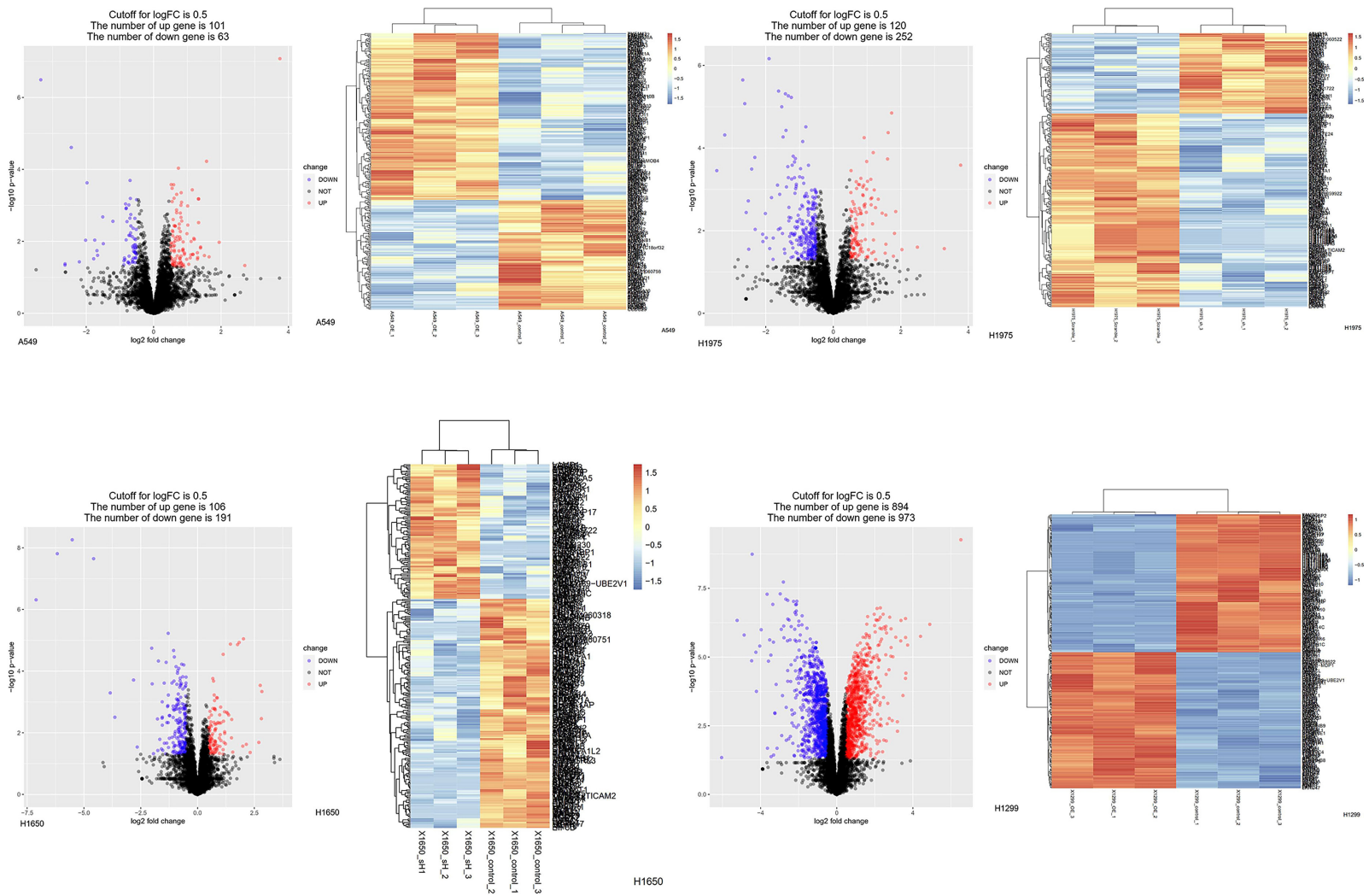


FIGURE 10 | Protein changes of LUAD cell lines induced by knockdown or overexpressed of ASF1B. Differentially expressed proteins in stable transfection cell lines compared to negative control. (Volcano plot) Red presents up-regulated proteins, blue represents down-regulated proteins, and black presents no significantly differentially expressed proteins. (Heatmap) The expression patterns of these differentially expressed proteins can distinguish between stable transfection cell lines and negative control.

(61–63). The onset and progression of cancer can be profoundly impacted by genetic and epigenetic changes, MSI, and TMB, and many of these mechanisms were correlated with ASF1B expression levels in different cancers in the present analysis.

In enrichment analyses, we found ASF1B was primarily associated with immune-, proliferation-, and autophagy-related pathways, some of which were enriched in both normal tissues and cancers although the associated genes differed. As such, we hypothesized that ASF1B may regulate immune cell infiltration by influencing genes in immune-related pathways.

We observed a close relationship between ASF1B and proliferation-related pathways including DNA replication and the cell cycle in LUAD. Our experimental results further confirmed that knocking down ASF1B impaired proliferation, altered cell cycle progression, and induced cell apoptosis in LUAD cells. In contrast, no impact of ASF1B overexpression was observed, possible because A549 and H1299 cells grow rapidly, and thus ASF1B overexpression may not further enhance their proliferation. The mechanisms whereby ASF1B can shape tumorigenesis remain poorly understood. Herein, we determined that in LUAD cells, ASF1B can indirectly regulate CKS1B, POLE3, and DHFR expression, and we found it positively correlated with the expression of these genes in most tumor and normal tissue samples. This indicates that ASF1B regulates cancer progression through these signaling pathways.

Notably, CKS1B is a CKS family protein that regulates cell cycle progression, growth, apoptosis, invasion metastasis, and chemical resistance in a range of cancer types (64–72). Wang et al. found that overexpression of CKS1B achieved in lung cancer cells through lentiviral infection enhanced drug resistance by inhibiting cisplatin (CDDP)- and doxorubicin (DOX)-induced apoptosis, supporting the critical role of CKS1B in lung cancer progression (73). A study has shown that CKS1B overexpression promoted drug resistance in myeloma. Moreover, research has demonstrated that CKS1B induces resistance to ubiquitin-like protein synthesis inhibitors such as bortezomib by inhibiting expression of the S-Phase Kinase Associated Protein 2/KIT Ligand (SCF/SKP2) substrate p21 (74, 75). DHFR is a ubiquitous enzyme and exists in a wide range of organisms (76). DHFR, a key enzyme in folate metabolism, converts dihydrofolate into tetrahydrofolate. It is well known that Pemetrexed and Methotrexate inhibits DHFR in the folate pathway, which is essential for the rapid cellular division and proliferation of cancer cells (77). Hence, the inhibition of DHFR can limit the growth and proliferation of cells. POLE3 is known subunits of DNA polymerase epsilon and more recently has been shown to form a newly identified histone H3-H4 chaperone complex that participates in the maintenance of chromatin integrity during DNA replication (78). Su et al. observed that POLE3-deficient cells displayed enhanced sensitivity to a Poly (ADP-Ribose) Polymerase (PA RP) inhibitor, an ATR inhibitor, and camptothecin (79, 80). Interestingly, above data demonstrated that targeting ASF1B may be an important method for cancer treatment. However, there are some limits. The detailed molecular mechanisms underlying the regulation of those key proteins by ASF1B need further explored in LUAD and other cancers. Nude mouse tumor formation experiment is also performed. Underlying mechanisms of immune infiltrate ion signaling pathways remain unclear, while function annotations and enrichment analysis of ASF1B are investigated.

In summary, we herein outlined the critical role played by ASF1B in LUAD cells, providing novel insight into its role as a regulator of cellular proliferation, cell cycle progression, and apoptotic induction. These data provide a more general framework for future studies of ASF1B in other cancer types and indicate that this protein may represent a viable therapeutic target in LUAD and other cancer types in the future.

DATA AVAILABILITY STATEMENT

The original contributions presented in the study are included in the article/**Supplementary Material**. Further inquiries can be directed to the corresponding author.

AUTHOR CONTRIBUTIONS

WC: also performs experimental operations. WZ: Analyzing data and writing manuscript. ZG, MG, and NL: Load raw data. GW: Concept and revised the manuscript. FJ: analyzing experiment data. All authors contributed to the article and approved the submitted version.

FUNDING

This study was funded by Wu Jieping Medical Foundation (320.6750.19 089-55) and by Tianjin Health Science and Technology Project (ZC20125).

SUPPLEMENTARY MATERIAL

The Supplementary Material for this article can be found online at: https://www.frontiersin.org/articles/10.3389/fonc.2021.731547/full#supplementary-material

Supplementary Figure 1 | CPG site correlated with prognosis of different cancers.

Supplementary Figure 2 | ASF1B mRNA expression in different immune subtypes in most cancers via TISIDB.

Supplementary Figure 3 | The mRNA expression of ASF1B in four cell lines were analyzed by using CCLE database.

Supplementary Figure 4 | SiRNA interference sequences were screened in the protein level.

Supplementary Figure 5 | The density levels were quantified and represented as a bar graph.

Supplementary Figure 6 | Western blot analysis of POLE3 in H1975 cells treated with knockdown-ASF1B and untreated controls cells. The density levels were quantified and represented as a bar graph.

Supplementary Figure 7 | Association ASF1B with CKS1B, POLE3 and DHFR in pan-cancers and normal tissues.

Supplementary Figure 8 | ASF1B is co-localized with CKS1B and POLE3 in cell nucleus.

Supplementary Figure 9 | Immunoprecipitation Mass spectrometry of A549 cell line induced by overexpressed of ASF1B. Differentially expressed proteins in stable ASF1B-OE cells compared to negative control. (Volcano plot) Red presents up-regulated proteins, blue represents down-regulated proteins, and black presents no significantly differentially expressed proteins. (Heatmap) The expression patterns of these differentially expressed proteins can distinguish between stable ASF1B-OE cell line and negative control.

Supplementary Figure 10 | CKS1B correlated with prognosis and clinicopathology.

Supplementary Figure 11 | Real-time PCR analysis of mRNA expression of ASF1B in H1975 Scramble cell lines compared to H1975 SH ASF1B cell lines.

Supplementary Table 1 | The results of LC-MS from four group cell lines were intersected(Log FC).

REFERENCES

1. Siegel RL, Miller KD, Jemal A. Cancer Statistics, 2018. *CA Cancer J Clin* (2018) 68(1):7–30. doi: 10.3322/caac.21442
2. Travis WD, Brambilla E, Noguchi M, Nicholson AG, Geisinger K, Yatabe Y, et al. International Association for the Study of Lung Cancer/American Thoracic Society/European Respiratory Society: International Multidisciplinary Classification of Lung Adenocarcinoma: Executive Summary. *Proc Am Thorac Soc* (2011) 8(5):381–5. doi: 10.1513/pats.201107-042ST
3. Yuan M, Huang LL, Chen JH, Wu J, Xu Q. The Emerging Treatment Landscape of Targeted Therapy in Non-Small-Cell Lung Cancer. *Signal Transduct Target Ther* (2019) 4:61. doi: 10.1038/s41392-019-0099-9
4. Liu WB, Wu JF, Du Y, Cao GW. Cancer Evolution-Development: Experience of Hepatitis B Virus-Induced Hepatocarcinogenesis. *Curr Oncol* (2016) 23(1): e49–56. doi: 10.3747/co.23.2836
5. Gatenby RA, Brown J. Mutations, Evolution and the Central Role of a Self-Defined Fitness Function in the Initiation and Progression of Cancer. *Biochim Biophys Acta Rev Cancer* (2017) 1867(2):162–6. doi: 10.1016/j.bbcan.2017.03.005
6. Abascal F, Corpet A, Gurard-Levin ZA, Juan D, Ochsenbein F, Rico D, et al. Subfunctionalization via Adaptive Evolution Influenced by Genomic Context: The Case of Histone Chaperones ASF1a and ASF1b. *Mol Biol Evol* (2013) 30 (8):1853–66. doi: 10.1093/molbev/mst086
7. Hattori N, Ushijima T. Compendium of Aberrant DNA Methylation and Histone Modifications in Cancer. *Biochem Biophys Res Commun* (2014) 455 (1-2):3–9. doi: 10.1016/j.bbrc.2014.08.140
8. Meng CF, Zhu XJ, Peng G, Dai DQ. Promoter Histone H3 Lysine 9 Di-Methylation is Associated With DNA Methylation and Aberrant Expression of P16 in Gastric Cancer Cells. *Oncol Rep* (2009) 22(5):1221–7. doi: 10.3892/or_00000558
9. Gurard-Levin ZA, Quivy JP, Almouzni G. Histone Chaperones: Assisting Histone Traffic and Nucle Osome Dynamics. *Annu Rev Biochem* (2014) 83:487–517. doi: 10.1146/annurev-biochem-060713-035536
10. Gurard-Levin ZA, Almouzni G. Histone Modifications and a Choice of Variant: A Language That Helps the Genome Express Itself. *F1000Prime Rep* (2014) 6:76. doi: 10.12703/P6-76
11. Avvakumov N, Nourani A, Cote J. Histone Chaperones: Modulators of Chromatin Marks. *Mol Cell* (2011) 41(5):502–14. doi: 10.1016/j.molcel.2011.02.013
12. Peng H, Nogueira ML, Vogel JL, Kristie TM. Transcriptional Coactivator HCF-1 Couples the Histone Chaperone Asf1b to HSV-1 DNA Replication Components. *Proc Natl Acad Sci USA* (2010) 107(6):2461–6. doi: 10.1073/pnas.0911128107
13. Messiaen S, Guiard J, Aigueperse C, Fliniaux I, Tourpin S, Barroca V, et al. Loss of the Histone Chaperone ASF1B Reduces Female Reproductive Capacity in Mice. *Reproduction* (2016) 151(5):477–89. doi: 10.1530/REP-15-0327
14. Paul PK, Rabaglia ME, Wang CY, Stapleton DS, Leng N, Kendziorski C, et al. Histone Chaperone ASF1B Promotes Human Beta-Cell Proliferation via Recruitment of Histone H3.3. *Cell Cycle* (2016) 15(23):3191–202. doi: 10.1080/15384101.2016.1241914
15. Feng Z, Zhang J, Zheng Y, Wang QZ, Tian TS. Elevated Expression of ASF1B Correlates With Poor Prognosis in Human Lung Adenocarcinoma. *Personalized Med* (2021) 18(12):115–27. doi: 10.2217/pme-2020-0112
16. Corpet A, De Koning L, Toedling J, Savignoni A, Berger F, Lemaitre C, et al. Asf1b, the Neces Sary Asf1 Isoform for Proliferation, is Predictive of Outcome in Breast Cancer. *EMBO J* (2011) 30(3):480–93. doi: 10.1038/emboj.2010.335
17. Han G, Zhang X, Liu P, Yu Q, Li Z, Yu Q, et al. Knockdown of Anti-Silencing Function 1B Histo Ne Chaperone Induces Cell Apoptosis via Repressing PI3K/Akt Pathway in Prostate Cancer. *Int J Oncol* (2018) 53(5):2056–66. doi: 10.3892/ijo.2018.4526
18. Liu X, Song J, Zhang Y, Wang H, Sun H, Feng X, et al. ASF1B Promotes Cervical Cancer Progre Ssion Through Stabilization of CDK9. *Cell Death Dis* (2020) 11(8):705. doi: 10.1038/s41419-020-02872-5
19. Jiangqiao Z, Tao Q, Zhongbao C, Xiaoxiong M, Long Z, Jilin Z, et al. Anti-Silencing Function 1B Histone Chaperone Promotes Cell Proliferation and Migration via Activation of the AKT Pathway in Clear Cell Renal Cell Carcinoma. *Biochem Biophys Res Commun* (2019) 511(1):165–72. doi: 10.1016/j.bbrc.2019.02.060
20. Goldman MJ, Craft B, Hastie M, Repeka K, Mcdade F, Kamath A, et al. Visualizing and Interpreting Cancer Genomics Data via the Xena Platform. *Nat Biotechnol* (2020) 38:675–8. doi: 10.1038/s41587-020-0546-8
21. Goldman LJ, Craft HM. The Genotype-Tissue Expression (GTEx) Project. *Biopreserv Biobank* (2015) 13(5):307–8. doi: 10.1089/bio.2015.29031.hmm
22. Alimonti A, Carracedo A, Clohessy JG, Trotman LC, Nardella C, Egia A, et al. Subtle Variations in Pten Dose Determine Cancer Susceptibility. *Nat Genet* (2010) 42(5):454–8. doi: 10.1038/ng.556
23. Chen CH, Lai JM, Chou TY, Chen CY, Su LJ, Lee YC, et al. VEGFA Upregulates FLJ10540 and Modulates Migration and Invasion of Lung Cancer via PI3K/AKT Pathway. *PLoS One* (2009) 4(4):e5052. doi: 10.1371/journal.pone.0005052
24. Chen X, Higgins J, Cheung ST, Li R, Mason V, Montgomery K, et al. Novel Endothelial Cell Markers in Hepatocellular Carcinoma. *Mod Pathol* (2004) 17 (10):1198–210. doi: 10.1038/modpathol.3800167
25. Crescenzo R, Abate F, Lasorsa E, Tabbo F, Gaudiano M, Chiesa N, et al. Convergent Mutations and Kinase Fusions Lead to Oncogenic STAT3 Activation in Anaplastic Large Cell Lymphoma. *Cancer Cell* (2015) 27 (4):516–32. doi: 10.1016/j.ccell.2015.03.006
26. Crescenzo R, Lee J, Nebozhyn M, Kim KM, Ting JC, Wong SS, et al. Molecular Analysis of Gastric Cancer Identifies Subtypes Associated With Distinct Clinical Outco Mes. *Nat Med* (2015) 21(5):449–56. doi: 10.1038/nm.3850
27. Curtis C, Shah SP, Chin SF, Turashvili G, Rueda OM, Dunning MJ, et al. The Genomic and Transcriptomic Architecture of 2,000 Breast Tumours Reveals Novel Subgroups. *Nature* (2012) 486(7403):346–52. doi: 10.1038/nature10983
28. D'Errico M, de Rinaldis E, Blasi MF, Viti V, Falchetti M, Calcagnile A, et al. Genome-Wide Expression Profile of Sporadic Gastric Cancers with Microsatellite Instability. *Eur J Cancer* (2009) 45(3):461–9. doi: 10.1016/j.ejca.2008.10.032
29. Garber ME, Troyanskaya OG, Schluens K, Petersen S, Thaesler Z, Pacyna-Gengelbach M, et al. Diversity of Gene Expression in Adenocarcinoma of the Lung. *Proc Natl Acad Sci USA* (2001) 98(24):13784–9. doi: 10.1073/pnas.241500798
30. Haferlach T, Kohlmann A, Wieczorek L, Basso G, Kronnie GT, Bene MC, et al. Clinical Utility of Microarray-Based Gene Expression Profiling in the Diagnosis and Subclassification of Leukemia: Report from the International Microarray Innovat Ions in Leukemia Study Group. *J Clin Oncol* (2010) 28 (15):2529–37. doi: 10.1200/JCO.2009.23.4732

31. Hou J, Aerts J, den Hamer B, van Ijcken W, den Bakker M, Riegman P, et al. Gene Expression-Based Classification of Non-Small Cell Lung Carcinomas and Survival Prediction. *PLoS One* (2010) 5(4):e10312. doi: 10.1371/journal.pone.0010312
32. Jones J, Otu H, Spentzos D, Kolia S, Inan M, Beecken WD, et al. Gene Signatures of Progression and Metastasis in Renal Cell Cancer. *Clin Cancer Res* (2005) 11(16):5730–9. doi: 10.1158/1078-0432.CCR-04-2225
33. Kim WJ, Kim EJ, Kim SK, Kim YJ, Ha YS, Jeong P, et al. Predictive Value of Progression-Related Gene Classifier in Primary Non-Muscle Invasive Bladder Cancer. *Mol Cancer* (2010) 9:3. doi: 10.1186/1476-4598-9-3
34. Li L, Zhang JW, Jenkins G, Xie F, Carlson EE, Fridley BL, et al. Genetic Variations Associated with Gemcitabine Treatment Outcome in Pancreatic Cancer. *Pharma Cogenet Genomics* (2016) 26(12):527–37. doi: 10.1097/FPC.0000000000000241
35. Li H, Zhang T, Jenkins Y, Xie Y, Carlson K, Fridley R, et al. Identification of Genes Upregulated in ALK-Positive and EGFR/KRAS/ALK-Negative Lung Adenocarcinomas. *Cancer Res* (2012) 72(1):100–11. doi: 10.1158/0008-5472.CAN-11-1403
36. Scotto L, Narayan G, Nandula SV, Arias-Pulido H, Subramaniyam S, Schneider A, et al. Identification of Copy Number Gain and Overexpressed Genes on Chromosome Arm 20q by an Integrative Genomic Approach in Cervical Cancer: Potential Role in Progression. *Genes Chromosomes Cancer* (2008) 47(9):755–65. doi: 10.1002/gcc.20577
37. Skrzypczak M, Goryca K, Rubel T, Paziewska A, Mikula M, Jarosz D, et al. Modeling Oncogenic Signaling In Colon Tumors by Multidirectional Analyses of Microarray Data Directed For Maximization of Analytical Reliability. *PLoS One* (2010) 5(10). doi: 10.1371/journal.pone.0013091
38. Yoon SS, Segal NH, Park PJ, Detwiller KY, Fernando NT, Ryeom SW, et al. Angiogenic Profile of Soft Tissue Sarcomas Based On Analysis of Circulating Factors and Microarray Gene Expression. *J Surg Res* (2006) 135(2):282–90. doi: 10.1016/j.jss.2006.01.023
39. Yoon K, Tajima A, Komata D, Yamamoto T, Kodama S, Fujiwara H, et al. Gene Expression Profiling of Advanced-Stage Serous Ovarian Cancers Distinguishes Novel Subclasses and Implicates ZEB2 in Tumor Progression and Prognosis. *Cancer Sci* (2009) 100(8):1421–8. doi: 10.1111/j.1349-7006.2009.01204.x
40. Sanchezcarbayo M, Socci ND, Lozano J, Saint F, Cordoncardo C. Defining Molecular Profiles of Poor Outcome in Patients with Invasive Bladder Cancer Using Oligonucleotide Microarrays. *J Clin Oncol Off J Am Soc Clin Oncol* (2006) 24(5):778–89. doi: 10.1200/JCO.2005.03.2375
41. Sun L, Hui AM, Su Q. Neuronal and Glioma-Derived Stem Cell Factor Induces Angiogenesis within the Brain. *Cancer Cell* (2006) 9(4):287–300. doi: 10.1016/jccr20603.003
42. Sun J, Grade M, Jung K, Camps J, et al. Mutated KRAS Results in Overexpression of DUSP4, a MAP-Kinase Phosphatase, and SMYD3, A Histone Methyltra Nsferase, in Rectal Carcinomas. *Genes Chromosomes Cancer* (2010) 49(11):24–34. doi: 10.1002/gcc.20811
43. Gaedcke J, Grade M, Jung K, Camps J, Jo P, Emons G, et al. Mutated KRAS Results in Overexpression of DUSP4, a MAP-Kinase Phosphatase, and SMYD3, A Histone Methyltra Nsferase, in Rectal Carcinomas. *Genes Chromosomes Cancer* (2010) 49(1):1024–34. doi: 10.1002/gcc.20811
44. Maia S, Haining WN, Ansén S, Xia AA, Ca Rdoso AA, et al. Gene Expression Profiling Identifies Bax-δ as A Novel Tumor Antigen in Acute Lymphoblastic Leukemia. *Cancer Research* (2005) 65(21):0050–8. doi: 10.1158/0008-5472.CAN-05-1574
45. Santegoets L, Baars RV, Terlou A, Heijmans-Antonissen C, Swagemakers S, Spek P, et al. Different DNA Damage and Cell Cycle Checkpoint Control in Low- And High-Risk Human Papillomavirus Infections of The Vulva. *Int J Cancer* (2012) 30(12):2874–85. doi: 10.1002/ijc.26345
46. Korkola JE, Heck S, Olshen AB, Feldman DR, Chaganti R. Development and Validation of a Gene-Based Model for Outcome Prediction in Germ Cell Tumors Using a Combined Genomic and Expression Profiling Approach. *PLoS One* (2015) 10(12):e0142846. doi: 10.1371/journal.pone.0142846
47. Vathipadiekal V, Wang V, Wei W, Waldron L, Drapkin R, Gillette M. Creation of a Human Secretome: A Novel Composite Library of Human Secreted Proteins: Validation Using Ovarian Cancer Gene Expression Data and a Virtual Secretome Array. *Clin Cancer Res* (2015) 21(21):4960–9. doi: 10.1158/1078-0432.CCR-14-3173
48. Barretina J, Taylor BS, Banerji S, Ramos AH, Singer S. Subtype-Specific Genomic Alterations Define New Targets for Soft-Tissue Sarcoma Therapy. *Nat Genet* (2010) 42(8):715–21. doi: 10.1038/ng.619
49. Modhukur V, Iljasenko T, Metsalu T, Lokk K, Laisk-Podar T, Vilo J. Methsurv: A Web Tool to Perform Multivariable Survival Analysis Using DNA Methylation Data. *Epigenomcs* (2017) epi-2017-0118. doi: 10.2217/epi-2017-0118
50. Liu CJ, Hu FF, Xia MX, Han L, Zhang Q, Guo AY. GSCALite: A Web Server for Gene Set Cancer Analysis. *Bioinformatics* (2018) 34(21):3771–2. doi: 10.1093/bioinformatics/bty411
51. Ru B, Wong CN, Tong Y, Zhong JY, Zhong SSW, Wu WC, et al. TISIDB: An Integrated Reposi Tory Portal for Tumor-Immune System Interactions. *Bioinformatics* (2019) 35(20):4200–2. doi: 10.1093/bioinformatics/btz210
52. Newman AM, Liu CL, Green MR, Gentles AJ, Feng W, Xu Y, et al. Robust Enumeration of Cell Subsets From Tissue Expression Profiles. *Nat Methods* (2015) 12(5):453–7. doi: 10.1038/nmeth.3337
53. O'Sullivan RJ, Arnoult N, Lackner DH, Oganesian L, Haggblom C, Corpet A, et al. Rapid Inducti on of Alternative Lengthening of Telomeres by Depletion of the Histone Chaperone ASF1. *Nat Struct Mol Biol* (2014) 21(2):167–74. doi: 10.1038/nsmb.2754
54. Qin Y, Wang J, Gong W, Zhang M, Tang Z, Zhang J, et al. UHRF1 Depletion Suppresses Growth of Gallbladder Cancer Cells Through Induction of Apoptosis and Cell Cycle Arrest. *Oncol Rep* (2014) 31(6):2635–43. doi: 10.3892/or.2014.3145
55. Ge S, Xia X, Ding C, Zhen B, Zhou Q, Feng J, et al. A Proteomic Landscape of Diffuse-Type Gastric Cancer. *Nat Commun* (2018) 9(1):1012. doi: 10.1038/s41467-018-03121-2
56. Hause RJ, Pritchard CC, Shendure J, Salipante SJ. Classification and Characterization of Microsa Tellite Instability Across 18 Cancer Types. *Nat Med* (2016) 22(11):1342–50. doi: 10.1038/nm.4191
57. Greillier L, Tomasini P, Barlesi F. The Clinical Utility of Tumor Mutational Burden in Non-Small Cell Lung Cancer. *Transl Lung Cancer Res* (2018) 7(6):639–46. doi: 10.21037/tlcr.2018.10.08
58. Otto JE, Kadoch C. A Two-Faced mSWI/SNF Subunit: Dual Roles for ARID1A in Tumor Supp Ression and Oncogenicity in the Liver. *Cancer Cell* (2017) 32(5):542–3. doi: 10.1016/j.ccell.2017.10.014
59. Rankin LC, Arpaia N. Treg Cells: A LAGging Hand Holds the Double-Edged Sword of the IL-23 Axis. *Immunity* (2018) 49(2):201–3. doi: 10.1016/j.immuni.2018.08.008
60. Zhao S, Zhang M, Zhang Y, Meng H, Wang Y, Liu Y, et al. The Prognostic Value of Programmed Cell Death Ligand 1 Expression in non-Hodgkin Lymphoma: A Meta-Analysis. *Cancer Biol Med* (2018) 15(3):290–8. doi: 10.20892/j.issn.2095-3941.2018.0047
61. Kondratova M, Czerwinska U, Sompairac N, Amigorena SD, Soumelis V, Barillot E, et al. A Multiscale Signalling Network Map of Innate Immune Response in Cancer Reveals Cell Hetero Gene Ity Signatures. *Nat Commun* (2019) 10(4808). doi: 10.1038/s41467-019-12270-x
62. Gerlinger M, Rowan AJ, Horswell S, Math M, Larkin J, Endesfelder D, et al. Intratumor Heterogeneity and Branched Evolution Revealed by Multiregion Sequencing. *N Engl J Med* (2012) 366(10):883–92. doi: 10.1056/NEJMoa1113205
63. McDonald KA, Kawaguchi T, Qi Q, Peng X, Asaoka M, Young J, et al. Tumor Heterogeneity Correlates With Less Immune Response and Worse Survival in Breast Cancer Patients. *Ann Surg Oncol* (2019) 26(7):2191–9. doi: 10.1245/s10434-019-07338-3
64. Bourne Y, Watson MH, Arvai AS, Bernstein SL, Reed SI, Tainer JA. Crystal Structure and Mutational Analysis of the Saccharomyces Cerevisiae Cell Cycle Regulatory Protein Cks1: Implica Tions for Domain Swapping, Anion Binding and Protein Interactions. *Structure* (2000) 8(8):841–50. doi: 10.1016/s0969-2126(00)00175-1
65. Slotky M, Shapira M, Ben-Izhak O, Linn S, Futerman B, Tsalic M, et al. The Expression of the Ubiquitin Ligase Subunit Cks1 in Human Breast Cancer. *Breast Cancer Res* (2005) 7(5):R737–44. doi: 10.1186/bcr1278
66. Lee SW, Kang SB, Lee DS, Lee JU. Akt and Cks1 are Related With Lymph Node Metastasis in Gastric Adenocarcinoma. *Hepatogastroenterology* (2013) 60(124):932–7. doi: 10.5754/hge121214
67. Wang JJ, Fang ZX, Ye HM, You P, Cai MJ, Duan HB, et al. Clinical Significance of Overex Pressed Cyclin-Dependent Kinase Subunits 1 and 2 in Esophageal Carcinoma. *Dis Esophagus* (2013) 26(7):729–36. doi: 10.1111/dote.12013

68. Shapira M, Ben-Izhak O, Bishara B, Futerman B, Minkov I, Krausz MM, et al. Alterations in the Expression of the Cell Cycle Regulatory Protein Cyclin Kinase Subunit 1 in Colorectal Carcinoma. *Cancer* (2004) 100(8):1615–21. doi: 10.1002/cncr.20172
69. Shapira M, Ben-Izhak O, Linn S, Futerman B, Minkov I, Hershko DD. The Prognostic Impact of the Ubiquitin Ligase Subunits Skp2 and Cks1 in Colorectal Carcinoma. *Cancer* (2005) 103(7):1336–46. doi: 10.1002/cncr.20917
70. Tsai YS, Chang HC, Chuang LY, Hung WC. RNA Silencing of Cks1 Induced G2/M Arrest and Apoptosis in Human Lung Cancer Cells. *IUBMB Life* (2005) 57(8):583–9. doi: 10.1080/15216540500215531
71. Lee EK, Kim DG, Kim JS, Yoon Y. Cell-Cycle Regulator Cks1 Promotes Hepatocellular Carcinoma by Supporting NF-Kbdependent Expression of Interleukin-8. *J Cancer Res* (2011) 71:6827–35. doi: 10.1158/0008-5472.CAN-10-435616
72. Zhan F, Colla S, Wu X, Chen B, Stewart JP, Kuehl WM, et al. CKS1B, Overexpressed in Aggressive Disease, Regulates Multiple Myeloma Growth and Survival Through SKP2- and p27Kip1- Dependent and -Independent Mechanisms. *J Blood* (2007) 109 (11):4995–5001. doi: 10.1182/blood-2006-07-038703
73. Wang H, Sun M, Guo J, Ma L, Jiang H, Gu L, et al. 3-O-(Z)-Coumaroyloleanolic Acid Overcomes Cks1b-Induced Chemoresistance in Lung Cancer by Inhibiting Hsp90 and MEK Pathways. *Biochem Pharmacol* (2017) 135(10):35–49. doi: 10.1016/j.bcp.2017.03.007
74. Shi L, Wang S, Zangari M, Xu H, Cao TM, Xu C, et al. Over-Expression of CKS1B Activates Both MEK/ERK and JAK/STAT3 Signaling Pathways and Promotes Myeloma Cell Drug-Resistance. *J Oncotarget* (2010) 1(1):22–33. doi: 10.18632/oncotarget.105
75. Huang J, Zhou Y, Thomas GS, Gu Z, Yang Y, Xu H, et al. Nedd8 Inhibition Overcomes Cks1b-Induced Drug Resistance by Upregulation of P21 in Multiple Myeloma. *Clin Cancer Res* (2015), 5532–42. doi: 10.1158/1078-0432.CCR-15-0254
76. Tobias AM, Toska D, Lange K, Eck T, Bhat R, Janson CA, et al. Expression, Purification, and Inhibition Profile of Dihydrofolate Reductase From the Filarial Nematode Wuchereria Bancrofti. *PloS One* (2018) 13(5):e0197173. doi: 10.1371/journal.pone.0197173
77. Chattopadhyay S, Moran RG and Goldman ID. Pemetrexed: Biochemical and Cellular Pharmaco Logy, Mechanisms, and Clinical Applications. *Mol Cancer Ther* (2007) 6(2):404–17. doi: 10.1158/1535-7163.MCT-06-0343
78. Bellelli R, Belan O, Pye VE, Clement C, Maslen SL, Skehel JM, et al. POLE3-POLE4 Is a Histone H3-H4 Chaperone That Maintains Chromatin Integrity During DNA Replication. *Mol Cell* (2018) 72(1):112–26.e5. doi: 10.1016/j.molcel.2018.08.043
79. Su D, Feng X, Colic M, Wang Y, Chen Y. CRISPR/CAS9-Based DNA Damage Response Screens Reveal Gene-Drug Interactions. *DNA Repair (Amst)* (2020) 87:102 803. doi: 10.1016/J.dnarep2020.102803
80. Hustedt N, Lvarez-Quilón A, Mcewan A, Yuan JY, Durocher D. A Consensus Set of Genetic Vulnerabilities to ATR Inhibition. *Open Biol* (2019) 9 (9):190156. doi: 10.1098/rsob.190156

Conflict of Interest: The authors declare that the research was conducted in the absence of any commercial or financial relationships that could be construed as a potential conflict of interest.

Publisher's Note: All claims expressed in this article are solely those of the authors and do not necessarily represent those of their affiliated organizations, or those of the publisher, the editors and the reviewers. Any product that may be evaluated in this article, or claim that may be made by its manufacturer, is not guaranteed or endorsed by the publisher.

Copyright © 2021 Zhang, Gao, Guan, Liu, Meng and Wang. This is an open-access article distributed under the terms of the Creative Commons Attribution License (CC BY). The use, distribution or reproduction in other forums is permitted, provided the original author(s) and the copyright owner(s) are credited and that the original publication in this journal is cited, in accordance with accepted academic practice. No use, distribution or reproduction is permitted which does not comply with these terms.

frontiers in Cell and Developmental Biology

ORIGINAL RESEARCH
published: 09 September 2021
doi: 10.3389/fcell.2021.714601

Circular RNA hsa_circ_0000073 Enhances Osteosarcoma Cells Malignant Behavior by Sponging miR-1252-5p and Modulating CCNE2 and MDM2

Zhijing Ren[1,2], Qinqin Yang[1], Jiajia Guo[1], Haifeng Huang[3], Bo Li[3], Zhen Yang[1,3] and Xiaobin Tian[1,4]**

[1] Medical College of Guizhou University, Guiyang, China, [2] Department of Clinical Laboratory, Guizhou Provincial People's Hospital, Guiyang, China, [3] Department of Orthopedics, Guizhou Provincial People's Hospital, Guiyang, China, [4] Department of Orthopedics, Affiliated Hospital of Guizhou Medical University, Guiyang, China

OPEN ACCESS

Edited by:
Ira Ida Skvortsova, Innsbruck Medical University, Austria

Reviewed by:
Haihao Wang, Huazhong University of Science and Technology, China
Fang Wang, The Second Affiliated Hospital of Harbin Medical University, China

***Correspondence:**
Zhen Yang
279754802@qq.com
Xiaobin Tian
txb1216@126.com

Specialty section:
This article was submitted to Molecular and Cellular Oncology, a section of the journal Frontiers in Cell and Developmental Biology

Received: *25 May 2021*
Accepted: *13 August 2021*
Published: *09 September 2021*

Citation:
Ren Z, Yang Q, Guo J, Huang H, Li B, Yang Z and Tian X (2021) Circular RNA hsa_circ_0000073 Enhances Osteosarcoma Cells Malignant Behavior by Sponging miR-1252-5p and Modulating CCNE2 and MDM2. Front. Cell Dev. Biol. 9:714601. doi: 10.3389/fcell.2021.714601

Objective: An increasing number of studies have demonstrated that circular RNAs (circRNAs) are involved in tumor progression. However, the role of hsa_circ_0000073 in osteosarcoma (OS) is still not fully elucidated.

Methods: Quantitative reverse transcription-polymerase chain reaction or Western blot was used to detect the gene expression. GeneChip analysis, bioinformatics, luciferase reporter, and RNA immunoprecipitation assays were adopted to predict and verify the relationships between genes. Counting Kit-8 Assay, clone formation assay, wound-healing assay, transwell assays, cell cycle assays, and *in vivo* tumorigenesis were used to evaluate cell function.

Results: hsa_circ_0000073 was highly expressed in OS cell lines and could promote OS progression, including proliferation, migration, invasion, and cell cycle *in vitro* as well as tumorigenesis *in vivo*. Mechanically, hsa_circ_0000073 could readily downregulate the expression of CCNE2 and MDM2 through miR-1252-5p. Rescue experiments validated miR-1252-5p mimics, or CCNE2/MDM2 short hairpin RNA could reverse the hsa_circ_0000073 overexpressing-induced impairment of malignant tumor behavior.

Conclusion: hsa_circ_0000073 functions as a tumor promoter in OS to increase malignant tumor behavior through sponging miR-1252-5p and regulating CCNE2 and MDM2 expression, which could be a novel target for OS therapy.

Keywords: hsa_circ_0000073, osteosarcoma, cell cycle, proliferation, miR-1252-5p, CCNE2, MDM2

INTRODUCTION

Osteosarcoma (OS), the most frequent bone tumor from malignant mesenchymal cells, is the leading cause of cancer mortality in children and teenagers. Unfortunately, although advanced surgery combined with chemotherapy has been practiced in clinical, the patients with OS have been shown to only approximately 65–70% in 5-year survival rate, and many patients suffer from potential distant metastasis (Zhou et al., 2016; Harrison et al., 2018).

It is widely accepted that patients with OS may benefit from the novel and efficacious treatment methods established, such as molecule-targeted therapies. However, little progress has been made in recent decades. Therefore, there is a pressing need to profoundly investigate the molecular mechanism underlying OS progress, especially complex gene regulation axes, which could help us develop robust interventions and therapies (Bishop et al., 2016; Otoukesh et al., 2018).

Circular RNAs (circRNAs) are a subclass of endogenous non-coding RNAs with no polyadenylated tail, which have a closed circular structure joined by the 3′ and 5′ ends (Kristensen et al., 2019). Increasing evidence has exhibited that multiple circRNAs have been involved in the generation and development of cancers, such as gene expression, migration, invasion, proliferation, cell cycle, among others (Arnaiz et al., 2019; Chen et al., 2020; Li R. et al., 2020; Wu P. et al., 2020). Currently, as many micro RNA (miRNA)-binding sites on circRNAs have been found, the most well-known function of circRNAs is to serve as miRNA sponges and subsequently regulate target gene expression (Lu et al., 2019; Wang H. Y. et al., 2020). In OS, extensive research has demonstrated that circRNAs could participate in the pathophysiological processes by exhibiting competitive binding to miRNAs, such as circ-XPR1, circTADA2A, hsa_circ_0005909, and hsa_circ_0000658 (Wu et al., 2019; Jiang and Chen, 2021; Mao et al., 2021; Zhang et al., 2021). However, studies of circRNAs in OS are just starting, and the underlying molecular mechanism of hsa_circ_0000073 is not fully understood. Here, we aimed to explore the function of hsa_circ_0000073 in proliferation, migration, invasion, and cell cycle of OS cells and unveiled a network among hsa_circ_0000073/miR-1252-5p/CCNE2 and MDM2, providing a potential target for OS therapy.

MATERIALS AND METHODS

Cell Culture

A normal human osteoblast cell line (hFOB1.19), three OS cell lines (MG63, U-2, and Saos2), were obtained from the Chinese Academy of Sciences (Shanghai, China) and cultured under standard conditions (temperature: 37°C; CO: 2.5%). For a complete medium, 100 U/ml penicillin G, streptomycins, and 10% fetal bovine serum were mixed in the Dulbecco's modified Eagle's medium (Gibco, United States).

Transfection of Cells

For transfection experiments, the empty vector (pcDNA3.1), overexpressing plasmids (hsa_circ_0000073), short hairpin RNAs (shRNAs) (sh-NC, sh-circ_0000073, sh-MDM2, and sh-CCNE2), miRNA mimics, and sponge (mimics-NC, miR-1252-5p mimics, sponge-NC, and miR-1252-5p sponge) were all designed and synthesized by General Biosystems (Anhui, China). Lipofectamine 3000 (Invitrogen, United States) was chosen for cell transfection. The shRNAs used are shown in **Supplementary Table 1**.

RNase R Treatment and Quantitative Reverse Transcription-Polymerase Chain Reaction

TRIzol (Takara, Japan) was taken for total RNA extraction. At 37°C, 2,000 ng of total RNA was incubated with or without RNase R (Epicenter Technologies, United States) for 15 min. The reverse transcription kit (Takara, Japan) and an SYBR Green PCR kit (Takara, Japan) were used for quantitative reverse transcription-polymerase chain reaction (qRT-PCR). The expression levels were normalized with glyceraldehyde 3-phosphate dehydrogenase or U6 and calculated with the $2^{-\Delta\Delta Ct}$. The primers used are displayed in **Supplementary Table 2**.

Counting Kit-8 Assay

Counting Kit-8 (CCK-8) reagent (Solarbio, China) was chosen to test cell proliferation. The transfected cells were cultured in 96-well plates. At 0, 24, 48, and 72 h, 10 μl of CCK-8 reagent was added to each well. After 2 h of incubation at 37°C, a microplate reader was taken to measure the optical density value at 450 nm.

Clone Formation Assay

Transfected cells were plated in 12-well plates for 1-week culture before being fixed in 4% paraformaldehyde. Crystal violet solution (0.1%, Solarbio, China) was used to stain. The images were captured for counting.

Wound-Healing Assay

Cells in the different groups were cultured in 12-well plates for 24 h. A 10-μl pipette tip was taken to scratch the cell surface. At 0 and 48 h after injury, the images were captured by a microscope. A relative migration rate was analyzed by measuring the migratory distance normalized to the 0-h control.

Transwell Assay

A transwell chamber coating matrigel on the upper side was taken to examine the cell invasion. The transfected cells with 200-μl serum-free media were added into the transwell chambers, whereas the outer chambers were packed with the complete medium. After 48 h of culture, the bottom surface cells were fixed with 4% paraformaldehyde and stained with 0.1% crystal violet (Solarbio, China). The images were captured for counting.

Cell Cycle Assay

The flow cytometer and a cell cycle analysis kit (Meilunbio, China) were used to detect the cell cycle stages. The cells were immobilized with 75% alcohol at −20°C for 24 h and added 500-μl propidium iodide solution [buffer:propidium iodide (20×):RNase A (50×) = 100:5:2] and incubated 30 min for the test.

Gene Expression Profiling Analysis and Bioinformatics Analysis

Cells transfected with sh-NC or sh-circ_0000073 were subjected to total RNA isolation using TRIzol reagent (Takara, Japan). Then, a GeneChip WT Pico Reagent Kit (Affymetrix,

United States) was taken to analyze the differentially expressed messenger RNAs with the conditions: fold change > 1.5 and $P < 0.05$. Gene Ontology (GO) (Yu et al., 2012) and Kyoto Encyclopedia of Genes and Genomes (KEGG) (Kanehisa et al., 2021) were taken to investigate the potential biological functions of hsa_circ_0000073 with the conditions: p.adj < 0.05 and q-value < 0.2. Protein–protein interaction (PPI) network and competing for endogenous RNA (ceRNA) network were created by STRING 11.0 (Szklarczyk et al., 2019) and Cytoscape 3.7.2 (Shannon et al., 2003).

Western Blot

Radioimmunoprecipitation assay buffer and BCA Protein assay kit (Beyotime, China) were used for protein extraction and protein concentration evaluation. Proteins were separated with a sodium dodecyl sulfate–polyacrylamide gel electrophoresis gel. The polyvinylidene fluoride membrane containing proteins was blocked with 5% milk. Then, specific primary antibodies (MDM2, Abcam; CCNE2, Abcam; and glyceraldehyde 3-phosphate dehydrogenase, Abcam) were applied to the membrane at 4°C overnight. After incubating with secondary antibodies, an ECL Western Blotting Substrate (Solarbio, China) was used to detect the protein blots.

RNA Immunoprecipitation

An EZ-Magna RNA Immunoprecipitation (RIP) Kit (Millipore, United States) was taken to AGO2-RIP experiments. The HEK-293 cells were lysed and incubated with human anti-Ago2 or mouse IgG-coated beads (Millipore, United States). qRT-PCR was used to analyze the immunoprecipitated RNAs.

Luciferase Reporter Assay

According to the target gene sites identified *via* Circbank (Liu et al., 2019), TargetScan (Agarwal et al., 2015), or ENCORI (Li et al., 2014), the wild-type or mutant sequence was plug into the vector (Tongyong, China) and transfected to cells. A double luciferase detection system was measured to the activity of the luciferase reporter gene.

Tumor Formation *in vivo*

BALB/C-nu mice (Sipeifu, China) were used to study tumor formation ability, in which 2×10^7 stably transfected MG63 cells were injected in the flank for 5 weeks. The tumor volume was monitored every week and calculated using the formula: length $\times$ width^2/2 (cubic millimeter). On week 5, mice were killed. The dissected tumors were weighed and collected. Formalin-fixed paraffin sections (4–6 μm) of tumor tissues were carried out for immunohistochemistry assay. The primary antibody (MDM2, Abcam; CCNE2, Abcam) and EnVision Detection System (DAKO, United States) were used according to the manufacturer's protocol. A microscope captured images. The Animal Ethics Committee of Guizhou Provincial People's Hospital approved this work.

Statistical Analysis

The data were represented as means ± SD and the Student's t-test, or one-factor analysis was taken to analyze the group comparison. Through SPSS 22.0 (IBM, United States) analysis, statistical significance was recording as $P < 0.05$.

RESULTS

hsa_circ_0000073 Was Upregulated in Osteosarcoma Cells

We analyzed the most upregulated circRNAs in OS cell lines from GSE96964 (**Figure 1A**). The hsa_circ_0032462, hsa_circ_0028173, and hsa_circ_0000073 were selected to further investigate by qRT-PCR. Comparing with hFOB1.19, the normal human osteoblast cell, the highest expression of hsa_circ_0000073 was observed in human OS cells, including MG63, U2OS, and Saos2 (**Figure 1B**). Then, hsa_circ_0000073 was chosen to be the main subject. Subsequently, we confirmed that hsa_circ_0000073 could only be detected from complementary DNA with divergent primers (**Figure 1C**) and undigested by RNase R, which showed strong stability due to the closed structure (**Figure 1D**). Moreover, the data of qRT-PCR proved that hsa_circ_0000073 was enriched in the cytoplasm (**Figure 1E**).

hsa_circ_0000073 Promoted Osteosarcoma Progression *in vitro*

Then, we designed two shRNAs that targeted the specific junction sites of hsa_circ_0000073. By qRT-PCR, we found that the sh-hsa_circ_0000073-1 had a better knockdown efficiency (**Figure 2A**). Thus, we chose the sh-hsa_circ_0000073-1 for further study. By contrast, we also designed an overexpressing plasmid of hsa_circ_0000073, which was verified that it could significantly upregulate the expression of hsa_circ_0000073 in OS cells (**Figure 2B**). Functionally, our results of the CCK-8 and colony formation assays confirmed that the hsa_circ_0000073 shRNA prominently weakened the cell proliferative ability, and the overexpression group was the opposite (**Figures 2C,D**). Moreover, the wound-healing and transwell assays also showed that the migrative and invasive abilities were similar to CCK-8 and colony formation assays (**Figures 2E,F**). Next, flow cytometry found that the S phase was higher by hsa_circ_0000073-silenced, whereas it was lower by overexpressing hsa_circ_0000073 (**Figure 2G**). In a word, hsa_circ_0000073 played an oncogenic role in OS progression.

Bioinformatics Predicted the Competing for Endogenous RNA Network of hsa_circ_0000073

To explore the complex underlying mechanisms, we first analyzed the gene expression profiling after transfected sh-hsa_circ_0000073 in MG-63 and Saos-2 cells. After hsa_circ_0000073 was silenced, the scatter plot showed there were 1,859 upregulated and 1,848 downregulated genes in MG-63 cells, as well as 2,339 upregulated and 1,255 downregulated genes in Saos-2 cells (**Figure 3A**). Subsequently, GO analyses showed that downregulated differentially expressed genes (DEGs) were enriched in a diverse cellular component, molecular function,

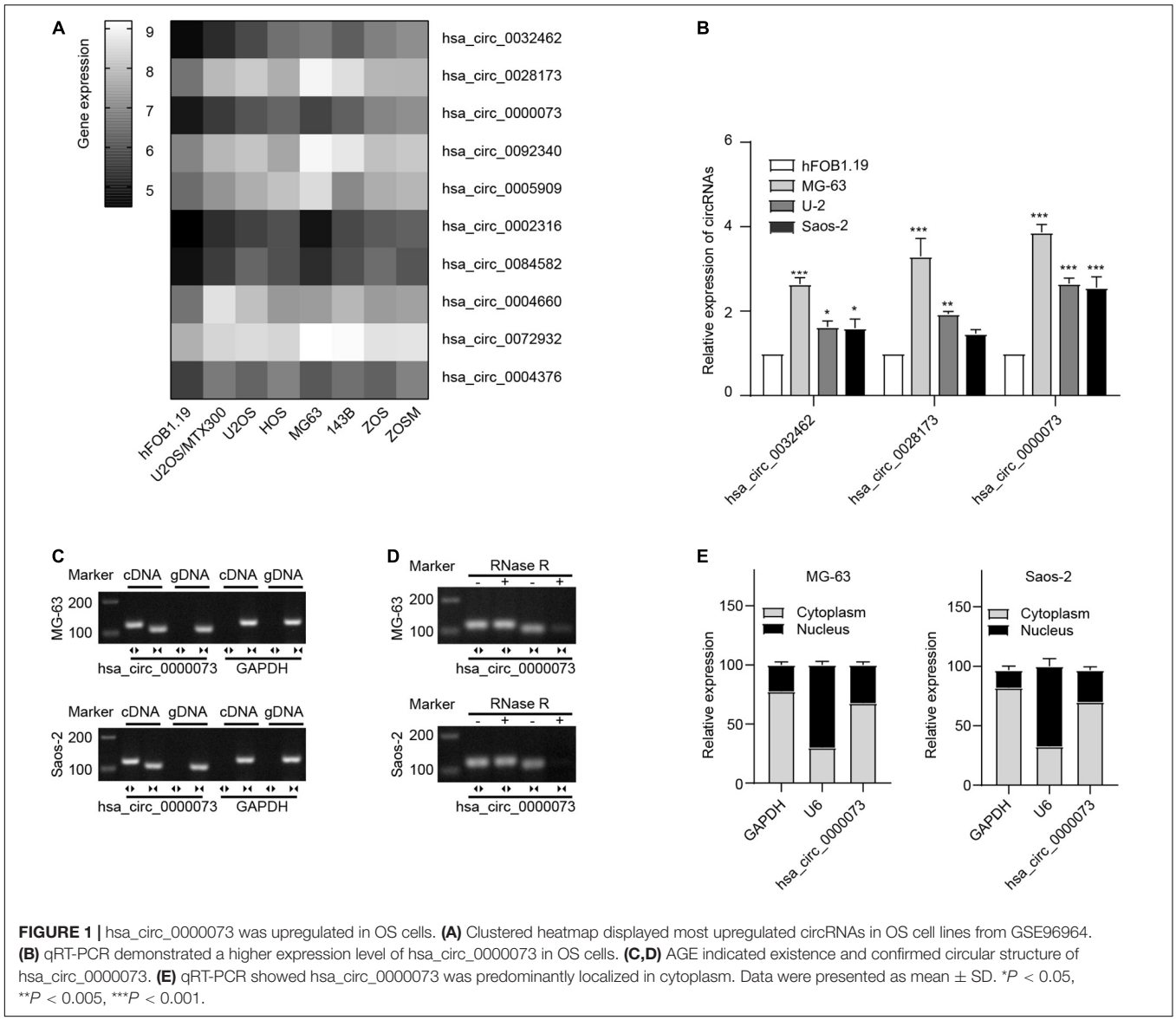


FIGURE 1 | hsa_circ_0000073 was upregulated in OS cells. **(A)** Clustered heatmap displayed most upregulated circRNAs in OS cell lines from GSE96964. **(B)** qRT-PCR demonstrated a higher expression level of hsa_circ_0000073 in OS cells. **(C,D)** AGE indicated existence and confirmed circular structure of hsa_circ_0000073. **(E)** qRT-PCR showed hsa_circ_0000073 was predominantly localized in cytoplasm. Data were presented as mean ± SD. $^{*}P < 0.05$, $^{**}P < 0.005$, $^{***}P < 0.001$.

or biological process (**Figure 3B**). Further KEGG pathways analysis indicated that "pathways in cancer" were one of the major pathways in both two cell lines (**Figure 3C**). Moreover, the Venn analysis revealed 16 genes in "pathways in cancer" that were co-downregulated in the two cell lines (**Figure 3D**). The details are displayed in **Supplementary Table 3**. By GO and KEGG analyses, the co-expressed DEGs were involved in cyclin-dependent protein, ubiquitin-binding, GTPase complex, and PI3K-Akt signaling pathway, which might imply to connect with cell growth and differentiation (**Figure 3E**). PPI network analysis showed the interaction of the 16 co-expressed DEGs and their relational genes (**Figure 3F**); the details of PPIs are shown in **Supplementary Table 4**.

Considering circRNAs are important in competing endogenous RNA networks, we searched the databases and found four miRNAs with several potential binding sites of hsa_circ_0000073 in circBank and ENCORI (**Figure 3G**). The ceRNA network analysis displayed the relationship among hsa_circ_0000073, miRNA, and target genes collected by co-expressed DEGs in "pathway in cancer" (**Figure 3H**). To sum up, based on bioinformatics, we made a potential ceRNA network of hsa_circ_0000073 that pointed out the direction for further research.

miR-1252-5p Combined With hsa_circ_0000073 and Suppressed Osteosarcoma Progression

Subsequently, we checked the expression of the four miRNAs after the knockdown of hsa_circ_0000073. The results of qRT-PCR uncovered that miR-1252-5p was significantly upregulated by hsa_circ_0000073 repression and was lowly expressed in OS cells (**Figures 4A–C**). Moreover, the binding between miR-1252-5p and hsa_circ_0000073 was further verified by the luciferase

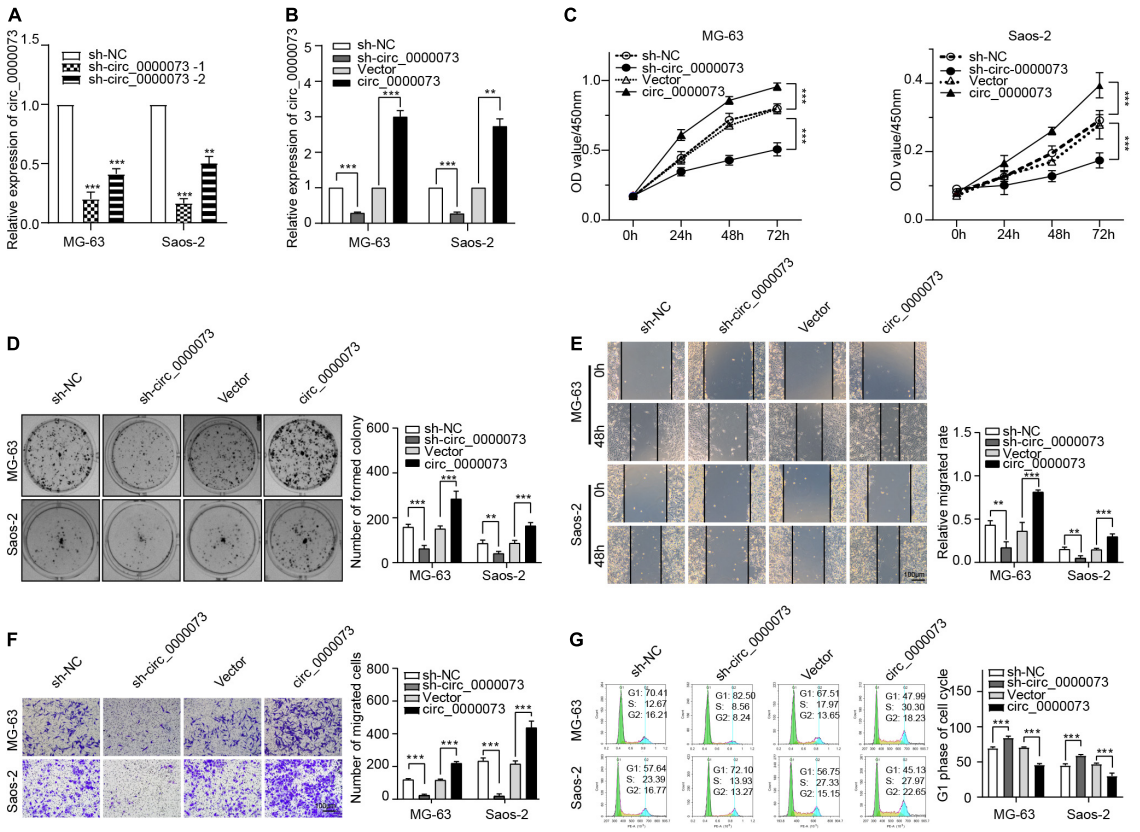


FIGURE 2 | hsa_circ_0000073 enhanced malignant behavior *in vitro*. **(A)** qRT-PCR qualified silenced efficiencies of hsa_circ_0000073. **(B)** qRT-PCR confirmed knockdown and overexpression of hsa_circ_0000073 by shRNA and overexpressing plasmid. **(C,D)** CCK-8 and clone formation assays showed hsa_circ_0000073 stimulated cell proliferation in OS cells. **(E,F)** Wound-healing and transwell assays verified hsa_circ_0000073 enhanced migration and invasion ability in OS cells with regulation, magnification, ×200. **(G)** Flow cytometry analysis revealed that hsa_circ_0000073-silenced induced S phase arrested in OS cells, whereas hsa_circ_0000073-overexpressed reductions. Data were presented as mean ± SD. $^{**}P < 0.005$, $^{***}P < 0.001$.

assay (**Figure 4D**). Thus, we chose miR-1252-5p for further study and designed the effective mimics and sponge of it (**Supplementary Figure 1**). Functionally, we further investigated the role of miR-1252-5p in OS progression, which found that miR-1252-5p could inhibit the carcinoma progression in proliferation, migration, invasion, and cell cycle (**Figures 4E–I**). Taken together, our study found and supported that miR-1252-5p could combine with hsa_circ_0000073 and suppresses the malignant behavior of OS cells.

hsa_circ_0000073 Sponging miR-1252-5p and Upregulated CCNE2 and MDM2 Expression

Next, based on the ceRNA network predicted by bioinformatics, the five genes related to miR-1252-5p were selected for further investigation, which found CCNE2 and MDM2 were the most dramatically downregulated genes by hsa_circ_0000073 silencing (**Figure 5A**). The further results of qRT-PCR and Western blot (WB) assay confirmed that hsa_circ_0000073 silencing observably downregulated the expression of CCNE2 and MDM2, whereas its overexpressing plasmid was the opposite (**Figures 5B,C**). Besides, we revealed that CCNE2 and MDM2 were dramatically increased in the OS cells and could be regulated by miR-1252-5p (**Figures 5D–F**). Furthermore, luciferase assay and RIP assays also confirmed the binding among hsa_circ_0000073, miR-1252-5p, CCNE2, or MDM2 (**Figures 5G,H**). Thus, we chose CCNE2 and MDM2 for further study and designed the effective shRNAs (**Supplementary Figure 2**). Moreover, the WB data validated that hsa_circ_0000073-overexpressed could upregulate the expression of CCNE2 and MDM2, and this upregulation could be attenuated by miR-1252-5p-overexpressed, CCNE2-silenced, or MDM2-silenced (**Figures 5I,J**). Collectively, our findings suggested that hsa_circ_0000073 could affect the expression of CCNE2 and MDM2 by regulating miR-1252-5p.

hsa_circ_0000073 Enhanced the Malignant Behavior of Osteosarcoma Cells by Targeting miR-1252-5p/CCNE2 and MDM2 Axis

Functionally, rescue experiments were performed to explore whether hsa_circ_0000073 could participate

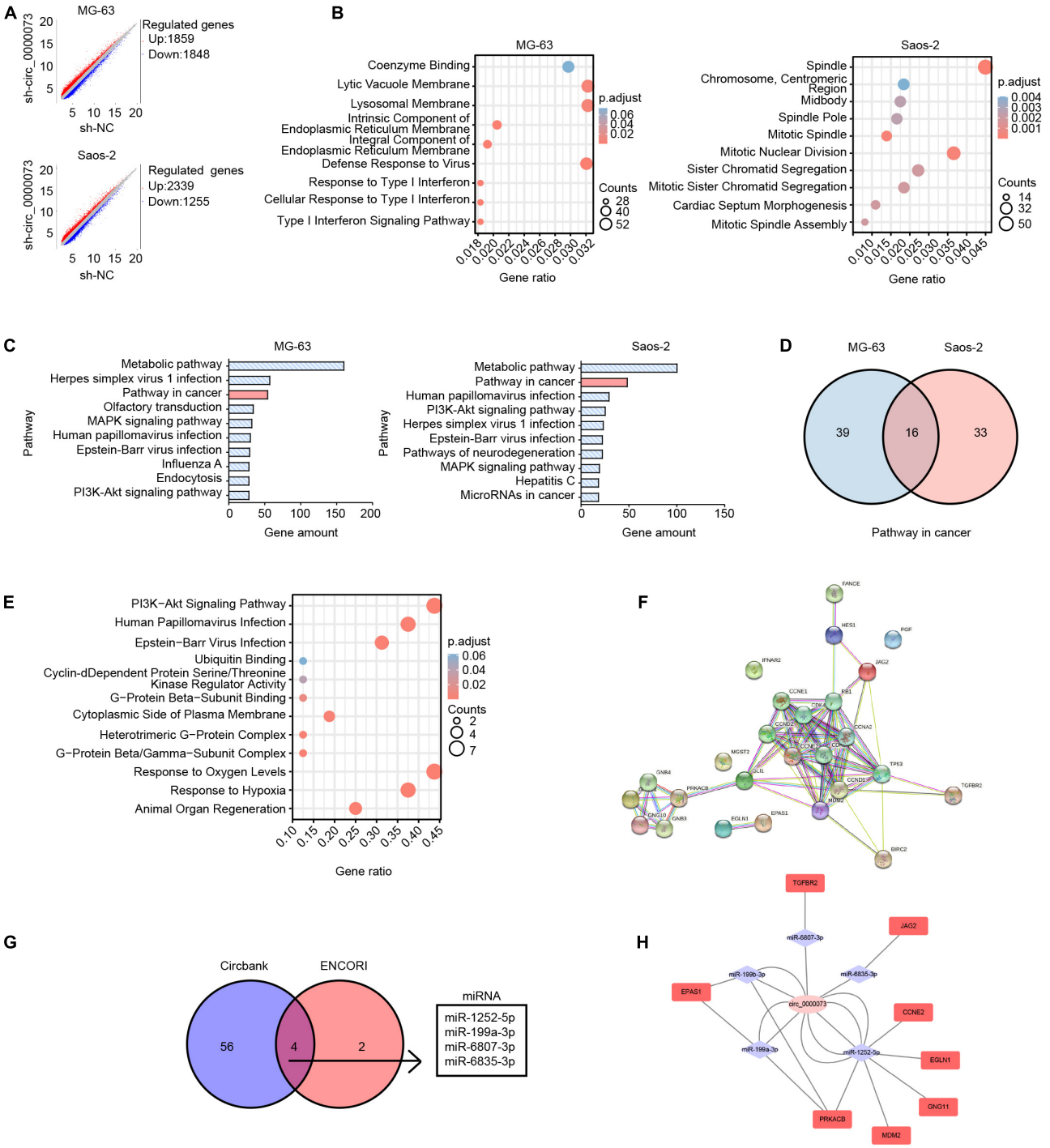


FIGURE 3 | Bioinformatics analysis of DEGs after hsa_circ_0000073 silencing. **(A)** Scatter plot of all DEGs between sh-NC group and sh- circ_0000073. **(B)** GO analyses showed enrichment of down-regulated DEGs. **(C)** KEGG pathways analysis of top 10 pathways. **(D)** Venn analysis revealed amount genes in "pathways in cancer" of two cell lines. **(E)** GO and KEGG analyses displayed enrichment of co-expressed DEGs. **(F)** PPI network analysis showed interaction of co-expressed DEGs as well as relational genes. **(G)** Databases predicted four miRNAs shared with hsa_circ_0000073. **(H)** ceRNA network displayed relationship among hsa_circ_0000073, miRNA, and target genes collected by co-expressed DEGs in "pathway in cancer."

in the progress of OS by sponging miR-1252-5p and regulating CCNE2 or MDM2 expression. The data of CCK-8, colony formation, transwell, wound-healing, and cell cycle assays verified that miR-1252-5p mimics, sh-CCNE2, or sh-MDM2 could reverse the malignant behavior caused by hsa_circ_0000073 overexpression in

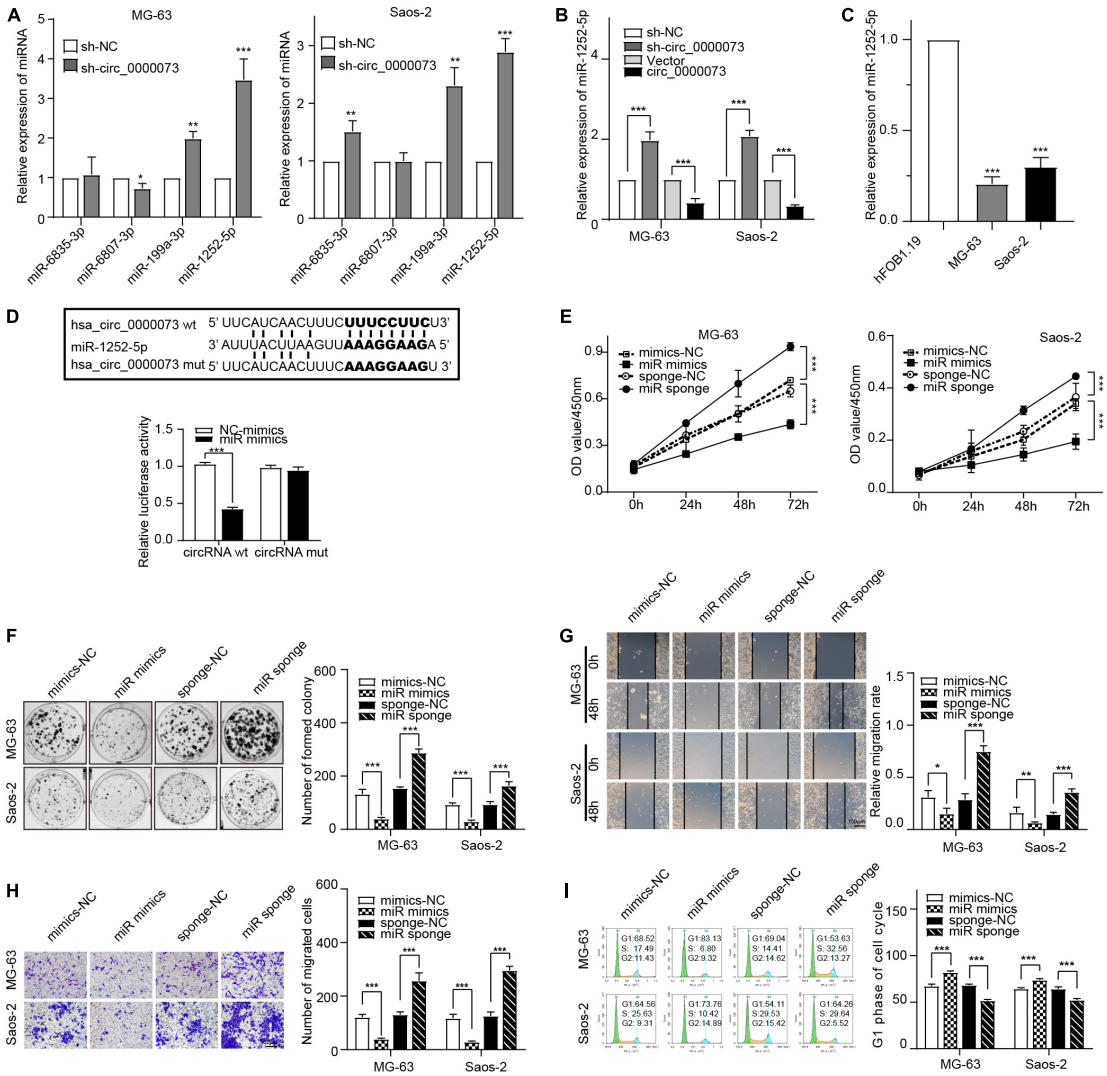


FIGURE 4 | hsa_circ_0000073 targets miR-1252-5p to promote OS progress. **(A)** qRT-PCR examined expression of four candidate miRNAs after hsa_circ_0000073 silencing. **(B)** qRT-PCR measured expression of miR-1252-5p in MG-63 and Saos-2 cells after overexpression or knockdown of hsa_circ_0000073. **(C)** qRT-PCR confirmed lower expression level of miR-1252-5p in OS cells. **(D)** Luciferase reporter assay confirmed relationship between hsa_circ_0000073 and miR-1252-5p in HEK293 cells. **(E,F)** CCK-8 and clone formation assays showed miR-1252-5p inhibited cell proliferation in OS cells. **(G,H)** Wound-healing and transwell assays revealed miR-1252-5p restrained migration and invasion ability in OS cells with regulation, magnification, ×200. **(I)** Flow cytometry analysis indicated upregulation of miR-1252-5p induced S phase arrested in OS cells whereas downregulation of reductions. Data were presented as mean ± SD. $^{*}P < 0.05$, $^{**}P < 0.005$, $^{***}P < 0.001$.

OS cells (**Figures 6A–E**). Overall, our results proved that hsa_circ_0000073 regulated CCNE2 or MDM2 through miR-1252-5p.

hsa_circ_0000073 Promotes the Tumorigenesis Through Sponging miR-1252-5p and Modulating CCNE2 and MDM2 Expression *in vivo*

A xenograft tumor model showed that the tumors derived from the cells transfected sh-hsa_circ_0000073 weighed less and grew more slowly than the control group (**Figure 7A**). Next, qRT-PCR confirmed the expression of miR-1252-5p was upregulated by hsa_circ_0000073 knockdown (**Figure 7B**). Meanwhile, the results of WB and immunohistochemistry showed that hsa_circ_0000073 silencing markedly reduced the expression of CCNE2 or MDM2 in tumor tissues (**Figures 7C,D**). To summarize, hsa_circ_0000073 enhances osteosarcoma cells' malignant behavior by sponging miR-1252-5p and modulating CCNE2 and MDM2 (**Figure 7E**).

DISCUSSION

Circular RNAs are an interesting class of RNA that do not have free ends. This special structure gives them excellent stability.

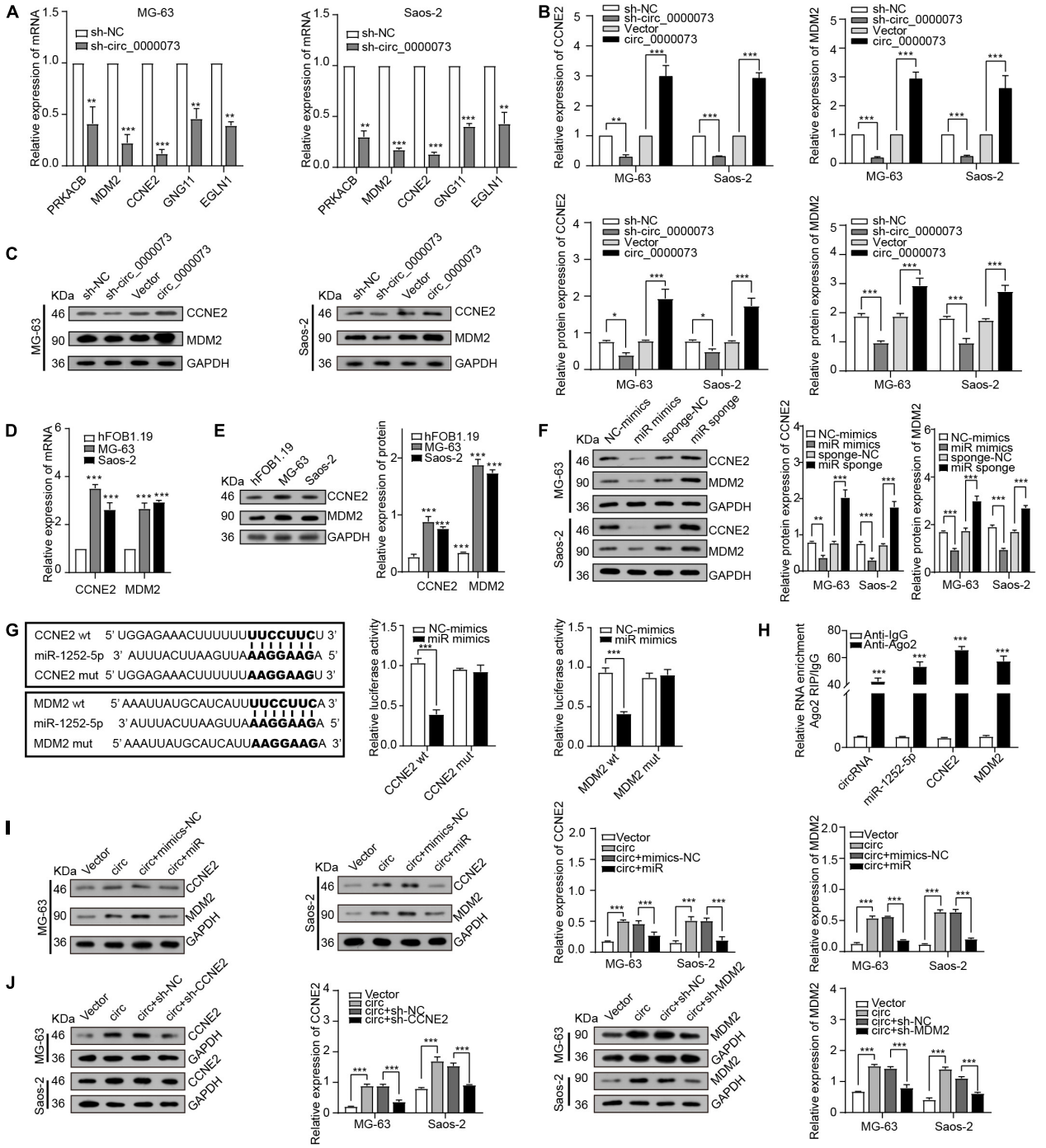


FIGURE 5 | hsa_circ_0000073 regulated expression of CCNE2 and MDM2 through miR-1252-5p. **(A)** qRT-PCR determined expression of five candidate genes after hsa_circ_0000073 silencing. **(B,C)** qRT-PCR and WB assays assessed expression of CCNE2 and MDM2 in OS cells with hsa_circ_0000073 regulation. **(D,E)** qRT-PCR and WB assays confirmed expression level of CCNE2 and MDM2 was higher in OS cells. **(F)** WB verified impacts of miR-1252-5p on CCNE2 and MDM2 expression in OS cells. **(G,H)** Luciferase reporter assay and RIP assays confirmed relationship among hsa_circ_0000073, miR-1252-5p, CCNE2, and MDM2 in HEK293 cells. **(I,J)** WB revealed rescue ability of miR-1252-5p, CCNE2, and MDM2 on overexpressed-hsa_circ_0000073 in MG-63 and Saos-2 cells. Data were presented as mean ± SD. $^{*}P < 0.05$, $^{**}P < 0.005$, and $^{***}P < 0.001$.

An *in vitro* study of 60 circRNAs confirmed that most circRNAs have longer half-lives than linear RNAs (Enuka et al., 2016). Their high stability, abundance, and many other characteristics make them become the potential to be an ideal target for clinical intervention (Jeck et al., 2013). Currently, emerging evidence has demonstrated that they have been involved in

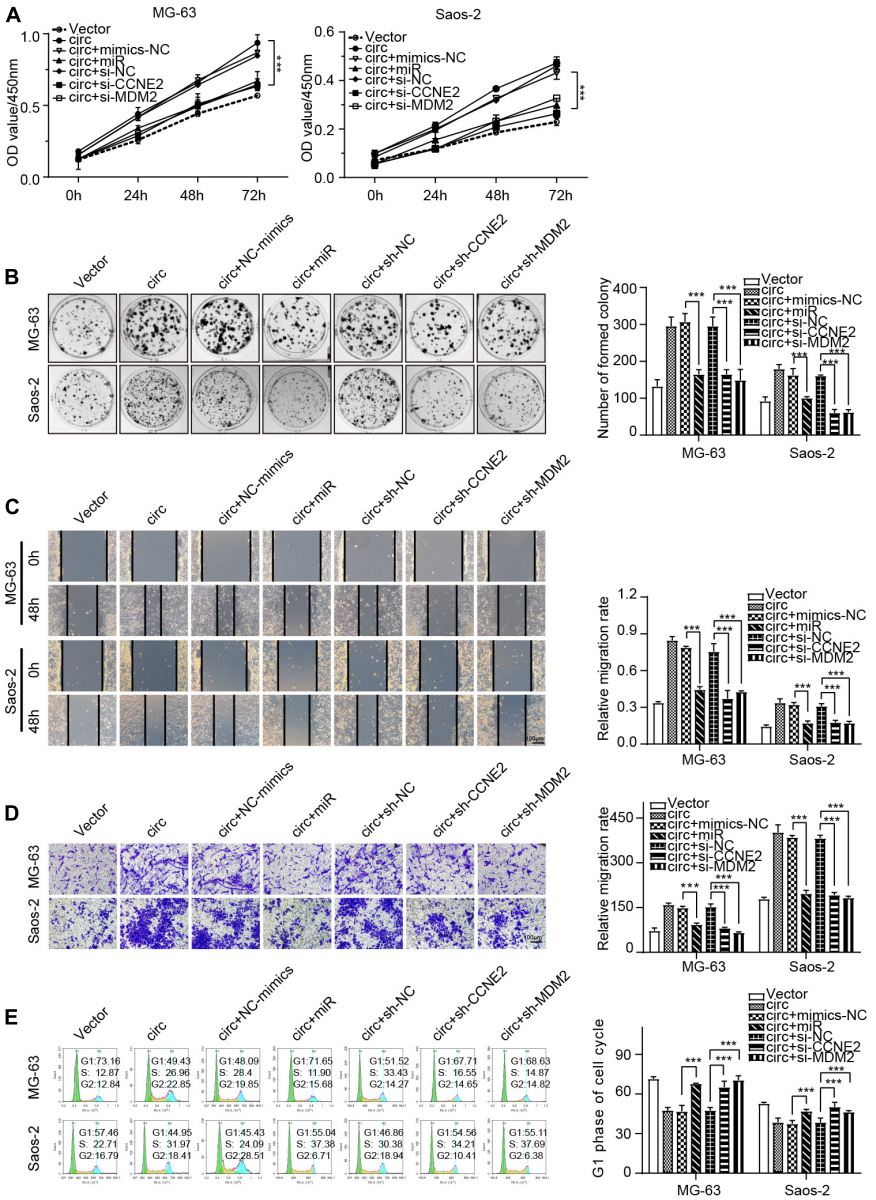


FIGURE 6 | hsa_circ_0000073 enhanced malignant behavior of OS cells by targeting miR-1252-5p and regulating CCNE2 and MDM2. **(A,B)** CCK-8 and colony formation assays demonstrated that overexpressed-miR-1252-5p, silenced-CCNE2, or MDM2 restored growth promotion induced by hsa_circ_0000073 overexpression. **(C,D)** Wound-healing and transwell assays evaluated cell migration and invasion in indicated groups, magnification, ×200. **(E)** Flow cytometry assay determined cell cycle under diverse conditions. Data were presented as mean ± SD ***$P < 0.001$.

multiple types of cancer and have great potentiality in regulating malignant tumor occurrence and development. For example, hsa_circ_0061825 could promote breast cancer progression, circ_SMAD4 contributes to gastric carcinogenesis, and circRNA-002178 acts as the tumor promoter in lung adenocarcinoma (Pan et al., 2020; Wang J. et al., 2020; Wang et al., 2021). Moreover, studies have found that different circRNAs have been shown to exhibit different effects and may act as the cancer-promoting or anticancer role in cancers. Such as in hepatocellular carcinoma, circTRIM33-12 could inhibit the progression, and circ_0008305 contributes to tumorigenesis (Zhang P. F. et al., 2019; Yan et al., 2021). However, the role of circRNAs in OS remains unclear. In this paper, we analyzed the most upregulated circRNAs in OS cell lines from GSE96964 and focused on the role and underlying mechanism of hsa_circ_0000073.

Based on our results, we verified hsa_circ_0000073 was highly expressed in OS cells and acted as an essential promotion factor in OS cells. Previously, Li X. et al. (2020) reported that hsa_circ_0000073 could enhance the proliferative, migrative, and invasive abilities of OS cells, which is also observed in our work. However, for the first time, our study revealed that the S phase of OS cells could arrest by hsa_circ_0000073

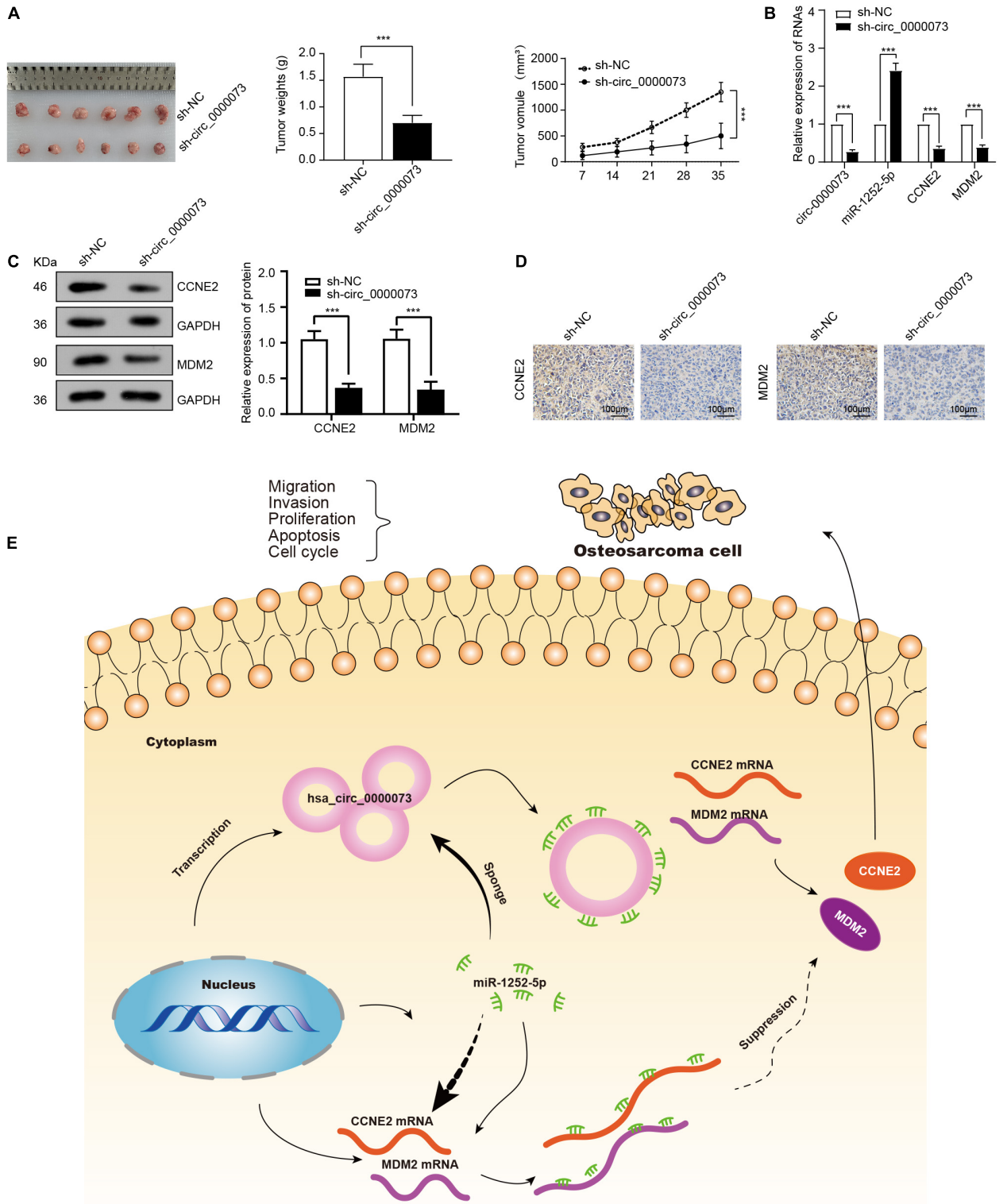


FIGURE 7 | Knockdown of hsa_circ_0000073 represses tumor growth through sponging miR-1252-5p and regulating CCNE2, and MDM2 *in vivo*. **(A)** Images, weight and growth curve of tumors after transfection with sh- hsa_circ_0000073 or sh-NC. **(B)** qRT-PCR determined expression of hsa_circ_0000073, miR-1252-5p, CCNE2, and MDM2 in tumors collected earlier. **(C,D)** WB and immunohistochemistry evaluated expression of CCNE2 and MDM2 when hsa_circ_0000073 was silenced, magnification, ×200. **(E)** Schematic illustration of final regulatory circuit among hsa_circ_0000073, miR-1252-5p, CCNE2, and MDM2. Data were presented as mean ± SD ***$P < 0.001$.

silencing. To explore the complex underlying mechanisms, we used the Affymetrix Gene Chip to analyze the DEGs after transfected sh-hsa_circ_0000073 in MG-63 and Saos-2 cells. Considering bioinformatics approaches are critical for handling and analyzing the deluge of information, bioinformatics analysis was performed to improve the accuracy of predicting target genes in our study. KEGG pathways analysis revealed that 16 DEGs were co-downregulated by hsa_circ_0000073 silencing in MG-63 and Saos-2 cell lines in "pathways in cancer." It is widely accepted that circRNAs are important in ceRNA networks. In OS, previous studies have reported that circ_0000337, hsa_circ_0136666, and hsa_circ_0032463 act as ceRNA contribute to OS progression (Fang and Long, 2020; Zhang et al., 2020; Qin and Wu, 2021). In our study, we searched the databases and found four miRNAs with several potential binding sites of hsa_circ_0000073 and created a potential ceRNA network among hsa_circ_0000073, 4 miRNAs, and the 16 target genes identified earlier.

Next, we deeply investigate the miRNAs with binding sites of hsa_circ_0000073, which found miR-1252-5p was regulated by hsa_circ_0000073 and was lowly in OS cells. Emerging researches have shown that miRNAs could function as a carcinogen or tumor suppressor involved in cancer progression (Song et al., 2019; Zhang L. et al., 2019). Indeed, miR-1252-5p has been verified to suppress cell proliferation and migration in several cancers (Gu and Liu, 2020; Chen et al., 2021). However, the role of miR-1252-5p in OS is unclear. In this paper, we first observed miR-1252-5p could suppress the malignant behavior of OS cells.

Subsequently, after knockdown of hsa_circ_0000073, the marked downregulation in messenger RNA and protein expression of two cancer-related genes, CCNE2 and MDM2, was verified by qRT-PCR and WB. Moreover, our data also demonstrated that CCNE2 and MDM2 have a higher expression level in MG-63 and Saos-2 cells than hFOB 1.19 cells. As previously reported, CCNE2, which is frequently observed in proliferation, or migration in various kinds of cancers, is one of the two regulatory subunits of cyclin-dependent kinase 2 and could regulate the progression from G1 to S phase in cells (Sonntag et al., 2018; Sun et al., 2020; Wu D. et al., 2020). On the other hand, several studies have confirmed that MDM2 has oncogenic properties, and targeted MDM2 is an especially attractive therapeutic strategy (Egorova et al., 2020; Konopleva et al., 2020). Here, we also observed CCNE2 and MDM2 could enhance the development of OS and could be regulated by hsa_circ_0000073. It suggested that hsa_circ_0000073 may prompt the progression of OS by sponging miR-1252-5p and modulating CCNE2 and MDM2 simultaneously.

However, although we have several preliminary findings to indicate the significance of hsa_circ_0000073/miR-1252-5p/CCNE2 or MDM2 axis in regulating OS progression, these conclusions were based on the responses of cell lines and mice. In the future, we believe that the clinical relevance and more animal experiments such as the survival curve and reverse experiment should be enrolled in our study. Also, more molecules and pathways working with hsa_circ_0000073 needed to be deeply investigated.

CONCLUSION

Our study confirms the key role of hsa_circ_0000073 in the regulation of malignant tumor behavior in OS cells, including proliferation, migration, invasion, and cell cycle *in vitro* as well as tumorigenesis *in vivo*. On the mechanisms, we first uncover hsa_circ_0000073 functions as a miR-1252-5p sponge and then affect CCNE2 and MDM2 expression, which providing a potential target for clinical treatment or prognosis of OS in the future.

DATA AVAILABILITY STATEMENT

The datasets presented in this study can be found in online repositories. The names of the repository/repositories and accession number(s) can be found below: GEO database and assigned GEO accession numbers as GSE176373.

ETHICS STATEMENT

This work was approved by the Animal Ethics Committee of the Guizhou Provincial People's Hospital.

AUTHOR CONTRIBUTIONS

XT, ZY, and ZR conceived and designed the experiments. ZR, QY, and JG performed the experiments. BL and ZY performed the statistical analysis. ZR and HH wrote the manuscript. All authors read and approved the final manuscript.

FUNDING

This work was supported by the National Natural Science Foundation of China (31660265, 31960208, 81060145, and 81560356), the Youth Fund of Guizhou Provincial People's Hospital [GZSYQN (2015) 06 and GZSYQN (2019) 15], the Subsidy Foundation of National Natural Science Foundation of Guizhou Provincial People's Hospital [Guizhou Science and Technology Platform (2017)5724], the Science and Technology Foundation of Guizhou Province [Guizhou Science and Technology J Word (2015)2096], and the Subsidy Foundation of National Natural Science Foundation of Guizhou Provincial People's Hospital (GPPH-NSFC-2019-1).

ACKNOWLEDGMENTS

Thanks to the persons who facilitated our work.

SUPPLEMENTARY MATERIAL

The Supplementary Material for this article can be found online at: https://www.frontiersin.org/articles/10.3389/fcell.2021.714601/full#supplementary-material

Supplementary Figure 1 | qRT-PCR analyzed the efficiency of miR-1252-5p mimics and sponge.

Supplementary Figure 2 | qRT-PCR and WB detected the knockdown effects of sh-CCNE2 and sh-MDM2.

REFERENCES

Agarwal, V., Bell, G. W., Nam, J. W., and Bartel, D. P. (2015). Predicting effective microRNA target sites in mammalian mRNAs. *eLife* 4:e05005. doi: 10.7554/eLife.05005

Arnaiz, E., Sole, C., Manterola, L., Iparraguirre, L., Otaegui, D., Lawrie, C. H., et al. (2019). CircRNAs and cancer: biomarkers and master regulators. *Semin. Cancer Biol.* 58, 90–99. doi: 10.1016/j.semcancer.2018.12.002

Bishop, M. W., Janeway, K. A., and Gorlick, R. (2016). Future directions in the treatment of osteosarcoma. *Curr. Opin. Pediatr.* 28, 26–33. doi: 10.1097/MOP.0000000000000298

Chen, R., Lei, S., Jiang, T., Zeng, J., Zhou, S., She, Y., et al. (2020). Roles of lncRNAs and circRNAs in regulating skeletal muscle development. *Acta Physiol.* 228:e13356. doi: 10.1111/apha.13356

Chen, X., Chen, H., Liu, M., Xiong, J., and Song, Z. (2021). Long noncoding RNA LINC00520 accelerates lung adenocarcinoma progression via miR-1252-5p/FOXR2 pathway. *Hum. Cell* 34, 478–490. doi: 10.1007/s13577-020-00478-9

Egorova, O., Lau, H. H., McGraphery, K., and Sheng, Y. (2020). Mdm2 and MdmX RING domains play distinct roles in the regulation of p53 responses: a comparative study of Mdm2 and MdmX RING domains in U2OS cells. *Int. J. Mol. Sci.* 21:1390. doi: 10.3390/ijms21041309

Enuka, Y., Lauriola, M., Feldman, M. E., Sas-Chen, A., Ulitsky, I., Yarden, Y., et al. (2016). Circular RNAs are long-lived and display only minimal early alterations in response to a growth factor. *Nucleic Acids Res.* 44, 1370–1383. doi: 10.1093/nar/gkv1367

Fang, Y., and Long, F. (2020). Circular RNA circ_0000337 contributes to osteosarcoma via the miR-4458/BACH1 pathway. *Cancer Biomark.* 28, 411–419. doi: 10.3233/CBM-190647

Gu, Z. R., and Liu, W. (2020). The LncRNA AL161431.1 targets miR-1252-5p and facilitates cellular proliferation and migration via MAPK signaling in endometrial carcinoma. *Eur. Rev. Med. Pharmacol. Sci.* 24, 2294–2302. doi: 10.26355/eurrev_202003_20495

Harrison, D. J., Geller, D. S., Gill, J. D., Lewis, V. O., and Gorlick, R. (2018). Current and future therapeutic approaches for osteosarcoma. *Expert. Rev. Anticancer Ther.* 18, 39–50. doi: 10.1080/14737140.2018.1413939

Jeck, W. R., Sorrentino, J. A., Wang, K., Slevin, M. K., Burd, C. E., Liu, J., et al. (2013). Circular RNAs are abundant, conserved, and associated with ALU repeats. *RNA* 19, 141–157. doi: 10.1261/rna.035667.112

Jiang, X., and Chen, D. (2021). Circular RNA hsa_circ_0000658 inhibits osteosarcoma cell proliferation and migration via the miR-1227/IRF2 axis. *J. Cell Mol. Med.* 25, 510–520. doi: 10.1111/jcmm.16105

Kanehisa, M., Furumichi, M., Sato, Y., Ishiguro-Watanabe, M., and Tanabe, M. (2021). KEGG: integrating viruses and cellular organisms. *Nucleic Acids Res.* 49, D545–D551. doi: 10.1093/nar/gkaa970

Konopleva, M., Martinelli, G., Daver, N., Papayannidis, C., Wei, A., Higgins, B., et al. (2020). MDM2 inhibition: an important step forward in cancer therapy. *Leukemia* 34, 2858–2874. doi: 10.1038/s41375-020-0949-z

Kristensen, L. S., Andersen, M. S., Stagsted, L. V. W., Ebbesen, K. K., Hansen, T. B., Kjems, J., et al. (2019). The biogenesis, biology and characterization of circular RNAs. *Nat. Rev. Genet.* 20, 675–691. doi: 10.1038/s41576-019-0158-7

Li, J. H., Liu, S., Zhou, H., Qu, L. H., and Yang, J. H. (2014). starBase v2.0: decoding miRNA-ceRNA, miRNA-ncRNA and protein-RNA interaction networks from large-scale CLIP-Seq data. *Nucleic Acids Res.* 42, D92–D97. doi: 10.1093/nar/gkt1248

Li, R., Jiang, J., Shi, H., Qian, H., Zhang, X., Xu, W., et al. (2020). CircRNA: a rising star in gastric cancer. *Cell Mol. Life Sci.* 77, 1661–1680. doi: 10.1007/s00018-019-03345-5

Li, X., Liu, Y., Zhang, X., Shen, J., Xu, R., Liu, Y., et al. (2020). Circular RNA hsa_circ_0000073 contributes to osteosarcoma cell proliferation, migration, invasion and methotrexate resistance by sponging miR-145-5p and miR-151-3p and upregulating NRAS. *Aging* 12, 14157–14173. doi: 10.18632/aging.103423

Liu, M., Wang, Q., Shen, J., Yang, B. B., and Ding, X. (2019). Circbank: a comprehensive database for circRNA with standard nomenclature. *RNA Biol.* 16, 899–905. doi: 10.1080/15476286.2019.1600395

Lu, G., Zhang, J., Liu, X., Liu, W., Cao, G., Lv, C., et al. (2019). Regulatory network of two circRNAs and an miRNA with their targeted genes under astilbin treatment in pulmonary fibrosis. *J. Cell Mol. Med.* 23, 6720–6729. doi: 10.1111/jcmm.14550

Mao, X., Guo, S., Gao, L., and Li, G. (2021). Circ-XPR1 promotes osteosarcoma proliferation through regulating the miR-214-5p/DDX5 axis. *Hum. Cell* 34, 122–131. doi: 10.1007/s13577-020-00412-z

Otoukesh, B., Boddouhi, B., Moghtadaei, M., Kaghazian, P., and Kaghazian, M. (2018). Novel molecular insights and new therapeutic strategies in osteosarcoma. *Cancer Cell Int.* 18:158. doi: 10.1186/s12935-018-0654-4

Pan, G., Mao, A., Liu, J., Lu, J., Ding, J., Liu, W., et al. (2020). Circular RNA hsa_circ_0061825 (circ-TFF1) contributes to breast cancer progression through targeting miR-326/TFF1 signalling. *Cell Prolif.* 53:e12720. doi: 10.1111/cpr.12720

Qin, G., and Wu, X. (2021). Circular RNA hsa_circ_0032463 acts as the tumor promoter in osteosarcoma by regulating the MicroRNA 498/LEF1 Axis. *Mol. Cell Biol.* 41:e0010021. doi: 10.1128/MCB.00100-21

Shannon, P., Markiel, A., Ozier, O., Baliga, N. S., Wang, J. T., Ramage, D., et al. (2003). Cytoscape: a software environment for integrated models of biomolecular interaction networks. *Genome Res.* 13, 2498–2504. doi: 10.1101/gr.1239303

Song, T., Xu, A., Zhang, Z., Gao, F., Zhao, L., Chen, X., et al. (2019). CircRNA hsa_circRNA_101996 increases cervical cancer proliferation and invasion through activating TPX2 expression by restraining miR-8075. *J. Cell Physiol.* 234, 14296–14305. doi: 10.1002/jcp.28128

Sonntag, R., Giebelera, N., Nevzorovaa, Y. A., Bangena, J.-M., Fahrenkampb, D., Lambertza, D., et al. (2018). Cyclin E1 and cyclin-dependent kinase 2 are critical for initiation, but not for progression of hepatocellular carcinoma. *Proc. Natl. Acad. Sci. U.S.A.* 115, 9282–9287. doi: 10.1073/pnas.1807155115

Sun, Q., Yu, R., Wang, C., Yao, J., and Zhang, L. (2020). Circular RNA circ-CSPP1 regulates CCNE2 to facilitate hepatocellular carcinoma cell growth via sponging miR-577. *Cancer Cell Int.* 20:202. doi: 10.1186/s12935-020-01287-8

Szklarczyk, D., Gable, A. L., Lyon, D., Junge, A., Wyder, S., Huerta-Cepas, J., et al. (2019). STRING v11: protein-protein association networks with increased coverage, supporting functional discovery in genome-wide experimental datasets. *Nucleic Acids Res.* 47, D607–D613. doi: 10.1093/nar/gky1131

Wang, H. Y., Wang, Y. P., Zeng, X., Zheng, Y., Guo, Q. H., Ji, R., et al. (2020). Circular RNA is a popular molecule in tumors of the digestive system (Review). *Int. J. Oncol.* 57, 21–42. doi: 10.3892/ijo.2020.5054

Wang, J., Zhao, X. H., Wang, Y. B., Ren, F. H., Sun, D. W., Yan, Y. B., et al. (2020). circRNA-002178 act as a ceRNA to promote PDL1/PD1 expression in lung adenocarcinoma. *Cell Death Dis.* 11:32. doi: 10.1038/s41419-020-2230-9

Wang, L., Li, B., Yi, X., Xiao, X., Zheng, Q., Ma, L., et al. (2021). Circ_SMAD4 promotes gastric carcinogenesis by activating wnt/beta-catenin pathway. *Cell Prolif.* 54:e12981. doi: 10.1111/cpr.12981

Wu, D., He, J., Wei, Zhang, Wang, K., Jin, S., Li, J., et al. (2020). CARM1 promotes non-small cell lung cancer progression through upregulating CCNE2 expression. *Aging* 12, 10578–10593. doi: 10.18632/aging.103280

Wu, P., Mo, Y., Peng, M., Tang, T., Zhong, Y., Deng, X., et al. (2020). Emerging role of tumor-related functional peptides encoded by lncRNA and circRNA. *Mol. Cancer* 19:22. doi: 10.1186/s12943-020-1147-3

Wu, Y., Xie, Z., Chen, J., Chen, J., Ni, W., Ma, Y., et al. (2019). Circular RNA circTADA2A promotes osteosarcoma progression and metastasis by sponging miR-203a-3p and regulating CREB3 expression. *Mol. Cancer* 18:73. doi: 10.1186/s12943-019-1007-1

Yan, F., Fan, B., Wang, J., Wei, W., Tang, Q., Lu, L., et al. (2021). Circ_0008305-mediated miR-660/BAG5 axis contributes to hepatocellular carcinoma tumorigenesis. *Cancer Med.* 10, 833–842. doi: 10.1002/cam4.3657

Yu, G., Wang, L. G., Han, Y., and He, Q. Y. (2012). clusterProfiler: an R package for comparing biological themes among gene clusters. *OMICS* 16, 284–287. doi: 10.1089/omi.2011.0118

Zhang, C., Na, N., Liu, L., and Qiu, Y. (2021). CircRNA hsa_circ_0005909 promotes cell proliferation of osteosarcoma cells by targeting miR-338-3p/HMGA1 Axis. *Cancer Manag. Res.* 13, 795–803. doi: 10.2147/CMAR.S285118

Zhang, C., Zhou, H., Yuan, K., Xie, R., and Chen, C. (2020). Overexpression of hsa_circ_0136666 predicts poor prognosis and initiates osteosarcoma tumorigenesis through miR-593-3p/ZEB2 pathway. *Aging* 12, 10488–10496. doi: 10.18632/aging.103273

Zhang, L., Liao, Y., and Tang, L. (2019). MicroRNA-34 family: a potential tumor suppressor and therapeutic candidate in cancer. *J. Exp. Clin. Cancer Res.* 38:53. doi: 10.1186/s13046-019-1059-5

Zhang, P. F., Wei, C. Y., Huang, X. Y., Peng, R., Yang, X., Lu, J. C., et al. (2019). Circular RNA circTRIM33-12 acts as the sponge of MicroRNA-191 to suppress hepatocellular carcinoma progression. *Mol. Cancer* 18:105. doi: 10.1186/s12943-019-1031-1

Zhou, C., Tan, W., Lv, H., Gao, F., and Sun, J. (2016). Hypoxia-inducible microRNA-488 regulates apoptosis by targeting Bim in osteosarcoma. *Cell Oncol.* 39, 463–471. doi: 10.1007/s13402-016-0288-2

Conflict of Interest: The authors declare that the research was conducted in the absence of any commercial or financial relationships that could be construed as a potential conflict of interest.

Publisher's Note: All claims expressed in this article are solely those of the authors and do not necessarily represent those of their affiliated organizations, or those of the publisher, the editors and the reviewers. Any product that may be evaluated in this article, or claim that may be made by its manufacturer, is not guaranteed or endorsed by the publisher.

Copyright © 2021 Ren, Yang, Guo, Huang, Li, Yang and Tian. This is an open-access article distributed under the terms of the Creative Commons Attribution License (CC BY). The use, distribution or reproduction in other forums is permitted, provided the original author(s) and the copyright owner(s) are credited and that the original publication in this journal is cited, in accordance with accepted academic practice. No use, distribution or reproduction is permitted which does not comply with these terms.

frontiers in Cell and Developmental Biology

ORIGINAL RESEARCH
published: 21 September 2021
doi: 10.3389/fcell.2021.722841

Classification of Estrogen Receptor-Positive Breast Cancer Based on Immunogenomic Profiling and Validation at Single-Cell Resolution

Xianxiong Ma[1†], Hengyu Chen[2†], Ming Yang[3], Zunxiang Ke[4], Mengyi Wang[5], Tao Huang[5] and Lei Li[5]*

[1] Department of Gastrointestinal Surgery, Union Hospital, Tongji Medical College, Huazhong University of Science and Technology, Wuhan, China, [2] Department of Breast and Thyroid Surgery, The Second Affiliated Hospital of Hainan Medical University, Haikou, China, [3] Department of Pancreatic Surgery, Union Hospital, Tongji Medical College, Huazhong University of Science and Technology, Wuhan, China, [4] Department of Emergency Surgery, Union Hospital, Tongji Medical College, Huazhong University of Science and Technology, Wuhan, China, [5] Department of Breast and Thyroid Surgery, Union Hospital, Tongji Medical College, Huazhong University of Science and Technology, Wuhan, China

OPEN ACCESS

Edited by:
Ira Ida Skvortsova, Innsbruck Medical University, Austria

Reviewed by:
David Linnaeus Gibbs, Institute for Systems Biology (ISB), United States
Wei Chong, Tianjin Medical University Cancer Institute and Hospital, China

***Correspondence:**
Lei Li
leili2008@hust.edu.cn

† These authors have contributed equally to this work and share first authorship

Specialty section:
This article was submitted to Molecular and Cellular Oncology, a section of the journal Frontiers in Cell and Developmental Biology

Received: *09 June 2021*
Accepted: *10 August 2021*
Published: *21 September 2021*

Citation:
Ma X, Chen H, Yang M, Ke Z, Wang M, Huang T and Li L (2021) Classification of Estrogen Receptor-Positive Breast Cancer Based on Immunogenomic Profiling and Validation at Single-Cell Resolution. Front. Cell Dev. Biol. 9:722841. doi: 10.3389/fcell.2021.722841

Background: The aim of this paper was to identify an immunotherapy-sensitive subtype for estrogen receptor-positive breast cancer (ER+ BC) patients by exploring the relationship between cancer genetic programs and antitumor immunity via multidimensional genome-scale analyses.

Methods: Multidimensional ER+ BC high-throughput data (raw count data) including gene expression profiles, copy number variation (CNV) data, single-nucleotide polymorphism mutation data, and relevant clinical information were downloaded from The Cancer Genome Atlas to explore an immune subtype sensitive to immunotherapy using the Consensus Cluster Plus algorithm based on multidimensional genome-scale analyses. One ArrayExpress dataset and eight Gene Expression Omnibus (GEO) datasets (GEO-meta dataset) as well as the Molecular Taxonomy of Breast Cancer International Consortium dataset were used as validation sets to confirm the findings regarding the immune profiles, mutational features, and survival outcomes of the three identified immune subtypes. Moreover, the development trajectory of ER+ BC patients from the single-cell resolution level was also explored.

Results: Through comprehensive bioinformatics analysis, three immune subtypes of ER+ BC (C1, C2, and C3, designated the immune suppressive, activation, and neutral subtypes, respectively) were identified. C2 was associated with up-regulated immune cell signatures and immune checkpoint genes. Additionally, five tumor-related pathways (transforming growth factor, epithelial–mesenchymal transition, extracellular matrix, interferon-γ, and WNT signaling) tended to be more activated in C2 than in C1 and C3. Moreover, C2 was associated with a lower tumor mutation burden, a decreased

neoantigen load, and fewer CNVs. Drug sensitivity analysis further showed that C2 may be more sensitive to immunosuppressive agents.

Conclusion: C2 (the immune activation subtype) may be sensitive to immunotherapy, which provides new insights into effective treatment approaches for ER+ BC.

Keywords: breast cancer, immune signature, TCGA, GEO, molecular subtypes, ER+, genomic mutation, single-cell sequencing

INTRODUCTION

Breast cancer (BC) is the most common cause of cancer-related death among females worldwide (Torre et al., 2017). The 5-year survival rate of BC patients is poor according to 2019 data (DeSantis et al., 2019). Estrogen receptor-positive (ER+) BC is the most common subtype of BC, accounting for approximately 75% of all BC cases (Burstein et al., 2010). The current treatments for ER+ BC include surgery, chemotherapy, and molecular targeted therapy (Bayraktar et al., 2019). However, treatment has been hindered by resistance in ER+ BC, which is related to the molecular heterogeneity and complex biological processes in these cases (Koren and Bentires-Alj, 2015). Thus, novel treatments are needed to improve the prognosis of ER+ BC patients.

Endocrine treatment is an important targeted therapy for patients with ER+ BC. However, quite a few BC patients with localized disease and most BC patients with metastasis develop resistance to endocrine therapy (No authors listed, 1998; Hurvitz and Pietras, 2008; Osborne and Schiff, 2011). Immunotherapy has gradually attracted the interest of many BC researchers. It is well known that an active immune microenvironment can hinder tumor growth and metastasis. Studies have suggested that tumor-infiltrating lymphocytes (TILs) were correlated with better cancer prognosis (Fridman et al., 2012). For example, Chu et al. (2019) reported that CD103(+) TILs predicted favorable prognosis in patients with esophageal squamous cell carcinoma. Hida et al. (2019) suggested that diffusely distributed TILs were a marker of improved prognosis in triple-negative BC (Adams et al., 2015). Loi et al. (2013) conducted a phase III randomized adjuvant trial of lymph node-positive BC patients (comparing doxorubicin plus docetaxel- vs doxorubicin-based chemotherapies) and revealed the prognostic and predictive values of TILs; the ER+ BC patients generally had low TIL levels, though a small proportion had very high TIL levels. However, no studies have reported a clear association between TILs and prognosis in ER+ BC patients' prognoses thus far, since the outcomes of the ER+ subgroup are highly heterogeneous (Ali et al., 2014; Dieci et al., 2015; Luen et al., 2016).

Therefore, our aim was to explore the relationship between the genomic landscape and antitumor immunity via multidimensional genome-scale analyses to identify an immune subtype of ER+ BC patients that may be sensitive to immunotherapy. RNA-sequencing data from The Cancer Genome Atlas (TCGA) database was used to identify three discrete immune subtypes of ER+ BC (regarded as immune suppressive, activation, and neutral phenotypes). Somatic mutation data and copy number variation (CNV) data were used to explore the associations between genetic features and the three immune subtypes. Additionally, a Gene Expression Omnibus (GEO)-meta dataset (composed of nine small datasets) and a Molecular Taxonomy of BC International Consortium (METABRIC) dataset were used as validation sets to confirm the value of the three identified immune subtypes. Moreover, the drug sensitivity of each ER+ BC immune subtype and the development trajectory of ER+ tumor microenvironment were investigated. The results improve our understanding of the immune microenvironment of the primary tumors in ER+ BC patients and provide new insights into immunotherapy for ER+ BC.

Abbreviations: BC, breast cancer; CNVs, copy number variations; SNP, single-nucleotide polymorphism; TCGA, The Cancer Genome Atlas; TMB, tumor mutation burden; TILs, tumor-infiltrating lymphocytes; PFS, progression-free survival; DFS, disease-free survival; DLDA, diagonal linear discriminant analysis; TGF-β, transforming growth factor-β; EMT, epithelial–mesenchymal transition.

MATERIALS AND METHODS

Data Presentation and Filtering

TCGA Dataset

Level 3 multidimensional BC high-throughput data including gene expression profiles, CNV data, single-nucleotide polymorphism (SNP) mutation data, and relevant clinical information were downloaded from TCGA using the "TCGAbiolinks" package (Colaprico et al., 2016). We excluded samples based on the following criteria: (1) incomplete overall survival (OS) or recurrence-free survival (RFS) data; (2) no ER+ BC samples; (3) para-cancer tissue samples of BC patients; and (4) datasets containing less than 40 samples. Thereafter, immune-associated genes were retrieved from the ImmPort database[1] (Bhattacharya et al., 2014). Eventually, gene expression data involving 1,811 immune-associated genes and 787 BC patients were used as the training dataset to identify a potentially immunotherapy-sensitive immune subtype among ER+ BC patients.

GEO-Meta Dataset

An ArrayExpress dataset (E-TABM-158, 83 samples) and eight GEO datasets (GSE1456, GSE2034, GSE2603, GSE45255, GSE4922, GSE6532, GSE7390, and GSE9195, containing 77, 209, 46, 58, 211, 201, 134, and 77 samples, respectively) along with a METABRIC dataset (1,435 samples) were used as external validation sets to confirm the findings regarding the immune

[1]http://www.immport.org

profiles, mutational features, and survival outcomes of the identified immune subtypes. As both GEO and ArrayExpress data were obtained using an Affymetrix microarray chip, we integrated the data to create the GEO-meta dataset (1,096 samples in total) for subsequent analyses. All GEO-meta sub-datasets contained progression-free survival (PFS)/RFS/disease-free survival (DFS) information, whereas only a few GEO-meta sub-datasets contained OS data. Therefore, only PFS/RFS/DFS were used to conduct a survival analysis in the GEO-meta dataset (while OS data were also used in the corresponding TCGA and METABRIC analyses). The GEO-meta ER+ BC samples with complete PFS/RFS/DFS data were included in the following analysis.

METABRIC Dataset

Level 3 METABRIC data including gene expression profiles, CNV data, SNP mutation data, and matched clinical information were obtained from the cBioPortal database (Pereira et al., 2016). The eligible criteria were the same as above. The detailed clinical information of all the included samples is shown in **Supplementary Table 1**.

Data Preprocessing

The immune-associated genes from the ImmPort database were used to identify the immune subtypes of ER+ BC and the immune cell profiles of these subtypes. The raw count matrix of level 3 TCGA mRNA data was converted to transcripts per million data. Genes with no expression in >50% of the samples were removed. Consequently, a TCGA training dataset consists of 1,295 immune-associated genes, and 787 ER+ BC samples were used in the cluster analysis. Regarding the GEO-meta sub-datasets, the raw data (CEL files) were normalized using the "rma" function in the "affy" package (Gautier et al., 2004). Regarding the METABRIC dataset, the normalized gene expression data were manually obtained directly from the cBioPortal website and used for subsequent analysis. In addition, the batch effects between different datasets were eliminated with the ComBat empirical Bayes method using the "sva" package (Chakraborty et al., 2012).

Identification of ER+ BC Subtypes in the Training Dataset and Validation of Molecular Subtypes in the GEO-Meta Dataset and METABRIC Dataset

To identify ER+ BC subtypes based on immune-associated gene expression profiles, the "ConsensusClusterPlus" 1.50.0 package (Wilkerson and Hayes, 2010) was applied to generate a consensus matrix plot. This involved 1,000 iterations, a maximum of eight clusters, sampling of 80% of the samples at each iteration, and use of the partitioning around medoids clustering method. The optimal cluster number was determined based on cumulative distribution function curves of the consensus score. The samples from two validation datasets were then classified according to specified classifiers trained in the TCGA dataset by using diagonal linear discriminant analysis (DLDA), which is a machine learning approach available in the "classpredict" package developed using BRB-ArrayTools modules (Simon et al., 2007).

Immune Profiles in ER+ BC Subtypes

First, the "GSVA" package and single-sample gene set enrichment analysis (ssGSEA; Bindea et al., 2013) were conducted with the expression signatures of 24 types of immune cells from a previous study (Hanzelmann et al., 2013). The resultant enrichment score for each of the 24 immune cell signatures represented the absolute enrichment of a particular gene set in each sample in the datasets (Subramanian et al., 2005). Second, for further validation, the "MCPcounter" package was also used to evaluate the absolute abundance of eight immune cell populations and two stromal cell populations based on gene expression profiles (Becht et al., 2016). Third, the "ESTIMATE" package was used to the estimate immune score and stromal score (Yoshihara et al., 2013), which were compared between subtypes. Fourth, the expression level of about 30 potentially targetable immune checkpoint molecules was compared between each subtype (Kim et al., 2019; Toor et al., 2019). Lastly, tumor mutation burden (TMB), neoantigen load, and CNV were compared between the subtypes, with the predicted neoantigen loads being calculated based on a previous analysis (Rooney et al., 2015). Thus, immune signature scores, immune checkpoint gene expression, and mutational features were compared between the three subtypes. The differences were assessed using the Mann–Whitney *U* test, with the Bonferroni correction being used to correct for multiple comparisons. Meanwhile, the LASSO regression model was used to construct a scoring system to quantify immune subtypes for individuals. The LASSO regression model was implemented via a publicly available R package "glmnet" (Engebretsen and Bohlin, 2019).

Prediction of the Benefit of Each Subclass From Immunotherapy and Targeted Therapy

Data from 47 melanoma patients treated with immunotherapy (a programmed cell death protein [PD]-1 inhibitor or a cytotoxic T-lymphocyte-associated protein [CTLA]-4 inhibitor) were used to assess the potential responses to immunotherapy of our three immune subtypes. This was done by assessing the similarities in gene expression profiles between our subtypes and the melanoma patients using a SubMap analysis in GenePattern (Roh et al., 2017). Additionally, sensitivity to two ER+ BC-targeted drugs (tamoxifen and fulvestrant) was evaluated in a SubMap analysis based on Genomics of Drug Sensitivity in Cancer cell line data (Iorio et al., 2016). 48 BC cell lines were ranked based on the half maximal inhibitory concentration (IC50) value, with 50% of cell lines with the highest IC50 values being considered drug resistant and the remainder being considered drug sensitive.

Single-Cell Development Analysis

We used single-cell data (GSE114725) to explore the development trajectory of the tumor microenvironment in ER+ BC patients. In total, 14,800 cells from four ER+ patients out of eight BC patients in the original dataset were included in our study. The raw count matrix of single-cell data was

downloaded from the GEO database. We successfully annotated 3,903 cells using "SingleR" packages (Aran et al., 2019), and a development trajectory analysis was performed using "Monocle" packages (Qiu et al., 2017). Furthermore, the annotation results regarding the 3,903 cells reported by Azizi et al. (2018) were used to validate our annotation results.

Additional Statistical Analyses

Chi-square and Fisher's exact tests were used to assess the associations between conventional clinical variables [age, ethnicity, cancer site, cancer stage, human epidermal growth factor receptor 2 (HER2) status, progesterone receptor status, and number of positive lymph nodes] and our three immune subtypes. Kaplan–Meier curves and log-rank tests were used to compare the survival of patients with the three immune subtypes. All analyses were performed using R software, unless otherwise specified.

RESULTS

ER+ BC Were Divided Into Three Subtypes Based on the ConsensusClusterPlus Algorithm

The study flowchart is presented in **Figure 1A**. The batch effect was removed from the standardized data before consensus clustering. The t-distributed stochastic neighbor embedding (t-SNE) performance before and after removing the batch effect is shown in **Figures 1B,C**, respectively. The expression profiles of 1,295 immune-associated genes were used to classify patients into K that consists of two to eight clusters, using the ConsensusClusterPlus algorithm (**Figure 1D**). $K = 3$ was optimal based on the cumulative distribution function curves of the consensus score (**Figures 1E,F**). The three subtypes were presented on a two-dimensional scatter plot based on the t-SNE algorithm and could be distinguished well (**Figure 1G**), which was largely concordant with the previous consensus clustering shown in **Figures 1E,F**.

The distributions of conventional clinic-related variables among the three molecular subtypes from the TCGA cohort are shown in **Table 1**. The association between age and three subtypes was significant ($p = 0.0003$). Meanwhile, there were also significant differences for age, HER2 status, number of positive lymph nodes, and ethnicity in C2 patients ($p = 0.0003$, $p < 0.001$, and $p < 0.0015$, respectively), whereas the other clinical variables are statistically non-significant.

Immune Cell Profiles of the Three Subtypes

The enrichment scores regarding the 24 immune cell signatures for each TCGA sample are shown in **Figure 2A** (top). Most of these immune signatures were up-regulated in C2 compared with C1 and C3, while Th2 cells were the most highly up-regulated cells in C1 and plasmacytoid dendritic cells (pDCs) and CD56 (bright) natural killer (NK) cells were mainly up-regulated cells in C3 (**Supplementary Figure 1**). Additionally, the distribution of eight immune cells and two stromal cells identified using the MCPcounter algorithm confirmed our initial immune cell signature results (**Figure 2A**, middle, and **Supplementary Figure 2**). Thereafter, the ESTIMATE algorithm was used to calculate immune and stromal scores. As expected, C2 had a higher score than C1 and C3 ($p < 0.001$; **Figures 2A–C**).

We also examined the expression level of >30 immune checkpoint molecules that have been reported to play important roles in T-cell regulation in the TCGA dataset (Kim et al., 2019; Toor et al., 2019). Most of the immune checkpoint molecules were more obviously up-regulated in C2 than in C1, and TNFRSF14 was the most regulated immune checkpoint molecule in C3 (**Figure 2A**, bottom; **Supplementary Figures 3A, 4, 5**). Taking into account the consistency of the up-regulated immune cell signatures and the immune checkpoint molecules in C2, followed by C3 and then C1, we designated C1, C2, and C3 as the immune suppressive, activation, and neutral subtypes, respectively.

We then compared the survival data between the three immune subtypes. Unexpectedly, both OS and DFS were longer for C2 (the immune activation subtype) than for C1 (the immune suppressive subtype; **Figures 2D,E** and **Supplementary Figures 3B,C**). The findings were contrary to current mainstream perception (Zhang et al., 2020), which suggests that increased immune cell infiltration leads to worse prognosis. Meanwhile, the samples were converted into dichotomous variables (C2 group and non-C2 group), and an eight-gene immune signature was developed and used to construct a scoring system to quantify immune subtypes for individuals using the following risk score formula: 0.10394*GAST + 0.56421*HFE + 0.80564*PLXNA3 + 0.40455*PLXNC1 + 0.1667*SEMA3A + 0.26431*TNFRSF11B + 1.16759*ZC3HAV1 − 0.12962*CCL14 (**Supplementary Figures 3D,E**).

Studies have reported that tumor-associated signatures such as the transforming growth factor (TGF)-β signature and epithelial–mesenchymal transition (EMT) signature play important roles in tumor progression and drug resistance (Oshimori et al., 2015; Xu et al., 2018; Tripathi et al., 2019). Unsurprisingly, the five tumor progression pathways [TGF-β signaling, EMT, extracellular matrix (ECM), interferon (IFN)-γ, and WNT signaling] were more activated in C2 than in C1 and C3 (**Figure 2A**, middle, and **Supplementary Figure 2**). This indicates that C2 may involve relatively advanced tumor stages, leading to increased immune cell recruitment to combat the tumor cells.

C2 Was Associated With a Lower TMB, a Decreased Neoantigen Load, and Fewer CNVs

Studies have reported that the genomic and mutational landscape is related to antitumor immunity. For example, Takahashi et al. (2020) revealed an association between a biologically aggressive phenotype in BC with a high mutation rate and an anticancer immunity counterbalance. Additionally, aneuploidy has been reported to be involved in immune evasion, which may reduce the effect of immunotherapy (Davoli et al., 2017). To explore

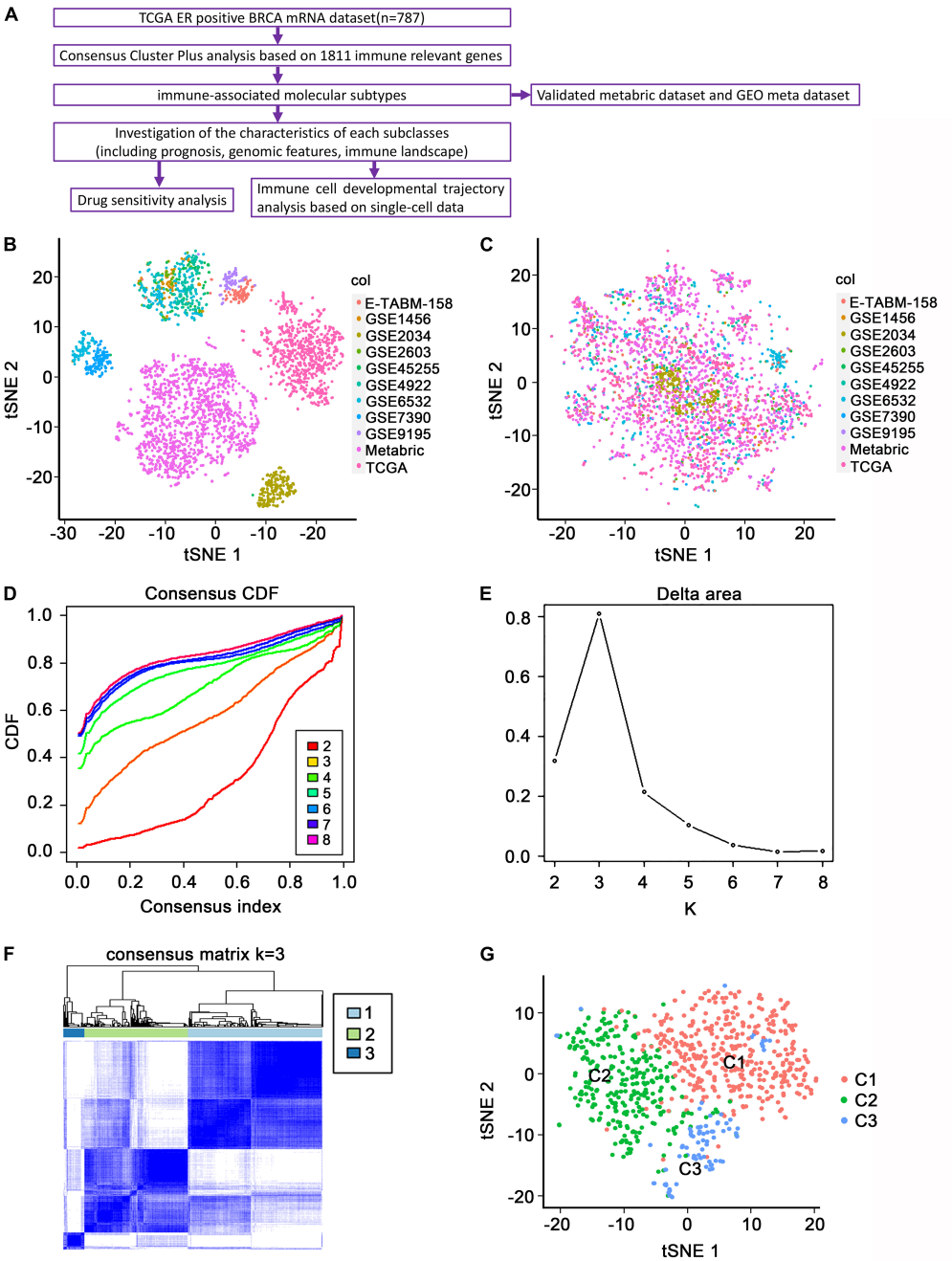


FIGURE 1 | Identification of immune-associated subtypes of ER+ BC in the TCGA dataset. **(A)** Flowchart of the present study. **(B)** The t-SNE distribution of all the enrolled patients before removing batch effects. Each point represents a single sample; different colors represent the included sub-datasets. **(C)** The t-SNE distribution of all the enrolled patients after removing batch effects. **(D)** The cumulative distribution function (CDF) curves in consensus cluster analysis. CDF curves of consensus scores by different subtype numbers (k = 2, 3, 4, 5, 6, 7, and 8) were displayed. **(E)** Relative change in area under the CDF curve for k = 2–8. **(F)** The consensus score matrix of all samples when k = 3. The higher the consensus score was, the more likely they were assigned to the same group. **(G)** The t-SNE distribution of TCGA ER+ BC samples by expression profile of global immune genes. Each point represents a single sample; different colors represent the three subtypes.

whether the TMB, neoantigen load, and CNV affect the immune microenvironment in ER+ BC patients in the TCGA dataset, we conducted a comprehensive analysis to examine the associations between these factors and the immune subtypes. The variants were mostly missense mutations, and SNPs were the most common variant type (**Figures 3A,B**). **Figure 3C** presented a panoramic view of ER+ mutations in each immune subtype: PIK3CA, TP53, CDH1, GATA3, and TTN were the genes with the highest mutation rates. C2 had a significantly lower TMB (**Figure 3D**) and a significantly decreased neoantigen

TABLE 1 | Association of three immune subtypes with clinical variables in the TCGA and METABRIC cohorts.

Characteristic		TCGA cohort				METABRIC cohort			
		C1	C2	C3	*p*-value	C1	C2	C3	*p*-value
Age					0.0003				< 0.001
	≥60	222	120	48		595	250	45	
	<60	184	177	36		303	221	21	
Site					0.41				0.31
	Left	216	143	44		459	220	33	
	Right	190	154	40		390	227	32	
	Unknown					49	24	1	
Stage					0.69				0.96
	Stage I	74	56	10		229	135	18	
	Stage II	229	160	49		372	207	26	
	Stage III	88	71	24		44	23	1	
	Stage IV	6	4	1		6	3	0	
	Unknown	9	6	0		1	1	0	
HER2 status					0.0003				0.3
	Positive	76	31	13		58	38	7	
	Negative	202	186	35		840	433	59	
	Indeterminate	128	80	36					
PR status					0.32				0.26
	Positive	342	259	66		621	307	42	
	Negative	62	37	18		277	164	24	
	Indeterminate	2	1	0					
No. of positive lymph nodes					< 0.001				0.12
	0	149	127	30		491	250	44	
	≥1	170	146	46		407	221	22	
	Unknown	87	24	8					
Ethnicity					0.0015				
	Hispanic/Latino	15	12	3					
	Not Hispanic/Latino	301	237	78					
	Unknown	90	48	3					

HER2: human epidermal growth factor receptor 2; PR: progesterone receptor.

load (**Figure 3E**) compared with C1. Furthermore, C2 had the significantly lowest CNV regarding both amplification and deletion (**Figures 3F,G**).

We further applied the MutSigCV algorithm to identify driver genes based on the TCGA mutation data, and 27 mutated genes were identified (FDR < 0.05, **Supplementary Table 2**). Among these genes, two (CDH1 and PIK3R1) were the marker genes (**Supplementary Table 3**) of three identified immune subtypes. It should be noted that CDH1 was a marker gene in all three subtypes. In other words, CDH1 expression was significantly different in each of the three subtypes, suggesting that CDH1 may be the mutation driver gene that modified the three immune subtypes. Unlike CDH1, PIK3R1 was a specific marker gene of the immune neutral subtype.

Three Immune Subtypes Were Validated in the GEO-Meta and METABRIC Datasets

The three immune subtypes identified in the TCGA training cohort were validated in two external cohorts using a DLDA classifier.

In the GEO-meta cohort, consistent with the TCGA cohort, C2 was shown to have high levels of most of the immune cell signatures (**Figure 4A**, top), while Th2 cells were most distinctly up-regulated in C1 and CD56 (bright) NK cells were most obviously up-regulated in C3. Additionally, Th17, Treg, and NK cells were also up-regulated in C3. Eosinophils were the most highly up-regulated cells in C1 (**Supplementary Figure 6**). Similar results were obtained using the MCPcounter algorithm except that the neutrophils were down-regulated in C2 (**Figure 4A**, middle). The ESTIMATE algorithm also demonstrated that the immune, stromal score and tumor purity were highest in C2 (**Figure 4A**, middle; **Figures 4B–D**, **Supplementary Figure 7**). Moreover, C2 had high expression levels of the immune checkpoint molecules (**Figure 4A**, bottom; **Supplementary Figures 8A, 9, 10**), and the Kaplan–Meier survival analysis revealed that C2 was associated with improved prognosis (**Figure 4E** and **Supplementary Figure 8B**).

In the METABRIC cohort, a majority of immune cells, most immune checkpoint molecule expression levels, and the immune score were increased in C2 (**Figures 5A–D** and **Supplementary Figures 11, 12, 14, 15**). TMB and neoantigen load were significantly lower in C1 and C2 than in C3, while there was no significant difference in TMB between C1 and C2, although it was lower in C2 than in C1 (**Figures 5E,F** and **Supplementary Figure 13**). Regarding CNV, C2 had the lowest CNV regarding amplification, which was significant (**Figure 5G**), while no significant differences in deletion were observed among C1, C2, and C3 (**Figure 5H**). In addition, the OS was better in C2 than in C1 (**Figure 5I** and **Supplementary Figure 13E**). The distributions of conventional clinical variables among the three immune subtypes in the METABRIC cohort are shown in **Table 1**.

The observations in both GEO-meta and METABRIC datasets were highly consistent with those in the TCGA cohort, indicating the robustness of our immune subtype classification.

Predictions of Differential Sensitivity to Immunotherapy and Targeted Therapies

As the effectiveness of immunotherapy varies due to different immune cell infiltration patterns (Li J. et al., 2018) and expression levels of immune checkpoint molecules, it was important to explore the potential immunotherapy sensitivity of each immune subtype. Using SubMap analysis, we mapped the expression profiles of three immune subtypes (C1, C2, and C3) with another published cohort involving 47 melanoma patients who were treated with a PD-1 or CTLA-4 immune checkpoint inhibitor. A significant association was observed when comparing the expression profile of C2 patients with that of the CTLA-4 inhibitor-responsive group ($p < 0.05$) in all three datasets assessed (**Figures 6A–C** and **Supplementary Table 4**). This indicates that C2 patients are more likely to respond to anti-CTLA-4 immunotherapy. Similar results were obtained when comparing the expression profile of C2 patients with that of the PD-1 inhibitor-responsive group, indicating that C2 patients may also respond to anti-PD-1 immunotherapy.

Moreover, we investigated the sensitivity of immune subtypes to targeted drugs (tamoxifen and fulvestrant) using SubMap

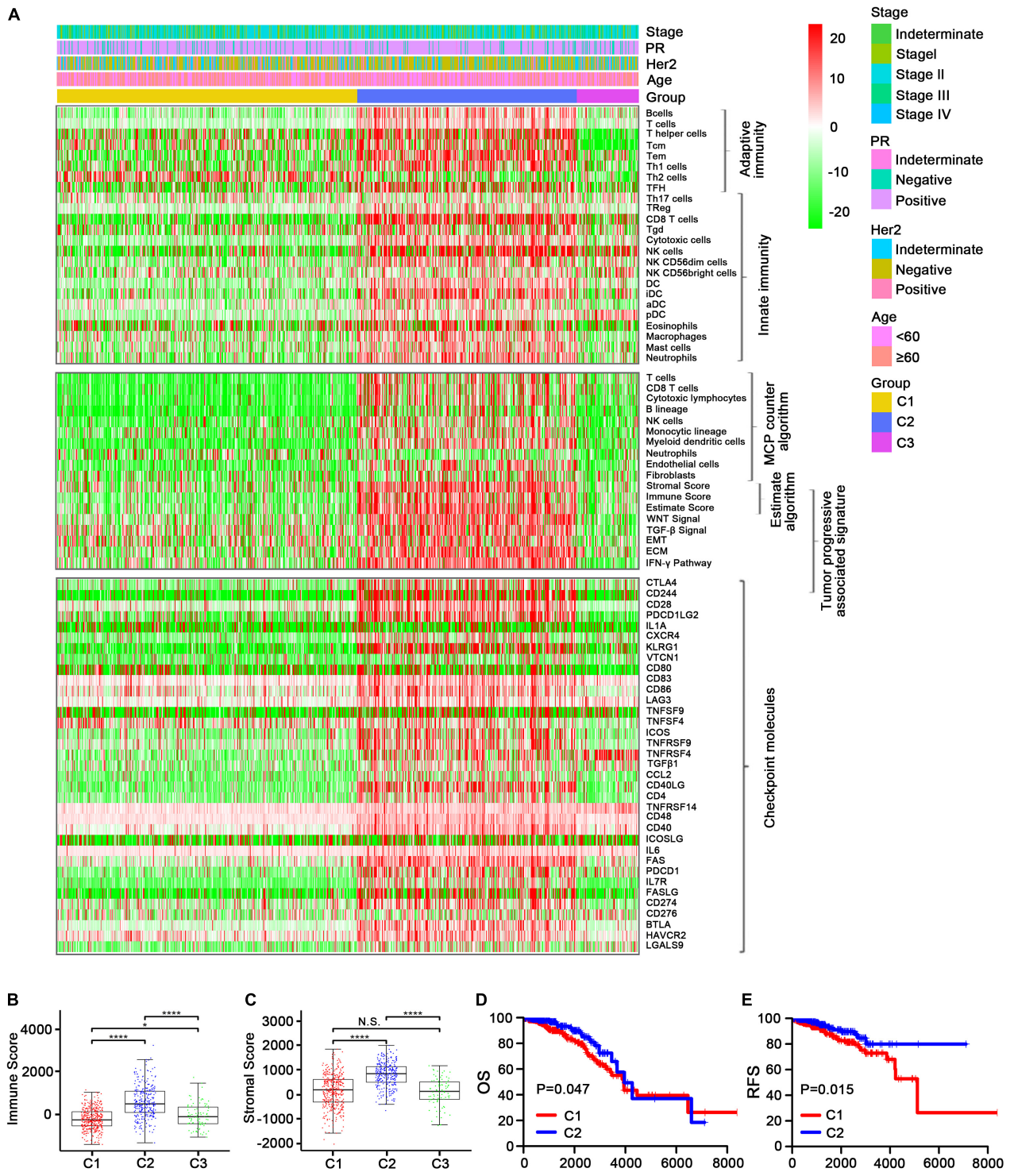


FIGURE 2 | Immune profiles of the three identified subclasses in the TCGA dataset. **(A)** The enrichment scores of 24 immune cell signatures and clinicopathologic features across three subclasses were presented in the upper panel. The middle panel indicated the abundance profile of 10 immune-related cells (eight immune cells and two stromal cells, MCPcounter algorithm) and immune-associated scores (ESTIMATE algorithm) as well as enrichment score of tumor progression-associated pathways (ssGSEA algorithm). The lower panel displayed the expression profile of immune checkpoint molecules across three subclasses. The heatmap represents the relative value of indicators, with red for high value and green for low value. Boxplot of the immune score **(B)** and stromal score **(C)** from ESTIMATE of three subclasses. The horizontal lines indicated 5, 25, 50, 75, and 95%. Comparisons between subtypes were performed by the Kruskal–Wallis test, and the *p*-values were labeled above each boxplot with asterisks (N.S. represents no significance, $*p < 0.05$, and $****p < 0.0001$). Kaplan–Meier curves show the distinct OS **(D)** and RFS **(E)** of patients in the immune activation (C2) class and immune suppressive class (C1). *p*-values were obtained using the log-rank test.

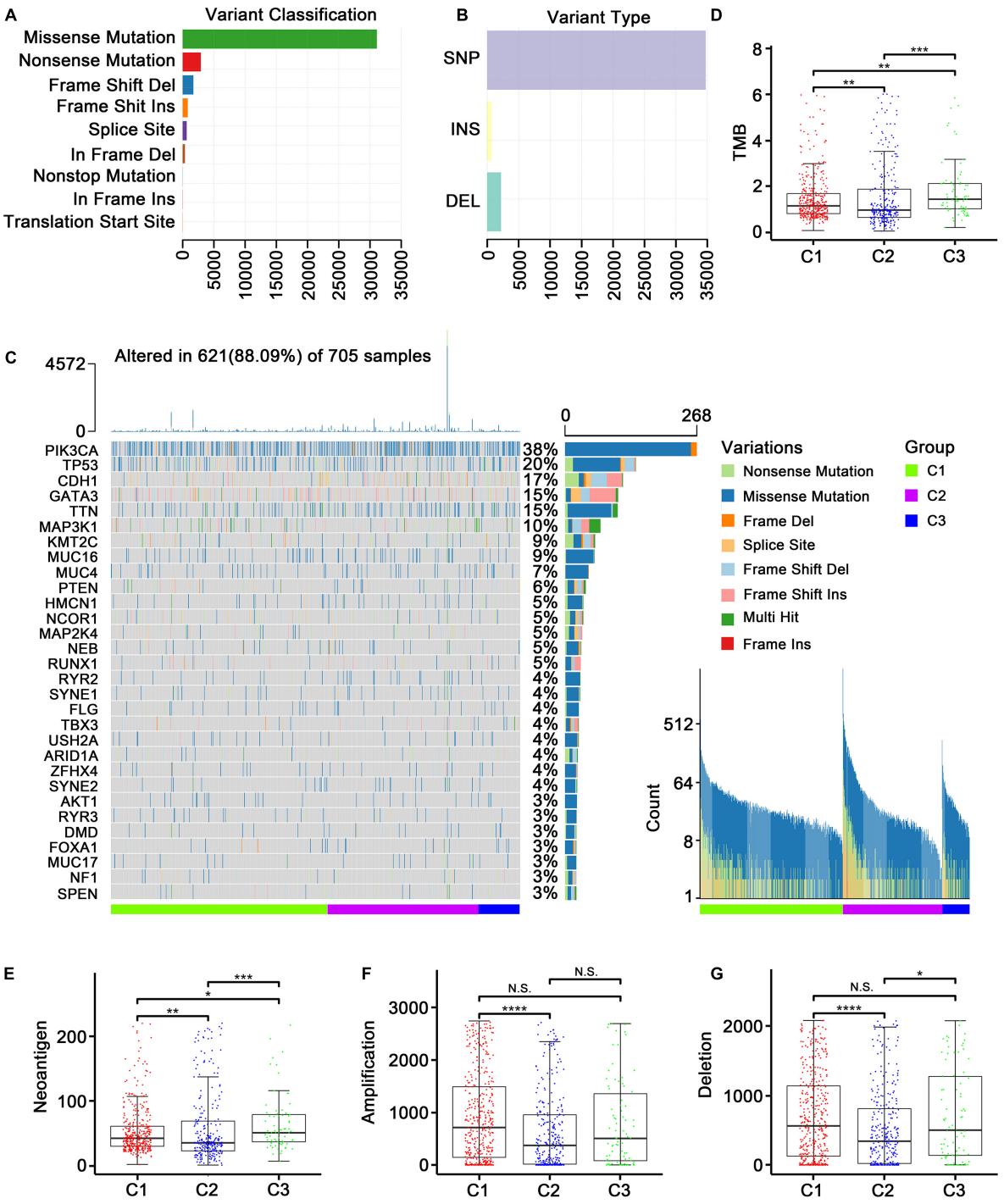


FIGURE 3 | Genomic and mutational landscape of three subtypes in TCGA cohort. **(A)** Barplot of variant classification distribution among TCGA ER+ BC patients. **(B)** Bar plot of variant type distribution among TCGA ER+ BC patients. **(C)** Oncoprint of mutation status of top 30 highly mutated genes across three subtypes (left) and ordered by mutation load (right). **(D–G)** Represent the boxplot of tumor mutation load, neoantigen load, copy number amplifications and copy number deletions, respectively. Comparisons between subtypes were performed by the Kruskal–Wallis test, and the *p*-values were labeled above each boxplot with asterisks (N.S. represents no significance, $^{*}p < 0.05$, $^{**}p < 0.01$, $^{***}p < 0.001$, and $^{****}p < 0.0001$).

analysis. Unexpectedly, C3 rather than C2 exhibited a significant association with the fulvestrant-sensitive group in both the TCGA and METABRIC cohorts ($p < 0.05$; **Figures 6D–F**). A similar but non-significant trend was observed in the GEO-meta cohort ($p = 0.1$; **Figure 6E**). Regarding tamoxifen, no significant associations were observed between any of the

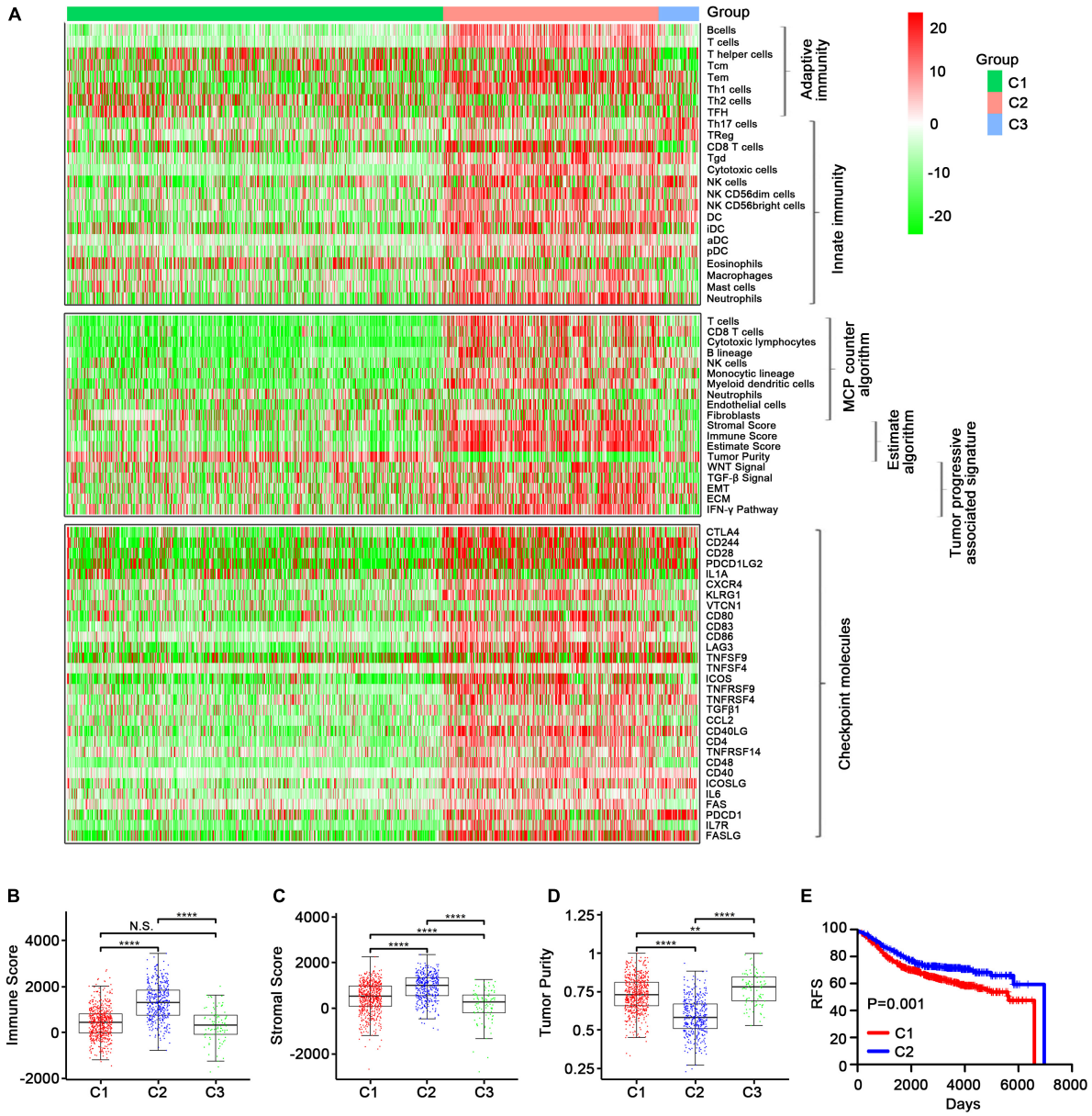


FIGURE 4 | Validation of the three immune-related subtypes in the GEO-meta cohort. **(A)** The enrichment scores of 24 immune cell signatures across three subclasses were presented in the upper panel. The middle panel indicated the abundance profile of 10 immune-related cells (eight immune cells and two stromal cells, MCPcounter algorithm) and immune-associated scores (ESTIMATE algorithm) as well as enrichment score of tumor progression-associated pathways (ssGSEA algorithm). The lower panel displayed the expression profile of immune checkpoint molecules across three subclasses. The heatmap represents the relative value of indicators, with red for high value and green for low value. Boxplot of the immune score **(B)** and stromal score **(C)** as well as tumor purity **(D)** from ESTIMATE algorithm of three subclasses. **(E)** Kaplan–Meier curves show the distinct RFS of patients in the immune activation (C2) class and immune suppressive class (C1). *p*-values were obtained using the log-rank test. (N.S. represents no significance, values are significant at $^{**}P < 0.01$, and $^{****}p < 0.0001$ as indicated).

immune subtypes and the tamoxifen-sensitive or tamoxifen-resistant groups (**Supplementary Table 4**).

Single-Cell Development Trajectory Analysis

The effectiveness of immunotherapy varies at different stages due to the different immune cell infiltration patterns and expression levels of immune checkpoint molecules (Li J. et al., 2018). The significant heterogeneity makes it difficult to identify effective treatment targets. However, single-cell data reflecting the diverse immune phenotypes help to avoid this issue. These data are useful for exploring tumor development trajectories and identifying more precise and effective treatment targets or biomarkers. The development trajectories of four patients, analyzed using Monocle, are presented in **Figure 7A**. As expected,

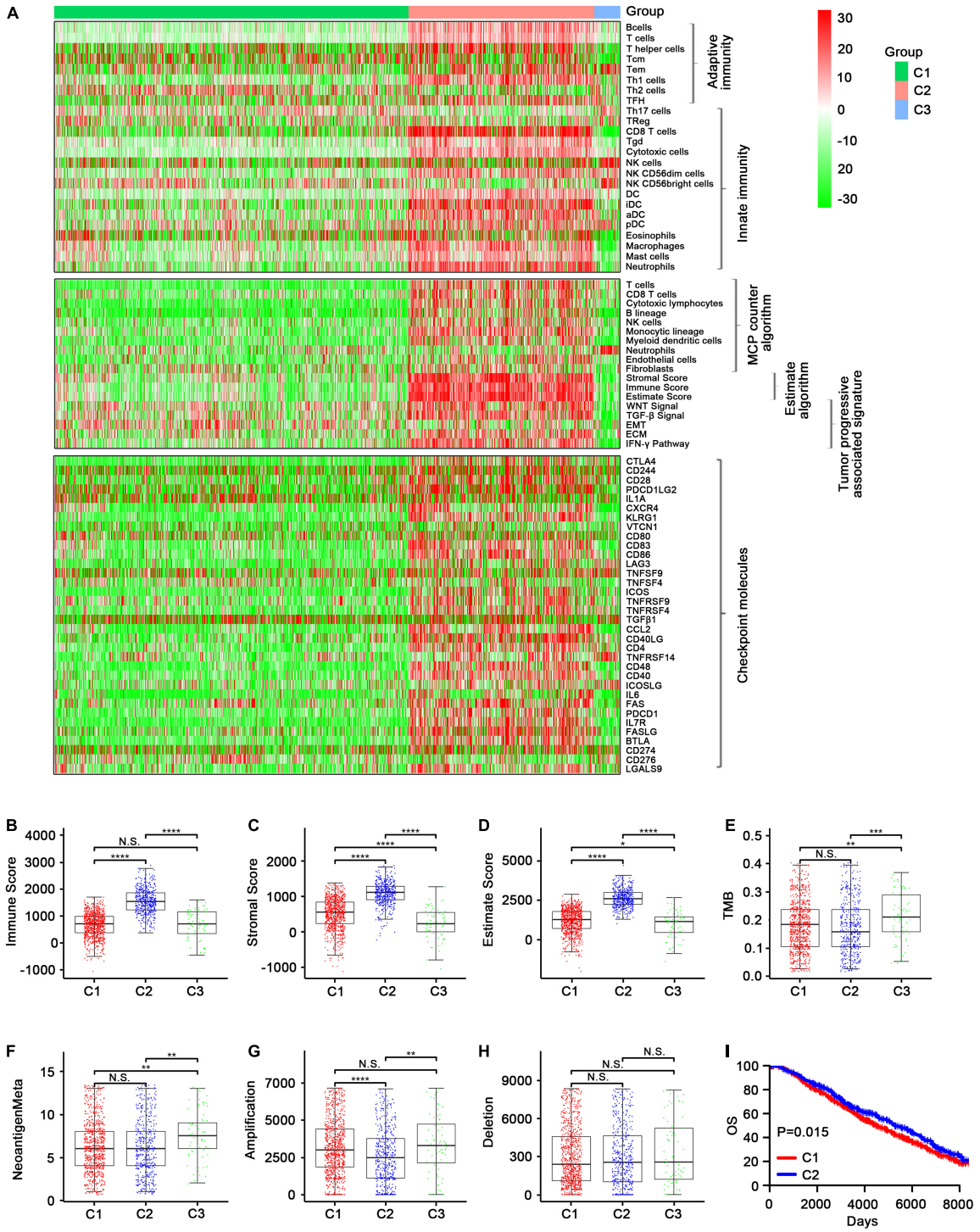


FIGURE 5 | Validation of the three immune-related subtypes in the Metabric cohort. **(A)** The enrichment scores of 24 immune cell signatures across three subclasses were presented in the upper panel. The middle panel indicated the abundance profile of ten immune-related cells (eight immune cells and two stromal cells, MCPcounter algorithm) and immune-associated scores (ESTIMATE algorithm) as well as enrichment score of tumor progression-associated pathways (ssGSEA algorithm). The lower panel displayed the expression profile of immune checkpoint molecules across three subclasses. The heatmap represents the relative value of indicator, with red for high value and green for low value. **(B–D)** Showed boxplot of immune score and stromal score as well as estimate score from ESTIMATE algorithm of three subclasses, respectively. **(E–H)** Represent the boxplot of tumor mutation load, neoantigen load, copy number amplifications, and copy number deletions, respectively. Comparisons between subtypes were performed by the Kruskal–Wallis test, and the *p*-values were labeled above each boxplot with asterisks. **(I)** Kaplan–Meier curves show the distinct OS of patients in immune activation (C2) class and immune suppressive class (C1). *p*-values were obtained using the log-rank test. (N.S. represents no significance, $^{*}p < 0.05$, $^{**}p < 0.01$, $^{***}p < 0.001$, and $^{****}p < 0.0001$).

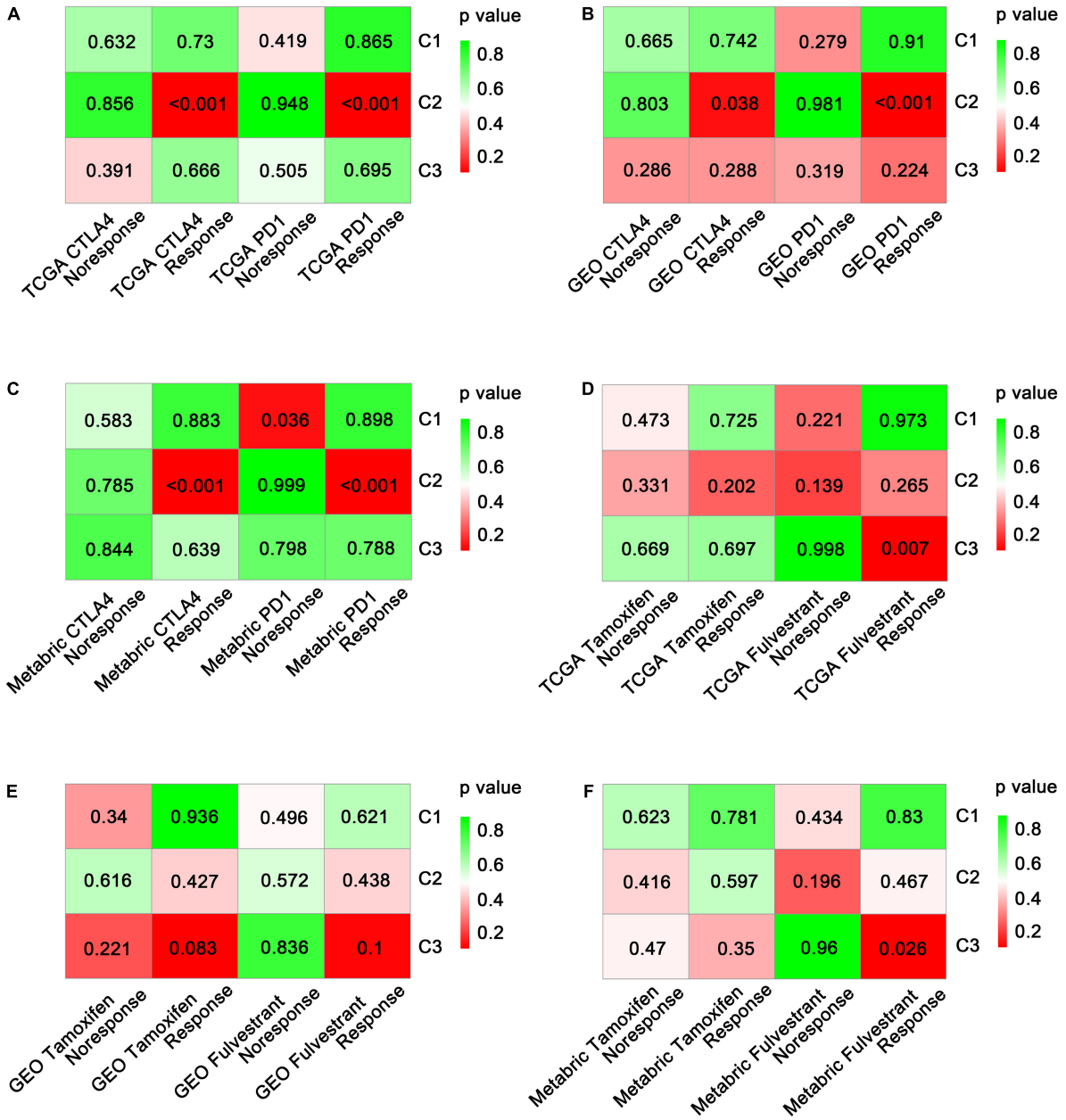


FIGURE 6 | Prediction of the benefit of each subtype from immunotherapy and targeted therapy. Significance of each subclass's drug sensitivity toward immune inhibitors (PD-1 and CTLA-4) in TCGA **(A)**, GEO **(B)**, and METABRIC **(C)** cohorts. Significance of each subclass's drug sensitivity toward targeted drugs (tamoxifen and fulvestrant) in TCGA **(D)**, GEO **(E)**, and METABRIC **(F)** cohorts.

the SingleR annotation results (**Figure 7B**) indicated similar development trajectories to those reported by Azizi et al. (**Figure 7C**) and Garvan et al. (**Figure 7D** and **Supplementary Table 5**), reflecting the same transition from innate immunity to adaptive immunity and the same immune cell infiltration pattern during tumor development. Three patients (BC1, BC2, and BC4) had most of the cells associated with adaptive immunity and were at a relatively late stage of the development trajectory, suggesting that these patients may be C2 patients (belonging to the immune activation subtype) or that these patients may have advanced-stage cancer and may be sensitive to immunotherapy.

DISCUSSION

In this study, we explored ER+ BC immune subtypes, identifying a subtype that may be sensitive to immunotherapy. Our ER+ BC subtype classification was developed based on level 3 multidimensional BC high-throughput data from the TCGA

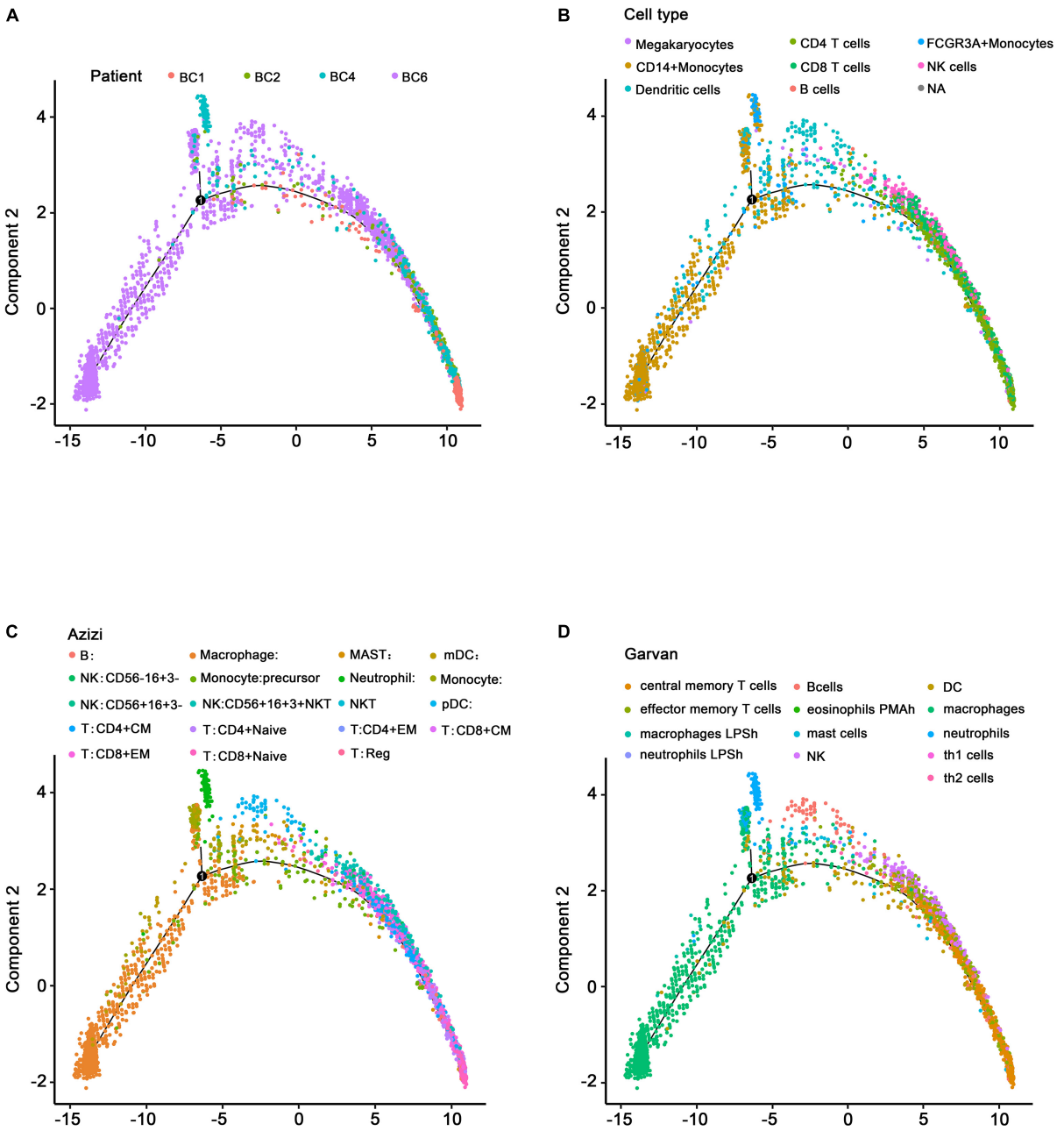


FIGURE 7 | Single-cell development trajectory analysis of ER+ BC patients. **(A)** Development trajectory distribution of four ER+ BC patients. Different colors represent different patients. **(B)** Development trajectory annotated by the SingleR package. **(C)** Development trajectory annotated by Azizi et al. **(D)** Development trajectory annotated by Garvan. Different colors represent different immune microenvironment-associated cells.

database. In addition, the GEO-meta dataset (composed of nine small datasets) and a METABRIC dataset were used to validate the identified immune subtypes. As a result, three subtypes of ER+ BC (C1, C2, and C3) were identified as immune suppressive, immune activation, and immune neutral subtypes, respectively, via a comprehensive bioinformatics analysis. Additionally, the immune cell signatures, activated signaling pathways, mutation features, and drug sensitivity of the subtypes were further explored. The results exhibited that C2 was related to many immune cell signatures and high expression levels of immune checkpoint genes, suggesting that C2 may be sensitive to CTLA-4 inhibitors and PD-1 inhibitors.

Previous studies have revealed several molecular subtypes of BC. For example, a study reported the genetic determinants of BC immune phenotypes based on integrative genome-scale analysis (Hendrickx et al., 2017), and Denkiewicz et al. (2019) identified BC subtype-specific microRNAs based on survival analysis to explore the roles of microRNAs in transcriptomic regulation.

In our study, we mainly concentrated on the overall immune profiles, which may offer more detailed information about the immune landscape of ER+ BC. Among our three subtypes, C2 exhibited an overall up-regulated immune profile relative to C1 and C3, indicating that C2 has increased lymphocyte infiltration. Additionally, C2 was associated with lower TMB, a decreased neoantigen load, and fewer CNVs. These findings suggest that the tumor microenvironment of C2 exhibits an increased immune status. Moreover, **Figure 2A** shows that pDCs and CD56 (bright) NK cells were mainly up-regulated in C3 in the TCGA cohort. A previous study reported that the level of circulating CD56 (bright) NK cells was inversely correlated with survival in melanoma patients (de Jonge et al., 2019). Schuster et al. suggested that pDCs surrounded and infiltrated some tumors such as malignant melanoma, head and neck cancer, ovarian cancer, and BC. We speculated that subtype C3 ER+ BC patients may have an unfavorable prognosis, as the presence of pDCs has been reported to be associated with poor prognosis (under the premise that these cells are unstimulated; Schuster et al., 2019). Our results confirmed this speculation (**Supplementary Figures 3C, 8B**). In addition, Th2 cells were the most highly up-regulated cells in C1 rather than in C2. The relationship between Th2 cells and cancer prognosis differs among cancer types. For example, Schreck et al. (2009) found that increased Th2 cells were related to significantly increased DFS in classical Hodgkin's lymphoma. In contrast, Chen et al. (2016) speculated that high expressions of Th2-related cytokines in hypopharyngeal cancer may contribute to cancer progression and metastasis, which may lead to poor prognosis. Those contradictory results may indicate that C2 was associated with a good prognosis, which indicated that the combined effect of immune cell infiltration in C2 may be favorable for prognosis.

A previous study indicated that neither neoantigen load nor TMB was related to T-cell response, while CNV may influence the immune response (Yang et al., 2020). Additionally, McGranahan et al. (2016) suggested that neoantigen quality instead of quantity could play a significant role in immune reactivity. In clinical practice, physicians may take immune molecular subtype, neoantigen quality, and CNV into consideration when identifying cancer patients, with a higher likelihood of responding to immunotherapy. Interestingly, identifying difference in the mutational features among immune subtypes may lead to biomarker identification. For example, Hao and Guo (2019) found that epidermal growth factor receptor mutation served as a novel prognostic factor related to immune infiltration in lower-grade glioma, while Zeng et al. (2016) suggested that the BRAF V600E mutation was associated with suppressive tumor immune microenvironment. We analyzed the TMB, neoantigen load, and CNV in the three immune subtypes. The result showed that C2 was significantly associated with a lower TMB, a decreased neoantigen load, and fewer CNVs in the TCGA and METABRIC datasets, which may provide insights into the identification of novel ER+ BC biomarkers.

Cancer immunotherapy aims to trigger a self-sustaining cancer-related immune response while minimizing therapy-associated autoinflammation (Karasaki et al., 2017). Several studies suggested that the immune checkpoints PD-1, CTLA-4, and T-cell immunoglobulin and mucin-domain containing-3 (TIM-3; Liu et al., 2017; Naoum et al., 2018; El Dika et al., 2019) are crucial indicators sustaining the pro-tumor immune microenvironment. They are also considered as perfect targets for carcinoma immunotherapy. **Figure 6** indicates that, based on comparisons of expression profiles, the C2 patients are more likely to respond to anti-CTLA-4 and anti-PD-1 immunotherapy. However, the frequent resistance exhibited against immune checkpoint inhibitors indicates that PD-1 or CTLA-4-targeted monotherapy may not fully offset the immunosuppression in the tumor microenvironment (Li X. et al., 2018). We hypothesize that other related immune checkpoints could be targeted in order to increase antitumor immunity. Nevertheless, the identification of C2 (the immune activation subtype) in this study may help to guide the choice of monotherapy or combination therapy for ER+ BC patients. Further validation in clinical trials is required before clinical application.

Figure 2 showed that five tumor-related pathways (TGF-β signaling, EMT, ECM, IFN-γ, and WNT signaling) were more activated in C2 than in C1 and C3. Previous research suggested that the TGF-β pathway has bidirectional effects in cancers (Metelli et al., 2018). In premalignant cells, TGF-β served as a tumor suppressor by inhibiting cell proliferation and facilitating apoptosis, whereas, in advanced tumors, TGF-β facilitated metastasis and induced a protumor immune microenvironment (David and Massagué, 2018). Donato et al. (2020) suggested that proliferation and migration of neural crest-derived cells involved the activation of the EMT pathway. Schomberg et al. (2020) found that luteolin-mediated inhibition of melanoma cell growth may involve simultaneously affecting various pathways such as the ECM, oncogenic signaling, and immune response pathways. Gao et al. (2016) suggested that the loss of the IFN-γ pathway genes in tumor cells may underlie resistance to anti-CTLA-4 treatment. Sun et al. (2019) found that miR-22 and miR-214 targeting BCL9L inhibited proliferation, metastasis, and EMT by down-regulating Wnt signaling in colon cancer. Nevertheless, clinical evidence and clinical trials are required to verify the combined effects of the above five pathways on tumor immunotherapy. Further exploration of these pathways may help to develop targeted antitumor therapy.

This study has several advantages that need to be expounded upon. Firstly, this is the first study to comprehensively describe the immune profile of ER+ BC cases, with data from three databases (TCGA, GEO-meta, and METABRIC datasets) involving a very large sample (3,318 samples) being combined to identify the ER+ BC immune subtypes. In other words, we performed multiple validations involving multiple datasets in order to confirm the identified immune subtypes, which made our findings more reliable. Secondly, three algorithms (ssGSEA, MCPcounter, and ESTIMATE) were applied to investigate the immune cell signatures in each immune subtype, and similar results were obtained, which indicated the robustness of our immune subtype classification. Thirdly, we explored the characteristics of each subtype not only based on gene expression but also based on mutational features (TMB, neoantigen load,

and CNV). Additionally, we predicted the drug susceptibility of each subtype and explored the developmental trajectory of BC patients. This multidimensional analysis provides a comprehensive picture of the clinical significance of each immune subtype and provides a foundation for improving clinical treatment.

CONCLUSION

We identified and verified a novel immune subtype classification of ER+ BC, which involves three robust subtypes: the immune suppressive, activation, and neutral subtypes. Patients with C2 (the immune activation subtype) represent the optimal candidates for anti-PD-1 and anti-CTLA-4 immunotherapy. Our classification may help to predict the prognosis of ER+ BC patients and provide clinicians a new basis for making accurate clinical diagnoses and selecting optimal treatments such as immunotherapy.

DATA AVAILABILITY STATEMENT

The data that support the findings of this study are available in the TCGA, GEO, and METABRIC databases.

ETHICS STATEMENT

This article does not contain any studies with human participants or animals performed by any of the authors.

AUTHOR CONTRIBUTIONS

XM and HC designed, extracted, analyzed, and interpreted the data from TCGA, GEO, and METABRIC databases. ZK and TH wrote the manuscript. MY and MW revised the manuscript. LL made substantial contributions to the conception of the work. XM, HC, and LL substantively revised it. All authors have read and approved the final manuscript.

FUNDING

This study was supported by the National Natural Science Foundation of China (NSFC; Grant Number: 81702397).

SUPPLEMENTARY MATERIAL

The Supplementary Material for this article can be found online at: https://www.frontiersin.org/articles/10.3389/fcell.2021.722841/full#supplementary-material

Supplementary Figure 1 | Boxplot of the distribution of 24 immune cells among three groups in the TCGA cohort (N.S. represents no significance, $*p < 0.05$, $**p < 0.01$, $***p < 0.001$, and $****p < 0.0001$).

Supplementary Figure 2 | Boxplot of the distribution of 10 immune-related cells and five tumor progression-related pathways among three groups in the TCGA cohort (N.S. represents no significance, $*p < 0.05$, $**p < 0.01$, $***p < 0.001$, and $****p < 0.0001$).

Supplementary Figure 3 | Heatmap of the top 10 marker genes of each subclass in the TCGA cohort **(A)** and Kaplan–Meier curves of each subclass **(B,C)**. Candidate immune gene selection using the LASSO regression model **(D,E)**.

Supplementary Figure 4 | Boxplot of the distribution of 35 checkpoint molecules among three groups in the TCGA cohort (N.S. represents no significance, $*p < 0.05$, $**p < 0.01$, $***p < 0.001$, and $****p < 0.0001$).

Supplementary Figure 5 | Coloring single samples on a dimensional reduction plot according to 23 checkpoint molecules in the TCGA cohort. **(A)** The t-SNE distribution of TCGA ER+ BC samples by expression profile of global immune genes. Each point represents a single sample; different colors represent the three subclasses. **(B–X)** Coloring single samples on a dimensional reduction plot according to 23 checkpoint molecules.

Supplementary Figure 6 | Boxplot of the distribution of 24 immune cells among three groups in the GEO-meta cohort (N.S. represents no significance, $*p < 0.05$, $**p < 0.01$, $***p < 0.001$, and $****p < 0.0001$).

Supplementary Figure 7 | Boxplot of the distribution of 10 immune-related cells and five tumor progression-related pathways among three groups in the GEO-meta cohort (N.S. represents no significance, $*p < 0.05$, $**p < 0.01$, $***p < 0.001$, and $****p < 0.0001$).

Supplementary Figure 8 | Heatmap of the top 10 marker genes of each subclass in the GEO-meta cohort **(A)** and Kaplan–Meier curves of each subclass **(B)**.

Supplementary Figure 9 | Boxplot of the distribution of 30 checkpoint molecules among three groups in the GEO-meta cohort (N.S. represents no significance, $*p < 0.05$, $**p < 0.01$, $***p < 0.001$, and $****p < 0.0001$).

Supplementary Figure 10 | Coloring single samples on a dimensional reduction plot according to 23 checkpoint molecules in the GEO-meta cohort. **(A)** The t-SNE distribution of GEO-meta ER+ BC samples by expression profile of global immune genes. Each point represents a single sample; different colors represent the three subclasses. **(B–X)** Coloring single samples on a dimensional reduction plot according to 23 checkpoint molecules.

Supplementary Figure 11 | Boxplot of the distribution of 24 immune cells among three groups in the METABRIC cohort (N.S. represents no significance, $*p < 0.05$, $**p < 0.01$, $***p < 0.001$, and $****p < 0.0001$).

Supplementary Figure 12 | Boxplot of the distribution of 10 immune-related cells and five tumor progression-related pathways among three groups in the METABRIC cohort (N.S. represents no significance, $*p < 0.05$, $**p < 0.01$, $***p < 0.001$, and $****p < 0.0001$).

Supplementary Figure 13 | Characteristics of identified subclasses in the METABRIC cohort. **(A)** Heatmap of the top 10 marker genes of each subclass in the METABRIC cohort. **(B)** Bar plot of variant classification distributions among METABRIC ER+ BC patients. **(C)** Bar plot of variant type distributions among METABRIC ER+ BC patients. **(D)** Oncoprint of mutation status of top 30 highly mutated genes across three subtypes (left) and ordered by mutation load (right). **(E)** Kaplan–Meier curves of three identified subclasses.

Supplementary Figure 14 | Boxplot of the distribution of 34 checkpoint molecules among three groups in the METABRIC cohort (N.S. represents no significance, $*p < 0.05$, $**p < 0.01$, $***p < 0.001$, and $****p < 0.0001$).

Supplementary Figure 15 | Coloring single samples on a dimensional reduction plot according to 23 checkpoint molecules in the METABRIC cohort. **(A)** The t-SNE distribution of METABRIC ER+ BC samples by expression profile of global immune genes. Each point represents a single sample; different colors represent the three subclasses. **(B–X)** Coloring single samples on a dimensional reduction plot according to 23 checkpoint molecules.

Supplementary Table 1 | Clinical information of enrolled patients.

Supplementary Table 2 | Identification of driver genes based on the TCGA ER+ mutation data.

Supplementary Table 3 | Identification of the marker genes of each subclass in the TCGA cohort.

Supplementary Table 4 | Datasets for SubMap analysis. **(A)** Melanoma dataset. **(B)** GDSC dataset. **(C)** TCGA dataset. **(D)** GEO dataset. **(E)** METABRIC dataset.

Supplementary Table 5 | Single-cell annotation results by Azizi and Garvan.

REFERENCES

Adams, S., Goldstein, L. J., Sparano, J. A., Demaria, S., and Badve, S. S. (2015). Tumor infiltrating lymphocytes (TILs) improve prognosis in patients with triple negative breast cancer (TNBC). *Oncoimmunology* 4:e985930. doi: 10.4161/2162402x.2014.985930

Ali, H. R., Provenzano, E., Dawson, S. J., Blows, F. M., Liu, B., Shah, M., et al. (2014). Association between CD8+ T-cell infiltration and breast cancer survival in 12,439 patients. *Annals Oncol.* 25, 1536–1543. doi: 10.1093/annonc/mdu191

Aran, D., Looney, A. P., Liu, L., Wu, E., Fong, V., Hsu, A., et al. (2019). Reference-based analysis of lung single-cell sequencing reveals a transitional profibrotic macrophage. *Nat. Immunol.* 20, 163–172. doi: 10.1038/s41590-018-0276-y

Azizi, E., Carr, A. J., Plitas, G., Cornish, A. E., Konopacki, C., Prabhakaran, S., et al. (2018). Single-Cell map of diverse immune phenotypes in the breast tumor microenvironment. *Cell* 174, 1293–1308.e36.

Bayraktar, S., Batoo, S., Okuno, S., and Glück, S. (2019). Immunotherapy in breast cancer. *J. Carcinogenesis* 18:2.

Becht, E., Giraldo, N. A., Lacroix, L., Buttard, B., Elarouci, N., Petitprez, F., et al. (2016). Estimating the population abundance of tissue-infiltrating immune and stromal cell populations using gene expression. *Genome Biol.* 17:218.

Bhattacharya, S., Andorf, S., Gomes, L., Dunn, P., Schaefer, H., Pontius, J., et al. (2014). ImmPort: disseminating data to the public for the future of immunology. *Immunol. Res.* 58, 234–239. doi: 10.1007/s12026-014-8516-1

Bindea, G., Mlecnik, B., Tosolini, M., Kirilovsky, A., Waldner, M., Obenauf, A. C., et al. (2013). Spatiotemporal dynamics of intratumoral immune cells reveal the immune landscape in human cancer. *Immunity* 39, 782–795. doi: 10.1016/j.immuni.2013.10.003

Burstein, H. J., Prestrud, A. A., Seidenfeld, J., Anderson, H., Buchholz, T. A., Davidson, N. E., et al. (2010). American society of clinical oncology clinical practice guideline: update on adjuvant endocrine therapy for women with hormone receptor-positive breast cancer. *J. Clin. Oncol.* 28, 3784–3796.

Chakraborty, S., Datta, S., and Datta, S. (2012). Surrogate variable analysis using partial least squares (SVA-PLS) in gene expression studies. *Bioinformatics* 28, 799–806. doi: 10.1093/bioinformatics/bts022

Chen, X., Wang, J., Wang, R., Su, Q., Luan, J., Huang, H., et al. (2016). Th1-, Th2-, and Th17-associated cytokine expression in hypopharyngeal carcinoma and clinical significance. *Eur. Arch. Oto-rhino-laryngology* 273, 431–438. doi: 10.1007/s00405-015-3779-2

Chu, Y., Liao, J., Li, J., Wang, Y., Yu, X., Wang, J., et al. (2019). CD103(+) tumor-infiltrating lymphocytes predict favorable prognosis in patients with esophageal squamous cell carcinoma. *J. Cancer* 10, 5234–5243. doi: 10.7150/jca.30354

Colaprico, A., Silva, T. C., Olsen, C., Garofano, L., Cava, C., Garolini, D., et al. (2016). TCGAbiolinks: an R/Bioconductor package for integrative analysis of TCGA data. *Nucleic Acids Res.* 44:e71. doi: 10.1093/nar/gkv1507

David, C. J., and Massagué, J. (2018). Contextual determinants of TGFβ action in development, immunity and cancer. *Nat. Rev. Mol. Cell Biol.* 19, 419–435. doi: 10.1038/s41580-018-0007-0

Davoli, T., Uno, H., Wooten, E. C., and Elledge, S. J. (2017). Tumor aneuploidy correlates with markers of immune evasion and with reduced response to immunotherapy. *Science* 355:eaaf8399. doi: 10.1126/science.aaf8399

de Jonge, K., Ebering, A., Nassiri, S., Maby-El Hajjami, H., Ouertatani-Sakouhi, H., Baumgaertner, P., et al. (2019). Circulating CD56(bright) NK cells inversely correlate with survival of melanoma patients. *Sci. Rep.* 9:4487.

Denkiewicz, M., Saha, I., Rakshit, S., Sarkar, J. P., and Plewczynski, D. (2019). Identification of breast cancer subtype specific MicroRNAs using survival analysis to find their role in transcriptomic regulation. *Front. Genet.* 10:1047. doi: 10.3389/fgene.2019.01047

DeSantis, C. E., Ma, J., Gaudet, M. M., Newman, L. A., Miller, K. D., Goding Sauer, A., et al. (2019). Breast cancer statistics, 2019. *CA Cancer J. Clin.* 69, 438–451.

Dieci, M. V., Mathieu, M. C., Guarneri, V., Conte, P., Delaloge, S., Andre, F., et al. (2015). Prognostic and predictive value of tumor-infiltrating lymphocytes in two phase III randomized adjuvant breast cancer trials. *Annals Oncol.* 26, 1698–1704. doi: 10.1093/annonc/mdv239

Donato, G., Presta, I., Arcidiacono, B., Vismara, M. F. M., Donato, A., Garo, N. C., et al. (2020). Innate and adaptive immunity linked to recognition of antigens shared by neural crest-derived tumors. *Cancers* 12:651.

El Dika, I., Khalil, D. N., and Abou-Alfa, G. K. (2019). Immune checkpoint inhibitors for hepatocellular carcinoma. *Cancer* 125, 3312–3319. doi: 10.1002/cncr.32076

Engebretsen, S., and Bohlin, J. (2019). Statistical predictions with glmnet. *Clin. Epigenet.* 11:123.

Fridman, W. H., Pagès, F., Sautès-Fridman, C., and Galon, J. (2012). The immune contexture in human tumours: impact on clinical outcome. *Nat. Rev. Cancer* 12, 298–306. doi: 10.1038/nrc3245

Gao, J., Shi, L. Z., Zhao, H., Chen, J., Xiong, L., He, Q., et al. (2016). Loss of IFN-γ pathway genes in tumor cells as a mechanism of resistance to Anti-CTLA-4 therapy. *Cell* 167, 397–404.e9.

Gautier, L., Cope, L., Bolstad, B. M., and Irizarry, R. A. (2004). affy–analysis of affymetrix GeneChip data at the probe level. *Bioinformatics* 20, 307–315. doi: 10.1093/bioinformatics/btg405

Hanzelmann, S., Castelo, R., and Guinney, J. (2013). GSVA: gene set variation analysis for microarray and RNA-seq data. *BMC Bioinform.* 14:7. doi: 10.1186/1471-2105-14-7

Hao, Z., and Guo, D. (2019). EGFR mutation: novel prognostic factor associated with immune infiltration in lower-grade glioma; an exploratory study. *BMC Cancer* 19:1184. doi: 10.1186/s12885-019-6384-8

Hendrickx, W., Simeone, I., Anjum, S., Mokrab, Y., Bertucci, F., Finetti, P., et al. (2017). Identification of genetic determinants of breast cancer immune phenotypes by integrative genome-scale analysis. *Oncoimmunology* 6:e1253654. doi: 10.1080/2162402x.2016.1253654

Hida, A. I., Watanabe, T., Sagara, Y., Kashiwaba, M., Sagara, Y., Aogi, K., et al. (2019). Diffuse distribution of tumor-infiltrating lymphocytes is a marker for better prognosis and chemotherapeutic effect in triple-negative breast cancer. *Breast Cancer Res. Treat.* 178, 283–294. doi: 10.1007/s10549-019-05390-x

Hurvitz, S. A., and Pietras, R. J. (2008). Rational management of endocrine resistance in breast cancer: a comprehensive review of estrogen receptor biology, treatment options, and future directions. *Cancer* 113, 2385–2397. doi: 10.1002/cncr.23875

Iorio, F., Knijnenburg, T. A., Vis, D. J., Bignell, G. R., Menden, M. P., Schubert, M., et al. (2016). A landscape of pharmacogenomic interactions in cancer. *Cell* 166, 740–754.

Karasaki, T., Nagayama, K., Kuwano, H., Nitadori, J. I., Sato, M., Anraku, M., et al. (2017). An immunogram for the cancer-immunity cycle: towards personalized immunotherapy of lung cancer. *J. Thoracic Oncol.* 12, 791–803. doi: 10.1016/j.jtho.2017.01.005

Kim, H. R., Park, H. J., Son, J., Lee, J. G., Chung, K. Y., Cho, N. H., et al. (2019). Tumor microenvironment dictates regulatory T cell phenotype: upregulated immune checkpoints reinforce suppressive function. *J. Immunotherapy Cancer* 7:339.

Koren, S., and Bentires-Alj, M. (2015). Breast tumor heterogeneity: source of fitness. Hurdle for Therapy. *Mol. Cell.* 60, 537–546. doi: 10.1016/j.molcel.2015.10.031

Li, J., Byrne, K. T., Yan, F., Yamazoe, T., Chen, Z., Baslan, T., et al. (2018). Tumor cell-intrinsic factors underlie heterogeneity of immune cell infiltration and response to immunotherapy. *Immunity* 49, 178–193.e7.

Li, X., Shao, C., Shi, Y., and Han, W. (2018). Lessons learned from the blockade of immune checkpoints in cancer immunotherapy. *J. Hematol. Oncol.* 11:31.

Liu, B., Song, Y., and Liu, D. (2017). Recent development in clinical applications of PD-1 and PD-L1 antibodies for cancer immunotherapy. *J. Hematol. Oncol.* 10:174.

Loi, S., Sirtaine, N., Piette, F., Salgado, R., Viale, G., Van Eenoo, F., et al. (2013). Prognostic and predictive value of tumor-infiltrating lymphocytes in a phase

III randomized adjuvant breast cancer trial in node-positive breast cancer comparing the addition of docetaxel to doxorubicin with doxorubicin-based chemotherapy: BIG 02-98. *J. Clin. Oncol.* 31, 860–867. doi: 10.1200/jco.2011.41.0902

Luen, S., Virassamy, B., Savas, P., Salgado, R., and Loi, S. (2016). The genomic landscape of breast cancer and its interaction with host immunity. *Breast (Edinburgh, Scotland)* 29, 241–250. doi: 10.1016/j.breast.2016.07.015

McGranahan, N., Furness, A. J., Rosenthal, R., Ramskov, S., Lyngaa, R., Saini, S. K., et al. (2016). Clonal neoantigens elicit T cell immunoreactivity and sensitivity to immune checkpoint blockade. *Science* 351, 1463–1469.

Metelli, A., Salem, M., Wallace, C. H., Wu, B. X., Li, A., Li, X., et al. (2018). Immunoregulatory functions and the therapeutic implications of GARP-TGF-β in inflammation and cancer. *J. Hematol. Oncol.* 11:24.

Naoum, G. E., Morkos, M., Kim, B., and Arafat, W. (2018). Novel targeted therapies and immunotherapy for advanced thyroid cancers. *Mol. Cancer* 17:51.

No authors listed (1998). Tamoxifen for early breast cancer: an overview of the randomised trials. early breast cancer trialists' collaborative group. *Lancet* 351, 1451–1467. doi: 10.1016/s0140-6736(97)11423-4

Osborne, C. K., and Schiff, R. (2011). Mechanisms of endocrine resistance in breast cancer. *Annu. Rev. Med.* 62, 233–247.

Oshimori, N., Oristian, D., and Fuchs, E. (2015). TGF-β promotes heterogeneity and drug resistance in squamous cell carcinoma. *Cell* 160, 963–976. doi: 10.1016/j.cell.2015.01.043

Pereira, B., Chin, S. F., Rueda, O. M., Vollan, H. K., Provenzano, E., Bardwell, H. A., et al. (2016). The somatic mutation profiles of 2,433 breast cancers refines their genomic and transcriptomic landscapes. *Nat. Commun.* 7:11479.

Qiu, X., Mao, Q., Tang, Y., Wang, L., Chawla, R., Pliner, H. A., et al. (2017). Reversed graph embedding resolves complex single-cell trajectories. *Nat. Methods* 14, 979–982. doi: 10.1038/nmeth.4402

Roh, W., Chen, P. L., Reuben, A., Spencer, C. N., Prieto, P. A., Miller, J. P., et al. (2017). Integrated molecular analysis of tumor biopsies on sequential CTLA-4 and PD-1 blockade reveals markers of response and resistance. *Sci. Trans. Med.* 9:eaah3560. doi: 10.1126/scitranslmed.aah3560

Rooney, M. S., Shukla, S. A., Wu, C. J., Getz, G., and Hacohen, N. (2015). Molecular and genetic properties of tumors associated with local immune cytolytic activity. *Cell* 160, 48–61. doi: 10.1016/j.cell.2014.12.033

Schomberg, J., Wang, Z., Farhat, A., Guo, K. L., Xie, J., Zhou, Z., et al. (2020). Luteolin inhibits melanoma growth in vitro and in vivo via regulating ECM and oncogenic pathways but not ROS. *Biochem. Pharmacol.* 177:114025. doi: 10.1016/j.bcp.2020.114025

Schreck, S., Friebel, D., Buettner, M., Distel, L., Grabenbauer, G., Young, L. S., et al. (2009). Prognostic impact of tumour-infiltrating Th2 and regulatory T cells in classical Hodgkin lymphoma. *Hematol. Oncol.* 27, 31–39. doi: 10.1002/hon.878

Schuster, P., Lindner, G., Thomann, S., Haferkamp, S., and Schmidt, B. (2019). Prospect of plasmacytoid dendritic cells in enhancing anti-tumor immunity of oncolytic herpes viruses. *Cancers* 11:651. doi: 10.3390/cancers11050651

Simon, R., Lam, A., Li, M. C., Ngan, M., Menenzes, S., and Zhao, Y. (2007). Analysis of gene expression data using BRB-ArrayTools. *Cancer Inform* 3, 11–17.

Subramanian, A., Tamayo, P., Mootha, V. K., Mukherjee, S., Ebert, B. L., Gillette, M. A., et al. (2005). Gene set enrichment analysis: a knowledge-based approach for interpreting genome-wide expression profiles. *Proc. Natl. Acad. Sci. U S A.* 102, 15545–15550. doi: 10.1073/pnas.0506580102

Sun, R., Liu, Z., Han, L., Yang, Y., Wu, F., Jiang, Q., et al. (2019). miR-22 and miR-214 targeting BCL9L inhibit proliferation, metastasis, and epithelial-mesenchymal transition by down-regulating Wnt signaling in colon cancer. *FASEB J.* 33, 5411–5424. doi: 10.1096/fj.201801798rr

Takahashi, H., Asaoka, M., Yan, L., Rashid, O. M., Oshi, M., Ishikawa, T., et al. (2020). Biologically aggressive phenotype and anti-cancer immunity counterbalance in breast cancer with high mutation rate. *Sci. Rep.* 10:1852.

Toor, S. M., Murshed, K., Al-Dhaheri, M., Khawar, M., Abu Nada, M., and Elkord, E. (2019). Immune checkpoints in circulating and tumor-infiltrating CD4(+) T Cell subsets in colorectal cancer patients. *Front. Immunol.* 10:2936. doi: 10.3389/fimmu.2019.02936

Torre, L. A., Islami, F., Siegel, R. L., Ward, E. M., and Jemal, A. (2017). Global cancer in women: burden and trends. *Cancer Epidemiol. Biomarkers Prevent.* 26, 444–457.

Tripathi, V., Shin, J. H., Stuelten, C. H., and Zhang, Y. E. (2019). TGF-β-induced alternative splicing of TAK1 promotes EMT and drug resistance. *Oncogene* 38, 3185–3200. doi: 10.1038/s41388-018-0655-8

Wilkerson, M. D., and Hayes, D. N. (2010). ConsensusClusterPlus: a class discovery tool with confidence assessments and item tracking. *Bioinformatics* 26, 1572–1573. doi: 10.1093/bioinformatics/btq170

Xu, X., Zhang, L., He, X., Zhang, P., Sun, C., Xu, X., et al. (2018). TGF-β plays a vital role in triple-negative breast cancer (TNBC) drug-resistance through regulating stemness, EMT and apoptosis. *Biochem. Biophys. Res. Commun.* 502, 160–165. doi: 10.1016/j.bbrc.2018.05.139

Yang, C., Huang, X., Liu, Z., Qin, W., and Wang, C. (2020). Metabolism-associated molecular classification of hepatocellular carcinoma. *Mol. Oncol.* 14, 896–913. doi: 10.1002/1878-0261.12639

Yoshihara, K., Shahmoradgoli, M., Martinez, E., Vegesna, R., Kim, H., Torres-Garcia, W., et al. (2013). Inferring tumour purity and stromal and immune cell admixture from expression data. *Nat. Commun.* 4:2612.

Zeng, K., Wang, Z., Ohshima, K., Liu, Y., Zhang, W., Wang, L., et al. (2016). BRAF V600E mutation correlates with suppressive tumor immune microenvironment and reduced disease-free survival in Langerhans cell histiocytosis. *Oncoimmunology* 5:e1185582. doi: 10.1080/2162402x.2016.1185582

Zhang, R., Liu, Q., Peng, J., Wang, M., Li, T., Liu, J., et al. (2020). CXCL5 overexpression predicts a poor prognosis in pancreatic ductal adenocarcinoma and is correlated with immune cell infiltration. *J. Cancer* 11, 2371–2381. doi: 10.7150/jca.40517

Conflict of Interest: The authors declare that the research was conducted in the absence of any commercial or financial relationships that could be construed as a potential conflict of interest.

The reviewer WC declared a shared affiliation, with one of the authors, HC, to the handling editor at time of review.

Publisher's Note: All claims expressed in this article are solely those of the authors and do not necessarily represent those of their affiliated organizations, or those of the publisher, the editors and the reviewers. Any product that may be evaluated in this article, or claim that may be made by its manufacturer, is not guaranteed or endorsed by the publisher.

Copyright © 2021 Ma, Chen, Yang, Ke, Wang, Huang and Li. This is an open-access article distributed under the terms of the Creative Commons Attribution License (CC BY). The use, distribution or reproduction in other forums is permitted, provided the original author(s) and the copyright owner(s) are credited and that the original publication in this journal is cited, in accordance with accepted academic practice. No use, distribution or reproduction is permitted which does not comply with these terms.

frontiers in Oncology

ORIGINAL RESEARCH
published: 27 September 2021
doi: 10.3389/fonc.2021.733175

RFWD2 Knockdown as a Blocker to Reverse the Oncogenic Role of TRIB2 in Lung Adenocarcinoma

Ruimin Hao[1†], Jinxia Hu[1†], Yuemei Liu[1†], Dongmin Liang[1†], Yan-Mei Li[2], Ranran Wang[1], Shucui Zhang[3], Pingyu Wang[1], You-Jie Li[1*] and Shuyang Xie[1*]*

[1] Department of Biochemistry and Molecular Biology, Binzhou Medical University, Yantai, China, [2] Department of Immune Rheumatism, Yantaishan Hospital, Yantai, China, [3] Key Laboratory of Cardiovascular Remodeling and Function Research, Qilu Hospital, Shandong University, Jinan, China

OPEN ACCESS

Edited by:
Yue Zhao,
University of Cologne, Germany

Reviewed by:
Ravi Manoharan,
University of Madras, India
Zhiqiang Liu,
Tianjin Medical University, China

***Correspondence:**
Shuyang Xie
shuyangxie@aliyun.com
You-Jie Li
youjie1979@163.com
Pingyu Wang
wpingyugirl@163.com

[†]These authors have contributed equally to this work

Specialty section:
This article was submitted to Molecular and Cellular Oncology, a section of the journal Frontiers in Oncology

Received: *30 June 2021*
Accepted: *06 September 2021*
Published: *27 September 2021*

Citation:
Hao R, Hu J, Liu Y, Liang D, Li Y-M, Wang R, Zhang S, Wang P, Li Y-J and Xie S (2021) RFWD2 Knockdown as a Blocker to Reverse the Oncogenic Role of TRIB2 in Lung Adenocarcinoma. Front. Oncol. 11:733175. doi: 10.3389/fonc.2021.733175

RFWD2, an E3 ubiquitin ligase, is overexpressed in numerous human cancers, including leukemia, lung cancer, breast cancer, renal cell carcinoma, and colorectal cancer. The roles of RFWD2 in cancer are related to the targeting of its substrates for ubiquitination and degradation. This study aimed to investigate the role of TRIB2 in relation to the regulation of protein degradation through RFWD2. inBio Discover™ results demonstrated that TRIB2 can perform its functions by interacting with RFWD2 or other factors. TRIB2 can interact with and regulate RFWD2, which further attends the proteasome-mediated degradation of the RFWD2 substrate p-IκB-α. TRIB2 colocalizes with RFWD2-related IκB-α to form a ternary complex and further affects the IκB-α degradation by regulating its phosphorylation. Specific domain analysis showed that TRIB2 may bind to RFWD2 *via* its C-terminus, whereas it binds to IκB *via* its pseudokinase domain. TRIB2 acts as an oncogene and promotes cancer cell proliferation and migration, whereas RFWD2 knockdown reversed the role of TRIB2 in promoting cancer cell growth and colony formation *in vitro* and *in vivo*. In summary, this study reveals that TRIB2 promotes the progression of cancer by affecting the proteasome-mediated degradation of proteins through the interaction with RFWD2.

Keywords: RFWD2, proteasome-mediated degradation, TRIB2, cancer therapy, target gene

INTRODUCTION

The ubiquitin (Ub) proteasome system plays important roles in regulating the cell cycle, cell proliferation, cell migration, and apoptosis by affecting the levels and activities of biological function-related proteins (1, 2). Substrate proteins are attached with a small and highly conserved Ub protein consisting of 76 amino acids (3). This attachment reaction is catalyzed by E1 Ub-activating enzyme, E2 Ub-conjugating enzyme, and E3 Ub-ligases (4). Then, the polyubiquitinated proteins are degraded timely by the Ub proteasome system (5), which is essential for maintaining cellular activity and homeostasis. Notably, about 80% of intracellular protein proteolysis depends on Ub, and the dysregulation of Ub proteasome system has been

involved in various diseases, including cancer (6). The components of Ub proteasome system are also mutated or abnormally expressed in multiple cancers. E3 Ub ligases can recognize and interact with ubiquity late protein substrates (7), which in several cases lead to the upregulation of oncogenic activities and downregulation of tumor-suppressor activities (8).

To date, about 600 putative E3 ligases have been found in the human genome (9). RFWD2 [also called constitutive photomorphogenic 1 (COP1)] is a RING finger containing protein and operates as an E3 Ub ligase for ubiquitination-mediated degradation by targeting its substrate proteins, thus playing an important role in regulating cell proliferation and apoptosis (10, 11). Based on datasets from Oncomine and Gene Expression Omnibus, RFWD2 is found to be overexpressed in various human cancers, including leukemia, lung cancer, breast cancer, renal cell carcinoma, colorectal cancer, ovarian cancer, and hepatocellular carcinoma (12). RFWD2 knockdown significantly suppresses cell proliferation and induces the apoptosis of human hepatocellular carcinoma cells (13). RFWD2-siRNA treatment can also suppress liver cancer growth and reduce tumor mass in nude mice (13). The overexpression of RFWD2 significantly promotes cell proliferation of human chronic lymphocytic leukemia cells (14). These studies demonstrated that RFWD2 is critically involved in tumorigenesis and may be a novel therapeutic target for cancer therapy.

The tribble (TRIB) pseudokinase protein family consists of three members: TRIB1, TRIB2, and TRIB3 (15). These proteins are predicted to contain three domains: an N-terminal PEST region, pseudokinase domain (containing an unusual N-lobe and canonical C-lobe), and C-terminal RFWD2-binding peptide region, which interacts in cis with a pocket formed adjacent to the unusual C-helix in the TRIB pseudokinase domain (15). Through structure–function analyses, Trib1 and Trib2 may act as adapters to recruit RFWD2-E3 Ub ligase by interacting with C-terminal RFWD2-binding motif (16, 17). In addition, RFWD2 accelerates the development of Trib1- and Trib2-induced acute myeloid leukemia in mouse models, which is abrogated when Rfwd2 or Trib1/2 is deleted or mutated (18, 19). These results suggest that RFWD2 forms a complex with Trib1 or Trib2 to exert its oncogenic roles in AML by promoting the ubiquitination and degradation of its related proteins.

We previously reported that TRIB2 promotes lung cancer development and may play an oncogenic role in lung cancers associated with poor outcomes (20). In this study, inBio Discover™ analysis showed that TRIB2 can perform its functions by interacting with RFWD2. To further study the mechanism of oncogenic TRIB2 and its interaction with RFWD2 in lung cancer, performed immunoprecipitation and immunofluorescence experiments showed that TRIB2 colocalizes with RFWD2-related IκB-α to form a ternary complex and further affected IκB-α degradation by regulating its phosphorylation. TRIB2, as an oncogene, promotes cancer cell proliferation and migration, which can be blocked by knocking down RFWD2.

MATERIALS AND METHODS

Lung Carcinoma Tissues

The experiments were approved by the Medical Ethics Committee of Binzhou Medical University. Severn paired samples of lung adenocarcinoma and adjacent noncancerous lung were obtained from patients who had undergone surgery between October 1, 2018 and July 31, 2019 at Yantaishan Hospital, the Affiliated Hospital of Binzhou Medical University (Yantai, China). Informed consent was obtained from all patients. The tissues were fixed in 10% neutral formalin for immunohistochemistry analysis or extracted with total protein for Western blotting.

Immunohistochemistry

Immunohistochemistry analysis of paraffin-embedded tissue was performed as follows. The sections were dewaxed with xylene, treated with gradient ethanol for hydration, and repaired with EDTA solution (pH 8.0), followed by blocking with goat serum and incubation with normal IgG. The sections were incubated overnight at 4°C with anti-TRIB2 antibody (1:200 Bioss, Beijing, China), and then incubated in biotin-conjugated second antibody. Proteins were visualized using a pv-9000 two-step detection kit (Zhongshan Jinqiao Biotechnology Co., Ltd., Beijing, China).

Cell Culture and siRNA Transfection

A549, H1975, and HeLa cells (Shanghai Institute of Cell Biology, Shanghai, China) were cultured in RPMI-1640 medium (Gibco, Grand Island, NY, USA) supplemented with 10% fetal bovine serum (Hyclone, Logan, UT, USA), 100 U/ml penicillin, and 100 μg/ml streptomycin at 37°C in a 5% CO_2 atmosphere.

Transfection of expression plasmids or short interfering RNAs (siRNAs) into HeLa, A549, and 293T cells was carried out using Lipofectamine™ 3000 (Thermo Fisher Scientific, Waltham, MA, USA; L3000015) according to the manufacturer's recommendations. All siRNAs were transfected into cells at a final concentration of 50 nM. The sequences of the siRNAs used in this study are shown (**Supplementary Table S1**).

Western Blotting

Total cell lysates were prepared using RIPA buffer (Beyotime, Shanghai, China). All proteins were separated *via* SDS-PAGE and transferred onto polyvinylidene fluoride membranes (Invitrogen, Carlsbad, CA, USA). The membranes were incubated overnight at 4°C with the following primary antibodies: p-IKB-α, IKB-α, RFWD2, ubiquitin (1:500, Bioworld Technology, Inc., Minneapolis, MN, USA), TRIB2 (1:1,000, Cell Signaling Technology, Danvers, MA, USA), and p-RFWD2 (1:500, Bioss Biotechnology). Next, the membranes were incubated with horseradish peroxidase-labeled secondary antibodies (1:6,000, Beijing Zhong Shan-Golden Bridge Technology Co., Ltd., Beijing, China), and the signals were detected with an Automatic Image Analysis System (Tanon 5200 Multi, Shanghai, China) following electrochemiluminescence immune reactions.

Plasmids

The DNA sequences of TRIB2-full and its truncated mutants were amplified using pcDNA-TRIB2 as a template. The primer sequences used are as shown in **Supplementary Table S2**. These DNA fragments were inserted into the p3×flag-CMV-9-10 vector plasmid. To construct the GFP-TRIB2-expressing plasmid, the cDNA for TRIB2 was amplified from pcDNA-TRIB2 using the same primers with Flag-TRIB2-full *via* PCR and ligated into the pEGFP-C3 plasmid containing an N-terminal GFP tag.

Immunoprecipitation

Cells were seeded into 10-cm plates and transfected with Flag-tagged expression plasmid vectors using Lipofectamine 2000 (Invitrogen) for 48 h. The total lysate was extracted with NP-40 buffer (50 mM Tris-Cl at pH 7.4, 150 mM NaCl, 1 mM EDTA, 1% NP-40, 0.5% SDS, protease inhibitor mixture) and incubated with 50 µl of Anti-Flag M2 Affinity Gel (Sigma-Aldrich, St. Louis, MO, USA) at 4°C for 2 h. Following centrifugation, the samples were washed with PBS and heated with 40 µl 1× loading buffer, and the supernatant was subjected to SDS-PAGE followed by immunoblotting.

To analyze the interactions among endogenous proteins, 500 µg of cell extracts were incubated with primary antibodies or control IgG overnight at 4°C, and then with protein G/A beads (Invitrogen) for 2 h at 4°C. The beads were washed with lysis buffer, mixed with protein loading buffer, and detected by SDS-PAGE.

Immunofluorescence Detection

Cells growing on glass coverslips were fixed with 4% paraformaldehyde, permeabilized with 0.1% NP-40, and incubated with rabbit antihuman IKB-α/RFWD2 (1:100; Bioworld Technology) overnight at 4°C. The cells were then incubated with Alexa Fluor 488 donkey antirabbit IgG (H+L) or Alexa Fluor 594 donkey antimouse IgG (H+L) (Molecular Probes, Eugene, OR, USA) at 37°C for 1 h. Immunofluorescence was observed using a microscope (DM6000B, Leica, Wetzlar, Germany).

3-(4,5-Dimethythiazol-2-yl)-2,5-Diphenyl tetrazolium Bromide Assay

Cells transfected with siRNAs (GenePharma, Shanghai, China; siRNA sequences were shown in **Supplementary Table S1**) or pcDNA-TRIB2 plasmids were cultured in 96-well plates for 48 h as described previously (20). Next, 10 µl 3-(4,5-dimethythiazol-2-yl)-2,5-diphenyl tetrazolium bromide (MTT; 5 mg/ml, Sigma-Aldrich) was added to the medium in each well. The medium was removed 4 h later, and 100 µl dimethyl sulfoxide (Sigma-Aldrich) was added, and the OD value (570 nm) was detected with a microplate reader (Multiskan FC, Thermo Fisher Scientific). Each experiment was performed in triplicate and repeated at least three times.

Analysis of Apoptotic Cells

Harvested cells were treated with Annexin V-FITC/PI (KeyGEN Biotech. Co., Ltd., Nanjing, China) according to the manufacturer's instructions and counted by flow cytometry (Beckman Coulter, Brea, CA, USA). Each experiment was performed in triplicate and repeated at last three times.

Colony-Formation Assay

Cells transfected with indicated siRNAs or plasmids were maintained in culture media for 14 days, followed by staining with crystal violet. Colonies containing more than 20 cells were counted. Each experiment was performed in triplicate and repeated at last three times.

Migration Assays

Cells (10^4 cells per well in 100 µl fetal bovine serum-free 1640 medium) were seeded into the upper chamber of a Corning Costar Transwell chamber (Sigma-Aldrich), and 600 µl of RPMI-1640 medium containing 20% calf serum was added to the lower chamber. After 16 h, cells in the upper chamber were removed using cotton swabs, and migrated cells in the lower chamber were fixed with 4% paraformaldehyde and incubated with 1% crystal violet (Sigma) for 15 min. After washing with ddH_2O, five fields per Transwell were examined under a microscope (DM6000B, Leica). The assay was repeated three times for each group.

Migration assays were also performed using an xCELLigence DP instrument following the manufacturer's instructions (ACEA Biosciences Inc., San Diego, CA, USA); 1.5×10^5 cells in 100 µl of medium were seeded into the upper compartment of a CIM plate in triplicate per group, after which 160 µl medium containing 20% fetal bovine serum was added to the lower compartment. The cell index, representing the number of migrated cells, was calculated *via* RECA (real-time cell analysis) software 1.2.1 (ACEA Biosciences).

A549 Lung Adenocarcinoma Cell Xenografts

Animals were grouped by simple randomization of using random number table. A549 cells stably expressing TRIB2 or treated with TRIB2-siRNA or RFWD2-siRNA were harvested, and 2×10^6 cells were injected subcutaneously into the backs of female BALB/C-nude mice aged 6–8 weeks (HFK Bio-Technology, Beijing, China) as previously described (20). The second siRNA was injected into the xenografts on day 14 after the initial treatment. Tumor volumes were measured daily using calipers. The animals were sacrificed by intraperitoneal injection of a barbiturate at 30 days after injection. All animal experiments were approved by the Committee on the Ethics of Animal Experiments of Binzhou Medical University.

Statistical Analysis

SPSS 22.0 software (IBM Corp., Armonk, NY, USA) was used to analyze statistical significance. Data were tested for normal distribution using a normality test. Data are expressed as mean ± SD. The Student's *t*-test was used to compare two averages. ANOVA was used for mean comparison of multiple groups; depending on whether the assumption of homogeneity of variance was satisfied or not, the LSD test or the Games-Howell test was used to compare means of different samples. Abnormally distributed data were expressed as median (interquartile range); the Mann-Whitney *U* test and Kruskal-

Wallis H test were used to compare two groups or multiple groups, respectively. Statistical significance was set at $P < 0.05$.

RESULTS

TRIB2 Promotes Cancer Cell Proliferation and Migration

TRIB2 acts as an oncogene in various tumors. Our previous study demonstrated that the overexpression of TRIB2 is related to the poor survival of patients with lung cancer, and miR-206 and miR-140 induce lung cancer cell death and suppress cell proliferation by regulating oncogenic TRIB2 promoter activity through p-Smad3 (20). To further determine the mechanism of TRIB2 in the progression and development of lung adenocarcinoma (LUAD), we detected the expression of TRIB2 in lung cancer and adjacent normal lung tissues by immunohistochemistry analysis. TRIB2 was overexpressed in lung cancer tissue compared with the adjacent normal lung tissue (**Figure 1A**). Next, we collected seven lung cancer and adjacent normal lung-tissue samples for Western blotting to detect the expression of TRIB2. We observed that TRIB2 was overexpressed in LUAD (**Figures 1B, C**). In a previous study, we transfected A549 cells with three pairs of siRNA-targeting TRIB2 and confirmed their effectiveness for knocking down TRIB2 (20). Next, we transiently transfected pcDNA-3.1-TRIB2 or siRNA into A549 cells to determine the role of TRIB2 in cancer after its overexpression or downregualtion (**Figures 1D, E**). The results of an MTT assay, which was performed to clarify the role of TRIB2 in cancer progression, showed that TRIB2 knockdown inhibited the proliferation of A549 cells (**Figure 1F**), whereas TRIB2 overexpression promoted the proliferation of A549 cells (**Figure 1G**). Plate colony formation indicated that cell clones, which were smaller and less abundant following TRIB2 knockdown in A549 cells ($p < 0.01$; **Figures 1H, I**), became

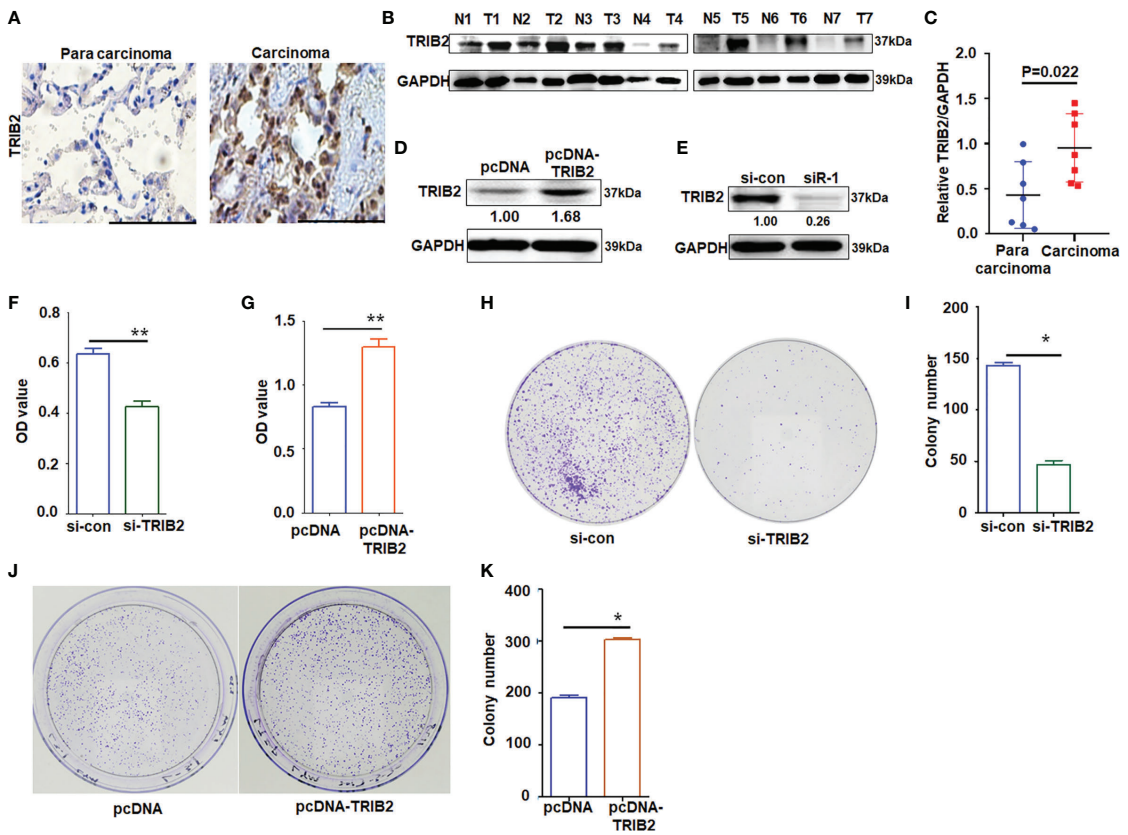


FIGURE 1 | Effects of TRIB2 on cancer cell proliferation. **(A)** Immunohistochemistry analysis of TRIB2 expression in one paired sample of lung anticarcinoma versus adjacent normal lung tissue; bar = 100 μm. **(B)** Total proteins from seven paired samples of lung adenocarcinoma (*T*) versus adjacent normal tissues (*N*) were extracted for Western blotting analysis with antibodies against TRIB2. **(C)** The levels of TRIB2 in seven lung adenocarcinoma and paired normal lung tissues of **(B)** was quantified with Image J (NIH, Bethesda, MD, USA) software and normalized to GAPDH, data were expressed as median (interquartile range). **(D, E)** TRIB2 expression in A549 cells treated with pcDNA-TRIB2 or TRIB2-siRNA and controls was assessed by Western blotting. GAPDH was used as the loading control. **(F)** TRIB2-siRNA inhibits A549 cell viability by MTT assay following siRNA transfection for 48 h Data represent the mean ± SD; for triplicate experiments. $^{**}p < 0.01$; LSD test. **(G)** Overexpression of TRIB2 increases viability of A549 cells by MTT assay. Data represent the mean ± SD; for triplicate experiments. $^{**}p < 0.01$; LSD test. **(H, I)** Knocking down TRIB2 inhibits colony formation of A549 cells. Data represent the mean ± SD; for triplicate experiments. $^{*}p < 0.05$; LSD test. **(J, K)** Overexpression of TRIB2 increased colony formation of A549 cells. Data represent the mean ± SD; for triplicate experiments. $^{*}p < 0.05$; LSD test.

larger and more abundant after TRIB2 overexpression ($p < 0.01$; **Figures 1J, K**).

Flow cytometry detection was conducted to investigate whether TRIB2-regulated cell proliferation is related to apoptosis. The results obtained demonstrated that the apoptotic rate of A549 cells significantly increased following TRIB2 knockdown but decreased following TRIB2 overexpression (**Supplementary Figures S1A, B**). Tumor cells often exhibit strong migration capabilities. Cell migration experiments indicated that TRIB2 knockdown significantly inhibited cell migration compared with that in the control group (**Supplementary Figures S1C, D**; $p < 0.05$). Following TRIB2 overexpression, the number of migrated cells increased significantly (**Supplementary Figures S1E, F**; $p < 0.05$), suggesting that TRIB2 promoted the migration of lung cancer cells. This finding was also supported by cell migration experiments using HeLa cells (**Supplementary Figure S2**).

TRIB2 Interacts With RFWD2

To investigate the mechanism of TRIB2 in promoting cancer cell proliferation, the interactions between TRIB2 and other proteins were analyzed with inBio Discover™ online (https://inbio-discover.com/#login). With inBio Discover™, we can explore the interactions between proteins, and gain valuable biological functions. The inBio Discover™ results demonstrated that TRIB2 can perform its functions by interacting with RFWD2, C/EBPα, WEE2, etc. (**Figure 2A**). TRIB2 is also specifically regulated by Wnt signaling in liver cancer cells, which is associated-Ub E3 ligase-TrCP, RFWD2, and Smurf1 reducing TCF4/β-catenin expression (21). To further verify whether the roles of TRIB2 are related to RFWD2 or other Ub E3 ligases, we extracted the total protein from 293T cells transiently expressing Flag-TRIB2 and performed coimmunoprecipitation experiments using an M2 affinity chromatography column binding anti-Flag antibodies. Our results confirmed the interaction between TRIB2 and RFWD2 but did not support the interaction between TRIB2 and polyubiquitin-C (**Figure 2B**). Coprecipitation experiments with the total lysates of 293T cells showed that anti-RFWD2 antibodies precipitated RFWD2, together with TRIB2 (**Figure 2C**). These results indicate that TRIB2 can interact with RFWD2, which may be related to TRIB2-regulating cancer cell proliferation.

TRIB2 With RFWD2 Attends Proteasome-Mediated Degradation of Proteins

RFWD2 is an E3 Ub ligase that plays a vital role in the regulation of cell proliferation and apoptosis (12). The abovementioned results showed that TRIB2 can interact with RFWD2, which indicates that the function of TRIB2 may affect the proteasome-mediated degradation of proteins through the interaction between TRIB2 and RFWD2. To investigate this hypothesis, we first detected the effect of TRIB2 on RFWD2 levels after the overexpression or knockdown of TRIB2 by Western blot. The levels of RFWD2 were significantly reduced following TRIB2 knockdown for 48 h in A549 cells but increased following TRIB2 overexpression (**Figure 2D**). These results indicate that the role of TRIB2 is related to its interaction with and effects on RFWD2. The roles of RFWD2 in cancer is related to targeting its substrates for ubiquitination and degradation, such as p-IκB-α (22), p53, Jun, STAT3, β-catenin, p27, and C/EBPα (12). Next, we detected the levels of RFWD2-related ubiquitination substrate p-IκB-α and p53 after the overexpression or knockdown of TRIB2 by Western blot. Our results showed that TRIB2 overexpression inhibited the p-IκB-α and p53 levels, whereas TRIB2 knockdown resulted in their increase (**Figures 2E, F**). The abovementioned results indicate that TRIB2 can affect p-IκB-α and p53 levels by regulating RFWD2.

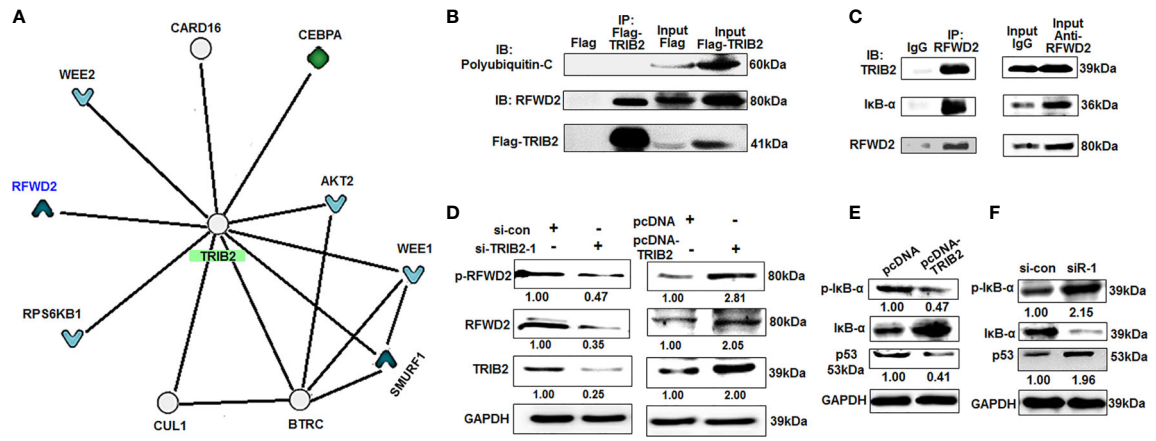


FIGURE 2 | TRIB2 interacts with RFWD2. **(A)** The results of inBio Discover™ showed that TRIB2 may interact with RFWD2, CEBPA, WEE2, etc. **(B)** 293T cells were transiently transfected with Flag-TRIB2 or Flag vector for 48 h, and then the total lysate was coimmunoprecipitated using M2 affinity gel. **(C)** Whole-cell lysate of 293T cells was immunoprecipited with RFWD2 antibody followed by immunoblotting with antibodies against indicated proteins. **(D)** TRIB2 positively regulates the expression of RFWD2 and si-TRIB2 inhibits p-RFWD2 and RFWD2 levels, as shown by Western blotting analysis. Expression levels of RFWD2 and TRIB2 quantified *via* ImageJ software and normalized to GAPDH. **(E, F)** Expression levels of IκB-α, p-IκB-α, and p53 in A549 cells treated with pcDNA-TRIB2 or TRIB2-siRNA and controls assessed by Western blotting. GAPDH was used as the loading control.

To further investigate the above hypothesis, we selected IκB-α as a research object for coprecipitation experiments with the total lysates of 293T cells. The results showed that anti-RFWD2 antibodies precipitated RFWD2, also together with IκB-α. Further coimmunoprecipitation experiments indicated that IκB-α also interacted with RFWD2 (**Figures 2C**, **3A**). To determine whether TRIB2 interacts directly with IκB-α, we conducted coimmunoprecipitation with cells overexpressing Flag-tagged TRIB2. The results demonstrated that anti-Flag M2 affinity gel precipitated TRIB2 with p-IκB-α (**Figure 3B**). We next confirmed the endogenous interaction between TRIB2 and p-IκB-α in 293T cells (**Figure 3C**). We further used eukaryotic expressed and purified TRIB2 and IκB-α proteins in coimmunoprecipitation experiments and observed that IκB-α antibodies may precipitate IκB-α and TRIB2 (**Figure 3D**). These results indicate that TRIB2, IκB-α, and RFWD2 form a ternary complex with RFWD2 though direct physical interactions, which may be related to the effect of TRIB2 on the proteasome-mediated degradation of proteins with RFWD2.

Prior studies also supported that TRIB2 regulates the degradation of certain proteins *via* the Ub-proteasome pathway (23, 24). To further test whether TRIB2 can regulate the degradation of IκB *via* the Ub–proteasome pathway, we treated A549 cells with various concentrations of MG132, an inhibitor of the proteasome degradation pathway. Western blotting indicated that p-IκB-α expression increased in an MG132 concentration-dependent manner (**Figure 3E**). The findings confirmed that IκB-α was phosphorylated and entered the ubiquitination degradation pathway. However, IκB-α degradation was blocked when A549 cells were treated with 20 μM MG132 following TRIB2 knockdown with siRNA, suggesting that TRIB2 affected IκB-α degradation by regulating its phosphorylation (**Figure 3F**).

TRIB2 Colocalizes With RFWD2-Related IκB-α

To test whether TRIB2 affects the proteasome-mediated degradation of protein IκB-α through a ternary complex TRIB2-RFWD2-IκB-α, we performed immunofluorescence staining to evaluate the interactions and colocalization among TRIB2, RFWD2, and IκB-α. Laser confocal microscopy revealed partial colocalization of exogenously expressed GFP-TRIB2 with FRWD2 in A549 cells (**Figure 4A**) and colocalization of endogenously expressed IκB-α with RFWD2 (**Figure 4B**). Following the transfection of A549 cells with Flag-TRIB2, immunofluorescence analysis revealed the colocalization of Flag-TRIB2 with IκB-α (**Figure 4C**). Altogether, these results support that TRIB2, IκB-α, and RFWD2 form a ternary complex. We also used a network tool (PRODIGY, https://nestor.science.uu.nl/prodigy/) to model the three-dimensional structures of TRIB2 and IκB-α and analyzed their potential for interaction with RFWD2. The PRODIGY results indicated that these three proteins directly interact (**Figure 4D**; **Supplementary Table S3**).

Mapping the Interaction of TRIB2, RFWD2, and IκB-α

TRIB2 contains an N-terminal PEST region, pseudokinase domain, and C-terminal region (25). To identify the specific domain associated with the interaction of TRIB2 with RFWD2 and IκB-α, we constructed Flag-tagged TRIB2-domain deletion

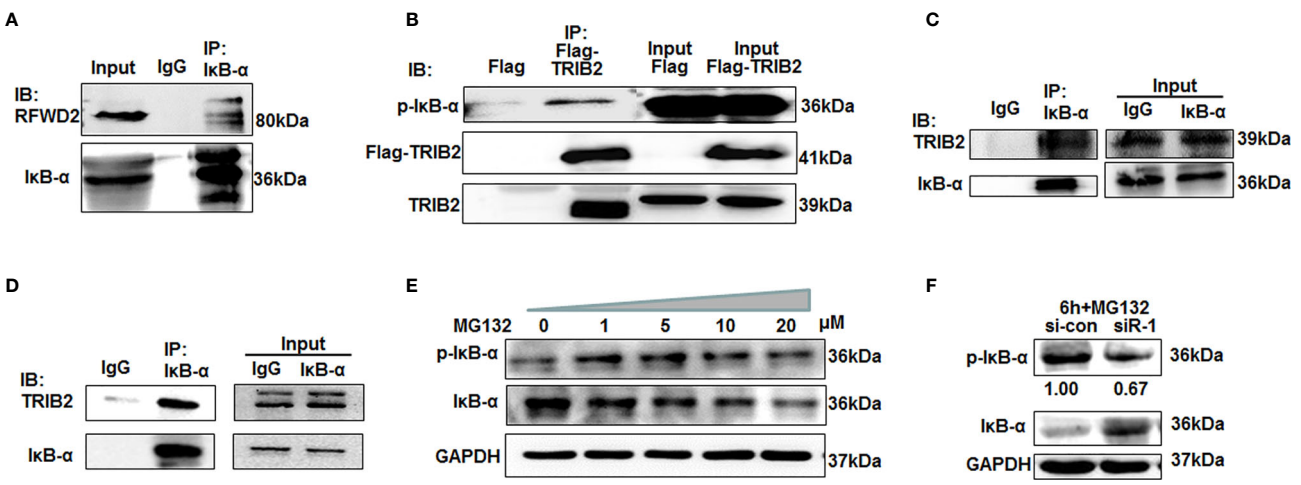


FIGURE 3 | TRIB2 with RFWD2 attend proteasome-mediated p-IκB-α degradation. **(A)** Coimmunoprecipitation with IKB-α antibodies showing interaction between RFWD2 and IκB-α in 293T cells. **(B)** Coimmunoprecipitation experiments were carried out using total lysates of 293T cells overexpressing Flag and Flag-TRIB2. M2 affinity gel precipitated TRIB2 together with p-IκB-α. **(C)** Coimmunoprecipitation using 293T lysate and anti-IκB-α antibodies. TRIB2 and IκB-α precipitated together. **(D)** Expressed and purified eukaryotic TRIB2 and IκB-α proteins used for coimmunoprecipitation experiments to further study the interaction between IκB-α and TRIB2. **(E)** p-IκB-α and IκB-α expression detected by Western blotting in A549 cells following treatment with various concentrations of MG132. **(F)** A549 cells were treated with 20 μM MG132 for 6 h following TRIB2 knockdown with siRNA and the total lysate was subjected to Western blotting to detect p-IκB-α and IκB-α expression levels.

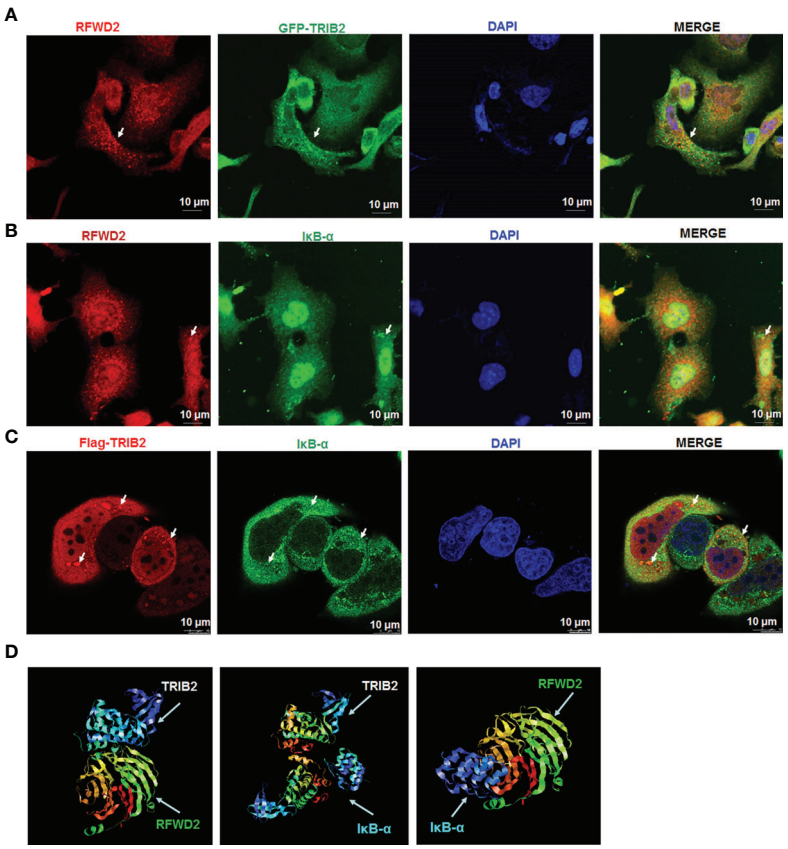


FIGURE 4 | Colocation analysis between TRIB2, RFWD2, and IκB-α. **(A)** Colocalization of RFWD2 (red) and GFP-TRIB2 (green) in A549 cells, observed *via* confocal microscopy. Immunostaining was performed with primary RFWD2 antibody after A549 cells were treated with GFP-TRIB2. Scale bar = 10 μm. **(B)** Immunostaining of A549 cells with antibodies against RFWD2 (red) and IκB-α (green). Scale bar = 10 μm. **(C)** A549 cells transfected with Flag-TRIB2 and subjected to immunostaining with antibodies against IκB-α (green) and TRIB2 (red). Scale bar = 10 μm. **(D)** Interactions between TRIB2, IκB-α, and RFWD2 analyzed *via* the PRODIGY Tool.

mutants (**Figure 5A**) and transiently transfected them into 293T cells. After 48 h, coimmunoprecipitation analysis of the total protein extract showed that RFWD2 precipitated together with Flag-TRIB2-Full, Flag-TRIB2-C, and Flag-TRIB2-E, indicating that TRIB2 interacted with RFWD2 mainly *via* its carboxyl terminus (**Figures 5B, C**). Flag-TRIB2-Full, Flag-TRIB2-B, and Flag-TRIB2-D coprecipitated with IκB-α, indicating that the pseudokinase domain is mainly required for the interaction between TRIB2 and IκB-α. Because of the affection of the binding of RFWD2 and the structure of mutant Flag-TRIB2-E, a relatively weak band was found in Flag-TRIB2-E. The abovementioned results indicate that TRIB2 may bind to RFWD2 *via* its C-terminus, whereas it binds to IκB *via* its pseudokinase domain. Therefore, the combination of TRIB2 with RFWD2 causes no effect on its interaction with IκB-α.

These above results indicate that TRIB2 can regulate the proteasome-mediated degradation of RFWD2. To further understand the biological role of RFWD2 in TRIB2 affecting the proteasome-mediated degradation of RFWD2-related protein, we screened siRNAs that effectively knock down RFWD2 (**Figure 5D**). siRNAs specific for RFWD2 were cotransfected with the control vector or TRIB2 expression plasmids into A549 cells, and the expression of related proteins was detected. The results showed that the levels of RFWD2-related protein p-IκB-α increased following the RFWD2 knockdown compared with the control treatment (**Figure 5E**). Our results indicate that the function of TRIB2 in regulating proteasome-mediated degradation requires the participation of RFWD2.

TRIB2 Promotes Cell Proliferation and Migration in a RFWD2-Dependent Manner

The abovementioned results showed that TRIB2 promoted cell proliferation and migration, and that the function of TRIB2 in regulating gene expression requires the participation of RFWD2. We next evaluated whether blocking the RFWD2 activity suppresses the oncogenic role of TRIB2. Using siRNA to knockdown RFWD2, we investigated the effect of RFWD2 on the proliferation and migration of A549 cells. MTT assay showed that proliferation was significantly inhibited in siRNA-treated cells compared with that in the control oligo treatment group ($p < 0.01$; **Figure 6A**). Fluorescence-activated cell sorting assay indicated that the apoptosis rate was elevated in siRNA-treated cells (**Figure 6B**). Real-time cell analysis of migration further

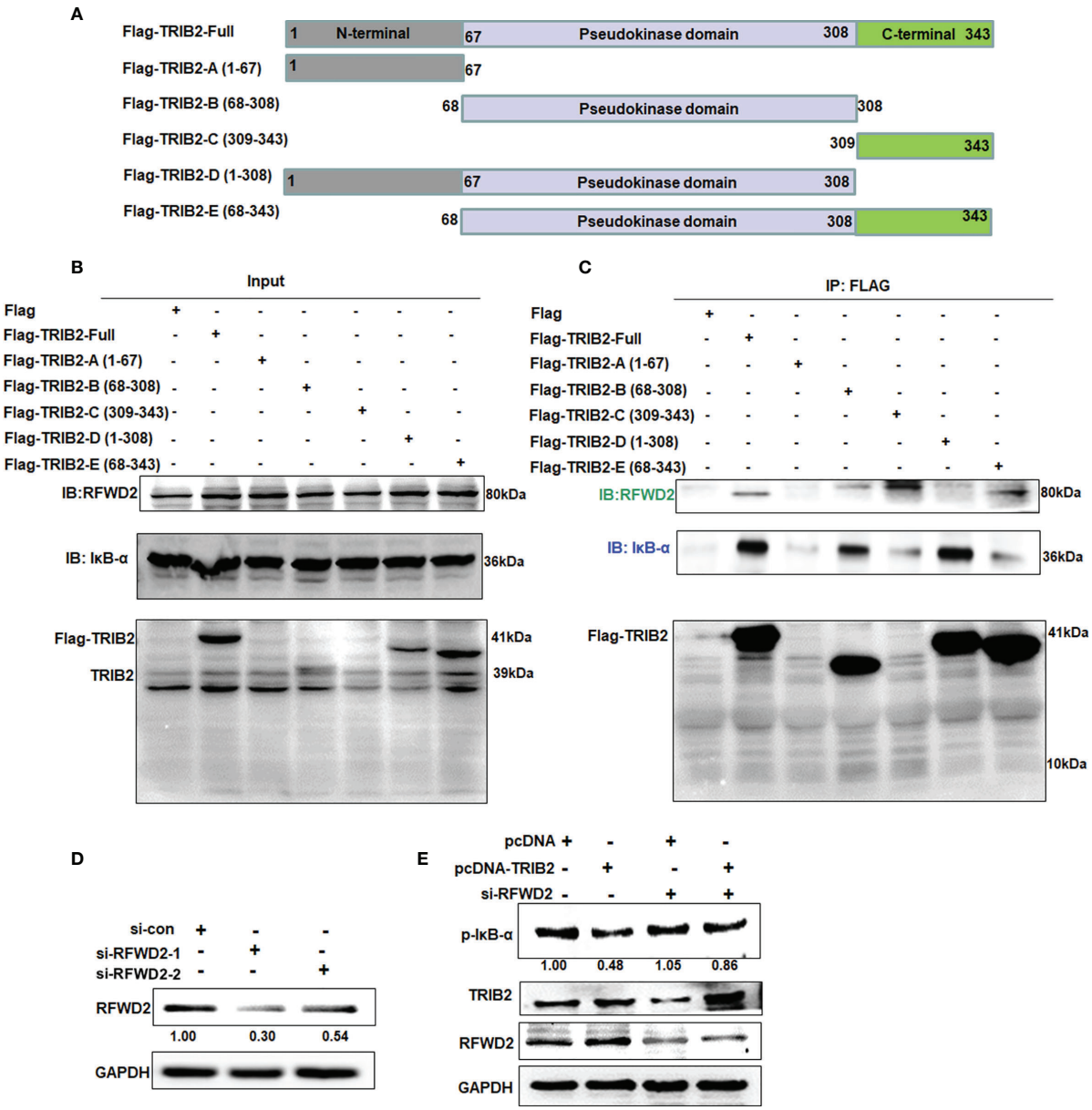


FIGURE 5 | Mapping interaction of TRIB2 with IκB-α or RFWD2. **(A)** Diagram showing constructs of Flag-TRIB2 and its deletion mutants. **(B, C)** Coimmunoprecipitation analysis of the domains of TRIB2 involved in the interaction with RFWD2 and IκB-α in 293T cells treated with Flag-TRIB2 deletion mutants. **(D)** Expression levels of RFWD2 were decreased in RFWD2-siRNA-treated A549 according to Western blotting. RFWD2 expression was normalized to GAPDH. **(E)** RFWD2 knockdown attenuated the role of TRIB2 in regulating the expression of p-IκB-α, as shown by Western blotting. Relative intensities of p-IκB-α were normalized to that of GAPDH.

showed that RFWD2 knockdown inhibited cell migration (**Figures 6C, D**; $p < 0.01$). The results in H1975 cells also supported that siRNA-RFWD2 inhibited cell proliferation and migration, and increased lung cancer cell apoptosis (**Supplementary Figure S3**). These results indicate that RFWD2 knockdown suppresses A549 cell proliferation.

Next, we analyzed the effect of RFWD2 on TRIB2-induced cell proliferation and migration. The MTT assay suggested that either TRIB2-siRNA or RFWD2-siRNA suppressed the proliferation of A549 cells; this suppressive effect was evident when both proteins were downregulated simultaneously (**Figure 6E**). Although TRIB2 overexpression promoted cell proliferation, knockdown of RFWD2 partially weakened the oncogenic role of *TRIB2* in A549 cells (**Figure 6F**). The apoptosis assay demonstrated that although the knockdown of either RFWD2 or TRIB2 individually increased the apoptosis rate, knocking them both down significantly increased the apoptotic rate of A549 cells (**Figure 6G**). Moreover, RFWD2 downregulation partially attenuated the role of TRIB2 (**Figure 6H**). The RTCA migration assay demonstrated that the simultaneous knockdown of TRIB2

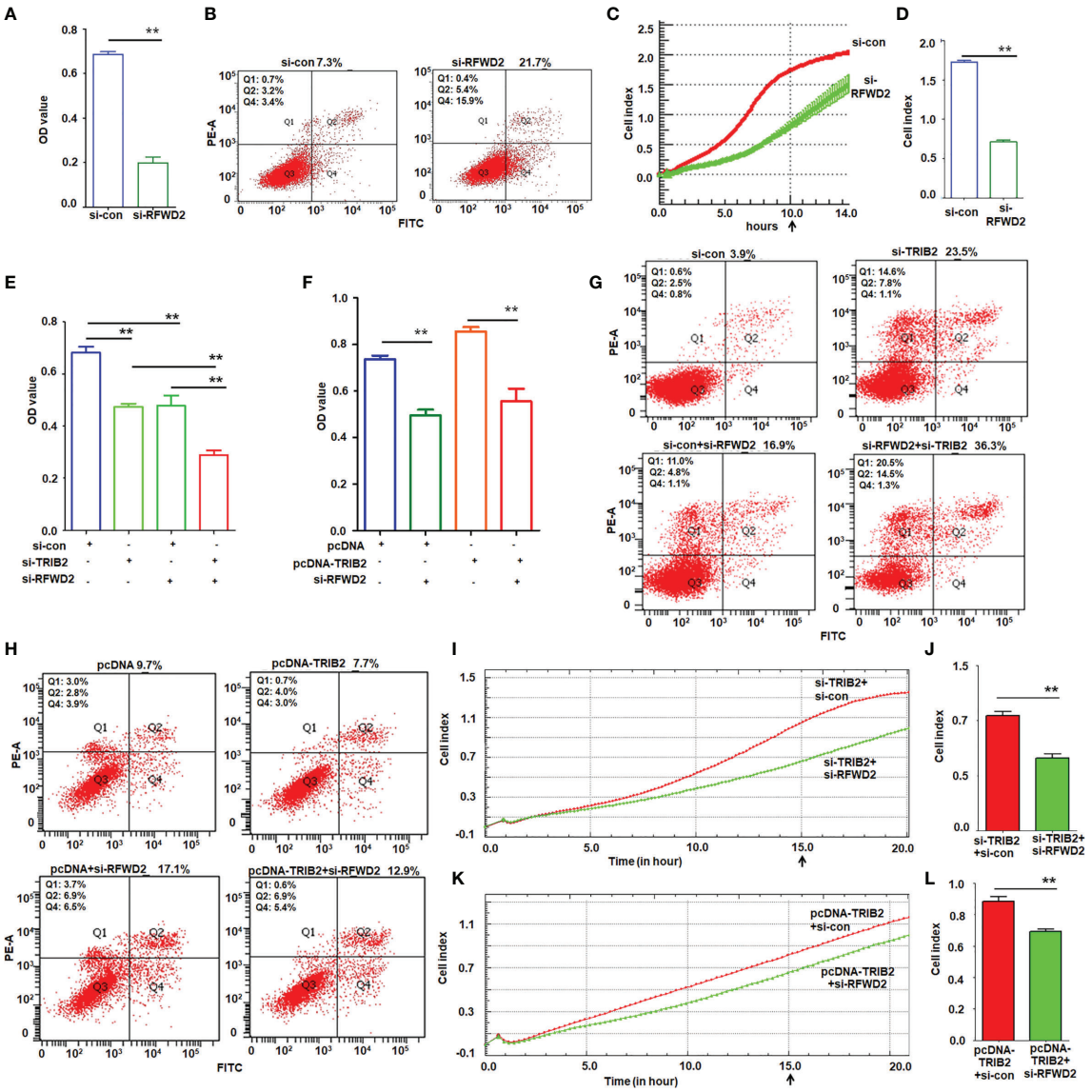


FIGURE 6 | TRIB2 promotion of cell growth and migration depends on RFWD2. **(A)** MTT assay showing that RFWD2 downregulation inhibited A549 cell proliferation. Data were expressed as the mean ± SD from triplicate experiments. $^{**}p < 0.01$; Student's *t*-test. **(B)** Apoptotic rate of A549 cells transfected with RFWD2-siRNA for 48 h measured *via* flow cytometry from triplicate experiments. **(C, D)** RFWD2 knockdown inhibited cell migration. A549 cells treated with siRNAs were analyzed *via* a real-time migration assay on an xCELLigence RTCS. Data are expressed as the mean ± SD of triplicate experiments. $^{**}p < 0.01$; Student's *t*-test. **(E)** Viability of A549 cells transfected with the indicated siRNAs analyzed *via* MTT assay. Data are expressed as the mean ± SD of triplicate experiments. $^{**}p < 0.01$; ANOVA. **(F)** Cell viability of A549 cells following treatment with the indicated plasmids or siRNAs, as analyzed by MTT assay. Data are expressed as the mean ± SD of triplicate experiments. $^{**}p < 0.01$; ANOVA. **(G)** TRIB2 and RFWD2 downregulation promotes apoptosis, as shown by flow cytometry assay performed in triplicate. **(H)** Cell apoptosis induced by RFWD2 knockdown is rescued by TRIB2 overexpression as evaluated in triplicate. **(I, J)** Real-time migration assay on an xCELLigence RTCS showed that simultaneous knockdown of RFWD2 and TRIB2 inhibited migration more strongly than TRIB2 knockdown alone. Cell index represents the mean ± SD of triplicate experiments. $^{**}p < 0.01$; Student's *t*-test. **(K, L)** Real-time migration assay on an xCELLigence RTCS showed that TRIB2 overexpression recused migration inhibition caused by RFWD2 knockdown. Cell index represents the mean ± SD of triplicate experiments. $^{**}p < 0.01$; Student's *t*-test.

and RFWD2 suppressed cell migration more substantially than the knockdown of TRIB2 alone (**Figures 6I, J**), and that knockdown of RFWD2 reduced the role of TRIB2 in cell migration (**Figure 6K, L**). The results in H1975 cells further supported that siRNA-RFWD2 can reverse the role of TRIB2 in cell proliferation, migration, and apoptosis (**Supplementary Figure S3**).

A plate colony-formation assay showed that RFWD2 knockdown inhibited the colony-forming ability of A549 cells (**Supplementary Figures S4A, B**); TRIB2 had the same effect. However, when both TRIB2 and RFWD2 were knocked down simultaneously, the suppressive effect on colony formation became much more remarkable (**Supplementary Figures S4C, D**).

Moreover, RFWD2 knockdown reversed the role of TRIB2 in promoting colony formation (**Supplementary Figures S4E, F**). These results indicate that the oncogenic role of TRIB2 is inseparable from RFWD2.

RFWD2 Level Is High in Cancer and RFWD2-siRNA Blocks TRIB2 Functions *In Vivo*

The abovementioned results demonstrated that RFWD2 knockdown suppressed cancer cell proliferation. To further analyze its roles in tumorigenesis, we investigated the RFWD2 expression in cancer based on datasets from The Cancer Genome Atlas online (http://ualcan.path.uab.edu/). The analyzed results demonstrated that RFWD2 is remarkably upregulated in the tissues of numerous kinds of tumors, including bladder urothelial carcinoma (BLCA), breast invasive carcinoma (BRCA), cervical squamous cell carcinoma (CESC), cholangiocarcinoma (CHOL), esophageal carcinoma (ESCA), glioblastoma multiforme (GBM), stomach adenocarcinoma (STAD), etc., compared with control tissues (**Figure 7A**). RFWD2 is also overexpressed in LUAD and lung squamous cell carcinoma (LUSC) tissues compared with normal tissues (**Figure 7B**). Kaplan-Meier plot analysis further (http://kmplot.com/analysis/) demonstrated that high RFWD2 levels from patients with lung cancer were related to extremely poor clinical outcomes (**Figure 7C**). These results indicate that RFWD2 may play an important role in promoting lung cancer cell proliferation.

Furthermore, siRNA- and control-treated cells were injected subcutaneously into the backs of BALB/C-nude mice to produce xenografts to investigate the effects of TRIB2 and RFWD2 on the tumorigenesis of lung cancer cells *in vivo*. On day 14, similar doses of siRNA and control were injected into the xenografts. After 4 weeks, the volume of transplanted tumors in the siRNA-TRIB2 and siRNA-RFWD2 groups was considerably smaller than that in the control group (**Figures 7D, E**). The tumor

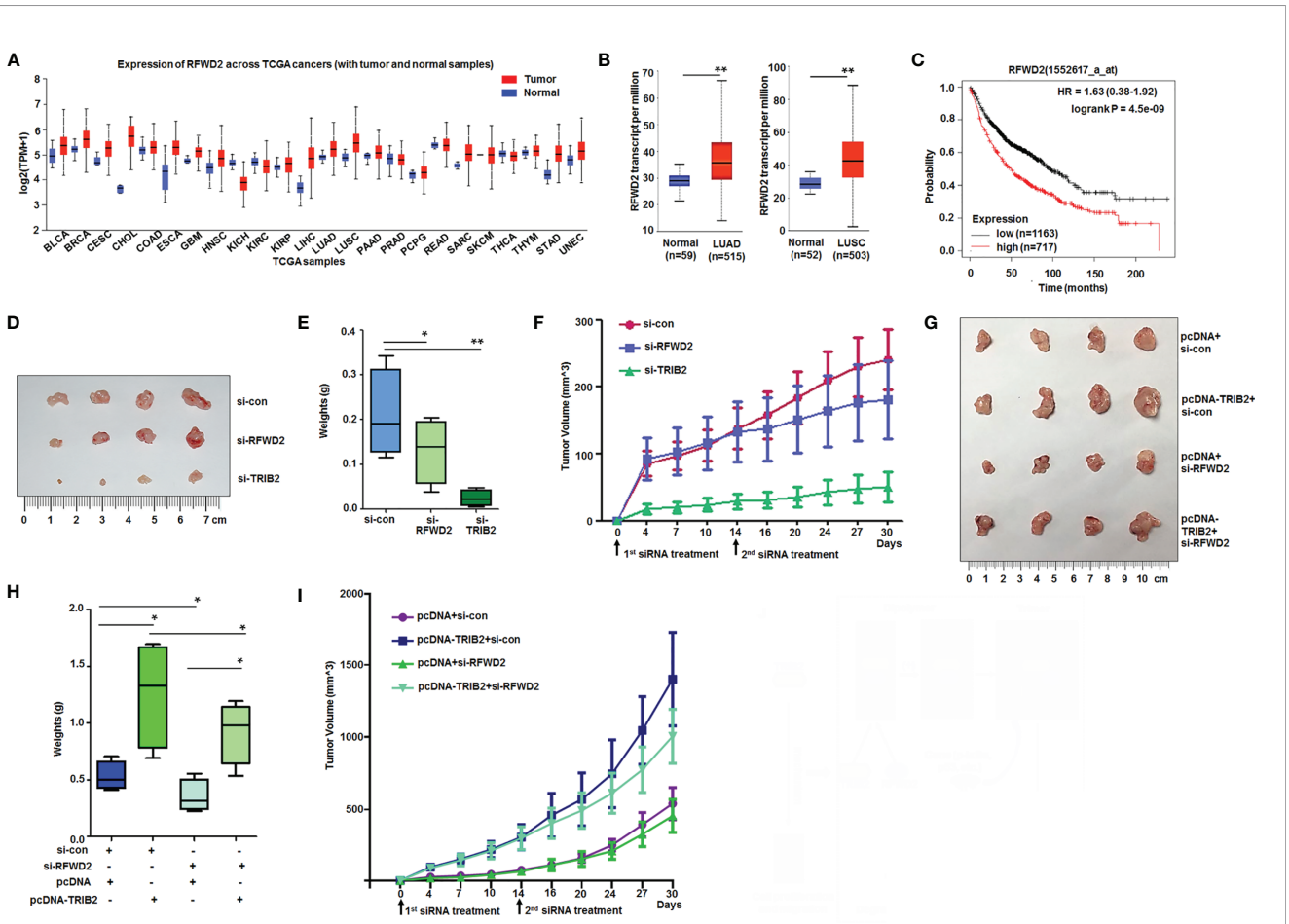


FIGURE 7 | High levels of RFWD2 in cancer and RFWD2 inhibition blocking functions of TRIB2 *in vivo*. **(A)** RFWD2 is obviously higher in the tissues of various kinds of tumors. **(B)** RFWD2 is overexpressed in lung adenocarcinoma and lung squamous cell carcinoma tissues. **(C)** Kaplan-Meier plot analysis of the relationship between RFWD2 levels and clinical outcome. **(D)** Suppressive role of TRIB2-siRNA and RFWD2-siRNA on A549 cell xenografts in BALB/C-nude mice. **(E)** The xenografts of each group ($n = 4$) were weighed, and data were expressed as median (interquartile range). $^{*}p < 0.05$, $^{**}p < 0.01$. **(F)** Volumes of xenografts from each group measured over time. **(G)** Effect of RFWD2 downregulation in xenografts of A549 cells stably overexpressing TRIB2. **(H)** Xenografts from each group ($n = 4$) were weighed, and data were expressed as median (interquartile range). $^{**}p < 0.05$. **(I)** Volumes of xenografts from each group measured over time.

growth curve further demonstrated that the downregulation of TRIB2 and RFWD2 inhibited tumor formation (**Figure 7F**).

To further verify whether the oncogenic role of *TRIB2* is inseparable from RFWD2 *in vivo*, we knocked down RFWD2 in A549 cell xenografts stably overexpressing TRIB2. The weight and growth curve of the xenografts showed that TRIB2 overexpression promoted tumor formation, whereas RFWD2 knockdown inhibited tumor formation and reduced tumorigenesis in xenografts stably expressing TRIB2 (**Figures 7G–I**). These results suggest that RFWD2 is important for the oncogenic roles of TRIB2 *in vitro and in vivo*.

DISCUSSION

TIRB2 is an oncogene involved in the development of several tumors, such as melanoma, colorectal cancer, acute myeloid leukemia, and liver cancer (25–28). In addition, the overexpression of TRIB2 in tumor tissues induces drug resistance by promoting phospho-AKT (at Ser473) *via* its COP1 domain. The highest TRIB2 protein expression from patients with cancer is related with an extremely poor clinical outcomes (29). Previously, we observed that TRIB2 promoted the proliferation and migration of lung cancer cells *in vitro* and *in vivo* (30, 31). The current study further verified whether the oncogenic role of TRIB2 depends on RFWD2 in regulating lung cancer cell proliferation. Our results showed that TRIB2 can promote cancer cell proliferation and migration, interact with RFWD2, and regulate RFWD2-related gene expression in lung cancer cells. Furthermore, our results indicated that TRIB2, RFWD2, and IκB-α form a ternary complex, which may be related to the effect of TRIB2 on the proteasome-mediated degradation of proteins with RFWD2. Therefore, we propose that TRIB2 may promote lung cancer cell proliferation *via* the following mechanisms (**Figure 8**): At first, TRIB2 binds RFWD2-E3 Ub ligase based on C-terminal RFWD2-binding motif to form a dipolymer, which increases phosphorylated RFWD2 levels. Next, RFWD2-E3 ubiquitin ligase further recruits and confers its substrate (p-IκB-α or others) specificity for Ub ligation. Then, TRIB2, RFWD2, and substrate p-IκB-α form a ternary complex, following which TRIB2 may regulate and drive the RFWD2-mediated degradation of the substrate *via* the ubiquitination pathway.

RFWD2, a ring-finger-type ubiquitin E3 ligase, was originally identified as a central regulator of photomorphogenesis in *Arabidopsis thaliana* (32). RFWD2 is highly conserved among different vertebrates and has been identified in mice and humans (33). The human RFWD2 gene is located on chromosome 1q24.1 (34). RFWD2 protein structure possesses three highly conserved domains, namely, a RING-finger region (N-terminal), a coiled-coil domain, and C-terminal domain with seven WD40 repeats, which are related to the modulation of protein–protein interactions (34, 35). Human RFWD2 shuttles between the cytoplasm and nucleus, which depends on distinct signals (36). Evidence shows that mammalian RFWD2 is expressed in the

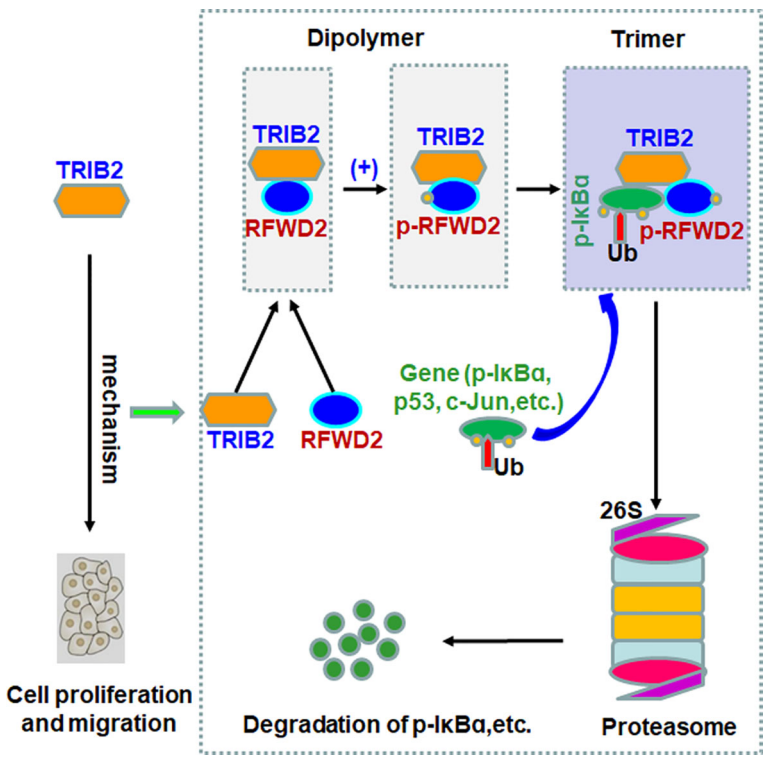


FIGURE 8 | Proposed model of the mechanism by which oncogenic roles of TRIB2 with RFWD2 in regulating proteasome-mediated degradation of proteins.

heart, lung, bladder, brain, pancreas, liver, spleen, kidney, aorta, skeletal muscle, ovary, prostate, and other tissues of humans and mice (34, 37). RFWD2 is also overexpressed in various kinds of human cancers (12), such as leukemia, lung cancer, breast cancer, lymphoma, glioma, melanoma, colorectal cancer, etc. We observed that RFWD2 levels were higher in lung cancer tissues compared with those in normal controls, and high levels of RFWD2 from patients with lung cancer showed a poor survival outcome. SiRNA-RFWD2 inhibited the proliferation of A549 and Hela cells and promoted the apoptosis and migration of cells. Our results showed that RFWD2 may play an important role in promoting lung cancer cell proliferation.

RFWD2, directly or indirectly, promotes protein degradation (38), and the substrates for human RFWD2 include the following: p-IκB-α (22); p53 (11, 39); C/EBPα (18); 14-3-3σ (40); β-catenin (12); activator protein-1 and c-Jun (10, 41); forkhead box protein O1 (42); p27Kip1 (12); transducer of regulated CREB activity 2 (43); and metastasis-associated protein (44). The roles of RFWD2 in cancer may be related to its promotion of the degradation of these proteins. We observed that siRNA-RFWD2 inhibited the proliferation of A549 and Hela cells and promoted the apoptosis and migration of cells, indicating that RFWD2 play important roles in tumorigenesis. We also revealed that RFWD2 interacts with p-IκB-α, and TRIB2 can affect p-IκB-α levels through regulating RFWD2. TRIB2, RFWD2, and IκB-α form a ternary complex with RFWD2 through direct physical interactions. Our results also demonstrated that the function of TRIB2 in regulating proteasome-mediated degradation of p-IκB-α requires the participation of RFWD2.

TRIB2 participates in the regulation of Wnt/β-catenin signaling (21), AP4/p21 signaling, and E2F1-C/EBPα feedback loop (26, 45). In most cases, the function of TRIB2 is related to the regulation of protein degradation. TRIB2 interacts with E3 Ub ligases (Smurf1, RFWD2, or β-TrCP), which further regulates the ubiquitination and degradation of specific protein signals (23). Moreover, the relationship between TRIB2 and the Ub proteasome system is complex, and may involve competition or cooperation with E3 ubiquitin ligase in binding TRIB2. Phosphorylated TRIB2 is also a target protein of Smurf1 and β-TrCP (46, 47), and it participates in the ubiquitination of TRIB2 and subsequently cause the degradation of TRIB2 to proteasome. In this study, inBio Discover™ results demonstrated that TRIB2 can perform its functions by interacting with RFWD2 or other factors. Next, we discovered that TRIB2 can regulate RFWD2 by interaction. The role of RFWD2 in cancer is related to the targeting of its substrates, such as p-IκB-α, for ubiquitination and degradation (22). Although IκBα is a substrate of E3 Ub ligases and TRIB1 knockdown inhibits the phosphorylation and degradation of IκBα (48), the relationship and regulation between TRIB2 and IκBα are unclear. All these results inspired us to study the effect of TRIB2 on IκB-α. We observed that TRIB2 overexpression increased the RFWD2 levels in cancer cells, indicating that the regulating action of TRIB2 may be related to its interaction with and effect on RFWD2. To further explore its role in TRIB2-promoted tumorigenesis in cancer, we used siRNA to knock down RFWD2. Our results demonstrated that RFWD2 knockdown inhibited the proliferation of A549 and Hela cells and promoted the apoptosis and migration of cells. We recorded that RFWD2 knockdown attenuated TRIB2-promoted colony formation. These data further suggest that RFWD2 assists TRIB2 in promoting cancer progression, and cooperates with TRIB2 to participate in the proteasome-mediated degradation of the RFWD2 substrate p-IκB-α.

Although the present study elucidated a potential mechanism through which TRIB2 interacts with E3 Ub ligases (RFWD2) and further regulates the ubiquitination and degradation of p-IκB-α *via* the TRIB2-IκB-α-RFWD2 ternary complex, several issues associated with this process remain unclear. Prior studies have reported that TrCP and RFWD2 may bind the C-terminus of TRIB2. TRIB2, RFWD2, and TrCP are involved in the degradation of β-catenin. Therefore, the involvement of TrCP in TRIB2 promoted IκB-α ubiquitination and degradation, and the competitive or synergistic nature of the role played by RFWD2 and TrCP in regulating IκBα degradation may require further study. Moreover, IκB-α is an important factor in NF-kB signaling pathway and the RFWD2-TRIB2 complex can regulate IκBα degradation, the effect of RFWD2 or TRIB2 on NF-kB signaling pathway also needs further study.

DATA AVAILABILITY STATEMENT

The original contributions presented in the study are included in the article/**Supplementary Material**. Further inquiries can be directed to the corresponding authors.

ETHICS STATEMENT

The studies involving human participants were reviewed and approved by the Medical Ethics of committee of Binzhou Medical University. The patients/participants provided their written informed consent to participate in this study. The animal study was reviewed and approved by the Ethics of Animal Experiments of Binzhou Medical University.

AUTHOR CONTRIBUTIONS

SX and Y-JL conceived the study and participated in the study design. SX, PW, RH, JH, YL, DL, Y-ML, RW, and SZ designed and performed most assays, analyzed data, and wrote the manuscript. SX, PW, RH, and Y-JL analyzed RNA expression. Y-JL, Y-ML, and SZ provided technical support. All authors contributed to the article and approved the submitted version.

FUNDING

The present study was supported by the National Natural Science Foundation of China (No. 81772281, 31371321, 81502536),

Shandong Science and Technology Committee (No. ZR2019MH022, ZR2020KH015), Education Department of Shandong Province (2019KJK014), Yantai Science and Technology Committee (2018XSCC051), and Shandong Province Taishan Scholar Project (ts201712067).

SUPPLEMENTARY MATERIAL

The Supplementary Material for this article can be found online at: https://www.frontiersin.org/articles/10.3389/fonc.2021.733175/full#supplementary-material.

REFERENCES

1. Narayanan S, Cai CY, Assaraf YG, Guo HQ, Cui Q, Wei L, et al. Targeting the Ubiquitin-Proteasome Pathway to Overcome Anti-Cancer Drug Resistance. *Drug Resist Update* (2020) 48:100663. doi: 10.1016/j.drup.2019.100663
2. Hershko A, Ciechanover A, Varshavsky A. Basic Medical Research Award. The Ubiquitin System. *Nat Med* (2000) 6:1073–81. doi: 10.1038/80384
3. Li W, Ye Y. Polyubiquitin Chains: Functions, Structures, and Mechanisms. *Cell Mol Life Sci* (2008) 65:2397–406. doi: 10.1007/s00018-008-8090-6
4. Hershko A, Heller H, Elias S, Ciechanover A. Components of Ubiquitin-Protein Ligase System. Resolution, Affinity Purification, and Role in Protein Breakdown. *J Biol Chem* (1983) 258:8206–14. doi: 10.1016/S0021-9258(20)82050-X
5. Christianson JC, Ye Y. Cleaning Up in the Endoplasmic Reticulum: Ubiquitin in Charge. *Nat Struct Mol Biol* (2014) 21:325–35. doi: 10.1038/nsmb.2793
6. Park J, Cho J, Song EJ. Ubiquitin-Proteasome System (UPS) as a Target for Anticancer Treatment. *Arch Pharm Res* (2020) 43:1144–61. doi: 10.1007/s12272-020-01281-8
7. Gatti V, Bernassola F, Talora C, Melino G, Peschiaroli A. The Impact of the Ubiquitin System in the Pathogenesis of Squamous Cell Carcinomas. *Cancers (Basel)* (2020) 12:1595. doi: 10.3390/cancers12061595
8. Senft D, Qi J, Ronai ZA. Ubiquitin Ligases in Oncogenic Transformation and Cancer Therapy. *Nat Rev Cancer* (2018) 18:69–88. doi: 10.1038/nrc.2017.105
9. Li W, Bengtson MH, Ulbrich A, Matsuda A, Reddy VA, Orth A, et al. Genome-Wide and Functional Annotation of Human E3 Ubiquitin Ligases Identifies MULAN, a Mitochondrial E3 That Regulates the Organelle's Dynamics and Signaling. *PloS One* (2008) 3:e1487. doi: 10.1371/journal.pone.0001487
10. Bianchi E, Denti S, Catena R, Rossetti G, Polo S, Gasparian S, et al. Characterization of Human Constitutive Photomorphogenesis Protein 1, A RING Finger Ubiquitin Ligase That Interacts With Jun Transcription Factors and Modulates Their Transcriptional Activity. *J Biol Chem* (2003) 278:19682–90. doi: 10.1074/jbc.M212681200
11. Dornan D, Wertz I, Shimizu H, Arnott D, Frantz GD, Dowd P, et al. The Ubiquitin Ligase COP1 Is a Critical Negative Regulator of P53. *Nature* (2004) 429:86–92. doi: 10.1038/nature02514
12. Song Y, Liu Y, Pan S, Xie S, Wang ZW, Zhu X. Role of the COP1 Protein in Cancer Development and Therapy. *Semin Cancer Biol* (2020) 67:43–52. doi: 10.1016/j.semcancer.2020.02.001
13. Lee YH, Andersen JB, Song HT, Judge AD, Seo D, Ishikawa T, et al. Definition of Ubiquitination Modulator COP1 as a Novel Therapeutic Target in Human Hepatocellular Carcinoma. *Cancer Res* (2010) 70:8264–9. doi: 10.1158/0008-5472.CAN-10-0749
14. Fu C, Gong Y, Shi X, Shi H, Wan Y, Wu Q, et al. Expression and Regulation of COP1 in Chronic Lymphocytic Leukemia Cells for Promotion of Cell Proliferation and Tumorigenicity. *Oncol Rep* (2016) 35:1493–500. doi: 10.3892/or.2015.4526
15. Eyers PA, Keeshan K, Kannan N. Tribbles in the 21st Century: The Evolving Roles of Tribbles Pseudokinases in Biology and Disease. *Trends Cell Biol* (2017) 27:284–98. doi: 10.1016/j.tcb.2016.11.002
16. Dedhia PH, Keeshan K, Uljon S, Xu L, Vega ME, Shestova O, et al. Differential Ability of Tribbles Family Members to Promote Degradation of C/EBPalpha and Induce Acute Myelogenous Leukemia. *Blood* (2010) 116:1321–8. doi: 10.1182/blood-2009-07-229450
17. Uljon S, Xu X, Durzynska I, Stein S, Adelmant G, Marto JA, et al. Structural Basis for Substrate Selectivity of the E3 Ligase Cop1. *Structure* (2016) 24:687–96. doi: 10.1016/j.str.2016.03.002
18. Yoshida A, Kato JY, Nakamae I, Yoneda-Kato N. COP1 Targets C/EBPalpha for Degradation and Induces Acute Myeloid Leukemia *via* Trib1. *Blood* (2013) 122:1750–60. doi: 10.1182/blood-2012-12-476101
19. Keeshan K, Bailis W, Dedhia PH, Vega ME, Shestova O, Xu L, et al. Transformation by Tribbles Homolog 2 (Trib2) Requires Both the Trib2 Kinase Domain and COP1 Binding. *Blood* (2010) 116:4948–57. doi: 10.1182/blood-2009-10-247361
20. Zhang YX, Yan YF, Liu YM, Li YJ, Zhang HH, Pang M, et al. Smad3-Related miRNAs Regulated Oncogenic TRIB2 Promoter Activity to Effectively Suppress Lung Adenocarcinoma Growth. *Cell Death Dis* (2016) 7:e2528. doi: 10.1038/cddis.2016.432
21. Xu S, Tong M, Huang J, Zhang Y, Qiao Y, Weng W, et al. TRIB2 Inhibits Wnt/beta-Catenin/TCF4 Signaling Through Its Associated Ubiquitin E3 Ligases, Beta-TrCP, COP1 and Smurf1, in Liver Cancer Cells. *FEBS Lett* (2014) 588:4334–41. doi: 10.1016/j.febslet.2014.09.042
22. Ma L, Pan Q, Sun F, Yu Y, Wang J. Cluster of Differentiation 166 (CD166) Regulates Cluster of Differentiation (CD44) *via* NF-KappaB in Liver Cancer Cell Line Bel-7402. *Biochem Biophys Res Commun* (2014) 451:334–8. doi: 10.1016/j.bbrc.2014.07.128
23. Liang KL, Paredes R, Carmody R, Eyers PA, Meyer S, Mccarthy TV, et al. Human TRIB2 Oscillates During the Cell Cycle and Promotes Ubiquitination and Degradation of CDC25C. *Int J Mol Sci* (2016) 17(9):1378. doi: 10.3390/ijms17091378
24. Link W. Tribbles Breaking Bad: TRIB2 Suppresses FOXO and Acts as an Oncogenic Protein in Melanoma. *Biochem Soc Trans* (2015) 43:1085–8. doi: 10.1042/BST20150102
25. Wang J, Zhang Y, Weng W, Qiao Y, Ma L, Xiao W, et al. Impaired Phosphorylation and Ubiquitination by P70 S6 Kinase (P70s6k) and Smad Ubiquitination Regulatory Factor 1 (Smurf1) Promote Tribbles Homolog 2 (TRIB2) Stability and Carcinogenic Property in Liver Cancer. *J Biol Chem* (2013) 288:33667–81. doi: 10.1074/jbc.M113.503292
26. Hou Z, Guo K, Sun X, Hu F, Chen Q, Luo X, et al. TRIB2 Functions as Novel Oncogene in Colorectal Cancer by Blocking Cellular Senescence Through AP4/p21 Signaling. *Mol Cancer* (2018) 17:172. doi: 10.1186/s12943-018-0922-x
27. Ma X, Zhou X, Qu H, Ma Y, Yue Z, Shang W, et al. TRIB2 Knockdown as a Regulator of Chemotherapy Resistance and Proliferation *via* the ERK/STAT3 Signaling Pathway in Human Chronic Myelogenous Leukemia K562/ADM Cells. *Oncol Rep* (2018) 39:1910–8. doi: 10.3892/or.2018.6249
28. Wang J, Park JS, Wei Y, Rajurkar M, Cotton JL, Fan Q, et al. TRIB2 Acts Downstream of Wnt/TCF in Liver Cancer Cells to Regulate YAP and C/EBPalpha Function. *Mol Cell* (2013) 51:211–25. doi: 10.1016/j.molcel.2013.05.013
29. Hill R, Madureira PA, Ferreira B, Baptista I, Machado S, Colaco L, et al. TRIB2 Confers Resistance to Anti-Cancer Therapy by Activating the Serine/Threonine Protein Kinase AKT. *Nat Commun* (2017) 8:14687. doi: 10.1038/ncomms14687
30. Wang PY, Sun YX, Zhang S, Pang M, Zhang HH, Gao SY, et al. Let-7c Inhibits A549 Cell Proliferation Through Oncogenic TRIB2 Related Factors. *FEBS Lett* (2013) 587:2675–81. doi: 10.1016/j.febslet.2013.07.004
31. Zhang C, Chi YL, Wang PY, Wang YQ, Zhang YX, Deng J, et al. miR-511 and miR-1297 Inhibit Human Lung Adenocarcinoma Cell Proliferation by Targeting Oncogene TRIB2. *PloS One* (2012) 7:e46090. doi: 10.1371/journal.pone.0046090
32. Deng XW, Caspar T, Quail PH. Cop1: A Regulatory Locus Involved in Light-Controlled Development and Gene Expression in Arabidopsis. *Genes Dev* (1991) 5:1172–82. doi: 10.1101/gad.5.7.1172
33. Wang H, Kang D, Deng XW, Wei N. Evidence for Functional Conservation of a Mammalian Homologue of the Light-Responsive Plant Protein COP1. *Curr Biol* (1999) 9:711–4. doi: 10.1016/s0960-9822(99)80314-5
34. Yi C, Wang H, Wei N, Deng XW. An Initial Biochemical and Cell Biological Characterization of the Mammalian Homologue of a Central Plant Developmental Switch, COP1. *BMC Cell Biol* (2002) 3:30. doi: 10.1186/1471-2121-3-30

35. Wertz IE, O'rourke KM, Zhang Z, Dornan D, Arnott D, Deshaies RJ, et al. Human De-Etiolated-1 Regulates C-Jun by Assembling a CUL4A Ubiquitin Ligase. *Science* (2004) 303:1371–4. doi: 10.1126/science.1093549
36. Yi C, Deng XW. COP1 - From Plant Photomorphogenesis to Mammalian Tumorigenesis. *Trends Cell Biol* (2005) 15:618–25. doi: 10.1016/j.tcb.2005.09.007
37. Holm M, Deng XW. Structural Organization and Interactions of COP1, A Light-Regulated Developmental Switch. *Plant Mol Biol* (1999) 41:151–8. doi: 10.1023/a:1006324115086
38. Marine JC. Spotlight on the Role of COP1 in Tumorigenesis. *Nat Rev Cancer* (2012) 12:455–64. doi: 10.1038/nrc3271
39. Yoneda-Kato N, Tomoda K, Umehara M, Arata Y, Kato JY. Myeloid Leukemia Factor 1 Regulates P53 by Suppressing COP1 *via* COP9 Signalosome Subunit 3. *EMBO J* (2005) 24:1739–49. doi: 10.1038/sj.emboj.7600656
40. Su CH, Zhao R, Zhang F, Qu C, Chen B, Feng YH, et al. 14-3-3sigma Exerts Tumor-Suppressor Activity Mediated by Regulation of COP1 Stability. *Cancer Res* (2011) 71:884–94. doi: 10.1158/0008-5472.CAN-10-2518
41. Migliorini D, Bogaerts S, Defever D, Vyas R, Denecker G, Radaelli E, et al. Cop1 Constitutively Regulates C-Jun Protein Stability and Functions as a Tumor Suppressor in Mice. *J Clin Invest* (2011) 121:1329–43. doi: 10.1172/JCI45784
42. Kato S, Ding J, Pisck E, Jhala US and Du K. COP1 Functions as a FoxO1 Ubiquitin E3 Ligase to Regulate FoxO1-Mediated Gene Expression. *J Biol Chem* (2008) 283:35464–73. doi: 10.1074/jbc.M801011200
43. Dentin R, Liu Y, Koo SH, Hedrick S, Vargas T, Heredia J, et al. Insulin Modulates Gluconeogenesis by Inhibition of the Coactivator TORC2. *Nature* (2007) 449:366–9. doi: 10.1038/nature06128
44. Ouyang M, Wang H, Ma J, Lu W, Li J, Yao C, et al. COP1, the Negative Regulator of ETV1, Influences Prognosis in Triple-Negative Breast Cancer. *BMC Cancer* (2015) 15:132. doi: 10.1186/s12885-015-1151-y
45. Rishi L, Hannon M, Salome M, Hasemann M, Frank AK, Campos J, et al. Regulation of Trib2 by an E2F1-C/EBPalpha Feedback Loop in AML Cell Proliferation. *Blood* (2014) 123:2389–400. doi: 10.1182/blood-2013-07-511683
46. Qiao Y, Zhang Y, Wang J. Ubiquitin E3 Ligase SCF(beta-TRCP) Regulates TRIB2 Stability in Liver Cancer Cells. *Biochem Biophys Res Commun* (2013) 441:555–9. doi: 10.1016/j.bbrc.2013.10.123
47. Salome M, Campos J, Keeshan K. TRIB2 and the Ubiquitin Proteasome System in Cancer. *Biochem Soc Trans* (2015) 43:1089–94. doi: 10.1042/BST20150103
48. Gendelman R, Xing H, Mirzoeva OK, Sarde P, Curtis C, Feiler HS, et al. Bayesian Network Inference Modeling Identifies TRIB1 as a Novel Regulator of Cell-Cycle Progression and Survival in Cancer Cells. *Cancer Res* (2017) 77:1575–85. doi: 10.1158/0008-5472.CAN-16-0512

Conflict of Interest: The authors declare that the research was conducted in the absence of any commercial or financial relationships that could be construed as a potential conflict of interest.

Publisher's Note: All claims expressed in this article are solely those of the authors and do not necessarily represent those of their affiliated organizations, or those of the publisher, the editors and the reviewers. Any product that may be evaluated in this article, or claim that may be made by its manufacturer, is not guaranteed or endorsed by the publisher.

Copyright © 2021 Hao, Hu, Liu, Liang, Li, Wang, Zhang, Wang, Li and Xie. This is an open-access article distributed under the terms of the Creative Commons Attribution License (CC BY). The use, distribution or reproduction in other forums is permitted, provided the original author(s) and the copyright owner(s) are credited and that the original publication in this journal is cited, in accordance with accepted academic practice. No use, distribution or reproduction is permitted which does not comply with these terms.

frontiers in Cell and Developmental Biology

ORIGINAL RESEARCH
published: 28 September 2021
doi: 10.3389/fcell.2021.736980

NR2F1-AS1 Promotes Pancreatic Ductal Adenocarcinoma Progression Through Competing Endogenous RNA Regulatory Network Constructed by Sponging miRNA-146a-5p/miRNA-877-5p

Dong Luo, Yunfei Liu, Zhiqiang Li, Hongwei Zhu† and Xiao Yu*†*

Department of Hepatopancreatobiliary Surgery, Third Xiangya Hospital, Central South University, Changsha, China

OPEN ACCESS

Edited by:
Ira Ida Skvortsova, Innsbruck Medical University, Austria

Reviewed by:
Rongjun Cui, Mudanjiang Medical University, China
Qian Guo, Shengjing Hospital of China Medical University, China

***Correspondence:**
Xiao Yu
yuxiaoyx4@126.com
Hongwei Zhu
zhuhongweizhw1987@126.com

†These authors share senior authorship

Specialty section:
This article was submitted to Molecular and Cellular Oncology, a section of the journal Frontiers in Cell and Developmental Biology

Received: *06 July 2021*
Accepted: *02 September 2021*
Published: *28 September 2021*

Citation:
Luo D, Liu Y, Li Z, Zhu H and Yu X (2021) NR2F1-AS1 Promotes Pancreatic Ductal Adenocarcinoma Progression Through Competing Endogenous RNA Regulatory Network Constructed by Sponging miRNA-146a-5p/miRNA-877-5p. Front. Cell Dev. Biol. 9:736980. doi: 10.3389/fcell.2021.736980

The role of NR2F1-AS1 in pancreatic ductal adenocarcinoma (PDAC) remains unknown. Therefore, we aimed to investigate the biological mechanism of NR2F1-AS1 in PDAC. The expression of NR2F1-AS1 was measured by using microarray data and real-time PCR. The effects of NR2F1-AS1 knockdown on proliferation, cell cycle progression, invasion *in vitro* and tumorigenesis *in vivo* were investigated. The mechanism of competitive endogenous RNAs was determined from bioinformatics analyses and validated by a dual-luciferase reporter gene assay. Potential target mRNAs from TargetScan 7.2 were selected for subsequent bioinformatics analysis. Key target mRNAs were further identified by screening hub genes and coexpressed protein-coding genes (CEGs) of NR2F1-AS1. NR2F1-AS1 was highly expressed in PDAC, and the overexpression of NR2F1-AS1 was associated with overall survival and disease-free survival. The knockdown of NR2F1-AS1 impaired PDAC cell proliferation, migration, invasion and tumorigenesis. NR2F1-AS1 competitively sponged miR-146a-5p and miR-877-5p, and low expression of the two miRNAs was associated with a poor prognosis. An integrative expression and survival analysis of the hub genes and CEGs demonstrated that the NR2F1-AS1–miR-146a-5p/miR-877-5p–GALNT10/ZNF532/SLC39A1/PGK1/LCO3A1/NRP2/LPCAT2/PSMA4 and CLTC ceRNA networks were linked to the prognosis of PDAC. In conclusion, NR2F1-AS1 overexpression was significantly associated with poor prognosis. NR2F1-AS1 functions as an endogenous RNA to construct a novel ceRNA network by competitively binding to miR-146a-5p/miR-877-5p, which may contribute to PDAC pathogenesis and could represent a promising diagnostic biomarker or potential novel therapeutic target in PDAC.

Keywords: NR2F1-AS1, miR-146a-5p/miR-877-5p, pancreatic ductal adenocarcinoma, ceRNA, bioinformatics analysis

INTRODUCTION

Pancreatic ductal adenocarcinoma (PDAC) remains a highly fatal disease with a 5-year survival rate of 10% (Siegel et al., 2021). PDAC accounts for almost as many deaths (466,000) as cases (496,000) because of its poor prognosis, and it is the seventh leading cause of cancer death in both sexes in 2020 (Sung et al., 2021) and projected to become the second leading cause of cancer-related death by 2030 (Rahib et al., 2014).

Pancreatic ductal adenocarcinoma is characterized by late diagnosis, metastasis and acquired resistance to chemotherapeutic agents in the clinic (Zheng et al., 2015; Sakamoto et al., 2020). Surgical resection with adjuvant systemic chemotherapy currently provides the only chance of long-term survival. However, only10–20% of PDAC patients are diagnosed with localized surgically resectable disease (Strobel et al., 2019). The prognosis for PDAC is still poor despite diagnostic progress and new chemotherapeutic regimens. Therefore, research on the genetic alterations and underlying molecular mechanism of PDAC is still urgently required to find new treatment strategies.

Endogenous genetic alterations, including KRAS oncogenes and mutations or losses of CDKN2A, TP53 and SMAD4, have been well characterized (Biankin et al., 2012; Rishi et al., 2015; Mizrahi et al., 2020). In addition, the critical role of dysregulation of epigenetic modifiers, such as non-coding RNAs, in the development and progression of many human cancer types, including PDAC, is also increasingly emphasized.

Emerging evidence has shown that long non-coding RNAs (lncRNAs) are major regulators in human cancers, including PDAC. LncRNAs are a class of measurably conserved and polyadenylated ncRNAs that are longer than 200 nucleotides, and they do not encode proteins (Lee, 2012; Slack and Chinnaiyan, 2019; Yao et al., 2019). LncRNAs are widely present in organisms and play an important role in various physiological and pathological processes at the level of epigenetic modification, transcription and posttranscriptional regulation.

Several groups have shown that dysregulated expression of lncRNAs is correlated with the initiation, progression, invasion, metastasis, angiogenesis, and drug resistance of PDAC (Lin et al., 2020; Pandya et al., 2020; Zhou et al., 2020). The functions and regulatory mechanisms of lncRNAs in PDAC include potential oncogenes and suppressors (Gong and Jiang, 2020). For lncRNAs as potential oncogenes, a negative correlation was observed in PDAC patients with higher MALAT-1 expression levels and disease-free survival (Liu et al., 2014). HOTAIR was a highly upregulated lncRNA and functioned as an oncogene in PDAC. Interestingly, the overexpression of HOTAIR was reported to have a positive correlation with increased cell growth, survival, migration and invasion in pancreatic carcinoma in a PRC2-dependent and PRC2-independent fashion (Kim et al., 2013; Li et al., 2017). In the context of PDAC, the HOTTIP lncRNA seemed to regulate HOX genes (HOXA9 and HOXA10), and the HOXA9 gene has been shown to promote cancer stem cell proliferation through the Wnt/β-catenin signaling pathway (Fu et al., 2017). On the other hand, overexpression of GAS5 inhibited PDAC cell proliferation, migration and gemcitabine resistance through miR-221/suppressor of cytokine signaling 3 (*SOCS3*)-mediated epithelial-mesenchymal transition (EMT; Liu et al., 2018a). Hu et al. (2016) found that MEG3 inhibits proliferation, induces apoptosis *via* p53 activation and is upregulated along with p53 by fenofibrate to reduce the proliferation of PDAC cells. For the regulatory mechanism, it has been reported that lncRNAs can act as competing endogenous RNAs (ceRNAs) or "RNA sponges," and they interact with microRNAs in a manner that can sequester these molecules and reduce their regulatory effect on target mRNAs (Cesana et al., 2011; Tay et al., 2014). For example, lncRNA THAP9-AS1 promoted PDAC and led to a poor clinical outcome by sponging miR-484 and interacting with YAP (Li et al., 2020).

The annotated potential lncRNA NR2F1-AS1 (NR2F1 antisense RNA 1) was previously reported to be expressed at low levels in certain human normal tissues, especially in the pancreas (Fagerberg et al., 2014). We found that NR2F1-AS1 was overexpressed in PDAC based on a bioinformatics analysis of publicly available datasets (e.g., Gene Expression Omnibus, GEO). NR2F1-AS1 has been reported to promote the growth of hepatocellular carcinoma (Huang H. et al., 2018), thyroid carcinoma (Yang et al., 2020), osteosarcoma (Li et al., 2019) and breast cancer (Sanchez et al., 2020). However, to the best of our knowledge, the biological role and clinical significance of NR2F1-AS1 and the mechanisms behind these events in PDAC have not been revealed.

The present study aimed to determine NR2F1-AS1 expression in PDAC, investigate the roles of NR2F1-AS1 in PDAC cells and elucidate the potential mechanisms of the ceRNA regulatory network underlying the effect of NR2F-AS1 on PDAC progression by combining experimental and bioinformatics analyses.

MATERIALS AND METHODS

Cell Lines and Culture

The PDAC cell lines PANC-1, CFPAC-1, Capan-2, SW1990, BXPC-3 and an immortalized human pancreatic ductal epithelial cell line (HPDE6) were kindly provided by Dr. Fang He and Hongwei Zhu (Chinese University of Hong Kong, Hong Kong, SAR China). HEK-293Ts were purchased from GENE (Shanghai, China). Cells were cultured in RPMI-1640 or DMEM (Gibco, United States) supplemented with 10% fetal bovine serum. HPDE6 cells were cultured in Keratinocyte-SFM (K-SFM) medium supplemented with Bovine Pituitary Extract (BPF) and Human Recombinant (EGF) [500 ml K-SFM)] medium contain 25 mg BPF and 2.5 μg EGF). Other cells were cultured in DMEM, IMDM, or RPMI 1640 (Gibco, United States) with 10% fetal bovine serum (FBS, Gibco). All cells were cultured at 37°C under 5% CO_2 in a humidified chamber.

Quantitative Real-Time PCR

Total RNA was extracted from the PDAC cells using TRIzol reagent (Invitrogen, United States). The RNA concentration and purity were measured at 260/280 nm using a NanoDrop ND-2000 spectrophotometer (Thermo Fisher Scientific,

United States). Next, according to the manufacturer's instructions, cDNA was synthesized with a reverse transcription kit (Toyobo, Osaka, Japan). qRT-PCR was performed on a LightCycler 480 (Roche, Switzerland) using a standard protocol from the SYBR Green PCR Kit (Toyobo, Japan). The qRT-PCR data were normalized to the expression of GAPDH. Primers used for qRT-PCR assays are listed in **Supplementary Table 1**. For the detection of miRNA expression, reverse transcription was performed and microRNAs were detected with Ploy-A primers purchased from GeneCopoeia (Guangzhou, China). U6 was used as the endogenous control. Relative fold changes were calculated using the comparative delta-delta CT method (2-ΔΔCt). All PCR assays were repeated three times.

Cell Transfection and Virus Infection

To establish stable transfectants *via* knockdown, shRNA sequences targeting NR2F1-AS1 (target sequence for sh-1#: 5′-GTAGATGAAACTCAAGAGA-3′; sh-2#: 5′-CCACAATATTAACCAGGAT-3′) were designed and inserted in lentiviral plasmids purchased from GENE (Shanghai, China). PANC-1 cells and CFPAC-1 cells were seeded in 6-well plates and infected with lentiviral particles expressing NR2F1-AS1 shRNA following the manufacturer's instructions to construct stably transfected cell lines. Puromycin (2 μg/ml) was added to the culture medium 72 h after infection and maintained for at least 1 week to select stably transfected cell lines (PANC-1/CFPAC-1-sh NR2F1-AS1 or PANC-1/CFPAC-1-sh-Control).

Cell Counting Kit-8 Assay

Cell viability was tested using a Cell Counting Kit-8 (CCK-8, Beyotime, Shanghai, China) according to the manufacturer's instructions and the transfected cells were grown in 96-well plates. Cellular viability was assessed every 24 h (for 96 h) through the measurement of the absorbance at a wavelength of 450 nm by a microplate reader (GEN5, United States).

Colony Formation Assay

Cells were plated onto 6-well plates (1×10^3 cells/well). The cells were cultured for 14 days and then stained with 0.1% crystal violet, and the number of colonies was counted using ImageJ.

Wound-Healing Scratch Assay

PANC-1 and CFPAC-1 cells were plated in 6-well plates and cultured in medium containing 10% FBS. After 24 h, the cells grew to almost total confluence. A scratch was created on the monolayer of cells with a 10 μl pipette tip. Subsequently, phosphate-buffered saline was used to wash the cells. Images of the cells that had migrated into the wound were obtained at 0 and 48 h using a microscope (OLYMPUS-IX71, Japan).

Transwell Invasion and Migration Assay

Approximately 1×10^5 stably transfected PDAC cells (PANC-1 and CFPAC-1) were suspended in serum-free medium and seeded in either chamber (Corning Costar, United States). Chambers not coated with Matrigel were used for migration assays, and chambers coated with Matrigel with 8-μm pores (Corning Costar, United States) were used for invasion assays. For both assays, medium containing 10% FBS was added to the lower chamber as a chemoattractant. After 24 h of incubation, the migrated and invaded cells on the lower membrane surface were fixed with formaldehyde for approximately 20 min. Optical microscopy was applied for cell counting and then stained with 1% purple crystal solution. Five random fields were counted per chamber by using an inverted microscope (OLYMPUS-IX71, Japan). Each experiment was repeated three times.

Apoptosis Analysis and Cell Cycle Analysis

Cell apoptosis status was determined by following the protocol of the Annexin V-FITC/PI-cell apoptosis Detection Kit (United States). Cells were trypsinized and resuspended in binding buffer containing Annexin V-FITC (United States) and propidium iodide (PI, BD Biosciences) for 20 min in the dark. Stained cells were analyzed using a flow cytometer. For analysis of cell cycle distribution, the cells were fixed with ice-cold 75% ethanol and incubated with PI (50 μg/mL) in the presence of RNase A (Sigma-Aldrich) for 30 min. The DNA content was analyzed by flow cytometry.

Animal Studies

BALB/C mice (male, 4–6 weeks old) were purchased from the Department of Animals and approved by the animal Ethics Committee of the Third Xiangya Hospital, Central South University. Animals were fed under sterile specific pathogen-free conditions. Each mouse was then injected with 100 μL of stably transfected PDAC (PANC-1 and CFPAC-1) cell suspension (2×10^6cells). Tumor volumes were monitored weekly. After 3 weeks, all mice were sacrificed using cervical dislocation, and tumor weight and volume were measured.

Luciferase Report Assay

293T cells were seeded onto 24-well plates and transfected with the reporter (NR2F1-AS1-MUT plasmid or NR2F1-AS1-WT) constructs together with the miR-146a-5p/miR-877-5p plasmid or empty vector using X-tremegene HP. The pRL-TK plasmid (Promega, Fitchburg, MA, United States) expressing Renilla luciferase was cotransfected to control for transfection efficiency. Forty-eight hours after transfection luciferase activities were measured using the Dual-Luciferase Reporter Assay System (Promega) according to the manufacturer's instructions, and the relative luciferase activity was determined after normalization against Renilla luciferase activity.

Fluorescence *in situ* Hybridization

Cy3-labeled lncRNA NR2F1-AS1 probes were purchased from RuiBo Biomedical Center. PANC-1 cells and CFPAC cells were fixed in 4% formaldehyde and permeabilized with 0.5% Triton

X-100. The cells were then hybridized with Cy3-probes. Nuclei were stained with DAPI. Slides were hybridized with probes overnight at 37°C and washed with 4× saline-sodium citrate (4× SSC), 2× SSC and 1× SSC at 42°C for 5 min. Glass slides were mounted using fluorescence mounting medium. Cells were observed and images were acquired using a fluorescence microscope (Olympus).

Bioinformatics Analysis

Microarray data of NR2F1-AS1 expression were obtained from the GEO dataset (GSE15471) (downloaded at).[1] The potential microRNA binding sites with NR2F1-AS 1 were predicted by the hTFtarget online[2] (Zhang Q. et al., 2020). MicroRNA-mRNA binding sites were obtained from TargetScan 7.2 (Agarwal et al., 2015). Database for Annotation, Visualization and Integrated Discovery (DAVID) 6.8 (Huang et al., 2009) was introduced to conduct Gene Ontology (GO) functional annotations and Kyoto Encyclopedia of Genes and Genomes (KEGG) pathway enrichment analyses for potential target mRNA genes. Then, the top 10 enriched GO terms and KEGG pathways were displayed using GraphPad Prism 8. We surveyed cellular signaling pathways involving miRNAs utilizing the miRNACancerMAP database (Tong et al., 2018). The PPI interaction networks between the potential target mRNA genes were constructed by the Search Tool for the Retrieval of Interacting Genes (STRING) database[3] (Szklarczyk et al., 2019). First, potential target mRNA genes were entered into the database. Then, high-resolution bitmaps were displayed and downloaded from the webpage. Only interactors with a combined confidence score $> = 0.4$ were shown in the bitmap. The hub genes in the PPI networks were identified using CytoHubba, a plugin in Cytoscape software (Version 3.7.2). According to the node degree, the top 10 hub genes were displayed in Cytoscape. Meanwhile, CEGs of NR2F1-AS1 were determined using a practical and user-friendly web interface called Co-LncRNA, which investigates the lncRNA combinatorial effects in GO annotations and KEGG pathways based on RNA-Seq data. A functional enrichment analysis of CEGs was performed using Metascape Analysis[4] (Zhou et al., 2019). A gene expression profiling interactive analysis (GEPIA)[5] was performed to analyze the expression level of NR2F1-AS1 (lncRNA) and key mRNA in PDAC from the pan-cancer analysis (Tang et al., 2017). We obtained a list of upregulated expressed genes in PDAC from a (GEPIA, see text footnote 5). The survival analysis of miRNA expression was based on OncomiR[6] (Wong et al., 2018). The prognostic values of lncRNAs and key target genes in PDAC were analyzed using the Kaplan-Meier plotter database (Nagy et al., 2018).

[1] http://www.ncbi.nlm.nih.gov/geo/

[2] http://bioinfo.life.hust.edu.cn/hTFtarget#!/

[3] https://string-db.org/cgi/input.pl?sessionId=LUwAMnwLiSDE&input_page_show_search=on

[4] https://metascape.org/gp/index.html#/main/step1

[5] http://gepia.cancer-pku.cn/

[6] http://www.oncomir.org/

Statistical Analysis

All data are presented as the mean value ± standard deviation (Mean ± SD). The *t*-test and the χ^2 test were used for comparisons between groups. Statistical analyses were performed using GraphPad Prism 8. Differences were deemed statistically significant at $p < 0.05$.

RESULTS

NR2F1-AS1 Is Upregulated in Pancreatic Ductal Adenocarcinoma and Correlated With Poor Prognosis

To identify eligible lncRNAs in PDAC, we queried public online datasets. We downloaded a total of 4711 lncRNAs (**Supplementary Table 2**), with valid names obtained from the HGNC database of human gene names when this work was initiated, they were analyzed by GEPIA. We were particularly interested in NR2F1-AS1 because its relative expression was the highest among the PDAC tumor samples relative to adjacent normal tissues in the pan-cancer analysis (**Supplementary Figure 1**), and this upregulation was confirmed (**Figure 1A**). A publicly accessible microarray dataset (GEO:GSE15471) from PDAC patients was analyzed, and the result was consistent with data from the GEPIA. We found that NR2F1-AS1 was significantly increased in the PDAC samples relative to the normal samples (**Figures 1B,C**). Moreover, NR2F1-AS1 expression in PDAC cell lines was also increased compared with HPDE6 based on RT-qPCR, especially in the PANC-1 and CFPAC-1 cell lines (**Figure 1D**). To clarify the prognostic value of NR2F1-AS1 among PDAC patients, the relationship between its expression and survival time was investigated by Kaplan–Meier plotter. This result indicated that PDAC patients with higher NR2F1-AS1 expression had shorter OS ($p = 0.024$) and RFS ($p = 0.005$) (**Figures 1E,F**). Collectively, these findings indicated that upregulated expression of NR2F1-AS1 might be closely associated with poor outcomes of PDAC. Therefore, we focused on NR2F1-AS1 for further characterization.

Knockdown of NR2F1-AS1 Suppresses Pancreatic Ductal Adenocarcinoma Growth *in vitro* and *in vivo*

To determine the biological function of NR2F1-AS1 in PDAC, loss-of function approaches were employed. PANC-1 and CFPAC-1 lines were selected to further investigate its effects in PDAC as described above (**Figure 1E**). First, NR2F1-AS1 was knocked down using shRNAs. Then, stable NR2F1-AS1 knockdown in the PANC-1 and CFPAC-1 lines expressing sh-1# or sh-2# (shRNAs) was established. NR2F1-AS1 expression was suppressed by shRNA transfection in the PANC-1 and CFPAC-1 cell lines (**Figure 2A**). Loss of NR2F1-AS1 significantly suppressed the proliferation of PANC-1 and CFPAC-1 cells (**Figures 2B,C**), as determined by CCK-8 assay. The colony-forming assay also showed that NR2F1-AS1 knockdown significantly inhibited the colony-forming capacity of PDAC

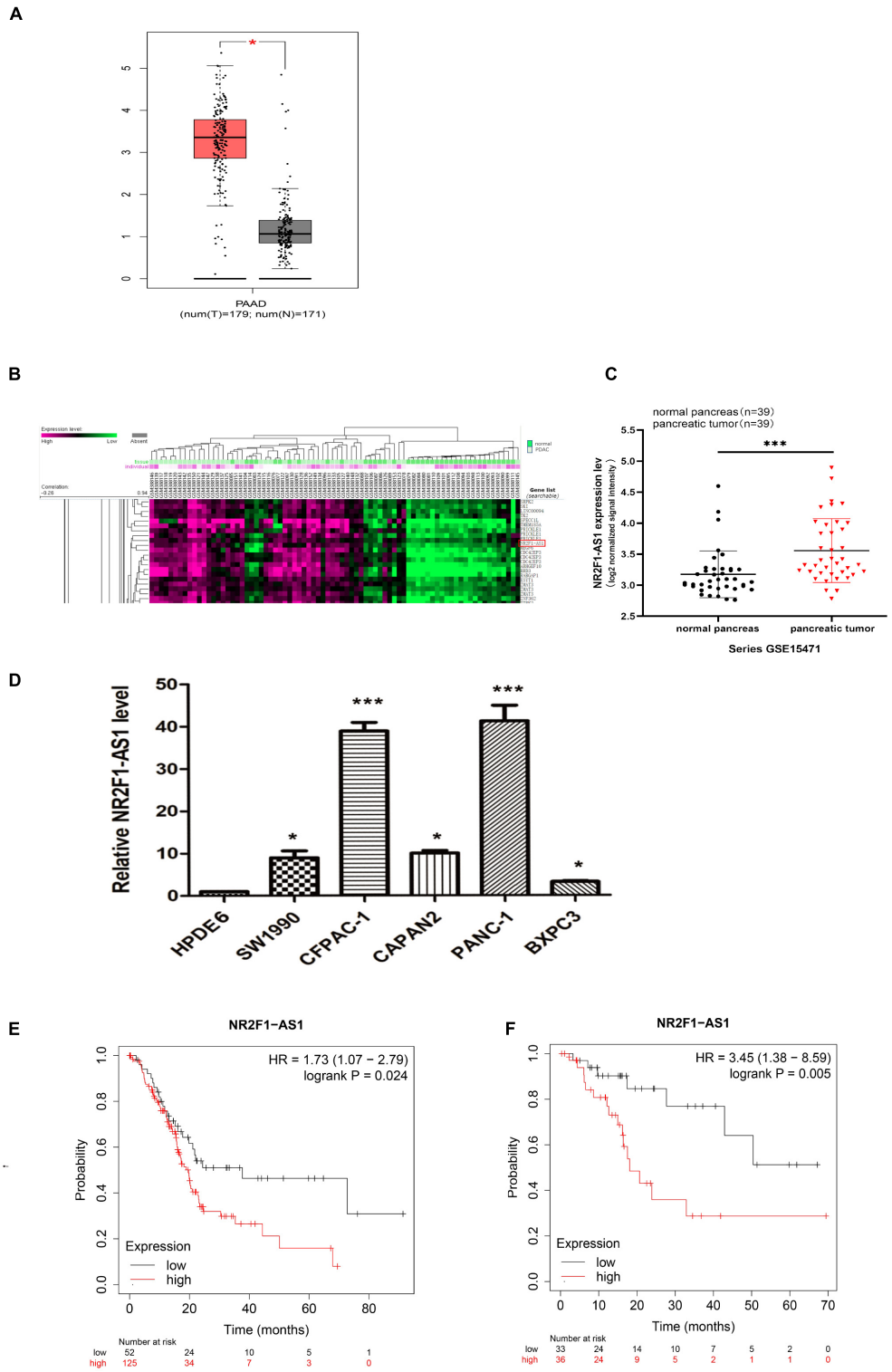


FIGURE 1 | NR2F1-AS1 is upregulated in PDAC and correlated with poor prognosis. **(A)** Boxplots comparing NR2F1-AS1 expression in PDAC samples (n = 179) and normal pancreatic tissue samples (n = 171). **(B)** Heatmap showing differentially expressed lncRNAs in the GEO dataset of GSE5471. **(C)** Microarray data from the GEO dataset GSE5471 were used to analyze the relative expression of NR2F1-AS1 in PDAC and adjacent normal tissue. **(D)** Relative expression levels of NR2F1-AS1 in PDAC cell lines. **(E,F)** Correlation analysis of NR2F1-AS1 expression with overall survival (OS) and recurrence-free survival (RFS) in PDAC patients obtained from the Kaplan–Meier plotter database. The P value was calculated by a log-rank test. HR, hazard ratio. Statistical significance: $^{*}p < 0.05$ and $^{***}p < 0.001$.

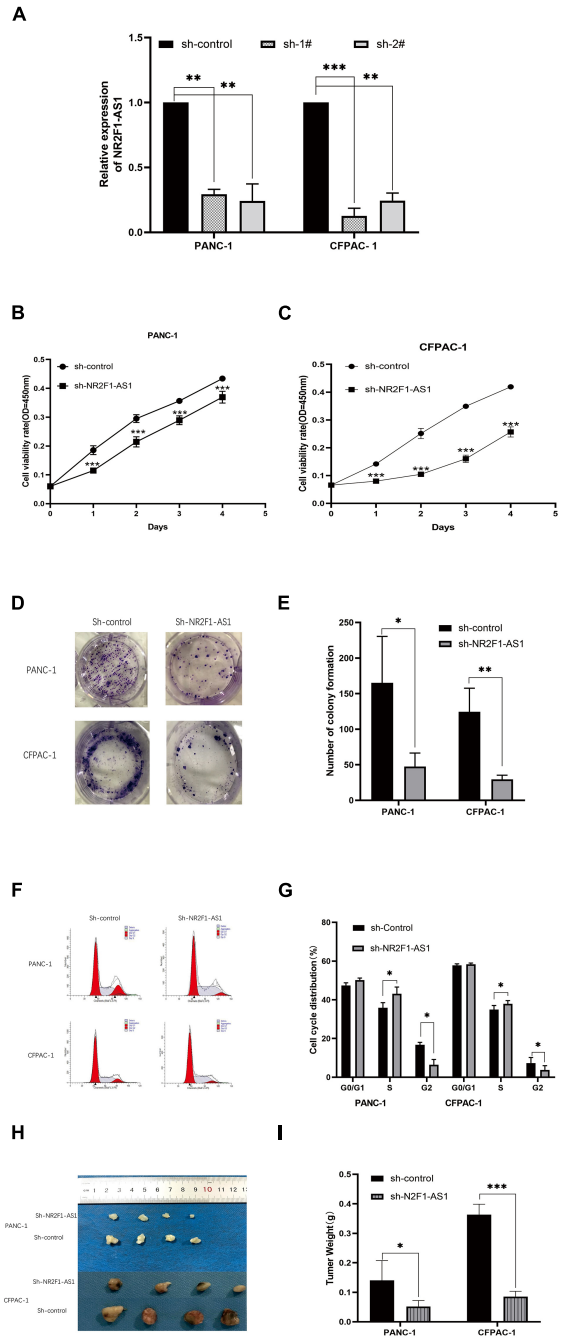


FIGURE 2 | Downregulation of NR2F1-AS1 expression suppresses PDAC cell proliferation and tumor growth *in vitro* and *in vivo*. **(A)** Expression of NR2F1-AS1 in PANC-1 and CFPAC-1 cells transfected with NR2F1-AS1 shRNA. **(B,C)** Knockdown of NR2F1-AS1 significantly suppressed proliferation in PANC-1 and CFPAC cells compared with the control group. Cell viability was determined by CCK-8 assay. **(D,E)** Colony forming assays after sh-NR2F1-AS1 transfection in PANC-1 and CFPAC-1 cells. **(F,G)** Flow cytometry was carried out to examine the cell cycle status of PANC-1 and CFPAC-1 cells after transfection with either sh-NR2F1-AS1 or sh-control. **(H,I)** Knockdown of NR2F1-AS1T reduces the tumor weight. The nude mice were sacrificed 21 days after the injection, and tumors from the respective groups are shown. **(H)** Image of the tumors; **(I)** tumor weight. $^{*}p < 0.05$, $^{**}p < 0.01$, and $^{***}p < 0.001$.

cells (**Figures 2D,E**). Next, we performed flow cytometry to examine whether NR2F1-AS1 could affect the proliferation of PDAC cells by altering cell cycle progression. The results showed that the cell cycle progression of sh-NR2F1-AS1 cells was arrested in S phase and the percentage of G2 phase cells was decreased compared with that of cells transfected with the sh-control (**Figures 2F,G**). However, the statistics showed no significant difference, downregulation of NR2F1-AS1 seemed to promote cell apoptosis (**Supplementary Figure 2**). To further test whether the level of NR2F1-AS1 expression could affect PDAC cell growth *in vivo*, NR2F1-AS1 stable knockdown cells and control cells were subcutaneously injected into BALB/C nude mice. Twenty-one days after the cells were injected, the mice were euthanized, and tumors were measured (**Figure 2H**). The tumor weight at the end of the experiment was markedly lower in the sh-NR2F1-AS1-transfected PANC-1 and CFPAC-1 groups than in the control group (**Figure 2I**). These results suggested that NR2F1-AS1 is a functionally important lncRNA in PDAC.

Knockout of NR2F1-AS1 Abrogates Migration and Invasion Ability in Pancreatic Ductal Adenocarcinoma

Pancreatic ductal adenocarcinoma is characterized by early metastasis or aggressive tumor spread. Given that high expression of NR2F1-AS1 was significantly associated with poor OS and DFS (**Figures 1E,F**), we hypothesized that NR2F1-AS1 expression is critical for cancer cell migration and invasion. We then assessed tumor cell migration and invasion abilities using wound-healing assays as well as Transwell migration and invasion assays. Knockdown of NR2F1-AS1 in PANC-1 or CFPAC-1 cells markedly suppressed cell migration and invasion compared with the corresponding control cells (**Figures 3A–G**).

NR2F1-AS1 Acts as a Sponge for miR-146a-5p/miR-877-5p in Pancreatic Ductal Adenocarcinoma

To explore the mechanism by which NR2F1-AS1 affects PDAC growth, we performed a bioinformatics analysis to search for miRNAs that can interact with NR2F1-AS1. After screening for miRNAs using the hTFtarget online tool. The results showed that NR2F1-AS1 harbors putative target sites for 40miRNAs (**Supplementary Table 3**), especially miR-146a-5p/miR-877-5p (**Figure 4A**). To determine the direct binding between NR2F1-AS1 and miR-146a-5p/miR-877-5p, dual-luciferase reporter assays were carried out. NR2F1-AS1-wt or NR2F1-AS1-mut was cotransfected into HEK293T cells with miR-146a-5p/miR-877-5p mimics or the negative control. The results revealed that miR-146a-5p/miR-877-5p overexpression considerably reduced the luciferase activity of the NR2F1-AS1-wt luciferase reporter vector compared with the negative control, while miR-146a-5p/miR-877-5p overexpression did not have any impact on the luciferase activity of NR2F1-AS1-mut (**Figures 4B,C**). RT-qPCR was then performed to determine the expression of miR-146a-5p and miR-877-5p among the PANC-1 and CFPAC-1 cell lines. The findings indicated that compared with HPDE6, the relative

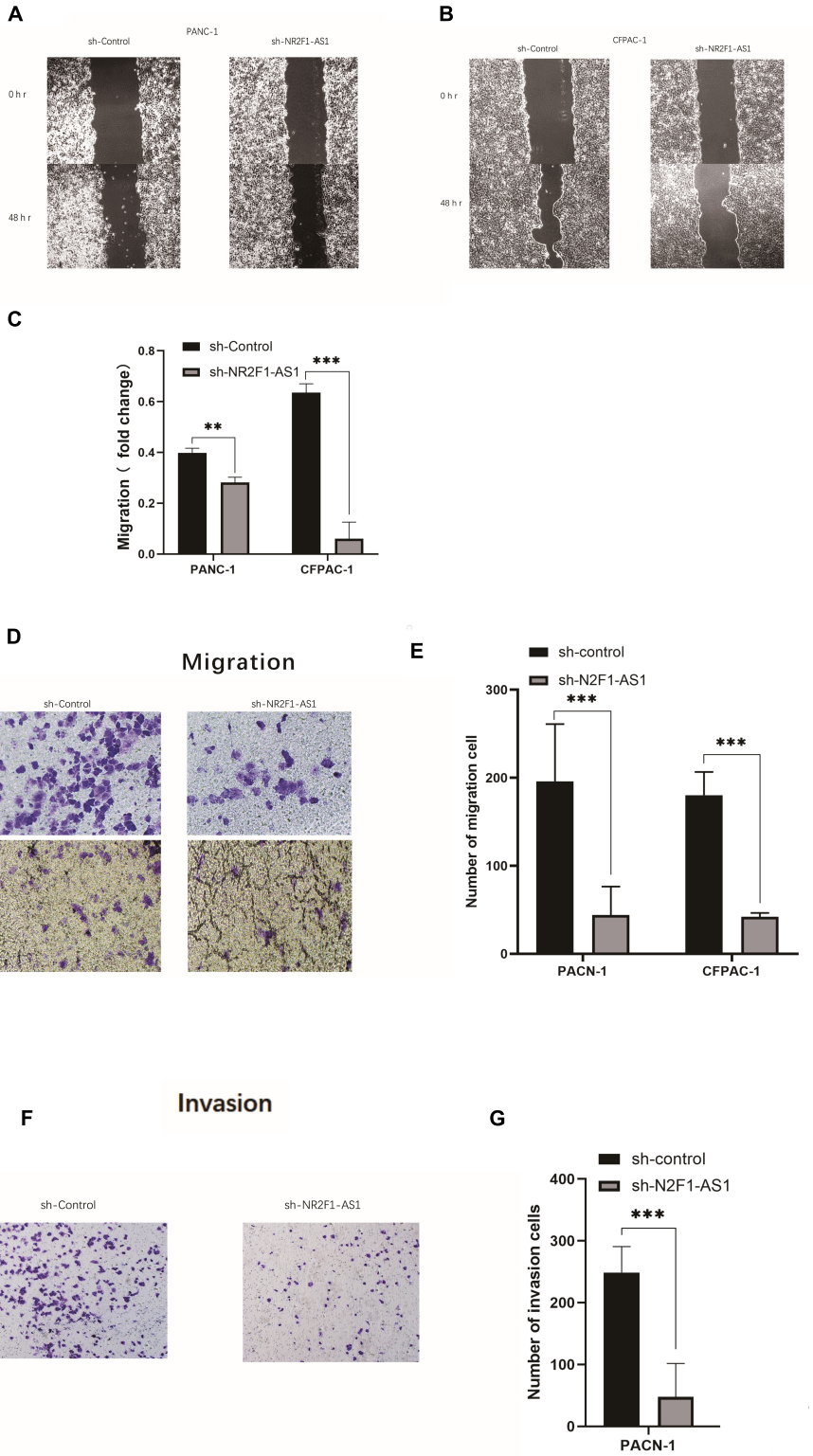


FIGURE 3 | Knockout of NR2F1-AS1 abrogates migration and invasion ability in PDAC. The migration and invasion abilities of tumor cells were assessed using wound healing assays as well as Transwell migration and invasion assays. **(A,B)** Wound healing assays (photographed after 0 and 48 h). **(C)** Histograms showing the change in healing area. **(D)** Transwell migration assays (photographed after 24 h). **(E)** Histograms showing the numbers of cells that migrated after 24 h. **(F)** Transwell invasion assays (photographed after 24 h). **(G)** Histograms showing the numbers of cells that invaded after 24 h. Statistical significance: $^{**}p < 0.01$ and $^{***}p < 0.001$.

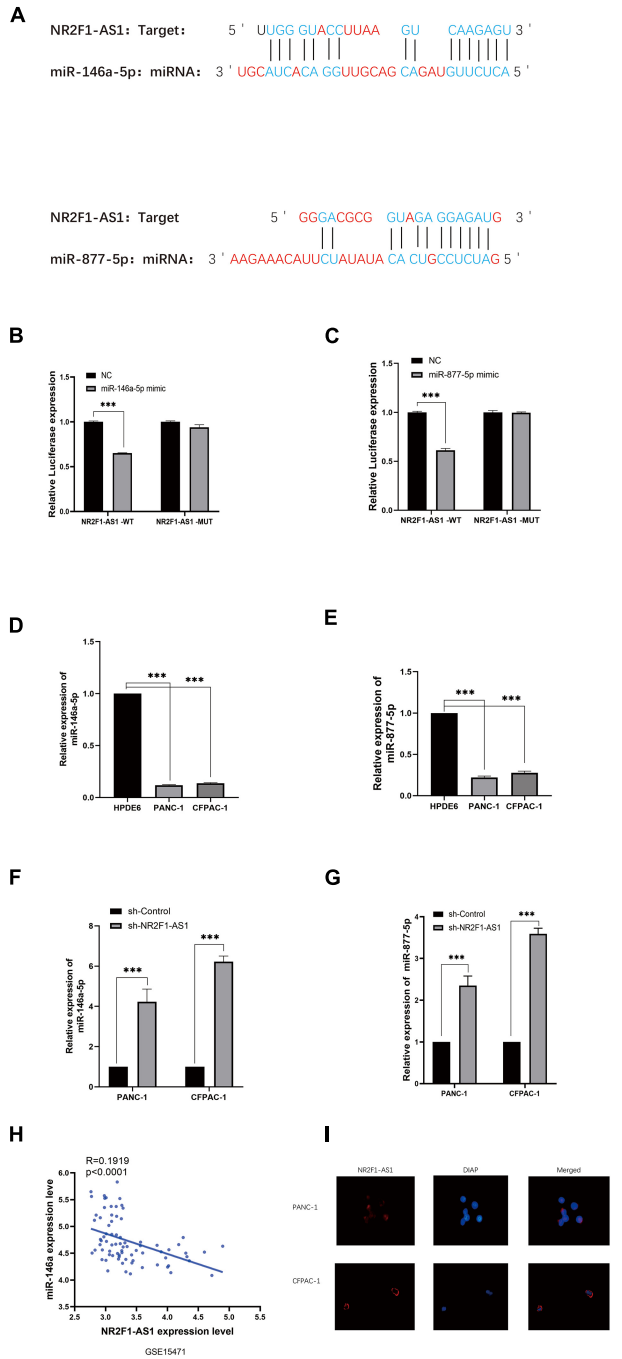


FIGURE 4 | NR2F1-AS1 interacts with miR-146a-5p/miR-877-5p in PDAC. **(A)** Prediction of target sites for miR-146a-5p/miR-877-5p in NR2F1-AS1 based on the online program. **(B,C)** Luciferase reporter assay showed that miR-146a-5p/miR-877-5p overexpression significantly suppressed the activity of the reporter containing wild-type NR2F1-AS1. **(D,E)** Expression levels of miR-146a-5p and miR-877-5p in PANC-1 and CFPAC-1 cells. **(F,G)** RT-PCR was performed with sh-NR2F1-AS1-transfected PANC-1 and CFPAC-1 cells to determine the effects of NR2F1-AS1 on miR-146a-5p and miR-877-5p. **(H)** Expression of NR2F1-AS1 was negatively associated with the expression of miR-146a-5p in 39 PDAC tissues from GSE15471. **(I)** FISH images showing the localization of NR2F1-AS1 in PANC-1 and CFPAC-1 cells. Statistical significance: $^{***}p < 0.001$.

expression of miR-146a-5p and miR-877-5p was markedly decreased (**Figures 4D,E**). The interaction between NR2F1-AS1 and miR-146a-5p/miR-877-5p was further investigated, and knockdown of NR2F1-AS1 expression markedly increased miR-146a-5p/miR-877-5p expression in both cell lines (**Figures 4F,G**). Furthermore, we found that the expression of NR2F1-AS1 was negatively associated with the expression of miR-146a-5p in 39 PDAC tissues from GSE15471 (**Figure 4H**). Finally, we performed a FISH analysis to identify the distribution of NR2F1-AS1 in PDAC cells. The results showed that NR2F1-AS1 was abundant in both the cytoplasm and nucleus and mainly located in the cytoplasm of PDAC cells (**Figure 4I**). These results suggested that NR2F1-AS1 directly targeted and negatively regulated miR-146a-5p/miR-877-5p in PDAC.

Prognostic Values of miR146a-5p/miR-877-5p and Signaling Pathways That May Be Involved in Downstream Targets in Pancreatic Ductal Adenocarcinoma

To further explore the clinical value of miR-146a-5p/miR-877-5p, we performed an analysis of the relationship between the expression of miR-146a-5p and miR-877-5p and clinicopathological features from OncomiR datasets. A survival analysis based on this database showed that low miR-146a-5p and miR-877-5p expression was associated with poor prognosis in PDAC patients (**Figures 5A,B**). Then, we surveyed cellular signaling pathways involving miR146a-5p and miR-877-5p by utilizing the miRNACancerMAP database. The results showed that these two miRNAs were involved in multiple tumors, including PDAC (**Figure 5C**). The results also showed that these two miRNAs with signaling cascades were closely related to tumor growth in PDAC. For miR146a-5p, its activity was associated with melanogenesis, the Wnt signaling pathway, the Hippo signaling pathway, purine metabolism, long-term depression and adherens junctions (**Figure 5D**). For miR-877-5p, its activity was associated with regulation of the actin cytoskeleton, PI3K-AKT signaling pathway, Dorso ventral axis formation, ECM receptor interaction, focal adhesion and Ras signaling pathway (**Figure 5E**).

Preliminary Construction of a Novel lncRNA-miRNA-mRNA (ceRNA) Regulatory Network

Subsequently, we predicted downstream target genes of miRNAs (miR-146a-5p and miR-877-5p) using TargetScan7.2. We obtained 152 and 131 potential target mRNA genes for miR-146a-5p and miR-877-5p, respectively (**Supplementary Tables 4, 5**). Based on the classical inverse relationship between miRNA and the target gene and considering that miR-146a-5p and miR-877-5p were downregulated in PDAC, we hypothesized that the downstream target mRNAs of the two miRNAs should be upregulated. Next, we identified a total of 2565 significantly upregulated DEGs in PDAC from

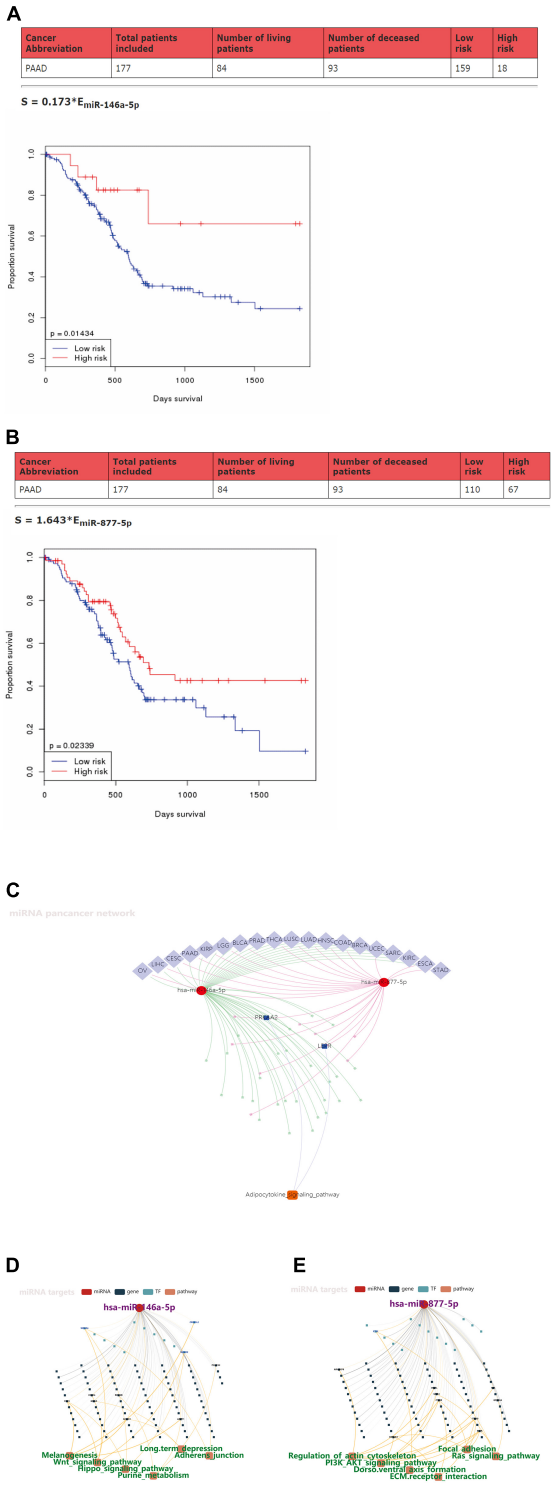


FIGURE 5 | Prognostic values of miR-146a-5p/miR-877-5p and the signaling pathways that may be involved in downstream targets in PDAC. **(A,B)** Kaplan–Meier survival analysis of miR146a-5p and miR-877-5p expression in pancreatic cancer based on OncomiR datasets. **(C)** Pan-cancer microRNA-gene-pathway network from miRNACancerMAP. **(D,E)** Regulatory networks of miR146a-5p/miR-877-5p and associated signaling pathways of putative targets in PDAC from miRNACancerMAP.

GEPIA (**Supplementary Table 6**) and further identified significant DEGs that were consistent between the two datasets (TargetScan 7.2 and GEPIA). A total of 39 significantly upregulated potential target genes for miR-146a-5p and miR-877-5p in PDAC were identified (**Figures 6A,B** and **Supplementary Table 6**). Finally, we found that miR-146a-5p and miR-877-5p could potentially regulate the expression of 39 key genes (**Supplementary Table 7**) and constructed a ceRNA regulatory network using Cytoscape software (**Figure 6C**).

Identification of Potential Key mRNA Genes in Pancreatic Ductal Adenocarcinoma by Hub Genes and Co-LncRNA Analysis

We obtained 152 and 131 potential target genes for miR-146a-5p and miR-877-5p, respectively (**Supplementary Tables 4, 5**), from TargetScan 7.2 as described above. To explore the underlying biological function and corresponding pathways of the potential target genes, the DAVID database was introduced to perform a functional enrichment analysis, which included three GO terms (BP: biological process; CC: cellular component; MF: molecular function) and KEGG pathways. The enriched GO functions included negative regulation of transcription from the RNA polymerase II promoter, positive regulation of cell proliferation and positive regulation of I-kappaB kinase NF-kappaB signaling in the BP category; Chromatin binding, RNA polymerase II core promoter proximal region sequence-specific DNA binding, RNA polymerase II transcription factor activity and sequence-specific DNA binding were identified for the MF category and nucleus was identified in the CC category (**Figures 7A,B**). The KEGG pathway enrichment analysis revealed that these potential target genes were significantly enriched in some cancer-associated pathways, such as the neurotrophin signaling pathway and pathways regulating stem cell pluripotency, pancreatic cancer, colorectal cancer and small cell lung cancer (**Figure 7C**). Based on the STRING database analysis, the PPI networks of these potential target genes were constructed (**Figure 7D**). Then, we identified the top 20 hub genes using Cytoscape software (**Figure 7E**). Subsequently, we identified 2 key potential target genes (CLTC and SPI1) by Venn analysis of the top 20 hub genes and 39 potential miRNA target genes (**Figure 7F**). Meanwhile, we identified CEGs of NR2F1-AS1 by using ColncRNA and downloaded a total of 2666 CEGs from Co-LncRNA (**Supplementary Table 8**). Subsequently, those 2666 CEGs were submitted into the online dataset Metascape for Gene Annotation & Enrichment Analysis. The results of the functional enrichment analysis mainly focused on metabolism of RNA, RNA splicing, cilium assembly, ribonucleoprotein complex biogenesis, cellular responses to stress and ncRNA metabolic processes (**Figure 7G**). Similarly, 9 key potential target genes (GALNT10, RPA3, ZNF532, SLC39A1, PKG1, SLCO3A1, NRP2, LPCAT2, and PSMA4) were identified by the Venn analysis of 2666 CEGs and 39 potential miRNA target genes (**Figure 7H**). Finally, we obtained 11 potential key target genes (**Supplementary Table 9**).

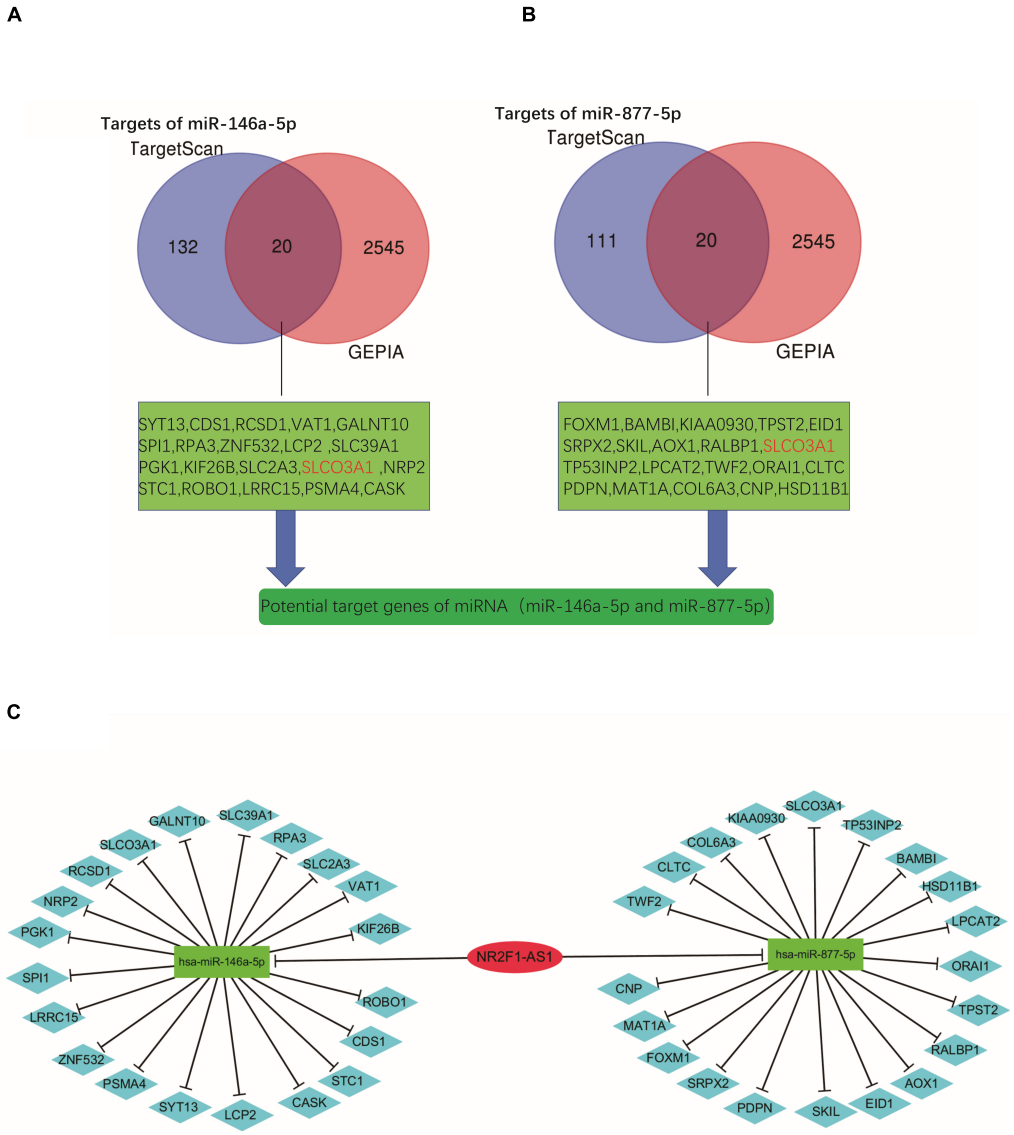


FIGURE 6 | Preliminary construction of a novel lncRNA-miRNA-mRNA (ceRNA) regulatory network. **(A,B)** Venn analysis for preliminary identification of potential target genes by combining prediction analyses and expression using TargetScan7.2 and GEPIA databases. **(C)** Construction of the lncRNA-miRNA-gene network using Cytoscape software.

Further Validation of Key Target Genes With Prognosis in Pancreatic Ductal Adenocarcinoma

A negative correlation is observed between miRNA and mRNA based on the ceRNA hypothesis. Thus, we analyzed the expression of these mRNAs in PDAC from the GEPIA database. All 11 potential key mRNAs were significantly upregulated in PDAC samples compared with normal samples (**Figure 8**). A subsequent survival analysis for the 11 potential key mRNA genes demonstrated that patients with high expression of GALNT10, ZNF532, SLC39A1, PGK1, SLCO3A1, NRP2, LPCAT2, PSMA4, and CLTC had unfavorable prognosis. A combined expression and survival analysis for these potential key mRNAs further confirmed 9 key mRNAs (GALNT10, ZNF532, SLC39A1, PGK1, SLCO3A1, NRP2, LPCAT2, PSMA4, and CLTC) (**Figure 8**).

Construction of a Novel lncRNA-miRNA-mRNA Network (NR2F1-AS1—miR-146a-5p/miR-877-5p-mRNA) in Pancreatic Ductal Adenocarcinoma

A novel triple regulatory network (lncRNA-miRNA-mRNA) with competitive endogenous RNA in PDAC was constructed by combining experimental and bioinformatics analyses. The network totally contained 2 lncRNA-miRNA pairs

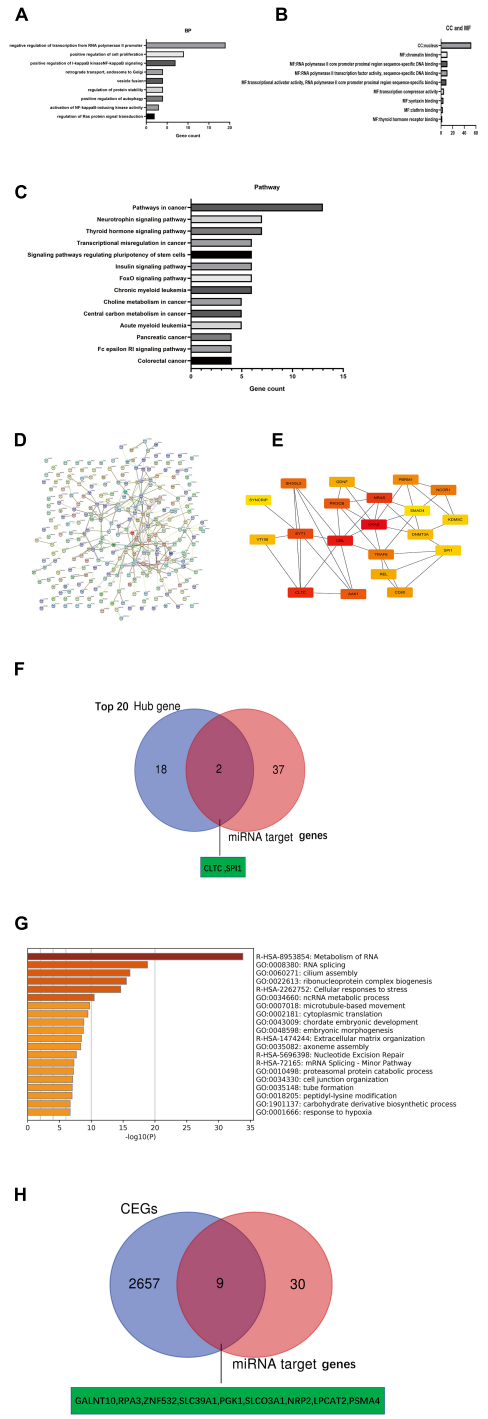


FIGURE 7 | Identification of key mRNA genes in PDAC by hub gene screening and Co-lncRNA analysis. **(A–C)** GO functional annotation and KEGG pathway enrichment analysis for the potential target genes of miRNAs by TargetScan 7.2. **(D,E)** Top 20 hub genes identified in protein-protein interaction (PPI) networks. **(F)** Intersection of the top 20 hub genes and 39 miRNA target genes by Venn analysis. **(G)** Bar graph of enriched terms across input gene lists [2,666 coexpressed protein-coding genes (CEGs) of NR2F1-AS1], colored by *p*-values from Metascape. **(H)** Intersection of 2666 coexpressed protein-coding genes (CEGs) of NR2F1-AS1 from Co-lncRNA and 39 miRNA target genes by Venn analysis.

(NR2F1-AS1—miR-146a-5p and NR2F1-AS1—miR-877-5p), 10 miRNA-mRNA pairs (miR-146a-5p—GALNT10, miR-146a-5p—ZNF532, miR-146a-5p—PGK1, miR-146a-5p—NRP2, miR-146a-5p—SLC39A, miR-146a-5p—LPCAT2, miR-146a-5p—PSMA4, miR-146a-5p—SLCO3A1, miR-877-5p—SLCO3A1, and miR-877-5p—CLTC) and 9 lncRNA-mRNA pairs (NR2F1-AS1—GALNT10, NR2F1-AS1—ZNF532, NR2F1-AS1—PGK1, NR2F1-AS1—NRP2, NR2F1-AS1—SLC39A, NR2F1-AS1—LPCAT2, NR2F1-AS1—PSMA4, NR2F1-AS1—SLCO3A1, and NR2F1-AS1—CLTC). This network is shown in **Figure 9**. We constructed a novel NR2F1-AS1—miR-146a-5p/miR-877-5p-mRNA network that was significantly associated with the prognosis of PDAC. We believe that NR2F1-AS1 may be a promising diagnostic biomarker or potential novel therapeutic target for PDAC.

DISCUSSION

The discovery of various lncRNAs in humans has dramatically changed our understanding of the mechanism of cancer. Emerging evidence has shown the important roles of lncRNAs in cancers, such as in the proliferation (Lin et al., 2020), metabolism (Tang et al., 2019), metastasis (Pan et al., 2020), EMT (Liang et al., 2018) and cell stemness of cancer (Zhan et al., 2020). Numerous lncRNAs are dysregulated in PDAC, and this aberration plays a key role in PDAC initiation and progression by regulating a variety of cancer-related biological events (Deng et al., 2018; Huang C.S. et al., 2018; Zeng et al., 2019; Pandya et al., 2020). Recently, Harvard Medical School proposed the hypothesis that competing endogenous RNA (ceRNA) regulates gene expression (Salmena et al., 2011). The ceRNA mechanism hypothesis proposed that these RNA transcripts act as ceRNAs or natural microRNA sponges. Therefore, lncRNAs act as molecular sponges to regulate the levels of mRNAs by competitively binding their same miRNAs targeting mRNAs (Fu et al., 2017; Thomson and Dinger, 2016; Zhong et al., 2018). This hypothesis was later confirmed (Tay et al., 2011; Karreth et al., 2015; Wang et al., 2016; Lin et al., 2020). Emerging evidence has demonstrated that endogenous lncRNAs may participate in posttranscriptional regulation by functioning as ceRNAs in PDAC (Cesana et al., 2011; Lei et al., 2019; Shi et al., 2019).

Initially, we predicted that NR2F1-AS1 was upregulated in PDAC based on public datasets, and the overexpression was further confirmed by a GEO dataset and PDAC cell lines. The upregulated expression of NR2F1-AS1 was associated with poor clinical outcomes by the bioinformatics analysis. After NR2F1-AS1 was knocked down, PDAC cell proliferation, colony formation, migration and invasion were all repressed. In addition, the knockdown of NR2F1-AS1 arrested PANC-1 and CFPAC-1 cells at the G2/M phase. Moreover, NR2F1-AS1 knockdown inhibited PDAC tumor growth *in vivo*. NR2F1-AS1 was also up-regulated in oxaliplatin-resistant hepatocellular carcinoma tissue and cells and NR2F1-AS1 knockdown reduced the invasion, migration in cells (Huang H. et al., 2018). These data validated the important role for NR2F1-AS1 in PDAC

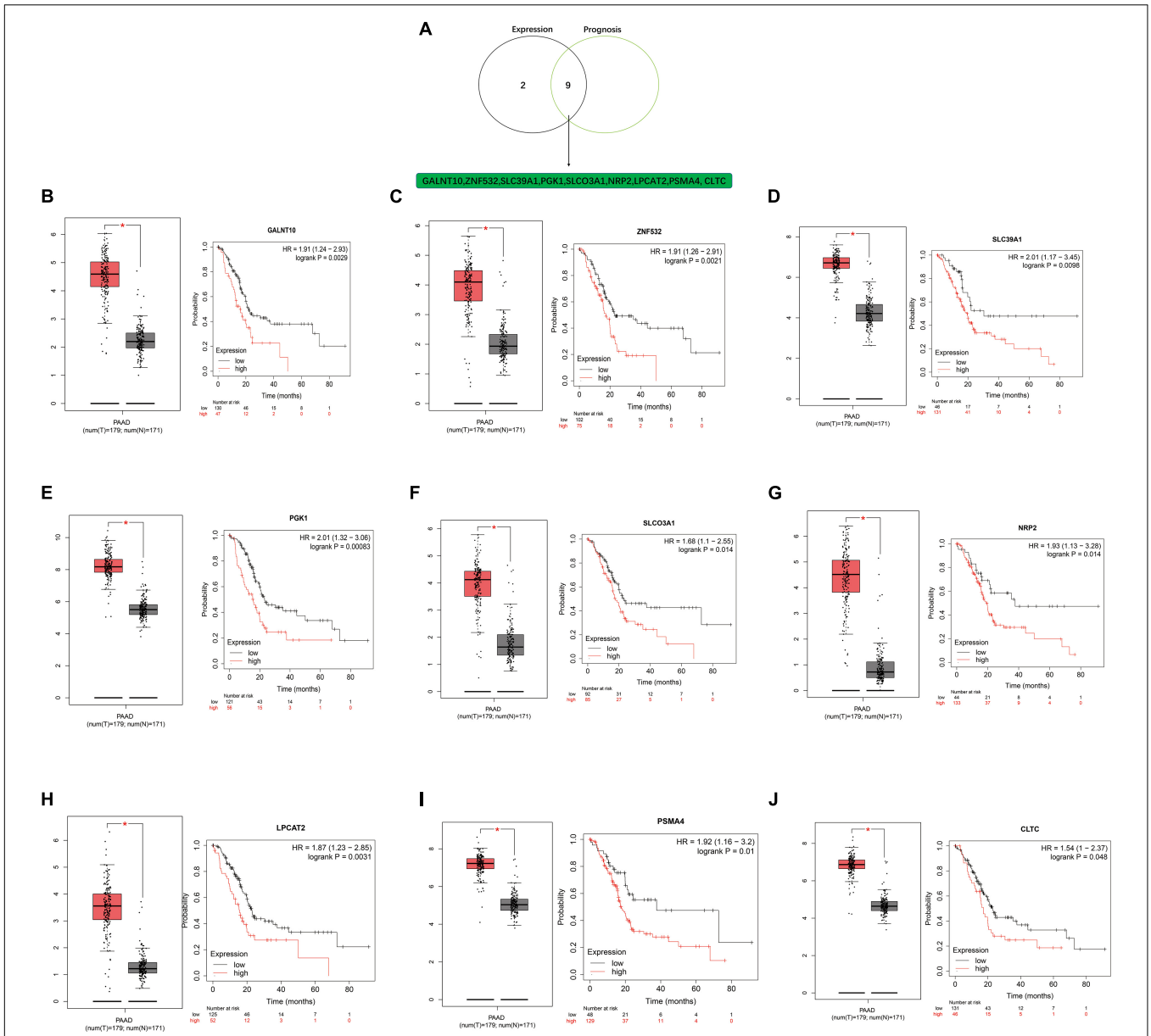


FIGURE 8 | Screening key mRNA (target genes) in PDAC. **(A)** Identification of key mRNAs among the 11 potential key mRNAs by combining expression and prognosis analyses using the GEPIA and Kaplan-Meier plotter databases. **(B)** Expression and prognostic value of GALNT10 in PDAC. **(C)** Expression and prognostic value of ZNF532 in PDAC. **(D)** Expression and prognostic value of SLC39A1 in PDAC. **(E)** Expression and prognostic value of PGK1 in PDAC. **(F)** Expression and prognostic value of SLCO3A1 in PDAC. **(G)** Expression and prognostic value of NRP2 in PDAC. **(H)** Expression and prognostic value of LPCAT2 in PDAC. **(I)** Expression and prognostic value of PSMA4 in PDAC. **(J)** Expression and prognostic value of CLTC in PDAC.

growth, thus highlighting the importance of NR2F1-AS1 as a PDAC promoter.

Bioinformatics prediction tools are an emerging assistant method to help researchers discover the underlying molecular mechanism within lncRNAs and miRNAs/mRNAs (Zhang and Yang, 2017). We first performed a bioinformatics analysis to predict potential lncRNA-miRNA interactions using the online tool hTFtarget. The results showed that NR2F1-AS1 harbors putative target sites for miR-146a-5p/miR-877-5p, which was confirmed through dual-luciferase reporter gene assays.

Mechanistically, NR2F1-AS1 can be negatively regulated by miR-146a-5p/miR-877-5p. We found that the expression of miR-146a-5p and miR-877-5p was markedly decreased in PDAC cells while knockdown of NR2F1-AS1 expression markedly increased miR-146a-5p/miR-877-5p expression in both cell lines. For example, we found that the expression of NR2F1-AS1 was negatively associated with the expression of miR-146a-5p in 39 PDAC tissues from GSE15471. Finally, the FISH results revealed that NR2F1-AS1 was mainly expressed in the cytoplasm. Study showed that NR2F1-AS1

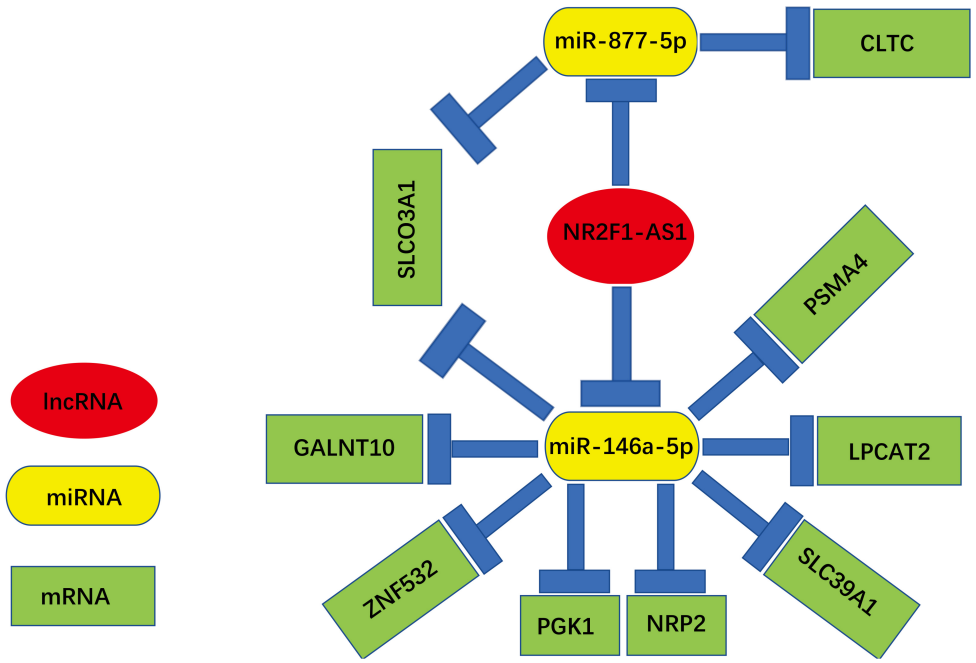


FIGURE 9 | Novel key lncRNA-miRNA-mRNA network competing endogenous RNA (ceRNA) regulatory network associated with the prognosis of PDAC.

is mainly located in the cytoplasm of osteosarcoma (OS) cells and plays an oncogenic role in OS through sponging miR-483-3p (Li et al., 2019). Taken together, NR2F1-AS1 confers an aggressive phenotype by sponging miR-146a-5p/miR-877-5p.

Previous studies have revealed that miR-146a-5p plays a tumor suppressive role in many cancers, such as leukemia (Su et al., 2020), cervical cancer (Dong et al., 2019), lung cancer (Mohamed et al., 2019), gastric cancer (Adami et al., 2019), and breast cancer (Long et al., 2019). Moreover, it has been previously reported that the expression of miR-146a-5p is downregulated in PDAC and acts as a tumor suppressor (Li et al., 2010; Meng et al., 2020). miR-877-5p has also been confirmed as a tumor suppressor in cancer, such as in hepatocellular carcinoma (Yan et al., 2018), gastric cancer (Wu et al., 2020) and cervical cancer (Liang J. et al., 2020). However, little is known about its function or link to NR2F1-AS1 in PDAC.

To the best of our knowledge, we are the first to demonstrate that NR2F1-AS1 acts as a ceRNA by sponging miR-146a-5p/miR-877-5p to regulate the development of PDAC. Subsequently, we found that down-regulated expression of miR-146a-5p and miR-877-5p was associated with poor prognosis in PDAC patients. In addition, miR-146a-5p and miR-877-5p may be involved in multiple tumors, including PDAC, and this result was consistent with the above discussion. The potential target genes of miR-146a-5p and miR-877-5p revealed their participation in several signaling cascades related to tumor development (e.g., Wnt signaling pathway, Hippo signaling pathway and Ras signaling pathway). Combining the potential target mRNAs for miR146a-5p and miR-877-5p in the TargetScan 7.2 database with data from GEPIA, we obtained 39 potential target genes and then preliminarily constructed a novel lncRNA-miRNA-mRNA (ceRNA) regulatory network.

We further identified key target mRNAs by screening hub genes and CEGs of NR2F1-AS1. On the one hand, enrichment analyses of target genes revealed their participation in some GO terms that were associated with cancer biological behaviors, including negative regulation of transcription from the RNA polymerase II promoter (Steinbach et al., 2019), chromatin binding (Heinonen et al., 2015)and nucleus (Kim et al., 2018). The KEGG pathway analysis showed that these target genes were mainly enriched in some cancer-associated pathways, such as pathways in cancer and signaling pathways regulating the pluripotency of stem cells and pancreatic cancer. A PPI network based on these genes was next constructed to obtain the top 20 hub genes and 2 potential key target mRNAs (CLTC and SPI1) were identified by Venn analysis between the top 20 hub genes and 39 potential miRNA target genes. On the other hand, 2,666 CEGs of NR2F1-AS1 were obtained, and the results of the functional enrichment analysis among these CEGs revealed that they were mainly focused on RNA metabolism, RNA splicing, ribonucleoprotein complex biogenesis, cellular responses to stress and ncRNA metabolic processes. Similarly, 9 potential key target genes were identified by the Venn analysis between the 2,666 CEGs and 39 potential miRNA target genes. Therefore, a total of 11 potential key target mRNAs were selected for further expression verification and survival analysis. Finally, a total of 9 key target genes (GALNT10, ZNF532, SLC39A1, PGK1, SLCO3A1, NRP2, LPCAT2, PSMA4, and CLTC) with poor prognosis were defined as key mRNAs in PDAC.

Intriguingly, these 9 key genes have been well investigated in multiple cancers (including PDAC). High GALNT10 expression confers an immunosuppressive microenvironment, promotes tumor progression, predicts poor clinical outcomes in high-grade ovarian serous cancer (HGSC; Zhang G. et al., 2020) and promotes proliferation and apoptosis resistance of hepatoma cells (Wu et al., 2015). ZNF532 drives dramatic mistargeting of active chromatin in NUT midline carcinoma (NMC; Alekseyenko et al., 2017). SLC39A1, one of the Zn^{2+} transporters of SLC families 39, is involved in specific functions in the pancreas, such as insulin synthesis and secretion and metallation of digestive proenzymes. Defective or dysregulated Zn^{2+} metabolism in the pancreas is associated with cancer (Schweigel-Rontgen, 2014). PGK1 regulates metabolism (glycolysis), promotes cell proliferation in brain tumors (Qian et al., 2019) and preferentially supports proliferation by functioning as a glycolytic enzyme in PDAC (Liang C. et al., 2020). SLCO3A1 could potentially be used to target anticancer drugs to PDAC (Hays et al., 2013). High expression of NRP2 is associated with poor overall survival for PDAC (Liu et al., 2018b) and hepatocellular carcinoma patients (Dong et al., 2017). Increased expression of LPCAT2 is associated with poor prognosis of PDAC patients (Idichi et al., 2018) and positively correlated with aggressive prostate cancer (Williams et al., 2014). PSMA4 plays a direct role in cell proliferation in lung carcinoma cell lines (Liu et al., 2009). CLTC promoted tumorigenesis in hepatocellular carcinoma (Huang et al., 2017) and cell growth in breast cancers (Ujihira et al., 2015). The above research can support the accuracy of our bioinformatics analyses.

Therefore, a prognosis-associated lncRNA-miRNA-mRNA network in PDAC was successfully established. Although highly interesting findings were obtained in a series of lab experiments and bioinformatics analyses in this study, more lab experiments need to be performed in the future.

CONCLUSION

In conclusion, this study suggests that NR2F1-AS1 is an independent prognostic factor in PDAC patients and promotes proliferation, migration and invasion in PDAC both *in vitro* and *in vivo*; moreover, a novel NR2F1-AS1-miR146a-5p/miR-877-5p-mRNA ceRNA regulatory network was constructed by integrated lab experiments and bioinformatics analysis, and all the RNAs in the network possess significant predictive value for prognosis in PDAC. In addition to identifying the prognostic value of this lncRNA-miRNA-mRNA network in PDAC, this study provided key insights for investigating the molecular mechanism in PDAC. However, additional studies should be conducted to further validate these findings.

DATA AVAILABILITY STATEMENT

The raw data that support the conclusion of this article will be made available by the authors, without undue reservation.

ETHICS STATEMENT

The animal study was reviewed and approved by the animal Ethics Committee of the Third Xiangya Hospital, Central South University.

AUTHOR CONTRIBUTIONS

DL and HZ: conceptualization and formal analysis. DL, YL, and ZL: data curation, investigation, and methodology. DL and XY: funding acquisition. DL: project administration and writing – original draft. DL, HZ, and XY: resources and writing – review and editing. DL and YL: software. HZ and XY: supervision and validation. All authors contributed to the article and approved the submitted version.

FUNDING

This project was supported by the self-exploration and innovation project for graduate student of Central South University in 2019 (Funding Number: 2019zzts365). The funders had no role in study design, data collection, data analysis, interpretation, and writing of the report.

ACKNOWLEDGMENTS

The authors thank all staffs of Department of Hepatopancreatobiliary Surgery, Third Xiangya Hospital, Central South University. The authors would like to thank the online datasets for their generous sharing of large amount of data.

SUPPLEMENTARY MATERIAL

The Supplementary Material for this article can be found online at: https://www.frontiersin.org/articles/10.3389/fcell.2021.736980/full#supplementary-material

Supplementary Figure 1 | Gene expression profile across all tumor samples and paired normal tissues from Gene Expression Profiling Interactive Analysis (GEPIA). The height of the bar represents the median expression of certain tumor types or normal tissues. ACC, adrenocortical carcinoma; BLCA, bladder urothelial carcinoma; BRCA, breast invasive carcinoma; CESC, cervical squamous cell carcinoma and endocervical adenocarcinoma; CHOL, cholangiocarcinoma; COAD, colon adenocarcinoma; ESCA, esophageal carcinoma; GBM, Glioblastoma multiforme; HNSC, head and neck squamous cell carcinoma; KICH, kidney chromophobe; KIRC, kidney renal clear cell carcinoma; KIRP, kidney renal papillary cell carcinoma; LAML, Acute Myeloid Leukemia; LGG, brain lower grade glioma; LIHC, liver hepatocellular carcinoma; LUAD, lung adenocarcinoma; LUSC, lung squamous cell carcinoma; MESO, mesothelioma; OV, ovarian serous cystadenocarcinoma; PAAD, pancreatic adenocarcinoma; PCPG, pheochromocytoma and paraganglioma; PRAD, prostate adenocarcinoma; READ, rectal adenocarcinoma; SARC, sarcoma; SKCM, skin cutaneous melanoma; STAD, stomach adenocarcinoma; TGCT, testicular germ cell tumors; THCA, thyroid carcinoma; THYM, thymoma; UCEC, uterine corpus endometrial carcinoma; UCS, uterine carcinosarcoma.

REFERENCES

Adami, B., Tabatabaeian, H., Ghaedi, K., Talebi, A., Azadeh, M., and Dehdashtian, E. (2019). MiR-146a is deregulated in gastric cancer. *J. Cancer Res. Ther.* 15, 108–114. doi: 10.4103/jcrt.JCRT_855_17

Agarwal, V., Bell, G. W., Nam, J. W., and Bartel, D. P. (2015). Predicting effective microRNA target sites in mammalian mRNAs. *eLife* 4:e05005. doi: 10.7554/eLife.05005

Alekseyenko, A. A., Walsh, E. M., Zee, B. M., Pakozdi, T., Hsi, P., Lemieux, M. E., et al. (2017). Ectopic protein interactions within BRD4-chromatin complexes drive oncogenic megadomain formation in NUT midline carcinoma. *Proc. Natl. Acad. Sci. U.S.A.* 114, E4184–E4192. doi: 10.1073/pnas.1702086114

Biankin, A. V., Waddell, N., Kassahn, K. S., Gingras, M. C., Muthuswamy, L. B., Johns, A. L., et al. (2012). Pancreatic cancer genomes reveal aberrations in axon guidance pathway genes. *Nature* 491, 399–405. doi: 10.1038/nature11547

Cesana, M., Cacchiarelli, D., Legnini, I., Santini, T., Sthandier, O., Chinappi, M., et al. (2011). A long noncoding RNA controls muscle differentiation by functioning as a competing endogenous RNA. *Cell* 147, 358–369. doi: 10.1016/j.cell.2011.09.028

Deng, S. J., Chen, H. Y., Ye, Z., Deng, S. C., Zhu, S., Zeng, Z., et al. (2018). Hypoxia-induced LncRNA-BX111 promotes metastasis and progression of pancreatic cancer through regulating ZEB1 transcription. *Oncogene* 37, 5811–5828. doi: 10.1038/s41388-018-0382-1

Dong, X., Guo, W., Zhang, S., Wu, T., Sun, Z., Yan, S., et al. (2017). Elevated expression of neuropilin-2 associated with unfavorable prognosis in hepatocellular carcinoma. *Onco Targets Ther.* 10, 3827–3833. doi: 10.2147/OTT.S139044

Dong, Z., Yu, C., Rezhiya, K., Gulijiahan, A., and Wang, X. (2019). Downregulation of miR-146a promotes tumorigenesis of cervical cancer stem cells via VEGF/CDC42/PAK1 signaling pathway. *Artif. Cells Nanomed. Biotechnol.* 47, 3711–3719. doi: 10.1080/21691401.2019.1664560

Fagerberg, L., Hallstrom, B. M., Oksvold, P., Kampf, C., Djureinovic, D., Odeberg, J., et al. (2014). Analysis of the human tissue-specific expression by genome-wide integration of transcriptomics and antibody-based proteomics. *Mol. Cell. Proteomics* 13, 397–406. doi: 10.1074/mcp.M113.035600

Fu, Z., Chen, C., Zhou, Q., Wang, Y., Zhao, Y., Zhao, X., et al. (2017). LncRNA HOTTIP modulates cancer stem cell properties in human pancreatic cancer by regulating HOXA9. *Cancer Lett.* 410, 68–81. doi: 10.1016/j.canlet.2017.09.019

Gong, R., and Jiang, Y. (2020). Non-coding RNAs in pancreatic ductal adenocarcinoma. *Front. Oncol.* 10:309. doi: 10.3389/fonc.2020.00309

Hays, A., Apte, U., and Hagenbuch, B. (2013). Organic anion transporting polypeptides expressed in pancreatic cancer may serve as potential diagnostic markers and therapeutic targets for early stage adenocarcinomas. *Pharm. Res.* 30, 2260–2269. doi: 10.1007/s11095-012-0962-7

Heinonen, H., Lepikhova, T., Sahu, B., Pehkonen, H., Pihlajamaa, P., Louhimo, R., et al. (2015). Identification of several potential chromatin binding sites of HOXB7 and its downstream target genes in breast cancer. *Int. J. Cancer* 137, 2374–2383. doi: 10.1002/ijc.29616

Hu, D., Su, C., Jiang, M., Shen, Y., Shi, A., Zhao, F., et al. (2016). Fenofibrate inhibited pancreatic cancer cells proliferation via activation of p53 mediated by upregulation of LncRNA MEG3. *Biochem. Biophys. Res. Commun.* 471, 290–295. doi: 10.1016/j.bbrc.2016.01.169

Huang, C. S., Chu, J., Zhu, X. X., Li, J. H., Huang, X. T., Cai, J. P., et al. (2018). The C/EBPβ-LINC01133 axis promotes cell proliferation in pancreatic ductal adenocarcinoma through upregulation of CCNG1. *Cancer Lett.* 421, 63–72. doi: 10.1016/j.canlet.2018.02.020

Huang, D. W., Sherman, B. T., and Lempicki, R. A. (2009). Systematic and integrative analysis of large gene lists using DAVID bioinformatics resources. *Nat. Protoc.* 4, 44–57. doi: 10.1038/nprot.2008.211

Huang, G. H., Shan, H., Li, D., Zhou, B., and Pang, P. F. (2017). MiR-199a-5p suppresses tumorigenesis by targeting clathrin heavy chain in hepatocellular carcinoma. *Cell Biochem. Funct.* 35, 98–104. doi: 10.1002/cbf.3252

Huang, H., Chen, J., Ding, C. M., Jin, X., Jia, Z. M., and Peng, J. (2018). LncRNA NR2F1-AS1 regulates hepatocellular carcinoma oxaliplatin resistance by targeting ABCC1 via miR-363. *J. Cell. Mol. Med.* 22, 3238–3245. doi: 10.1111/jcmm.13605

Idichi, T., Seki, N., Kurahara, H., Fukuhisa, H., Toda, H., Shimonosono, M., et al. (2018). Molecular pathogenesis of pancreatic ductal adenocarcinoma: impact of passenger strand of pre-miR-148a on gene regulation. *Cancer Sci.* 109, 2013–2026. doi: 10.1111/cas.1361

Karreth, F. A., Reschke, M., Ruocco, A., Ng, C., Chapuy, B., Leopold, V., et al. (2015). The BRAF pseudogene functions as a competitive endogenous RNA and induces lymphoma in vivo. *Cell* 161, 319–332. doi: 10.1016/j.cell.2015.02.043

Kim, D. H., Hah, J., and Wirtz, D. (2018). Mechanics of the cell nucleus. *Adv. Exp. Med. Biol.* 1092, 41–55. doi: 10.1007/978-3-319-95294-9_3

Kim, K., Jutooru, I., Chadalapaka, G., Johnson, G., Frank, J., Burghardt, R., et al. (2013). HOTAIR is a negative prognostic factor and exhibits pro-oncogenic activity in pancreatic cancer. *Oncogene* 32, 1616–1625. doi: 10.1038/onc.2012.193

Lee, J. T. (2012). Epigenetic regulation by long noncoding RNAs. *Science* 338, 1435–1439. doi: 10.1126/science.1231776

Lei, S., He, Z., Chen, T., Guo, X., Zeng, Z., Shen, Y., et al. (2019). Long noncoding RNA 00976 promotes pancreatic cancer progression through OTUD7B by sponging miR-137 involving EGFR/MAPK pathway. *J. Exp. Clin. Cancer Res.* 38:470. doi: 10.1186/s13046-019-1388-4

Li, C. H., Xiao, Z., Tong, J. H., To, K. F., Fang, X., Cheng, A. S., et al. (2017). EZH2 coupled with HOTAIR to silence MicroRNA-34a by the induction of heterochromatin formation in human pancreatic ductal adenocarcinoma. *Int. J. Cancer* 140, 120–129. doi: 10.1002/ijc.30414

Li, N., Yang, G., Luo, L., Ling, L., Wang, X., Shi, L., et al. (2020). LncRNA THAP9-AS1 promotes pancreatic ductal adenocarcinoma growth and leads to a poor clinical outcome via sponging miR-484 and interacting with YAP. *Clin. Cancer Res.* 26, 1736–1748. doi: 10.1158/1078-0432.CCR-19-0674

Li, S., Zheng, K., Pei, Y., Wang, W., and Zhang, X. (2019). Long noncoding RNA NR2F1-AS1 enhances the malignant properties of osteosarcoma by increasing forkhead box A1 expression via sponging of microRNA-483-3p. *Aging* 11, 11609–11623. doi: 10.18632/aging.102563

Li, Y., Vandenboom, T. N., Wang, Z., Kong, D., Ali, S., Philip, P. A., et al. (2010). MiR-146a suppresses invasion of pancreatic cancer cells. *Cancer Res.* 70, 1486–1495. doi: 10.1158/0008-5472.CAN-09-2792

Liang, C., Shi, S., Qin, Y., Meng, Q., Hua, J., Hu, Q., et al. (2020). Localisation of PGK1 determines metabolic phenotype to balance metastasis and proliferation in patients with SMAD4-negative pancreatic cancer. *Gut* 69, 888–900. doi: 10.1136/gutjnl-2018-317163

Liang, H., Yu, T., Han, Y., Jiang, H., Wang, C., You, T., et al. (2018). LncRNA PTAR promotes EMT and invasion-metastasis in serous ovarian cancer by competitively binding miR-101-3p to regulate ZEB1 expression. *Mol. Cancer* 17:119. doi: 10.1186/s12943-018-0870-5

Liang, J., Zhang, S., Wang, W., Xu, Y., Kawuli, A., Lu, J., et al. (2020). Long non-coding RNA DSCAM-AS1 contributes to the tumorigenesis of cervical cancer by targeting miR-877-5p/ATXN7L3 axis. *Biosci. Rep.* 40:BSR20192061. doi: 10.1042/BSR20192061

Lin, Z., Lu, S., Xie, X., Yi, X., and Huang, H. (2020). Noncoding RNAs in drug-resistant pancreatic cancer: a review. *Biomed. Pharmacother.* 131:110768. doi: 10.1016/j.biopha.2020.110768

Liu, B., Wu, S., Ma, J., Yan, S., Xiao, Z., Wan, L., et al. (2018a). LncRNA GAS5 reverses EMT and tumor stem cell-mediated gemcitabine resistance and metastasis by targeting miR-221/SOCS3 in pancreatic cancer. *Mol. Ther. Nucleic Acids* 13, 472–482. doi: 10.1016/j.omtn.2018.09.026

Liu, B., Yang, H., Taher, L., Denz, A., Grutzmann, R., Pilarsky, C., et al. (2018b). Identification of prognostic biomarkers by combined mRNA and miRNA expression microarray analysis in pancreatic cancer. *Transl. Oncol.* 11, 700–714. doi: 10.1016/j.tranon.2018.03.003

Liu, J. H., Chen, G., Dang, Y. W., Li, C. J., and Luo, D. Z. (2014). Expression and prognostic significance of lncRNA MALAT1 in pancreatic cancer tissues. *Asian Pac. J. Cancer Prev.* 15, 2971–2977. doi: 10.7314/apjcp.2014.15.7.2971

Liu, Y., Liu, P., Wen, W., James, M. A., Wang, Y., Bailey-Wilson, J. E., et al. (2009). Haplotype and cell proliferation analyses of candidate lung cancer susceptibility genes on chromosome 15q24-25.1. *Cancer Res.* 69, 7844–7850. doi: 10.1158/0008-5472.CAN-09-1833

Long, J. P., Dong, L. F., Chen, F. F., and Fan, Y. F. (2019). MiR-146a-5p targets interleukin-1 receptor-associated kinase 1 to inhibit the growth, migration, and invasion of breast cancer cells. *Oncol. Lett.* 17, 1573–1580. doi: 10.3892/ol.2018.9769

Meng, Q., Liang, C., Hua, J., Zhang, B., Liu, J., Zhang, Y., et al. (2020). A miR-146a-5p/TRAF6/NF-kB p65 axis regulates pancreatic cancer chemoresistance:

functional validation and clinical significance. *Theranostics* 10, 3967–3979. doi: 10.7150/thno.40566

Mizrahi, J. D., Surana, R., Valle, J. W., and Shroff, R. T. (2020). Pancreatic cancer. *Lancet* 395, 2008–2020. doi: 10.1016/S0140-6736(20)30974-0

Mohamed, R. H., Pasha, H. F., Gad, D. M., and Toam, M. M. (2019). MiR-146a and miR-196a-2 genes polymorphisms and its circulating levels in lung cancer patients. *J. Biochem.* 166, 323–329. doi: 10.1093/jb/mvz044

Nagy, A., Lanczky, A., Menyhart, O., and Gyorffy, B. (2018). Validation of miRNA prognostic power in hepatocellular carcinoma using expression data of independent datasets. *Sci. Rep.* 8:9227. doi: 10.1038/s41598-018-27521-y

Pan, J., Fang, S., Tian, H., Zhou, C., Zhao, X., Tian, H., et al. (2020). LncRNA JPX/miR-33a-5p/Twist1 axis regulates tumorigenesis and metastasis of lung cancer by activating Wnt/beta-catenin signaling. *Mol. Cancer* 19:9. doi: 10.1186/s12943-020-1133-9

Pandya, G., Kirtonia, A., Sethi, G., Pandey, A. K., and Garg, M. (2020). The implication of long non-coding RNAs in the diagnosis, pathogenesis and drug resistance of pancreatic ductal adenocarcinoma and their possible therapeutic potential. *Biochim. Biophys. Acta Rev. Cancer* 1874:188423. doi: 10.1016/j.bbcan.2020.188423

Qian, X., Li, X., Shi, Z., Xia, Y., Cai, Q., Xu, D., et al. (2019). PTEN suppresses glycolysis by dephosphorylating and inhibiting autophosphorylated PGK1. *Mol. Cell* 76, 516–527. doi: 10.1016/j.molcel.2019.08.006

Rahib, L., Smith, B. D., Aizenberg, R., Rosenzweig, A. B., Fleshman, J. M., and Matrisian, L. M. (2014). Projecting cancer incidence and deaths to 2030: the unexpected burden of thyroid, liver, and pancreas cancers in the United States. *Cancer Res.* 74, 2913–2921. doi: 10.1158/0008-5472.CAN-14-0155

Rishi, A., Goggins, M., Wood, L. D., and Hruban, R. H. (2015). Pathological and molecular evaluation of pancreatic neoplasms. *Semin. Oncol.* 42, 28–39. doi: 10.1053/j.seminoncol.2014.12.004

Sakamoto, H., Attiyeh, M. A., Gerold, J. M., Makohon-Moore, A. P., Hayashi, A., Hong, J., et al. (2020). The evolutionary origins of recurrent pancreatic cancer. *Cancer Discov.* 10, 792–805. doi: 10.1158/2159-8290.CD-19-1508

Salmena, L., Poliseno, L., Tay, Y., Kats, L., and Pandolfi, P. P. (2011). A ceRNA hypothesis: the rosetta stone of a hidden RNA language? *Cell* 146, 353–358. doi: 10.1016/j.cell.2011.07.014

Sanchez, C. A., Yamamoto, T., Kawamura, Y., Hironaka-Mitsuhashi, A., Ono, M., Tsuda, H., et al. (2020). Long non-coding NR2F1-AS1 is associated with tumor recurrence in estrogen receptor-positive breast cancers. *Mol. Oncol.* 14, 2271–2287. doi: 10.1002/1878-0261.12704

Schweigel-Rontgen, M. (2014). The families of zinc (SLC30 and SLC39) and copper (SLC31) transporters. *Curr. Top. Membr.* 73, 321–355. doi: 10.1016/B978-0-12-800223-0.00009-8

Shi, W., Zhang, C., Ning, Z., Hua, Y., Li, Y., Chen, L., et al. (2019). Long non-coding RNA LINC00346 promotes pancreatic cancer growth and gemcitabine resistance by sponging miR-188-3p to derepress BRD4 expression. *J. Exp. Clin. Cancer Res.* 38:60. doi: 10.1186/s13046-019-1055-9

Siegel, R. L., Miller, K. D., Fuchs, H. E., and Jemal, A. (2021). Cancer Statistics, 2021. *CA Cancer J. Clin.* 71, 7–33. doi: 10.3322/caac.21654

Slack, F. J., and Chinnaiyan, A. M. (2019). The role of non-coding RNAs in oncology. *Cell* 179, 1033–1055. doi: 10.1016/j.cell.2019.10.017

Steinbach, N., Hasson, D., Mathur, D., Stratikopoulos, E. E., Sachidanandam, R., Bernstein, E., et al. (2019). PTEN interacts with the transcription machinery on chromatin and regulates RNA polymerase II-mediated transcription. *Nucleic Acids Res.* 47, 5573–5586. doi: 10.1093/nar/gkz272

Strobel, O., Neoptolemos, J., Jager, D., and Buchler, M. W. (2019). Optimizing the outcomes of pancreatic cancer surgery. *Nat. Rev. Clin. Oncol.* 16, 11–26. doi: 10.1038/s41571-018-0112-1

Su, Y. L., Wang, X., Mann, M., Adamus, T. P., Wang, D., Moreira, D. F., et al. (2020). Myeloid cell-targeted miR-146a mimic inhibits NF-kappaB-driven inflammation and leukemia progression in vivo. *Blood* 135, 167–180. doi: 10.1182/blood.2019002045

Sung, H., Ferlay, J., Siegel, R. L., Laversanne, M., Soerjomataram, I., Jemal, A., et al. (2021). global cancer statistics 2020: GLOBOCAN estimates of incidence and mortality worldwide for 36 Cancers in 185 Countries. *CA Cancer J. Clin.* 71, 209–249. doi: 10.3322/caac.21660

Szklarczyk, D., Gable, A. L., Lyon, D., Junge, A., Wyder, S., Huerta-Cepas, J., et al. (2019). STRING v11: protein-protein association networks with increased coverage, supporting functional discovery in genome-wide experimental datasets. *Nucleic Acids Res.* 47, D607–D613. doi: 10.1093/nar/gky1131

Tang, J., Yan, T., Bao, Y., Shen, C., Yu, C., Zhu, X., et al. (2019). LncRNA GLCC1 promotes colorectal carcinogenesis and glucose metabolism by stabilizing c-Myc. *Nat. Commun.* 10:3499. doi: 10.1038/s41467-019-11447-8

Tang, Z., Li, C., Kang, B., Gao, G., Li, C., and Zhang, Z. (2017). GEPIA: a web server for cancer and normal gene expression profiling and interactive analyses. *Nucleic Acids Res.* 45, W98–W102. doi: 10.1093/nar/gkx247

Tay, Y., Kats, L., Salmena, L., Weiss, D., Tan, S. M., Ala, U., et al. (2011). Coding-independent regulation of the tumor suppressor PTEN by competing endogenous mRNAs. *Cell* 147, 344–357. doi: 10.1016/j.cell.2011.09.029

Tay, Y., Rinn, J., and Pandolfi, P. P. (2014). The multilayered complexity of ceRNA crosstalk and competition. *Nature* 505, 344–352. doi: 10.1038/nature12986

Thomson, D. W., and Dinger, M. E. (2016). Endogenous microRNA sponges: evidence and controversy. *Nat. Rev. Genet.* 17, 272–283. doi: 10.1038/nrg.2016.20

Tong, Y., Ru, B., and Zhang, J. (2018). MiRNACancerMAP: an integrative web server inferring miRNA regulation network for cancer. *Bioinformatics* 34, 3211–3213. doi: 10.1093/bioinformatics/bty320

Ujihira, T., Ikeda, K., Suzuki, T., Yamaga, R., Sato, W., Horie-Inoue, K., et al. (2015). MicroRNA-574-3p, identified by microRNA library-based functional screening, modulates tamoxifen response in breast cancer. *Sci. Rep.* 5:7641. doi: 10.1038/srep07641

Wang, Y., Hou, J., He, D., Sun, M., Zhang, P., Yu, Y., et al. (2016). The emerging function and mechanism of ceRNAs in cancer. *Trends Genet.* 32, 211–224. doi: 10.1016/j.tig.2016.02.001

Williams, K. A., Lee, M., Hu, Y., Andreas, J., Patel, S. J., Zhang, S., et al. (2014). A systems genetics approach identifies CXCL14, ITGAX, and LPCAT2 as novel aggressive prostate cancer susceptibility genes. *PLoS Genet.* 10:e1004809. doi: 10.1371/journal.pgen.1004809

Wong, N. W., Chen, Y., Chen, S., and Wang, X. (2018). OncomiR: an online resource for exploring pan-cancer microRNA dysregulation. *Bioinformatics* 34, 713–715. doi: 10.1093/bioinformatics/btx627

Wu, K., Yu, Z., Tang, Z., Wei, W., Xie, D., Xie, Y., et al. (2020). MiR-877-5p suppresses gastric cancer cell proliferation through targeting FOXM1. *Onco Targets Ther.* 13, 4731–4742. doi: 10.2147/OTT.S251916

Wu, Q., Liu, H. O., Liu, Y. D., Liu, W. S., Pan, D., Zhang, W. J., et al. (2015). Decreased expression of hepatocyte nuclear factor 4alpha (Hnf4alpha)/microRNA-122 (miR-122) axis in hepatitis B virus-associated hepatocellular carcinoma enhances potential oncogenic GALNT10 protein activity. *J. Biol. Chem.* 290, 1170–1185. doi: 10.1074/jbc.M114.601203

Yan, T. H., Qiu, C., Sun, J., and Li, W. H. (2018). MiR-877-5p suppresses cell growth, migration and invasion by targeting cyclin dependent kinase 14 and predicts prognosis in hepatocellular carcinoma. *Eur. Rev. Med. Pharmacol. Sci.* 22, 3038–3046. doi: 10.26355/eurrev_201805_15061

Yang, C., Liu, Z., Chang, X., Xu, W., Gong, J., Chai, F., et al. (2020). NR2F1-AS1 regulated miR-423-5p/SOX12 to promote proliferation and invasion of papillary thyroid carcinoma. *J. Cell. Biochem.* 121, 2009–2018. doi: 10.1002/jcb.29435

Yao, R. W., Wang, Y., and Chen, L. L. (2019). Cellular functions of long noncoding RNAs. *Nat. Cell Biol.* 21, 542–551. doi: 10.1038/s41556-019-0311-8

Zeng, Z., Xu, F. Y., Zheng, H., Cheng, P., Chen, Q. Y., Ye, Z., et al. (2019). LncRNA-MTA2TR functions as a promoter in pancreatic cancer via driving deacetylation-dependent accumulation of HIF-1alpha. *Theranostics* 9, 5298–5314. doi: 10.7150/thno.34559

Zhan, Y., Chen, Z., He, S., Gong, Y., He, A., Li, Y., et al. (2020). Long non-coding RNA SOX2OT promotes the stemness phenotype of bladder cancer cells by modulating SOX2. *Mol. Cancer* 19:25. doi: 10.1186/s12943-020-1143-7

Zhang, G., Lu, J., Yang, M., Wang, Y., Liu, H., and Xu, C. (2020). Elevated GALNT10 expression identifies immunosuppressive microenvironment and dismal prognosis of patients with high grade serous ovarian cancer. *Cancer Immunol. Immunother.* 69, 175–187. doi: 10.1007/s00262-019-02454-1

Zhang, G., and Yang, P. (2017). Bioinformatics genes and pathway analysis for chronic neuropathic pain after spinal cord injury. *Biomed. Res. Int.* 2017:6423021. doi: 10.1155/2017/6423021

Zhang, Q., Liu, W., Zhang, H. M., Xie, G. Y., Miao, Y. R., Xia, M., et al. (2020). HTFtarget: a comprehensive database for regulations of human transcription

factors and their targets. *Genomics Proteomics Bioinformatics* 18, 120–128. doi: 10.1016/j.gpb.2019.09.006

Zheng, X., Carstens, J. L., Kim, J., Scheible, M., Kaye, J., Sugimoto, H., et al. (2015). Epithelial-to-mesenchymal transition is dispensable for metastasis but induces chemoresistance in pancreatic cancer. *Nature* 527, 525–530. doi: 10.1038/nature16064

Zhong, Y., Du, Y., Yang, X., Mo, Y., Fan, C., Xiong, F., et al. (2018). Circular RNAs function as ceRNAs to regulate and control human cancer progression. *Mol. Cancer* 17:79. doi: 10.1186/s12943-018-0827-8

Zhou, W., Chen, L., Li, C., Huang, R., Guo, M., Ning, S., et al. (2020). The multifaceted roles of long noncoding RNAs in pancreatic cancer: an update on what we know. *Cancer Cell Int.* 20:41. doi: 10.1186/s12935-020-1126-1

Zhou, Y., Zhou, B., Pache, L., Chang, M., Khodabakhshi, A. H., Tanaseichuk, O., et al. (2019). Metascape provides a biologist-oriented resource for the analysis of systems-level datasets. *Nat. Commun.* 10:1523. doi: 10.1038/s41467-019-09234-6

Conflict of Interest: The authors declare that the research was conducted in the absence of any commercial or financial relationships that could be construed as a potential conflict of interest.

Publisher's Note: All claims expressed in this article are solely those of the authors and do not necessarily represent those of their affiliated organizations, or those of the publisher, the editors and the reviewers. Any product that may be evaluated in this article, or claim that may be made by its manufacturer, is not guaranteed or endorsed by the publisher.

Copyright © 2021 Luo, Liu, Li, Zhu and Yu. This is an open-access article distributed under the terms of the Creative Commons Attribution License (CC BY). The use, distribution or reproduction in other forums is permitted, provided the original author(s) and the copyright owner(s) are credited and that the original publication in this journal is cited, in accordance with accepted academic practice. No use, distribution or reproduction is permitted which does not comply with these terms.

frontiers in Cell and Developmental Biology

ORIGINAL RESEARCH
published: 29 September 2021
doi: 10.3389/fcell.2021.737723

The Prognostic Model Based on Tumor Cell Evolution Trajectory Reveals a Different Risk Group of Hepatocellular Carcinoma

*Haoren Wang[1,2†], Shizhe Yu[1,3†], Qiang Cai[1], Duo Ma[1], Lingpeng Yang[1], Jian Zhao[1], Long Jiang[1], Xinyi Zhang[1] and Zhiyong Yu[1]**

[1] Department of Hepatobiliary Surgery, The Affiliated Hospital of Yunnan University, Kunming, China, [2] Department of Oncology, The First Affiliated Hospital of Zhengzhou University, Zhengzhou, China, [3] Department of Surgery, The First Affiliated Hospital of Zhengzhou University, Zhengzhou, China

OPEN ACCESS

Edited by:
Ira Ida Skvortsova, Innsbruck Medical University, Austria

Reviewed by:
Tao Wang, Sichuan University, China
Yufang Hou, Institute of Materia Medica, Chinese Academy of Medical Sciences and Peking Union Medical College, China

***Correspondence:**
Zhiyong Yu
xsrsyby@sohu.com

† These authors have contributed equally to this work and share first authorship

Specialty section:
This article was submitted to Molecular and Cellular Oncology, a section of the journal Frontiers in Cell and Developmental Biology

Received: *07 July 2021*
Accepted: *30 August 2021*
Published: *29 September 2021*

Citation:
Wang H, Yu S, Cai Q, Ma D, Yang L, Zhao J, Jiang L, Zhang X and Yu Z (2021) The Prognostic Model Based on Tumor Cell Evolution Trajectory Reveals a Different Risk Group of Hepatocellular Carcinoma. Front. Cell Dev. Biol. 9:737723. doi: 10.3389/fcell.2021.737723

Hepatocellular carcinoma (HCC) is one of the leading causes of cancer-related death worldwide, and heterogeneity of HCC is the major barrier in improving patient outcome. To stratify HCC patients with different degrees of malignancy and provide precise treatment strategies, we reconstructed the tumor evolution trajectory with the help of scRNA-seq data and established a 30-gene prognostic model to identify the malignant state in HCC. Patients were divided into high-risk and low-risk groups. C-index and receiver operating characteristic (ROC) curve confirmed the excellent predictive value of this model. Downstream analysis revealed the underlying molecular and functional characteristics of this model, including significantly higher genomic instability and stronger proliferation/progression potential in the high-risk group. In summary, we established a novel prognostic model to overcome the barriers caused by HCC heterogeneity and provide the possibility of better clinical management for HCC patients to improve their survival outcomes.

Keywords: hepatocellular carcinoma, single-cell transcriptomics, tumor heterogeneity, tumor evolution, copy number aberration, prognosis, cell state transition, genomic diversity

INTRODUCTION

Hepatocellular carcinoma (HCC), with more than one million new cases annually and a 5-year survival rate <20% in most countries, is the fastest growing malignancy both in terms of incidence and mortality (Allemani et al., 2018; Bray et al., 2018). Despite the clinical efficacy of systemic therapies such as tyrosine kinase inhibitors (TKIs) and immune checkpoint inhibitors (ICIs), primary and secondary drug resistance is inevitable and ultimately leads to treatment failure (Llovet et al., 2008, 2018; Abou-Alfa et al., 2018; Pinter et al., 2021). This ability of HCC to adapt to pharmacologic pressures can be described as tumor evolution and can be attributed to the heterogeneity of HCC (Amirouchene-Angelozzi et al., 2017), which refers to the different genetic or epigenetic alterations within the same lesion (intratumor heterogeneity) or in different lesions in the same patient (inter-tumor heterogeneity). Thus, the understanding of the potential mechanisms underlying HCC heterogeneity and its impact on therapeutic intervention is paramount for treatment success and overall survival (OS; Llovet et al., 2021).

The traditional bulk RNA-seq only provides the average number of genes expressed in a pooled population of cells and cannot detect the wide transcriptome heterogeneity in cell populations (Wang et al., 2020). Thus, researchers previously classified cells by purpose-related features and focused on a set of genes, ignoring the continuity of the tumor evolution process (Bidkhori et al., 2018; Chaudhary et al., 2018; Long et al., 2019b; Sarathi and Palaniappan, 2019; Sun et al., 2020; Zhang et al., 2020; Zhu et al., 2020). However, with the advent of single-cell RNA sequencing (scRNA-seq), a novel technology that allows transcriptomic analyses of individual cells, researchers can explore the heterogeneity and plasticity of tumor cells, which can result in early recurrence and drug resistance in the process of tumor evolution on single cell resolution. Given the large number of cells, we can reasonably hypothesize that the sequencing results include every distinct point of the dynamic process (Losic et al., 2020; Marjanovic et al., 2020; Rajewsky et al., 2020; Sun et al., 2021). Several studies have profiled the single-cell landscape of tumor generation and progression (Kim et al., 2018; Durante et al., 2020; Losic et al., 2020; Marjanovic et al., 2020). Furthermore, scRNA-seq is a promising tool that can facilitate individualized therapy owing to its ability to define cell subsets with potential treatment targets.

Here, we reconstructed the evolution trajectory of tumor cells with the help of scRNA-seq data and established a prognostic model to classify different risk groups of HCC. Our findings provide a strategy for precision medicine on the basis of tumor heterogeneity, and we also identified a wide range of potential therapeutic targets, thus improving the survival of patients with HCC.

MATERIALS AND METHODS

Data Sources

The normalized gene-level RNA-Seq data and clinical information for 364 patients LIHC-TCGA cohorts were downloaded from UCSC Xena[1] with R package UCSC Xena Tools (Wang and Liu, 2019). To obtain 258 patients LIRI-JP validation set, RNA-seq data, and related clinic pathological data were downloaded from the ICGC website[2] (Zhang J. et al., 2019). The scRNA-seq barcode sequences and raw gene expression matrix were downloaded from the CNP0000650 (Sun et al., 2021). Mutation data that contained somatic variants were stored in Mutation Annotation Format (MAF) form and were downloaded from Genomic Data Commons (GDC).[3]

Processing of Single-Cell RNA-Seq Data

Dimension Reduction and Unsupervised Clustering

Single-cell RNA sequencing data were processed for dimension reduction and unsupervised clustering by following the workflow in Seurat (v4.0.2) (Butler et al., 2018). In brief, first, the read counts for each cell were divided by the total counts for that cell and multiplied by the scale factor (10,000), and then natural-log transformed. A principal component analysis (PCA) matrix with 50 components were calculated to reveal the main axes of variation and the data were denoised by using "Run PCA" function with default parameter. For visualization, the dimensionality of each dataset was further reduced using Uniform Manifold Approximation and Projection (UMAP) implemented in "Run UMAP" function (Becht et al., 2019). We retained cell clustering based on the original study. The cluster-specific marker genes were identified by using the "Find All Markers" function with MAST algorithm (Finak et al., 2015).

Define Subpopulations of Aneuploid Tumor Cells

TPM gene expression matrix was extracted from the Seurat object as recommended in the "prepare the read count input file" section (CopyKAT). For each patient, normal reference T cells and malignant cells were selected and identified from the annotated clusters as determined above. Quality control filtering was performed to select the highest quality cells by only including malignant cells with at least five genes in each chromosome to calculate DNA copy numbers. We extracted aneuploid cells that are considered as tumor cells in aneuploid tumors to define two copy number subpopulations of single tumor cells using default parameters in CopyKAT (Gao et al., 2021).

Construct Tumor Cell Evolution Trajectory

Malignant cells were identified from the annotated clusters as determined above. This resulted in six high-quality malignant clusters to use for this analysis. Single-cell pseudo-time trajectories were constructed with Monocle 2 (2.10.1) (Qiu et al., 2017). Genes for trajectory inference were selected using the "dispersion table" function to calculate a smooth function describing how variance in each gene's expression across cells varies according to the mean. Only genes with mean expression greater than or equal to 0.1 were used for the analysis. The "reduce Dimension" function was utilized with the DDRTree reduction method with default parameters. Results were visualized using the "plot cell trajectory" and "plot complex cell trajectory" functions and annotated with cell type, subclones, and calculated cell states. Once the pseudo-space trajectory was defined, we used the Tradeseq (Trajectory Differential Expression analysis for Sequencing data) R package to select genes that were differentially expressed along the trajectory (Van den Berge et al., 2020). Association Test function was used to test whether the average gene expression is significantly changing along pseudotime. The top 500 gene upregulated genes and Top 500 downregulated genes decrease along the inferred pseudo-time trajectory with a q-value less than 0.01 were separated with hierarchical clustering using the "plot multiple ranches heatmap" function with num clusters = 3 and "branches" set to the terminal branchpoints for aneuploid tumor cells.

Development and Validation of the Tumor Evolution Signature for Hepatocellular Carcinoma

Select differential genes based on single cell tumor evolution trajectory to reduce the impact of non-tumor cells. The cases from the TCGA LIHC datasets were used as the training cohort

[1] https://xenabrowser.net/

[2] https://dcc.icgc.org/projects/LIRI-JP

[3] https://portal.gdc.cancer.gov/

to establish the LASSO model. Univariate analysis and logRank test were used to identify genes with prognostic ability. For the genes with prognostic ability, Cox proportional hazards model (iteration = 1,000) with a lasso penalty was used to find the best gene model utilizing an R package called "glmnet" (Friedman et al., 2010). The best gene model was used to establish the tumor evolution signature. The risk score for each patient was calculated with the LASSO model weighting coefficient as follows:

$$riskscores = \sum_{i=1}^{n} Coef_j * X_j$$

In this formula, n represents the number of key genes, $Coef_j$ is the LASSO coefficient of Gene j, and X_j is the normalized expression value of Gene j (**Supplementary Table 4**). Then, the concordance (c)-index proposed by Harrell[24] was applied to validate the predictive ability of the signature in all datasets, by using the "survcomp" R package (Haibe-Kains et al., 2008). The larger c-index indicated the more accurate predictive ability of the model.

Survival Analysis

To verify the trend of this tumor evolution trajectory, Kaplan–Meier (K–M) analysis was performed. The top 10 end-genes were extracted and the potential prognostic significance of these genes was assessed with the LIHC data from GEPIA2.[4] The K–M survival curves were also generated to graphically demonstrate the OS to the high-risk group and low-risk group, which were stratified by the tumor evolution signature. The R package called "survminer" was utilized to perform the survival analysis, and the optimal cutoff was ascertained by the "surv_cutpoint" function.

Somatic Mutation and Copy-Number Aberration Analysis

Mutation comment file (MAF) of TCGA-LIHC cohort was downloaded from the GDC client. Differential analysis and visualization of somatic mutations was done using Maftools (The Cancer Genome Atlas Research Network et al., 2013; Mayakonda et al., 2018). This difference between high- and low-risk group was detected using function "mafComapre," which performs Fisher's exact test on all genes between two groups to detect differentially mutated genes.

Composite copy number profiles were generated to highlight differences between high- and low- risk group. Segment file of TCGA-LIHC cohort was downloaded from FIREHOSE and samples were further divided into high- and low-risk groups. Then we ran the GISTIC 2.0 pipeline to generate discrete copy number data file. Chromosomes reference objects were from the "BSgenome.Hsapiens.UCSC.hg19" R package.

As in the previous study, a non-synonymous mutation from the TCGA database was used as the raw mutation count, and it was divided by 38 MB to quantify TMB (Chalmers et al., 2017). The samples were sorted according to the value of the median TMB from low to high.

[4]http://gepia2.cancer-pku.cn/#index

Bioinformatics Analyses

Gene Enrichment Analysis (GSEA) was further used to investigate the functional enrichment of risk score-associated genes using the R package "clusterProfiler" (Yu et al., 2012). The Benjamini–Hochberg method was used to adjust nominal p-values (false discovery rate, FDR) for multiple testing.

The Maftools package was used to illustrate the respective mutation profiling of the two risk group levels by waterfall plot, and differentially mutated genes were identified by using the "mafCompare" function where genes mutated in greater than 5% of LIHC samples in the TCGA cohort were considered (Mayakonda et al., 2018).

Statistical Analysis

Student's *t-test* was conducted to make statistical comparison. The "pheatmap" R package was applied to generate heatmaps. Survival analysis was completed using Kaplan–Meier method, and the prediction performance of the risk model was evaluated using receiver operating characteristic (ROC) *via* "time-ROC" R package. Multivariate COX regression analyses were used to investigate the prognostic value of risk-score. Hazard ratio (HR) and 95% confidence intervals (CI) for each variable were also calculated where needed. A value of $p < 0.05$ was defined as statistically significant difference. All of our analyses were conducted using R software version 4.0.2.[5]

The whole process of data analysis is depicted in **Figure 1**.

RESULTS

Classification of the Malignant Cell Clusters With Single-Cell RNA Sequencing Data

Unsupervised dimensionality reduction and graph-based clustering analysis were performed with the data from CNP0000650, and 24 clusters (**Figure 2A**) were visualized by the UMAP method (Becht et al., 2019; Sun et al., 2021). The immune cells mainly consisted of myeloid-derived cells, T cells, B cells, plasma cells, and natural killer (NK) cells, while non-immune cells included endothelial cells, hepatic stellate cells, apparently normal epithelial cells, and HCC malignant cells. To contrast the difference among different patients, we classified the cells by patient origin (**Figure 2B**), and the result showed that tumor cells contained obvious heterogeneity, while non-tumor cells kept homogeneous, proving that the differences between tumor cell clusters are mainly due to the tumor heterogeneity, rather than batch effects between samples. No normal liver cells were detected, likely because of the technical limitations, resulting in no comparison between normal and malignant liver cells.

We further extracted the varied tumor cell clusters for the analysis of tumor heterogeneity (**Figure 2C**), and two major sub-clones were defined by the clustered heat maps of single cell copy number profiles (**Figure 2D**). Compared with sub-clone 2 (green), the heatmap showed that sub-clone 1 (red)

[5]https://www.r-project.org/

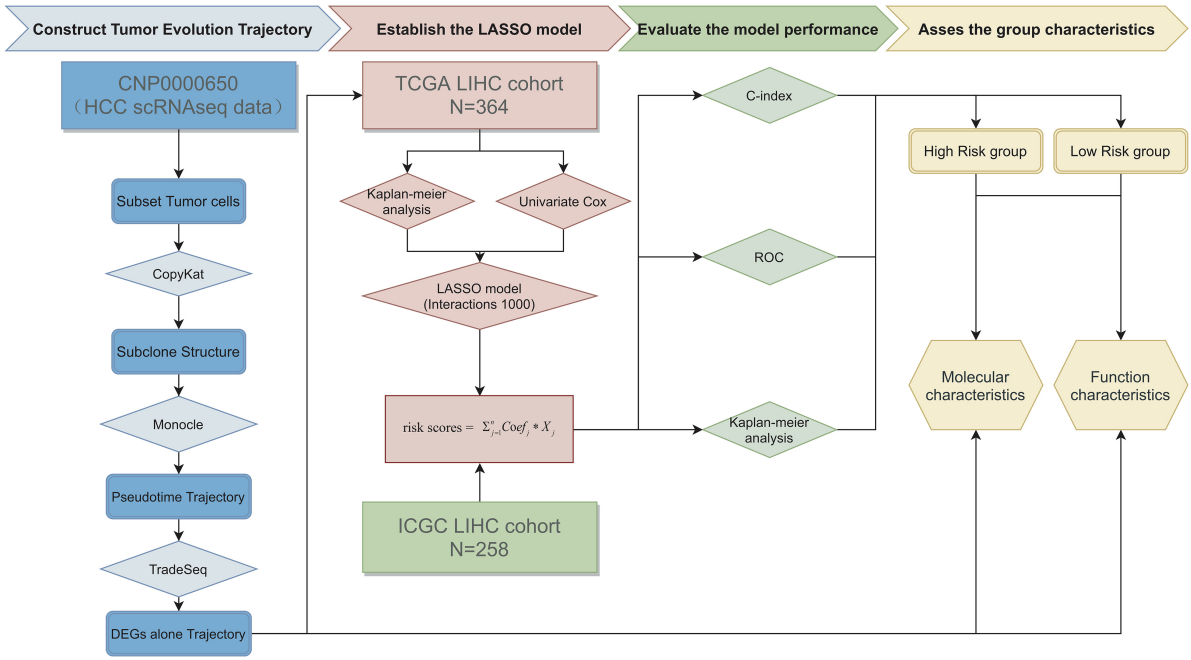


FIGURE 1 | The whole process of data analysis.

contained more CNAs, implying that sub-clone 1 might be more malignant (**Figure 2E**).

Reconstruction of Tumor Cells Progression Trajectory

To determine the relationship between malignant cell clusters, we performed single-cell trajectory analysis with scRNA-seq data using Monocle (Qiu et al., 2017). As is well known, genomic mutations accumulate over time in the process of tumor evolution (Turajlic et al., 2019; Craig et al., 2020; Losic et al., 2020). Thus, we defined the cell cluster with a lower CNA burden as the root, while the cell cluster with a higher CNA burden was defined as the end of the trajectory. We noticed that sub-clone 2, comprising cells with obvious liver characteristics, was concentrated at the beginning of the trajectory, while sub-clone 1, comprising cells with less specificity of origins, was concentrated at the end of the trajectory, indicating that the trajectory model fits the process of tumor evolution well (**Figures 3A,B**).

During the process of transition of tumor cells from a lower to higher malignant state, some genes are silenced, while others become newly active. We used Tradeseq, a powerful generalized additive model framework based on the negative binomial distribution, to interpret the within lineage differential expression (**Figure 3C** and **Supplementary Table 1**). To verify the malignant trend of this trajectory, we extracted the top 10 downregulated genes (root genes) and top 10 upregulated genes (end genes) for Kaplan–Meier (K-M) analysis. The high expression of the top 10 root genes represented a benign prognosis, while the high expression of the top 10 end genes represented a poor prognosis (**Figures 3F,G**). Furthermore, along the trajectory, liver characteristics such as *ALB* (**Figure 3D**) were gradually lost, while stemness and malignant marker genes such as *TWIST1* (**Figure 3E**), gradually increased, suggesting that the malignant state was advancing.

The gene set variation analysis (GSVA; Hänzelmann et al., 2013) was used to further analyze the underlying biological processes along the trajectory. In the Molecular Signature Database (MSigDB) "hallmark" collection of major biological categories (Liberzon et al., 2015), the upregulated genes of sub-clone 1 were enriched in the tumor-promoting pathway ("Wnt/β-catenin signaling") and proliferation pathway ("G2M checkpoint," "E2F Targets," "MYC Targets"), while the downregulated genes of sub-clone 1 were enriched in the tumor-suppressor pathway ("P53 pathway") and essential liver function pathway ("Complement," "Fatty acid metabolism," "Adipogenesis") (**Figure 3H**), which were consistent with the characteristics of cells that progressed from the lower malignant state to the higher malignant state (Maley et al., 2017; Losic et al., 2020; Marjanovic et al., 2020; Llovet et al., 2021).

Establishment of the 30-Gene Prognostic Model

Although the top 10 genes had a certain predictive effect, we preferred optimizing gene combination to obtain a better prognostic model. With the selection criteria of $p < 0.01$, the intersection of univariate Cox regression analysis and K-M analysis identified 200 credibly survival-related genes. We used TCGA data as the training cohort and ICGC data as the external validation cohort (The Cancer Genome Atlas Research Network et al., 2013; Zhang J. et al., 2019). Lasso-penalized Cox

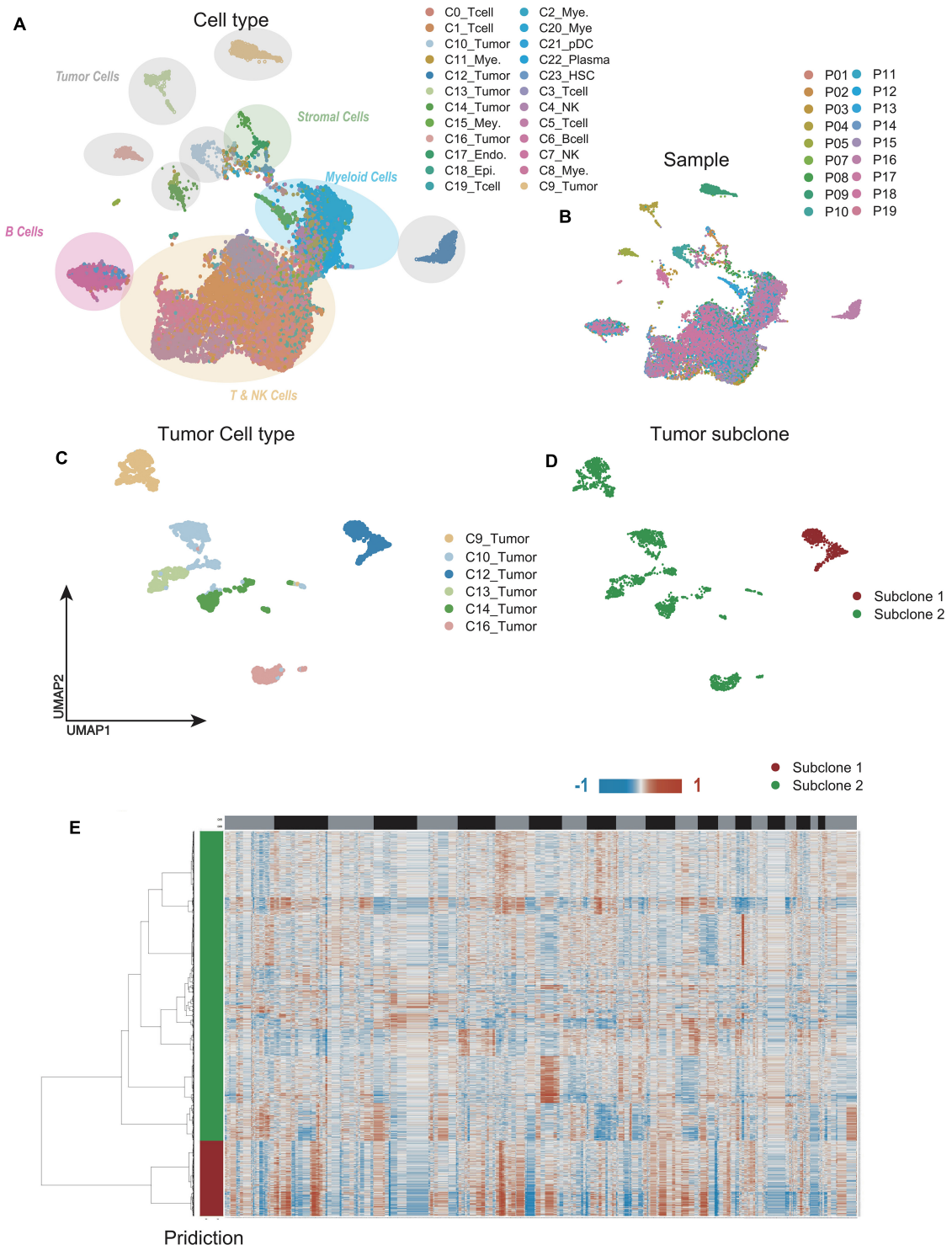


FIGURE 2 | Single-cell RNA sequencing (scRNA-seq) profiling of different malignant cell clusters. **(A,B)** The Uniform Manifold Approximation and Projection (UMAP) plot showing the annotation and color codes for cell types in hepatocellular carcinoma (HCC) **(A)**. Cells were further shown in different color by patient origin **(B)**. **(C)** The UMAP plot, showing only malignant cell clusters by Louvain algorithm. **(D)** With CopyKAT, malignant cell clusters were delineated into two subclones by single-cell copy number profiles inferred from scRNA-seq data. **(E)** Clustered heat maps of single HCC malignant cell copy number profiles in two major subclones.

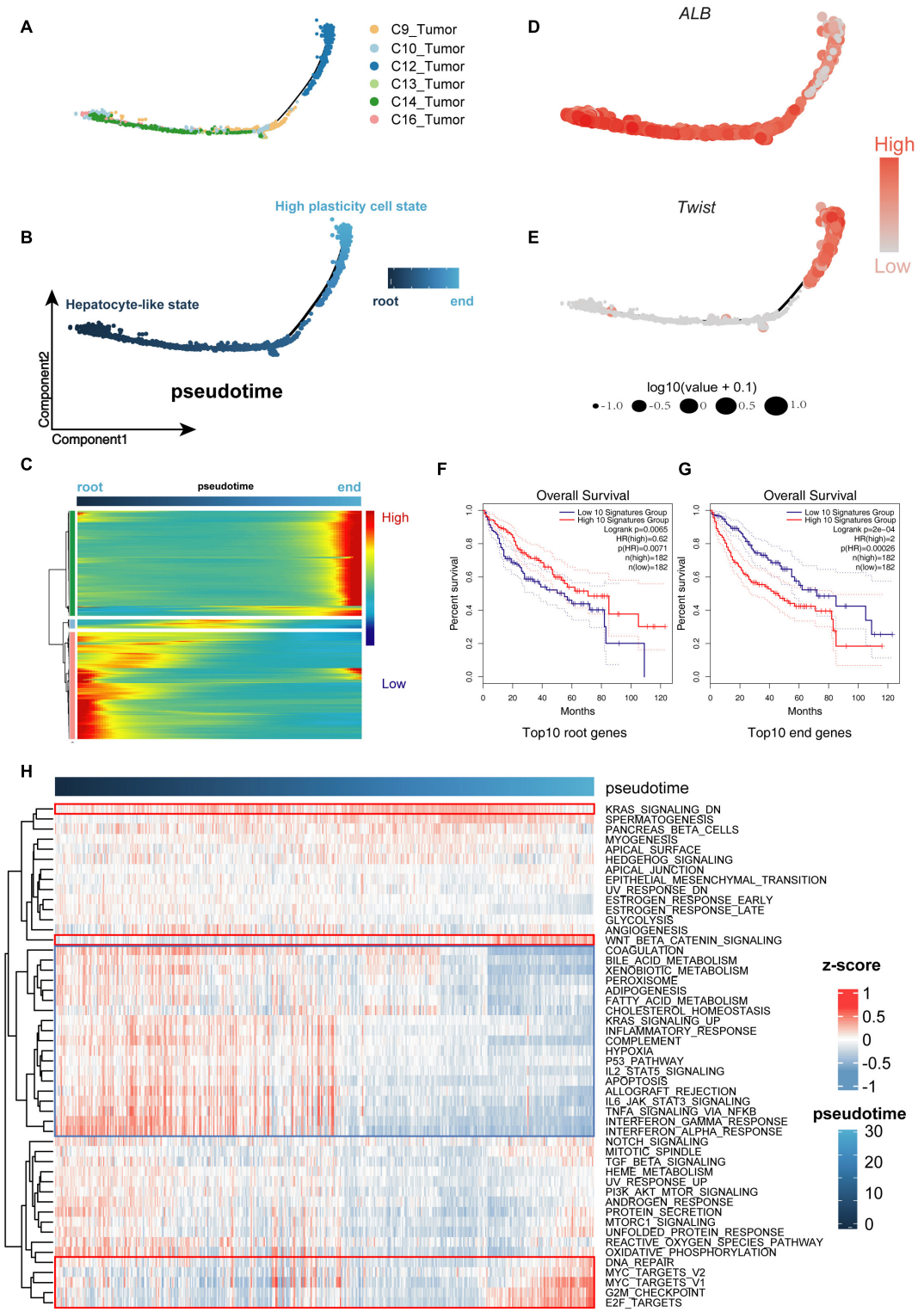


FIGURE 3 | Cells were sorted by progression from lower malignant state to higher malignant state. **(A,B)** Cell Trajectory performing the route of low- to high-malignant cells, which can serve as a model to describe malignant cell differences. **(C)** Expression levels for differentially expressed genes (rows), with cells (columns) shown in pseudo-time order. **(D,E)** ALB and Twist genes confirming the trusty of the cell progression trajectory model. **(F,G)** The Kaplan–Meier (K-M) analysis of the top 10 downregulated genes (root genes) and top 10 upregulated genes (end genes) from 1,000 differential genes group capturing the overall survival (OS) differences between low- and high-malignant cell groups. **(H)** Gene set variation analysis (GSVA) heat map showing the mainly differential signaling pathways between low- and high-malignant cell groups.

analysis was subsequently performed 1,000 times in the TCGA training cohort with 10-fold cross-validation to evaluate and eliminate variables that contributed less to the model, and a 30-gene signature with the most powerful predictive features were selected (**Figures 4A**,**C**,**D**). To validate the credibility of this model, C-index was assessed in the TCGA training cohort and ICGC validation cohort, which was confirmed as 0.79 and 0.73, respectively (**Figure 4B**), suggesting that our model had favorable efficacy for predicting prognosis (Harrell, 1982). Based on the 30-gene prognostic model, TCGA and ICGC samples were clustered into high-risk and low-risk groups, and the OS time of patients in the high-risk group was remarkably decreased (**Figures 4E**,**F**).

Evaluation of the Prognostic Model in TCGA Cohort and ICGC Cohort

The K–M analysis and time-dependent ROC was used to assess the prognostic capacity of the 30-gene prognostic model in the TCGA cohort and ICGC cohort, respectively. The K–M analysis illustrated that patients in the low-risk group had significantly longer OS than those in the high-risk group, both in the TCGA cohort (**Figure 5A**) and the ICGC cohort (**Figure 5B**). The area under the ROC curve (AUC) for the 1-, 3-, and 5-year OS was 0.843, 0.848, and 0.824 in the TCGA cohort, while it was 0.77, 0.796, and 0.774 in the ICGC cohort (**Figures 5C**,**D**), indicating that this 30-gene prognostic model had high sensitivity and specificity for survival prediction.

Gender, age, stage, vascular invasion, bile duct invasion, fibrosis, and the risk score of the prognostic model were included in the multivariate Cox regression model, and the risk score was revealed to be independent predictor for OS, showing splendid predictive performance ability, with HR: 6.432, 95% CI: 4.095–10.103, $p < 0.001$ in TCGA cohort, and HR: 3.751, 95% CI: 1.419–9.918, $p < 0.001$ in ICGC cohort. Taken together, the 30-gene prognostic model was completely reliable for the precise prediction of OS in HCC (**Figure 5E**).

Comparison of Genomic Aberrations in Different Risk Groups

Increasing mutation frequency is a typical feature of human cancer. To identify the divergence of genomic aberrations between the high-risk and low-risk groups in the TCGA database, CNAs data were downloaded from the GDC portal and analyzed with GISTIC 2.0, with which the high-risk group had an obviously higher genomic aberration burden than the low-risk group (**Figure 6A**). Meanwhile, the top 20 genes with high genomic mutation frequency in the high-risk and low-risk groups were constructed by Maftools (Mayakonda et al., 2018; **Figures 6B**,**C**). To analyze the discrepancy between the high-risk and low-risk groups, the differentially mutated gene type and frequency were compared by Fisher's exact tests. The results showed three significantly differential genes—*TP53* (47 versus 19%), *OBSCN* (18 versus 5%), and *RB1* (11 versus 2%) (**Figure 6D**). The six genes most recurrently mutated were *TP53* (47 versus 19%), *TTN* (31 versus 27%), *CTNNB1* (26 versus 28%), *MUC16* (19 versus 16%), *OBSCN* (18 versus 5%), and *ALB* (12 versus 13%) (**Figure 6E** and **Supplementary Table 2**). These findings suggested that some mutated genes such as *TP53* and *OBSCN* that were notably different compared with the high-risk and low-risk groups could be related to the malignant progression and can continuously accumulate mutations over time; whereas, the others such as *CTNNB1* and *ALB*, which remained stable from the low-risk state to high-risk state, likely contribute to the essential neoplastic process rather than malignant progression.

The tumor mutation burden (TMB) is also considered an essential factor impacting on the occurrence and progression of the tumor. The distribution plot shows TMB distribution of different cancer types (**Figure 6F**). The three types including low-risk HCC, all HCC samples (liver hepatocellular carcinoma, LIHC), and high-risk HCC were apparently distinct from each other, and the TMB gradually increased from low-risk type to high-risk type, which suggested that our model had excellent distinguishing capability.

Gene Enrichment Analysis of the 30-Gene Prognostic Model

To explore the underlying molecular mechanisms of this prognostic model, we conducted GSEA to compare the low-risk group with the high-risk group in TCGA cohorts (Yu et al., 2012). In the MsigDB "hallmark" collection of major biological categories, proliferative signaling pathways ("E2F targets," "G2M checkpoint," "KARS signaling"), and the invasion and metastasis-related signaling pathways ("EMT" and "myogenesis") were dramatically increased in the high-risk group (**Figure 7B**). This was consistent with the data at the single-cell level. Notably, the low-risk group was enriched in inflammation-related gene pathways such as "inflammatory response," "interferon-α response," and "interferon-γ response," which suggested that the secretion of inflammatory factors might originate from the tumor cells, indicating a strong proinflammation potential in the early tumorigenesis stage (**Figure 7A**). A similar phenomenon had been reported in melanoma, breast cancer, and colorectal cancer, where the expression of immune-related genes was also presented by tumor cells and could likely be an independent influence on their prognostic differences (Sconocchia et al., 2014; Forero et al., 2016; Buetow et al., 2019; McCaw et al., 2019; Jin et al., 2020).

DISCUSSION

Hepatocellular carcinoma is one of the leading causes of cancer-related mortality worldwide. Previous studies have proved that the heterogeneity, which was thought to be evolutionarily selected for increasing fitness of tumor cells, might be the major barrier for improving patients outcome (Chaudhary et al., 2018; Llovet et al., 2018, 2021; Long et al., 2019b,a; Yang et al., 2019; Craig et al., 2020). Thus, there is a critical need to stratify HCC patients accurately on the basis of heterogeneity and provide precise treatment strategies.

In this study, we analyzed CNAs in tumor cells using CopyKat and classified them into two major subclones, wherein subclone 1 had a higher CNA burden than that of subclone 2. Then, we defined the cells in hepatocyte-like state as the root and cells in high-plasticity state as the end, and

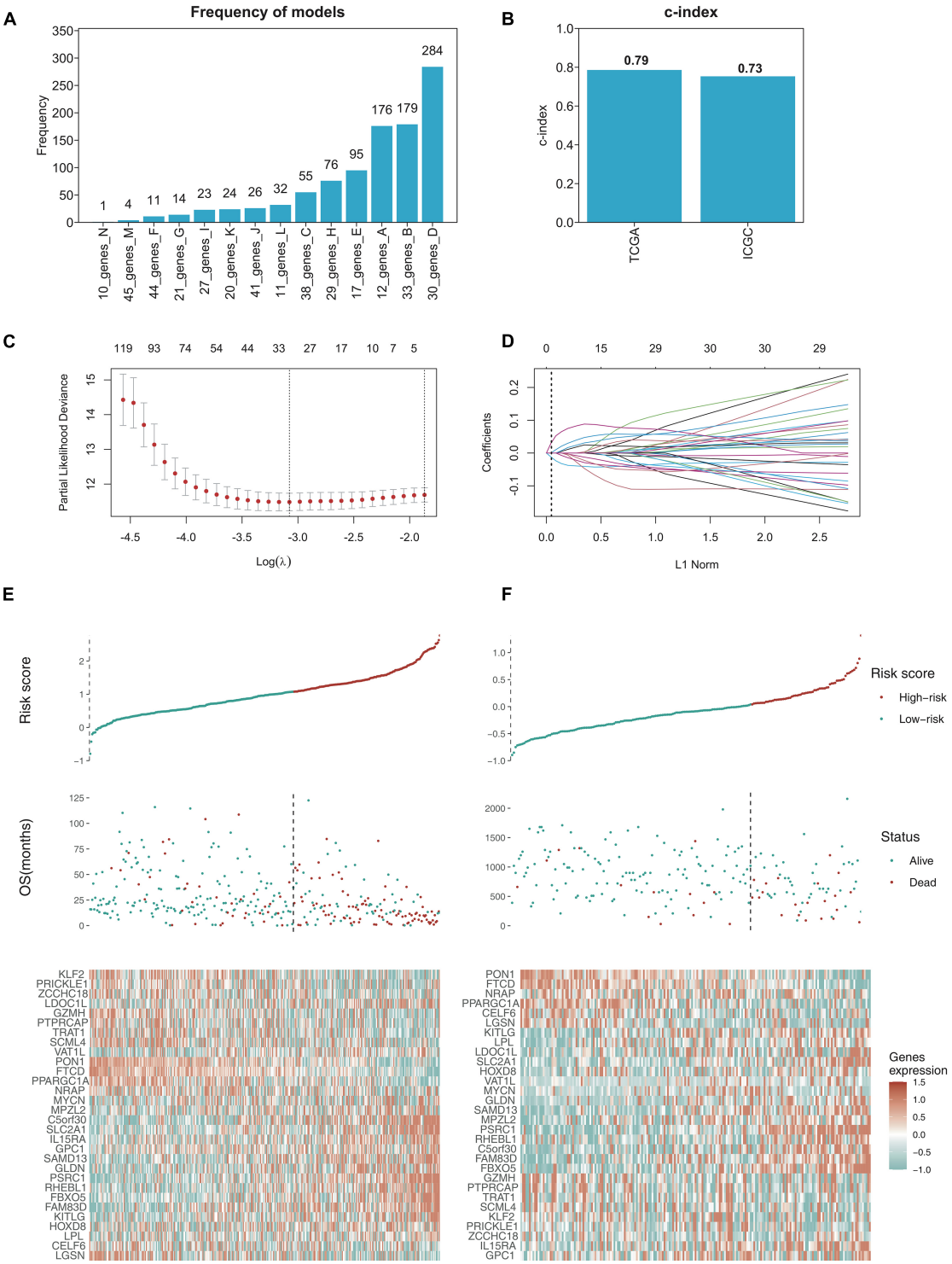
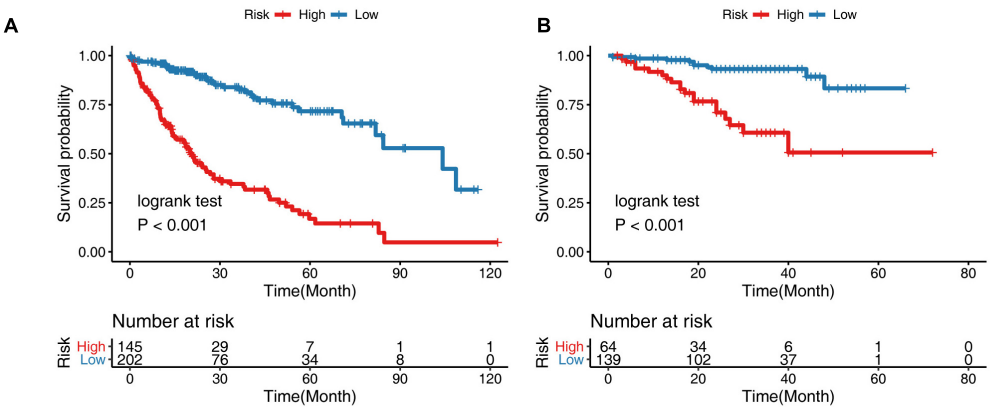
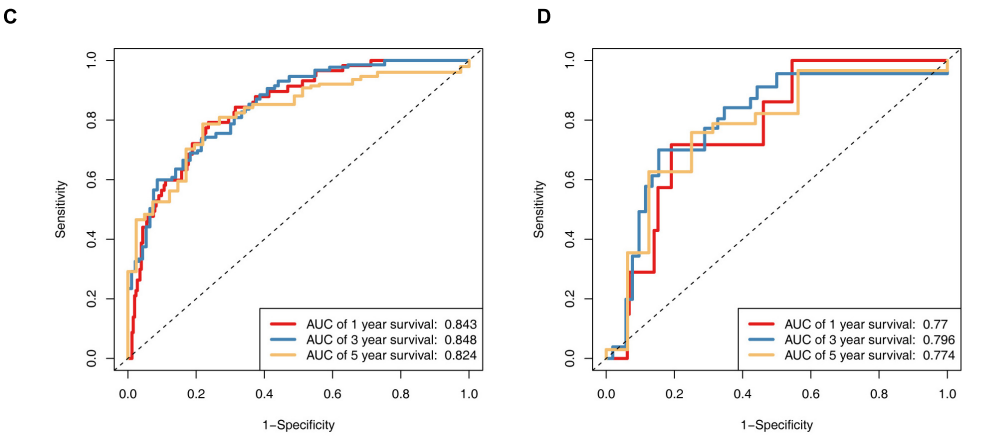


FIGURE 4 | Establishing the 30-gene prognostic model with LASSO regression analysis. **(A)** LASSO regression analysis performed the frequency of different gene combination models and finally determined the 30-gene signature for OS prediction. **(B)** C-index of 30-gene prognostic model was 0.79 in TCGA training cohort, while 0.73 in ICGC validation cohort. **(C)** LASSO coefficient profiles of the gene features. **(D)** Ten-time cross-validation for tuning parameter selection in the LASSO model. **(E,F)** The risk score distribution and survival status distribution of 30-gene prognostic model in TCGA training cohort and ICGC validation cohort, and the heat map of gene expression are shown below with color, red (high) and green (low).





E

Variable	HR	lower 95%CI	upper 95%CI	pvalue
TCGA				
GENDER MALE	0.725	0.463	1.138	1.62e−01
AGE	1.016	0.999	1.033	7.34e−02
AJCC_STAGE1 Stage II	0.828	0.437	1.569	5.63e−01
AJCC_STAGE1 Stage III&IV	1.183	0.680	2.060	5.52e−01
VASCULAR_INVASION Micro	0.802	0.460	1.398	4.36e−01
VASCULAR_INVASION Macro	0.910	0.413	2.002	8.14e−01
risk.score	6.432	4.095	10.103	6.46e−16
ICGC				
AGE	1.009	0.970	1.050	6.42e−01
GENDER Male	0.347	0.152	0.795	1.23e−02
T_stage II	2.213	0.494	9.913	2.99e−01
T_stage III	4.078	0.850	19.577	7.90e−02
T_stage IV	8.860	1.636	47.982	1.14e−02
VEIN_INVASION	1.569	0.803	3.068	1.88e−01
BILE_DUCT_INVASION	0.749	0.314	1.788	5.15e−01
FIBROSIS	1.052	0.779	1.423	7.40e−01
risk.score	3.751	1.419	9.918	7.69e−03

FIGURE 5 | Prognostic performance of 30-gene signature in TCGA Training Cohort and ICGC Validation Cohort. **(A,B)** K–M survival curve for risk score in TCGA training cohort **(A)** and ICGC validation cohort **(B)**. **(C,D)** Receiver operating characteristic (ROC) curve of the 30-gene prognostic model in TCGA cohort **(C)** and ICGC cohort **(D)**. **(E)** Multivariate Cox regression analysis of clinical parameters and prognostic model for OS.

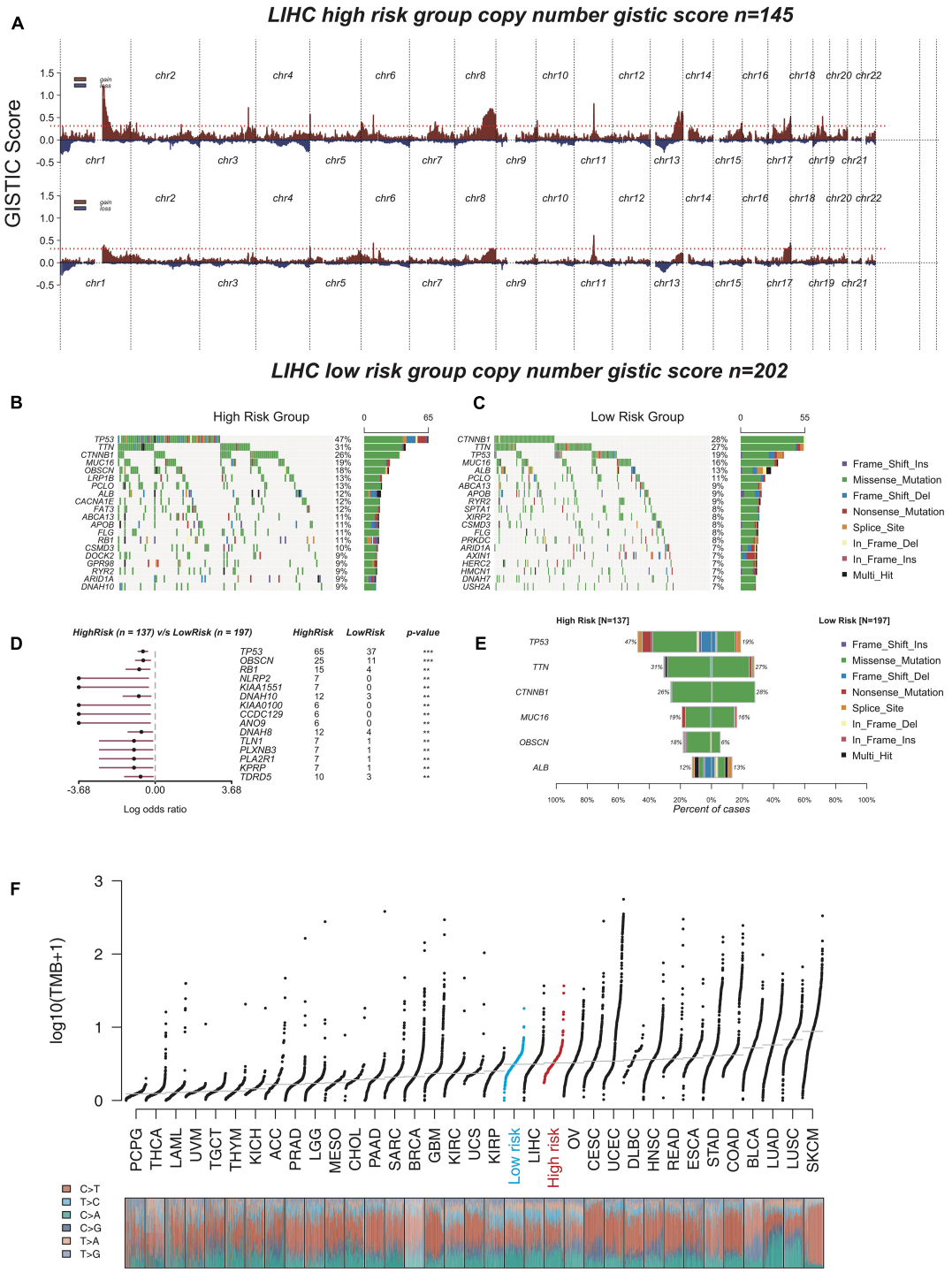


FIGURE 6 | The analysis of genomic aberrations in high-risk group and low-risk group. **(A)** Recurrent copy number aberrations of high-risk group and low-risk group in TCGA cohort. Regions of recurrent copy number amplifications (red) and deletions (blue) were above and below baseline (0.0), respectively, in the targeted array were identified by GISTIC 2.0. (Red line represented GISTIC score of 0.3). **(B,C)** Oncoplot displaying the somatic landscape of high-risk group **(B)** and low-risk group **(C)**. Genes were arranged according to their mutation frequency. The *Y*-axis was the gene name and the abscissa was the sample name. Different colors represented different mutation types. **(D)** Forest plot showed differentially mutated genes between high-risk group and low-risk group. The adjacent table included the number of samples in high-risk group and low-risk group with the mutations in the highlighted gene. The *p*-value indicated significance threshold: ***$p < 0.001$; **$p < 0.01$; Fisher's exact test. **(E)** Co-bar plots showed the most recurrently mutated genes in high-risk group and low-risk group. **(F)** The distribution plot shows tumor mutation burden (TMB) distribution of different cancer types. Liver hepatocellular carcinoma (LIHC) patients were divided into low-risk group and high-risk group.

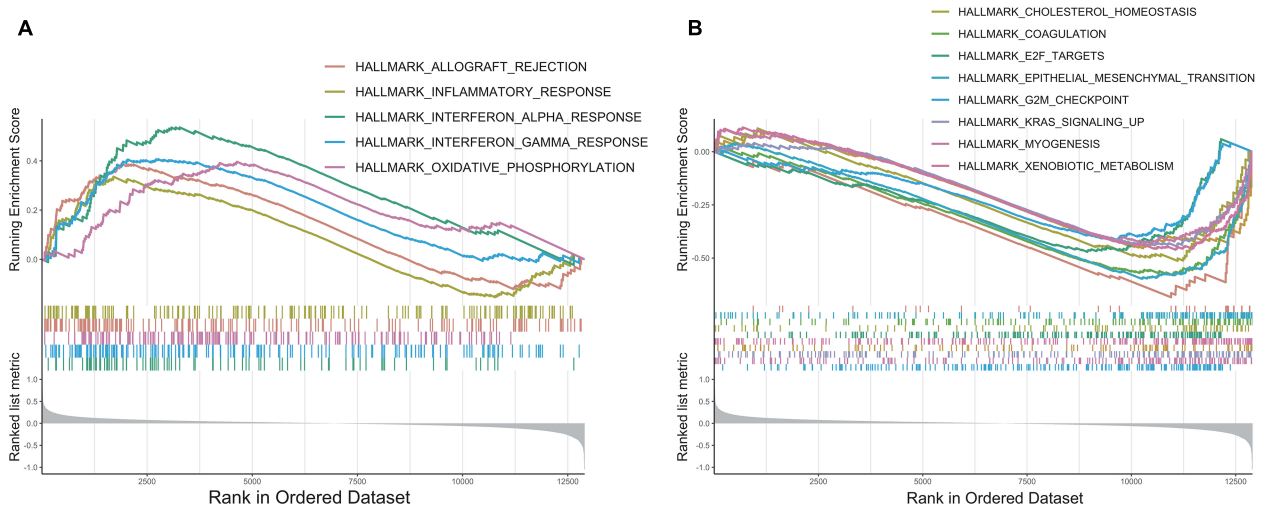


FIGURE 7 | GSEA enrichment analysis. **(A)** The enrichment plot of upregulated gene sets in low-risk group. **(B)** The enrichment plot of downregulated gene sets in low-risk group.

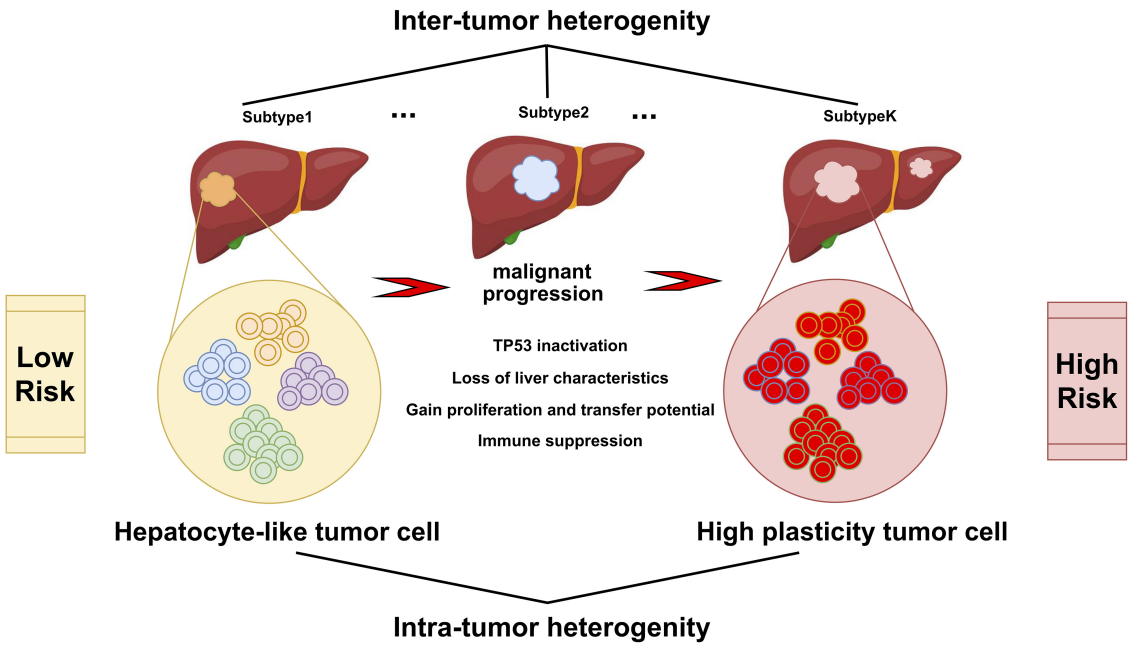


FIGURE 8 | Varied malignant cell subgroups contribute to the inter-tumor and intra-tumor heterogeneity of HCC. Hepatocyte-like tumor cells could progress to high plasticity tumor cells, accompanied by the inactivation of tumor suppressor pathways such as TP53, the disappearance of the inherent characteristics of hepatocytes, the enhancement of proliferation, invasion and metastasis ability, and the appearance of immune suppression.

reconstructed the tumor evolution trajectory with the help of scRNA-seq data. Consistent with previous studies of other tumors (Zhang L. et al., 2019; Marjanovic et al., 2020), GSVA analysis revealed that along the trajectory, cells gradually lost their intrinsic characteristics and transformed into a high plasticity state. Based on this evolutionary trajectory, we further constructed a 30-gene prognostic model. C-index and multivariate analysis confirmed that compared with the other three existing prognostic models (Bidkhori et al., 2018; Chaudhary et al., 2018; Liang et al., 2020; Sun et al., 2020; Zhang et al., 2020; Deng et al., 2021), this model possessed high predictive efficacy and accuracy. Finally, we also performed GSEA analysis to explore the underlying biological mechanisms of this model.

To investigate the heterogeneity and potential progression trajectory of HCC cells on single-cell resolution, high-quality scRNA-seq data were necessary. Thus, we reviewed associated studies of liver cancer published in recent years to identify the

most suitable single-cell dataset (**Supplementary Table 3**; Zheng et al., 2018; Ma et al., 2019; Zhang Q. et al., 2019; Losic et al., 2020; Sharma et al., 2020; Sun et al., 2021). Two key points need to be considered, namely, the number of tumor cells and the quality of sequencing data. Dissociating tissues is one of the difficulties of single-cell sequencing. Epithelial cells require more stringent dissociation conditions than immune cells and need to be enriched with FACs. However, in early studies, few authors noticed this point, making their results got a large proportion of immune cells and stromal cells instead of tumor cells. This was also the reason why some HCC studies focused on the immune microenvironment (Ma et al., 2019; Ramachandran et al., 2019; Massalha et al., 2020; Sun et al., 2021). To obtain enough cells, we narrowed the range into the data of Sun and Sharma (Sharma et al., 2020; Sun et al., 2021). Regarding the quality of sequencing data, a major factor is the sequencing platform. The plate-based SMART-seq2 full-length method provides in-depth coverage for a smaller number of cells, but the droplet-based 10× Genomics Chromium approach captures cells on a larger scale but with the limitation of inadequate gene coverage. The gene capturing rate of 20 cells by SMART-seq2 was comparable with that of 1,000 cells by 10× (Ding et al., 2019; Zhang Q. et al., 2019). Unfortunately, at least half of the tumor cells from the data of Sharma et al. (2020) based on the 10× platform, could not meet the input threshold of CopyKat, which would introduce a large bias in the downstream analysis (Sharma et al., 2020; Gao et al., 2021). To explore a more refined dynamic change process, we finally chose the data of Sun et al. (2021) for the downstream analysis.

As our model was based on tumor heterogeneity and the trajectory was highly similar to the natural process of tumor evolution, genes included in this model and the underlying biological mechanisms were complicated. Some upregulated genes were found to be associated with cell proliferation and progression. The upregulation of *GPC1* had been reported to be dramatically correlated with the reduced OS time for HCC patients (Wang et al., 2021). *MYCN*, a member of the *Myc* family, was positively correlated with the recurrence of *de novo* HCC (Qin et al., 2018). Furthermore, *EVA1* expression was significantly increased in HCC and was also associated with a poor prognosis and recurrence in these patients. Overexpression of *EVA1* promoted cell growth, invasion, and migration *in vitro*, while knockdown of *EVA1* expression inhibited proliferation and migration *in vitro* (Ni et al., 2020). Some downregulated genes were considered to function as tumor suppressor genes, such as *PPARGC1A*, also known as *PGC-1*α, a master regulator of mitochondrial biogenesis and oxidative phosphorylation. A previous study had reported that low levels of *PPARGC1A* expression were correlated with poor survival, vascular invasion, and large tumor size (Huang et al., 2020; Zuo et al., 2021). *PRICKLE1* has been reported to be a negative regulator of the Wnt/beta-catenin signaling pathway and is a putative tumor suppressor gene in HCC (Chan et al., 2006).

Our study has some limitations. First, RNA-Seq detected more of the content specific to Affymetrix and Illumina microarrays than either of the microarray platforms on the same samples, and many of the feature genes included in our analysis were not detected on the microarray platform (Zhao et al., 2014). Thus, we only used cohorts based on RNA-seq platform. Second, our retrospective findings need to be further validated in prospective research, and complex mechanisms involved in the progression of liver cancer cells still need to be further explored.

In conclusion, this study integrated the scRNA-seq data and bulk multi-omics data to reconstruct the tumor evolution trajectory and establish a novel prognostic model to clarify different risk groups of HCC, which might help in clinical decision making for individual treatment and improve patient outcomes (**Figure 8**).

DATA AVAILABILITY STATEMENT

The datasets presented in this study can be found in online repositories. The names of the repositories and accession numbers can be found in section "Materials and Methods."

AUTHOR CONTRIBUTIONS

HW, SY, and ZY contributed to conception and design of the study. SY, HW, and QC performed the statistical analysis. HW wrote the first draft of the manuscript. DM, LY, XZ, and JZ wrote sections of the manuscript. All authors contributed to manuscript revision, read, and approved the submitted version.

SUPPLEMENTARY MATERIAL

The Supplementary Material for this article can be found online at: https://www.frontiersin.org/articles/10.3389/fcell.2021.737723/full#supplementary-material

REFERENCES

Abou-Alfa, G. K., Meyer, T., Cheng, A.-L., El-Khoueiry, A. B., Rimassa, L., Ryoo, B.-Y., et al. (2018). Cabozantinib in patients with advanced and progressing hepatocellular carcinoma. *N. Engl. J. Med.* 379, 54–63. doi: 10.1056/NEJMoa1717002

Allemani, C., Matsuda, T., Di Carlo, V., Harewood, R., Matz, M., Nikšić, M., et al. (2018). Global surveillance of trends in cancer survival 2000-14 (CONCORD-3): analysis of individual records for 37 513 025 patients diagnosed with one of 18 cancers from 322 population-based registries in 71 countries. *Lancet* 391, 1023–1075. doi: 10.1016/S0140-6736(17)33326-3

Amirouchene-Angelozzi, N., Swanton, C., and Bardelli, A. (2017). Tumor evolution as a therapeutic target. *Cancer Discov.* 7, 805–817. doi: 10.1158/2159-8290.CD-17-0343

Becht, E., McInnes, L., Healy, J., Dutertre, C.-A., Kwok, I. W. H., Ng, L. G., et al. (2019). Dimensionality reduction for visualizing single-cell data using UMAP. *Nat. Biotechnol.* 37, 38–44. doi: 10.1038/nbt.4314

Bidkhori, G., Benfeitas, R., Klevstig, M., Zhang, C., Nielsen, J., Uhlen, M., et al. (2018). Metabolic network-based stratification of hepatocellular carcinoma reveals three distinct tumor subtypes. *Proc. Natl. Acad. Sci. U.S.A.* 115, E11874–E11883. doi: 10.1073/pnas.1807305115

Bray, F., Ferlay, J., Soerjomataram, I., Siegel, R. L., Torre, L. A., and Jemal, A. (2018). Global cancer statistics 2018: GLOBOCAN estimates of incidence and

mortality worldwide for 36 cancers in 185 countries. *CA Cancer J. Clin.* 68, 394–424. doi: 10.3322/caac.21492

Buetow, K. H., Meador, L. R., Menon, H., Lu, Y.-K., Brill, J., Cui, H., et al. (2019). High GILT expression and an active and intact MHC Class II antigen presentation pathway are associated with improved survival in melanoma. *J. I.* 203, 2577–2587. doi: 10.4049/jimmunol.1900476

Butler, A., Hoffman, P., Smibert, P., Papalexi, E., and Satija, R. (2018). Integrating single-cell transcriptomic data across different conditions, technologies, and species. *Nat. Biotechnol.* 36, 411–420. doi: 10.1038/nbt.4096

Chalmers, Z. R., Connelly, C. F., Fabrizio, D., Gay, L., Ali, S. M., Ennis, R., et al. (2017). Analysis of 100,000 human cancer genomes reveals the landscape of tumor mutational burden. *Genome Med.* 9:34. doi: 10.1186/s13073-017-0424-2

Chan, D. W., Chan, C.-Y., Yam, J. W. P., Ching, Y.-P., and Ng, I. O. L. (2006). Prickle-1 negatively regulates Wnt/beta-catenin pathway by promoting Dishevelled ubiquitination/degradation in liver cancer. *Gastroenterology* 131, 1218–1227. doi: 10.1053/j.gastro.2006.07.020

Chaudhary, K., Poirion, O. B., Lu, L., and Garmire, L. X. (2018). Deep learning–based multi-omics integration robustly predicts survival in liver cancer. *Clin. Cancer Res.* 24, 1248–1259. doi: 10.1158/1078-0432.CCR-17-0853

Craig, A. J., von Felden, J., Garcia-Lezana, T., Sarcognato, S., and Villanueva, A. (2020). Tumour evolution in hepatocellular carcinoma. *Nat. Rev. Gastroenterol. Hepatol.* 17, 139–152. doi: 10.1038/s41575-019-0229-4

Deng, T., Hu, B., Jin, C., Tong, Y., Zhao, J., Shi, Z., et al. (2021). A novel ferroptosis phenotype-related clinical-molecular prognostic signature for hepatocellular carcinoma. *J. Cell Mol. Med.* 25, 6618–6633. doi: 10.1111/jcmm.16666

Ding, J., Adiconis, X., Simmons, S. K., Kowalczyk, M. S., Hession, C. C., Marjanovic, N. D., et al. (2019). Systematic comparative analysis of single cell RNA-sequencing methods. *Genomics* 38, 737–746. doi: 10.1101/632216

Durante, M. A., Rodriguez, D. A., Kurtenbach, S., Sanchez, M. I., Decatur, C. L., Snyder, H., et al. (2020). Single-cell analysis reveals new evolutionary complexity in uveal melanoma. *Nat. Commun.* 11:496.

Finak, G., McDavid, A., Yajima, M., Deng, J., Gersuk, V., Shalek, A. K., et al. (2015). MAST: a flexible statistical framework for assessing transcriptional changes and characterizing heterogeneity in single-cell RNA sequencing data. *Genome Biol.* 16:278. doi: 10.1186/s13059-015-0844-5

Forero, A., Li, Y., Chen, D., Grizzle, W. E., Updike, K. L., Merz, N. D., et al. (2016). Expression of the MHC class II pathway in triple-negative breast cancer tumor cells is associated with a good prognosis and infiltrating lymphocytes. *Cancer Immunol. Res.* 4, 390–399. doi: 10.1158/2326-6066.CIR-15-0243

Friedman, J., Hastie, T., and Tibshirani, R. (2010). Regularization paths for generalized linear models via coordinate descent. *J. Stat. Soft.* 33, 1–22. doi: 10.18637/jss.v033.i01

Gao, R., Bai, S., Henderson, Y. C., Lin, Y., Schalck, A., Yan, Y., et al. (2021). Delineating copy number and clonal substructure in human tumors from single-cell transcriptomes. *Nat. Biotechnol.* 39, 599–608. doi: 10.1038/s41587-020-00795-2

Haibe-Kains, B., Desmedt, C., Sotiriou, C., and Bontempi, G. (2008). A comparative study of survival models for breast cancer prognostication based on microarray data: does a single gene beat them all? *Bioinformatics* 24, 2200–2208. doi: 10.1093/bioinformatics/btn374

Hänzelmann, S., Castelo, R., and Guinney, J. (2013). GSVA: gene set variation analysis for microarray and RNA-Seq data. *BMC Bioinformatics* 14:7. doi: 10.1186/1471-2105-14-7

Harrell, F. E. (1982). Evaluating the yield of medical tests. *JAMA* 247, 2543–2546. doi: 10.1001/jama.1982.03320430047030

Huang, Y., Chen, S., Qin, W., Wang, Y., Li, L., Li, Q., et al. (2020). A novel RNA binding protein-related prognostic signature for hepatocellular carcinoma. *Front. Oncol.* 10:580513. doi: 10.3389/fonc.2020.580513

Jin, S., Li, R., Chen, M.-Y., Yu, C., Tang, L.-Q., Liu, Y.-M., et al. (2020). Single-cell transcriptomic analysis defines the interplay between tumor cells, viral infection, and the microenvironment in nasopharyngeal carcinoma. *Cell Res.* 30, 950–965. doi: 10.1038/s41422-020-00402-8

Kim, C., Gao, R., Sei, E., Brandt, R., Hartman, J., Hatschek, T., et al. (2018). Chemoresistance evolution in triple-negative breast cancer delineated by single-cell sequencing. *Cell* 173, 879.e13–893.e13. doi: 10.1016/j.cell.2018.03.041

Liang, J., Wang, D., Lin, H., Chen, X., Yang, H., Zheng, Y., et al. (2020). A novel ferroptosis-related gene signature for overall survival prediction in patients with hepatocellular carcinoma. *Int. J. Biol. Sci.* 16, 2430–2441. doi: 10.7150/ijbs.45050

Liberzon, A., Birger, C., Thorvaldsdóttir, H., Ghandi, M., Mesirov, J. P., and Tamayo, P. (2015). The molecular signatures database hallmark gene set collection. *Cell Syst.* 1, 417–425. doi: 10.1016/j.cels.2015.12.004

Llovet, J. M., Kelley, R. K., Villanueva, A., Singal, A. G., Pikarsky, E., Roayaie, S., et al. (2021). Hepatocellular carcinoma. *Nat. Rev. Dis. Primers* 7:6. doi: 10.1038/s41572-020-00240-3

Llovet, J. M., Montal, R., Sia, D., and Finn, R. S. (2018). Molecular therapies and precision medicine for hepatocellular carcinoma. *Nat. Rev. Clin. Oncol.* 15, 599–616. doi: 10.1038/s41571-018-0073-4

Llovet, J. M., Ricci, S., Mazzaferro, V., Hilgard, P., Gane, E., Blanc, J.-F., et al. (2008). Sorafenib in advanced hepatocellular carcinoma. *N. Engl. J. Med.* 359, 378–390. doi: 10.1056/NEJMoa0708857

Long, J., Chen, P., Lin, J., Bai, Y., Yang, X., Bian, J., et al. (2019a). DNA methylation-driven genes for constructing diagnostic, prognostic, and recurrence models for hepatocellular carcinoma. *Theranostics* 9, 7251–7267. doi: 10.7150/thno.31155

Long, J., Wang, A., Bai, Y., Lin, J., Yang, X., Wang, D., et al. (2019b). Development and validation of a TP53-associated immune prognostic model for hepatocellular carcinoma. *EBioMedicine* 42, 363–374. doi: 10.1016/j.ebiom.2019.03.022

Losic, B., Craig, A. J., Villacorta-Martin, C., Martins-Filho, S. N., Akers, N., Chen, X., et al. (2020). Intratumoral heterogeneity and clonal evolution in liver cancer. *Nat. Commun.* 11:291. doi: 10.1038/s41467-019-14050-z

Ma, L., Hernandez, M. O., Zhao, Y., Mehta, M., Tran, B., Kelly, M., et al. (2019). Tumor cell biodiversity drives microenvironmental reprogramming in liver cancer. *Cancer Cell* 36, 418.e6–430.e6. doi: 10.1016/j.ccell.2019.08.007

Maley, C. C., Aktipis, A., Graham, T. A., Sottoriva, A., Boddy, A. M., Janiszewska, M., et al. (2017). Classifying the evolutionary and ecological features of neoplasms. *Nat. Rev. Cancer* 17, 605–619. doi: 10.1038/nrc.2017.69

Marjanovic, N. D., Hofree, M., Chan, J. E., Canner, D., Wu, K., Trakala, M., et al. (2020). Emergence of a high-plasticity cell state during lung cancer evolution. *Cancer Cell* 38, 229.e13–246.e13. doi: 10.1016/j.ccell.2020.06.012

Massalha, H., Bahar Halpern, K., Abu-Gazala, S., Jana, T., Massasa, E. E., Moor, A. E., et al. (2020). A single cell atlas of the human liver tumor microenvironment. *Mol. Syst. Biol.* 16:e9682. doi: 10.15252/msb.20209682

Mayakonda, A., Lin, D.-C., Assenov, Y., Plass, C., and Koeffler, H. P. (2018). Maftools: efficient and comprehensive analysis of somatic variants in cancer. *Genome Res.* 28, 1747–1756. doi: 10.1101/gr.239244.118

McCaw, T. R., Li, M., Starenki, D., Cooper, S. J., Liu, M., Meza-Perez, S., et al. (2019). The expression of MHC class II molecules on murine breast tumors delays T-cell exhaustion, expands the T-cell repertoire, and slows tumor growth. *Cancer Immunol. Immunother.* 68, 175–188. doi: 10.1007/s00262-018-2262-5

Ni, Q., Chen, Z., Zheng, Q., Xie, D., Li, J.-J., Cheng, S., et al. (2020). Epithelial V-like antigen 1 promotes hepatocellular carcinoma growth and metastasis via the ERBB-PI3K-AKT pathway. *Cancer Sci.* 111, 1500–1513. doi: 10.1111/cas.14331

Pinter, M., Scheiner, B., and Peck-Radosavljevic, M. (2021). Immunotherapy for advanced hepatocellular carcinoma: a focus on special subgroups. *Gut* 70, 204–214. doi: 10.1136/gutjnl-2020-321702

Qin, X.-Y., Suzuki, H., Honda, M., Okada, H., Kaneko, S., Inoue, I., et al. (2018). Prevention of hepatocellular carcinoma by targeting MYCN-positive liver cancer stem cells with acyclic retinoid. *Proc. Natl. Acad. Sci. U.S.A.* 115, 4969–4974. doi: 10.1073/pnas.1802279115

Qiu, X., Mao, Q., Tang, Y., Wang, L., Chawla, R., Pliner, H. A., et al. (2017). Reversed graph embedding resolves complex single-cell trajectories. *Nat. Methods* 14, 979–982. doi: 10.1038/nmeth.4402

Rajewsky, N., Almouzni, G., Gorski, S. A., Aerts, S., Amit, I., et al. (2020). LifeTime and improving European healthcare through cell-based interceptive medicine. *Nature* 587, 377–386. doi: 10.1038/s41586-020-2715-9

Ramachandran, P., Dobie, R., Wilson-Kanamori, J. R., Dora, E. F., Henderson, B. E. P., Luu, N. T., et al. (2019). Resolving the fibrotic niche of human liver cirrhosis at single-cell level. *Nature* 575, 512–518. doi: 10.1038/s41586-019-1631-3

Sarathi, A., and Palaniappan, A. (2019). Novel significant stage-specific differentially expressed genes in hepatocellular carcinoma. *BMC Cancer* 19:663. doi: 10.1186/s12885-019-5838-3

Sconocchia, G., Eppenberger-Castori, S., Zlobec, I., Karamitopoulou, E., Arriga, R., Coppola, A., et al. (2014). HLA Class II antigen expression in colorectal

carcinoma tumors as a favorable prognostic marker. *Neoplasia* 16, 31–42. doi: 10.1593/neo.131568

Sharma, A., Seow, J. J. W., Dutertre, C.-A., Pai, R., Blériot, C., Mishra, A., et al. (2020). Onco-fetal reprogramming of endothelial cells drives immunosuppressive macrophages in hepatocellular carcinoma. *Cell* 183, 377.e21–394.e21. doi: 10.1016/j.cell.2020.08.040

Sun, X., Yu, S., Zhang, H., Li, J., Guo, W., and Zhang, S. (2020). A signature of 33 immune-related gene pairs predicts clinical outcome in hepatocellular carcinoma. *Cancer Med.* 9, 2868–2878. doi: 10.1002/cam4.2921

Sun, Y., Wu, L., Zhong, Y., Zhou, K., Hou, Y., Wang, Z., et al. (2021). Single-cell landscape of the ecosystem in early-relapse hepatocellular carcinoma. *Cell* 184, 404.e16–421.e16. doi: 10.1016/j.cell.2020.11.041

The Cancer Genome Atlas Research Network, Weinstein, J. N., Collisson, E. A., Mills, G. B., Shaw, K. R. M., Ozenberger, B. A., et al. (2013). The cancer genome atlas pan-cancer analysis project. *Nat. Genet.* 45, 1113–1120. doi: 10.1038/ng.2764

Turajlic, S., Sottoriva, A., Graham, T., and Swanton, C. (2019). Resolving genetic heterogeneity in cancer. *Nat. Rev. Genet.* 20, 404–416. doi: 10.1038/s41576-019-0114-6

Van den Berge, K., Roux de Bézieux, H., Street, K., Saelens, W., Cannoodt, R., Saeys, Y., et al. (2020). Trajectory-based differential expression analysis for single-cell sequencing data. *Nat. Commun.* 11:1201. doi: 10.1038/s41467-020-14766-3

Wang, J.-Y., Wang, X.-K., Zhu, G.-Z., Zhou, X., Yao, J., Ma, X.-P., et al. (2021). Distinct diagnostic and prognostic values of Glypicans gene expression in patients with hepatocellular carcinoma. *BMC Cancer* 21:462. doi: 10.1186/s12885-021-08104-z

Wang, S., and Liu, X. (2019). The UCSCXenaTools R package: a toolkit for accessing genomics data from UCSC Xena platform, from cancer multi-omics to single-cell RNA-seq. *JOSS* 4:1627. doi: 10.21105/joss.01627

Wang, Y., Mashock, M., Tong, Z., Mu, X., Chen, H., Zhou, X., et al. (2020). Changing technologies of RNA sequencing and their applications in clinical oncology. *Front. Oncol.* 10:447. doi: 10.3389/fonc.2020.00447

Yang, J. D., Hainaut, P., Gores, G. J., Amadou, A., Plymoth, A., and Roberts, L. R. (2019). A global view of hepatocellular carcinoma: trends, risk, prevention and management. *Nat. Rev. Gastroenterol. Hepatol.* 16, 589–604. doi: 10.1038/s41575-019-0186-y

Yu, G., Wang, L.-G., Han, Y., and He, Q.-Y. (2012). clusterProfiler: an R package for comparing biological themes among gene clusters. *OMICS* 16, 284–287. doi: 10.1089/omi.2011.0118

Zhang, B., Tang, B., Gao, J., Li, J., Kong, L., and Qin, L. (2020). A hypoxia-related signature for clinically predicting diagnosis, prognosis and immune microenvironment of hepatocellular carcinoma patients. *J. Transl. Med.* 18:342. doi: 10.1186/s12967-020-02492-9

Zhang, J., Bajari, R., Andric, D., Gerthoffert, F., Lepsa, A., Nahal-Bose, H., et al. (2019). The international cancer genome consortium data portal. *Nat. Biotechnol.* 37, 367–369. doi: 10.1038/s41587-019-0055-9

Zhang, L., He, X., Liu, X., Zhang, F., Huang, L. F., Potter, A. S., et al. (2019). Single-cell transcriptomics in medulloblastoma reveals tumor-initiating progenitors and oncogenic cascades during tumorigenesis and relapse. *Cancer Cell* 36, 302.e7–318.e7. doi: 10.1016/j.ccell.2019.07.009

Zhang, Q., He, Y., Luo, N., Patel, S. J., Han, Y., Gao, R., et al. (2019). Landscape and dynamics of single immune cells in hepatocellular carcinoma. *Cell* 179, 829.e7–845.e7. doi: 10.1016/j.cell.2019.10.003

Zhao, S., Fung-Leung, W.-P., Bittner, A., Ngo, K., and Liu, X. (2014). Comparison of RNA-Seq and microarray in transcriptome profiling of activated T Cells. *PLoS One* 9:e78644. doi: 10.1371/journal.pone.0078644

Zheng, H., Pomyen, Y., Hernandez, M. O., Li, C., Livak, F., Tang, W., et al. (2018). Single-cell analysis reveals cancer stem cell heterogeneity in hepatocellular carcinoma. *Hepatology* 68, 127–140. doi: 10.1002/hep.29778

Zhu, Y., Wang, R., Chen, W., Chen, Q., and Zhou, J. (2020). Construction of a prognosis-predicting model based on autophagy-related genes for hepatocellular carcinoma (HCC) patients. *Aging* 12, 14582–14592. doi: 10.18632/aging.103507

Zuo, Q., He, J., Zhang, S., Wang, H., Jin, G., Jin, H., et al. (2021). PPARγ Coactivator-1α suppresses metastasis of hepatocellular carcinoma by inhibiting warburg effect by PPARγ-Dependent WNT/β-Catenin/Pyruvate dehydrogenase kinase isozyme 1 axis. *Hepatology* 73, 644–660. doi: 10.1002/hep.31280

Conflict of Interest: The authors declare that the research was conducted in the absence of any commercial or financial relationships that could be construed as a potential conflict of interest.

Publisher's Note: All claims expressed in this article are solely those of the authors and do not necessarily represent those of their affiliated organizations, or those of the publisher, the editors and the reviewers. Any product that may be evaluated in this article, or claim that may be made by its manufacturer, is not guaranteed or endorsed by the publisher.

Copyright © 2021 Wang, Yu, Cai, Ma, Yang, Zhao, Jiang, Zhang and Yu. This is an open-access article distributed under the terms of the Creative Commons Attribution License (CC BY). The use, distribution or reproduction in other forums is permitted, provided the original author(s) and the copyright owner(s) are credited and that the original publication in this journal is cited, in accordance with accepted academic practice. No use, distribution or reproduction is permitted which does not comply with these terms.

frontiers in Oncology

ORIGINAL RESEARCH
published: 07 October 2021
doi: 10.3389/fonc.2021.710525

A Novel ZNF304/miR-183-5p/FOXO4 Pathway Regulates Cell Proliferation in Clear Cell Renal Carcinoma

Li-Xin Ren[1], *Bo-Wen Zeng*[2], *Meng Zhu*[1], *An-Ning Zhao*[1], *Bei Shi*[1], *Hong Zhang*[1], *Dan-Dan Wang*[1], *Jun-Fei Gu*[1*] *and Zhan Yang*[1*]

[1] *Department of Urology, The Second Hospital of Hebei Medical University, Shijiazhuang, China,* [2] *Department of Urology, Affiliated Hospital of Sergeant School of Army Medical University, Shijiazhuang, China*

Zinc-finger protein 304 (ZNF304) plays a critical role in silencing genes through transcription, regulating cell survival, proliferation, apoptosis, and differentiation during development. However, the roles of transcription factor ZNF304 and its clinical significance in clear cell renal carcinoma (ccRCC) remain unclear. In this study, we found that the expression of ZNF304 was downregulated in ccRCC tissues. Lower levels of ZNF304 were correlated with poor survival. Downregulation of ZNF304 promoted ccRCC cell growth *in vitro*, whereas overexpression of ZNF304 inhibited growth. Our results indicated that miR-183-5p/FOXO4 mediated ZNF304 regulation of cell growth. Interestingly, we revealed that ZNF304 promoted FOXO4 expression in ccRCC cells. Mechanistically, ZNF304 binds to miR-183 promoter and inhibits miR-183-5p transcription. Furthermore, the expression of miR-183-5p wes increased in ccRCC tissues, and the upregulation of miR-183-5p was related to the poor prognosis of ccRCC patients. miR-183-5p upregulation repressed the expression of FOXO4 and promoted ccRCC progression. These results demonstrated that ZNF304/miR-183-5p/FOXO4 axis played essential role in promoting ccRCC progression, which suggests that disruption of this axis may be a potential therapeutic target in ccRCC.

Keywords: zinc-finger protein 304, proliferation, FOXO4, miR-183-5p, clear cell renal carcinoma (ccRCC)

OPEN ACCESS

Edited by:
Simona Kranjc Brezar, Institute of Oncology Ljubljana, Slovenia

Reviewed by:
Camilla Abbehausen, State University of Campinas, Brazil
Xixi Zhou, University of New Mexico, United States

****Correspondence:***
Jun-Fei Gu
Junfei_Gu2020@hebmu.edu.cn
Zhan Yang
yangzhan@hb2h.com

Specialty section:
This article was submitted to Molecular and Cellular Oncology, a section of the journal Frontiers in Oncology

Received: *16 May 2021*
Accepted: *15 September 2021*
Published: *07 October 2021*

Citation:
Ren L-X, Zeng B-W, Zhu M, Zhao A-N, Shi B, Zhang H, Wang D-D, Gu J-F and Yang Z (2021) A Novel ZNF304/miR-183-5p/FOXO4 Pathway Regulates Cell Proliferation in Clear Cell Renal Carcinoma. Front. Oncol. 11:710525. doi: 10.3389/fonc.2021.710525

INTRODUCTION

Renal cell carcinoma (RCC), which is one of the most common malignant tumors in humans, is also the most deadly urinary tract tumor (1). In 2020, there were 76,080 new RCC cases and more than 13,000 deaths in the United States (2). Moreover, the incidence and mortality caused by RCC are increasing. Among them, clear cell RCC (ccRCC) accounts for 75%–80% of renal cell carcinoma cases, and is the

Abbreviations: ZNF304, Zinc-finger protein 304; ccRCC, clear cell renal carcinoma; ChIP, Chromatin immunoprecipitation; RCC, Renal cell carcinoma; FOXO4, Forkhead box O 4; CRC, colorectal cancer; mRCC, Metastatic renal cell carcinoma; miR, microRNA; RT-qPCR, Real-time quantitative PCR; WT, wild-type; MTT, 3-(4,5-dimethylthiazol-2-yl)-2,5-diphenyltetrazolium bromide; shZNF304, short hairpin RNA ZNF304; shFOXO4, short hairpin RNA FOXO4; oeZNF304, overexpression ZNF304.

most common histological subtype in renal cell carcinoma (3, 4). Surgical resection of the tumor usually prolongs progression-free and overall survival of patients (5, 6). However, more than 25% of patients have developed the metastatic RCC (mRCC) at the time of diagnosis (7). Unfortunately, the clinical results for kidney cancer patients were not satisfactory in the past decade; even though tyrosine kinase inhibitor (CTKI) drugs, rapamycin protein (mTOR) inhibitor drugs and immunotherapy showed promise for treatment (8–10), 30% of newly diagnosed locally advanced kidney cancer patients will metastasize (11). Therefore, understanding the molecular mechanisms underlying malignant ccRCC is of great significance, as it will aide in determining new drug targets and treatment strategies.

The occurrence and development of tumors is a complex process involving the abnormal expression of multiple genes, such as up-regulated proto-oncogenes and down-regulated tumor suppressor factors (12–15). Unfortunately, many current studies have focused on up-regulated genes in tumors, and have ignored the research on down-regulated genes. In fact, these abnormal genes play an equally important role in the tumor process (16). Zinc-finger protein 304 (ZNF304), which is a transcription factor, belongs to the Krueppel C2H2-type zinc-finger family protein (17). ZNF304 often function as f transcriptional repressor and plays a role in gene silencing (18). ZNF304 binds to the promoters of INK4-ARF and other CpG island methylator phenotype genes, and facilitates transcriptional silencing by recruiting co-repressor complexes (19). ZNF304 binds to the ITGB1 promoter and upregulates the transcription of β-1 integrin (18). However, the expression and function of ZNF304 and its downstream effectors in ccRCC are not well understood.

Forkhead box O 4 (FOXO4) transcription factor is one of the Forkhead box O family proteins which also contain FOXO1, FOXO3a, and FOXO6 (20). FOXO factors are involved in the regulation of the insulin signaling pathway, and implicated in regulating cellular processes such as cell viability, proliferation, energy production and immune responses (21). FOXO4 acts as a tumor suppressor in multiple human cancers, such as lung, leukemia, cervical, pancreatic and CRCs etc. (22–24). In glioblastomas, FOXO4 inhibits the malignant phenotype of cells *in vitro* and *in vivo* (25). Importantly, overexpression of FOXO4 promotes apoptosis of ccRCC cells by repressing Bim expression (26).

Here, we demonstrate that ZNF304 and FOXO4 are downregulated in ccRCC tissue, where lower levels of these proteins are associated with poor prognosis of patient survival. Downregulation of ZNF304 promotes ccRCC cell growth *in vitro*. Mechanistically, ZNF304 bound directly to the miR-183 promoter and inhibited miR-183-5p expression by transcriptional activation. The results revealed that ZNF304/miR-183-5p/FOXO4 axis plays a critical key role in ccRCC growth and may serve as a potential therapeutic target.

METHODS

Clinical Samples

Human primary clear cell renal cell carcinoma and corresponding normal kidney tissue were collected from the Department of Urology, the Second Hospital of Hebei Medical University. All patients were ccRCC patients from July 2015 to June 2020. All patients underwent radical nephrectomy for treatment. Fresh ccRCC and corresponding normal kidney tissue were washed with saline and quickly frozen in liquid nitrogen or formaldehyde to fix for further used. The research protocol has been approved by the Ethics Committee of the Second Hospital of Hebei Medical University, and each patient's written consent has been obtained.

Cell Lines and Transfection

Human ccRCC cell lines (SW839, A498, Caki-1, 786-0) were purchased from ATCC (Rockville, Maryland, USA), and are preserved in our laboratory. The 293A cell line is deposited in our laboratory. The above-mentioned cells were cultured in low-sugar dulbecco's modified eagle medium (DMEM) supplemented with 10% fetal bovine serum (Clark Bio, Claymont, DE, USA) and 1% penicillin/streptomycin (Solarbio, Beijing). The cells are cultured in a humidified condition of 95% air and 5% CO_2. All cells were transfected using Lipofectamine 2000 (Invitrogen) according to the manufacturer's operating manual. Briefly (27), 786-O and SW839 cells (1×10^5 cells/ml) were seeded into plates in growth medium (DMEM). Until the required number of cells (80% confluence) is obtained at the time of transfection. The cells were washed twice with PBS and the transfected lipoplex (prepared as described in the operating manual) was added to each well. It was mixed gently by rocking the plate back and forth. The cells were cultured in DMEM (without FBS), 5% CO_2, and 37°C humidified incubator for 4-6 hours. Then the cells were washed twice with PBS, replaced with complete medium, and cultured for 48 hours.

RNA Isolation and RT-qPCR

Use RNAeasy Mini Elute Kit (QIAGEN) according to the manufacturer's manual for total RNA isolation. The NanoDrop 2000 system detects RNA concentration and quality. The first strand of cDNA was synthesized using M-MLV First Strand Kit (Life Technologies) with random hexamer primers. Dilute the first strand of cDNA 5-10 times as needed, and use Platinum SYBR Green qPCR Super Mix UDG kit (Invitrogen) to perform real-time quantitative PCR (qRT-PCR) analysis on mRNA in ABI 7500 FAST System (Life Technologies). The relative transcriptional expression level of gene mRNA was standardized with GAPDH as an internal reference gene. The calculation was carried out using the $2^{-\Delta\Delta Ct}$ formula according to the previous description (28). ZNF304-F:GACCGGGTTC AGAGTTGTGT; ZNF304-R:CCACGTGTGCACAGTTTCTG; FOXO4-F:GGGAAAAGGCCATTGAAAGCG; FOXO4-R: TGTGGCGGATCGAGTTCTTC; GAPDH-F:ATGAATGGGC AGCCGTTAGG; GAPDH-R:TGGAATTTGCCATGGGTGGA; Cyclin D1-F:CTGATTGGACAGGCATGGGT; Cyclin D1-R: GTGCCTGGAAGTCAACGGTA; miR-23-3p-F:GGCACATT GCCAGGGATTTC; miR-96-5p-F:GGTTTGGCACTAGCACA TTTTTG; miR-128-3p-F:GGCTCACAGTGAACCGGTCTC; miR-142-3p-F:GGCCGTAGTGTTTCCTACTTTATG; miR-150-5p-F:GCTCTCCCAACCCTTGTACCAG; miR-183-5p-F: GGCTATGGCACTGGTAGAATTCAC; miR-216b-5p-F:GCA AATCTCTGCAGGCAAATGTG; miR-217-F:GTACTGCATC

AGGAACTGATTGG; miR-449a-5p-F:GGTGGCAGTGTATTG TTAGCTGG; miR-1271-5p-F:CTTGGCACCTAGCAAGCACTC.

Western Blot Analysis

Western blot analysis was performed as previously described (28). Polyvinylidene fluoride (PVDF) membranes (Millipore), were incubated with primary antibodies anti-ZNF304 (1:500, HPA050531), anti-FOXO4 (1:1000, ab128908), anti-cyclin D1 (1:500, 26939-1-AP), and anti-β-actin (1:1000, sc-47778). An HRP-conjugated secondary antibody (1:5000, Rockland) was used and detection was by ECL (enhanced chemiluminescence) Fuazon Fx (Vilber Lourmat). Images were captured and processed by FusionCapt Advance Fx5 software (Vilber Lourmat). All experiments were repeated three times.

Vector Construction and Luciferase Reporter Assay

Lentiviral pLKO-ZNF304 (shZNF304), pWPI-ZNF304 (overexpression ZNF304, oeZNF304) and pLKO-FOXO4 (shFOXO4) plasmids were designed and constructed from Biocaring Biotechnology Co., Ltd (Shijiazhuang). Briefly (28), ZNF304 cDNA was inserted into EcoRI and XhoI restriction endonuclease digested pWPI empty vector (Addgene, #12254) and then Sanger sequencing for confirming. ZNF304 and FOXO4 shRNA were inserted into BsmBI restriction endonuclease digested pLKO (Addgene, #14748) and then Sanger sequencing for confirming. The 3' UTR sequences of FOXO4 containing wild-type (WT) or mutant (mut) forms of the miR-183-5p target site were inserted into restriction endonucleases XhoI (Xho1) and SalI (Sal1) along with pmirGLO Dual-Luciferase miRNA Target Expression Vector (Promega, Madison, WI, USA). FOXO4 reporter construct (WT or mut) or the empty reporter vector were co-transfected into SW839 cells with miR-183-5p mimic or mimic control and plasmid Renilla luciferase-thymidine kinase. Luciferase activity was measured by Dual-Glo Luciferase Assay System (Promega) with a Flash and Glow reader (LB955; Berthold Technologies, Bad Wildbad, Germany). The specific target activity was expressed as the relative activity ratio of firefly luciferase to Renilla luciferase.

Morphometry and Histology

Human ccRCC and normal kidney tissues were fixed in formalin and then processed for routine paraffin embedding (29). Ten 5-μm-thick consecutive sections were prepared for hematoxylin and eosin staining. Images were acquired using a Leica microscope (Leica DM6000B, Switzerland) and digitized with LAS V.4.4 (Leica).

MTT Assay

Cell viability was detected by an MTT [3-(4,5-dimethylthiazol-2-yl)-2,5-diphenyltetrazolium bromide] colorimetric assay as previously described (29). Briefly, SW839 and 786-0 cells were plated and transfected with the indicated vector or treated with AZD6244 for 24 h. Absorbance at 570nm was measured using a microplate reader (Thermo Fisher, USA).

Colony Formation Assay

100 cells/well were seeded into six-well plates, cultured for 1 week and fixed in a glacial acetic acid/methanol solution. Then, 0.5% crystal violet was used to stain the colonies. Colony numbers were counted under a microscope (30).

ChIP Assay

The chromatin immunoprecipitation (ChIP) assay was performed as previously described (30). Briefly, SW839 cells were treated with formaldehyde. The cross-linked chromatin was sonicated to an average size of 400–600 bp. Samples were precleared with protein A-agarose/salmon sperm DNA and the DNA fragments were immunoprecipitated overnight at 4°C with anti-ZNF304 or anti-IgG antibodies. After reversal of cross-linking, ZNF304 occupancy on the miR-183-5p promoter was examined. Results were determined by qRT-PCR with miR-183-prom-F1: GGGCCTTCAGGTGGAGATAGGAG; miR-183-prom-R1:CCCTGCGGAGAGACCAGCGG; miR-183-prom-F2: CAGTCTGGCCCAATCTGGTCTGG; miR-183-prom-R2: GGAGAGGCAAGCAGCTGGCCAG; miR-183-prom-F3: GGGTGCCAGCTCCCCAGAGACC; miR-183-prom-R3: CTGCAGCCACCCAGGTGGCTTG.

Statistical Analysis

Statistical analysis as previously described (28). Data were presented as the mean ± SEM. Student's t test was used to analyze differences between two groups. Spearman's correlation analysis was used to evaluate the correlation analysis. Values of $p < 0.05$ were considered statistically significant. GraphPad Prism 7.0 software was used for the statistical analysis (GraphPad Software).

RESULTS

The Expression of ZNF304 Is Down-Regulated in ccRCC Tissue, and the Lower Level of ZNF304 Indicates a Poor Prognosis for Patients

To investigate the expression level of ZNF304 in ccRCC, firstly, we collected clinical samples and located the ccRCC tumor and an area of normal kidney tissue by using hematoxylin and eosin staining (**Figure 1A**). Compared with normal kidney tissue, the mRNA and protein levels of ZNF304 in ccRCC tissue (T) are significantly reduced (**Figures 1B–D**). Data from the TCGA database show that the mRNA expression level of ZNF304 in ccRCC tissue is significantly lower than that in normal kidney tissue (**Figure 1E**). And the higher levels of ZNF304 indicates a good prognosis for patients in patients with ccRCC (**Figure 1F**). Furthermore, clinicopathologic factors of ZNF304 mRNA expression level was markedly negative associated with tumor grade but not with age, sex and tumor size etc (**Table 1**). Next, we detected ZNF304 expression in cell lines. 786-0 and SW839 cells expressed much lower levels of ZNF304 compared with the other cell lines (**Figures 1G–I**). These results suggest that downregulation of ZNF304 may be associated with ccRCC progression.

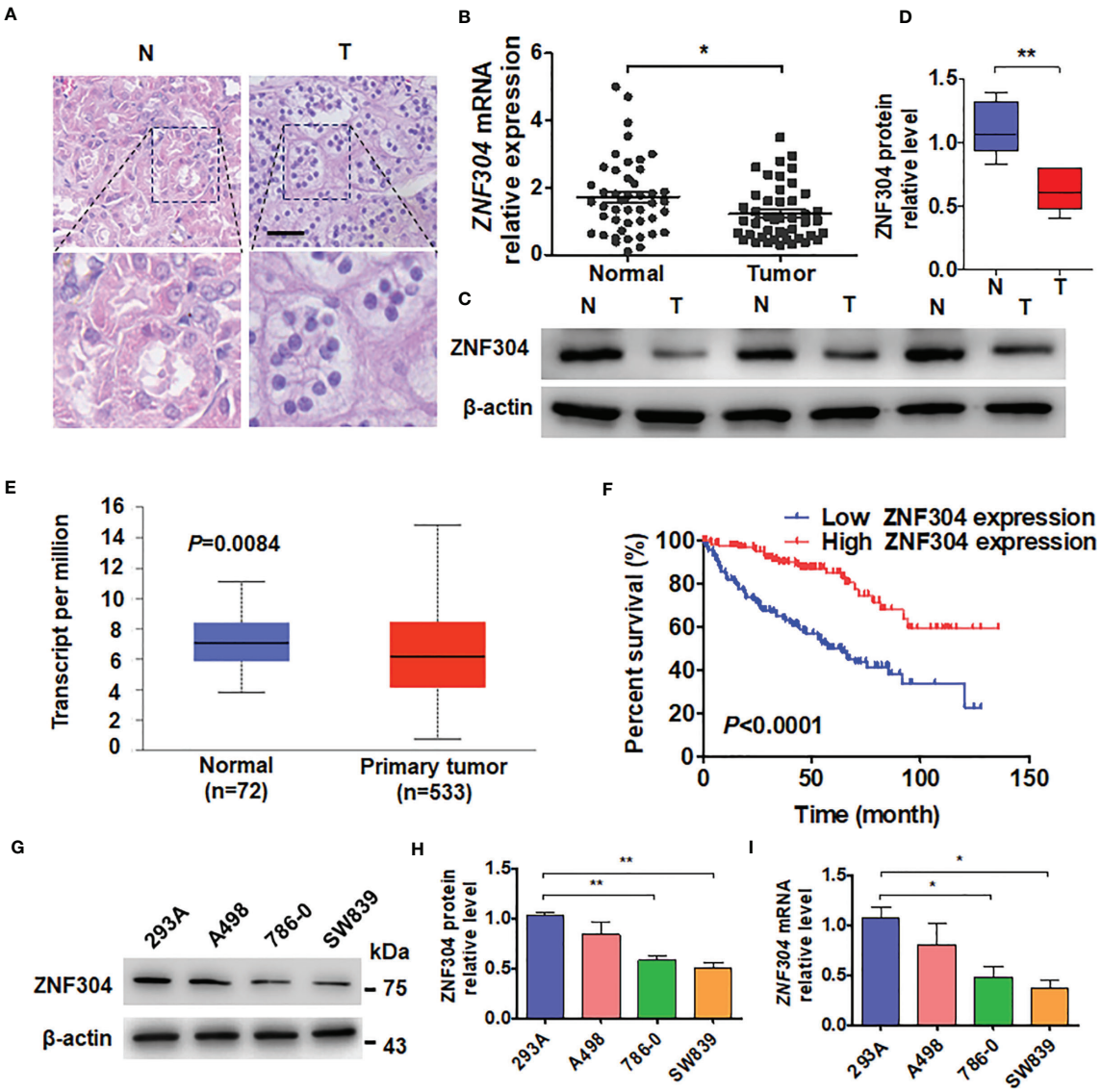


FIGURE 1 | ZNF304 downregulation in ccRCC is correlated with good prognosis. **(A)** Staining of Hematoxylin and eosin in ccRCC (T) and normal (N) kidney tissues. Scale Bar = 50 μm. **(B)** RT-qPCR was use to examine ZNF304 mRNA level in ccRCC (T, n = 43) and normal kidney (N, n = 43) tissues. **(C)** Western blot analysis detected the protein levels of ZNF304 in ccRCC (T) and normal (N) kidney tissues **(D)** Quantitative analysis of **(C)**. **(E)** ZNF304 mRNA levels were analyzed from data of the TCGA database. **(F)** Kaplan–Meier analysis of the overall survival of ccRCC patients in the TCGA database with low (n = 130) and high (n = 130) ZNF304 levels (cutoff value is 25%). **(G)** Western blot was used to measure the proteins level of ZNF304 in 293A and RCC cell lines (A498, 786-0, and SW839). **(H)** Quantitative analysis of **(G)**. **(I)** qRT-PCR was performed to detect the ZNF304 mRNA level in the above cell lines. All data are from three independent experiments and expressed as the mean ± SEM. *P < 0.05, **P < 0.01 vs. the corresponding controls.

ZNF304 Inhibits Cell Proliferation in ccRCC

Previous studies revealed ZNF304 to be a transcriptional repressor involved in cancer cell survival (18). Overexpression of ZNF304 with a lentiviral vector markedly increased ZNF304 mRNA and protein levels, whereas transfection with shZNF304 significantly reduced ZNF304 expression (**Figures 2A–C**). The MTT assay showed that ZNF304 overexpression inhibited growth of both 786-0 and SW839 cells, whereas ZNF304 downregulation accelerated cell line proliferation (**Figure 2D**). The colony formation assay confirmed these findings (**Figures 2E, F**). Taken together, these data reveal that ZNF304 inhibits ccRCC cell growth.

ZNF304 Repression of Cell Growth *In Vitro* Is Mediated by FOXO4

To elucidate the molecular pathway underlying ccRCC cell growth regulation by ZNF304, we analyzed the correlation of

TABLE 1 | Clinicopathological characteristics.

Characteristics	Number of patients (%)	ZNF304 expression		
		Low (%)	High (%)	*P* value
No. of patients	45	22	23	
Age				
≤60	22	11 (50.00)	11 (50.00)	1.000
>60	23	11 (47.83)	12 (52.17)	
Gender				
Male	30	16 (53.33)	14 (46.67)	0.530
Female	15	6 (40.00)	9 (60.00)	
Tumor size (cm)				
≤5	27	12 (44.44)	15 (55.56)	0.550
>5	18	10 (55.56)	8 (44.44)	
pT status				
pT_1–pT_2	18	11 (61.11)	7 (38.89)	0.125
pT_3–pT_4	27	9 (33.33)	18 (66.67)	
pN status				
pN0	30	14 (46.67)	16 (53.33)	0.758
pN1–pN3	15	8 (53.33)	7 (46.67)	
TNM stage				
I–II	28	10 (35.71)	18 (64.29)	0.033
III–IV	17	12 (70.59)	5 (29.41)	

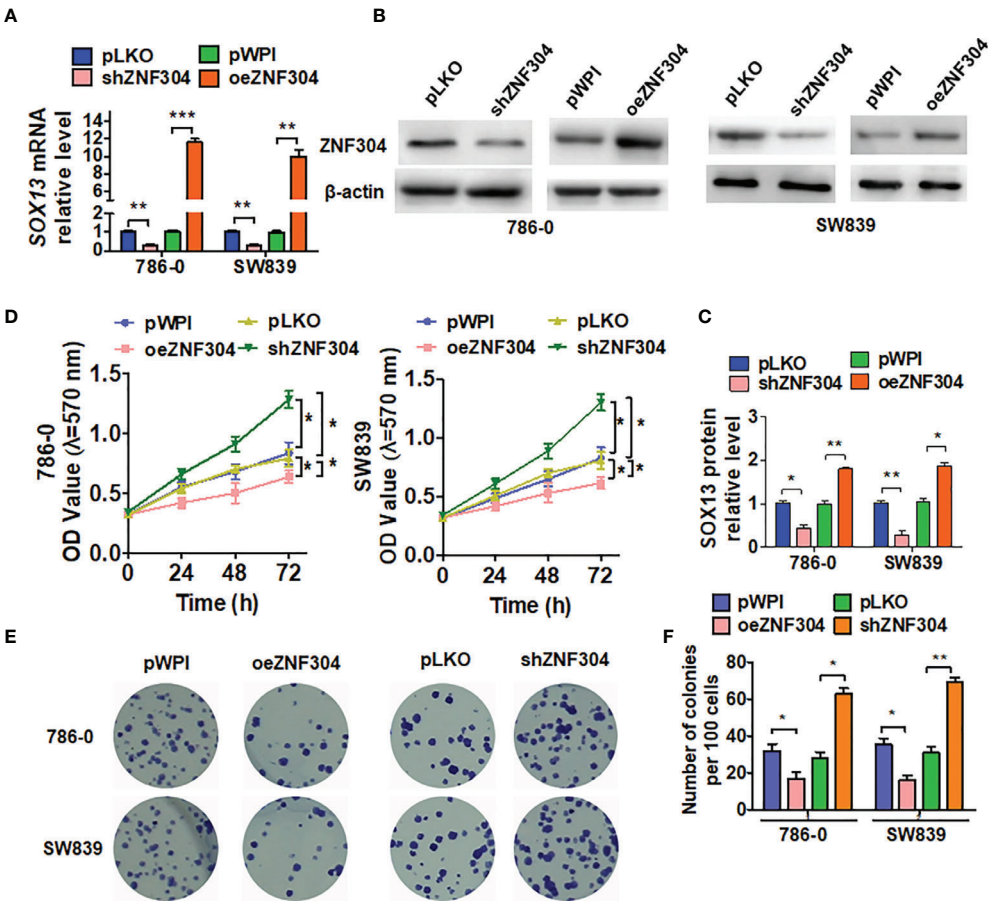


FIGURE 2 | ZNF304 inhibits ccRCC cell growth. **(A)** The shZNF304, oeZNF304 and control vectors were transfected to SW839 and 786-0 cell, and then qRT-PCR was used to examine the mRNA level of ZNF304. **(B)** SW839 and 786-0 cells were transfected as in **(A)**, and the protein level ZNF304 was measured by Western blot. **(C)** Quantitative analysis of **(B)**. **(D–F)** Cells were transfected as in **(A)**, and cell viability was examined by MTT **(D)** and colony formation assays **(E, F)**. All data are from three independent experiments and expressed as the mean ± SEM. *P < 0.05, **P < 0.01, ***P < 0.001 vs. the corresponding controls.

gene expression with ZNF304 in ccRCC tissues from the TCGA database (**Supplementary Figure 1**). The transcription factor FOXO4 appeared to be implicated in this. Knockdown of ZNF304 reduced FOXO4 protein level while ZNF304 overexpression upregulated FOXO4 (**Figures 3A, B**). FOXO4 was also detected in ccRCC and normal kidney tissues. Compared to normal kidney tissues, the expression of FOXO4 was obviously decreased in ccRCC tissues (T) (**Figure 3C**). The data from TCGA databases also show that FOXO4 mRNA levels were downregulated in ccRCC (**Figure 3D**). And the lower expression level of FOXO4 was associated with poor overall survival in ccRCC patients (**Figure 3E**). Moreover, we confirmed that FOXO4 has a positive correlation with ZNF304 in ccRCC using PCR data (**Figure 3F**). The MTT assay showed that depletion of FOXO4 facilitated cell proliferation and reversed the inhibition caused by ZNF304 overexpression (**Figure 3G**). Surprisingly, overexpression or depletion of ZNF304 did not affect FOXO4 mRNA levels (**Figure 3H**). These findings show that FOXO4 underlies the regulation of ccRCC cell proliferation by ZNF304.

miR-183-5p Mediates ZNF304-Promoted FOXO4 Expression

Regulation of FOXO4 protein expression level by ZNF304, without influence in FOXO4 mRNA, suggests that ZNF304 regulates FOXO4 at the epigenetic regulation. Because microRNAs (miRNAs) are one of critical regulators in the regulation of gene expression at the posttranscriptional level, we predicted miRNAs that may target the FOXO4 3′-UTR from TargetScan, miRanda, and RNA22 database (**Figure 4A**). FOXO4 3′-UTR containing biotin-labeled uracil was generated by a T7 RNA transcriptase. Then, we performed a pull-down assay combined with RT-PCR to detect the enrichment of these candidate miRNA levels (**Figure 4B**). The result showed that 6

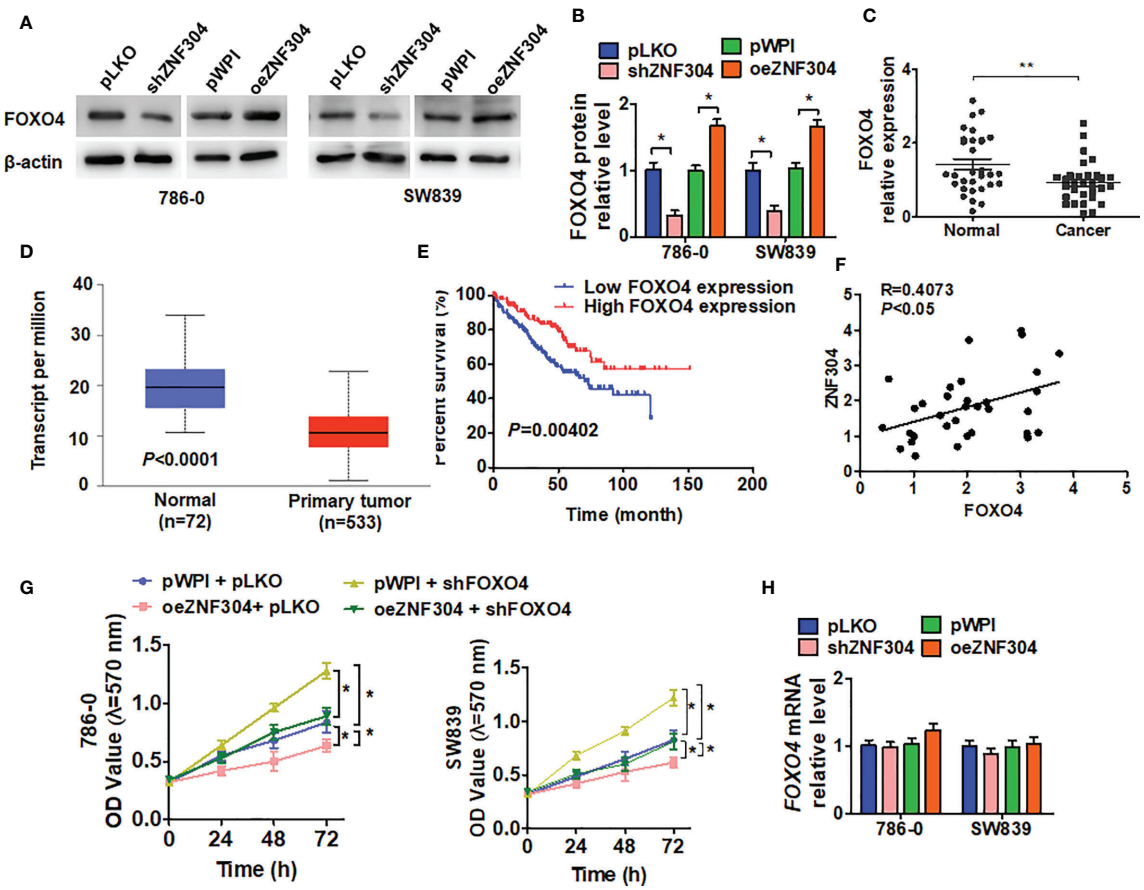


FIGURE 3 | FOXO4 regulates ZNF304-mediated cell proliferation. **(A)** 786-0 and SW839 cells were transfected with pKLO, shZNF304, pWPI, and oeZNF304 vectors, and then protein expression of FOXO4 was measured by western blot. **(B)** Quantitative analysis of **(A)**. **(C)** The expression of FOXO4 mRNA was measured by qRT-PCR in ccRCC (T, n = 43) and normal kidney (N, n = 43) tissues. **(D)** the overall survival of ccRCC patients from the TCGA database was analyzed by Kaplan–Meier analysis. FOXO4 levels low (n = 130) and high (n = 130) (cutoff value is 25%). **(E)** The correlation between ZNF304 and FOXO4 mRNA expression in PCa tissues was analyzed by Pearson correlation analysis of our clinical data (R = 0.4073, $P < 0.05$). **(F)** 786-0 and SW839 cells were transfected with oeZNF304, shFOXO4, oeZNF304 + shFOXO4 and control vectors, and cell viability was measured by MTT. **(G)** Cells were prepared as in **(A)**, and FOXO4 mRNA was detected by RT-qPCR. **(H)** Cells were prepared as in **(A)**, and cell viability was measured by MTT **(D)** and colony formation assays **(E, F)**. All data are from three independent experiments and expressed as the mean ± SEM. *P < 0.05, **P < 0.01 vs. the corresponding controls.

high enrichment miRNAs were changed after up- and downregulation of ZNF304. However, only miR-183-5p was increased in shZNF304 transfected cells and decreased in ZNF304 overexpressing cells (**Figure 4C**). In addition, the luciferase reporter assay demonstrated that miR-183-5p can target the 3′UTR of FOXO4 (**Figures 4D, E**). Furthermore, western blot also confirmed that FOXO4 was a directly target of miR-183-5p (**Figures 4F, G**). miR-183-5p mimic facilitated cell proliferation and reversed cell growth inhibition caused by ZNF304 overexpression (**Figure 4H**). Totally, these finding indicated that miR-183-5p, which was regulated by ZNF304, directly targets 3′URT and repressed FOXO4 expression.

ZNF304 Regulates miR-183-5p Transcription

In order to confirm whether ZNF304 directly regulated miR-183-5p expression through transcription, we first analyzed the potential ZNF304 binding sites in the miR-183 2-kb 5'-promoter region on the nsembl and PROMO 3.0 websites. The results showed that there were three potential binding sites for ZNF304 in this region. (**Figure 5A**). ChIP analysis proved that ZNF304 mainly bound to the -80 to -65 bp region of the transcription start site in the miR-183 promoter (**Figure 5B**). Furthermore, in RCC cells where ZNF304 was downregulated pre-miR-183-5p expression was promoted and ZNF304 downregulation inhibited pre-miR-183-5p expression (**Figure 5C**). Compare to the normal kidney tissues, miR-183-5p level was significantly upregulation in ccRCC tissues (T) (**Figure 5D**). And the higher expression level of miR-183-5p in ccRCC patients were associated with poor overall survival (**Figure 5E**). Additionally, the mRNA level of miR-183-5p was positively correlated with ZNF304 in ccRCC tissues (**Figure 5F**). These findings reveal that ZNF304 directly promotes miR-183-5p transcription.

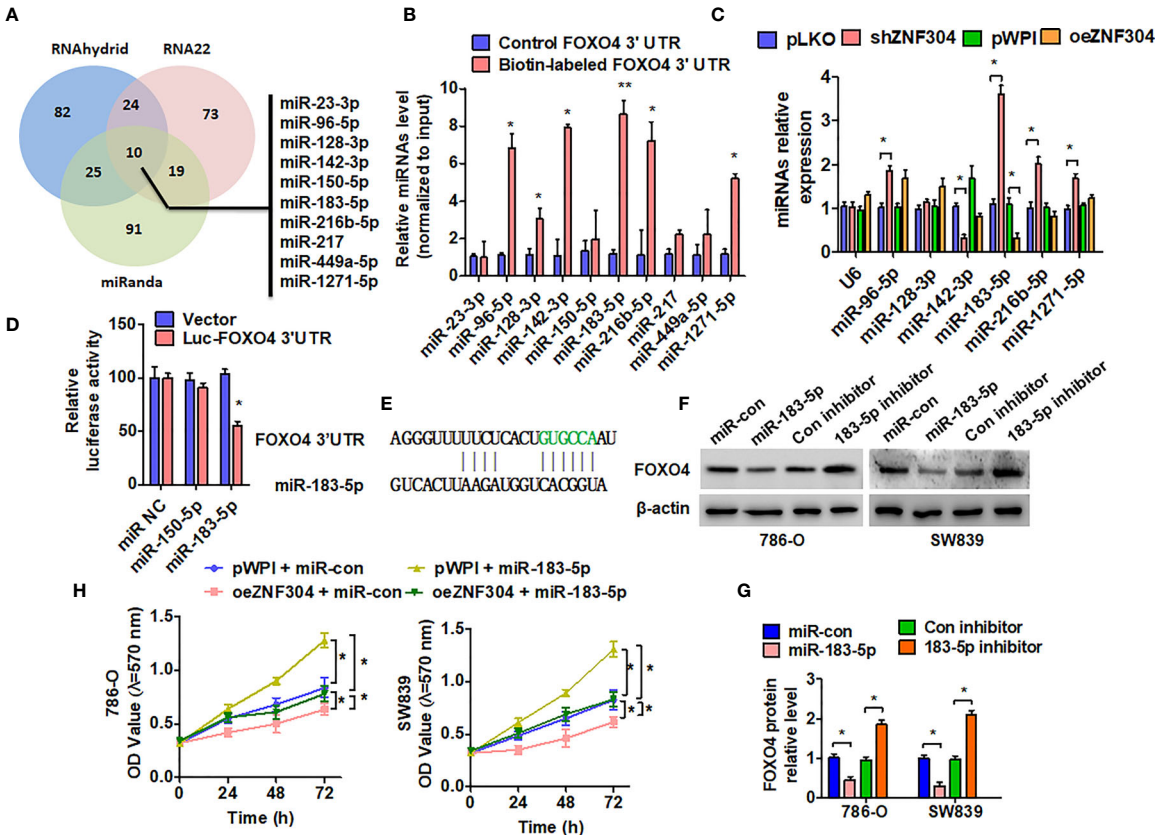


FIGURE 4 | miR-183-5p mediates ZNF304-regulated FOXO4 expression in ccRCC. **(A)** Potential microRNAs targeted 3′UTR of FOXO4 were predicted in three online target-prediction programs, and showed with venn diagram. **(B)** Biotin pull-down assay was used to enrich miRNAs, and RT-qPCR was used to detect these candidate miRNAs. **(C)** 786-0 cells were transfected with oeZNF304 or shZNF304 or control vectors. Candidate miRNAs were detected by using RT-qPCR. U6 served as a negative control. **(D)** 786-0 cells were co-transfected with the FOXO4 3′UTR and miR-183-5p or miR-150-5p mimics. Luciferase reporter assays showed that miR-183-5p reduced FOXO4 3′UTR luciferase activity. **(E)** The prediction of miR-183-5p binding site in the FOXO4 3′UTR. **(F, G)** 786-0 and SW839 cells were transfected with the indicated miRNAs, and then FOXO4 protein expression was measured by western blotting. **(H)** 786-0 and SW839 cells were co-transfected with the indicated miRNAs and vectors, and cell viability was measured by MTT. All data are from three independent experiments and expressed as the mean ± SEM. *P < 0.05, **P < 0.01 vs. the corresponding controls.

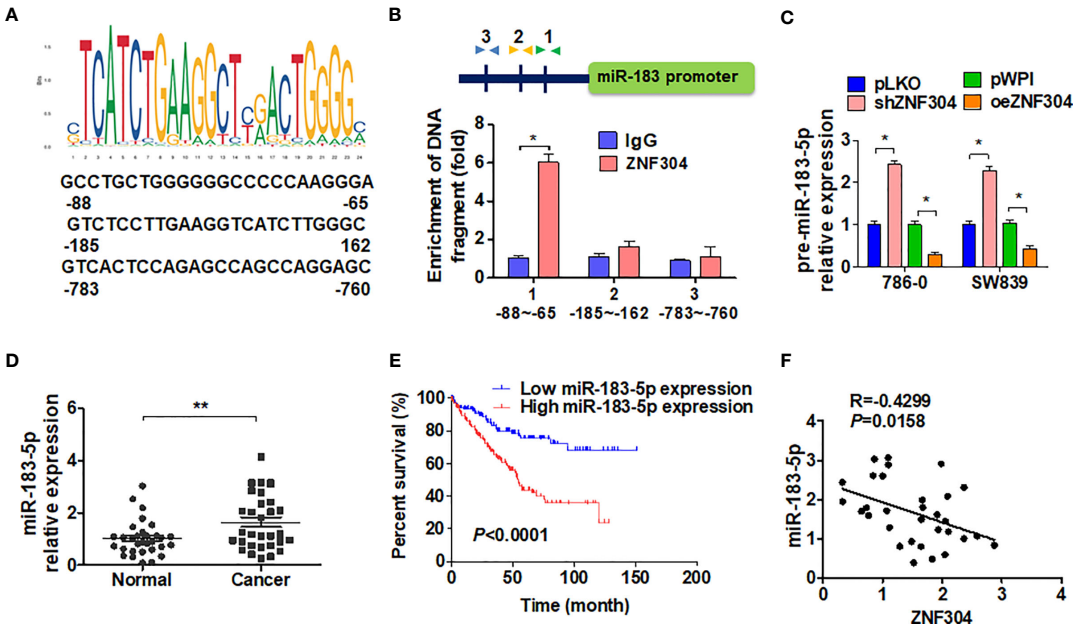


FIGURE 5 | ZNF304 downregulates miR-183-5p expression by transcriptional repression. **(A)** The level of miR-183-5p was detected by qRT-PCR in ccRCC (T, n = 43) and normal kidney (N, n = 43) tissues. **(B)** According to the expression level of miR-183-5p in the TCGA database, kaplan-Meier was used to analyze the overall survival of ccRCC patients (cutoff value is 25%). **(C)** Pearson correlation analysis ZNF304 and miR-183-5p correlation (R = 0.4299, *P* = 0.0158). **(D)** JASPAR (http://jaspar.genereg.net/) predicted the potential binding site for ZNF304 in the miR-183-5p promotor. **(E)** Binding site of ZNF304 in miR-183-5p promoter region was confirmed by using ChIP-qPCR in 786-0 cell. The position of the primer is indicated by the arrowheads. **(F)** 786-0 and SW839 cells were transfected with oeZNF304 or shZNF304 or control vectors, and pre-miR-183-5p expression was measured by RT-qPCR. All data are from three independent experiments and expressed as the mean ± SEM. *P < 0.05, **P < 0.01 vs. the corresponding controls.

Disruption of ZNF304/miR-183-5p/FOXO4 Axis Inhibits ccRCC Progression

Overexpression of ZNF304 increased FOXO4 protein level and reduced cyclin D1 level, and the regulation of FOXO4 was enhanced by miR-183-5p inhibitor co-transfection (**Figures 6A, B**). Depletion of FOXO4 promoted cyclin D1 expression, while miR-183-5p inhibitor co-transfection reversed the promotion of FOXO4 (**Figures 6C, D**). Finally, we used a xenograft model to examine whether disruption of ZNF304/miR-183-5p/FOXO4 axis inhibits cell growth *in vivo*. Injection of 786-0 cells with stable depletion of miR-183-5p, to block ZNF304/miR-183-5p/FOXO4 axis, yielded smaller tumors in nude mice than in those injected with sham-transfected cells (**Figures 6E, F**). Similarly, stable knockdown of miR-183-5p also resulted in a smaller wet tumor weight (**Figure 6G**). Western blot analysis also revealed that silence of miR-183-5p significantly increased FOXO4 but reduced cyclin D1 proteins level compared to tumors derived from control cells (**Figure 6H**). These findings suggest that disruption of ZNF304/miR-183-5p/FOXO4 axis inhibits cell proliferation in ccRCC cells *in vivo*.

DISCUSSION

The main discovery in this study is that ZNF304, which is significantly decreased in ccRCC tissues, acts as a critical upstream regulator of FOXO4. Overexpression of ZNF304 resulted in antitumor activity and inhibited RCC cell growth *in vitro* through FOXO4 upregulation. Low level of ZNF304 mRNA was associated with poor survival of ccRCC patients. Interestingly, ZNF304 positively regulated FOXO4 protein expression but not mRNA level. Mechanistically, ZNF304 bound to miR-183 promoter and activated miR-183-5p transcription. Upregulation of miR-183-5p directly bound to 3′ UTR of FOXO4 and repressed its expression (**Figure 7**). Our findings suggest ZNF304/miR-183-5p/FOXO4 pathway plays a vital role in regulation of cell survival in ccRCC.

The occurrence and development of tumors is a complex process involving multi-step, multi-stage, and multi-factor regulation (31). This process also involves the abnormal expression of many genes, such as the upregulation of proto-oncogenes and the downregulation of tumor suppressor genes (12–15). However, many current studies have focused on upregulated genes in tumors, and have ignored the research on downregulated genes. In fact, these abnormal genes play an equally important role in the tumor process (16). On the technical level, it is easier for researchers to develop targeted inhibitors or targeted suppression of upregulated genes than targeted downregulated genes. However, genes whose expression is downregulated can also achieve tumor suppression through the development of agonists or targeted upregulation. In the present study, we demonstrated that ZNF304 downregulated in ccRCC and downregulation of ZNF304 promoted

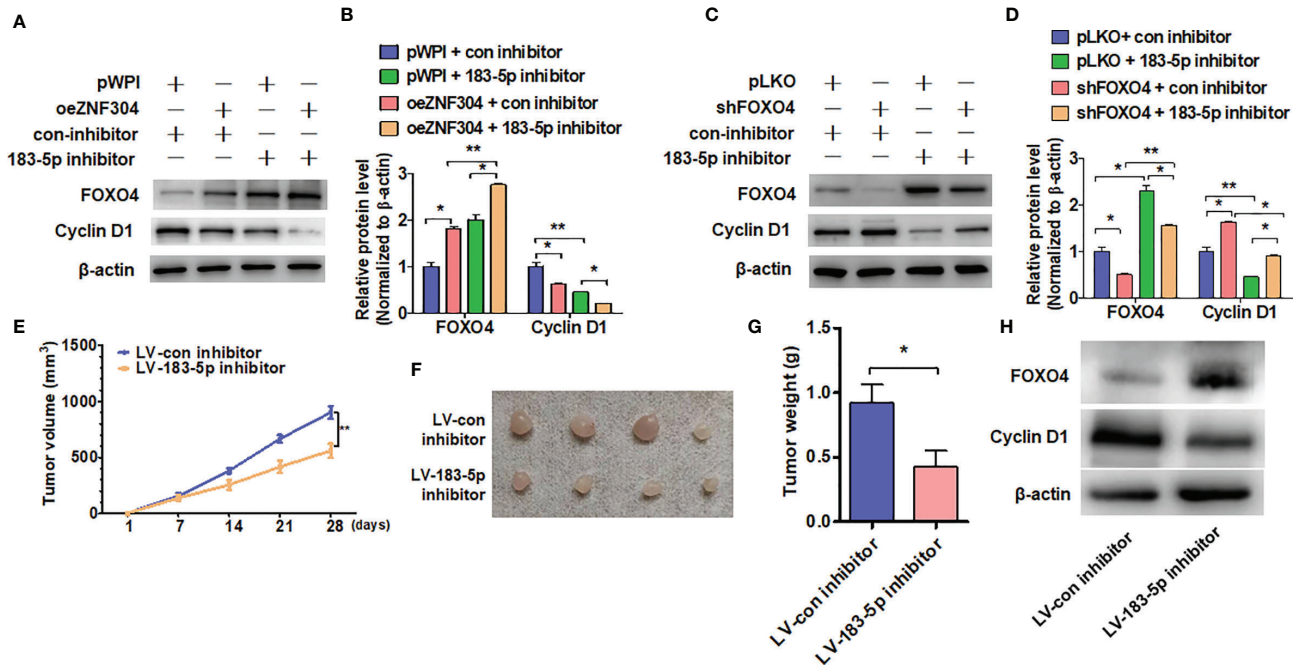


FIGURE 6 | ZNF304/miR-183-5p/FOXO4 axis inhibits ccRCC progression. **(A, B)** 786-0 cells were transfected with the oeZNF304, 183-5p inhibitor or co-transfected with both and then subjected to western blot analysis the FOXO4 and Cyclin D1 protein level. **(C, D)** Indicated RNA and vectors were used to transfect into 786-0 cells and the FOXO4 and Cyclin D1protein level were detected by Western blot. **(E–G)** xenograft tumors were performed by injecting 786-0 cells with stably downregulated miR-183-5p in nude mice and tumor volumes **(E, F)** or tumor weight **(G)** were measured by direct measurement. **(H)** FOXO4 and Cyclin D1 proteins level in xenograft tumors were examined by using western blot. All data are from three independent experiments and expressed as the mean ± SEM. *P < 0.05, **P < 0.01 vs. the corresponding controls.

expression of miR-183-5p which is a upstream molecular of FOXO4. *In vivo* and *in vitro* results indicate that overexpression of ZNF304 or targeted inhibition of miR-183-5p can effectively inhibit tumor progression. Therefore, development of ZNF304 or FOXO4 agonists or the use of technologies such as CRISPR-Cas9 (32, 33) to target upregulation of these genes expression, or the use of miR-183-5p antagonists are expected to achieve the inhibition of tumor progression. Therefore, we believe that the downstream pathway of ZNF304 is possible as a potential anti-tumor pathway. We plan to explore the upstream regulator of ZNF304 and FOXO4 in our next study.

FOXO4, as a transcription inhibitor, one of its important functions is to inhibit tumor growth (21). Downregulation of FOXO4 in nasopharyngeal carcinoma is significant and related to distant metastasis, tumor recurrence and low overall patient survival rate (34). Concomitantly, the expression of FOXO4 is negatively correlated with the level of miR-150, and overexpression of FOXO4 significantly reduces tumor cell invasion *in vitro* (34). FOXO4 overexpression inhibits breast cancer cell growth and delays the occurrence and development of tumors in nude mice (35). Cholangiocarcinoma cell growth *in vitro* is repressed by FOXO4 *via* induction of G0/G1 arrest (36). FOXO4 also limits glioblastoma development by inhibiting the malignant phenotype of cells (25). In addition, FOXO4 has been shown to inhibit cervical cancer, gastric cancer, liver and nasopharyngeal cancer cell growth and tumor progression (37–40). However, little is known about the function of FOXO4 in ccRCC.

miRNA participates in a variety of biological processes through post-transcriptional regulation, including cell growth, migration and invasion, cell cycle progression and apoptosis (41). Abnormally expressed miRNAs may have an oncogene or tumor suppressor effect, often depending on the biological function of its target (42). In previous studies, we found that miR-193a-5p silencing inhibited the resistance of prostate cancer cells to docetaxel (29). miR-193a-5p mediates the p53-RBM25-circAMOTL1L axis to regulate Pcdha expression in the epithelial-mesenchymal transition of prostate cancer cells (30, 43). Our recent study found that miR-212-5p/miR-449a inhibits the expression of E2F5 and mediates circCDK13/CDK13 feedback regulation to promote the occurrence and development of prostate cancer (28). Depletion of miR-183-5p reduces radio-resistance in colorectal cancer through direct retinal ATG5 (44). In addition, miR-183-5p facilitates growth and metastasis of hepatocellular carcinoma cells by targeting IRS1 and is associated with patient survival (45). Similar to our study, Li et al. reported that higher level of miR-183-5p was associated with poor survival of patients after RCC surgery (46). In the present study, we demonstrated that level of miR-183-5p was significantly elevated in ccRCC tissues compared to normal kidney tissues. The higher level of miR-183-5p predicted poor overall survival of patients with ccRCC. By targeting 3′UTR of FOXO4, miR-183-5p inhibited FOXO4

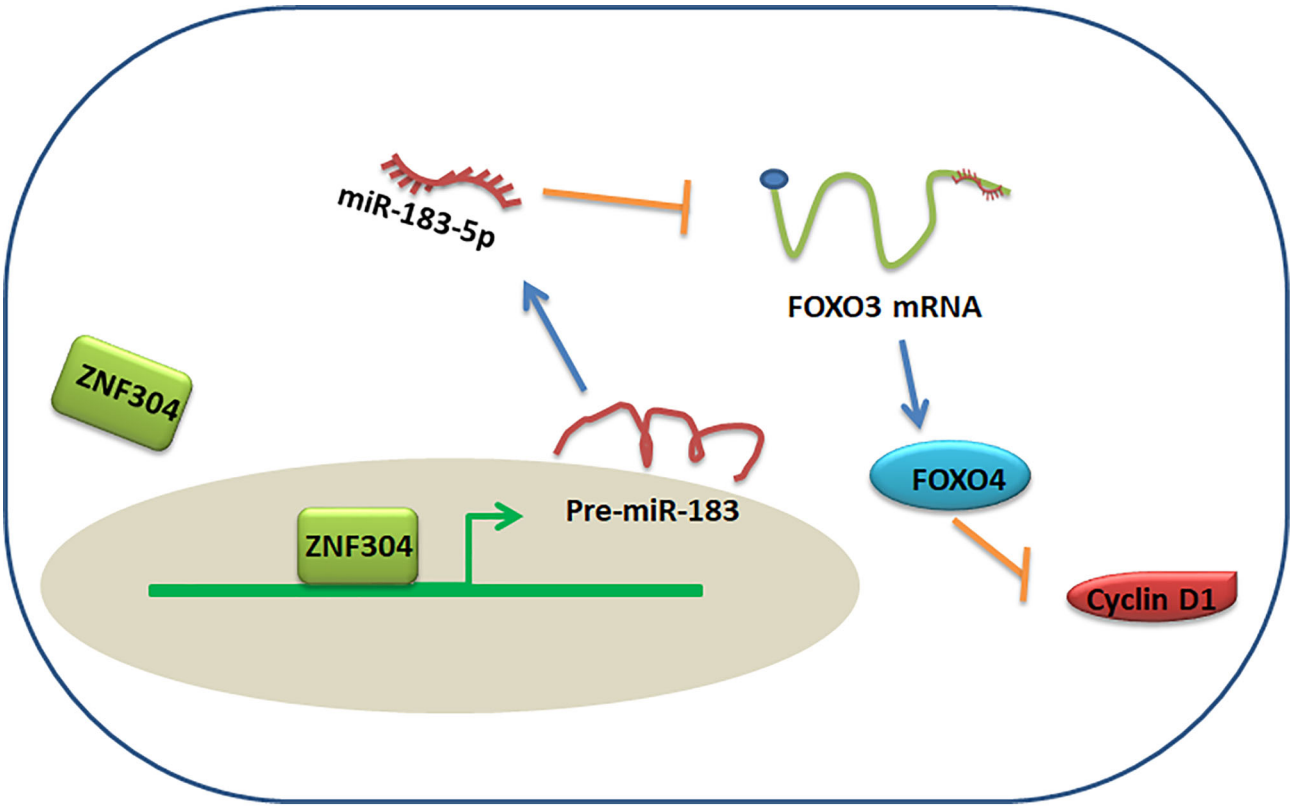


FIGURE 7 | Proposed model for ZNF304/miR-183-5p/FOXO4 regulation of ccRCC progression.

expression in RCC cells. Interestingly, ZNF304, which is a upstream regulator of FOXO4, bound to miR-183 promoter and repressed miR-183-5p transcription.

CONCLUSION

In summary, our results demonstrated that downregulation of ZNF304 affected miR-183-5p/FOXO4 axis, further repressing cell growth in ccRCC. These data provide theoretical evidence that ZNF304/miR-183-5p/FOXO4 pathway plays a critical role in ccRCC progression. Therefore, a comprehensive understanding of the mechanism responsible for regulating this axis will promote the development of an effective therapeutic strategy to inhibit ccRCC progression.

DATA AVAILABILITY STATEMENT

The original contributions presented in the study are included in the article/**Supplementary Material**. Further inquiries can be directed to the corresponding authors.

ETHICS STATEMENT

The studies involving human participants were reviewed and approved by The Ethics Committee of the Second Hospital of Hebei Medical University. The patients/participants provided their written informed consent to participate in this study.

AUTHOR CONTRIBUTIONS

ZY, J-FG, and L-XR contributed to conception and design of the study. L-XR, BS, HZ, D-DW, and MZ organized the database. B-WZ performed the statistical analysis. L-XR and ZY wrote the first draft of the manuscript. ZY, J-FG, B-WZ, and L-XR wrote sections of the manuscript. All authors contributed to the article and approved the submitted version.

FUNDING

This study was partially supported by The National Natural Science Foundation of China (No. 81970216, 82072842), Excellent Youth Science Foundation of Hebei Province (H2019206536).

SUPPLEMENTARY MATERIAL

The Supplementary Material for this article can be found online at: https://www.frontiersin.org/articles/10.3389/fonc.2021.710525/full#supplementary-material

REFERENCES

1. Gray RE, Harris GT. Renal Cell Carcinoma: Diagnosis and Management. *Am Fam Physician* (2019) 99(3):179–84.
2. Siegel RL, Miller KD, Fuchs HE, Jemal A. Cancer Statistics, 2021. *CA Cancer J Clin* (2021) 71(1):7–33. doi: 10.3322/caac.21654
3. Ricketts CJ, De Cubas AA, Fan H, Smith CC, Lang M, Reznik E, et al. The Cancer Genome Atlas Comprehensive Molecular Characterization of Renal Cell Carcinoma. *Cell Rep* (2018) 23(1):313–26.e5. doi: 10.1016/j.celrep.2018.03.075
4. Hsieh JJ, Purdue MP, Signoretti S, Swanton C, Albiges L, Schmidinger M, et al. Renal Cell Carcinoma. *Nat Rev Dis Primers* (2017) 3:17009. doi: 10.1038/nrdp.2017.9
5. Petejova N, Martinek A. Renal Cell Carcinoma: Review of Etiology, Pathophysiology and Risk Factors. *BioMed Pap Med Fac Univ Palacky Olomouc Czech Repub* (2016) 160(2):183–94. doi: 10.5507/bp.2015.050
6. Gershman B, Thompson RH, Boorjian SA, Lohse CM, Costello BA, Cheville JC, et al. Radical Versus Partial Nephrectomy for Ct1 Renal Cell Carcinoma. *Eur Urol* (2018) 74(6):825–32. doi: 10.1016/j.eururo.2018.08.028
7. Cheng SK, Chuah KL. Metastatic Renal Cell Carcinoma to the Pancreas: A Review. *Arch Pathol Lab Med* (2016) 140(6):598–602. doi: 10.5858/arpa.2015-0135-RS
8. Deleuze A, Saout J, Dugay F, Peyronnet B, Mathieu R, Verhoest G, et al. Immunotherapy in Renal Cell Carcinoma: The Future Is Now. *Int J Mol Sci* (2020) 21(7):2532–54. doi: 10.3390/ijms21072532
9. Choueiri TK, Motzer RJ. Systemic Therapy for Metastatic Renal-Cell Carcinoma. *N Engl J Med* (2017) 376(4):354–66. doi: 10.1056/NEJMra1601333
10. Choueiri TK, Escudier B, Powles T, Mainwaring PN, Rini BI, Donskov F, et al. Cabozantinib Versus Everolimus in Advanced Renal-Cell Carcinoma. *N Engl J Med* (2015) 373(19):1814–23. doi: 10.1056/NEJMoa1510016
11. Wiechno P, Kucharz J, Sadowska M, Michalski W, Sikora-Kupis B, Jonska-Gmyrek J, et al. Contemporary Treatment of Metastatic Renal Cell Carcinoma. *Med Oncol* (2018) 35(12):156. doi: 10.1007/s12032-018-1217-1
12. Liu Y, Ao X, Ding W, Ponnusamy M, Wu W, Hao X, et al. Critical Role of FOXO3a in Carcinogenesis. *Mol Cancer* (2018) 17(1):104. doi: 10.1186/s12943-018-0856-3
13. Dey P, Li J, Zhang J, Chaurasiya S, Strom A, Wang H, et al. Oncogenic KRAS-Driven Metabolic Reprogramming in Pancreatic Cancer Cells Utilizes Cytokines From the Tumor Microenvironment. *Cancer Discov* (2020) 10(4):608–25. doi: 10.1158/2159-8290.CD-19-0297
14. Beuselinck B, Jean-Baptiste J, Couchy G, Job S, De Reynies A, Wolter P, et al. RANK/OPG Ratio of Expression in Primary Clear-Cell Renal Cell Carcinoma is Associated With Bone Metastasis and Prognosis in Patients Treated With Anti-VEGFR-TKIs. *Br J Cancer* (2015) 113(9):1313–22. doi: 10.1038/bjc.2015.352
15. Xu YP, Lv L, Liu Y, Smith MD, Li WC, Tan XM, et al. Tumor Suppressor TET2 Promotes Cancer Immunity and Immunotherapy Efficacy. *J Clin Invest* (2019) 129(10):4316–31. doi: 10.1172/JCI129317
16. Kontomanolis EN, Koutras A, Syllaios A, Schizas D, Mastoraki A, Garmpis N, et al. Role of Oncogenes and Tumor-Suppressor Genes in Carcinogenesis: A Review. *Anticancer Res* (2020) 40(11):6009–15. doi: 10.21873/anticanres.14622
17. Sabater L, Ashhab Y, Caro P, Kolkowski EC, Pujol-Borrell R, Dominguez O. Identification of a KRAB-Containing Zinc Finger Protein, ZNF304, by AU-Motif-Directed Display Method and Initial Characterization in Lymphocyte Activation. *Biochem Biophys Res Commun* (2002) 293(3):1066–72. doi: 10.1016/S0006-291X(02)00344-3
18. Aslan B, Monroig P, Hsu MC, Pena GA, Rodriguez-Aguayo C, Gonzalez-Villasana V, et al. The ZNF304-Integrin Axis Protects Against Anoikis in Cancer. *Nat Commun* (2015) 6:7351. doi: 10.1038/ncomms8351
19. Serra RW, Fang M, Park SM, Hutchinson L, Green MR. A KRAS-Directed Transcriptional Silencing Pathway That Mediates the CpG Island Methylator Phenotype. *Elife* (2014) 3:e02313. doi: 10.7554/eLife.02313
20. Tia N, Singh AK, Pandey P, Azad CS, Chaudhary P, Gambhir IS. Role of Forkhead Box O (FOXO) Transcription Factor in Aging and Diseases. *Gene* (2018) 648:97–105. doi: 10.1016/j.gene.2018.01.051
21. Jiang S, Yang Z, Di S, Hu W, Ma Z, Chen F, et al. Novel Role of Forkhead Box O 4 Transcription Factor in Cancer: Bringing Out the Good or the Bad. *Semin Cancer Biol* (2018) 50:1–12. doi: 10.1016/j.semcancer.2018.04.007
22. Beretta GL, Corno C, Zaffaroni N, Perego P. Role of FoxO Proteins in Cellular Response to Antitumor Agents. *Cancers (Basel)* (2019) 11(1):90–106. doi: 10.3390/cancers11010090
23. Coomans de Brachene A, Demoulin JB. FOXO Transcription Factors in Cancer Development and Therapy. *Cell Mol Life Sci* (2016) 73(6):1159–72. doi: 10.1007/s00018-015-2112-y
24. Sheng Z, Ma L, Sun JE, Zhu LJ, Green MR. BCR-ABL Suppresses Autophagy Through ATF5-Mediated Regulation of mTOR Transcription. *Blood* (2011) 118(10):2840–8. doi: 10.1182/blood-2010-12-322537
25. Qi M, Sun LA, Jiang XC, Han YL, Wang L, Niu WH, et al. FOXO4 Expression Associates With Glioblastoma Development and FOXO4 Expression Inhibits Cell Malignant Phenotypes *In Vitro* and *In Vivo*. *Life Sci* (2020) 247:117436. doi: 10.1016/j.lfs.2020.117436
26. Wang W, Zhou PH, Hu W. Overexpression of FOXO4 Induces Apoptosis of Clear-Cell Renal Carcinoma Cells Through Downregulation of Bim. *Mol Med Rep* (2016) 13(3):2229–34. doi: 10.3892/mmr.2016.4789
27. Cui S, Wang B, Zhao Y, Chen H, Ding H, Zhi D, et al. Transmembrane Routes of Cationic Liposome-Mediated Gene Delivery Using Human Throat Epidermis Cancer Cells. *Biotechnol Lett* (2014) 36(1):1–7. doi: 10.1007/s10529-013-1325-0
28. Qi JC, Yang Z, Lin T, Ma L, Wang YX, Zhang Y, et al. CDK13 Upregulation-Induced Formation of the Positive Feedback Loop Among Circcdk13, miR-212-5p/miR-449a and E2F5 Contributes to Prostate Carcinogenesis. *J Exp Clin Cancer Res* (2021) 40(1):2. doi: 10.1186/s13046-020-01814-5
29. Yang Z, Chen JS, Wen JK, Gao HT, Zheng B, Qu CB, et al. Silencing of miR-193a-5p Increases the Chemosensitivity of Prostate Cancer Cells to Docetaxel. *J Exp Clin Cancer Res* (2017) 36(1):178. doi: 10.1186/s13046-017-0649-3
30. Yang Z, Qu CB, Zhang Y, Zhang WF, Wang DD, Gao CC, et al. Dysregulation of P53-RBM25-Mediated circAMOTL1L Biogenesis Contributes to Prostate Cancer Progression Through the circAMOTL1L-miR-193a-5p-Pcdha Pathway. *Oncogene* (2019) 38(14):2516–32. doi: 10.1038/s41388-018-0602-8
31. Mo Y, Wang Y, Zhang L, Yang L, Zhou M, Li X, et al. The Role of Wnt Signaling Pathway in Tumor Metabolic Reprogramming. *J Cancer* (2019) 10(16):3789–97. doi: 10.7150/jca.31166
32. Roberston MJ, Raghunathan S, Potaman VN, Zhang F, Stewart MD, McConnell BK, et al. CRISPR-Cas9-Induced IGF1 Gene Activation as a Tool for Enhancing Muscle Differentiation via Multiple Isoform Expression. *FASEB J* (2020) 34(1):555–70. doi: 10.1096/fj.201901107RR
33. Osborn MJ, Lees CJ, McElroy AN, Merkel SC, Eide CR, Mathews W, et al. CRISPR/Cas9-Based Cellular Engineering for Targeted Gene Overexpression. *Int J Mol Sci* (2018) 19(4):946–66. doi: 10.3390/ijms19040946
34. Liu B, Tan Z, Jiang Y, Chen Y, Chen Y, Ling K. Correlation Between the Expression of miR150 and FOXO4 and the Local Recurrence and Metastasis of Nasopharyngeal Carcinoma After Intensive Radiotherapy. *J BUON* (2018) 23(6):1671–78.
35. Yang H, Zhao R, Yang HY, Lee MH. Constitutively Active FOXO4 Inhibits Akt Activity, Regulates P27 Kip1 Stability, and Suppresses HER2-Mediated Tumorigenicity. *Oncogene* (2005) 24(11):1924–35. doi: 10.1038/sj.onc.1208352
36. Intuyod K, Chomwong S, Thongpon P, Vaeteewoottacharn K, Pairojkul C, Pinlaor P, et al. Expression of FOXO4 Inhibits Cholangiocarcinoma Cell Proliferation *In Vitro via* Induction of G0/G1 Arrest. *Anticancer Res* (2020) 40(12):6899–905. doi: 10.21873/anticanres.14713
37. Li J, Hu L, Tian C, Lu F, Wu J, Liu L. microRNA-150 Promotes Cervical Cancer Cell Growth and Survival by Targeting FOXO4. *BMC Mol Biol* (2015) 16:24. doi: 10.1186/s12867-015-0052-6
38. Zhang T, Wan C, Shi W, Xu J, Fan H, Zhang S, et al. The RNA-Binding Protein Sam68 Regulates Tumor Cell Viability and Hepatic Carcinogenesis by Inhibiting the Transcriptional Activity of FOXOs. *J Mol Histol* (2015) 46(6):485–97. doi: 10.1007/s10735-015-9639-y
39. Su L, Liu X, Chai N, Lv L, Wang R, Li X, et al. The Transcription Factor FOXO4 is Down-Regulated and Inhibits Tumor Proliferation and Metastasis in Gastric Cancer. *BMC Cancer* (2014) 14:378. doi: 10.1186/1471-2407-14-378
40. Chen L, Tang Y, Wang J, Yan Z, Xu R. miR-421 Induces Cell Proliferation and Apoptosis Resistance in Human Nasopharyngeal Carcinoma via Downregulation of FOXO4. *Biochem Biophys Res Commun* (2013) 435(4):745–50. doi: 10.1016/j.bbrc.2013.05.056
41. He L, Hannon GJ. MicroRNAs: Small RNAs With a Big Role in Gene Regulation. *Nat Rev Genet* (2004) 5(7):522–31. doi: 10.1038/nrg1379

42. Wiemer EA. The Role of microRNAs in Cancer: No Small Matter. *Eur J Cancer* (2007) 43(10):1529–44. doi: 10.1016/j.ejca.2007.04.002
43. Atala A. Re: Dysregulation of P53-RBM25-Mediated circAMOTL1L Biogenesis Contributes to Prostate Cancer Progression Through the circAMOTL1L-miR-193a-5p-Pcdha Pathway. *J Urol* (2020) 203(2):256–57. doi: 10.1097/01.JU.0000613432.22169.0b
44. Zheng S, Zhong YF, Tan DM, Xu Y, Chen HX, Wang D. miR-183-5p Enhances the Radioresistance of Colorectal Cancer by Directly Targeting ATG5. *J Biosci* (2019) 44(4):92–103. doi: 10.1007/s12038-019-9918-y
45. Yan R, Li K, Yuan D, Wang H, Chen W, Zhu K, et al. miR-183-5p Promotes Proliferation and Migration in Hepatocellular Carcinoma by Targeting IRS1 and Its Association With Patient Survival. *Int J Biol Markers* (2020) 35(3):83–9. doi: 10.1177/1724600820951572
46. Li H, Pan X, Gui Y, Quan J, Li Z, Zhao L, et al. Upregulation of miR-183-5p Predicts Worse Survival in Patients With Renal Cell Cancer After Surgery. *Cancer Biomark* (2019) 24(2):153–58. doi: 10.3233/CBM-182047

Conflict of Interest: The authors declare that the research was conducted in the absence of any commercial or financial relationships that could be construed as a potential conflict of interest.

Publisher's Note: All claims expressed in this article are solely those of the authors and do not necessarily represent those of their affiliated organizations, or those of the publisher, the editors and the reviewers. Any product that may be evaluated in this article, or claim that may be made by its manufacturer, is not guaranteed or endorsed by the publisher.

Copyright © 2021 Ren, Zeng, Zhu, Zhao, Shi, Zhang, Wang, Gu and Yang. This is an open-access article distributed under the terms of the Creative Commons Attribution License (CC BY). The use, distribution or reproduction in other forums is permitted, provided the original author(s) and the copyright owner(s) are credited and that the original publication in this journal is cited, in accordance with accepted academic practice. No use, distribution or reproduction is permitted which does not comply with these terms.

frontiers in Oncology

ORIGINAL RESEARCH
published: 12 October 2021
doi: 10.3389/fonc.2021.651692

MiRNA-146a/AKT/β-Catenin Activation Regulates Cancer Stem Cell Phenotype in Oral Squamous Cell Carcinoma by Targeting CD24

Sangeeta Ghuwalewala[1†], Dishari Ghatak[1†], Sumit Das[2], Stuti Roy[3], Pijush Das[1], Ramesh Butti[2], Mahadeo Gorain[2], Somsubhra Nath[3], Gopal C. Kundu[2] and Susanta Roychoudhury[1,3]*

[1] Cancer Biology and Inflammatory Disorder Division, Council of Scientific and Industrial Research (CSIR)-Indian Institute of Chemical Biology, Kolkata, India, [2] Laboratory of Tumor Biology, Angiogenesis and Nanomedicine Research, National Centre for Cell Science (NCCS), Pune, India, [3] Division of Research, Saroj Gupta Cancer Centre and Research Institute, Kolkata, India

OPEN ACCESS

Edited by:
Ira Ida Skvortsova, Innsbruck Medical University, Austria

Reviewed by:
Minal Garg, University of Lucknow, India
Taichi Isobe, Kyushu University, Japan
Rakesh Rawal, Gujarat University, India

***Correspondence:**
Susanta Roychoudhury
susantarc@gmail.com

[†]These authors have contributed equally to this work

Specialty section:
This article was submitted to Molecular and Cellular Oncology, a section of the journal Frontiers in Oncology

Received: *10 January 2021*
Accepted: *16 September 2021*
Published: *12 October 2021*

Citation:
Ghuwalewala S, Ghatak D, Das S, Roy S, Das P, Butti R, Gorain M, Nath S, Kundu GC and Roychoudhury S (2021) MiRNA-146a/AKT/β-Catenin Activation Regulates Cancer Stem Cell Phenotype in Oral Squamous Cell Carcinoma by Targeting CD24. Front. Oncol. 11:651692. doi: 10.3389/fonc.2021.651692

$CD44^{high}CD24^{low}$ population has been previously reported as cancer stem cells (CSCs) in Oral Squamous Cell Carcinoma (OSCC). Increasing evidence suggests potential involvement of microRNA (miRNA) network in modulation of CSC properties. MiRNAs have thus emerged as crucial players in tumor development and maintenance. However, their role in maintenance of OSCC stem cells remains unclear. Here we report an elevated expression of miR-146a in the $CD44^{high}CD24^{low}$ population within OSCC cells and primary HNSCC tumors. Moreover, over-expression of miR-146a results in enhanced stemness phenotype by augmenting the $CD44^{high}CD24^{low}$ population. We demonstrate that miR-146a stabilizes β-catenin with concomitant loss of E-cadherin and CD24. Interestingly, CD24 is identified as a novel functional target of miR-146a and ectopic expression of CD24 abrogates miR-146a driven potential CSC phenotype. Mechanistic analysis reveals that higher CD24 levels inhibit AKT phosphorylation leading to β-catenin degradation. Using stably expressing miR-146a/CD24 OSCC cell lines, we also validate that the miR-146a/CD24/AKT loop significantly alters tumorigenic ability *in vivo*. Furthermore, we confirmed that β-catenin trans-activates miR-146a, thereby forming a positive feedback loop contributing to stem cell maintenance. Collectively, our study demonstrates that miR-146a regulates CSCs in OSCC through CD24-AKT-β-catenin axis.

Keywords: mir-146a, β-catenin, Wnt-AKT signalling, CD24, stemness, OSCC

INTRODUCTION

OSCC is the most prevalent form of head and neck cancers worldwide with more than 60% individuals diagnosed with advanced tumors (1). The oral CSCs are held responsible for tumor aggressiveness leading to treatment failures, relapse and development of metastases (2, 3). Over the past decade, epigenetic re-programming has emerged as a crucial mechanism of regulating cancer stem cell dynamics (4, 5). These include DNA methylation, histone modifications and chromatin

remodeling having robust effect upon cellular fate and stem cell potential. Another such epigenetic regulatory mechanism that has recently gained considerable importance in tumor biology are the miRNAs. MiRNAs are small ncRNAs of 20-22 nucleotides, de-regulation of which may have critical roles in disease development. They can act either as oncogenes or as tumor-suppressors depending upon the specific genes targeted (6, 7). MiRNA associated signatures are now considered for cancer specific diagnostic and prognostic purposes (8, 9).

MiRNAs not only regulate primary cellular functions like proliferation, differentiation, migration and invasion, but also directly or indirectly influence CSC functions (10). These are mostly attributed to altered signaling pathways including cell surface markers, pluripotency factors, chemo-resistance and epithelial-to-mesenchymal transition (EMT) markers (11–14). Role of miR-34a, miR-145a and miR-200bc family in regulating CD44, Oct4, Sox2, KLF4, Bmi1, Zeb1/2 and Notch1 has been well established (15–17). Thus, by precisely regulating the CSC related genes, miRNAs themselves have emerged as inherent modulators of cancer stem cells. MiR-146a is predominantly an onco-miR, which directly targets *IRAK1*, *traf6*, and *numb* genes in OSCC and imparts tumorigenicity (18, 19). Emerging evidence on miR-146a suggests that it directs the self-renewal process in colorectal cancer stem cells by regulating Snail-β-catenin axis which also contributes to EMT (20). High nuclear accumulation of β-catenin, along with lowering of E-cadherin is frequently associated with higher tumor grade and poor prognosis in various cancers (21). Given the role of Wnt/β-catenin signaling in CSC maintenance and the miRNAs in regulating wnt pathway, understanding the stepwise regulation of its mediators is crucial (22).

Our recent study has characterized $CD44^{high}CD24^{low}$ cells as the potential CSC population in OSCC (2). CD24, a small cell surface protein, was identified as a critical determinant of differentiation in hematopoietic cells and mammary epithelial cells (23). Besides its role in adhesion, cadherin switching and migration, CD24 is involved in diverse signaling networks that promotes oncogenesis or regression (24). Although role of CD44 is well established (3), the involvement of CD24 in determining stemness is less explored, particularly in oral CSCs. In this study, we show that miR-146a confers $CD44^{high}CD24^{low}$status to OSCC cells by targeting CD24 (25). We also observed that CD24 downregulation caused by miR-146a leads to β-catenin stabilization through the AKT pathway. We propose that miR-146a/CD24/AKT/β-catenin axis influences the stemness characteristics of oral cancer cells.

MATERIALS AND METHODS

Cell Culture and Transfection

Human OSCC cell lines SCC131, SCC084 and SCC036 were obtained from Dr. Sussane Gollin, University of Pittsburgh (26). SCC131 and SCC036 were derived from new primary tumors while SCC084 from recurrent ones. The characteristics and phenotype of SCC cell lines are described in **Supplementary File 2**, **Table 1**. These cells were maintained in 5% CO_2 at 37°C in DMEM medium supplemented with 10% fetal bovine serum (FBS) and antibiotics (Life Technologies, Thermo Fisher Scientific Inc., MA, USA). The ATCC (American Type Culture Collection) oral cancer cell line, SCC25 was cultured in complete DMEM-F12 medium and 400ng/ml Hydrocortisone (Sigma Aldrich) under similar conditions. Magnetic assisted cell sorting was used to isolate $CD44^{high}CD24^{low}$ cells in a sequential separation method. Briefly, 10^6 OSCC cells were first incubated with CD24 antibody which got depleted using magnetic bead-based enrichment. The $CD24^{low}$ cells were then incubated with CD44 antibody to enrich CD44 expressing cells i.e. $CD44^{high}CD24^{low}$ population. The $CD24^{high}$ population from the previous step was used to obtain the $CD44^{high}CD24^{high}$ cells by same method. All these populations were further confirmed and characterized by flow cytometry analysis as shown in our previous work (2). For transfection, Lipofectamine™ 2000 (Invitrogen) was used in serum free medium. Transfected cells were harvested after 48 hrs or 72 hrs for over-expression or knockdown studies respectively.

Plasmid Constructs, miRNA inhibitors and siRNAs

We obtained mir-146a and mir-146a SDM (mutated by site-directed mutagenesis) expressing pU61 construct from Dr. Nitai. P. Bhattacharjee (SINP, Kolkata). The TOP-flash/FOP-flash reporters, dnTCF4, Numb, and pcDNA3.1 empty vector along with miR-146a promoter LucA, LucB and mLucA Luciferase constructs were kind gifts from Muh-Hwa Yang (Taiwan). Human CTNNB1 expression plasmid deposited by Eric Fearon was purchased from Addgene (#16828). CD24 cDNA cloned into the pCDNA3.1 vector and the full-length 3'-UTR of CD24 cloned into pMIR (Ambion) were obtained from Heike Allgayer (University of Heidelberg, Germany). Anti-miR-146a (ID: AM17120) was obtained from Ambion, CD24 siRNA (a pool of 3 target specific siRNAs), UBE2C siRNA (sc-61742) and scramble siRNA from Santa Cruz. CTNNB1 shRNA constructs (Addgene # 18803) were provided by Dr. Mrinal Kanti Ghosh, IICB, Kolkata. The generation of CTNNB1 shRNA lines are discussed in supplementary methods (**Supplementary File 5**). MiR-146a over-expression cassette was sub-cloned from pU61 into the pLKO.1 TRC vector (Addgene plasmid #10878). Packaging plasmids psPAX2 (Addgene plasmid # 12260) and pMD2.G (Didier Trono, Addgene plasmid# 12259) was used to generate the miR-146a over-expression lentiviral particles and target cells were infected following the manufacturer's protocol. Stable transduced cells were selected by puromycin (Gibco) and over-expression efficiencies were verified by qRT-PCR and western blotting. CD24 was co-transfected, and clones were selected by G418.

Quantitative Real Time PCR

TRIzol (Invitrogen, Thermo Fisher Scientific Inc., MA USA) method was used for isolation of total RNA as per manufacturer's instructions. 250 ng of RNA were converted to

Abbreviations: OSCC, oral squamous cell carcinoma; CSCs, cancer stem cells; mi-RNAs, micro-RNAs; HNSCC, Head and Neck Squamous cell carcinoma.

cDNAs using stem-loop primers specific for reverse transcription of individual miRNAs (27). MiRNA cDNAs were amplified with forward primers specific for individual miRNAs and a URP (universal reverse primer), with U6 snRNA as an endogenous reference control. For mRNA expression changes, protocol was similar to that described previously (2). SYBR Green master mix (Roche, USA) was used to perform qRT-PCR in the 7500 Fast Real-Time PCR instrument (Applied Biosystems, USA). Relative quantification ($2^{\wedge -\Delta CT}$*100) was plotted for most of the q-PCR experiments. In some cases, fold changes ($2^{-\Delta\Delta CT}$) or Log transformed [Log10 ($2^{\wedge -\Delta CT}$)] values were calculated and plotted. The delCts or log fold changes were subjected to unpaired t-tests in GraphPad prism 8. All analysis was done using results from three independent experiments taking mean values of at least 2 technical replicates from each experiment. Technical replicates include pipetting repetitions for q-PCR. Primer sequences of genes, miRNA forward and loop primers are listed in **Supplementary File 1**.

Analysis of TCGA and NCI-60 Datasets

RNA and miRNA-seq data were acquired for a total of 292 HNSCC tumor specimens from TCGA (The Cancer Genome Atlas) data portal (https://tcga-data.nci.nih.gov/tcga/). The percentage of CSCs can vary largely depending on the origin, stage, location, age and a number of other physiological attributes associated with a tumor. Since the TCGA data is obtained from bulk tumor, average expression values of CD44 and CD24 across these samples were found to be extremely heterogenous and so was miR-146a levels. To eliminate the discrepancy of medium expression levels and compare between relatively pure CSC and non-CSC populations, we first grouped top 25% of CD44 high and CD44 low expressing tumors and then further sub-grouped 25% of these tumors based on CD24 expression. These samples (n=19) were designated as $CD44^{high}CD24^{low}$ and $CD44^{low}CD24^{high}$, wherein we checked the differential expression of miR-146a and calculated statistical significance using R Limma Package (unpaired t-test). Node status of these patients was also correlated with miR-146a expression using GraphPad Prism5 software. NCI-60 miRNA expression dataset (GEO accession number GSE26375) was analyzed to compare the miR-146a expression between the epithelial and mesenchymal groups as classified earlier (16) using Mann Whitney's u test.

Flow Cytometry

CD44-PE and CD24-FITC (BD Pharmingen) conjugated antibodies were used for double staining of miR-146a transfected cells. Cells were then washed and subjected to flow cytometry on the BD LSRFortessa and analyzed using BD FACSDiva 6.2 software. Isotype controls were included for the non-specific staining. The gating strategy for the flow analysis has been schematically described in **Figure S2A**. Relative fluorescence intensity of CD44 and CD24 for different experimental conditions were plotted respectively and p-values were calculated by one-sample t-test on log fold change in GraphPad prism 8.

Sphere Forming Assay

MiR-146a transfected cells were trypsinised and a single cell suspension was ensured. Low attachment 6-well plate were used for re-seeding the cells at a density of 5000 cells/ml in DMEM-F-12 serum free media containing 1% B27 supplement, 20 ng/ml of EGF and 20 ng/ml of bFGF (Invitrogen). 500 µl of media was added every 2-3 days. Photographs of the spheres were taken under inverted microscope (Leica TCS SP8; Germany) with 20X magnification at 7-14 days. All experiments were done in biological triplicates. Spheres were counted for a number of fields shown as overlaid dots onto the bar graphs and statistical significance was determined by Mann-Whitney's unpaired-test in GraphPad prism 8.

Immuno-Fluorescence

Sorted populations of SCC131 were grown on cover-slips overnight and then fixed with chilled aceto-methanol (1:1). 0.03% Saponin (Calbiochem, Germany) was used for permeabilization followed by blocking with 3% BSA. Rabbit monoclonal antibody against β-catenin and mouse monoclonal antibody against CD24, CD44 (Cell signaling technology) were added at a dilution of 1:200 and incubated overnight. It was then probed with anti-rabbit-FITC and anti-mouse Alexa-Flour 633nm conjugated secondary antibody (molecular probes) and counter stained with DAPI (Invitrogen) for nuclear staining. Images were taken under a confocal microscope (Andor Spinning Disc Confocal Microscope, Andor Technology, Belfast, Ireland) at 60X magnification.

Western Blotting

Cell lysates were prepared after 48 hrs of transfection in NP-40 lysis buffer (Invitrogen) and protease inhibitor cocktail (1X). Equivalent amounts of denatured protein samples were subjected to SDS-PAGE (8%-10%), separated by size and transferred on to PVDF membrane (Millipore, Billerica, USA). Antibodies used for immuno-blotting were polyclonal β-catenin, E-cadherin, CD44 and CD24, Involucrin (Santa Cruz Biotechnology, CA, USA), polyclonal Oct4 and Sox2 (Abcam), polyclonal C-myc, Akt and phospho-Akt (Cell Signaling Technology, USA) and UBE2C (Abcam). Bands were obtained using ECL substrate (Thermo Scientific, USA) from HRP-conjugated secondary antibody (Sigma). Proteasome Inhibitor MG132 (Calbiochem) and Akt inhibitor LY294002 (Cell signaling Technology, USA) were both used at a concentration of 50 µM. Transfected cells were treated for 4 hours before harvesting. Band intensities of each protein were analyzed by ImageJ to obtain densitometric values for their quantification. These were normalized to β-actin for individual experimental sets and fold change calculated. All the histograms were expressed as means ± S.D. of three different experiments and p values computed in GraphPad Prism 5 (Student's two tailed t test).

In Vivo Tumor Xenograft Experiments

Animal experiments were performed following guidelines of the Institutional Animal Ethics Committee (IAEC) of National Centre for Cell Science, Pune. All the animals were issued

under the project IAEC/2012/B183. To investigate the effect of miR-146a overexpression on OSCC growth *in vivo*, 3×10^6 empty vector- and microRNA overexpression construct-containing SCC084 cells were injected subcutaneously into the dorsal flanks of eight NOD/SCID male mice (18 weeks old) on left and right side respectively. When palpable tumors could be seen, the mice were segregated into groups of four each. Mice in one of the groups were injected with 25 mg/kg of body weight of Quercetin (Sigma) on every alternate day for a period of 15 days. The experiment was terminated when the average miR-146a over-expressing SCC084 tumor volumes in the group which received no quercetin reached about 1200 mm^3. At the termination of the experiment, the animals were sacrificed by CO_2 asphyxiation and the tumors were collected for further analysis. Tumor diameters were measured each time the quercetin was injected and at the termination of the experiment using digital Vernier Caliper. Excised tumor tissues were weighed and then stored in RNAlater solution (ThermoFisher Scientific) in -20°C freezer. Tumor volumes were determined using the following formula: $\pi/6[(d1\times d2)^{3/2}]$; where d1 and d2 are two different diameters of a tumor. In another experiment, to investigate effect of simultaneous overexpression of miR-146a and CD24 on OSCC growth *in vivo*, 3×10^6 empty vector- and miR-146a and CD24 overexpression constructs-containing SCC084 cells were injected subcutaneously into the dorsal flanks of four NOD/SCID male mice (15 weeks old) on left and right side respectively. Tumor volumes were measured when palpable growth could be observed. The experiment was terminated when tumor volumes reached 1300 mm^3. The animals were euthanized by CO_2 asphyxiation and the tumors were collected. Tumor tissues were processed as described previously for the other experiment. Tumor volumes were calculated intermittently before final termination and a 2-way ANOVA was performed to determine p-value that consider difference at all timepoints in GraphPad prism 8. Tumor weights were measured at end point and unpaired student's t-test was done to calculate significance.

Immunohistochemistry

Formalin fixed xenograft tumors were embedded in paraffin and 5µm sections were cut for immunohistochemical staining. The sections were baked (stretched) at 65°C for 20 minutes, deparaffinized in xylene and rehydrated in grades of ethanol. Heat mediated antigen retrieval was performed in citrate buffer (10mM sodium citrate, 0.05% Tween 20, pH 6.0) followed by quenching of the endogenous peroxidase activity by 0.3% H_2O_2 for 7 minutes. Beta-catenin antibody (sc-7199) was used at 1:100 dilution and incubated overnight at 4°C. Next day, the primary antibody was washed, and the sections were probed with HRP-conjugated secondary antibody (Sigma). The antigen-antibody complexes were visualized using diaminobenzidine (D8001, Sigma Aldrich). The sections were counterstained with Mayer's hematoxylin, dehydrated in ethanol series and mounted using DPX. Images were acquired using Lawrence and Mayo's LM-52-1704 binocular microscope using 40X objective and processed using the ScopeImage 9.0 software.

Reporter Assays

Cells seeded in 24 well plates were co-transfected with miR-146a OE plasmid and either CD24 3'UTR or miR-146a promoter luciferase construct using Lipofectamine™ 2000 (Invitrogen). The TOP-Flash and FOP-Flash reporters were also used under similar conditions. Promega dual luciferase assay system was performed according to the manufacturer's protocol. After 48 hr of transfection, medium was washed off with 1x PBS and cells were lysed with Passive Lysis Buffer (Promega) and luminescence was measured in Promega Glomax 20/20 luminometer. The luminescence values were transfection normalized with the internal control pRL-TK (50 ng, Renilla Luciferase; Promega). Experiments were performed with three biological replicates. One-sample t-test (on log fold change of control vs experiment) were performed to calculate p-value in GraphPad prism 8.

Chromatin Immunoprecipitation

Cells seeded in 10cm dishes were transfected with either Scr or CD24 siRNA for endogenous ChIP on the miR-146a promoter. For transient ChIP assays, miR-146a LucA/m-LucA/LucB promoter with or without CD24 over-expression was used. After 48hrs, 1X formaldehyde solution was added for DNA-protein crosslinking. Cells were lysed in SDS lysis buffer followed by sonication in Bioruptor (Diagenode) to obtain 200-1000 bp chromatin fragments. ChIP dilution buffer was used to dilute the sheared chromatin followed by preclearing with Protein G Agarose beads (Sigma) for 30min. After preclearing, 20% of the lysate was kept aside as the input and the remaining was divided equally for IP and IgG. Immunoprecipitation was carried out using 5µg of β-catenin (Santa Cruz) and normal IgG control (Sigma) and incubated overnight. The following day, Protein G Agarose beads were added to collect the Antibody/Antigen/Chromatin complex. The complex was washed briefly with cold low salt immune complex wash followed by high salt immune complex buffer, lithium chloride immune complex buffer and Tris-EDTA buffer. It was then reverse-crosslinked and the DNA purified using Phenol/Chloroform extraction method. PCR amplification of the immunoprecipitated DNA was carried out using primers listed in **Supplementary File 1**. Composition of the ChIP buffers are provided in **Supplementary Methods** (**Supplementary File 5**).

Statistical Analyses

Two to three experimental repetitions consisting of at least three biological replicates were used in the study for statistical inference. Various experimental data were subjected to an independent two-tailed Student's *t* test; one-sample-t-test or unpaired t-tests (with either equal or unequal variance) to measure the significance value as was applicable. We confirmed that data must be normally distributed for p-value calculations by t-test or ANOVA, In case of fold changes, we have log transformed the data, beforehand to approximate normal distribution. One-sample t-tests have been used instead of usual two-sample t-tests in case of ratio data, using log FC (fold change) of control vs experimental group. Non-parametric tests were used for the data that are not normally distributed.

All the statistical tests were performed using graph-pad prism and their versions are mentioned in the respective methods as well as legends. In some cases, R package version 3.5.0 was used to generate the correlation graphs and calculate p values. For miRNA discovery, we used multiple correction analysis as shown in **Supplementary File 2**, **Table 2**, and the selection was based on FDR cut off for adjusted p <0.05. Individual data points used are shown onto the respective bar graphs and p-values indicated.

RESULTS

MiR-146a Is Over-Expressed in $CD44^{high}CD24^{low}$ Population of OSCC Cell Lines and Primary Tumors

To identify the cellular miRNAs regulating CSC phenotype of OSCC cells, we initially screened nine miRNAs that are aberrantly expressed in human cancers with their reported role in cancer stemness and EMT (14–18). The expression of these miRNAs was investigated in the $CD44^{high}CD24^{low}$ (CSCs) and $CD44^{low}CD24^{high}$ (non-CSCs) populations of SCC25 cells, which were purified and characterized as previously described (2). QRT-PCR data showed significant difference in the expression of, miR-138, miR-34a, and miR-146a between $CD44^{high}CD24^{low}$ and $CD44^{low}CD24^{high}$ population of SCC25 cells (**Figure 1A**). Amongst them, we focused on miR-146a in view of its context dependent role in various cancers (19, 28, 29). MiR-146a is consistently over-expressed in oral CSCs (18, 19), therefore it was intriguing to explore its possible connection with stemness and the underlying mechanisms. Up-regulation of miR-146a was further confirmed in the $CD44^{high}CD24^{low}$ population of SCC131 and SCC25 cell lines (**Figure 1B**). MiR-146a expression was found to be increased in the sphere forming culture conditions of SCC131 derived $CD44^{high}CD24^{low}$ cells, suggesting it as an important determinant of oral cancer stemness and maintenance (**Figure 1C**). Increased miR-146a expression has been earlier shown to predict poor survival of OSCC patients (18). Interestingly, the analyses in TCGA Head and Neck Squamous Cell Carcinoma (HNSCC) patient's cohort (30), showed increased miR-146a expression in patients with $CD44^{high}CD24^{low}$profile compared to those with $CD44^{low}CD24^{high}$, complementing our cell line data (**Figure 1D**). While there was not much difference in the histological stage of the tumors across the two categories, most of the $CD44^{low}CD24^{high}$ tumors were free of lymph node metastasis (**Figure S1A**, **Supplementary File 3**). Moreover, miR-146a expression of the node positive patients was relatively higher than that of the node negative ones, although not statistically significant (**Figure S1B**). Together, our data suggests possible correlation of high miR-146a expression with CSC-like phenotype in oral tumors.

Ectopic Expression of miR-146a Induces CSC Characteristics

We next investigated whether ectopic expression of miR-146a affect the proportion of CSCs by flow cytometry and found a significant increase in the relative proportion of $CD44^{high}CD24^{low}$ population in SCC131 cells (**Figure 2A**). Similar results were also obtained with SCC036, SCC084 and SCC25 cells, respectively (**Figure S2B**). Characteristic sphere forming ability of miR-146a expressing SCC131 and SCC036 cells were also markedly enhanced (**Figure 2B**). In several studies, the cancer stem cells have been found to express Yamanaka factors which are indicators of stemness, and show loss of epithelial differentiation markers (31). We also observed that ectopic expression of miR-146a led to the increased expression of intracellular stem cell markers such as Oct4, Sox2 and C-myc and loss of Involucrin (32) (**Figure 2C**). However, in SCC131 cells the levels of Oct4 and Involucrin did not show a dose dependent change upon miR-146a over-expression (**Figure 2C**). Additionally, a pronounced decrease in CD24 protein levels upon ectopic miR-146a expression was evident in SCC036, SCC131 and SCC084 cells (**Figure 2A**, **S2B** and **2C**). Altered expression of CSC markers upon knockdown of miR-146a was also evident in SCC131 cells (**Figure S2C**). The modulation in the expression of miR-146a upon ectopic expression or knockdown was validated by qRT-PCR (**Figures S2D, E**). Transfection of miR-146a containing mutated seed sequence, however, did not alter the levels of stem-related proteins in a statistically significant manner (**Figure 2D**). These results demonstrate that miR-146a contributes to enrichment of CSCs in OSCC through increased expression of stem cell markers and lowered CD24 levels.

MiR-146a Activates Wnt/β-Catenin Pathway and Promotes EMT in Oral CSCs

It is known that Wnt, Notch and Hedgehog signaling pathways are often involved in self-renewal property of stem cells and hence its niche maintenance (33). Accordingly, we observed increased expression of β-catenin and Cleaved Notch1 in $CD44^{high}CD24^{low}$ population of SCC25 and SCC131 cells (**Figure S3A**). We also observed higher expression of β-catenin at RNA level in $CD44^{high}CD24^{low}$ cells compared to $CD44^{low}CD24^{high}$ cells (**Figure S3B**). To specifically decipher the role of CD24, we began to compare the $CD44^{high}CD24^{low}$ population with the $CD44^{high}CD24^{high}$ cells only (34). Interestingly, β-catenin protein levels were remarkably high in SCC084 $CD24^{low}$ compared to $CD24^{high}$ cells that correlated well with the expression of stemness markers in these cells (**Figure 3A**). We have previously reported the purity levels of these sub-populations and shown that $CD44^{high}CD24^{high}$ cells are less stem-like than the $CD44^{high}CD24^{low}$ ones (2). In addition, we detected nuclear localization of β-catenin in the $CD44^{high}CD24^{low}$ population of SCC131 cells, whereas it remained membrane bound in $CD44^{high}CD24^{high}$cells (**Figure 3B**). Enhanced transcriptional activity of β-catenin in $CD44^{high}CD24^{low}$ cells compared to $CD44^{high}CD24^{high}$ was observed by measuring the relative wnt reporter activity in the respective cell populations of SCC084 (**Figure S3C**). Interestingly, upon stable knockdown of β-catenin, not only the stem cell markers were reduced but also a modest increase in CD24 expression was observed along with E-cadherin (**Figure S3D**).

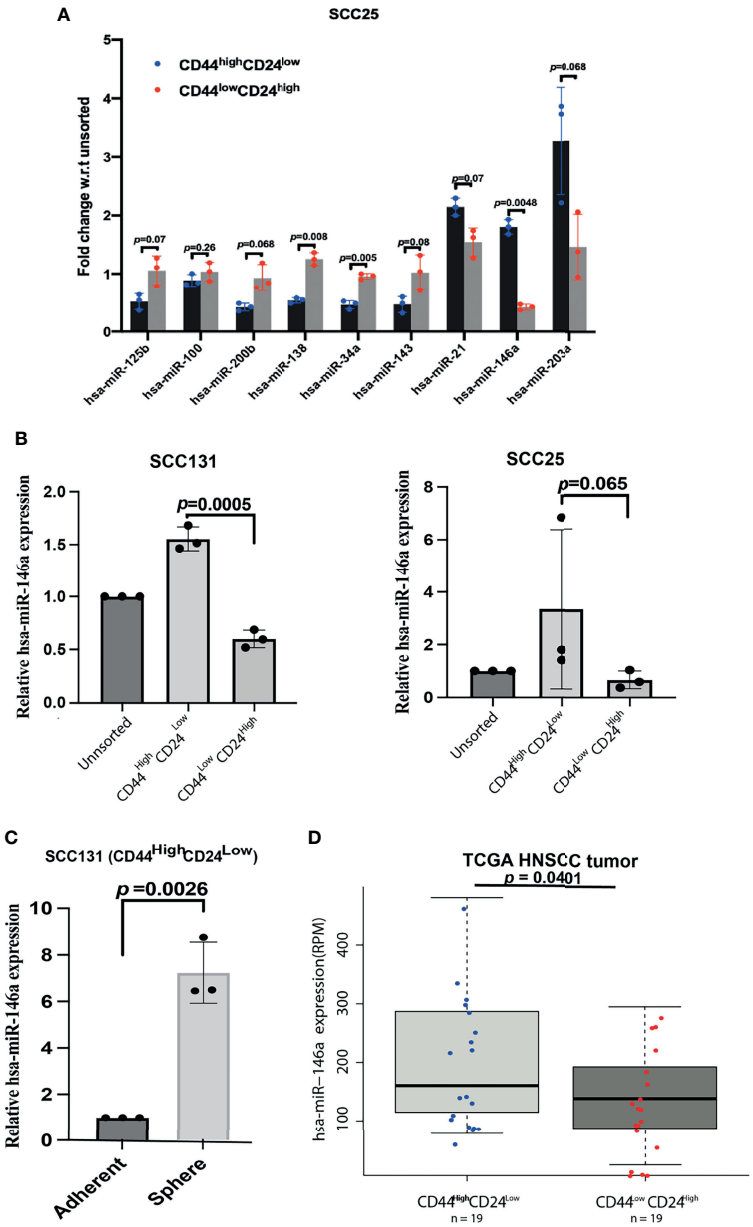


FIGURE 1 | Over-expression of miR-146a in CD44^{high}CD24^{low} cells of Oral Squamous Cell Carcinoma. **(A)** Total RNA extracted from the stem (CD44^{high}CD24^{low}) and the non-stem (CD44^{low}CD24^{high}) sub-populations of SCC25 cells were reverse-transcribed using stem-loop primers specific for subsequent Real time PCR analysis of various miRNAs using respective forward primers and Universal reverse primer (**Supplementary File 1**). Fold changes w.r.t the unsorted population have been plotted and their adjusted p-values are shown on respective miRNAs (calculated using multiple correction FDR analysis as shown in **Supplementary File 2**, **Table 2**). **(B)** Expression of miR-146a was re-analyzed in UPCI: SCC131 and UPCI: SCC25 by qRT-PCR. Fold change values were plotted and log FC subjected to unpaired t-tests to calculate *p*-values using GraphPad prism 8. **(C)** Quantification of miR-146a transcripts in the spheres enriched from CD44^{high}CD24^{low} cells of SCC131 compared to that grown under differentiating adherent conditions. Data is representative of 3 independent experiments and fold change is shown with mean ± SD (p-value calculated on log FC). U6snRNA was used to normalize relative expression values. **(D)** Box-Scatter plot showing the differential expression of miR-146a in the CD44^{high}CD24^{low}and CD44^{low}CD24^{high} subgroup of HNSCC tumors obtained from TCGA. (p-value from unpaired t-test was calculated in R package to show statistical significance).

These results suggest a possible cross talk between CD24 and β-catenin in conferring stemness and EMT to these cells.

The clue that β-catenin level might influence stemness in OSCC cells led us to investigate whether miR-146a directly regulates β-catenin. We did find that over-expression of miR-146a lead to the dose dependent increment in β-catenin levels with concordant decrease in E-cadherin (**Figure 3C**). It is already known that miR-146a targets the 3'UTR of Numb, a protein that

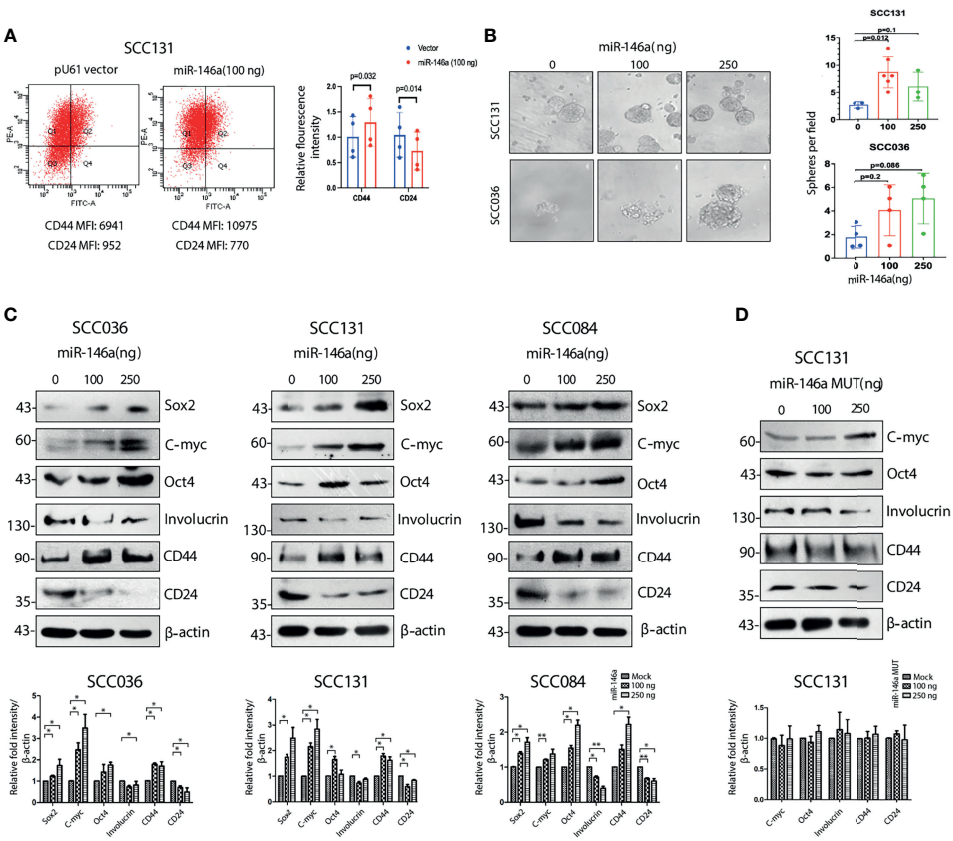


FIGURE 2 | Cancer stem cell characteristics induced by miR-146a in OSCC cell lines. **(A)** MiR-146a transfected SCC131 cells were analyzed by flow cytometry and fold change for the respective mean fluorescence values of CD44 (PE) and CD24 (FITC) have been plotted (p values calculated using one sample t-test on logFC). **(B)** Equal number of vector and miR-146a transfected UPCI: SCC131 and UPCI: SCC036 cells were seeded in ultralow-attachment 6-well plate at clonal density. Sphere forming structures was captured at five random fields at 20X magnification using phase contrast microscope (Leica CTR4000) with scale bar equal to 50 μm. Number of spheres per field were counted and plotted (p-value calculated by Mann whitney's u test in GraphPad prism 8). **(C)** Representative images of western blots showing dose dependent increment of Sox2, C-myc, Oct-4, Involucrin and CD44, decrease in CD24 in the UPCI: SCC036, UPCI: SCC131 and UPCI: SCC084 upon ectopic expression of miR-146a. β-actin bands was used to normalize the data. Band intensities of each protein has been quantified from three biological replicates and the average ± sd is plotted in GraphPad prism 5 showing statistical significance in the respective graphs (below) (*P < 0.05, **P < 0.01) **(D)** Similar western blots upon transfection of miR-146a with mutated seed sequences in UPCI : SCC131 and its graphical representation (below).

promotes lysosomal degradation of β-catenin and Cleaved Notch1 (35). We indeed, confirmed reduced levels of Numb upon miR-146a over-expression along with stabilization of Cleaved Notch1 (**Figure S3E**). Conversely, inhibition of miR-146a activity led to β-catenin degradation along with the loss of Oct4 as expected of its ability to alter stem cell markers (**Figure 3D**). Notably, we did not observe these changes upon mutant miR-146a over-expression indicating that this effect of miR-146a is sequence specific (**Figure S3F**). To emphasize the contribution of β-catenin in miR-146a induced stemness, we transfected miR-146a in β-catenin shRNA expressing cells and found no change in expression of CSC markers (**Figure S3G**) as compared to that of non-silencing controls. Strikingly, the ability of anchorage independent growth of SCC131 cells induced by miR-146a was also reduced in the absence of β-catenin (**Figure S3H**) suggesting that the tumorigenic role of miR-146a in OSCC is β-catenin dependent.

To show the generality in the relationships among miR-146a, CD24 and β-catenin, we checked the correlation between miR-146a and β-catenin/CD24 expression across the NCI-60 cell lines and found it to be positively correlated (**Figure 3E**). Similarly, examination of $CD44^{high}$ HNSCC tumors from TCGA dataset revealed a positive correlation between miR-146a expression and β-catenin/CD24 ratio, showing their clinical relationship (**Figure 3F**). Further, the observed down-regulation of E-cadherin upon miR-146a expression prompted us to address the miR-146a driven EMT phenomenon in OSCC. Indeed, miR-146a was found to be significantly over-expressed in the mesenchymal (MS) cell lines showing higher CD44 and lower CD24 expression (2), compared to the epithelial (EP) cell lines of the NCI-60 panel (**Figure 3G**) (16). In addition, the miR-146a expression in TCGA tumor samples was negatively correlated with the E-cadherin to Vimentin ratio (**Figure 3H**). Based on these observations, we propose that miR-146a induced stemness

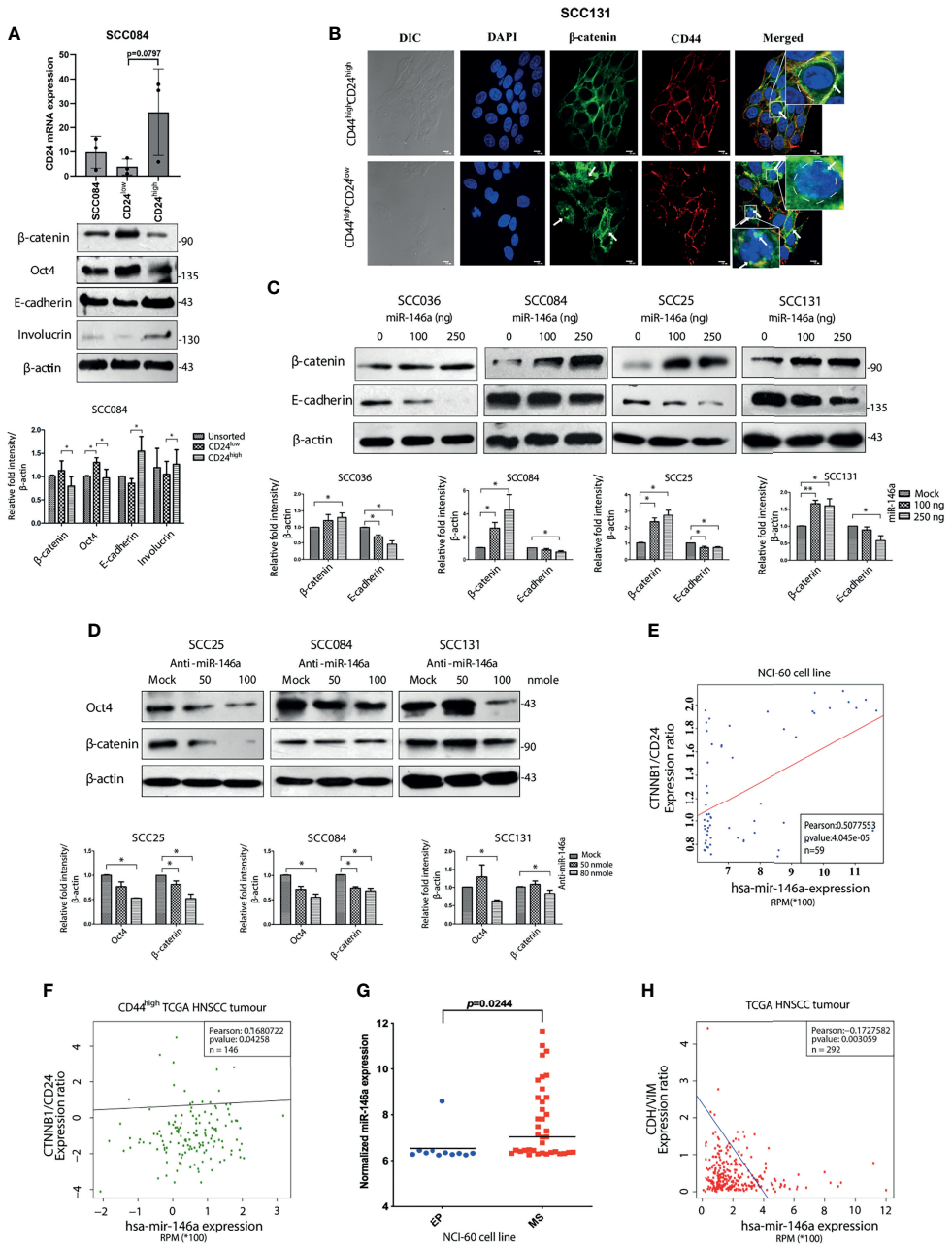


FIGURE 3 | MiR-146a induced β-catenin/Wnt Signaling in CD44^{high}CD24^{low} population. **(A)** Validation of CD24^{low} and CD24^{high} cells from SCC084, as shown by qRT-PCR of CD24 (unpaired t-test on delCT values). 18srRNA served as an endogenous control. Western blot images of β-catenin, Oct-4, E-cadherin and Involucrin in the respective populations along with its quantitative plot indicating the statistical data. **(B)** Representative confocal immunofluorescence images (60X magnification) of CD44^{high}CD24^{high} and CD44^{high}CD24^{low} subpopulation of SCC131 showing β-catenin (green) and CD44 (red) counterstained with DAPI (blue) (scale bar equal to 10 μm). Enlarged image is shown in inset. **(C)** Each of the SCC cell lines were subjected to western blot analysis of β-catenin and E-cadherin upon increasing doses of miR-146a. **(D)** β-catenin and Oct-4 immunoblotting upon increasing doses of anti-miR-146a. Data normalized with β-actin. All the data has been graphically represented beneath the respective figures (*P < 0.05, **P < 0.01, ***P < 0.001). **(E)** Association of miR-146a expression with β-catenin/CD24 in the NCI-60 cell lines (n = 59) and **(F)** with β-catenin/CD24 ratio in the CD44^{high} tumors of the TCGA HNSCC patients (n = 146). Statistical significance was determined by Pearson correlation test. Pearson correlation coefficient is shown in each plot. **(G)** Box plots showing miR-146a expression in NCI-60 cell lines classified as epithelial (EP) and mesenchymal (MS) subgroups. p value has been calculated using mann-whitney's u-test using GraphPad prism 8. **(H)** Correlation (Pearson) of miR-146a with CDH1/VIM expression ratio based on the RNA-Seq data from 292 TCGA HNSCC specimens.

and EMT in OSCC is potentially mediated through lowering of CD24 followed by activation of β-catenin.

MiR-146a Targets CD24 in Oral CSCs

Since, we observed a negative correlation between miR-146a and CD24 expression both experimentally and in patient cohort analysis, we assumed CD24 as a putative target of miR-146a through which it might impart stemness in OSCC. Although, *in silico* identification of miRNA targets using the prediction software did not reveal CD24 as the probable target, we did find matching of miR-146a seed sequence in the CD24 3'UTR in miRanda (**Supplementary File 4**). Despite one mismatch, the maximum free energy of miRNA-mRNA binding was favorable enough for hybridization and targeting (**Figure 4A**). In **Figure 2C**, we had already examined that CD24 expression was significantly depleted upon miR-146a transfection in a dose dependent manner in SCC036, SCC131 and SCC084 cells. Alongside, it was also up-regulated upon inhibition of miR-146a in SCC131 cells (**Figure 4B**). We also observed an expected trend in CD24 transcript levels in both SCC131 and SCC084 upon modulation of miR-146a, although it was not statistically significant in some cases (**Figures 4C, D**). To further confirm that CD24 is a direct target of miR-146a, we co-transfected luciferase reporter vector containing the 3'UTR fragment of CD24 gene with either miR-146a expressing vector or anti-miR-146a in SCC131 cells. As shown in **Figures 4E, F**, miR-146a over-expression reduced the luciferase activity of CD24 3'UTR, while miR-146a inhibitor elevated the same. On the contrary, transfection with mutated mir-146a did not alter the CD24 3'UTR luciferase activity significantly (**Figure 4G**). Thus, this data experimentally validates the ability of miR-146a to directly target CD24 gene by binding to its 3'UTR. This justifies the involvement of miR-146a in negative regulation of CD24 expression in oral cancer stem cells.

MiR-146a Stabilizes β-Catenin by Down-Regulating CD24

We documented in the previous sections that miR-146a expression enhances β-catenin level (**Figure 3**) and miR-146a targets CD24 (**Figure 4**). To gain mechanistic insight into the miR-146a mediated β-catenin stabilization, CD24 was over-expressed in miR-146a over-expressing cells. Interestingly, CD24 not only abolished the stemness markers but also the expression of β-catenin and CD44 (**Figure 5A** and **Figure S4A**). This indicated that down-regulation of CD24 by miR-146a (**Figure 4**) was instrumental in maintaining high β-catenin levels (**Figure 3**) and consequently the downstream stemness phenotype. This was further exemplified as CD24 over-expression alone could lead to decreased expression of β-catenin protein and the associated stem cell markers, while the siRNA mediated knockdown of CD24 showed an opposite effect (**Figures 5B, C**). Wnt target gene *C-myc* was significantly

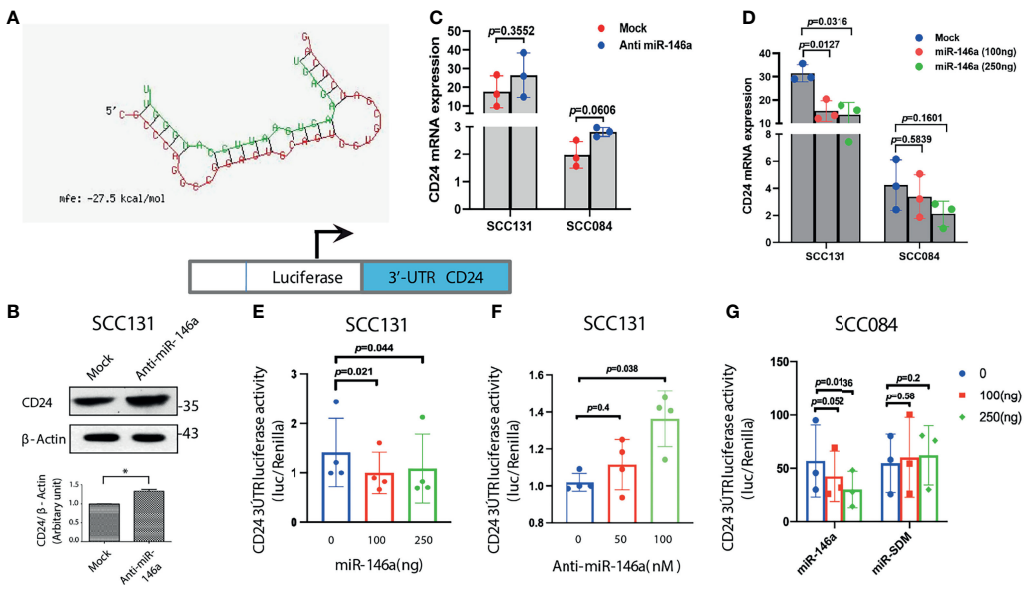


FIGURE 4 | MiR-146a targets CD24 post-transcriptionally. **(A)** Secondary structure prediction of CD24 3'UTR base pairing with the seed sequences of miR-146a with negative free energy allowing favorable binding. **(B)** Immunoblotting of CD24 in SCC131 cells subjected to miR-146a knockdown showing significant up-regulation upon normalization with β-actin. **(C)** qRT-PCR to detect CD24 transcripts in the anti-miR-146a treated or **(D)** miR-146a over-expressed SCC131 and SCC084 cells.18srRNA served as an endogenous control and p-values calculated by unpaired t-test (n = 3) on delCT values that was plotted. Schematic representation of the CD24 3'UTR luciferase constructs (below). **(E)** CD24 3'UTR reporter activity upon miR-146a over-expression and **(F)** miR-146a knockdown in SCC131 cells. **(G)** Luciferase activity of the CD24 3'UTR reporter gene in SCC084 cells with increasing expression of miR-146a or miR-SDM (site-directed mutant miR-146a). Data in **(E–G)** are mean ± SD, normalized with pRL-TK vector and statistical significance was measured by one sample t-test in GraphPad prism 8, from three or four independent experiments.

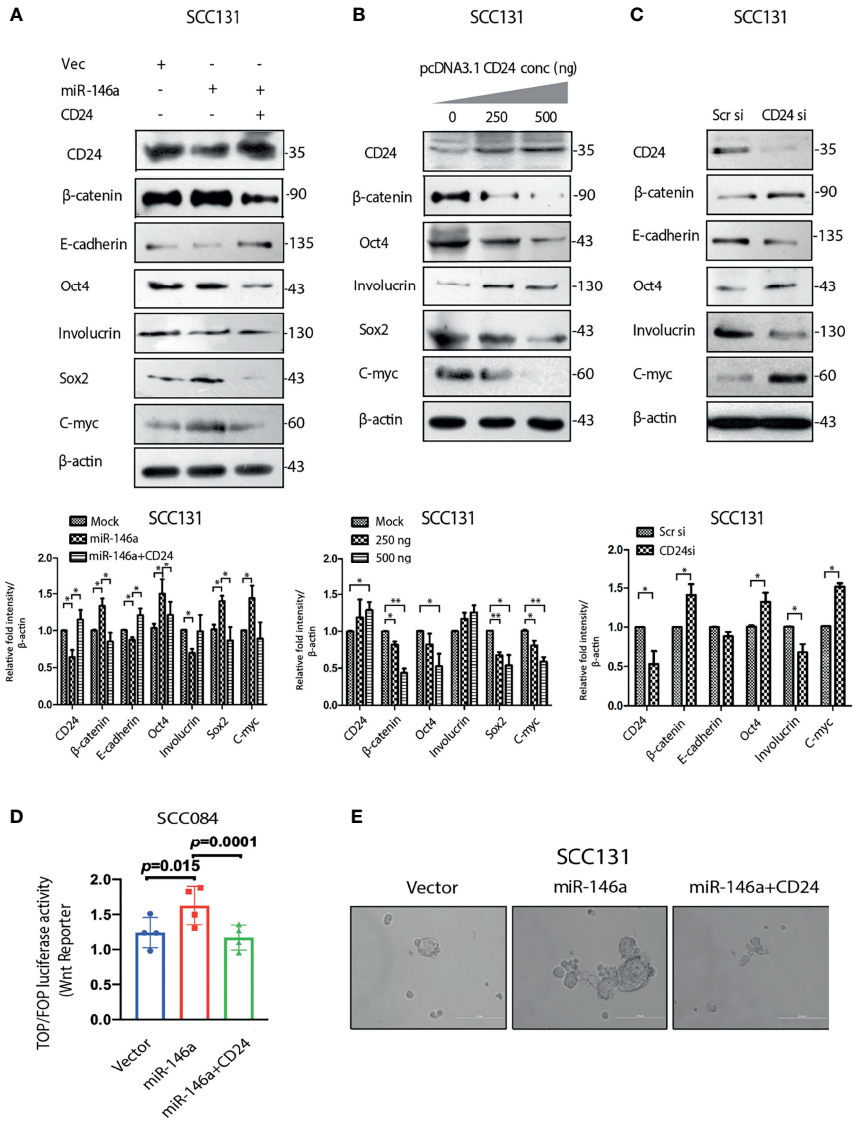


FIGURE 5 | MiR-146a promotes stemness by down-regulating CD24 **(A)** Immunoblot analysis of SCC131 transfected with either a vector control, miR-146a with or without CD24 showing rescued expression of β-catenin and E-cadherin as well as Involucrin Oct-4, Sox2, C-myc. **(B)** Immunoblotting of the same proteins with increasing dose of CD24 expression and **(C)** upon knockdown of CD24 in SCC131 cells. β-actin is loaded as an endogenous control. Histograms show fold changes in the densitometric values of band intensity and shown as means ± S.D. of 3 individual experiments. **(D)** Wnt reporter activity as measured by Top-Flash vs Fop-Flash luciferase construct in SCC084 mock, miR-146a with or without CD24 transfection, as indicated (p-value computed by one sample t-test). **(E)** Sphere formation ability under similar conditions as described in **(D)** (Scale bar = 200 μm).

depleted upon CD24 over-expression in cells expressing miR-146a, although β-catenin mRNA levels remain unchanged (**Figure S4B**). Other wnt targets, *CD44* and *CCND1* were also altered however were not significant at the level of p value<0.05. (**Figure S4B**). These observations suggest an inverse correlation between CD24 and β-catenin signaling in OSCC cells. It was further confirmed by the inhibition of miR-146a-induced β-catenin nuclear mobilization upon ectopic expression of CD24 (**Figure S4C**). In addition, miR-146a driven increased wnt reporter activity was found to be reduced upon CD24 over-expression (**Figure 5D**). To further investigate its downstream effect on stemness phenotype, we performed an *in vitro* sphere-formation assay. We observed a considerably defective spheroid forming ability of miR-146a transfected cells in the presence of CD24 (**Figure 5E**). Together, these observations suggest the possible contribution of CD24 in regulating Wnt pathway through β-catenin, thereby affecting CSC-like traits.

Involvement of pAKT in CD24 Mediated Degradation of β-Catenin

Next, to elucidate the cause of β-catenin reduction in the presence of CD24, we treated SCC084 and SCC036 cells with

MG132, a proteasomal inhibitor and found β-catenin levels returned to that of un-transfected controls (**Figure 6A**). This confirms that unlike Numb, which is known to degrade β-catenin lysosomally (35), CD24 degrades β-catenin in a proteasomal dependent manner. The restored β-catenin also re-established the expression of stem cell marker Oct4 irrespective of CD24 over-expression in both SCC036 and SCC084 cells (**Figure 6A**), suggesting that CD24 acts upstream of β-catenin stabilization. E-cadherin levels, however, remained high in the presence of CD24, irrespective of β-catenin stability (**Figure 6A**). Notably, CD24 did not affect Numb expression, corroborating the independent participation of CD24 in regulating β-catenin (**Figure S5A**). To gain mechanistic insights into the CD24 mediated β-catenin degradation, we speculated that CD24 may lead to β-catenin destabilization *via* AKT-GSK-3β pathway (36, 37). Towards this, we did find that CD24 over-expression rescued the miR-146a mediated increase in pAKT (Ser 473) levels (**Figure 6B**), although it remained stable during MG132 treatment (**Figure S5B**). It may be noted that over-expression of CD24 alone caused direct down-regulation of total AKT protein resembling mTOR mediated targeting (38) (**Figure S5C**). Hence the pAKT/AKT ratio remains unchanged upon CD24 expression as noted in **Figure 6B**. On the contrary, knockdown of CD24 in SCC036 increased pAKT and β-catenin levels (**Figure 6C**). We confirmed that CD24 siRNA targeting was specific by checking the effect of an unrelated siRNA UBE2C upon the stem cell markers (**Figure S5D**). Moreover, pAKT was found to be accumulated in the $CD44^{high}CD24^{low}$ fraction of SCC25 cells thereby indicating its prior involvement in stemness (**Figure S5E**). In addition, we observed significant depletion of β-catenin upon treatment with pAKT inhibitor (LY294002) which again confirmed its regulation by miR-146a-CD24 pAKT axis (**Figure 6D**).

This was further supported by the soft agar tumorigenesis assays, which clearly showed that CD24 over-expression or AKT inhibition, both reduced the miR-146a induced colony formation in OSCC cells (**Figure 7A**). These cell line related observations was further validated using mouse xenograft model. To check the effect of miR-146a on *in*-vivo tumor formation, SCC084 cells harboring either an empty vector (SCC084/EV) or stably expressing miR-146a (SCC084/miR-146a), were generated and the over-expression of miR-146a with subsequent downregulation of CD24 was confirmed by both qRT-PCR and western blotting (**Figures S6A–C**). SCC084/EV and SCC084/miR-146a cells were then introduced in the right and left flanks of NOD/SCID mice respectively and allowed to form subcutaneous tumor (**Figures S6D, E**). It is interesting to note that in stable lines, there is an enhancement in β-catenin mRNA level, which is most likely due to prolonged miR-146a expression that may have potentiated a stable CSC phenotype (**Figure S6B**) (20, 39). A significant increase in tumor volume and tumor weight was observed in SCC084 xenografts stably over-expressing miR-146a suggesting enhanced tumorigenic potential of these cells (**Figures 7B, C**). Further, to explore the effect of AKT signaling on miR-146a induced tumor, mice with palpable tumors generated from SCC084/EV and SCC084/miR-146a cells were treated with quercetin, a known PI3K/AKT signaling pathway blocker (**Figures S6D, E**) (40). As expected, the tumor formation ability of miR-146a cells was significantly attenuated *in vivo* upon administration of quercetin at regular intervals (**Figures 7B, C**). While there was no effect of quercetin on miR-146a and CD24 levels, β-catenin over-expression in miR-146a tumors was compromised in presence

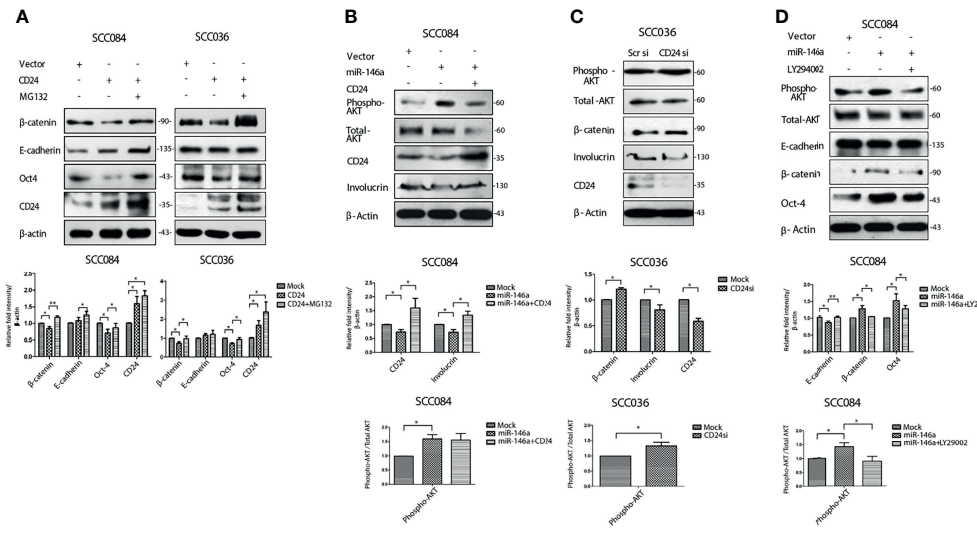


FIGURE 6 | MiR-146a leads to AKT mediated stabilization of β-catenin. **(A)** Western blot analysis revealed degradation of β-catenin upon CD24 over-expression revived with MG132 treatment in SCC084, SCC036. **(B)** Phospho-AKT levels upon ectopic expression of miR-146a alone or in combination with CD24. Total AKT is also shown. **(C)** Phospho-AKT and Total AKT levels upon siRNA mediated down-regulation of CD24 in SCC036 cells. **(D)** Effect of pAKT inhibitor (LY294002) on β-catenin levels in SCC084 cells. Histograms showing fold change in the densitometric values of band intensity is represented as avg ± S.D. of n different experiments (n = 3) (*P < 0.05, **P < 0.01).

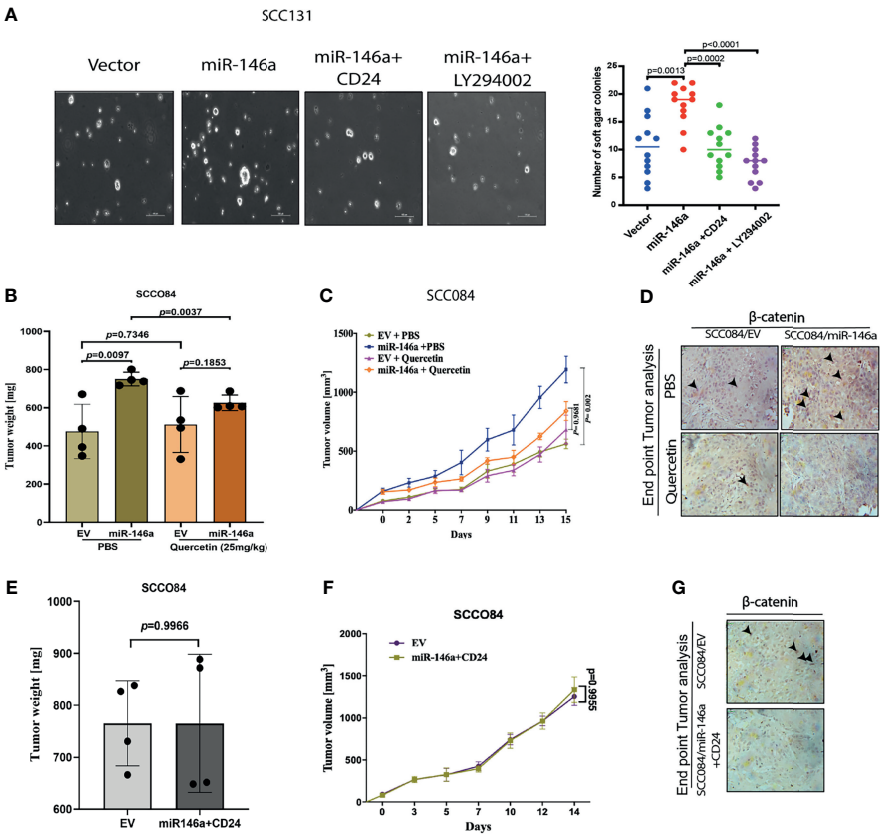


FIGURE 7 | MiR-146a promotes *in vivo* tumor growth which is rescued upon CD24/AKT modulation **(A)** Representative pictures of the colonies from the soft agar assay performed under given transfections and treatment conditions as shown (Left) (Scale bar=100 μm). Number of similar sized colonies were counted for each field and avg ± sd were plotted and graphically represented. *p*-values are measured by mann-whitney u- test between 2 independent experiments (* P < 0.05). **(B)** Bar graphs showing relative weight (mg) of the xenograft tumors generated from control or miR-146a expressing SCC084 treated without or with Quercetin. Data represent mean ± SD (n = 4). P-values were computed using unpaired t-test. **(C)** Line graph showing relative growth rate of tumors in response to Quercetin in SCC084 cells harboring either control vector or stably expressing miR-146a. Once tumors reached a palpable size, one set of mice were injected with Quercetin (10 mg/kg) intraperitoneally and after 10 successive treatment, change in tumor volume was measured at regular interval up to 20 days. Data represent mean ± SD (n = 4) and *p*-values shown using 2-way ANOVA in GraphPad prism 8. **(D)** Immunohistochemistry showing nuclear β-catenin levels in the xenograft tumors obtained from the experiment described in b) (scale bar = 20 μM). **(E)** Bar graphs showing relative weight (mg) of the tumors described in xenograft tumors generated from SCC084 harboring either control vector or stably expressing miR146a and CD24. Data represent mean ± SD (n = 4). P-values were assessed using unpaired t-test **(F)** Line graph showing relative growth rate of tumors described in **(E)**. Data represent mean ± SD (n = 4). For all the time-course experiments, *p*-values were calculated using ANOVA in graph-pad prism8. **(G)** Immunohistochemistry showing nuclear β-catenin levels in the xenograft tumor obtained from the experiment described in **(E)** (scale bar = 20 μM).

of quercetin (**Figures S6F, G**). In order to investigate the effect of CD24 upon the acquired tumorigenicity of miR-146a expressing cancer cells *in vivo*, we examined xenograft tumors generated from SCC084/miR-146a cells harboring CD24 expression construct (**Figures S6A–C, H, I**). Notably, compared to the control tumors, volume and weight of CD24 expressing SCC084/miR-146a tumors were not significantly (p-value = 0.7360) altered (**Figures 7E, F**) suggesting loss of miR-146a driven tumor formation ability. Xenograft tumor subjected to qRT-PCR analysis confirms the overexpression of miR-146a and CD24 in these cells while β-catenin is down-regulated (**Figures S6J, K**). Immunohistochemical analyses further confirmed the increased β-catenin protein levels in miR-146a expressing tumor specimens which is diminished upon either quercetin treatment or CD24 over-expression (**Figures 7D, G**). Collectively, these results indicate that CD24/AKT/β-catenin axis plays an important role in miR-146a mediated tumor growth *in-vivo*.

β-Catenin Transactivates miR-146a Expression Contributing to Positive Feedback Loop

The upstream regulators of miRNAs have always been involved in feedback regulatory mechanisms and are not much investigated. Analysis of miR-146a promoter has revealed the binding sites for *NF-κB, TCF4/β-catenin* and *STAT3*, suggesting possible transcriptional modulation (20, 41, 42). Our data suggests that β-catenin directly enhance stemness features by driving the intracellular levels of *c-Myc* and Oct4 (**Figure 8A**).

This apparently contributes to the enhanced tumorigenic properties which was observed in response to high miR-146a levels. Interestingly, we found that β-catenin in turn also promotes the expression of miR-146a, which might augment the stemness acquiring ability of the cancer cells (**Figure 8B**). However, expression of miR-146a was significantly reduced in the presence of both dn*TCF4* which inhibits β-catenin binding to the promoter and numb which degrades it respectively (**Figure 8C**). Change in miR-146a promoter activity under similar conditions suggests that β-catenin is involved in trans-

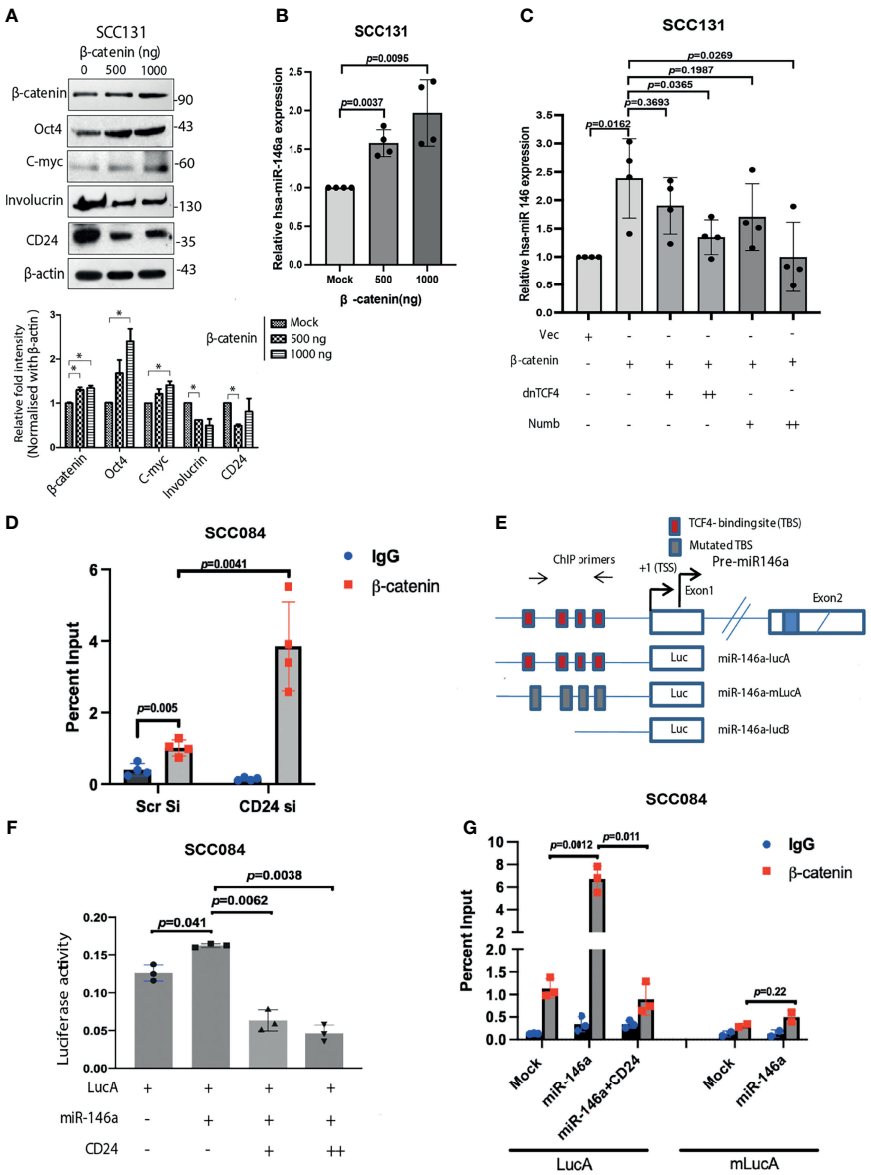


FIGURE 8 | β-catenin transactivates miR-146a mediating a positive feedback loop. **(A)** Increase in stemness markers upon β-catenin over-expression as revealed by western blot and the densitometric analysis of its band intensities (right below). Data was normalized with corresponding β-actin (*P < 0.05). **(B)** Concomitant fold change of miR-146a expression in β-catenin transfected SCC131 as quantified by qPCR. **(C)** Increase in miR-146a transcripts upon β-catenin over-expression is dose dependently inhibited in the presence of either dnTCF4 or Numb. Unpaired student's t-test were performed on log transformed fold change values in GraphPad prism 8. **(D)** Chromatin Immunoprecipitation assays in SCC084 cells transfected with either scramble siRNA or CD24 siRNA showing recruitment of β-catenin upon endogenous miR-146a promoter. We used unpaired t-tests on %input to calculate *p*-values. **(E)** Schematic of miR-146a promoter locus and reporter constructs namely LucA: wild-type; mLucA: TCF-4 binding site (TBS) mutation; LucB: TBS deletion (20). **(F)** Relative luciferase activity of LucA in SCC084 cells under various transfections as indicated (one sample t-test was used to compute p-values). Data represent average of n = 3 individual experiments. **(G)** Transient ChIP assay with same constructs as shown. The percentage enrichment of amplified product was normalized to input and graphically presented. Data represent mean ± sd and n = 3 different experiments. We used unpaired t-tests calculate *p*-values.

activation of miR-146a promoter (**Figure S7A**). We hypothesize that β-catenin mediated induction of miR-146a contributes to β-catenin mediated CD24 reduction as shown earlier (**Figure 8A**). ChIP-qPCR assay using β-catenin antibody confirmed that β-catenin binds to the miR-146a promoter *in vivo* (**Figure 8D**). Further, the recruitment of β-catenin was found to be significantly enhanced upon knockdown of CD24 suggesting negative regulation of β-catenin by CD24 (**Figure 8D**). Moreover, miR-146a promoter activity was significantly increased in presence of miR-146a, while reduced upon ectopic expression of CD24 (**Figures 8E, F**). However, the constructs with either mutated (m-LucA) or deleted (LucB) TCF4 binding sites showed reduced difference in promoter activity in presence of miR-146a (**Figure S7B**). This may be due to the alternating levels of β-catenin which shoots up in miR-146a over-expression condition and gets depleted in presence of CD24. Transient ChIP assays with the same luciferase constructs also confirmed that β-catenin indeed binds to miR-146a promoter, which is impeded upon CD24 over-expression (**Figure 8G**). These data positively confirm the feedback activation loop by β-catenin that further trans-activates miR-146a expression to shift the equilibrium towards CSC maintenance.

DISCUSSION

Oral cancer progression has been largely attributed to both genetic and epigenetic alterations of the cellular genome. Tumorigenic cells can arise from the non-tumorigenic cancer cells owing to spontaneous conversion to a stem-like state (43). The origin and plasticity of such cells, called cancer stem cells (CSCs), have always been a matter of debate and is most likely attributed to transient molecular changes. Nevertheless, CSCs are suspected to be responsible for the underlying chemo-resistance, recurrence and metastasis of a tumor (34). Detail molecular characterization of CSCs is therefore a pre-requisite for identifying and eliminating them from its roots. However, no single molecular marker can exclusively be assigned to distinguish CSCs from other cancer cell types. CD24 has been routinely used in combination with CD44 for the prospective isolation of CSCs in colorectal, prostate and breast cancers (34, 44). Expression of Aldehyde dehydrogenase, drug transporters like *ABCG2* and various other signaling molecules are also known to mark CSCs in a given tumor (32). It is assumed that the cellular miRNAs regulating these CSC markers may provide an important target for anticancer therapy (19, 45). For instance, targeting of CD44 by miRNAs in NSCLC, prostate and ovarian cancer has been demonstrated to attenuate stemness (46). However, miRNA mediated regulation of CD24 remains to be determined.

Consistent with its oncogenic functions, miR-146a promotes symmetric division of colorectal CSCs, thereby promoting stemness (20). This miRNA is also involved in the development of melanoma by activating Notch1 signaling leading to drug resistance (47). However, little is known about its role in regulating expression of CSC-related CD markers in oral cancer. In the present study, we provide evidence that miR-146a mediated downregulation of CD24 confers CSC phenotype in oral cancers. We also show that decreased level of CD24 leads to stabilization of β-catenin due to degradation of AKT. Firstly, we demonstrated significantly higher expression of miR-146a in $CD44^{high}CD24^{low}$ population of OSCC cell lines as well as in tumor specimens. We therefore investigated whether miR-146a expression maintains CSC traits or miR-146a accumulation is a consequence of induced stemness. Notably, ectopic expression of miR-146a induced enrichment of $CD44^{high}CD24^{low}$ population together with increased β-catenin activity in OSCC cell lines. The molecular connection for miR-146a induced CD44 expression was understandable as CD44 is a well-known transcriptional target of β-catenin (20). However, the effect of miR-146a upon CD24 expression under these conditions was particularly unknown. Hence, we examined whether CD24 is a direct target of miR-146a and experimentally confirmed that miR-146a binds to the 3'UTR of CD24 thereby repressing it post-transcriptionally. This observation was quite intriguing as direct targeting of cell surface CSC markers by miRNA could be therapeutically beneficial. However, we cannot rule out that there are alternative targets of mir-146a, which could also possibly contribute synergistically to the effect in oral cancer stemness. Besides, miR-146a is known to be expressed in normal tissue with some relevant physiological roles that may be hindered (48). This adds to the potential limitations for using miR-146a in therapy and needs further investigation. From this study, loss of E-cadherin upon miR-146a over-expression and positive correlation with the mesenchymal marker vimentin was also evident. Hence, in addition to its novel role in acquiring stemness, our results also confirmed miR-146a as a key regulator of EMT (49).

Wnt/β-catenin signaling has shown great potential for CSC-targeting in cancer (33). Our study shows that CSC characteristics in OSCC is attributed to the elevated β-catenin along with depleted CD24 levels. The anticipation that CD24 leads to proteasomal degradation of β-catenin was found to be true and apparently it also abolished the β-catenin mediated stemness. This is a novel functional interaction through which miR-146a regulates β-catenin in oral cancer cells. Nuclear localization of β-catenin in stable miR-146a expressing tumor was evident, however, less pronounced upon transient expression in cell lines, which likely indicates the equilibrium shift towards CSCs, due to prolonged expression of miR-146a with consequent reduction of CD24. Our study, thus points towards the tumor-suppressor functions of CD24, supporting our previous observation of reduced CD24 expression in oral tumors compared to the normal tissue (2). Although growth inhibition was achieved by knocking down CD24 in colorectal and pancreatic cancer, no such effects were observed in oral cancer. Perhaps the variable cell-type specific effect underlies the paradoxical role of CD24 in oral cancer (50).

Activated PI3K-AKT pathway is one of the primary events in carcinogenesis (51). Its contribution to stem cell self-renewal and proliferation has also been extensively studied. Receptor Tyrosine Kinase (RTKs) mediated growth signals (through EGF, IL-6, TGF-β etc.) impinges upon AKT through activation of the PI3K kinase. This RTK mediated activation of AKT *via* PI3K is also negatively regulated by PTEN which again is known

to be regulated by miR-21 (52, 53). Stability of phospho-AKT and other kinases play key role in maintaining its activity in cancer stem cells of chronic myeloid leukemia (CML), NSCLC, breast, prostate and colorectal cancer (54). Further, signaling pathways like WNT are often linked with AKT activation that eventually contribute to expression of stem cells-related factors, chemo-resistance genes, and CSC markers (51, 55). Here we show that CD24, the cell surface CSC marker lie upstream of AKT protein, along with TWIST and FOXO transcription factors which in turn is also known to inhibit CD24 (56). However, the precise mechanism by which expression/stability of AKT protein is regulated by CD24 is still unknown. CD24 has been shown to possibly modulate phospho-AKT levels (57), which might affect its downstream targets such as GSK-3β (37). Activated GSK-3β mediates phosphorylation and ubiquitination of β-catenin, thereby leading to its degradation (37). Therefore, it was incumbent on us to ask whether CD24 mediates inhibition of AKT and subsequently affect β-catenin stability in oral CSCs. Indeed, MG132 treatment was found to re-stabilize β-catenin by relieving pAKT inhibition in cells over-expressing CD24. Moreover, direct AKT inhibition in miR-146a expressing cells depleted β-catenin, irrespective of CD24 level suggesting AKT is downstream of CD24. Thus, we logically elucidated the molecular mechanism underlying CD24 mediated β-catenin degradation *via* AKT in oral cancer cells.

Our findings thus not only supported the importance of signaling molecules in CSC maintenance, but also elucidated an upstream regulatory network that may be broadly applicable for other pathways. We have specifically shown that CD24 over-expression decrease levels of phospho-AKT leading to β-catenin instability. The role of miR-146a/CD24/AKT/β-catenin axis in maintaining the oral cancer stem cell populations is thus mechanistically evident. Studies from in-vivo tumor model system also confirms that this molecular mechanism directly affects tumorigenesis in OSCC. Further, the recruitment of β-catenin onto the miR-146a promoter was found to be negatively regulated by CD24 which might contribute to the fine tuning of stemness. These results clearly establish a cross-regulatory network between miR-146a and β-catenin, governed by a stem-related marker, CD24 in OSCC cells.

CONCLUSIONS

Our study thus provides strong evidence which suggest that miR-146a promotes CSC characteristics of oral cancer cells by down-regulating CD24. Repression of CD24 leads to AKT stabilization followed by activation of Wnt/β-catenin signaling. Based on our observation, we propose a model wherein, AKT activity is an important determinant of miR-146a dependent β-catenin signaling (Graphical abstract). It should be noted, however, that β-catenin mediated CSC induction might be due to the induction of miR-146a expression or vice-versa. Taken together, the present study highlights a novel mechanism of miR-146a mediated self-renewal capacity of Oral CSCs that may have a prognostic or therapeutic value in oral cancer.

DATA AVAILABILITY STATEMENT

The original contributions presented in the study are included in the article/**Supplementary Material**. Further inquiries can be directed to the corresponding author.

ETHICS STATEMENT

The animal study was reviewed and approved by National Centre for Cell Science, Pune.

AUTHOR CONTRIBUTIONS

SG and SuR conceived and designed the study. Some experiments were designed by DG and SD. Experiments, data collection and statistical analyses were performed by SG, DG, SD, StR and PD. Some experiments were performed by RB and MG. The manuscript was written and edited by SG, DG, SD, SN, GCK, and SuR. All authors contributed to the article and approved the submitted version.

FUNDING

The work was supported by CSIR –Mayo Clinic Collaboration for Innovation and Translational Research Grant CMPP-08 and J.C. Bose National Fellowship grant JCB/2017/000005 awarded to SuR. SN is supported by Early Career Award, Science & Engineering Research Board (SERB)-Dept. of Science and Technology (DST), Govt of India (File No. ECR/2015/000206) and Grant-in-Aid, Department of Science & Technology and Biotechnology, Govt. of West Bengal (ST/P/S&T/9G-21/2016). SG, DG and PD are supported by fellowship from the Council of Scientific and Industrial Research (New Delhi, India). SD and RB are supported by Dr. Shyama Prasad Mukherjee Senior Research Fellowship (SPM-SRF) and Senior Research Fellowship from CSIR respectively. StR is supported by University Grants Commission- Junior Research Fellowship (UGC Ref. No.:771/CSIR-UGC NET-2017).

ACKNOWLEDGMENTS

We thank Prof. Nitai. P. Bhattacharjee (SINP), Dr. Muh-Hwa Yang (National Yang-Ming University, Taiwan) and Dr. Heike Allgayer (University of Heidelberg, Germany) for providing us the necessary plasmids. We thank Dr. Raghunath Chatterjee (Indian Statistical Institute, Kolkata, India) for helping us with the statistical analysis and performing the RNA-hybrid analysis in miRanda software. We thank Tanmoy Dalui and Diptadeep Sarkar (CSIR-Indian Institute of Chemical Biology, Kolkata, India) for helping us with Flow Cytometry and Confocal Microscopy respectively. We thank Dr. Arindam Datta (CSIR-Indian Institute of Chemical Biology, Kolkata, India) for assisting

TCGA and NCI-60 dataset analysis. The article is available on the preprint server bioRxiv: https://www.biorxiv.org/content/10.1101/429068v2.

SUPPLEMENTARY MATERIAL

The Supplementary Material for this article can be found online at: https://www.frontiersin.org/articles/10.3389/fonc.2021.651692/full#supplementary-material

Supplementary File 1 | List of Primers for the qRT-PCR (Excel File)

Supplementary File 2 | Supplementary Figure and Figure Legends (S1, S2, S3, S4, S5, S6, S7)

Supplementary File 3 | Analysis of TCGA data for Head and Neck Squamous Cell Carcinoma patients (Excel File)

Supplementary File 4 | Snapshots of miRanda analysis for miR-146a-5p seed sequence and CD24 3'UTR matching showing their free energy of binding (pdf)

Supplementary File 5 | Supplementary methods

REFERENCES

1. Suh Y, Amelio I, Guerrero Urbano T, Tavassoli M. Clinical Update on Cancer: Molecular Oncology of Head and Neck Cancer. *Cell Death Dis* (2014) 5:e1018. doi: 10.1038/cddis.2013.548
2. Ghuwalewala S, Ghatak D, Das P, Dey S, Sarkar S, Alam N, et al. CD44(high) CD24(low) Molecular Signature Determines the Cancer Stem Cell and EMT Phenotype in Oral Squamous Cell Carcinoma. *Stem Cell Res* (2016) 16:405–17. doi: 10.1016/j.scr.2016.02.028
3. Prince ME, Sivanandan R, Kaczorowski A, Wolf GT, Kaplan MJ, Dalerba P, et al. Identification of a Subpopulation of Cells With Cancer Stem Cell Properties in Head and Neck Squamous Cell Carcinoma. *Proc Natl Acad Sci USA* (2007) 104:973–8. doi: 10.1073/pnas.0610117104
4. Munoz P, Iliou MS, Esteller M. Epigenetic Alterations Involved in Cancer Stem Cell Reprogramming. *Mol Oncol* (2012) 6:620–36. doi: 10.1016/j.molonc.2012.10.006
5. Lund AH, van Lohuizen M. Epigenetics and Cancer. *Genes Dev* (2004) 18:2315–35. doi: 10.1101/gad.1232504
6. Calin GA, Croce CM. MicroRNA Signatures in Human Cancers. *Nat Rev Cancer* (2006) 6:857–66. doi: 10.1038/nrc1997
7. Courthod G, Franco P, Palermo L, Pisconti S, Numico G. The Role of microRNA in Head and Neck Cancer: Current Knowledge and Perspectives. *Molecules* (2014) 19:5704–16. doi: 10.3390/molecules19055704
8. Min A, Zhu C, Peng S, Rajthala S, Costea DE, Sapkota D. MicroRNAs as Important Players and Biomarkers in Oral Carcinogenesis. *BioMed Res Int* (2015) 2015:186904. doi: 10.1155/2015/186904
9. Toden S, Kunitoshi S, Cardenas J, Gu J, Hutchins E, Van Keuren-Jensen K, et al. Cancer Stem Cell-Associated miRNAs Serve as Prognostic Biomarkers in Colorectal Cancer. *JCI Insight* (2019) 4:1–15. doi: 10.1172/jci.insight.125294
10. Liu C, Tang DG. MicroRNA Regulation of Cancer Stem Cells. *Cancer Res* (2011) 71:5950–4. doi: 10.1158/0008-5472.CAN-11-1035
11. Sun X, Jiao X, Pestell TG, Fan C, Qin S, Mirabelli E, et al. MicroRNAs and Cancer Stem Cells: The Sword and the Shield. *Oncogene* (2014) 33:4967–77. doi: 10.1038/onc.2013.492
12. Chen D, Sun Y, Yuan Y, Han Z, Zhang P, Zhang J, et al. miR-100 Induces Epithelial-Mesenchymal Transition But Suppresses Tumorigenesis, Migration and Invasion. *PloS Genet* (2014) 10:e1004177. doi: 10.1371/journal.pgen.1004177
13. Tiwari A, Shivananda S, Gopinath KS, Kumar A. MicroRNA-125a Reduces Proliferation and Invasion of Oral Squamous Cell Carcinoma Cells by Targeting Estrogen-Related Receptor Alpha: Implications for Cancer Therapeutics. *J Biol Chem* (2014) 289:32276–90. doi: 10.1074/jbc.M114.584136
14. Yu Z, Li Y, Fan H, Liu Z, Pestell RG. miRNAs Regulate Stem Cell Self-Renewal and Differentiation. *Front Genet* (2012) 3:191. doi: 10.3389/fgene.2012.00191
15. Liu C, Kelnar K, Liu B, Chen X, Calhoun-Davis T, Li H, et al. The microRNA miR-34a Inhibits Prostate Cancer Stem Cells and Metastasis by Directly Repressing CD44. *Nat Med* (2011) 17:211–5. doi: 10.1038/nm.2284
16. Park SM, Gaur AB, Lengyel E, Peter ME. The miR-200 Family Determines the Epithelial Phenotype of Cancer Cells by Targeting the E-Cadherin Repressors ZEB1 and ZEB2. *Genes Dev* (2008) 22:894–907. doi: 10.1101/gad.1640608
17. Xu N, Papagiannakopoulos T, Pan G, Thomson JA, Kosik KS. MicroRNA-145 Regulates OCT4, SOX2, and KLF4 and Represses Pluripotency in Human Embryonic Stem Cells. *Cell* (2009) 137:647–58. doi: 10.1016/j.cell.2009.02.038
18. Hung PS, Liu CJ, Chou CS, Kao SY, Yang CC, Chang KW, et al. miR-146a Enhances the Oncogenicity of Oral Carcinoma by Concomitant Targeting of the IRAK1, TRAF6 and NUMB Genes. *PloS One* (2013) 8:e79926. doi: 10.1371/journal.pone.0079926
19. Paik JH, Jang JY, Jeon YK, Kim WY, Kim TM, Heo DS, et al. MicroRNA-146a Downregulates NFkappaB Activity *via* Targeting TRAF6 and Functions as a Tumor Suppressor Having Strong Prognostic Implications in NK/T Cell Lymphoma. *Clin Cancer Res* (2011) 17:4761–71. doi: 10.1158/1078-0432.CCR-11-0494
20. Hwang WL, Jiang JK, Yang SH, Huang TS, Lan HY, Teng HW, et al. MicroRNA-146a Directs the Symmetric Division of Snail-Dominant Colorectal Cancer Stem Cells. *Nat Cell Biol* (2014) 16:268–80. doi: 10.1038/ncb2910
21. Gottardi CJ, Wong E, Gumbiner BM. E-Cadherin Suppresses Cellular Transformation by Inhibiting Beta-Catenin Signaling in an Adhesion-Independent Manner. *J Cell Biol* (2001) 153:1049–60. doi: 10.1083/jcb.153.5.1049
22. Liu Y, Huang T, Zhao X, Cheng L. MicroRNAs Modulate the Wnt Signaling Pathway Through Targeting Its Inhibitors. *Biochem Biophys Res Commun* (2011) 408:259–64. doi: 10.1016/j.bbrc.2011.04.009
23. Vegfors J, Petersson S, Kovacs A, Polyak K, Enerback C. The Expression of Psoriasin (S100A7) and CD24 Is Linked and Related to the Differentiation of Mammary Epithelial Cells. *PloS One* (2012) 7:e53119. doi: 10.1371/journal.pone.0053119
24. Muppala S, Mudduluru G, Leupold JH, Buergy D, Sleeman JP, Allgayer H. CD24 Induces Expression of the Oncomir miR-21 *via* Src, and CD24 and Src Are Both Post-Transcriptionally Downregulated by the Tumor Suppressor miR-34a. *PloS One* (2013) 8:e59563. doi: 10.1371/journal.pone.0059563
25. Chen D, Wang CY. Targeting Cancer Stem Cells in Squamous Cell Carcinoma. *Precis Clin Med* (2019) 2:152–65. doi: 10.1093/pcmedi/pbz016
26. White JS, Weissfeld JL, Ragin CCR, Rossie KM, Martin CL, Shuster M, et al. The Influence of Clinical and Demographic Risk Factors on the Establishment of Head and Neck Squamous Cell Carcinoma Cell Lines. *Oral Oncol* (2007) 43(7):701–12. doi: 10.1016/j.oraloncology.2006.09.001
27. Chen C, Ridzon DA, Broomer AJ, Zhou Z, Lee DH, Nguyen JT, et al. Real-Time Quantification of microRNAs by Stem-Loop RT-PCR. *Nucleic Acids Res* (2005) 33:e179. doi: 10.1093/nar/gni178
28. Shi Z, Johnson JJ, Jiang R, Liu Y, Stack MS. Decrease of miR-146a Is Associated With the Aggressiveness of Human Oral Squamous Cell Carcinoma. *Arch Oral Biol* (2015) 60:1416–27. doi: 10.1016/j.archoralbio.2015.06.007
29. Zhang Z, Zhang Y, Sun XX, Ma X, Chen ZN. microRNA-146a Inhibits Cancer Metastasis by Downregulating VEGF Through Dual Pathways in Hepatocellular Carcinoma. *Mol Cancer* (2015) 14:5. doi: 10.1186/1476-4598-14-5
30. The Cancer Genome Atlas Network. Comprehensive Genomic Characterization of Head and Neck Squamous Cell Carcinomas. *Nature* (2015) 517:576–82. doi: 10.1038/nature14129
31. Seymour T, Twigger A-J, Kakulas F. Pluripotency Genes and Their Functions in the Normal and Aberrant Breast and Brain. *Int J Mol Sci* (2015) 16:27288–301. doi: 10.3390/ijms161126024
32. Huang CF, Xu XR, Wu TF, Sun ZJ, Zhang WF. Correlation of ALDH1, CD44, OCT4 and SOX2 in Tongue Squamous Cell Carcinoma and Their Association With Disease Progression and Prognosis. *J Oral Pathol Med* (2014) 43:492–8. doi: 10.1111/jop.12159

33. Takebe N, Miele L, Harris PJ, Jeong W, Bando H, Kahn M, et al. Hedgehog, and Wnt Pathways in Cancer Stem Cells: Clinical Update. *Nat Rev Clin Oncol* (2015) 12:445–64. doi: 10.1038/nrclinonc.2015.61
34. Vikram R, Chou WC, Hung SC, Shen CY. Tumorigenic and Metastatic Role of CD44(-/Low)/CD24(-/Low) Cells in Luminal Breast Cancer. *Cancers (Basel)* (2020) 12:1–23. doi: 10.3390/cancers12051239
35. McGill MA, McGlade CJ. Mammalian Numb Proteins Promote Notch1 Receptor Ubiquitination and Degradation of the Notch1 Intracellular Domain. *J Biol Chem* (2003) 278:23196–203. doi: 10.1074/jbc.M302827200
36. Li J, Zhou BP. Activation of Beta-Catenin and Akt Pathways by Twist Are Critical for the Maintenance of EMT Associated Cancer Stem Cell-Like Characters. *BMC Cancer* (2011) 11:49. doi: 10.1186/1471-2407-11-49
37. Zhao S, Fu J, Liu X, Wang T, Zhang J, Zhao Y. Activation of Akt/GSK-3beta/Beta-Catenin Signaling Pathway Is Involved in Survival of Neurons After Traumatic Brain Injury in Rats. *Neurol Res* (2012) 34:400–7. doi: 10.1179/1743132812Y.0000000025
38. Wu Y-T, Ouyang W, Lazorchak AS, Liu D, Shen H-M, Su B. mTOR Complex 2 Targets Akt for Proteasomal Degradation via Phosphorylation at the Hydrophobic Motif*. *J Biol Chem* (2011) 286:14190–8. doi: 10.1074/jbc.M111.219923
39. Shang S, Hua F, Hu ZW. The Regulation of Beta-Catenin Activity and Function in Cancer: Therapeutic Opportunities. *Oncotarget* (2017) 8:33972–89. doi: 10.18632/oncotarget.15687
40. Lim W YC, Park S, Bazer FW, Song G. Inhibitory Effects of Quercetin on Progression of Human Choriocarcinoma Cells Are Mediated Through PI3K/AKT and MAPK Signal Transduction Cascades. *J Cell Physiol* (2017) 232 (6):1428–40. doi: 10.1002/jcp.25637
41. Sun X, Zhang J, Hou Z, Han Q, Zhang C, Tian Z. miR-146a Is Directly Regulated by STAT3 in Human Hepatocellular Carcinoma Cells and Involved in Anti-Tumor Immune Suppression. *Cell Cycle* (2014) 14:243–52. doi: 10.4161/15384101.2014.977112
42. Taganov KD, Boldin MP, Chang KJ, Baltimore D. NF-KappaB-Dependent Induction of microRNA miR-146, an Inhibitor Targeted to Signaling Proteins of Innate Immune Responses. *Proc Natl Acad Sci USA* (2006) 103:12481–6. doi: 10.1073/pnas.0605298103
43. Chaffer CL, Brueckmann I, Scheel C, Kaestli AJ, Wiggins PA, Rodrigues LO, et al. Normal and Neoplastic Nonstem Cells can Spontaneously Convert to a Stem-Like State. *Proc Natl Acad Sci USA* (2011) 108:7950–5. doi: 10.1073/pnas.1102454108
44. Jaggupilli A, Elkord E. Significance of CD44 and CD24 as Cancer Stem Cell Markers: An Enduring Ambiguity. *Clin Dev Immunol* (2012) 2012:708036. doi: 10.1155/2012/708036
45. Ling H, Fabbri M, Calin GA. MicroRNAs and Other Non-Coding RNAs as Targets for Anticancer Drug Development. *Nat Rev Drug Discov* (2013) 12:847–65. doi: 10.1038/nrd4140
46. Cheng W, Liu T, Wan X, Gao Y, Wang H. MicroRNA-199a Targets CD44 to Suppress the Tumorigenicity and Multidrug Resistance of Ovarian Cancer-Initiating Cells. *FEBS J* (2012) 279:2047–59. doi: 10.1111/j.1742-4658.2012.08589.x
47. Forloni M, Dogra SK, Dong Y, Conte DJr., Ou J, Zhu LJ, et al. miR-146a Promotes the Initiation and Progression of Melanoma by Activating Notch Signaling. *Elife* (2014) 3:e01460. doi: 10.7554/eLife.01460
48. Zhao JL, Starczynowski DT. Role of microRNA-146a in Normal and Malignant Hematopoietic Stem Cell Function. *Front Genet* (2014) 5:219. doi: 10.3389/fgene.2014.00219
49. Wang X, Lu H, Li T, Yu L, Liu G, Peng X, et al. Kruppel-Like Factor 8 Promotes Tumorigenic Mammary Stem Cell Induction by Targeting miR-146a. *Am J Cancer Res* (2013) 3(4):356–73.
50. Cremers N, Neeb A, Uhle T, Dimmler A, Rothley M, Allgayer H, et al. CD24 Is Not Required for Tumor Initiation and Growth in Murine Breast and Prostate Cancer Models. *PloS One* (2016) 11:e0151468. doi: 10.1371/journal.pone.0151468
51. Zhang HF, Wu C, Alshareef A, Gupta N, Zhao Q, Xu XE, et al. The PI3K/AKT/c-MYC Axis Promotes the Acquisition of Cancer Stem-Like Features in Esophageal Squamous Cell Carcinoma. *Stem Cells* (2016) 34(8):2040–51. doi: 10.1002/stem.2395
52. Dubrovska A, Kim S, Salamone RJ, Walker JR, Maira SM, Garcia-Echeverria C, et al. The Role of PTEN/Akt/PI3K Signaling in the Maintenance and Viability of Prostate Cancer Stem-Like Cell Populations. *Proc Natl Acad Sci USA* (2009) 106:268–73. doi: 10.1073/pnas.0810956106
53. Meng F, Henson R, Wehbe-Janek H, Ghoshal K, Jacob ST, Patel T. MicroRNA-21 Regulates Expression of the PTEN Tumor Suppressor Gene in Human Hepatocellular Cancer. *Gastroenterology* (2007) 133:647–58. doi: 10.1053/j.gastro.2007.05.022
54. Xia P, Xu XY. PI3K/Akt/mTOR Signaling Pathway in Cancer Stem Cells: From Basic Research to Clinical Application. *Am J Cancer Res* (2015) 5(5):1602–9.
55. Huang TS, Li L, Moalim-Nour L, Jia D, Bai J, Yao Z, et al. A Regulatory Network Involving Beta-Catenin, E-Cadherin, PI3k/Akt, and Slug Balances Self-Renewal and Differentiation of Human Pluripotent Stem Cells In Response to Wnt Signaling. *Stem Cells* (2015) 33:1419–33. doi: 10.1002/stem.1944
56. Farhad Vesuna AL, Kimble B, Raman V. Twist Modulates Breast Cancer Stem Cells by Transcriptional Regulation of CD24 Expression. *Neoplasia* (2009) 11:1318–28. doi: 10.1593/neo.91084
57. Hosonaga M, Arima Y, Sugihara E, Kohno N, Saya H. Expression of CD24 Is Associated With HER2 Expression and Supports HER2-Akt Signaling in HER2-Positive Breast Cancer Cells. *Cancer Sci* (2014) 105:779–87. doi: 10.1111/cas.12427

Conflict of Interest: The authors declare that the research was conducted in the absence of any commercial or financial relationships that could be construed as a potential conflict of interest.

Publisher's Note: All claims expressed in this article are solely those of the authors and do not necessarily represent those of their affiliated organizations, or those of the publisher, the editors and the reviewers. Any product that may be evaluated in this article, or claim that may be made by its manufacturer, is not guaranteed or endorsed by the publisher.

Copyright © 2021 Ghuwalewala, Ghatak, Das, Roy, Das, Butti, Gorain, Nath, Kundu and Roychoudhury. This is an open-access article distributed under the terms of the Creative Commons Attribution License (CC BY). The use, distribution or reproduction in other forums is permitted, provided the original author(s) and the copyright owner(s) are credited and that the original publication in this journal is cited, in accordance with accepted academic practice. No use, distribution or reproduction is permitted which does not comply with these terms.

frontiers in Cell and Developmental Biology

ORIGINAL RESEARCH
published: 20 October 2021
doi: 10.3389/fcell.2021.746194

Overexpression of NREP Promotes Migration and Invasion in Gastric Cancer Through Facilitating Epithelial-Mesenchymal Transition

Yuan-jie Liu[1,2,3†], Shu-hong Zeng[2,3†], Yi-dou Hu[1], Yong-hua Zhang[1] and Jie-pin Li[1,3*]*

[1] Department of Oncology, Zhangjiagang TCM Hospital Affiliated to Nanjing University of Chinese Medicine, Zhangjiagang, Jiangsu, China, [2] Affiliated Hospital of Nanjing University of Chinese Medicine, Jiangsu Province Hospital of Chinese Medicine, Nanjing, Jiangsu, China, [3] No. 1 Clinical Medical College, Nanjing University of Chinese Medicine, Nanjing, Jiangsu, China

The identification of biomarkers and effective therapeutic targets for gastric cancer (GC), the most common cause of cancer-related deaths around the world, is currently a major focus area in research. Here, we examined the utility of Neuronal Regeneration Related Protein (*NREP*) as a prognostic biomarker and therapeutic target for GC. We assessed the clinical relevance, function, and molecular role of *NREP* in GC using bioinformatics analysis and experimental validation. Our results showed that in GC, *NREP* overexpression was significantly associated with a poor prognosis. Our findings also suggested that *NREP* may be involved in the activation of cancer-associated fibroblasts and the epithelial–mesenchymal transition (EMT), with transforming growth factor β1 mediating both processes. In addition, *NREP* expression showed a positive correlation with the abundance of M2 macrophages, which are potent immunosuppressors. Together, these results indicate that *NREP* is overexpressed in GC and affects GC prognosis. Thus, *NREP* could be a prognostic biomarker and therapeutic target for GC.

Keywords: NREP, gastric cancer, bioinformatics, epithelial–mesenchymal transition, cancer-associated fibroblasts, M2 macrophages

OPEN ACCESS

Edited by:
Ira Ida Skvortsova, Innsbruck Medical University, Austria

Reviewed by:
Zhigang Bai, Beijing Friendship Hospital, China
Yufang Hou, Institute of Materia Medica, Chinese Academy of Medical Sciences and Peking Union Medical College, China

***Correspondence:**
Yong-hua Zhang
zjgzy043@njucm.edu.cn
Jie-pin Li
zjgzy027@njucm.edu.cn

† These authors share first authorship

Specialty section:
This article was submitted to Molecular and Cellular Oncology, a section of the journal Frontiers in Cell and Developmental Biology

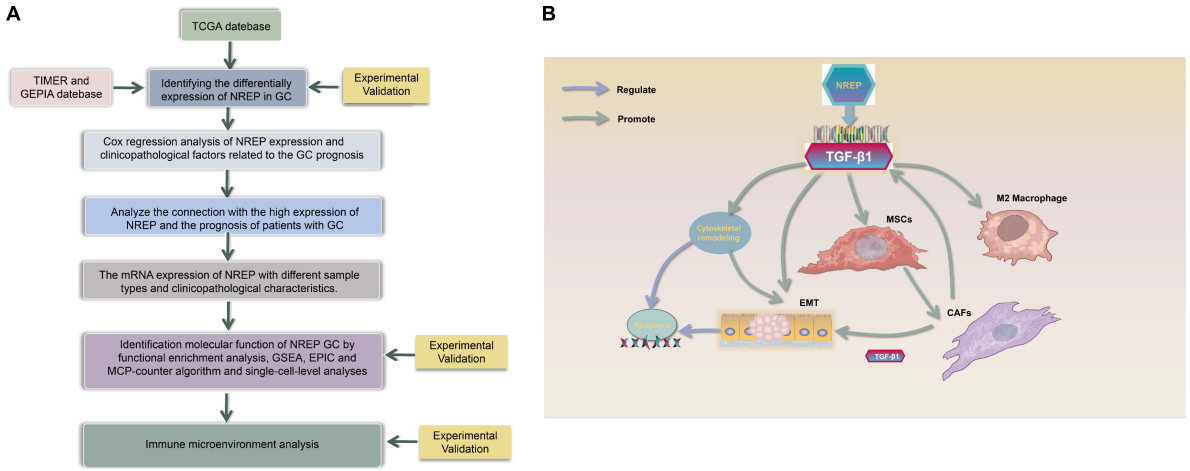
Received: *23 July 2021*
Accepted: *01 October 2021*
Published: *20 October 2021*

Citation:
Liu Y-j, Zeng S-h, Hu Y-d, Zhang Y-h and Li J-p (2021) Overexpression of NREP Promotes Migration and Invasion in Gastric Cancer Through Facilitating Epithelial-Mesenchymal Transition. Front. Cell Dev. Biol. 9:746194. doi: 10.3389/fcell.2021.746194

INTRODUCTION

Gastric cancer (GC) is the third most prevalent cancer globally (Son et al., 2021). Both perioperative chemotherapy and preoperative chemoradiotherapy are recommended for the treatment of resectable GC around the world. Of these strategies, perioperative chemotherapy is used most frequently (Al-Batran et al., 2020). The period between the decision to perform surgery and the completion of surgical treatment is called the perioperative period. This period includes the pre-operative, intra-operative, and post-operative stages. Radical surgery is currently the primary curative treatment for resectable GC. In contrast, adjuvant chemoradiotherapy is the standard treatment for unresectable and metastatic GC (De Steur et al., 2021). While chemotherapy improves patient survival, the response to treatment can be variable and unpredictable, with many patients experiencing recurrence and distant metastasis. In advanced GC, the 5-year overall survival (OS) continues to be low at 20–30% (Smyth et al., 2020).

In this era of individualized and precision medicine, molecular targeted therapies and immunotherapies are developing very rapidly, and they have shown great promise in the treatment of GC (Liu and Meltzer, 2017; Pauli et al., 2017). Although previous research has largely focused on targeting malignant cancer cells, an increasing number of studies are now



GRAPHICAL ABSTRACT | (A) Study Flow chart, **(B)** Diagram depicting the regulation mechanism of *NREP* in the tumorigenesis of gastric cancer.

focusing on the tumor microenvironment (TME; Wu and Dai, 2017), which includes all non-malignant host cells and non-cellular components, including immune, blood, and endothelial cells; extracellular matrix (ECM); fibroblasts; and mesenchymal stromal cells (MSCs; Rojas et al., 2020).

There has been recent progress in molecular targeted therapies for GC. Trastuzumab in combination with chemotherapy has been found to improve survival in human epidermal growth factor receptor 2-positive GC (Meric-Bernstam et al., 2019). However, few anti-vascular molecular targeted agents have been identified for advanced GC. Although ramucirumab and apatinib have been approved for second- and third-line treatment, a drug for first-line treatment is still unavailable (Wilke et al., 2014; Scott, 2018). This is likely because of the complex TME of GC and the lack of accurate predictive biomarkers. Therefore, identifying specific biomarkers, targeting the tumorigenic stroma, and reducing the number of immunosuppressive macrophages may be helpful in GC treatment and may also hold the key to improving survival in this cancer.

Neuronal Regeneration Related Protein, which binds to the transforming growth factor β1 (TGF-β1) latency-related protein, is an intracellular polypeptide (8 kDa, 68 amino acids long) that is highly conserved across species and is expressed in the brain, smooth muscles, regenerated tissue, and malignant glioblastomas (Stradiot et al., 2018). *NREP* regulates the expression of TGF-β1 not only at the translational but also at the transcriptional level (Li et al., 2016). *NREP* also regulates myofibroblast differentiation and fibrosis and promotes embryo development, wound healing, and nerve and lung regeneration (Studler et al., 1993; Duan et al., 2019). The molecular physiology of wound healing is thought to be very similar to that of cancer progression (Margadant and Sonnenberg, 2010). During wound healing, epithelial-mesenchymal transition (EMT) confers motility and invasiveness to epithelial cells, thereby allowing them to travel to the wound site and repair tissue damage. Similarly, once cancer cells enter the EMT phase, they become locally invasive, and this is the first step in tumor metastasis. Many important signaling pathways and molecules involved in wound healing also regulate tumor cell proliferation and metastasis (Derynck and Weinberg, 2019). Given these findings and the results of enrichment analysis for *NREP*-related genes, we hypothesized that NREP may have a powerful role in promoting EMT in tumors. Further, we speculated that TGF-β1 could be an important mediator in the effects of NREP. TGF-β1 is a well-known key factor in the TME and can promote the reprogramming of tumor-infiltrating cells, including tumor-associated macrophages (TAMs) and tumor-associated fibroblasts, enabling them to play a decisive role in tumor survival and progression. Signaling crosstalk between cancer cells and mesenchymal cells ultimately leads to an environment that supports tumor growth and metastasis. Recently, high *NREP* expression was observed around the rims of invasive human glioma tumors. Furthermore, *NREP* knockdown in human glioma cells (SF767) has been found to reduce their migration ability *in vitro* (Mariani et al., 2001; Yao et al., 2015, 2017). However, data on the role played by *NREP* in tumorigenesis, particularly in GC, are limited. Therefore, we examined the mechanistic role of *NREP* in GC and its development. We also assessed its prognostic value in GC along with its potential as a target for cancer therapy.

MATERIALS AND METHODS

Antibodies and Reagents

A complete list of reagents and antibodies is provided in **Supplementary Material 1**. All the concentrations were chosen based on previous studies or manufacturer's instructions. The detailed screening protocol is also presented in **Supplementary Material 1**.

Cell Culture

AGS (moderately differentiated GC cells), HGC27 (undifferentiated GC cells), GES-1 (healthy gastric epithelial cells), and THP-1 cells (human monocytic cells) were purchased from the cell bank of the Chinese Academy of Sciences (Shanghai, China). MKN74 and MKN45 cells (well and poorly differentiated

GC cells, respectively) were purchased from the Japanese Collection of Research Bioresources Cell Bank. Human MSCs were purchased from Cyagen Biosciences (Guangzhou, China). GC and THP-1 cells were cultured in RPMI-1640 medium with 10% fetal bovine serum (FBS), and GES-1 cells and human MSCs were cultured in DMEM with 10% FBS. All cells were incubated at 37°C in 5% CO_2.

RNA Extraction and Real-Time Quantitative PCR

Quantitative RT-PCR was performed using the protocol provided in previous studies (Bustin et al., 2005). Total RNA was extracted from cells using the TRIzol reagent. cDNA was synthesized via reverse transcription using the manufacturer's protocol. β-actin was chosen as the internal control. The primers were as follows: β-*actin* (F): 5′-GCGTGACATTAAGGAGAAGC-3′; β-*actin* (R): 5′-ACGTCACACTTCATGATGG-3′; *NREP* (F):5′ TTGAGCGAATGCTACCAGAG-3′; and *NREP* (R):5′-AGGCG AGGCTACGGAAAG -3′.

Western Blot Assessment

The protocol for western blotting was based on previous studies (Hnasko and Hnasko, 2015). Target/β-actin bands were identified with a gel image processing system (ChemiDoc XRS+). Subsequently, relative protein levels were calculated.

Ethics Statement and Specimen Collection

The study's protocol was approved by the ethics committee of the Jiangsu Province Hospital of Chinese Medicine, and informed consent was obtained from clinicians and patients (2019NL-166-02). GC tissue and the surrounding non-tumorous tissue (margin, 5 cm) were collected during surgery from 30 previously treatment-naïve patients with GC at the Jiangsu Provincial Hospital of Traditional Chinese Medicine. Tumors were staged and graded using the 8th edition of the American Joint Committee on Cancer tumor-node-metastasis staging system (Ji et al., 2018). After extraction, tissue specimens were washed with cold phosphate-buffered saline and immediately placed in liquid nitrogen. They were then transferred and stored at −80°C until further examination.

Immunohistochemistry

The protocol used for Immunohistochemistry (IHC) was based on earlier studies (Nizioł et al., 2021). Images were obtained using a NIKON Eclipse Ni-E microscope (NIKON, Japan; original magnification, ×400). The H-SCORE (range 0–300, higher scores indicating stronger positive staining) was calculated as described previously (Yang et al., 2019).

Lentiviral Vector Construction and Transfection

We used lentiviral vectors for overexpressing and knocking down *NREP*. Viruses were designed, synthesized, and produced by GeneChem Corporation. Transfection was performed according to the supplier's protocol. HGC27 and MKN74 cells were transduced with the recombinant lentiviruses using 2 μg/mL polybrene for 24 h. Subsequently, we identified stably transfected GFP-expressing cells using 1.5 μg/mL puromycin. We assessed *NREP* overexpression and knockdown as well as transduction efficiency using western blots.

Enzyme-Linked Immunosorbent Assay

We examined cell supernatants for TGF-β1 levels using the TGF-β1 Enzyme-linked immunosorbent assay (ELISA) Kit based on the given instruction manual. A microplate reader (BioTek Synergy HT) was used to examine optical density at 450 nm.

Colony Formation Assays

We assessed the clonogenic ability of cells using a clone formation assay, as described previously (Li et al., 2012). The number of colonies was counted using a compound light microscope (Olympus BX53, Japan).

Xenograft Tumor Model

All animal experiments were approved by the ethics committee of the Jiangsu Province Hospital of Chinese Medicine (2021-5-062). Twenty-four 4-week-old male BALB/c nude mice were obtained from the Beijing Institute of Biomedicine (Beijing, China; Certificate No. SYXK2019-0010). MKN74 cells transfected with sh-NREP, oe-NREP, and NC and control cells (4×10^6 cell/mouse) were injected subcutaneously into the right armpit region of the mice ($n = 6$ per group). 7 days later, tumor formation was observed beneath the skin. The maximum (a) and minimum tumor diameter (b) were measured twice weekly. On day 15, the mice were euthanized and all tumors were collected. Tumor volume was calculated ($V = 1/2ab^2$), and the growth curves of the subcutaneous xenografts were drawn.

Wound Healing Assay

The protocol used for the wound healing assay was based on earlier studies (Pasquale et al., 2020). Cell migration toward the scratch zone was photographed using an inverted fluorescence microscope (Olympus CKX-41, Japan; ×200 magnification) every 12 h.

Transwell Migration Assay

Cell invasion was assessed using a transwell assay based on a previously published protocol (Misra et al., 2021). The membrane in the chamber was cut and imaged using light microscopy (Olympus BX53, Japan; ×200 magnification), and cell counts were obtained using Image J software.

TUNEL Staining

The TUNEL apoptosis detection kit was used to perform the TUNEL assay, as described previously (Telegina et al., 2019). TUNEL-negative (blue) and TUNEL-positive (red) cells were observed using a fluorescence microscope (Olympus CKX-41, Japan; ×200 magnification).

Immunofluorescence Staining

The protocol used for immunofluorescence staining was based on earlier studies (Donaldson, 2015). Immunofluorescence staining was observed using an epi-fluorescence microscope (Olympus, BX60-32FB2-A03) and different filters and imaged using an Olympus, DP50 camera (×400 magnification).

Establishment of a Co-culture Unit

A non-contact co-culture unit of MSCs and GC cells was established using a co-culture transwell system (upper chamber, GC cells; lower chamber, MSCs; Long et al., 2019). The culture medium was changed every 48 h. After 4 days of non-contact co-culture, the culture in the lower chamber was terminated and cells were harvested for other experiments.

THP-1 cells (1×10^5 cells/mL) were treated with phorbol 12-myristate 13-acetate (PMA; 10 ng/mL) for 48 h to allow the induction of macrophage differentiation (Genin et al., 2015). PMA-containing medium was replaced with serum-free medium, and the cells were cultured for 24 h. 2 days before the co-culture experiment, cells (1×10^5 cells/mL) from the control, knock-down (sh-NREP), overexpression (oe-NREP), and negative control (NC) groups were seeded onto 0.4-μM transwell inserts. For co-culture, the culture medium in the inserts with GC cells was removed and transferred to the top of the pates with differentiated THP-1 cells. After 48 h of further co-culturing, cells were obtained, and immunofluorescence staining was performed.

Statistical Analysis

Data were reported as the mean ± standard deviation. We used *t*-tests and one-way ANOVA to perform comparisons between two groups and among multiple groups, respectively. All data were analyzed using SPSS 26.0 (SPSS Inc., United States) and illustrated using GraphPad Prism 8.0 (GraphPad Software, Inc., United States). All experiments were carried out at least thrice. $^{**}P < 0.01$ and $^{*}P < 0.05$ were considered statistically significant.

Expression Analysis

The expression of *NREP* in GC was first investigated using the TIMER and[1] and GEPIA databases[2] (Pan et al., 2019; Yuan et al., 2019). The Cancer Genome Atlas (TCGA)-Stomach Adenocarcinoma (STAD) cohort and Fei et al. (2018), Li et al (2020), and Shan et al. (2021) datasets were then used to further confirm the differential expression of *NREP* (Rossari et al., 2018; Tian et al., 2018). The Human Protein Atlas database[3], which contains data on >11,200 unique proteins, is the biggest, most comprehensive database on protein distribution in human tissues and cells (Thul and Lindskog, 2018).

Cox Model Establishment and Clinical Value Analysis of NREP in Gastric Cancer

Multivariate Cox regression analysis of TCGA-STAD data was used to identify whether *NREP* could be an independent prognosticator for GC. *P* values, hazard ratios (HRs), and 95% confidence intervals (CIs) were obtained using the "forest plot" R package.

The differences in *NREP* levels were analyzed based on various classification parameters, such as the T/N/M stage, pathologic stage, and histologic grade.

Differences in survival based on *NREP* expression were examined using Kaplan–Meier survival analysis and log-rank tests. *P* values, HRs, and 95% CIs were obtained using log-rank tests and univariate Cox proportional hazards regression. Time receiver operating characteristic (ROC) analysis was applied to calculate the accuracy of prognostication based on *NREP* levels.

Gene Enrichment Analysis

The GeneMANIA database was used to identify genes that showed *NREP*-lined expression and to explore their potential functions (Franz et al., 2018). Genes co-expressed with *NREP* were identified based on TCGA-STAD data (criteria: $|\log FC > 3|$ and $P < |0.05|$). Subsequently, we conducted functional enrichment analysis of *NREP* and the identified genes using the Enrichr database (Kuleshov et al., 2016).

To analyze the connections among proteins, genes co-expressed with *NREP* were assessed using the Search Tool for the Retrieval of Interacting Genes database (STRING)[4] (Szklarczyk et al., 2021); we visualized the results obtained after setting the minimum interaction score to 0.4 in Cytoscape (Doncheva et al., 2019). In addition, based on the constructed protein–protein interaction network (PPI), important modules were screened out using the Molecular Complex Detection (MCODE) tool. Hub genes were obtained by setting the following cutoffs: degree cutoff value = 2, node density cutoff value = 0.1, node score cutoff value = 0.2, k-core = 2, and maximum depth = 100. Finally, the relationship between the levels of these hub genes and GC prognosis was examined using TCGA-STAD data.

Gene set enrichment analysis (GSEA) was performed using the Broad Institute GSEA software 3.0. The geneset "subset of GO (Gene Ontology)" (Molecular Signatures Databases; http://www.gsea-msigdb.org/gsea/msigdb/index.jsp) was used for GO enrichment analysis (Powers et al., 2018). Statistical significance was defined at a normal *P* value < 0.05. The GSCALite online tool was used to explore the relationship between the 10 hub genes and EMT, and we calculated the co-expression relationship between NREP and 6 classical factors of EMT using TCGA-STAD data (Liu et al., 2018). In addition, single-cell analysis was conducted based on GSE134520 to find more evidence on the potential functions of NREP.

Immune Cell and Stromal Cell Analysis

The correlation between *NREP* expression levels and fibroblast levels was first calculated based on the Explicitly Parallel Instruction Code (EPIC) and Mixed Complementarity Problem (MCP)-counter algorithm from the TIMER web tool (Sturm et al., 2019). GC patients were grouped into high- and low-expression cohorts based on the median *NREP* expression, and differential analysis was performed

[1]https://cistrome.shinyapps.io/timer/

[2]https://www.oncomine.org/

[3]https://www.proteinatlas.org/

[4]https://string-db.org/

to identify the differentially abundant cells. Furthermore, CIBERSORT — a high-performance computational method used for quantifying cellular components from bulk-tissue gene expression profiles — was used to accurately estimate immune infiltration (Chen et al., 2018). Spearman's rank correlation coefficients were calculated for pairwise correlation comparisons; $P < 0.05$ was defined as statistically significant. All findings were illustrated using "ggplot2" and "pheatmap."

RESULTS

NREP Expression in Gastric Tumors

The Cancer Genome Atlas-Stomach Adenocarcinoma data showed that *NREP* expression was higher in GC tissues than in normal tissues (**Figure 1A**; $P < 0.05$). Moreover, the analysis of TIMER and TCGA data also showed high *NREP* expression in GC (**Figure 1B**).

We further explored the expression of *NREP* in GC tissues using data from the Gene Expression Omnibus (GEO) database. Data from the Fei et al. (2018), Li et al (2020), and Shan et al. (2021) datasets indicated a significant difference in NREP expression between GC tissues and adjacent tissues (**Figures 1C–E**). Western blot, RT-PCR, and IHC staining also revealed that NREP was over-expressed in GC cells and tissue. The mean H-SCOREs for NREP expression in GC and paracancerous tissue were 93.15 ± 18.21 and 10.49 ± 3.94, respectively (**Figures 1F–J**; $P < 0.01$, ANOVA). NREP protein expression in GC was further verified using IHC data from The Human Protein Atlas. NREP was found to be primarily expressed in the cell membrane and cytoplasm (**Figure 1H**).

Prognostic Value of NREP Expression in Gastric Cancer

Multivariate analysis of TCGA-STAD data revealed that *NREP* overexpression, age, and tumor stage were related with a poor prognosis in GC ($P < 0.001$; **Figure 2A**). In particular, *NREP* levels were identified as an independent predictor of survival in GC patients. The relationship of *NREP* levels with the clinicopathological characteristics of GC patients — including T/N/M stage, histologic grade, pathologic stage, gender, and race — is illustrated in **Figure 2B**. The mRNA levels of *NREP* only showed a correlation with T stage ($P < 0.01$, $P < 0.001$), and no such relationship was observed for other clinical features. Further analysis of the prognostic value of *NREP* using TCGA-STAD data showed that the low-risk group had a longer duration of survival than did the high-risk group (**Figure 2C**; $P < 0.05$). Additionally, according to TCGA-STAD data, the areas under the ROC curves of *NREP* expression for 1-, 3-, and 5-year OS were 0.589, 0.651, and 0.708, respectively, (**Figure 2D**). In summary, the results showed that *NREP* overexpression could be used as an indicator for OS in GC.

Functional Enrichment Analysis of NREP

The functional network of *NREP* and its neighboring genes obtained using GeneMANIA is displayed in **Figure 3A**. We identified genes showing expression levels positively or negatively correlated with *NREP* expression using TCGA-STAD data and the "DESeq" R package (**Figure 3B**). The 73 differentially expressed genes (DEGs) were imported into the DEG PPI (**Figure 3C**). After applying Cytotype MCODE, we identified 10 hub genes among which 8 were up-regulated and 2 were down-regulated (**Figure 3D** and **Supplementary Figures 1A–J**). The GSCALite online tool was used to elucidate the relationship between the 10 hub genes and EMT (**Figure 3E**). Further enrichment analysis suggested that *NREP* may be associated with "extracellular structure organization," "external encapsulating structure organization," "extracellular matrix organization," "collagen-containing extracellular matrix," "platelet-derived growth factor binding," "focal adhesion," and "ECM-receptor interaction" (**Figures 3F–I**).

Additional survival analysis revealed that the levels of 5 up-regulated genes were associated with the prognosis of GC patients (**Supplementary Figures 1K–T**).

Relationship Between NREP and EMT and Its Underlying Mechanism

In vitro NREP silencing in HGC27 and MKN74 cells using shRNA constructs significantly down-regulated *NREP* expression (**Supplementary Figure 2**; $P < 0.01$). *NREP* silencing also decreased tumor cell clone formation (**Figure 4A**). In contrast, the opposite trend was observed in cells overexpressing *NREP*. Moreover, stable *NREP* overexpression in MKN74 cells promoted the formation of subcutaneous xenograft tumors *in vivo* (**Figures 4B–D**; $P < 0.01$). GSEA for *NREP* revealed the potential role of *NREP* in "epithelial–mesenchymal transition" and "TGF-beta signaling." Analyses using TIMER data revealed a positive correlation between NREP and TGF-β1 expression ($R = 0.520$, $P < 0.001$; **Figure 4E**). Subsequent *in vitro* experiments using ELISA revealed a reduction in TGF-β1 levels in culture medium after *NREP* silencing ($P < 0.05$; **Figure 4F**), and the opposite trend was observed when *NREP* was overexpressed. *NREP* overexpression was also found to increase EMT-related phenotypes such as the migration and invasion of GC cells and the expression of EMT-associated proteins. However, this effect was attenuated after treatment with the TGF-β signaling kinase inhibitor LY364947 (**Figures 4G–J**). In addition, cell viability assays showed that the selected concentration of LY364947 did not affect cell proliferation (**Supplementary Material 1**). Further analyses based on TIMER data also revealed a positive correlation between the expression of *NREP* and that of *CDH2* ($R = 0.64$, $P < 0.001$), *MMP2* ($R = 0.65$, $P < 0.001$), *MMP9* ($R = 0.13$ $P = 0.01$), and *VIM* ($R = 0.69$, $P < 0.001$). Further, *NREP* expression was found to show a negative correlation with *CDH1* expression ($R = -0.130$, $P = 0.01$; **Figure 4K**). Therefore, *NREP* silencing and overexpression altered the levels of EMT-related proteins (**Figures 4L,M**).

Relationship of NREP Expression With Cytoskeletal Remodeling and Gastric Cancer Cell Apoptosis

Gene set enrichment analysis also revealed functional enrichment for *NREP* under the "ACTIN FILAMENT ORGANIZATION" and "ACTIN_CYTOSKELETON" domains

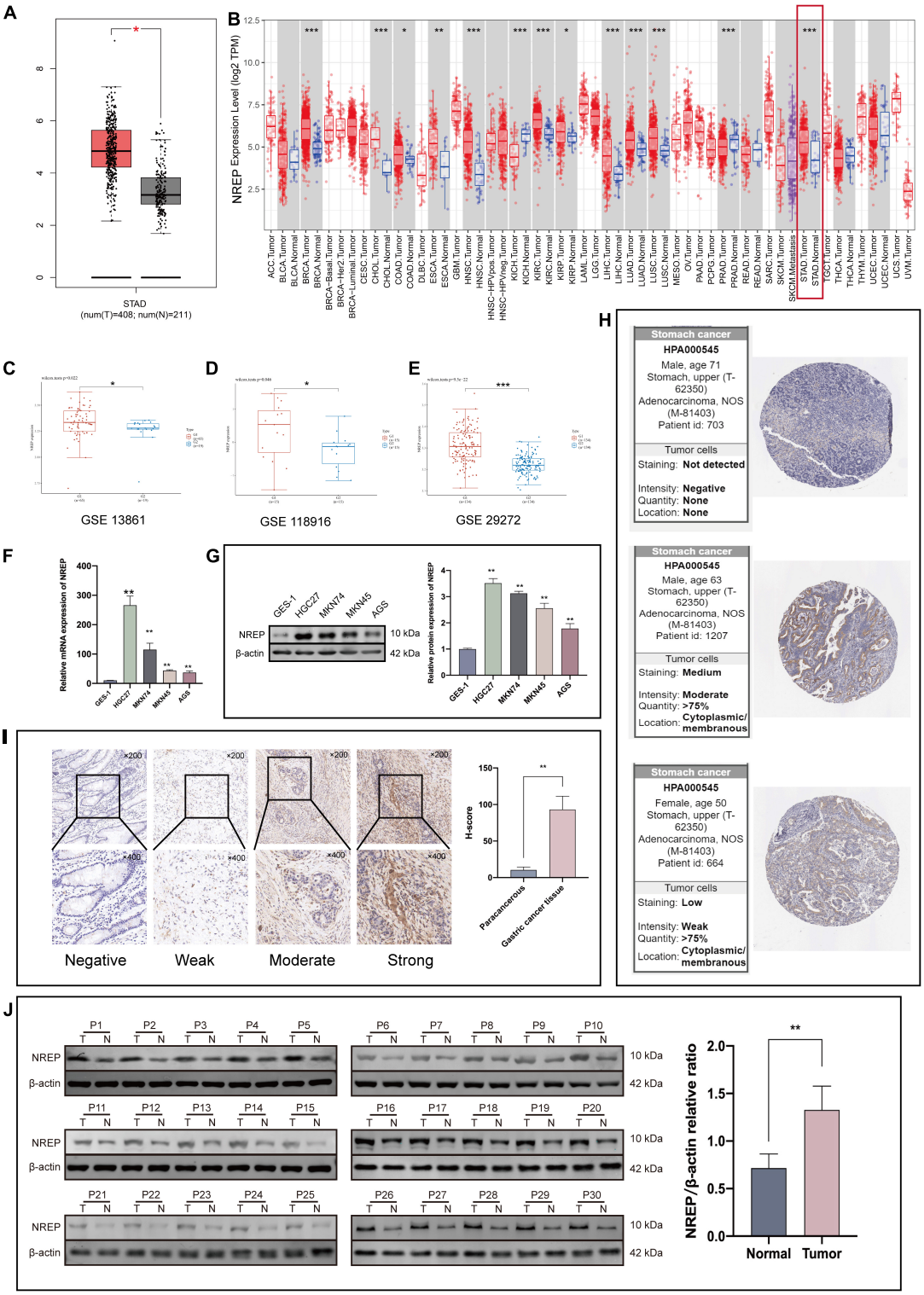


FIGURE 1 | *NREP* levels in gastric cancer (GC) tissue. **(A)** Expression levels of *NREP* in GC based on The Cancer Genome Atlas (TCGA)-STAD data. **(B)** *NREP* mRNA levels in GC and normal tissue based on the TIMER database. **(C–E)** Public datasets from Gene Expression Omnibus (Fei et al., 2018; Li et al, 2020; Shan et al., 2021) used to verify *NREP* mRNA levels in GC. **(F,G)** *NREP* mRNA **(F)** and protein expression **(G)** in normal gastric epithelial cells and GC cells. **(H)** NREP immunohistochemistry in GC tissue based on data from the Human Protein Atlas. **(I)** Intensity of NREP immunohistochemistry staining and NREP expression levels in paracancerous and GC tissue ($n = 30$). **(J)** NREP expression in GC tissues (T) and paired non-tumorous tissue (N) evaluated using western blotting ($n = 30$). (NS: not significant, $^*P < 0.05$, $^{**}P < 0.01$, and $^{***}P < 0.001$).

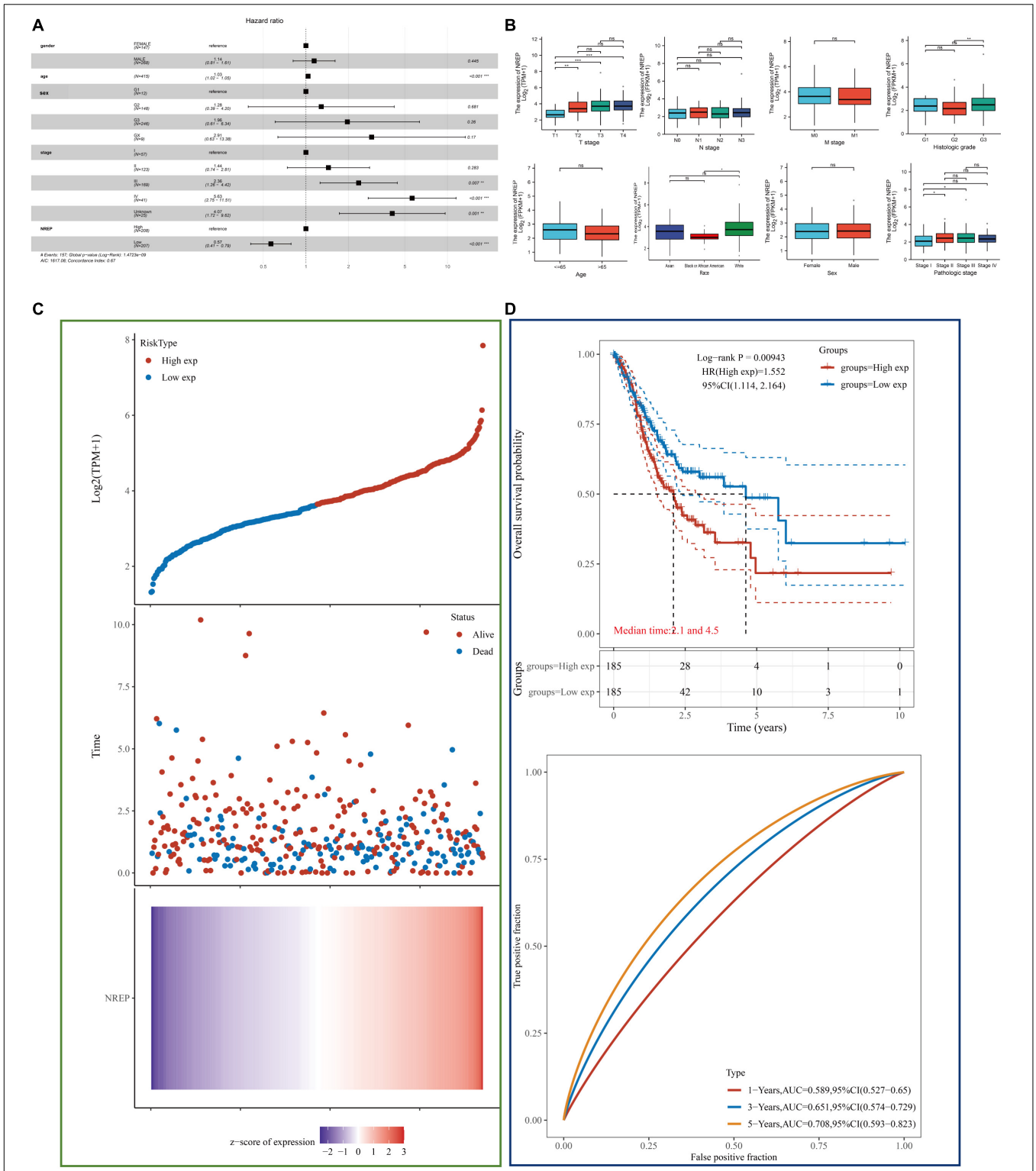


FIGURE 2 | Diagnostic value of *NREP* expression in gastric cancer (GC) based on clinical characteristics. **(A)** Forest plot showing data on Sex, Age, tumor Grade/Stage, and *NREP* expression. **(B)** Association of *NREP* mRNA expression with T/N/M stage, histologic grade, pathologic stage, sex, race, and age in GC patients. **(C)** Patients were divided into low- and high-risk groups according to the median *NREP* expression. From top to bottom: The curve of risk score. Survival status of the patients and more dead patients corresponding to the higher risk score. Heatmap of *NREP* expression. The horizontal coordinates all represent samples, and the samples are ordered consistently. **(D)** Kaplan–Meier survival analysis and time-dependent receiver operating characteristic analysis based on *NREP* levels. (ns: no significance, $^{*}P < 0.05$, $^{**}P < 0.01$, $^{***}P < 0.001$).

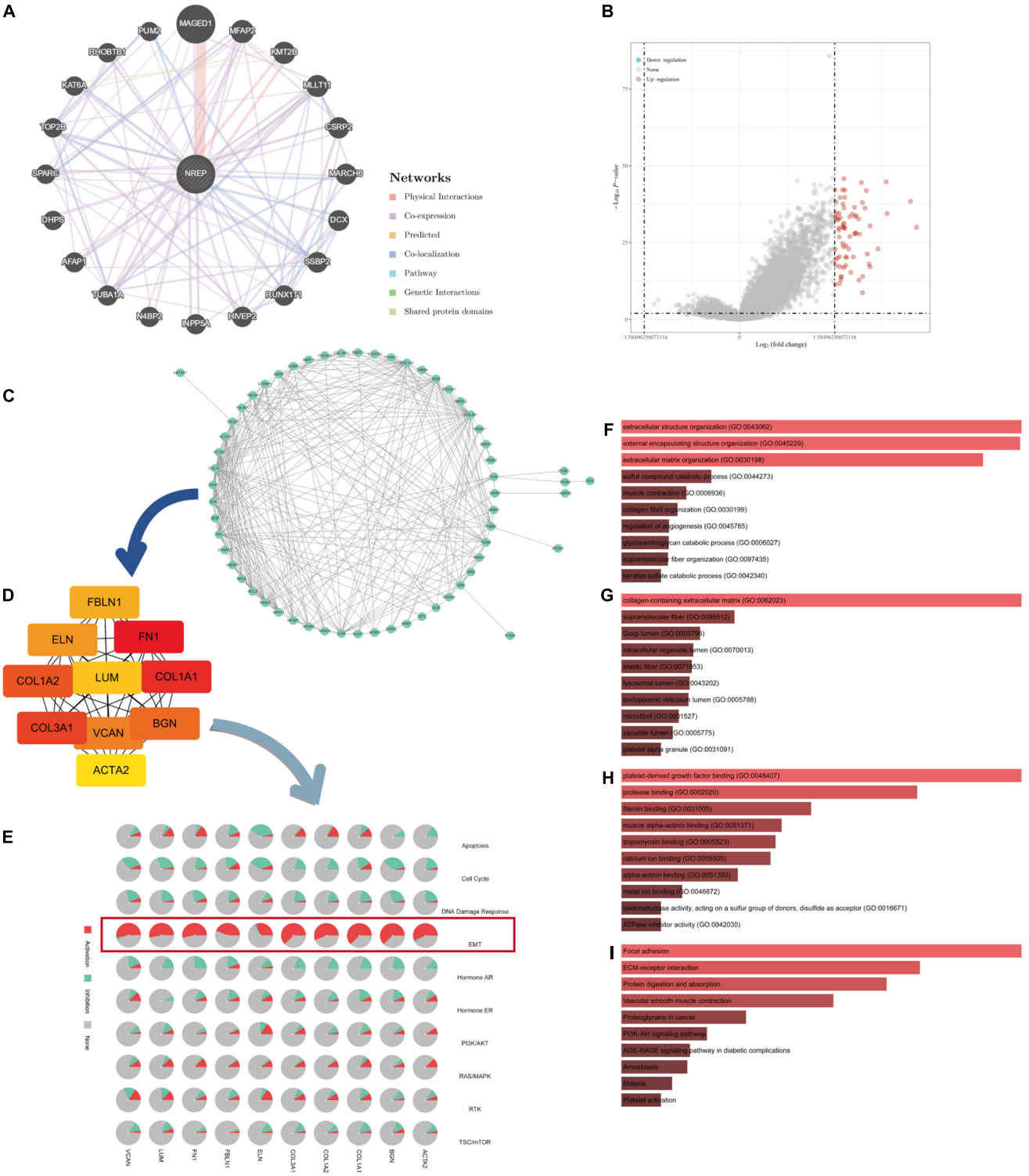


FIGURE 3 | Protein–protein interaction (PPI) network and enrichment analysis. **(A)** GeneMANIA-based PPI; *NREP* is at the core of this network. **(B)** Volcano map of genes showing differential expression after a change in *NREP* levels. Red dots, up-regulated genes; blue dots, down-regulated genes; abscissa, differences in gene expression (log2 fold change); and ordinate, significance of these differences (−log10 padj). **(C)** Network of *NREP* and genes with *NREP*-linked expression (positive). **(D)** Hub gene network of *NREP*. **(E)** Relationship between hub genes and epithelial–mesenchymal transition. **(F–I)** Functional enrichment analysis of *NREP*-related genes. **(F)** Biological Processes (BP), **(G)** Cellular Components (CC), **(H)** Molecular Functions (MF), and **(I)** Kyoto Encyclopedia of Genes and Genomes (KEGG).

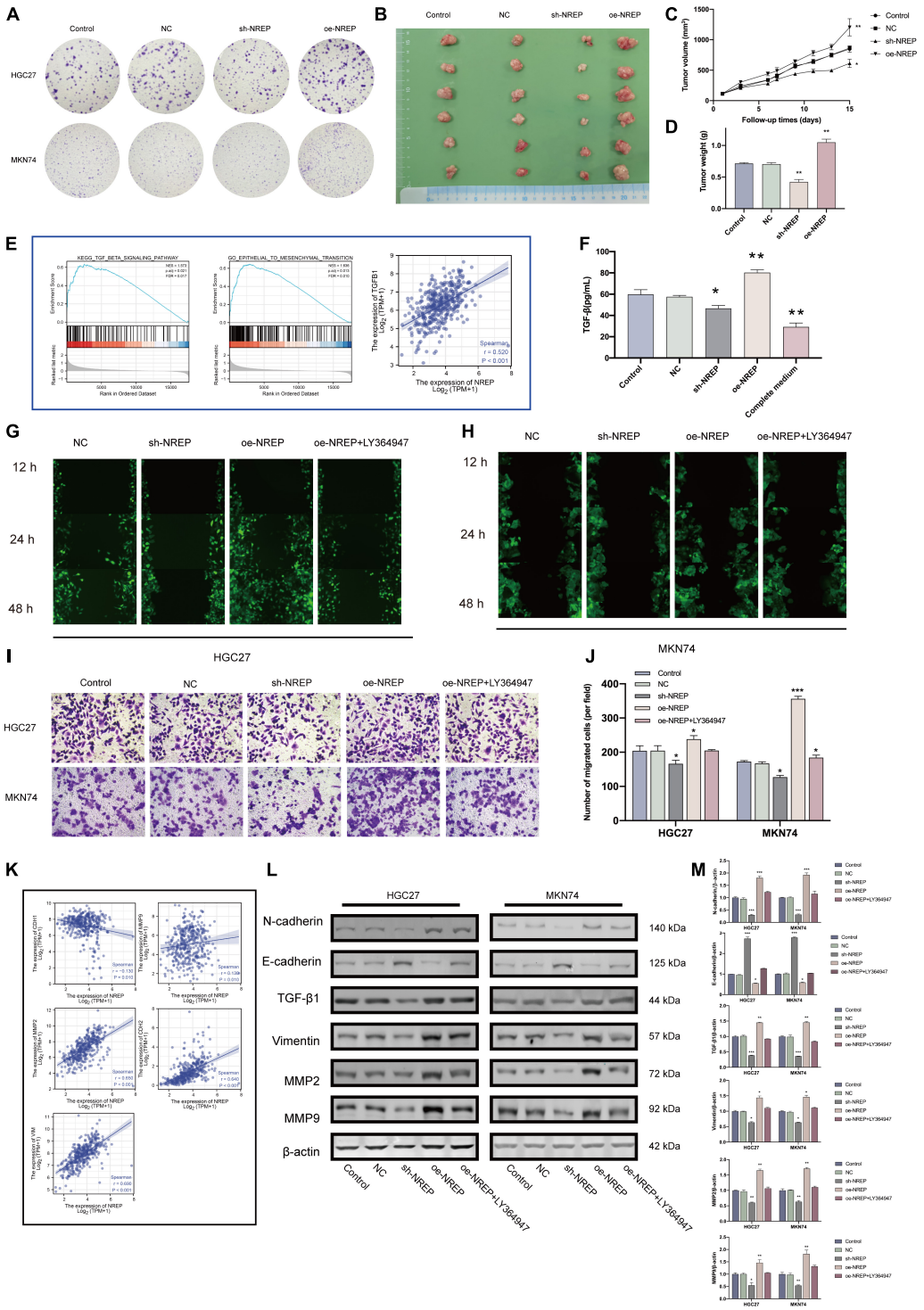


FIGURE 4 | *NREP* overexpression promotes a malignant phenotype in gastric cancer (GC). **(A)** Clone formation capacity of GC cells transfected with the NC, sh-NREP, and oe-NREP constructs assessed using the clone formation assay. **(B)** Xenograft tumors from nude mice. **(C,D)** Tumor volume **(C)** and weights **(D)** of xenografts from nude mice **(E)** Gene Set Enrichment Analysis (GSEA) of *NREP* and correlation analysis between *NREP* and *TGF-β1* expression using TIMER. **(F)** TGF-β1 levels in the supernatant of GC cells transfected with NC, sh-NREP, and oe-NREP examined using ELISA. **(G,H)** Migratory ability of different group of GC cells [**(G)**: HGC27, **(H)**: MKN74] examined using wound healing assays. **(I,J)** The invasion ability of GC cells after transfection **(I**; magnification, ×200); the relative invasive cell number is shown toward the right in **(J)**. **(K)** Correlation coefficient circles for NREP and EMT-related genes (TIMER). **(L)** Expression of EMT-related proteins examined using western blots after the transfection of GC cells with NC, sh-NREP, and oe-NREP constructs and treatment with 5 μM LY364947, an inhibitor specific to TGF-β type I receptor. **(M)** Statistical analysis of western blot results. (*$P < 0.05$, **$P < 0.01$, and ***$P < 0.001$).

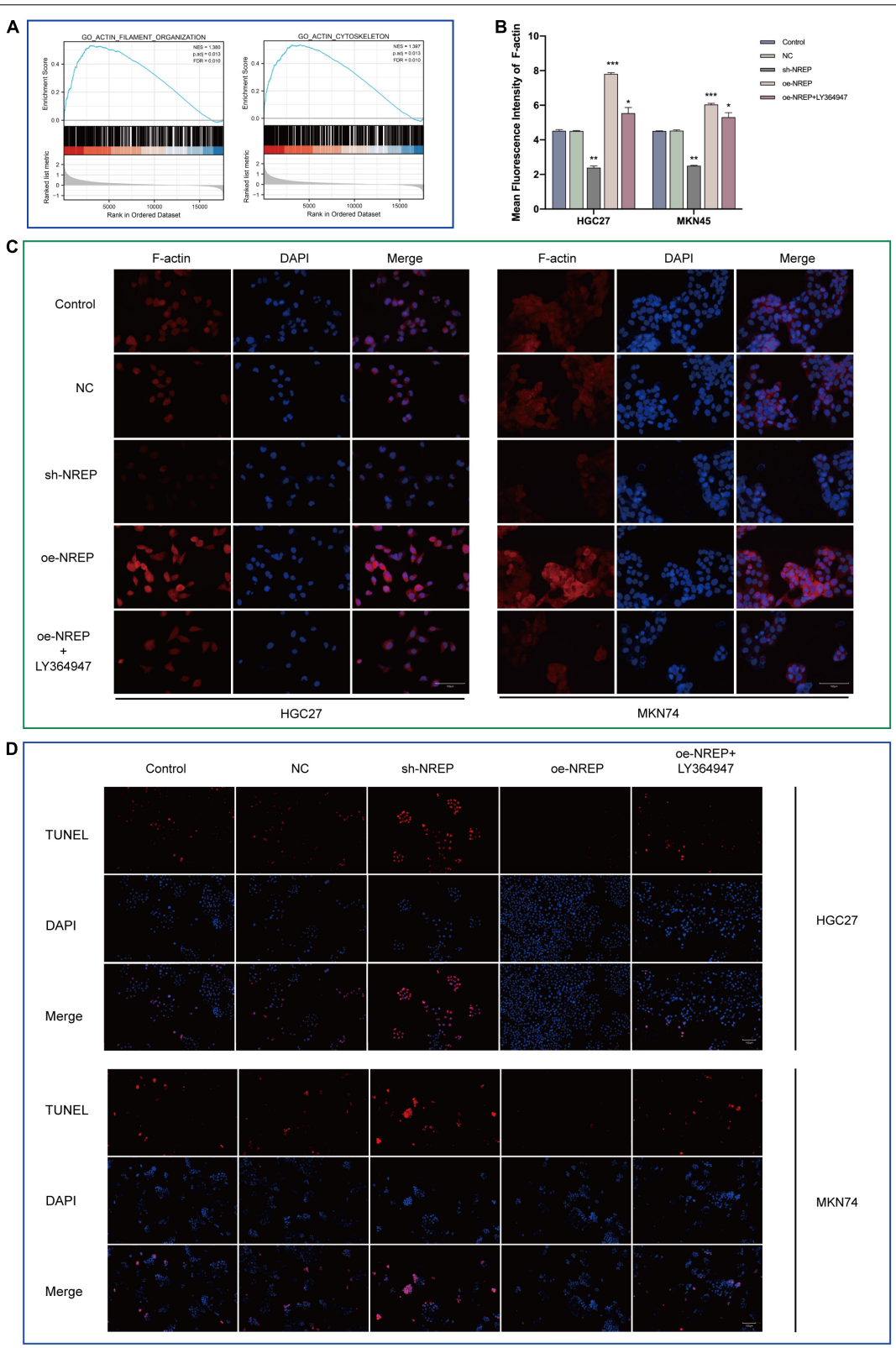


FIGURE 5 | Relationship between NREP and *F*-actin cytoskeleton and cell apoptosis. **(A)** Gene Set Enrichment Analysis (GSEA) of NREP. **(B)** Immunofluorescence intensities. **(C)** *F*-actin levels in gastric cancer (GC) cells (control cells and GC cells transfected with the NC, sh-NREP, and oe-NREP constructs) treated with 5 μM LY364947 detected using immunofluorescence staining (magnification, ×400). **(D)** Apoptosis assessed using a TUNEL assay (TUNEL-positive cells indicated in red; magnification, ×200). (*$P < 0.05$, **$P < 0.01$, ***$P < 0.001$).

(**Figure 5A**). Subsequent *in vitro* experiments revealed that *NREP* overexpression caused the up-regulation of F-actin (**Figures 5B,C**; $P < 0.01$). Moreover, after TUNEL staining, no TUNEL-positive cells were detected in cells overexpressing *NREP*. In contrast, *NREP* knockdown and LY364947 treatment increased the number of TUNEL-positive cells (**Figure 5D**).

Relationship of NREP Expression With the Differentiation of Mesenchymal Stromal Cells Into Cancer-Associated Fibroblasts

The abundance of cancer-associated fibroblasts (CAFs) was found to be a potential prognostic factor in GC (**Table 1**). Using the EPIC and MCP-counter algorithms and TCGA-STAD data (**Figures 6A,B**), we found that *NREP* expression was positively correlated with CAF abundance (EPIC: $R = 0.715$, $P = 1.13e\text{-}60$ and MCP-counter: $R = 0.761$, $P = 5.74e\text{-}73$). Subsequent single-cell-level analyses revealed that *NREP* was mainly expressed in fibroblasts, which are important players in EMT (**Figures 6C–F**).

Local and recruited MSCs are known to transform into CAFs at close proximity to tumor cells. To test whether *NREP* overexpression in GC facilitates the conversion of MSCs into CAFs, we co-cultured MSCs with GC cells (**Figure 6G**). After the co-culture of MSCs with GC cells, CAF markers were remarkably up-regulated in MSCs (**Figure 6H**; $P < 0.01$, $P < 0.001$). Furthermore, we co-cultured MSCs with GC cells showing different levels of *NREP* expression for 4 days. Immunofluorescence staining revealed that α-SMA and Vimentin levels were up-regulated in the *NREP* overexpression group, whereas they were down-regulated in the sh-*NREP* group (**Figures 6I,J**; $P < 0.05$, $P < 0.01$). Interestingly, ELISA revealed a 4-fold increase in the levels of TGF-β1 in the cell supernatant after MSCs were co-cultured with *NREP*-overexpressing cells (**Figure 6K**; $P < 0.05$, $P < 0.05$, and $P < 0.001$). Consistent with our previous results, these findings also showed that a TGF-β inhibitor can decrease the ability of MSCs to differentiate into CAFs in a co-culture unit.

Recently, two modes of cancer cell invasion have been defined: collective cancer cell invasion and fibroblast-led collective invasion. Next, we examined the effect of *NREP* overexpression on CAF recruitment through a transwell experiment. We observed that with an increase in *NREP* expression, the ability of GC cells to recruit CAFs was significantly enhanced (**Figures 6L,M**).

Together, these results indicated that *NREP* may contribute to GC progression by recruiting and activating fibroblasts.

TABLE 1 | The Cox analysis of the Cancer associated fibroblast (CAFs).

	Coef	HR	Se(coef)	95%CI_l	95%CI_u	*p* value
Cancer associated fibroblast_EPIC	1.546	4.692	0.629	1.368	16.093	0.014
Age	0.036	1.036	0.009	1.017	1.055	0
Stage2	0.339	1.404	0.341	0.719	2.74	0.32
Stage3	0.849	2.338	0.318	1.254	4.356	0.007
Stage4	1.567	4.793	0.372	2.31	9.946	0
Gendermale	0.153	1.166	0.191	0.801	1.696	0.423
Purity	−0.422	0.655	0.357	0.326	1.319	0.237

Coef: regression coefficient; HR: hazard ratio; se (coef): standard error of regression coefficient; CI-L: confidence interval low; and CI-U: confidence interval up.

Relationship of NREP Expression With M2 Macrophage Infiltration

Using CIBERSORT, we found that the proportion of tumor-infiltrating cells was positively correlated with *NREP* levels and the presence of M2 macrophages in patients with GC ($P < 0.001$; **Figure 7A**). Subsequently, the relationship of *NREP* expression with macrophage polarization was assessed using the Li et al, 2020 and Fei et al., 2018 datasets. The correlation between *NREP* expression and immune cell subpopulations is shown in **Figure 7B**. Interestingly, *NREP* expression levels were found to be positively correlated with M2 macrophage abundance (**Figure 7C**).

Therefore, we calculated the correlation of *NREP* with M2 surface markers using the TIMER database and observed a positive correlation between *NREP* expression and *MRC1* (CD206; $R = 0.34$, $P < 0.001$) and *CD163* ($R = 0.37$, $P < 0.001$) expression (**Figure 7D**). This series of results suggested the presence of a positive association between *NREP* expression and M2 macrophage infiltration. To further investigate the influence of *NREP* overexpression on M2 macrophage abundance in GC, we established a tumor–macrophage cell co-culture model using a transwell non-contact co-culture unit (**Figure 7E**). We observed that *NREP* overexpression significantly up-regulated the surface markers of M2 TAMs (CD206 and CD163; **Figures 7F,G**).

Hence, our findings confirmed the positive correlation between *NREP* levels and the abundance of M2 macrophage infiltration.

DISCUSSION

Gastric cancer is a very common form of cancer (Machlowska et al., 2020). Previous studies have shown that a large number of genetic and epigenomic alterations in oncogenes as well as genetic instability together govern gastric carcinogenesis, a multistep process that involves the interactive regulation of numerous molecular networks (Chia and Tan, 2016). Thus, the search for new oncogenes and biomarkers not only helps in developing new antitumor drugs, but also helps to broaden the known tumor-associated molecular network (Gyurkó et al., 2013). However, gastric tumors contain more than just cancer cells; they are a complex ecosystem composed of several different types of cells and cytokines, all of which greatly influence the proliferation, adhesion, movement, invasion, and metastasis of GC. During tumor formation, tumor cells must adhere closely to the ECM and communicate with other cells to form a stromal microenvironment suitable for proliferation and eventually metastasis (Mierke, 2019; Zeng et al., 2019).

As a potentially useful target gene for tumor therapy, *NREP* can not only directly affect the biological characteristics of tumor cells, but also reshape the TME and influence patient prognosis. The association between *NREP* and the TGF-β1 pathway has been clearly demonstrated (Yue et al., 2014). TGF-β1 is the

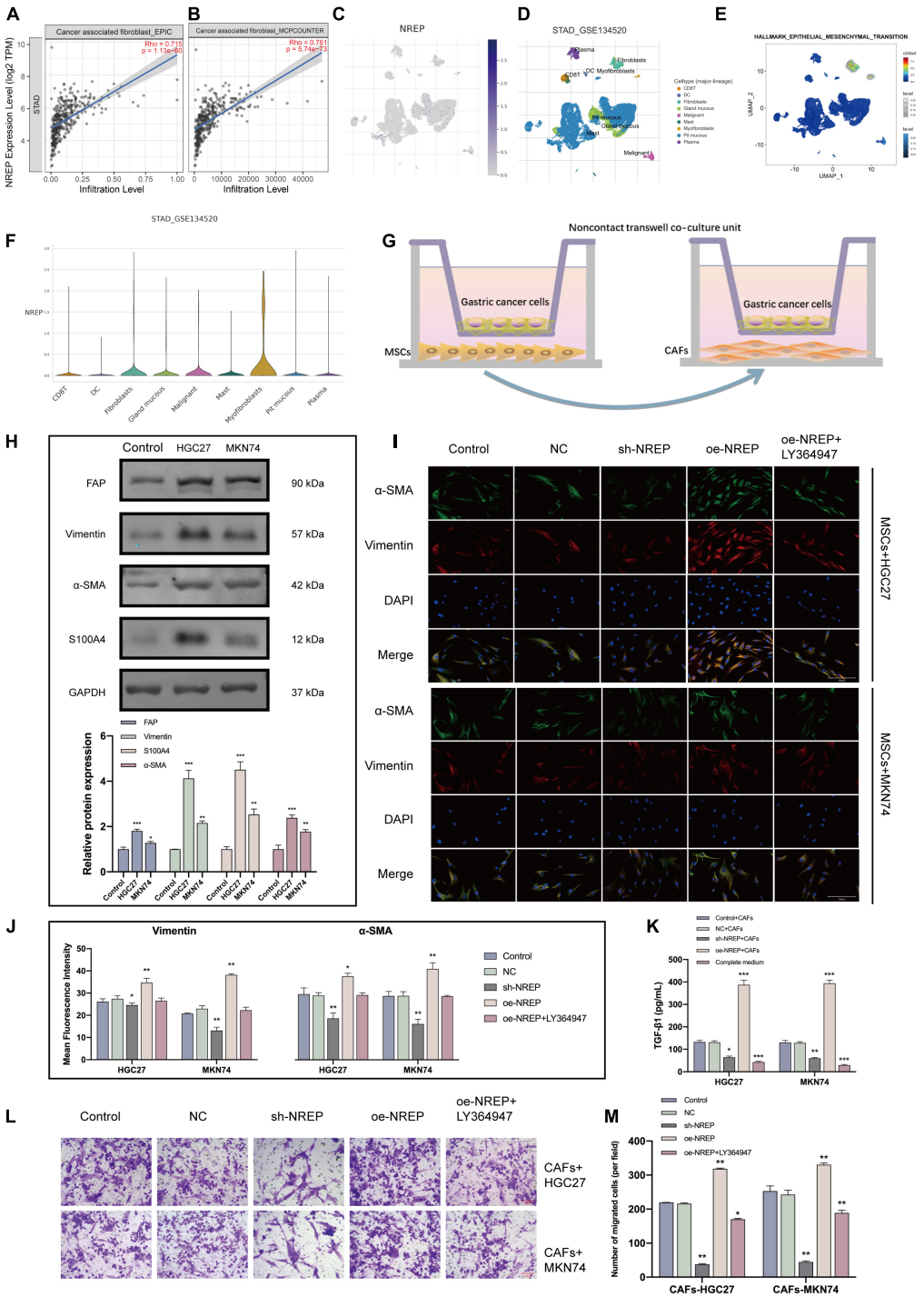


FIGURE 6 | NREP upregulation in gastric cancer (GC) promotes the activation and recruitment of cancer-associated fibroblasts (CAFs). **(A,B)** Correlation of NREP expression with CAFs based on the Fei et al., 2018 **(A)** and Li et al, 2020 **(B)** datasets. **(C)** Uniform manifold approximation and projection (UMAP) plots illustrating the expression of NREP clusters. **(D)** UMAP plots illustrating the GC cell landscape. We found nine cell clusters across 56,440 cells after quality control, dimensionality reduction, and clustering. **(E)** Enrichment score for genes from the Hallmark hypoxia gene set in each cell, obtained using gene set variation analysis. **(F)** Violin plots for GC cell cluster marker genes and *NREP* in different cell types. Expression was measured as log 2 (TP10K + 1). **(G)** A non-contact co-culture unit of MSCs and GC cells established by incubating MSCs with GC cells at a 1:1 ratio. **(H)** After co-culture with GC cells for 4 days, CAF-related markers were examined using western blots. **(I)** Immunofluorescence staining of MSCs co-cultured with GC cells (control cells and GC cells transfected with the NC, sh-NREP, and oe-NREP constructs) treated with 5 μM LY364947 (magnification, ×400). **(K)** After co-culture with different groups of GC cells for 4 days, ELISA assays were used to demonstrate an increase in the TGF-β1 protein levels in the supernatant of the co-culture system. **(L)** The transwell system was used to investigate the ability of GC cells to recruit CAFs. (magnification, ×200). **(M)** The number of migrated cells was counted using Image **(J)**. (*$P < 0.05$, **$P < 0.01$, and ***$P < 0.001$).

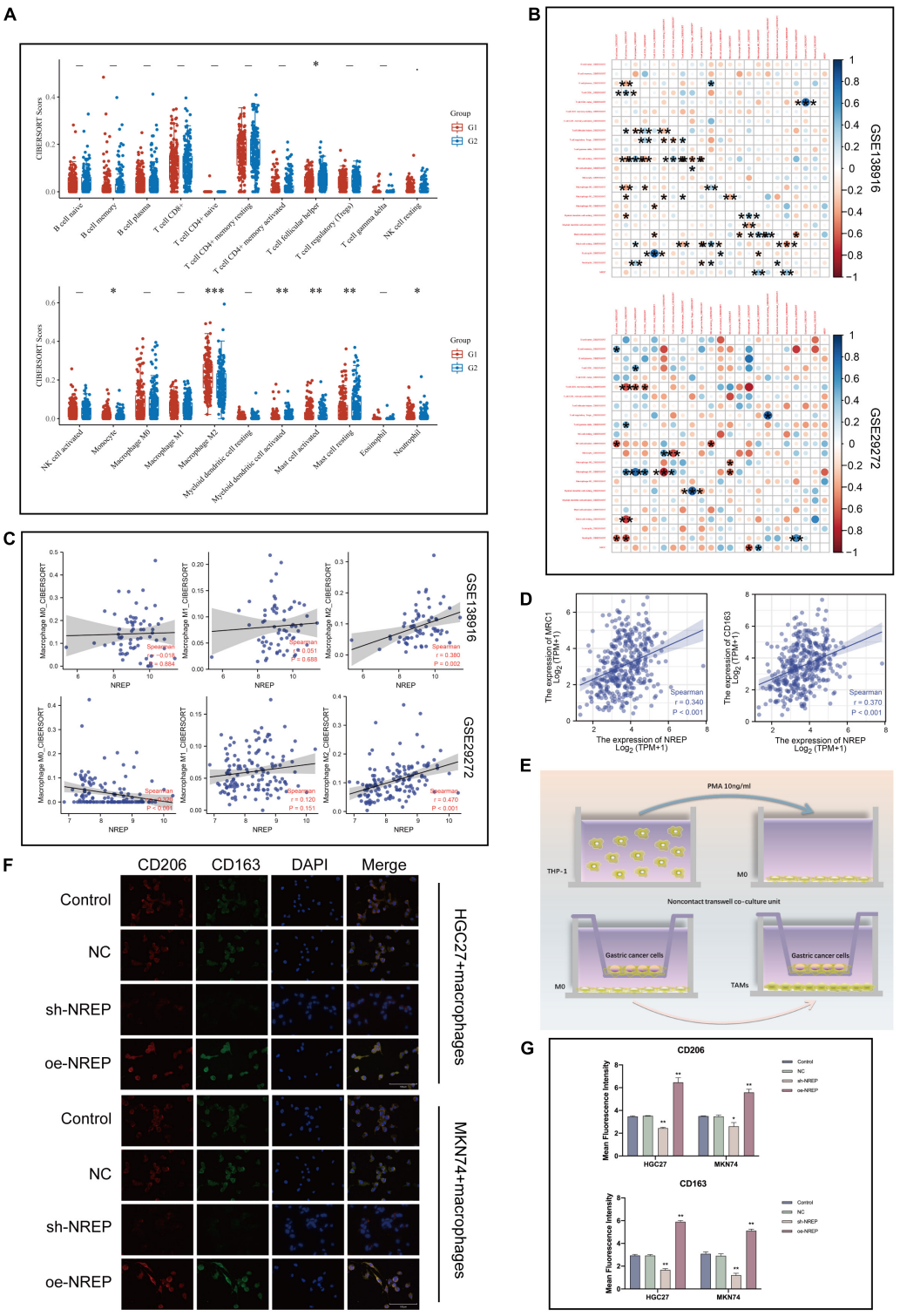


FIGURE 7 | Association of *NREP* expression with the abundance of M2 tumor-associated macrophage infiltration. **(A)** Score distribution of immune cells in gastric cancer (GC) and normal tissues. Horizontal axis, different groups; vertical axis, distribution of gene expression; G1, high *NREP* expression group; and G2, low *NREP* expression group. **(B)** Correlation matrix showing the abundance of 22 types of immune cells. **(C)** Correlation of *NREP* expression levels with macrophage abundance based on Fei et al., 2018 and Li et al, 2020 datasets. **(D)** Correlation of *NREP* expression levels with M2 macrophage markers. **(E)** Schematic diagram for the tumor–macrophage cell co-culture. **(F)** Immunofluorescence staining for CD206 (green) and CD163 (red; magnification, ×400). **(G)** Immunofluorescence expression. (*$P < 0.05$, **$P < 0.01$, and ***$P < 0.001$).

most effective inductor of EMT and has been found to be up-regulated in a variety of tumors (Chen et al., 2017). *NREP* is thought to stimulate the expression of TGF-β1 by promoting the methylation of the *NREP* promoter and activating the *TGF-β1* 5′/3′ UTR (Li et al., 2016). Recent studies have revealed that *NREP* promotes renal fibrosis via the TGF-β1 signaling pathway and that the deletion of *NREP* results in delayed burn wound healing (Stradiot et al., 2018). The process of tumor development has been frequently compared to wound healing owing to several shared molecular and biological processes, including neovascularization, ECM remodeling, and fibrosis (Chang et al., 2004). Therefore, it is reasonable to speculate that *NREP* supports cancer metastasis and the formation of the tumor stromal microenvironment.

It is well known that EMT is a very dynamic process and causes several changes in the cellular phenotype, leading to dramatic cytoskeleton remodeling and the facilitation of cell motility (Pastushenko and Blanpain, 2019). After pooling the genes with *NREP*-linked expression levels, we detected a significant enrichment for EMT-related pathways, including growth factor binding and integrin binding. To further validate this result, we predicted the functions of 10 hub genes using the GSCALite online tool and found that they contribute positively toward the EMT phenotype. Further experiments confirmed that the overexpression of *NREP* significantly up-regulated TGF-β1 and activated the EMT phenotype.

Cancer-associated fibroblasts, important constituents of the tumor stromal microenvironment, play a vital role in tumor–stroma crosstalk, promoting tumor development and progression (Liao et al., 2019). They also secrete oncogenic growth factors, produce ECM, and promote EMT (Pape et al., 2020). TGF-β1-mediated signaling in CAFs has been identified as a pivotal mediator (Porcelli et al., 2019). The TIMER online tool showed that the abundance of CAF infiltration was positively correlated with the expression levels of *NREP*. We also performed single-cell-level analyses and found that *NREP* was predominantly expressed in myofibroblasts, which are a subset of activated fibroblasts characterized by the expression of α-SMA. It has been well-documented that myofibroblasts can be derived from pre-existing stromal fibroblasts and drive tumor progression by establishing TGF-β autocrine signaling in a cell-autonomous manner (Kojima et al., 2010). Considering that bone marrow-derived precursors and bone marrow MSCs are among the multiple origins of CAFs (Borriello et al., 2017), we first co-cultured *NREP*-overexpressing GC cells with MSCs and observed a significant increase in the abundance of CAFs. Further experiments showed that *NREP*-overexpressing GC cells had a stronger ability to recruit CAFs. It has been well-established that CAFs are powerful inducers of EMT activation, and therefore, our findings indicate that *NREP* has a vital function in this process.

An essential step in migration is the remodeling of the cytoskeleton — involving the reorganization and rebuilding of the actin cortical cytoskeleton — which promotes movement (Urra et al., 2018). CAF-derived chemokines influence tumor cell motility by modifying the formin-assembled F-actin cytoskeleton (Zhai et al., 2019). In the present study, GSEA suggested that *NREP* may be involved in cytoskeletal remodeling, and subsequent experiments also confirmed that *NREP* significantly up-regulated F-actin expression levels. Our data demonstrated that *NREP* promotes the activation and chemotaxis of CAFs. Therefore, CAFs may be one of the key factors mediating the promotion of cytoskeletal remodeling by *NREP* in GC cells. Notably, *F*-actin depolymerization and the changes in its cellular distribution, i.e., the transfer of actin filaments from the cytoplasm to the nucleus, are obvious in apoptotic cells (May and Machesky, 2001). The manipulation of F-actin remodeling is used as a therapeutic strategy for inducing apoptosis. Resistance to apoptosis is a well-recognized feature of cancer (Giampazolias and Tait, 2016). Subsequent TUNEL staining showed that the overexpression of *NREP* promoted tumor progression in GC, at least in part, by inhibiting apoptosis.

Normal fibroblasts can acquire a CAF phenotype through communication with cancer cells (Kalluri, 2016). CAFs can be derived from a variety of sources, such as endothelial cells, tumor cells that transdifferentiate into mesenchymal cells via EMT, and bone marrow-MSCs. The recruitment of CAFs from the microenvironment is essential for remodeling the tumor's ECM and allowing tumor motility and metastasis (Monteran and Erez, 2019). Our findings directly confirm the involvement of *NREP* in this complex process.

During the development of GC, a large number of peripheral blood mononuclear cells are attracted to the tumor mesenchyme and transform into TAMs (Sica et al., 2006). Phenotypic analysis has revealed that in progressive GC, infiltrating TAMs often show the immunosuppressive M2 phenotype and play a key role in promoting tumor EMT (Suarez-Carmona et al., 2017). Recent studies have found that tumor cells undergoing EMT promote the M2 phenotype in macrophages by secreting tumor metabolites, and M2 macrophages in turn secrete a variety of cytokines to promote tumor transformation to the mesenchyme, leading to a vicious cycle (Li et al., 2019). CAFs are also known to enhance TAM recruitment in the TME, creating a positive feedback loop between CAFs and TAMs and the ECM (Cho et al., 2018). Therefore, we first analyzed the relationship between the levels of *NREP* and the infiltration of multiple immune cells based on TCGA-STAD data and found that the level of M2 macrophage infiltration was positively correlated with *NREP* expression; moreover, this correlation showed the highest statistical significance. Similar results were obtained from two other independent GEO datasets. Our co-culture experiments also confirmed the positive effect of *NREP* on the levels of CD163 and CD206 (MRC1), which are surface markers of M2 macrophages. Therefore, our findings indicate that NREP promotes M2 macrophage activation — a process that is considered strongly carcinogenic.

Taken together, our results demonstrate that *NREP* is elevated in GC cells and tissues. High *NREP* levels are associated with some clinicopathological features of GC and a poor patient prognosis. Our results show that *NREP* may act as an important player in the complex gene regulatory machinery driving GC via processes such as EMT activation, CAF activation, actin cytoskeleton remodeling, and M2 macrophage infiltration, ultimately promoting tumor development. However, our study has a few limitations. First, *in vivo* experimental evidence was

lacking, and there was insufficient clinical evidence. Therefore, more focused research is needed to elucidate the detailed biological functions and mechanistic roles of *NREP* in GC and to uncover the functional and regulatory niches of this gene.

DATA AVAILABILITY STATEMENT

The original contributions presented in the study are included in the article/**Supplementary Material**, further inquiries can be directed to the corresponding author/s.

ETHICS STATEMENT

The studies involving human participants were reviewed and approved by the Ethics Committee of the Jiangsu Province Hospital of Chinese Medicine. The patients/participants provided their written informed consent to participate in this study. The animal study was reviewed and approved by the Ethics Committee of the Jiangsu Province Hospital of Chinese Medicine.

AUTHOR CONTRIBUTIONS

J-pL and Y-hZ developed the experimental plan. Y-jL and S-hZ performed all experiments. S-hZ and Y-dH analyzed the data. Y-jL and J-pL wrote the manuscript. All authors have read and approved the final manuscript.

FUNDING

The present study was supported by the Youth Science and Technology Project of Suzhou (No. KJXW2019059); the Suzhou Science and Technology Development Plan (No. SYSD2019006); and the Zhangjiagang TCM Hospital Youth Science and Technology Project (No. ZZYQ1915).

ACKNOWLEDGMENTS

We are grateful to all the participants of the present study.

SUPPLEMENTARY MATERIAL

The Supplementary Material for this article can be found online at: https://www.frontiersin.org/articles/10.3389/fcell.2021.746194/full#supplementary-material

Supplementary Figure 1 | Prognostic roles of 10 hub genes and relationship with sample types in patients from the TCGA-STAD dataset. **(A–J)** Expression of *FBLN1*, *ELN*, *FN1*, *COL1A2*, *LUM*, *COL1A1*, *COL3A1*, *VCAN*, *BGN*, and *ACTA2* in different sample types (normal vs. tumor) based on the TCGA-STAD dataset. High expression, red; low expression, blue. TPM: Transcripts Per Kilobase Million. **(K–T)** Survival analysis based on *FBLN1*, *ELN*, *FN1*, *COL1A2*, *LUM*, *COL1A1*, *COL3A1*, *VCAN*, *BGN*, and *ACTA2* expression.

Supplementary Figure 2 | Validation of cell transfection efficiency.

REFERENCES

Al-Batran, S. E., Pauligk, C., and Götze, T. O. (2020). Perioperative chemotherapy for gastric cancer in FLOT4 - Authors' reply. *Lancet* 395:e4. doi: 10.1016/s0140-6736(19)32516-4

Borriello, L., Nakata, R., Sheard, M. A., Fernandez, G. E., Sposto, R., Malvar, J., et al. (2017). Cancer-Associated Fibroblasts Share Characteristics and Protumorigenic Activity with Mesenchymal Stromal Cells. *Cancer Res.* 77, 5142–5157. doi: 10.1158/0008-5472.Can-16-2586

Bustin, S. A., Benes, V., Nolan, T., and Pfaffl, M. W. (2005). Quantitative real-time RT-PCR–a perspective. *J. Mol. Endocrinol.* 34, 597–601. doi: 10.1677/jme.1.01755

Chang, H. Y., Sneddon, J. B., Alizadeh, A. A., Sood, R., West, R. B., Montgomery, K., et al. (2004). Gene expression signature of fibroblast serum response predicts human cancer progression: similarities between tumors and wounds. *PLoS Biol.* 2:E7. doi: 10.1371/journal.pbio.0020007

Chen, B., Khodadoust, M. S., Liu, C. L., Newman, A. M., and Alizadeh, A. A. (2018). Profiling Tumor Infiltrating Immune Cells with CIBERSORT. *Methods Mol. Biol.* 1711, 243–259. doi: 10.1007/978-1-4939-7493-1_12

Chen, Q., Yang, W., Wang, X., Li, X., Qi, S., Zhang, Y., et al. (2017). TGF-β1 Induces EMT in Bovine Mammary Epithelial Cells Through the TGFβ1/Smad Signaling Pathway. *Cell Physiol. Biochem.* 43, 82–93. doi: 10.1159/000480321

Chia, N. Y., and Tan, P. (2016). Molecular classification of gastric cancer. *Ann. Oncol.* 27, 763–769. doi: 10.1093/annonc/mdw040

Cho, H., Seo, Y., Loke, K. M., Kim, S. W., Oh, S. M., Kim, J. H., et al. (2018). Cancer-Stimulated CAFs Enhance Monocyte Differentiation and Protumoral TAM Activation via IL6 and GM-CSF Secretion. *Clin. Cancer Res.* 24, 5407–5421. doi: 10.1158/1078-0432.Ccr-18-0125

De Steur, W. O., van Amelsfoort, R. M., Hartgrink, H. H., Putter, H., Meershoek-Klein Kranenbarg, E., van Grieken, N. C. T., et al. (2021). Adjuvant chemotherapy is superior to chemoradiation after D2 surgery for gastric cancer in the per-protocol analysis of the randomized CRITICS trial. *Ann. Oncol.* 32, 360–367. doi: 10.1016/j.annonc.2020.11.004

Derynck, R., and Weinberg, R. A. (2019). EMT and Cancer: more Than Meets the Eye. *Dev. Cell* 49, 313–316. doi: 10.1016/j.devcel.2019.04.026

Donaldson, J. G. (2015). Immunofluorescence Staining. *Curr. Protoc. Cell Biol.* 69, 41–47. doi: 10.1002/0471143030.cb0403s69

Doncheva, N. T., Morris, J. H., Gorodkin, J., and Jensen, L. J. (2019). Cytoscape StringApp: network Analysis and Visualization of Proteomics Data. *J. Proteome Res.* 18, 623–632. doi: 10.1021/acs.jproteome.8b00702

Duan, F. F., Barron, G., Meliton, A., Mutlu, G. M., Dulin, N. O., and Schuger, L. (2019). P311 Promotes Lung Fibrosis via Stimulation of Transforming Growth Factor-β1, -β2, and -β3 Translation. *Am. J. Respir. Cell Mol. Biol.* 60, 221–231. doi: 10.1165/rcmb.2018-0028OC

Fei, H. J., Chen, S. C., Zhang, J. Y., Li, S. Y., Zhang, L. L., Chen, Y. Y., et al. (2018). Identification of significant biomarkers and pathways associated with gastric carcinogenesis by whole genome-wide expression profiling analysis. *Int. J. Oncol.* 52, 955–966. doi: 10.3892/ijo.2018.4243

Franz, M., Rodriguez, H., Lopes, C., Zuberi, K., Montojo, J., Bader, G. D., et al. (2018). GeneMANIA update 2018. *Nucleic Acids Res.* 46, W60–W64. doi: 10.1093/nar/gky311

Genin, M., Clement, F., Fattaccioli, A., Raes, M., and Michiels, C. (2015). M1 and M2 macrophages derived from THP-1 cells differentially modulate the response of cancer cells to etoposide. *BMC Cancer* 15:577. doi: 10.1186/s12885-015-1546-9

Giampazolias, E., and Tait, S. W. (2016). Mitochondria and the hallmarks of cancer. *FEBS J.* 283, 803–814. doi: 10.1111/febs.13603

Gyurkó, D. M., Veres, D. V., Módos, D., Lenti, K., Korcsmáros, T., and Csermely, P. (2013). Adaptation and learning of molecular networks as a description of cancer development at the systems-level: potential use in anti-cancer therapies. *Semin. Cancer Biol.* 23, 262–269. doi: 10.1016/j.semcancer.2013.06.005

Hnasko, T. S., and Hnasko, R. M. (2015). The Western Blot. *Methods Mol. Biol.* 1318, 87–96. doi: 10.1007/978-1-4939-2742-5_9

Ji, X., Bu, Z. D., Yan, Y., Li, Z. Y., Wu, A. W., Zhang, L. H., et al. (2018). The 8th edition of the American Joint Committee on Cancer tumor-node-metastasis staging system for gastric cancer is superior to the 7th edition: results from a Chinese mono-institutional study of 1663 patients. *Gastric Cancer* 21, 643–652. doi: 10.1007/s10120-017-0779-5

Kalluri, R. (2016). The biology and function of fibroblasts in cancer. *Nat. Rev. Cancer* 16, 582–598. doi: 10.1038/nrc.2016.73

Kojima, Y., Acar, A., Eaton, E. N., Mellody, K. T., Scheel, C., Ben-Porath, I., et al. (2010). Autocrine TGF-beta and stromal cell-derived factor-1 (SDF-1) signaling drives the evolution of tumor-promoting mammary stromal myofibroblasts. *Proc. Natl. Acad. Sci. U. S. A.* 107, 20009–20014. doi: 10.1073/pnas.1013805107

Kuleshov, M. V., Jones, M. R., Rouillard, A. D., Fernandez, N. F., Duan, Q., Wang, Z., et al. (2016). Enrichr: a comprehensive gene set enrichment analysis web server 2016 update. *Nucleic Acids Res.* 44, W90–W97. doi: 10.1093/nar/gkw377

Li, H., Yao, Z., He, W., Gao, H., Bai, Y., Yang, S., et al. (2016). P311 induces the transdifferentiation of epidermal stem cells to myofibroblast-like cells by stimulating transforming growth factor β1 expression. *Stem Cell Res. Ther.* 7:175. doi: 10.1186/s13287-016-0421-1

Li, S., Zhao, W., and Sun, M. (2020). An analysis regarding the association between the *ISLR* gene and gastric carcinogenesis. *Front. Genet.* 11:620. doi: 10.3389/fgene.2020.00620

Li, W., Li, D. M., Chen, K., Chen, Z., Zong, Y., Yin, H., et al. (2012). Development of a gene therapy strategy to target hepatocellular carcinoma based inhibition of protein phosphatase 2A using the α-fetoprotein promoter enhancer and pgk promoter: an in vitro and in vivo study. *BMC Cancer* 12:547. doi: 10.1186/1471-2407-12-547

Li, W., Zhang, X., Wu, F., Zhou, Y., Bao, Z., Li, H., et al. (2019). Gastric cancer-derived mesenchymal stromal cells trigger M2 macrophage polarization that promotes metastasis and EMT in gastric cancer. *Cell Death Dis.* 10:918. doi: 10.1038/s41419-019-2131-y

Liao, Z., Tan, Z. W., Zhu, P., and Tan, N. S. (2019). Cancer-associated fibroblasts in tumor microenvironment - Accomplices in tumor malignancy. *Cell Immunol.* 343:103729. doi: 10.1016/j.cellimm.2017.12.003

Liu, C. J., Hu, F. F., Xia, M. X., Han, L., Zhang, Q., and Guo, A. Y. (2018). GSCALite: a web server for gene set cancer analysis. *Bioinformatics* 34, 3771–3772. doi: 10.1093/bioinformatics/bty411

Liu, X., and Meltzer, S. J. (2017). Gastric Cancer in the Era of Precision Medicine. *Cell. Mol. Gastroenterol. Hepatol.* 3, 348–358. doi: 10.1016/j.jcmgh.2017.02.003

Long, X., Xiong, W., Zeng, X., Qi, L., Cai, Y., Mo, M., et al. (2019). Cancer-associated fibroblasts promote cisplatin resistance in bladder cancer cells by increasing IGF-1/ERβ/Bcl-2 signalling. *Cell Death Dis.* 10:375. doi: 10.1038/s41419-019-1581-6

Machlowska, J., Baj, J., Sitarz, M., Maciejewski, R., and Sitarz, R. (2020). Gastric Cancer: epidemiology, Risk Factors, Classification, Genomic Characteristics and Treatment Strategies. *Int. J. Mol. Sci.* 21:4012. doi: 10.3390/ijms21114012

Margadant, C., and Sonnenberg, A. (2010). Integrin-TGF-beta crosstalk in fibrosis, cancer and wound healing. *EMBO Rep.* 11, 97–105. doi: 10.1038/embor.2009.276

Mariani, L., Mcdonough, W. S., Hoelzinger, D. B., Beaudry, C., Kaczmarek, E., Coons, S. W., et al. (2001). Identification and validation of *P311* as a glioblastoma invasion gene using laser capture microdissection. *Cancer Res.* 61, 4190–4196.

May, R. C., and Machesky, L. M. (2001). Phagocytosis and the actin cytoskeleton. *J. Cell Sci.* 114, 1061–1077.

Meric-Bernstam, F., Johnson, A. M., Dumbrava, E. E. I., Raghav, K., Balaji, K., Bhatt, M., et al. (2019). Advances in HER2-Targeted Therapy: novel Agents and Opportunities Beyond Breast and Gastric Cancer. *Clin. Cancer Res.* 25, 2033–2041. doi: 10.1158/1078-0432.Ccr-18-2275

Mierke, C. T. (2019). The matrix environmental and cell mechanical properties regulate cell migration and contribute to the invasive phenotype of cancer cells. *Rep. Prog. Phys.* 82:064602. doi: 10.1088/1361-6633/ab1628

Misra, S., Ghatak, S., Moreno-Rodriguez, R. A., Norris, R. A., Hascall, V. C., and Markwald, R. R. (2021). Periostin/Filamin-A: a Candidate Central Regulatory Axis for Valve Fibrogenesis and Matrix Compaction. *Front. Cell Dev. Biol.* 9:649862. doi: 10.3389/fcell.2021.649862

Monteran, L., and Erez, N. (2019). The Dark Side of Fibroblasts: cancer-Associated Fibroblasts as Mediators of Immunosuppression in the Tumor Microenvironment. *Front. Immunol.* 10:1835. doi: 10.3389/fimmu.2019.01835

Nizioł, M., Zińczuk, J., Zaręba, K., Guzińska-Ustymowicz, K., and Pryczynicz, A. (2021). Immunohistochemical Analysis of the Expression of Adhesion Proteins: TNS1, TNS2 and TNS3 in Correlation with Clinicopathological Parameters in Gastric Cancer. *Biomolecules* 11:640. doi: 10.3390/biom11050640

Pan, J. H., Zhou, H., Cooper, L., Huang, J. L., Zhu, S. B., Zhao, X. X., et al. (2019). LAYN Is a Prognostic Biomarker and Correlated With Immune Infiltrates in Gastric and Colon Cancers. *Front. Immunol.* 10:6. doi: 10.3389/fimmu.2019.00006

Pape, J., Magdeldin, T., Stamati, K., Nyga, A., Loizidou, M., Emberton, M., et al. (2020). Cancer-associated fibroblasts mediate cancer progression and remodel the tumouroid stroma. *Br. J. Cancer* 123, 1178–1190. doi: 10.1038/s41416-020-0973-9

Pasquale, V., Ducci, G., Campioni, G., Ventrici, A., Assalini, C., Busti, S., et al. (2020). Profiling and Targeting of Energy and Redox Metabolism in Grade 2 Bladder Cancer Cells with Different Invasiveness Properties. *Cells* 9:2669. doi: 10.3390/cells9122669

Pastushenko, I., and Blanpain, C. (2019). EMT Transition States during Tumor Progression and Metastasis. *Trends Cell Biol.* 29, 212–226. doi: 10.1016/j.tcb.2018.12.001

Pauli, C., Hopkins, B. D., Prandi, D., Shaw, R., Fedrizzi, T., Sboner, A., et al. (2017). Personalized In Vitro and In Vivo Cancer Models to Guide Precision Medicine. *Cancer Discov.* 7, 462–477. doi: 10.1158/2159-8290.Cd-16-1154

Porcelli, L., Iacobazzi, R. M., Di Fonte, R., Serratì, S., Intini, A., Solimando, A. G., et al. (2019). CAFs and TGF-β Signaling Activation by Mast Cells Contribute to Resistance to Gemcitabine/Nabpaclitaxel in Pancreatic Cancer. *Cancers* 11:330. doi: 10.3390/cancers11030330

Powers, R. K., Goodspeed, A., Pielke-Lombardo, H., Tan, A. C., and Costello, J. C. (2018). GSEA-InContext: identifying novel and common patterns in expression experiments. *Bioinformatics* 34, i555–i564. doi: 10.1093/bioinformatics/bty271

Rojas, A., Araya, P., Gonzalez, I., and Morales, E. (2020). Gastric Tumor Microenvironment. *Adv. Exp. Med. Biol.* 1226, 23–35. doi: 10.1007/978-3-030-36214-0_2

Rossari, F., Minutolo, F., and Orciuolo, E. (2018). Past, present, and future of Bcr-Abl inhibitors: from chemical development to clinical efficacy. *J. Hematol. Oncol.* 11:84. doi: 10.1186/s13045-018-0624-2

Scott, L. J. (2018). Apatinib: a Review in Advanced Gastric Cancer and Other Advanced Cancers. *Drugs* 78, 747–758. doi: 10.1007/s40265-018-0903-9

Shan M. J., Meng, L. B., Guo, P., Zhang, Y. M., Kong, D., and Liu Y.B. (2021). Screening and identification of key biomarkers of gastric cancer: three genes jointly predict gastric cancer. *Front. Oncol.* 11:591893. doi: 10.3389/fonc.2021.591893

Sica, A., Schioppa, T., Mantovani, A., and Allavena, P. (2006). Tumour-associated macrophages are a distinct M2 polarised population promoting tumour progression: potential targets of anti-cancer therapy. *Eur. J. Cancer* 42, 717–727. doi: 10.1016/j.ejca.2006.01.003

Smyth, E. C., Nilsson, M., Grabsch, H. I., van Grieken, N. C., and Lordick, F. (2020). Gastric cancer. *Lancet* 396, 635–648. doi: 10.1016/s0140-6736(20)31288-5

Son, S. E., Kim, N. J., and Im, D. S. (2021). Development of Free Fatty Acid Receptor 4 (FFA4/GPR120) Agonists in Health Science. *Biomol. Ther.* 29, 22–30. doi: 10.4062/biomolther.2020.213

Stradiot, L., Mannaerts, I., and van Grunsven, L. A. (2018). P311, Friend, or Foe of Tissue Fibrosis? *Front. Pharmacol.* 9:1151. doi: 10.3389/fphar.2018.01151

Studler, J. M., Glowinski, J., and Lévi-Strauss, M. (1993). An abundant mRNA of the embryonic brain persists at a high level in cerebellum, hippocampus and olfactory bulb during adulthood. *Eur. J. Neurosci.* 5, 614–623. doi: 10.1111/j.1460-9568.1993.tb00527.x

Sturm, G., Finotello, F., Petitprez, F., Zhang, J. D., Baumbach, J., Fridman, W. H., et al. (2019). Comprehensive evaluation of transcriptome-based cell-type quantification methods for immuno-oncology. *Bioinformatics* 35, i436–i445. doi: 10.1093/bioinformatics/btz363

Suarez-Carmona, M., Lesage, J., Cataldo, D., and Gilles, C. (2017). EMT and inflammation: inseparable actors of cancer progression. *Mol. Oncol.* 11, 805–823. doi: 10.1002/1878-0261.12095

Szklarczyk, D., Gable, A. L., Nastou, K. C., Lyon, D., Kirsch, R., Pyysalo, S., et al. (2021). The STRING database in 2021: customizable protein-protein networks, and functional characterization of user-uploaded gene/measurement sets. *Nucleic Acids Res.* 49, D605–D612. doi: 10.1093/nar/gkaa1074

Telegina, D. V., Suvorov, G. K., Kozhevnikova, O. S., and Kolosova, N. G. (2019). Mechanisms of Neuronal Death in the Cerebral Cortex during Aging and Development of Alzheimer's Disease-Like Pathology in Rats. *Int. J. Mol. Sci.* 20:5632. doi: 10.3390/ijms20225632

Thul, P. J., and Lindskog, C. (2018). The human protein atlas: a spatial map of the human proteome. *Protein Sci.* 27, 233–244. doi: 10.1002/pro.3307

Tian, J., Guo, S., Chen, H., Peng, J. J., Jia, M. M., Li, N. S., et al. (2018). Combination of Emricasan with Ponatinib Synergistically Reduces Ischemia/Reperfusion Injury in Rat Brain Through Simultaneous Prevention of Apoptosis and Necroptosis. *Transl. Stroke Res.* 9, 382–392. doi: 10.1007/s12975-017-0581-z

Urra, H., Henriquez, D. R., Cánovas, J., Villarroel-Campos, D., Carreras-Sureda, A., Pulgar, E., et al. (2018). IRE1α governs cytoskeleton remodelling and cell migration through a direct interaction with filamin A. *Nat. Cell Biol.* 20, 942–953. doi: 10.1038/s41556-018-0141-0

Wilke, H., Muro, K., Van Cutsem, E., Oh, S. C., Bodoky, G., Shimada, Y., et al. (2014). Ramucirumab plus paclitaxel versus placebo plus paclitaxel in patients with previously treated advanced gastric or gastro-oesophageal junction adenocarcinoma (RAINBOW): a double-blind, randomised phase 3 trial. *Lancet Oncol.* 15, 1224–1235. doi: 10.1016/s1470-2045(14)70420-6

Wu, T., and Dai, Y. (2017). Tumor microenvironment and therapeutic response. *Cancer Lett.* 387, 61–68. doi: 10.1016/j.canlet.2016.01.043

Yang, Y., Xiao, M., Song, Y., Tang, Y., Luo, T., Yang, S., et al. (2019). H-score of 11β-hydroxylase and aldosterone synthase in the histopathological diagnosis of adrenocortical tumors. *Endocrine* 65, 683–691. doi: 10.1007/s12020-019-02022-8

Yao, Z., Li, H., He, W., Yang, S., Zhang, X., Zhan, R., et al. (2017). P311 Accelerates Skin Wound Reepithelialization by Promoting Epidermal Stem Cell Migration Through RhoA and Rac1 Activation. *Stem Cells Dev.* 26, 451–460. doi: 10.1089/scd.2016.0249

Yao, Z., Yang, S., He, W., Li, L., Xu, R., Zhang, X., et al. (2015). P311 promotes renal fibrosis via TGFβ1/Smad signaling. *Sci. Rep.* 5:17032. doi: 10.1038/srep17032

Yuan, Q., Sun, N., Zheng, J., Wang, Y., Yan, X., Mai, W., et al. (2019). Prognostic and Immunological Role of FUN14 Domain Containing 1 in Pan-Cancer: friend or Foe?. *Front. Oncol.* 9:1502. doi: 10.3389/fonc.2019.01502

Yue, M. M., Lv, K., Meredith, S. C., Martindale, J. L., Gorospe, M., and Schuger, L. (2014). Novel RNA-binding protein P311 binds eukaryotic translation initiation factor 3 subunit b (eIF3b) to promote translation of transforming growth factor β1-3 (TGF-β1-3). *J. Biol. Chem.* 289, 33971–33983. doi: 10.1074/jbc.M114.609495

Zeng, D., Li, M., Zhou, R., Zhang, J., Sun, H., Shi, M., et al. (2019). Tumor Microenvironment Characterization in Gastric Cancer Identifies Prognostic and Immunotherapeutically Relevant Gene Signatures. *Cancer Immunol. Res.* 7, 737–750. doi: 10.1158/2326-6066.Cir-18-0436

Zhai, J., Shen, J., Xie, G., Wu, J., He, M., Gao, L., et al. (2019). Cancer-associated fibroblasts-derived IL-8 mediates resistance to cisplatin in human gastric cancer. *Cancer Lett.* 454, 37–43. doi: 10.1016/j.canlet.2019.04.002

Conflict of Interest: The authors declare that the research was conducted in the absence of any commercial or financial relationships that could be construed as a potential conflict of interest.

Publisher's Note: All claims expressed in this article are solely those of the authors and do not necessarily represent those of their affiliated organizations, or those of the publisher, the editors and the reviewers. Any product that may be evaluated in this article, or claim that may be made by its manufacturer, is not guaranteed or endorsed by the publisher.

Copyright © 2021 Liu, Zeng, Hu, Zhang and Li. This is an open-access article distributed under the terms of the Creative Commons Attribution License (CC BY). The use, distribution or reproduction in other forums is permitted, provided the original author(s) and the copyright owner(s) are credited and that the original publication in this journal is cited, in accordance with accepted academic practice. No use, distribution or reproduction is permitted which does not comply with these terms.

frontiers in Cell and Developmental Biology

REVIEW
published: 06 January 2022
doi: 10.3389/fcell.2021.792555

Extrachromosomal Circular DNA (eccDNA): From Chaos to Function

*Shanru Zuo[1,2], Yihu Yi[3], Chen Wang[4], Xueguang Li[2], Mingqing Zhou[5], Qiyao Peng[6,7], Junhua Zhou[2], Yide Yang[2] and Quanyuan He[2]**

[1]Department of Pharmacy, The Third Xiangya Hospital, Central South University, Changsha, China, [2]The Key Laboratory of Model Animals and Stem Cell Biology in Hunan Province, School of Medicine, Hunan Normal University, Changsha, China, [3]Department of Orthopaedics, Wuhan Union Hospital, Wuhan, China, [4]Department of Obstetrics and Gynecology, The Third Xiangya Hospital of Central South University, Changsha, China, [5]Zhongshan Hospital Affiliated to Sun Yat-Sen University, Zhongshan People's Hospital, Zhongshan, China, [6]Institute of Chinese Medicine, Hunan Academy of Traditional Chinese Medicine and Innovation Centre for Science and Technology, Hunan University of Chinese Medicine, Changsa, China, [7]Chongqing Key Laboratory for Pharmaceutical Metabolism Research, College of Pharmacy, College of Traditional Chinese Medicine, Chongqing Medical University, Chongqing, China

Extrachromosomal circular DNA (eccDNA) is a type of double-stranded circular DNA that is derived and free from chromosomes. It has a strong heterogeneity in sequence, length, and origin and has been identified in both normal and cancer cells. Although many studies suggested its potential roles in various physiological and pathological procedures including aging, telomere and rDNA maintenance, drug resistance, and tumorigenesis, the functional relevance of eccDNA remains to be elucidated. Recently, due to technological advancements, accumulated evidence highlighted that eccDNA plays an important role in cancers by regulating the expression of oncogenes, chromosome accessibility, genome replication, immune response, and cellular communications. Here, we review the features, biogenesis, physiological functions, potential functions in cancer, and research methods of eccDNAs with a focus on some open problems in the field and provide a perspective on how eccDNAs evolve specific functions out of the chaos in cells.

Keywords: eccDNA, circulome, biogenesis, cancer, biomarker

OPEN ACCESS

Edited by:
Yue Zhao,
University of Cologne, Germany

Reviewed by:
Richard Chahwan,
University of Zurich, Switzerland
Kui Ming Chan,
City University of Hong Kong, Hong Kong SAR, China

****Correspondence:***
Quanyuan He
hqyone@gmail.com

Specialty section:
This article was submitted to Molecular and Cellular Oncology, a section of the journal Frontiers in Cell and Developmental Biology

Received: *10 October 2021*
Accepted: *16 December 2021*
Published: *06 January 2022*

Citation:
Zuo S, Yi Y, Wang C, Li X, Zhou M, Peng Q, Zhou J, Yang Y and He Q (2022) Extrachromosomal Circular DNA (eccDNA): From Chaos to Function. Front. Cell Dev. Biol. 9:792555. doi: 10.3389/fcell.2021.792555

INTRODUCTION

EccDNA refers to a type of double-stranded circular DNA that is derived and free from chromosomes. In 1965, Alix Bassel and Yasuo Hoota first observed eccDNA in boar sperm using the electron microscope (Hotta and Bassel, 1965). From there, many efforts have been taken to figure out the features and functions of eccDNAs (**Figure 1**). It is clear now that eccDNA is ubiquitous in eukaryotic cells and has been identified in yeasts, plants, *Oxytricha*, *Xenopus*, pigeons, and human cells. (Cohen and Méchali, 2002; Møller et al., 2015; Hull et al., 2019; Yerlici et al., 2019; Molin et al., 2020a, Molin et al., 2020b; Møller et al., 2020; Sin et al., 2021; Wang K et al., 2021; Zhu et al., 2021). It can be derived from everywhere in a genome with sizes ranging from hundreds of base pairs (bp) to several mega bases (Mb). According to the size and origin, eccDNAs can be categorized into mitochondria DNAs (mtDNAs), episomes, double minutes (DMs) (100kb~3 Mb), telomeric circle (t-circles), small polydispersed circular DNA (spcDNA) (100bp~10 kb), and microDNA (100–400 bp) (Wang M et al., 2021).Some studies revealed that episomes can be polymerized into DMs in cancer cells suggesting the possibility that one type of eccDNA can be transformed to others by polymerization or fragmentation with subsequent recircularization (Wahl et al., 1984; Carroll et al., 1988).

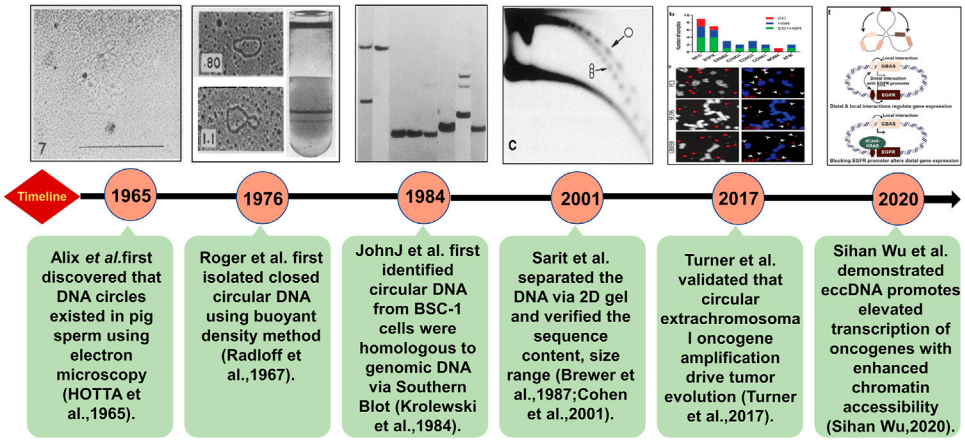


FIGURE 1 | Brief discovery history of eccDNA. The technologies and key discoveries were illustrated following the timeline of the milestone studies. The detailed descriptions are as following: in 1965, Alix Bassel and Yasuo Hoota first observed eccDNAs in boar sperm under the electron microscope (Hotta and Bassel, 1965). The Roger's group extracted eccDNA in HeLa cells by CsCl gradient purification in 1976 (Radloff et al., 1967). In 1984, Krolewski found that eccDNA molecules were homologous to genomic DNA (Krolewski et al., 1984) using Southern blot indicating that eccDNAs may be derived from chromosomes. Neutral–neutral two-dimensional (2D) gel electrophoresis combined with standard procedures of Southern blots and hydridization verified useful for characterizing eccDNA including its size range and sequence content, and it can prove eccDNA organized as discrete multimers (Brewer and Fangman, 1987; Cohen and Mechali, 2001). With rapid advances in high-throughput DNA sequencing, more eccDNAs have been identified and quantified on a global level (Turner et al., 2017). Furthermore, the architecture of eccDNA can be directly observed by super resolution (SR) confocal microscopy (Sihan Wu, 2020).

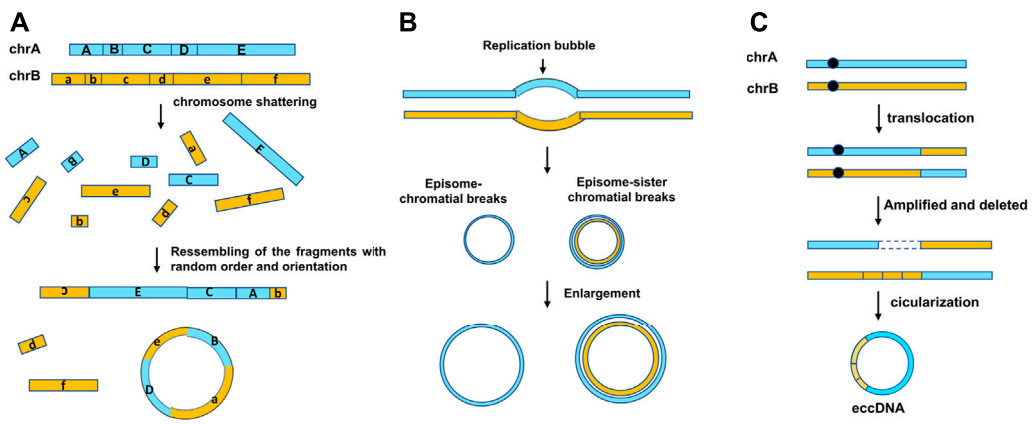


FIGURE 2 | Three mechanisms of eccDNA biogenesis. **(A)** "Chromothripsis" model, chromothripsis is the generation of DNA double-strand breaks. Fragments are joined together in a random order and orientation by DNA repair machineries. The new chromosomes may contain complex structural rearrangements and structural variants. **(B)** Episome model, DNA bidirectionally replicates leading to two replication forks, and the region between them is the replication bubble. The replication fork collapse when the error in replication take place, and then, the replication bubbles drop and form shape of an episome. They can enlarge to form eccDNAs by replication and recombination. **(C)** Translocation–excision–deletion–amplification model. Gene translocation occurs near the chromosome. The fragment next to the translocation positions can be amplified, deleted, and circularized, generating the genesis of eccDNA.

As the counts, compositions, origin, and expression patterns of eccDNA are dramatically dynamic and diverse in cells and tissues, characterizing the functions and underline mechanisms of eccDNAs are extremely challenging (Turner et al., 2017). Many fundamental open questions about eccDNAs remained unanswered. For example, is eccDNA a byproduct or essential player of cellular procedures? Do the sequences of eccDNAs matter for their functions? What is the role of eccDNAs in cancer initiation and progression? et al. Some excellent reviews (Cao et al., 2021; Ling et al., 2021; Wang T et al., 2021) have summarized the characteristics and functions of eccDNA. Here, we review the last progress in the field and try to find the clues to answer the above questions.

THE BIOGENESIS OF ECCDNA

Several models of the eccDNA biogenesis have been proposed: 1) The chromothripsis model (**Figure 2A**): Chromothripsis is the catastrophic shattering of a chromosome followed by massive

genomic rearrangement in a random order, leading to complex genomic structural rearrangements in confined genomic regions. As the "shattering" procedure results in clustered DNA double-strand breaks (DSBs), following by DNA repairing or aberrant DNA replication, and which make it a perfect circumstance to generate eccDNA (Nazaryan-Petersen et al., 2020); in 2021, Wang's team (Wang Y et al., 2021) reported that apoptosis can promote eccDNA generation in human and mouse cells. It is not surprising; apoptosis, just like chromothripsis, can induce DNA fragmentation and may provide massive DNA fragments for eccDNA formation; 2) Episome model (**Figure 2B**). Replication fork stalling may result in replication fork collapse, and the replication bubble subsequently falls off the chromosome, transforms into an extrachromosomal circular molecule named as episome (Gu et al., 2020); 3) Translocation–excision–deletion–amplification model (**Figure 2C**) (Boon et al., 2001; Van Roy et al., 2006). In this model, DNA rearrangements take place close to translocation sites on the chromosome. The fragment in proximity to the translocation breakpoints can be amplified, deleted, and circularized, resulting in the accumulation of eccDNAs.

The above studies indicated that the DNA damage repairing pathways including homologous recombination (HR) or nonhomologous end-joining (NHEJ) and microhomology-mediated end-joining (MMEJ) are involved in the formation of microDNAs (Dillon et al., 2015; Paulsen et al., 2021). The cells lack 53BP1 and XRCC4 promoting the canonical-NHEJ (c-NHEJ), resulting in more microDNA. On the contrary, the deficiency of NBS1, POLQ, RAD54, MLH1, MSH2, MSH3, FAN1, and NBS results in the decrease of microDNA (Paulsen et al., 2021). The short, reverted repeats at both ends of junction sites provide perfect places to initialize homologous recombination (HR) during eccDNA formation. Furthermore, some key players in NHEJ and MMEJ pathways, such as DNA ligases IV and III, were found to contribute to the eccDNA generation (Cohen et al., 2006; Wang K et al., 2021). Additionally, DNA replication and transcription were also proposed as the mechanisms underlying the formation of eccDNAs. For instance, the most transcribed protein-coding gene in the muscle, titin (TTN), has the greatest amount of eccDNAs (Møller et al., 2018). On the contrary, noncoding gene areas show a lower correlation with the eccDNA frequency (Dillon et al., 2015; Møller et al., 2018).

It is widely accepted that eccDNA origination is not restricted to a particular locus in the genome (Møller et al., 2020; Wang T et al., 2021). However, the pattern of eccDNA distribution is still controversial. Some studies reported that the vast majority of eccDNA originates from repetitive elements (Motejlek et al., 1993; Cohen and Mechali, 2001; Moller et al., 2015); others suggested that they prefer to reside in some hotspots such as UTRs of genes, GC islands, and transcriptionally activated chromatins (Shibata et al., 2012; Mehanna et al., 2017). A recent study supported an even distribution model in drug-induced apoptosis cells (Wang Y et al., 2021). Although the driving force of these patterns is still unknown, it is reasonable to speculate that eccDNA origination may be determined by the mechanisms of eccDNA generation under different cellular conditions (**Figure 3**).

THE AMPLIFICATION OF ECCDNA

Most of eccDNA will be degraded rapidly except the ones who can amplify themselves. However, what are the mechanisms of eccDNA amplification is controversial. Some studies suggested that eccDNA amplification relies on DNA replication and mitosis (Baker and Grant, 2007; Herrup and Yang, 2007); others have found that the eccDNA level increases when the ongoing replication is blocked by inhibitors (Sunnerhagen et al., 1986) or even in the absence of any DNA replication (Cohen et al., 2009). However, it is not clear whether these eccDNA levels increasing are a result from amplification or higher levels of biogenesis. We speculate that eccDNAs can be amplified in a way independent of mitosis because many of them don't have replication origins which are required by regular DNA replication.

REGULATORY MECHANISMS OF ECCDNA

Accumulated evidence suggested that eccDNA may regulate many cellular procedures (see the function sections below) through distinct mechanisms (**Figure 3**): 1) Biogenesis of eccDNAs containing whole gene may lead to a gain in the gene copy number and enhance the transcription of the gene (Turner et al., 2017); 2) Forming R-loop by hybridization with mRNA to regulate its translational efficiency (Wiedemann et al., 2016); 3) Titrating the components of the replication or transcription machinery and result in an inability to replicate or transcribe genomic DNA, which eventually induces cell growth arrest and death; (Paulsen et al., 2019; Zhu, et al., 2021); 4) Acting as trans-acting factors (such as super enhancer) to regulate the gene expression by regulating the epigenetic statue and/or accessibility of the targeting gene (Wu et al., 2019); 5) Function as a cytokine to stimulate immune responses or mediate the intercellular communication (Poirier et al., 2018); 6. Genetic rearrangements by the reinsertion of eccDNA into the genome DNA (Pavri, 2017); 7. Protecting the telomeres in ALT cells (McEachern, 2000; Cech, 2004).

PHYSIOLOGICAL FUNCTIONS OF ECCDNA

It is already known that eccDNA plays an important role in a variety of physiological procedures including the following: 1) Stress resistance and evolution. In plants, eccDNA plays a role to amplify and transmit the herbicide resistance gene in crop weeds which result in rapid glyphosate resistance and adaptive evolution (Koo et al., 2018). Furthermore, eccDNA was identified in the *C.elegans* germ line and may serve as genetic materials to be inherited by the offspring (Shoura et al., 2017); 2) Functional enhancement. In humans, the most transcribed protein-coding gene in the muscle, titin (TTN), has the greatest amount of eccDNAs (Møller et al., 2018), and suggesting eccDNA may help host cell fulfill their function. 3) Aging. EccDNA has been found accumulated in old cells and inducing aging in yeast (Hull et al., 2019). It was also amplified during aging in senescence-resistant SAM-R mice and associated with premature aging and shorter lifespan (Yamagishi et al., 1985). Accumulated results highlighted

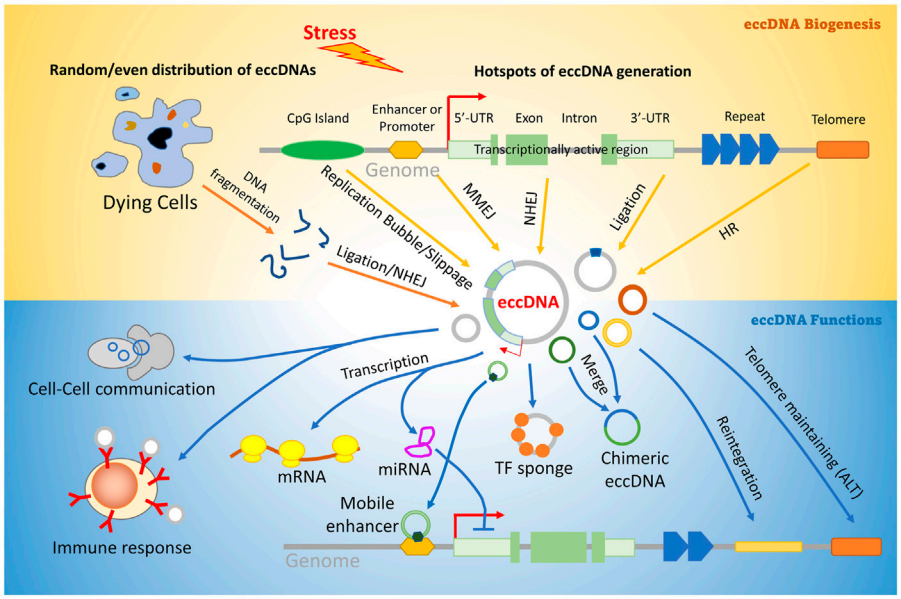


FIGURE 3 | Pathways involved in eccDNA biogenesis and function. Stress may induce aberrant DNA replication, transcription, or even genomic DNA broken into random fragments, and generate linear DNA fragments. Some of them are ligated and circularized by DNA damage repair pathways including HR (homologous recombination), NHEJ (Non-homologous end joining), Ligation by DNA ligases IV and III, and MMEJ (microhomology mediated end-joining). EccDNAs can regulate many downstream biological procedures including transcription, telomere protection, gene translocation, immune response, and cell–cell communication. Description about details can be found in the text.

the proposed role of eccDNAs in age-related CNS diseases, but direct evidence is still absent (Shibata et al., 2012); 4) Genome stability maintenance. Certain types of eccDNAs were originated from telomeres (t-circles) and centromeres (major satellite repeats), that are fundamental structures to maintain genome integrity. Especially, t-circle is essential to maintain telomeres in ATL cells (Neumann et al., 2013); 5) Immune response. As not protected by chromatin, eccDNA may become an endogenous antigen to active autoimmune cells (Collins et al., 2004). Recently, the role of eccDNA in triggering innate immune response was uncovered (Wang M et al., 2021). Surprisingly, the study demonstrated that it is the circular nature but not the sequence of eccDNA critical to the immune response activation; 6) Cell-to-cell communications. The high stability, high mobility, and self-replication ability of eccDNA make it a perfect messenger to transduce and amplify signals among cells. Recent studies confirmed that eccDNA (especially microDNA) can be emitted and sensed by human and mouse cells efficiently *in vitro* (Wang T et al., 2021). In addition, the eccDNAs released by normal and tumor cells have been detected in the peripheral blood (Møller et al., 2018). These data suggested a potential role of eccDNA contributing to both local and long-range signal transduction between cells.

FUNCTIONS OF ECCDNA IN CANCER

EcDNA refers to large eccDNA exclusively detected in tumors. Furthermore, DM is a specific type of ecDNA, which usually contains intact oncogenes and/or drug-resistance genes, which has been detected in most (182/200) kinds of human tumors (Fan et al., 2011). EcDNA, as the vehicles for oncogene and drug-resistance genes, enables them to be rapidly amplified, and lead to overexpression consequently (Turner et al., 2017). For instance, oncogenes EGFR and c-MYC were found in ecDNA and amplified in human cancer tissues than normal tissues (L'Abbate et al., 2014). In tumor cells from a SCLC (small cell lung cancer) patient who received methotrexate (MTX), a large quantity of DMs containing dihydrofolate reductase (DHFR), a drug-resistance gene, was amplified and overexpressed (Curt et al., 1983). Lacking a high-order chromatin structure, suppressing histone modifications, and insulator shackle make ecDNAs more accessible than their genome counterparts which may facilitate promoter–enhancer interactions, transcription initialization, and achieving additional expression (Morton et al., 2019). Furthermore, recent studies also suggested that ecDNA/DMs can function as mobile super-enhancers to enhance targeting genes transcription in genome-wide (Y. Zhu, et al., 2021). Additionally, the unbalanced segregation of ecDNA during mitotic divisions provides an additional layer of tumor heterogeneity which ultimately cause tumor adaptation to the microenvironment stresses and various therapies such as radiotherapy and chemotherapy. This may be the reason that tumors with ecDNA are frequently more aggressive, related to poorer survival outcomes (Bruckert et al., 2000).

The role of smaller eccDNAs (e.g., microDNAs) in cancer biology remains controversial. As they usually are too small to contain the full length of the gene (except for miRNA genes),

whether its transcriptional products have any effects on cancer progression is unknown. However, they may be important for molecular sponging. As often originated from the 5′-UTRs of its parental gene, microDNA may provide additional binding sites for related transcription factors and therefore, acting as a sponge for transcription factors to control the gene expression and transcription homeostasis indirectly (Reon and Dutta, 2016; Paulsen et al., 2018). Additionally, Wang et al. reported that the microDNAs released from dying cells can dramatically induce type I interferon expression and innate immunostimulatory response. It is suspected that drug treatment on cancer cells may induce cell apoptosis with eccDNA generation and subsequent change in the tumor microenvironment dramatically. This work highlighted the potential role of microDNA in drug resistance of cancer cells and shed new light on cancer immunotherapy (Wang Y et al., 2021).

APPLICATIONS OF ECCDNA IN MEDICINE

The entire set of circular DNA (Circulome) varies as a function of tissue type and health and disease conditions and can be used as a fingerprint of disease. Extracellular free eccDNAs are more stable than linear cell-free DNAs (cfDNAs) and have been detected in cancer tissues and peripheral blood of cancer patients (Kumar et al., 2017), suggesting the potential applying them as a novel type of biomarkers in liquid biopsy for the early detection of diseases, the monitoring of drug treatment response, and cancer survival.

Although many efforts have been made, the application of eccDNA in medicine is still at an early stage. In the mammalian repertoire of eccDNA, microDNAs may be the most promising biomarkers because they have smaller size, higher mobility, and higher abundance (account for up to 84% of the entire circulome) (Shibata et al., 2012; Dillon et al., 2015) than others. Furthermore, it exhibited lineage-specific or cell type-specific patterns in human cells (Hotta and Bassel, 1965; Dillon et al., 2015). However, the functions of microDNA are largely unknown, and very few of them are shared by patients, which raise the questions whether the sequence is a matter for them or not. Large cohort studies are needed to identify clinic-relevant microDNA patterns. Another potential eccDNA biomarker is mtDNA. Some studies have reported that the mtDNA copy number variation was correlated with cancer (Sozzi et al., 2003). For example, a high mtDNA copy number in peripheral blood leukocytes (PBLs) was associated with the increased risk of prostate cancer (PCa) and high tumor burden in PCa patients (Zhou et al., 2014). And paradoxically, another report indicated that low mtDNA abundance in PBLs correlated with aggressive PCa at diagnosis (Tu et al., 2015). Similarly, the mtDNA copy number was significantly lower in PBLs of patients with endometrial cancer than normal controls (Sun et al., 2016). As these associations between mtDNA amount and cancer risk are inconsistent and the underlying mechanisms are still unknown, huge gap needs to be filled before the clinical application of mtDNAs. Moreover, it remains unclear about eccDNAs' presence in other bodily fluids such as saliva and urine. It is worthwhile to check the existence of eccDNAs in other bodily fluids.

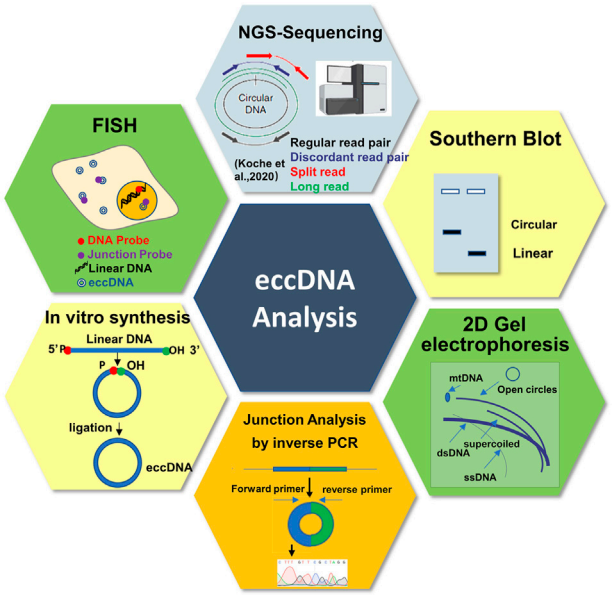


FIGURE 4 | Schematic representation of the different approaches and tools to study circular DNA.

ADVANCE OF ECCDNA RESEARCH METHODS

Many conventional methods were used to characterize the sequence, copy number, subcellular localization, and biological functions of eccDNAs (**Figure 4**), and which was reviewed by elsewhere (Wang T et al., 2021). However, these methods usually provide little information about eccDNA sequences and cannot provide the global view for the whole circulome. Currently, the next/third generation sequencing technologies (such as long-read sequencing (Nanopore and PacBio SMRT sequencing) and single cell sequencing (SC-Seq)) and the improved methods (such as Circle-seq, 4C-seq, PLAC-seq, and ATAC-seq) provide us revolutionary tools to investigate the circulome from various perspectives and with single base-pair and single-cell resolutions (Turner et al., 2017; Prada-Luengo et al., 2019; Rajkumar et al., 2019; Kumar et al., 2020; Mehta et al., 2020; Sin et al., 2020). Especially, the long-read sequencing coupled with the PCR-free eccDNA purification technology present a promising solution to overcome the limitation of short-read sequencing in detecting big eccDNAs and provide unbiased circulomics profiles (Wang M et al., 2021). Furthermore, we speculated that the SC-Seq may be the next dominant technology to decode the rule of eccDNA segregation to rebuild the evolutionary history of the tumor (van den Bos et al., 2018). Additionally, recently, many bioinformatics analysis tools and database for eccDNAs have been proposed (Rajkumar et al., 2019; Wu et al., 2019), which facilitate the rapid development of eccDNA research significantly. However, taking the extreme complexity of the circulome into consideration, the data about eccDNA are still very limited; intensive studies need to be carried out to accumulate and annotate eccDNAs in the future.

PERSPECTIVE: FROM CHAOS TO FUNCTION

For most of eccDNAs, the story may begin with a chaos result from certain internal and external stresses. The stress induces aberrant transcription, DNA replication, and recombination leading to the release of DNA fragments from some hotspots which were consequently recognized and "repaired" by DNA damage repairing mechanisms to form a circulated DNA. In dying or apoptosis cell, global genome DNA fragmentation generate a lot of DNA fragments in a random fashion; some of them were also "rescued" by DNA damage repairing mechanisms to form eccDNAs. We speculate that the former mechanism may majorly contribute to the formation of relatively longer eccDNAs (episomes and DMs), and the latter one is for shorter eccDNAs (spcDNA and microDNA). Most of the eccDNAs will be degraded rapidly, and only the ones who have the ability to amplify themselves and provide adaptive advantage to cells can survive. During the procedure of evolutionary selection, eccDNAs may migrate through cells to search for a good host. They can merge with others to create a new one and novel functions which may provide further advantages of the survival of themselves and hosts. Some eccDNAs may be even more "lucky" to get the chance to integrate into genomic DNA, which eventually fixes themselves in the cell's genome. In tumors, this story may happen everywhere and all the time. EccDNAs help cancer cells develop drug resistance and escape from immune attack. Furthermore, it may also be possible that the eccDNAs originated from the cancer cell can transform target cells remotely through circulation and mediate the metastasis. In germ line, eccDNAs may serve as the secondary genetic materials and were passed to progeny and create additional genetic diversity in population. For somatic cells, too much random eccDNAs may be a burden. However, highly specific functional eccDNA may be a big help for them to fulfill their functions especially under stress conditions (Møller et al., 2018).

CONCLUSION

The discovery of eccDNA may reshape our current understanding of the heredity, evolution, and diseases. EccDNA, as a new kind of genetic material, is mobile, flexible, functionable, tremendous diverse, and everywhere (Wang T et al., 2021). It lets all the cells different and makes quick adaptation and evolution possible. The biological significance of eccDNAs may be heavily underestimated. The eccDNA study is still in its infancy.

Future studies need to focus on 1) Figuring out the chromatin structural features and sequence characteristics of eccDNA on the circulome level; 2) Discovering key regulators and interaction partners of eccDNAs; 3) Exploring the eccDNA segregation procedure at the single cell level to understanding cancer development; 4) Applying it as a liquid biopsy biomarker to improve disease diagnosis, prognosis, and treatment selection; 5) Developing more convenience and sensitive detection methods and advanced tools to support eccDNA research. All these works will deepen our understanding of the nature of eccDNAs and open up new opportunities for cancer diagnosis and therapy.

AUTHOR CONTRIBUTIONS

SZ and QH conceived the present idea and researched the background of the study. YY, CW, XL, QP, MZ, YY, and JZ prepared the figures. SZ, YY, CW, and QH wrote the manuscript. QH revised the manuscript. All the authors read and approved the final manuscript.

FUNDING

This work was supported by the National Natural Science Foundation of China (31771445), the Major Scientific and Technological Project for Collaborative Prevention and Control of Birth Defect in Hunan Province (2019SK1012), and the High-Level Talent Program in Hunan Province (2019RS1035).

ACKNOWLEDGMENTS

We acknowledge and appreciate our colleagues for their valuable suggestions and technical assistance for this study.

REFERENCES

Baker, S. P., and Grant, P. A. (2007). The SAGA Continues: Expanding the Cellular Role of a Transcriptional Co-Activator Complex. *Oncogene.* 26 (37), 5329–5340. doi:10.1038/sj.onc.1210603

Boon, K., Caron, H. N., van Asperen, R., Valentijn, L., Hermus, M.-C., van Sluis, P., et al. (2001). N-myc Enhances the Expression of a Large Set of Genes Functioning in Ribosome Biogenesis and Protein Synthesis. *Embo J.* 20 (6), 1383–1393. doi:10.1093/emboj/20.6.1383

Brewer, B. J., and Fangman, W. L. (1987). The Localization of Replication Origins on ARS Plasmids in S. Cerevisiae. *Cell.* 51 (3), 463–471. doi:10.1016/0092-8674(87)90642-8

Bruckert, P., Kappler, R., Scherthan, H., Link, H., Hagmann, F.-G., and Zankl, H. (2000). Double Minutes and C-MYC Amplification in Acute Myelogenous Leukemia. *Cancer Genet. Cytogenet.* 120 (1), 73–79. doi:10.1016/S0165-4608(99)00235-6

Cao, X., Wang, S., Ge, L., Zhang, W., Huang, J., and Sun, W. (2021). Extrachromosomal Circular DNA: Category, Biogenesis, Recognition, and Functions. *Front. Vet. Sci.* 8, 693641. doi:10.3389/fvets.2021.693641

Carroll, S. M., DeRose, M. L., Gaudray, P., Moore, C. M., Needham-Vandevanter, D. R., Von Hoff, D. D., et al. (1988). Double Minute Chromosomes Can Be Produced from Precursors Derived from a Chromosomal Deletion. *Mol. Cell. Biol.* 8 (4), 1525–1533. doi:10.1128/mcb.8.4.1525-1533.1988

Cech, T. R. (2004). Beginning to Understand the End of the Chromosome. *Cell.* 116 (2), 273–279. doi:10.1016/s0092-8674(04)00038-8

Cohen, S., and Mechali, M. (2001). A Novel Cell-free System Reveals a Mechanism of Circular DNA Formation from Tandem Repeats. *Nucleic Acids Res.* 29 (12), 2542–2548. doi:10.1093/nar/29.12.2542

Cohen, S., and Méchali, M. (2002). Formation of Extrachromosomal Circles from Telomeric DNA in *Xenopus laevis*. *EMBO Rep.* 3 (12), 1168–1174. doi:10.1093/embo-reports/kvf240

Cohen, Z., Bacharach, E., and Lavi, S. (2006). Mouse Major Satellite DNA Is Prone to eccDNA Formation via DNA Ligase IV-dependent Pathway. *Oncogene.* 25 (33), 4515–4524. doi:10.1038/sj.onc.1209485

Cohen, Z., Lavi, S., and Sullivan, B. A. (2009). Replication Independent Formation of Extrachromosomal Circular DNA in Mammalian Cell-Free System. *PLoS One.* 4 (7), e6126. doi:10.1371/journal.pone.0006126

Collins, L. V., Hajizadeh, S., Holme, E., Jonsson, I.-M., Tarkowski, A., Sahlgrenska, A., et al. (2004). Endogenously Oxidized Mitochondrial DNA Induces *In Vivo* and *In Vitro* Inflammatory Responses. *J. Leukoc. Biol.* 75 (6), 995–1000. doi:10.1189/jlb.0703328

Curt, G. A., Carney, D. N., Cowan, K. H., Jolivet, J., Bailey, B. D., Drake, J. C., et al. (1983). Unstable Methotrexate Resistance in Human Small-Cell Carcinoma Associated with Double Minute Chromosomes. *N. Engl. J. Med.* 308 (4), 199–202. doi:10.1056/NEJM198301273080406

Dillon, L. W., Kumar, P., Shibata, Y., Wang, Y.-H., Willcox, S., Griffith, J. D., et al. (2015). Production of Extrachromosomal MicroDNAs Is Linked to Mismatch Repair Pathways and Transcriptional Activity. *Cell Rep.* 11 (11), 1749–1759. doi:10.1016/j.celrep.2015.05.020

Fan, Y., Mao, R., Lv, H., Xu, J., Yan, L., Liu, Y., et al. (2011). Frequency of Double Minute Chromosomes and Combined Cytogenetic Abnormalities and Their Characteristics. *J. Appl. Genet.* 52 (1), 53–59. doi:10.1007/s13353-010-0007-z

Gu, X., Yu, J., Chai, P., Ge, S., and Fan, X. (2020). Novel Insights into Extrachromosomal DNA: Redefining the Onco-Drivers of Tumor Progression. *J. Exp. Clin. Cancer Res.* 39 (1), 215. doi:10.1186/s13046-020-01726-4

Herrup, K., and Yang, Y. (2007). Cell Cycle Regulation in the Postmitotic Neuron: Oxymoron or New Biology? *Nat. Rev. Neurosci.* 8 (5), 368–378. doi:10.1038/nrn2124

Hotta, Y., and Bassel, A. (1965). Molecular Size and Circularity of Dna in Cells of Mammals and Higher Plants. *Proc. Natl. Acad. Sci.* 53, 356–362. doi:10.1073/pnas.53.2.356

Hull, R. M., King, M., Pizza, G., Krueger, F., Vergara, X., and Houseley, J. (2019). Transcription-induced Formation of Extrachromosomal DNA during Yeast Ageing. *Plos Biol.* 17 (12), e3000471. doi:10.1371/journal.pbio.3000471

Koo, D.-H., Molin, W. T., Saski, C. A., Jiang, J., Putta, K., Jugulam, M., et al. (2018). Extrachromosomal Circular DNA-Based Amplification and Transmission of Herbicide Resistance in Crop weedAmaranthus Palmeri. *Proc. Natl. Acad. Sci. USA.* 115 (13), 3332–3337. doi:10.1073/pnas.1719354115

Krolewski, J. J., Schindler, C. W., and Rush, M. G. (1984). Structure of Extrachromosomal Circular DNAs Containing Both the Alu Family of Dispersed Repetitive Sequences and Other Regions of Chromosomal DNA. *J. Mol. Biol.* 174 (1), 41–54. doi:10.1016/0022-2836(84)90364-4

Kumar, P., Dillon, L. W., Shibata, Y., Jazaeri, A. A., Jones, D. R., and Dutta, A. (2017). Normal and Cancerous Tissues Release Extrachromosomal Circular DNA (eccDNA) Into the Circulation. *Mol. Cancer Res.* 15 (9), 1197–1205. doi:10.1158/1541-7786.MCR-17-0095

Kumar, P., Kiran, S., Saha, S., Su, Z., Paulsen, T., Chatrath, A., et al. (2020). ATAC-seq Identifies Thousands of Extrachromosomal Circular DNA in Cancer and Cell Lines. *Sci. Adv.* 6 (20), a2489. doi:10.1126/sciadv.aba2489

L'Abbate, A., Macchia, G., D'Addabbo, P., Lonoce, A., Tolomeo, D., Trombetta, D., et al. (2014). Genomic Organization and Evolution of Double Minutes/Homogeneously Staining Regions withMYCamplification in Human Cancer. *Nucleic Acids Res.* 42 (14), 9131–9145. doi:10.1093/nar/gku590

Ling, X., Han, Y., Meng, J., Zhong, B., Chen, J., Zhang, H., et al. (2021). Small Extrachromosomal Circular DNA (eccDNA): Major Functions in Evolution and Cancer. *Mol. Cancer* 20 (1), 113. doi:10.1186/s12943-021-01413-8

McEachern, M. J., Krauskopf, A., and Blackburn, E. H. (2000). Telomeres and Their Control. *Annu. Rev. Genet.* 34, 331–358. doi:10.1146/annurev.genet.34.1.331

Mehanna, P., Gagné, V., Lajoie, M., Spinella, J.-F., St-Onge, P., Sinnett, D., et al. (2017). Characterization of the microDNA Through the Response to Chemotherapeutics in Lymphoblastoid Cell Lines. *PLoS One.* 12 (9), e0184365. doi:10.1371/journal.pone.0184365

Mehta, D., Cornet, L., Hirsch-Hoffmann, M., Zaidi, S. S.-e. -A., and Vanderschuren, H. (2020). Full-length Sequencing of Circular DNA Viruses and Extrachromosomal Circular DNA Using CIDER-Seq. *Nat. Protoc.* 15 (5), 1673–1689. doi:10.1038/s41596-020-0301-0

Molin, W. T., Yaguchi, A., Blenner, M., and Saski, C. A. (2020a). Autonomous Replication Sequences from the Amaranthus Palmeri eccDNA Replicon Enable Replication in Yeast. *BMC Res. Notes.* 13 (1), 330. doi:10.1186/s13104-020-05169-0

Molin, W. T., Yaguchi, A., Blenner, M., and Saski, C. A. (2020b). The EccDNA Replicon: A Heritable, Extranuclear Vehicle That Enables Gene Amplification and Glyphosate Resistance in Amaranthus Palmeri. *Plant Cell.* 32 (7), 2132–2140. doi:10.1105/tpc.20.00099

Møller, H. D., Larsen, C. E., Parsons, L., Hansen, A. J., Regenberg, B., and Mourier, T. (2016). Formation of Extrachromosomal Circular DNA from Long Terminal Repeats of Retrotransposons in *Saccharomyces cerevisiae*. *G3 (Bethesda).* 6 (2), 453–462. doi:10.1534/g3.115.025858

Møller, H. D., Mohiyuddin, M., Prada-Luengo, I., Sailani, M. R., Halling, J. F., Plomgaard, P., et al. (2018). Circular DNA Elements of Chromosomal Origin Are Common in Healthy Human Somatic Tissue. *Nat. Commun.* 9 (1), 1069. doi:10.1038/s41467-018-03369-8

Møller, H. D., Parsons, L., Jørgensen, T. S., Botstein, D., and Regenberg, B. (2015). Extrachromosomal Circular DNA Is Common in Yeast. *Proc. Natl. Acad. Sci. USA.* 112 (24), E3114–E3122. doi:10.1073/pnas.1508825112

Møller, H. D., Ramos-Madrigal, J., Prada-Luengo, I., Gilbert, M. T. P., and Regenberg, B. (2020). Near-Random Distribution of Chromosome-Derived Circular DNA in the Condensed Genome of Pigeons and the Larger, More Repeat-Rich Human Genome. *Genome Biol. Evol.* 12 (2), 3762–3777. doi:10.1093/gbe/evz281

Morton, A. R., Dogan-Artun, N., Faber, Z. J., MacLeod, G., Bartels, C. F., Piazza, M. S., et al. (2019). Functional Enhancers Shape Extrachromosomal Oncogene Amplifications. *Cell.* 179 (6), 1330–1341. doi:10.1016/j.cell.2019.10.039

Motejlek, K., Schindler, D., Assum, G., and Krone, W. (1993). Increased Amount and Contour Length Distribution of Small Polydisperse Circular DNA (spcDNA) in Fanconi Anemia. *Mutat. Research/DNA Repair.* 293 (3), 205–214. doi:10.1016/0921-8777(93)90071-n

Nazaryan-Petersen, L., Bjerregaard, V. A., Nielsen, F. C., Tommerup, N., and Tümer, Z. (2020). Chromothripsis and DNA Repair Disorders. *J. Clin. Med.* 9 (3), 613. doi:10.3390/jcm9030613

Neumann, A. A., Watson, C. M., Noble, J. R., Pickett, H. A., Tam, P. P. L., and Reddel, R. R. (2013). Alternative Lengthening of Telomeres in Normal Mammalian Somatic Cells. *Genes Dev.* 27 (1), 18–23. doi:10.1101/gad.205062.112

Paulsen, T., Kumar, P., Koseoglu, M. M., and Dutta, A. (2018). Discoveries of Extrachromosomal Circles of DNA in normal and Tumor Cells. *Trends Genet.* 34 (4), 270–278. doi:10.1016/j.tig.2017.12.010

Paulsen, T., Malapati, P., Shibata, Y., Wilson, B., Eki, R., Benamar, M., et al. (2021). MicroDNA Levels Are Dependent on MMEJ, Repressed by C-NHEJ Pathway, and Stimulated by DNA Damage. *Nucleic Acids Res.* 49, 11787–11799. doi:10.1093/nar/gkab984

Paulsen, T., Shibata, Y., Kumar, P., Dillon, L., and Dutta, A. (2019). Small Extrachromosomal Circular DNAs, microDNA, Produce Short Regulatory RNAs that Suppress Gene Expression Independent of Canonical Promoters. *Nucleic Acids Res.* 47 (9), 4586–4596. doi:10.1093/nar/gkz155

Pavri, R. (2017). R Loops in the Regulation of Antibody Gene Diversification. *Genes.* 8 (6), 154. doi:10.3390/genes8060154

Poirier, E. Z., Goic, B., Tomé-Poderti, L., Frangeul, L., Boussier, J., Gausson, V., et al. (2018). Dicer-2-Dependent Generation of Viral DNA from Defective Genomes of RNA Viruses Modulates Antiviral Immunity in Insects. *Cell Host & Microbe.* 23 (3), 353–365. doi:10.1016/j.chom.2018.02.001

Prada-Luengo, I., Krogh, A., Maretty, L., and Regenberg, B. (2019). Sensitive Detection of Circular DNAs at Single-Nucleotide Resolution Using Guided Realignment of Partially Aligned Reads. *BMC Bioinformatics.* 20 (1), 663. doi:10.1186/s12859-019-3160-3

Radloff, R., Bauer, W., and Vinograd, J. (1967). A Dye-Buoyant-Density Method for the Detection and Isolation of Closed Circular Duplex DNA: The Closed Circular DNA in HeLa Cells. *Proc. Natl. Acad. Sci.* 57 (5), 1514–1521. doi:10.1073/pnas.57.5.1514

Rajkumar, U., Turner, K., Luebeck, J., Deshpande, V., Chandraker, M., Mischel, P., et al. (2019). EcSeg: Semantic Segmentation of Metaphase Images Containing Extrachromosomal DNA. *iScience.* 21, 428–435. doi:10.1016/j.isci.2019.10.035

Reon, B. J., and Dutta, A. (2016). Biological Processes Discovered by High-Throughput Sequencing. *Am. J. Pathol.* 186 (4), 722–732. doi:10.1016/j.ajpath.2015.10.033

Shibata, Y., Kumar, P., Layer, R., Willcox, S., Gagan, J. R., Griffith, J. D., et al. (2012). Extrachromosomal MicroDNAs and Chromosomal Microdeletions in Normal Tissues. *Science.* 336 (6077), 82–86. doi:10.1126/science.1213307

Shoura, M. J., Gabdank, I., Hansen, L., Merker, J., Gotlib, J., Levene, S. D., et al. (2017). Intricate and Cell Type-Specific Populations of Endogenous Circular DNA (eccDNA) in *Caenorhabditis elegans* and *Homo sapiens*. *G3 (Bethesda).* 7 (10), 3295–3303. doi:10.1534/g3.117.300141

Sin, S. T. K., Ji, L., Deng, J., Jiang, P., Cheng, S. H., Heung, M. M. S., et al. (2021). Characteristics of Fetal Extrachromosomal Circular DNA in Maternal Plasma: Methylation Status and Clearance. *Clin. Chem.* 67 (5), 788–796. doi:10.1093/clinchem/hvaa326

Sin, S. T. K., Jiang, P., Deng, J., Ji, L., Cheng, S. H., Dutta, A., et al. (2020). Identification and Characterization of Extrachromosomal Circular DNA in Maternal Plasma. *Proc. Natl. Acad. Sci. USA.* 117 (3), 1658–1665. doi:10.1073/pnas.1914949117

Sozzi, G., Conte, D., Leon, M., Cirincione, R., Roz, L., Ratcliffe, C., et al. (2003). Quantification of Free Circulating DNA as a Diagnostic Marker in Lung Cancer. *J. Clin. Oncol.* 21 (21), 3902–3908. doi:10.1200/JCO.2003.02.006

Sun, Y., Zhang, L., Ho, S. S., Wu, X., and Gu, J. (2016). Lower Mitochondrial DNA Copy Number in Peripheral Blood Leukocytes Increases the Risk of Endometrial Cancer. *Mol. Carcinog.* 55 (6), 1111–1117. doi:10.1002/mc.22373

Sunnerhagen, P., SjÖberg, R.-M., Karlsson, A.-L., Lundh, L., and Bjursell, G. (1986). Molecular Cloning and Characterization of Small Polydisperse Circular DNA from Mouse 3T6 Cells. *Nucl. Acids Res.* 14 (20), 7823–7838. doi:10.1093/nar/14.20.7823

Tu, H., Gu, J., Meng, Q. H., Kim, J., Davis, J. W., He, Y., et al. (2015). Mitochondrial DNA Copy Number in Peripheral Blood Leukocytes and the Aggressiveness of Localized Prostate Cancer. *Oncotarget.* 6 (39), 41988–41996. doi:10.18632/oncotarget.5889

Turner, K. M., Deshpande, V., Beyter, D., Koga, T., Rusert, J., Lee, C., et al. (2017). Extrachromosomal Oncogene Amplification Drives Tumour Evolution and Genetic Heterogeneity. *Nature.* 543 (7643), 122–125. doi:10.1038/nature21356

van den Bos, H., Bakker, B., Spierings, D. C. J., Lansdorp, P. M., and Foijer, F. (2018). Single-cell Sequencing to Quantify Genomic Integrity in Cancer. *Int. J. Biochem. Cell Biol.* 94, 146–150. doi:10.1016/j.biocel.2017.09.016

Van Roy, N., Vandesompele, J., Menten, B., Nilsson, H., De Smet, E., Rocchi, M., et al. (2006). Translocation-Excision-Deletion-Amplification Mechanism Leading to Nonsyntenic Coamplification ofMYC andATBF1. *Genes Chromosom. Cancer.* 45 (2), 107–117. doi:10.1002/gcc.20272

Wahl, G. M., Robert de Saint Vincent, B., and DeRose, M. L. (1984). Effect of Chromosomal Position on Amplification of Transfected Genes in Animal Cells. *Nature.* 307 (307), 516–520. doi:10.1038/307516a0

Wang, K., Tian, H., Wang, L., Wang, L., Tan, Y., Zhang, Z., et al. (2021). Deciphering Extrachromosomal Circular DNA in Arabidopsis. *Comput. Struct. Biotechnol. J.* 19, 1176–1183. doi:10.1016/j.csbj.2021.01.043

Wang, M., Chen, X., Yu, F., Ding, H., Zhang, Y., and Wang, K. (2021). Extrachromosomal Circular DNAs: Origin, Formation and Emerging Function in Cancer. *Int. J. Biol. Sci.* 17 (4), 1010–1025. doi:10.7150/ijbs.54614

Wang, T., Zhang, H., Zhou, Y., and Shi, J. (2021). Extrachromosomal Circular DNA: A New Potential Role in Cancer Progression. *J. Transl. Med.* 19 (1), 257. doi:10.1186/s12967-021-02927-x

Wang, Y., Wang, M., Djekidel, M. N., Chen, H., Liu, D., Alt, F. W., et al. (2021). EccDNAs Are Apoptotic Products with High Innate Immunostimulatory Activity. *Nature.* 599, 308–314. doi:10.1038/s41586-021-04009-w

Wiedemann, E.-M., Peycheva, M., and Pavri, R. (2016). DNA Replication Origins in Immunoglobulin Switch Regions Regulate Class Switch Recombination in an R-loop-dependent Manner. *Cell Rep.* 17 (11), 2927–2942. doi:10.1016/j.celrep.2016.11.041

Wu, S., Turner, K. M., and Nguyen, N. (2019). Circular ecDNA Promotes Accessible Chromatin and High Oncogene Expression. *Nature.* 575, 699. doi:10.1038/s41586-019-1763-5

Yamagishi, H., Kunisada, T., and Takeda, T. (1985). Amplification of Extrachromosomal Small Circular DNAs in a Murine Model of Accelerated Senescence. A Brief Note. *Mech. Ageing Development.* 29 (1), 101–103. doi:10.1016/0047-6374(85)90051-x

Yerlici, V. T., Lu, M. W., Hoge, C. R., Miller, R. V., Neme, R., Khurana, J. S., et al. (2019). Programmed Genome Rearrangements in Oxytricha Produce Transcriptionally Active Extrachromosomal Circular DNA. *Nucleic Acids Res.* 47 (18), 9741–9760. doi:10.1093/nar/gkz725

Zhou, W., Zhu, M., Gui, M., Huang, L., Long, Z., Wang, L., et al. (2014). Peripheral Blood Mitochondrial DNA Copy Number Is Associated with Prostate Cancer Risk and Tumor burden. *PLoS One.* 9 (10), e109470. doi:10.1371/journal.pone.0109470

Zhu, Y., Gujar, A. D., Wong, C.-H., Tjong, H., Ngan, C. Y., Gong, L., et al. (2021). Oncogenic Extrachromosomal DNA Functions as mobile Enhancers to Globally Amplify Chromosomal Transcription. *Cancer Cell.* 39, 694–707. doi:10.1016/j.ccell.2021.03.006

Conflict of Interest: The authors declare that the research was conducted in the absence of any commercial or financial relationships that could be construed as a potential conflict of interest.

Publisher's Note: All claims expressed in this article are solely those of the authors and do not necessarily represent those of their affiliated organizations, or those of the publisher, the editors, and the reviewers. Any product that may be evaluated in this article, or claim that may be made by its manufacturer, is not guaranteed or endorsed by the publisher.

Copyright © 2022 Zuo, Yi, Wang, Li, Zhou, Peng, Zhou, Yang and He. This is an open-access article distributed under the terms of the Creative Commons Attribution License (CC BY). The use, distribution or reproduction in other forums is permitted, provided the original author(s) and the copyright owner(s) are credited and that the original publication in this journal is cited, in accordance with accepted academic practice. No use, distribution or reproduction is permitted which does not comply with these terms.

frontiers in Cell and Developmental Biology

ORIGINAL RESEARCH
published: 12 January 2022
doi: 10.3389/fcell.2021.779169

SIPA1 Enhances Aerobic Glycolysis Through HIF-2α Pathway to Promote Breast Cancer Metastasis

*Chenguang Yao[1†], Jun Weng[1†], Lingyun Feng[1†], Wanjun Zhang[1], Yan Xu[2], Peijing Zhang[1], Yoshimasa Tanaka[3] and Li Su[1]**

[1]Key Laboratory of Molecular Biophysics of Ministry of Education, College of Life Science and Technology, Huazhong University of Science and Technology, Wuhan, China, [2]Medical Innovation Center, Graduate School of Medicine, Kyoto University, Kyoto, Japan, [3]Center for Medical Innovation, Nagasaki University, Nagasaki, Japan

Increased dependence on aerobic glycolysis is characteristic of most cancer cells, whereas the mechanism underlying the promotion of aerobic glycolysis in metastatic breast cancer cells under ambient oxygen has not been well understood. Here, we demonstrated that aberrant expression of signal-induced proliferation-associated 1 (SIPA1) enhanced aerobic glycolysis and altered the main source of ATP production from oxidative phosphorylation to glycolysis in breast cancer cells. We revealed that SIPA1 promoted the transcription of *EPAS1*, which is known as the gene encoding hypoxia-inducible factor-2α (HIF-2α) and up-regulated the expression of multiple glycolysis-related genes to increase aerobic glycolysis. We also found that blocking aerobic glycolysis by either knocking down SIPA1 expression or oxamate treatment led to the suppression of tumor metastasis of breast cancer cells both *in vitro* and *in vivo*. Taken together, aberrant expression of SIPA1 resulted in the alteration of glucose metabolism from oxidative phosphorylation to aerobic glycolysis even at ambient oxygen levels, which might aggravate the malignancy of breast cancer cells. The present findings indicate a potential target for the development of therapeutics against breast cancers with dysregulated SIPA1 expression.

Keywords: aerobic glycolysis, breast cancer, EPAS1, HIF-2α, signal-induced proliferation-associated 1

OPEN ACCESS

Edited by:
Yue Zhao,
University of Cologne, Germany

Reviewed by:
Aiyun Wang,
Nanjing University of Chinese Medicine, China
Keith R. Laderoute,
Consultant, Redwood City, CA, United States

****Correspondence:***
Li Su
lisu@hust.edu.cn

†These authors have contributed equally to this work and share first authorship

Specialty section:
This article was submitted to Molecular and Cellular Oncology, a section of the journal Frontiers in Cell and Developmental Biology

Received: *18 September 2021*
Accepted: *17 December 2021*
Published: *12 January 2022*

Citation:
Yao C, Weng J, Feng L, Zhang W, Xu Y, Zhang P, Tanaka Y and Su L (2022) SIPA1 Enhances Aerobic Glycolysis Through HIF-2α Pathway to Promote Breast Cancer Metastasis. Front. Cell Dev. Biol. 9:779169. doi: 10.3389/fcell.2021.779169

INTRODUCTION

Cancer cells rely on aerobic glycolysis for energy resources, even under the condition of ambient oxygen levels (Hanahan and Weinberg, 2011). This aberrant metabolic process is of great benefit for rapid energy production and increased levels of intermediates for other metabolic pathways, and continuously yields acidic lactate altering microenvironment, impairing tumor immune responses and stromal cell integrity, and ultimately leading to tumor progression (Kroemer and Pouyssegur, 2008; Simoes et al., 2015; Garcia-Canaveras et al., 2019). Although aerobic glycolysis is characteristic for some cancer cells, the mechanism underlying the conversion of metabolic pathway of aerobic glycolysis has not been fully elucidated yet.

Breast cancer is a heterogeneous disease characterized by metabolic rewriting from oxidative phosphorylation to aerobic glycolysis in a specific malignant mass, whereas functional mitochondria is pivotal for the survival of cancer cells (Jeon et al., 2013; Lanning et al., 2017; Wang et al., 2020). Hypoxia-inducible factor-1 (HIF-1α) is an essential regulatory factor for aerobic glycolysis and other neoplastic bioprocesses in cancer cells in both hypoxic as well as oxygenated regions of tumors

(Denko, 2008). By inducing glycolysis-related genes products such as hexokinase 2 (HK2), lactate dehydrogenase A (LDHA), and glucose transporter 1 (GLUT1, also known as solute carrier family A1, SLC2A1), HIF-1α switches the glucose metabolism of hypoxic tumor cells to the glycolytic pathway. This metabolic switch might cause a shift in energy production in cancer cells (Denko, 2008). Whereas HIF-1α was initially identified as a key factor in response to hypoxia, accumulating evidence has revealed that HIF-1α could be also regulated by hypoxia-independent pathways such as oncogene activation or loss of tumor suppressors, which links metabolic reprogramming to tumorigenesis and cancer metastasis (Denko, 2008; Rankin and Giaccia, 2016; Zhang et al., 2019). As one of the oncogenic transcriptional factors regulating the glycolytic phenotype of breast cancer, c-myc can drive glycolytic programming by directly up-regulating the transcription of glycolysis-related genes including GLUTs, HK2, and LDHA (Hsieh et al., 2015). In addition, p53 and K-ras were demonstrated to be involved in the regulation of glycolysis in hepatocarcinoma (Kawada et al., 2017; Kim et al., 2019). Moreover, HIF-2α, which is encoded by *EPAS1* gene, having 48% homology to HIF-1α at an amino acid sequence, is expressed in many tumor cells and facilitates aerobic glycolysis by targeting and transcriptionally activating glycolysis-related genes (Warnecke et al., 2004; Kim et al., 2009; Chen et al., 2017), and promotes breast cancer cell epithelial-mesenchymal transition (EMT) and invasion (Yang et al., 2019). It has been reported that HIF-2α activates c-myc in a way that mimics a response to hypoxia and then triggers the expression of glutamine transporter ASCT2 and of glutaminase 1 (GLS1), resulting in an increase in glutamine uptake and catabolism in SiHa and HeLa cervical carcinoma cells (Perez-Escuredo et al., 2016). Although these regulators have been shown to be responsible for aerobic glycolysis, the precise mechanism how breast cancer cells switch this metabolic process has not been well delineated yet.

Signal-induced proliferation-associated 1 (SIPA1), a member of Rap1GAP family (Wada et al., 1997), is aberrantly expressed in breast cancer, colorectal cancer, melanoma and prostate cancer cells, participating in the regulation of tumor cell proliferation, adhesion, invasion and metastasis (Shimizu et al., 2011; Ji et al., 2012; Mathieu et al., 2012; Zhang et al., 2015). Recent studies confirmed that SIPA1 interacted with promoters of integrin subunit β1 (*ITGB1*) and cluster of differentiation 44 (*CD44*) and activated their transcription (Zhang et al., 2015; Wang et al., 2020). It is, however, not clear whether SIPA1 could regulate or alter the metabolism in breast cancer cells.

In the present study, we set out to clarify the effect of aberrant expression of SIPA1 on glucose metabolism in breast cancer cells and demonstrated that SIPA1 enhanced aerobic glycolytic flux and up-regulated the expression of glycolysis-related genes in breast cancer cells through transcriptionally activating HIF-2α. The SIPA1/HIF-2α axis shifted the ATP source from conventional oxidative phosphorylation to aerobic glycolysis, even in the presence of functional mitochondria, and promoted breast cancer invasion and metastasis both *in vitro* and *in vivo*. The findings strongly suggested that the SIPA1/HIF-2α axis is critical for aerobic glycolysis and pivotal for metastasis in breast cancers highly expressing SIPA1.

RESULTS

SIPA1 Modulates Aerobic Glycolysis in Breast Cancer Cells

To examine the status of aerobic glycolysis in metastatic breast cancer cells with ambient oxygen, we first determined the lactate production and glucose consumption in four different breast cancer cell lines. As shown in **Supplementary Figure S1A**, three triple-negative breast cancer (TNBC) cell lines, SUM159, MDA-MB-231 and BT549, all with high level of SIPA1 expression, consumed more glucose and produced more lactate than MCF7, a non-TNBC cell line with low SIPA1 expression (**Supplementary Figures S1A–S1C**), indicating that a high level of SIPA1 expression might be responsible for high aerobic glycolysis in breast cancer cells. To verify the correlation between SIPA1 and aerobic glycolysis, we established MDA-MB-231 and BT549 cell lines expressing a low level of SIPA1 and an MCF7 cell line overexpressing a high level of SIPA1 (MCF7/SIPA1) (**Figure 1A** and **Supplementary Figure S2A**), and we found knocking down SIPA1 decreased the levels of lactate production and glucose consumption, whereas forced expression of SIPA1 exhibited the opposite effects in these cells (**Figures 1B,C** and **Supplementary Figures S2B–C**). Furthermore, we examined the transcriptional levels of glycolysis-related genes of parental and SIPA1-knockdown MDA-MB-231 cells, as well as those of parental and SIPA1-overexpressing MCF7 cells by RNA sequencing. As shown in **Figure 1D**, knocking down SIPA1 down-regulated mRNA levels of nearly all glycolysis-related genes in MDA-MB-231 cells, whereas overexpressing SIPA1 up-regulated them in MCF7 cells. It was then confirmed by qRT-PCR assay that SIPA1 modulated the transcription levels of the glycolysis-related genes in MDA-MB-231, BT549 and MCF7 cells (**Figure 1E** and **Supplementary Figure S3**). The expression of key enzymes HK2 and LDHA was detected by Western blotting and we confirmed that knocking down SIPA1 significantly down-modulated the expression of HK2 and LDHA in MDA-MB-231 cells, whereas overexpressing SIPA1 up-regulated them in MCF7 cells (**Figure 1F**). Since LDHA is a critical enzyme for the conversion of pyruvate to lactate at the final step of aerobic glycolysis, we set out to determine whether LDH activity was modulated by SIPA1 in breast cancer cells. As shown in **Figures 1G,H**, knocking down SIPA1 in MDA-MB-231 cells significantly decreased both extracellular and intracellular LDH activities, whereas forced-expression of SIPA1 in 231si cells increased both LDH activities. In MCF7 cells, overexpressing SIPA1 also greatly increased both LDH activities (**Figures 1G,H**).

Additionally, it is worthy of note that HIF-1α and c-myc have been reported to serve as dominant regulators of glycolysis by targeting multiple glycolysis-related genes in a variety of cancers

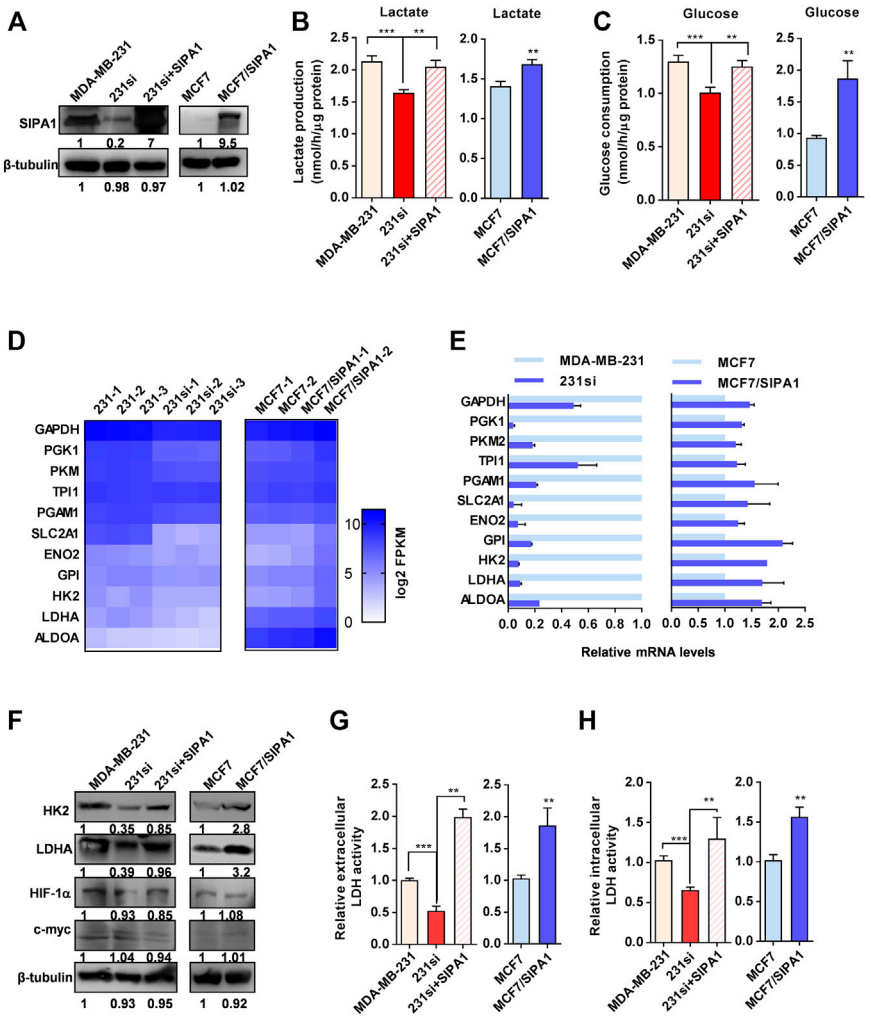


FIGURE 1 | SIPA1 enhances aerobic glycolysis in breast cancer cells under a normoxic condition. **(A)** SIPA1 protein expression levels in breast cancer cells were determined by Western blotting analysis. 231si (SIPA1-knocked down MDA-MB-231); 231si + SIPA1 (SIPA1-resumed 231si); MCF7/SIPA1 (SIPA1 overexpressed MCF7). β-tubulin was included as a loading control. **(B–C)** Effect of SIPA1 on the lactate production **(B)** and the glucose consumption **(C)** in breast cancer cell lines. **(D)** Heatmap of mRNA levels of major glycolysis-related genes in three independent parental and SIPA1-knockdown MDA-MB-231 cells, and two independent MCF7 and MCF/SIPA1 cells were presented with Log_2 FPKM by transcriptome sequencing and analysis. **(E)** mRNA levels of glycolysis-related genes were determined by qRT-PCR. Data were shown as mean ± s.d. The experiments were conducted in triplicate. Mitochondrial succinate dehydrogenase cytochrome b560 subunit (SDHC) was included as an endogenous control. **(F)** Expression of HK2, LDHA, HIF-1α and c-myc were determined by Western blotting. β-tubulin was included as a control. **(G–H)** the extracellular lactate dehydrogenase (LDH) activity **(G)** and intracellular LDH activity **(H)** were determined. Data are shown as mean ± s.d triplicate measuements (n = 3). $^{**}p < 0.01$, $^{***}p < 0.001$. (Student's *t*-test).

(Gatenby and Gillies, 2004). The expression levels of HIF-1α and c-myc were, however, not affected by SIPA1 both in MDA-MB-231 and MCF7 cells (**Figure 1C**). Taken together, SIPA1 might be a modulator of aerobic glycolysis under normoxia in breast cancer cells.

SIPA1 Alters ATP Production Source in Breast Cancer Cells

When breast cancer cells were incubated with glucose as an exclusive carbon source, as shown in **Figure 2A** (left panel), the cellular ATP level was increased by knocking down SIPA1 in MDA-MB-231 and restored by forced expression of SIPA1 in 231si cells. A decrease in the level of ATP was also observed in MCF7 cells overexpressing SIPA1 (**Figure 2B**, left).

Since overexpressing SIPA1 in breast cancer cell lines increased glucose consumption and lactate production (**Figures 1D,E**), but decreased ATP production (**Figures 2A,B**), it is likely that there might exist a SIPA1-induced energy production switch from respiration to fermentation in breast cancer cells. To address this hypothesis, we treated cells with the mitochondrial ATPase inhibitor oligomycin, and found that 100 nM oligomycin treatment decreased ATP levels in breast cancer cells (**Figures 2A,B**, left panel). Notably, the ATP level in 231si cells was significantly decreased to one-sixth of its original value after oligomycin treatment, suggesting that a significant amount of ATP (about 80%) was produced by

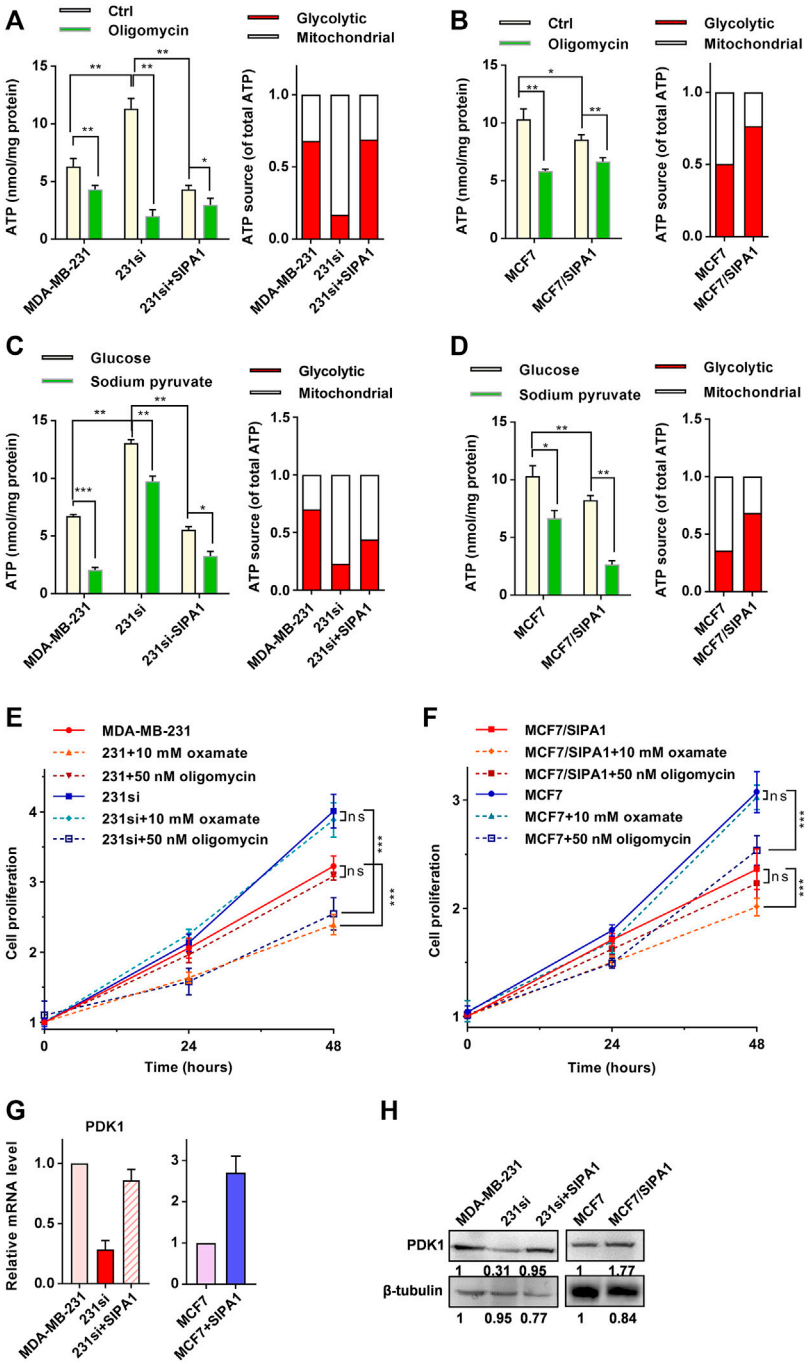


FIGURE 2 | SIPA1 alters ATP production source from respiration to aerobic glycolysis. **(A–B)** ATP levels in MDA-MB-231 **(A)** and MCF7 **(B)** with various SIPA1 expression levels after treatment with oligomycin or not. A mitochondria ATP level was calculated by the following formula ($ATP_{(m)} = ATP_{(T)} - ATP_{(g)}$), in which total ATP level ($ATP_{(T)}$) was measured after incubating cells with 15 mM glucose and the glycolytic ATP ($ATP_{(g)}$) were measured after incubating cells with 15 mM glucose and 100 nM oligomycin for 5 h. Yellow bars: control; green bars: oligomycin (left panel). Based on the left panel, the contribution of each ATP source on cellular ATP production was estimated. Red: aerobic glycolysis; white: mitochondrial respiration (right panel). **(C–D)** Effect of sodium pyruvate as a sole carbon source on ATP production in MDA-MB-231 **(C)** and MCF7 cells **(D)** with various SIPA1 expression levels. Cells were grown in the medium containing glucose or sodium pyruvate as a sole carbon source, and the cellular ATP level was measured. Yellow bars, glucose; green bars, sodium pyruvate (left panel). Based on the left panel, the contribution of each ATP source on cellular ATP production was estimated. Red: aerobic glycolysis; white: mitochondrial respiration (right panel). **(E–F)** Effect of oxamate and oligomycin on the proliferation of MDA-MB-231 **(E)** and MCF7 cells **(F)**. **(G)** mRNA levels of PDK1 were determined by qRT-PCR. **(H)** Protein levels of PDK1 were determined by Western blotting. Data were shown as mean ± s.d of triplicate measurements (n = 3). $^{*}p < 0.05$, $^{**}p < 0.01$, $^{***}p < 0.001$, ns, no significance. (Student's *t*-test).

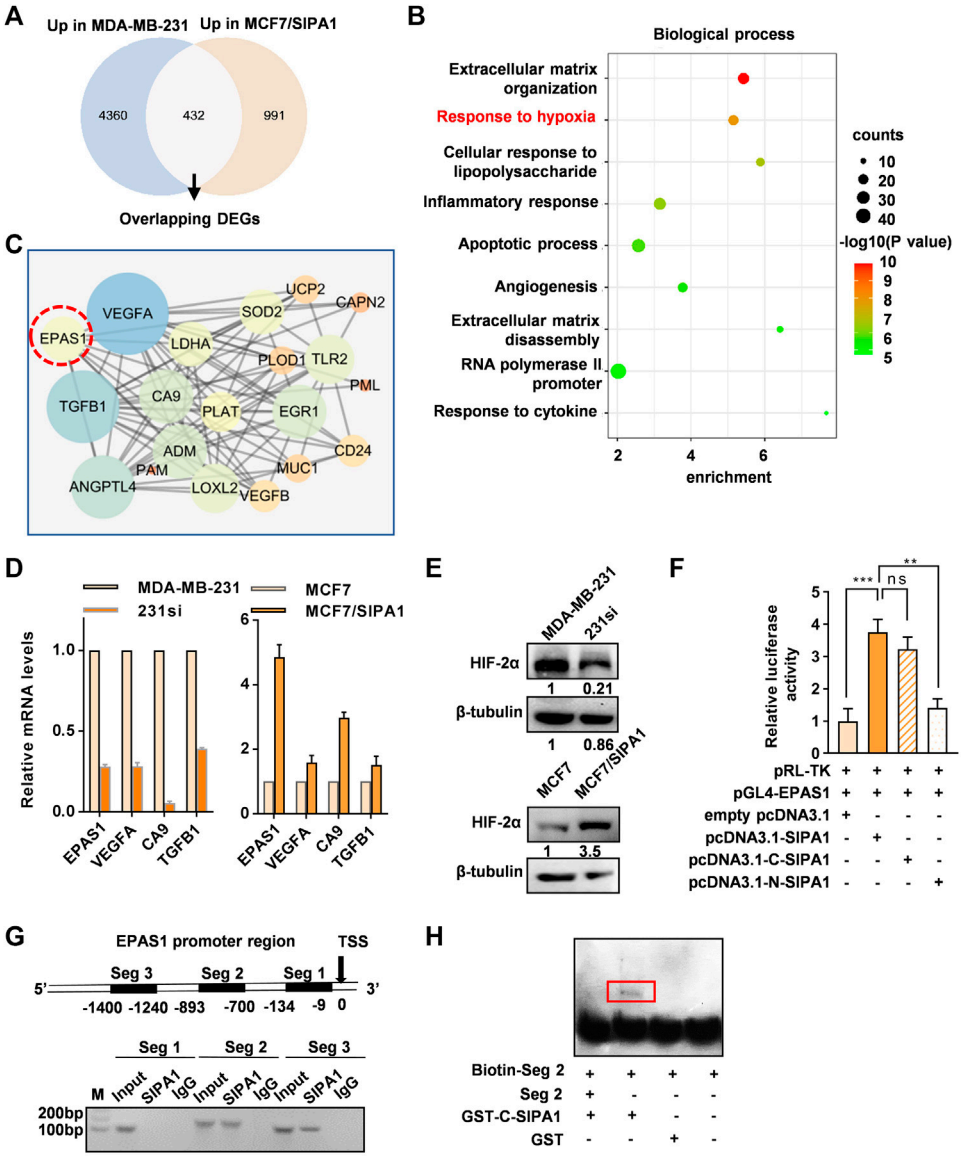


FIGURE 3 | SIPA1 upregulates EPAS1 transcription by binding to its promoter region. **(A)** Transcriptome sequencing datasets of two pairs of cells (MDA-MB-231 vs 231si, MCF7 vs MCF7/SIPA1) were analyzed and 432 overlapping candidate genes which were positively regulated by SIPA1 were selected in the Venn diagram. **(B)** GO biological process enrichment analyses of the 432 genes positively correlated with SIPA1. Top nine GO terms were listed with *p* values, counts and enrichment scores. **(C)** Genes allocated to "responses to hypoxia" in **(B)** were plotted as a protein-protein interaction network. **(D)** qRT-PCR analyses of EPAS1 and its downstream gene candidates, *TGFB1*, *VEGFA* and *CA9*. Data were shown as mean ± s.d. The experiments were conducted in triplicate. SDHC was included as an endogenous control. **(E)** Western blotting analyses of HIF-2α expression in breast cancer cells with various SIPA1 levels. β-tubulin was included as an internal control. **(F)** The effect of SIPA1 on *EPAS1* promoter activity were accessed by a luciferase reporter assay. **(G)** Interaction of SIPA1 with *EPAS1* gene promoter revealed by ChIP-PCR. Seg 1, Seg 2 and Seg 3 represented the indicated promoter regions. TSS, transcription start site. **(H)** Interactions of truncated SIPA1 protein (540-1042aa) with *EPAS1* gene promoter segment 2 were revealed by EMSA. Data shown are mean ± s.d. of triplicate measurements (n = 3).

respiratory pathway in 231si cells, whereas as much as 70% ATP were produced *via* aerobic glycolysis in MDA-MB-231 cells or 231si cells with forced-expression of SIPA1 (**Figure 2A**, right panel). Similarly, about 50% ATP were derived from respiratory processes in parental MCF7 cells, whereas about 20% ATP were attributed to mitochondrial respiration in MCF7/SIPA1 cells (**Figure 2B**, right panel). These results strongly suggested that SIPA1 switched energy sources from respiration to fermentation.

We further examined the effect of SIPA1 on the mitochondrial ATP production. When cells were cultured with sodium pyruvate as a sole carbon source, the level of ATP production was significantly higher in SIPA1 low-expression cells than in SIPA1 high-expression

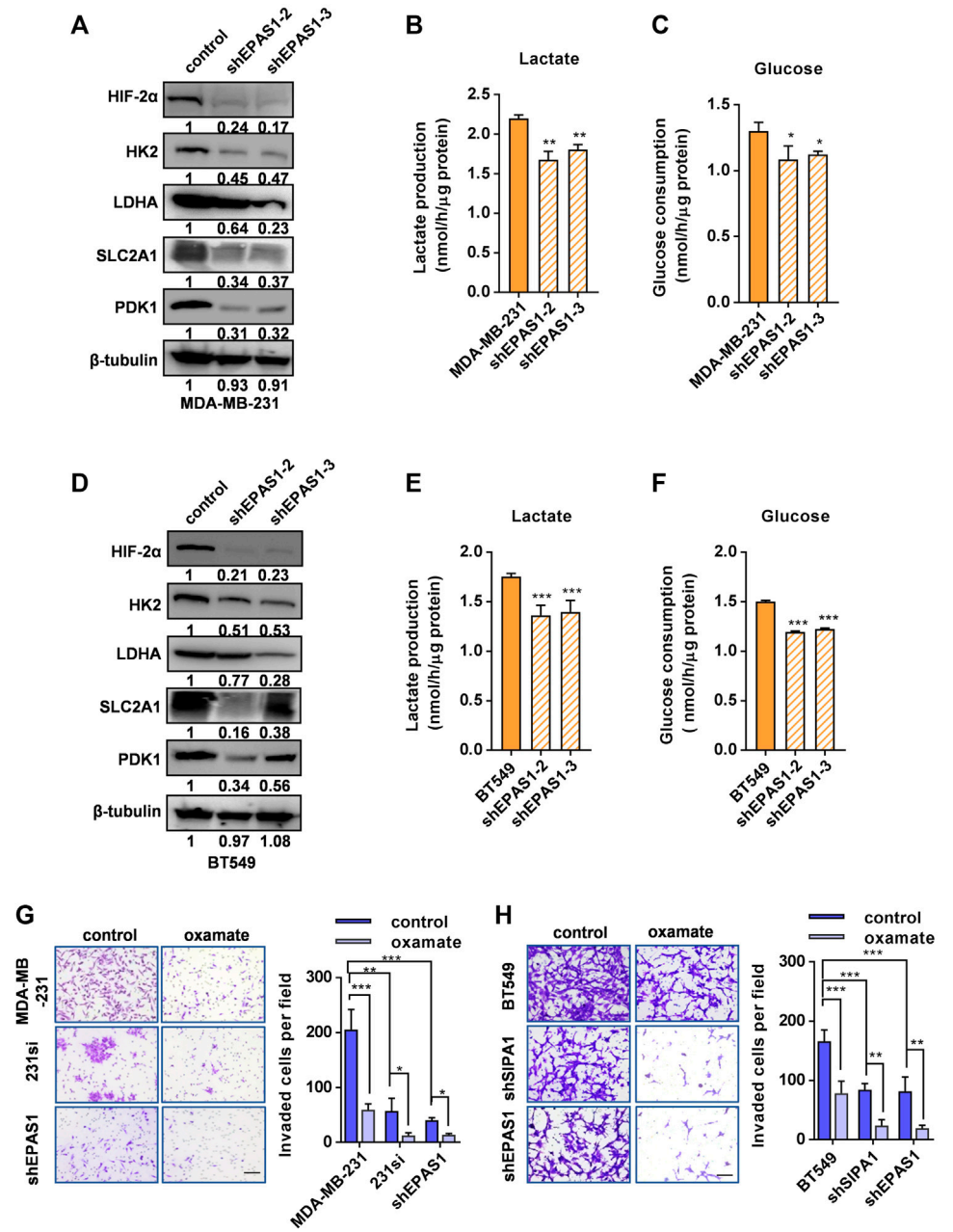


FIGURE 4 | Knocking down HIF-2α suppresses aerobic glycolysis and invasion of breast cancer cells. **(A)** HIF-2α and glycolytic-related proteins in parental and HIF-2α-knockdown MDA-MB-231 cells were determined by Western blotting analysis. β-tubulin was included as an internal control. Production of lactate **(B)** and glucose consumption **(C)** in parental and HIF-2α knockdown MDB-MB-231 cells. **(D)** HIF-2α and glycolysis-related protein levels were determined by Western blotting in parental and HIF-2α knockdown BT549 cells. β-tubulin was included as an internal control. Production of lactate **(E)** and glucose consumption **(F)** in parental and HIF-2α knockdown BT549 cells. **(G–H)** Invasion of MDA-MB-231 **(G)** and BT549 **(H)** and their derivatives treated with or without 20 mM oxamate was analyzed by a transwell assay sistern. Data are shown as mean ± s.d of triplicate measurements (n = 3). $^{*}p < 0.05$, $^{**}p < 0.01$, $^{***}p < 0.001$. (Student's *t*-test).

cells (**Figures 2C,D**, green bars). It is, therefore, likely that a high level of SIPA1 expression down-modulated the intracellular ATP generation by switching the ATP source to aerobic glycolysis (**Figures 2C,D**, right panel). These results suggest that SIPA1 suppressed oxidative phosphorylation in mitochondria of breast cancer cells.

To address whether the alteration of ATP source by SIPA1 affects the sensitivity of cells to glycolytic and mitochondrial inhibitors, we treated the SIPA1-overexpressing or -knockdown breast cancer cells with 10 mM oxamate (an LDH inhibitor) or 50 nM oligomycin. As shown in **Figure 2E**, suppression of SIPA1 significantly increased the proliferation of MDA-MB-231. When MDA-MB-231 cells were

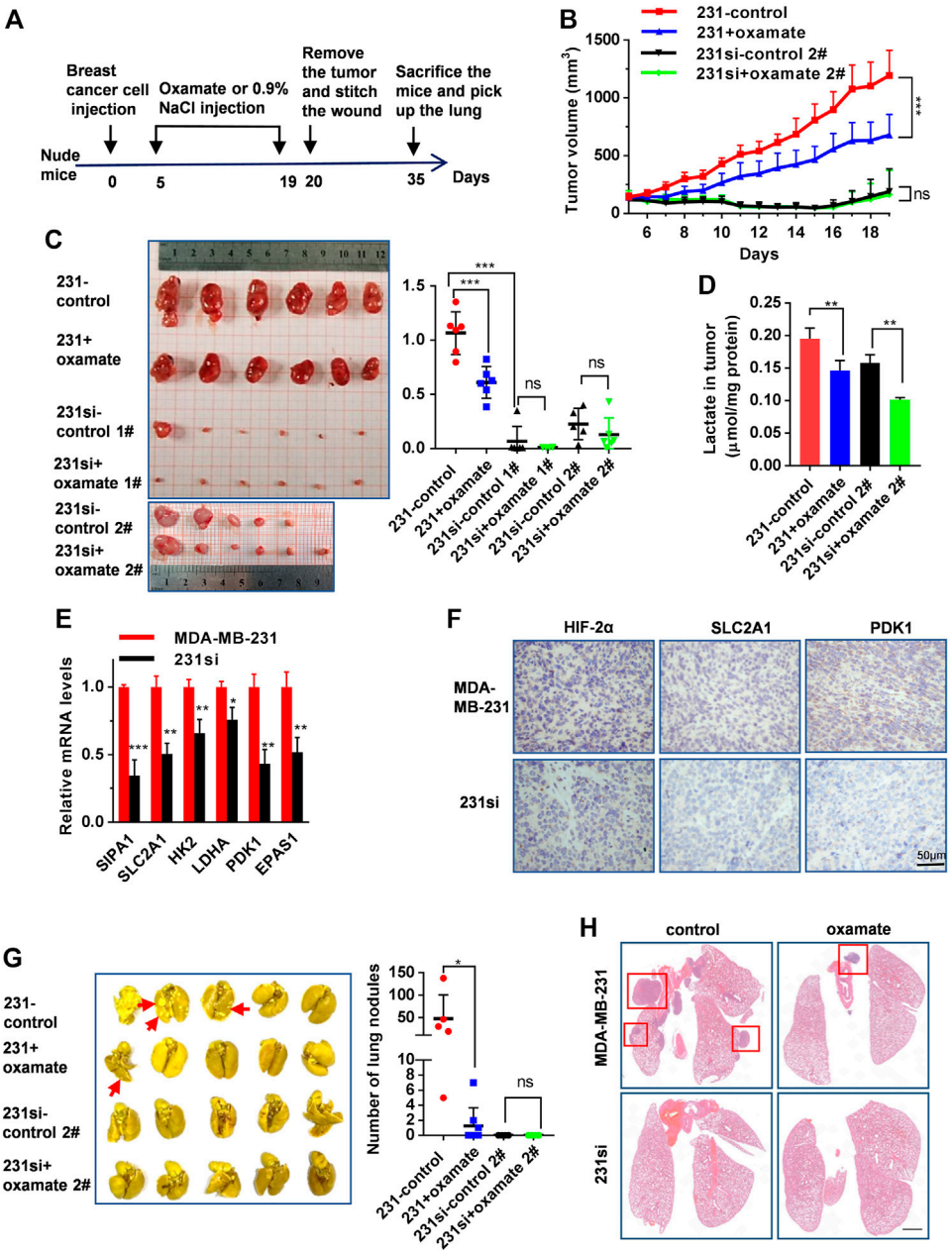


FIGURE 5 | SIPA1/HIF-2α axis blockade suppresses aerobic glycolysis and breast cancer growth and metastasis in a xenograft mouse model. **(A)** The schematic overview of the xenograft experimental workflow. Oxamate treatment on 231si cell xenografted tumor formation experiment was done twice (1# and 2#). **(B)** Tumor volumes in the four groups of mice were measured from day 5 to day 19. **(C)** The tumors in each group were photographed and weighed. **(D)** Lactate levels in tumor tissues were determined in each group, n = 3. **(E)** mRNA levels of glycolytic rate-limiting genes in tumor tissues of mice (n = 3 in each group) were determined by qRT-PCR. Data are shown as mean ± *s*.d. The experiments were done in triplicate. **(F)** Immunohistochemical analyses of HIF-2α, SLC2A1 and PDK1 in tumor tissues derived from two groups of mice were performed. **(G)** Lungs from four groups of mice were photographed (left panel) and the number of nodules observed on the lung surface were counted (right panel). **(H)** Representative histopathological images of HE staining in the lungs were presented. Scale bar: 1 mm. Data are mean ± s.d. of triplicate measurements. $^{*}p < 0.05$, $^{**}p < 0.01$, $^{***}p < 0.001$. (Student's *t*-test).

treated with oxamate, the proliferation was significantly decreased, whereas the proliferation of MDA-MB-231 was not affected by the addition of oligomycin. Conversely, treatment of 231si cells with oligomycin greatly suppressed the cell proliferation, while oxamate had no effect on the proliferation of 231si cells. Additionally, overexpressing SIPA1 in MCF7 cells significantly reduced the cell proliferation. Interestingly, oligomycin treatment greatly decreased the proliferation of parental MCF7 cells, while no effect was observed

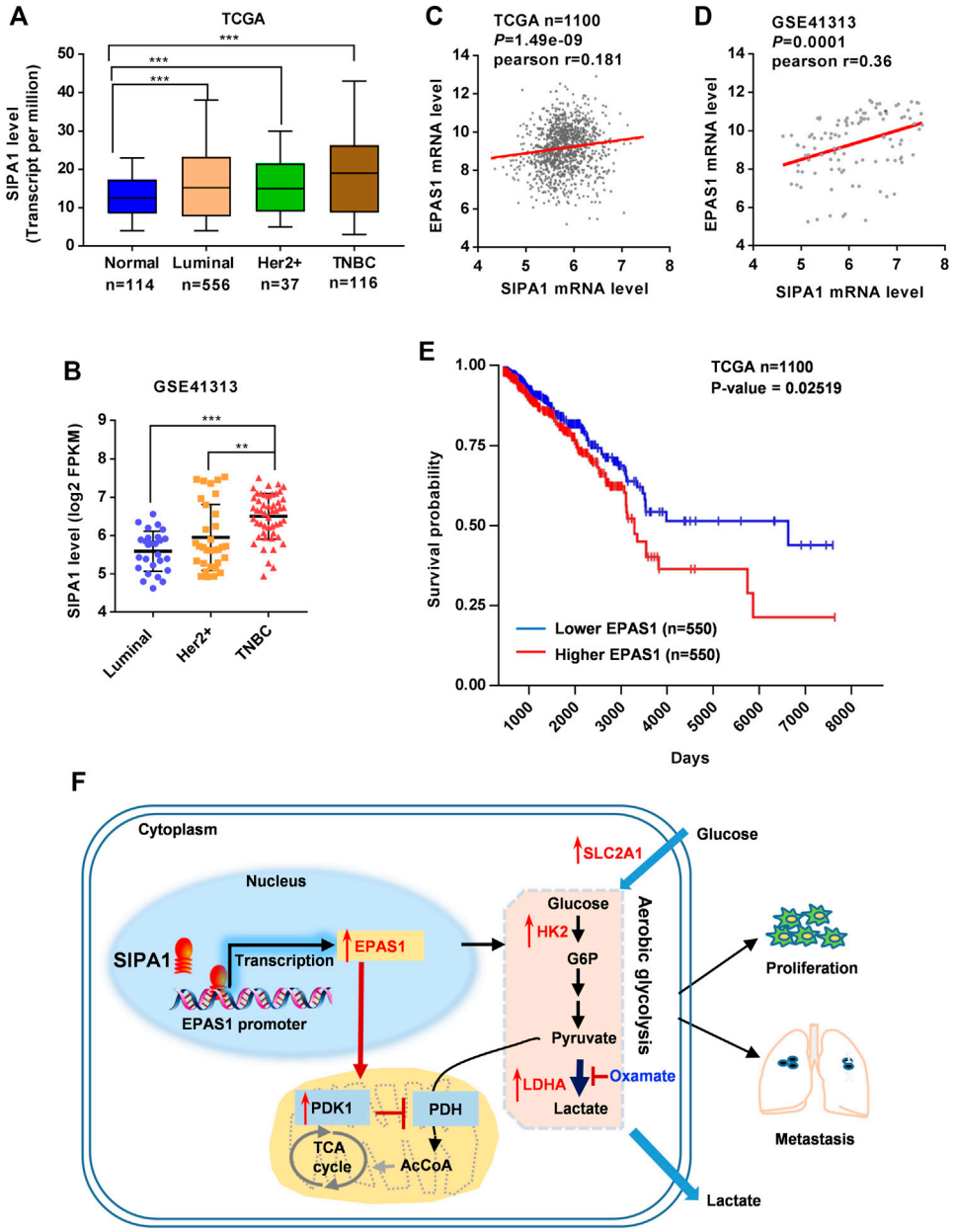


FIGURE 6 | SIPA1/EPAS1 axis is a poor prognosis predictor of breast cancer. **(A–B)** mRNA level of SIPA1 in breast cancer subtypes in TCGA **(A)** and GSE41313 dataset **(B)**. **(C–D)** The relationship between SIPA1 and EPAS1 was analyzed based on TCGA **(C)** and GSE41313 datasets **(D)**. Pearson correlation coefficients (Pr) for SIPA1 and EPAS1 gene expression levels were shown. **(E)** Kaplan-Meier survival analysis for survival probability of breast cancer patient in TCGA according to EPAS1 expression status. The *p* value was presented using the log-rank test. **(F)** A proposed diagram for SIPA1-mediated aerobic glycolysis and breast cancer cell metastasis.

for oxamate treatment. On the contrary, oxamate significantly suppressed the proliferation of MCF7/SIPA1 cells, but oligomycin failed to exhibit the suppressive activity (**Figure 2F**).

Pyruvate dehydrogenase kinase 1 (PDK1) is a key switch of tricarboxylic acid (TCA) cycle in mitochondria and inhibits mitochondrial oxidation of glucose by blocking the catalytic activity of pyruvate dehydrogenase (PDH) that converts pyruvate to acetyl-CoA (Dupuy et al., 2015). Interestingly, knocking down SIPA1 down-regulated PDK1 at both mRNA and protein expression levels in MDA-MB-231 and BT549 cells, whereas overexpression of SIPA1 up-regulated PDK1 expression in 231si and MCF7 cells (**Figures 2G,H** and **Supplementary Figure S2**). It is thus likely that a high level of SIPA1 expression alters the glucose metabolism from respiration to aerobic glycolysis by promoting the expression of glycolysis-related gene products and inhibiting the mitochondrial TCA cycle *via* up-regulating PDK1.

SIPA1 Promotes *EPAS1* Transcription by Binding to its Promoter

In order to elucidate the pathway by which SIPA1 modulates the expression of glycolysis-related genes and *PDK1*, we analyzed RNA-seq data from two pairs of breast cancer cell lines: parental and SIPA1-knowndown MDA-MB-231 cells and parental and SIPA1-overexpressing MCF7 cells. Differentially-expressed genes (DEGs) analysis revealed that 4,972 genes were down-regulated and 5,726 genes were up-regulated by knocking-down SIPA1 in MDA-MB-231 cells. In case of overexpressing SIPA1 in MCF7 cells, 1,423 genes were up-regulated and 1,352 genes were down-regulated. The DEGs which were positively correlated with SIPA1 expression in both cell lines were selected, from which 432 bilateral candidate genes were extracted (**Figure 3A**). Then 432 genes were subjected to GO enrichment analysis, and two annotations named "extracellular matrix organization" and "response to hypoxia" with significant enrichment score and statistically significant *p*-values were noted among the top 9 annotations (**Figure 3B**). We plotted the protein-protein interaction (PPI) network of the DEGs nominated in the annotation of "response to hypoxia" involved in cellular hypoxic responses as well as aerobic glycolysis processes. *EPAS1* that encodes HIF-2α was identified as a hub gene to link its downstream genes including *TGFB1*, *VEGFA* and *CA9* in sight of the PPI network (**Figure 3C**). The mRNA levels of *EPAS1* as well as *TGFB1*, *VEGFA* and *CA9*, were confirmed to be positively correlated with those of SIPA1 in these two pairs of breast cancer cells (**Figure 3D**) and BT549, another TNBC cell line (**Supplementary Figure S3**). Meanwhile, knocking-down SIPA1 decreased HIF-2α expression in MDA-MB-231 cells, and overexpressing SIPA1 in MCF7 cells increased HIF-2α expression at a protein level (**Figure 3E**).

It was previously demonstrated that SIPA1 up-regulated the promoter activity of certain target genes in breast cancer cells (Zhang et al., 2015; Wang et al., 2020). In this study, we also demonstrated that SIPA1 could be located in the nuclei of MCF7/SIPA1 and three TNBC cells (**Supplementary Figure S4**). Dual luciferase reporter assay further revealed that overexpression of SIPA1 and its C-terminal region (540-1042aa), but not the N-terminal region (1-539aa), increased the transcriptional activity of the *EPAS1* promoter transcriptional activity by three-fold, compared to controls (**Figure 3F**). We then conducted a chromatin immunoprecipitation (ChIP) assay to examine the direct interaction between SIPA1 and the *EPAS1* promoter. Three pairs of specific primers corresponding to three segments of the *EPAS1* promoter, Seg 1, Seg 2, and Seg 3 were employed (**Figure 3G**, upper panel). As shown in the lower panel of **Figure 3G**, Seg 2 (−1,400 to −1,240 bp) and Seg 3 (−893 to −700 bp) were specifically amplified from the cell lysates immunopecipitatated with anti-SIPA1 antibody. Moreover, the direct interaction between SIPA1 protein and the *EPAS1* promoter segments was observed by EMSA, in which GST-tagged C-terminal SIPA1 specifically pulled down the biotin-labeled Seg 2, (**Figure 3H**). It is thus likely that SIPA1 directly interacted with the *EPAS1* promoter, enhanced its promoter activity and promoted HIF-2α expression in breast cancer cells.

Knocking Down HIF-2α Suppresses Aerobic Glycolysis and invasion of Breast Cancer Cells

We next established stable HIF-2α knockdown MDA-MB-231 cell lines (**Figure 4A**) to address the hypothesis that the increased dependence of SIPA1-overexpressing breast cancer cells on aerobic glycolysis was mediated by HIF-2α. It was demonstrated that knocking-down HIF-2α in MDA-MB-231 breast cancer cells significantly decreased the expression of glycolysis-related gene products, such as HK2, LDHA, SLC2A1 and PDK1 (**Figure 4A**), consisting with the suppression of mRNA levels of glycolysis- and hypoxia-related genes (**Supplementary Figure S5**). In addition, lactate production and glucose consumption were also decreased in MDA-MB-231 cells by knocking down of HIF-2α (**Figures 4B,C**). Essentially, the same results were observed in BT549 breast cancer cells (**Figures 4D–F**).

We then compared the invasiveness of the breast cancer cells with SIPA1 or HIF-2α knockdown with that of parental cells by using a transwell assay. As shown in **Figure 4G**, knocking down either SIPA1 or HIF-2α significantly inhibited the invasion of MDA-MB-231 cells *in vitro* and the tumor cell translocation was further inhibited by the treatment with 20 mM oxamate. BT549 breast cancer cells behaved similarly after gene manipulation and drug treatment (**Figure 4H**). These results suggest that SIPA1 could enhance the aerobic glycolysis by up-regulating the expression of HIF-2α to promote the invasion of breast cancer cells *in vitro*.

Blockade of SIPA1/HIF-2α-Mediated Aerobic Glycolysis Suppresses Breast Cancer Growth and Metastasis in Xenografted Mice

We then examined the role of SIPA1/HIF-2α-mediated aerobic glycolysis in breast tumor growth and metastasis *in vivo*. We set up four groups of mice xenografted with (1) MDA-MB-231 breast cancer cells followed by 0.9% NaCl treatment (n = 6), (2) MDA-MB-231 followed by oxamate treatment (n = 6), (3) 231si cells followed by 0.9% NaCl treatment (1#: n = 6, 2#: n = 6), and (4) 231si cells followed by oxamate treatment (1#: n = 6, 2#: n = 6) under the xenograft experimental workflow (**Figure 5A**). No significant difference was observed on the body weight of mice in all the four groups during the treatments (**Supplementary Figure S6**). For two groups of mice inoculated with MDA-MB-231 cells, oxamate treatment significantly suppressed the tumor volumes and weights, compared to the group without oxamate treatment. As for the mice inoculated with 231si cells, the tumor growth rate was significantly lower than that of mice xenografted with parental MDA-MB-231 cells (**Figures 5B,C**).

Furthermore, the level of lactate in MDA-MB-231 xenograft tumors was much higher than that in 231si xenograft tumors. On the other hand, oxamate treatment decreased the level of lactate both in MDA-MB-231 and 231si xenograft tumors (**Figure 5D**). Also, SIPA1 knockdown decreased the expressions of EPAS1, glycolysis-related products and PDK1 in tumor tissues at mRNA and protein levels (**Figures 5E,F**).

Regarding lung metastasis, the number of nodules on the surface of the lungs in 231si xenografted mice was significantly fewer than that in MDA-MB-231 xenografted mice. In addition, the oxamate treatment further reduced the number of lung nodules in MDA-MB-231 xenografted mice (**Figure 5G**). The histopathological images of HE staining revealed that the numbers of tumors and the area of each nodule were decreased in the lungs in mice received 231si cells, compared to those inoculated with MDA-MB-231 cells. In addition, the oxamate treatment reduced the number of tumor nodules (**Figure 5H**). These results indicate that knocking down SIPA1 decreased breast tumor metastasis, which might be associated with the suppression of glycolysis.

HIF-2α expression Positively Correlates With SIPA1 Expression and Poor Clinical Outcomes

To determine the clinical relevance of the above findings in breast cancers, we analyzed the TCGA database and found that SIPA1 was up-regulated in some breast cancer subtypes including luminal, Her2+ and TNBC (**Figure 6A**). In addition, we found that SIPA1 was aberrantly expressed in TNBC cells when compared to the other subtypes in GSE41313 dataset (**Figure 6B**). We also found a positive correlation between mRNA levels of *SIPA1* and *EPAS1* genes in both datasets (**Figures 6C,D**). A survival analysis by the log-rank test indicated that patients with *EPAS1*-high tumors had significantly lower rates of survival probability than patients with *EPAS1*-low tumors in TCGA (**Figure 6E**). These data suggest that SIPA1 induced the expression of HIF-2α and the expression of HIF-2α in tumor cells might result in poor prognosis in breast cancer patients.

Taken together, SIPA1/HIF-2α axis could be a key regulator of aerobic glycolysis, contributing to the switch from oxidative phosphorylation to aerobic glycolysis in breast cancer cells under an ambient oxygen condition, leading to tumor invasion and metastasis (**Figure 6F**).

DISCUSSION

Accumulating evidence indicates that SIPA1 is highly expressed in various solid tumors and that its expression is correlated with metastasis and poor prognosis in many types of cancers (Liu et al., 2020). In the present study, we demonstrated that SIPA1 was aberrantly expressed in some breast cancer cells, especially in TNBC cells, and promoted aerobic glycolysis, leading to tumor invasion and metastasis *in vivo*.

It has been reported that HIF-1α and c-myc are two master regulators of aerobic glycolysis by targeting multiple glycolysis-related genes. Under normoxic conditions, however, SIPA1 enhanced aerobic glycolysis without affecting the expression of HIF-1α and c-myc in breast cancer cells, suggesting additional mechanisms rather than HIF-1α/c-myc pathway are involved.

SIPA1 knockdown led to down-regulation of nearly all glycolysis-related genes and increased dependence on respiration, instead of glycolysis, in the generation of ATP, suggesting that the network for glycolytic flux in breast cancer cells could be modulated by SIPA1. It is noted that SIPA1 decreased a total cellular ATP content in spite of marked enhancement of aerobic glycolysis. In fact, SIPA1 shifted ATP production from mitochondrial respiration to fermentation *via* aerobic glycolysis. It has been reported that an increase in glycolysis, especially aerobic glycolysis, and a decrease in mitochondrial functions are characteristic of breast cancer cells with a metastatic phenotype (Lu et al., 2010). On the contrary, other reports indicated that an increase in mitochondrial activity was also important for the metastatic phenotype (LeBleu et al., 2014; Dupuy et al., 2015; Andrzejewski et al., 2017). In the present study, we showed that metabolic transformation to decreased glycolysis and increased mitochondrial oxidative phosphorylation induced by SIPA1 knockdown led to poor metastatic properties of breast cancer cells. It suggests that breast cancer cells exhibit metabolic plasticity that balances energy production sources between glycolysis and mitochondrial oxidative phosphorylation and modulates proliferation and metastatic properties.

In the present study, we comprehensively searched for candidate genes that might link between SIPA1 and glycolysis-related factors by employing transcriptome analyses. We then demonstrated that HIF-2α (encoded by *EPAS1*) was directly regulated by SIPA1 in breast cancer cells. It was previously shown that HIF-2α protein was gradually accumulated in tumor cells and contributed to the prolonged activation of hypoxia-related genes, in which HIF-2α regulated a glycolytic flux by targeting several glycolysis-related genes such as SLC2A1 and LDHA. In addition, HIF-2α was shown to regulate angiogenesis-related signaling pathways by targeting genes including vascular endothelial growth factor A (VEGFA) to promote an aggressive phenotype of tumor cells (Holmquist-Mengelbier et al., 2006; Chen et al., 2017).

Herein, we found that SIPA1 could enhance HIF-2α expression and that HIF-2α knockdown decreased the aerobic glycolytic flux and expression of glycolysis-related genes such as HK2, SLC2A1, and LDHA under normoxia, suggesting that HIF-2α is a potent mediator controlling the hypoxic phenotype including aerobic glycolysis. Under normoxia, HIF-1α protein could be hydroxylated on the proline residues due to the action of prolyl hydroxylase 2 and be rapidly digested by 26S proteasomes. (Semenza, 2003). HIF-2α protein is, however, more stable and active than HIF-1α under resembling end capillary oxygen conditions (Holmquist-Mengelbier et al., 2006). Whereas it is challenging to address the long-standing mystery why cancer cells adapt the less efficient glycolysis for energy sources even with ambient oxygen supply, it would be important to shed light on the SIPA1/HIF-2α axis that regulates aerobic glycolysis under normoxia for better understanding of cancer metastasis.

Interestingly, 231si cells with reduced expression of SIPA1 grew faster than the parental MDA-MB-231 cells at 48 h under a normoxic condition *in vitro*. In contrast, the xenografted tumor in the mice inoculated with MDA-MB-231 cells was much larger than that in mice injected with 231si cells, indicating that MDA-MB-231 cells grew faster than 231si cells *in vivo*. In our study, MDA-MB-231 cells were characterized by a glycolytic phenotype

evidenced by higher glucose consumption, higher lactate production, higher expression of glycolytic genes, main source of glycolytic ATP, and lower mitochondrial activity due to high expression of PDK1 (a mitochondrial inhibitor, which inhibits conversion of pyruvate into acetyl-CoA). Given that 231si cells were equipped with functionally active mitochondria to generate much more ATP than MDA-MB-231 cells, evidenced by their lower expression of glycolytic genes and PDK1, the mitochondria provide advantages for 231si cells in proliferation under normoxia *in vitro*. Tumor cells generally undergo hypoxia condition *in vivo* due to limited supply and increased demand of oxygen during rapid expansion (Hanahan and Weinberg, 2011). This context preferentially supports MDA-MB-231 cells favoring glycolytic metabolism.

In the present study, we demonstrated that SIPA1 could up-regulate the expression of PDK1 through HIF-2α. PDK1 was originally characterized as a suppressor of TCA cycle by inhibiting PDH activity to decrease the conversion of pyruvate to acetyl-CoA in mitochondria. Breast cancer cells highly expressing SIPA1 greatly depend on glycolysis in the production of ATP, and thus have advantages in cell proliferation under hypoxia like in solid tumor tissues. In fact, SIPA1 knockdown breast cancer cells exhibited impaired growth in xenografted mice, whereas rapid proliferation was observed *in vitro* under normoxia.

Animal models further showed that the SIPA1/HIF-2α axis could play an important role in aerobic glycolysis and metastasis of breast cancer cells *in vivo*. SIPA1 knockdown as well as LDH inhibitor oxamate administration markedly inhibited breast cancer cell metastasis from primary xenografted sites to the lungs, suggesting that the blockade of glycolysis mediated by SIPA1/HIF-2α axis is an efficacious strategy for the treatment of aggressive breast cancer that expresses SIPA1. Taken together, the present study revealed a novel regulatory mechanism how breast cancer cells, especially TNBC cells highly expressing SIPA1, facilitated cancer progression *via* a metabolic shift from respiration to aerobic glycolysis.

MATERIALS AND METHODS

Plasmids and Cells

Plasmids of pcDNA3-SIPA1, pcDNA3-N-SIPA1 encoding N-terminal half part of SIPA1 (1-539aa) and pcDNA3-C-SIPA1 encoding C-terminal half part of SIPA1 (540-1042aa) were constructed as previously described (Ma et al., 2021). SIPA1 and EPAS1 shRNA nucleotides (**Supplementary Table S1**) were cloned into pLKO.1-GFP (RRID: Addgene_30323) to construct pLKO.1-GFP-SIPA1 and pLKO.1-GFP-EPAS1, respectively. Lentivirus packaging plasmids, psPAX2 (RRID: Addgene_12260) and pMD2. G (RRID: Addgene_12259), and a reporter plasmid pRL-TK (RRID: Addgene_11313) were purchased from Merck & Co. (Kenilworth, NJ). EPAS1 promoter region (-1618bp to transcription starting site) was cloned into pGL4 (RRID: Addgene_48744) to give pGL4-EPAS1. pGEX-C-SIPA1 was constructed to express GST-tagged C-terminal half part SIPA1 protein.

Human cell lines MDA-MB-231, MCF7, and HEK293T were purchased and authorized from China Center for Type Culture Collection (CCTCC, Wuhan, China). BT549 was purchased from Procell (Wuhan, China) with short tandem repeat authentication. SUM159 were gifted from Dr. Peijing Zhang (Yao et al., 2018). Cells were cultured according to the previous study (Ma et al., 2021). The stable knockdown cells were established following the previous study (Zhang et al., 2015).

Measurement of Glucose Consumption, Lactate Production, Intracellular and Extracellular Lactate Dehydrogenase Activity

To detect glucose consumption and lactate production, 5×10^4 cells were placed into wells and incubated in modified RPMI1640 medium with 15 mM glucose in the absence of glutamine and pyruvate for 5 h. After being washed with PBS, the culture medium and cells were harvested separately. Concentrations of glucose and lactate in the culture medium were measured using a glucose assay kit and a lactate assay kit (Nanjing Jiancheng Bioengineering Institute, Nanjing, China) according to the manufacturer's instructions, respectively. To measure lactate in tumor tissues, 30 mg tumor specimens were pulverized in liquid nitrogen and lysed in 300 μl NP40 lysis buffer. After centrifugation for 5 min at 13,000 rpm at 4oC, the supernatant was harvested and examined for lactate and protein concentrations.

For the determination of the intracellular lactate dehydrogenase (LDH) activity, 1×10^5 cells were seeded into the wells and incubated in media for 24 h. After being washed with PBS, cells were harvested and examined for LDH activity with an LDH assay kit (Nanjing Jiancheng Bioengineering Institute) according to the manufacturer's instructions. For extracellular LDH activity assay, 2×10^5 cells were seeded into the wells and incubated with medium for 5 h, and then supernatants were collected and examined for LDH activity by using an LDH assay kit.

Measurement of ATP Level

ATP levels in breast cancer cells were measured using an ATP assay kit (Beyotime, Nanjing, China) according to the manufacturer's instructions. The amount of total ATP was calculated based on luminescence measured on a FlexStation 3 luminescence reader (Molecular Devices, San Jose, CA). To measure the levels of glycolytic ATP production, 5×10^4 cells were seeded into wells and incubated in media containing 100 nM oligomycin (Thermo Fisher Scientific) for 5 h. After being washed with PBS, the cells were lysed and examined for ATP levels using an ATP assay kit according to the manufacturer's protocol. To measure the ATP production in mitochondria, 5×10^4 cells were seeded into wells and incubated in media containing 10 mM pyruvate in the absence of glucose and glutamine for 5 h. After being washed with PBS, the cells were lysed and examined for ATP levels and protein concentrations.

qRT-PCR and ChIP-PCR

Quantitative real-time polymerase chain reaction (qRT-PCR) and chromatin immunoprecipitation PCR (ChIP-PCR) were conducted as previously described (Zhang et al., 2015).

The specific primers are listed in **Supplementary Tables S2 and S3**.

Transcriptome Sequencing and Analysis

Total RNA was isolated using TRIzol reagent (Thermo Fisher Scientific). Transcriptome sequencing was conducted by Novogene Co. Ltd. (Beijing, China). Gene expression levels for each transcript were estimated as the number of reads per kilobase of exon model per million mapped reads (RPKM) using only uniquely mapped reads in exonic regions. A gene was considered differentially expressed if its expression differed between any two samples with the fold change >2 and the p value <0.05. DAVID (RRID: SCR_001881) online tool (https://david.abcc.ncifcrf.gov) was used for Gene Ontology (GO) enrichment analysis and KEGG (RRID: SCR_012773) pathway enrichment analysis. STRING (RRID: SCR_005223) online tool (https://string-db.org) was used to assess the protein-protein interaction of cluster genes.

Luciferase Reporter Assay

EPAS1 promoter region was amplified by PCR from MDA-MB-231 genomic DNA, and cloned into a pGL-4 basic luciferase expression vector (Promega, Madison, WI). Reporter assays were performed using HEK293T cells transfected with the indicated plasmids and analyzed using a Dual-Luciferase Reporter Assay kit (Promega). The luciferase activity was measured by FlexStation 3 (Molecular Devices). The expression levels were normalized with respect to those for cells co-transfected with a renilla plasmid.

Western Blotting and Immunohistochemistry

Cell lyzates, cytoplasmic lyzates, and nuclear extracts were prepared as previously described (Zhang et al., 2015). Primary antibodies for SIPA1 (Abcam, ab85928, RRID: AB_1925436), LDHA (Abcam, ab47010, RRID: AB_1952042), HK2 (Abcam, ab104836, RRID: AB_10710018), SLC2A1 (Abcam, ab115730), HIF-2α (Abcam, ab207607, RRID: AB_2618694), HIF-1α (Abcam, ab179483), c-myc (Cell Signaling Technology, Danvers, MA, 9,402), PDK1 (Abcam, ab207450), and secondary antibodies (Cell Signaling Technology, 91196 and 7,074) were used for blotting, and β-tubulin (Absin Bioscience Inc., Shanghai, China, abs830032) was included as a control. The relative amount of protein was quantitated by an ImageJ software.

For immunohistochemistry, the xenograft tumor tissue slides underwent deparaffinization, rehydration, and antigen-retrieval and were then incubated with the primary antibody: HIF-2α (Abcam, ab207607), SLC2A1 (Abcam, ab115730) or PDK1 (Abcam, ab207450). Staining image was monitored using 80i fluorescence microscope (Nikon, Tokyo, Japan).

Electrophoretic Mobility Shift Assay

GST-tagged C-terminal half of SIPA1 was expressed in *E. coli* BL21 (DE3) and purified using glutathione-Sepharose beads. The purified protein (2 μg) was incubated with competitive biotin-labeled double-stranded DNA segments on ice for 5 min. Then, 1 μ mole of unlabeled double-stranded DNA segments, which had been amplified from EPAS1 promoter, were added to the mixture, and the protein/DNA mixture was incubated at room temperature for 30 min. The proteins bound to biotin-labeled Seg 2 were resolved by native 6.5% PAGE and imaged by immunoblot assay.

Cell Proliferation and invasion Assay

Cell growth and invasion *in vitro* was measured as described previously (Zhang et al., 2015).

Animal Studies

All animal studies were conducted after approval by the Institutional Animal Care Committee of Huazhong University of Science and Technology. For xenograft experiments, female BALB/c nude mice were divided into two groups, and MDA-MB-231 and 231si cells (2×10^6/mouse) were subcutaneously injected with matrigel (v/v = 3:1) into the right mammary pad for each group, respectively. Five days later, a subset of 6 mice in each group received an intraperitoneal injection with 15 mg oxamate or 0.9% NaCl. The administration was done every 24 h for the next 14 days. The tumor volume was determined every 24 h with vernier caliper according to the following formula: volume (mm^3) = [width (mm)]^2 × [length (mm)]/2. Subsequently, all the tumors were surgically removed and weighed, and the wounds were stitched with surgical suture to maintain animals for 15 additional days. Finally, all the mice were sacrificed by cervical dislocation, and the lungs of each mouse were dissected and immersed in formalin, then analyzed by haematoxylin and eosin (HE) staining.

GEO and TCGA Data Analysis

Dataset GSE41313 was downloaded from GEO (Riaz et al., 2013). In GSE41313, mRNA expression levels in 153 samples from 51 breast cancer cell lines were extracted from the general public license (GPL) 13158 platform (Affymetrix, Santa Clara, CA). Fragments per kilobase of exon model per million mapped fragments (FPKM) were used to compare gene expressions in different groups. Data acquisition and application from The Cancer Genome Atlas (TCGA) were performed in accordance with TCGA publication guidelines and data access policies (Chandrashekar et al., 2017).

Statistical Analysis

The data were presented as mean ± s.d. Student's t-test was used to evaluate p values. One-way or two-way ANOVA were used to compare multiple testing correction within multiple groups. A p-value of 0.05 or lower is considered to be statistically significant.

Associated Data

The raw sequence data reported in this paper have been deposited in the Genome Sequence Archive (Chen et al., 2021) in National Genomics Data Center (CNCB-NGDC Members and Partners, 2021), China National Center for Bioinformation/Beijing Institute of Genomics, Chinese Academy of Sciences, under accession number HRA001265 that are publicly accessible at https://ngdc.cncb.ac.cn/gsa-human.

DATA AVAILABILITY STATEMENT

The datasets presented in this study can be found in online repositories. The names of the repository/repositories and accession number(s) can be found in the article/**Supplementary Material**.

ETHICS STATEMENT

The animal study was reviewed and approved by the Institutional Animal Care Committee of Huazhong University of Science and Technology.

AUTHOR CONTRIBUTIONS

Conceptualization, CY, JW, and LS; methodology, CY, JW, and LS; formal analysis, CY, JW, and LS; investigation, CY, LF, and WZ; original draft preparation, CY, and JW; manuscript review and editing, CY, JW, YX, PZ, YT, and LS; visualization, CY, JW, and LS; supervision, JW and LS; project administration, LS; funding acquisition, LS.

FUNDING

This work was supported by grants from MOST-Key Program for International S and T Cooperation Projects of China (2017YFE0129100) and NSFC (81872154 and 31271504).

SUPPLEMENTARY MATERIAL

The Supplementary Material for this article can be found online at: https://www.frontiersin.org/articles/10.3389/fcell.2021.779169/full#supplementary-material

REFERENCES

Andrzejewski, S., Klimcakova, E., Johnson, R. M., Tabariès, S., Annis, M. G., McGuirk, S., et al. (2017). PGC-1α Promotes Breast Cancer Metastasis and Confers Bioenergetic Flexibility against Metabolic Drugs. *Cel Metab.* 26, 778–787. doi:10.1016/j.cmet.2017.09.006

Chandrashekar, D. S., Bashel, B., Balasubramanya, S. A. H., Creighton, C. J., Ponce-Rodriguez, I., Chakravarthi, B. V. S. K., et al. (2017). UALCAN: A Portal for Facilitating Tumor Subgroup Gene Expression and Survival Analyses. *Neoplasia* 19, 649–658. doi:10.1016/j.neo.2017.05.002

Chen, D., Wu, L., Liu, L., Gong, Q., Zheng, J., Peng, C., et al. (2017). Comparison of HIF1A-AS1 and HIF1A-AS2 in Regulating HIF-1α and the Osteogenic Differentiation of PDLCs under Hypoxia. *Int. J. Mol. Med.* 40, 1529–1536. doi:10.3892/ijmm.2017.3138

Chen, T., Chen, X., Zhang, S., Zhu, J., Tang, B., Wang, A., et al. (2021). The Genome Sequence Archive Family: Toward Explosive Data Growth and Diverse Data Types. *Genomics Proteomics Bioinformatics*, S1672-0229(21)00163-7. doi:10.1016/j.gpb.2021.08.001

CNCB-NGDC Members and Partners (2021). Database Resources of the National Genomics Data Center, China National Center for Bioinformation in 2021. *Nucleic Acids Res.* 49, D18–D28. doi:10.1093/nar/gkaa1022

Denko, N. C. (2008). Hypoxia, HIF1 and Glucose Metabolism in the Solid Tumour. *Nat. Rev. Cancer* 8, 705–713. doi:10.1038/nrc2468

Dupuy, F., Tabariès, S., Andrzejewski, S., Dong, Z., Blagih, J., Annis, M. G., et al. (2015). PDK1-Dependent Metabolic Reprogramming Dictates Metastatic Potential in Breast Cancer. *Cel Metab.* 22, 577–589. doi:10.1016/j.cmet.2015.08.007

García-Cañaveras, J. C., Chen, L., and Rabinowitz, J. D. (2019). The Tumor Metabolic Microenvironment: Lessons from Lactate. *Cancer Res.* 79, 3155–3162. doi:10.1158/0008-5472.can-18-3726

Gatenby, R. A., and Gillies, R. J. (2004). Why Do Cancers Have High Aerobic Glycolysis? *Nat. Rev. Cancer* 4, 891–899. doi:10.1038/nrc1478

Hanahan, D., and Weinberg, R. A. (2011). Hallmarks of Cancer: the Next Generation. *Cell* 144, 646–674. doi:10.1016/j.cell.2011.02.013

Holmquist-Mengelbier, L., Fredlund, E., Löfstedt, T., Noguera, R., Navarro, S., Nilsson, H., et al. (2006). Recruitment of HIF-1α and HIF-2α to Common Target Genes Is Differentially Regulated in Neuroblastoma: HIF-2α Promotes an Aggressive Phenotype. *Cancer Cell* 10, 413–423. doi:10.1016/j.ccr.2006.08.026

Hsieh, A. L., Walton, Z. E., Altman, B. J., Stine, Z. E., and Dang, C. V. (2015). MYC and Metabolism on the Path to Cancer. *Semin. Cel Develop. Biol.* 43, 11–21. doi:10.1016/j.semcdb.2015.08.003

Jeon, H. M., Kim, D. H., Jung, W.-H., and Koo, J. S. (2013). Expression of Cell Metabolism-Related Genes in Different Molecular Subtypes of Triple-Negative Breast Cancer. *Tumori* 99, 555–564. doi:10.1177/030089161309900419

Ji, K., Ye, L., Toms, A. M., Hargest, R., Martin, T. A., Ruge, F., et al. (2012). Expression of Signal-Induced Proliferation-Associated Gene 1 (SIPA1), a RapGTPase-Activating Protein, Is Increased in Colorectal Cancer and Has Diverse Effects on Functions of Colorectal Cancer Cells. *Cancer Genomics Proteomics* 9, 321–327.

Kawada, K., Toda, K., and Sakai, Y. (2017). Targeting Metabolic Reprogramming in KRAS-Driven Cancers. *Int. J. Clin. Oncol.* 22, 651–659. doi:10.1007/s10147-017-1156-4

Kim, J., Yu, L., Chen, W., Xu, Y., Wu, M., Todorova, D., et al. (2019). Wild-Type P53 Promotes Cancer Metabolic Switch by Inducing PUMA-dependent Suppression of Oxidative Phosphorylation. *Cancer Cell* 35, 191–203. doi:10.1016/j.ccell.2018.12.012

Kim, W. Y., Perera, S., Zhou, B., Carretero, J., Yeh, J. J., Heathcote, S. A., et al. (2009). HIF2α Cooperates with RAS to Promote Lung Tumorigenesis in Mice. *J. Clin. Invest.* 119, 2160–2170. doi:10.1172/jci38443

Kroemer, G., and Pouyssegur, J. (2008). Tumor Cell Metabolism: Cancer's Achilles' Heel. *Cancer Cell* 13, 472–482. doi:10.1016/j.ccr.2008.05.005

Lanning, N. J., Castle, J. P., Singh, S. J., Leon, A. N., Tovar, E. A., Sanghera, A., et al. (2017). Metabolic Profiling of Triple-Negative Breast Cancer Cells Reveals Metabolic Vulnerabilities. *Cancer Metab.* 5, 6. doi:10.1186/s40170-017-0168-x

LeBleu, V. S., O'Connell, J. T., Gonzalez Herrera, K. N., Wikman, H., Pantel, K., Haigis, M. C., et al. (2014). PGC-1α Mediates Mitochondrial Biogenesis and Oxidative Phosphorylation in Cancer Cells to Promote Metastasis. *Nat. Cel Biol* 16, 992–1003. doi:10.1038/ncb3039

Liu, C., Jiang, W. G., Hargest, R., and Martin, T. A. (2020). The Role of SIPA1 in the Development of Cancer and Metastases (Review). *Mol. Clin. Oncol.* 13, 32. doi:10.3892/mco.2020.2102

Lu, X., Bennet, B., Mu, E., Rabinowitz, J., and Kang, Y. (2010). Metabolomic Changes Accompanying Transformation and Acquisition of Metastatic Potential in a Syngeneic Mouse Mammary Tumor Model. *J. Biol. Chem.* 285, 9317–9321. doi:10.1074/jbc.c110.104448

Ma, Y., Weng, J., Wang, N., Zhang, Y., Minato, N., and Su, L. (2021). A Novel Nuclear Localization Region in SIPA1 Determines Protein Nuclear Distribution and Epirubicin-Sensitivity of Breast Cancer Cells. *Int. J. Biol. Macromolecules* 180, 718–728. doi:10.1016/j.ijbiomac.2021.03.101

Mathieu, V., Pirker, C., Schmidt, W. M., Spiegl-Kreinecker, S., Lötsch, D., Heffeter, P., et al. (2012). Aggressiveness of Human Melanoma Xenograft Models Is Promoted by Aneuploidy-Driven Gene Expression Deregulation. *Oncotarget* 3, 399–413. doi:10.18632/oncotarget.473

Pérez-Escuredo, J., Dadhich, R. K., Dhup, S., Cacace, A., Van Hée, V. F., De Saedeleer, C. J., et al. (2016). Lactate Promotes Glutamine Uptake and Metabolism in Oxidative Cancer Cells. *Cell Cycle* 15, 72–83. doi:10.1080/15384101.2015.1120930

Rankin, E. B., and Giaccia, A. J. (2016). Hypoxic Control of Metastasis. *Science* 352, 175–180. doi:10.1126/science.aaf4405

Riaz, M., van Jaarsveld, M. T., Hollestelle, A., Prager-van der Smissen, W. J., Heine, A. A., Boersma, A. W., et al. (2013). miRNA Expression Profiling of 51 Human Breast Cancer Cell Lines Reveals Subtype and Driver Mutation-specific miRNAs. *Breast Cancer Res.* 15, R33. doi:10.1186/bcr3415

Semenza, G. L. (2003). Targeting HIF-1 for Cancer Therapy. *Nat. Rev. Cancer* 3, 721–732. doi:10.1038/nrc1187

Shimizu, Y., Hamazaki, Y., Hattori, M., Doi, K., Terada, N., Kobayashi, T., et al. (2011). SPA-1 Controls the Invasion and Metastasis of Human Prostate Cancer. *Cancer Sci.* 102, 828–836. doi:10.1111/j.1349-7006.2011.01876.x

Simões, R. V., Serganova, I. S., Kruchevsky, N., Leftin, A., Shestov, A. A., Thaler, H. T., et al. (2015). Metabolic Plasticity of Metastatic Breast Cancer Cells: Adaptation to Changes in the Microenvironment. *Neoplasia* 17, 671–684. doi:10.1016/j.neo.2015.08.005

Wada, Y., Kubota, H., Maeda, M., Taniwaki, M., Hattori, M., Imamura, S., et al. (1997). Mitogen-InducibleSIPA1Is Mapped to the Conserved Syntenic Groups of Chromosome 19 in Mouse and Chromosome 11q13.3 Centromeric toBCL1in Human. *Genomics* 39, 66–73. doi:10.1006/geno.1996.4464

Wang, N., Weng, J., Xia, J., Zhu, Y., Chen, Q., Hu, D., et al. (2020). SIPA1 Enhances SMAD2/3 Expression to Maintain Stem Cell Features in Breast Cancer Cells. *Stem Cel Res.* 49, 102099. doi:10.1016/j.scr.2020.102099

Wang, Z., Jiang, Q., and Dong, C. (2020). Metabolic Reprogramming in Triple-Negative Breast Cancer. *Cancer Biol. Med.* 17, 44–59. doi:10.20892/j.issn.2095-3941.2019.0210

Warnecke, C., Zaborowska, Z., Kurreck, J., Erdmann, V. A., Frei, U., Wiesener, M., et al. (2004). Differentiating the Functional Role of Hypoxia-inducible Factor (HIF)-1α and HIF-2α (EPAS-1) by the Use of RNA Interference: Erythropoietin Is a HIF-2α Target Gene in Hep3B and Kelly Cells. *FASEB j.* 18, 1462–1464. doi:10.1096/fj.04-1640fje

Yang, H., Geng, Y. H., Wang, P., Zhou, Y. T., Yang, H., Huo, Y. F., et al. (2019). Extracellular ATP Promotes Breast Cancer Invasion and Epithelial-mesenchymal Transition via Hypoxia-inducible Factor 2α Signaling. *Cancer Sci.* 110, 2456–2470. doi:10.1111/cas.14086

Yao, F., Zhou, Z., Kim, J., Hang, Q., Xiao, Z., Ton, B. N., et al. (2018). SKP2- and OTUD1-Regulated Non-proteolytic Ubiquitination of YAP Promotes YAP Nuclear Localization and Activity. *Nat. Commun.* 9, 2269. doi:10.1038/s41467-018-04620-y

Zhang, T., Suo, C., Zheng, C., and Zhang, H. (2019). Hypoxia and Metabolism in Metastasis. *Adv. Exp. Med. Biol.* 1136, 87–95. doi:10.1007/978-3-030-12734-3_6

Zhang, Y., Gong, Y., Hu, D., Zhu, P., Wang, N., Zhang, Q., et al. (2015). Nuclear SIPA1 Activates Integrin β1 Promoter and Promotes Invasion of Breast Cancer Cells. *Oncogene* 34, 1451–1462. doi:10.1038/onc.2014.36

Conflict of Interest: The authors declare that the research was conducted in the absence of any commercial or financial relationships that could be construed as a potential conflict of interest.

Publisher's Note: All claims expressed in this article are solely those of the authors and do not necessarily represent those of their affiliated organizations, or those of the publisher, the editors and the reviewers. Any product that may be evaluated in this article, or claim that may be made by its manufacturer, is not guaranteed or endorsed by the publisher.

Copyright © 2022 Yao, Weng, Feng, Zhang, Xu, Zhang, Tanaka and Su. This is an open-access article distributed under the terms of the Creative Commons Attribution License (CC BY). The use, distribution or reproduction in other forums is permitted, provided the original author(s) and the copyright owner(s) are credited and that the original publication in this journal is cited, in accordance with accepted academic practice. No use, distribution or reproduction is permitted which does not comply with these terms.

frontiers in Cell and Developmental Biology

ORIGINAL RESEARCH
published: 17 February 2022
doi: 10.3389/fcell.2021.673904

Disruption of LTBP4 Inhibition-Induced TGFβ1 Activation Promoted Cell Proliferation and Metastasis in Skin Melanoma by Inhibiting the Activation of the Hippo-YAP1 Signaling Pathway

*Lina Wang[1], Dongrun Tang[2], Tong Wu[2] and Fengyuan Sun[2]**

[1]Sichuan Eye Hospital, AIER Eye Hospital Group, Chengdu, China, [2]Tianjin International Joint Research and Development Centre of Ophthalmology and Vision Science, Eye Institute and School of Optometry, Tianjin Medical University Eye Hospital, Tianjin, China

Melanoma is a malignant tumor derived from melanocytes, which is the most fatal skin cancer. The present study aimed to explore and elucidate the candidate genes in melanoma and its underlying molecular mechanism. A total of 1,156 differentially expressed genes were obtained from the GSE46517 dataset of Gene Expression Omnibus database using the package "limma" in R. Based on two algorithms (LASSO and SVM-RFE), we obtained three candidate DEGs (LTBP4, CDHR1, and MARCKSL1). Among them, LTBP4 was identified as a diagnostic marker of melanoma (AUC = 0.985). Down-regulation of LTBP4 expression was identified in melanoma tissues and cells, which predicted poor prognosis of patients with melanoma. Cox analysis results discovered that LTBP4 with low expression was an independent prognostic factor for overall survival in patients with melanoma. LTBP4 inhibition reduced cell apoptosis and promoted cell proliferation and metastasis. These changes were correlated with the expression levels of caspase-3, Ki67 and E-cadherin. Further, as indicated by tumor formation study of nude mice, LTBP4 silencing improved the tumorigenic ability of melanoma cells. Knockdown of LTBP4 increased the percentage of active TGFβ1 secreted by melanoma cells. CTGF, Gyr61, and Birc5 expression levels were reduced, YAP1 phosphorylation was inhibited, and YAP1 was translocated from the cytoplasm to the nucleus in melanoma cells treated with TGF-β1. These effects were reversed by LTBP4 overexpression. As evidenced by immunofluorescent staining, Western blotting and luciferase reporter assay, LTBP4 overexpression activated the Hippo signaling pathway, which was characterized by the increased nuclear-cytoplasmic translocation of YAP1 and the enhanced phosphorylation of YAP1, MST1, and MOB1. In addition, the effects of LTBP4 overexpression on inhibiting CTGF, Cyr61 and Birc5 expression, promoting the apoptosis, and inhibiting the metastasis and proliferation of melanoma cells were reversed by the

OPEN ACCESS

Edited by:
Simona Kranjc Brezar, Institute of Oncology Ljubljana, Slovenia

Reviewed by:
Luciana N. S. Andrade, Universidade de São Paulo, Brazil
Guohua Hua, Huazhong Agricultural University, China

***Correspondence:**
Fengyuan Sun
ydyk2016@126.com

Specialty section:
This article was submitted to Molecular and Cellular Oncology, a section of the journal Frontiers in Cell and Developmental Biology

Received: *28 February 2021*
Accepted: *21 December 2021*
Published: *17 February 2022*

Citation:
Wang L, Tang D, Wu T and Sun F (2022) Disruption of LTBP4 Inhibition-Induced TGFβ1 Activation Promoted Cell Proliferation and Metastasis in Skin Melanoma by Inhibiting the Activation of the Hippo-YAP1 Signaling Pathway. Front. Cell Dev. Biol. 9:673904. doi: 10.3389/fcell.2021.673904

Abbreviations: GEO database, Gene Expression Omnibus database; LTBP4, Latent transforming growth factor beta binding protein 4; DEG, Differentially expression gene; OS, Overall survival; OE, Overexpression; KD, Knockdown; YAP. Yes1-associated transcriptional regulator; MST1, Macrophage stimulating 1; MOB1, Mps one binder protein 1; CTGF, Connective tissue growth factor; Birc5, Baculoviral IAP repeat containing 5; TGF-β, Transforming growth factor-β; TGF-βRII, Transforming growth factor-β receptor II.

overexpression of YAP1 or MST1. In conclusion, the LTBP4-TGFβ1-Hippo-YAP1 axis is a critical pathway for the progression of skin melanoma.

Keywords: Ltbp4, proliferation, metastasis, melanoma, hippo, Yap1

BACKGROUND

Melanoma is a malignant tumor that originates from melanocytes in the skin and other tissues (Dong et al., 2020). Malignant melanoma is the most invasive skin cancer. Surgery is an effective treatment for early melanoma, however, many patients with advanced melanoma are associated with dismal prognosis and are not the candidates for surgery. For these patients, immunotherapy, radiation therapy, chemotherapy, or combination therapy (Altonsy et al., 2020). Therefore, it is very important to identify the effective potential targets and explore its related molecular mechanisms for the diagnosis and treatment of skin melanoma.

Latent transforming growth factor binding protein (LTBP) is an extracellular matrix (ECM) glycoprotein belonging to the LTBP/fibrillins superfamily, which mainly includes four subtypes of LTBP1, LTBP2, LTBP3, and LTBP4 (Koli et al., 2008; Rifkin et al., 2018). LTBP1 and LTBP3 are lowly expressed in epithelial cancer, ovarian cancer (Higashi et al., 2001), and liver cancer (Hou et al., 2017; Deryugina et al., 2018), respectively. LTBP2 functions as a component of ECM microfibers, which plays a role in cell adhesion (Vehviläinen et al., 2003; Enomoto et al., 2018; Pang et al., 2020). Studies have shown that there is a molecular interaction between LTBP4 and TGFβR2, and LTBP4 gene knockdown reduces the abundance of TGFβ receptor, resulting in the increased TGF-β1 level (Su et al., 2015; Ruan et al., 2019; Cao et al., 2020). It has also been shown that active TGF-β1 affects the activation of Hippo signaling pathway and the function of YAP1, thereby regulating the proliferation of tumor cells (Patel et al., 2019). The knockdown of LTBP4 can increase the percentage of active TGF-β1 secreted by liver cancer cell lines (Yang et al., 2020). The Hippo signaling pathway, which is involved in regulating the homeostasis of various cells and organs, is related to the occurrence and development of melanoma (Zhang et al., 2020). The hippo signaling pathway is mainly composed of a series of kinase complexes and transcription activating factors, including MST1/2, SAV1, LATS1/2, MOB1, and YAP1/TAZ. In addition, the Hippo pathway oncoprotein YAP can promote cell invasion and spontaneous metastasis in skin melanoma (Nallet-Staub et al., 2014; Zhang et al., 2019). Our previous results showed that LTBP4 was not only significantly down-regulated in melanoma tumor tissues, but also served as a diagnostic marker for melanoma in the GSE46517 dataset (Gutzmer et al., 2020). Therefore, we hypothesized that LTBP4 was a gene closely related to the occurrence and development of skin melanoma, and explored its related molecular mechanisms in this study.

METHODS

Melanoma Cancer Database and Data Processing

GSE46517 dataset containing mRNA expression profiles were downloaded from the Gene Expression Omnibus (GEO) database (http://www.ncbi.nlm.nih.gov/geo/). GSE46517 dataset included 121 samples, which among is seven normal skin samples, one normal epithelial melanocytes sample, and 113 melanoma samples (73 metastatic melanoma samples and 40 primary melanoma samples). Because normal epithelial melanocytes sample does not belong to tissue sample, seven normal skin samples were included in the control group and 113 melanoma samples were included in the experiment group in this study.

Data Processing and DEG Screening

The limma package of R (http://www.bioconductor.org/) was used for background correction, normalization between arrays, and differential expression analysis between 113 MM and seven control samples. Samples with an adjusted false discovery rate $p < 0.05$ and $|\log \text{fold change (FC)}| > 1$ were considered as the threshold points for DEGs.

Candidate Diagnostic Biomarker Screening

To identify significant prognostic variables, two machine-learning algorithms were used to predict disease status. The least absolute shrinkage and selection operator (LASSO) is a regression analysis algorithm that uses regularization to improve the prediction accuracy. The LASSO regression algorithm was carried out using the "glmnet" package in R to identify the genes significantly associated with the discrimination of melanoma and normal samples. Support vector machine (SVM) is a supervised machine-learning technique widely utilized for both classification and regression. To avoid overfitting, an RFE algorithm was employed to select the optimal genes from the meta-data cohort. Therefore, to identify the set of genes with the highest discriminative power, support vector machine recursive feature elimination (SVM-RFE) was carried out using the "e1071" package, "kernlab" package, and "caret" package in R to select the appropriate features. The overlapping genes between the two algorithms were included and the expression levels of candidate genes were further validated in the GSE46517 dataset.

Diagnostic Value of Feature Biomarkers in Melanoma

To test the predictive value of the identified biomarkers, we generated an ROC curve using the mRNA expression data from 113 melanoma and seven control samples. The area under the ROC curve (AUC) value was utilized to determine the diagnostic effectiveness in discriminating MM from control samples and further validated in the GSE46517 dataset.

Expression and Survival Analysis of LTBP4

TCGAportal (http://www.tcgaportal.org) and GEPIA (http://gepia.cancer-pku.cn/) were used to investigate survival probability and LTBP4 expression in tumor tissues and corresponding para-carcinoma tissues.

TABLE 1 | Correlation between LTBP4 expression and clinicopathological parameters of patients with melanoma.

Parameters	Number of patients		*p*-value	χ^2
	Low LTBP4 expression (n)	High LTBP4 expression (n)		
Age (years)				
<60	25	15	0.901	0.015
≥60	22	14		
Sex				
Male	28	14	0.336	0.926
Female	19	15		
Invasion				
T0-T2	14	20	0.001*	11.135
T3-T4	33	9		
TNM stage				
I-II	12	20	0.000*	13.879
III-IV	35	9		
Distal metastasis				
Yes	37	8	0.000*	19.418
No	10	21		
Lymph node metastasis				
Yes	32	9	0.002*	9.909
No	15	20		

*TNM stage, Tumor-Lymph Node-Metastasis stage; LTBP4, Latent transforming growth factor beta binding protein 4; *p < 0.05 was considered as significant.*

Immunofluorescent Staining

Cells on the coverslips were fixed with 4% paraformaldehyde and incubated with the primary antibody against YAP (diluted 1:100; CST, 14074) at 4°C overnight. After washing with PBS, cells were then incubated with fluorescence-conjugated secondary antibody (Invitrogen, Carlsbad, CA), and subsequently, the coverslips were treated with 4,6-diamidino-2-phenylindole (DAPI; Life Technology) for 5 min for nuclear staining and then mounted on glass slides. Images were acquired using a fluorescence microscope (Olympus).

Cells and Surgical Specimens

Five melanoma cell lines used in this study. A101D, SK-MEL-1, VMM5A, A375, and MeWo cells and control cells (human epidermal melanocytes: PEM cell) were purchased from the Cell Culture Collection of the Chinese Academy of Sciences (Beijing, China) and cultured in DMEM medium containing 10% fetal bovine serum (HyClone, Logan, UT, United States), 100 mg/ml streptomycin, and 100 U/mL penicillin in a humidified incubator containing 5% CO_2 at 37°C for 2–3 days. Melanoma tumor tissues and corresponding normal tissues were collected from 76 patients with melanoma between October 2018 and October 2019, following surgical resection at Tianjin Medical University Eye Hospital. All patients have not received neoadjuvant treatment before surgery. All experiments were approved by the Medical Ethics Committee of Tianjin Medical University Eye Hospital and written informed consent documents were signed by all of the patients. **Table 1** lists the clinical characteristics of the enrolled patients.

LTBP4 Gene Silencing and OE and Cell Transfection

Two different shRNAs (shRNA-1 and shRNA-2; purchased from GeneChem, Shanghai, China) were used to target the LTBP4 gene KD. A nonsilencing shRNA (NC) was used as control (GeneChem). LTBP4 expressing plasmids (constructed using a pcDNA 3.1 vector) (Invitrogen; Thermo Fisher Scientific, Inc., Waltham, MA, United States) to induce LTBP4 OE. Cells were transfected with 10 nM of shRNAs or pcDNA3.1 when cells reached about 50% confluence. After 8 h of transfection using Lipofectamine-2000 (Life Technologies) according to the manufacturer's protocol, cells were returned to normal medium in the incubator. When cells reached 85% confluence, cell supernatant, protein, and RNA were collected for later experiments.

A101D cells transfected with pcDNA3.1-LTBP4 were treated with 0, 5 ng/ml TGF-β1 (Zhang et al., 2017) (biolab Science and Technology Ltd., Beijing, China) for 48 h. Then, protein and mRNA were collected for later experiments.

Luciferase Reporter Assay

A luciferase reporter assay was performed to detect YAP transcriptional activity in A101D and A375 cells exposed to pcDNA3.1-LTBP4 transfection, or shRNA-1-LTBP4 transfection. Briefly, the 8xGTIIC-luciferase plasmid, which contains a YAP -responsive synthetic promoter driving luciferase expression, was co-transfected into cells with a β-gal plasmid (Ambion, United States) using LipofectamineTM 2000. After 72 h, luciferase activity was examined. β-Gal activity was used as a normalization control for luciferase activity.

YAP1 Gene or MST1 Genes OE and Cell Transfection

YAP1 expressing plasmids or MST1 expressing plasmids (constructed using a pcDNA 3.1 vector) (Invitrogen; Thermo Fisher Scientific, Inc.) to induce YAP1 OE or MST1 OE. SK-MEL-1 and A375 cells were transfected with 10 nM of pcDNA3.1 when cells reached 30–50% confluence using Lipofectamine-2000 (Life Technologies) according to the manufacturer's protocol.

After transfection for 48 h, the transfection efficiency was determined using RT-PCR assay.

Rescue Experiment

This experiment was divided into the following four groups:1) SK-MEL-1 or A375 cells without any treatment was viewed as CTRL group; 2) SK-MEL-1 or A375 cells transfected with LTBP4 OE was viewed as LTBP4-OE group; 3) SK-MEL-1 or A375 cells co-transfected with LTBP4 OE and YAP1 OE was viewed as LTBP4-OE + YAP1-OE group; 4) SK-MEL-1 or A375 cells co-transfected with LTBP4 OE and MST1 OE was viewed as LTBP4-OE + MST1-OE group. Cell proliferation, apoptosis, migration and invasion in above groups were measured using CCK-8, colony formation, flow cytometry, transwell and wound healing assays.

Cell Viability Assay

Cell viability was detected using CCK-8 kit instructions (Beyotime, Shanghai, China). Logarithmically growing cells were picked out, digested with 0.25% trypsin (Gibco). Transfected cells were seeded at a density of 5×10^3 cells/well in 96-well plates and cultured in a 5% CO_2 at 37°C incubators for 2 h to adhere to cells. After cells being cultured for 0, 6, 12, 24, 48 and 72 h, CCK-8 reagent was added (10 μL/well) and incubated for 4 h. The optical density was determined at 450 nm by the microplate reader. The dual-wavelength microplate reader (Beckman Coulter, United States) was used to measure the detection wavelength of 450 nm.

Colony Formation

For the colony formation assay, 600 cells per group were plated in triplicates in a six-well plate. Dishes were taken out when the cell colonies in each well were more than 25. The numbers of cell clones were counted following staining with 1% crystal violet (Beyotime) for 5 min at room temperature, and images were captured by an optical microscope (Olympus, CX23).

Flow Cytometry Analysis

For apoptosis measurements, the percentages of apoptotic cells were determined by flow cytometry using the Annexin V-FITC/PI cell apoptosis detection kit (Promega) according to the manufacturer's instructions. The Q2 and Q3 were identified as the apoptotic quadrant.

Wound-Healing Assay

Cells (4.5×10^5/ml) were seeded on a six-well plate to form a confluent monolayer in a 10% FBS-containing medium. The monolayer cells were scratched by a plastic tip and washed with PBS to remove cell debris; 0.5% FBS-containing F12K or RPMI1640 were then added to each well, and the scratched monolayer was incubated in a 37°C incubator with 5% CO_2 for 24 h. Wound closure was measured in five random fields at ×200 magnification using ImageJ software and an inverted microscope (Olympus). Percentage of wound healing was calculated as follows: migrated cell surface area/total surface area × 100, in which, migrated cell surface area = length of cell migration (mm) × 2 × length of defined areas, total surface area = beginning width × length of defined areas.

Transwell Invasion Assays

Cells (4×10^5/ml) were seeded onto the upper chamber of each 24-well plate (Corning, NY, United States) with serum-free medium. The pore size of upper chamber was 8.0 μm. The lower chamber was filled with 600 μL of medium with 10% FBS. After the cells were incubated for 48 h, the cells attached to the reverse phase of the membrane were fixed with 4% paraformaldehyde for 15 min and the cells on the upper chamber were removed using cotton swabs. Then the cells located on the lower surface were stained with 0.1% crystal violet for 5 min. Cells were photographed at least five fields using a light microscope (Olympus).

Total and Active TGFβ1 Detection

1) After determining the number of cells, the plates were washed 4 times and treated with 50 μL assay buffer C. 2) This was followed by the addition of 50 μL of diluted standards or samples. 3) The plates were washed another four times and 100 μL of detection antibody solution was added. 3) The plates were washed four more times and 100 μL of avidin-HRP D solution was added. 4) The plates were washed five times and 100 μL of substrate solution was added. 5) Finally, 100 μL of stop solution was added to the plates. The absorbance was read at 450 nM.

In vivo Tumorigenesis in Nude Mice

Animal experiments were done according to Institutional Animal Care and Use Committee (IACUC) protocol and approved by Tianjin Medical University Animal Center for Use and Care of Animals. The establishment of the subcutaneous melanoma tumor model was treated by subcutaneous injection of SK-MEL-1 with transiently transfected siRNA-LTBP4 and A101D cells with transiently transfected pcDNA 3.1-LTBP4. Four-week-old female BALB/C nude mice (n = 24; Tianjin Medical University Animal Center, Tianjin, China) were required to establish melanoma model mice for 4 weeks (Wu et al., 2020a). Tumor volumes were measured every 3 days. The tumor volume was calculated using the following formula: volume = (length × width^2)/2. Mice were sacrificed 32 days after the injection and the size of the tumor was measured by vernier caliper and the weight of the tumor was measured by electronic balance.

Immunohistochemistry (IHC) Staining

LTBP4 expression between melanoma tissues and adjacent noncancerous tissues in patients with melanoma was determined by IHC staining. For IHC, sections were incubated with anti-LTBP4 (1:300 dilution) antibody. LTBP4 staining was scored by two independent pathologists. LTBP4 or cleaved caspase-3 expression between LTBP4-OE group and LTBP4-KD group in tumor tissues of BALB/C nude mice was determined by IHC staining. Sections were photographed in at least five fields using a light microscope. For IHC, sections were incubated with anti-LTBP4 (1:500 dilution) antibody, anti-cleaved caspase-3 (1:200 dilution) antibody, anti-Ki67 (1:600 dilution) antibody, anti-E-cadherin (1:500 dilution) antibody, anti-YAP1 (1:800 dilution) antibody, and anti-N-cadherin (1: 500 dilution) antibody. Protein's staining was

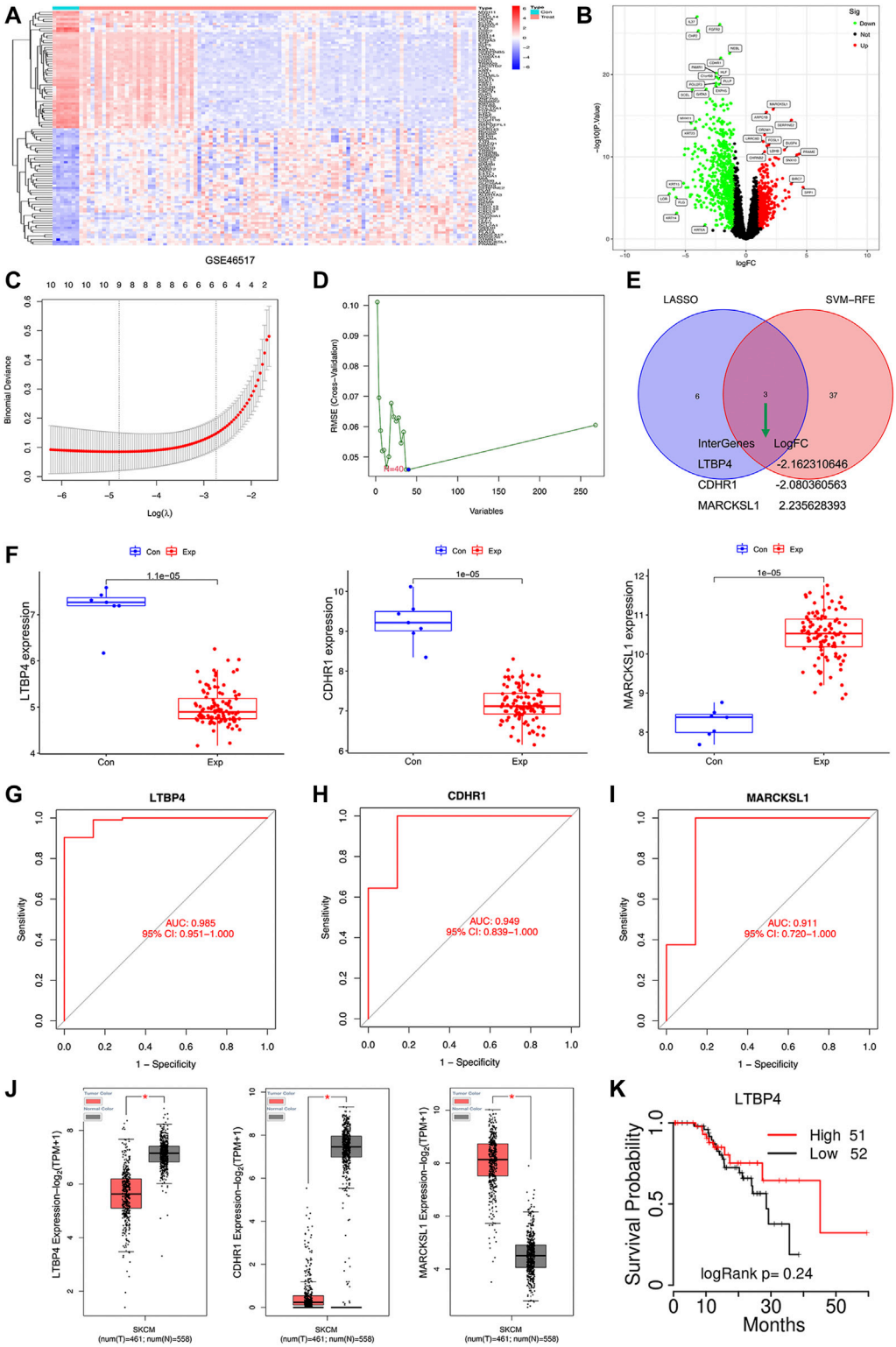


FIGURE 1 | Bioinformatics analysis of DEGs. The heatmap plot of DEGs **(A)** and Venn plot of DEGs **(B)** in the GSE46517 dataset. **(C)** Tuning feature selection in the least absolute shrinkage and selection operator model. **(D)** A plot of biomarkers selection via support vector machine-recursive feature elimination (SVM-RFE) algorithm. **(E)** Venn diagram demonstrating four diagnostic markers shared by the least absolute shrinkage and selection operator and SVM-RFE algorithms. **(F)** Validation of the expression of diagnostic biomarkers (LTBP4, CDHR1, and MARCKSL1) in the GSE46517 dataset. The receiver operating characteristic (ROC) curve of the diagnostic effectiveness of LTBP4 **(G)**, CDHR1 **(H)**, and MARCKSL1 **(I)** **(J)** LTBP4 expression was determined via using the GEPIA database **(K)** The survival probability of LTBP4 was determined via using the TCGAportal database.

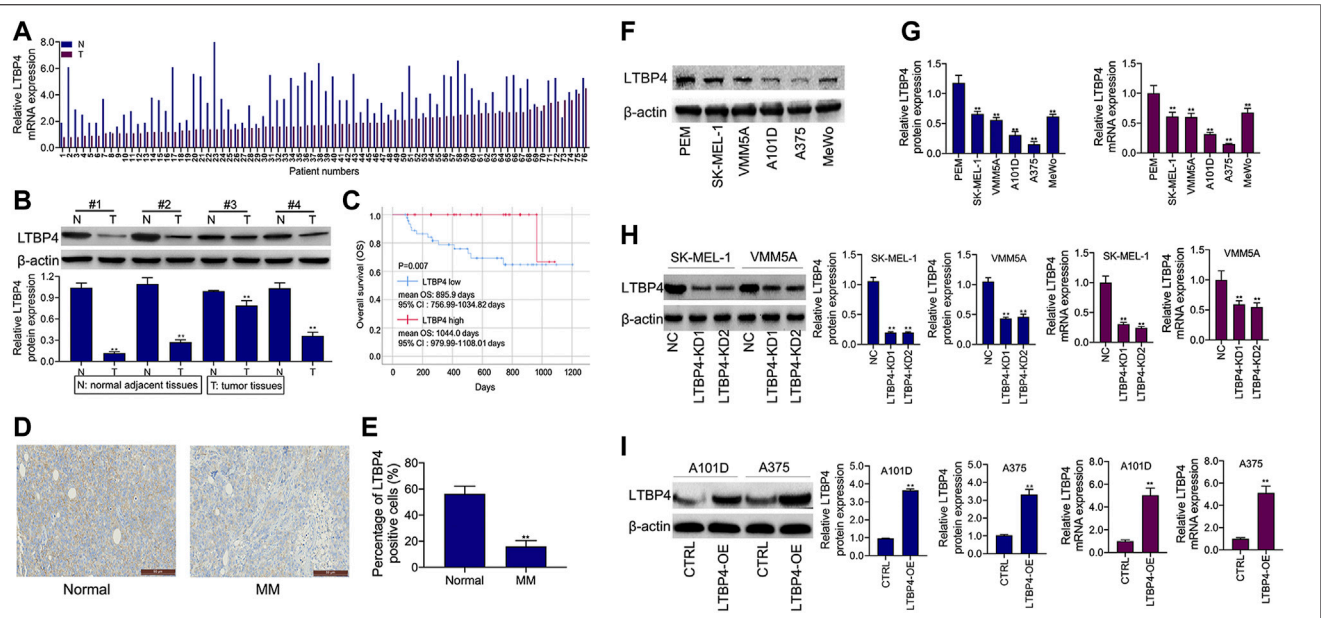


FIGURE 2 | LTBP4 expression was down-regulation in melanoma tissues and cell lines, which was closely related to the poor survival for patients with melanoma. **(A)** The mRNA level of LTBP4 in melanoma tissues was detected by RT-PCR assay. **(B)** The protein level of LTBP4 in melanoma tissues was detected by western blotting assay. **(C)** Survival curve was performed by using the Kaplan-Meier method, and differences between the curves in LTBP4 high expression group and LTBP4 low expression group were determined by log-rank test **(D** and **E)** LTBP4 expression in melanoma tissues was determined by IHC staining. **(F)** The protein level of LTBP4 in melanoma cell lines was detected by western blotting assay. **(G)** The mRNA level of LTBP4 in melanoma cell lines was detected by RT-PCR assay. **(H)** shRNA-LTBP4#1 or #2 was transfected into SK-MEL-1 and VMM5A cells, the protein and mRNA levels of LTBP4 were detected by western blotting and RT-PCR assays. **(I)** LTBP4 expressing plasmids were transfected into A101D and A375 cells, the protein and mRNA levels of LTBP4 were detected by western blotting and RT-PCR assays. β-actin was used as a load control. Data are presented as the mean ± standard deviation. $^{**}p < 0.01$ vs NC/normal/HaCaT group.

scored by researcher. The scoring system was based on the staining intensity and extent. Staining intensity was classified as 0 (negative), 1 (weak), 2 (moderate), and 3 (strong). Staining extent depended on the percentage of positive cells and was divided into 0 (<5%), 1 (5–25%), 2 (26–50%), 3 (51–75%), and 4 (>75%). According to the staining intensity and the staining extent scores, the IHC result was classified as 0–1, negative (−); 2–4, weakly positive (+); 5–8, moderately positive (++); and 9–12, strongly positive (+++).

Western Blotting

Protein lysates were prepared from cells using 500 μL of RIPA buffer with 1 mM phenylmethane sulfonyl fluoride. A total of 40 ug protein was separated by 10% (SDS)-polyacrylamide gel for electrophoresis and then transferred onto polyvinylidene difluoride (PVDF) membrane. The membranes were blocked with PBS containing 0.1% Tween-20 (PBST) and 5% nonfat milk (w/v) for 1 h at room temperature. After they were washed with PBST, the membranes were probed with antibodies overnight at 4°C. Antibody against LTBP4 was obtained from Shanghai Yu Bo Biotech Co.,Ltd. (Shanghai, China); antibody against cleaved caspase-3/Ki67/E-cadherin/YAP1/MST1/CTGF/Cyr61//TGFβR2 and phosph-YAP1/MST1 antibody was obtained from Abcam (Cambridge, UK); antibody against MOB1 and phospho-MOB1 were obtained from Cell Signaling Technology, Inc. (United States); antibody against Birc5 and phosphor-Birc5 were obtained from CUSABIO engineering co. Ltd. (Wuhan, Hubei, China); antibody against β-actin or LaminB were obtained from Beyotime (China). The membranes were washed again with PBST, then horseradish peroxidase-labeled IgG at 1:5,000 dilution was added at room temperature for 1 h, and the blots were developed using

TABLE 2 | Univariate Cox proportional hazards analyses of LTBP4 expression and overall survival for patients with melanoma.

Parameters	Univariate analysis	
	HR (95% CI)	*p*-value
Invasion		
T0-T2 vs T3-T3	0.799 (0.228–2.797)	0.726
TNM stage		
I-II vs III-IV	0.650 (0.165–2.556)	0.537
Distal metastasis		
Yes vs No	1.278 (0.342–4.781)	0.715
Lymph node metastasis		
Yes vs No	1.176 (0.365–3.790)	0.786
Age		
<60 vs ≥ 60	1.406 (0.434–4.550)	0.570
Sex		
Male vs Female	1.013 (0.303–3.390)	0.983
LTBP4 expression		
Low vs High	0.062 (0.006–0.694)	0.024*

*TNM stage, Tumor-Lymph Node-Metastasis stage; LTBP4, Latent transforming growth factor beta binding protein 4; HR, hazard ratio; CI, confidence interval. *p < 0.05 was considered as significant.*

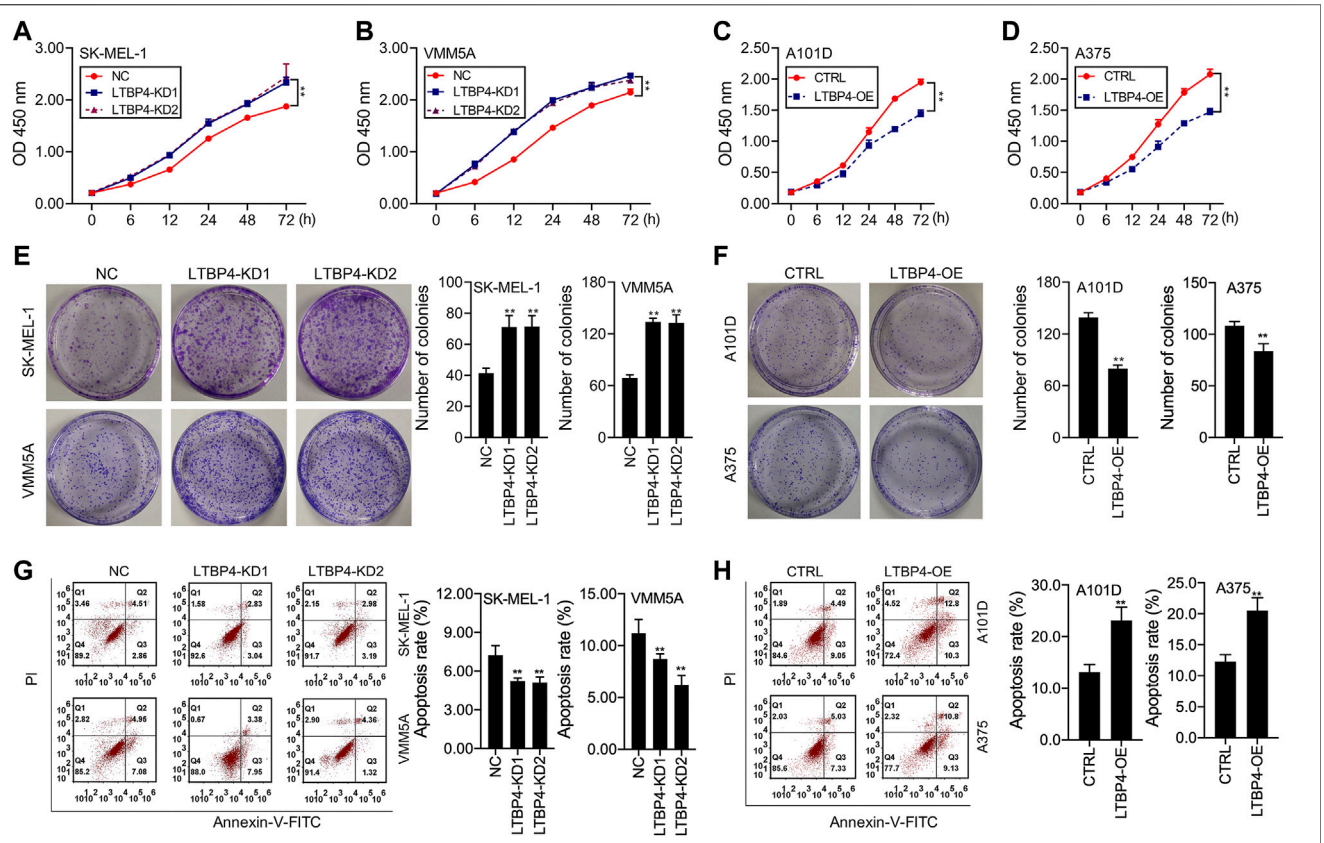


FIGURE 3 | LTBP4 significantly regulated the proliferation and apoptosis in melanoma cell lines **(A** and **B)** The viability of shRNA-LTBP4#1 or #2 transfected SK-MEL-1 and VMM5A cells was detected by CCK-8 assay **(C** and **D)** The viability of LTBP4 expressing plasmids transfected A101D and A375 cells was detected by CCK-8 assay. **(E)** The proliferation of shRNA-LTBP4#1 or #2 transfected SK-MEL-1 and VMM5A cells was detected by colony formation assay. **(F)** The proliferation of LTBP4 expressing plasmids transfected A101D and A375 cells was detected by colony formation assay. **(G)** The apoptosis level of shRNA-LTBP4#1 or #2 transfected SK-MEL-1 and VMM5A cells was detected by flow cytometry assay. **(H)** The apoptosis level of LTBP4 expressing plasmids transfected A101D and A375 cells by flow cytometry assay. Data are presented as the mean ± standard deviation. $^{**}p < 0.01$ vs NC/CTRL group.

enhanced chemiluminescence western blotting reagents. β-actin or LaminB was used as an internal control.

Real-Time PCR (RT-PCR)

Real-time PCR was performed on a Step Two Real-Time PCR System (Applied Biosystems) using the comparative Ct quantization method. Real-time PCR Master Mix (Toyobo) was used to detect and quantify the expression level of the target gene. β-actin and GAPDH were used as the internal control (Lin and Redies, 2012). The primers used were as follows: CTGF, 5′- AGT GCATCCGTACTCCCAAA-3' (F) and 5′- CCGTCGGTACAT ACTCCACA-3' (R); Cyr61, 5′- GCAGCGTTTCCCTTCTAC AG-3' (F) and 5′- ATGAGTCCCATCACCCACAC-3' (R); Birc5, 5′- AACAGTGGCTGCTTCTCTCT-3' (F) and 5′- GCC TTCTTCCTCCCTCACTT-3' (R); β-actin, 5′- ACTCTTCCAGCC TTCCTTCC-3' (F), 5′-CAATGCCAGGGTACATGGTG-3' (R); LTBP4, 5′- CGACATGCCAGACTTTGAGG-3' (F) and 5′- ACCAGCATAGCTTCCACCTT-3' (R); TGFβR2, 5′-CCCCAG GTAAGGATAGCAG-3' (F) and 5′-CCAGGTAGGCAGTGG AAA-3' (R); GAPDH, 5′-CCTTCCGTGTCCCCACT-3' (F) and 5′-GCCTGCTTCACCACCTTC-3' (R).

Statistical Analysis

Statistical analyses were performed using SPSS 19.0 (IBM, Armonk, NY, United States). Correlations between LTBP4 expression and the clinicopathological variables were analyzed using the Pearson $\chi 2$ analysis. The average value of LTBP4 > 1.925 as high expression. Survival was analyzed using the Kaplan-Meier method, and differences were evaluated using the log-rank test. The Cox proportional hazards model was used for univariate analysis to examine the potential prognostic value of different variables on OS. Data were evaluated using ANOVA with LSD test for multiple comparisons and Student's t-test between two groups. $p < 0.05$ was considered to indicate a statistically significant difference.

RESULTS

LTBP4 Is a Feature Biomarker for Melanoma

There were 1,155 DEGs (including 738 down-regulated and 417 up-regulated) between normal tissue samples and melanoma

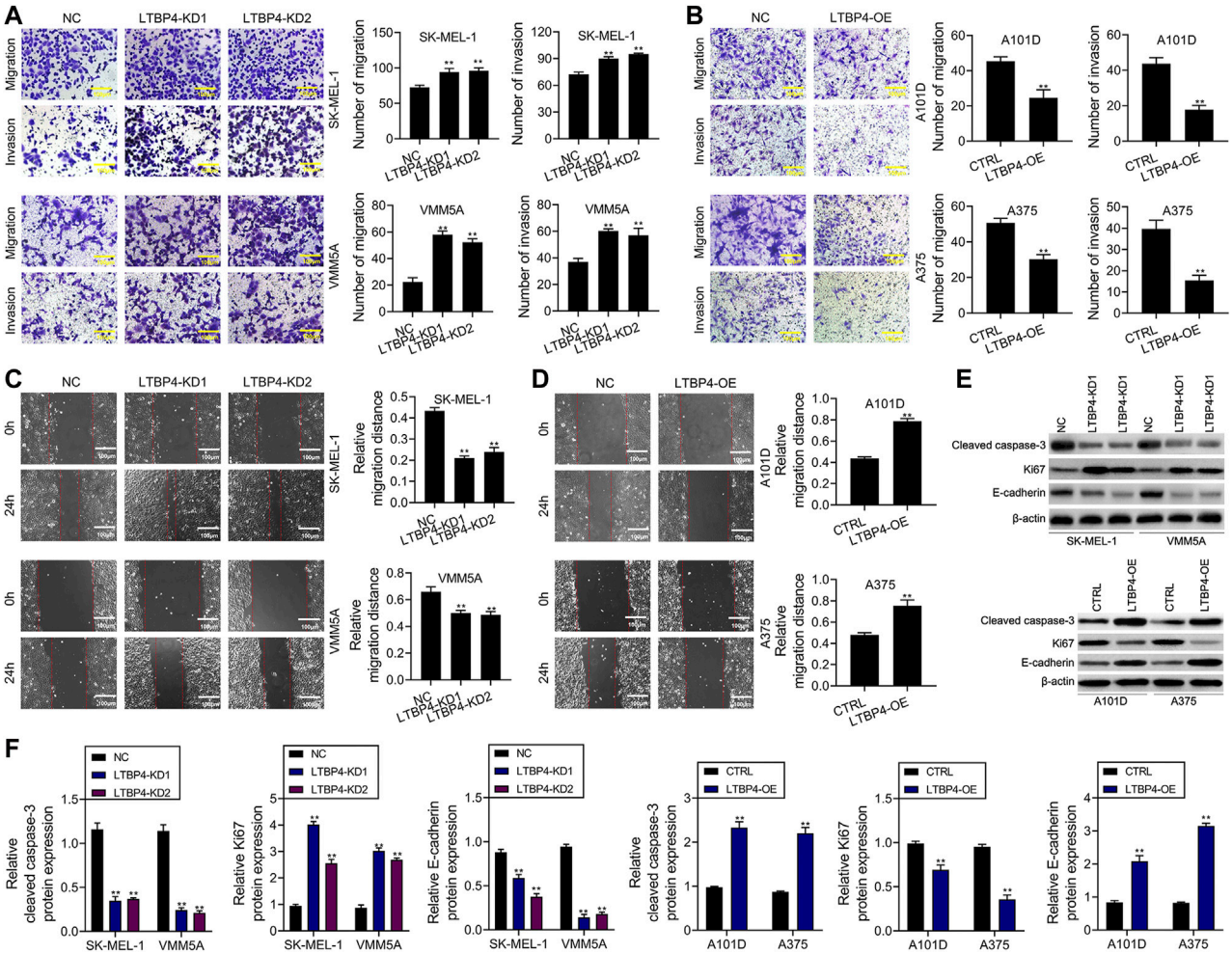


FIGURE 4 | LTBP4 significantly regulated the invasion and migration in melanoma cell lines, and closely related to the expressions of cleaved caspase-3, Ki67 and E-cadherin. **(A)** The migration and invasion of shRNA-LTBP4#1 or #2 transfected SK-MEL-1 and VMM5A cells was detected by transwell assay. **(B)** The migration and invasion of LTBP4 expressing plasmids transfected A101D and A375 cells was detected by transwell assay. **(C)** The migration of shRNA-LTBP4#1 or #2 transfected SK-MEL-1 and VMM5A cells was detected by transwell assay. **(D)** The migration of LTBP4 expressing plasmids transfected A101D and A375 cells was detected by wound healing assay **(E** and **F)** The protein levels of cleaved caspase-3, Ki67, and E-cadherin in shRNA-LTBP4#1 or #2 transfected SK-MEL-1 and VMM5A cells or LTBP4 expressing plasmids transfected A101D and A375 cells were detected by western blotting assay. β-actin was used as a load control. Data are presented as the mean ± standard deviation. $^{**}p < 0.01$ vs NC/CTRL group.

samples in the GSE46517 dataset (**Figures 1A,B**). Two different algorithms were used to screen potential biomarkers. Thereafter, the number of DEGs was narrowed down using the LASSO regression algorithm, and nine variables were identified as the diagnostic biomarkers for melanoma (**Figure 1C**). A subset of 40 features among the DEGs was determined using the SVM-RFE algorithm (**Figure 1D**). Ultimately, the three overlapping features (LTBP4, CDHR1, and MARCKSL1) between these two algorithms were selected (**Figure 1E**). Furthermore, to generate the more accurate and reliable results, the GSE46517 dataset was utilized to verify the expression levels of the three features. The expression levels of LTBP4 and CDHR1 in melanoma tissues were notably lower than those in the control group, while MARCKSL1 expression in melanoma tissues was notably higher than that in the control group (**Figure 1F**). Therefore, the three identified genes were incorporated to establish a diagnostic model using the logistic regression algorithm in the metadata cohort. Next, the diagnostic ability of these three biomarkers in discriminating melanoma from the control samples demonstrated favorable diagnostic value, with the AUC values of 0.985 (95% CI 0.951–1.000) in LTB4 (**Figure 1G**), 0.949 (95% CI 0.839–1.000) in CDHR1 (**Figure 1H**), and 0.911 (95% CI 0.720–1.000) in MARCKSL1 (**Figure 1I**). Moreover, more powerful discrimination ability was confirmed in the GSE60993 dataset, with the AUC value of 0.985 (95% CI 0.951–1.000) in LTB4, indicating that these feature biomarkers achieved high diagnostic ability. Then, the GEPIA database similarly showed that LTBP4 was significantly down-regulated in melanoma tissues (**Figure 1J**), and the TCGAportal database demonstrated no significant difference in the ability of

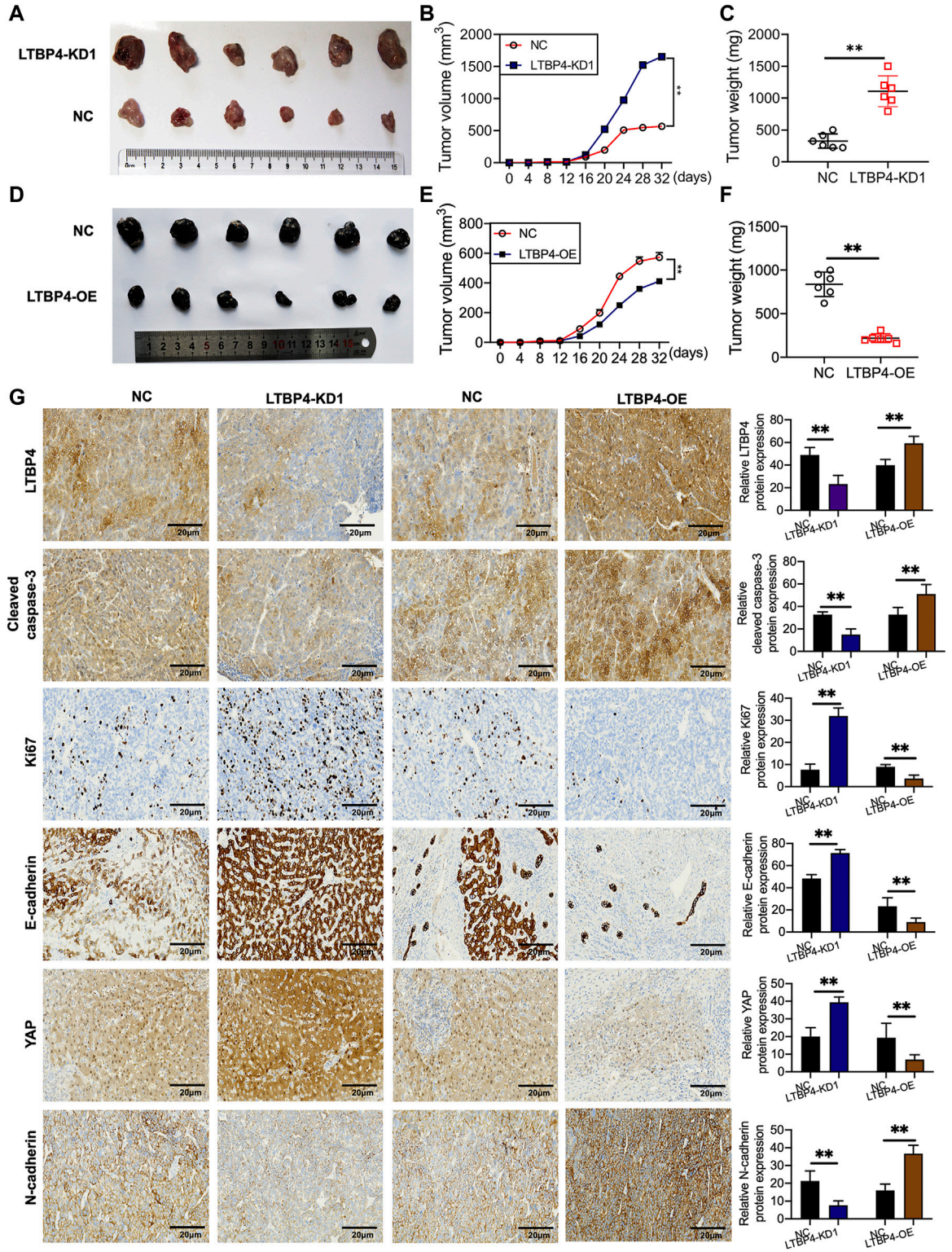


FIGURE 5 | LTBP4 affected the oncogenicity of melanoma cell *in vivo*. SK-MEL-1 cells transfected with shRNA-LTBP4, or NC were subcutaneously injected into the nude mice, **(A)** The nude mice were sacrificed, and the tumors were collected after 32 days; **(B)** the volume of the tumors were determined; **(C)** the weight of the tumors were determined; A101D cells transfected with LTBP4 overexpression or NC were subcutaneously injected into the nude mice, **(D)** The nude mice were sacrificed, and the tumors were collected after 30 days; **(E)** the volume of the tumors were determined; **(F)** the weight of the tumors were determined; **(G)** the expression of Ki67, cleaved caspase-3, Ki67, E-cadherin, YAP, and N-cadherin in the tumors collected from different groups were determined using IHC staining. Data are presented as the mean ± standard deviation. $^{**}p < 0.01$ vs NC group.

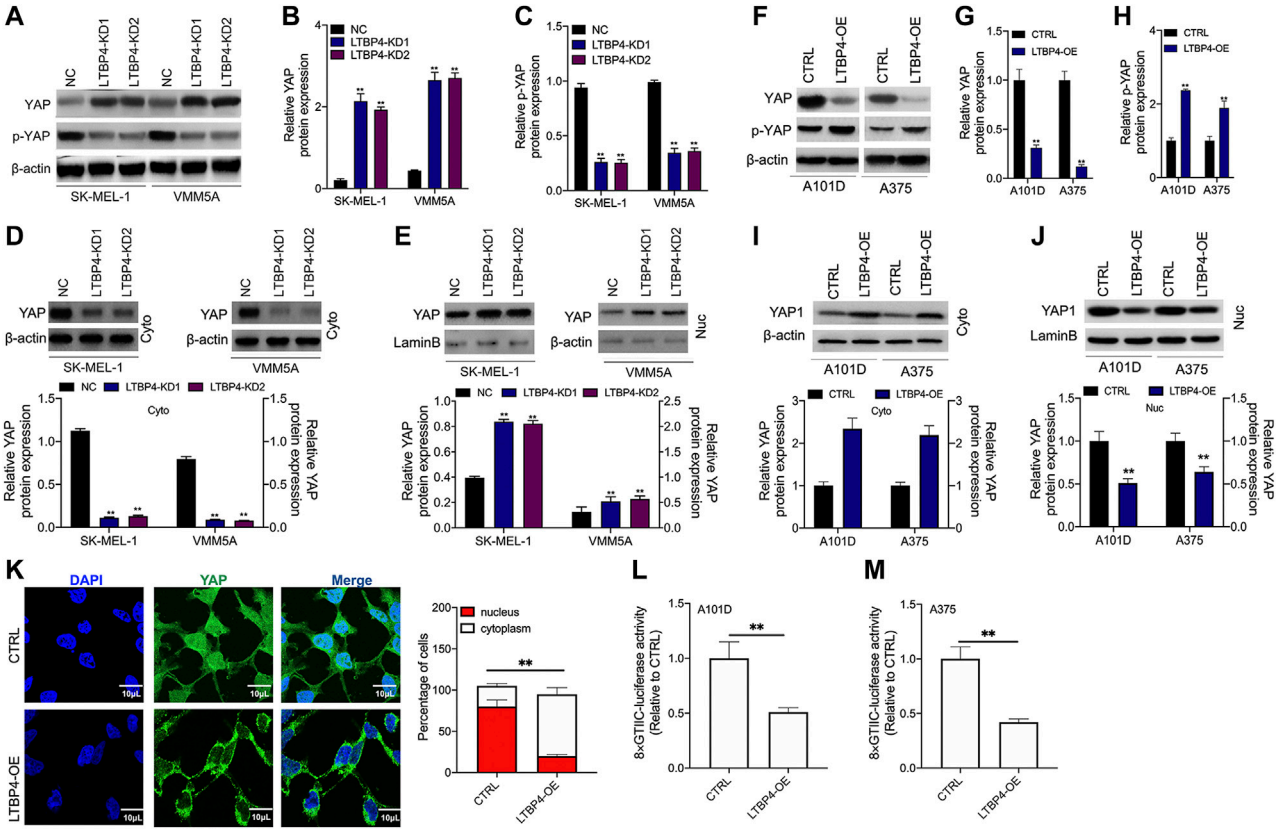


FIGURE 6 | LTBP4 inhibited the transcriptional activity of YAP1 by promoting YAP1 nuclear-cytoplasmic translocation and its phosphorylation. After shRNA-LTBP4#1 or #2 was transfected into SK-MEL-1 and VMM5A cells, the expressions of MST1 and MOB1 **(A,B)**, the phosphorylation level of MST1 and MOB1 **(C)**, and cytoplasmic YAP1 expression **(D)** and nuclear YAP1 expression **(E)** were detected by western blotting. After LTBP4 expressing plasmids transfected A101 and A375 cells, the expressions of MST1 and MOB1 **(F,G)**, the phosphorylation level of MST1 and MOB1 **(H)**, and cytoplasmic YAP1 expression **(I)** and nuclear YAP1 expression **(J)** were detected by western blotting **(K)** The nuclear-cytoplasmic translocation of YAP1 in A101D cells transfected with LTBP4-overexpression vector was examined by immunofluorescence assay **(L** and **M)** The luciferase activity of 8xGTIIC-luciferase, a YAP-responsive synthetic promoter driving luciferase expression plasmid, was evaluated in A101D and A375 cells following LTBP4-overexpression vector transfection or no transfection. β-actin and LaminB were used as a load control. Data are presented as the mean ± standard deviation. $^{**}p < 0.01$ vs CTRL group.

LTBP4 to predict survival probability between its high expression group and low expression group (**Figure 1K**). But when the survival time exceeded 15 months, the survival rate of patients with low LTBP4 expression was lower than that of patients with high LTBP4 expression.

Down-Regulation of LTBP4 Is Closely Related to the Poor Survival of Patients With Melanoma

As shown by the results of RT-PCR and Western blotting assays, LTBP4 was significantly down-regulated in cancer tissues from 76 patients with melanoma, which was associated with invasion, TNM stage, distal metastasis, and lymph node metastasis (**Figures 2A,B** and **Table 1**). We divided the 76 melanoma patients into high and low LTBP4 expression groups according to the average LTBP4 expression level (average = 1.925). Kaplan-Meier curve was performed to estimate survival, and the log-rank test was used to compare the curves. The OS of high LTBP4 expression group was longer (mean OS: 1,044.0 days, 95% CI: 979.99–1,108.01 days) than that of low LTBP4 expression group (mean OS: 895.9 days, 95% CI: 756.99–1,034.82 days) ($p = 0.007$) (**Figure 2C**). Univariate Cox regression analysis revealed that low LTBP4 expression [hazard ratio (HR), 0.062; 95% confidence interval (CI), 0.006–0.694; $p = 0.024$] was associated with patient survival (**Table 2**). While invasion, TNM stage, distal metastasis, lymph node metastasis, age, and sex were not associated with survival (all $p > 0.05$). Likewise, the LTBP4 protein expression was significantly downregulated in melanoma tissues, as revealed by IHC staining (**Figures 2D,E**). Subsequently, we found that LTBP4 expression was significantly down-regulated in melanoma cell lines, as evidenced by RT-PCR and Western blotting assays (**Figures 2F,G**). LTBP4 expression in SK-MEL-1 and VMM5A cells was significantly higher than that in A101D and A375 cells. shRNA-LTBP4 # one or # two was transfected into SK-MEL-1 and VMM5A cells to inhibit LTBP4 expression, whereas the LTBP4 expressing plasmids were

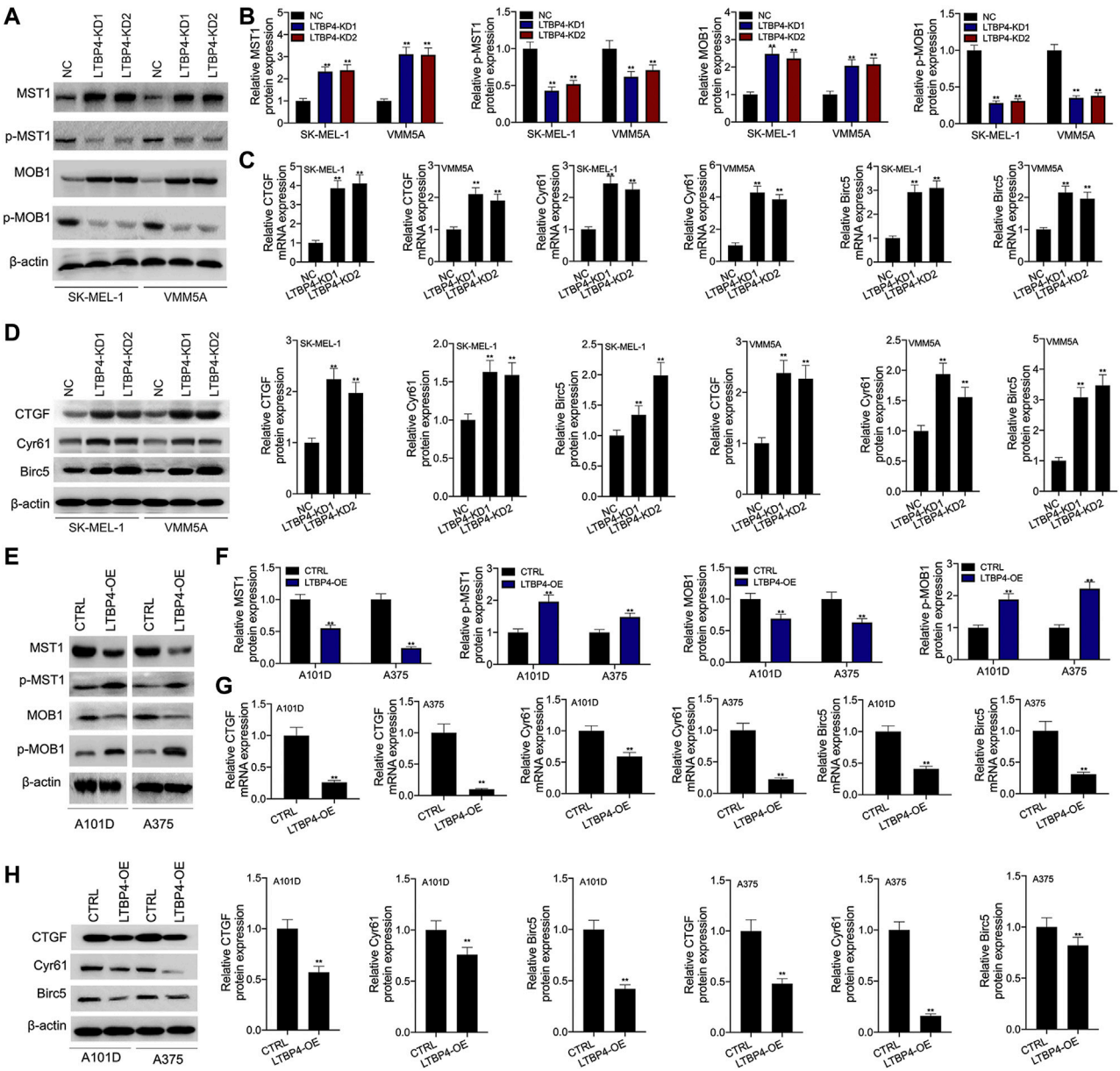


FIGURE 7 | LTBP4 inhibited the activation of Hippo signaling pathway *in vitro*. After shRNA-LTBP4#1 or #2 was transfected into SK-MEL-1 and VMM5A cells **(A** and **B)** the expressions of MST1 and MOB1 and the phosphorylation level of MST1 and MOB1 were detected by western blotting assay, **(C)** the mRNA levels of CTGF, Cyr61, and Birc5 were detected by RT-PCR assay, **(D)** the protein levels of CTGF, Cyr61, and Birc5 were detected by western blotting assay. After LTBP4 expressing plasmids transfected A101 and A375 cells **(E** and **F)** the expressions of MST1 and MOB1 and the phosphorylation level of MST1 and MOB1 were detected by western blotting assay, **(G)** the mRNA levels of CTGF, Cyr61, and Birc5 were detected by RT-PCR assay, and **(H)** the protein levels of CTGF, Cyr61, and Birc5 were detected by western blotting assay. β-actin was used as a load control. Data are presented as the mean ± standard deviation. $^{**}p < 0.01$ vs CTRL/or NC group.

transfected into A101D and A375 cells to over-express LTBP4 expression (**Figures 2H,I**).

LTBP4 Regulates the Proliferation and Apoptosis of Melanoma Cell Lines

Our results showed that LTBP4 knockdown promoted the viability of SK-MEL-1 and VMM5A cells (**Figures 3A,B**), whereas LTBP4 overexpression inhibited the viability of A101D and A375 cells (**Figures 3C,D**). Besides, CCK8 analysis showed that the doubling time of SK-MEL-1 cells was 12 h (**Figure 3A**), while that of VMM5A cells was 8 h (**Figure 3B**), that of A101D cells was 18 h (**Figure 3C**), and that of A375 cells was 16 h (**Figure 3D**). Unsurprisingly, the results of clone formation assay indicated that LTBP4 knockdown promoted the proliferation of SK-MEL-1 and VMM5A cells (**Figure 3E**), while LTBP4 overexpression inhibited the

proliferation of A101D and A375 cells (**Figure 3F**). Flow cytometry results demonstrated that the apoptosis of SK-MEL-1 and VMM5A cells was significantly suppressed by LTBP4-KD1 or LTBP4-KD2; meanwhile, the apoptosis of A101D and A375 cells was significantly promoted by LTBP4 OE (**Figures 3G,H**). However, there was no significant difference in cell viability, proliferation or apoptosis between LTBP4-KD1 group and LTBP4-KD2 group.

LTBP4 Significantly Regulates the Invasion and Migration of Melanoma Cell Lines

According to results of Transwell assay, LTBP4 silencing significantly promoted the invasion of SK-MEL-1 and VMM5A cells (**Figure 4A**), whereas LTBP4 overexpression markedly restrained the invasion of A101D and A375 cells (**Figure 4B**). Conversely, wound healing assay suggested that LTBP4 silencing significantly promoted the migration of SK-MEL-1 and VMM5A cells (**Figure 4C**), while LTBP4 overexpression markedly restrained the migration of A101D and A375 cells (**Figure 4D**). Next, changes in the expression of cleaved caspase-3, Ki67, and E-cadherin proteins within melanoma cell lines with LTBP4 knockdown or overexpression were determined by Western blotting. The results showed that LTBP4 silencing significantly inhibited the expression levels of cleaved caspase-3 and E-cadherin, and increased Ki67 expression in SK-MEL-1 and VMM5A cells. Meanwhile, LTBP4 overexpression significantly increased the expression levels of cleaved caspase-3 and E-cadherin, but suppressed Ki67 expression in A101D and A375 cells (**Figures 4E,F**).

LTBP4 Affects the Oncogenicity of Melanoma Cells *in vivo*

shRNA-LTBP4 was first of all transfected into SK-MEL-1 cells, then the transfected cells were injected into the nude mice subcutaneously, and the tumor weight and volume were measured using the electronic balance and vernier caliper, respectively (**Figure 5A**). As a result, LTBP4 knockdown promoted tumor growth (**Figures 5B,C**), whereas LTBP4 overexpression inhibited tumor growth (**Figures 5D–F**). Next, IHC staining results showed that the expression of LTBP4, cleaved caspase-3, and N-cadherin was inhibited by LTBP4 knockdown, while that of Ki67, E-cadherin, and YAP1 was promoted by LTBP4 knockdown (**Figure 5G**). Unsurprisingly, overexpression of LTBP4 increased the expression of LTBP4, cleaved caspase-3, and N-cadherin, but inhibited that of Ki67, E-cadherin, and YAP1 in tumor tissues of mice.

LTBP4 Inhibited the Transcriptional Activity of YAP1 by Promoting YAP1 Nuclear-Cytoplasmic Translocation and Its Phosphorylation

YAP1 has been shown to contribute to melanoma progression, therefore, we wondered whether LTBP4 affected YAP1 activity. Our Western blotting results showed that silencing of LTBP4 up-regulated YAP1 expression and suppressed the phosphorylation level of YAP1 in SK-MEL-1 and VMM5A cells (**Figures 6A–C**). Furthermore, YAP1 was lowly expressed in the cytoplasm of SK-MEL-1 and VMM5A cells transfected with shRNA-LTBP4 (**Figure 6D**). At the same time, YAP1 was highly expressed in the nuclei of SK-MEL-1 and VMM5A cells transfected with shRNA-LTBP4 (**Figure 6E**). Afterwards, LTBP4 overexpression was found to suppress YAP1 expression and enhance the phosphorylation of YAP1 in A101D and A375 cells (**Figures 6F–H**). Differently, LTBP4 overexpression increased the cytoplasmic YAP1 expression and inhibited its nuclear expression (**Figures 6I,J**). Consistently, the nuclear-cytoplasmic translocation of YAP1 was promoted by LTBP4 overexpression (**Figure 6K**). Furthermore, we conducted luciferase reporter assay, which showed that LTBP4 overexpression decreased the YAP1 transcriptional activity, which was characterized by the decreased activity of 8xGTIIC luciferase, a YAP-responsive synthetic promoter that drove luciferase expression (Fig. 6L-m).

LTBP4 Inhibits the Activation of the Hippo Signaling Pathway *in vitro*

Our Western blotting results indicated that the silencing of LTBP4 up-regulated the expression of MST1 and MOB1, but suppressed the phosphorylation levels of MST1 and MOB1 in SK-MEL-1 and VMM5A cells (**Figures 7A,B**). Next, the mRNA and protein levels of CTGF, Cyr61, and Birc5 in SK-MEL-1 and VMM5A cells transfected with shRNA-LTBP4 were significantly up-regulated, as evidenced by RT-PCR and Western blotting assays (**Figure 7D**). In addition, there was no significant difference in the expression of YAP1, MST1, MOB1, CTGF, Cyr61, or Birc5 within SK-MEL-1 and VMM5A cells between LTBP4-KD1 group and LTBP4-KD2 group.

Furthermore, our results demonstrated that LTBP4 overexpression down-regulated the expression of MST1 and MOB1, but promoted the phosphorylation of MST1 and MOB1 in A101D and A375 cells (**Figures 7E,F**). Next, the mRNA and protein levels of CTGF, Cyr61, and Birc5 in A101D and A375 cells transfected with LTBP4 expression plasmids were significantly down-regulated, as evidenced by RT-PCR and Western blotting assays (**Figures 7G,H**).

LTBP4 Suppresses the Secretion of Active TGFβ1, the Active TGFβ1-Stimulated YAP1 Nuclear-Cytoplasmic Translocation and the Hippo Signaling Pathway

According to our findings, LTBP4 overexpression promoted TGFβR2 expression, while LTBP4 knockdown inhibited TGFβR2 expression (**Figure 8A**). The secretion of active TGFβ1 significantly increased in LTBP4 knockdown transfected A101D cells but decreased in LTBP4 overexpression transfected SK-MEL-1 cells, and the total TGFβ1 did not significantly increase in the two states (**Figure 8B**). We further investigated the activation of Hippo-YAP1 signaling pathway in A101D cells treated with TGF-β1. As a result, TGF-β1 treatment inhibited YAP1 phosphorylation (**Figure 8C**). Consistent with the decreased phosphorylation of YAP1, TGF-β1 treatment induced YAP1 translocation from the cytoplasm to the nucleus (**Figure 8D**). Next, the luciferase reporter assay showed that TGFβ1 treatment increased the

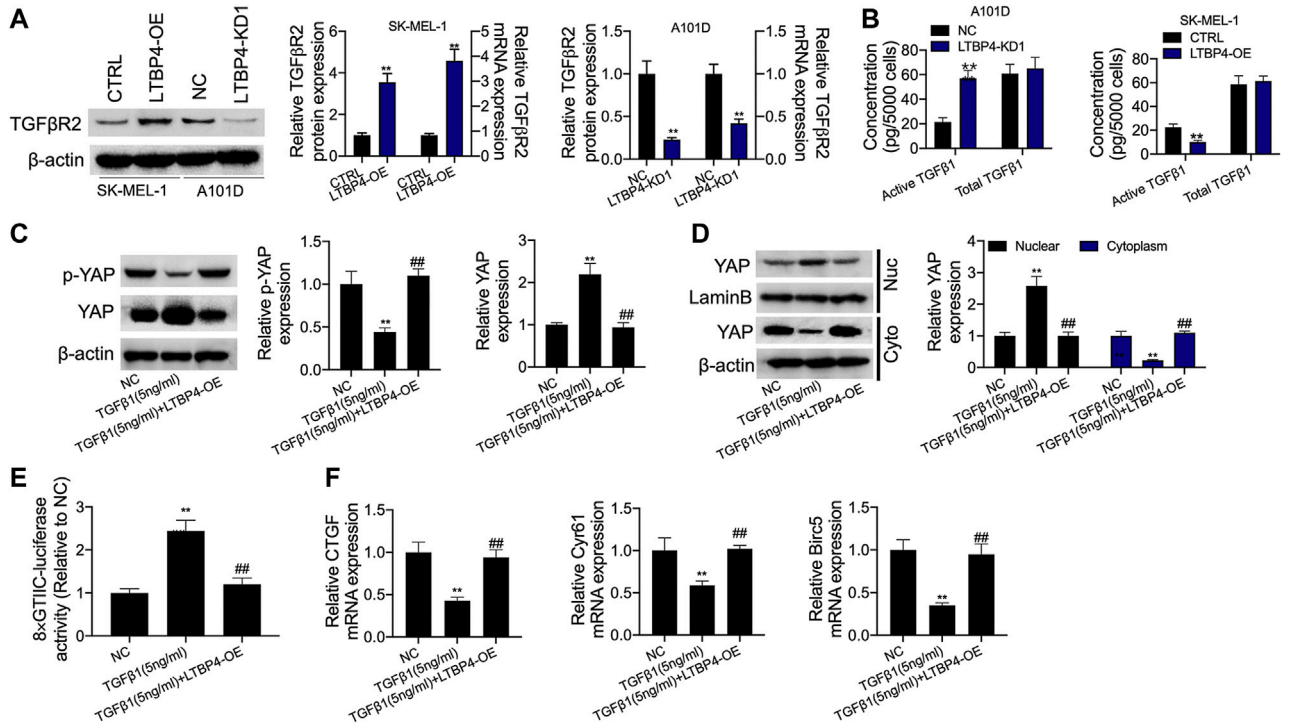


FIGURE 8 | LTBP4 suppressed secretion of active TGFβ1 as well as active TGFβ1-stimulated YAP1 nuclear-cytoplasmic translocation and the Hippo signaling inhibition. **(A)** Western blot, RT-PCR and ELISA analysis of TGFβRII expression **(A)** and total and active TGFβ1 **(B)** in shRNA-LTBP4#1 transfected SK-MEL-1 cells and LTBP4 expressing plasmids transfected A101 cells. A101D cells transfected with pcDNA3.1-LTBP4 were treated with 5 ng/ml TGF-β1, then, western blot analysis of YAP phosphorylation **(C)**, cytoplasmic YAP1 expression and nuclear YAP1 expression **(D)**, the luciferase activity of 8xGTIIC-luciferase analysis of YAP1 transcriptional activity **(E)**, and RT-PCR analysis of CTGF, Cyr61, and Birc5 expression **(F)**. β-actin and LaminB were used as a load control. Data are presented as the mean ± standard deviation. $^{**}p < 0.01$ vs CTRL/or NC group.

YAP1 transcriptional activity (**Figure 8E**) but inhibited the expression of CTGF, Cyr61, and Birc5 (**Figure 8F**). However, these effects were reversed by the transfection of LTBP4 overexpression.

LTBP4 Overexpression Inhibits the Proliferation, Invasion, and Migration, and Promoted the Apoptosis of Melanoma Cells via the Hippo-YAP Signaling Pathway

YAP1 or MST1 expression plasmid was transfected into SK-MEL-1 and A375 cells to induce the overexpression of YAP1 or MST1 by RT-PCR and Western blotting assays (**Figures 9A,B**). The results of CCK-8 and colony formation assays indicated that the functions of LTBP4 overexpression in inhibiting the viability and proliferation of SK-MEL-1 and A375 cells were reversed by YAP1 overexpression or MST1 overexpression (**Figures 9C,D**). In addition, YAP1 overexpression or MST1 overexpression significantly abolished the effects of LTBP4 overexpression on promoting the apoptosis of SK-MEL-1 and A375 cells (**Figure 9E**). In addition, the functions of LTBP4 overexpression in inhibiting the invasion and migration of SK-MEL-1 and A375 cells were reversed by YAP1 overexpression or MST1/2 overexpression (**Figures 9F,G**). Similarly, Western blotting results showed that the effects of LTBP4 overexpression on increasing the expression of cleaved caspase-3 and E-cadherin and reducing the Ki67 expression were counteracted by YAP1 overexpression or MST1 overexpression in SK-MEL-1 and A375 cells (**Figures 10A–D**). Next, both YAP1 overexpression and MST1 overexpression inhibited the functions of LTBP4 overexpression in decreasing CTGF, Cyr61, and Birc5 expression in SK-MEL-1 and A375 cells (**Figures 10E–H**).

DISCUSSION

The GEO database possesses expression profile data of a wide range of cancers, which has greatly reduced the time needed for the researchers to screen genes closely associated with cancer development (Song et al., 2020). We selected one melanoma-related dataset from the GEO data, namely GSE46517 (Xu et al., 2020). LASSO analysis and SVM-RFE analysis identified LTBP4 as a key feature biomarker for melanoma. Besides, results from the TCGaportal database revealed no significant difference in the survival between patients with low and high LTBP4 expression. However, our results indicated that patients with low LTBP4 expression had significantly lower survival than those with high LTBP4 expression. This may be ascribed to the small sample size (n = 76) and individual differences. However, the TCGaportal database also suggested that after 15 months, the survival rate

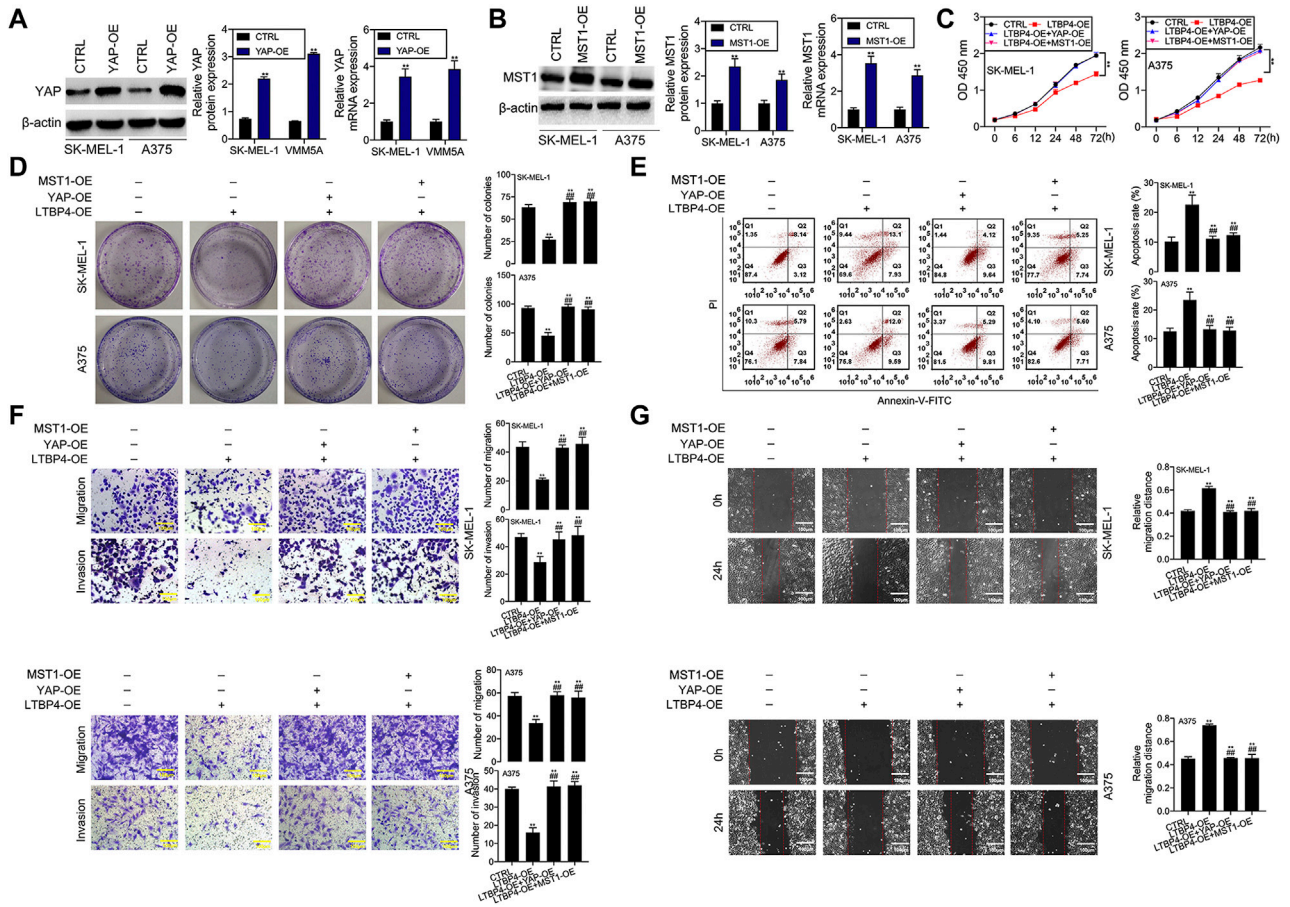


FIGURE 9 | Overexpression of LTBP4 inhibited the proliferation, invasion and migration, and promoted the apoptosis of melanoma cells via the Hippo-YAP1 signaling. **(A)** The protein and mRNA levels of YAP1 in YAP1 expressing plasmids transfected SK-MEL-1 and A375 cells were detected by western blotting and RT-PCR assays. **(B)** The protein and mRNA levels of MST1 in MST1 expressing plasmids transfected SK-MEL-1 and A375 cells were detected by western blotting and RT-PCR assays. After LTBP4 expressing plasmids and YAP1/or MST1 expressing plasmids were co-transfected into SK-MEL-1 and A375 cells, **(C)** the viability was detected by CCK-8 assay, **(D)** the proliferation was detected by colony formation assay, **(E)** the apoptosis level was detected by flow cytometry assay, **(F)** the migration and invasion were detected by transwell assay, and **(G)** the migration was detected by wound healing assay. β-actin was used as a load control. Data are presented as the mean ± standard deviation. $^{**}p < 0.01$ vs CTRL group and $^{\#\#}p < 0.01$ vs LTBP4-OE group.

of patients with low LTBP4 expression began to be significantly lower than that of patients with high LTBP4 expression. Based on the above results, it was confirmed that patients with low LTBP4 expression had poorer prognosis. Next, further experimental results indicated that LTBP4 showed significantly lower expression in tumor tissues from melanoma patients and melanoma cell lines. As revealed by cell and animal studies, LTBP4 silencing promoted cell proliferation, invasion, and migration, inhibited cell apoptosis, and significantly enhanced the tumorigenicity of melanoma cells, which in turn inhibited the progression of malignant melanoma. Of course, the expression of proteins related to proliferation, apoptosis, and migration, and invasion changed significantly during this process. Caspase-3 and Ki67 are the important proteins related to proliferation and apoptosis, which are abnormally expressed in numerous types of malignant tumors (Rodrigues et al., 2016). E-cadherin is a critical tumor suppressor gene related to tumor metastasis, whose expression is significantly down-regulated in malignant tumor cells with great migration and invasion (van Roy and Berx, 2008). Unsurprisingly, our results showed that LTBP4 silencing significantly inhibited the expression of cleaved caspase-3 and E-cadherin, but up-regulated that of Ki67 in melanoma cells, while these effects were abolished by LTBP4 overexpression, consistent with the above studies. These data suggest that LTBP4 is downregulated in malignant melanoma patients, which promotes tumor growth by accelerating cell proliferation, thus aggravating the occurrence and development of melanoma.

Studies have shown that LTBP4, a key molecule in the stabilization of the TGF-β receptor complex, can regulate the activity of TGF-β1, while TGF-β1 can regulate the nuclear translocation of YAP protein (Su et al., 2015; Patel et al., 2019). Thus, it is speculated that LTBP4 regulates the nuclear translocation of YAP protein by affecting TGF-β1 activity

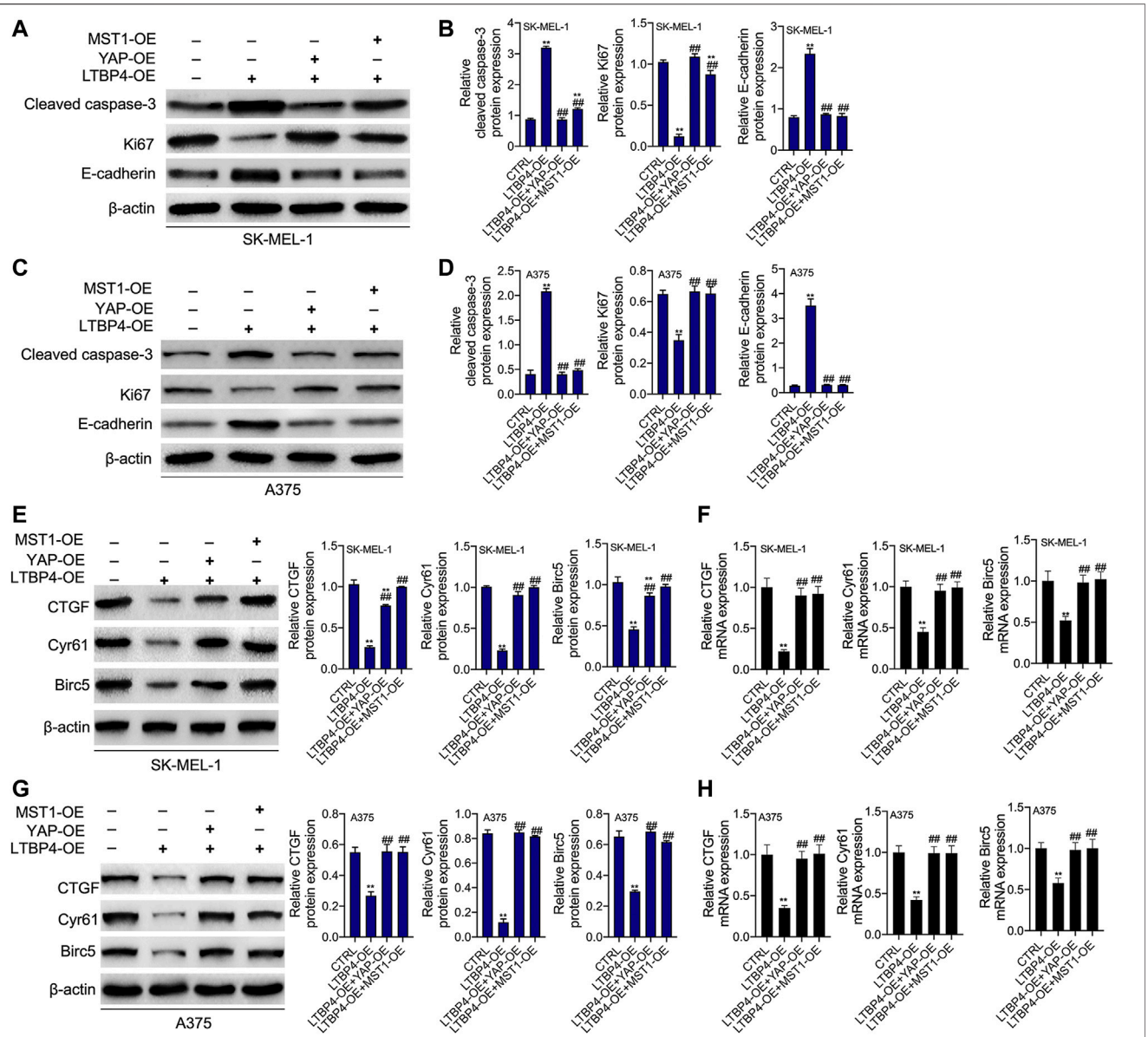


FIGURE 10 | The functions of overexpression of LTBP4 regulating cleaved caspase-3, Ki67, E-cadherin, CTGF, Cyr61, and Birc5 were reversed by YAP1 OE or MST1 OE in melanoma cells. After LTBP4 expressing plasmids and YAP1/or MST1 expressing plasmids were co-transfected into SK-MEL-1 and A375 cells **(A** and **B)** the protein levels of cleaved caspase-3, Ki67, and E-cadherin in SK-MEL-1 cells were detected by western blotting assay **(C** and **D)** the protein levels of cleaved caspase-3, Ki67, and E-cadherin in A375 cells were detected by western blotting assay **(E** and **F)** the protein and mRNA levels of CTGF, Cyr61, and Birc5 in SK-MEL-1 cells were detected by western blotting and RT-PCR assays, and **(G** and **H)** the protein and mRNA levels of CTGF, Cyr61, and Birc5 in A375 cells were detected by western blotting and RT-PCR assays. β-actin was used as a load control. Data are presented as the mean ± standard deviation. $^{**}p < 0.01$ vs CTRL group and $^{\#\#}p < 0.01$ vs LTBP4-OE group.

through acting on the TGF-β receptors, ultimately affecting the activation of the Hippo signaling pathway. The inactivation of the Hippo pathway fails to promote the phosphorylation of YAP protein so that cell proliferation is promoted (Boopathy and Hong, 2019). The high expression of YAP has been reported to promote tumor growth and accelerate cancer progression (Zanconato et al., 2016; Mello et al., 2017; Huang et al., 2020). In this study, tumor formation experiments in nude mice showed that YAP was highly expressed in the cytoplasm and nuclei of tumor tissues in mice transfected with LTBP4-silencing cells. In addition, LTBP4 silencing also increased the expression of YAP and inhibited its phosphorylation. At the same time, expression of the downstream transcriptional activators of the Hippo signaling pathway, including CTGF, CYR61, and BIRC5 (Wu et al., 2020b), elevated by LTBP4 silencing. Certainly, the effect of LTBP4 overexpression was also investigated in the above processes,

and the results showed that high expression of LTBP4 promoted the phosphorylation of YAP, but inhibited the expression of CTGF, CYR61, and BIRC5. Therefore, these data confirm that LTBP4 plays an anticancer role in melanoma by promoting YAP phosphorylation to activate the Hippo signaling pathway, thereby inhibiting tumor growth and metastasis. However, the unphosphorylated YAP will translocate into the nucleus and accumulate in the nucleus, where it plays a role of transcriptional co-activator to promote the expression of related genes that contribute to cell proliferation and survival (Hasegawa et al., 2021). Our results also showed that LTBP4 silencing promoted the nuclear translocation of YAP and increased the enrichment of YAP in the nucleus. The nuclear enrichment of YAP also promoted the expression of CTGF, CYR61, and BIRC5. In addition, LTBP4 silencing inhibited the expression of TGFβR2 and induced the activation of TGFβ1. The functions of TGFβ1 treatment in stimulating YAP1 nuclear-cytoplasmic translocation and inhibiting the activation of the Hippo signaling were abolished by LTBP4 overexpression. This directly indicates that the active TGF-β1 enhances its role in promoting the cytoplasmic-nuclear translocation of YAP1. Moreover, rescue experimental results suggested that the functions of LTBP4 overexpression in inhibiting the viability, proliferation, invasion, and migration, and promoting the apoptosis of melanoma cells were reversed by YAP1 overexpression or MST1 overexpression (the core molecule of Hippo signaling pathway). Meanwhile, the functions of LTBP4 overexpression in inhibiting the expression of cleaved caspase-3 and E-cadherin and inhibiting that of Ki67, CTGF, Cyr61 and Birc5 in melanoma cells were abolished by YAP1 overexpression or MST1 overexpression. Therefore, these results indicate that LTBP4 activates TGF-β1 through co-expression with TGFβR2. It then promotes the phosphorylation of YAP and reduces its nuclear translocation, eventually inhibiting its nuclear enrichment to lead to the activation of the Hippo signaling pathway, which slows the pathogenesis of skin melanoma.

CONCLUSION

The downregulation of LTBP4 is found in melanoma tissues and cell lines, which predicts poor survival of patients with melanoma. LTBP4 silencing promotes the growth and metastasis of melanoma *in vivo* and *in vitro*. We further prove that LTBP4 knockdown increases YAP1 transcriptional activity and promotes YAP1 cytoplasmic-nuclear translocation by inducing the secretion of the active TGFβ1. Therefore, LTBP4 regulates the progression of skin melanoma via the TGFβ1/Hippo/YAP1 signaling pathway. These results also raise the possibility that LTBP4 may function as an important new biomarker

DATA AVAILABILITY STATEMENT

The datasets presented in this study can be found in online repositories. The names of the repository/repositories and accession number(s) can be found in the article/ **Supplementary Material**.

ETHICS STATEMENT

The studies involving human participants were reviewed and approved by Medical Ethics Committee of Tianjin Medical University Eye Hospital. The patients/participants provided their written informed consent to participate in this study. The animal study was reviewed and approved by Medical Ethics Committee of Tianjin Medical University Eye Hospital.

AUTHOR CONTRIBUTIONS

LW wrote the main manuscript and analyzed the data. LW, DT and TW performed the experiments. LW and FS designed the study. All authors read and approved the final manuscript.

ACKNOWLEDGMENTS

The authors of the present work are truly grateful to the GEO database for the availability of the data.

SUPPLEMENTARY MATERIAL

The Supplementary Material for this article can be found online at: https://www.frontiersin.org/articles/10.3389/fcell.2021.673904/full#supplementary-material

REFERENCES

Altonsy, M. O., Ganguly, A., Amrein, M., Surmanowicz, P., Li, S. S., Lauzon, G. J., et al. (2020). Beta3-Tubulin Is Critical for Microtubule Dynamics, Cell Cycle Regulation, and Spontaneous Release of Microvesicles in Human Malignant Melanoma Cells (A375). *Int. J. Mol. Sci.* 21, 1656. doi:10.3390/ijms21051656

Boopathy, G. T. K., and Hong, W. (2019). Role of Hippo Pathway-YAP/TAZ Signaling in Angiogenesis. *Front. Cel Dev. Biol.* 7, 49. doi:10.3389/fcell.2019.00049

Cao, J., Liu, D., Zhao, S., Yuan, L., Huang, Y., Ma, J., et al. (2020). Estrogen Attenuates TGF-B1-Induced EMT in Intrauterine Adhesion by Activating Wnt/β-Catenin Signaling Pathway. *Braz. J. Med. Biol. Res.* 53, e9794. doi:10.1590/1414-431x20209794

Deryugina, E. I., Zajac, E., Zilberberg, L., Muramatsu, T., Joshi, G., Dabovic, B., et al. (2018). LTBP3 Promotes Early Metastatic Events during Cancer Cell Dissemination. *Oncogene* 37, 1815–1829. doi:10.1038/s41388-017-0075-1

Dong, Z., Yang, J., Li, L., Tan, L., Shi, P., Zhang, J., et al. (2020). FOXO3a-SIRT6 axis S-uppresses A-erobic G-lycolysis in M-elanoma. *Int. J. Oncol.* 56 (3), 728–742. doi:10.3892/ijo.2020.4964

Enomoto, Y., Matsushima, S., Shibata, K., Aoshima, Y., Yagi, H., Meguro, S., et al. (2018). LTBP2 Is Secreted from Lung Myofibroblasts and Is a Potential Biomarker for Idiopathic Pulmonary Fibrosis. *Clin. Sci. (Lond).* 132, 1565–1580. doi:10.1042/cs20180435

Gutzmer, R., Stroyakovskiy, D., Gogas, H., Robert, C., Lewis, K., Protsenko, S., et al. (2020). Atezolizumab, Vemurafenib, and Cobimetinib as First-Line Treatment for Unresectable Advanced BRAFV600 Mutation-Positive Melanoma (IMspire150): Primary Analysis of the Randomised, Double-Blind, Placebo-Controlled, Phase 3 Trial. *The Lancet* 395, 1835–1844. doi:10.1016/s0140-6736(20)30934-x

Hasegawa, K., Fujii, S., Matsumoto, S., Tajiri, Y., Kikuchi, A., and Kiyoshima, T. (2021). YAP Signaling Induces PIEZO1 to Promote Oral Squamous Cell Carcinoma Cell Proliferation. *J. Pathol.* 253, 80–93. doi:10.1002/path.5553

Higashi, T., Sasagawa, T., Inoue, M., Oka, R., Shuangying, L., and Saijoh, K. (2001). Overexpression of Latent Transforming Growth Factor-Bl (TGF-Bl) Binding Protein 1 (LTBP-1) in Association with TGF-B1 in Ovarian Carcinoma. *Jpn. J. Cancer Res.* 92, 506–515. doi:10.1111/j.1349-7006.2001.tb01123.x

Hou, Z., Xu, X., Fu, X., Tao, S., Zhou, J., Liu, S., et al. (2017). HBx-Related Long Non-coding RNA MALAT1 Promotes Cell Metastasis via Up-Regulating LTBP3 in Hepatocellular Carcinoma. *Am. J. Cancer Res.* 7, 845–856.

Huang, C., Yuan, W., Lai, C., Zhong, S., Yang, C., Wang, R., et al. (2020). EphA2-to-YAP Pathway Drives Gastric Cancer Growth and Therapy Resistance. *Int. J. Cancer* 146, 1937–1949. doi:10.1002/ijc.32609

Koli, K., Ryynänen, M. J., and Keski-Oja, J. (2008). Latent TGF-β Binding Proteins (LTBPs)-1 and -3 Coordinate Proliferation and Osteogenic Differentiation of Human Mesenchymal Stem Cells. *Bone* 43, 679–688. doi:10.1016/j.bone.2008.06.016

Lin, J., and Redies, C. (2012). Histological Evidence: Housekeeping Genes Beta-Actin and GAPDH Are of Limited Value for Normalization of Gene Expression. *Dev. Genes Evol.* 222, 369–376. doi:10.1007/s00427-012-0420-x

Mello, S. S., Valente, L. J., Raj, N., Seoane, J. A., Flowers, B. M., McClendon, J., et al. (2017). A P53 Super-tumor Suppressor Reveals a Tumor Suppressive P53-Ptpn14-Yap Axis in Pancreatic Cancer. *Cancer Cell* 32, 460–473. e466. doi:10.1016/j.ccell.2017.09.007

Nallet-Staub, F., Marsaud, V., Li, L., Gilbert, C., Dodier, S., Bataille, V., et al. (2014). Pro-invasive Activity of the Hippo Pathway Effectors YAP and TAZ in Cutaneous Melanoma. *J. Invest. Dermatol.* 134, 123–132. doi:10.1038/jid.2013.319

Pang, X. F., Lin, X., Du, J. J., and Zeng, D. Y. (2020). LTBP2 Knockdown by siRNA Reverses Myocardial Oxidative Stress Injury, Fibrosis and Remodelling during Dilated Cardiomyopathy. *Acta Physiol.* 228, e13377. doi:10.1111/apha.13377

Patel, S., Tang, J., Overstreet, J. M., Anorga, S., Lian, F., Arnouk, A., et al. (2019). Rac-GTPase Promotes Fibrotic TGF-β1 Signaling and Chronic Kidney Disease via EGFR, P53, and Hippo/YAP/TAZ Pathways. *FASEB j.* 33, 9797–9810. doi:10.1096/fj.201802489RR

Rifkin, D. B., Rifkin, W. J., and Zilberberg, L. (2018). LTBPs in Biology and Medicine: LTBP Diseases. *Matrix Biol.* 71-72, 90–99. doi:10.1016/j.matbio.2017.11.014

Rodrigues, H., Carvalho, M. I., Pires, I., Prada, J., and Queiroga, F. L. (2016). Clinicopathological Significance of Caspase-3 and Ki-67 Expression in Canine Mammary Gland Tumours. *Acta Veterinaria Hungarica* 64, 78–89. doi:10.1556/004.2016.009

Ruan, H., Lv, Z., Liu, S., Zhang, L., Huang, K., Gao, S., et al. (2019). Anlotinib Attenuated Bleomycin-Induced Pulmonary Fibrosis via the TGF-B1 Signalling Pathway. *J. Pharm. Pharmacol.* 72, 44–55. doi:10.1111/jphp.13183

Song, X., Du, R., Gui, H., Zhou, M., Zhong, W., Mao, C., et al. (2020). Identification of Potential Hub Genes Related to the Progression and Prognosis of Hepatocellular Carcinoma through Integrated Bioinformatics Analysis. *Oncol. Rep.* 43, 133–146. doi:10.3892/or.2019.7400

Su, C.-T., Huang, J.-W., Chiang, C.-K., Lawrence, E. C., Levine, K. L., Dabovic, B., et al. (2015). Latent Transforming Growth Factor Binding Protein 4 Regulates Transforming Growth Factor Beta Receptor Stability. *Hum. Mol. Genet.* 24, 4024–4036. doi:10.1093/hmg/ddv139

van Roy, F., and Berx, G. (2008). The Cell-Cell Adhesion Molecule E-Cadherin. *Cell. Mol. Life Sci.* 65, 3756–3788. doi:10.1007/s00018-008-8281-1

Vehviläinen, P., Hyytiäinen, M., and Keski-Oja, J. (2003). Latent Transforming Growth Factor-β-Binding Protein 2 Is an Adhesion Protein for Melanoma Cells. *J. Biol. Chem.* 278, 24705–24713. doi:10.1074/jbc.M212953200

Wu, L., Zhu, L., Li, Y., Zheng, Z., Lin, X., and Yang, C. (2020). LncRNA MEG3 Promotes Melanoma Growth, Metastasis and Formation through Modulating miR-21/e-Cadherin axis. *Cancer Cel Int* 20, 12. doi:10.1186/s12935-019-1087-4

Wu, Z., Wang, C., Chen, Y., Sun, Z., and Yan, W. (2020). SRPX2 Promotes Cell Proliferation and Invasion in Osteosarcoma through Regulating Hippo Signaling Pathway. *OncoTargets Ther.* 13, 1737–1749. doi:10.2147/ott.S225602

Xu, Y., Mu, Y., Wang, L., and Zhang, X. (2020). Detailed Analysis of Molecular Mechanisms in Primary and Metastatic Melanoma. *J. Comput. Biol.* 27, 9–19. doi:10.1089/cmb.2019.0197

Yang, X., Ye, X., Zhang, L., Zhang, X., and Shu, P. (2020). Disruption of LTBP4 Induced Activated TGFβ1, Immunosuppression Signal and Promoted Pulmonary Metastasis in Hepatocellular Carcinoma. *OncoTargets Ther.* 13, 7007–7017. doi:10.2147/ott.S246766

Zanconato, F., Cordenonsi, M., and Piccolo, S. (2016). YAP/TAZ at the Roots of Cancer. *Cancer Cell* 29, 783–803. doi:10.1016/j.ccell.2016.05.005

Zhang, X., Fan, Q., Li, Y., Yang, Z., Yang, L., Zong, Z., et al. (2017). Transforming Growth Factor-Beta1 Suppresses Hepatocellular Carcinoma Proliferation via Activation of Hippo Signaling. *Oncotarget* 8, 29785–29794. doi:10.18632/oncotarget.14523

Zhang, X., Tang, J. Z., Vergara, I. A., Zhang, Y., Szeto, P., Yang, L., et al. (2019). Somatic Hypermutation of the YAP Oncogene in a Human Cutaneous Melanoma. *Mol. Cancer Res.* 17, 1435–1449. doi:10.1158/1541-7786.Mcr-18-0407

Zhang, X., Yang, L., Szeto, P., Abali, G. K., Zhang, Y., Kulkarni, A., et al. (2020). The Hippo Pathway Oncoprotein YAP Promotes Melanoma Cell Invasion and Spontaneous Metastasis. *Oncogene* 39, 5267–5281. doi:10.1038/s41388-020-1362-9

Conflict of Interest: The authors declare that the research was conducted in the absence of any commercial or financial relationships that could be construed as a potential conflict of interest.

Publisher's Note: All claims expressed in this article are solely those of the authors and do not necessarily represent those of their affiliated organizations, or those of the publisher, the editors and the reviewers. Any product that may be evaluated in this article, or claim that may be made by its manufacturer, is not guaranteed or endorsed by the publisher.

Copyright © 2022 Wang, Tang, Wu and Sun. This is an open-access article distributed under the terms of the Creative Commons Attribution License (CC BY). The use, distribution or reproduction in other forums is permitted, provided the original author(s) and the copyright owner(s) are credited and that the original publication in this journal is cited, in accordance with accepted academic practice. No use, distribution or reproduction is permitted which does not comply with these terms.

frontiers in Cell and Developmental Biology

ORIGINAL RESEARCH
published: 01 March 2022
doi: 10.3389/fcell.2022.770550

An Aging-Related Gene Signature-Based Model for Risk Stratification and Prognosis Prediction in Lung Squamous Carcinoma

Wen-Yu Zhai[1,2†], *Fang-Fang Duan*[3†], *Si Chen*[1,2†], *Jun-Ye Wang*[1], *Ze-Rui Zhao*[1,2], *Yi-Zhi Wang*[1,2], *Bing-Yu Rao*[1,2], *Yao-Bin Lin*[1,2*] *and Hao Long*[1,2*]

[1]State Key Laboratory of Oncology in Southern China, Collaborative Innovation Center for Cancer Medicine, Department of Thoracic Surgery, Sun Yat-Sen University Cancer Center, Guangzhou, China, [2]Lung Cancer Research Center, Sun Yat-Sen University, Guangzhou, China, [3]State Key Laboratory of Oncology in Southern China, Collaborative Innovation Center for Cancer Medicine, Department of Medical Oncology, Sun Yat-Sen University Cancer Center, Guangzhou, China

OPEN ACCESS

Edited by:
Hamid Morjani,
Université de Reims Champagne-Ardenne, France

Reviewed by:
Elena Ciaglia,
University of Salerno, Italy
Jianchun Duan,
Chinese Academy of Medical Sciences and Peking Union Medical College, China

***Correspondence:**
Yao-Bin Lin
linyaob@sysucc.org.cn
Hao Long
longhao@sysucc.org.cn

[†]These authors have contributed equally to this work

Specialty section:
This article was submitted to Molecular and Cellular Oncology, a section of the journal Frontiers in Cell and Developmental Biology

Received: 04 September 2021
Accepted: 04 February 2022
Published: 01 March 2022

Citation:
Zhai W-Y, Duan F-F, Chen S, Wang J-Y, Zhao Z-R, Wang Y-Z, Rao B-Y, Lin Y-B and Long H (2022) An Aging-Related Gene Signature-Based Model for Risk Stratification and Prognosis Prediction in Lung Squamous Carcinoma. Front. Cell Dev. Biol. 10:770550. doi: 10.3389/fcell.2022.770550

Aging is an inevitable process characterized by a decline in many physiological activities, and has been known as a significant risk factor for many kinds of malignancies, but there are few studies about aging-related genes (ARGs) in lung squamous carcinoma (LUSC). We designed this study to explore the prognostic value of ARGs and establish an ARG-based prognosis signature for LUSC patients. RNA-sequencing and corresponding clinicopathological data of patients with LUSC were downloaded from The Cancer Genome Atlas (TCGA) and Gene Expression Omnibus (GEO). The ARG risk signature was developed on the basis of results of LASSO and multivariate Cox analysis in the TCGA training dataset (n = 492). Furthermore, the GSE73403 dataset (n = 69) validated the prognostic performance of this ARG signature. Immunohistochemistry (IHC) staining was used to verify the expression of the ARGs in the signature. A five ARG-based signature, including A2M, CHEK2, ELN, FOS, and PLAU, was constructed in the TCGA dataset, and stratified patients into low- and high-risk groups with significantly different overall survival (OS) rates. The ARG risk score remained to be considered as an independent indicator of OS in the multivariate Cox regression model for LUSC patients. Then, a prognostic nomogram incorporating the ARG risk score with T-, N-, and M-classification was established. It achieved a good discriminative ability with a C-index of 0.628 (95% confidence interval [CI]: 0.586–0.671) in the TCGA cohort and 0.648 (95% CI: 0.535–0.762) in the GSE73403 dataset. Calibration curves displayed excellent agreement between the actual observations and the nomogram-predicted survival. The IHC staining discovered that these five ARGs were overexpression in LUSC tissues. Besides, the immune infiltration analysis in the TCGA cohort represented a distinctly differentiated infiltration of anti-tumor immune cells between the low- and high-risk groups. We identified a novel ARG-related prognostic signature, which may serve as a potential biomarker for individualized survival predictions and personalized therapeutic recommendation of anti-tumor immunity for patients with LUSC.

Keywords: lung squamous carcinoma (LUSC), aging, prognostic signature, risk stratification, anti-tumor immune cells infiltration

INTRODUCTION

Lung cancer (LC), the second most commonly diagnosed malignancy annually, is the leading cause of tumor-related death worldwide (Sung et al., 2020). Lung squamous carcinoma (LUSC), one of the major histological types of LC (Santarpia et al., 2018), occupies about 25% to 30% of non-small cell lung cancer (NSCLC) (Travis et al., 2015). The diagnosis and treatment of LC, especially targeted therapy, have substantially improved during the last decades. Unlike patients with lung adenocarcinoma (LUAD), only few patients with LUSC benefit due to the different gene mutation profiles (Yu et al., 2016; Oberndorfer and Müllauer, 2018). And the improvement of overall survival (OS) in LUSC patients remains dissatisfactory (Piperdi et al., 2014; Siegel et al., 2019). Until now, the tumor-node-metastasis (TNM) system has been commonly adopted to predict individual clinical outcomes, but it contains limited factors and neglects genetic characteristics (Balachandran et al., 2015). Thus, it is vital to develop individual antineoplastic protocols and exploit new prognostic biomarkers for identifying heterogeneous patients with LUSC and guiding personalized therapeutic care.

Aging, which is characterized by gradual functional deterioration of many tissues, is an inevitable and important biological process overtime, lastly generating numerous chronic and age-related pathologies, and is a powerful risk factor for several kinds of diseases, including neoplastic, neurodegenerative, metabolic, and cardiovascular diseases (havlakadze, 2019; Armanios et al., 2015; Benayoun et al., 2019; Smetana et al., 2016). Cytologically speaking, aging is correlated with mitochondrial dysfunction, genomic instability, cellular senescence, and so on, which is accompanied by the accumulation of irreparable damage and lethal substances in cells (Yin and Chen, 2005; López-Otín et al., 2013). Aging has been found to have an effect of irreversibly arresting cell growth and development, inhibiting the uncontrolled proliferation of tumor cells (Mosteiro et al., 2016; He and Sharpless, 2017; Calcinotto et al., 2019). A large flat morphology and reduced motility in senescent cells may contribute to suppress invasion, escape, cell migration, and metastasis (Zhao et al., 2015). However, the mechanisms and impact of cell aging on malignant tumors are quite complicated. Aging-related genes (ARGs) play a vital role in initiation and regulation of cell aging, and potentially affect tumor cells in complex ways. Regulation of tumor cellular senescence by ARGs can inhibit tumors, but ARGs can potentially promote tumor initiation, development, and metastasis (Johnson et al., 2013; Mosteiro et al., 2016; Galluzzi et al., 2018; Calcinotto et al., 2019; Lee and Schmitt, 2019). Lately, the potential diagnostic or prognostic value of ARGs have been explored and confirmed in colorectal cancer and LUAD (Xu and Chen, 2021; Yue et al., 2021). But its prognostic values and potential mechanisms in LUSC remain unknown, and no precise ARG-based risk signature has been developed for LUSC patients.

A comprehensive model with multi-genes shows stronger predictive capacity than a model with one gene (Srivastava and Gopal-Srivastava, 2002). Thus, in the current study, we made use of The Cancer Genome Atlas (TCGA) database to establish an ARG-based signature to predict individual prognosis for LUSC, and the data of a Gene Expression Omnibus (GEO) dataset validated the prognostic value of the ARG-based signature. Finally, a predictive nomogram including the ARG-based signature and TNM system was developed for precise survival predictions of LUAC.

MATERIALS AND METHODS

Data Collection and Preparation

Data of gene expression and clinical information of LUSC patients were downloaded from the TCGA (https://tcga-data.nci.nih.gov/tcga/) and GEO databases (https://www.ncbi.nlm.nih. gov/geo/). After excluding cases with incomplete clinical information and follow-up of less than 1 day, 492 patients from the TCGA dataset were analyzed as a training set and 69 patients from the GSE73403 dataset were used for validation. The scale method from the 'limma' R package was performed to normalize gene expression profiles. The Masked Somatic Mutation data (varscan. Somatic. Maf) were downloaded and analyzed by the "maftools" R package (Mayakonda and Koeffler, 2016). A total of 309 human ARGs were obtained from the Human Aging Genomic Resources 3 (**Supplementary Table S1**).

Construction and Validation of the Prognostic ARG Signature

A log2 | fold change | > 2 and false discovery rate (FDR) < 0.05 were defined as the cut-off values. The differentially expressed genes (DEGs) in LUSC tumor tissues and normal tissues were analyzed by the R software "limma" package. The ARG candidates for the prognostic-related signature were firstly selected using univariate Cox regression analysis ($p < 0.05$) in the TCGA cohort. Secondly, we used the least absolute shrinkage and selection operator (LASSO) regression model to further narrow down the number of prognostic-related ARG candidates. Then, the multivariate Cox model was used to assess the prognostic contributions of each ARG candidate in OS and determine the best weighting coefficient of each prognostic-related ARG candidate. Finally, the signature enrolled all the differentially expressed prognostic-related ARGs. The risk score of each patient was summed up by normalized expression levels of ARGs and their corresponding regression coefficients. The specific formula was as follows: Risk score = sum (each ARG's expression level × corresponding coefficients). According to the cut-off point of risk scores derived from maximally selected log-rank statistics, LUSC patients in the TCGA training cohort were divided into low- and high-risk groups. The Kaplan-Meier method was utilized to estimate OS and the log-rank test was used to compare the differences of OS between the two groups.

To validate this prognostic signature, the risk score of patients in the GSE73043 dataset was calculated according to the same formula as the TCGA cohort. Patients in the GSE73043 validation cohort were also divided into two groups according to the cut-off

points of risk scores from maximally selected log-rank statistics. Kaplan-Meier curves and the log-rank test were performed to identified the relation between the ARG signature and OS in the validation cohort.

Gene Set Enrichment Analyses

To explore the potential molecular mechanisms of the ARGs, we performed Gene Set Enrichment Analysis (GSEA) to find enriched terms between high- and low-risk patients (Subramanian et al., 2005). GSEA was performed in Java GSEA v. 4.0.1 with Kyoto Encyclopedia of Genes and Genomes (KEGG) pathways in C2 and Gene Ontology (GO) terms in C5. After performing 1,000 permutations, genes with a false discovery rate $q < 0.05$ were seen as significantly enriched.

Immune Infiltration and Tumor Mutation Burden Analyses

After normalizing the expression data in the TCGA dataset, we used single-sample GSEA (ssGSEA) to evaluate 28 immune cells in the R package "GSVA" (Tamborero, et al., 2018) with 782 genes included in the gene sets (http://software.broadinstitute.org/gsea/msigdb/index.jsp). With the perm set to 1,000, the CIBERSORT algorithm was used in the CIBERSORT software package to evaluate the proportion of 22 types of infiltrating immune cells based on LM22 (Newman et al., 2015). Immune scores and stromal scores in low- and high-risk groups were calculated by the R package 'ESTIMATE'. According to the length of the human exon, the TMB calculated for each patient was equal to the total mutation frequency/35 MB. Dividing the total number of mutations by the size of the coding region of the target results in TMB per megabase. The Wilcoxon test and Mann-Whitney *U* test were performed to contrast the differential abundances of immune infiltrates, expression level of PD-1, PD-L1, PD-L2, and CTLA4, TMB, immune score, and stromal score between the low- and high-risk groups.

Establishment and Validation of a Predictive Nomogram

In the TCGA dataset, we established a nomogram integrating the ARG signature and TNM staging system for predicting individual survival. Besides, calibration curves for 1-, 3-, and 5 years OS were calculated to evaluate the predictive accuracy of our nomogram in the TCGA dataset as well as the GSE73403 validation dataset.

Immunohistochemistry

Tumor and adjacent non-tumorous tissue specimens from 10 LUSC samples from Sun Yat-Sen University Cancer Center between January 2016 and January 2017 were collected for the immunohistochemistry (IHC) assay. The formalin-fixed, paraffin-embedded tissue sections were dewaxed and rehydrated followed by antigen retrieval and blocking.

The slides were incubated with primary antibodies, rabbit anti-CHEK2 polyclonal antibody (1:2000; ab207446; ABCAM), rabbit anti-A2M polyclonal antibody (1:500; ab109422; ABCAM), rabbit anti-ELN polyclonal antibody (1:2000; ab213720; ABCAM), rabbit anti-c-FOS polyclonal antibody (1:2000; ab214672; ABCAM), and rabbit anti-PLAU polyclonal antibody (1:150; ab133563; ABCAM) overnight in 4°C.

After being incubated with anti-rabbit secondary antibody, HRP-conjugated rabbit polymer (1:500; ab97051; ABCAM) and liquid diaminobenzidine tetrahydrochloride plus substrate (DAB chromogen, Changjia) were used for visualization followed by counterstaining with hematoxylin. The samples were photographed by microscope (Nikon), and images were analyzed using ImageJ FIJI v2.1.0.

Ten random fields were analyzed per tissue section for semi-quantitative scoring, and the scoring method was as follows: 1) Positive cell rate score 0 for <10% positive cells, one for 10~25% positive cells, two for 25~50% positive cells, three for 50~75% positive cells, and four for >75% positive cells.

We also used the Human Protein Atlas database to identify the protein expression of immunohistochemical staining of these five ARGs in LUSC patients.

Statistical Analysis

Continuous data were shown as the mean ± SD and compared by Student's *t*-test. Categorical variables were listed as frequencies with percentages and tested using the chi-square (χ^2) test. According to an outcome-oriented approach for OS, maximally selected log-rank statistics from the "maxstat" R package were collated to decide the optimal cut-off value of risk scores for risk stratification (Hothorn and Zeileis, 2008). Survival curves were estimated by the Kaplan-Meier method, and differences between these two different risk groups were compared with the log-rank test. Based on results from the multivariate Cox model, we established a predictive nomogram using the "rms" R package, and assessed its predictive accuracy by calibration curves and compared its discriminate ability using time-dependent receiver operating characteristic (ROC) curves. Statistical analysis was conducted using SPSS (version 22.0) and R software (version 4.0.1); a p value <0.05 was considered as statistical significant.

RESULTS

Identifying a Prognosis-Related ARG Signature

As represented in the flowchart (**Figure 1**), gene differential expression analysis was performed in the TCGA dataset between 502 tumor tissues and 49 normal tissues. We discovered 1924 upregulated and 2,639 downregulated DEGs including 45 differentially expressed ARGs. After excluding 9 cases lacking survival or important clinical data, 492 cases from the TCGA training cohort were included in this study to decide prognosis-related ARGs as well as construct the ARG-based signature. In addition, 69 cases from the GSE73403 validation cohort were used to validate the ARG-based signature. Clinicopathological factors of the TCGA training cohort and the GSE73403 cohort are shown in **Table 1**.

After univariate Cox analysis by using mRNA expression profiles of each differentially expressed ARG, five OS-related ARGs from TCGA were identified (**Supplementary Table S2**), which were also significant in the LASSO Cox regression analysis (**Figures 2A,B**) and entered the multivariate Cox regression analysis (**Figure 2C**). Finally, a five-ARG risk signature was

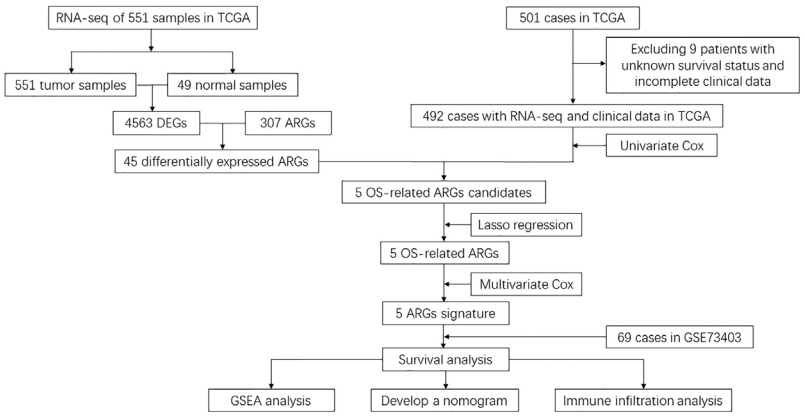


FIGURE 1 | Flowchart of data collection and analysis.

constructed according to 492 LUSC cases in the TCGA dataset, whose risk score was specifically calculated based on a linear combination of gene expression levels and their corresponding regression coefficients from the multivariate Cox analysis. The specific formula was as follows: Risk score = *A2M* × 2.952e-7 - *CHEK2* × 1.347e-4 + *ELN* × 1.222e-5 + *FOS* × 7.953e-6 + *PLAU* × 1.858e-5.

Prognostic Value of the ARG Signature in the Training Cohort

In the training cohort, the cut-off value of risk scores was defined as 0.35 by means of the maximally selected log-rank statistics (**Figure 3A**), according to which we divided cases into low-risk and high-risk groups. **Figure 3B** shows the distribution of risk scores. As shown in **Figure 3C**, there were significantly fewer deaths due to LUSC in the low-risk patients than high-risk patients. We plotted a heatmap to show different expression levels of these five ARGs between the two risk groups (**Figure 3D**). Additionally, patients in the low-risk group had a significantly better OS than patients in the high-risk group (p = 1.352e-08) (**Figure 3E**). After integrating age, gender, smoking history, and T, N, and M classification, the risk score was still significantly associated with OS (HR = 2.68, 95%CI = 1.86–3.86, p < 0.001) (**Figure 3F**).

TABLE 1 | Patients' characteristics.

	TCGA training cohort *n* = 492	GEO validation cohort *n* = 69
Gender		
Male	364 (74.0)	65 (94.2)
Female	128 (26.0)	4 (5.8)
Age (year)	61.3 ± 9.6	58.3 ± 8.5
≤65	171 (34.8)	44 (63.8)
>65	321 (65.2)	25 (36.2)
Smoking history		
Yes or ever or unknown	474 (96.3)	58 (84.1)
No	18 (3.7)	11 (15.9)
T stage		
T1	114 (23.2)	4 (5.8)
T2	286 (58.1)	42 (60.9)
T3	69 (14.0)	20 (29.0)
T4	23 (4.7)	3 (4.3)
N stage		
N0	320 (65.0)	35 (50.7)
N1	127 (25.8)	17 (24.6)
N2	40 (8.1)	17 (24.6)
N3	5 (1.0)	0 (0)
M stage		
M0	486 (98.8)	69 (100)
M1	6 (1.2)	0 (0)

Prognostic Value of the ARG Signature in the Validation Cohort

In our validation cohort, 69 patients with LUSC were divided into high-risk (N = 33) and low-risk (N = 36) groups on the basis of the cut-off value of the risk score from the maximally selected log-rank statistics. The distribution of risk score is presented in **Figure 4A**. Similar with the training cohort, more deaths in the high-risk group were significantly found compared with the low-risk group (**Figure 4B**). As shown in **Figure 4C**, expression profiles of the five ARGs between low-risk and high-risk groups were plotted in the heatmap. The Kaplan-Meier curves revealed that patients in the low-risk group had an apparently longer OS than patients in the high-risk group (p = 1.108e-02) (**Figure 4D**). Further, the multivariate Cox model revealed the ARG risk score as an independent indicator for OS after controlling other clinical factors (HR = 9.51e+18, 95%CI = 752.28–1.20e+35, p = 0.02) (**Table 2**).

Gene Set Enrichment Analysis for Important Pathways

To explore the potential functional mechanisms associated with the prognosis-related ARGs in patients with LUSC, we performed GSEA using GO and KEGG pathway enrichment

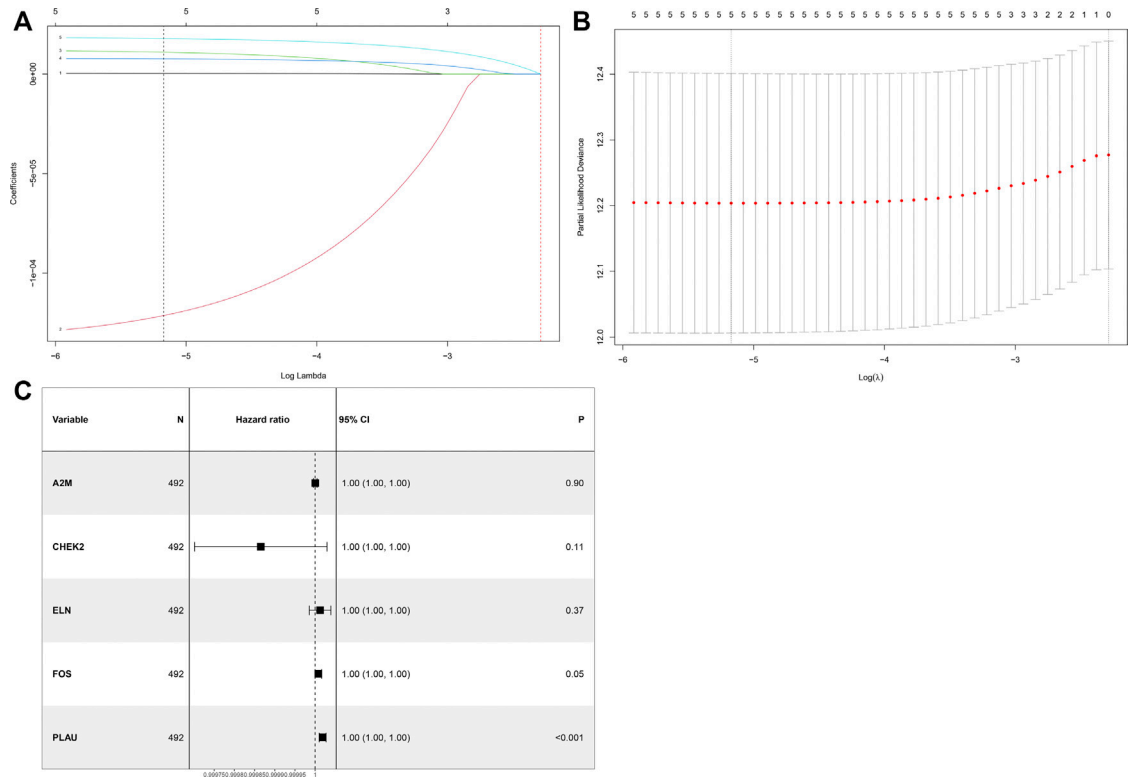


FIGURE 2 | Identification of a prognosis-related ARG-based signature in the TCGA training cohort. **(A)** Selection of the optimal candidate genes in the LASSO model. **(B)** LASSO coefficients of prognosis-associated ARGs, each curve represents a gene. **(C)** Forest plots showing results of univariate Cox regression analysis between the candidate ARG expression and overall survival.

analysis in the low-risk and high-risk groups in the TCGA training dataset. In patients with high-risk, genes were primarily enriched in collagen fibril organization, regulation of extracellular matrix organization, cell substrate junction, collagen binding, extracellular matrix structural constituent, ECM receptor interaction, focal adhesion, nod-like receptor signaling pathway, natural killer cell-mediated cytotoxicity, and B-cell receptor signaling pathway. In patients with low-risk, genes were primarily enriched in cell cycle DNA replication, DNA-dependent DNA replication, NADH dehydrogenase complex, respiratory chain complex, NADPH dehydrogenase quinone activity, base excision repair, DNA replication, homologous recombination, mismatch repair, and RNA polymerase (**Figures 5A,B**).

Tumor Immunity Landscape and TMB in LUSC

To explore the association between ARG risk scores and anti-tumor immunity, ssGSEA and the CIBERSORT algorithm were used to evaluate the immunity landscape between low-risk and high-risk groups in the TCGA dataset. The heatmap showed the results of ssGSEA in 28 immune cells, which demonstrated that these two risk groups had significantly different proportions of different immune cell infiltration (**Figure 6A**). Similar results were also seen in the CIBERSORT algorithm analysis of 22 immune cells (**Figure 6B**). Correlations among the 22 immune cell types are plotted in **Figure 6C**. As shown in **Figure 6D**, infiltrating proportions of naive B cells, $CD8^+$ T cells, activated $CD4^+$ memory T cells, follicular helper T cells, M1 macrophages, resting mast cells, and monocytes were apparently higher in low-risk patients while infiltrating proportions of M0 macrophages, activated mast cells, and neutrophils were significantly higher in high-risk patients. A significantly higher calculated immune score and stromal score with the characteristic of "hot tumor" were found in the high-risk group (**Figures 6E,F**). Compared with LUSC patients in the low-risk group, patients in the high-risk group tended to have a higher expression of PD-1 (**Figure 7A**), but no significant difference in the expression level of PD-L1 was found (**Figure 7B**). Patients with high-risk had an apparently higher expression level of PD-L2 and CTLA4 (**Figures 7C,D**), but patients with low-risk had a significantly higher TMB (**Figure 7E**).

Nomogram Based on ARG Signature for LUSC

We established a visualized predictive nomogram model incorporating the ARG risk scores and T-, N-, and

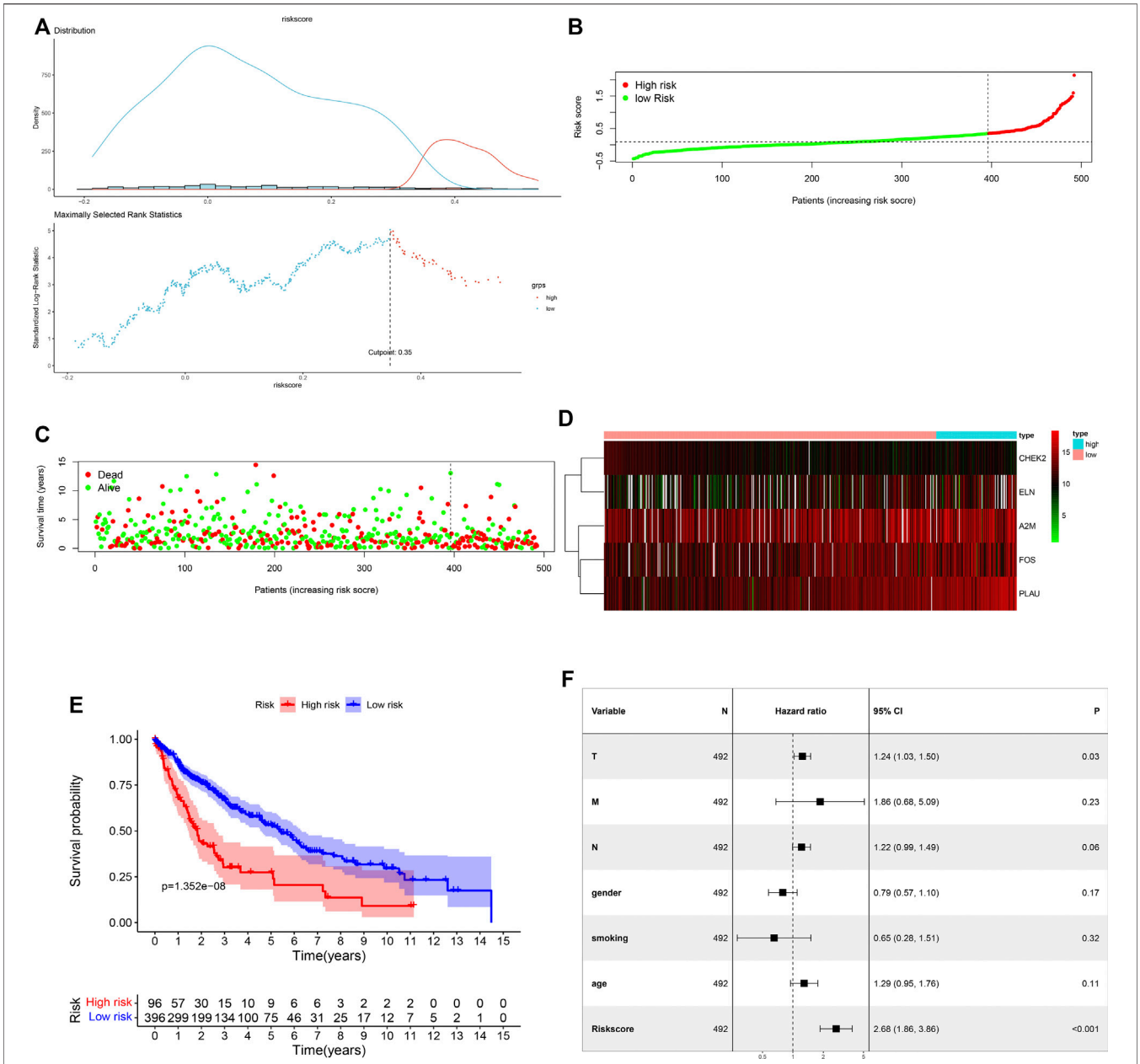


FIGURE 3 | Assessment of prognostic value of the ARG signature model in the TCGA training cohort. **(A)** Determination of cut-off value of ARG risk scores by the maximally selected log-rank statistics. **(B)** The distribution of risk scores in the TCGA cohort. **(C)** Patient distribution in the high- and low-risk groups according to overall survival status. **(D)** The heatmap showing expression profiles of the five ARGs. **(E)** Kaplan-Meier curves for the overall survival of patients in the high- and low-risk groups. **(F)** Multivariate Cox regression analysis of the ARG signature and other clinicopathological factors.

M-classification to predict individual OS probability at 1-, 3-, and 5 years using the data of the training cohort (**Figure 8A**). Bootstrap validation was performed in this nomogram. The C-index of the TCGA training cohort was 0.628 (95% CI: 0.586–0.671) and the C-index of the GSE73403 validation cohort was 0.648 (95% CI: 0.535–0.762), which suggested its good performance in predicting OS for LUSC patients. Calibration curves were drawn in both the TCGA cohort (**Figure 8B**) and the GSE73403 validation cohort (**Figure 8C**), which showed the good consistency between the actual survival and the nomogram-predicted survival at 1-, 3-, and 5-years. The time-dependent ROC curves showed that ARG risk scores combined with the TNM system has better capability in predicting OS for both training and validation cohorts (**Figures 8D,E**).

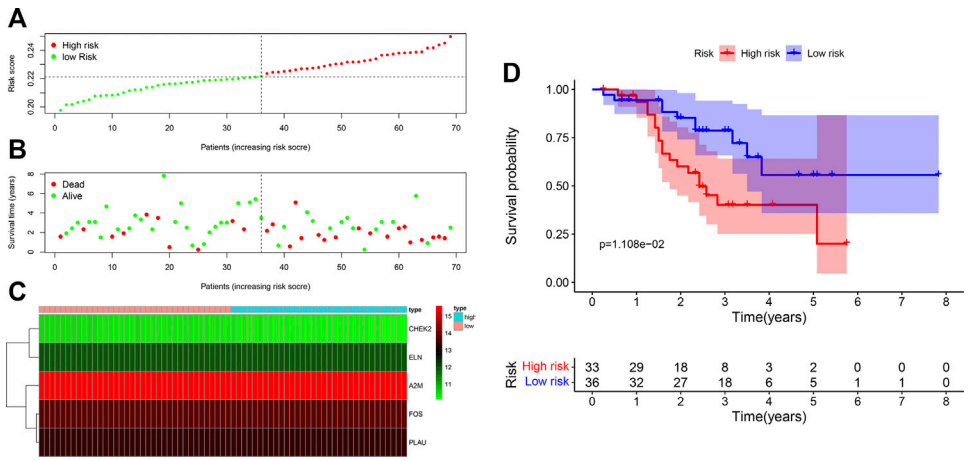


FIGURE 4 | Assessment of prognostic value of the ARG signature model in the GSE20685 validation cohort. **(A)** The distribution of risk scores in the GSE20685 cohort. **(B)** Patient distribution in the high- and low-risk groups according to overall survival status. **(C)** The heatmap showing expression profiles of the five ARGs. **(D)** Kaplan-Meier curves for the overall survival of patients in the high- and low-risk groups.

TABLE 2 | Multivariate Analysis of GEO validation.

Factors	Multivariate analysis	
	HR (95%CI)	*p* Value
Gender		
Female		References
Male	1.68 (0.25–11.36)	0.59
Age (year)		
≤65		References
>65	1.01 (0.96–1.05)	0.81
Smoking history	1.77 (0.44–7.08)	0.42
T stage	1.86 (1.02–3.41)	0.04
N stage	1.50 (0.92–2.44)	0.10
M stage	—	—
Risk score	9.51e+18 (752.28–1.20e+35)	0.02

Validation of the Expression Levels of Five ARGs in LUSC and Paracancerous Normal Tissues

To verify the reliability of the results, tumor and adjacent non-tumorous tissue specimens from 10 LUSC samples were collected to test the expression levels of the five ARGs by IHC. The representative images of IHC staining of A2M, CHEK2, FOS, PLAU, and ELN are shown in **Figures 9A–E**. We also obtained the IHC staining images of A2M, CHEK2, FOS, and PLAU from the Human Protein Atlas database (**Figures 9F–I**). We found that the IHC scores of the five ARGs in tumor tissues were higher than those in the normal lung tissues (**Figure 9J**).

DISCUSSION

In the current study, we investigated the relationship between the expression levels of ARGs and survival of LUSC patients, and established a novel prognostic ARG signature consisting of five ARGs, i.e., A2M, CHEK2, FOS, ELN, and PLAU. In the TCGA training dataset, multivariate Cox analysis further revealed the independent prognostic value of the ARG signature. Then a predictive nomogram integrating this ARG signature and the TNM staging system was developed for predicting individual prognosis, and we validated its prognostic accuracy in the GSE73403 validation cohort. Furthermore, we explored the relation between the ARG risk signature and immune cell infiltration in patients with LUSC.

With the accessibility of getting free data from the public TCGA and GEO databases, more and more studies focus on the relation between RNA-seq data of specific gene sets and individual outcomes (Wu et al., 2019; Qu et al., 2020; Zhu et al., 2020). These studies were limited to autophagy, immune infiltration, and so on, and they lacked clinical extension. Besides, studies about the prognostic role of ARGs in LUSC are rare. Biologically speaking, along with the decline of function, aging is spontaneous and inevitable (Shavlakadze et al., 2019). Pathophysiologically speaking, metabolic disorders, declining immune response, and malnutrition occur during the aging process, and are a risk factor of many chronic illnesses, such as cancer (Smetana et al., 2016; Lee and Schmitt, 2019). Aging may also promote occurrence, development, and metastasis of tumors (Johnson et al., 2013; Mosteiro et al., 2016; Galluzzi et al., 2018; Calcinotto et al., 2019; Lee and Schmitt, 2019). A previous study revealed that ARGs were associated with the prognosis of lung carcinoma (Xu and Chen, 2021). Understanding the association between the ARGs and LUSC is also necessary and meaningful.

The ARG risk score formula of this study indicated that a high level of plasminogen activator urokinase (PLAU) gene expression was mostly unfavorable for individualized survival. Belonging to the plasminogen activator family, PLAU is a protease which is involved in cell migration and adhesion by

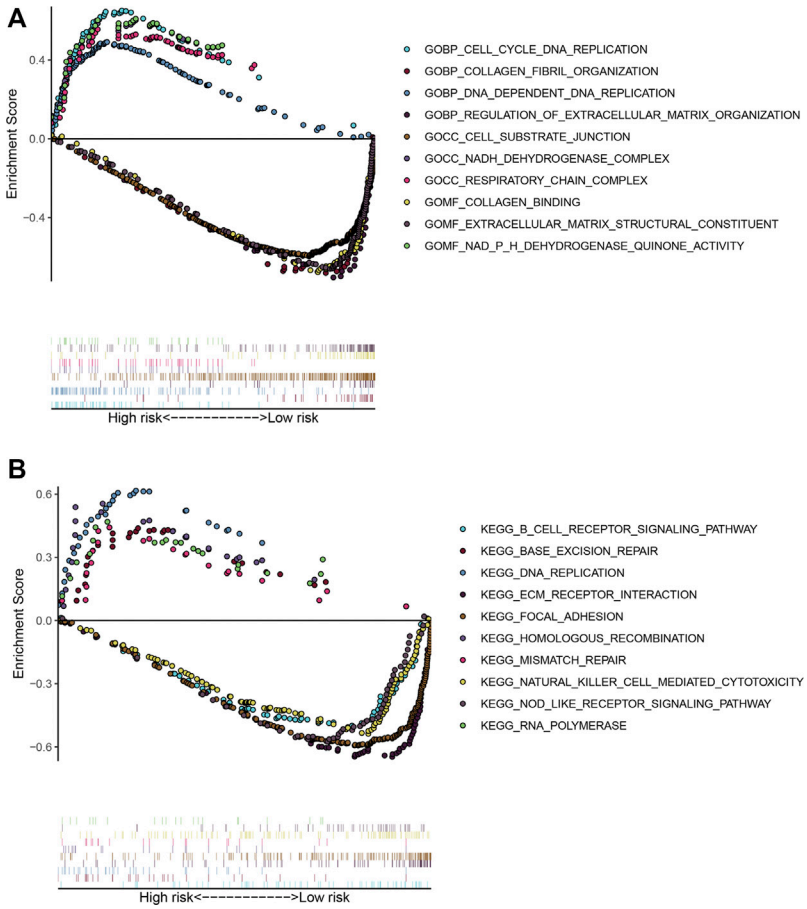


FIGURE 5 | Gene set enrichment analysis between the low- and high-risk subgroups. **(A)** Enriched GO terms between high- and low-risk groups. **(B)** Enriched KEGG pathways between high- and low-risk groups.

activating several signaling pathways. A previous study reported that PLAU was associated with immune cell infiltration in LUSC (Zhang et al., 2020). Elastin (ELN), a fibrous protein, provides characteristic elasticity properties in several tissues (Salesse et al., 2018) and aberrant expression of ELN was a risk factor for lung fibrotic diseases (Li et al., 2020). But the underlying mechanisms and function of ELN have not been exhaustively studied in LUSC. The expression product of the FOS gene is c-FOS protein, which can dimerize with JUN family proteins to regulate downstream gene expression and participate in proliferation, invasion, metastasis, angiogenesis, and apoptosis of tumors (Angel and Karin, 1991; Hennigan et al., 1994; Milde-Langosch, 2005). The overexpression of FOS was also related to poor survival outcomes of LUSC (Volm et al., 1993). The protein encoded by A2M is alpha-2-macroglobulin, which may promote tumor progression in mice (Kurz et al., 2018). A previous study revealed that A2M was a hub gene significantly associated with the occurrence and development of LUSC (Zhang et al., 2019). Checkpoint kinase two is a pluripotent kinase encoded by the CHEK2 gene, which is associated with DNA repair, cell cycle regulation, and causes apoptosis when DNA damage occurs (Wang et al., 2014). CHEK2 gene mutation is also a pathogenic mutation in lung cancer and increases susceptibility to lung cancer (Liu et al., 2020). IHC staining discovered that the four ARGs, A2M, ELN, FOS, and PLAU, were overexpressed in LUSC, which is consistent with our ARG signature. However, IHC staining revealed that CHEK2 was overexpressed in tumor tissues. The IHC images in the Human Protein Atlas also demonstrate that CHEK2 was overexpressed in tumor tissues. Therefore, the possible mechanism of CHEK2 in LUSC needs further study.

Cellular senescence can lead to cancer-related immune responses, and the immune cellular infiltration in the tumor microenvironment contributes to the response of immunotherapy (Zhao et al., 2015). However, the relationship between immune cellular infiltration and aging in LUSC is poorly known. In this study, we discovered that patients in the low-risk group had an apparent increase in $CD8^+$ T cell, activated $CD4^+$ memory T cell, follicular helper T cell, and M1 macrophage infiltration. Results of the CIBERSORT algorithm show a favorable immune status in the low-risk group, which is associated with

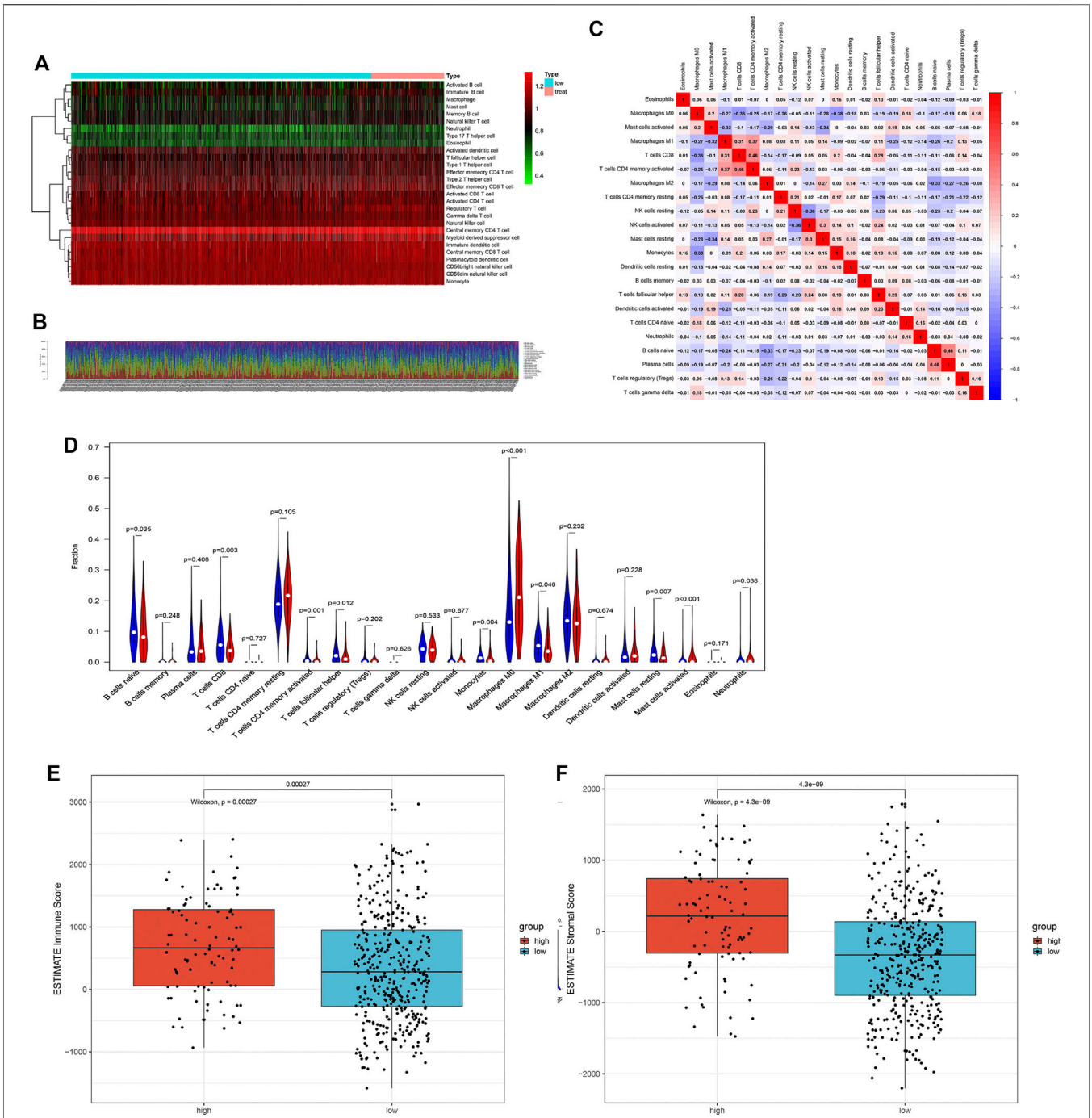


FIGURE 6 | The landscape of immune cell infiltration between the high- and low-risk groups in the TCGA training cohort. **(A)** Heatmap of the 28 tumor-infiltrating cell proportions in ssGSEA. **(B)** Barplot of 22 immune cell infiltrations in CIBERSORT. **(C)** Correlation matrix of the association between the expression level of the five ARGs and tumor-infiltrating immune cell infiltrations. **(D)** Violin plot showing differences of infiltrating immune cell types between the low- and the high-risk groups. **(E)** Expression of the immune score between the low- and the high-risk groups. **(F)** Expression of the stromal score between the low- and the high-risk groups.

prolonged survival (Sebestyen et al., 2020; Zhang et al., 2020). However, the results of the ESTIMATE algorithm showed that patients with high-risk had a higher immune score and stromal score and a higher expression level of PD-L2 and CTLA4, which indicated that patients with a high-risk score had a more complex tumor immune microenvironment and more immune cell infiltration, although the immune cell infiltration in high-risk tumors did not show an anti-tumor effect. These results suggested that the high-risk group had greater potential to benefit from immunotherapy. In addition, patients in the low-risk group

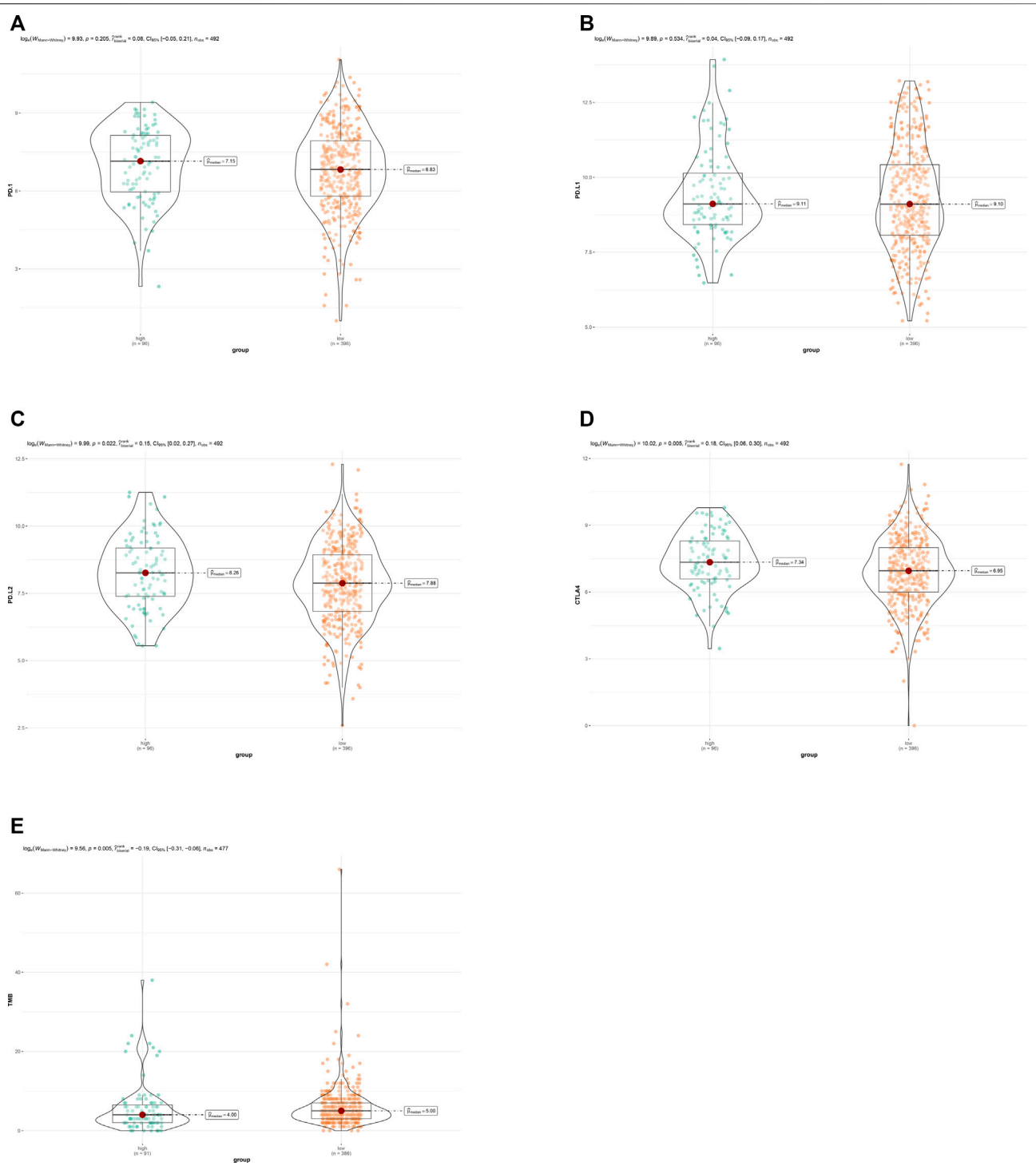


FIGURE 7 | (A) Expression of PD-1 between the low- and the high-risk groups. **(B)** Expression of PD-L1 between the low- and the high-risk groups. **(C)** Expression of PD-L2 between the low- and the high-risk groups. **(D)** Expression of CTL4 between the low- and the high-risk groups. **(E)** TMB between the low- and the high-risk groups.

had a higher TMB, which related to a poor prognosis in NSCLC (Devarakonda et al., 2018). The Checkmate 026 trial determined that NSCLC patients with TMB ≥10/MB could benefit from immunotherapy (Carbone, et al., 2017), given both risk groups had a TMB less than 10/MB, TMB in this study could not be used as a predictor of immunotherapy.

There remain some limitations in our study. Firstly, this ARG prognostic model was only established by bioinformatic analysis

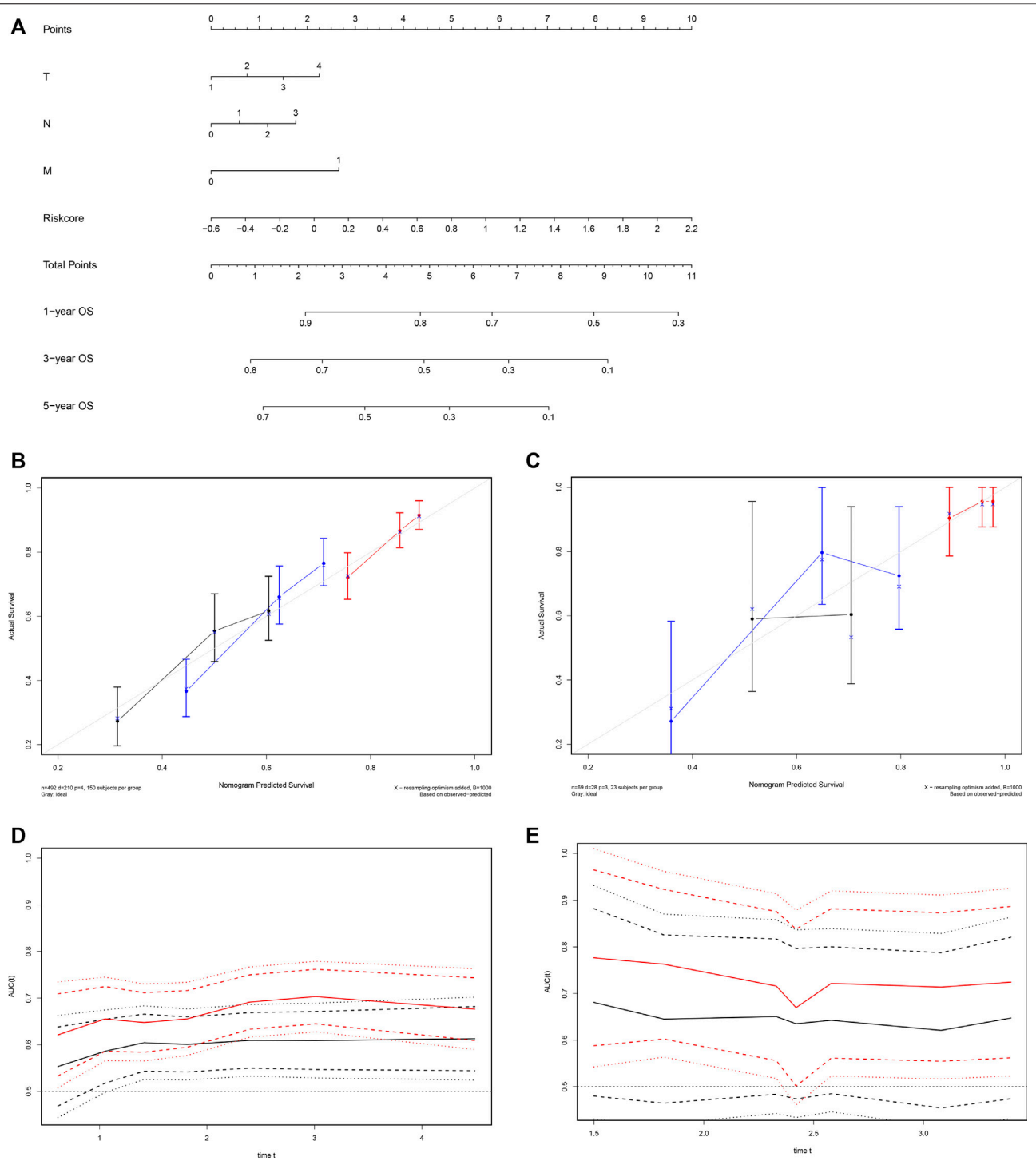


FIGURE 8 | Development of a nomogram based on the ARG signature for predicting overall survival of patients with LUSC. **(A)** The nomogram plot integrating ARG risk score and T-, N-, and M-classification in the TCGA training cohort. **(B)** The calibration plot for the probability of 1-, 3-, and 5 years OS in the TCGA training cohort; 1-year: red; 3 years: blue; 5 years: black. **(C)** The calibration plot for the probability of 1-, 3-, and 5 years OS in the GSE73403 validation cohort; 1 year: red; 3 years: blue; 5 years: black. **(D)** Time-dependent ROC curves comparing the prognostic accuracy of the risk score combining ARGs and the TNM system in the training cohort; risk score + TNM: red; TNM only: black. **(E)** Time-dependent ROC curves comparing the prognostic accuracy of the risk score combining ARGs and the TNM system in the validation cohort; risk score + TNM: red; TNM only: black.

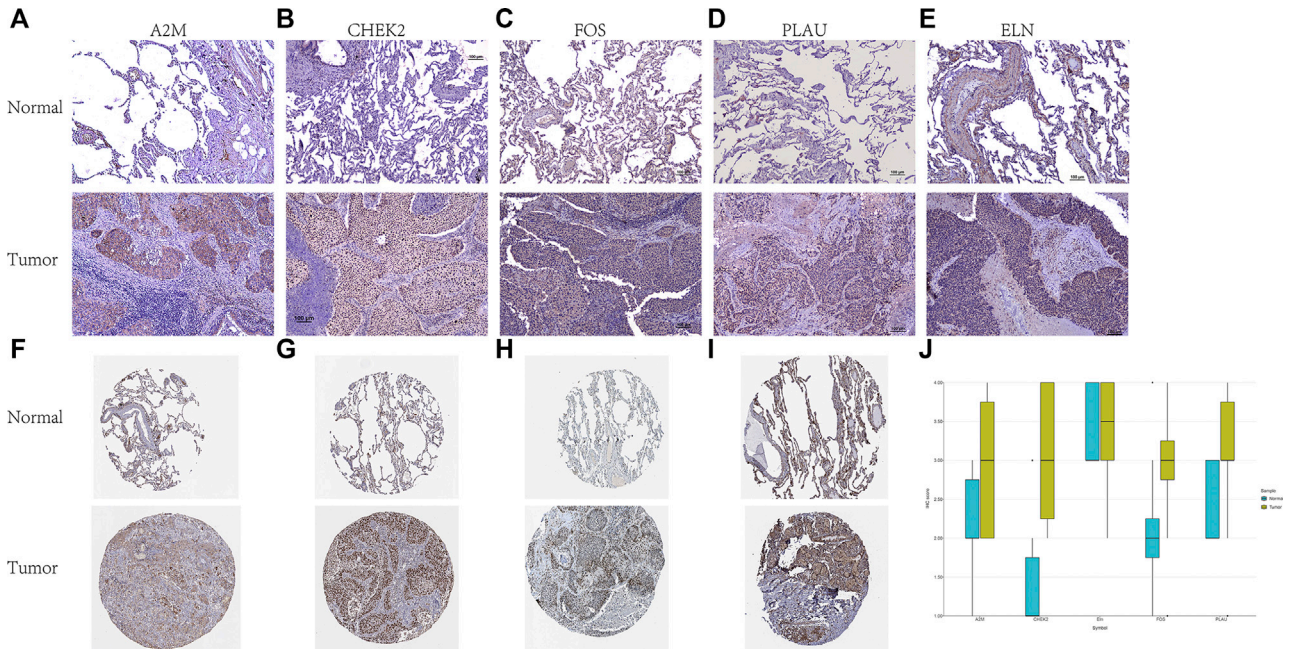


FIGURE 9 | The representative images of IHC staining of five ARGs from SYSUCC. **(A)** A2M; **(B)** CHEK2; **(C)** FOS; **(D)** PLAU; and **(E)** ELN. The representative images of IHC staining of four ARGs from Human Protein Atlas. **(F)** A2M; **(G)** CHEK2; **(H)** FOS; and **(I)** PLAU. **(J)** The IHC score of 5 ARGs.

from the public TCGA and GEO databases, results of this study need further validation from prospective, multicenter, or experimental data. Secondly, this study preliminarily explored the potential relationship between the ARG risk signature and anti-tumor immunity cell infiltration, studies are needed to reveal the underlying mechanisms by experimental data. Thirdly, although the ARG signature and TNM staging system were integrated in our prognostic nomogram, we cannot identify the contribution of each ARG in this signature.

In conclusion, the ARG risk score was associated with OS in patients with LUSC, we developed and validated a predictive nomogram for LUSC including the ARG risk signature and TNM staging system for predicting individual clinical prognosis. Moreover, we identified that patients with a high ARG risk score may have higher sensitivity to immunotherapy.

DATA AVAILABILITY STATEMENT

Publicly available datasets were analyzed in this study. This data can be found here: TCGA databases (https://tcga-data.nci.nih.gov/tcga/), GEO databases (https://www.ncbi.nlm.nih.gov/geo/) and Human Protein Atlas (https://www.proteinatlas.org/).

ETHICS STATEMENT

The studies involving human participants were reviewed and approved by The Institutional Review Board of the SYSUCC. Written informed consent for participation was not required for this study in accordance with the national legislation and the institutional requirements.

AUTHOR CONTRIBUTIONS

Author Contribution Conception and design: HL and Y-BL; provision of study materials or patients: W-YZ, F-FD, and SC; collection and assembly of data: J-YW, Z-RZ, Y-ZW, and B-YR; data analysis and interpretation: W-YZ, F-FD, and SC; manuscript writing and editing: W-YZ and F-FD; final approval of manuscript: All authors.

FUNDING

This work was supported by the Natural Science Foundation of Guangdong Province of China (Grant number: 2019A1515011601).

SUPPLEMENTARY MATERIAL

The Supplementary Material for this article can be found online at: https://www.frontiersin.org/articles/10.3389/fcell.2022.770550/full#supplementary-material

REFERENCES

Angel, P., and Karin, M. (1991). The Role of Jun, Fos and the AP-1 Complex in Cell-Proliferation and Transformation. *Biochim. Biophys. Acta* 1072 (2-3), 129–157. doi:10.1016/0304-419x(91)90011-9

Armanios, M., de Cabo, R., Mannick, J., Partridge, L., van Deursen, J., and Villeda, S. (2015). Translational Strategies in Aging and Age-Related Disease. *Nat. Med.* 21 (12), 1395–1399. doi:10.1038/nm.4004

Balachandran, V. P., Gonen, M., Smith, J. J., and DeMatteo, R. P. (2015). Nomograms in Oncology: More Than Meets the Eye. *Lancet Oncol.* 16 (4), e173–e180. doi:10.1038/nm.400410.1016/s1470-2045(14)71116-7

Benayoun, B. A., Pollina, E. A., Singh, P. P., Mahmoudi, S., Harel, I., Casey, K. M., et al. (2019). Remodeling of Epigenome and Transcriptome Landscapes with Aging in Mice Reveals Widespread Induction of Inflammatory Responses. *Genome Res.* 29 (4), 697–709. doi:10.1101/gr.240093.118

Calcinotto, A., Kohli, J., Zagato, E., Pellegrini, L., Demaria, M., and Alimonti, A. (2019). Cellular Senescence: Aging, Cancer, and Injury. *Physiol. Rev.* 99 (2), 1047–1078. doi:10.1152/physrev.00020.2018

Carbone, D. P., Reck, M., Paz-Ares, L., Creelan, B., Horn, L., Steins, M., et al. (2017). First-Line Nivolumab in Stage IV or Recurrent Non-small-cell Lung Cancer. *N. Engl. J. Med.* 376 (25), 2415–2426. doi:10.1056/NEJMoa1613493

Devarakonda, S., Rotolo, F., Tsao, M.-S., Lanc, I., Brambilla, E., Masood, A., et al. Tumor Mutation Burden as a Biomarker in Resected Non-small-cell Lung Cancer. *Jco* 36 (30), 2995–3006. doi:10.1200/jco.2018.78.1963

Galluzzi, L., Vitale, I., Aaronson, S. A., Abrams, J. M., Adam, D., Agostinis, P., et al. (2018). Molecular Mechanisms of Cell Death: Recommendations of the Nomenclature Committee on Cell Death 2018. *Cell Death Differ* 25 (3), 486–541. doi:10.1038/s41418-017-0012-4

havlakadze, T., Morris, M., Fang, J., Wang, S. X., Zhu, J., Zhou, W., et al. (2019). Age-Related Gene Expression Signature in Rats Demonstrate Early, Late, and Linear Transcriptional Changes from Multiple Tissues. *Cell Rep* 28 (12), 3263–3273.e3263. doi:10.1016/j.celrep.2019.08.043

He, S., and Sharpless, N. E. (2017). Senescence in Health and Disease. *Cell* 169 (6), 1000–1011. doi:10.1016/j.cell.2017.05.015

Hennigan, R. F., Hawker, K. L., and Ozanne, B. W. (1994). Fos-transformation Activates Genes Associated with Invasion. *Oncogene* 9 (12), 3591–3600.

Hothorn, T., and Zeileis, A. (2008). Generalized Maximally Selected Statistics. *Biometrics* 64 (4), 1263–1269. doi:10.1111/j.1541-0420.2008.00995.x

Johnson, S. C., Rabinovitch, P. S., and Kaeberlein, M. (2013). mTOR Is a Key Modulator of Ageing and Age-Related Disease. *Nature* 493 (7432), 338–345. doi:10.1038/nature11861

Kurz, S., Thieme, R., Amberg, R., Groth, M., Jahnke, H. G., Pieroh, P., et al. (2018). Correction: The Anti-tumorigenic Activity of A2M-A Lesson from the Naked Mole-Rat. *PloS one* 13 (3), e0195169. doi:10.1371/journal.pone.0195169

Lee, S., and Schmitt, C. A. (2019). The Dynamic Nature of Senescence in Cancer. *Nat. Cel Biol* 21 (1), 94–101. doi:10.1038/s41556-018-0249-2

Li, J., Xu, X., Jiang, Y., Hansbro, N. G., Hansbro, P. M., Xu, J., et al. (2020). Elastin Is a Key Factor of Tumor Development in Colorectal Cancer. *BMC cancer* 20 (1), 217. doi:10.1186/s12885-020-6686-x

Liu, M., Liu, X., Suo, P., Gong, Y., Qu, B., Peng, X., et al. (2020). The Contribution of Hereditary Cancer-Related Germline Mutations to Lung Cancer Susceptibility. *Transl Lung Cancer Res.* 9 (3), 646–658. doi:10.21037/tlcr-19-403

López-Otín, C., Blasco, M. A., Partridge, L., Serrano, M., and Kroemer, G. (2013). The Hallmarks of Aging. *Cell* 153 (6), 1194–1217. doi:10.1016/j.cell.2013.05.039

Mayakonda, A., and Koeffler, H. P. (2016). Maftools: Efficient Analysis, Visualization and Summarization of MAF Files from Large-Scale Cohort Based Cancer Studies. *bioRxiv*, 052662.

Milde-Langosch, K. (2005). The Fos Family of Transcription Factors and Their Role in Tumourigenesis. *Eur. J. Cancer* 41 (16), 2449–2461. doi:10.1016/j.ejca.2005.08.008

Mosteiro, L., Pantoja, C., Alcazar, N., Marión, R. M., Chondronasiou, D., Rovira, M., et al. (2016). Tissue Damage and Senescence Provide Critical Signals for Cellular Reprogramming *In Vivo*. *Science* 354, 6315. doi:10.1126/science.aaf4445

Newman, A. M., Liu, C. L., Green, M. R., Gentles, A. J., Feng, W., Xu, Y., et al. (2015). Robust Enumeration of Cell Subsets from Tissue Expression Profiles. *Nat. Methods* 12 (5), 453–457. doi:10.1038/nmeth.3337

Oberndorfer, F., and Müllauer, L. (2018). Molecular Pathology of Lung Cancer: Current Status and Perspectives. *Curr. Opin. Oncol.* 30 (2), 69–76. doi:10.1097/CCO.0000000000000429

Piperdi, B., Merla, A., and Perez-Soler, R. (2014). Targeting Angiogenesis in Squamous Non-small Cell Lung Cancer. *Drugs* 74 (4), 403–413. doi:10.1007/s40265-014-0182-z

Qu, Y., Cheng, B., Shao, N., Jia, Y., Song, Q., Tan, B., et al. (2020). Prognostic Value of Immune-Related Genes in the Tumor Microenvironment of Lung Adenocarcinoma and Lung Squamous Cell Carcinoma. *Aging* 12 (6), 4757–4777. doi:10.18632/aging.102871

Salesse, S., Odoul, L., Chazée, L., Garbar, C., Duca, L., Martiny, L., et al. (2018). Elastin Molecular Aging Promotes MDA - MB -231 Breast Cancer Cell Invasiveness. *FEBS open bio* 8 (9), 1395–1404. doi:10.1002/2211-5463.12455

Santarpia, M., Liguori, A., D'Aveni, A., Karachaliou, N., Gonzalez-Cao, M., Daffinà, M. G., et al. (2018). Liquid Biopsy for Lung Cancer Early Detection. *J. Thorac. Dis.* 10 (Suppl. 7), S882–s897. doi:10.21037/jtd.2018.03.81

Sebestyen, Z., Prinz, I., Déchanet-Merville, J., Silva-Santos, B., and Kuball, J. (2020). Translating Gammadelta (γδ) T Cells and Their Receptors into Cancer Cell Therapies. *Nat. Rev. Drug Discov.* 19 (3), 169–184. doi:10.1038/s41573-019-0038-z

Siegel, R. L., Miller, K. D., and Jemal, A. (2019). Cancer Statistics, 2019. *CA A. Cancer J. Clin.* 69 (1), 7–34. doi:10.3322/caac.21551

Smetana Jr., K., Jr., Lacina, L., Szabo, P., Dvořánková, B., Brož, P., and Šedo, A. (2016). Ageing as an Important Risk Factor for Cancer. *Ar* 36 (10), 5009–5018. doi:10.21873/anticanres.11069

Srivastava, S., and Gopal-Srivastava, R. (2002). Biomarkers in Cancer Screening: a Public Health Perspective. *J. Nutr.* 132 (8 Suppl. l)–2475Ss2475s. doi:10.1093/jn/132.8.2471S-

Subramanian, A., Tamayo, P., Mootha, V. K., Mukherjee, S., Ebert, B. L., Gillette, M. A., et al. (2005). Gene Set Enrichment Analysis: a Knowledge-Based Approach for Interpreting Genome-wide Expression Profiles. *Proc. Natl. Acad. Sci.* 102 (43), 15545–15550. doi:10.1073/pnas.0506580102

Sung, H., Ferlay, J., Siegel, R. L., Laversanne, M., Soerjomataram, I., Jemal, A., et al. (2021). Global Cancer Statistics 2020: GLOBOCAN Estimates of Incidence and Mortality Worldwide for 36 Cancers in 185 CountriesGLOBOCAN Estimates of Incidence and Mortality Worldwide for 36 Cancers in 185 Countries. *CA Cancer J. Clin.* 71 (3), 209–249. doi:10.3322/caac.21660

Tamborero, D., Rubio-Perez, C., Muiños, F., Sabarinathan, R., Piulats, J. M., Muntasell, A., et al. (2018). A Pan-Cancer Landscape of Interactions between Solid Tumors and Infiltrating Immune Cell Populations. *Clin. Cancer Res.* 24 (24), 3717–3728. doi:10.1158/1078-0432.CCR-17-3509

Travis, W. D., Brambilla, E., Nicholson, A. G., Yatabe, Y., Austin, J. H. M., Beasley, M. B., et al. (2015). The 2015 World Health Organization Classification of Lung Tumors. *J. Thorac. Oncol.* 10 (9), 1243–1260. doi:10.1097/JTO.0000000000000630

Volm, M., Drings, P., and Wodrich, W. (1993). Prognostic Significance of the Expression of C-Fos, C-Jun and C-erbB-1 Oncogene Products in Human Squamous Cell Lung Carcinomas. *J. Cancer Res. Clin. Oncol.* 119 (9), 507–510. doi:10.1007/BF01686458

Wang, Y., McKay, J. D., Rafnar, T., Wang, Z., Timofeeva, M. N., Broderick, P., et al. (2014). Rare Variants of Large Effect in BRCA2 and CHEK2 Affect Risk of Lung Cancer. *Nat. Genet.* 46 (7), 736–741. doi:10.1038/ng.3002

Wu, P., Wang, Y., Wu, Y., Jia, Z., Song, Y., and Liang, N. (2019). Expression and Prognostic Analyses of ITGA11, ITGB4 and ITGB8 in Human Non-small Cell Lung Cancer. *PeerJ* 7, e8299. doi:10.7717/peerj.8299

Xu, Q., and Chen, Y. (2021). An Aging-Related Gene Signature-Based Model for Risk Stratification and Prognosis Prediction in Lung Adenocarcinoma. *Front. Cel Dev. Biol.* 9, 685379. doi:10.3389/fcell.2021.685379

Yin, D., and Chen, K. (2005). The Essential Mechanisms of Aging: Irreparable Damage Accumulation of Biochemical Side-Reactions. *Exp. Gerontol.* 40 (6), 455–465. doi:10.1016/j.exger.2005.03.012

Yu, K.-H., Zhang, C., Berry, G. J., Altman, R. B., Ré, C., Rubin, D. L., et al. (2016). Predicting Non-small Cell Lung Cancer Prognosis by Fully Automated Microscopic Pathology Image Features. *Nat. Commun.* 7, 12474. doi:10.1038/ncomms12474

Yue, T., Chen, S., Zhu, J., Guo, S., Huang, Z., Wang, P., et al. (2021). The Aging-Related Risk Signature in Colorectal Cancer. *Aging* 13 (5), 7330–7349. doi:10.18632/aging.202589

Zhang, J., Zhang, J., Yuan, C., Luo, Y., Li, Y., Dai, P., et al. (2020). Establishment of the Prognostic index of Lung Squamous Cell Carcinoma Based on Immunogenomic Landscape Analysis. *Cancer Cel Int* 20, 330. doi:10.1186/s12935-020-01429-y

Zhang, N., Wang, H., Xie, Q., Cao, H., Wu, F., Di Wu, D. B., et al. (2019). Identification of Potential Diagnostic and Therapeutic Target Genes for Lung Squamous Cell Carcinoma. *Oncol. Lett.* 18 (1), 169–180. doi:10.3892/ol.2019.10300

Zhao, L., Zhang, Y., Gao, Y., Geng, P., Lu, Y., Liu, X., et al. (2015). JMJD3 Promotes SAHF Formation in Senescent WI38 Cells by Triggering an Interplay between Demethylation and Phosphorylation of RB Protein. *Cel Death Differ* 22 (10), 1630–1640. doi:10.1038/cdd.2015.6

Zhu, J., Wang, M., and Hu, D. (2020). Development of an Autophagy-Related Gene Prognostic Signature in Lung Adenocarcinoma and Lung Squamous Cell Carcinoma. *PeerJ* 8, e8288. doi:10.7717/peerj.8288

Conflict of Interest: The authors declare that the research was conducted in the absence of any commercial or financial relationships that could be construed as a potential conflict of interest.

Publisher's Note: All claims expressed in this article are solely those of the authors and do not necessarily represent those of their affiliated organizations, or those of the publisher, the editors and the reviewers. Any product that may be evaluated in this article, or claim that may be made by its manufacturer, is not guaranteed or endorsed by the publisher.

Copyright © 2022 Zhai, Duan, Chen, Wang, Zhao, Wang, Rao, Lin and Long. This is an open-access article distributed under the terms of the Creative Commons Attribution License (CC BY). The use, distribution or reproduction in other forums is permitted, provided the original author(s) and the copyright owner(s) are credited and that the original publication in this journal is cited, in accordance with accepted academic practice. No use, distribution or reproduction is permitted which does not comply with these terms.

frontiers in Oncology

REVIEW
published: 04 March 2022
doi: 10.3389/fonc.2022.841381

The Emerging Role of PRMT6 in Cancer

Zhixian Chen[1,2†], *Jianfeng Gan*[1,2†], *Zhi Wei*[1,2], *Mo Zhang*[1,2], *Yan Du*[1,2], *Congjian Xu*[1,2*] *and Hongbo Zhao*[1,2*]

[1] *Shanghai Key Laboratory of Female Reproductive Endocrine Related Diseases, Obstetrics and Gynecology Hospital, Fudan University, Shanghai, China,* [2] *Department of Obstetrics and Gynecology of Shanghai Medical School, Fudan University, Shanghai, China*

Protein arginine methyltransferase 6 (PRMT6) is a type I PRMT that is involved in epigenetic regulation of gene expression through methylating histone or non-histone proteins, and other processes such as alternative splicing, DNA repair, cell proliferation and senescence, and cell signaling. In addition, PRMT6 also plays different roles in various cancers *via* influencing cell growth, migration, invasion, apoptosis, and drug resistant, which make PRMT6 an anti-tumor therapeutic target for a variety of cancers. As a result, many PRMT6 inhibitors are being utilized to explore their efficacy as potential drugs for various cancers. In this review, we summarize the current knowledge on the function and structure of PRMT6. At the same time, we highlight the role of PRMT6 in different cancers, including the differentiation of its promotive or inhibitory effects and the underlying mechanisms. Apart from the above, current research progress and the potential mechanisms of PRMT6 behind them were also summarized.

Keywords: PRMT6, arginine methylation, cancers, regulation, PRMT6 inhibitors

OPEN ACCESS

Edited by:
Simona Kranjc Brezar, Institute of Oncology Ljubljana, Slovenia

Reviewed by:
Donghang Cheng, University of Texas MD Anderson Cancer Center, United States
Lin Shan, Capital Medical University, China

***Correspondence:**
Hongbo Zhao
zhaohongbo01@sina.com
Congjian Xu
xucongjian@gmail.com

†*These authors have contributed equally to this work*

Specialty section:
This article was submitted to Cancer Molecular Targets and Therapeutics, a section of the journal Frontiers in Oncology

Received: *22 December 2021*
Accepted: *09 February 2022*
Published: *04 March 2022*

Citation:
Chen Z, Gan J, Wei Z, Zhang M, Du Y, Xu C and Zhao H (2022) The Emerging Role of PRMT6 in Cancer. Front. Oncol. 12:841381. doi: 10.3389/fonc.2022.841381

INTRODUCTION

Epigenetic regulation includes modification of DNA or histones to affect gene expression and function through methylation, acetylation, phosphorylation, ubiquitination, and chromatin remodeling, while restoring complete DNA sequences. Therefore, epigenetic disorders have become a common mechanism in the occurrence and development of cancer (1). Arginine methylation was first reported in 1971 (2) and was viewed as a key epigenetic regulation of post-translational modification by adding methyl groups to nitrogen atoms of arginine residues in polypeptides, and participating in the regulation of various cellular processes, including splicing, transcription, translation, and signaling (3, 4). It changes the metabolic landscape of cells and further leads to cancer metastasis (5), DNA damage (6), and parasitic infection (7). But interests in the post-translational modification (PTM) did not expand until PRMT1 was cloned in the mid-1990s. Compared with other PTMs, the research progress of arginine methylation is relatively slow mainly due to the lack of reliable arginine-methyl antibodies and effective small-molecule inhibitors. In eukaryotes, there are three distinct forms of arginine methylation, monomethylarginines (MMAs), asymmetric dimethylarginines (ADMAs) and symmetric dimethylarginines (SDMAs). The production of larger and more hydrophobic residues during methylation may influence the interactions with other proteins or nucleic acids (8–10).

A large number of recent reports have confirmed that protein arginine methyltransferases (PRMTs) are a family of enzymes that methylate arginine residues of substrate proteins, and the main mechanism of PRMTs affecting cell activity is epigenetic regulation. Much of this activity can be attributed to their ability to methylate histone tails. However, at the same time, the PRMT family can also methylate non-histone proteins in transcription (11, 12). To sum up, the role of PRMT family can be reflected in many aspects, such as the major regulators of epigenetic-mediated gene expression, mRNA splicing, DNA damage responses, stem cell function, and immune responses (11, 13). PRMTs can be subdivided according to their methylation pattern: type I PRMTs (PRMT1, 2, 3, 4, 6 and 8) mainly catalyze the synthesis of MMA and ADMA; type II PRMTs (PRMT5 and PRMT9) catalyze the synthesis of MMA and SDMA; and type III PRMT (PRMT7) regulates monomethylation. There is another type IV PRMT that produces δ-NG-monomethylarginine in fungi (14, 15). PRMTs are recruited to target genes by transcription factors and act as a part of multicomponent transcription complexes. Although cancer-related mutations in PRMTs are uncommon, PRMTs expression levels are usually elevated in patients and are associated with poor prognosis (16, 17). These findings have led to a widespread interest in PRMTs as new cancer drug targets.

Protein arginine methyltransferase 6 (PRMT6) is a type I PRMT that asymmetrically dimethylates protein substrates on arginine residues and has functions in epigenetic regulation of gene expression (18–21), alternative splicing (13, 22), development and differentiation (23–25), DNA repair (26), cell proliferation and senescence (27–29), DNA methylation (30), mitosis (31, 32), inflammation (33–35), congenital antiviral immunity (36), spermatogenesis (37), transactivation of nuclear receptors (13, 38) and cell signaling (39, 40). In addition, the dysregulation of PRMT6 is also associated with viral diseases (41, 42), cancer (43) and cardiac dystrophy (44). At the same time, PRMT6 plays a role in a variety of hitherto unidentified cellular functions (45). PRMT6 is predominantly located in the nucleus, in sharp contrast to PRMT3 and PRMT5, which are predominantly present in the cytoplasm. Other members of the PRMT family are present in both the nucleus and cytosol. PRMT6 is expressed in a variety of tissues, and significantly increased in kidney and testes (21). Moreover, it also exists in regulatory DNA regions of important cell cycle regulators such as CDKN1A, CDKN1B, CDKN2A and p53, thus acts as a transcription inhibitor in these regions (28, 29, 46, 47). It produces asymmetric dimethylation in histone 3 at arginine 2, arginine 17, arginine 42 (H3R2me2a, H3R17me2a, and H3R42me2a) (18–20, 48, 49), arginine 26 (H2AR26me2a) (50) and is involved in epigenetic regulation of gene expression. In addition, PRMT6 can methylate a variety of non-histone proteins and regulate a variety of biological functions.

Since PRMT6 was identified more than 20 years ago, many studies have been performed to identify the characteristics and molecular functions of PRMT6 in cancer (**Figure 1**). Asymmetric dimethylation of histone H3 at arginine 2 (H3R2me2a) was catalyzed by protein arginine methyltransferase 6 (PRMT6). PRMT6-dependent H3R2me2a can be detected on active genes at promoters and enhancer sites. That is, PRMT6 interferes with the deposition of adjacent histone markers through H3R2me2a and regulates the activity of important differentiation-related genes through reverse transcriptional effects. Depending on its genomic location, H3R2me2a can exhibit either inhibitory or activating properties: transcriptional inhibition at promoters and transcriptional activation at enhancers, respectively. Therefore, PRMT6 can promote or inhibit cancer development, and its effect is not single and fixed (51). For example, PRMT6 knockdown can significantly inhibit the growth of bladder cancer and lung cancer cells (43). In addition, PRMT6 knockdown results in upregulation of tumor suppressor genes p21 and p27 (28, 29, 46). Therefore, PRMT6 promotes cell growth and prevents senescence, thus becoming an anti-tumor therapeutic target for various types of cancer. Furthermore, PRMT6 is involved in regulating gene expression of TSP-1, a potent natural inhibitor of angiogenesis (52, 53), RUNX1, a group of target genes involved in hematopoietic stem/progenitor cell differentiation (54), and genes participated in maintaining embryonic stem cell characteristics (24). In addition, studies have confirmed that PRMT6 is involved in regulating drug resistance of tumor cells. $p21^{CDKN1A}$, as an effective inhibitor of cyclin-dependent kinase (CDK), regulates the cell cycle in a p53-dependent manner in response to a variety of stimuli, including DNA damage. PRMT6 methylates p21 at arginine 156 and promotes phosphorylation of threonine 145 on p21, resulting in the increased cytoplasmic localization of p21. The cytoplasmic presence of p21 makes cancer cells more resistant to cytotoxic drugs (55). PRMT6 can also act as a limiting factor of viral replication, acting on the pathogenesis of human immunodeficiency virus through methylation of TAT and other HIV proteins (41). In this review, we will summarize some recent studies on PRMT family, and focus on the different roles of PRMT6 in tumor. We will also note that PRMT6 is a potential target for cancer therapy.

TUMOR PROMOTING ROLES OF PRMT6 IN CANCERS

Endometrial Cancer

Endometrial carcinoma (EMC) ranks the fourth most frequently diagnosed cancer among women. In 2020, 130,051 newly diagnosed cases and 29,963 EMC-related deaths were estimated (56). *In vitro* and *in vivo* studies showed that PRMT6 was up-regulated at mRNA and protein levels in EMC. PRMT6 exerts carcinogenic activity by activating the AKT/mTOR pathway, promoting cell proliferation and migration in EMC. Data showed that the expression of PRMT6 in EMC was controlled by miR-372-3p, which targeted the 3'UTR of PRMT6 promoter to inhibit its expression. Down-regulation of miR-372-3p and its inhibitory effect on proliferation and migration of endometrial cancer cells have been reported (57). MiR-372-3p functions through the AKT/mTOR pathway, studies have shown that PHLPP2 was the

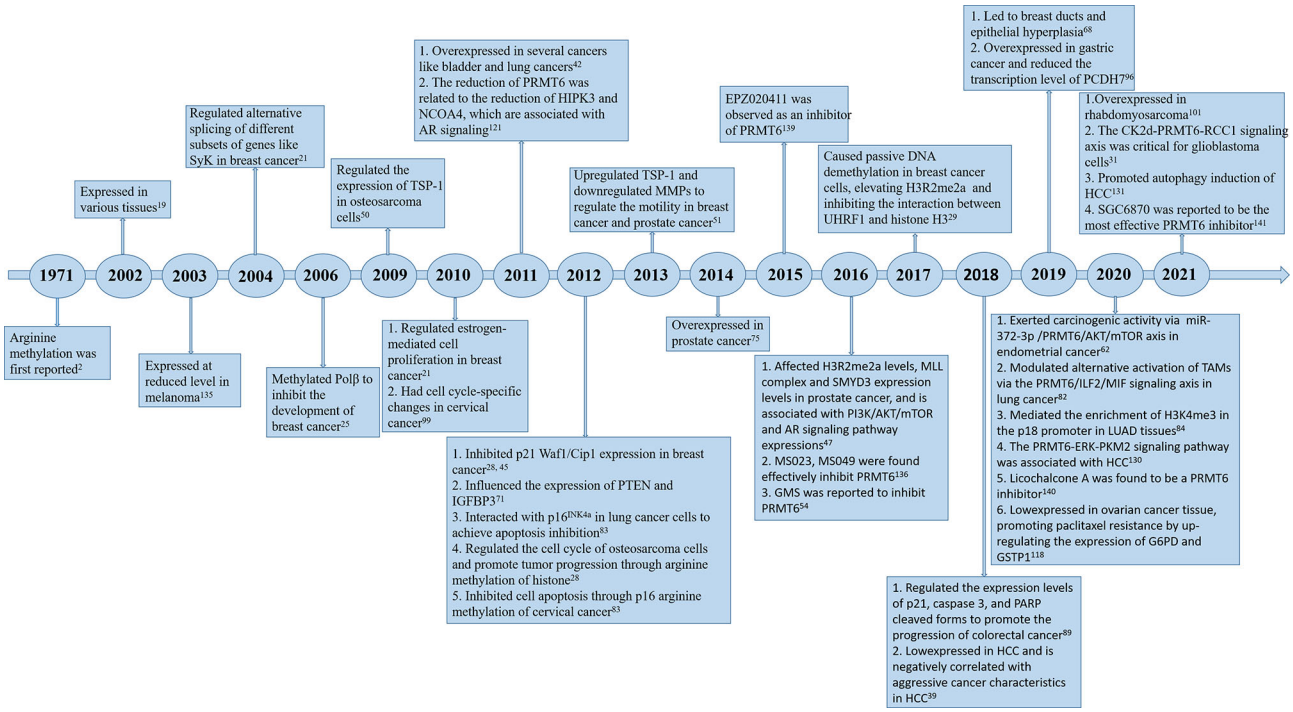


FIGURE 1 | Timeline of *PRMT6* research. A brief history of functional and pharmacological studies of PRMT6.

theoretical target gene of miR-372. PHLPP2 belongs to a novel Ser/Thr protein phosphatase family that negatively regulates AKT, PKC, MAPK, and Mst1-activated signaling pathways and plays a central role in maintaining cell survival inhibition. This was confirmed by the fact that miR-372 gene knockout inhibited the phosphorylation levels of major components of the PI3k/AKT pathway, including AKT, mTOR, and P70S6K (58). Therefore, it can be inferred that miR-372-3p/PRMT6/AKT/mTOR axis can serve as both a prognostic factor and therapeutic target for EMC (59).

Breast Cancer

Breast cancer is one of the most widespread invasive cancers, accounting for 25-30% of new cancers in women, ~15% of cancer-related deaths in women, and ~6.5% of all cancer-related deaths (60). In previous studies on the relationship between PRMTs family and breast cancer, PRMT1 is verified overexpressed in breast cancer tumor samples, and its expression degree is related to tumor grade (43, 61). Meanwhile, CARM1 was found to methylate a large number of proteins with a variety of biological functions, including regulation of intracellular estrogen receptor-mediated signaling, chromatin organization and chromatin remodeling. CARM1 can recruit the coactivator protein tumor-domain-containing protein 3 (TDRD3) to its binding enhancer through hypermethylation of these proteins to activate the estrogen/ERα-target genes. Therefore, CARM1 can promote the proliferation of ERα -positive breast cancer cells and tumor growth in mice *in vivo* (62). PRMT1 is also overexpressed in breast cancer tumor samples, and its expression degree is related to tumor grade (43, 61).

Since the role of CARM1 in estrogen-dependent breast cancer was confirmed (62), PRMT6-siRNA-1 assay showed that PRMT6 also played a role in estrogen signaling, and the survival rate of MCF-7 cells was significantly reduced, participating in estrogen-stimulated ERα-expressing breast cancer cell proliferation (13). Since PRMT6 and CARM1 can play a synergistic role in estrogen signal transduction, when they are knocked out together, a synergistic effect is observed in the regulation of estrogen-induced proliferation (13). PRMT6 has also been shown to regulate alternative splicing of different subsets of genes in MCF-7 cells in hormone-independent way. For example, in VEGF genes, whilst reduction of PRMT6 transcription increases the ratio of VEGF189 to VEGF165 by more than 2 times. In Syk genes, PRMT6 knockout will lead to a significant increase in the ratio of Syk [L]: Syk [S] (22). Therefore, it can be concluded that PRMT6 is an essential component of estrogen signaling pathway in breast cancer cells. In addition to regulating transcription initiation in estrogen signaling pathway, it can also affect various aspects of RNA progression, especially alternative splicing (13). Meanwhile, PRMT6 negatively regulates DNA methylation, and the upregulation of PRMT6 contributes to global DNA hypomethylation in cancer. Depletion or inhibition of PRMT6 could restore global DNA methylation of MCF7 cells. Mechanistically, PRMT6 overexpression impairs chromatin binding of UHRF1, a cofactor of DNMT1, leading to passive DNA demethylation. This effect may be due to

elevated H3R2me2a, which inhibits the interaction between UHRF1 and histone H3 (30). PRMT6 can also directly inhibit the p21 promotor. PRMT6 gene knock-down (KD) results in a p21 derepression in breast cancer cells, which is p53-independent, and leads to cell cycle arrest, cellular senescence and reduced growth in soft agar assays, and severe combined immune deficiency (SCID). Bypassing the p21-mediated arrest rescues PRMT6 KD cells from senescence and restores their ability to grow on soft agar. And it directly inhibits p21 Waf1/Cip1 expression by targeting the promoter gene region (29, 46). It has also been found that K5-driven conditional overexpression of PRMT1, CARM1 and PRMT6 leads to breast ducts and epithelial hyperplasia to varying degrees at different time points. In the context of Neu-induced carcinogenesis, overexpression of PRMT1 and PRMT6 significantly accelerated breast tumor onset, while CARM1 increased tumor progression only at tumorigenesis. These results suggest that all three type I PRMTs have carcinogenic activity that predisposed mouse mammary gland to tumorigenesis, and support the targeting of these PRMTs for breast cancer patients (63). PRMT6 methylation of H3R2 promotes transcriptional inhibition of HoxA10 (52), a protein whose upregulation promotes increased p53 expression and reduced invasive potential in breast cancer (64).

In addition, Affymetrixexon microarray (Santa Clara, CA) was used to demonstrate that PRMT6-dependent gene signature influences long-term survival in breast cancer patients, which included (i) reduced level of the tumor inhibition, PTEN in breast cancer patient samples and increased PTEN mRNA expression after loss of PRMT6 in breast cancer cells, and (ii) differential splicing of genes involved in centrosome targeting, cell invasion, apoptosis, p21-interacting proteins, and other genes which involved in cell cycle regulation. In addition, they demonstrated that abnormal expression of PRMT6 and PRMT6-dependent gene signature is associated with poorer clinical prognosis in patients with ER+ breast cancer (22). Experiments have also observed that PRMT6 mRNA expression level in the invasive ductal carcinoma (IDC) breast cancer is significantly lower than that in normal breast tissues. When PRMT6 is knocked down in the MCF-7 cell lines, the expressions of PTEN and IGFBP3 are increased. PTEN is a tumor suppressor gene that inhibits the PI3K pathway (65). Loss of PTEN leads to the activation of many kinases and subsequent cell cycle progression (66), and IGFBP3 has an anti-proliferative effect and induces apoptosis of breast cancer cells (67). This suggests that lower PRMT6 expression may lead to increased expressions of PTEN and IGFBP3, decreased cell cycle progression and increased apoptosis of breast cancer cells (22). Therefore, PRMT6 plays an essential role on the development, metastasis, treatment, drug resistance and many other aspects of breast cancer.

Prostate Cancer

Prostate cancer (PCa) is the fourth most frequently diagnosed malignant tumor in men and the second leading cause of cancer-related mortality worldwide which just behind lung cancer (56). Because intracellular CARM1 levels are important for estrogen and androgen receptor signaling, it has previously been shown to be altered in breast and prostate cancer tissues (68, 69). PRMT6 was also found to be overexpressed in prostate tumor tissue, which was distinguishable from normal prostate tissue (70). Overexpression at the transcription and protein levels was associated with poorer disease-free survival in PCa, suggesting a carcinogenic effect. Stable PRMT6 knockdown attenuated the malignant phenotype in PC-3. At the molecular level, PRMT6 silencing was associated with decreased H3R2me2a levels and increased expression of the MLL complex and SMYD3. PRMT6 silencing increased p21, p27 and CD44, decreased the expression of MMP-9, which was associated with downregulation of PI3K/AKT/mTOR and increased androgen receptor (AR) signaling pathway (71). The potential clinical relevance of restoring AR expression in Sh-PRMT6 PC-3 suggests that PRMT6 inhibition may re-sensitize androgen-insensitive tumor cells to ADT, providing a new approach for the treatment of castration-resistant prostate cancer (CRPC) (71).

Lung Cancer

Lung cancer is the leading cause of cancer-related deaths worldwide (18% of the total cancer deaths) with an estimated 1.6 million deaths each year and imposes a heavy burden on health care system (56, 72). Previous studies have proved that PRMT1, PRMT5 and PRMT7 in the PRMT family are all highly expressed in lung cancer tissues (43, 73–76). It was confirmed that PRMT6 is upregulated in lung cancer and can promote the growth of tumor cells (43). Depletion of PRMT6 can reduce cell proliferation, cell migration and anchorage-independent growth of NSCLC cells. There is a protein-protein interaction (PPI) between PRMT6 and interleukin-enhancer binding protein 2 (ILF2), and the PRMT6-ILF2 signaling axis is a novel regulator of macrophage migration inhibitor factor (MIF). Therefore, PRMT6 promotes lung tumor progression by modulating the alternate activation of tumor-associated macrophages (TAMs). Targeting the newly identified PRMT6/ILF2/MIF axis may open new possibilities for lung cancer intervention (77). PRMT6 can also interact with p16, overexpression of PRMT6 can counteract the cell cycle arrest at G1 phase caused by p16 in NSCLC A549 cells and decrease the association intensity of p16-CDK4, suggesting that PRMT6 probably achieves its cell apoptosis restraint role in NSCLC through p16 arginine methylation and provide a new idea for NSCLC treatment (78). Besides, it was also found that PRMT6 gene knockdown can significantly increase the enrichment of H3K4me3 in the p18 promoter in lung adenocarcinoma (LUAD) tissues, which leads to upregulation of p18, thus mediating G1/S phase cell cycle arrest and inhibiting the proliferation of LUAD cells *in vitro* and *in vivo*. This negative correlation between PRMT6 and p18 suggests that p18 may be a downstream target of PRMT6, which acts as an oncogene in the disease and epigenetically inhibits the expression of p18 and interferes with G1/S phase transition of LUAD cells (79). In terms of treatment, a study has identified the combination of PARP inhibitors and type I PRMT inhibitors offers new therapeutic opportunities for MTAP-negative NSCLC and cancers that are resistant to PARP inhibitors (80).

Colorectal Cancer

Colorectal cancer (CRC) is one of the most commonly diagnosed cancers in the world and a leading cause of cancer death, among men, colorectal cancer ranks third in both incidence and mortality (56). Previously, overexpression of three major types of type I PRMTs has been observed in CRC, including PRMT1 (81) and CARM1 (82, 83). PRMT6 is observed up-regulated in CRC tissues, its activity plays a key role in tumor cell differentiation. PRMT6 gene knockdown (KD) promotes CRC cells apoptosis by upregulating the tumor suppressor p21 protein in CRC cells. It also increases the expression of the cleavage forms of caspase 3 and PARP, thereby inhibiting the growth and colony formation of CRC cell lines, which indicated that PRMT6 played an important role in promoting the proliferation and progression of CRC (84). Recently, the protein arginine methyl transferase (PRMT) type 1 inhibitor MS023 was found to be an effective inducer of alkaline phosphatase (ALP) activity promoting cell differentiation phenotype, significantly delaying the growth of CRC cells. Therefore, it was selected as a probe with the potential to modulate the CRC phenotype. PRMT1 has been confirmed as a target of MS023, and PRMT6, as a member of type 1 PRMT family, is also promising as a new anticancer target (85).

Osteosarcomas

Osteosarcoma is the most common malignant primary bone tumor in children and adolescents, characterized by the formation of immature bone or osteoid tissue from the sarcoma cells that develop mainly in the long bones (86, 87). It has been confirmed that overexpression of CARM1 in the PRMT family promotes human osteosarcoma cell proliferation through the PGSK3β/β -catenin/cyclin D1 signaling pathway (88). In PRMT6-deficient osteosarcoma cells U2OS cells, the expression of TSP-1 gene promoter was increased and the loss of H3R2me2a and the corresponding increase of H3K4me3 were observed at the TSP-1 promoter, inhibiting the migration of U2OS cells. These results suggest that PRMT6 regulates the expression of TSP-1 in osteosarcoma cells by regulating epigenetic markers at the TSP-1 promoter level (52). It has been found that down-regulation of PRMT6 leads to up-regulation of p21 and p27, two members of the cyclin-dependent kinase (CDK) inhibitor CIP/KIP family, and accumulation of human osteosarcoma cell line U2OS at the G2 checkpoint. PRMT6 also involves the methylation of arginine-2 of histone H3, so PRMT6 can regulate the cell cycle of osteosarcoma cells and promote tumor progression through arginine methylation of histone (29).

Bladder Cancer

As one of the most common malignant tumors of the urinary system, bladder cancer (BCa) ranks tenth with high morbidity and mortality worldwide, with approximately 573,000 new cases and 213,000 deaths (56). It was found that PRMT1 and PRMT6 were significantly upregulated in bladder tumor tissues. When PRMT1 and PRMT6 genes were knocked down, the growth of bladder cancer cell lines (SW780 and RT4) was significantly inhibited, and the cells in the S phase were significantly reduced, while those in G0 and G1 phases were increased simultaneously. These results indicated that PRMT1 and PRMT6 play an important role in the G1-S transformation of bladder cancer cells. Meanwhile, real-time quantitative RT-PCR analysis of gene microarray data suggested that PRMT1 and PRMT6 could lead to the carcinogenesis of bladder cancer by regulating RNA processing and DNA replication. Therefore, PRMT1 and PRMT6 may be a promising target for bladder cancer therapy, and their inhibitors may be ideal candidates for molecular targeted therapy of bladder cancer (43).

Gastric Cancer

Gastric cancer (GC) is the fifth most commonly diagnosed cancer type and the third leading cause of cancer-related deaths, with more than 1 million new cases diagnosed and more than 780,000 deaths per year (8.2% of all cancer deaths) (56). In the studies on the effect of PRMT family on GC, it was previously concluded that PRMT5 (89) and PRMT8 (90) expressions were both significantly increased in GC tissues, and were both significantly correlated with the short-term survival rate of GC patients. It was also found that the expression level of PRMT6 in GC was significantly higher than that in non-cancer tissues, and overexpression of PRMT6 enhanced the aggressiveness of gastric cancer cells and increased the expression level of H3R2me2a in GC cells through the direct pathway of transcriptional inhibition of tumor suppressor gene procadherin 7 (PCDH7), and the expression level of H3R2me2a was an independent prognostic indicator of GC. Therefore, PRMT6 may have carcinogenic properties, and its overexpression may contribute to GC progression and become a new therapeutic target for GC (91).

Cervical Cancer

Cervical cancer (CC) is a serious and common gynecological malignant tumor disease located in the cervix, with high morbidity and mortality. In recent years, the age of onset is gradually younger, and the incidence is on the rise (92). Previous studies have shown that PRMT5, a type II PRMT, is highly expressed in cervical cancer, and arginine methyltransferase inhibitor 1 (AMI-1) can inhibit solid tumors of cervical cancer by targeting PRMT5 (93). At the same time, PRMT8 expression was also observed to be elevated in cervical cancer (90). It was found that the level of PRMT6 was upregulated from G0/G1 to G1 phases in HeLa cells and recovered to the level of G1 phase after the M phase. Meanwhile, aDMA-methylated 64kDA CstF-64, which is involved in mRNA metabolism, 80kDa hnRNPR and their 68kDa subfamily, which are involved in post-transcriptional processing of mRNA, and 25 kDa TPI regulating glycolysis and gluconiogenesis were also upregulated in G0/G1 phase, suggesting that PRMT6 has cell cycle-specific changes in cervical cancer cells and is most likely to modulate the cellular growth and proliferation during HeLa cell cycle (94). In HeLa cells, PRMT6 can also interact with p16 to methylate it and reduce the association of p16 and CDK4, suggesting that PRMT6 inhibits cell apoptosis through p16 arginine methylation, which

also makes p16-associated gene therapy for cervical cancer a possible new strategy (78).

Rhabdomyosarcoma

Rhabdomyosarcoma (RMS) is a rare malignancy neoplasm that originates in the mesenchyme or neuroectoderm, which is arisen from skeletal muscle progenitor cells. Despite its low incidence (4.5 cases per million children), it is the most common soft tissue sarcoma in children, nearly 20% of patients presenting with locally aggressive and/or metastatic disease (95). The expression of PRMT1, CARM1, PRMT5, PRMT7, PRMT8 and PRMT9 were all elevated in rhabdomyosarcoma (96), CARM1 and its direct interaction with histone acetyltransferase PCAF jointly were also detected to exert an increased expression of myogenin gene and lead to rhabdomyosarcoma cell differentiation (9). It was observed that the expression of gene encoding PRMT6 was increased in rhabdomyosarcoma cell lines, and PRMT inhibitors (AMI-1 and SAH) effectively reduced the invasive phenotype of RMS cells by inhibiting the proliferation rate, cell viability and colony formation ability of rhabdomyosarcoma cell lines. These inhibitors also attenuate the activity of the PI3K-Akt signaling pathway, resulting in decreased levels of cyclin D1 and Bcl-xL and increased level of GADD45G protein, thus halting the cell cycle and promoting apoptosis (96). Therefore, PRMT6 is expected to be a new therapeutic target for rhabdomyosarcoma.

Others

The tumor-promoting effect of PRMT6 is also seen in other systems, such as the blood system, and can be seen in leukemia. Leukaemias are commonly divided into chronic or acute leukaemias and as lymphocytic or myelogenous leukaemias; the subtypes include chronic lymphocytic leukemia (CLL), chronic myeloid leukemia (CML), acute myeloid leukemia (AML), and acute lymphocytic leukemia (ALL) among others (97). More and more evidences show that PRMT family plays an important role in malignant hematopoiesis. PRMT1 has been found to interact with AML1-ETO, which acts as an oncogenic transcription factor and occurs in 15% of *de novo* AML cases, and methylate its fusion protein, thereby promoting transcriptional activation and self-renewal capability (98). PRMT1 can also collaborate with some MLL fusion proteins in MLL leukemia, and the enzyme activity of PRMT1 has been shown to be critical for MLL-mediated transformation (99–101). It has also been found that increased activity of PRMT5 promoted the growth of AML *in vitro* and *in vivo*, while downregulation of PRMT5 decreased the growth of AML (102), and elevated levels of PRMT5 in some leukemia and lymphoma cells lead to H3R8 and H4R3 hypermethylation and transcriptional silencing in promoter regions of the RB tumor suppressor family, which suggest that PRMTs can regulate the expression of miRNAs (103). It was also found that N1-(2-((2-chlorophenyl)thio)benzyl) -N1-methylethane-1,2-diamine (28d, DCPR049_12), a highly potent inhibitor of type I PRMTs, effectively inhibited cell proliferation and reduced asymmetric arginine dimethylation levels in several leukemia cell lines. 28d, as a potent inhibitor, demonstrates the cell killing mechanisms in both cell cycle arrest and apoptotic effects as well as downregulation of the pivotal mixed lineage leukemia (MLL) fusion target genes such as HOXA9 and MEIS1, reflecting the critical roles of type I PRMTs in MLL leukemia (104). It was also found that the transcriptional co-repressors PRMT5 and PRMT6 were overexpressed in hematocarcinoma and inhibited the expression level of tumor suppressor genes (5).

This effect has also been seen in brain tumors such as glioblastoma. Gliomas are the most common malignant tumors of the central nervous system with high intra- and inter-tumor heterogeneity, and the most destructive form of glioma is grade IV astrocytoma, known as glioblastoma (GBM) (105). It has been found that abnormal expression of PRMT is associated with the development of brain tumors such as glioblastoma and medulloblastoma, for example, PRMT1 (106) is known as a contributor to the development of GBM, PRMT2 is also speculated to be involved in the pathogenesis of GBM by promoting cell stemness (107), CARM1/PRMT4 can also regulate the production of miR-17-92a, thus affecting the differentiation and production of neuronal and glial cells (108), PRMT8 depletion can increase cellular markers associated with gliomagenesis (109), the increased expression of PRMT5 has also been implicated in tumorigenesis and is associated with worse GBM prognosis (110). PRMT6 and subunits of polycomb repressor complexes 1 and 2 bind regulatory regions of HOXA genes were found to affect neuronal differentiation (111). PRMT6 was also found to promote RCC1 chromatin association, thereby enhancing the mitotic activity of GBM cells, while casein kinase 2α (CK2α) phosphorylates and stabilizes PRMT6. The CK2α-PRMT6-RCC1 signaling axis is critical for GBM cell mitosis. Inhibition of PRMT6 can reduce the tumogenesis of GBM cells and enhance the cytotoxic activity of radiotherapy (RT) (32).

TUMOR SUPPRESSIVE ROLES OF PRMT6 IN CANCERS

Ovarian Cancer

Ovarian cancer is a malignant tumor only found in female reproductive system, with high morbidity and mortality, the most dominant pathological subtype is epithelial OC, including five major tissue types, differ in origin, pathogenesis, molecular changes, risk factors, and prognosis (112).. Previous studies have found that in the PRMT family, the expression level of PRMT8 in ovarian cancer is significantly increased and is associated with increased survival rate of patients (90). Compared with normal ovarian tissues, PRMT6 mRNA expression levels were decreased, while glucose-6-phosphate dehydrogenase (G6PD) and glutathione S-transferase P1 (GSTP1) protein expression levels were significantly up-regulated, and the three changes were correlated with each other. GSTP1 can detoxify several anticancer drugs and mediate specific S-glutathionylation of ER-resident proteins to induce chemotherapy resistance in tumors and stress response, suggesting that the decrease of PRMT6 expression and subsequent increase of G6PD expression give ovarian cancer cells resistance to paclitaxel by

regulating GSTP1 expression. These results suggest that PRMT6 may be a new potential target for overcoming paclitaxel resistance in ovarian cancer (113).

Breast Cancer: Invasive Ductal Carcinoma

Experiments have shown that the reduction of PRMT6 in the MCF-7 and T47D ER+ cell lines leads to the reduction of HIPK3 and NCOA4, two transcriptional co-activators originally associated with androgen receptor (AR) signaling. This suggests that in addition to the co-activation of steroid hormone-dependent genes, PRMT6 is also involved in the expression of genes that promote steroid hormone signaling. Interestingly, AR signaling in ER+ breast cancer is thought to be associated with favorable prognosis (114, 115), and the reduction of HIPK3 and NCOA4 may negatively affect AR signaling and ER+ breast cancer prognosis. Conversely, the reduction of the NCOA4 full-length isoform in MCF-7 cells was associated with increased breast cancer metastasis (116), while NCOA4 knockdown in MCF-7 cells led to reduced cell proliferation (117). Therefore, the exact role NCOA4 plays in breast cancer is not fully established and requires further research (22). PRMT6 was observed overexpressed in breast cancer MCF7 cell lines, while the levels of thrombospondin-1 (TSP-1), an effective natural inhibitor of angiogenesis, were highly up-regulated in PRMT6-overexpressing cells. Significant down-regulations of MMP-2 and MMP-9 were also observed in PRMT6-overexpressing cells. Compared with control GFP expressing cells, the growth rate and colony formation ability of PRMT6 overexpressed cells were significantly reduced, which suggest that PRMT6 overexpression is involved in the regulation of motility and invasion in human breast cancer cells through up-regulation of TSP-1 and down-regulation of MMPs (53).

However, these results are inconsistent with previous observations that TSP-1 is a transcriptional inhibitory target of PRMT6 and blocks secretory TSP-1 erythrocyte migration in PRMT6-deficient osteosarcoma cells (U2OS) (52). One possible reason for this analysis is that the cellular system (MCF7 vs U2OS) is different between the two studies, the other is the difference between PRMT6 overexpression system and PRMT6 knock-down system. In knock-down system, the absence of PRMT6 could not write the inhibitory epigenetic marker H3R2me2a on the TSP-1 promoter region, resulting in increased TSP-1 expression. However, in the overexpression system, overexpressed PRMT6 may inhibit the expression of some inhibitory complexes of TSP-1 transcriptional inhibition by generating H3R2me2a on their expression region, such as txr-1 and id-1 (118), thus transforming into TSP-1 transcriptional activation (53). It was also found that PRMT6 methylates DNA polymerase β (Polβ), an enzyme involved in DNA base excision and repair. PRMT6 methylation of Polβ arginine residues 83 and 152 is required to stimulate Polβ's DNA-binding ability and promote its processability (26). Low Polβ mRNA and protein expression was associated with breast cancer incidence, higher tumor grade, positive lymph node status, increased ER+ tumor aggressiveness, and poor patient survival (119). This suggests that PRMT6 methylation of Polβ is a mechanism that promotes genomic stability and thus may inhibit the development of breast cancer. Therefore, PRMT6 may be served as a therapeutic marker for breast cancer, but its exact effects on breast cancer need further study (120).

Hepatocellular Carcinoma

Hepatocellular carcinoma (HCC) is one of the most common cancers worldwide, and the main type of primary liver cancers, accounting for approximately 90% of human liver cancer and the third leading cause of cancer-related deaths (121). PRMT2 (122), PRMT9 (123) had previously been shown to accelerate the development, invasion and metastasis of hepatocellular carcinoma, however, PRMT5 was found to inhibit the growth of HCC (124). It has been found that PRMT6 is frequently down-regulated in HCC, and its expression is negatively correlated with aggressive cancer characteristics in HCC patients. In a DEN+ CCL4HCC-induced PRMT6 knockout mouse model, deletion of PRMT6 expression exacerbates the occurrence of liver tumors. The silencing of PRMT6 promotes tumor initiation, metastasis, and anti-therapeutic potential in HCC cell lines and patient-derived organoids. PRMT6 interacts with CRAF on arginine 100 to interfere with its binding to RAS/RAF binding domain, reduce its RAS binding potential and alter its downstream MEK/ERK signaling, thereby maintaining a key inhibitory function of HCC cells (40). The use of 2-deoxyglucose (a glycolysis inhibitor) reverses tumorigenicity and sorafenib resistance mediated by PRMT6 deficiency in HCC. Most tumor cells utilize aerobic glycolysis (the Warburg effect) to support anabolic growth, promoting tumorigenicity and drug resistance. PRMT6 regulates aerobic glycolysis in HCC through nuclear relocalization of pyruvate kinase M2 subtype (PKM2), a key regulator of the Warburg effect. PRMT6 methylates CRAF at arginine 100 and interferes with its RAS/RAF binding potential, thereby altering the ERK-mediated translocation of PKM2 to the nucleus. REST is a novel target of PRMT6 hypoxia, linking PRMT6 with hypoxia to drive glycolysis events. Use of the glycolysis inhibitor 2-deoxyglucose (2DG) reverses tumorigenicity and sorafenib resistance caused by PRMT6 defect mediated glycolysis events in HCC. Therefore, the regulatory axis of PRMT6-ERK-PKM2 has a mechanistic association with tumorigenicity of HCC, sorafenib resistance, and Warburg effect of tumor cells, and is an important determinant factor (125). Since autophagy is a key survival factor for cancer cells, it can maintain cellular homeostasis by degrading damaged organelles and unwanted proteins and support cellular biosynthesis in response to stress.

It was found that deficiency of PRMT6 promotes autophagy induction in HCC in response to nutrient/oxygen starvation and drug-induced stress, the catalytically active domain of PRMT6 plays an important role in autophagy regulation of HCC. The enhanced autophagic flux of HCC cells was negatively correlated with the expression of PRMT6, and the catalytic domain of PRMT6 was critical in mediating these autophagy activities. PRMT6 physically interacts and methylates BAG5 to enhance the degradation of its interaction partner HSC70 (a well-known autophagy participant), and a reverse correlation between PRMT6 and HSC70 expression in HCC tissues was observed. The therapeutic potential of gene targeting BAG5 to reverse

tumogenesis and sorafenib resistance mediated by PRMT6 defects in HCC has also been demonstrated *in vivo* models. In conclusion, PRMT6 deficiency regulates BAG5-related HSC70 stability through post-translational methylation of BAG5, thereby inducing autophagy to promote tumorigenicity and cell survival in the malignant microenvironment of HCC tumors. Therefore, targeting BAG5 by inhibiting autophagy and inducing the sensitivity of HCC cells to sorafenib may be an attractive strategy for the treatment of HCC (126). Therefore, PRMT6 can be viewed as a new target for liver cancer research, and its specific mechanism of action remains to be further studied.

Prostate Cancer

It was observed that the growth rate and colony formation ability of PRMT6 overexpressed cells were significantly reduced in PC3 cell lines, and the expression of thrombospondin-1 (TSP-1), an effective natural inhibitor of angiogenesis, was highly up-regulated in PRMT6-overexpressing cells. When TSP-1 was specifically knocked down, the inhibition of migration and invasion by overexpression of PRMT6 was significantly saved. Concomitantly, down-regulation of MMP-2 and MMP-9 expressions were observed in PRMT6-overexpressing cells. These results indicated that PRMT6 overexpression could inhibit the migration and invasion of prostate cancer cells by up-regulating TSP-1 and down-regulating MMPs (53).

Melanoma

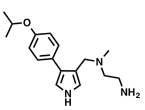
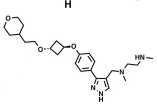
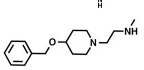
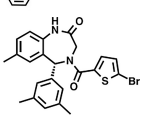
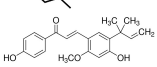
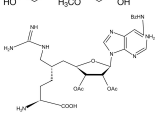
Malignant melanoma (MM) is a skin tumor that originates in melanocytes and is responsible for melanin production and its metastasis to keratinocytes (127). Previous study has found that the expression of most PRMTs in primary tumours and metastases remains unchanged compared with normal melanocytes, and only PRMT4/CARM1 was significantly induced during tumor development (128). PRMT1 has also been found to be overexpressed in human melanoma, and PRMT1 may regulate tumor growth and metastasis by targeting activated leukocyte cell adhesion molecule (ALCAM) (129). PRMT6 was found to be expressed at reduced levels in melanoma compared to melanocytes, early studies have shown that the expression of methylthioadenosine phosphorylase (MTAP), which is involved in tumorigenesis, is significantly reduced in melanoma (130). Due to lack of MTAP expression, the processing of the metabolite MTA is impaired and thus accumulates in and outside the cell, and MTA has been described as a potential inhibitor of PRMT activity. Therefore, in melanoma cells, the loss of MTAP expression leads to a significant decrease in protein methylation through accumulation of MTA. This suggests that metabolism changes may lead to global cellular changes that support tumor development and aggressiveness (128).

PRMT6 INHIBITORS

As PRMT6 has been found to have the ability to regulate cell cycle and inhibit the expression of tumor suppressor genes in a variety of tumors, with oncogene-like properties, it is often found to be significantly overexpressed in tumor tissues, and is associated with poor prognosis. Therefore, PRMT6 can be regarded as a new research target for tumor therapy, and the study of PRMT6 inhibitors has also become a hot spot to explore potential cancer treatment approaches (**Table 1**).

Many inhibitors of PRMT6 exert their effects based on the specific structural basis of PRMT6. All the PRMT proteins have a core region of conservative catalytic domain with variable

TABLE 1 | PRMT6 inhibitors.

Inhibitor	Structure	Mode of action	PRMT6 IC50 (nM)	Cancer type(s) tested	References
MS023		Inhibition (methyltransferase activity)	4-119	Breast cancer, colorectal cancer	(131)
EPZ020411		Changes of biochemical structure	10	Melanoma	(132, 133)
MS049		Inhibition (methyltransferase activity)	34-43	NA	(131, 133, 134)
SGC6870		Allosteric inhibitor	77 ± 6	NA	(135)
Licochalcone A		Competitive (substrates)	22.3	Breast cancer	(136)
GMS		Competitive (substrates and SAM)	90	NA	(137)

NA, not available.

N-terminal fragment that has been observed to regulate methyltransfer activity and substrate specificity. The PRMT6 structure consists of three structural components: (i) the N-terminal Rossmann fold, containing the SAM binding pocket, (ii) the C-terminal β-barrel domain and (iii) a dimerization helix located between the β6 and β7 strands of the C-terminal β-barrel domain, cis-conformation of cis-proline (Pro186) connects the N-terminal Rossmann fold to the C-terminal β-barrel domain (137, 138). PRMT6 exists as a dimer, with the dimerization arm (helix α4-6) from one monomer packing against helixes αY/Z and α1/2 of the Rossmann domain from the other monomers, forming a circulate dimer structure. The SAH molecule binds in an extended conformation in a pocket formed by the Rossmann fold domain. The invariant residues in Rossmann's folded SAM binding pocket interact with the homocysteine carboxylate, adenine ring and ribose of SAH *via* a series of hydrogen bonds and salt bridges (**Figure 2**) (137). The N-terminal fragment of PRMT6 has long been thought to play an important role in substrate specificity and to be necessary and sufficient for its binding with other binding partners (139).

Several PRMT6 inhibitors have been introduced in several studies. Compounds 1-6 were found when evaluated in biochemical analysis using tritiated SAM (3H-SAM) as the methyl donor. Compound 1 with a triazole core is weak against most type I PRMTs, but it is most effective against PRMT6 (IC50 = 230 ± 12 nM). Considering that the pyrrole core is superior to triazole core in inhibiting type I PRMTs, compound 2 was found to be about 10 times more potent against PRMT6 than compound 1, and showed a higher inhibitory effect against PRMT6 (IC50 = 9 ± 0.9 nM). In addition, it was found that changing the meta-trifluoromethyl group (compound 2) to the para-isopropoxy (compound 3) improved the efficacy against all type I PRMT family. For example, MS023 (compound 3) effectively inhibited PRMT6 (IC50 = 4 ± 0.5 nM) (131). Based on the discovery of cocrystal structure of PRMT6-MS023, the first effective, selective and cytoactive irreversible inhibitor of PRMT6, compound 4 (MS117) was also reported. Mass of spectrometry (MS), kinetics studies and a eutectic structure were used to detect the covalent binding mode of compound 4 to PRMT6. Compound 4 does not covalently modify other type I PRMTs, only effectively inhibits PRMT6 in cells, and has higher selectivity to PRMT6 than other methyltransferases, and is more effective than compound 5, which is a similar analogue of compound 4 and also acts as a potent and cell-active reversible inhibitor of PRMT6 (140). At the same time, Jin et al. (140) also developed two control compounds with similar structures, 5 (MS167), a potent and cellular activity reversible PRMT6 inhibitor, and 7 (MS168), a very poor inhibitor of PRMT6, but with the same reaction warhead as compound 4.

In addition, a dual inhibitor of both CARM1 and PRMT6 called 17(MS049) was developed through structure-activity relationship (SAR) studies based on a previously designed potent selective inhibitor of the type I PRMT family inhibitor 3(MS023). The inhibition mechanism of MS049 may be as follows: (i) because MS049 has similar chemical structure to CARM1, it may occupy the substrate binding site of CARM1 and PRMT6; (ii) The binding of MS049 to the protein will cause conformational changes in the protein, which will disable the traditional enzyme kinetics (131, 134).

Based on studies of type I inhibitors, structural optimization was performed to obtain inhibitors, such as EPZ020411 with high valence (IC50 = 10 nM) and moderate selectivity (approx. 12-fold) against PRMT6, which can be used in animal models to reduce H3R2me2a levels, and the eutectic structure of PRMT6-SAH-EPZ020411 indicates that the inhibitor occupies the arginine binding site. However, as the first effective and selective small molecule tool compound of PRMT6 inhibitor, EPZ020411 is still in the stage of preclinical development, and its specific disease indications need to be further explored (132).

At the same time, systematic studies using human breast cancer cell lines demonstrated that licochalcone A, a natural compound, is a novel, reversible and selective, non-S-adenosyl L-methionine (SAM) binding site competitive PRMT6 inhibitor. In breast cancer MCF-7 cells, licochalcone A inhibits PRMT6-dependent methylation of histone H3 at arginine 2 (H3R2), resulting in a significant inhibition of estrogen receptor activity.

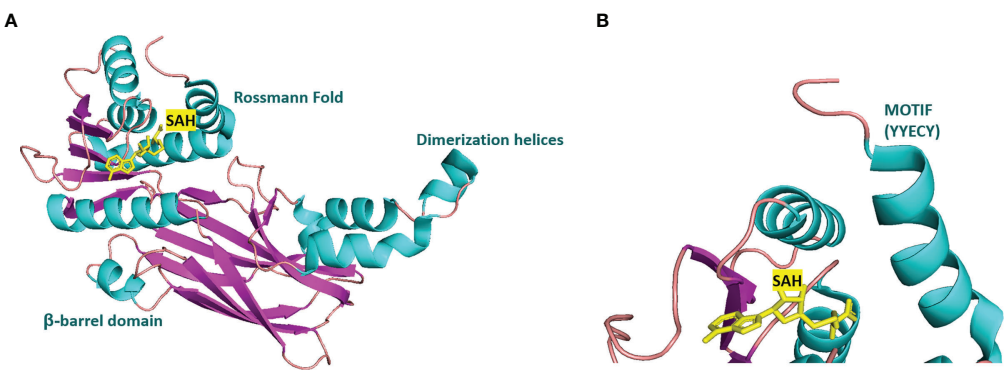


FIGURE 2 | Structural attributes of PRMT6. **(A)** Overall crystal structure of human PRMT6 (PDB: 6W6D, this work) in complex with SAH (marine yellow). **(B)** Structual superimposition of the conserved motif from PRMT6 (Motif: YYECY).

Licochalcone A showed cytotoxicity to human MCF-7 breast cancer cells but no cytotoxicity to MCF-10A breast epithelial cells by up-regulating p53 expression, blocking G2/M cell cycle progression, and then inhibiting apoptosis. These results also indicate that licochalcone A, one of the main flavonoids extracted from licorice root, is the first natural inhibitor of PRMT6 with higher specificity (136). There is also a study identified a bisubstrate inhibitor called 6'-methyleneamine sinefungin (GMS), which is an analog of sinefungin, and its inhibitory activity is stronger than other cofactor competitive inhibitors. The compound can occupy the substrate arginine binding site (PDB:4QQK) and cofactor binding pockets (137).

It has also been reported that (R)-2 (SGC6870) was the most effective PRMT6 inhibitor (IC50 = 77 ± 6nM) in a series of more than 60 derivatives. In view of the structural differences between SGC6870 and other known substrate-competitive and SAM-competitive PRMT inhibitors. Enzyme kinetics and X-ray crystallography method validation study results show that there is a noncompetitive inhibition in the case of both the peptide substrate and SAM cofactor, suggests that it is not a SAM competitive inhibitor. SGC6870 combined without the substrate binding pocket, and the conformation of the most significant changes associated with the double-E loop, which reshaped and moved away from β-barrels of domain structure, thus forming the allosteric site. In conclusion, SGC6870 engages PRMT6 and effectively inhibits its methyltransferase activity in cells and acts as a novel allosteric inhibitor of PRMT6 (135).

CONCLUSIONS AND PERSPECTIVES

As a member of type I PRMT family, PRMT6 can regulate gene expression, promote proliferation and migration of cancer cells, activate or inhibit signal transduction, regulate cancer cell metabolism, and promote self-renewal and differentiation of tumor stem cells by methylating histone or non-histone proteins. The various biological processes associated with these functions of PRMT6 are consistent with the various proteins methylated by PRMT6 in cells. No doubt, during the course of future research, this aspect of research will be further expanded. As mentioned above, the context-specific function of PRMT6 may result from its interacting proteins. Several studies have begun to explore the binding partner proteins of PRMT6 using techniques such as co-immunoprecipitation or adjacent

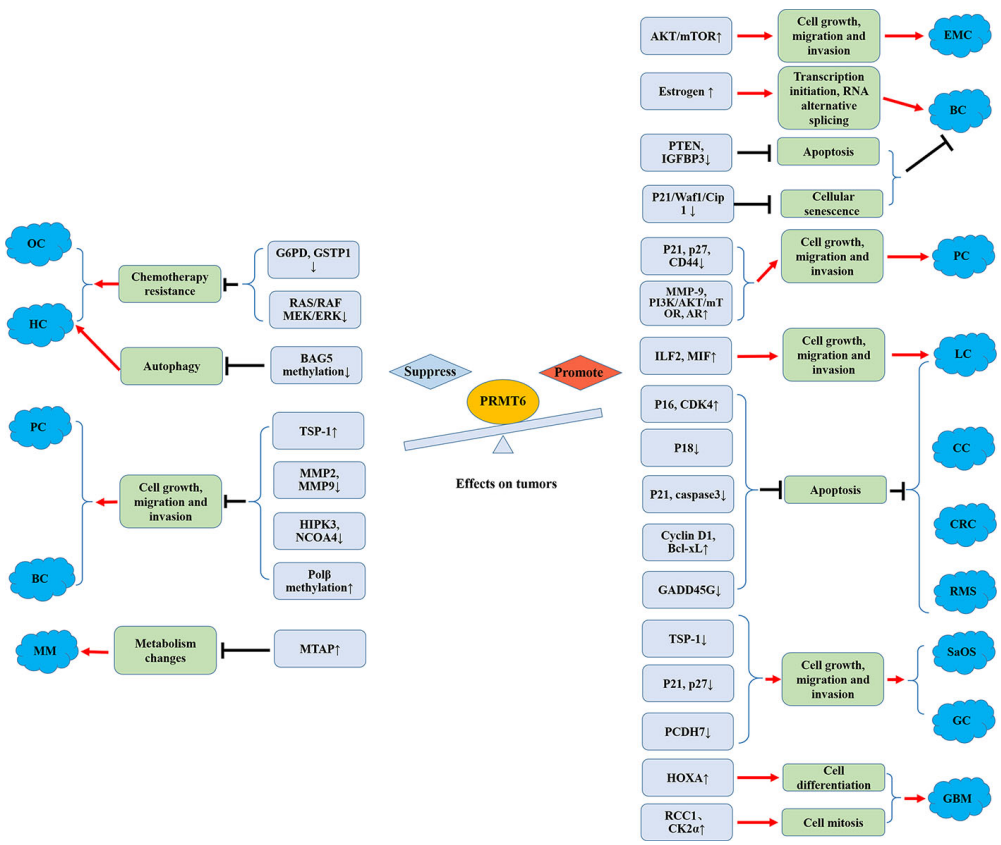


FIGURE 3 | Promoting and suppressing effects of PRMT6 on different cancers. OC, ovarian cancer; HCC, hepatocellular carcinoma; MM, melanoma; PC, prostate cancer; BC, breast cancer; EMC, endometrial carcinoma; CRC, colorectal cancer; SaOS, osteosarcoma; GC, gastric cancer; CC, cervical cancer; LC, lung cancer; RMS, rhabdomyosarcoma; GBM, glioblastoma; AR, androgen receptor; Polβ, DNA polymerase β.

biotinylation, and such mechanistic studies are necessary to elucidate the importance of PRMT6-driven methylation. However, more experiments are needed to verify and explore the mechanism behind why PRMT6 overexpression has different effects on different tumor types. Therefore, further studies on PRMT6 expression levels, mechanisms of action, substrates and interaction partners, as well as interactions with other PRMT family members, will contribute to be conducted for further understanding of the function of PRMT6. At present, immunotherapy of tumor is a new hotspot with great exploration space in the field of tumor therapy. However, the research of PRMT6 in tumor immunotherapy is still weak, which provides a new research direction for cancer prevention and treatment in the future. In addition, the discoveries *in vivo* which show the specific regulation of PRMT6 is still needed to be further verified. The research of more PRMT6 substrates is also a promising study direction, which can lay more foundation for subsequent experiments. Since PRMT6 regulation occurs in the nucleus or cytoplasm, it is difficult to use PRMT6 expression as a biomarker to predict cancer status before obtaining tumor tissue. As the technical tools for drug development continue to evolve, exploratory studies on specific PRMT6 inhibitors are being improved, and the mechanisms underlying the therapeutic potential of PRMT6 inhibitors will be a promising research area. Several PRMT6 inhibitors have shown positive results in mouse models and are currently undergoing clinical trials. PRMT6 inhibitors may be used for cancer treatment alone or in combination with other current or future therapies. PRMT6 inhibitors may be beneficial in patients with tumors that have not responded to checkpoint inhibitor therapy. PRMT6 inhibitors may be very effective in cancer therapy through synergistic effects on tumor cells and tumor microenvironment components and are expected to become new tumor therapeutic targets.

In conclusion, systematic approaches to arginine methylation, including the issues mentioned above (**Figure 3**), will not only help us better understand the tumor-related biological phenomena, but also help develop a novel class of anticancer drugs.

AUTHOR CONTRIBUTIONS

ZC and JG contributed equally to this paper. ZC: extensive literature search and drafting. JG: figures. ZW: extensive literature search. MZ and YD: literature search and critical revision. HZ: conception of the work and final version approval. All authors read and approved the final manuscript.

FUNDING

This work was funded by the National Natural Science Foundation of China (grant number: 81971394, 81571457). The Shanghai Pujiang Program (grant number: 15PJ1400900).

REFERENCES

1. Mohammad HP, Barbash O, Creasy CL. Targeting Epigenetic Modifications in Cancer Therapy: Erasing the Roadmap to Cancer. *Nat Med* (2019) 25 (3):403–18. doi: 10.1038/s41591-019-0376-8
2. Brostoff S, Eylar E. Localization of Methylated Arginine in the A1 Protein From Myelin. *Proc Natl Acad Sci United States America* (1971) 68(4):765–9. doi: 10.1073/pnas.68.4.765
3. Walsh G. Post-Translational Modifications of Protein Biopharmaceuticals. *Drug Discovery Today* (2010) 15(17-18):773–80. doi: 10.1016/j.drudis.2010.06.009
4. Morales Y, Caceres T, May K, Hevel JM. Biochemistry and Regulation of the Protein Arginine Methyltransferases (PRMTs). *Arch Biochem Biophys* (2016) 590:138–52. doi: 10.1016/j.abb.2015.11.030
5. Yang Y, Bedford MT. Protein Arginine Methyltransferases and Cancer. *Nat Rev Cancer* (2013) 13(1):37–50. doi: 10.1038/nrc3409
6. Karkhanis V, Wang L, Tae S, Hu YJ, Imbalzano AN, Sif S. Protein Arginine Methyltransferase 7 Regulates Cellular Response to DNA Damage by Methylating Promoter Histones H2A and H4 of the Polymerase Delta Catalytic Subunit Gene, POLD1. *J Biol Chem* (2012) 287(35):29801–14. doi: 10.1074/jbc.M112.378281
7. Ferreira TR, Alves-Ferreira EV, Defina TP, Walrad P, Papadopoulou B, Cruz AK. Altered Expression of an RBP-Associated Arginine Methyltransferase 7 in Leishmania Major Affects Parasite Infection. *Mol Microbiol* (2014) 94(5):1085–102. doi: 10.1111/mmi.12819
8. Carlson SM, Gozani O. Emerging Technologies to Map the Protein Methylome. *J Mol Biol* (2014) 426(20):3350–62. doi: 10.1016/j.jmb.2014.04.024
9. Gao X, Pan WS, Dai H, Zhang Y, Wu NH, Shen YF. CARM1 Activates Myogenin Gene *via* PCAF in the Early Differentiation of TPA-Induced Rhabdomyosarcoma-Derived Cells. *J Cell Biochem* (2010) 110(1):162–70. doi: 10.1002/jcb.22522
10. Blanc RS, Richard S. Arginine Methylation: The Coming of Age. *Mol Cell* (2017) 65(1):8–24. doi: 10.1016/j.molcel.2016.11.003
11. Guccione E, Richard S. The Regulation, Functions and Clinical Relevance of Arginine Methylation. *Nat Rev Mol Cell Biol* (2019) 20(10):642–57. doi: 10.1038/s41580-019-0155-x
12. Suresh S, Huard S, Dubois T. CARM1/PRMT4: Making Its Mark Beyond Its Function as a Transcriptional Coactivator. *Trends Cell Biol* (2021) 31 (5):402–17. doi: 10.1016/j.tcb.2020.12.010
13. Harrison MJ, Tang YH, Dowhan DH. Protein Arginine Methyltransferase 6 Regulates Multiple Aspects of Gene Expression. *Nucleic Acids Res* (2010) 38 (7):2201–16. doi: 10.1093/nar/gkp1203
14. Skaar JR, Pagan JK, Pagano M. SCF Ubiquitin Ligase-Targeted Therapies. *Nat Rev Drug Discovery* (2014) 13(12):889–903. doi: 10.1038/nrd4432
15. Baldwin G, Carnegie P. Specific Enzymic Methylation of an Arginine in the Experimental Allergic Encephalomyelitis Protein From Human Myelin. *Sci (New York NY)* (1971) 171(3971):579–81. doi: 10.1126/science.171.3971.579
16. Chiang K, Zielinska AE, Shaaban AM, Sanchez-Bailon MP, Jarrold J, Clarke TL, et al. PRMT5 Is a Critical Regulator of Breast Cancer Stem Cell Function *via* Histone Methylation and FOXP1 Expression. *Cell Rep* (2017) 21 (12):3498–513. doi: 10.1016/j.celrep.2017.11.096
17. Stopa N, Krebs JE, Shechter D. The PRMT5 Arginine Methyltransferase: Many Roles in Development, Cancer and Beyond. *Cell Mol Life Sci* (2015) 72 (11):2041–59. doi: 10.1007/s00018-015-1847-9
18. Guccione E, Bassi C, Casadio F, Martinato F, Cesaroni M, Schuchlautz H, et al. Methylation of Histone H3R2 by PRMT6 and H3K4 by an MLL Complex are Mutually Exclusive. *Nature* (2007) 449(7164):933–7. doi: 10.1038/nature06166
19. Iberg AN, Espejo A, Cheng D, Kim D, Michaud-Levesque J, Richard S, et al. Arginine Methylation of the Histone H3 Tail Impedes Effector Binding. *J Biol Chem* (2008) 283(6):3006–10. doi: 10.1074/jbc.C700192200
20. Hyllus D, Stein C, Schnabel K, Schiltz E, Imhof A, Dou Y, et al. PRMT6-Mediated Methylation of R2 in Histone H3 Antagonizes H3 K4 Trimethylation. *Genes Dev* (2007) 21(24):3369–80. doi: 10.1101/gad.447007

21. Frankel A, Yadav N, Lee J, Branscombe TL, Clarke S, Bedford MT. The Novel Human Protein Arginine N-Methyltransferase PRMT6 is a Nuclear Enzyme Displaying Unique Substrate Specificity. *J Biol Chem* (2002) 277 (5):3537–43. doi: 10.1074/jbc.M108786200
22. Dowhan DH, Harrison MJ, Eriksson NA, Bailey P, Pearen MA, Fuller PJ, et al. Protein Arginine Methyltransferase 6-Dependent Gene Expression and Splicing: Association With Breast Cancer Outcomes. *Endocr-Relat Cancer* (2012) 19(4):509–26. doi: 10.1530/ERC-12-0100
23. Zhao XX, Zhang YB, Ni PL, Wu ZL, Yan YC, Li YP. Protein Arginine Methyltransferase 6 (Prmt6) Is Essential for Early Zebrafish Development Through the Direct Suppression of Gadd45alphaa Stress Sensor Gene. *J Biol Chem* (2016) 291(1):402–12. doi: 10.1074/jbc.M115.666347
24. Lee YH, Ma H, Tan TZ, Ng SS, Soong R, Mori S, et al. Protein Arginine Methyltransferase 6 Regulates Embryonic Stem Cell Identity. *Stem Cells Dev* (2012) 21(14):2613–22. doi: 10.1089/scd.2011.0330
25. Lausen J. Contributions of the Histone Arginine Methyltransferase PRMT6 to the Epigenetic Function of RUNX1. *Crit Rev Eukar Gene* (2013) 23 (3):265–74. doi: 10.1615/CritRevEukaryotGeneExpr.2013007527
26. El-Andaloussi N, Valovka T, Toueille M, Steinacher R, Focke F, Gehrig P, et al. Arginine Methylation Regulates DNA Polymerase Beta. *Mol Cell* (2006) 22(1):51–62. doi: 10.1016/j.molcel.2006.02.013
27. Ma WL, Wang L, Liu LX, Wang XL. Effect of Phosphorylation and Methylation on the Function of the P16(INK4a) Protein in non-Small Cell Lung Cancer A549 Cells. *Oncol Lett* (2015) 10(4):2277–82. doi: 10.3892/ol.2015.3617
28. Stein C, Riedl S, Ruthnick D, Notzold RR, Bauer UM. The Arginine Methyltransferase PRMT6 Regulates Cell Proliferation and Senescence Through Transcriptional Repression of Tumor Suppressor Genes. *Nucleic Acids Res* (2012) 40(19):9522–33. doi: 10.1093/nar/gks767
29. Kleinschmidt MA, de Graaf P, van Teeffelen HA, Timmers HT. Cell Cycle Regulation by the PRMT6 Arginine Methyltransferase Through Repression of Cyclin-Dependent Kinase Inhibitors. *PloS One* (2012) 7(8):e41446. doi: 10.1371/journal.pone.0041446
30. Veland N, Hardikar S, Zhong Y, Gayatri S, Dan J, Strahl BD, et al. The Arginine Methyltransferase PRMT6 Regulates DNA Methylation and Contributes to Global DNA Hypomethylation in Cancer. *Cell Rep* (2017) 21(12):3390–7. doi: 10.1016/j.celrep.2017.11.082
31. Kim S, Kim NH, Park JE, Hwang JW, Myung N, Hwang KT, et al. PRMT6-Mediated H3R2me2a Guides Aurora B to Chromosome Arms for Proper Chromosome Segregation. *Nat Commun* (2020) 11(1):612. doi: 10.1038/s41467-020-14511-w
32. Huang T, Yang Y, Song X, Wan X, Wu B, Sastry N, et al. PRMT6 Methylation of RCC1 Regulates Mitosis, Tumorigenicity, and Radiation Response of Glioblastoma Stem Cells. *Mol Cell* (2021) 81(6):1276–91 e9. doi: 10.1016/j.molcel.2021.01.015
33. Di Lorenzo A, Yang Y, Macaluso M, Bedford MT. A Gain-of-Function Mouse Model Identifies PRMT6 as a NF-kappaB Coactivator. *Nucleic Acids Res* (2014) 42(13):8297–309. doi: 10.1093/nar/gku530
34. Tsai KD, Lee WX, Chen W, Chen BY, Chen KL, Hsiao TC, et al. Upregulation of PRMT6 by LPS Suppresses Klotho Expression Through Interaction With NF-kappaB in Glomerular Mesangial Cells. *J Cell Biochem* (2018) 119(4):3404–16. doi: 10.1002/jcb.26511
35. Stavride P, Arampatzi P, Papamatheakis J. Differential Regulation of MHCII Genes by PRMT6, *via* an AT-Hook Motif of RFX5. *Mol Immunol* (2013) 56 (4):390–8. doi: 10.1016/j.molimm.2013.05.235
36. Zhang H, Han C, Li T, Li N, Cao X. The Methyltransferase PRMT6 Attenuates Antiviral Innate Immunity by Blocking TBK1-IRF3 Signaling. *Cell Mol Immunol* (2019) 16(10):800–9. doi: 10.1038/s41423-018-0057-4
37. Luo M, Li Y, Guo H, Lin S, Chen J, Ma Q, et al. Protein Arginine Methyltransferase 6 Involved in Germ Cell Viability During Spermatogenesis and Down-Regulated by the Androgen Receptor. *Int J Mol Sci* (2015) 16(12):29467–81. doi: 10.3390/ijms161226186
38. Scaramuzzino C, Casci I, Parodi S, Lievens PMJ, Polanco MJ, Milioto C, et al. Protein Arginine Methyltransferase 6 Enhances Polyglutamine-Expanded Androgen Receptor Function and Toxicity in Spinal and Bulbar Muscular Atrophy. *Neuron* (2015) 85(1):88–100. doi: 10.1016/j.neuron.2014.12.031
39. Feng J, Dang Y, Zhang W, Zhao X, Zhang C, Hou Z, et al. PTEN Arginine Methylation by PRMT6 Suppresses PI3K-AKT Signaling and Modulates pre-mRNA Splicing. *Proc Natl Acad Sci U.S.A.* (2019) 116(14):6868–77. doi: 10.1073/pnas.1811028116
40. Chan LH, Zhou L, Ng KY, Wong TL, Lee TK, Sharma R, et al. PRMT6 Regulates RAS/RAF Binding and MEK/ERK-Mediated Cancer Sternness Activities in Hepatocellular Carcinoma Through CRAF Methylation. *Cell Rep* (2018) 25(3):690–+. doi: 10.1016/j.celrep.2018.09.053
41. Boulanger MC, Liang C, Russell RS, Lin R, Bedford MT, Wainberg MA, et al. Methylation of Tat by PRMT6 Regulates Human Immunodeficiency Virus Type 1 Gene Expression. *J Virol* (2005) 79(1):124–31. doi: 10.1128/JVI.79.1.124-131.2005
42. Xie B, Invernizzi CF, Richard S, Wainberg MA. Arginine Methylation of the Human Immunodeficiency Virus Type 1 Tat Protein by PRMT6 Negatively Affects Tat Interactions With Both Cyclin T1 and the Tat Transactivation Region. *J Virol* (2007) 81(8):4226–34. doi: 10.1128/JVI.01888-06
43. Yoshimatsu M, Toyokawa G, Hayami S, Unoki M, Tsunoda T, Field HI, et al. Dysregulation of PRMT1 and PRMT6, Type I Arginine Methyltransferases, is Involved in Various Types of Human Cancers. *Int J Cancer* (2011) 128 (3):562–73. doi: 10.1002/ijc.25366
44. Raveendran VV, Al-Haffar K, Kunhi M, Belhaj K, Al-Habeeb W, Al-Buraiki J, et al. Protein Arginine Methyltransferase 6 Mediates Cardiac Hypertrophy by Differential Regulation of Histone H3 Arginine Methylation. *Heliyon* (2020) 6(5):e03864. doi: 10.1016/j.heliyon.2020.e03864
45. Lo Sardo A, Altamura S, Pegoraro S, Maurizio E, Sgarra R, Manfioletti G. Identification and Characterization of New Molecular Partners for the Protein Arginine Methyltransferase 6 (PRMT6). *PloS One* (2013) 8(1): e53750. doi: 10.1371/journal.pone.0053750
46. Phalke S, Mzoughi S, Bezzi M, Jennifer N, Mok WC, Low DHP, et al. P53-Independent Regulation of p21Waf1/Cip1 Expression and Senescence by PRMT6. *Nucleic Acids Res* (2012) 40(19):9534–42. doi: 10.1093/nar/gks858
47. Neault M, Mallette FA, Vogel G, Michaud-Levesque J, Richard S. Ablation of PRMT6 Reveals a Role as a Negative Transcriptional Regulator of the P53 Tumor Suppressor. *Nucleic Acids Res* (2012) 40(19):9513–21. doi: 10.1093/nar/gks764
48. Casadio F, Lu X, Pollock SB, LeRoy G, Garcia BA, Muir TW, et al. H3R42me2a is a Histone Modification With Positive Transcriptional Effects. *Proc Natl Acad Sci USA* (2013) 110(37):14894–9. doi: 10.1073/pnas.1312925110
49. Cheng D, Gao G, Di Lorenzo A, Jayne S, Hottiger MO, Richard S, et al. Genetic Evidence for Partial Redundancy Between the Arginine Methyltransferases CARM1 and PRMT6. *J Biol Chem* (2020) 295 (50):17060–70. doi: 10.1074/jbc.RA120.014704
50. Waldmann T, Izzo A, Kamieniarz K, Richter F, Vogler C, Sarg B, et al. Methylation of H2AR29 is a Novel Repressive PRMT6 Target. *Epigenet Chromatin* (2011) 4(1):11–21. doi: 10.1186/1756-8935-4-11
51. Bouchard C, Sahu P, Meixner M, Notzold RR, Rust MB, Kremmer E, et al. Genomic Location of PRMT6-Dependent H3R2 Methylation Is Linked to the Transcriptional Outcome of Associated Genes. *Cell Rep* (2018) 24 (12):3339–52. doi: 10.1016/j.celrep.2018.08.052
52. Michaud-Levesque J, Richard S. Thrombospondin-1 is a Transcriptional Repression Target of PRMT6. *J Biol Chem* (2009) 284(32):21338–46. doi: 10.1074/jbc.M109.005322
53. Kim NH, Kim SN, Seo DW, Han JW, Kim YK. PRMT6 Overexpression Upregulates TSP-1 and Downregulates MMPs: Its Implication in Motility and Invasion. *Biochem Biophys Res Commun* (2013) 432(1):60–5. doi: 10.1016/j.bbrc.2013.01.085
54. Herglotz J, Kuvardina ON, Kolodziej S, Kumar A, Hussong H, Grez M, et al. Histone Arginine Methylation Keeps RUNX1 Target Genes in an Intermediate State. *Oncogene* (2013) 32(20):2565–75. doi: 10.1038/onc.2012.274
55. Nakakido M, Deng ZZ, Suzuki T, Dohmae N, Nakamura Y, Hamamoto R. PRMT6 Increases Cytoplasmic Localization of P21(CDKN1A) in Cancer Cells Through Arginine Methylation and Makes More Resistant to Cytotoxic Agents. *Oncotarget* (2015) 6(31):30957–67. doi: 10.18632/oncotarget.5143
56. Sung H, Ferlay J, Siegel RL, Laversanne M, Soerjomataram I, Jemal A, et al. Global Cancer Statistics 2020: GLOBOCAN Estimates of Incidence and Mortality Worldwide for 36 Cancers in 185 Countries. *CA Cancer J Clin* (2021) 71(3):209–49. doi: 10.3322/caac.21660

57. Liu BL, Sun KX, Zong ZH, Chen S, Zhao Y. MicroRNA-372 Inhibits Endometrial Carcinoma Development by Targeting the Expression of the Ras Homolog Gene Family Member C (RhoC). *Oncotarget* (2016) 7 (6):6649–64. doi: 10.18632/oncotarget.6544
58. Chen X, Hao B, Han G, Liu Y, Dai D, Li Y, et al. miR-372 Regulates Glioma Cell Proliferation and Invasion by Directly Targeting PHLPP2. *J Cell Biochem* (2015) 116(2):225–32. doi: 10.1002/jcb.24949
59. Jiang N, Li QL, Pan W, Li J, Zhang MF, Cao T, et al. PRMT6 Promotes Endometrial Cancer *via* AKT/mTOR Signaling and Indicates Poor Prognosis. *Int J Biochem Cell Biol* (2020) 120:105681. doi: 10.1016/j.biocel.2019.105681
60. Ferlay J, Soerjomataram I, Dikshit R, Eser S, Mathers C, Rebelo M, et al. Cancer Incidence and Mortality Worldwide: Sources, Methods and Major Patterns in GLOBOCAN 2012. *Int J Cancer* (2015) 136(5):E359–86. doi: 10.1002/ijc.29210
61. Mathioudaki K, Scorilas A, Ardavanis A, Lymberi P, Tsiambas E, Devetzi M, et al. Clinical Evaluation of PRMT1 Gene Expression in Breast Cancer. *Tumour Biol* (2011) 32(3):575–82. doi: 10.1007/s13277-010-0153-2
62. Peng BL, Li WJ, Ding JC, He YH, Ran T, Xie BL, et al. A Hypermethylation Strategy Utilized by Enhancer-Bound CARM1 to Promote Estrogen Receptor Alpha-Dependent Transcriptional Activation and Breast Carcinogenesis. *Theranostics* (2020) 10(8):3451–73. doi: 10.7150/thno.39241
63. Bao J, Di Lorenzo A, Lin K, Lu Y, Zhong Y, Sebastian MM, et al. Mouse Models of Overexpression Reveal Distinct Oncogenic Roles for Different Type I Protein Arginine Methyltransferases. *Cancer Res* (2019) 79(1):21–32. doi: 10.1158/0008-5472.CAN-18-1995
64. Chu MC, Selam FB, Taylor HS. HOXA10 Regulates P53 Expression and Matrigel Invasion in Human Breast Cancer Cells. *Cancer Biol Ther* (2004) 3 (6):568–72. doi: 10.4161/cbt.3.6.848
65. Chow LM, Baker SJ. PTEN Function in Normal and Neoplastic Growth. *Cancer Lett* (2006) 241(2):184–96. doi: 10.1016/j.canlet.2005.11.042
66. Guertin DA, Sabatini DM. An Expanding Role for mTOR in Cancer. *Trends Mol Med* (2005) 11(8):353–61. doi: 10.1016/j.molmed.2005.06.007
67. Kim HS, Lee WJ, Lee SW, Chae HW, Kim DH, Oh Y. Insulin-Like Growth Factor Binding Protein-3 Induces G1 Cell Cycle Arrest With Inhibition of Cyclin-Dependent Kinase 2 and 4 in MCF-7 Human Breast Cancer Cells. *Horm Metab Res* (2010) 42(3):165–72. doi: 10.1055/s-0029-1243190
68. El Messaoudi S, Fabbrizio E, Rodriguez C, Chuchana P, Fauquier L, Cheng D, et al. Coactivator-Associated Arginine Methyltransferase 1 (CARM1) is a Positive Regulator of the Cyclin E1 Gene. *Proc Natl Acad Sci USA* (2006) 103 (36):13351–6. doi: 10.1073/pnas.0605692103
69. Majumder S, Liu Y, Ford OH3rd, Mohler JL, Whang YE. Involvement of Arginine Methyltransferase CARM1 in Androgen Receptor Function and Prostate Cancer Cell Viability. *Prostate* (2006) 66(12):1292–301. doi: 10.1002/pros.20438
70. Vieira FQ, Costa-Pinheiro P, Ramalho-Carvalho J, Pereira A, Menezes FD, Antunes L, et al. Deregulated Expression of Selected Histone Methylases and Demethylases in Prostate Carcinoma. *Endocr Relat Cancer* (2014) 21(1):51–61. doi: 10.1530/ERC-13-0375
71. Almeida-Rios D, Graça I, Vieira F, Ramalho-Carvalho J, Pereira-Silva E, Martins A, et al. Histone Methyltransferase PRMT6 Plays an Oncogenic Role of in Prostate Cancer. *Oncotarget* (2016) 7(33):53018–28. doi: 10.18632/oncotarget.10061
72. Siegel RL, Miller KD, Jemal A. Cancer Statistics, 2018. *CA Cancer J Clin* (2018) 68(1):7–30. doi: 10.3322/caac.21442
73. Wei TY, Juan CC, Hisa JY, Su LJ, Lee YC, Chou HY, et al. Protein Arginine Methyltransferase 5 is a Potential Oncoprotein That Upregulates G1 Cyclins/Cyclin-Dependent Kinases and the Phosphoinositide 3-Kinase/AKT Signaling Cascade. *Cancer Sci* (2012) 103(9):1640–50. doi: 10.1111/j.1349-7006.2012.02367.x
74. Gu Z, Gao S, Zhang F, Wang Z, Ma W, Davis RE, et al. Protein Arginine Methyltransferase 5 is Essential for Growth of Lung Cancer Cells. *Biochem J* (2012) 446(2):235–41. doi: 10.1042/BJ20120768
75. He L, Hu Z, Sun Y, Zhang M, Zhu H, Jiang L, et al. PRMT1 is Critical to FEN1 Expression and Drug Resistance in Lung Cancer Cells. *DNA Repair (Amst)* (2020) 95:102953. doi: 10.1016/j.dnarep.2020.102953
76. Cheng D, He Z, Zheng L, Xie D, Dong S, Zhang P. PRMT7 Contributes to the Metastasis Phenotype in Human non-Small-Cell Lung Cancer Cells Possibly Through the Interaction With HSPA5 and EEF2. *Onco Targets Ther* (2018) 11:4869–76. doi: 10.2147/OTT.S166412
77. Avasarala S, Wu PY, Khan SQ, Yanlin S, Van Scoyk M, Bao J, et al. PRMT6 Promotes Lung Tumor Progression *via* the Alternate Activation of Tumor-Associated Macrophages. *Mol Cancer Res* (2020) 18(1):166–78. doi: 10.1158/1541-7786.MCR-19-0204
78. Wang X, Huang Y, Zhao J, Zhang Y, Lu J, Huang B. Suppression of PRMT6-Mediated Arginine Methylation of P16 Protein Potentiates its Ability to Arrest A549 Cell Proliferation. *Int J Biochem Cell Biol* (2012) 44(12):2333–41. doi: 10.1016/j.biocel.2012.09.015
79. Tang J, Meng Q, Shi R, Xu Y. PRMT6 Serves an Oncogenic Role in Lung Adenocarcinoma *via* Regulating P18. *Mol Med Rep* (2020) 22(4):3161–72. doi: 10.3892/mmr.2020.11402
80. Dominici C, Sgarioto N, Yu Z, Sesma-Sanz L, Masson JY, Richard S, et al. Synergistic Effects of Type I PRMT and PARP Inhibitors Against non-Small Cell Lung Cancer Cells. *Clin Epigenet* (2021) 13(1):54. doi: 10.1186/s13148-021-01037-1
81. Mathioudaki K, Papadokostopoulou A, Scorilas A, Xynopoulos D, Agnanti N, Talieri M. The PRMT1 Gene Expression Pattern in Colon Cancer. *Br J Cancer* (2008) 99(12):2094–9. doi: 10.1038/sj.bjc.6604807
82. Ou CY, LaBonte MJ, Manegold PC, So AY, Ianculescu I, Gerke DS, et al. A Coactivator Role of CARM1 in the Dysregulation of Beta-Catenin Activity in Colorectal Cancer Cell Growth and Gene Expression. *Mol Cancer Res* (2011) 9(5):660–70. doi: 10.1158/1541-7786.MCR-10-0223
83. Kim YR, Lee BK, Park RY, Nguyen NTX, Bae JA, Kwon DD, et al. Differential CARM1 Expression in Prostate and Colorectal Cancers. *BMC Cancer* (2010) 10(1):197–210. doi: 10.1186/1471-2407-10-197
84. Lim Y, Yu S, Yun JA, Do IG, Cho L, Kim YH, et al. The Prognostic Significance of Protein Arginine Methyltransferase 6 Expression in Colon Cancer. *Oncotarget* (2018) 9(10):9010–20. doi: 10.18632/oncotarget.23809
85. Plotnikov A, Kozer N, Cohen G, Carvalho S, Duberstein S, Almog O, et al. PRMT1 Inhibition Induces Differentiation of Colon Cancer Cells. *Sci Rep* (2020) 10(1):20030. doi: 10.1038/s41598-020-77028-8
86. Bielack SS, Smeland S, Whelan JS, Marina N, Jovic G, Hook JM, et al. Methotrexate, Doxorubicin, and Cisplatin (MAP) Plus Maintenance Pegylated Interferon Alfa-2b Versus MAP Alone in Patients With Resectable High-Grade Osteosarcoma and Good Histologic Response to Preoperative MAP: First Results of the EURAMOS-1 Good Response Randomized Controlled Trial. *J Clin Oncol* (2015) 33(20):2279–87. doi: 10.1200/JCO.2014.60.0734
87. Piperno-Neumann S, Le Deley M-C, Rédini F, Pacquement H, Marec-Bérard P, Petit P, et al. Zoledronate in Combination With Chemotherapy and Surgery to Treat Osteosarcoma (OS2006): A Randomised, Multicentre, Open-Label, Phase 3 Trial. *Lancet Oncol* (2016) 17(8):1070–80. doi: 10.1016/S1470-2045(16)30096-1
88. Li S, Cheng D, Zhu B, Yang Q. The Overexpression of CARM1 Promotes Human Osteosarcoma Cell Proliferation Through the Pgsk3beta/Beta-Catenin/cyclinD1 Signaling Pathway. *Int J Biol Sci* (2017) 13(8):976–84. doi: 10.7150/ijbs.19191
89. Zhang B, Zhang S, Zhu L, Chen X, Zhao Y, Chao L, et al. Arginine Methyltransferase Inhibitor 1 Inhibits Gastric Cancer by Downregulating Eif4e and Targeting PRMT5. *Toxicol Appl Pharmacol* (2017) 336:1–7. doi: 10.1016/j.taap.2017.10.002
90. Hernandez SJ, Dolivo DM, Dominko T. PRMT8 Demonstrates Variant-Specific Expression in Cancer Cells and Correlates With Patient Survival in Breast, Ovarian and Gastric Cancer. *Oncol Lett* (2017) 13(3):1983–9. doi: 10.3892/ol.2017.5671
91. Okuno K, Akiyama Y, Shimada S, Nakagawa M, Tanioka T, Inokuchi M, et al. Asymmetric Dimethylation at Histone H3 Arginine 2 by PRMT6 in Gastric Cancer Progression. *Carcinogenesis* (2019) 40(1):15–26. doi: 10.1093/carcin/bgy147
92. Olusola P, Banerjee HN, Philley JV, Dasgupta S. Human Papilloma Virus-Associated Cervical Cancer and Health Disparities. *Cells* (2019) 8(6):622–34. doi: 10.3390/cells8060622
93. Dong SH, Wang X, Tian SC, Ma NQ, Zhang XY, Liu Y, et al. Arginine Methyltransferase Inhibitor 1 Exhibits Antitumor Effects Against Cervical Cancer *In Vitro* and In Vivo. *Pharmazie* (2018) 73(5):269–73. doi: 10.1691/ph.2018.8365

94. Kim C, Lim Y, Yoo BC, Won NH, Kim S, Kim G. Regulation of Post-Translational Protein Arginine Methylation During HeLa Cell Cycle. *Biochim Biophys Acta* (2010) 1800(9):977–85. doi: 10.1016/j.bbagen.2010.06.004
95. Dagher R, Helman L. Rhabdomyosarcoma: An Overview. *Oncologist* (1999) 4(1):34–44. doi: 10.1634/theoncologist.4-1-34
96. Janisiak J, Kopytko P, Tkacz M, Roginska D, Peruzynska M, Machalinski B, et al. Protein Arginine Methyltransferase (PRMT) Inhibitors-AMI-1 and SAH Are Effective in Attenuating Rhabdomyosarcoma Growth and Proliferation in Cell Cultures. *Int J Mol Sci* (2021) 22(15):8023–41. doi: 10.3390/ijms22158023
97. Balla B, Tripon F, Banescu C. From Descriptive to Functional Genomics of Leukemias Focusing on Genome Engineering Techniques. *Int J Mol Sci* (2021) 22(18):10065–85. doi: 10.3390/ijms221810065
98. Shia WJ, Okumura AJ, Yan M, Sarkeshik A, Lo MC, Matsuura S, et al. PRMT1 Interacts With AML1-ETO to Promote its Transcriptional Activation and Progenitor Cell Proliferative Potential. *Blood* (2012) 119(21):4953–62. doi: 10.1182/blood-2011-04-347476
99. Cheung N, Chan LC, Thompson A, Cleary ML, So CW. Protein Arginine-Methyltransferase-Dependent Oncogenesis. *Nat Cell Biol* (2007) 9(10):1208–15. doi: 10.1038/ncb1642
100. Cheung N, Fung TK, Zeisig BB, Holmes K, Rane JK, Mowen KA, et al. Targeting Aberrant Epigenetic Networks Mediated by PRMT1 and KDM4C in Acute Myeloid Leukemia. *Cancer Cell* (2016) 29(1):32–48. doi: 10.1016/j.ccell.2015.12.007
101. Zhu YH, He X, Lin YC, Dong HJ, Zhang L, Chen XW, et al. Targeting PRMT1-Mediated FLT3 Methylation Disrupts Maintenance of MLL-Rearranged Acute Lymphoblastic Leukemia. *Blood* (2019) 134(15):1257–68. doi: 10.1182/blood.2019002457
102. Tarighat SS, Santhanam R, Frankhouser D, Radomska HS, Lai H, Anghelina M, et al. The Dual Epigenetic Role of PRMT5 in Acute Myeloid Leukemia: Gene Activation and Repression *via* Histone Arginine Methylation. *Leukemia* (2016) 30(4):789–99. doi: 10.1038/leu.2015.308
103. Mallappa C, Hu YJ, Shamulailatpam P, Tae S, Sif S, Imbalzano AN. The Expression of Myogenic microRNAs Indirectly Requires Protein Arginine Methyltransferase (Prmt)5 But Directly Requires Prmt4. *Nucleic Acids Res* (2011) 39(4):1243–55. doi: 10.1093/nar/gkq896
104. Wang C, Jiang H, Jin J, Xie Y, Chen Z, Zhang H, et al. Development of Potent Type I Protein Arginine Methyltransferase (PRMT) Inhibitors of Leukemia Cell Proliferation. *J Med Chem* (2017) 60(21):8888–905. doi: 10.1021/acs.jmedchem.7b01134
105. Ostrom QT, Gittleman H, Truitt G, Boscia A, Kruchko C, Barnholtz-Sloan JS. CBTRUS Statistical Report: Primary Brain and Other Central Nervous System Tumors Diagnosed in the United States in 2011-2015. *Neuro Oncol* (2018) 20(suppl_4):iv1–iv86. doi: 10.1093/neuonc/noy131
106. Favia A, Salvatori L, Nanni S, Iwamoto-Stohl LK, Valente S, Mai A, et al. The Protein Arginine Methyltransferases 1 and 5 Affect Myc Properties in Glioblastoma Stem Cells. *Sci Rep* (2019) 9(1):15925. doi: 10.1038/s41598-019-52291-6
107. Samuel SF, Barry A, Greenman J, Beltran-Alvarez P. Arginine Methylation: The Promise of a 'Silver Bullet' for Brain Tumours? *Amino Acids* (2021) 53(4):489–506. doi: 10.1007/s00726-020-02937-x
108. Bryant JP, Heiss J, Banasavadi-Siddegowda YK. Arginine Methylation in Brain Tumors: Tumor Biology and Therapeutic Strategies. *Cells* (2021) 10(1):124–45. doi: 10.3390/cells10010124
109. Simandi Z, Czipa E, Horvath A, Koszeghy A, Bordas C, Poliska S, et al. PRMT1 and PRMT8 Regulate Retinoic Acid-Dependent Neuronal Differentiation With Implications to Neuropathology. *Stem Cells* (2015) 33(3):726–41. doi: 10.1002/stem.1894
110. Banasavadi-Siddegowda YK, Russell L, Frair E, Karkhanis VA, Relation T, Yoo JY, et al. PRMT5-PTEN Molecular Pathway Regulates Senescence and Self-Renewal of Primary Glioblastoma Neurosphere Cells. *Oncogene* (2017) 36(2):263–74. doi: 10.1038/onc.2016.199
111. Stein C, Notzold RR, Riedl S, Bouchard C, Bauer UM. The Arginine Methyltransferase PRMT6 Cooperates With Polycomb Proteins in Regulating HOXA Gene Expression. *PloS One* (2016) 11(2):e0148892. doi: 10.1371/journal.pone.0148892
112. Reid BM, Permuth JB, Sellers TA. Epidemiology of Ovarian Cancer: A Review. *Cancer Biol Med* (2017) 14(1):9–32. doi: 10.20892/j.issn.2095-3941.2016.0084
113. Feng Q, Li X, Sun W, Sun M, Li Z, Sheng H, et al. Targeting G6PD Reverses Paclitaxel Resistance in Ovarian Cancer by Suppressing GSTP1. *Biochem Pharmacol* (2020) 178:114092. doi: 10.1016/j.bcp.2020.114092
114. Castellano I, Allia E, Accortanzo V, Vandone AM, Chiusa L, Arisio R, et al. Androgen Receptor Expression is a Significant Prognostic Factor in Estrogen Receptor Positive Breast Cancers. *Breast Cancer Res Treat* (2010) 124(3):607–17. doi: 10.1007/s10549-010-0761-y
115. Park S, Koo JS, Kim MS, Park HS, Lee JS, Lee JS, et al. Androgen Receptor Expression is Significantly Associated With Better Outcomes in Estrogen Receptor-Positive Breast Cancers. *Ann Oncol* (2011) 22(8):1755–62. doi: 10.1093/annonc/mdq678
116. Wu X, Chen F, Sahin A, Albarracin C, Pei Z, Zou X, et al. Distinct Function of Androgen Receptor Coactivator ARA70alpha and ARA70beta in Mammary Gland Development, and in Breast Cancer. *Breast Cancer Res Treat* (2011) 128(2):391–400. doi: 10.1007/s10549-010-1131-5
117. Hua S, Kallen CB, Dhar R, Baquero MT, Mason CE, Russell BA, et al. Genomic Analysis of Estrogen Cascade Reveals Histone Variant H2A.Z Associated With Breast Cancer Progression. *Mol Syst Biol* (2008) 4:188. doi: 10.1038/msb.2008.25
118. Lih CJ, Wei W, Cohen SN. Txr1: A Transcriptional Regulator of Thrombospondin-1 That Modulates Cellular Sensitivity to Taxanes. *Genes Dev* (2006) 20(15):2082–95. doi: 10.1101/gad.1441306
119. Abdel-Fatah TM, Russell R, Agarwal D, Moseley P, Abayomi MA, Perry C, et al. DNA Polymerase Beta Deficiency is Linked to Aggressive Breast Cancer: A Comprehensive Analysis of Gene Copy Number, mRNA and Protein Expression in Multiple Cohorts. *Mol Oncol* (2014) 8(3):520–32. doi: 10.1016/j.molonc.2014.01.001
120. Morettin A, Baldwin RM, Cote J. Arginine Methyltransferases as Novel Therapeutic Targets for Breast Cancer. *Mutagenesis* (2015) 30(2):177–89. doi: 10.1093/mutage/geu039
121. Forner A, Reig M, Bruix J. Hepatocellular Carcinoma. *Lancet* (2018) 391(10127):1301–14. doi: 10.1016/S0140-6736(18)30010-2
122. Hu G, Yan C, Xie P, Cao Y, Shao J, Ge J. PRMT2 Accelerates Tumorigenesis of Hepatocellular Carcinoma by Activating Bcl2 *via* Histone H3R8 Methylation. *Exp Cell Res* (2020) 394(2):112152. doi: 10.1016/j.yexcr.2020.112152
123. Jiang H, Zhou Z, Jin S, Xu K, Zhang H, Xu J, et al. PRMT9 Promotes Hepatocellular Carcinoma Invasion and Metastasis *via* Activating PI3K/Akt/GSK-3beta/Snail Signaling. *Cancer Sci* (2018) 109(5):1414–27. doi: 10.1111/cas.13598
124. Zhang B, Dong S, Li Z, Lu L, Zhang S, Chen X, et al. Targeting Protein Arginine Methyltransferase 5 Inhibits Human Hepatocellular Carcinoma Growth *via* the Downregulation of Beta-Catenin. *J Transl Med* (2015) 13:349. doi: 10.1186/s12967-015-0721-8
125. Wong TL, Ng KY, Tan KV, Chan LH, Zhou L, Che N, et al. CRAF Methylation by PRMT6 Regulates Aerobic Glycolysis-Driven Hepatocarcinogenesis *via* ERK-Dependent PKM2 Nuclear Relocalization and Activation. *Hepatology* (2020) 71(4):1279–96. doi: 10.1002/hep.30923
126. Che N, Ng KY, Wong TL, Tong M, Kau PW, Chan LH, et al. PRMT6 Deficiency Induces Autophagy in Hostile Microenvironments of Hepatocellular Carcinoma Tumors by Regulating BAG5-Associated HSC70 Stability. *Cancer Lett* (2021) 501:247–62. doi: 10.1016/j.canlet.2020.11.002
127. Lin JY, Fisher DE. Melanocyte Biology and Skin Pigmentation. *Nature* (2007) 445(7130):843–50. doi: 10.1038/nature05660
128. Limm K, Ott C, Wallner S, Mueller DW, Oefner P, Hellerbrand C, et al. Deregulation of Protein Methylation in Melanoma. *Eur J Cancer* (2013) 49(6):1305–13. doi: 10.1016/j.ejca.2012.11.026
129. Li L, Zhang Z, Ma T, Huo R. PRMT1 Regulates Tumor Growth and Metastasis of Human Melanoma *via* Targeting ALCAM. *Mol Med Rep* (2016) 14(1):521–8. doi: 10.3892/mmr.2016.5273
130. Behrmann I, Wallner S, Komyod W, Heinrich PC, Schuierer M, Buettner R, et al. Characterization of Methylthioadenosin, Phosphorylase (MTAP) Expression in Malignant Melanoma. *Am J Pathol* (2003) 163(2):683–90. doi: 10.1016/S0002-9440(10)63695-4

131. Eram MS, Shen Y, Szewczyk M, Wu H, Senisterra G, Li F, et al. A Potent, Selective, and Cell-Active Inhibitor of Human Type I Protein Arginine Methyltransferases. *ACS Chem Biol* (2016) 11(3):772–81. doi: 10.1021/acschembio.5b00839
132. Mitchell LH, Drew AE, Ribich SA, Rioux N, Swinger KK, Jacques SL, et al. Aryl Pyrazoles as Potent Inhibitors of Arginine Methyltransferases: Identification of the First PRMT6 Tool Compound. *ACS Med Chem Lett* (2015) 6(6):655–9. doi: 10.1021/acsmedchemlett.5b00071
133. Ferreira de Freitas R, Eram MS, Szewczyk MM, Steuber H, Smil D, Wu H, et al. Discovery of a Potent Class I Protein Arginine Methyltransferase Fragment Inhibitor. *J Med Chem* (2016) 59(3):1176–83. doi: 10.1021/acs.jmedchem.5b01772
134. Shen Y, Szewczyk MM, Eram MS, Smil D, Kaniskan HU, de Freitas RF, et al. Discovery of a Potent, Selective, and Cell-Active Dual Inhibitor of Protein Arginine Methyltransferase 4 and Protein Arginine Methyltransferase 6. *J Med Chem* (2016) 59(19):9124–39. doi: 10.1021/acs.jmedchem.6b01033
135. Shen Y, Li F, Szewczyk MM, Halabelian L, Chau I, Eram MS, et al. A First-In-Class, Highly Selective and Cell-Active Allosteric Inhibitor of Protein Arginine Methyltransferase 6. *J Med Chem* (2021) 64(7):3697–706. doi: 10.1021/acs.jmedchem.0c02160
136. Gong S, Maegawa S, Yang Y, Gopalakrishnan V, Zheng G, Cheng D. Licochalcone A is a Natural Selective Inhibitor of Arginine Methyltransferase 6. *Biochem J* (2020) 478(2):389–406. doi: 10.1042/BCJ20200411
137. Wu H, Zheng W, Eram MS, Vhuiyan M, Dong A, Zeng H, et al. Structural Basis of Arginine Asymmetrical Dimethylation by PRMT6. *Biochem J* (2016) 473(19):3049–63. doi: 10.1042/BCJ20160537
138. Bonnefond L, Stojko J, Mailliot J, Troffer-Charlier N, Cura V, Wurtz JM, et al. Functional Insights From High Resolution Structures of Mouse Protein Arginine Methyltransferase 6. *J Struct Biol* (2015) 191(2):175–83. doi: 10.1016/j.jsb.2015.06.017
139. Goulet I, Gauvin G, Boisvenue S, Cote J. Alternative Splicing Yields Protein Arginine Methyltransferase 1 Isoforms With Distinct Activity, Substrate Specificity, and Subcellular Localization. *J Biol Chem* (2007) 282(45):33009–21. doi: 10.1074/jbc.M704349200
140. Shen Y, Li F, Szewczyk MM, Halabelian L, Park KS, Chau I, et al. Discovery of a First-In-Class Protein Arginine Methyltransferase 6 (PRMT6) Covalent Inhibitor. *J Med Chem* (2020) 63(10):5477–87. doi: 10.1021/acs.jmedchem.0c00406

Conflict of Interest: The authors declare that the research was conducted in the absence of any commercial or financial relationships that could be construed as a potential conflict of interest.

Publisher's Note: All claims expressed in this article are solely those of the authors and do not necessarily represent those of their affiliated organizations, or those of the publisher, the editors and the reviewers. Any product that may be evaluated in this article, or claim that may be made by its manufacturer, is not guaranteed or endorsed by the publisher.

Copyright © 2022 Chen, Gan, Wei, Zhang, Du, Xu and Zhao. This is an open-access article distributed under the terms of the Creative Commons Attribution License (CC BY). The use, distribution or reproduction in other forums is permitted, provided the original author(s) and the copyright owner(s) are credited and that the original publication in this journal is cited, in accordance with accepted academic practice. No use, distribution or reproduction is permitted which does not comply with these terms.

frontiers | Frontiers in Oncology

REVIEW
published: 04 May 2022
doi: 10.3389/fonc.2022.861959

Recent Advances of Autophagy in Non-Small Cell Lung Cancer: From Basic Mechanisms to Clinical Application

Weina Guo[1†], *Keye Du*[2†], *Shanshan Luo*[3] *and Desheng Hu*[1,4,5*]

[1] Department of Integrated Traditional Chinese and Western Medicine, Union Hospital, Tongji Medical College, Huazhong University of Science and Technology, Wuhan, China, [2] Department of Neurosurgery, Union Hospital, Tongji Medical College, Huazhong University of Science and Technology, Wuhan, China, [3] Institute of Hematology, Union Hospital, Tongji Medical College, Huazhong University of Science and Technology, Wuhan, China, [4] Key Laboratory of Biological Targeted Therapy, The Ministry of Education, Wuhan, China, [5] Department of immunology, Hubei Clinical Research Center of Cancer Immunotherapy, Wuhan, China

OPEN ACCESS

Edited by:
Simona Kranjc Brezar,
Institute of Oncology Ljubljana, Slovenia

Reviewed by:
Sujit Kumar Bhutia,
National Institute of Technology Rourkela, India
Juan Zhou,
Shanghai Pulmonary Hospital, China

***Correspondence:**
Desheng Hu
desheng.hu@hust.edu.cn

[†]These authors have contributed equally to this work and share first authorship

Specialty section:
This article was submitted to Cancer Molecular Targets and Therapeutics, a section of the journal Frontiers in Oncology

Received: 25 January 2022
Accepted: 04 April 2022
Published: 04 May 2022

Citation:
Guo W, Du K, Luo S and Hu D (2022) Recent Advances of Autophagy in Non-Small Cell Lung Cancer: From Basic Mechanisms to Clinical Application. Front. Oncol. 12:861959. doi: 10.3389/fonc.2022.861959

Lung cancer is characterized by the most common oncological disease and leading cause of cancer death worldwide, of which a group of subtypes known as non-small cell lung cancer (NSCLC) accounts for approximately 85%. In the past few decades, important progression in the therapies of NSCLC has enhanced our understanding of the biology and progression mechanisms of tumor. The application of immunotherapy and small molecule tyrosine kinase inhibitors has brought significant clinical benefits in certain patients. However, early metastasis and the emergence of resistance to antitumor therapy have resulted in the relatively low overall cure and survival rates for NSCLC. Autophagy is a conserved process that allows cells to recycle unused or damaged organelles and cellular components. It has been reported to be related to the progression of NSCLC and resistance to targeted therapy and cytotoxic chemotherapy. Therefore, autophagy is considered as a potential therapeutic target for NSCLC. Mounting results have been reported about the combination of tyrosine kinase inhibitors and inhibitors of autophagy in models of NSCLC. This review aims to provide a comprehensive review on the roles of autophagy in NSCLC, focusing on related clinical data of agents that regulate autophagy in NSCLC. Furthermore, this study will provide a theoretical basis for further improvement of autophagy-based cancer therapy.

Keywords: non-small cell lung cancer, immunotherapy, resistance, tyrosine kinase inhibitors, autophagy

1 INTRODUCTION

Lung cancer including non-small cell lung cancer (NSCLC) and small-cell lung cancer (SCLC), has been reported to account for 11.6% and 18.4% of global cancer morbidity and mortality, respectively (1, 2). According to histological classification, approximately 85% of patients belong to the subtype referred to as NSCLC, among which the most common subtypes are lung squamous cell carcinoma (LUSC) and lung adenocarcinoma (LUAD) (3, 4). Over the past few decades, therapies for NSCLC

have progressed from cytotoxic treatment to effective and better tolerated regimens that are designed to target to specific molecular subtypes (3, 5, 6). The identification of target gene alterations is an evolution for the lung cancer management, with the combination of tumor genotyping making personalized treatment possible, and it is of great benefit to patients treated with kinase inhibitors (TKIs) for EGFR, ALK, ROS1, BRAF, or MET (7–11). Furthermore, the introduction of immune checkpoint blockers (ICBs) such as monoclonal antibodies that target programmed death-1 (PD-1) or programmed death ligand-1 (PD-L1) and antibodies against cytotoxic T-lymphocyte antigen-4 (CTLA-4) have indicated a new direction for lung cancer care (12, 13). To further improve the treatment efficiency, there is an urgent need to deeply understand the mechanisms of acquired resistance so as to provide a theoretical basis for effective treatments at the time of emergence.

In 2016, Yoshinori Ohsumi was awarded the Nobel Prize in Medicine for his contributions in elucidating the genetic basis of autophagy (14, 15). autophagy is generally believed to be an evolutionarily conserved physiological process, which is triggered by cellular stress or nutrient depletion, leading to the circulation of intracellular compounds. The vesicle fuses with lysosomes, and through subsequent degradation, new metabolites are produced to meet cell metabolism and energy requirements (9, 16, 17). Actually, in mammalian cells, protein degradation during autophagy occurs through three different mechanisms, including macroautophagy, and two other relatively less studied types, namely microautophagy and chaperone-mediated autophagy (CMA) (18). In macroautophagy, double-membrane vesicles are formed through a closed restriction membrane, which separates cargo proteins from the rest of the cytoplasmic components. Interestingly, proteins enter the lysosome cavity through the invagination of the lysosomal membrane surface in microautophagy (18). Different from the above, the selective pool of cytosolic proteins degraded by CMA are directly translocated across the lysosomal membrane (19, 20).

As a matter of fact, autophagy has a Janus character in the initiation and progression of cancer. On the one hand, autophagy prevents carcinogenesis by reducing the damage of cells (including DNA), but once carcinogenesis occurs, the role of autophagy in energy balance would help in cultivating cancer cells, thereby helping these aggressive cancer cells to grow in the stress environment (21). This makes the role of autophagy not only limited to protecting the host, it also has a function that is not welcomed, including the promotion the recurrence and invasion of cancer. Results from genetically engineered mouse models (GEMMs) of lung cancer, pancreatic cancer and melanoma induced by mutations in RAS or BRAF indicated that autophagy inhibited the growth of early benign tumors, but accelerated the growth of advanced cancers (22–26). Furthermore, there is accumulating evidence indicating that autophagy inhibition could be a potential approach in the treatment of advanced cancer (27). Therefore, a more in-depth understanding of how autophagy affects events in cancer cells and the response of patients to treatment may contribute to the improvement of treatment regimen for NSCLC.

In this article, we will review the research progress on the role of autophagy in NSCLC progression, the mechanism of autophagy affecting NSCLC progression, as well as clinical results obtained so far using autophagy inhibitors in NSCLC. With the increasing results of clinical research focusing on autophagy, the review of these topics is particularly timely, which would enable us to target autophagy effectively to improve the clinical prognosis of patients with NSCLC.

2 THE PROCESS OF AUTOPHAGY

Macroautophagy (hereafter referred to autophagy) is a multistep lysosomal degradation pathway that supports nutrient recycling and metabolic adaptation, which has been implicated as a process that regulates cancer (14). Mastering the mechanisms of autophagy flux can promote the development of effective compounds, thus ultimately treating autophagy-related cancers. Based on our current knowledge, the autophagy pathway includes at least 5 steps, which are initiation, vesicle nucleation, vesicle maturation, vesicle fusion and cargo degradation (**Figure 1**).

Autophagy is initiated by activation of Unc-51-like kinase 1 (ULK1) complex, which comprises ULK1, ULK2, autophagy-related gene 13 (ATG13), focal adhesion kinase interacting protein 200 kDa (FIP200) and ATG101. ULK1 complex can integrate two main stress signals in cells, including nutrient regulator (mTOR) and energy stress factor (AMPK). The ULK1 complex is usually inactive, and it is activated when mTORC1 is inhibited or AMPK is activated.

Once ULK1 kinase is activated, it would trigger the phosphorylation and activation of the Beclin1 -VPS34 (a class III phosphatidylinositol 3-kinase (PI3K)) complex, which includes Beclin1, VPS34, and other proteins such as activating molecule in BECN1-regulated autophagy protein 1 (AMBRA1), VPS15, ATG14, and UV radiation resistance associated gene protein (UVRAG), which depends on the subcellular localization of the complex (28). The activated Beclin1-VPS34 complex achieves vesicle nucleation through the formation of phosphatidylinositol 3-phosphate (PI3P) on membranes that can be derived from the endoplasmic reticulum (ER), mitochondria, plasma membrane (29–31).

During the maturation process, the formation of autophagosomes requires two unique protein conjugation events (32, 33): 1) ATG7 and ATG10 conjugate ATG5 to ATG12, and then ATG5-ATG12 binds to ATG16L1 to form a complex, and the ATG5-ATG12-ATG16L1 complex gets anchored onto PI3P produced by VPS34 on neonatal autophagosome through WIPI2B scaffold (34); 2) ATG4 cleaves pro-LC3 to generate soluble LC3-I, which is then conjugated to lipid phosphatidylethanolamine (PE) on the surface of the emerging autophagosome by ATG3 and ATG7, and further follows the guidance of the ATG5-ATG12-ATG16L1 complex (35). Once LC3-I is conjugated to lipid, it becomes

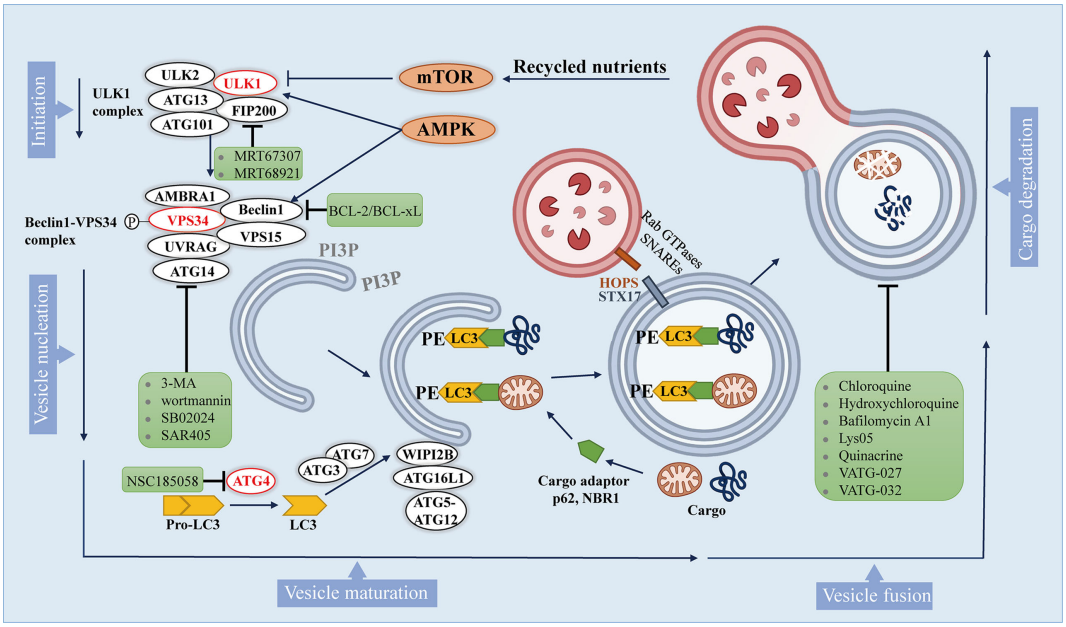


FIGURE 1 | The autophagy pathway and multiple stages can be inhibited. The autophagy pathway consists 5 steps. Intracellular membranes are prepared by initiation and vesicle nucleation to form AVs through the formation of PI3P on membranes. Next, LC3-I is conjugated to PE on emerging AVs. Subsequently, LC3 is docked with the cargo adapter so that the cargo can be loaded into the AVs. After AVs matures, it fuses with lysosomes to complete the degradation of cargo and the recycling of nutrients. Autophagy inhibitors are shown in green boxes.

inserted on the surface of the emerging autophagic vesicles (AVs) (36). On gel electrophoresis, the lipid-conjugated form of LC3 (LC3-II) migrates faster than LC3-I, so that the ratio of LC3-II and LC3-I can be used as an approximation of the number of AVs.

In addition to being a marker for AVs, LC3 on AVs is also a docking site for receptors of autophagy cargo, bringing autophagy cargo to AVs. Cargo receptors such as SQSTM1 (p62) and the neighbor of BRCA1 (NBR1) bind to proteins and organelles through ubiquitin labeling, and then undergo autophagy degradation (37). Specific cargo receptors will preferentially bind to specific cargoes, which may provide selectivity for the autophagy process (38). Once the isolation membrane is enclosed, it is called the autophagosome (27).

After autophagosomes are formed and cargos are sequestered, the cargo-bound autophagosomes are transported to the perinuclear region, where lysosomes exist (39). The membrane-tethering complexes (HOPS complex, VPS genes), Rab GTPases and soluble N-ethylmaleimide-sensitive factor attachment protein receptors (SNARE) along with syntaxin 17 (STX17) help the fusion of the autophagosomes to the lysosome (40, 41). Lastly, autophagic cargo are degraded by lysosomal hydrolases, and recycled contents are discharged through nutrient transporters, thereby fueling cell growth (42).

Although these 5 steps of autophagy are well established, additional autophagy regulators are still being discovered. These steps in the autophagy pathway represent potential drug targets, which provide pathways to influence autophagy positively and negatively.

3 THE ROLE OF AUTOPHAGY IN NSCLC PROGRESSION

Evidence suggests that the role of autophagy in tumorigenesis may be dichotomous. On the one hand, mice with allelic loss of Beclin1 are tumor prone and liver-specific deletion of ATG5 or ATG7 induces benign hepatomas, which suggest a role for autophagy in tumor suppression (43–45). On the other hand, autophagy enables cancer cells to survive from metabolically stressed and hypoxic regions in solid tumors (46–48).

Interestingly, Rao et al. (49) found that the inactivation of the essential autophagy gene ATG5 at early stage increased the number and volume of hyperplastic regions and adenomas in the mouse model of KRAS-driven NSCLC. Conversely, at later stages, autophagy is required for the progression of adenomas to adenocarcinomas. Indeed, the role of autophagy in cancer is environment-dependent, and its upregulation is necessary for cancer cells to survive in hypoxic tumor regions (50). Moreover, the transformation of the oncogene RAS up-regulates the basal level of autophagy to meet the needs of maintaining mitochondrial metabolism and tumor progression (23, 51, 52). Data from several studies revealed that, in $KRAS^{G12D}$-and BrafV600E-NSCLC in adult mice, loss of ATG7 caused tumors to accumulate defective mitochondria and leaded to impaired metabolism. On the other hand, in the absence of ATG7, cancer cell proliferation is inhibited, and the tumor develops into benign eosinophil tumor instead of adenoma and cancer, thereby prolonging the lifespan of mice (53–55). Karsli-Uzunbas (56) et al. found that, in the models of NSCLC, 5 weeks of acute reduction in autophagy transformed lung

adenocarcinoma into oncocytomas, and blocked the signal transduction of mTOR and MAP kinase, as well as cell proliferation and survival.

Tumors that have formed are more dependent on autophagy than newly developed tumors and normal tissues. This indicates that there may be a therapeutic target to inhibit tumorigenesis by appropriately controlling the extent and timing of autophagy inhibition, while preserving most of the normal tissues. Therefore, a comprehensive understanding of tumor dependence on the autophagy pathway driven by specific oncogenic events can promote autophagy regulation as an effective and specific cancer treatment strategy.

4 THE MECHANISM OF AUTOPHAGY AFFECTING NSCLC PROGRESSION

4.1 Autophagy Shapes the Tumor Microenvironment of NSCLC

The tumor microenvironment (TME) is shaped by several processes, such as autophagy and immune responses (57). The TME takes advantage of autophagy to meet the metabolic needs of cancer stem cells (CSCs), sounding immune cells, cancer associated fibroblasts (CAF), angiogenesis, neural connections, as well as extracellular matrix (**Figure 2**) (21). Furthermore, recent studies have shown that there is a complex interaction between autophagy and epithelial-mesenchymal transition (EMT), through which cancer cells acquire invasive phenotype and metastatic potential (58, 59).

4.1.1 CSCs

CSCs are a subgroup of cancer cells, which can promote the occurrence and development of cancer and are related to the production of drug resistance. Interestingly, it is reported that CSCs promote and maintain tumor heterogeneity by activating EMT, Juxtacrine and inflammatory signals in TME (60). It has been revealed that Lung CSCs can degrade p53 through the autophagy pathway, thereby enhancing Zeb1 expression and regulating stemness, suggesting that the autophagy-p53-Zeb1 axis regulates the self-renewal ability of CSCs (61). Moreover, in lung cancer stem cells, miR-138-5p mimic can inhibit ATG7-dependent regulation of autophagy and self-renewal (62).

4.1.2 CAFs

NSCLC has a high stromal content, which contribute to low response rates to current therapies and a poor long-term survival (63). As one of the most abundant cell types in the tumor stroma, CAFs have a tremendous influence on remodeling the stromal compartment within the TME through collagen deposition and matrix metalloproteinase secretion (64). *In vitro* and *in vivo* analysis using xenograft models of lung cancer indicated that CAFs produced IGF1/2, CXCL12 and β-hydroxybutyrate and increased the level of reactive oxygen species (ROS), which resulted in mTOR inactivation and autophagy increasement in cancer cells after irradiation (65). In addition, by triggering ROS-mediated autophagy in neighboring CAFs, cancer cells can use high-energy metabolites like glutamine and lactic acid to carry out the tricarboxylic acid (TCA) cycle under stress conditions, thereby supporting tumor growth and progression (21).

4.1.3 EMT

Recently, autophagy has been connected to EMT, an indispensable multistep process required for cancer cells' invasion and metastasis (66, 67). Moreover, studies have also shown that EMT induced by transforming growth factor (TGF)-β1 in NSCLC is autophagy-dependent (68). In addition,

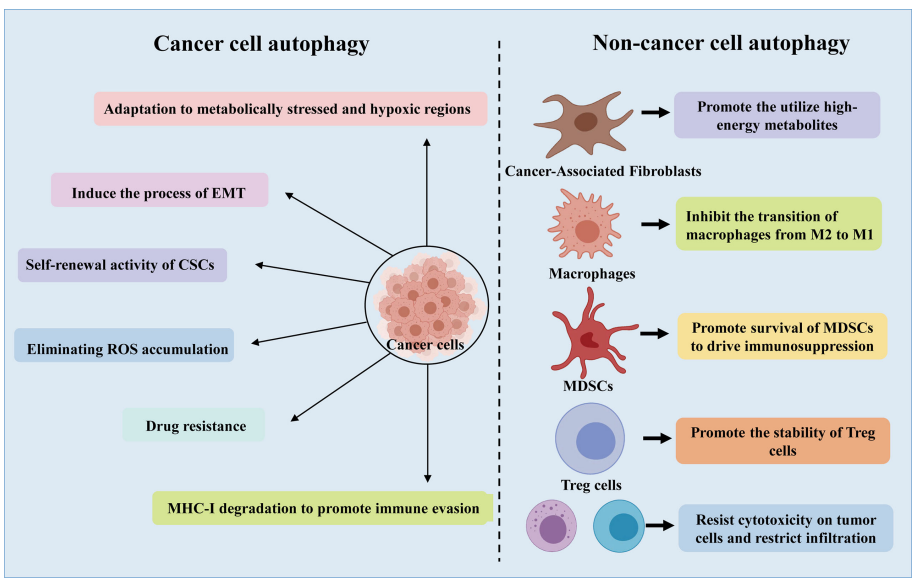


FIGURE 2 | A schematic representation of the role of autophagy in cancer cells and non-cancer cells.

rapamycin-induced autophagy can activate cell migration, invasion and the expression of EMT markers, and knockdown of Beclin1 can reverse this phenomenon (69). Another hepatocellular carcinoma model showed that inhibiting autophagy *in vitro* did not alter migration, invasion and EMT marker expression, while inhibition of autophagy *in vivo* caused cells to be sensitive to anoikis and reduced lung metastases (70).

There still exists many questions for cancer and TME treatment targeting autophagy. To unravel the signal transduction that controls the interaction between cancer cells and other components of TME, one of the future focuses may be to develop new models. For example, the development of 3D co-cultivation system might reveal some important metabolic interactomes in the TME. In order to have a better future for autophagy targeted cancer therapy, further basic research and translation studies are needed to clarify new findings and solve unanswered questions, like the role of bacterial components in the tumor microbiome.

4.2 Autophagy and Metabolic Reprogramming in NSCLC

Some studies have proved the importance of autophagy in maintaining the growth and survival of cancer cells by regulating the metabolism of cancer cells. Interestingly, autophagy enhances glucose uptake by up-regulating the expression of glucose transporter type 1 (GLUT1) on the cell surface, while blocking autophagy leads to accumulation of GLUT1 in late endosomes (71). Moreover, it is reported that during glucose starvation, hexokinase-2 (HK2) converts cell metabolism to autophagy-dependent pathway from glycolysis-dependent ones through the inhibition of mTORC1 (72). Deregulation of HK2 in Tongue Squamous Cell Carcinoma inhibited autophagic activity and weakened the invasiveness (73). Furthermore, cystine transporter SLC7A11-mediated cystine introduction depends on autophagy-mediated localization on the cell, and inhibition of autophagy would result in inactivation of SLC7A11 (74).

As an important event involved in the processing of metabolites and biosynthesis, autophagy can promote the metabolic adaptation of cancer cells in the survival of TME (**Figure 2**). Guo et al. found that glutamine or glutamate can rescue the starving ATG7-deficient KRAS-driven lung cancer cells, revealing the important role of autophagy in supporting the cyclic metabolites of TCA and nucleotide synthesis (25). In addition, adult mice with acute systemic loss of ATG7 died during fasting. The mice showed obvious muscle atrophy and died of hypoglycemia, which indicated that autophagy is necessary to maintain glucose homeostasis (56). Interestingly, the survival rate of cancer cell lines lacking ATG7 and p53 is reduced, and lipid cysts are formed, showing dysfunction of lipid metabolism (55). Additionally, in patients with NSCLC expressing a mutant form of EGFR, c-Jun n-terminal kinase (JNK)-induced autophagy results in high levels of glycolysis. Based on these phenomena, inhibition of autophagy may be a potential therapy for the treatment of lung adenocarcinoma.

4.3 Autophagy and ROS

ROS participates in the occurrence and development of cancer by oxidizing cell lipids, damaging the integrity of DNA and proteins, which also makes them more susceptible to the aggression of cancer (21). Autophagy has been shown to closely interplay with ROS (75–77). In the process of tumorigenesis, the production of ROS is related to the accumulation of dysfunctional organelles, which activates the autophagy pathway to clear the damaged organelles in the cells. In turn, the loss of autophagy can further induce ROS formation, leading to DNA damage (78). Autophagy eliminates accumulated ROS and relieves the metabolic stress of cancer cells in the TME, thereby promoting tumor survival (23, 42) (**Figure 2**). Cancer cells produce ROS under hypoxic conditions, and the transfer of ROS to CAFs promotes autophagy, thereby providing nutrition for the growth of cancer cells (21). Significant increase in ROS levels can cause DNA damage and the transformation of metabolism from OXPHOS to glycolysis, proving that autophagy could promote cancer cell growth by controlling ROS levels and energy metabolism (23). However, the role of ROS in the regulation of the progression of NSCLC by autophagy remains to be further determined.

5 CLINICAL RELEVANCE OF AUTOPHAGY IN NSCLC

5.1 Autophagy and Drug Resistance in NSCLC

It is worth noting that more and more studies have shown that autophagy is closely related to drug resistance in NSCLC. For a long time, the emergence of resistance to EGFR inhibitors has been a crucial clinical issue (79). Erlotinib can induce apoptosis and autophagy in NSCLC cells with EGFR activating mutations, and inhibiting the autophagy process can enhance the cytotoxicity of erlotinib to cancer cells (80). In addition, by inhibiting autophagy in NSCLC cells with wild-type EGFR, the resistance of NSCLC cells to erlotinib can be eliminated (81). Moreover, the inhibition of autophagy in TKI-resistant lung cancer cells can significantly enhance the sensitivity of lung cancer cells to erlotinib by regulating the endoplasmic reticulum stress (82). Coincidentally, Han W and other studies have shown that EGFR-TKIs, such as gefitinib and erlotinib, can activate autophagy of human lung cancer cells, and then the growth inhibitory effect of EGFR-TKIs on cancer cells is weakened (83). *In vitro* study using cell lines and clinical samples showed that one of the mechanisms of EGFR-TKI resistance is LC3a-mediated autophagy activation (79). Furthermore, other pre-clinical studies have demonstrated that the inhibition of autophagy can overcome the emergence of resistance to tyrosine kinase inhibitors in NSCLC and ALK-positive lung cancer (84, 85). Beyond that, it has been proven that hypoxia-induced autophagy in lung cancer leads to resistance to the chemotherapy drug cisplatin (86). Based on the phenomenon that EGFR-TKIs induce autophagy (83, 87), and autophagy may lead to chemotherapy resistance (88), researchers speculate that autophagy may be a protective mechanism for cancer cells and contribute to the emergence of drug resistance in NSCLC.

Elucidating the role of autophagy in drug resistance will aid in exploring how to manipulate autophagy to maximize the effect of cancer therapy. As the link between autophagy and drug resistance continues to strengthen, autophagy will undoubtedly become a promising target in cancer therapy. At the same time, it is also urgent to advance the combination therapy of autophagy modulators and existing antitumor drugs in clinical trials.

5.2 Autophagy Promotes Tumor Evasion in Antitumor Immune Responses

Autophagy has been reported to modulate immune components, mainly containing T and B lymphocytes, natural killer (NK) cells, tumor-associated macrophage (TAMs), and dendritic cells (DCs), Myeloid-derived suppressor cells (MDSCs), thereby interfering with host innate and adaptive immune responses. Autophagy in immune cells located in TME controls host antitumor immunity and induces an immunosuppressive microenvironment (**Figure 2**).

Upon systemic autophagy inhibition by chloroquine (CQ), as well as tumor-specific autophagy inhibition, infiltration of $CD8^+$ T cells and an increase of MHC-I molecules on the surface of cancer cell make them sensitive towards ICB, thereby inhibiting the growth of tumors (89, 90). The combination of anti-PD-1/PD-L1 blockade and Vps34 inhibition promotes the mass production of pro-inflammatory cytokines and chemokines CCL5, CXCL10 and IFN-γ, as well as the accumulation of $CD4^+$, $CD8^+$ T and NK cells, DCs and M1 macrophages, thus enhancing the efficacy of treatment (**Figure 3**) (91). In addition, autophagy can inhibit the antitumor immune responses by triggering the degradation of cytotoxic granules released from $CD8^+$ T and NK cells (92, 93). Furthermore, the combination of antitumor drug 5-FU and CQ can augment the response of $CD8^+$ T cells to HCT-116 colon cancer cells and promote the maturation of DCs (94). It is worth noting that the conditional deletion of ATG7 in $KRAS^{G12D}$-driven lung cancers closely correlated with abundant tumor infiltration by CTLs and macrophages (55, 95). Interestingly, Ma et al. found that SKIL promoted tumorigenesis and immune escape of NSCLC cells through upregulation of TAZ/autophagy axis and inhibition of downstream STING pathway, resulting in decreased T cell infiltration and release of chemokines such as CXCL10, CCL5 and IFN-β (96).

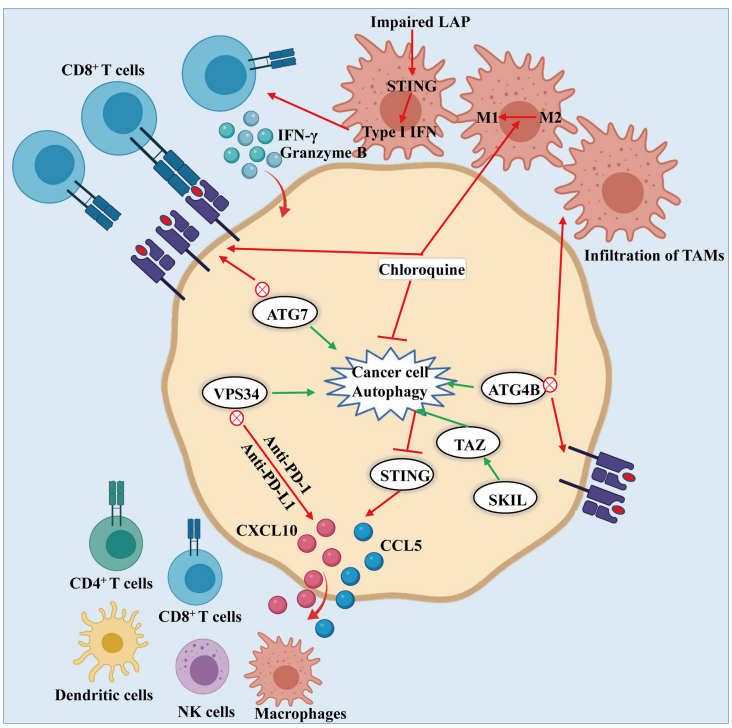


FIGURE 3 | Autophagy-mediated immune evasion of cancer cells: Knockdown of ATG7, or dominant negative expression of ATG4B or treatment of chloroquine leads to the inhibition of autophagy, which induces the accumulation of MHC-I on the surface of cancer cell. The MHC-I accumulation promotes the recognition and effect of $CD8^+$ T cells on cancer cells. Likewise, inhibiting autophagy results in the infiltration of TAMs and the conversion of macrophages from M2 to M1 phenotype, thereby enhancing the antitumor activity. What is noteworthy is that impairment of LAP results in activation of T cells mediated by STING, producing granzyme B and IFN-γ to kill the cancer cells. In addition, the combination of PIK3C3/VPS34 inhibitors with anti-PD-1 and PD-L1 therapy could increase the numbers of NK and $CD8^+$, $CD4^+$ T cells, macrophages and dendritic cells along with CCL5 and CXCL10 infiltrating in tumor environment. Moreover, SKIL promoted tumorigenesis and immune escape of NSCLC cells by up-regulating the TAZ/autophagy axis and inhibition on downstream STING pathway, thereby resulting in reducing T cell infiltration and release of chemokines including CXCL10, CCL5 and IFN-β.

Besides that, specific deletion of two essential genes, ATG7 or ATG5, in Treg cells impaired their survival fitness and lineage stability, leading to loss of Treg and greater tumor resistance (97). In addition, it was shown that by inducing autophagy to promote the survival of MDSCs, the high mobility group box 1 can induce an immunosuppressive tumor microenvironment, thereby promoting tumor progression (98). Furthermore, glycolysis inhibits the formation of autophagy, and enhances the expression of autophagy-mediated partial hepatic enrichment activating factors, thereby promoting the expression of granulocyte-macrophage colony stimulating factor, which supports the development of MDSCs in tumors (99).

In most solid tumors, autophagy plays a crucial role in controlling macrophages at different stages, especially the polarization. Interestingly, in B16 melanoma and H22 liver cancer tumor-bearing mouse models, CQ treatment promotes the antitumor immunity mediated by $CD8^+$ T cells *via* activating the inflammatory cytokines, thereby causing TAMs to deviate from conversion of M2 phenotype to M1 phenotype (100). Interestingly, LC3-associated phagocytosis (LAP) has been shown to contribute to the polarization of macrophages towards M2 phenotype in TME (101). Larissa D et al. found that, upon phagocytosis of dying cancer cells, LAP-deficient TAMs induce antitumor T cell responses by triggering STING-mediated type-I interferon responses and augmenting the expression of pro-inflammatory gene (101).

It is noteworthy that inactivation of the autophagy gene ATG5 leads to accelerated tumorigenesis at early stages by promoting the infiltration of Treg cells in a mouse model of NSCLC (49). Therefore, great importance should be attached to the right staging and grading of tumors to maximize the efficacy of autophagy inhibitors from the perspective of clinical application.

5.3 Biomarkers of Autophagy in NSCLC

A major challenge in all of the clinical studies has been identifying appropriate pharmacodynamic biomarkers which are specific in evaluating changes within autophagy. Nevertheless, there are few effective and specific autophagy-related biomarkers currently identified, which are crucial for selecting patients for autophagy inhibitor-related clinical trials and evaluating the effect of treatment. See **Table 1** for some examples of autophagy-related proteins with biomarker potential.

5.3.1 LC3B

Microtubule-associated protein 1 light chain 3B (MAP1LC3B, LC3B) is one of the best studied proteins in autophagy-related proteins, and has been utilized as an autophagy marker in multiple trials *in vivo* and *in vitro*. Accumulating evidence showed that the high expression of LC3B is related to the high aggressiveness and adverse prognosis of many types of cancers, including colorectal cancers (102), breast cancer (103) and hepatocellular carcinoma (104). It's worth noting that a recent study of NSCLC evaluated the relationship between the expression levels of LC3B and p62 and prognosis, and found that high punctate expression of LC3B may be associated with a good prognosis (105).

TABLE 1 | Autophagy-related proteins as biomarkers.

Biomarker	Setting	Study object	Clinical significance	Reference
LC3B	Colorectal cancers (CRC)	127 CRC patients with known KRAS mutational status	LC3 overexpression was significantly associated with decreased overall survival (OS) in the KRAS-mutated CRC subgroup	(102)
	Breast cancer	20 breast cancer patients	Elevated expression of LC3B was associated with increased nuclear grade and shortened survival.	(103)
	Hepatocellular carcinoma (HCC)	156 operable HCC patients	Overexpression of LC3B correlates with malignant progression and predicts a poor prognosis in HCC	(104)
	non-small cell lung cancer (NSCLC)	466 stage I/II NSCLC patients	High LC3B levels may be correlated with lower tumor aggressiveness	(105)
LC3A	breast carcinomas	102 operable breast carcinomas patients	"Stone-like" structure (SLS) distribution of LC3A was related to high-grade tumors and a less favorable outcome	(106)
	NSCLC	115 patients with NSCLC treated with surgery	Elevated presence of SLSs is strongly linked to a poor outcome in NSCLC	(107)
p62	NSCLC	466 stage I/II NSCLC patients	High expression of p62 was significantly associated with higher tumor aggressiveness	(105)
		104 NSCLC patients	High expression of p62 was significantly associated with shorter survival	(108)
		109 NSCLC patients	The accumulation of p62 was associated with worse lung cancer-specific survival	(109)
ULK1/2	HCC	156 operable HCC patients	ULK1 expression was negatively correlated with 5-year progression free survival	(110)
Beclin1	NSCLC	104 NSCLC patients	Low expression of Beclin1 was significantly associated with shorter survival	(108)
		244 primary NSCLC patients	Low expression of Beclin1 showed significantly inferior OS and progression-free survival	(111)
		1159 patients with NSCLC	High level of Beclin1 was significantly associated with better OS in NSCLC	(112)
ATG4B	Oral squamous cell carcinoma (OSCC)	498 OSCC patients	High protein levels of ATG4B were significantly associated with worse disease-specific survival	(113)
LAMP2A and HSC70	Pulmonary squamous cell carcinomas (pSQCC)	402 patients with primary resected pSQCC	High LAMP2A and HSC70 expression were associated with worse OS and disease-free survival	(114)
Autophagy-related lncRNAs	Lung adenocarcinoma (LUAD)	Data from The Cancer Genome Atlas database	16 autophagy-related lncRNAs were identified to have significant prognostic value for LUAD patients	(115)

5.3.2 LC3A

Early studies reported that there are three different distribution patterns of LC3A in solid tumors through immunohistochemical staining, including diffuse distribution in the cytoplasm, paranuclear and "stone-like" structure (SLS) distribution (106), and each distribution pattern represents a different prognostic result. It is worth noting that the increase in the number of SLS is related to the adverse prognosis of NSCLC (107).

5.3.3 p62

In the process of autophagosome formation, p62 acts as a bridge linking LC3 and its substrates (116). Since p62 is degraded in the autophagy flux, it is generally believed that the accumulation of p62 protein in the cell is a sign of the inhibition of autophagy (19). In NSCLC, the high expression of p62 significantly related to the tumor's high aggressiveness and poor prognosis (108, 109).

5.3.4 ULK-1/2

ULK-1 and ULK-2 are the only serine/threonine kinases in the process of autophagy (117, 118), and small molecule inhibitors for ULK-1/2 are under development (118, 119). In hepatocellular carcinoma, ULK1 expression was reported to be negatively correlated with 5-year progression free survival (110). However, no association of ULK-1/2 with prognosis in NSCLC is available from current researches. To better determine the prognostic value of ULK1 and ULK2 in different cancer types, more studies are urgently needed in larger patient cohorts.

5.3.5 Beclin1 and VPS34

As a key regulator of autophagy, Beclin1 was reported to be an independent prognostic biomarker in the NSCLC (111). Similarly, Zheng et al. (112) reported that the high expression of Beclin1 is related to the better prognosis of NSCLC, indicating that Beclin1 may become a favorable prognostic marker of NSCLC.

5.3.6 ATG4B

As the enzymatic roles of cysteine protease ATG4B are of great significance in the process of autophagy, it is currently referred as one of the potential therapeutic targets (120, 121). Intense presence of ATG4B was significantly associated with worse disease-specific survival in oral squamous cell carcinoma (113). Previous researches revealed increased expression of ATG4B in lung cancer cells (122), but its prognostic value for different cancers is poorly understood.

5.3.7 Additional Autophagy-Related Biomarkers

Of course, there are also reports on the potential of other autophagy-related proteins as biomarkers. For instance, in primary resected squamous cell carcinomas of the lung, chaperone-mediated autophagy markers LAMP2A and HSC70 have been identified as independent poor prognostic markers (114). In addition, Jiang et al. (115) identified 16 autophagy-related long non-coding RNAs (lncRNAs) which have significant prognostic value for LUAD patients.

5.4 Autophagy Can be Inhibited at Multiple Stages

Formation of the autophagosome requires the assistance of various genes called autophagy related (ATG) genes, which are evolutionarily-conserved (123). Interestingly, accumulating evidence revealed that autophagy can be inhibited at multiple stages (**Figure 1**). It's reported that two drugs MRT67307 and MRT68921 have been synthesized to inhibit ULK1 and ULK2 specifically, which lead to the inhibition of autophagy flux (119).

After the phosphorylation of Beclin1 by ULK1, it promotes the localization of autophagic proteins to the phagophore. It is being proved that the pro-autophagic activity of Beclin1 can be attenuated since BCL-2 and BCL-xL can interact with Beclin1 at the BH3 domain (124). In addition, phosphorylation of VPS34 (also known as PIK3C3) reduces its interaction with Beclin1, which can be targeted pharmacologically within the upstream by 3-methyladenine (3-MA) and wortmannin (125) which can inhibit PI3K, or VPS34 inhibitors, like RNAi or SB02024, SAR405 (91, 126).

The process of growing double membranes undergoing maturation and finally forming autophagosomes requires the participation of a variety of enzymes, including ATG4B, ATG7, and ATG10. Studies have shown that the ATG4B inhibitor NSC185058 (121) have both *in vitro* and *in vivo* antitumor activity. Besides, another study found that inhibition of autophagy by knocking down ATG7 or expressing dominant negative ATG4B in cancer cells resulted in a significant increase in the number of $CD8^+$ T cells infiltrating in pancreatic tumors (89).

Later on, protein STX17 promotes the fusion of autophagosomes and lysosomes to produce autolysosomes. In this regard, CQ or hydroxychloroquine (HCQ) and bafilomycin A1 can inhibit the fusion of autophagosomes with lysosomes, and lysosomal inhibitors such as Lys05, quinacrine, VATG-027 and VATG-032 can also be utilized to target this process to inhibit autophagy (127–131).

As an autophagy inhibitor, the clinical efficacy of CQ undoubtedly illustrates the promise of autophagy inhibition as a therapeutic strategy, but also highlights the critical need for new inhibitors of autophagy, including the development of new compounds, as well as promotion of translation into clinical medicine. In this regard, certain inhibitors mentioned above are showing initial promise.

5.5 Clinical Trials Targeting Autophagy in NSCLC

Indeed, clinical intervention trials targeting autophagy in cancer treatment are already underway, most of which focus on inhibition of autophagy. In March 2022, a search for the search term "autophagy and cancer" on the ClinicalTrials.gov website showed 91 studies, mainly focusing on inhibiting and evaluating autophagy to improve prognosis of cancer patients.

As the only drugs used to inhibit autophagy in current clinical practice, CQ and hydroxychloroquine (HCQ) can prevent the degradation of cargo by deacidifying the lysosome and blocking the fusion of autophagosomes with lysosomes (132). Early

clinical evidence for improving treatment effects by inhibiting autophagy comes from a small trial involving 18 patients with glioblastoma, which revealed that the median survival of patients receiving CQ combined with radiotherapy and temozolomide alkylation treatment was significantly prolonged compared with the control group (133). Hereafter, a randomized, double-blind, placebo-controlled trial demonstrated that administration of CQ in addition to the conventional treatment of glioblastoma multiforme can improve the mid-term survival rate (134).

The integrated results of published clinical trials (**Table 2**) indicate that HCQ is safe for the treatment of NSCLC. Interestingly, a dose-escalation phase I study was conducted with erlotinib and HCQ in patients with advanced NSCLC who had previously temporarily benefited from EGFR inhibitor therapy. They found that taking HCQ 1000 mg daily was tolerable and safe for patients. One patient had a partial response to the combination of erlotinib and HCQ, and the overall response rate was 5% (135). Furthermore, seventy-three patients with NSCLC or breast cancer with brain metastasis were randomly grouped, with patients receiving full brain radiotherapy and 150 mg of CQ per day for 4 weeks or the same schedule of full brain radiotherapy and a matching placebo. In their study, they found that combination of full brain radiotherapy and CQ improved the control of brain metastasis with no increase in toxicity (136). In addition, a phase Ib/II report of chemotherapy with HCQ revealed that addition of HCQ could reverse chemotherapy resistance in advanced NSCLC (137).

Clinical trials, in which CQ or HCQ were utilized as autophagy inhibitors that targeting lysosomes, have proved the safety of targeting autophagy in the treatment of cancer. In addition to lysosomal inhibitors, other autophagy-specific inhibitors are still under development, including drugs targeting early steps, such as ATG4B and ULK1. Although preliminary data are encouraging, these compounds are still in early preclinical studies (138).

6 CONCLUSION AND FUTURE PERSPECTIVE

As the leading cause of cancer-related death, NSCLC remains difficult to cure. Elucidating the molecular mechanisms of NSCLC and discovering new biomarkers will aid in developing more specific and efficient therapies. Autophagy is an important physiological activity that controls cell survival and death, affecting cell homeostasis and clinical therapeutics. With an increasing understanding of the role and mechanisms of autophagy, the problems we currently face are clearly more complex than initially anticipated. Above all, we need to identify some reliable compounds targeting key components of autophagy to deepen our understanding of the consequences of pharmacological regulation of autophagy and help translate it into clinical use. In clinical trials, investigating the clinical efficacy of currently available autophagy-modulating compounds will improve our understanding of the effects of these autophagy-modulating agents and promote its translation in clinical applications. In clinical trials, studying the clinical efficacy of currently available autophagy-modulating compounds helps to deepen our understanding of the effects of these autophagy-modulating agents, thus establishing relevance to preclinical models.

Autophagy is essential for maintaining glucose homeostasis and tumor growth in lung cancer (139). Based on this fact, it's reasonable to assume that tumor growth can be restricted through the inhibition of autophagy. Notably, there is also evidence that autophagy deficiency triggers inhibition of antitumor immunosurveillance (49), which undoubtedly points to other therapeutic concepts. Overall, the fact that autophagy has been described as both tumor suppressor and tumor promoter in NSCLC does not mean that it cannot be therapeutically modulated. The overwhelming evidence points to inhibition of autophagy in NSCLC, and the results of the combination of chemotherapeutics and autophagy inhibition have led to the initiation of several clinical trials of chemoradiotherapy in combination with hydroxychloroquine (NCT01649947; NCT00728845). The predictive value of mouse models is limited due to the significant differences in immune system function between mice and humans, as well as the inherent limitations of oncogenic induction and genetically engineered models. Therefore, the impact of modulating autophagy on antitumor immune responses still needs to be evaluated in clinical trials.

There is still no complete and reliable system to assess autophagy in human samples, including blood and tumors, which undoubtedly limits our ability to evaluate autophagy regulation in clinical trials. In order to have a better future for autophagy targeted cancer therapy, further studies should focus on developing better biomarkers as pharmacodynamic markers for the efficacy of autophagy inhibitors and patient selection in the treatment. At the same time, it is obvious that, as tool compounds and autophagy inhibitors, stronger and specific autophagy inhibitors are needed.

TABLE 2 | The ongoing clinical trials using therapy targeting autophagy in NSCLC.

Clinical trial identifier	Autophagy Inhibitor	Clinical trial Phase	Additional treatment
NCT01649947	Hydroxychloroquine	II	Paclitaxel Carboplatin Bevacizumab
NCT00728845	Hydroxychloroquine	II	Paclitaxel Carboplatin Bevacizumab

AUTHOR CONTRIBUTIONS

Conceptualization, WG and KD. Investigation, WG and KD. Writing—original draft preparation, WG and KD. Writing—review and editing, WG, KD, SL, and DH. Project administration, SL and DH. All authors have read and agreed to the published version of the manuscript.

FUNDING

This work was funded by the National Key R&D Program of China (no. 2019YFC1316204), the National Natural Science Foundation of China (82161138003, 81974249, 82070136), the Natural Science Foundation of Hubei Province (2020BHB016).

REFERENCES

1. Imyanitov EN, Iyevleva AG, Levchenko EV. Molecular Testing and Targeted Therapy for Non-Small Cell Lung Cancer: Current Status and Perspectives. *Crit Rev Oncol Hematol* (2021) 157:103194. doi: 10.1016/j.critrevonc.2020.103194
2. Bray F, Ferlay J, Soerjomataram I, Siegel RL, Torre LA, Jemal A. Global Cancer Statistics 2018: GLOBOCAN Estimates of Incidence and Mortality Worldwide for 36 Cancers in 185 Countries. *CA Cancer J Clin* (2018) 68 (6):394–424. doi: 10.3322/caac.21492
3. Herbst RS, Morgensztern D, Boshoff C. The Biology and Management of Non-Small Cell Lung Cancer. *Nature* (2018) 553(7689):446–54. doi: 10.1038/nature25183
4. Molina JR, Yang P, Cassivi SD, Schild SE, Adjei AA. Non-Small Cell Lung Cancer: Epidemiology, Risk Factors, Treatment, and Survivorship. *Mayo Clin Proc* (2008) 83(5):584–94. doi: 10.4065/83.5.584
5. Cancer Genome Atlas Research N. Author Correction: Comprehensive Molecular Profiling of Lung Adenocarcinoma. *Nature* (2018) 559(7715): E12. doi: 10.1038/s41586-018-0228-6
6. Cancer Genome Atlas Research N. Comprehensive Genomic Characterization of Squamous Cell Lung Cancers. *Nature* (2012) 489 (7417):519–25. doi: 10.1038/nature11404
7. Lemmon MA, Schlessinger J, Ferguson KM. The EGFR Family: Not So Prototypical Receptor Tyrosine Kinases. *Cold Spring Harb Perspect Biol* (2014) 6(4):a020768. doi: 10.1101/cshperspect.a020768
8. Lin JJ, Riely GJ, Shaw AT. Targeting ALK: Precision Medicine Takes on Drug Resistance. *Cancer Discov* (2017) 7(2):137–55. doi: 10.1158/2159-8290.CD-16-1123
9. Shaw AT, Ou SH, Bang YJ, Camidge DR, Solomon BJ, Salgia R, et al. Crizotinib in ROS1-Rearranged Non-Small-Cell Lung Cancer. *N Engl J Med* (2014) 371(21):1963–71. doi: 10.1056/NEJMoa1406766
10. Hyman DM, Puzanov I, Subbiah V, Faris JE, Chau I, Blay JY, et al. Vemurafenib in Multiple Nonmelanoma Cancers With BRAF V600 Mutations. *N Engl J Med* (2015) 373(8):726–36. doi: 10.1056/NEJMoa1502309
11. Paik PK, Drilon A, Fan PD, Yu H, Rekhtman N, Ginsberg MS, et al. Response to MET Inhibitors in Patients With Stage IV Lung Adenocarcinomas Harboring MET Mutations Causing Exon 14 Skipping. *Cancer Discov* (2015) 5(8):842–9. doi: 10.1158/2159-8290.CD-14-1467
12. Leach DR, Krummel MF, Allison JP. Enhancement of Antitumor Immunity by CTLA-4 Blockade. *Science* (1996) 271(5256):1734–6. doi: 10.1126/science.271.5256.1734
13. McGranahan N, Furness AJ, Rosenthal R, Ramskov S, Lyngaa R, Saini SK, et al. Clonal Neoantigens Elicit T Cell Immunoreactivity and Sensitivity to Immune Checkpoint Blockade. *Science* (2016) 351(6280):1463–9. doi: 10.1126/science.aaf1490
14. Amaravadi RK, Kimmelman AC, Debnath J. Targeting Autophagy in Cancer: Recent Advances and Future Directions. *Cancer Discov* (2019) 9 (9):1167–81. doi: 10.1158/2159-8290.CD-19-0292
15. Levine B, Klionsky DJ. Autophagy Wins the 2016 Nobel Prize in Physiology or Medicine: Breakthroughs in Baker's Yeast Fuel Advances in Biomedical Research. *Proc Natl Acad Sci USA* (2017) 114(2):201–5. doi: 10.1073/pnas.1619876114
16. Bagherniya M, Butler AE, Barreto GE, Sahebkar A. The Effect of Fasting or Calorie Restriction on Autophagy Induction: A Review of the Literature. *Ageing Res Rev* (2018) 47:183–97. doi: 10.1016/j.arr.2018.08.004
17. He L, Zhang J, Zhao J, Ma N, Kim SW, Qiao S, et al. Autophagy: The Last Defense Against Cellular Nutritional Stress. *Adv Nutr* (2018) 9(4):493–504. doi: 10.1093/advances/nmy011
18. Mizushima N, Levine B, Cuervo AM, Klionsky DJ. Autophagy Fights Disease Through Cellular Self-Digestion. *Nature* (2008) 451(7182):1069–75. doi: 10.1038/nature06639
19. Klionsky DJ, Abdelmohsen K, Abe A, Abedin MJ, Abeliovich H, Acevedo Arozena A, et al. Guidelines for the Use and Interpretation of Assays for Monitoring Autophagy (3rd Edition). *Autophagy* (2016) 12(1):1–222. doi: 10.1080/15548627.2015.1100356
20. Orenstein SJ, Cuervo AM. Chaperone-Mediated Autophagy: Molecular Mechanisms and Physiological Relevance. *Semin Cell Dev Biol* (2010) 21 (7):719–26. doi: 10.1016/j.semcdb.2010.02.005
21. Mukhopadhyay S, Mahapatra KK, Praharaj PP, Patil S, Bhutia SK. Recent Progress of Autophagy Signaling in Tumor Microenvironment and Its Targeting for Possible Cancer Therapeutics. *Semin Cancer Biol* (2021) S1044-579X(21)00227-3. doi: 10.1016/j.semcancer.2021.09.003
22. Strohecker AM, White E. Targeting Mitochondrial Metabolism by Inhibiting Autophagy in BRAF-Driven Cancers. *Cancer Discov* (2014) 4(7):766–72. doi: 10.1158/2159-8290.CD-14-0196
23. Yang S, Wang X, Contino G, Liesa M, Sahin E, Ying H, et al. Pancreatic Cancers Require Autophagy for Tumor Growth. *Genes Dev* (2011) 25 (7):717–29. doi: 10.1101/gad.2016111
24. Yang A, Kimmelman AC. Inhibition of Autophagy Attenuates Pancreatic Cancer Growth Independent of TP53/TRP53 Status. *Autophagy* (2014) 10 (9):1683–4. doi: 10.4161/auto.29961
25. Guo JY, Teng X, Laddha SV, Ma S, Van Nostrand SC, Yang Y, et al. Autophagy Provides Metabolic Substrates to Maintain Energy Charge and Nucleotide Pools in Ras-Driven Lung Cancer Cells. *Genes Dev* (2016) 30 (15):1704–17. doi: 10.1101/gad.283416.116
26. Guo JY, Xia B, White E. Autophagy-Mediated Tumor Promotion. *Cell* (2013) 155(6):1216–9. doi: 10.1016/j.cell.2013.11.019
27. Tanida I. Autophagosome Formation and Molecular Mechanism of Autophagy. *Antioxid Redox Signal* (2011) 14(11):2201–14. doi: 10.1089/ars.2010.3482
28. Behrends C, Sowa ME, Gygi SP, Harper JW. Network Organization of the Human Autophagy System. *Nature* (2010) 466(7302):68–76. doi: 10.1038/nature09204
29. Shibutani ST, Yoshimori T. A Current Perspective of Autophagosome Biogenesis. *Cell Res* (2014) 24(1):58–68. doi: 10.1038/cr.2013.159
30. Ravikumar B, Moreau K, Jahreiss L, Puri C, Rubinsztein DC. Plasma Membrane Contributes to the Formation of Pre-Autophagosomal Structures. *Nat Cell Biol* (2010) 12(8):747–57. doi: 10.1038/ncb2078
31. Hailey DW, Rambold AS, Satpute-Krishnan P, Mitra K, Sougrat R, Kim PK, et al. Mitochondria Supply Membranes for Autophagosome Biogenesis During Starvation. *Cell* (2010) 141(4):656–67. doi: 10.1016/j.cell.2010.04.009
32. Walczak M, Martens S. Dissecting the Role of the Atg12-Atg5-Atg16 Complex During Autophagosome Formation. *Autophagy* (2013) 9(3):424–5. doi: 10.4161/auto.22931
33. Onorati AV, Dyczynski M, Ojha R, Amaravadi RK. Targeting Autophagy in Cancer. *Cancer* (2018) 124(16):3307–18. doi: 10.1002/cncr.31335
34. Wilson MI, Dooley HC, Tooze SA. WIPI2b and Atg16L1: Setting the Stage for Autophagosome Formation. *Biochem Soc Trans* (2014) 42(5):1327–34. doi: 10.1042/BST20140177
35. Kraya AA, Piao S, Xu X, Zhang G, Herlyn M, Gimotty P, et al. Identification of Secreted Proteins That Reflect Autophagy Dynamics Within Tumor Cells. *Autophagy* (2015) 11(1):60–74. doi: 10.4161/15548627.2014.984273

36. Ichimura Y, Kirisako T, Takao T, Satomi Y, Shimonishi Y, Ishihara N, et al. A Ubiquitin-Like System Mediates Protein Lipidation. *Nature* (2000) 408 (6811):488–92. doi: 10.1038/35044114
37. Lamark T, Kirkin V, Dikic I, Johansen T. NBR1 and P62 as Cargo Receptors for Selective Autophagy of Ubiquitinated Targets. *Cell Cycle* (2009) 8 (13):1986–90. doi: 10.4161/cc.8.13.8892
38. Gatica D, Lahiri V, Klionsky DJ. Cargo Recognition and Degradation by Selective Autophagy. *Nat Cell Biol* (2018) 20(3):233–42. doi: 10.1038/s41556-018-0037-z
39. Fass E, Shvets E, Degani I, Hirschberg K, Elazar Z. Microtubules Support Production of Starvation-Induced Autophagosomes But Not Their Targeting and Fusion With Lysosomes. *J Biol Chem* (2006) 281 (47):36303–16. doi: 10.1074/jbc.M607031200
40. Takats S, Pircs K, Nagy P, Varga A, Karpati M, Hegedus K, et al. Interaction of the HOPS Complex With Syntaxin 17 Mediates Autophagosome Clearance in Drosophila. *Mol Biol Cell* (2014) 25(8):1338–54. doi: 10.1091/mbc.E13-08-0449
41. Nakamura S, Yoshimori T. New Insights Into Autophagosome-Lysosome Fusion. *J Cell Sci* (2017) 130(7):1209–16. doi: 10.1242/jcs.196352
42. Kimmelman AC, White E. Autophagy and Tumor Metabolism. *Cell Metab* (2017) 25(5):1037–43. doi: 10.1016/j.cmet.2017.04.004
43. Qu X, Yu J, Bhagat G, Furuya N, Hibshoosh H, Troxel A, et al. Promotion of Tumorigenesis by Heterozygous Disruption of the Beclin 1 Autophagy Gene. *J Clin Invest* (2003) 112(12):1809–20. doi: 10.1172/JCI20039
44. Takamura A, Komatsu M, Hara T, Sakamoto A, Kishi C, Waguri S, et al. Autophagy-Deficient Mice Develop Multiple Liver Tumors. *Genes Dev* (2011) 25(8):795–800. doi: 10.1101/gad.2016211
45. Yue Z, Jin S, Yang C, Levine AJ, Heintz N. Beclin 1, an Autophagy Gene Essential for Early Embryonic Development, Is A Haploinsufficient Tumor Suppressor. *Proc Natl Acad Sci USA* (2003) 100(25):15077–82. doi: 10.1073/pnas.2436255100
46. Degenhardt K, Mathew R, Beaudoin B, Bray K, Anderson D, Chen G, et al. Autophagy Promotes Tumor Cell Survival and Restricts Necrosis, Inflammation, and Tumorigenesis. *Cancer Cell* (2006) 10(1):51–64. doi: 10.1016/j.ccr.2006.06.001
47. Karantza-Wadsworth V, Patel S, Kravchuk O, Chen G, Mathew R, Jin S, et al. Autophagy Mitigates Metabolic Stress and Genome Damage in Mammary Tumorigenesis. *Genes Dev* (2007) 21(13):1621–35. doi: 10.1101/gad.1565707
48. Mathew R, Kongara S, Beaudoin B, Karp CM, Bray K, Degenhardt K, et al. Autophagy Suppresses Tumor Progression by Limiting Chromosomal Instability. *Genes Dev* (2007) 21(11):1367–81. doi: 10.1101/gad.1545107
49. Rao S, Yang H, Penninger JM, Kroemer G. Autophagy in Non-Small Cell Lung Carcinogenesis: A Positive Regulator of Antitumor Immunosurveillance. *Autophagy* (2014) 10(3):529–31. doi: 10.4161/auto.27643
50. White E. Deconvoluting the Context-Dependent Role for Autophagy in Cancer. *Nat Rev Cancer* (2012) 12(6):401–10. doi: 10.1038/nrc3262
51. Guo JY, Chen HY, Mathew R, Fan J, Strohecker AM, Karsli-Uzunbas G, et al. Activated Ras Requires Autophagy to Maintain Oxidative Metabolism and Tumorigenesis. *Genes Dev* (2011) 25(5):460–70. doi: 10.1101/gad.2016311
52. Lock R, Kenific CM, Leidal AM, Salas E, Debnath J. Autophagy-Dependent Production of Secreted Factors Facilitates Oncogenic RAS-Driven Invasion. *Cancer Discov* (2014) 4(4):466–79. doi: 10.1158/2159-8290.CD-13-0841
53. Guo JY, White E. Autophagy Is Required for Mitochondrial Function, Lipid Metabolism, Growth, and Fate of KRAS(G12D)-Driven Lung Tumors. *Autophagy* (2013) 9(10):1636–8. doi: 10.4161/auto.26123
54. Strohecker AM, Guo JY, Karsli-Uzunbas G, Price SM, Chen GJ, Mathew R, et al. Autophagy Sustains Mitochondrial Glutamine Metabolism and Growth of BrafV600E-Driven Lung Tumors. *Cancer Discov* (2013) 3 (11):1272–85. doi: 10.1158/2159-8290.CD-13-0397
55. Guo JY, Karsli-Uzunbas G, Mathew R, Aisner SC, Kamphorst JJ, Strohecker AM, et al. Autophagy Suppresses Progression of K-Ras-Induced Lung Tumors to Oncocytomas and Maintains Lipid Homeostasis. *Genes Dev* (2013) 27(13):1447–61. doi: 10.1101/gad.219642.113
56. Karsli-Uzunbas G, Guo JY, Price S, Teng X, Laddha SV, Khor S, et al. Autophagy Is Required for Glucose Homeostasis and Lung Tumor Maintenance. *Cancer Discov* (2014) 4(8):914–27. doi: 10.1158/2159-8290.CD-14-0363
57. Bustos SO, Antunes F, Rangel MC, Chammas R. Emerging Autophagy Functions Shape the Tumor Microenvironment and Play a Role in Cancer Progression - Implications for Cancer Therapy. *Front Oncol* (2020) 10:606436. doi: 10.3389/fonc.2020.606436
58. Wu H, Huang S, Chen Z, Liu W, Zhou X, Zhang D. Hypoxia-Induced Autophagy Contributes to the Invasion of Salivary Adenoid Cystic Carcinoma Through the HIF-1alpha/BNIP3 Signaling Pathway. *Mol Med Rep* (2015) 12(5):6467–74. doi: 10.3892/mmr.2015.4255
59. Singla M, Bhattacharyya S. Autophagy as a Potential Therapeutic Target During Epithelial to Mesenchymal Transition in Renal Cell Carcinoma: An *In Vitro* Study. *BioMed Pharmacother* (2017) 94:332–40. doi: 10.1016/j.biopha.2017.07.070
60. Bocci F, Gearhart-Serna L, Boareto M, Ribeiro M, Ben-Jacob E, Devi GR, et al. Toward Understanding Cancer Stem Cell Heterogeneity in the Tumor Microenvironment. *Proc Natl Acad Sci USA* (2019) 116(1):148–57. doi: 10.1073/pnas.1815345116
61. Wang J, Liu D, Sun Z, Ye T, Li J, Zeng B, et al. Autophagy Augments the Self-Renewal of Lung Cancer Stem Cells by the Degradation of Ubiquitinated P53. *Cell Death Dis* (2021) 12(1):98. doi: 10.1038/s41419-021-03392-6
62. Zhou Q, Cui F, Lei C, Ma S, Huang J, Wang X, et al. ATG7-Mediated Autophagy Involves in miR-138-5p Regulated Self-Renewal and Invasion of Lung Cancer Stem-Like Cells Derived From A549 Cells. *Anticancer Drugs* (2021) 32(4):376–85. doi: 10.1097/CAD.0000000000000979
63. Turley SJ, Cremasco V, Astarita JL. Immunological Hallmarks of Stromal Cells in the Tumour Microenvironment. *Nat Rev Immunol* (2015) 15 (11):669–82. doi: 10.1038/nri3902
64. Kalluri R. The Biology and Function of Fibroblasts in Cancer. *Nat Rev Cancer* (2016) 16(9):582–98. doi: 10.1038/nrc.2016.73
65. Yan Y, Chen X, Wang X, Zhao Z, Hu W, Zeng S, et al. The Effects and the Mechanisms of Autophagy on the Cancer-Associated Fibroblasts in Cancer. *J Exp Clin Cancer Res* (2019) 38(1):171. doi: 10.1186/s13046-019-1172-5
66. Rojas-Sanchez G, Cotzomi-Ortega I, Pazos-Salazar NG, Reyes-Leyva J, Maycotte P. Autophagy and Its Relationship to Epithelial to Mesenchymal Transition: When Autophagy Inhibition for Cancer Therapy Turns Counterproductive. *Biol (Basel)* (2019) 8(4):71. doi: 10.3390/biology8040071
67. Marcucci F, Ghezzi P, Rumio C. The Role of Autophagy in the Cross-Talk Between Epithelial-Mesenchymal Transitioned Tumor Cells and Cancer Stem-Like Cells. *Mol Cancer* (2017) 16(1):3. doi: 10.1186/s12943-016-0573-8
68. Alizadeh J, Glogowska A, Thliveris J, Kalantari F, Shojaei S, Hombach-Klonisch S, et al. Autophagy Modulates Transforming Growth Factor Beta 1 Induced Epithelial to Mesenchymal Transition in Non-Small Cell Lung Cancer Cells. *Biochim Biophys Acta Mol Cell Res* (2018) 1865(5):749–68. doi: 10.1016/j.bbamcr.2018.02.007
69. Shen H, Yin L, Deng G, Guo C, Han Y, Li Y, et al. Knockdown of Beclin-1 Impairs Epithelial-Mesenchymal Transition of Colon Cancer Cells. *J Cell Biochem* (2018) 119(8):7022–31. doi: 10.1002/jcb.26912
70. Peng YF, Shi YH, Ding ZB, Ke AW, Gu CY, Hui B, et al. Autophagy Inhibition Suppresses Pulmonary Metastasis of HCC in Mice *via* Impairing Anoikis Resistance and Colonization of HCC Cells. *Autophagy* (2013) 9 (12):2056–68. doi: 10.4161/auto.26398
71. Sun M, Zhao S, Duan Y, Ma Y, Wang Y, Ji H, et al. GLUT1 Participates in Tamoxifen Resistance in Breast Cancer Cells Through Autophagy Regulation. *Naunyn Schmiedebergs Arch Pharmacol* (2021) 394(1):205–16. doi: 10.1007/s00210-020-01893-3
72. Roberts DJ, Tan-Sah VP, Ding EY, Smith JM, Miyamoto S. Hexokinase-II Positively Regulates Glucose Starvation-Induced Autophagy Through TORC1 Inhibition. *Mol Cell* (2014) 53(4):521–33. doi: 10.1016/j.molcel.2013.12.019
73. Chen G, Zhang Y, Liang J, Li W, Zhu Y, Zhang M, et al. Deregulation of Hexokinase II Is Associated With Glycolysis, Autophagy, and the Epithelial-Mesenchymal Transition in Tongue Squamous Cell Carcinoma Under Hypoxia. *BioMed Res Int* (2018) 2018:8480762. doi: 10.1155/2018/8480762
74. Mukhopadhyay S, Biancur DE, Parker SJ, Yamamoto K, Banh RS, Paulo JA, et al. Autophagy Is Required for Proper Cysteine Homeostasis in Pancreatic Cancer Through Regulation of SLC7A11. *Proc Natl Acad Sci USA* (2021) 118 (6):e2021475118. doi: 10.1073/pnas.2021475118

75. Chen Y, McMillan-Ward E, Kong J, Israels SJ, Gibson SB. Mitochondrial Electron-Transport-Chain Inhibitors of Complexes I and II Induce Autophagic Cell Death Mediated by Reactive Oxygen Species. *J Cell Sci* (2007) 120(Pt 23):4155–66. doi: 10.1242/jcs.011163
76. Scherz-Shouval R, Shvets E, Fass E, Shorer H, Gil L, Elazar Z. Reactive Oxygen Species Are Essential for Autophagy and Specifically Regulate the Activity of Atg4. *EMBO J* (2007) 26(7):1749–60. doi: 10.1038/sj.emboj.7601623
77. Dewaele M, Maes H, Agostinis P. ROS-Mediated Mechanisms of Autophagy Stimulation and Their Relevance in Cancer Therapy. *Autophagy* (2010) 6 (7):838–54. doi: 10.4161/auto.6.7.12113
78. Mathew R, Karp CM, Beaudoin B, Vuong N, Chen G, Chen HY, et al. Autophagy Suppresses Tumorigenesis Through Elimination of P62. *Cell* (2009) 137(6):1062–75. doi: 10.1016/j.cell.2009.03.048
79. Nihira K, Miki Y, Iida S, Narumi S, Ono K, Iwabuchi E, et al. An Activation of LC3A-Mediated Autophagy Contributes to *De Novo* and Acquired Resistance to EGFR Tyrosine Kinase Inhibitors in Lung Adenocarcinoma. *J Pathol* (2014) 234(2):277–88. doi: 10.1002/path.4354
80. Li YY, Lam SK, Mak JC, Zheng CY, Ho JC. Erlotinib-Induced Autophagy in Epidermal Growth Factor Receptor Mutated Non-Small Cell Lung Cancer. *Lung Cancer* (2013) 81(3):354–61. doi: 10.1016/j.lungcan.2013.05.012
81. Zou Y, Ling YH, Sironi J, Schwartz EL, Perez-Soler R, Piperdi B. The Autophagy Inhibitor Chloroquine Overcomes the Innate Resistance of Wild-Type EGFR Non-Small-Cell Lung Cancer Cells to Erlotinib. *J Thorac Oncol* (2013) 8(6):693–702. doi: 10.1097/JTO.0b013e31828c7210
82. Bouhsira E, Franc M, Lienard E, Bouillin C, Gandoin C, Geurden T, et al. The Efficacy of a Selamectin (Stronghold ®) Spot on Treatment in the Prevention of Bartonella Henselae Transmission by Ctenocephalides Felis in Cats, Using a New High-Challenge Model. *Parasitol Res* (2015) 114(3):1045–50. doi: 10.1007/s00436-014-4271-4
83. Han W, Pan H, Chen Y, Sun J, Wang Y, Li J, et al. EGFR Tyrosine Kinase Inhibitors Activate Autophagy as a Cytoprotective Response in Human Lung Cancer Cells. *PloS One* (2011) 6(6):e18691. doi: 10.1371/journal.pone.0018691
84. Liu JT, Li WC, Gao S, Wang F, Li XQ, Yu HQ, et al. Autophagy Inhibition Overcomes the Antagonistic Effect Between Gefitinib and Cisplatin in Epidermal Growth Factor Receptor Mutant Non–Small-Cell Lung Cancer Cells. *Clin Lung Cancer* (2015) 16(5):e55-66. doi: 10.1016/j.cllc.2015.03.006
85. Ji C, Zhang L, Cheng Y, Patel R, Wu H, Zhang Y, et al. Induction of Autophagy Contributes to Crizotinib Resistance in ALK-Positive Lung Cancer. *Cancer Biol Ther* (2014) 15(5):570–7. doi: 10.4161/cbt.28162
86. Mizushima N, Klionsky DJ. Protein Turnover *via* Autophagy: Implications for Metabolism. *Annu Rev Nutr* (2007) 27:19–40. doi: 10.1146/annurev.nutr.27.061406.093749
87. Gorzalczany Y, Gilad Y, Amihai D, Hammel I, Sagi-Eisenberg R, Merimsky O. Combining an EGFR Directed Tyrosine Kinase Inhibitor With Autophagy-Inducing Drugs: A Beneficial Strategy to Combat Non-Small Cell Lung Cancer. *Cancer Lett* (2011) 310(2):207–15. doi: 10.1016/j.canlet.2011.07.002
88. Amaravadi RK, Lippincott-Schwartz J, Yin XM, Weiss WA, Takebe N, Timmer W, et al. Principles and Current Strategies for Targeting Autophagy for Cancer Treatment. *Clin Cancer Res* (2011) 17(4):654–66. doi: 10.1158/1078-0432.CCR-10-2634
89. Yamamoto K, Venida A, Yano J, Biancur DE, Kakiuchi M, Gupta S, et al. Autophagy Promotes Immune Evasion of Pancreatic Cancer by Degrading MHC-I. *Nature* (2020) 581(7806):100–5. doi: 10.1038/s41586-020-2229-5
90. Yamamoto K, Venida A, Perera RM, Kimmelman AC. Selective Autophagy of MHC-I Promotes Immune Evasion of Pancreatic Cancer. *Autophagy* (2020) 16(8):1524–5. doi: 10.1080/15548627.2020.1769973
91. Noman MZ, Parpal S, Van Moer K, Xiao M, Yu Y, Viklund J, et al. Inhibition of Vps34 Reprograms Cold Into Hot Inflamed Tumors and Improves Anti-PD-1/PD-L1 Immunotherapy. *Sci Adv* (2020) 6(18):eaax7881. doi: 10.1126/sciadv.aax7881
92. Baginska J, Viry E, Berchem G, Poli A, Noman MZ, van Moer K, et al. Granzyme B Degradation by Autophagy Decreases Tumor Cell Susceptibility to Natural Killer-Mediated Lysis Under Hypoxia. *Proc Natl Acad Sci USA* (2013) 110(43):17450–5. doi: 10.1073/pnas.1304790110
93. Noman MZ, Janji B, Kaminska B, Van Moer K, Pierson S, Przanowski P, et al. Blocking Hypoxia-Induced Autophagy in Tumors Restores Cytotoxic T-Cell Activity and Promotes Regression. *Cancer Res* (2011) 71(18):5976–86. doi: 10.1158/0008-5472.Can-11-1094
94. Zamame Ramirez JA, Romagnoli GG, Falasco BF, Gorgulho CM, Sanzochi Fogolin C, Dos Santos DC, et al. Blocking Drug-Induced Autophagy With Chloroquine in HCT-116 Colon Cancer Cells Enhances DC Maturation and T Cell Responses Induced by Tumor Cell Lysate. *Int Immunopharmacol* (2020) 84:106495. doi: 10.1016/j.intimp.2020.106495
95. Guerriero JL. Macrophages: Their Untold Story in T Cell Activation and Function. *Int Rev Cell Mol Biol* (2019) 342:73–93. doi: 10.1016/bs.ircmb.2018.07.001
96. Ma F, Ding MG, Lei YY, Luo LH, Jiang S, Feng YH, et al. SKIL Facilitates Tumorigenesis and Immune Escape of NSCLC *via* Upregulating TAZ/autophagy Axis. *Cell Death Dis* (2020) 11(12):1028. doi: 10.1038/s41419-020-03200-7
97. Wei J, Long L, Yang K, Guy C, Shrestha S, Chen Z, et al. Autophagy Enforces Functional Integrity of Regulatory T Cells by Coupling Environmental Cues and Metabolic Homeostasis. *Nat Immunol* (2016) 17(3):277–85. doi: 10.1038/ni.3365
98. Parker KH, Horn LA, Ostrand-Rosenberg S. High-Mobility Group Box Protein 1 Promotes the Survival of Myeloid-Derived Suppressor Cells by Inducing Autophagy. *J Leukoc Biol* (2016) 100(3):463–70. doi: 10.1189/jlb.3HI0715-305R
99. Li W, Tanikawa T, Kryczek I, Xia H, Li G, Wu K, et al. Aerobic Glycolysis Controls Myeloid-Derived Suppressor Cells and Tumor Immunity *via* a Specific CEBPB Isoform in Triple-Negative Breast Cancer. *Cell Metab* (2018) 28(1):87–103.e6. doi: 10.1016/j.cmet.2018.04.022
100. Chen D, Xie J, Fiskesund R, Dong W, Liang X, Lv J, et al. Chloroquine Modulates Antitumor Immune Response by Resetting Tumor-Associated Macrophages Toward M1 Phenotype. *Nat Commun* (2018) 9(1):873. doi: 10.1038/s41467-018-03225-9
101. Cunha LD, Yang M, Carter R, Guy C, Harris L, Crawford JC, et al. LC3-Associated Phagocytosis in Myeloid Cells Promotes Tumor Immune Tolerance. *Cell* (2018) 175(2):429–441.e16. doi: 10.1016/j.cell.2018.08.061
102. Schmitz KJ, Ademi C, Bertram S, Schmid KW, Baba HA. Prognostic Relevance of Autophagy-Related Markers LC3, P62/Sequestosome 1, Beclin-1 and ULK1 in Colorectal Cancer Patients With Respect to KRAS Mutational Status. *World J Surg Oncol* (2016) 14(1):189–9. doi: 10.1186/s12957-016-0946-x
103. Lazova R, Camp RL, Klump V, Siddiqui SF, Amaravadi RK, Pawelek JM. Punctate LC3B Expression Is A Common Feature of Solid Tumors and Associated With Proliferation, Metastasis, and Poor Outcome. *Clin Cancer Res* (2012) 18(2):370–9. doi: 10.1158/1078-0432.Ccr-11-1282
104. Wu DH, Jia CC, Chen J, Lin ZX, Ruan DY, Li X, et al. Autophagic LC3B Overexpression Correlates With Malignant Progression and Predicts a Poor Prognosis in Hepatocellular Carcinoma. *Tumour Biol* (2014) 35(12):12225–33. doi: 10.1007/s13277-014-2531-7
105. Schläfli AM, Adams O, Galván JA, Gugger M, Savic S, Bubendorf L, et al. Prognostic Value of the Autophagy Markers LC3 and P62/SQSTM1 in Early-Stage Non-Small Cell Lung Cancer. *Oncotarget* (2016) 7(26):39544–55. doi: 10.18632/oncotarget.9647
106. Sivridis E, Koukourakis MI, Zois CE, Ledaki I, Ferguson DJ, Harris AL, et al. LC3A-Positive Light Microscopy Detected Patterns of Autophagy and Prognosis in Operable Breast Carcinomas. *Am J Pathol* (2010) 176 (5):2477–89. doi: 10.2353/ajpath.2010.090049
107. Karpathiou G, Sivridis E, Koukourakis MI, Mikroulis D, Bouros D, Froudarakis ME, et al. Light-Chain 3A Autophagic Activity and Prognostic Significance in Non-Small Cell Lung Carcinomas. *Chest* (2011) 140(1):127–34. doi: 10.1378/chest.10-1831
108. Wang X, Du Z, Li L, Shi M, Yu Y. Beclin 1 and P62 Expression in Non-Small Cell Lung Cancer: Relation With Malignant Behaviors and Clinical Outcome. *Int J Clin Exp Pathol* (2015) 8(9):10644–52.
109. Inoue D, Suzuki T, Mitsuishi Y, Miki Y, Suzuki S, Sugawara S, et al. Accumulation of P62/SQSTM1 Is Associated With Poor Prognosis in Patients With Lung Adenocarcinoma. *Cancer Sci* (2012) 103(4):760–6. doi: 10.1111/j.1349-7006.2012.02216.x

110. Wu DH, Wang TT, Ruan DY, Li X, Chen ZH, Wen JY, et al. Combination of ULK1 and LC3B Improve Prognosis Assessment of Hepatocellular Carcinoma. *BioMed Pharmacother* (2018) 97:195–202. doi: 10.1016/j.biopha.2017.10.025
111. Zhou W, Yue C, Deng J, Hu R, Xu J, Feng L, et al. Autophagic Protein Beclin 1 Serves as an Independent Positive Prognostic Biomarker for Non-Small Cell Lung Cancer. *PloS One* (2013) 8(11):e80338. doi: 10.1371/journal.pone.0080338
112. Zheng T, Li D, He Z, Feng S, Zhao S. Prognostic and Clinicopathological Significance of Beclin-1 in Non-Small-Cell Lung Cancer: A Meta-Analysis. *Onco Targets Ther* (2018) 11:4167–75. doi: 10.2147/ott.S164987
113. Liu PF, Chen HC, Cheng JS, Tsai WL, Lee HP, Wang SC, et al. Association of ATG4B and Phosphorylated ATG4B Proteins With Tumorigenesis and Prognosis in Oral Squamous Cell Carcinoma. *Cancers (Basel)* (2019) 11 (12):1854. doi: 10.3390/cancers11121854
114. Losmanová T, Janser FA, Humbert M, Tokarchuk I, Schläfli AM, Neppl C, et al. Chaperone-Mediated Autophagy Markers LAMP2A and HSC70 Are Independent Adverse Prognostic Markers in Primary Resected Squamous Cell Carcinomas of the Lung. *Oxid Med Cell Longev* (2020) 2020:8506572. doi: 10.1155/2020/8506572
115. Jiang A, Liu N, Bai S, Wang J, Gao H, Zheng X, et al. Identification and Validation of an Autophagy-Related Long Non-Coding RNA Signature as a Prognostic Biomarker for Patients With Lung Adenocarcinoma. *J Thorac Dis* (2021) 13(2):720–34. doi: 10.21037/jtd-20-2803
116. Puissant A, Fenouille N, Auberger P. When Autophagy Meets Cancer Through P62/SQSTM1. *Am J Cancer Res* (2012) 2(4):397–413.
117. Lin MG, Hurley JH. Structure and Function of the ULK1 Complex in Autophagy. *Curr Opin Cell Biol* (2016) 39:61–8. doi: 10.1016/j.ceb.2016.02.010
118. Egan DF, Chun MG, Vamos M, Zou H, Rong J, Miller CJ, et al. Small Molecule Inhibition of the Autophagy Kinase ULK1 and Identification of ULK1 Substrates. *Mol Cell* (2015) 59(2):285–97. doi: 10.1016/j.molcel.2015.05.031
119. Petherick KJ, Conway OJ, Mpamhanga C, Osborne SA, Kamal A, Saxty B, et al. Pharmacological Inhibition of ULK1 Kinase Blocks Mammalian Target of Rapamycin (mTOR)-Dependent Autophagy. *J Biol Chem* (2015) 290 (18):11376–83. doi: 10.1074/jbc.C114.627778
120. Nguyen TG, Honson NS, Arns S, Davis TL, Dhe-Paganon S, Kovacic S, et al. Development of Fluorescent Substrates and Assays for the Key Autophagy-Related Cysteine Protease Enzyme, ATG4B. *Assay Drug Dev Technol* (2014) 12(3):176–89. doi: 10.1089/adt.2013.561
121. Akin D, Wang SK, Habibzadegah-Tari P, Law B, Ostrov D, Li M, et al. A Novel ATG4B Antagonist Inhibits Autophagy and has a Negative Impact on Osteosarcoma Tumors. *Autophagy* (2014) 10(11):2021–35. doi: 10.4161/auto.32229
122. Wu S, Su J, Qian H, Guo T. SLC27A4 Regulate ATG4B Activity and Control Reactions to Chemotherapeutics-Induced Autophagy in Human Lung Cancer Cells. *Tumour Biol* (2016) 37(5):6943–52. doi: 10.1007/s13277-015-4587-4
123. Mizushima N, Yoshimori T, Ohsumi Y. The Role of Atg Proteins in Autophagosome Formation. *Annu Rev Cell Dev Biol* (2011) 27:107–32. doi: 10.1146/annurev-cellbio-092910-154005
124. Levine B, Sinha S, Kroemer G. Bcl-2 Family Members: Dual Regulators of Apoptosis and Autophagy. *Autophagy* (2008) 4(5):600–6. doi: 10.4161/auto.6260
125. Moon EK, Kim SH, Hong Y, Chung DI, Goo YK, Kong HH. Autophagy Inhibitors as a Potential Antiamoebic Treatment for Acanthamoeba Keratitis. *Antimicrob Agents Chemother* (2015) 59(7):4020–5. doi: 10.1128/aac.05165-14
126. Mao X, Nanzhang, Xiao J, Wu H, Ding K. Hypoxia-Induced Autophagy Enhances Cisplatin Resistance in Human Bladder Cancer Cells by Targeting Hypoxia-Inducible Factor-1α. *J Immunol Res* (2021) 2021:8887437. doi: 10.1155/2021/8887437
127. McAfee Q, Zhang Z, Samanta A, Levi SM, Ma X-H, Piao S, et al. Autophagy Inhibitor Lys05 has Single-Agent Antitumor Activity and Reproduces the Phenotype of a Genetic Autophagy Deficiency. *Proc Natl Acad Sci USA* (2012) 109(21):8253–8. doi: 10.1073/pnas.1118193109
128. Goodall ML, Wang T, Martin KR, Kortus MG, Kauffman AL, Trent JM, et al. Development of Potent Autophagy Inhibitors That Sensitize Oncogenic BRAF V600E Mutant Melanoma Tumor Cells to Vemurafenib. *Autophagy* (2014) 10(6):1120–36. doi: 10.4161/auto.28594
129. Pellegrini P, Strambi A, Zipoli C, Hägg-Olofsson M, Buoncervello M, Linder S, et al. Acidic Extracellular pH Neutralizes the Autophagy-Inhibiting Activity of Chloroquine: Implications for Cancer Therapies. *Autophagy* (2014) 10(4):562–71. doi: 10.4161/auto.27901
130. Wang T, Goodall ML, Gonzales P, Sepulveda M, Martin KR, Gately S, et al. Synthesis of Improved Lysomotropic Autophagy Inhibitors. *J Med Chem* (2015) 58(7):3025–35. doi: 10.1021/jm501586m
131. Mauvezin C, Neufeld TP. Bafilomycin A1 Disrupts Autophagic Flux by Inhibiting Both V-ATPase-Dependent Acidification and Ca-P60A/SERCA-Dependent Autophagosome-Lysosome Fusion. *Autophagy* (2015) 11 (8):1437–8. doi: 10.1080/15548627.2015.1066957
132. Yang YP, Hu LF, Zheng HF, Mao CJ, Hu WD, Xiong KP, et al. Application and Interpretation of Current Autophagy Inhibitors and Activators. *Acta Pharmacol Sin* (2013) 34(5):625–35. doi: 10.1038/aps.2013.5
133. Briceño E, Reyes S, Sotelo J. Therapy of Glioblastoma Multiforme Improved by the Antimutagenic Chloroquine. *Neurosurg Focus* (2003) 14(2):e3. doi: 10.3171/foc.2003.14.2.4
134. Sotelo J, Briceño E, López-González MA. Adding Chloroquine to Conventional Treatment for Glioblastoma Multiforme: A Randomized, Double-Blind, Placebo-Controlled Trial. *Ann Intern Med* (2006) 144 (5):337–43. doi: 10.7326/0003-4819-144-5-200603070-00008
135. Goldberg SB, Supko JG, Neal JW, Muzikansky A, Digumarthy S, Fidias P, et al. A Phase I Study of Erlotinib and Hydroxychloroquine in Advanced Non-Small-Cell Lung Cancer. *J Thorac Oncol* (2012) 7(10):1602–8. doi: 10.1097/JTO.0b013e318262de4a
136. Rojas-Puentes LL, Gonzalez-Pinedo M, Crismatt A, Ortega-Gomez A, Gamboa-Vignolle C, Nuñez-Gomez R, et al. Phase II Randomized, Double-Blind, Placebo-Controlled Study of Whole-Brain Irradiation With Concomitant Chloroquine for Brain Metastases. *Radiat Oncol* (2013) 8:209. doi: 10.1186/1748-717x-8-209
137. Malhotra J, Jabbour S, Orlick M, Riedlinger G, Guo Y, White E, et al. Phase Ib/II Study of Hydroxychloroquine in Combination With Chemotherapy in Patients With Metastatic Non-Small Cell Lung Cancer (NSCLC). *Cancer Treat Res Commun* (2019) 21:100158. doi: 10.1016/j.ctarc.2019.100158
138. Pasquier B. Autophagy Inhibitors. *Cell Mol Life Sci* (2016) 73(5):985–1001. doi: 10.1007/s00018-015-2104-y
139. Guo JY, White E. Autophagy, Metabolism, and Cancer. *Cold Spring Harb Symp Quant Biol* (2016) 81:73–8. doi: 10.1101/sqb.2016.81.030981

Conflict of Interest: The authors declare that the research was conducted in the absence of any commercial or financial relationships that could be construed as a potential conflict of interest.

Publisher's Note: All claims expressed in this article are solely those of the authors and do not necessarily represent those of their affiliated organizations, or those of the publisher, the editors and the reviewers. Any product that may be evaluated in this article, or claim that may be made by its manufacturer, is not guaranteed or endorsed by the publisher.

Copyright © 2022 Guo, Du, Lu and Hu. This is an open-access article distributed under the terms of the Creative Commons Attribution License (CC BY). The use, distribution or reproduction in other forums is permitted, provided the original author(s) and the copyright owner(s) are credited and that the original publication in this journal is cited, in accordance with accepted academic practice. No use, distribution or reproduction is permitted which does not comply with these terms.

Frontiers in
Cell and Developmental Biology

Explores the fundamental biological processes of life, covering intracellular and extracellular dynamics.

The world's most cited developmental biology journal, advancing our understanding of the fundamental processes of life. It explores a wide spectrum of cell and developmental biology, covering intracellular and extracellular dynamics.

Discover the latest Research Topics

See more →



Frontiers

Avenue du Tribunal-Fédéral 34
1005 Lausanne, Switzerland
frontiersin.org

Contact us

+41 (0)21 510 17 00
frontiersin.org/about/contact